

3 5 ✓

THE JOURNAL OF PHYSICAL CHEMISTRY

Volume 70

MAY—AUGUST 1966

PAGES 1341—2708

FREDERICK T. WALL, *Editor*

BERNARD KIRTMAN, GLENN H. MILLER, AND HENRY W. OFFEN, *Assistant Editors*

EDITORIAL BOARD

L. F. DAHL
B. P. DAILEY
F. S. DAINTON
J. R. FRESCO
G. J. HILLS
C. J. HOCHANADEL
C. KEMBALL

W. KLEMPERER
A. KUPPERMAN
F. A. LONG
J. L. MARGRAVE
J. P. McCULLOUGH
W. J. MOORE
W. A. NOYES, JR.

R. G. PARR
G. PORTER
B. S. RABINOVITCH
W. G. SCHNEIDER
S. I. WEISSMAN
W. WEST
B. ZIMM

CHARLES R. BERTSCH, *Senior Production Editor*

RICHARD H. BELKNAP
Assistant Director of Publications
Director of Research Journals

RICHARD L. KENYON
Director of Publications

JOSEPH H. KUNEY
Director of Business Operations
Director of Publications Research

EASTON, PA.
MACK PRINTING COMPANY
1966

THE JOURNAL OF PHYSICAL CHEMISTRY

FREDERICK T. WALL, *Editor*

BERNARD KIRTMAN, GLENN H. MILLER, HENRY W. OFFEN, *Assistant Editors*

EDITORIAL BOARD: L. F. DAHL (1965-1969), B. P. DAILEY (1963-1967),
F. S. DAINTON (1962-1966), J. R. FRESCO (1965-1969), G. J. HILLS (1966-1970),
C. J. HOCHANADEL (1963-1966), C. KEMBALL (1964-1968),
W. KLEMPERER (1964-1968), A. KUPPERMAN (1965-1969), F. A. LONG (1964-1968),
J. L. MARGRAVE (1963-1967), J. P. McCULLOUGH (1962-1966),
W. J. MOORE (1964-1968), W. A. NOYES, JR. (1965-1969), R. G. PARR (1963-1967),
G. PORTER (1963-1967), B. S. RABINOVITCH (1966-1970), W. G. SCHNEIDER (1966-1970),
S. I. WEISSMAN (1966-1970), W. WEST (1962-1966), B. ZIMM (1964-1968)

CHARLES R. BERTSCH, *Senior Production Editor*

AMERICAN CHEMICAL SOCIETY PUBLICATIONS, 1155 Sixteenth St., N.W., Washington, D. C. 20036

RICHARD L. KENYON, *Director of Publications*

RICHARD H. BELKNAP, *Assistant Director of Publications and Director of Research Journals*

JOSEPH H. KUNEY, *Director of Business Operations and Director of Publications Research*

Copyright, 1966, by the American Chemical Society. Published monthly by the American Chemical Society at 20th and Northampton Sts., Easton, Pa. 18042. Second-class postage paid at Easton, Pa.

The Journal of Physical Chemistry is devoted to the publication of contributed papers in the broad field of physical chemistry. Preference for publication in *The Journal of Physical Chemistry* is given to papers dealing with fundamental concepts, atomic and molecular phenomena, and systems in which clearly defined models are applicable. Manuscripts containing extensive reviews, reevaluations of existing data, applied chemical data, or measurements on materials of ill-defined nature are, in general, not acceptable for publication. Symposium papers may be published as a group, but only through special arrangement with the Editor.

Except as immediately following, all manuscripts should be sent to *The Journal of Physical Chemistry*, Department of Chemistry, University of California, Santa Barbara, Calif. 93106. Manuscripts originating in the British Isles, Europe, and Africa should be sent to F. C. TOMPKINS, The Faraday Society, 6 Gray's Inn Square, London, W. C. 1, England.

All manuscripts should be submitted in duplicate, including an original typewritten, double-spaced copy. Original drawings should accompany the manuscript. Lettering at the sides of graphs (black on white or blue) may be pencilled in and will be typeset. Figures and tables should be held to a minimum consistent with adequate presentation of information. All footnotes and references to the literature should be numbered consecutively and placed in the manuscript at the proper places. Initials of authors referred to in citations should be given. Nomenclature should conform to that used in *Chemical Abstracts*, mathematical characters should be marked for italic, Greek letters carefully made or annotated, and subscripts and superscripts clearly shown.

Articles should be written as briefly as possible consistent with clarity, avoiding historical background unnecessary for specialists. They should cover their subjects with reasonable thoroughness and completeness and should not depend for their usefulness on papers to be published later. A brief abstract, generally not exceeding 300 words, should appear at the beginning of each article. All articles are subject to critical reviews by referees.

Notes are similar to Articles, but are shorter and not accompanied by abstracts. The length of a Note, including tables, figures, and text, must not exceed 1.5 journal pages (1500 words or the equivalent). A Note treats a limited subject with reasonable completeness and should not be considered a preliminary notice. Like Articles, Notes are subject to critical review by referees.

Communications to the Editor are divided into two categories, Letters and Comments. The length of a Communication, including tables, figures, and text, must not exceed three-fourths of a page (750 words or the equivalent).

Letters should report preliminary results of immediate interest.

It is expected that the material in Letters may be republished in *The Journal of Physical Chemistry* at a later date in more complete form. Communications in this category will be treated expeditiously but are subject to review by the Editor and readily available experts.

Comments include significant remarks on the work of others or observations of unusual interest which the authors do not intend to pursue. In the former case, the authors of the work being discussed will, ordinarily, be allowed to reply. Comments are not refereed but are published at the discretion of the Editor.

Additions and Corrections are published once yearly in the December issue. See Volume 69, Number 12 for the proper form.

Extensive or unusual alterations in an article after it has been set in type are made at the author's expense, and it is understood that by entering such alterations on proofs the author agrees to defray the cost thereof.

The American Chemical Society and the Editor of *The Journal of Physical Chemistry* assume no responsibility for the statements and opinions advanced by contributors.

Correspondence regarding accepted copy, proofs, and reprints should be directed to Research Journals Production Office, American Chemical Society, 20th and Northampton Sts., Easton, Pa. 18042. Senior Production Editor: CHARLES R. BERTSCH. Assistant Senior Production Editor: MARIANNE C. BROGAN. Assistant Editors: EDWARD A. BORGER and CELIA B. McFARLAND.

Advertising Office: Reinhold Publishing Corporation, 430 Park Ave., New York, N. Y. 10022.

Business and Subscription Information

Remittances and orders for subscriptions and for single copies, notices of changes of address and new professional connections, and claims for missing numbers should be sent to the Subscription Service Department, American Chemical Society, 1155 Sixteenth St., N.W., Washington, D. C. 20036. Four weeks should be allowed for changes of address. Please include an old address label with the notification.

Claims for missing numbers will not be allowed (1) if received more than sixty days from date of issue, (2) if loss was due to failure of notice of change of address to be received before the date specified in the preceding paragraph, or (3) if the reason for the claim is "missing from files."

Subscription rates (1966): members of the American Chemical Society, \$12.00 for 1 year; to nonmembers, \$24.00 for 1 year. Postage to Canada and countries in the Pan-American Union, \$2.00; all other countries, \$3.00. Single copies for current year: \$2.50. Postage, single copies: to Canada and countries in the Pan-American Union, \$0.15; all other countries, \$0.20. Rates for back issues are available from the Special Issues Sales Department, 1155 Sixteenth St., N.W., Washington, D. C. 20036.

Look at it this way... and you'll buy Kimax

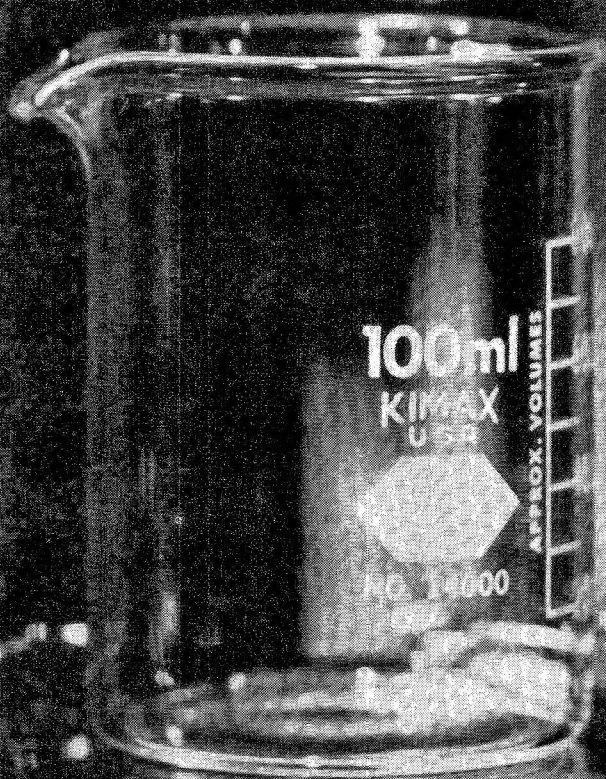
This cross-sectional view shows why KIMAX® beakers are a cut above the ordinary. Walls that are uniform and heavier... rugged rims built to withstand long hard use... an improved pour-out design. And note the printed volume scale — another thoughtful improvement you now get at no extra cost. Altogether, quite a change from the beakers on the market just a few years ago.

Kimble now is offering beakers and Erlenmeyer flasks *in lower case quantities*, for convenience and economy.

Shouldn't you look at it this way, for the best value in scientific glassware?

OWENS-ILLINOIS

Maker of Kimble Products
Toledo, Ohio 43601

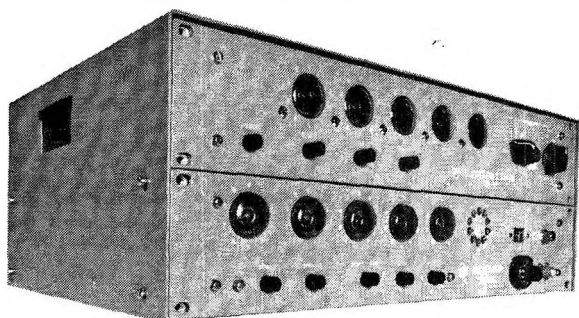


THE JOURNAL OF
PHYSICAL CHEMISTRY

Volume 70, Number 5 May 1966

| | | |
|--|--|------|
| The Yield of Scavengable Hydrogen Atoms from the Radiolysis of Saturated Hydrocarbons | Richard A. Holroyd | 1341 |
| Equilibrium Studies of the Reaction $2\text{Al(l)} + \text{AlCl}_3\text{(g)} \rightleftharpoons 3\text{AlCl(g)}$ | D. Bhogeswara Rao and V. V. Dadape | 1349 |
| Distribution of Benzoic Acid between Benzene and Water and Dimerization of Benzoic Acid in Benzene | A. K. M. Shamsul Huq and S. A. K. Lodhi | 1354 |
| The Effect of Solvent on the Rate of Formation of Monoacetylacetonatocopper(II) Ion | Raymond C. Barile, Michael Cefola, Philip S. Gentile, and Alfred V. Celiano | 1358 |
| Considerations on the Distribution of Ions between an Organic Solution of Alkylammonium Salts and an Aqueous Solution of Inorganic Salts in the Presence of Homopolymers and Heteropolymers in the Organic Phase | G. Scibona | 1365 |
| Dielectric Dispersion of Deoxyribonucleic Acid. II | Shiro Takashima | 1372 |
| The Concept of Length in the Thermodynamics of Elastic Bodies | Hans J. Kuhn | 1380 |
| Kinetics of Formation and Growth of Colloidal Silver Bromide Particles. II | E. J. Meehan and Grace Chiu | 1384 |
| Electron Spin Resonance Studies of γ -Irradiated High Surface Area Silica. I. Identification of Defects | G. M. Muha | 1390 |
| Electron Spin Resonance Studies of γ -Irradiated High Surface Area Silica. II. Effect of Adsorbed Molecules | G. M. Muha and D. J. C. Yates | 1399 |
| Kinetics of the Water-Gas Equilibrium Reaction. I. The Reaction of Carbon Dioxide with Hydrogen | G. L. Tingey | 1406 |
| Infrared Spectroscopic Investigations of Zeolites and Adsorbed Molecules. II. Adsorbed Carbon Monoxide | C. L. Angell and Paul C. Schaffer | 1413 |
| Radiolysis of Oxalate Alkaline Solutions in the Presence of Oxygen | Z. D. Draganić, I. G. Draganic, and M. M. Kosanić | 1418 |
| Effect of Pressure on Conductance. II. Walden Products and Ionic Association in Methanol | James F. Skinner and Raymond M. Fuoss | 1426 |
| Intramolecular Hydrogen Bonding in the Hydrogen Anions of Some Carboxylic Acids in Water and Water-Methanol Mixtures. Evidence from Proton Magnetic Resonance | Brian L. Silver, Z. Luz, S. Peller, and J. Reuben | 1434 |
| Photochemistry of the Fluoro Ketones. 1,1,3,3-Tetrafluoroacetone | G. O. Pritchard and J. T. Bryant | 1441 |
| Arsenic(IV) as an Intermediate in the Photochemical Oxidation of Ferrous Sulfate in the Presence of Arsenic Acid | R. Woods | 1446 |
| Structure and Transition in the Solid State of a Helical Macromolecule | A. J. McKinnon and A. V. Tobolsky | 1453 |
| Theoretical Calculations on Ions and Radicals. I. A Restricted Hartree-Fock Perturbation Method for the Calculation of Spin Densities | J. E. Bloor, B. R. Gilson, and P. N. Daykin | 1457 |
| The Thermal Decomposition of Methyl Ketene | P. G. Blake and K. J. Hole | 1464 |
| The N-Isopropylcarbazole-Picryl Chloride System | Paul Cherin and Michael Burack | 1470 |
| Ion-Solvent Size Ratio as a Factor in the Thermodynamics of Electrolytes | B. E. Conway and R. E. Verrall | 1473 |

TRANSISTORIZED SCALER/TIMER



No other company can offer this quality and accuracy for such a low price. NUCLEAR SUPPLIES Scaler/Timer can be used with GM, Scintillation, Gas flow, Proportional, Bf, and solid state detectors. It is used in hospitals, medical centers, for experimentation, classroom demonstration and industrial quality control. Reliable and rugged plug-in transistorized circuit boards are used throughout.

\$990

Manufactured exclusively for NUCLEAR SUPPLIES by the world's first company to successfully build transistorized nuclear equipment, Kobe Industries Corp. of Japan. Complete line of instruments, modules, automatic systems and accessories listed in new catalog. Write to: NUCLEAR SUPPLIES Incorporated, P.O. Box 312, Encino, California, Phone Area Code 213, 787-1722.

SCALER

MODEL SA-250

300-3000 volts, adjustable high voltage
1 μ second resolving time
5 μ A pulses can be scaled
Push button aural speaker
999,999 total counts
Transistorized printed circuit boards
19" w. | 3½" h. | 14" d.

Price \$495

TIMER


MODEL TM-12

9999.9 switch selected mins. or secs.
Preset time dual selection
Push button start | stop | reset control
Time base 60 c/s line frequency
Ambient temperature, -25C to +55C
Transistorized printed circuit boards
19" w. | 3½" h. | 14" d.

Price \$495



2333 Boron tribromide, 99.5%
\$5.00/10g, \$24.00/100g.
6462 Sodium trichloroacetate
\$22.50/kg.




RARE CHEMICALS FINE

CATALOG
NUMBER 5

SEND FOR CATALOG #5

TELEPHONE
AREA CODE 516
GENERAL 3-6262



TWX 516-433-8184
TELEX 01-26464
CABLE: KALABOR PLAINVIEWNEWYORK
LABORATORIES, INC.
122 EXPRESS STREET, ENGINEERS HILL, PLAINVIEW, NEW YORK

FUEL CELL SYSTEMS

ADVANCES IN CHEMISTRY SERIES 47

Theory and technology of fuel cell systems are developed in 25 papers from symposia sponsored by the American Chemical Society's Division of Fuel Chemistry, including such topics as:

- Fuel cells for submarines and satellites
 - Molten carbonate fuel cells
 - Theory of polarization of porous electrodes
 - Olefins and paraffin fuels
 - Solid-state fuel cells
 - A coal-burning fuel cell power plant
- and many others.

Cloth bound, 360 pages, \$8.00 postpaid in U.S. and Canada; plus 20 cents foreign and PUAS.

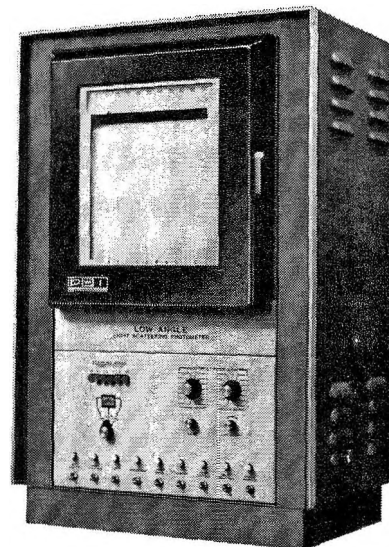
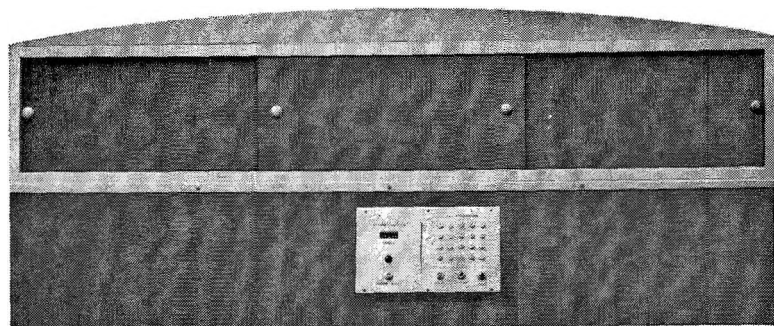
Set of L.C. cards supplied free on library orders.

Order from: **Special Issues Sales**
American Chemical Society
1155 Sixteenth St., N.W.
Washington, D. C. 20036

| | | |
|---|---|------|
| The Reaction of Pyrophoric Lead with Oxygen | J. Charles, P. W. Kopf, and S. Toby | 1478 |
| Infrared Study of the Reaction of Hydrogen Chloride with the Surface of γ -Alumina and Its Effect on Surface "Acid" Sites | J. B. Peri | 1482 |
| Liquid Ammonia Solutions. III. The Nature of Solutions of the Alkali and Alkaline Earth Iodides | J. T. Nelson, R. E. Cuthrell, and J. J. Lagowski | 1492 |
| Thermodynamic Properties of Nonaqueous Solutions. II. Free Energies, Entropies, and Activity Coefficients of Selected Alkali Metal Halides in Anhydrous N-Methylformamide | Eugene Luksha and Cecil M. Criss | 1496 |
| Transference Numbers and Ionic Conductances in Formamide at 25° | J. M. Notley and M. Spiro | 1502 |
| Condensed-Phase Behavior of the Aluminum Chloride-Zirconium Chloride System | A. J. Shor, William T. Smith, Jr., and M. A. Bredig | 1511 |
| Gas-Liquid Partition Chromatography of Perdeuterioethane. Isotope Effects on Vaporization from Solution | W. Alexander Van Hook and James T. Phillips | 1515 |
| Vibrational Intensities. XII. An Optical-Mechanical System from Infrared Attenuated Total Reflection Measurements | A. C. Gilby, John Burr, Jr., and Bryce Crawford, Jr. | 1520 |
| Vibrational Intensities. XIII. Reduction of Attenuated Total Reflection Data to Optical Constants | A. C. Gilby, John Burr, Jr., William Krueger, and Bryce Crawford, Jr. | 1525 |
| Vibrational Intensities. XIV. The Relation of Optical Constants to Molecular Parameters | A. A. Clifford and Bryce Crawford, Jr. | 1536 |
| Proton Resonance Spectrum of Butatriene | Stephen G. Frankiss and Ikuo Matsubara | 1543 |
| Nitrous Oxide Dosimetry. Effects of Temperature, Pressure, and Electric Field | F. T. Jones and T. J. Sworski | 1546 |
| Diffusion of Iron in Single-Crystal Nickel Oxide | K. J. Richards and F. E. Wagstaff | 1553 |
| Spin-Free Quantum Chemistry. III. Bond Functions and the Pauling Rules | F. A. Matsen, A. A. Cantu, and R. D. Poshusta | 1558 |
| Spin-Free Quantum Chemistry. IV. The p^n Electron Configuration | F. A. Matsen | 1568 |
| Intramolecular Kinetic Carbon Isotope Effect in the Gas Phase Decomposition of Deuteriooxalic Acid | Gabriel Lapidus, Donald Barton, and Peter E. Yankwich | 1575 |
| Abstraction of Halogen Atoms by Methyl Radicals | D. M. Tomkinson and H. O. Pritchard | 1579 |
| Polymer Formation in Irradiated Liquid Pyridine | Carol K. Pearce and Joseph E. Ellison, Jr. | 1582 |
| Membrane Potentials. Measurement of Electromotive Force of Cells Containing "Untreated" Collodion Membrane | N. Lakshminarayanaiah | 1588 |
| The Significant Structure Theory Applied to the Hydrides of Elements of the Fifth Group | Mu Shik Jhon, Joe Grosh, Taikyue Ree, and Henry Eyring | 1591 |
| A Hydrogen Electrode in Ice | P. N. Krishnan, I. Young, and R. E. Salomon | 1595 |
| Further Studies on the Decarboxylation of Oxalic Acid in Polar Solvents | Louis Watts Clark | 1597 |
| Short-Range Order in Fused Salts. I. Coordination States of Nickel(II) in Molten Zinc Chloride-Potassium Chloride Mixtures | C. A. Angell and D. M. Gruen | 1601 |
| Ultrasonic Absorption in Aqueous Polyethylene Glycol Solutions | Gordon G. Hammes and Thomas B. Lewis | 1610 |
| The Interaction of Acridine Orange with Poly- α -L-glutamic Acid | Gordon G. Hammes and Colin D. Hubbard | 1615 |
| Kinetics of Excited Molecules. V. Photochemistry of Hexafluoroacetone | Peter G. Bowers and Gerald B. Porter | 1622 |
| Positive Hole Migration and Trapping in γ -Irradiated 3-Methylpentane at -196° | David W. Skelly and William H. Hamill | 1630 |
| Gravimetric Adsorption Studies of Thorium Oxide. II. Water Adsorption at 25.00° | E. L. Fuller, Jr., H. F. Holmes, and C. H. Secoy | 1633 |
| Photochemical Equilibrium Studies of Carbon Dioxide and Their Significance for the Venus Atmosphere | Robert R. Reeves, Jr., Paul Harteck, Barbara A. Thompson, and Roger W. Waldron | 1637 |

designed to yield size and shape information on particles in the 0.2 to 200 micron diameter range...

**THE NEW PHOENIX
AUTOMATIC SCANNING
LOW-ANGLE
LIGHT-SCATTERING PHOTOMETER**



WRITE FOR INSTRUMENTATION DATA SHEET 1LA-265

PHOENIX PRECISION INSTRUMENT COMPANY

A Subsidiary of CENCO INSTRUMENTS CORP.

3803-05 NORTH 5TH STREET, PHILADELPHIA, PENNSYLVANIA. 19140, U.S.A.

World Wide Sales & Service



**Opportunity for Senior
Research Scientists
in Magnetics
at Honeywell,
Minneapolis, Minnesota**

Join Honeywell's well equipped Corporate Research Center where you will work in an atmosphere of true scientific professionalism, where personal dedication replaces the confining supervision you may find in other companies.

Magnetics

PhD in Physical Chemistry. Candidate interested in doing basic studies in electrochemistry and/or electrodeposited magnetic materials. Some experience in magnetics preferred but not essential.

PhD in Physics or Physical Chemistry. Prefer candidate with several years' experience and an interest in doing basic studies on thin ferromagnetic films with ultimate applicability to memory and logic devices. The work includes studies of anisotropy, coupled magnetic films and basic studies of films prepared by various deposition techniques. Must have a strong background in ferromagnetism, magnetic films or soft magnetic materials.

WE INVITE YOUR INQUIRY

Please air mail resume including salary requirements to: Mr. Marc D. Wanvig, Placement Administrator, 2701 Fourth Avenue South, Minneapolis, Minnesota 55408.

Honeywell

An equal opportunity employer (M & F)

BORON-NITROGEN CHEMISTRY

ADVANCES IN CHEMISTRY SERIES 42

contains thirty-two papers presented at the Boron-Nitrogen Chemistry Symposium sponsored by the U. S. Army Research Office—Durham. These papers contain contributions from many subdisciplines of chemistry and emphasize the close collaboration of classical chemistry with advanced techniques and modern theoretical treatments.

Principal topics discussed: Amineboranes and related compounds, 6 papers; physical chemistry of amino-boranes, 4 papers; preparative aspects of aminoboranes, 5 papers; pseudoaromatic B-N compounds, 6 papers; general B-N chemistry, 11 papers.

330 pages, clothbound \$7.50 postpaid U. S. and Canada; plus 20 cents foreign and PUAS.

**Order from: Special Issues Sales
American Chemical Society
1155 Sixteenth St., N. W.
Washington, D. C. 20036**

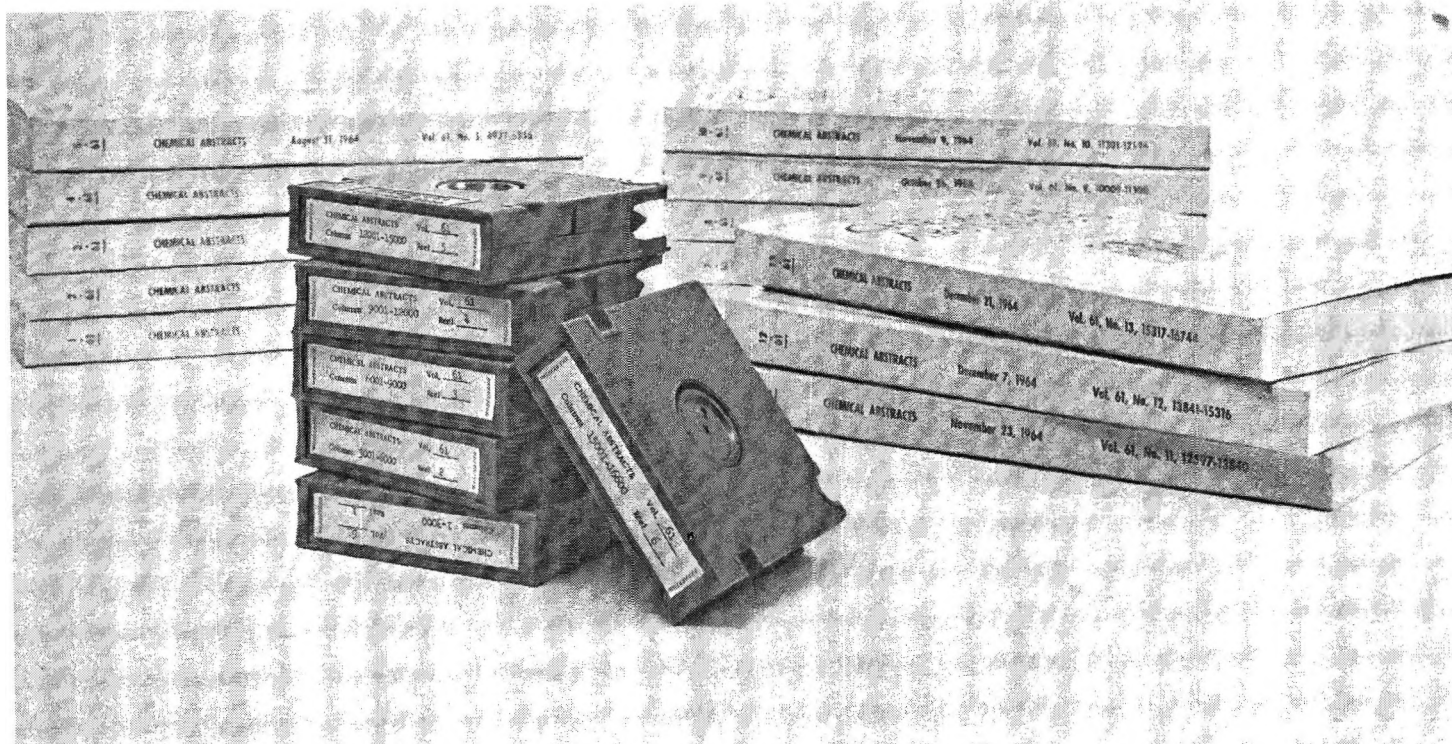
| | | |
|---|--|------|
| Osmotic and Activity Coefficients of Acidopentaamminecobalt(III) Complexes | L. H. Berka and W. L. Masterton | 1641 |
| Nitro- <i>p</i> -terphenyls. I. Dual Charge-Transfer Properties and Spectral Correlations | Richard L. Hansen | 1646 |
| Nitro- <i>p</i> -terphenyls. II. The Relation between Charge-Transfer Properties and Polarographic Oxidation and Reduction Potentials | Richard L. Hansen, P. E. Toren, and R. H. Young | 1653 |

NOTES

| | | |
|---|---|------|
| Nitro- <i>p</i> -terphenyls. III. Electron Paramagnetic Resonance Spectra of the Radical Anions | Richard L. Hansen, R. H. Young, and P. E. Toren | 1657 |
| Radiation Chemistry of Aqueous Solution of Silver Ion | Gideon Czapski and A. O. Allen | 1659 |
| Evidence for the Existence of ^{11}B - ^{10}B Coupling in NaB_2H_6 and B_4H_{10} | Arlan D. Norman and Riley Schaeffer | 1662 |
| Observations in Relation with Surface Phenomena of Rotating Liquids | M. Borneas | 1664 |
| Exchange of Chlorine between Hydrogen Chloride and Metal Chlorides | J. R. Wilson and J. E. Willard | 1665 |
| Chemical Shifts of Methyl Protons in Methylated Polynuclear Aromatic Hydrocarbons | I. C. Lewis | 1667 |
| Changes in Dielectric Relaxation during Dehydration and Rehydration of Rochelle Salt | P. G. Hall and F. C. Tompkins | 1669 |
| Solubilities of Potassium, Triisooamylbutylammonium, and Tetrabutylammonium Tetraphenylborides and Picrates in Water and Methanol and Their Medium Effects at 25° | Orest Popovych and Robert M. Friedman | 1671 |
| Effects of Divalent Cations on Multiionic Diffusion across a Weak-Acid Membrane | T. M. Ellison and H. G. Spencer | 1673 |
| Scaling in Carbon Monoxide and Nitrogen | J. Goodisman | 1675 |
| The Electron Spin Resonance Absorption of Solid 1,1-Diphenyl-2-picrylhydrazyl Mixtures. Surface and Aging Effects | Kedma H. Bar-Eli and Karl Weiss | 1677 |
| Adsorption of Propane on Carbon Black | G. L. Taylor and J. H. Atkins | 1678 |
| Doubly Charged Transition Metal Carbonyl Ions | Robert E. Winters and Robert W. Kiser | 1680 |
| The Nature of the Acidic Sites on Silica-Alumina. A Reevaluation of the Relative Absorption Coefficients of Chemisorbed Pyridine | Michael R. Basila and Theodore R. Kantner | 1681 |
| Nuclear Magnetic Resonance Studies of Inorganic Fluorides. II. Solvent Effects on $J(^{29}\text{Si}-^{19}\text{F})$ in Silicon Tetrafluoride | T. D. Coyle, R. B. Johannesen, F. E. Brinckman, and T. C. Farrar | 1682 |
| The Dissociation Rate of Molecular Fluorine. | Daniel J. Seery | 1684 |
| Viscoelastic Behavior of Dilute Polystyrene Solutions in an Extended Frequency Range | John D. Ferry, Larry A. Holmes, J. Lamb, and A. J. Matheson | 1685 |

COMMUNICATIONS TO THE EDITOR

| | | |
|--|---------------------------------------|------|
| Kinetics of Iodination of Mercury Dimethyl in Various Solvents | Allan Lord and H. O. Pritchard | 1689 |
| The Thermodynamic Properties of the Aluminum Silicates | J. L. Holm and O. J. Kleppa | 1690 |



Chemical Abstracts on Microfilm

Does your present information program provide:

- Photocopies of abstracts published in *Chemical Abstracts*?
- Abstract bulletins to staff members?
- A complete set of *Chemical Abstracts*?
- Rapid access to abstracts of papers published in more than 10,000 serial publications (current and historical) and to abstracts of patents issued in 24 countries?

You can provide all of these services when you add the microfilmed abstract issues of *Chemical Abstracts* to your information program. All of the abstract issues which have been published from 1907 to date have been filmed on 16 mm microfilm. Thus, this traditional information tool has been adapted to fast, modern methods of use. Special codes permit you to reach any portion of the microfilm quickly when you use either manual or automatic microfilm reader-printer equipment.

Current subscribers to *Chemical Abstracts* may lease the microfilmed abstract issues on a yearly basis and the Chemical Abstracts Service will maintain and update the microfilm collection.

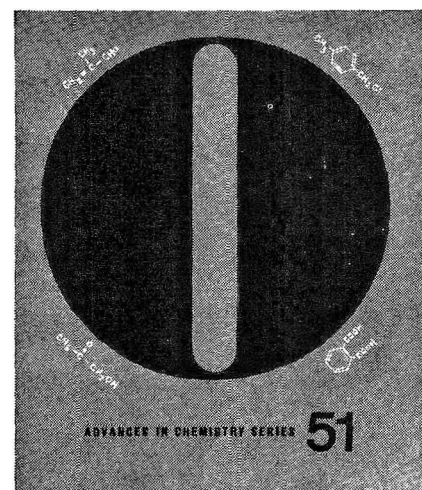
Put this new form of *Chemical Abstracts* to work in your present information program and find out for yourself how much easier it is to use *CA* and how much more information you can obtain from its pages.

For subscription information, contact the Service Division, Chemical Abstracts Service, Box 1378, Columbus, Ohio 43216 (telephone 614 293-5022).

AUTHOR INDEX

- Allen, A. O., 1659
 Angell, C. A., 1601
 Angell, C. L., 1413
 Atkins, J. H., 1678
- Bar-Eli, K. H., 1677
 Barile, R. C., 1358
 Barton, D., 1575
 Basila, M. R., 1681
 Berka, L. H., 1641
 Blake, P. G., 1464
 Bloor, J. E., 1457
 Borneas, M., 1664
 Bowers, P. G., 1622
 Bredig, M. A., 1511
 Brinckman, F. E., 1682
 Bryant, J. T., 1441
 Burack, M., 1470
 Burr, J., Jr., 1520, 1525
- Cantu, A. A., 1558
 Cefola, M., 1358
 Celiano, A. V., 1358
 Charles, J., 1478
 Cherin, P., 1470
 Chiu, G., 1384
 Clark, L. W., 1597
 Clifford, A. A., 1536
 Conway, B. E., 1473
 Coyle, T. D., 1682
 Crawford, B., Jr., 1520, 1525, 1536
 Criss, C. M., 1496
 Cuthrell, R. E., 1492
 Czapski, G., 1659
- Dadape, V. V., 1349
 Daykin, P. N., 1457
 Draganić, I. G., 1418
 Draganić, Z. D., 1418
- Ellison, J. E., Jr., 1582
 Ellison, T. M., 1673
 Eyring, H., 1591
- Farrar, T. C., 1682
 Ferry, J. D., 1685
 Frankiss, S. G., 1543
 Friedman, R. M., 1671
 Fuller, E. L., Jr., 1633
 Fuoss, R. M., 1426
- Gentile, P. S., 1358
 Gilby, A. C., 1520, 1525
 Gilson, B. R., 1457
 Goodisman, J., 1675
 Grosh, J., 1591
 Gruen, D. M., 1601
- Hall, P. G., 1669
 Hamill, W. H., 1630
 Hammes, G. G., 1610, 1615
 Hansen, R. L., 1646, 1653, 1657
 Harteck, P., 1637
 Hole, K. J., 1464
 Holm, J. L., 1690
 Holmes, H. F., 1633
 Holmes, L. A., 1685
- Holroyd, R. A., 1341
 Hubbard, C. D., 1615
 Huq, A. K. M. S., 1354
- Jhon, M. S., 1591
 Johannesen, R. B., 1682
 Jones, F. T., 1546
- Kantner, T. R., 1681
 Kiser, R. W., 1680
 Kleppa, O. J., 1690
 Kopf, P. W., 1478
 Kosanić, M. M., 1418
 Krishnan, P. N., 1595
 Krueger, W., 1525
 Kuhn, H. J., 1380
- Lagowski, J. J., 1492
 Lakshminarayanaiah, N., 1588
 Lamb, J., 1685
 Lapidus, G., 1575
 Lewis, I. C., 1667
 Lewis, T. B., 1610
 Lodhi, S. A. K., 1354
 Lord, A., 1689
 Luksha, E., 1496
 Luz, Z., 1434
- Masterton, W. L., 1641
 Matheson, A. J., 1685
 Matsen, F. A., 1558, 1568
 Matsubara, I., 1543
- McKinnon, A. J., 1453
 Meehan, E. J., 1384
 Muha, G. M., 1390, 1399
- Nelson, J. T., 1492
 Norman, A. D., 1662
 Notley, J. M., 1502
- Pearce, C. K., 1582
 Peller, S., 1434
 Peri, J. B., 1482
 Phillips, J. T., 1515
 Popovych, O., 1671
 Porter, G. B., 1622
 Poshusta, R. D., 1558
 Pritchard, G. O., 1441
 Pritchard, H. O., 1579, 1689
- Rao, D. B., 1349
 Ree, T., 1591
 Reeves, R. R., Jr., 1637
 Reuben, J., 1434
 Richards, K. J., 1553
- Salomon, R. E., 1595
 Schaffer, P. C., 1413
 Schaeffer, R., 1662
 Scibona, G., 1365
 Secoy, C. H., 1633
 Seery, D. J., 1684
 Shor, A. J., 1511
 Silver, B. L., 1434
- Skelly, D. W., 1630
 Skinner, J. F., 1426
 Smith, W. T., Jr., 1511
 Spencer, H. G., 1673
 Spiro, M., 1502
 Sworski, T. J., 1546
- Takashima, S., 1372
 Taylor, G. L., 1678
 Thompson, B. A., 1637
 Tingey, G. L., 1406
 Tobolsky, A. V., 1453
 Toby, S., 1478
 Tomkinson, D. M., 1579
 Tompkins, F. C., 1669
 Toren, P. E., 1653, 1657
- Van Hook, W. A., 1515
 Verrall, R. E., 1473
- Wagstaff, F. E., 1553
 Waldron, R. W., 1637
 Weiss, K., 1677
 Willard, J. E., 1665
 Wilson, J. R., 1665
 Winters, R. E., 1680
 Woods, R., 1446
- Yankwich, P. E., 1575
 Yates, D. J. C., 1399
 Young, I., 1595
 Young, R. H., 1653, 1657

Do oxidation processes, products, and mechanisms interest you?
"Selective Oxidation Processes"
ADVANCES IN CHEMISTRY
SERIES No. 51 surveys a number
of processes and details research
on improving the range, selectivity,
and mechanisms of such processes.



The book includes discussions of hydroxylating selected aromatics and olefins, pyrolysis of isobutylene—all of these by vapor phase processes. Among liquid phase processes are three general methods for oxidizing aromatics, sulfur dioxide as oxidant for a number of products, use of nitrogen dioxide catalyzed by selenium dioxide, and ozone as a selective oxidant. The last chapter is a broad survey of carbanion oxidation. The book is based on a symposium sponsored by the ACS Division of Petroleum Chemistry.

177 pages with index Cloth bound (1965) \$6.50

Other books in ADVANCES IN CHEMISTRY SERIES on topics of Industrial interest include:

No. 48 Plasticization and Plasticizer Processes. Seventeen papers survey recent studies on plasticizer action, properties, and production. Includes chapters on glass transition, plasticizer mobility, processes for phthalates and other plasticizers, and antiplasticizers.

200 pages with index Cloth bound (1965) \$7.00

No. 46 Patents for Chemical Inventions. What to do about your patentable idea before you call the attorney.

117 pages with index Cloth bound (1964) \$4.00

No. 38 Saline Water Conversion—II. Fourteen papers from two symposia; includes recovery of minerals from sea water, minimizing scale formation, wiped thin-film distillation, diffusion still, solar flash evaporation, osmosis, electro dialysis (3 papers), research in Israel, hydrate process.

199 pages Paper bound (1963) \$6.00

No. 34 Polymerization and Polycondensation Processes. An I&EC Division symposium with emphasis on unit processes. Twenty-one papers on addition polymerization, polycondensation reactions, commercial polymerization processes, and equipment design.

260 pages Paper bound (1962) \$8.00

No. 27 Saline Water Conversion. A Water and Waste Chemistry Division symposium; includes thermodynamics of desalting, solvent extraction, freezing, cen-

trifugal phase barrier recompression distillation, multi-stage flash evaporation, ion exchange, osmosis, and electrochemical demineralization.

246 pages Paper bound (1960) \$5.85

No. 24 Chemical Marketing in the Competitive Sixties. Twenty articles survey the challenge in marketing drugs, agricultural chemicals, industrial organics, inorganic and heavy chemicals, and plastics; the role of advertising; sales; delivering goods to the customer; monitoring sales performance; market research; technical service, and application research.

147 pages Paper bound (1959) \$3.50

No. 21 Ozone Chemistry and Technology. Sixty papers from the International Ozone Conference; includes ozone chemistry, high concentration ozone, ozone analysis and technology, formation in electrical discharge, toxicity, sterilization and water purification.

465 pages Cloth bound (1959) \$7.00

No. 19 Handling and Uses of Alkali Metals. Nineteen articles on the chemistry, manufacture, and use of the alkali metals; five are devoted solely or partly to lithium, two to potassium, the remainder to sodium.

177 pages Paper bound (1957) \$4.75

No. 10 Literature Resources for Chemical Process Industries. Information sources on market research (13 papers), resins and plastics (7 papers), textile chemistry (6 papers), food industry (10 papers), petroleum (10 papers), literature searching and language problems (13 papers).

582 pages with index Paper bound (1954) \$7.50

No. 5 Progress in Petroleum Technology. Survey of 25 years of progress at the ACS Diamond Jubilee. Thirty-two papers on all aspects of petroleum processing and products.

392 pages Cloth bound (1951) \$6.50

Order from Special Issues Sales
American Chemical Society
1155 Sixteenth St., N.W.
Washington, D. C. 20036

THE JOURNAL OF PHYSICAL CHEMISTRY

Volume 70, Number 6 June 1966

| | | |
|--|---|------|
| The Vapor Phase Reaction of Methyl Radicals with Crotonaldehyde | Eric R. Allen and James N. Pitts, Jr. | 1691 |
| Nature of Bonding in Dye Aggregates | K. K. Rohatgi and G. S. Singhal | 1695 |
| On the Use of Ellipsometry for Adsorption Measurements below Monolayer Coverage | A. C. Hall | 1702 |
| The Mechanism of the Photoreduction of Azo Dyes in the Presence of DL-Mandelic Acid and in the Absence of Oxygen | H. C. A. van Beek and P. M. Heertjes | 1704 |
| Absorption Spectra and Transient Species Found in the Pulse Radiolysis of Alkaline Aqueous Benzoate Solutions | D. F. Sangster | 1712 |
| Note on Experimental Tests of Theories for the Excluded Volume Effect in Polymer Coils | Hiroshi Inagaki, Hidematsu Suzuki, Makoto Fujii, and Togoro Matsuo | 1718 |
| Radiometric Determination of the Solubility of Cadmium in Molten Cadmium Chloride | J. Mościński and L. Suski | 1727 |
| Electronic Structure of Nonalternant Hydrocarbons, Their Analogs and Derivatives. VII. Electronic Spectra of Some Benzologs of the Cyclopentadienylium Cation | J. Michl, R. Zahradnik, and P. Hochmann | 1732 |
| Structures of Some C_2H_4O Compounds Adsorbed on Nickel | G. Blyholder and Laurence D. Neff | 1738 |
| Infrared Spectra and Structures of Some C_2H_4O Compounds Adsorbed on Silica-Supported Iron, Cobalt, and Nickel | G. Blyholder and William V. Wyatt | 1745 |
| The Heat of Formation of Silylgermane | Stuart R. Gunn and John H. Kindsvater | 1750 |
| Mass Spectra of Volatile Hydrides. IV. Silylgermane | Fred E. Saalfeld and Harry J. Svec | 1753 |
| The Dispersion of Electric Birefringence | S. H. Lin, C. Y. Lin, and H. Eyring | 1756 |
| Vapor Pressure and Heat of Sublimation of Cerium(III) Fluoride | Mahnjick Lim and Alan W. Searcy | 1762 |
| Isotopic Exchange of Exited Oxygen Atoms with Carbon Monoxide | E. A. Th. Verdurmen | 1767 |
| Surface Equation of State for Ionized Surfactants | E. H. Lucassen-Reynders | 1777 |
| Shock Wave Studies with a Quadrupole Mass Filter. I. Experimental Apparatus: Its Design and Performance | David Gutman, Arthur J. Hay, and R. Linn Belford | 1786 |
| Shock Wave Studies with a Quadrupole Mass Filter. II. The Thermal Decomposition of Nitrous Oxide | David Gutman, R. Linn Belford, Arthur J. Hay, and Roy Pancirov | 1793 |
| The Adsorption of Polyfunctional Esters. A Test of the Frisch-Simha Polymer Adsorption Isotherm | B. J. Fontana | 1801 |
| The High-Pressure Solubility of Nitrogen in Fused Sodium Nitrate. Temperature and Pressure Dependences and the Heat and Entropy of Solution | James L. Copeland and Lawrence Seibles | 1811 |
| Solvent Effects in Proton Magnetic Resonance | John C. Schug | 1816 |
| Hydrolysis and Precipitates in Carboxylate Soap Solutions | J. Lucassen | 1824 |
| Activity Coefficients for the Systems Water-Urea and Water-Urea-Sucrose at 25° from Iospiestic Measurements | H. David Ellerton and Peter J. Dunlop | 1831 |
| Surface Tension of Molten Salts: Solutions of the Alkaline Earth Halides in the Alkali Halides | G. Bertozzi and G. Soldani | 1838 |

| | | |
|--|---|------|
| The Thermodynamics of Cation Exchange. V. The Excess Enthalpies of Some Mixed Resinates of Dowex 50 | D. S. Flett and P. Meares | 1841 |
| Seeding of Supercooled Polyethylene with Extended Chain Crystals | Bernhard Wunderlich and C. M. Cormier | 1844 |
| The Parahydrogen Conversion on Alloys of the Noble Metals with Palladium | A. Couper and A. Metcalfe | 1850 |
| Diffusion in Molten Salts at Constant Volume | M. K. Nagarajan and J. O'M. Bockris | 1854 |
| The Direct Estimation of Continuous Molecular Weight Distributions by Equilibrium Ultracentrifugation | Thomas H. Donnelly | 1862 |
| Dynamic Measurements of Silver Bromide Crystal Growth | C. R. Berry and D. C. Skillman | 1871 |
| Heats of Mixing of Aqueous Electrolytes. III. A Test of the General Equations with Quaternary Mixtures | Robert H. Wood and Henry L. Anderson | 1877 |
| An Experimental Comparison of the Gouy and the Diaphragm Cell Methods for Studying Isothermal Ternary Diffusion | E. L. Cussler, Jr., and Peter J. Dunlop | 1880 |
| Dielectric Relaxation in the Clathrate Hydrates of Some Cyclic Ethers | R. E. Hawkins and D. W. Davidson | 1889 |
| Stereoregularity in Poly(isopropyl acrylate). I. Chain Dimensions by Viscometry and Osmometry | J. E. Mark, R. A. Wessling, and R. E. Hughes | 1895 |
| Stereoregularity in Poly(isopropyl acrylate). II. Light-Scattering Results and Intrinsic Viscosity-Molecular Weight Relationships at High Chain Extension | R. A. Wessling, J. E. Mark, E. Hamori, and R. E. Hughes | 1903 |
| Stereoregularity in Poly(isopropyl acrylate). III. Phase Equilibrium Studies | R. A. Wessling, J. E. Mark, and R. E. Hughes | 1909 |
| Vaporization Study of the Titanium-Tellurium System | Akio Suzuki and P. G. Wahlbeck | 1914 |
| Evaluation of Ion-Pair Dissociation Constants from Osmotic Coefficients | W. L. Masterton and L. H. Berka | 1924 |
| Mean Activity Coefficient of Polyelectrolytes. II. Measurements of Sodium Salts of Polyvinyl Alcohols Partially Acetalized with Glyoxylic Acid | Norio Ise and Tsuneo Okubo | 1930 |
| Apparent Catalysis of Graphitization. I. Possible Mechanisms | M. L. Pearce and E. A. Heintz | 1935 |
| The Kinetics of the Reaction between Vanadium(III) and Uranium(VI) in Acid Perchlorate Solutions. Evidence for a Binuclear Intermediate | T. W. Newton and F. B. Baker | 1943 |
| Some Reactions of Oxygen Atoms. I. C_2F_4 , C_3F_6 , C_2H_2 , C_2H_4 , C_3H_6 , $1-C_4H_8$, C_2H_6 , $c-C_3H_6$, and C_3H_8 | Dennis Saunders and Julian Heicklen | 1950 |
| Heats of Mixing of Nonelectrolyte Solutions. III. Solutions of the Five Hexane Isomers with Hexadecane | John A. Larkin, David V. Fenby, Theodore S. Gilman, and Robert L. Scott | 1959 |
| The Reduction of Nitrate by Molybdenum(V) | E. Park Guymon and Jack T. Spence | 1964 |
| The Reaction of Methylene with Isopentane Vapor | Robert W. Carr, Jr. | 1970 |
| Random Monomer Distribution in Copolymers. Copolymerizations of Ethylene-Vinyl Chloride and Ethylene-Vinyl Acetate | Jacob Schaefer | 1975 |
| Raman and Far-Infrared Spectra of Some Four-Membered Ring Molecules | James R. Durig, W. H. Green, and N. C. Hammond | 1989 |
| The Excess Free Energy of Mixtures of Cyclohexane and <i>n</i> -Dodecane | José D. Gómez-Ibáñez, Julia J. C. Shieh, and Erlind M. Thorsteinson | 1998 |
| Entropy Titration. A Calorimetric Method for the Determination of ΔG , ΔH , and ΔS from a Single Thermometric Titration | J. J. Christensen, R. M. Izatt, L. D. Hansen, and J. A. Partridge | 2003 |
| The Infrared Spectra of the Anion and Weak Charge-Transfer Complexes of Tetracyanoethylene | Jack Stanley, Donald Smith, Bobby Latimer, and J. P. Devlin | 2011 |
| High-Temperature Equation of State—Argon | H. L. Frisch, J. L. Katz, E. Praestgaard, and J. L. Lebowitz | 2016 |
| Heats of Solution of Some Tetraalkylammonium Salts in Water and in Propylene Carbonate and Ionic Enthalpies of Transfer from Water to Propylene Carbonate | Yung-Chi Wu and Harold L. Friedman | 2020 |

| | | |
|---|--|------|
| Equilibria between Cyclic and Linear Molecules in Aqueous Formaldehyde | Kurt Moedritzer and John R. Van Wazer | 2025 |
| Cyclic Silthiazanes | Kurt Moedritzer and John R. Van Wazer | 2030 |
| Ionic Reactions in Gaseous Amines | M. S. B. Munson | 2034 |
| Sorption of Vapors by Proteins. I. Sorption of Water Vapor and Ethanol Vapor by Egg Albumin | Adolf Fogiel and Wilfried Heller | 2039 |

NOTES

| | | |
|--|--|------|
| The Potential of Zero Charge of Platinum and Its pH Dependence | E. Gileadi, S. D. Argade, and J. O'M. Bockris | 2044 |
| Substituent Effects V. Correlation of C ¹³ Chemical Shifts by Pairwise Interactions | Edmund R. Malinowski, Theodore Vladimiroff, and Robert F. Tavares | 2046 |
| Dissociation of Iridium Oxide | Wayne E. Bell, M. Tagami, and R. E. Inyard | 2048 |
| Thermodynamics of an Epimer Equilibrium | T. H. Siddall, III | 2050 |
| On the Radiolytic Isotopic Exchange of Gaseous Nitrogen | M. Anbar and P. Perlstein | 2052 |
| Solvent Shifts of Electronic Energy Levels of Acetone and Benzene | K. Keith Innes | 2053 |
| Reactions of Sulfur Dioxide in Hydrogen Flames | A. S. Kallend | 2055 |
| Metastable Transitions in the Mass Spectrum of Iron Pentacarbonyl | Robert E. Winters and Jerome H. Collins | 2057 |
| Mass Spectrometric Method for the Determination of the Activity Coefficient of Ammonia in Aqueous Salt Solutions | Richard A. Durst, Paul G. Schmidt, and Irwin Feldman | 2058 |
| Free Radical Addition of Perfluoroacetonitrile to Vinyl Fluoride | G. J. Janz and J. B. Flannery | 2061 |

COMMUNICATIONS TO THE EDITOR

| | | |
|---|---|------|
| Improved Methods for Preparing Hydrocarbon Cation Radicals | P. A. Malacheksy, L. S. Marcoux, and R. N. Adams | 2064 |
| Departure from Henry's Law for Solution in a Semiconductor | M. O'Keeffe | 2065 |
| Intramolecular Energy Transfer: Photoelimination of Halogen Atoms from Aromatic Ketones | E. J. Baum and J. N. Pitts, Jr. | 2066 |
| Charge Separation and Recombination without External Current at Nonideal Polarized Electrodes | Paul Delahay | 2067 |
| Complex Modulus of Concentrated Polymer Solutions in Steady Shear | Ian F. Macdonald and R. Byron Bird | 2068 |
| Reactivity of Charge-Transfer Complexes. Exchange Reaction of Hydrogen between Acetylene and Charge-Transfer Complexes of Various Phthalocyanines with Sodium | Masaru Ichikawa, Mitsuyuki Soma, Takaharu Onishi, and Kenzi Tamaru | 2069 |
| Emission at 2537 Å Produced by Quenching the 6(¹ P ₁) State of Mercury with Nitrogen or Carbon Monoxide | T. A. Gover and H. G. Bryant, Jr. | 2070 |
| Catalyzed Enhancement of Chemi-Ionization in Atomic Nitrogen and Oxygen Mixtures | Arthur Fontijn and Pieter H. Vree | 2071 |

AUTHOR INDEX

- Adams, R. N., 2064
 Allen, E. R., 1691
 Anbar, M., 2052
 Anderson, H. L., 1877
 Argade, S. D., 2044
- Baker, F. B., 1943
 Baum, E. J., 2066
 Belford, R. L., 1786, 1793
 Bell, W. E., 2048
 Berka, L. H., 1924
 Berry, C. R., 1871
 Bertozzi, G., 1838
 Bird, R. B., 2068
 Blyholder, G., 1738, 1745
 Bockris, J. O'M., 1854, 2044
 Bryant, H. G., Jr., 2070
- Carr, R. W., Jr., 1970
 Christensen, J. J., 2003
 Collins, J. H., 2057
 Copeland, J. L., 1811
 Cormier, C. M., 1844
 Couper, A., 1850
 Cussler, E. L., Jr., 1880
- Davidson, D. W., 1889
 Delahay, P., 2067
 Devlin, J. P., 2011
 Donnelly, T. H., 1862
 Dunlop, P. J., 1831, 1880
- Durig, J. R., 1989
 Durst, R. A., 2058
- Ellerton, H. D., 1831
 Eyring, H., 1756
- Feldman, I., 2058
 Fenby, D. V., 1959
 Flannery, J. B., 2061
 Flett, D. S., 1841
 Fogiel, A., 2039
 Fontana, B. J., 1801
 Fontijn, A., 2071
 Friedman, H. L., 2020
 Frisch, H. L., 2016
 Fujii, M., 1718
- Gileadi, E., 2044
 Gilman, T. S., 1959
 Gómez-Ibáñez, J. D., 1998
 Gover, T. A., 2070
 Green, W. H., 1989
 Gunn, S. R., 1750
 Gutman, D., 1786, 1793
 Guymon, E. P., 1964
- Hall, A. C., 1702
 Hammond, N. C., 1989
 Hamori, E., 1903
 Hansen, L. D., 2003
 Hawkins, R. E., 1889
 Hay, A. J., 1786, 1793
 Heertjes, P. M., 1704
 Heicklen, J., 1950
 Heintz, E. A., 1935
- Heller, W., 2039
 Hochmann, P., 1732
 Hughes, R. E., 1895, 1903, 1909
- Ichikawa, M., 2069
 Inagaki, H., 1718
 Innes, K. K., 2053
 Inyard, R. E., 2048
 Ise, N., 1930
 Izatt, R. M., 2003
- Janz, G. J., 2061
- Kallend, A. S., 2055
 Katz, J. L., 2016
 Kindsvater, J. H., 1750
- Larkin, J. A., 1959
 Latimer, B., 2011
 Lebowitz, J. A., 2016
 Lim, M., 1762
 Lin, C. Y., 1756
 Lin, S. H., 1756
 Lucassen, J., 1824
 Lucassen-Reynders, E. H., 1777
- Macdonald, I. F., 2068
 Malachuk, P. A., 2064
 Malinowski, E. R., 2046
 Marcoux, L. S., 2064
 Mark, J. E., 1895, 1903, 1909
 Masterton, W. L., 1924
 Matsuo, T., 1718
- Meares, P., 1841
 Metcalfe, A., 1850
 Michl, J., 1732
 Moedritzer, K., 2025, 2030
 Mościński, J., 1727
 Munson, M. S. B., 2034
- Nagarajan, M. K., 1854
 Neff, L. D., 1738
 Newton, T. W., 1943
- O'Keeffe, M., 2065
 Okubo, T., 1930
 Onishi, T., 2069
- Pancirov, R., 1793
 Partridge, J. A., 2003
 Pearce, M. L., 1935
 Perlstein, P., 2052
 Pitts, J. N., Jr., 1691, 2066
 Praestgaard, E., 2016
- Rohatgi, K. K., 1695
- Saalfeld, F. E., 1753
 Sangster, D. F., 1712
 Saunders, D., 1950
 Schaefer, J., 1975
 Schmidt, P. G., 2058
 Schug, J. C., 1816
 Scott, R. L., 1959
 Searcy, A. W., 1762
 Seibles, L., 1811
 Shieh, J. J. C., 1998
 Siddall, T. H., III, 2050
- Singhal, G. S., 1695
 Skillman, D. C., 1871
 Smith, D., 2011
 Soldani, G., 1838
 Soma, M., 2069
 Spence, J. T., 1964
 Stanley, J., 2011
 Suski, L., 1727
 Suzuki, A., 1914
 Suzuki, H., 1718
 Svec, H. J., 1753
- Tagami, M., 2048
 Tamaru, K., 2069
 Tavares, R. F., 2046
 Thorsteinson, E. M., 1998
- van Beek, H. C. A., 1704
 Van Wazer, J. R., 2025, 2030
 Verdurmen, E. A. Th., 1767
 Vladimiroff, T., 2046
 Vree, P. H., 2071
- Wahlbeck, P. G., 1914
 Wessling, R. A., 1895, 1903, 1909
 Winters, R. E., 2057
 Wood, R. H., 1877
 Wu, Y.-C., 2020
 Wunderlich, B., 1844
 Wyatt, W. V., 1745
- Zahradník, R., 1732

THE JOURNAL OF PHYSICAL CHEMISTRY

Volume 70, Number 7 July 1966

| | | |
|---|--|------|
| Dissociation of Acetic Acid- d_4 in Deuterium Oxide from 5 to 50° and Related Isotope Effects | Maya Paabo, Roger G. Bates, and R. A. Robinson | 2073 |
| Adsorption Thermodynamics of the Interaction of Water and Various Silica Powders | Donald E. Meyer and Norman Hackerman | 2077 |
| The Electronegativity of Multiply Bonded Groups | James E. Huheey | 2086 |
| The Pulse Radiolysis of Deaerated Aqueous Bromide Solutions | M. S. Matheson, W. A. Mulac, J. L. Weeks, and J. Rabani | 2092 |
| The Pulse Radiolysis of Deaerated Aqueous Carbonate Solutions. I. Transient Optical Spectrum and Mechanism. II. pK for OH Radicals | James L. Weeks and Joseph Rabani | 2100 |
| Determination of the Roughness Factor of a Powdered Solid | Sydney Ross and Ian J. Wiltshire | 2107 |
| The Vapor Pressure of Boron Oxide over the Range 1946-2419°K | Frank T. Greene and John L. Margrave | 2112 |
| The Rate of Reaction of Chloroacetate Ion with Thiocyanate in Concentrated Solutions | Thomas I. Crowell, Jackson E. Hicks, and Ching Chih Lai | 2116 |
| The Effect of Cyclic Oxygen Adsorption and Reduction on a Silver Surface | A. W. Czanderna | 2120 |
| Interactions in Aqueous Nonelectrolyte Solutions. I. Solute-Solvent Equilibria | R. H. Stokes and R. A. Robinson | 2126 |
| Dissolution of Solid Oxides in Oxide Melts. The Rate of Dissolution of Solid Silica in Na_2SiO_2 and K_2O-SiO_2 Melts | Klaus Schwerdtfeger | 2131 |
| Some Aspects of Interionic Charge-Transfer Interactions of Alkylpyridinium Ions in Ion Pairs and on Micelles | Ashoka Ray and Pasupati Mukerjee | 2138 |
| Charge-Transfer Interactions and the Polarity at the Surface of Micelles of Long-Chain Pyridinium Iodides | Pasupati Mukerjee and Ashoka Ray | 2144 |
| The Specificity of Counterion Adsorption to Micelles of Dodecylpyridinium Iodide and Their Critical Concentrations | Pasupati Mukerjee and Ashoka Ray | 2150 |
| A Study of Concentration-Dependent Three-Component Diffusion | P. F. Mijnlief and H. A. Vreedenberg | 2158 |
| Heats of Immersion in Water of Characterized Silicas of Varying Specific Surface Area | J. A. G. Taylor and J. A. Hockey | 2169 |
| The Promotion of a Nickel Catalyst by Electronic Interaction with Germanium Supports | Raymond F. Baddour and Max C. Deibert | 2173 |
| The Viscosity of Water under Pressure | R. A. Horne and D. S. Johnson | 2182 |
| Reactions of the Ethyl Radical. VIII. A Molecular Orbital Approach to the Energetics of the Addition Reaction | J. E. Bloor, A. C. R. Brown, and D. G. L. James | 2191 |
| Triplet State Zero-Field Splittings of Some Structurally Related Aromatic Hydrocarbon and Heterocyclic Molecules | Seymour Siegel and Henry S. Judeikis | 2201 |
| A Magnetophotoselection Study of the Polarizations of the Absorption Bands of Some Structurally Related Hydrocarbons and Heterocyclic Molecules | Seymour Siegel and Henry S. Judeikis | 2205 |

| | | |
|---|--|------|
| A Study of Some Free-Radical Reactions in Aqueous γ Radiolysis by Direct Measurements of Cu^+ Intermediates during Irradiation | Olga Mićić and Ivan Draganić | 2212 |
| Electron Spin Resonance Studies of Fundamental Processes in Radiation and Photochemistry. II. Photochemical Reactions in γ -Irradiated Nitriles at 77°K | P. B. Ayscough, R. G. Collins, and T. J. Kemp | 2220 |
| Hydrogen Iodide as a Radical Scavenger in the Radiolysis of Hydrocarbons | D. Perner and Robert H. Schuler | 2224 |
| Scavenger Kinetics in the Radiolysis of Cyclohexane Solutions. I. Pure Cyclohexane | Inder Mani and Robert J. Hanrahan | 2233 |
| The Electrical Conductivities of Boron Trifluoride in Pure and Mixed Halogen Fluorides | Madeline S. Toy and William A. Cannon | 2241 |
| Spectroscopic Evidence for the Enol Imine-Keto Enamine Tautomerism of N-(<i>o</i> - and <i>p</i> -Hydroxybenzylidene) Anils in Solution | John W. Ledbetter, Jr. | 2245 |
| Nonequivalence of Protons and Related Phenomena in Some Organonitrogen and Organophosphorus Compounds | T. H. Siddall, III | 2249 |
| Catalysis over Supported Metals. V. The Effect of Crystallite Size on the Catalytic Activity of Nickel | J. L. Carter, J. A. Cusumano, and J. H. Sinfelt | 2257 |
| Rapid Reactions in Methanol-Water Solvents | Ronald P. Jensen, Edward M. Eyring, and William M. Walsh | 2264 |
| Normal Stress Effect in Dilute Polymer Solutions. II. Polystyrene in Chlorinated Diphenyl | Kunihiro Osaki, Katsuhisa Tanaka, Michio Kurata, and Mikio Tamura | 2271 |
| Electrolysis with Constant Potential. Diffusion Currents of Metal Species Dissolved in Spherical Mercury Electrodes | William G. Stevens and Irving Shain | 2276 |
| The Photochemistry of Phosphorus Compounds. IV. Photolysis of Sodium Hydrogen Phosphate in Aqueous Solution | M. Halmann and I. Platzner | 2281 |
| The Apparent Molal Volumes of the Alkali Metal Chlorides in Aqueous Solution and Evidence for Salt-Induced Structure Transitions | Fred Vaslow | 2286 |
| Thermodynamic Properties in the Exchange of Silver with Sodium Ions in Cross-Linked Polystyrene Sulfonate Cation Exchangers | F. Vaslow and G. E. Boyd | 2295 |
| Measurements of the Intradiffusion Coefficients at 25° of the Ternary Systems (Labeled L- α -Alanine)-(DL- α -Alanine)-Water and (Labeled β -Alanine)-(β -Alanine)-Water | J. G. Albright | 2299 |
| Photochemistry of the Fluoro Ketones. Pentafluoroethyl Ethyl Ketone | R. L. Thommarson and G. O. Pritchard | 2307 |
| The Zero-Charge Potential of Indium Amalgams in Perchloric Acid | James N. Butler | 2312 |
| Chemical Relaxation Spectra: Calculation of Relaxation Times for Complex Mechanisms | Gordon G. Hammes and Paul R. Schimmel | 2319 |
| The Effect of Solvent Structure on the Mobility of Symmetrical Ions in Aqueous Solution | Robert L. Kay and D. Fennell Evans | 2325 |
| Viscosity <i>B</i> Coefficients for the Tetraalkylammonium Halides | Robert L. Kay, T. Vituccio, C. Zawoyski, and D. F. Evans | 2336 |
| Thermal Diffusion in an Oxidation-Reduction Thermocell—the Bismuth-Bismuth Iodide System | Jordan D. Kellner | 2341 |
| Temperature Coefficient of the Unperturbed Dimension of Linear Polyethylene from Intrinsic Viscosity Measurements in θ Solvents | R. Chiang | 2348 |
| Ion-Molecule Reactions in Acetonitrile and Propionitrile | J. L. Franklin, Yasuo Wada, P. Natalis, and P. M. Hierl | 2353 |
| The Radiation-Induced Isomerization of Stilbene in Benzene and Cyclohexane | Robert R. Hentz, D. B. Peterson, S. B. Srivastava, Helmut F. Barzynski, and Milton Burton | 2362 |
| Electrode Processes without <i>a Priori</i> Separation of Double-Layer Charging | Paul Delahay | 2373 |
| Observations on Trapped Electrons and Allyl Radicals Formed in 2-Methylpentene-1 by γ Radiolysis at Low Temperature | D. R. Smith and J. J. Pieroni | 2379 |

| | | |
|---|--|------|
| The Electrical Conductivity of Solutions of Metals in Their Molten Halides. VIII. Alkaline Earth Metal Systems | A. S. Dworkin, H. R. Bronstein, and M. A. Bredig | 2384 |
| The Saturation Thermodynamic Functions for Bismuth Chloride from 298°K to the Critical Point | Daniel Cubicciotti, H. Eding, F. J. Keneshea and J. W. Johnson | 2389 |
| Thermodynamic Properties of Gases in Propellants and Oxidizers. I. Solubilities of He, N ₂ , O ₂ , Ar, and N ₂ O ₃ in Liquid N ₂ O ₄ | E. T. Chang and N. A. Gokcen | 2394 |
| Mean Activity Coefficient of Polyelectrolytes. III. Measurements of Hydrochlorides of Polyethylenimine and Its Low Molecular Weight Analogs. | Norio Ise and Tsuneo Okubo | 2400 |

NOTES

| | | |
|---|--|------|
| Infrared Spectra of Ethylene Chemisorbed on Nickel and Platinum in Relation to the Activity of These Metals as Hydrogenation Catalysts | B. A. Morrow and N. Sheppard | 2406 |
| Concentration Dependence of Activity of a Macromolecular Component or Species | Norio Ise and Tsuneo Okubo | 2407 |
| Absorption Spectrum of the Hydroxyl Radical | J. K. Thomas, J. Rabani, M. S. Matheson, E. J. Hart, and S. Gordon | 2409 |
| A New Σ -Plot Treatment of Equilibrium Data and Its Application to the Vaporization of Bismuth Chloride | Daniel Cubicciotti | 2410 |
| Transition Energies for a Merocyanine Dye in Aqueous Electrolyte Solutions. Solvent Polarity Indicator Transition Energy-Internal Pressure Relations | John E. Gordon | 2413 |

COMMUNICATIONS TO THE EDITOR

| | | |
|--|--|------|
| The Thermodynamics of the System Pentafluorobenzene-Benzene | William A. Duncan and Findlay L. Swinton | 2417 |
| Isomeric Transition-Induced Reactions of Iodine-130 in Cyclohexane | J. A. Merrigan, J. B. Nicholas, R. M. Lambrecht, N. J. Parks, and E. P. Rack | 2417 |
| Anomalous Effect of Pressure on the Protolytic Dissociation of Excited States of Nitrophenols | S. D. Hamann | 2418 |
| Carbon Dioxide Adsorbed on Linde X and Y Zeolites | C. L. Angell | 2420 |
| The Reactions of Thermal Hydrogen Atoms with Ethanol and Ethanol Free Radicals at 77°K | R. H. Johnsen, A. K. E. Hagopian, and H. B. Yun | 2420 |
| The Radiolysis of Pure Decaborane-14 | T. J. Kligen and J. M. O'Neal | 2421 |

AUTHOR INDEX

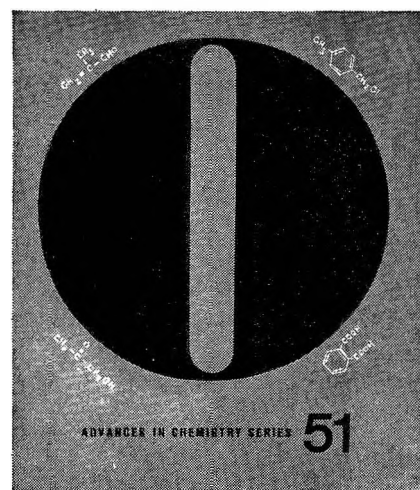
- Albright J. G., 2299
 Angell, C. L., 2420
 Ayscough, P. B., 2220
- Baddour, R. F., 2173
 Barzynski, H. F., 2362
 Bates, R. G., 2073
 Bloor, J. E., 2191
 Boyd, G. E., 2295
 Bredig, M. A., 2384
 Bronstein, H. R., 2384
 Brown, A. C. R., 2191
 Burton, M., 2362
 Butler, J. N., 2312
- Cannon, W. A., 2241
 Carter, J. L., 2257
 Chang, E. T., 2394
 Chiang, R., 2348
 Collins, R. G., 2220
 Crowell, T. I., 2116
 Cubicciotti, D., 2389,
 2410
 Cusumano, J. A., 2257
 Czanderna, A. W., 2120
- Deibert, M. C., 2173
 Delahay, P., 2373
 Draganić, I., 2212
 Duncan, W. A., 2417
 Dworkin, A. S., 2384
- Eding, H., 2389
 Evans, D. F., 2325, 2336
 Eyring, E. M., 2264
- Franklin, J. L., 2353
- Gokcen, N. A., 2394
 Gordon, J. E., 2413
 Gordon, S., 2409
 Greene, F. T., 2112
- Hackerman, N., 2077
 Hagopian, A. K. E.,
 2420
 Halmann, M., 2281
 Hamann, S. D., 2418
 Hammes, G. G., 2319
 Hanrahan, R. J., 2233
 Hart, E. J., 2409
 Hentz, R. R., 2362
 Hicks, J. E., 2116
 Hierl, P. M., 2353
 Hockey, J. A., 2169
 Horne, R. A., 2182
 Huheey, J. E., 2086
- Ise, N., 2400, 2407
- James, D. G. L., 2191
 Jensen, R. P., 2264
- Johnsen, R. H., 2420
 Johnson, D. S., 2182
 Johnson, J. W., 2389
 Judeikis, H. S., 2201,
 2205
- Kay, R. L., 2325, 2336
 Kellner, J. D., 2341
 Kemp, T. J., 2220
 Keneshea, F. J., 2389
 Kligen, T. J., 2421
 Kurata, M., 2271
- Lai, C. C., 2116
 Lambrecht, R. M., 2417
 Ledbetter, J. W., Jr.,
 2245
- Mani, I., 2233
 Margrave, J. L., 2112
 Matheson, M. S., 2092,
 2409
 Merrigan, J. A., 2417
 Meyer, D. E., 2077
 Micić, O., 2212
 Mijnlief, P. F., 2158
 Morrow, B. A., 2406
 Mukerjee, P., 2138,
 2144, 2150
 Mulac, W. A., 2092
- Natalis, P., 2353
 Nicholas, J. B., 2417
- Okubo, T., 2400, 2407
 O'Neal, J. M., 2421
 Osaki, K., 2271
- Paabo, M., 2073
 Parks, N. J., 2417
 Perner, D., 2224
 Peterson, D. B., 2362
 Pieroni, J. J., 2379
 Platzner, I., 2281
 Pritchard, G. O., 2307
- Rabani, J., 2092, 2100,
 2409
 Rack, E. P., 2417
 Ray, A., 2138, 2144,
 2150
 Robinson, R. A., 2073,
 2126
 Ross, S., 2107
- Schimmel, P. R., 2319
 Schuler, R. H., 2224
 Schwerdtfeger, K., 2131
 Shain, I., 2276
 Sheppard, N., 2406
- Siddall, T. H., III, 2249
 Siegel, S., 2201, 2205
 Sinfelt, J. H., 2257
 Smith, D. R., 2379
 Srivastava, S. B., 2362
 Stevens, W. G., 2276
 Stokes, R. H., 2126
 Swinton, F. L., 2417
- Tamura, M., 2271
 Tanaka, K., 2271
 Taylor, J. A. G., 2169
 Thomas, J. K., 2409
 Thommarson, R. L.,
 2307
 Toy, M. S., 2241
- Vaslow, F., 2286, 2295
 Vituccio, T., 2336
 Vreedenberg, H. A.,
 2158
- Wada, Y., 2353
 Walsh, W. M., 2264
 Weeks, J. L., 2092, 2100
 Wiltshire, I. J., 2107
- Yun, H. B., 2420
- Zawoyski, C., 2336

THE JOURNAL OF PHYSICAL CHEMISTRY

Volume 70, Number 8 August 1966

| | |
|---|------|
| Heats of Dilution of Aqueous Rare Earth Chloride Solutions at 25° F. H. Spedding, D. A. Csejka, and C. W. DeKock | 2423 |
| Relative Viscosities of Some Aqueous Rare Earth Chloride Solutions at 25° F. H. Spedding and M. J. Pikal | 2430 |
| Apparent Molal Volumes of Some Aqueous Rare Earth Chloride and Nitrate Solutions at 25° F. H. Spedding, M. J. Pikal, and B. O. Ayers | 2440 |
| Heat Capacities of Aqueous Rare Earth Chloride Solutions at 25° F. H. Spedding and K. C. Jones | 2450 |
| Reactions of NO(A ₂ Σ) with Hydrogen, Methane, and Ethane Julian Heicklen | 2456 |
| The Prediction of Stable States F. E. Diebold and C. L. Hiltrop | 2462 |
| Thermodynamics of Vaporization in the Aluminum Oxide-Boron Oxide System Paul E. Blackburn, Alfred Büchler, and James L. Stauffer | 2469 |
| The Gas Phase Photolysis of Acetone at 3130 Å in the Presence of Hydrogen Bromide. A Study of the Primary Photochemical Decomposition Processes of Acetone Carl W. Larson and H. Edward O'Neal | 2475 |
| Electron Spin Resonance Spectrum and Electronic Structure of the PO ₃ ²⁻ Radical in an X-Ray Irradiated Single Crystal of Ammonium Fluorophosphate F. G. Herring, J. H. Hwang, W. C. Lin, and C. A. McDowell | 2487 |
| Cryoscopic Behavior of Selected Solutes in the Molten Alkali Nitrates. I. Molten Lithium Nitrate R. E. Isbell, E. W. Wilson, Jr., and D. F. Smith | 2493 |
| Liquid Diffusivities in the Glycol-Water System Charles H. Byers and C. Judson King | 2499 |
| The Role of Excited States in the Photolysis of Carbon Suboxide R. B. Cundall, A. S. Davies, and T. F. Palmer | 2503 |
| Heats of Exchange of Halide Ions in Variously Cross-Linked Strong-Base Anion Exchangers F. Vaslow and G. E. Boyd | 2507 |
| Hysteresis of Contact Angle in the Galena-Water-Nitrogen System N. Sarkar and A. M. Gaudin | 2512 |
| Gibbs Free Energies of Formation of Thorium Phosphides from Solid-State Electromotive Force Measurements K. A. Gingerich and S. Aronson | 2517 |
| The Kinetics of the Decarboxylation of Methylmalonic Acid and Octadecylmalonic Acid in the Molten State Louis Watts Clark | 2523 |
| Nuclear Magnetic Resonance Study of Poly(vinyl chloride) Kermit C. Ramey | 2525 |
| Radiolysis of Frozen Solutions. VI. Electron and Excited Water Reactions in Nitrate Ices Larry Kevan | 2529 |
| The Reaction of Propylene Adsorbed on Silica with Hydrogen Atoms R. D. Gonzalez and R. J. Kokes | 2535 |
| Hydrogenation of Ethylene and Propylene over Palladium Hydride R. J. Rennard, Jr., and R. J. Kokes | 2543 |
| Ultrasonic Absorption in Solutions of Tetra- <i>n</i> -butylammonium Bromide in Two Isodielectric Solvent Mixtures Sergio Petrucci and Gordon Atkinson | 2550 |

Selective Oxidation Processes



Do oxidation processes, products, and mechanisms interest you? "Selective Oxidation Processes" **ADVANCES IN CHEMISTRY SERIES No. 51** surveys a number of processes and details research on improving the range, selectivity, and mechanisms of such processes.

The book includes discussions of hydroxylating selected aromatics and olefins, pyrolysis of isobutylene—all of these by vapor phase processes. Among liquid phase processes are three general methods for oxidizing aromatics, sulfur dioxide as oxidant for a number of products, use of nitrogen dioxide catalyzed by selenium dioxide, and ozone as a selective oxidant. The last chapter is a broad survey of carbanion oxidation. The book is based on a symposium sponsored by the ACS Division of Petroleum Chemistry.

177 pages with index Cloth bound (1965) \$6.50

Other books in **ADVANCES IN CHEMISTRY SERIES** on topics of Industrial interest include:

No. 48 Plasticization and Plasticizer Processes. Seventeen papers survey recent studies on plasticizer action, properties, and production. Includes chapters on glass transition, plasticizer mobility, processes for phthalates and other plasticizers, and antiplasticizers.
200 pages with index Cloth bound (1965) \$7.00

No. 46 Patents for Chemical Inventions. What to do about your patentable idea before you call the attorney.
117 pages with index Cloth bound (1964) \$4.00

No. 38 Saline Water Conversion—II. Fourteen papers from two symposia; includes recovery of minerals from sea water, minimizing scale formation, wiped thin-film distillation, diffusion still, solar flash evaporation, osmosis, electrodialysis (3 papers), research in Israel, hydrate process.
199 pages Paper bound (1963) \$6.00

No. 34 Polymerization and Polycondensation Processes. An I&EC Division symposium with emphasis on unit processes. Twenty-one papers on addition polymerization, polycondensation reactions, commercial polymerization processes, and equipment design.
260 pages Paper bound (1962) \$8.00

No. 27 Saline Water Conversion. A Water and Waste Chemistry Division symposium; includes thermodynamics of desalting, solvent extraction, freezing, cen-

trifugal phase barrier recompression distillation, multi-stage flash evaporation, ion exchange, osmosis, and electrochemical demineralization.

246 pages Paper bound (1960) \$5.85

No. 24 Chemical Marketing in the Competitive Sixties. Twenty articles survey the challenge in marketing drugs, agricultural chemicals, industrial organics, inorganic and heavy chemicals, and plastics; the role of advertising; sales; delivering goods to the customer; monitoring sales performance; market research; technical service, and application research.

147 pages Paper bound (1959) \$3.50

No. 21 Ozone Chemistry and Technology. Sixty papers from the International Ozone Conference; includes ozone chemistry, high concentration ozone, ozone analysis and technology, formation in electrical discharge, toxicity, sterilization and water purification.
465 pages Cloth bound (1959) \$7.00

No. 19 Handling and Uses of Alkali Metals. Nineteen articles on the chemistry, manufacture, and use of the alkali metals; five are devoted solely or partly to lithium, two to potassium, the remainder to sodium.
177 pages Paper bound (1957) \$4.75

No. 10 Literature Resources for Chemical Process Industries. Information sources on market research (13 papers), resins and plastics (7 papers), textile chemistry (6 papers), food industry (10 papers), petroleum (10 papers), literature searching and language problems (13 papers).
582 pages with index Paper bound (1954) \$7.50

No. 5 Progress in Petroleum Technology. Survey of 25 years of progress at the ACS Diamond Jubilee. Thirty-two papers on all aspects of petroleum processing and products.
392 pages Cloth bound (1951) \$6.50

Order from **Special Issues Sales**
American Chemical Society
1155 Sixteenth St., N.W.
Washington, D. C. 20036

AUTHOR INDEX

- Affsprung, H. E., 2691
 Agarwal, R. K., 2568
 Anbar, M., 2660
 Aronson, S., 2517
 Atkinson, G., 2550
 Ayers, B. O., 2440

 Bafus, D. A., 2614
 Bender, C. F., 2675
 Bevan, R. B., Jr., 2609
 Blackburn, P. E., 2469
 Boyd, G. E., 2507
 Büchler, A., 2469
 Burer, T., 2663
 Busey, R. H., 2609
 Byers, C. H., 2499

 Calvert, L. D., 2689
 Campbell, G. M., 2703
 Chattoraj, D. K., 2687
 Christian, S. D., 2691
 Clark, L. W., 2523
 Csejka, D. A., 2423

 Cundall, R. B., 2503
 Davidson, E. R., 2675
 Davies, A. S., 2503
 DeKock, C. W., 2423
 Delahay, P., 2601
 Dickie, R. A., 2594
 Diebold, F. E., 2462
 Doty, P., 2620
 Dunn, R. L., 2555

 Edwards, O. W., 2555
 Evans, J. C., 2702

 Farhataziz, 2696
 Ferry, J. D., 2594

 Gallegos, E. J., 2614
 Gaudin, A. M., 2512
 Gayer, K. H., 2609
 Gilbert, R. A., 2609
 Gingerich, K. A., 2517
 Gonzalez, R. D., 2535

 Hatfield, J. D., 2555
 Hecklen, J., 2456
 Henderson, R. M., 2694
 Herring, F. G., 2487
 Hiltrop, C. L., 2462
 Hoernschemeyer, D.,
 2628
 Hummel, R. W., 2685
 Hwa, S. C. P., 2572
 Hwang, J. H., 2487

 Isbell, R. E., 2493

 Janz, G. J., 2562
 Jones, K. C., 2450

 Katzin, L. I., 2663
 Kevan, L., 2529
 King, C. J., 2499
 Kiser, R. W., 2614
 Klotzkin, M. P., 2562
 Kokes, R. J., 2535,
 2543

 Lakshminarayanan,
 G. R., 2562
 Lamola, A. A., 2634
 Larson, C. W., 2475
 Leary, J. A., 2703
 Lin, W. C., 2487
 Lo, G. Y-S., 2702

 McDiarmid, R., 2620
 McDowell, C. A., 2487
 Meyerstein, D., 2660
 Miller, D. G., 2639
 Mueller, D. D., 2691
 Mukerjee, P., 2708

 Nayak, B., 2568
 Neta, P., 2660

 O'Neal, H. E., 2475

 Palmer, T. F., 2503
 Petrucci, S., 2550
 Pikal, M. J., 2430, 2440

 Ramey, K. C., 2525
 Rennard, R. J., Jr.,
 2543
 Roquette, B. C., 2699

 Sargent, D. F., 2689
 Sarkar, N., 2512
 Sharp, L. J., 2634
 Smith, D. F., 2493
 Solon, E., 2601
 Spedding, F. H., 2423,
 2430, 2440, 2450
 Stauffer, J. L., 2469
 Susbilles, G. G., 2601

 Vaslow, F., 2507

 Willi, A. V., 2705
 Wilson, E. W., Jr., 2493
 Wood, G. O., 2691

 Ziegler, W. T., 2572

THE JOURNAL OF PHYSICAL CHEMISTRY

Registered in U. S. Patent Office © Copyright, 1966, by the American Chemical Society

VOLUME 70, NUMBER 5 MAY 16, 1966

The Yield of Scavengable Hydrogen Atoms from the Radiolysis of Saturated Hydrocarbons¹

by Richard A. Holroyd

Atomics International, a Division of North American Aviation, Inc., Canoga Park, California
(Received December 28, 1966)

The purpose of this study was to establish the extent that thermal hydrogen atoms are present in irradiated hydrocarbons. Ethylene, present as a solute in the hydrocarbon being irradiated, was used as a specific scavenger of hydrogen atoms. The yield of ethyl radicals, formed by the addition of hydrogen atoms to ethylene, was measured with the ¹⁴CH₃ radical sampling technique. $G(\text{H})$ was found to be 1.3 for *n*-pentane, 1.8 for 2,4-dimethylpentane, and 1.6 for 2,2,4-trimethylpentane. The ratio of $G(\text{H})$ to the total yield of cycloalkyl radicals was found to be 0.45 and 0.46 for cyclohexane and cyclopentane, respectively. If the total cycloalkyl radical yield is assumed to be 4.0, then these data indicate $G(\text{H})$ is 1.8 for the cycloalkanes. The yield of thermal hydrogen atoms apparently is not markedly dependent on structural factors. The yield of $G(\text{H})$ observed with ethylene for *n*-pentane and the cycloalkanes is less than one-half the yield reported in studies where scavengers such as methyl methacrylate and benzoquinone were used. These data suggest that the latter solutes reduce the hydrogen yield not only by scavenging thermal hydrogen atoms but also by reacting with other precursors of H₂.

Introduction

The yield of thermal hydrogen atoms, $G(\text{H})$, formed in the radiolysis of saturated hydrocarbons is a subject of considerable controversy. One of the methods frequently used to measure $G(\text{H})$ involves determining the change in yield of hydrogen gas $\Delta G(\text{H}_2)$ induced by the addition of a solute which is assumed to be a hydrogen atom scavenger. The use of this method in cyclohexane gave conflicting values for $G(\text{H})$ of 0.2,² 2.0,³ 3.1,⁴ and 3.2⁵ when benzene, iodine, methyl methacrylate, and benzoquinone, respectively, were used as scavengers.

A more direct method to evaluate $G(\text{H})$ consists of measuring the yield of the product, HS, which is produced when hydrogen atoms react with a scavenger, S.



(1) This paper is based on studies conducted for the U. S. Atomic Energy Commission under Contract AT(11-1)-GEN-8.

(2) J. F. Merklin and S. Lipsky, *J. Phys. Chem.*, **68**, 3297 (1964).

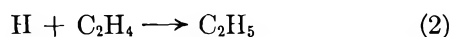
(3) C. E. Klots, Y. Raef, and R. H. Johnson, *ibid.*, **68**, 2040 (1964).

(4) T. J. Hardwick, *ibid.*, **66**, 1611 (1962).

(5) G. E. Adams, J. H. Baxendale, and R. D. Sedgewick, *ibid.*, **63**, 854 (1959).

It is necessary in this case that the product formed in reaction 1 be not only stable and detectable but also uniquely formed by this reaction. Iodine is a solute which has been employed for this purpose. The yield of HI, which is identified with $G(\text{H})$, was found to be 2.2 in the case of cyclopentane and 2.1 in the case of cyclohexane.⁶ Unfortunately, the use of iodine at the high concentrations required to scavenge all the hydrogen atoms is complicated since reaction of iodine with a charged species may also occur. In a similar fashion, methyl iodide has been used to determine $G(\text{H})$. The products of the reaction of methyl iodide with H atoms are initially $\text{CH}_3 + \text{HI}$, but cage reaction of these products, forming CH_4 and I atoms, occurs with a large probability. A value of $G(\text{H}) = 0.7$ was obtained for several hydrocarbons including cyclopentane from measurements of the CH_4 produced.⁷

In view of the discrepancies in reported values of $G(\text{H})$, several saturated hydrocarbons have been reinvestigated with a new and more direct method. The scavenger in this case is ethylene and the yield of hydrogen atoms is obtained from the yield of ethyl radicals produced by



Under the conditions of the experiment, the abstraction reaction

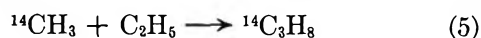


also occurs in competition with reaction 2. It is essential in this method that ethyl radicals are formed from ethylene only by reaction 2. Ethylene was chosen as a scavenger because it is not expected to react with other intermediates for the following reasons: ethylene is reputed to be a poor electron trap,⁸ energy transfer to ethylene from hydrocarbons is expected to be unimportant at low concentrations;⁹ and charge exchange from the hydrocarbon ion is energetically unfavorable.¹⁰ Thus, it is reasonable to assume that the only reaction of ethylene, at concentrations employed in this work, is to scavenge hydrogen atoms.

The yield of ethyl radicals, $G(\text{C}_2\text{H}_5)$, formed by reaction 2 can be determined by the methyl radical sampling technique.¹¹ In this method small amounts of $^{14}\text{CH}_3$ radicals are generated from solute $^{14}\text{CH}_3\text{I}$ by



High dose rates are employed to favor radical-combination reactions and the propane- ^{14}C formed by



serves as a quantitative measure of the ethyl radical yield.

From eq 2-4, the relationship

$$\frac{1}{G(\text{C}_2\text{H}_5) - G(\text{C}_2\text{H}_5)^\circ} = \frac{1}{G(\text{H})} + \frac{k_3(\text{RH})}{k_2 G(\text{H})(\text{C}_2\text{H}_4)} \left\{ 1 + \frac{k_4(\text{CH}_3\text{I})}{k_3(\text{RH})} \right\} \quad (I)$$

may be derived if the steady-state assumption is made for the concentration of hydrogen atoms, where $G(\text{C}_2\text{H}_5)^\circ$ is the yield of ethyl radicals that is produced directly from the radiolysis of the hydrocarbon in the absence of ethylene. The methyl iodide concentration is kept approximately constant and the hydrocarbon concentration is of course constant so that the final term in eq I is essentially constant and nearly unity.¹² Thus, from plots of $\{G(\text{C}_2\text{H}_5) - G(\text{C}_2\text{H}_5)^\circ\}^{-1}$ vs. the reciprocal of the ethylene concentration, the values of $G(\text{H})$ and k_3/k_2 may be derived from a least-squares analysis of the data if a linear relationship is observed.

Experimental Section

All hydrocarbons (Phillips Research Grade) were dried with silica gel and degassed prior to use. The methyl- ^{14}C iodide (Volk Radiochemical Co.) was diluted with unlabeled methyl iodide to a specific activity of ~ 0.5 mcurie/mmole and purified by gas chromatography. The specific activity was determined by irradiating a dilute solution of the $^{14}\text{CH}_3\text{I}$ in cyclopentane and measuring, with the proportional counter (see below), the specific activity of the methane produced.

Samples were irradiated in copper cells which were cylindrical in shape, 0.5 in. in diameter and 0.5 in. deep. A 0.001-in. brass window was soldered on the top of the cell to pass the electron beam which entered the cell vertically. The sample size was generally 0.3 ml of hydrocarbon solution. The sample was introduced into the evacuated cell through a Viton O-ring type stopcock connected to the cell by a Kovar seal. A measured amount of ethylene was added to the cell and the

(6) G. Meshitsuka and M. Burton, *Radiation Res.*, **10**, 499 (1959).

(7) S. Z. Toma and W. H. Hamill, *J. Am. Chem. Soc.*, **86**, 1478 (1964).

(8) (a) J. P. Guarino and W. H. Hamill, *ibid.*, **86**, 781 (1964); (b) C. F. Cullis, J. M. Francis, and A. J. Swallow, *Proc. Roy. Soc. (London)*, **A287**, 15 (1965).

(9) R. W. Fessenden and R. H. Schuler, *Discussions Faraday Soc.*, **36**, 147 (1963).

(10) Although ionization potentials are lower in the liquid phase, the evidence indicates that for both unsaturated and saturated hydrocarbons the ionization potential is reduced equally; cf. C. Vermeil, M. Matheson, S. Leach, and F. Muller, *J. Chim. Phys.*, **61**, 596 (1964).

(11) (a) R. A. Holroyd and G. W. Klein, *J. Appl. Radiation Isotopes*, **15**, 633 (1964); (b) *J. Phys. Chem.*, **68**, 194 (1965).

(12) The term $k_4(\text{CH}_3\text{I})/k_3(\text{RH})$, which represents the fraction of H atoms which react with methyl iodide forming $^{14}\text{CH}_3$ radicals, was neglected since $G(^{14}\text{CH}_3) \cong 0.15$ and $G(\text{H}) \sim 1.5$.

concentration of the ethylene in solution determined from Henry's law: $X_E = kP_E$ where X_E is the mole fraction of ethylene in solution and P_E is the ethylene pressure in atmospheres. Values of k at 23° were experimentally determined to be 0.007 for pentane, 0.019 for 2,4-dimethylpentane, 0.016 for 2,2,4-trimethylpentane, 0.007 for cyclopentane, and 0.011 for cyclohexane.

A Van de Graaff accelerator provided a beam of 2.0-Mev electrons for the irradiations. The beam current was 5 to 10 μ a. The beam was defined by a 0.25 in. diameter slit, and a pneumatic aluminum shutter was used to turn the electron beam on and off. Irradiation times of 0.5 to 2 sec were employed. The yield of hydrogen from pure cyclopentane was used as a dosimeter. The relative dose was determined by integrating the beam current to the irradiation cell. Samples received a dose of $2-4 \times 10^{19}$ ev/ml.

Irradiated samples were analyzed with a gas chromatograph (Loenco Model 16). The column employed was 40 ft long and contained GC-22 support, 30-60 mesh, coated with silicon grease. The effluent from the chromatograph passed directly into a proportional counter (Atomic Accessories Model VPC-164) for measurement of the radioactivity yield in each component of the sample. The counter was operated at 2450 v by a high-voltage supply (RIDL 40-9). Pulses from the counter were amplified (RIDL 30-23), passed into a single-channel analyzer (RIDL 33-10) and counted both with a scaler (RIDL 49-26) and a ratemeter (RIDL 35-7). The ratemeter output was recorded on a two-channel recorder, which also recorded the output of the thermal conductivity detector. An event-marking pen was employed which recorded every hundredth count from the scaler. This in effect provided automatic integration of the radioactivity yield in each product.

In a typical experiment, from 2000 to 10,000 counts would be observed in a single product corresponding to a product yield of 7.0 to 40 nmoles. A lower limit of ~ 2 nmoles of product could be detected with this technique.

Results

n-Pentane. The labeled hydrocarbons formed from 0.5 mM solutions of $^{14}\text{CH}_3\text{I}$ in *n*-pentane were those which were expected to be formed by combination of $^{14}\text{CH}_3$ radicals with the radicals known to be intermediates.¹³ The addition of ethylene enhanced the $^{14}\text{C}_3\text{H}_8$ yield. Only the yields of labeled propane, butane, and *n*-hexane, corresponding to ethyl, *n*-propyl, and *n*-pentyl radicals, respectively, were determined as a function of ethylene concentration. The results in terms of ratios of these yields are given in Table I. The actual observed yields of radioactive products were

quite low; for example, $G(^{14}\text{C}_3\text{H}_8)$ was from 0.03 to 0.13 for the experiments reported in Table I. This is typical of the method in that the radicals present are sampled and not completely scavenged. It has been shown

Table I: *n*-Pentane^a

| [C ₂ H ₄], mM | $G(n-^{14}\text{C}_4\text{H}_{10})$ | $G(n-^{14}\text{C}_6\text{H}_{14})$ | $G(\text{C}_2\text{H}_5)$ | |
|---|-------------------------------------|-------------------------------------|---------------------------|--------|
| | $G(^{14}\text{C}_3\text{H}_8)$ | $G(^{14}\text{C}_3\text{H}_8)$ | Eq II | Eq III |
| 20.8 | 0.227 | 0.360 | 1.45 | 1.81 |
| 17.3 | 0.247 | 0.430 | 1.34 | 1.51 |
| 11.5 | 0.288 | 0.466 | 1.15 | 1.39 |
| 8.56 | 0.292 | 0.539 | 1.13 | 1.21 |
| 6.58 | 0.304 | 0.550 | 1.09 | 1.18 |
| 5.16 | 0.352 | 0.670 | 0.94 | 0.97 |
| 3.10 | 0.441 | 0.725 | 0.75 | 0.90 |
| 1.23 | 0.605 | 1.15 | 0.55 | 0.56 |
| 0 | ... | ... | 0.47 | 0.47 |

^a $^{14}\text{CH}_3\text{I}$ concentration, 0.4 ± 0.1 mM; dose, $2-4 \times 10^{19}$ ev/ml.

that the ratio of any two radical yields is proportional to the yields of the corresponding labeled hydrocarbons.¹¹ In this case the yield of $^{14}\text{C}_3\text{H}_8$ is a measure of the ethyl radical yield and similarly the yields of $^{14}\text{C}_4\text{H}_{10}$ and $n-^{14}\text{C}_6\text{H}_{14}$ are proportional to the propyl and *n*-pentyl radical yields, respectively. Thus the yield of ethyl radicals may be calculated from either of the equations¹⁴

$$G(\text{C}_2\text{H}_5) = G(\text{C}_3\text{H}_7) \times G(^{14}\text{C}_3\text{H}_8)/G(^{14}\text{C}_4\text{H}_{10}) \quad (\text{II})$$

$$G(\text{C}_2\text{H}_5) = G(n-\text{C}_5\text{H}_{11}) \times 1.06G(^{14}\text{C}_3\text{H}_8)/1.10G(n-^{14}\text{C}_6\text{H}_{14}) \quad (\text{III})$$

providing that $G(\text{C}_3\text{H}_7)$ and $G(n-\text{C}_5\text{H}_{11})$ are independent of ethylene concentration. In the absence of ethylene these yields are 0.33¹⁵ and 0.68,^{11a} respectively. The propyl radical yield should not be affected by ethylene if the latter scavenges only hydrogen atoms. It was at first thought that $G(n-\text{C}_5\text{H}_{11})$ would similarly be unaffected since hydrogen atoms abstract mainly from CH_2 groups in pentane. The values of $G(\text{C}_2\text{H}_5)$ calculated from the data with eq II and III are shown in Table I. Values calculated with eq III are consistently higher than those from eq II and the discrepancy is greater at

(13) R. A. Holroyd and G. W. Klein, *J. Am. Chem. Soc.*, **84**, 4000 (1962).

(14) The disproportionation factor in the denominator of eq III is 1.10 since for the reaction of methyl with *n*-pentyl radicals the ratio of disproportionation to combination is 0.10; cf. M. H. J. Wijnen, *ibid.*, **83**, 3752 (1961).

(15) This value is from ref 13 and has been corrected for a beam-current measurement error which resulted in the values reported in that paper being 10% too high.

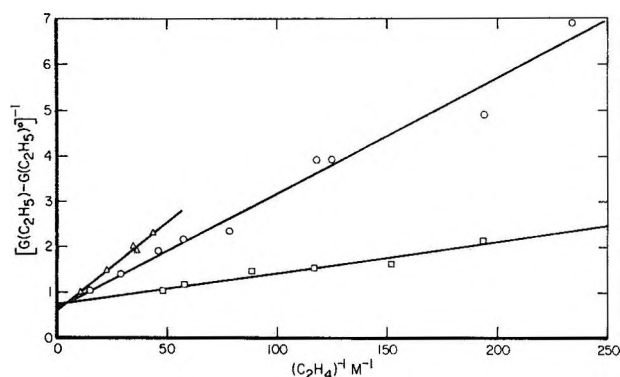


Figure 1. Plot of $[G(\text{C}_2\text{H}_5) - G(\text{C}_2\text{H}_5)^\circ]^{-1}$ vs. $[\text{C}_2\text{H}_4]^{-1}$; units of G are molecules per 100 ev: Δ , 2,4-dimethylpentane; \circ , 2,2,4-trimethylpentane; and \square , n -pentane.

higher ethylene concentration. This is attributed to the fact that $G(n\text{-C}_5\text{H}_{11})$ is not constant but decreases slightly with increasing ethylene concentration since approximately one-sixth of the radicals formed in reaction 3 are n -pentyl radicals¹⁶ and the yield from this source will decrease with increasing ethylene concentration. Because of this effect, only the values of $G(\text{C}_2\text{H}_5)$ obtained with eq II were used in the plot of $[G(\text{C}_2\text{H}_5) - G(\text{C}_2\text{H}_5)^\circ]^{-1}$ vs. $1/[\text{C}_2\text{H}_4]$ in Figure 1. $G(\text{C}_2\text{H}_5)^\circ$ was taken to be 0.47.¹⁵ It was found from a least-squares analysis of the data that $G(\text{H}) = 1.3$ and $k_3/k_2 = 0.0010$.¹²

2,4-Dimethylpentane. The radicals formed when 2,4-dimethylpentane is irradiated are reported in detail elsewhere.¹⁶ The major fragment radicals are isopropyl and isobutyl; in this study the ethyl radical yield was determined relative to the yield of these radicals. The labeled hydrocarbons which correspond to these radicals are isobutane and isopentane and the observed yields of these labeled products relative to that of propane-¹⁴C are reported in Table II. The maximum observed yield of the propane-¹⁴C was ~ 0.06 molecule/100 ev. In a manner analogous to the treatment of the n -pentane data, the ethyl radical yields were calculated from the equations

$$G(\text{C}_2\text{H}_5) = G(i\text{-C}_4\text{H}_9) \times \frac{1.06G(^{14}\text{C}_3\text{H}_8)}{G(i\text{-}^{14}\text{C}_5\text{H}_{12})} \quad (\text{IV})$$

$$G(\text{C}_2\text{H}_5) = G(i\text{-C}_3\text{H}_7) \times \frac{1.06G(^{14}\text{C}_3\text{H}_8)}{1.22G(i\text{-}^{14}\text{C}_4\text{H}_{10})} \quad (\text{V})$$

and the observed yields of $G(i\text{-C}_4\text{H}_9) = 0.54$ and $G(i\text{-C}_3\text{H}_7) = 0.53$.¹⁶ The yields of these two radicals are independent of ethylene concentration.¹⁶ The disproportionation factors for the reactions of methyl with isobutyl and methyl with isopropyl are 1.0¹⁷ and 1.22,¹⁸

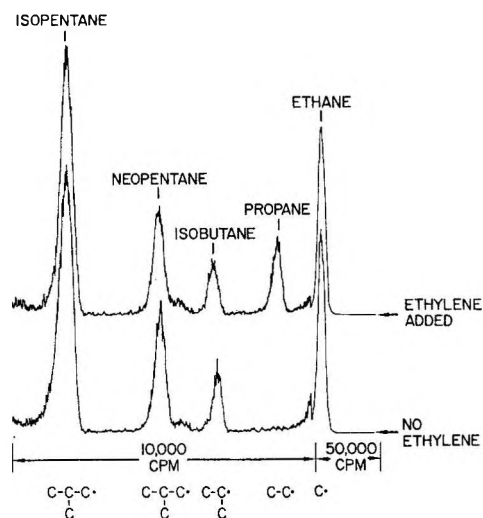


Figure 2. H atoms in 2,2,4-trimethylpentane. Recorder trace of radioactivity in various products. Lower trace is for no ethylene added and upper trace is the result when ethylene is present.

respectively. The reciprocal of the average values of $G(\text{C}_2\text{H}_5)$ are plotted in Figure 1 ($G(\text{C}_2\text{H}_5)^\circ$ is in this case zero¹⁶). A least-squares analysis of the data gave $G(\text{H}) = 1.78$ and $k_3/k_2 = 0.0105$.¹²

Table II: 2,4-Dimethylpentane^a

| $[\text{C}_2\text{H}_4]$, mM | $\frac{G(i\text{-}^{14}\text{C}_5\text{H}_{12})}{G(^{14}\text{C}_2\text{H}_6)}$ | $\frac{G(i\text{-}^{14}\text{C}_4\text{H}_{10})}{G(^{14}\text{C}_3\text{H}_8)}$ | $G(\text{C}_2\text{H}_5)$ | |
|----------------------------------|---|---|---------------------------|------|
| | | | Eq IV | Eq V |
| 93.0 | 0.539 | 0.471 | 1.06 | 0.98 |
| 44.1 | 0.815 | 0.700 | 0.70 | 0.66 |
| 29.1 | 1.07 | 0.995 | 0.54 | 0.46 |
| 27.8 | 1.10 | 0.862 | 0.52 | 0.53 |
| 23.0 | 1.39 | 1.00 | 0.41 | 0.46 |

^a $[^{14}\text{CH}_3\text{I}]$ is 0.8 ± 0.2 mM; dose, 2×10^{19} ev/ml.

2,2,4-Trimethylpentane. The fragment alkyl radicals present in irradiated 2,2,4-trimethylpentane are methyl, neopentyl, t -butyl, isopropyl, and isobutyl.¹⁶ The yields of isopropyl and isobutyl, 0.13 and 0.80, respectively, were used to monitor the ethyl radical yield. Radioactive propane is observed only when ethylene is present (see Figure 2). Equations IV and V were used to calculate $G(\text{C}_2\text{H}_5)$. Results are presented in Table III in terms of the ratio of yields of the labeled hydrocarbons,

(16) R. A. Holroyd, to be published.

(17) R. A. Holroyd and T. E. Pierce, *J. Phys. Chem.*, **68**, 1392 (1964).

(18) J. A. Kerr and A. F. Trotman-Dickenson, *J. Chem. Soc.*, 1609 (1960).

isobutane and isopentane, to the yield of labeled propane. The yield of $^{14}\text{C}_3\text{H}_8$ detected varied from 0.03 to 0.07 molecules/100 ev. The average values of the reciprocal of $G(\text{C}_2\text{H}_5)$ are plotted in Figure 1 (again $G(\text{C}_2\text{H}_5)^\circ = 0$) and in this case a least-squares analysis of the data gave $G(\text{H}) = 1.63$ and $k_3/k_2 = 0.0063$.¹²

Table III: 2,2,4-Trimethylpentane^a

| [C ₂ H ₄], mM | G(i- ¹⁴ C ₈ H ₁₈) G(¹⁴ C ₈ H ₈) | G(i- ¹⁴ C ₇ H ₁₆) G(¹⁴ C ₇ H ₈) | G(C ₂ H ₅) | |
|---|---|---|-----------------------------------|-----------------|
| | | | Eq IV | Eq V |
| 66.2 | 0.80 | ... | 1.06 | Nd ^b |
| 34.6 | 1.02 | 0.158 | 0.83 | 0.72 |
| 21.7 | 1.37 | 0.219 | 0.62 | 0.52 |
| 17.5 | 1.65 | 0.235 | 0.51 | 0.48 |
| 12.8 | 1.88 | 0.243 | 0.45 | 0.46 |
| 8.46 | 2.80 | 0.444 | 0.29 | 0.255 |
| 7.98 | 3.03 | 0.423 | 0.28 | 0.27 |
| 5.15 | 3.74 | 0.544 | 0.23 | 0.21 |
| 4.27 | 5.10 | 0.777 | 0.166 | 0.145 |

^a CH₃I concentration, ~1.0 mM; dose, 2-4 × 10¹⁹ ev/ml.

^b Not determined.

A few experiments were done with both nitrous oxide and ethylene as scavengers. The nitrous oxide presumably reacts with the electron and the ethylene should scavenge any thermal hydrogen atoms. Unfortunately, quantitative results could not be obtained, but a sizable yield of $^{14}\text{C}_3\text{H}_8$, indicating C₂H₅ radicals were formed, was observed at 30 mM N₂O, showing that hydrogen atoms were present.

Cyclopentane. Cyclopentyl radicals constitute 90% of the alkyl radical yield in cyclopentane.¹⁹ The labeled hydrocarbon formed by reaction of cyclopentyl with methyl radicals is methylcyclopentane which was the only labeled product, besides methane, ethane, and propane, observed to be formed in significant amounts.²⁰ The ratio of radical yields: $G(\text{cyclo-C}_5\text{H}_9)/G(\text{C}_2\text{H}_5)$, was calculated from the ratio of yields of the corresponding labeled products (Table IV) utilizing the relationship

$$\frac{G(\text{cyclopentyl})}{G(\text{C}_2\text{H}_5)} = \frac{G(\text{methylcyclopentane-}^{14}\text{C})}{G(^{14}\text{C}_3\text{H}_8)} \quad (\text{VI})$$

The disproportionation factor for the reaction, methyl + cyclopentyl →, was taken as 1.06.²¹ Since the yield of cyclopentyl radicals is expected to vary with ethylene concentration, $G(\text{C}_2\text{H}_5)$ could not be calculated for each run and thus a plot of the data according to eq I could not be made. However, it may be assumed that the yield of cyclopentyl radicals, $G(\text{cyclo-C}_5\text{H}_9)$, is equal to the total cyclopentyl radical yield in the absence of

Table IV: Cyclopentane^a

| [C ₂ H ₄], mM | G(methylcyclopentane- ¹⁴ C) | G(cyclo-C ₅ H ₉) |
|---|--|---|
| | G(¹⁴ C ₃ H ₈) | G(C ₂ H ₅) |
| 68.9 | 1.93 | 1.93 |
| 57.9 | 2.18 | 2.18 |
| 28.2 | 3.12 | 3.12 |
| 17.0 | 4.38 | 4.38 |
| 12.2 | 5.85 | 5.85 |
| 9.04 | 7.15 | 7.15 |

^a CH₃I concentration, ~0.3 mM; dose, 4 × 10¹⁹ ev/ml.

solute less $G(\text{C}_2\text{H}_5)$. The total cyclopentyl radical yield is just the initial yield, $G(\text{cyclopentyl})^\circ$, formed in primary processes plus $G(\text{H})$, since hydrogen atoms in the absence of scavenger abstract to form additional cyclopentyl radicals. Thus it follows from eq I that

$$\frac{G(\text{cyclopentyl})}{G(\text{C}_2\text{H}_5)} = \frac{G(\text{cyclopentyl})^\circ}{G(\text{H})} + \frac{k_3 [\text{RH}]}{k_2 [\text{C}_2\text{H}_4]} \left[\frac{G(\text{cyclopentyl})^\circ}{G(\text{H})} + 1 \right] \quad (\text{VII})$$

The ratio $G(\text{cyclopentyl})/G(\text{C}_2\text{H}_5)$ is plotted vs. $[\text{C}_2\text{H}_4]^{-1}$ in Figure 3. By least-squares analysis it is found that $G(\text{H}) = 0.835 G(\text{cyclopentyl})^\circ$ and $k_3/k_2 = 0.0024$. Therefore, $G(\text{H})$ is 0.455 times the total cyclopentyl radical yield. Values of 2.6,²² 2.9,²³ and 4.1¹⁹ have been reported for the total cyclopentyl radical yield. It is unlikely that the yield is much greater than 4.1, and the smaller values, which were obtained with iodine, are expected to be low since rate constant considerations would indicate that at the iodine concentrations employed in these studies hydrogen atoms would be partially scavenged by iodine. Owing to this uncertainty in the actual yield of cyclopentyl radicals in the pure solvent, the result obtained here for $G(\text{H})$ is uncertain. If we assume that the total cyclopentyl radical yield is 4 ± 1 then $G(\text{H})$ is 1.8 ± 0.4 .

Considerable amounts of $^{14}\text{CH}_4$ are formed in all of these systems only a fraction of which can be attributed to disproportionation reactions; the excess methane, denoted $G(^{14}\text{CH}_4)$, is presumably formed by geminate

(19) R. A. Holroyd and G. W. Klein, *J. Am. Chem. Soc.*, **87**, 4985 (1965).

(20) Although methylcyclopentene-3-¹⁴C, 1-hexene-¹⁴C, and *n*-hexane-¹⁴C were presumably formed, their yields were too low to allow accurate measurement.

(21) Calculated from an empirical relationship; cf. R. A. Holroyd and G. W. Klein, *J. Phys. Chem.*, **67**, 2273 (1963).

(22) G. A. Muccini and R. H. Schuler, *ibid.*, **64**, 1436 (1960).

(23) J. Dauphin, Proceedings of the Conference on Radioisotopes in the Physical Sciences and Industry, IAEA-UNESCO, Copenhagen, Vol. III, Globus, Vienna, 1962, p 471.

recombination of the products of reaction 4. The ratio of yields, $G(^{14}\text{CH}_3)/[G(^{14}\text{CH}_3) + G(^{14}\text{CH}_4)]$, is a measure of the fraction of methyl radicals formed which escape cage recombination. This ratio of yields was found to be 0.41 ± 0.04 in the case of cyclopentane.

Cyclohexane. The radioactive products formed when solutions of $^{14}\text{CH}_3\text{I}$ (0.4 mM) and ethylene in cyclohexane were irradiated were methane, ethane, propane, and methylcyclohexane. Analysis of the products on a silica gel column showed that the C_3 activity was entirely propane (not propylene), indicating that vinyl radicals were not produced from the ethylene. Since no other significant peaks were observed in the C_7 region it is concluded that cyclohexyl radicals are the major radical species in cyclohexane.

The results are given in Table V. The ratio of radical yields in the final column was calculated from the relationship

$$G(\text{cyclohexyl})/G(\text{C}_2\text{H}_5) = \frac{1.22G(\text{methylcyclohexane-}^{14}\text{C})}{1.06G(^{14}\text{C}_3\text{H}_8)} \quad (\text{VIII})$$

The disproportionation factor for the reaction of methyl with cyclohexyl radicals is 1.22.²¹ Values of the ratio, $G(\text{cyclohexyl})/G(\text{C}_2\text{H}_5)$, are plotted as a function of the reciprocal of the ethylene concentration in Figure 3. The best straight line through the points, as determined

Table V: Cyclohexane^a

| $[\text{C}_2\text{H}_4]$, mM | $\frac{G(\text{methylcyclohexane-}^{14}\text{C})}{G(^{14}\text{C}_3\text{H}_8)}$ | $\frac{G(\text{cyclo-C}_6\text{H}_{11})}{G(\text{C}_2\text{H}_5)}$ |
|----------------------------------|--|--|
| 71.7 | 2.05 | 2.36 |
| 39.7 | 2.20 | 2.53 |
| 36.3 | 2.69 | 3.10 |
| 22.6 | 4.03 | 4.62 |
| 21.6 | 4.16 | 4.79 |
| 15.7 | 4.97 | 5.72 |
| 9.85 | 7.52 | 8.64 |

^a CH_3I concentration, ~ 0.4 mM; dose, $\sim 2 \times 10^{19}$ ev/ml.

by least squares, indicated $G(\text{H}) = 0.82 G(\text{cyclohexyl})^\circ$, and $k_3/k_2 = 0.0037$. It is necessary to know the total cyclohexyl radical yield in order to evaluate $G(\text{H})$ from these data. The yield of cyclohexyl iodide from iodine solutions is a measure of this quantity and was found to be 3.4²² at 3 mM I_2 and 3.9⁷ at 6 mM I_2 ; this would indicate $G(\text{H})$ is between 1.5 and 1.7. However, it is known that at the concentrations of iodine employed to obtain these yields, $G(\text{H}_2)$ is lowered to some extent and iodine may be scavenging hydrogen atoms or some other

precursor of cyclohexyl radicals. On the other hand, the total radical yield based on the yield of iodine uptake from a 0.4 mM solution is 4.8.²⁴ At this low concentration complications due to interaction of iodine with ions and hydrogen atoms are minimal. This yield of 4.8 should represent the total radical yield of which from 90 to 95% would be cyclohexyl radicals, indicating $G(\text{H})$ is 2.0 ± 0.1 .

It was found that the average value of the ratio of yields $G(^{14}\text{CH}_3)/[G(^{14}\text{CH}_3) + G(^{14}\text{CH}_4)]$ was 0.54 ± 0.04 .

Discussion

The results are summarized in Table VI where they are compared with results of other work. The results of this work indicate that the yield of thermal hydrogen atoms is from 1.3 to 1.8 for the five hydrocarbons studied. The yield of thermal hydrogen atoms is apparently not markedly dependent on structural factors.

To establish the validity of the results obtained in this work it is important to reexamine what is known about the mode of interaction of ethylene in liquid hydrocarbons. It has been shown that ethyl radicals are produced from ethylene when the latter is present during the radiolysis of an alkane.^{25,26} These observations have been attributed to hydrogen atom scavenging. In confirmation of this we note that there is a correspondence between the suppression of the yield of H_2 and the yield of ethyl radicals produced; that is, the addition of 40 mM ethylene to cyclopentane reduces the yield of H_2 from 5.78²⁷ to 4.7²⁵ or $\Delta G(\text{H}_2) = 1.08$. From Figure 3, $G(\text{C}_2\text{H}_5)$ is 1.1 at this concentration if it is assumed that the total cyclopentyl radical yield is 4.0. This agreement is perhaps fortuitous but does indicate that only ethyl radicals result from hydrogen atom addition to ethylene.

The rate constant data obtained in this work further support the supposition that ethylene interacts only by hydrogen atom scavenging. The values of k_3/k_2 are summarized in Table VII. Gas phase ratios of k_3/k_2 are also listed for comparison. The latter were obtained in a study in which ethylene was used to scavenge hydrogen atoms generated from hydrocarbons by photolysis. The gas phase values of k_3/k_2 are generally higher (by a factor of 2–4) than the liquid phase values but similar trends in the two sets of data are apparent, i.e., molecules with tertiary hydrogen atoms and the cycloalkanes are more reactive than *n*-pentane, and the

(24) P. J. Horner and A. J. Swallow, *J. Phys. Chem.*, **65**, 953 (1961).

(25) R. A. Holroyd, *ibid.*, **66**, 730 (1962).

(26) R. W. Fessenden and R. H. Schuler, *J. Chem. Phys.*, **39**, 2147 (1963).

(27) T. J. Hardwick, *J. Phys. Chem.*, **65**, 101 (1961).

Table VI: Summary of $G(H)$

| Hydrocarbon | Scavenger | Ref | Yield measured | $G(H)^a$ |
|------------------------|-------------------------------|-----------|-----------------|------------------|
| <i>n</i> -Pentane | C ₂ H ₄ | This work | $G(C_2H_5)$ | 1.3 |
| | MMA ^b | 4 | $\Delta G(H_2)$ | 4.2 |
| 2,4-Dimethylpentane | C ₂ H ₄ | This work | $G(C_2H_5)$ | 1.8 |
| | MMA | 4 | $\Delta G(H_2)$ | 2.6 |
| 2,2,4-Trimethylpentane | C ₂ H ₄ | This work | $G(C_2H_5)$ | 1.6 |
| | MMA | 4 | $\Delta G(H_2)$ | 1.7 |
| Cyclopentane | C ₂ H ₄ | This work | $G(C_2H_5)$ | 1.8 ± 0.4 |
| | MMA | 4 | $\Delta G(H_2)$ | 3.1 |
| | I ₂ | 6 | $G(HI)$ | 2.2 |
| | CH ₃ I | 7 | $G(CH_4)$ | 1.0 ^c |
| Cyclohexane | C ₂ H ₄ | This work | $G(C_2H_5)$ | 1.8 ± 0.3 |
| | MMA | 4 | $\Delta G(H_2)$ | 3.1 |
| | I ₂ | 3 | $\Delta G(H_2)$ | ≥ 2.0 |
| | I ₂ | 6 | $G(HI)$ | 2.1 |
| | Benzene | 2 | $\Delta G(H_2)$ | 0.2 |
| | Benzoquinone | 5 | $\Delta G(H_2)$ | 3.2 |
| | Benzoquinone | <i>d</i> | <i>e</i> | 2.1 |
| | HI | 32 | $G(HD)$ | 1.7 |
| | Cyclohexene- ¹⁴ C | <i>f</i> | <i>g</i> | 3.7 |

^a Units are atoms/100 ev. ^b Methyl methacrylate. ^c See footnote 31. ^d F. C. Goodspeed and J. G. Burr, *J. Am. Chem. Soc.*, **87**, 1643 (1965). ^e Value of $G(H)$ deduced from $\Delta G(H_2)$, $G(\text{quinhydrone})$, $G(\text{cyclohexylquinone})$, $G(\text{cyclohexene})$, and $G(\text{dicyclohexyl})$. ^f M. Cher, C. S. Hollingsworth, and B. Browning, *J. Chem. Phys.*, **41**, 2270 (1964). ^g Values of $G(H)$ deduced from $\Delta G(H_2)$, $G(\text{cyclohexane-}^{14}\text{C})$, and the yields of various labeled C₁₂ products.

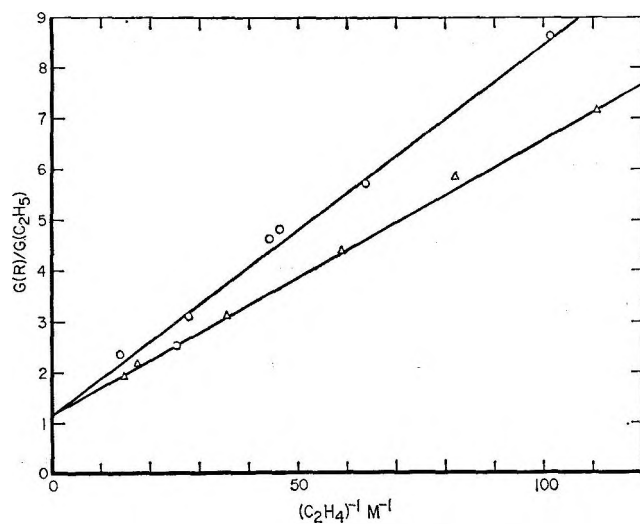


Figure 3. Plot of $G(R)/G(C_2H_5)$ vs. $[C_2H_4]^{-1} (M^{-1})$: Δ , R is cyclopentyl; and \circ , R is cyclohexyl.

rate of reaction of hydrogen atoms with a molecule having two tertiary hydrogen atoms is nearly twice the rate for a molecule with only one. Thus, the kinetic rate data as well as other evidence support the contention that the interaction of ethylene in irradiated liquid hydrocarbons is to scavenge hydrogen atoms forming C₂H₅ radicals.

 Table VII: Values of k_3/k_2

| Hydrocarbon | This work | Gas phase ^a |
|------------------------|-----------|------------------------|
| <i>n</i> -Pentane | 0.0010 | 0.0037 |
| 2,4-Dimethylpentane | 0.010 | (0.021) ^b |
| 2,2,4-Trimethylpentane | 0.063 | (0.012) ^c |
| Cyclopentane | 0.0024 | 0.009 |
| Cyclohexane | 0.0037 | ... |

^a Reference 31. ^b Value of ratio observed for 2,3-dimethylbutane. ^c Value of ratio observed for 2-methylpentane.

It is essential to the interpretation given here that ethylene does not interact in any other independent way. That is, if ethylene also scavenged the ions and excited states, which may be precursors of the free radicals that are formed, the assumed constancy of the yields of these radicals with varying ethylene concentration would be invalid. As pointed out earlier, electron capture by ethylene is unlikely and charge transfer cannot occur. The only reaction with ions which is at all likely to occur is proton transfer. The reaction of propane ions with ethylene to give C₂H₅⁺ has been observed in mass spectrometers and is therefore exother-

(28) R. A. Holroyd and G. W. Klein, *J. Phys. Chem.*, **67**, 2273 (1963).

mic.²⁹ The occurrence of the analogous reactions of the molecular ions of the hydrocarbons studied here has not been reported; we have assumed they are unimportant.

The results obtained for $G(H)$ here agree reasonably well with other *direct* determinations of this quantity. For *n*-hexane, which should be similar to *n*-pentane, $G(H)$ was found to be 1.5 based on the yield of HD from a concentrated solution of D₂S in *n*-hexane.³⁰ For the branched hydrocarbons, no direct measurements of $G(H)$ have been made. For cyclopentane, values of 2.2 and 1.0³¹ have been reported (Table VI). The latter which is based on the yield of methane formed from solutions of methyl iodide should be regarded as a lower limit because of the high concentration (8%) of solute employed. Other direct determinations of $G(H)$ for cyclohexane vary from 1.7³² to 2.1. The lower value is based on the yield of HD from a 0.7 mole % solution of HI in perdeuteriocyclohexane.

However, much higher values have been reported for $G(H)$, especially for the normal and cycloalkanes, where the indirect method based on the change in the hydrogen yield was employed. Data obtained by this method are presently open to question (see ref 3) since it is now known that certain solutes reduce the hydrogen yield by scavenging other precursors of H₂; for example, N₂O reduces the hydrogen yield without scavenging hydrogen atoms.³³ That N₂O does not scavenge hydrogen atoms was confirmed by our observation of ethyl radicals from 2,2,4-trimethylpentane with 30 mM N₂O present. It has been postulated by Dyne³⁴ that many additives, including cyclohexene, benzoquinone, and carbon tetrachloride reduce the hydrogen yield by capturing electrons or reacting with positive ions.³⁴ The high measured values of the rate constants for the reactions of benzoquinone and carbon tetrachloride with the solvated electron³⁵ support this postulate.

If methyl methacrylate at the concentration employed by Hardwick⁴ to measure $G(H)$ is capable of reacting with other precursors of H₂ besides H atoms,

this explains the high yields observed of 3.1 for the cycloalkanes and 4.2 for *n*-pentane (see Table VI).

Although the use of methyl methacrylate to determine $G(H)$ gave values much higher than those reported here for the cyclo- and normal alkanes, it gave a value for 2,2,4-trimethylpentane of 1.67, only slightly larger than that obtained with ethylene. This is understandable if we consider that the total hydrogen yield is low, either 2.3³⁶ or 2.9,⁴ for 2,2,4-trimethylpentane, and much higher, between 5 and 6, for *n*-pentane and the cycloalkanes. Thus the yield of H₂ from precursors other than thermal H atoms is about 4 for *n*-pentane and between 0.7 and 1.3 for 2,2,4-trimethylpentane.

It follows that the yield of H₂ which does not arise from hydrogen atoms is strikingly dependent on molecular structure and is large in the normal and cycloalkanes and small in the highly branched alkanes. Thus any effect of methyl methacrylate to scavenge other precursors of H₂ would be minimal in 2,2,4-trimethylpentane and of most importance in the normal and cycloalkanes. Consequently, the two techniques give values of $G(H)$ in near agreement for 2,2,4-trimethylpentane.

Acknowledgment. The assistance of H. H. Neely, D. Hogan, D. R. Warner, and W. Goepfinger in operating the Van de Graaff accelerator is gratefully acknowledged.

(29) V. L. Tal'rose and E. L. Frankevitch, *J. Am. Chem. Soc.*, **80**, 2344 (1958).

(30) G. Meisner and A. Henglein, *Ber. Bunsenges*, **69**, 264 (1965).

(31) Toma and Hamill⁷ actually reported $G(H) = 0.74$. They used as the probability of geminate recombination a value of 0.80 based on the photolysis of ethyl iodide. However, we find for recombination of CH₃ with HI (*cf.* reaction 4) a value of 0.59, indicating their value should be corrected; *i.e.*, $0.74 \times 0.8/0.59 = 1.0$.

(32) J. R. Nash and W. H. Hamill, *J. Phys. Chem.*, **66**, 1097 (1962).

(33) G. Scholes and M. Simic, *Nature*, **202**, 895 (1964).

(34) P. J. Dyne, *Can. J. Chem.*, **43**, 1080 (1965).

(35) E. J. Hart, *Science*, **146**, 3640 (1964).

(36) R. H. Schuler and R. R. Kuntz, *J. Phys. Chem.*, **67**, 1004 (1963).

Equilibrium Studies of the Reaction $2\text{Al(l)} + \text{AlCl}_3\text{(g)} \rightleftharpoons 3\text{AlCl(g)}$

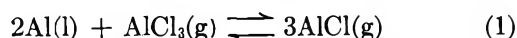
by D. Bhogswara Rao and V. V. Dadape

Communication No. 776 from the National Chemical Laboratory, Poona, India (Received April 7, 1965)

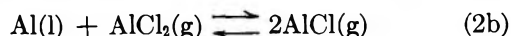
The equilibrium reaction $2\text{Al(l)} + \text{AlCl}_3\text{(g)} \rightleftharpoons 3\text{AlCl(g)}$ was studied between 1125 and 1425°K, employing a transpiration technique. Over the temperature range the ΔH_r was found to be 90.86 ± 1.6 kcal. The $\Delta S_{r_{1275}}$ was 60.12 ± 1.3 cal deg⁻¹. From the available thermal functions the second-law $\Delta H_{f_{298}}$ obtained was -12.57 ± 1.6 kcal mole⁻¹ for AlCl(g), which compared favorably with the third-law value of -10.41 ± 0.22 kcal mole⁻¹.

Introduction

Ever since the vapor phase existence of monovalent chloride of aluminum was established by Bhaduri and Fowler,¹ the equilibrium reaction

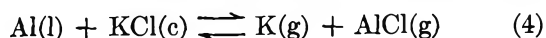
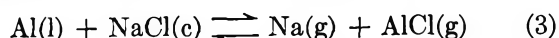


has been studied by several workers at high temperatures (the range being 880–1800°K). The chemical literature has a number of references to the heat of formation of the subhalide, but the values are not in good agreement with one another though similar techniques have been employed.^{2–5} Experimental values of Heimgartner⁴ disagree with the calculated ones, and consequently the equilibrium reaction (1) was rejected, and the following reactions were proposed



the AlCl₂(g) being considered as the main species. However, there is no evidence in the literature about the stability of AlCl₂(g) species at high temperatures. The ΔH_{f_0} values of Weiss,² Russell, *et al.*,³ and Semenkovich⁵ were -17 , -10.7 , and -16 kcal mole⁻¹, respectively, for the molecule AlCl(g).

The heat of formation ($\Delta H_{f_0} = -10.7$ kcal) obtained from equilibrium studies by Russell, *et al.*,³ compared well with that deduced ($\Delta H_{f_{298}} = -11.58$ kcal) by Gross, *et al.*⁶ However, in the latter work, the following reactions have been investigated in conjunction



with reaction 1. The $\Delta H_{f_{298}}$ values of AlCl(g) from reactions 3 and 4 did not correspond with that obtained from reaction 1. The observed difference of more than 4 kcal in the free energy of reaction has been attributed to the unreliable thermochemical data for AlCl₂(g) and to the fact that the equilibrium might not have been reached during the experiment. In reaction 1, the matter appears to be complicated by the possibility of the formation of AlCl₂(g).⁴

Foster, *et al.*,⁷ and Heise and Wieland⁸ have calculated from spectroscopic measurements the ΔH_{f_0} of AlCl(g) molecule giving the values -13.8 and -10.5 ± 2 kcal, respectively. Widely differing values of dissociation energies calculated from the spectra of diatomic molecules have been reported by Gaydon⁹ ($D_{298}^\circ = 117.6$ kcal) and Herzberg¹⁰ ($D_{298}^\circ = 71.5$ kcal.). The corresponding heats of formation $\Delta H_{f_{298}}$ were -11.6 and $+34.5$ kcal mole⁻¹, respectively.

Considering the above discrepancies in the thermochemical data, the equilibrium reaction (1) has been

(1) B. N. Bhaduri and A. Fowler, *Proc. Roy. Soc. (London)*, **A145**, 321 (1934).

(2) P. Weiss, *Z. Erzbergbau Metallhuettenw.*, **3**, 241 (1950).

(3) A. S. Russell, *et al.*, *J. Am. Chem. Soc.*, **73**, 1466 (1951).

(4) R. Heimgartner, *Schweiz. Arch. Angew. Wiss. Tech.*, **18**, 241 (1952).

(5) S. A. Semenkovich, *Zh. Prikl. Khim.*, **33**, 1281 (1960); *J. Appl. Chem. USSR*, **33**, 1269 (1960).

(6) P. Gross, *et al.*, *Discussions Faraday Soc.*, **4**, 206 (1948).

(7) L. M. Foster, *et al.*, *J. Am. Chem. Soc.*, **72**, 2580 (1950).

(8) M. Heise and K. Wieland, *Helv. Chim. Acta*, **34**, 2182 (1951).

(9) A. G. Gaydon, "Dissociation Energies and Spectra of Diatomic Molecules," Chapman and Hall Ltd., London, 1953.

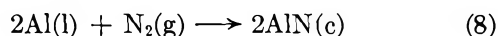
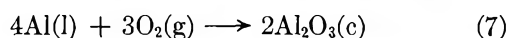
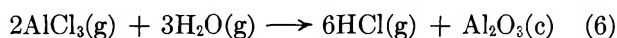
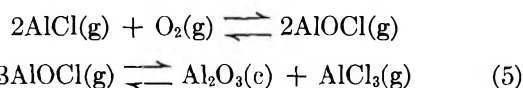
(10) G. Herzberg, "Spectra of Diatomic Molecules," D. Van Nostrand Co., Inc., New York, N. Y., 1963.

studied at high temperatures (1125–1425°K) employing the transpiration technique, which has been reviewed by Margrave.¹¹ The studies have also been carried out in regard to the corrosive nature of the molecule AlCl(g).

Experimental Section

Materials. Aluminum wire having 99.98% purity (BDH AR quality) was melted in an argon atmosphere to expel the dissolved gases (if any), and the resulting ingot was cut into chips. These chips were degreased and used. Spectrographic analysis of the sample indicated that it contained trace impurities (nearly 200 ppm), *viz.* Fe, Cu, and Si. Aluminum chloride with 99.9% purity (E. Merck grade) was resublimed in an inert atmosphere before use. Resublimed product contained 0.04% ferric chloride and 0.02% alumina.

Purification of Argon. Argon was used as a carrier gas. It is necessary to purify argon, as the impurities like oxygen, nitrogen, and moisture will react with aluminum or with the monochloride or trichloride as given below, thus affecting the apparent concentrations.



The purification process used by Gross, *et al.*,⁶ served well during the present work. In addition, sodalite (sodalime containing a little manganic acid) was also used to remove carbon dioxide.

Apparatus and Procedure. The experimental setup to study the high-temperature reaction between aluminum and aluminum trichloride was essentially similar to that reported by Hildenbrand, *et al.*¹² It may be described as follows.

A Kyanite refractory tube 60 cm in length and 2 cm in internal diameter was introduced in a Kanthal-wound tube furnace which gave a constant-temperature zone ($\pm 3^\circ$) of 25-cm length at temperatures between 1125 and 1425°K. To maintain a constant power supply, the Kanthal heating elements were connected to the 230-v main source, through a voltage stabilizer. The constant-temperature zone was long enough to accommodate a Kyanite boat (length 15 cm, width 1.5 cm, and height 1.5 cm) containing a sample of aluminum metal. Sections of Pyrex glass tubing of suitable sizes were connected to either end of the reaction tube with a high-alumina refractory cement (Accocet-50) which helped to give cemented gas-tight joints. In the

Pyrex tube at the upstream end a glass boat containing anhydrous aluminum chloride was introduced. The temperature of the Pyrex glass section was maintained at $150 \pm 3^\circ$ to facilitate the transport of the halide by argon gas. From the downstream end a Kyanite thermocouple sheath entered the reaction tube and was positioned over the center of the refractory boat. Initially, a chromel–alumel thermocouple calibrated up to the melting point of copper (1083°) served to measure the temperature during the experiment. A flowmeter was employed to measure the rate of flow of argon, and arrangements were also made to collect the gas during the run.

The rate of passage of pure argon was brought up to the desired value, and the experiment was started. After running the experiment for a definite time, the boat containing aluminum metal was pushed out of the hot zone by a refractory rod. The heating of the reaction tube and the Pyrex tube was stopped. The system was allowed to cool in an argon atmosphere. The rate of transport of aluminum trichloride as a function of the temperature and the rate of flow of argon gas were previously determined by a series of experiments.

The vapor pressure of aluminum monochloride formed during the reaction at high temperatures was calculated from

$$\frac{P_a}{P_t} = \frac{P_a}{P_a + P_b + P_f} = \frac{n_a}{n_a + n_b + n_f} \quad (9)$$

where P_a = the partial pressure of AlCl(g), P_t = total pressure = 720 mm, n_a = number of moles of AlCl(g) formed, n_b = number of moles of unreacted AlCl₃(g), n_f = number of moles of argon collected during the run. In each run the amount of AlCl₃ passed and the amount of chemically transported aluminum were found out by weight loss measurements. A good agreement was noticed between the loss in weight of the boat and the AlCl₃ collected. Loss in weight of aluminum was also checked by chemical analysis of the residual aluminum.

Results

In the transpiration method it is necessary to determine the limits of the flow rates of the carrier gas which is saturated with the gaseous reaction products. This helps us to know the extent to which the experimental results are being influenced by diffusion transport. If an equilibrium between a gaseous phase and a condensed phase is established with negligible diffusion

(11) J. L. Margrave, "Physicochemical Measurements at High Temperatures," J. O. M. Bockris, J. L. White, and J. D. Mackenzie, Ed., Butterworth Scientific Publications Ltd., London, 1959, Chapter 10.

(12) D. L. Hildenbrand, *et al.*, *J. Chem. Phys.*, **39**, 1973 (1963).

effects, the amount of vapor transported per unit time varies linearly with the flow rate of the gas mixture.¹³

In the present experiment the transport of vapor is directly proportional to the loss in weight of metal aluminum, and hence it was studied at a reaction temperature of 1183°K by varying the flow rate of a carrier gas (containing AlCl_3 vapor) between 25 and 130 ml/min. When the weight loss data were plotted against the flow rates in the above range, the weight loss increased linearly up to the flow rate of 107 ml/min, thereby indicating that the flow gas was saturated with the gaseous reaction products. The curve on interpolation passed through the origin showing that the diffusion effects were negligible. The equilibrium constant calculated at each one of the flow rates between 25 and 107 ml/min agreed well ($\pm 2\%$), which suggests that within these limits the reaction is independent of the flow rate of the carrier gas.

In a few preliminary experiments it was observed that the refractory boat (weight of the boat, 16.1740 g) increased in weight at the end of a run of 2 hr. After each succeeding run, the increase in weight progressively reduced. The boat showed almost negligible (less than 0.04%) increase in weight, after a total reaction period of 16 hr. Blank experiments carried out with aluminum metal only or by transporting AlCl_3 vapor over an empty boat at 1183°K showed no perceptible increase in the weight of the boat. In addition to the attack of aluminum monochloride on the boat material, it was also observed that the inner surface of the Kaynite tube got covered with a thin layer of a black refractory material in the initial runs. To ensure complete passivation of the inner surface of the tube, a series of experiments was carried out by placing a number of boats containing aluminum metal throughout the length of the tube. Consistent results in the equilibrium studies could be obtained only after the two surfaces were passivated. A small amount of black shining product (containing 81–83% silica, 14–15% aluminum, and 2–2.5% iron) as a result of this attack was collected. The behavior of the material toward heat treatment and the reaction with aluminum monochloride vapor was studied. It did not show any loss in weight even after several hours of heating at about 1650°K, nor did it react with aluminum chloride vapor at 1300°K. Once the boat was covered with the film of the above black material, the equilibrium reaction between molten aluminum and aluminum chloride vapor could be studied over a wide temperature range (1125–1425°K) without any difficulty.

Treatment of the Data

In the study of the equilibrium reaction (1) over the

temperature range 1125–1425°K, the experimentally determined weight loss data of Al and $\text{AlCl}_3(g)$ were converted to partial pressures of $\text{AlCl}(g)$. The equilibrium constant for reaction 1 was calculated by substituting the pressures into the expression

$$K = \frac{P_{\text{AlCl}}^3}{P_{\text{AlCl}_3}} \quad (10)$$

The free energy and heats of reaction at various temperatures were calculated employing the equations

$$\Delta F^\circ = -RT \ln K \quad (11)$$

$$\frac{\Delta H^\circ_{298}}{T} = -R \ln K - \sum \frac{F^\circ_T - H^\circ_{298}}{T} (\text{products}) + \sum \frac{F^\circ_T - H^\circ_{298}}{T} (\text{reactants}) \quad (12)$$

The free energy functions $(F^\circ_T - H^\circ_{298})/T$ for the products and the reactants were taken from the "JANAF Tables."¹⁴

Discussion

The experimental data for reaction 1 have been summarized in Table I. Employing the well-known van't Hoff equation

$$(d \ln K)/d(1/T) = -(\Delta H/R) \quad (13)$$

the heat of reaction, ΔHr , has been determined from the plot of the logarithm of the equilibrium constant *vs.* the reciprocal of the absolute temperature (Figure 1). The slope of the line obtained by the method of least squares gave the heat of reaction $\Delta Hr = 90.86 \pm 1.6$ kcal. This value of ΔHr represents the mean value over the temperature range studied and does not take into account the effect of ΔC_p . From the functions cited in the "JANAF Tables,"¹⁴ $\Delta(H_{1275} - H_{298})$ for reaction 1 has been found to be -6.34 kcal. ΔHr_{298} thus becomes 97.20 ± 1.6 kcal, and its deviation from the third-law heat (103.69) may be due to the temperature-dependent errors which contribute significantly to the second-law calculations. The second-law heat of reaction thus permits the heat of formation of $\text{AlCl}(g)$ to be calculated from the equation

$$\Delta Hf_{298}\text{AlCl}(g) = \frac{1}{3}[\Delta Hr_{298} + \Delta Hf_{298}\text{AlCl}_3(g) + \Delta Hf_{298}2\text{Al}(l)] \quad (14)$$

as -12.57 ± 1.6 kcal mole⁻¹, and the corresponding third-law value gives -10.41 ± 0.23 kcal mole⁻¹. The

(13) U. Merten, *J. Phys. Chem.*, **63**, 443 (1959).

(14) "JANAF Thermochemical Tables," revised ed, The Dow Chemical Co., Midland, Mich., 1964.

Table I: Transpiration Data and Related Third-Law Heats for the Reaction $2\text{Al}(l) + \text{AlCl}_3(g) \rightleftharpoons 3\text{AlCl}(g)^a$

| Temp, °K | No. of moles of argon passed | AlCl ₃ passed, g | Loss in Al wt, g | P _{AlCl} , atm | Log K | -RT ln K | ΔH _{r298} | ΔH _{f298} |
|----------|------------------------------|-----------------------------|------------------|-------------------------|---------|----------|--------------------|--------------------|
| 1125 | 0.5358 | 10.6495 | 0.1695 | 0.0144 | -4.5839 | 23.5969 | 103.69 | -10.40 |
| 1183 | 0.3247 | 10.8900 | 0.2495 | 0.0319 | -3.7350 | 20.2011 | 103.49 | -10.47 |
| 1183 | 0.5358 | 10.7477 | 0.3929 | 0.0324 | -3.6622 | 19.8241 | 103.88 | -10.34 |
| 1220 | 0.5464 | 10.9053 | 0.5630 | 0.0457 | -3.0368 | 16.0529 | 103.00 | -10.63 |
| 1225 | 0.5258 | 10.4902 | 0.5335 | 0.0450 | -3.0584 | 17.1434 | 103.38 | -10.51 |
| 1270 | 0.5464 | 10.9578 | 0.8417 | 0.0672 | -2.4993 | 14.5251 | 103.53 | -10.46 |
| 1280 | 0.5358 | 10.7626 | 0.8340 | 0.0679 | -2.4850 | 14.5548 | 104.18 | -10.24 |
| 1336 | 0.5154 | 10.8912 | 1.3324 | 0.1084 | -1.8157 | 11.0998 | 104.11 | -10.26 |
| 1373 | 0.5358 | 11.5390 | 1.9512 | 0.1479 | -1.3270 | 8.3370 | 103.60 | -10.43 |
| 1420 | 0.4958 | 10.7429 | 2.4808 | 0.1955 | -0.8173 | 5.3085 | 103.46 | -10.48 |
| 1425 | 0.5358 | 10.9600 | 2.4695 | 0.1834 | -0.8972 | 5.8497 | 104.29 | -10.20 |

Av -10.41 ± 0.22
kcal

^a Duration of each run is 2 hr.

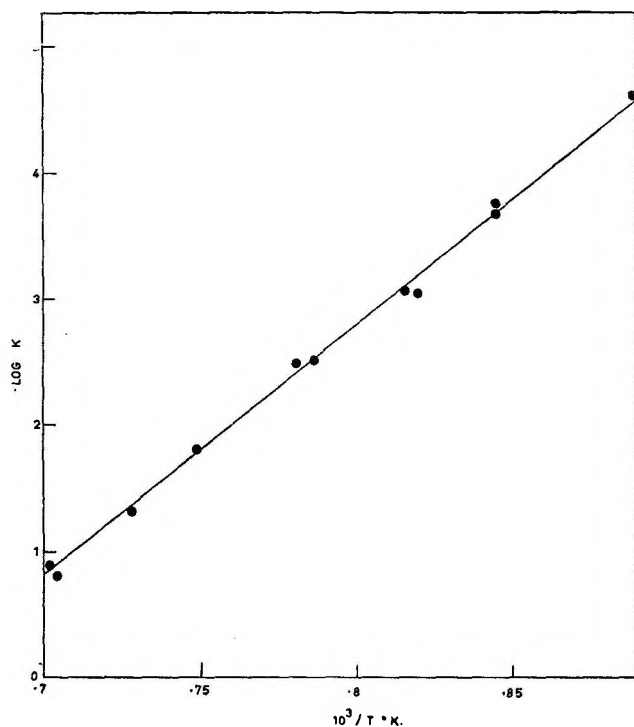


Figure 1. Plot of $\log K$ vs. $(1/T)$ from transpiration studies of the reaction $2\text{Al}(l) + \text{AlCl}_3(g) \rightleftharpoons 3\text{AlCl}(g)$.

uncertainties reported in this work are only those due to the statistical analysis of the data. The ΔH_{f298} for AlCl_2 and the heat of fusion for Al have been taken from the "JANAF Tables."¹⁴ To facilitate comparison, $\log K$ values at different temperatures reported by several workers have been recorded in Table II.

Table II: Comparison of the Values for Equilibrium Constants ($\log K$)

| Temp, °K | | | | Ref |
|----------|-------|-------|-------|--------------|
| 1000 | 1100 | 1300 | 1500 | |
| -Log K | | | | |
| -7.1 | -5.3 | -2.5 | -0.4 | 3 |
| -5.3 | -4.8 | -1.4 | 0.3 | 5 |
| -6.94 | -5.09 | -2.25 | -0.17 | 6 |
| -5.5 | -3.8 | -1.1 | -0.9 | 7 |
| -7.1 | -5.2 | -2.4 | -0.4 | 8 |
| -6.76 | -4.96 | -2.18 | -0.14 | Present work |

The entropy of reaction ΔS_r is obtained from the second law of thermodynamics

$$\Delta F_r = \Delta H_r - T\Delta S_r \quad (15)$$

Employing the values of ΔF_r and ΔH_r at 1275°K, a value of $60.12 \pm 1.3 \text{ cal deg}^{-1}$ for ΔS_{r1275} is obtained. This value agrees well with the theoretical value of $\Delta S_{r1273} = 60.5 \text{ cal deg}^{-1}$ reported by Heimgartner⁴ and also agrees well with $\Delta S_{r1275} = 61.26 \text{ cal deg}^{-1}$ calculated from the data given in the "JANAF Tables."¹⁴ This good agreement suggests that the entropy of $\text{AlCl}_3(g)$ at elevated temperatures may have considerable validity. The results of the present work are in very good agreement with those reported by Gross, *et al.*,⁶ as can be seen from Table II. It also shows that the presence of AlCl_2 species (as suggested by Heimgartner⁴) is not important in the temperature range studied.

While this manuscript was under the process of reviewing, the study of reaction 1 by Frisch, *et al.*,¹⁵ appeared, employing the molecular flow effusion technique over the temperature range 930–1034°K. An excellent agreement has been noted between their data and that of the present work. These authors have also derived the entropy of $\text{AlCl}_2(g)$ from the entropy of reaction 1 and the value of S°_{982} for $\text{AlCl}_3(g)$ is essentially 4 cal/deg/mole higher than the estimated value.¹⁵ Their value of $\Delta S^\circ_{982} = 55.1 \pm 1.1$ cal/deg mole differs by 5.0 cal/deg mole from the value calculated from "JANAF Thermochemical Tables." They have also concluded that the value of S°_{298} for $\text{AlCl}_3(g)$ as given in the "JANAF" tables is uncertain by at least 2 cal/deg mole.

The $\Delta S^\circ_{1275} = 60.12 \pm 1.3$ cal/deg reported in the

present work agrees well with the calculated value using "JANAF" tables and the difference was within the stated uncertainties. However, there is a difference of 6.5 kcal between the second-law and the third-law heats of reaction. The second-law heat may be in error due to the uncertainties in the thermodynamic functions of $\text{AlCl}_3(g)$, particularly in the reduction to 298°K. A revision, therefore, of these functions of $\text{AlCl}_3(g)$ may be of great help.

Acknowledgment. The authors wish to thank the Council of Scientific and Industrial Research for the award of a Junior Research Fellowship to D. B. R., which made possible the execution of this work.

(15) M. A. Frisch, M. A. Greenbaum, and M. Farber, *J. Phys. Chem.*, **69**, 3001 (1965).

Distribution of Benzoic Acid between Benzene and Water and Dimerization of Benzoic Acid in Benzene^{1a}

by A. K. M. Shamsul Huq^{1b}

Chemistry Department, Karachi University, Karachi, Pakistan

and S. A. K. Lodhi

*Physics Division, Pakistan Council of Scientific and Industrial Research, Karachi, Pakistan
(Received May 14, 1965)*

Distribution of benzoic acid between water and benzene has been determined at seven temperatures between 5 and 35°. The distribution ratio of undissociated monomeric benzoic acid molecules between water and benzene ($[HA]_B/[HA]_W$) and the equilibrium constant for the dissociation of benzoic acid dimers in benzene have been evaluated for each of the seven temperatures. Standard enthalpy, Gibbs free energy, and entropy values have been evaluated at the standard temperature of 25°. The values of ΔH° , ΔG° , and ΔS° for the distribution process are, respectively, 2100 ± 100 cal/mole, -241 ± 11 cal/mole, and 7.88 ± 0.35 cal/mole deg, and for the dissociation process are, respectively, 7500 ± 350 cal/mole, 3260 ± 35 cal/mole, and 14.2 ± 1.2 cal/mole deg.

Introduction

A general treatment given by Moelwyn-Hughes² permits, from distribution measurements alone, the examination of two equilibria, *viz.*, dimerization of benzoic acid in benzene and distribution of benzoic acid monomers between water and benzene. This treatment has been successfully tested by extensive works by Moelwyn-Hughes and his co-workers³ on acetic and propionic acids distributed between water and a variety of organic solvents in which these acids dimerize.

At a constant temperature, the ratio of total concentrations of benzoic acid in benzene, C_B , and in water, C_W , is given by

$$C_B/C_W(1 - \alpha) = C_B/[HA] = \frac{K_1 + 2K_1^2/K_2[HA]}{1} \quad (1)$$

where K_1 ($[HA]_B/[HA]_W$) is the equilibrium constant for distribution of benzoic acid monomers between water and benzene, K_2 is that for dissociation of benzoic acid dimers in benzene, and α is the degree of ionization of benzoic acid in water. $[HA]$, the concentration of un-ionized benzoic acid molecules in water, is given by

$$[HA] = \alpha^2 C_W^2 \gamma_{\pm}^2 / K_a \quad (2)$$

where K_a is the ionization constant of benzoic acid in water and γ_{\pm} is the mean activity coefficient of ionized benzoic acid. The activity coefficient of un-ionized benzoic acid molecules is taken as unity. A plot of $C_B/[HA]$ vs. $[HA]$ thus yields the value of K_1 from the intercept and of K_2 from the slope of eq 1. Gibbs free energy values, ΔG° , are obtained from the corresponding K values. Temperature coefficients of K values give the corresponding values of ΔH° and ΔS° through the usual thermodynamic relations.

Hendrixson⁴ measured the distribution of benzoic acid between water and benzene at 10 and 40° and found the enthalpy of dimerization of benzoic acid in benzene to be 8710 cal/mole. By means of a vapor pressure method working at 32, 44, and 56°, Wall and Rouse⁵

(1) (a) The experimental work was performed in the Central Laboratories of the Pakistan Council of Scientific and Industrial Research, Karachi, Pakistan; (b) Atomic Energy Centre, P. O. Box 164, Dacca-2, East Pakistan.

(2) E. A. Moelwyn-Hughes, *J. Chem. Soc.*, 850 (1940).

(3) M. Davies, P. Jones, D. Patnaik, and E. A. Moelwyn-Hughes, *ibid.*, 1249 (1951).

(4) W. S. Hendrixson, *Z. Anorg. Allgem. Chem.*, 13, 6 (1897).

Equilibrium was established by first vigorously shaking the flasks for 3 hr, followed by allowing the flasks to stand upright without shaking for 6 hr for phase separation. Known volumes of solution from both layers were separately titrated with carbonate-free NaOH solution using phenolphthalein as indicator. The alkali solution was standardized against recrystallized reagent grade succinic acid. Atmospheric CO₂ was excluded by using soda lime guard tubes at the openings of the automatic burets used. A mean of three titrations was taken. Experiments were performed at seven temperatures: 5, 10, 15, 20, 25, 30, and 35°.

Results

The basic data are presented in Table I. The titration data were first expressed as total concentrations of benzoic acid in millimoles per liter of solution in the water layer, C_w , and in benzene layer, C_B . C_B and C_w are shown in columns 1 and 2 of the table. The calculated values of α at the appropriate concentrations and temperatures are shown in column 3.

α has been evaluated from eq 2. Jones and Parton⁶ determined the thermodynamic ionization constants of benzoic acid in water at 20, 25, 30, and 35° by a cell without liquid junction. K_a values in molarity units have been calculated from their data. γ_{\pm} was calculated by means of an extended Debye-Hückel equation

$$-\log \gamma_{\pm} = A \sqrt{C_i} / (1 + B\sqrt{C_i}) \quad (3)$$

where A and B are constants⁷ and C_i is the concentration of benzoate ion in water. The computation of α was done by an IBM 704 computer using a successive approximation method. Two stages of approximation gave α values which agreed within 1%, which was considered acceptable for our purpose.

Least-squares values of the constants K_1 and $2K_1^2/K_2$ and hence of K_2 in eq 1 were computed. From these values of K_1 and K_2 , the values of the ratio $C_B/[HA]$ were calculated back. The standard deviations between these calculated and the observed values of this ratio are shown in column 4 of Table II for each temperature. The least-squares values of K_1 and K_2 are presented as plots of $\log K$ vs. $1/T$ in Figure 1. The least-squares straight lines of these plots expressed by the equations

$$\log K_1 = 1.7112 - 0.4556 \times 10^3/T \quad (4)$$

and

$$\log K_2 = 3.1273 - 1.6348 \times 10^3/T \quad (5)$$

are drawn between the seven experimental points.

The K values at the corresponding $1/T$ values are tabulated in Table II.

Table II

| $t, ^\circ\text{C}$ | K_1 | $K_2 \times 10^3$ | S.D. ^a |
|---------------------|-------|-------------------|-------------------|
| 5 | 1.17 | 1.75 | 0.120 |
| 10 | 1.23 | 1.90 | 0.083 |
| 15 | 1.40 | 2.96 | 0.093 |
| 20 | 1.43 | 3.18 | 0.081 |
| 25 | 1.49 | 3.85 | 0.055 |
| 30 | 1.54 | 4.46 | 0.055 |
| 35 | 1.72 | 6.76 | 0.065 |

^a Standard deviation of the ratio $C_B/[HA]$.

ΔH_1° and ΔH_2° values are assumed constant within experimental error in the measured temperature range and are evaluated from the slopes of the least-squares lines in Figure 1. The values of ΔG° and ΔS° calculated at 25° with their standard deviations are shown in Table III.

Table III: Values of Standard Thermodynamic Functions of Water-Benzoic Acid-Benzene System at 25° (Errors Are Standard Deviations)

| Distribution of benzoic acid monomer between water and benzene | Dissociation of benzoic acid dimers in benzene |
|--|--|
| $\log K_1 = 0.1772 \pm 0.0078$ | $\log K_2 = -2.389 \pm 0.025$ |
| $\Delta H_1^\circ = 2100 \pm 100$ cal/mole | $\Delta H_2^\circ = 7500 \pm 350$ cal/mole |
| $\Delta G_1^\circ = -241 \pm 11$ cal/mole | $\Delta G_2^\circ = 3260 \pm 35$ cal/mole |
| $\Delta S_1^\circ = 7.88 \pm 0.35$ cal/mole deg | $\Delta S_2^\circ = 14.2 \pm 1.2$ cal/mole deg |

Discussion

Enthalpy of dissociation of benzoic acid dimers in benzene obtained in the present work, 7500 ± 350 cal/mole, using the distribution method is somewhat lower than the value found by Hendrixson⁴ also using the distribution method, 8710 cal/mole, and by Wall and Rouse⁵ using a vapor pressure method, 9000 ± 400 cal/mole. The value of K_2 calculated at 10° from Hendrixson's data, using somewhat better values for α and K_1 , is 1.4×10^{-2} ; from Wall and Rouse's data the value is 2.14×10^{-3} , and from our data it is 1.90×10^{-3} .

Although Hendrixson's analytical accuracy should be considered perhaps as good as ours, the following

(6) A. V. Jones and H. N. Parton, *Trans. Faraday Soc.*, **48**, 8 (1952).

(7) J. N. Butler, "Ionic Equilibrium," Addison-Wesley, Reading, Mass., 1964, p 428.

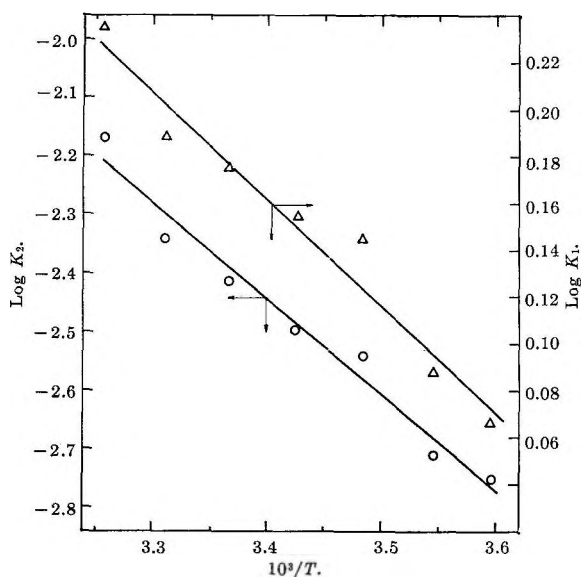


Figure 1. Temperature dependence of K_1 and K_2 . Arrows on the lines indicate the scale to be used; open circles and open triangles are observed points; lines are least-squares fits.

factors, however, tend to introduce greater uncertainty in his enthalpy value. (i) His measurements were made at two temperatures only, 10 and 40°, whereas ours were made in the same temperature range at seven temperatures, from 5 to 35° at an interval of 5°. (ii) Apparently, he used one single value, 6×10^{-5} , for the ionization constant of benzoic acid for both temperatures, whereas the values are different. (iii) He made no activity coefficient correction for α . (iv) His concentration range of aqueous layer was 40 to 460 mM compared to ours of 0.3 to 5 mM. This approximately 100-fold concentration would introduce an even larger uncertainty in α .

In our analysis we have neglected the possibility that the slight solubility of water in benzene (4.02×10^{-4} mole fraction⁸ at 25°) may influence the calculated value of K_2 because the presence of water could produce an additional species in the benzene phase. We would then have to consider not only the dissociation of dimers, $HA_2 \rightleftharpoons 2HA$, but also the hydration of benzoic acid, $HA + H_2O \rightleftharpoons HA \cdot H_2O$. This would introduce a systematic error in our values for K_1 which could tend to make K_2 as much as 6% smaller than the value we have obtained. Thus, this factor could not account for the difference between our value and Wall and Rouse's value⁴ which was obtained in the absence of water. The fact that these values agree within 10% is consistent with the possible systematic errors in both experiments and implies that the presence of water in benzene does not have a major effect on K_2 , as Lassette⁹ has predicted.

Wall and Rouse's enthalpy value, which is also somewhat higher than ours and in better agreement with Hendrixson's, is free from the above criticisms, as they used a vapor pressure method. However, the concentration range of benzoic acid in benzene in which they worked was 70 to 200 mM, whereas our concentration range was 0.3 to 25 mM. If it is assumed that a higher concentration of benzoic acid in benzene leads to higher orders of polymerization of benzoic acid like formation of trimers and tetramers,⁹ a higher enthalpy value would be expected. The same comment should apply to the value reported by Hendrixson, whose concentration range of benzoic acid in benzene was also high, *viz.*, 140 to 780 mM. Within our concentration range, however, the slope of the $C_B/[HA]$ vs. $[HA]$ line, which gave K_2 , did not show any systematic trend at different concentrations, hence showing no significant evidence of higher order of polymerization beyond dimerization.

The values for the thermodynamic functions for distribution of benzoic acid monomers between water and benzene presented in Table III show smaller deviations compared to the corresponding values for dimerization of benzoic acid in benzene. The values of the equilibrium constant K_1 , from which the other thermodynamic values were calculated, obtained as intercepts of the $C_B/[HA]$ vs. $[HA]$ lines, are comparatively less sensitive to experimental error. Our enthalpy and entropy values for benzoic acid are in the same range for propionic acid distributed between water and a number of organic solvents including benzene, as reported by Moelwyn-Hughes and his co-workers.³ For example, our values for the enthalpy and entropy of distribution of benzoic acid monomers between water and benzene are 2100 cal/mole and 7.88 cal/mole deg compared to their values of 3935 cal/mole and 7.16 cal/mole deg for the enthalpy and entropy of distribution of propionic acid between the same solvents.

Acknowledgments. The authors wish to extend their thanks to Dr. S. Siddiqi, Director, Council of Scientific and Industrial Research, Karachi, Pakistan, for providing laboratory facilities and to Dr. R. J. Wineman, Director, Monsanto Research Corp. Boston Laboratory, for permitting us to use the Monsanto Computer facilities. Thanks are due to Miss Sharon Lee Wilson, mathematician, Computer Center, Central Research Department of the Monsanto Co., who performed the

(8) F. Franks, M. Gent, and H. H. Johnson, *J. Chem. Soc.*, 2716 (1963).

(9) E. N. Lassette, *Chem. Rev.*, 20, 259 (1937).

computer calculations, and to Mr. E. N. Wescott of the Monsanto Research Corp. Boston Laboratory for assistance in problem preparation. Finally, A. K.

M. S. H. wishes to thank Dr. J. N. Butler of Tyco Laboratories, Inc., Waltham, Mass., for helpful discussions during the preparation of this paper.

The Effect of Solvent on the Rate of Formation of Monoacetylacetonatocopper(II) Ion

by Raymond C. Barile,

Department of Chemistry, Manhattan College, Bronx, New York

Michael Cefola, Philip S. Gentile,

Department of Chemistry, Fordham University, Bronx, New York 10458

and Alfred V. Celiano

Department of Chemistry, Seton Hall University, South Orange, New Jersey (Received June 28, 1965)

The kinetics of the reaction of copper(II) ion + acetylacetonone \rightleftharpoons monoacetylacetonatocopper(II) ion in mixed solvents of methanol-water and ethanol-water was investigated conductometrically in the temperature range -20 to 0° . In all solvents the reaction obeyed second-order kinetics, first order with respect to the concentration of copper ion and first order with respect to the concentration of the enol form of acetylacetonone. The initial rate in representative solvents was independent of initial hydrogen ion concentration, indicating that the reaction does not involve prior ionization of acetylacetonone but most likely a direct combination of the two reacting species. The log of the forward rate constant, k_1 , was found to be a linear function of the reciprocal of the macroscopic dielectric constant of the solvent over a range of 80 to 40. The energy of activation, E_a , was separated into a contribution due to change of dielectric constant, $(E_a)_T$, and into a contribution due to a change of temperature, $(E_a)_D$.

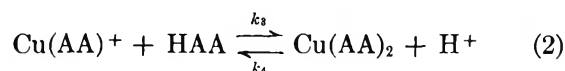
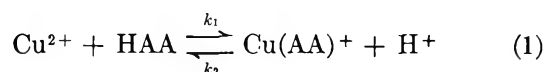
Introduction

The reactions between metal ions and β -diketones have been the subject of considerable investigation. In the sphere of kinetics of complex ions interest has been focused mainly on the mechanism of substitution reactions rather than the rate of complex formation.¹⁻⁶

According to principles enunciated by Bjerrum,⁷

complex formation of copper ion with acetylacetonone (HAA) takes place in a series of two reversible steps

- (1) D. W. Margerum, *J. Am. Chem. Soc.*, **78**, 4211 (1956).
- (2) T. Leo, I. Kolthoff, and D. Leussing, *ibid.*, **70**, 3596 (1948).
- (3) P. Krumholz, *J. Phys. Chem.*, **60**, 87 (1956).
- (4) J. H. Baxendale and P. George, *Trans. Faraday Soc.*, **46**, 736 (1950).



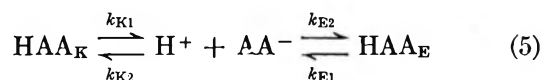
Assuming a concerted mechanism for reaction 1, $K_1 = k_1/k_2$, and for reaction 2, $K_2 = k_3/k_4$, then the first complex formation constant is

$$K_1 = \frac{k_1}{k_2} = \frac{[\text{Cu}(\text{AA})^+][\text{H}^+]}{[\text{Cu}^{2+}][\text{HAA}]} \quad (3)$$

and the second complex formation constant is

$$K_2 = \frac{k_3}{k_4} = \frac{[\text{Cu}(\text{AA})_2][\text{H}^+]}{[\text{Cu}(\text{AA})^+][\text{HAA}]} \quad (4)$$

The values of the formation constants determined under many experimental conditions⁵ indicate the ratio of $K_1/K_2 \geq 10$. The conversion between the tautomeric forms of acetylacetone is believed to follow the mechanism⁸



where HAA_K is the keto form, HAA_E is the enol form, AA^- is the enolate ion, $k_{K1} = 1.4 \times 10^{-2} \text{ sec}^{-1}$, and $k_{E2} = 3 \times 10^{10} \text{ M}^{-1} \text{ sec}^{-1}$. From the data of Eigen⁸ and Celiano⁶ the rate of first complex formation of Cu^{2+} with acetylacetone is much greater than the rate of conversion of the keto form to the enol form of acetylacetone. In the present study, the forward rate constant for the first complex formation, k_1 , was measured conductometrically in solvents of varying compositions of methanol-water and ethanol-water at temperatures of 0, -10, and -20°. The enol content of acetylacetone was measured in all the solvents at each experimental temperature.

Experimental Section

Materials. ACS grade methanol was refluxed for 1 hr over magnesium methoxide⁹ and then distilled through a 90-cm column. The first portion of the distillate was discarded, and a second distillation was made over 2,4,6-trinitrobenzoic acid through a 15-plate Oldershaw column; bp 64.70° (lit.¹⁰ 64.75°). ACS grade 95% ethanol was refluxed for 1 hr and then distilled through an Oldershaw column. The first portion of the distillate was discarded, and the constant boiling point fraction was collected; bp 78.15° (lit.¹¹ 78.15°). Fisher Purified 1-propanol was refluxed over Mg ribbon and then distilled through a 15-plate Oldershaw column. The first fraction was discarded, and the second fraction was collected at a temperature

of $97.1 \pm 0.1^\circ$ (lit.¹² 97.4°). Laboratory-distilled water was passed through a Fisher demineralizer, and the eluent water had a specific conductance less than 10^{-6} mho. CP grade acetylacetone was used without further purification. Analytical reagent grade copper perchlorate hexahydrate (G. Frederick Smith) was used without further purification. Complexometric and ion-exchange analyses¹³ gave assays of $\text{Cu}(\text{ClO}_4)_2 \cdot 6\text{H}_2\text{O}$ between 99.20 and 99.60%. Analytical reagent grade anhydrous NaClO_4 (G. Frederick Smith) was dried in a finely powdered form at 200°¹⁴ and was used without further purification. Aqueous perchloric acid (70%), doubly distilled and lead free (G. Frederick Smith), was used without further purification.

Solutions. Calibrated glassware and weights were used throughout. Stock solutions of $\text{Cu}(\text{ClO}_4)_2$ in the various alcohol-water solvents were standardized by complexometric titration with 0.1 N EDTA. Sodium perchlorate stock solutions in the different alcohol-water solvents were standardized by an ion-exchange method. Perchloric acid stock solutions in the alcohol-water solvents were standardized by titration with 0.1 N NaOH. The alcohol-water solvents were made up by weight in a 50-l. bottle and stored under nitrogen. The exact composition of the solvent was determined by measurement of the density *in vacuo* at 25°. All stock solutions were kept in automatic burets and protected from atmospheric moisture and CO_2 . Solutions employed in the kinetic determinations were made from stock solutions. All kinetic determinations were made in solutions containing $1.04 \times 10^{-2} \text{ M}$ sodium perchlorate. The reasons for employing a neutral salt are twofold: it decreases the percentage change in the ionic strength during the reaction and allows the initial resistance of the acetylacetone and the copper perchlorate solutions to be adjusted to within 500 ohms of

(5) R. Taft and E. Cook, *J. Am. Chem. Soc.*, **81**, 46 (1959).

(6) A. V. Celiano, M. Cefola, and P. S. Gentile, *ibid.*, **65**, 2194 (1961).

(7) J. Bjerrum, "Metal Ammine Formation in Aqueous Solution," P. Haase and Son, Copenhagen, 1941.

(8) M. Eigen and L. DeMaeyer in "Techniques of Organic Chemistry," Vol. VIII, Part II, Interscience Publishers, Inc., New York, N. Y., 1963, p 1037.

(9) A. Weissberger, "Techniques of Organic Chemistry," Vol. VII, Interscience Publishers, Inc., New York, N. Y., 1955, p 336.

(10) G. E. Coates and J. E. Coates, *J. Am. Chem. Soc.*, **55**, 2733 (1933).

(11) R. W. Merriam, *J. Chem. Soc.*, **103**, 628 (1913).

(12) F. G. Keyes and W. J. Winninghoff, *J. Am. Chem. Soc.*, **38**, 1178 (1916).

(13) F. J. Welcher, "The Analytical Uses of Ethylenediamine Tetraacetic Acid," D. Van Nostrand Co., Inc., New York, N. Y., 1958, p 242.

(14) C. Duval, "Inorganic Thermogravimetric Analysis," Elsevier Publishing Co., New York, N. Y., 1953.

each other.⁶ Acetylacetone was weighed in a pycnometer-type cell having 0.5-mm capillary side arms to prevent vaporization. The enol content of 0.04 *M* solutions of acetylacetone in the alcohol-water solvents containing 1.04×10^{-2} *M* NaClO₄ was determined by the Kurt Meyer titration method as modified by Cooper and Barnes.¹⁵

Apparatus. The reaction of copper(II) ion + acetylacetone \rightleftharpoons monoacetylacetonatocopper(II) ion + hydrogen ion is far too rapid to be followed by conventional techniques, and thus a continuous-flow apparatus was adopted. The apparatus employed in this study was modified by Celiano⁶ from the original design by Dalziel.¹⁶

Measurements. Ideal operation of the apparatus involves mixing of equal amounts of material from both reagent containers. The experimental mixing ratio (MR) was determined at all temperatures and fluid drive pressures in all solvents by mixing in the apparatus an approximately 0.1 *N* HClO₄ solution from the right reagent container with solvent from the left reagent container. Aliquots of the diluted acid, undiluted acid, and the solvent (blank) were titrated in excess water with NaOH to a phenolphthalein end point. Mixing efficiency was assessed by the physical dilution process in which a solution of HClO₄ was mixed with the pure solvent. The efficiency of mixing was evaluated by comparing the experimentally measured resistance of the flowing solutions after mixing with the resistance calculated for perfect mixing by $1/R_c = MR(1/R_a) + (1 - MR)(1/R_s)$, where R_c = calculated resistance, MR = mixing ratio, R_a = measured resistance of acid solution, and R_s = experimentally measured resistance of the solvent. The tests for mixing efficiency were performed in the most viscous solvents at a flow rate less than the flow rate employed in the reaction rate studies. The lowest mixing efficiency at the second electrode was found to be $98.0 \pm 0.5\%$.

The reaction time was determined to ± 0.0003 sec, indirectly from a knowledge of the reactor volume and the flow rate. The reactor volumes were obtained from Celiano.¹⁷ The flow rates were determined at all temperatures, fluid drive pressures, and in all solvents.

It is known that pressure applied to a system affects the electrical resistance of a solution.¹⁸ The expected decrease of resistance with increase in pressure was observed to be a linear relationship in all solvents and at all temperatures employed in this study. All resistance values were corrected to a reference pressure of 10 psi, at which pressure the initial resistances, calibration resistances, and resistance ratios were determined. In order to correlate the resistance

measurements at each electrode, the eighth electrode was used as a reference electrode. The resistances measured at other electrodes were related to the eighth electrode through resistance ratios. The resistance ratios were determined at every temperature and in every solvent employed in this study. The initial resistance of the metal and ligand solutions, respectively, was determined while flowing through the apparatus at a pressure of 10 psi. The initial resistance after mixing is calculated by the parallel resistance law with the proper dilution factors.

In each solvent system an experimental curve relating concentration of hydrogen ion formed to the resistance of the solution was determined. The experimental calibration curve was based on the assumption made by Monk, *et al.*, in the determination of the dissociation constant of condensed phosphates,¹⁹ namely, that the ratio of mobilities and hence conductances of two similar ions are equal to the ratio of their ionic charges. We assumed the mobility of the solvated Cu²⁺ to be twice that of the solvated first complex, CuAA⁺, and accordingly made up solutions covering the range of concentrations of products formed in the reaction. Calibration curves were determined for every solvent at all experimental temperatures. A linear calibration curve was found in all solvents, with the exception of those most viscous. In these solvents the experimental calibration curve was concave toward the resistance axis. In order to demonstrate that the concave curvature of the calibration curve had no relation to the hydrolysis between copper ion and the solvent, solutions of increasing concentration of NaClO₄ in the solvent were prepared, and the resistance was measured at the eighth electrode. A plot of resistance of NaClO₄ exhibited the same curvature. This indicates that measurable hydrolysis of copper ion was not obtained in any experimental solvents.

Results and Discussion

Order of Reaction. The order of reaction of Cu²⁺ and acetylacetone was evaluated from the van't Hoff equation²⁰ in all solvent systems and found to be overall second order, first order with respect to the concentration of Cu²⁺, and first order with respect to the

(15) S. R. Cooper and R. P. Barnes, *Ind. Eng. Chem., Anal. Ed.*, **10**, 379 (1939).

(16) K. Dalziel, *J. Biol. Chem.*, **55**, 79 (1953).

(17) A. V. Celiano, Thesis, Fordham University, 1960.

(18) G. F. Kortum and J. Bockris, "Electrochemistry," Elsevier Publishing Co., New York, N. Y., 1951.

(19) R. W. Jones, C. B. Monk, and C. W. Davies, *J. Chem. Soc.*, **152**, 2693 (1949).

(20) A. A. Frost and R. G. Pearson, "Kinetics and Mechanism," 2nd ed, John Wiley and Sons, Inc., New York, N. Y., 1961.

concentration of acetylacetonone. The fact that the integrated rate equation could be applied to evaluate the specific rate constant, for all solvent systems, was taken as further evidence that the reaction is over-all second order.

The Effect of Hydrogen Ion on the Rate of Complex Formation. The acid dissociation constant of acetylacetonone²¹ at 0° was found to vary approximately from 10⁻⁹ in H₂O to 10⁻¹³ in MeOH. With the concentrations of acetylacetonone employed in our experiments, the contribution of hydrogen ion from the dissociation of acetylacetonone would be less than 10⁻⁶ M. Experimentally, 10⁻³ M acetylacetonone was not found to have a measurable effect upon the conductance of a 10⁻² M NaClO₄ in all solvents. Thus, we may conclude that solutions of 10⁻³ M acetylacetonone in mixed alcohol-water solvents have a hydrogen ion content of less than 10⁻⁶ M.

The rate of formation of the products, in all solvent systems, was measured under identical conditions for two runs, one of which differed only in the initial hydrogen ions added. Table I indicates the measured concentration of products (*x*) at varying experimental times for the two runs and the difference (Δ) between the concentrations of products for the runs with and without initial hydrogen ions, respectively.

Table I^a

| Time $\times 10^3$, sec | 10 ³ (H ⁺), M | | 10 ³ Δ , M |
|-----------------------------|--------------------------------------|--------------------|---------------------------------|
| | Run A ^b | Run B ^c | |
| 19.64 | 0.201 | 0.196 | 0.005 |
| 22.78 | 0.228 | 0.220 | 0.008 |
| 44.08 | 0.338 | 0.320 | 0.018 |
| 51.15 | 0.370 | 0.351 | 0.021 |
| 69.01 | 0.485 | 0.455 | 0.030 |
| 80.04 | 0.516 | 0.504 | 0.012 |
| 81.13 | 0.553 | 0.523 | 0.022 |
| 94.32 | 0.585 | 0.542 | 0.040 |
| 108.5 | 0.630 | 0.588 | 0.042 |

^a Solvent composition: 49.96% MeOH-H₂O; temperature -10.00°; (Cu²⁺)₀ = 4.988 $\times 10^{-3}$ M; (HAAE)₀ = 0.9447 $\times 10^{-3}$ M. ^b (H⁺)₀ = 10⁻⁶ M. ^c (H⁺)₀ = 2 $\times 10^{-4}$ M.

The value of Δ at the beginning of the reaction is within the experimental error of the measured concentration of products, and thus the initial rates of complex formation for the two runs are approximately equal and independent of hydrogen ion. It appears, therefore, that prior ionization of acetylacetonone is not involved in the mechanism of complex formation,⁶ but rather a direct combination of the reacting species occurs. As the extent of reaction increases, the value of

Δ increases indicating that the concentration of products is affected by initial hydrogen ion only insofar as the rate of the reverse reaction is accelerated.

Specific Rate Constants. Complex formation can be represented by a stepwise process according to eq 1 and 2 where the equilibrium constant for the first and second complex formation are given by eq 3 and 4, respectively. The integrated rate equation for an irreversible second-order reaction²⁰ is

$$k_1 t = \frac{2.303}{a-b} \log \frac{b(a-x)}{a(b-x)} \quad (6)$$

where *a* = initial concentration of Cu²⁺, *b* = initial concentration of the enol form of acetylacetonone, *x* = concentration of products measured at time *t*, and *k* = specific rate constant for first complex formation. Plotting log [(*a*-*x*)/(*b*-*x*)] vs. time, we have an equation of the form *y* = *mx* + *B* where the slope is

$$m = \frac{k_1(a-b)}{2.303} \quad (7)$$

and the intercept is

$$B = \log (a/b) \quad (8)$$

The specific rate constants for the first complex formation were determined by graphically evaluating the slope of log [(*a*-*x*)/(*b*-*x*)] vs. time and by using eq 7.

Celiano⁶ has shown that irreversible second-order kinetics may be employed up to 60% completion of the reaction yielding *k*₁ which deviates by only 2% from the true value. In considering the plots of log [(*a*-*x*)/(*b*-*x*)] vs. time for the different solvent systems, linearity was obtained, within experimental error, over the whole experimental concentration-time range studied in solvents of dielectric constant greater than 38. This fact was interpreted to indicate that the measured concentrations of products were only affected by the forward reaction for complex formation. With solvents of lower dielectric constant, we found an upward drift after approximately 60% reaction. Analysis of the data for the solvent 91.04% EtOH-H₂O showed that within 100 msec more hydrogen ion had been formed than the enol initially present. Since the conversion of the keto to the enol form is believed to follow the mechanism given by eq 5, the change of an appreciable amount of the keto to the enol form could not possibly occur in the experimental time range of our study. In all probability, therefore, the upward drift may be due to the second complex formation reaction of Cu(AA)⁺ with the enol form first and then

(21) P. S. Gentile, M. Cefola, and A. V. Celiano, *J. Phys. Chem.*, **67**, 1083 (1963).

by interaction with the keto form especially in solvents of lower dielectric constants. Table II lists the specific rate constants and the conditions under which they were determined.

Table II: Specific Rate Constants for First Complex Formation

| Wt % alcohol | D | % enol | Temp, °K | $10^3 a, M$ | $10^3 b, M$ | $10^{-3} k, M^{-1} \text{ sec}$ |
|--------------|-------|--------|----------|-------------|-------------|---------------------------------|
| 49.58 MeOH | 63.02 | 49.83 | 273.16 | 5.041 | 0.968 | 2.49 |
| 50.42 MeOH | 62.74 | 50.41 | 273.16 | 5.070 | 0.677 | 1.97 |
| 49.60 MeOH | 66.50 | 48.43 | 263.16 | 5.063 | 1.052 | 2.01 |
| 49.60 MeOH | 66.50 | 48.43 | 263.16 | 5.063 | 0.806 | 1.85 |
| 49.80 MeOH | 62.84 | 50.00 | 273.16 | 4.989 | 0.856 | 2.63 |
| 46.37 MeOH | 68.21 | 46.02 | 263.16 | 5.002 | 0.904 | 2.03 |
| 49.96 MeOH | 66.31 | 48.70 | 263.16 | 4.966 | 0.844 | 1.72 |
| 49.96 MeOH | 66.31 | 48.70 | 263.16 | 4.993 | 0.947 | 1.81 |
| 49.96 MeOH | 66.31 | 48.70 | 263.16 | 4.988 | 0.947 | 2.00 |
| 49.96 MeOH | 66.31 | 48.70 | 263.16 | 2.494 | 0.943 | 1.78 |
| 49.96 MeOH | 66.31 | 48.70 | 263.16 | 4.986 | 0.943 | 1.73 |
| 70.37 MeOH | 55.02 | 63.88 | 263.16 | 4.986 | 1.978 | 2.20 |
| 70.37 MeOH | 55.02 | 63.88 | 263.16 | 4.986 | 1.903 | 2.24 |
| 70.37 MeOH | 51.93 | 63.90 | 273.16 | 4.986 | 1.904 | 3.51 |
| 70.37 MeOH | 51.93 | 63.90 | 273.16 | 4.986 | 1.904 | 3.42 |
| 87.33 MeOH | 42.30 | 72.75 | 273.16 | 4.986 | 3.078 | 3.62 |
| 87.33 MeOH | 44.72 | 75.36 | 263.16 | 4.986 | 3.284 | 2.45 |
| 87.33 MeOH | 44.72 | 75.36 | 263.16 | 4.986 | 2.844 | 2.54 |
| 87.56 MeOH | 47.24 | 77.33 | 253.16 | 4.999 | 3.192 | 1.73 |
| 87.56 MeOH | 47.24 | 77.33 | 253.16 | 4.999 | 3.180 | 1.77 |
| 79.95 MeOH | 51.93 | 72.19 | 253.16 | 4.475 | 2.682 | 1.59 |
| 79.95 MeOH | 51.93 | 72.19 | 253.16 | 4.475 | 2.719 | 1.56 |
| 69.86 MeOH | 58.52 | 63.70 | 253.16 | 4.475 | 2.523 | 1.41 |
| 69.86 MeOH | 58.52 | 63.70 | 253.16 | 4.475 | 2.512 | 1.49 |
| 91.02 EtOH | 36.55 | 86.17 | 253.16 | 4.337 | 3.958 | 2.28 |
| 91.02 EtOH | 36.55 | 86.17 | 253.16 | 4.337 | 3.968 | 3.24 |
| 91.04 EtOH | 34.36 | 85.05 | 263.16 | 5.263 | 3.433 | 7.29 |
| 91.04 EtOH | 34.36 | 85.05 | 263.16 | 4.503 | 3.403 | 7.25 |
| 91.04 EtOH | 32.31 | 83.42 | 273.16 | 4.995 | 3.347 | 13.9 |
| 91.04 EtOH | 32.31 | 83.42 | 273.16 | 4.995 | 3.354 | 14.0 |
| 69.70 PrOH | 35.85 | 77.77 | 273.16 | 5.058 | 2.682 | 1.16 |
| 69.70 PrOH | 35.85 | 77.77 | 273.16 | 5.064 | 2.803 | 1.16 |
| 80.06 EtOH | 38.05 | 77.84 | 273.16 | 4.974 | 2.943 | 4.33 |
| 80.06 EtOH | 38.05 | 77.84 | 273.16 | 4.974 | 2.934 | 4.35 |
| 18.20 EtOH | 76.87 | 32.89 | 273.16 | 5.183 | 0.709 | 2.16 |
| 18.20 EtOH | 76.87 | 32.89 | 273.16 | 5.183 | 0.417 | 1.87 |

Effect of Solvent on the Specific Rate Constant. Considering the reaction of ionic species with neutral molecules, Laidler and Eyring,²² using the theory of absolute reaction rates, showed that

$$\frac{d(\log k^0)}{d(1/D)} = \frac{Z_A^2 e^2}{2kT} \left(\frac{1}{R_A} - \frac{1}{R_M^*} \right) \quad (9)$$

where k^0 = specific rate constant at zero ionic strength, D = macroscopic dielectric constant, R_A = radius of ionic species, R_M^* = radius of activated complex, k =

Boltzmann's constant, Z_A = ionic charge, e = electronic charge, and T = absolute temperature.

Applying the above equation to the reaction of copper ion with the enol form of acetylacetone and neglecting the polar nature of the latter, the rate constant, k_1 , measured at an ionic strength of 0.025 is taken as equal to the rate constant at zero ionic strength, k_1^0 . For a reaction between an ion and a polar molecule, the influence of ionic strength on the specific rate constant has been shown^{23,24} to be practically nil below an ionic strength of 0.10. Ignoring the polar character of the enol form does not essentially change the basic nature of the relation of $\log k^0$ with the dielectric constant which follows

$$\log k_1^0 = A \left(\frac{1}{D} \right) + B \quad (10)$$

Figures 1-3 are the plots of $\log k_1^0$ ^{25,26} vs. $1/D$ at $t = 0, -10, \text{ and } -20^\circ$, respectively. Treating the data by the method of least squares, the equations were derived

$$\log k_1^0 = 21.81 \frac{1}{D} + 3.067 \text{ at } t = 0^\circ \quad (11)$$

$$\log k_1^0 = 18.77 \frac{1}{D} + 2.960 \text{ at } t = -10^\circ \quad (12)$$

$$\log k_1^0 = 20.96 \frac{1}{D} + 2.799 \text{ at } t = -20^\circ \quad (13)$$

From Figures 1-3 the plots of $\log k_1^0$ vs. $1/D$ are linear over the range of $1/D$ from 0.0125 to 0.0250 and then rise sharply. The upward deviation from linearity begins at different dielectric constants depending upon whether the solvent system is EtOH-H₂O or MeOH-H₂O. This seems to imply the existence of some factor(s), dependent on the mole fraction of alcohol, as the contributing cause for the nonlinear behavior beyond a certain dielectric constant. Furthermore, deviations from linearity appear to be smaller at the lower temperatures when compared at values of $t = 0, -10, \text{ and } -20^\circ$. Thus, there is also reason to believe that deviation from linearity is influenced by some dielectric constant dependent factor.

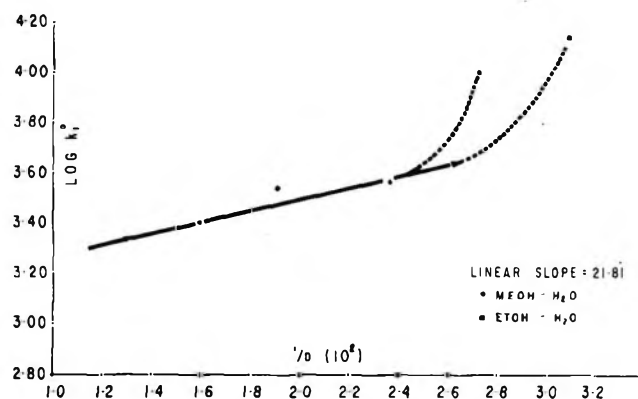
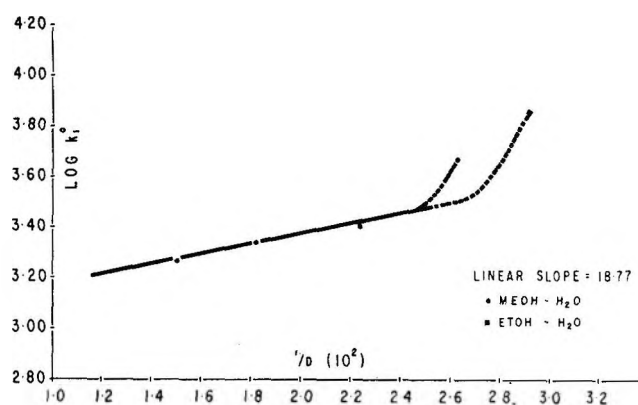
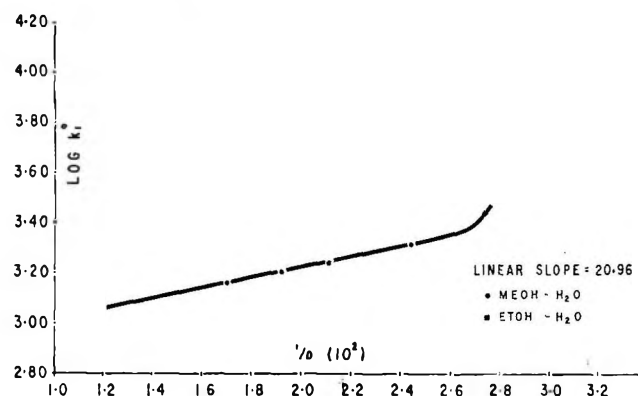
(22) K. J. Laidler and H. Eyring, *Ann. N. Y. Acad. Sci.*, **39**, 303 (1940).

(23) J. N. Brønsted and W. F. K. Wynne-Jones, *Trans. Faraday Soc.*, **25**, 59 (1929).

(24) A. Long, J. McDevitt, and P. Dunkle, *J. Phys. Colloid Chem.*, **55**, 819 (1951).

(25) The values of the specific rate constants are for the average values of those in Table II.

(26) Values of k_1^0 in 98.76% MeOH-H₂O were obtained by interpolating the data of Cellano.

Figure 1. $\text{Log } k_1^0$ as a function of $1/D$ at 0° .Figure 2. $\text{Log } k_1^0$ as a function of $1/D$ at -10° .Figure 3. $\text{Log } k_1^0$ as a function of $1/D$ at -20° .

Data on the coordination of metal ions in alcohol-water solvents have indicated that the fully coordinated aquo complex is not found when stoichiometric amounts of H_2O are available for the metal ion. For Co^{2+} in $\text{EtOH-H}_2\text{O}$ ²⁷, Dy^{3+} in $\text{MeOH-H}_2\text{O}$ ²⁸, and Cu^{2+} in $\text{EtOH-H}_2\text{O}$,²⁹ the hexaquo complex is found exclusively at concentrations of H_2O greater than $10 M$.

It is a known fact³⁰ that the axially coordinated H_2O molecules in such a distorted octahedron are replaced at a faster rate than the equatorially situated H_2O molecules. Thus, the occupation of an axial position by an alcohol molecule should result in a larger rate constant. A factor dependent upon dielectric constant, which could account for the upward deviation from linearity, is the instability of ionic species in solvents of low dielectric constant ($D < 35$).

Separation of Energy of Activation. In comparing reactions in the gas state and in solution one would like to compare activation energies of the gas state with those in solution which are independent of the properties of the solution. Since the rate constant is a function of temperature, dielectric constant, and ionic strength in solution,³¹⁻³³ the energy of activation and other thermodynamic properties of activation are functions of these parameters.

Svirbely and Warner³³ described a method of separating the temperature and dielectric effects on the energy of activation. For a system at zero ionic strength, one may write

$$\log k^0 = f(D, T) \quad (14)$$

Obtaining the general differential expression

$$d \log k^0 = \left[\frac{\delta \log k^0}{\delta T} \right]_D dT + \left[\frac{\delta \log k^0}{dD} \right]_T dD \quad (15)$$

dividing through by dT , and multiplying by $2.3RT^2$, we obtain

$$2.3RT^2 \left[\frac{d \log k^0}{dT} \right] = 2.3RT^2 \left[\frac{\delta \log k^0}{\delta T} \right]_D + 2.3RT^2 \left[\frac{\delta \log k^0}{\delta D} \right]_T \frac{dD}{dT} \quad (16)$$

Equation 16 can simply be stated as

$$(E_a)_{FC} = (E_a)_D + (E_a)_T \quad (17)$$

where $(E_a)_{FC}$ is the energy of activation at a fixed composition, the Arrhenius activation energy, $(E_a)_D$ is the contribution to the energy of activation at a fixed dielectric constant, and $(E_a)_T$ is the contribution to the energy of activation at a constant temperature. In

(27) C. K. Jorgensen, *Acta Chem. Scand.*, **8**, 175 (1954).

(28) J. Bjerrum and C. K. Jorgensen, *ibid.*, **7**, 953 (1953).

(29) N. J. Friedman and R. A. Plane, *Inorg. Chem.*, **2**, 11 (1963).

(30) L. DeMaeyer and K. Kustin, *Ann. Rev. Phys. Chem.*, **14**, 8 (1963).

(31) E. S. Amis and V. K. La Mer, *J. Am. Chem. Soc.*, **61**, 905 (1939).

(32) W. J. Svirbely and J. Lander, *ibid.*, **60**, 1616 (1938).

(33) W. J. Svirbely and J. C. Warner, *ibid.*, **57**, 1883 (1935).

previous works,³¹⁻³³ $(E_a)_D$ was evaluated by using isodielectric solvents at different temperatures. $(E_a)_T$ was obtained by subtracting $(E_a)_D$ from $(E_a)_{FC}$ which is evaluated by the Arrhenius equation.

To eliminate the extra weight placed upon a point in using isodielectric solvents, an analytical method of evaluating $(E_a)_D$ was adopted from the work of Cefola, Gentile, and Celiano.³⁴ Instead of using isodielectric solvents, a function of the dielectric constant is chosen which gives a linear relationship with $\log k^0$ over the range of dielectric constants of interest. At each temperature, an equation of the form $\log k^0 = Af(D) + B$ is obtained. For a fixed dielectric constant $\log k^0$ can be calculated at each temperature at which the above expression has been evaluated, then $(E_a)_D$ can be obtained. In this work $\log k_1^0$ is a linear function of $1/D$ over the range of $D = 40$ to 80 . Equations 11-13 represent these linear functions at 0 , -10 , and -20° , respectively. In order to demonstrate the additivity of $(E_a)_D + (E_a)_T = (E_a)_{FC}$, $(E_a)_D$, $(E_a)_T$, and $(E_a)_{FC}$ are evaluated for $t = -10$ and solvents of $D = 40, 50, 60, 70$, and 80 .

$(E_a)_{FC}$ was evaluated by using the Arrhenius expression

$$(E_a)_{FC} = -2.3R \frac{(\log k_1^0)_1 - (\log k_1^0)_2}{(1/T_1) - (1/T_2)} \quad (18)$$

where the rate constants are evaluated using eq 11 and 13 at 0 and -20° for the fixed compositions corresponding to $D = 40, 50, 60, 70$, and 80 at -10° .

$(E_a)_D$ is given by the expression

$$(E_a)_D = 2.3RT^2 \left[\frac{\delta \log k_1^0}{\delta T} \right]_D \quad (19)$$

which is equivalent to

$$(E_a)_D = -2.3R \left[\frac{\delta \log k_1^0}{\delta(1/T)} \right]_D \quad (20)$$

$\log k_1^0$ is determined at 0 and -20° using eq 11 and 13 for $D = 40, 50, 60, 70$, and 80 , and $[\partial \log k_1^0 / \partial(1/T)]_D$ is evaluated for each D and $(E_a)_D$ is calculated.

$(E_a)_T$ is given by the expression

$$(E_a)_T = 2.3RT^2 \left[\frac{\delta \log k_1^0}{\delta D} \right]_T \frac{dD}{dT} \quad (21)$$

which is equivalent to

$$(E_a)_T = -2.3RT^2 \frac{1}{D^2} \left[\frac{\delta \log k_1^0}{\delta(1/D)} \right]_T \frac{dD}{dT} \quad (22)$$

dD/dT is evaluated by the data of Akerlöf³⁵ and $[\partial \log k_1^0 / \partial(1/D)]_T$ is the least-squares slope of the equation of $\log k_1^0$ vs. $1/D$ for $t = -10^\circ$ derived from eq 11 and 13 at 0 and -20° .

Table III contains the tabulation of $(E_a)_T$, $(E_a)_D$, $(E_a)_T + (E_a)_D$, and $(E_a)_{FC}$ for each D .

Table III: Energy of Activation for the Formation of Monoacetylacetonatocopper(II) Ion at Constant Temperature, Fixed Dielectric Constant, and Fixed Composition as a Function of Dielectric Constant of MeOH-H₂O Mixtures at -10°

| D | $(E_a)_D$, kcal/mole | $(E_a)_T$, kcal/mole | $(E_a)_T +$ $(E_a)_D$, kcal/mole | $(E_a)_{FC}$, kcal/mole |
|-----|--------------------------|--------------------------|---|-----------------------------|
| 40 | 4.56 | 0.918 | 5.48 | 5.50 + 0.02 |
| 50 | 4.50 | 0.775 | 5.28 | 5.27 - 0.01 |
| 60 | 4.47 | 0.633 | 5.10 | 5.08 - 0.02 |
| 70 | 4.43 | 0.507 | 4.94 | 4.92 - 0.02 |
| 80 | 4.40 | 0.417 | 4.82 | 4.81 - 0.01 |

The additivity of $(E_a)_T$ and $(E_a)_D$ is found to be within ± 20 cal/mole. $(E_a)_D$ varies only slightly with dielectric constant, but $(E_a)_T$ is a linear function of $\log D$ over the range of solvent compositions in which $\log k_1^0$ is linear with $1/D$. Thus, the variation of the Arrhenius activation energy with a change in solvent composition is due mainly to the variation of the contribution to the energy of activation at a constant temperature with solvent composition.

Acknowledgment. We are grateful to the Atomic Energy Commission for support of this work under Contract AT(30-1)-906.

(34) P. S. Gentile, M. Cefola, and A. V. Celiano, *J. Phys. Chem.*, **67**, 1447 (1963).

(35) G. Akerlöf, *J. Am. Chem. Soc.*, **54**, 4125 (1932).

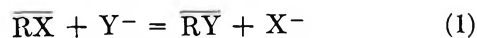
Considerations on the Distribution of Ions between an Organic Solution of Alkylammonium Salts and an Aqueous Solution of Inorganic Salts in the Presence of Homopolymers and Heteropolymers in the Organic Phase

by G. Scibona^{1a}

Laboratory for Nuclear Science, Department of Chemistry,^{1b} Massachusetts Institute of Technology, Cambridge, Massachusetts, and Centro Studi Nucleari Casaccia, Rome, Italy (Received July 6, 1965)

The distribution of a monovalent simple anion, Y^- , or of a monovalent metal complex anion, MX_{n+1}^- , between an aqueous solution of the supporting electrolyte CX and a water-immiscible solution of an alkylammonium salt \overline{RX} has been described considering the presence in the organic phase of the homopolymers $(\overline{RX})_i$, $(\overline{RY})_j$, and of the heteropolymers $(\overline{RX})_a(\overline{RY})_b$. A set of equations has been derived that show the dependence of the experimental distribution data on the concentration of the alkylammonium salt and the extracted anion. A successful reinterpretation of the data existing in the literature on the distribution of $UO_2(NO_3)_2$ between aqueous nitrate solution and alkylammonium nitrate solutions has been carried out. The presence of a mixed tetramer and of monomer terms seems to fit the experimental data.

The distribution of the anion Y^- between an organic solution (water immiscible) of an alkylammonium salt, \overline{RX} , and an aqueous solution of the salt MY in the presence of the supporting electrolyte MX has been described by the exchange reaction^{2,3}



with the bar indicating the organic salt.

The equilibrium constant of reaction 1 in terms of the concentration, m , and of the activity coefficient, γ , of each species is given by the equation

$$K = \overline{m}_{RY} \overline{\gamma}_{RY} m_{MX} \gamma_X / \overline{m}_{RX} \overline{\gamma}_{RX} m_{MY} \gamma_Y \quad (2)$$

Introducing the mean activity coefficients for the aqueous phase, eq 2 reduces to

$$K = \overline{m}_{RY} \overline{\gamma}_{RY} m_{MX} \gamma_{\pm MX(MY)}^2 / \overline{m}_{RX} \overline{\gamma}_{RX} m_{MY} \gamma_{\pm MY(MX)}^2 \quad (3)$$

with $\gamma_{\pm MX(MY)}$ and $\gamma_{\pm MY(MX)}$ mean activity coefficients of MX and MY in the presence of MY and MX , respectively.

Equations 1-3 are based on the assumptions that only monomeric species, RX and RY , are involved in the exchange and that the ratio of the organic activity

coefficients, Γ , takes into account the nonideality of the organic phase.

The validity of these assumptions can be established only by reference to experimental facts. At very low concentrations of alkylammonium salt the existence of only monomeric species can be accepted, and eq 1 probably describes the exchange reaction. Experimental results indicate that the monomer is the predominant species in $10^{-4} M$ solutions of tertiary ammonium chloride, nitrate, and perchlorate salts in an organic solvent of low dielectric constant.⁴⁻⁶ However, it seems unlikely that reaction 1 can describe the dis-

(1) (a) Centro Studi Nucleari Casaccia, Rome, Italy; (b) this work has been supported in part by the U. S. Atomic Energy Commission, Contract No. AT(30-1)905.

(2) (a) C. F. Coleman, "Amine Extraction in Reprocessing, Atomic Energy Review," Vol. 2, No. 2, I.A.E.A., Vienna, 1964; (b) F. Baroncelli, G. Scibona, and M. Zifferero, *J. Inorg. Nucl. Chem.*, **24**, 547 (1962).

(3) S. Lindenbaum and G. E. Boyd, *J. Phys. Chem.*, **66**, 1383 (1962).

(4) G. Scibona, S. Basol, P. R. Danesi, and F. Orlandini, *J. Inorg. Nucl. Chem.*, submitted.

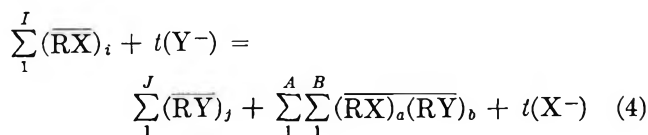
(5) J. I. Bucker and R. M. Diamond, *J. Phys. Chem.*, **69**, 1565 (1965).

(6) E. Hogfeldt, *Svensk Kem. Tidskr.*, **76**, 4 (1964), and references therein.

tribution of anions between phases if the concentration of ammonium salt is in the range where dimers, trimers, and higher polymers are known to exist. A more suitable reaction would take into account all species existing in the organic phase since the number and type of species in the initial and equilibrium phase can be different.

It should be pointed out that eq 2 accounts for structural changes of the organic phase with the activity coefficient ratio Γ . However, it is a more realistic approach to consider all of the species participating in the distribution process and to account for a part of the solute-solute interactions in terms of n -mer existing in the organic phase. If, in addition, an inert diluent is chosen to give a minimum of specific solvent-solute interactions, the activity coefficient of each species in the organic solution approaches unity.

In the presence of species in addition to monomers, the exchange process can be described by the equilibrium



with i, j, a , and b integer numbers 1, 2, 3, ..., n . I, J, A , and B indicate the maximum polymerization in the system. The term with the double sum, $\Sigma\Sigma$, accounts for the presence of mixed aggregates that can be formed between RX and RY .

The idea of polymerization of the organic phase has been used in the past by different authors⁷⁻⁹ to describe in general the partition of solutes between two immiscible liquid phases.

It must be pointed out, however, that a detailed development of this idea applied to the ammonium salt has not been done. A treatment of this kind can give us some equation useful for the handling of partition data of ions, simple or complex, between aqueous electrolyte solution and organic solutions of ammonium salts.

In order to give a physical picture of the exchange process and to describe equilibrium 4 in terms of measurable quantities, we can imagine the following mechanism. Of all of the $(\overline{RX})_i$ species in equilibrium, only the monomeric species RX exchanges with Y to form RY ; RY is itself in equilibrium with the $(\overline{RY})_i$ species and with the heteropolymers $(\overline{RX})_a (\overline{RY})_b$.

The following equations and their relative equilibrium constants are then to be considered



$K_{(1,X,Y)}$ is the equilibrium constant for the exchange between the monomers. Equilibria 7 and 8 account for the formation of i - and j -mers. Equilibrium 9 deals with the heteropolymer formation. In the following sections these equilibria will be used to derive the distribution coefficient for simple and complex monovalent anions.

Distribution Coefficient of Simple Monovalent Anion

In the equilibrium distribution experiments of the anion Y^- between an organic solution of the salt \overline{RX} and an aqueous solution of the salt MY in mixture with the electrolyte CX the distribution coefficient of Y^- is given by the expression

$$D = (Y)_{org}/(Y)_{aq} \quad (9)$$

where $(Y)_{org}$ and $(Y)_{aq}$ are the concentrations of Y^- in the organic and aqueous media, respectively.

Considering equilibria 4-8, the following expression for the distribution coefficient is obtained

$$D = K_{(1,X,Y)} (\overline{RX})(X)^{-1} F^{-1} + \left[\sum_2^J j K_{(1,X,Y)}^j K_{(j,Y)} (\overline{RX})^j (Y)^{j-1} (X)^{-j} F^{-j} + \sum_1^A \sum_1^B b K_{(1,X,Y)}^b K_{(a,b)} (\overline{RX})^{a+b} (Y)^{b-1} (X)^{-b} F^{-b} \right] \quad (10)$$

F is the ratio of the mean-square aqueous activity coefficients. The first term on the right part of eq 10 is the distribution coefficient when the simple mass action law is followed. The terms in brackets account for the presence of $(\overline{RY})_j$ species and for the formation of heteropolymer $(\overline{RX})_a (\overline{RY})_b$. The use of the monomer concentration (RX) accounts for the aggregation of the salt RX .

From eq 10 the difference $\Delta D = D - [K_{(1,X,Y)} (\overline{RX})(X)^{-1} F^{-1}]$ can be calculated if experimental values for D are available in the low concentration range, where the monomer predominates. In this condition ΔD is given by the term in brackets.

$$\Delta D = \left[\sum_2^J j K_{(1,X,Y)}^j K_{(j,Y)} (\overline{RX})^j (Y)^{j-1} (X)^{-j} F^{-j} + \sum_1^A \sum_1^B b K_{(1,X,Y)}^b K_{(a,b)} (\overline{RX})^{a+b} (Y)^{b-1} (X)^{-b} F^{-b} \right] \quad (11)$$

(7) H. Irving, F. J. C. Rossotti, and R. J. P. Williams, *J. Chem. Soc.*, 1906 (1956).

(8) J. Saldick, *J. Phys. Chem.*, **60**, 500 (1956).

(9) R. Diamond, *ibid.*, **61**, 69 (1957).

On a logarithmic plot of D vs. (\overline{RX}) , ΔD is represented by the difference between the experimental D values and the line with slope 1. To draw the line with slope 1, it was assumed that the D values of the lowest ammonium salt concentration used in the experiment matches the assumption that simple mass action law is followed. The definition of a concentration range where the plot of $\log D$ vs. $\log (\overline{RX})$ follows a straight line with slope 1 is sometimes experimentally difficult. It is then more suitable to obtain an expression connected with D that allows a limit operation to zero (\overline{RX}) values.

A new function, Q , is obtained by multiplying eq 10 by $(\overline{RX})^{-1}(X)^F$

$$Q = K_{(1,X,Y)} + \sum_2^J jK_{(1,X,Y)}^j K_{(j,Y)} (\overline{RX})^{j-1} (Y)^{j-1} \times (X)^{-(j-1)} F^{-(j-1)} + \sum_1^A \sum_1^B bK_{(1,X,Y)}^b K_{(a,b)} \times (\overline{RX})^{a+b-1} (Y)^{b-1} (X)^{-(b-1)} F^{-(b-1)} \quad (12)$$

From eq 12 the values of $K_{(1,X,Y)}$ can be obtained as the limit of the function $Q = f(\overline{RX})$

$$\lim_{(\overline{RX}) \rightarrow 0} Q = K_{(1,X,Y)} \quad (13)$$

It must also be noted that $K_{(1,X,Y)}$ can be obtained using the total ammonium concentration as the variable in calculating the limit by the extrapolation method even if the presence of i -mers has been detected.

From eq 12 and 13 it is possible to calculate a new function ΔQ

$$\Delta Q = Q - K_{(1,X,Y)} = \sum_2^J jK_{(1,X,Y)}^j K_{(j,Y)} (\overline{RX})^{j-1} \times (Y)^{j-1} (X)^{-(j-1)} F^{-(j-1)} + \sum_1^A \sum_1^B bK_{(1,X,Y)}^b K_{(a,b)} \times (\overline{RX})^{a+b-1} (Y)^{b-1} (X)^{-(b-1)} F^{-(b-1)} \quad (14)$$

The function $\Delta Q = f(\overline{RX})$, as well as $\Delta D = f(\overline{RX})$, can be used to analyze the presence of $(\overline{RY})_j$ species in the organic phase. If different $(\overline{RX})_i$ species are present, the free monomer concentration (\overline{RX}) at equilibrium must be used for this analysis. Equations 10 and 12 show that ΔD and ΔQ depend on both (\overline{RX}) and (Y) .

In ref 10 the distribution data of ReO_4^- ion between aqueous electrolyte solutions and tertiary ammonium salt in organic solvent have been analyzed using eq 12. The analysis has been successful and the formation constant of the mixed dimer $(\overline{RX})_1(\overline{RY})_1$ with $X = \text{Cl}, \text{NO}_3, \text{Br}$ and $Y = \text{ReO}_4$ has been calculated.

Distribution Coefficient of Anionic Metal Complex

The simple case of a monovalent anionic metal complex will be considered. In the case of a metal ion, M^{n+} , of valence n forming an anionic complex with the ligand X^- (anion of the supporting electrolyte CX) the distribution coefficient is given by the ratio of the metal concentration in the organic and in the aqueous phases

$$D = (M)_{\text{org}} / (M)_{\text{aq}} \quad (15)$$

Considering the equilibrium formation of the species MX_i with $i = 0, 1, \dots, n+1$



its equilibrium constant $K_{(i,\text{aq})}$ is given by the expression

$$K_{(i,\text{aq})} = (\text{MX}_i^{n-i}) / (X^-)^i (M^{n+}) F'_i \quad (17)$$

where parentheses indicate concentrations and F'_i is an activity coefficient function that takes into account the activity coefficient of each species in equilibrium 16. When $i = 0$, it is $K_{(i,\text{aq})} = 1$. The total aqueous concentration of the metal is then given by the expression

$$(M)_{\text{aq}} = (M^{n+}) \sum_i K_{(i,\text{aq})} (X^-)^i (F'_i)^{-1} \quad (18)$$

It will be convenient to the following discussion to express the activity function F' in terms of mean activity coefficients when $i = n+1$. The equation (17) for $i = n+1$ reduces to

$$K_{(n+1,\text{aq})} = (\text{MX}_{n+1}^-) / (M^{n+})(X^-) \times \gamma_{\pm \text{MX}_{n+1}(\text{CX})}^2 / \gamma_{\pm \text{MX}_n(\text{CX})} \gamma_{\pm \text{CX}(0)}^2 \quad (19)$$

where $\gamma_{\pm \text{MX}_{n+1}(\text{CX})}$ is the mean activity coefficient of the electrolyte $\text{C}^+ \text{MX}_{n+1}^-$ (with C the monovalent cation of the supporting electrolyte CX) in the presence of CX , $\gamma_{\pm \text{MX}_n(\text{CX})}$ is the mean activity coefficient of the electrolyte MX_n in the presence of CX , and $\gamma_{\pm \text{CX}(0)}$ is the mean activity coefficient of the supporting electrolyte in the presence of the other species. The use of the mean activity coefficient of CX , $\gamma_{\pm \text{CX}}$, in place of $\gamma_{\pm \text{CX}(0)}$ is justified when $\text{CX} \gg \text{MX}_n$.

The distribution of the metal complexes can be described by means of a set of equations equivalent to eq 3, 5, 7, and 9, considering the anionic complex MX_{n+1}^- in place of Y^- . Of course, all of the considerations concerning these equations are still valid.

Considering equilibrium 4 and eq 5-9, the distribu-

(10) G. Scibona, R. A. Nathan, A. S. Kertes, and J. W. Irvine, Jr., *J. Phys. Chem.*, **70**, 375 (1966).

tion coefficient of the anionic metal complex will be given by

$$D = \left[K_F(\overline{RX})(X^-)^n \gamma + \sum_2^J j K_F^j K_{(j,K)} (M^{n+})^{j-1} \times (\overline{RX})^j (X^-) \gamma^j + \sum_1^A \sum_1^B b K_F^b K_{(a,b)} (\overline{RX})^{a+b} (M^{n+})^{b-1} \times (X^-)^{nb} \gamma^b \right] \left[\sum_i K_{(i,aq)} (X^-)^i (F'_i)^{-1} \right]^{-1} \quad (20)$$

with $K_F = K_{(1,X,Y)} K_{(n+1,aq)}$ and $\gamma = \gamma^{n+1}_{\pm MX(CX)}$.

At fixed aqueous ionic strength a logarithmic plot of D vs. (\overline{RX}) must give a straight line with slope 1 if only monomers are present in the organic phase. In presence of other species, a positive deviation from the line of slope 1.0 is expected, and the function $\Delta D = f(\overline{RX})$ can be calculated as well as has been done in eq 11.

Let us now define the function Z^{-1}

$$Z^{-1} = K_{(n+1,aq)} (X^-)^n \gamma / \sum_i K_{(i,aq)} (X^-)^i (F'_i)^{-1} \quad (21)$$

(It must be noted that we can obtain the molar fraction of the complex MX_{n+1} multiplying Z^{-1} by $(X^-) \cdot \gamma^2_{\pm CX(0)} \gamma^{-2}_{\pm MX_{n+1}(CX)}$.) Multiplying eq 20 by Z and $(\overline{RX})^{-1}$, the expression is obtained

$$Q = K_{(1,X,Y)} + \sum_2^J j K_{(1,X,Y)}^j K_{(j,X)} (M^{n+})^{j-1} \times (X^-)^{nj-n} \gamma^{j-1} + \sum_1^A \sum_1^B b K_{(1,X,Y)}^b K_{(a,b)} \times (\overline{RX})^{a+b-1} (M^{n+})^{b-1} (X^-)^{nb-n} \gamma^{b-1} \quad (22)$$

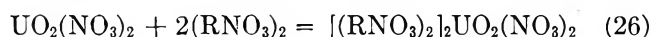
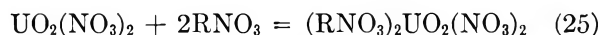
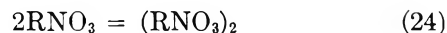
Equation 22 is the twin of eq 12 for the case of monovalent metal-anionic complex. The value of $K_{(1,X,Y)}$ can be obtained by calculating the limit for $RX \rightarrow 0$ of the function $Q = f(\overline{RX})$. The eventual partition of the species MY_n at the place of MX_{n+1} will require the use of $K_{(n,aq)}$ instead of $K_{(n+1,aq)}$ in eq 20-22.

From eq 22 the function $\Delta Q = f(\overline{RX})$ can be obtained

$$\Delta Q = Q - K_{(1,X,Y)} = \sum_2^J j K_{(1,X,Y)}^j K_{(j,X)} (M^{n+})^{j-1} \times (\overline{RX})^{j-1} (X^-)^{nj-n} \gamma^{j-1} + \sum_1^A \sum_1^B b K_{(1,X,Y)}^b K_{(a,b)} \times (\overline{RX})^{a+b-1} (M^{n+})^{b-1} (X^-)^{nb-n} \gamma^{b-1} \quad (23)$$

An application of the approach here developed for the distribution of metal ion forming complexes with ligands will be made using the data of ref 11.

In ref 11 the extraction of $UO_2(NO_3)_2$ by tridodecylammonium nitrate in toluene has been suggested by the authors to fit the experimental results.



To avoid a long explanation of the model, assumptions, and conditions, a careful reading of the quoted reference is suggested. Briefly, it can be said that the authors describe the extraction of $UO_2(NO_3)_2$ as involving equilibria between amine nitrate monomer and dimer species, extraction of uranium by both of these species, and extraction of HNO_3 by amine nitrate.

Now it is interesting to handle the data of Tables I and II of ref 11 using eq 22 and 23 and forgetting the model suggested in the quoted reference. Since eq 22 and 23 ask for the use of the monomer concentration, (\overline{RX}) , and these data are not available for toluene solutions of the salt RNO_3 , we have used the monomer concentration values of benzene solutions of tridodecylammonium nitrate salt.⁴ It seems reasonable to us that the use of toluene in place of benzene does not affect the values of the monomer concentration appreciably.

The extraction of UO_2^{2+} from nitrate media by monomeric RNO_3 can be represented by either of the following reactions, which are thermodynamically indistinguishable



The experimental distribution coefficient is described by eq 20. Tables I and II give the values of Q' obtained by dividing the distribution coefficient by the concentration of monomeric alkylammonium nitrate.

Table I

| Amine concn, M | (RNO_3) monomer, M | D | Q' | $\Delta Q'$ | $\frac{\Delta Q'}{(RNO_3)^2}$ |
|---------------------|------------------------|--------|------|-------------|-------------------------------|
| 0.346 ^a | | 2.91 | | | |
| 0.210 ^a | 0.052 | 1.04 | 32.7 | 32.3 | 1.0×10^6 |
| 0.109 ^a | 0.023 | 0.254 | 11 | 10.7 | 8.5×10^5 |
| 0.0501 ^a | 0.015 | 0.0624 | 4 | 3.7 | 1.0×10^6 |
| 0.0210 ^a | 0.0086 | 0.0141 | 1.6 | 1.3 | 2.0×10^6 |
| 0.0101 ^a | 0.0057 | 0.0030 | 0.5 | 0.2 | 1.0×10^6 |

^a From ref 11. Amine in equilibrium with 2.75 M NO_3^- and 0.010 M H^+ .

(11) R. J. Lloyd and E. A. Mason, *J. Phys. Chem.*, **68**, 3120 (1964).

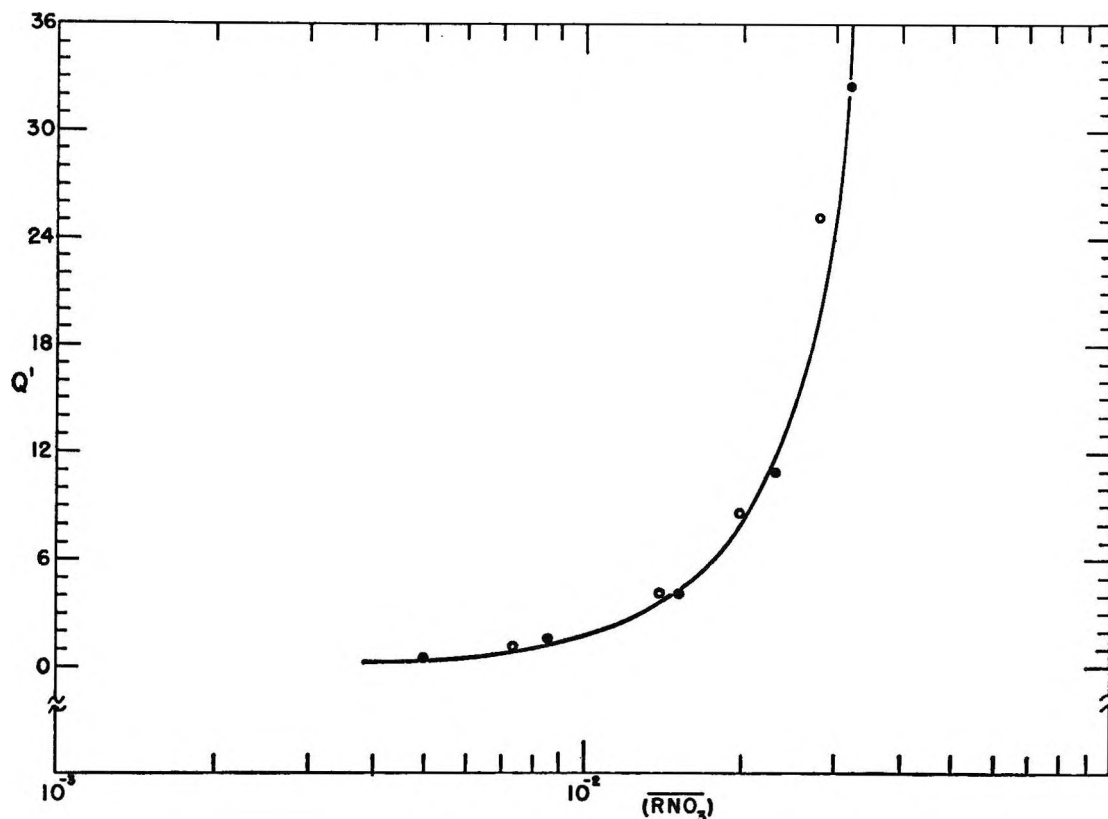


Figure 1. Plot of Q' against $(\overline{RNO_3})$. The solid points refer to data of Table I; the empty circles refer to data of Table II.

Table II

| Amine concn, M | B | $(\overline{RNO_3})$ monomer, M | D | Q' | $\Delta Q'$ | $\frac{\Delta Q'}{(\overline{RNO_3})^3}$ |
|---------------------|--------|-----------------------------------|--------|------|-------------|--|
| 0.339 ^a | 0.246 | 0.035 | 1.45 | 41.4 | 41 | 9.6×10^6 |
| 0.204 ^a | 0.153 | 0.028 | 0.706 | 25.4 | 25 | 1.1×10^6 |
| 0.103 ^a | 0.079 | 0.020 | 0.169 | 8.5 | 8 | 1.0×10^6 |
| 0.0515 ^a | 0.039 | 0.0137 | 0.060 | 4.3 | 4 | 1.6×10^6 |
| 0.0208 ^a | 0.016 | 0.0074 | 0.0084 | 1.1 | 0.8 | 2.0×10^6 |
| 0.0105 ^a | 0.0081 | 0.0048 | 0.0006 | 0.4 | 0.1 | 1.0×10^6 |

^a From ref 11. Amine in equilibrium with 2.95 M NO_3^- and 0.93 M H^+ .

Table III

| Amine concn, M | B | $(\overline{RNO_3})$ monomer, M | D |
|--------------------|-------|-----------------------------------|------|
| 0.346 ^a | 0.318 | 0.044 ^b | 3.27 |
| 0.346 ^a | 0.282 | 0.040 ^b | 2.37 |
| 0.346 ^a | 0.225 | 0.033 | 1.18 |
| 0.346 ^a | 0.175 | 0.029 | 0.59 |
| 0.346 ^a | 0.116 | 0.023 | 0.32 |

^a From ref 11. Amine in equilibrium with 2.72 M NO_3^- and 0.0047 M H^+ . ^b The monomer concentration has been arbitrarily extrapolated from the experimental data of ref 4.

In the experimental conditions of ref 11 the equilibrium nitrate concentration in the aqueous solution is 2.85 ± 0.15 . The aqueous ionic strength, therefore the term (X) in eq 20 and 22, can be considered constant. Although Z is nearly constant under these conditions, it cannot be evaluated since $K_{(i,aq)}$ and F'_i are not known. Consequently, we will not multiply D by Z , with the result that all of the terms of eq 22 are multiplied by the constant term $K_{(n+1,aq)} \cdot (X)^n$ and that the values in Tables I-IV are $Q' =$

$QK_{(n+1,aq)}(X)^n \gamma$. A very rough estimation of Z from eq 21, using the $K_{(i,aq)}$ at 35° of ref 12 and neglecting F'_i , gives $Z = 1.2$.

The data in Tables III and IV refer to D values obtained using the same initial ammonium salt concentration and aqueous uranium concentrations such as to give appreciable loading of the organic phase. The two different sets of data in Tables III and IV refer to different H^+ concentrations.

The D values in Tables I and II obtained at $H^+ 0.01 M$ have been obtained at such conditions as to

Table IV

| Amine concn, M | B | $(\overline{RNO_3})$ monomer, M | D |
|--------------------|-------|-----------------------------------|-------|
| 0.339 ^a | 0.196 | 0.031 | 1.18 |
| 0.339 ^a | 0.165 | 0.029 | 0.775 |
| 0.339 ^a | 0.127 | 0.025 | 0.503 |
| 0.339 ^a | 0.056 | 0.0165 | 0.305 |
| 0.339 ^a | 0.048 | 0.015 | 0.281 |

^a From ref 11. Amine in equilibrium with 2.92 M NO_3^- , 0.940 M H^+ .

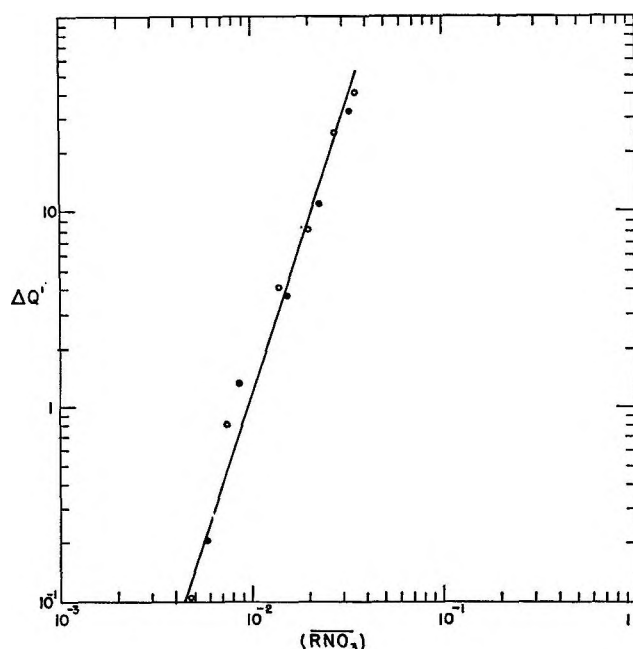


Figure 2. Logarithmic plot of Q' against $(\overline{RNO_3})$. The solid points refer to data of Table I; the empty circles refer to data of Table II.

make negligible both the uranium loading of the organic phase and the extraction of HNO_3 in excess with respect to the stoichiometry of the salt.

The monomer concentrations of the salt corresponding to each amine concentration have been obtained from ref 4 and are reported in Table I.

A plot of Q' vs. $(\overline{RNO_3})$ is in Figure 1. In Figure 2 the logarithmic plot of $\Delta Q'$ vs. $(\overline{RNO_3})$ shows a straight line with slope 3.0. The values of $\Delta Q'$ have been obtained using the same procedure indicated to calculate ΔQ (see previous sections). This result fits well with the presence of the heteropolymer $(\overline{RNO_3})_3(\overline{RUO_2(NO_3)_3})_1$. From eq 22 the presence of such species in the organic phase asks for the independence of D on the metal concentration. The existing data in the literature¹¹ do not give the chance to check this point.

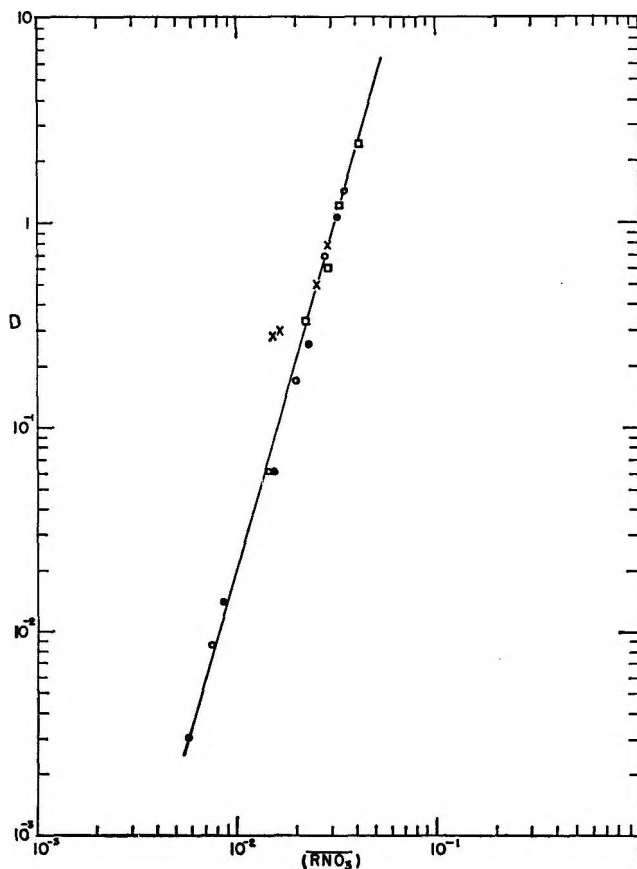


Figure 3. Logarithmic plot of D against $(\overline{RNO_3})$. The solid points refer to data of Table I; the empty circles refer to data of Table II. The squares refer to Table III; the crosses (\times) refer to the data of Table IV.

The existence of the 3:1 heteropolymer is then assumed on the basis of the good fitting of the experimental data with this hypothesis. Equation 22, using Q' at the place of Q , then reduces to

$$Q' = K' + K''(RX)^3 \quad (29)$$

with $K' = K_F(X)^{n\gamma}$ and $K'' = K'K_{(3,1)}$. In Tables I and II the values of Q' and $Q'/(\overline{RNO_3})^3 = K''$ are reported.

If the D values are obtained in such conditions where there is excess HNO_3 in the organic phase and significant uranium loading of the organic phase, it is necessary to know the nature of the salts in the organic phase in order to calculate the concentration of monomer. This information is not available at this time. However, an approximation can be tried. Assuming that the average aggregation number of the free ammonium salt is not affected by the presence of the heteropolymers and HNO_3 - $\overline{RNO_3}$ complexes, the free ammonium salt concentration, B , can be calculated by using the expression

$$B = C_i - C_{\text{HNO}_3} - (C_{\text{U(a)}} + 4C_{\text{U(b)}}) \quad (30)$$

C_i , C_{HNO_3} , $C_{\text{U(a)}}$, and $C_{\text{U(b)}}$ are the initial amine concentration, the excess HNO_3 concentration in the organic phase, the organic uranium concentration due to the monomer, and the organic uranium concentration under form of heteropolymer, respectively.

The calculation of B from eq 30 asks for the knowledge of $C_{\text{U(a)}}$ and $C_{\text{U(b)}}$. The calculation of B can be simplified using an average of 2.5 organic ammonium salt molecules per uranium atom. The value of 2.5 is obtained assuming equal contribution of the monomer and of the heteropolymers to the organic uranium concentration.

$$B = C_i - C_{\text{HNO}_3} - 2.5C_{\text{U}} \quad (31)$$

C_{U} is the total organic uranium concentration in the organic phase. For small uranium concentration it is relatively unimportant how many ammonium salt molecules are bound to U in calculating B .

Values of B are reported in Tables II–IV. From ref 4 the monomer concentration for each B value is obtained, except for the highest B values, and is reported in Tables II–IV.

In Figure 1 the values of D vs. the monomer concentration ($\overline{\text{RNO}_3}$) are reported for the four sets of data of Tables I–IV. All of the points are on the line of slope 3.3 except for the last two points of Table IV. The D values for the highest ammonium salt concentrations are not reported as a consequence of the uncertainty of the monomer values obtained by extrapolation. The slope of 3.3 is consistent with the idea of a monomer–tetramer (with regard to ammonium salt molecules) species in solution. A slope ranging from 1 to 4 is, in fact, expected for these species when the ammonium concentration changes from low to high values. The value 3.3 indicates that we are observing

only a portion of the curve D vs. monomer concentration.

Of course, all of the points on the straight line are satisfied by the same parameters. This means that all four sets of data fit the model of a monomer and a 3:1 heteropolymer in the organic phase. $Q/(\text{RNO}_3)^3 = K''$ values are reported in Table II. K'' values are not calculated in Tables III and IV since there are no K values available at low RNO_3 concentrations.

The two points far from the straight line are obtained at high loading conditions of the organic phase. The assumptions involved in eq 30 could not be satisfied in this condition. This analysis does not exclude the presence of other species that cannot be detected as a consequence of the precision of the distribution data.

From this discussion it seems that the approach here developed is able to carry out a satisfactory explanation of the data. The existence of a mixed tetramer in the organic phase does not disagree with the observation that the ultraviolet spectra show the pattern of trinitratouranyl ion $\text{UO}_2(\text{NO}_3)_3^-$.¹¹ Dipole–dipole interactions are in fact possible in the organic phase.

It must be also pointed out that eq 20 gives a satisfactory explanation for noninteger slope found by different authors in the extraction of uranyl nitrate by amine nitrate.^{12–14} Furthermore, it suggests that the use of a semiempirical equation of the form $D = K(C_i - mC_{\text{U}})^n$ used in the literature^{15,16} must be carefully considered. In fact, this equation does not use the monomer concentrations necessary for the correct interpretation of the distribution process.

(12) F. Baroncelli, G. Scibona, and M. Zifferero, *J. Inorg. Nucl. Chem.*, **24**, 547 (1962).

(13) V. B. Shevchenko, *Zh. Neorgan. Khim.*, **5**, 2354 (1960).

(14) V. M. Vdovenko, *et al.*, *Radiokhimiya*, **3**, 555 (1961).

(15) K. B. Brown, Report CF-61-3141, 1961.

(16) C. F. Coleman, *Nucl. Sci. Eng.*, **17**, 274 (1963).

Dielectric Dispersion of Deoxyribonucleic Acid. II¹

by Shiro Takashima

Electromedical Division, Moore School of Electrical Engineering, University of Pennsylvania, Philadelphia, Pennsylvania (Received July 12, 1965)

Dielectric dispersion of deoxyribonucleic acid (DNA) solution is measured with a high-precision low-frequency bridge between 50 cps and 200 kcps. The measurements are carried out with DNA samples with widely different molecular dimension. It is found that the dielectric increment and the relaxation time of helical DNA are proportional to the square of the length of molecule. The dielectric increment and the relaxation time of coiled DNA are distinctly smaller than the values for helical DNA. This relationship seems to hold for different types of DNA. The measurements of flow birefringence is conducted simultaneously with the dielectric measurement. The rotary relaxation time is compared with the dielectric relaxation time. It is found that the agreement of both relaxation times is fairly good in a low molecular weight region. The disparity, however, becomes pronounced when DNA is larger, and the rotary relaxation time is greater than the dielectric relaxation time by a factor of 20.

Introduction

Dielectric dispersion of DNA was first measured by Allgen, Jungner, and Jungner.² They reached a conclusion, on the basis of their experimental results, that DNA had a permanent dipole in the transverse direction. They also concluded that electric polarization of DNA is caused by the rotation of the molecule around the major axis in its entirety. The dielectric dispersion of DNA was also studied by Jerrard and Simmons.³ These previous measurements are, however, limited to a narrow frequency region and also limited to low molecular weight DNA samples. Recently, Takashima⁴ extended the measurement to a low-frequency region. He measured the dielectric dispersion of various DNA samples with molecular weights ranging from 400,000 to 6,000,000 between 50 cps and 1 Mcps. He observed that DNA had a dielectric dispersion in a lower frequency region than previously observed. He found that the dipole moment and the relaxation time were proportional to the molecular weight of DNA. He concluded from these results that DNA had a dipole moment in the direction of the major instead of the minor axis. The present work is an extension of the previous experiments to provide further evidence for the conclusion described above.

It is known that DNA exhibits a negative flow birefringence. By measuring the extinction angle, we

can calculate the rotary diffusion constant. This is in turn converted into the relaxation time. The conclusion drawn by Allgen and Jungner is based on the fact that the dielectric relaxation time they observed (10^{-7} sec) differs substantially from the rotary relaxation time observed by Edsall⁵ (10^{-3} sec). As mentioned above, Takashima found a dielectric dispersion in a lower frequency region. The relaxation time he obtained is indeed in the range of 1 msec, which indicates that the dielectric relaxation time is close to the rotary relaxation time. In this experiment, measurements of dielectric dispersion and flow birefringence are carried out simultaneously. A more careful comparison of dielectric relaxation time with rotary relaxation time is attempted.

Experimental Section

A Wheatstone bridge designed by Schwan⁶ was used.

(1) This work was supported by National Institutes of Health Grant GM-12083-01.

(2) L. G. Allgen, *Acta Physiol. Scand., Suppl.*, **22**, 76 (1950); G. Jungner, I. Jungner, and L. G. Allgen, *Nature*, **63**, 849 (1949).

(3) H. G. Jerrard and B. A. W. Simmons, *ibid.*, **184**, 1715 (1959).

(4) S. Takashima, *J. Mol. Biol.*, **7**, 455 (1963).

(5) J. T. Edsall, "Proteins, Amino Acids and Peptides," E. J. Cohn and J. T. Edsall, Ed., Reinhold Publishing Corp., New York, N. Y., 1943, p 450.

(6) H. P. Schwan, "Physical Techniques in Biological Research," Vol. 6, Academic Press, Inc., New York, N. Y., 1963, Chapter 6.

Measurements were carried out between 50 cps and 200 kcps. The bridge was designed for measurement with conductive materials and is suitable for DNA solution. The conductance of dilute DNA solution is usually 20 to 50 μ mhos at a concentration of 0.01–0.03%. The magnitude of experimental error in lossy solutions was already discussed in detail by Schwan.⁶

The major source of experimental error with conductive solutions is due to electrode polarization. Two methods are applied to eliminate this effect. (1) The platinum electrodes are very carefully plated with platinum black according to the method developed by Maczuk and Schwan.⁶ This is to increase the surface area of the electrodes. The measured capacity of the solution can be expressed by the following equation,⁶ where C_s is the true capacity, C_p is the elec-

$$C = C_s + 1/[C_p^2 \omega^2 R] \quad (1)$$

trode capacity, ω is the angular frequency, and R is the resistivity of the solution. To make the second term of eq 1 small, either R or C_p must be made large. We cannot make the resistivity of DNA solution very large because the resistivity of water is at most 1 megohm and DNA is a highly charged molecule. Moreover, DNA is unstable at very low ionic strength and one must keep the ionic strength above a certain level. An increase in the electrode capacity is, therefore, a more feasible method of decreasing the second term of the equation. The effect of electrode polarization can still be considerable with conductive solutions, even with a good plating. This gives rise to a difficulty in determining the low-frequency dielectric constant. As will be mentioned later, the dispersion of DNA depends largely on the length of the molecule. The effect of electrode polarization is not serious for small DNA molecules because the dielectric dispersion is in a relatively high frequency region. For large molecules, however, further correction is essential. A dielectric cell was constructed in which the distance of the electrodes was variable. Measurements were repeated twice at two electrode distances, say at 10 and 1 cm. Electrode polarization is independent of the electrode distance and it can be eliminated by using the following equation;⁶ C_s is the true capacity

$$C_s = \left[C_1 - C_2 \left(\frac{R_2}{R_1} \right)_{5kc} \right] / \left[1 - \left(\frac{R_2}{R_1} \right)_{5kc} \right] \quad (2)$$

at 10 cm, C_1 and C_2 are the capacities at electrode distance 10 and 1 cm, respectively, and R_1 and R_2 are the resistivities at those electrode distances, respectively.

The capacity and conductivity of the solution can be measured down to 100 cps with a reasonable accuracy. High molecular weight DNA, however, has an anomalous

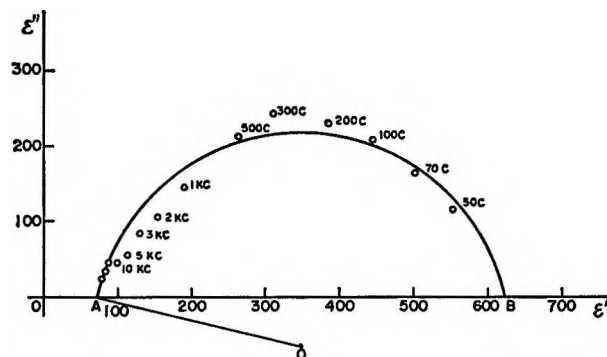


Figure 1. The Cole-Cole plot of salmon sperm DNA. The ordinate is the imaginary part and the abscissa is the real part of dielectric constant. The numbers in the figure are frequencies. A and B gives the high- and low-frequency dielectric constant.

ous dispersion in a very low frequency region. The low-frequency plateau of the dielectric dispersion of these samples seems to appear even below 100 cps. The measurement of capacity of DNA solution becomes much more difficult below 100 cps. One cannot obtain the low-frequency plateau by extrapolating the dispersion curve without considerable arbitrariness. In a case like this, the use of a Cole-Cole plot⁷ is very helpful. As shown in Figure 1, the Cole-Cole plot of DNA is symmetrical. Thus, we can estimate the low-frequency dielectric constant from the intersection of the circle with the abscissa. The value of the low-frequency dielectric constant obtained by this method is much more reliable and less arbitrary. In the present experiment, the low-frequency dielectric constant is always obtained by this method.

The imaginary part of the dielectric constant (dielectric loss ϵ'') is calculated by the formula

$$\epsilon'' = (\kappa - \kappa_0)/2\pi f \epsilon_\gamma \quad (3)$$

κ_0 is the low-frequency conductivity in micromhos and ϵ_γ is the absolute value of dielectric constant of vacuum ($1/36 \pi \times 10^{11}$). The dispersion of conductivity is shown in Figure 2. It is evident from eq 3 that a small error in the conductivity measurement can cause a considerable error in the dielectric loss at low frequency. The measurement of conductivity is performed with the error of $\pm 0.001 \mu$ mho. Although the temperature of the solution is controlled by circulating the thermostated water, the fluctuation of conductivity cannot be prevented. The correction method for the drift of conductivity is given in the previous publication.⁸ The random error of the conductivity

(7) K. S. Cole and R. H. Cole, *J. Chem. Phys.*, **9**, 341 (1941).

(8) J. Maczuk, Intramural Report of University of Pennsylvania, 1957. This method is described also in ref 4.

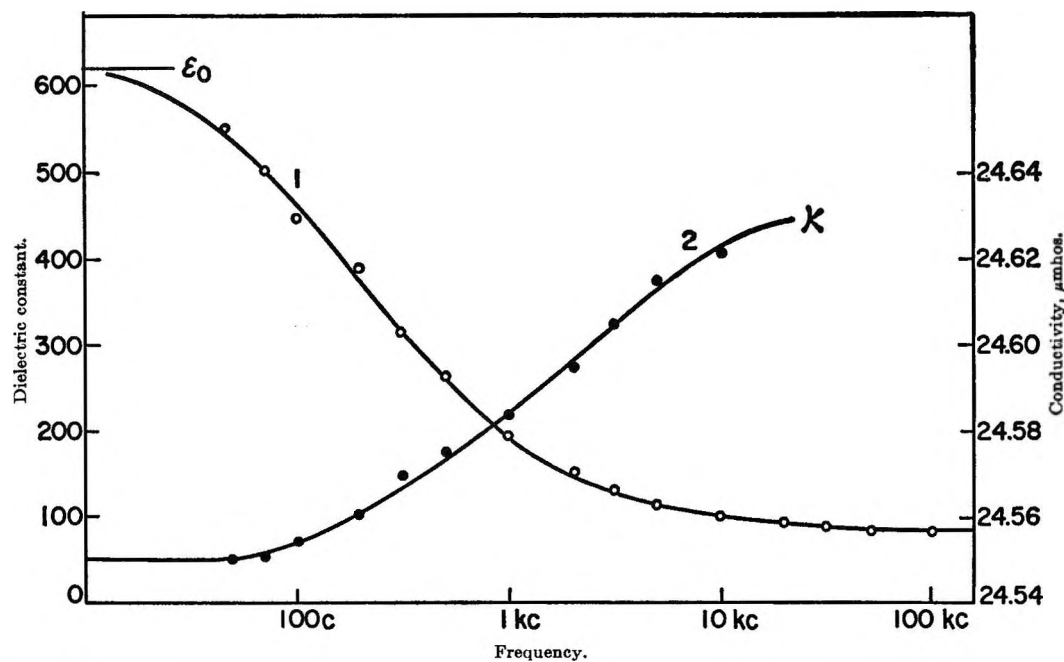


Figure 2. Dielectric dispersion of salmon sperm DNA: curve 1, dielectric constant; curve 2, conductivity. The concentration is 0.01%. The horizontal line designated ϵ_0 indicates the low-frequency dielectric constant obtained from Cole-Cole plot.

reading is sufficiently small for the determination of the dielectric loss.

The flow birefringence and the extinction angle of DNA solution are measured with a Rao birefringence apparatus Model-B-22. The extinction angle χ is related to a parameter α^9 in the equation by Boeder¹⁰ and that by Peterlin and Stuart.¹¹

$$\chi = \frac{1}{2} \tan^{-1} \frac{6}{\alpha} = \frac{\pi}{4} - \frac{\alpha}{12} [1 - f(\alpha, a, b)] \quad (4)$$

The value of α is tabulated in the paper by Edsall, *et al.*,¹² for various axial ratios. The rotary diffusion constant is related to the parameter α by eq 5, where β

$$\alpha = \beta/\theta \quad (5)$$

is the velocity gradient. The rotary relaxation time is calculated from the rotary diffusion constant by eq 6. The length of DNA is calculated by using the

$$\tau = \theta/2 \quad (6)$$

Perrin equation¹³

$$\theta_b = \frac{3kT}{16\pi\eta a^3} \left(2 \ln \frac{2a}{b} - 1 \right) \quad (7)$$

where θ_b is the rotary diffusion constant around the minor axis, η is the viscosity of the solvent in poises, a and b are the semimajor and semiminor axes in centimeters. The axis a is not necessarily the fully stretched length of DNA and the b is not necessarily the radius

of double helix. Since the Perrin equation cannot be solved analytically, a computer IBM 1710 is used to obtain the solution for the length of DNA molecule.¹⁴

Calf thymus and salmon sperm DNA were used in this experiment. The length of calf thymus DNA ranged from 10,500 to 1500 A and that of salmon sperm DNA was from 7400 to 1300 A. A 20-kc sonic oscillation was applied to produce smaller DNA samples. Viscosity and rotary diffusion constant were measured each time. Viscosity was measured with a Rao couette-type viscometer with varying shearing stress. The viscosity was obtained by extrapolating the consistency curve to zero shear.

DNA was dissolved in freshly deionized water. The pH of the water was carefully examined each time. Distilled water becomes acidic on storage. Since DNA is unstable at low ionic strength, the pH of the water must be maintained close to neutral to avoid the denaturation. If DNA was dissolved in acidic water, it did not exhibit flow birefringence nor large dielectric increment. This indicates denaturation,

(9) This parameter should not be confused with the Cole-Cole parameter, α .

(10) P. Boeder, *Z. Physik*, **75**, 273 (1932).

(11) A. Peterlin and H. A. Stuart, *ibid.*, **112**, 1, 129 (1939).

(12) H. A. Scheraga, J. T. Edsall, and J. O. Gadd, *J. Chem. Phys.*, **19**, 1101 (1951).

(13) F. Perrin, *J. Phys. Radium*, **7**, 5, 497 (1934).

(14) The author is grateful to Mr. B. Pennock for his help for the programming.

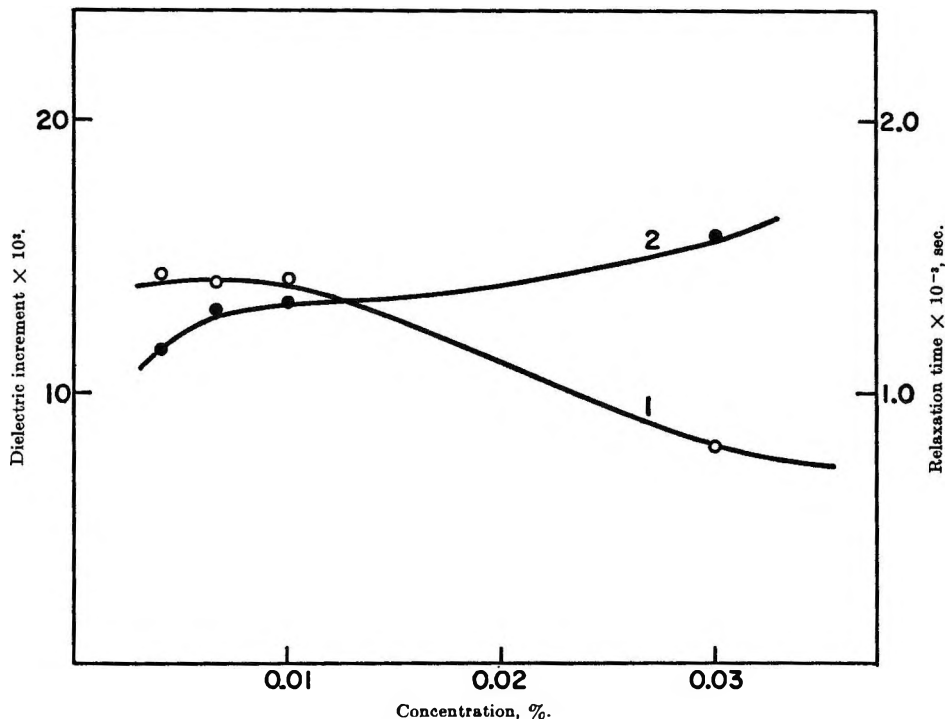


Figure 3. Dependence of specific dielectric increment and relaxation time on concentration, grams per 100 ml. Specific dielectric increment is $\Delta\epsilon$ per gram per 100 ml: curve 1, dielectric increment; curve 2, relaxation time.

probably strand separation. It was found that calf thymus DNA is more stable than salmon sperm DNA. The concentration of DNA was 0.01% unless otherwise stated.

Results

(a) *Native DNA.* The dielectric dispersion of salmon sperm DNA is shown in Figure 2. The dielectric constant of DNA solution rises far above the dielectric constant of water and is still increasing at 50 cps. Thus, it is difficult to estimate the low-frequency dielectric constant from the dispersion curve with a reasonable accuracy. As explained in the previous section, the use of the Cole-Cole plot is very helpful for obtaining the low- and high-frequency dielectric constant. The Cole-Cole plot of DNA solution is shown in Figure 1. The low and high dielectric constant as obtained from this plot are 620 and 80, respectively. The horizontal line in Figure 2 is the low-frequency dielectric constant obtained by the Cole-Cole plot. The value thus obtained seems to be in reasonable agreement with the value obtained by the extrapolation of the dispersion curve. The dispersion of conductivity is shown in Figure 2. The increment of the conductivity is about 0.08 μmho . This indicates that the measurement of conductivity dispersion is much more difficult than that of dielectric constant. The distribution parameter is calculated

from the angle OAB ($\alpha^\tau/2$). Here α is the Cole-Cole distribution parameter. It was observed that the dielectric increment depended on the concentration of DNA.⁴ Schwarz and Eigen¹⁵ also observed, in the study of orienting field effect, that the polarizability and the orientational relaxation time of DNA were dependent on the solute concentration. Figure 3 shows the dependence of specific increment and the dielectric relaxation time on concentration. One observes a considerable dependence of dielectric increment on concentration in the high concentration region; however, it becomes rather constant below 0.01%. Relaxation time also changes with concentration, particularly below 0.002%. From this figure, it is obvious that 0.01% seems to be the best concentration to carry out the dielectric measurement. The subsequent measurements were carried out at 0.01% unless otherwise stated.

Figure 4 illustrates the dispersion curves of salmon sperm DNA with various lengths. It is found that the dielectric increment as well as the relaxation time decrease with the decrease of the length. Particularly, the decrease in the dielectric increment is pronounced. Curve 1 in Figure 5 shows the relationship between the length of the molecule and the dielectric increment.

(15) M. Eigen and G. Schwarz, "Electrolytes," B. Pesce, Ed., Pergamon Press Ltd., London, 1962.

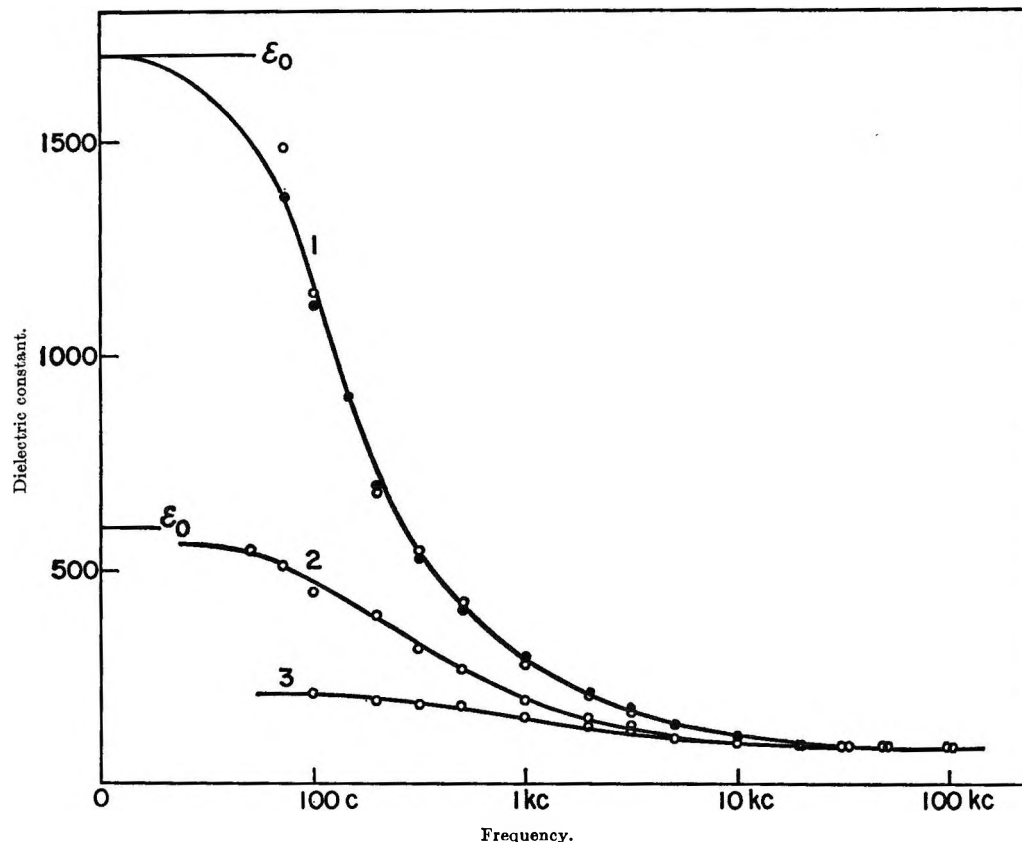


Figure 4. Dielectric dispersion of salmon sperm DNA. The lengths of DNA samples are 7400 (curve 1), 5600 (curve 2), and 1300 A (curve 3). The concentration is 0.01%. Curve 1 shows the result of two measurements.

The following relationship between the length and the dielectric increment is obtained

$$\Delta\epsilon = 0.29 \times 10^{-5} \times L^2 = AL^2 \quad (8)$$

The relaxation time is calculated by using

$$\tau = 1/2\pi f_c \quad (9)$$

where τ is the relaxation time and f_c is the critical frequency. The relationship between the relaxation time and the length is shown in Figure 6. The relationship is expressed by the empirical formula

$$\tau = 1.6 \times 10^{-5} \times L^2 = BL^2 \quad (10)$$

Curve 2 in Figure 5 illustrates the relationship between the dielectric increment of calf thymus DNA and its length. Curve 2 in Figure 6 illustrates the size dependence of relaxation time of calf thymus DNA. The relationships are very much the same as that of salmon sperm DNA. The dielectric increment and the relaxation time of this DNA can be expressed by using eq 8 and 10.

(b) *Denatured DNA.* Figure 7 illustrates the dielectric dispersion of heat-denatured DNA. It is

known that DNA undergoes a transition from a double helical configuration to a single-strand random-coil configuration. The transition is caused by heating or by an extreme pH. The dispersion curve shown here represents a dielectric dispersion of heat-denatured coil-form DNA. The denaturation is confirmed by the decrease of viscosity and by the disappearance of flow birefringence. It must be noted that the scale of the ordinate in Figure 7 is greatly enlarged. Although the magnitude of dielectric increment is much smaller than that of helical DNA, one can still observe a considerable increment and its dependency on frequency. Undoubtedly, the dielectric dispersion of the coil form exists in a higher frequency region than that of the helical form.

(c) *Comparison between the Rotary and Dielectric Relaxation Time.* The conclusion drawn by Allgen and Jungner was based on the fact that the dielectric relaxation time they observed was widely different from the rotary relaxation time. As was mentioned, the dielectric relaxation time observed in this experiment is considerably larger than those observed by Allgen and Jungner. A comparison of dielectric relaxa-

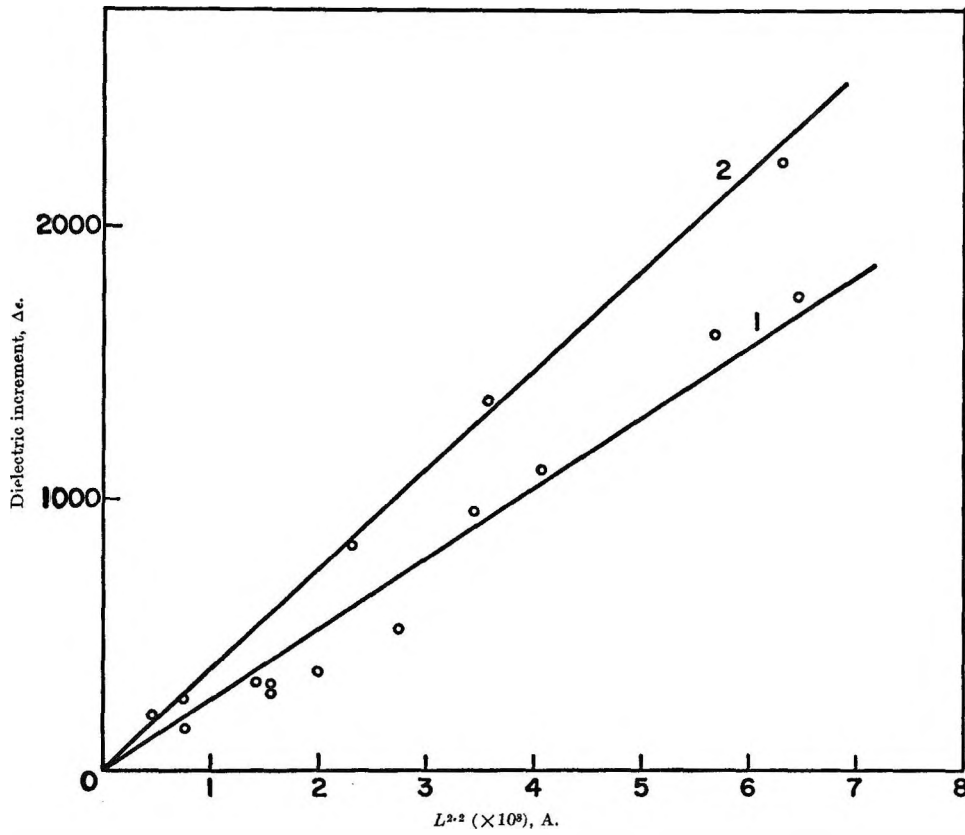


Figure 5. The plot of dielectric increment against the length of DNA: curve 1, salmon sperm DNA; curve 2, calf thymus DNA. The ordinate is dielectric increment as measured and the abscissa is the 2.2 power of the length in angstroms. Concentration is 0.01%.

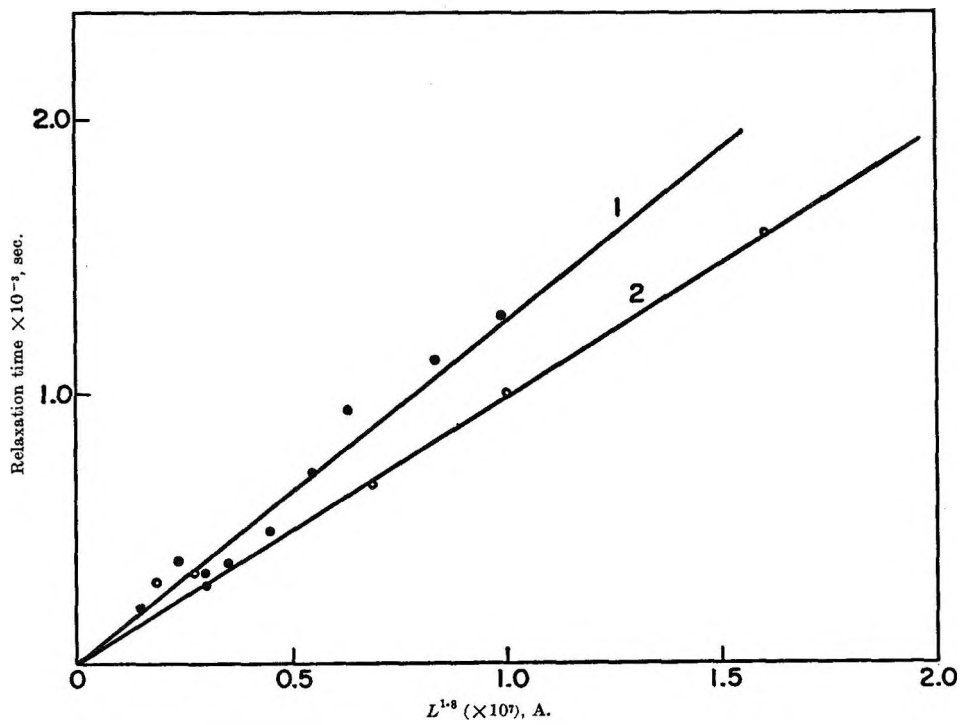


Figure 6. The plot of dielectric relaxation time against the length of DNA: curve 1, salmon sperm DNA; curve 2, calf thymus DNA. The abscissa is the 1.8 power of the length in angstroms.

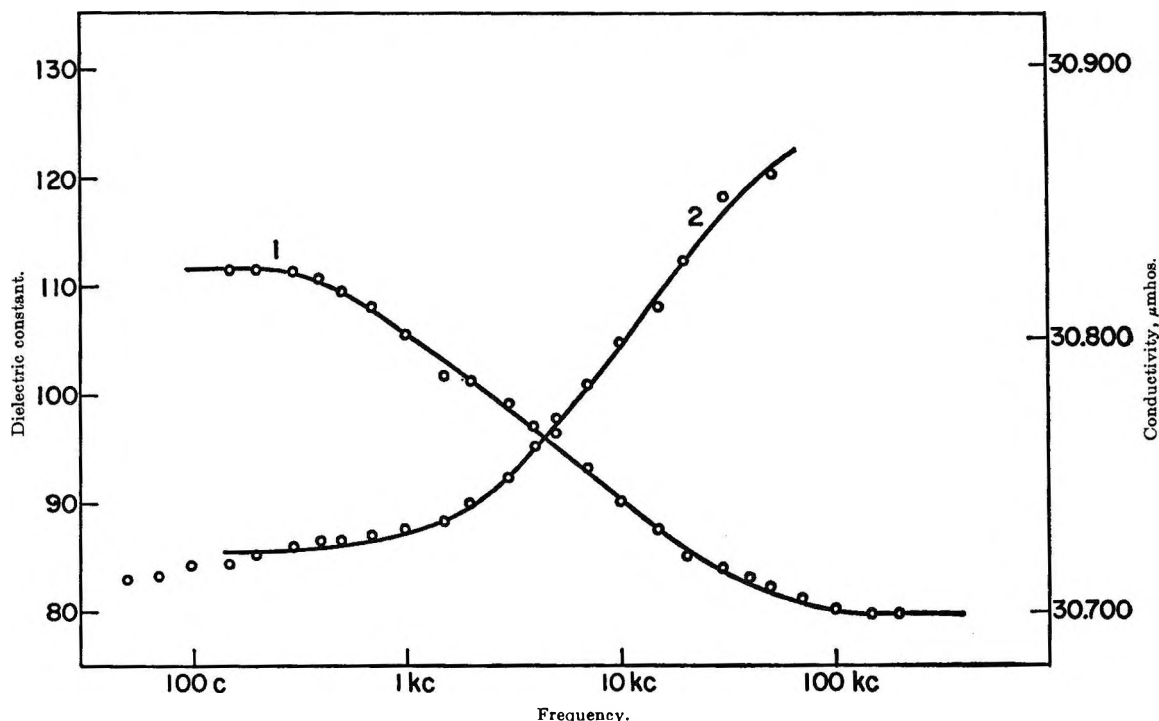


Figure 7. Dielectric dispersion of heat-denatured DNA: curve 1, dielectric constant; curve 2, conductivity in micromhos. Concentration is 0.03%.

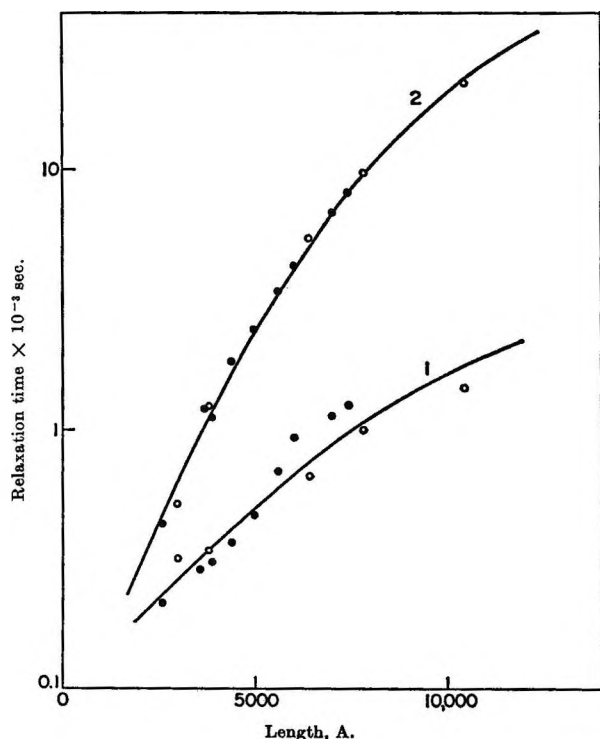


Figure 8. Dielectric relaxation time and rotary relaxation time of DNA plotted against the length of the DNA molecule; curve 1, dielectric relaxation time; curve 2, rotary relaxation time: \circ , salmon sperm DNA; \bullet , calf thymus DNA. The ordinate is in logarithmic scale.

tion time and the rotary relaxation time is attempted. The rotary and the dielectric relaxation time are measured simultaneously with the same DNA sample. The results obtained with calf thymus DNA are tabulated in Table I. To show the relationship more clearly, those relaxation times are plotted in Figure 8 for both DNA's. In both cases dielectric and rotary relaxation

Table I: Comparison between Rotary Diffusion and Dielectric Relaxation

| Length, A | Rotary relaxation time, sec $\times 10^3$ | Dielectric relaxation time, sec $\times 10^3$ |
|-----------|---|---|
| 10,400 | 21.2 | 1.57 |
| 7,800 | 9.6 | 1.0 |
| 6,400 | 5.36 | 0.66 |
| 3,800 | 1.21 | 0.33 |
| 3,000 | 0.52 | 0.31 |

times are close to each other in the low molecular weight region. This result is in contrast with the observation by Allgen and Jungner. They observed a 1000-fold difference between these relaxation times in the same molecular weight range. Undoubtedly, the discrepancy between the present results and theirs is

beyond the experimental error. The deviation of both relaxation times becomes more pronounced with increasing molecular weight. This is not really surprising because the rotary diffusion constant is proportional to the cube of the length and dielectric relaxation time is proportional to the square of the length. It was originally expected that the curves would be either far apart from each other or cross each other at some point. This expectation is because of the different size dependency of both relaxation times. Although the rotary and dielectric relaxation times are different by a factor of about 20 or more at the molecular weight of 5,000,000, this discrepancy is still much smaller than the difference observed previously by Allgen and Jungner.

Discussion

As has been mentioned, there are considerable discrepancies between our observations and those by previous workers. First of all, the magnitude of dipole moment and relaxation time is widely different. The difference is undoubtedly beyond the experimental error. Above all, it was observed¹ that the relaxation time of their DNA was around 10^{-7} sec and far smaller than the rotary relaxation time observed by Edsall, *et al.*⁵ We observe that the dielectric relaxation time is about 1–2 msec and also that the dielectric relaxation time and the rotary relaxation are not drastically different for the DNA samples used in this experiment. Considering the facts mentioned above, we have good reasons to believe that there is a missing link between our measurements and theirs. Recently, O'Konski¹⁶ reported that DNA had two dielectric dispersions, the one in a low-frequency region and the other in the megacycle region. The magnitude of the latter dispersion is smaller than the former. Apparently, Allgen and Jungner observed only the second dispersion and our conclusion is based on the observation on the low-frequency dispersion alone. According to the results presented above, the magnitude of the second dispersion is much smaller than the first one and seems to be less significant. The discussion concerning the second dispersion, therefore, will be presented elsewhere.

It is clear from Figure 8 that the dielectric relaxation time does not quite agree with the rotational relaxation time. Both quantities are similar only in the low molecular weight region, but the disparity is more and more pronounced as the molecular weight increases. Eigen and Schwarz¹⁵ state that in an orienting field (field strength above 1000 v/cm), an induced dipole is created and the whole molecule orients itself in the direction of the field. They found that the relaxation time of

DNA in an orienting field is approximately 10 msec. The rotational relaxation time in a flow was found to be about 10 msec with a slightly larger DNA in this experiment. Indeed, the value they found is of the same order of magnitude as that of rotary relaxation time in a mechanical flow. This strongly indicates that the orienting field effect is rather more similar to a rotary diffusion process in a mechanical flow than to dielectric relaxation (field strength about 0.5 v/cm). The dielectric relaxation time is smaller than the others and, moreover, is proportional to the square of the length. It is, therefore, unlikely that dielectric relaxation is similar to either mechanical orientation or orienting field effect. There is some indication that dielectric relaxation is similar to mechanical orientation in the low molecular weight region. However, the situation seems to be more complicated in a larger molecule.

Pollack¹⁷ calculated the dielectric relaxation time on the basis of the Maxwell-Wagner theory¹⁸ for an ellipsoid. He found that the relaxation time in the longitudinal direction is proportional to the square of the length, which is in qualitative agreement with the present results. His theory is, however, restricted to special cases because of the assumptions he used.

Recently, Pennock and Takashima¹⁹ extended the counterion polarization theory by Schwarz²⁰ to cylindrical molecules with a parallel external field. They obtained the following equations for dielectric increment and relaxation time

$$\Delta\epsilon = \frac{p}{1+p} \frac{e^2\sigma a^2}{kT b} \quad (11)$$

$$\tau = \frac{a^2 + b^2}{2ukT} \quad (12)$$

where p is the fraction of DNA, e is the electronic charge, σ is the charge density per square centimeter, a and b are the major and minor axes, and u in eq 12 is the mobility of counterions. According to eq 11, the increment is proportional to a^2/b . Since b is almost independent of the molecular weight, we can assume, without serious error, that b is a constant. Therefore, we can conclude that $\Delta\epsilon$ is proportional to a^2 , the square

(16) N. C. Stellwagen, M. Shirai, and C. T. O'Konski, Abstracts, Annual Biophysical Society Meeting, San Francisco, Calif., Feb 24, 1965.

(17) M. Pollack, *J. Chem. Phys.*, **43**, 3, 908 (1965).

(18) K. W. Wagner, *Arch. Electrotech.*, **3**, 83 (1914).

(19) B. E. Pennock and S. Takashima, to be published.

(20) G. Schwarz, *J. Phys. Chem.*, **66**, 2636 (1962).

of the major axis. Likewise, the relaxation time is proportional to $a^2 + b^2$. Since b is negligibly small compared with a , we can conclude that the relaxation time also is proportional to the square of the major axis. Thus the counterion polarization theory seems to ex-

plain the dielectric relaxation of DNA. This theory will be discussed in a forthcoming paper.

Acknowledgment. The author is indebted to Professor H. P. Schwan for his continuing interest and valuable advice.

The Concept of Length in the Thermodynamics of Elastic Bodies

by Hans J. Kuhn

Institute of Physical Chemistry, University of Basel, Basel, Switzerland (Received July 20, 1965)

Several experimental findings related to the thermodynamic behavior of elastic bodies call for a new basic principle: the postulate of inaccessibility of states under isometric conditions. It follows from this postulate that functions of state of elastic bodies can only be calculated if changes of length are measured on a new scale. This physical scale of length is a universal function of the force only. Physical length changes, *i.e.*, length changes measured on the physical scale of length, are constructed in analogy to the construction of entropy by Carathéodory. Variables of state of an elastic body are physical length, temperature, mole numbers, and exchange numbers. Entropy is a function of state of these variables. Internal energy, however, is a mere definition and is not a function of state. It is shown that, as a consequence of the concept of physical length, neither chemical nor thermal energy can be completely converted into useful mechanical work.

1. Introduction

A state of a gas or a liquid is characterized by a homogeneous pressure within the sample, and the shape of the gas or the liquid does not influence the properties of such samples. Tensorial force components which depend on the shape of the solid determine the state of a solid which is described with reference to a standard state. The differences between gases or liquids and solids are an idealization which may be nullified in reality.

Ordinary thermodynamics is founded on gases or liquids.¹ The shape of a solid, especially the shape of the body in the state of reference, is a quality at random. One has to ask if this random shape of the reference state has consequences for the future states or if it affects only the reference state. In this paper is presented evidence that the present state and all future

states of each elastic system are linked to the random shape of the initial state, a fact which cannot be circumvented by any approximation.

2. Mathematics

A system is defined by a set of variables: x, y_1, \dots, y_n or z_1, \dots, z_n .

(i) A Pfaffian dR is integrable

$$dR = R_x dx + \sum_{j=1}^n R_j dy_j = \varphi(x, y_j) d\rho \quad (2.1)$$

i.e., integrating denominators φ and perfect differentials ρ exist, if R_x and R_j are finite and continuous functions of the variables and if in any vicinity of a point of the system there are other points which are not accessible

(1) C. Carathéodory, *Math. Ann.*, **67**, 355 (1909).

from the initial point on curves which are solutions of the equation $dR = 0$.^{1,2}

(ii) (a) Two independent systems shall be additive with respect to dR . (b) A contacting variable shall exist for the systems in series; *i.e.*, a variable (x in (2.1)) can have at the same time the same value for each single system and for the systems in series; (c) R_x and R_x^{-1} in (2.1) shall not be identically equal to zero. Under these assumptions one can construct integrating denominators which are only functions of the contacting variable^{1,2}

$$dR = \phi(x)d\rho^* \left[\frac{\partial\phi}{\partial y_j} = 0 \text{ for } j = 1, \dots, n \right] \quad (2.2)$$

(iii) The line integral over dR for a system which satisfies (i) and (ii) is, according to Stoke's theorem, given by

$$\oint dR = -\sum_{j=1}^n \iint \frac{1}{\phi} \frac{\partial\phi}{\partial x} R_j dx dy_j \quad (2.3)$$

(iv) A differential form $d\pi = \sum_{j=1}^n (a_j - b_j)\beta_j dz_j$ [$a_j = a_j(z_k)$ and $\beta_j = \beta_j(z_k)$ are functions of the variables z_k and the b_j are parameters] yields for $d\pi = 0$ in the limit $a_j \rightarrow b_j$ the relations

$$\beta_j \frac{\partial a_j}{\partial z_k} = \beta_k \frac{\partial a_k}{\partial z_j} \quad (2.4)$$

3. The Postulate of Isometric Inaccessibility

(i) To overcome difficulties in the physical interpretation of tensions and deformation tensors, a primitive elastic system (PES) is discussed in this paper. A PES is a parallelepiped which consists of one phase and which can only be deformed by changes of its variables. A PES has the characteristics of a solid.

(ii) Variables of a PES are (a) the gas temperature T , (b) the mole number N_α ($\alpha = 1, \dots, A$) of the chemical components, (c) the force f which acts normally to two opposite faces of the parallelepiped.

A PES exhibits a mechanical relaxation: in general, an elongation is observed if temperature, mole numbers, and force are constant. In the case of swollen macromolecular networks this pure mechanical relaxation may be attributed to a redistribution of netpoints within the gel. This diffusion is often controlled by the reaction rate of the cross-links with the gel matrix. There may exist catalysts and inhibitors for such a cross-linking reaction. Under the action of inhibitors the gel is in a blocked equilibrium, and the pure mechanical relaxation is approximated by a set of blocked equilibria. The technique of isotopic tracers allows for a determination of the exchange number between

two blocked equilibria. Although the exchange number of a PES may be difficult to detect, it is always possible to measure the exchange of certain molecules with respect to an ordered structure of any solid.

The different states of polymeric systems for different exchange numbers have been described by statistical models.^{3,4} According to these models it is necessary to know the pathway by which a gel is brought to mechanical equilibrium. James and Guth³ and Green and Tobolsky⁴ have generalized the earlier calculations⁵ of the retractive force by observing that the distributions of the different netpoints in their native states determine the elastic moduli. This view is generally accepted today.⁶

(d) A further variable of a PES is the exchange number m_β ($\beta = 1, \dots, B$).

(iii) Under isometric conditions the length L of a PES, *i.e.*, the distance between the marked faces of the hexahedron, is constant

$$dL = L_f df + L_T dT + \sum_{\alpha=1}^A L_{N,\alpha} dN_\alpha + \sum_{\beta=1}^B L_{m,\beta} dm_\beta = 0 \quad (3.1)$$

The functions L_j (for $j = f, T, N_\alpha, m_\alpha$) are determinable from experiment. The solid characteristics of a PES implies that L_f and L_f^{-1} are not identically equal to zero.

(iv) Length changes are not perfect differentials. Consider isothermic processes at constrained mole numbers on an annealed system. In a plane of force and one exchange number, the point b (Figure 1) may be reached from point a *via* two different pathways. On path a-c (Figure 1) the unloaded system endures a change of the exchange number Δm . On this path a perfectly annealed sample shows no change in length. On paths c-b and a-d an annealed system endures, therefore, the same increase in length for the same load. On path d-b (Figure 1) the system flows. The length in b after the path a-d-b is greater than the length

(2) M. Born, *Physik. Z.*, **22**, 218, 249, 282 (1921); "Natural Philosophy of Cause and Chance," Oxford University Press, London, 1949, and Dover Publications, New York, N. Y., 1964; H. A. Buchdahl, *Am. J. Phys.*, **17**, 41, 44, 212 (1949); **22**, 182 (1954); P. T. Landsberg, "Thermodynamics," Interscience Publishers, Inc., New York, N. Y., 1961; J. F. Lay, "Thermodynamics," C. E. Merriell, Columbus, Ohio, 1963; R. Giles, "Mathematical Foundations of Thermodynamics," Pergamon Press Ltd., Oxford, 1964.

(3) H. M. James and F. Guth, *J. Chem. Phys.*, **11**, 455 (1943); **15**, 669 (1947); **21**, 1039 (1953).

(4) M. S. Green and A. V. Tobolsky, *ibid.*, **14**, 806 (1946).

(5) E. Wöhlisch, *Verh. Phys. Med. Ges. Würzb. N. F.*, **51**, 53 (1926); K. H. Meyer, *Biochem. Z.*, **208**, 23 (1929); W. Kuhn, *Kolloid-Z.*, **68**, 2 (1934); E. Guth and H. Mark, *Monatsh.*, **65**, 93 (1935).

(6) See, for instance, A. J. Stavermann, "Handbuch der Physik," Vol. XIII, S. Flügge, Ed., Springer-Verlag, Berlin, 1962, p 399.

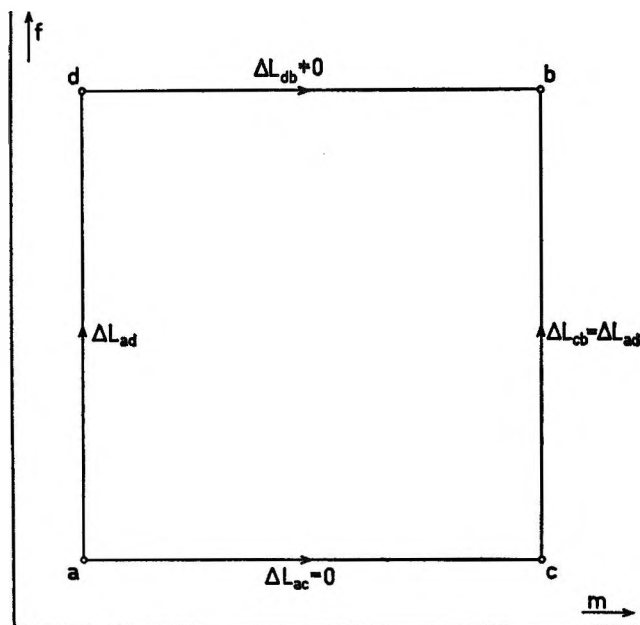


Figure 1. Changes of length in a plane of force f and exchange number m .

after the path a-c-b; the length is not a function of state.

(v) A general physical property of elastic systems is as follows. In any vicinity of an initial point P_0 of a PES there exist other points P_{0-1} which are not accessible from the initial point on isometric curves $dL = 0$. This principle of isometric inaccessibility implies that a force $f > 0$ which acts on a PES in a set of blocked equilibria can, at constant temperature and constant mole numbers, not increase.

(vi) The length changes of two PES in series are additive.

(vii) The force which acts at the same time on two or more contacting PES in series is, according to Archimedes, a contacting variable. Relating 3(iii), 3(v)-3(vii) to 2(i) and 2(ii), one obtains

$$dL = \chi(f)d\Lambda \quad (3.2)$$

The modulus $\chi(f)$ in (3.2) does not depend on either the temperature, the mole number, or the exchange numbers, but is a universal function of the force. The modulus χ cannot be a constant [3(iv)], but rather defines a scale for a function of state, the physical length Λ . The difference between the empirical length L and the physical length Λ can be discussed easily. Consider a system which is, at constrained exchange numbers, subjected to cyclic variations of the force and of one mole number, N , via an isothermal pathway. From (2.3) and (3.2) one obtains for the increase in length ΔL during such a cycle

$$\Delta L = \oint dL = -\iint \frac{\chi'}{\chi} L_N dNdf \quad (3.3)$$

Because ΔL and L_N (the increase in length per mole) are directly observed, it is possible to obtain the derivative of $\ln \chi$ from experiments.

4. Thermodynamics

The physical length is a function of state, if temperature, force, mole numbers, and exchange numbers are chosen as independent variables. As another set of variables, we can also use the temperature, the physical length, the mole numbers, and the exchange numbers. These variables generate another function of state, the entropy. The entropy, S , can be constructed from an empirical entropy⁷ or from the postulate of Lord Kelvin or from the equivalent⁸ postulate of Carathéodory.^{1,2} The heat absorbed during a quasi-static process is related to the entropy

$$dQ' = TdS \quad (4.1)$$

The change in the internal energy, dE , is defined as the sum of the mechanical and chemical work supplied to the system and the heat absorbed by the system. If the increase in length, dL , is expressed in terms of the change in physical length, $d\Lambda$, one obtains for the increase in internal energy a modified fundamental relation of Gibbs

$$dE = TdS + f\chi(f)d\Lambda + \sum_{\alpha=1}^A \mu_{\alpha} dN_{\alpha} \quad (4.2)$$

In (4.2) one has to observe that quasi-static changes of the exchange numbers are effected without chemical work and that the internal energy is not a function of state. The force f in (4.2) is in general a function of the exchange number; i.e., $\partial f/\partial m = \partial^2 E/\partial m \partial f$ is not identically equal to zero. However, according to (4.2), $\partial E/\partial m$ and, therefore, $\partial^2 E/\partial f \partial m$ are identically equal to zero.

Since the internal energy of a PES is not a function of state, no Maxwell relations between the coupling coefficients T , $f\chi(f)$, and μ_{α} , of the internal energy can exist. In the following thermodynamic discussion the exchange numbers are constrained and chemical reactions are excluded. In thermodynamics the reaction of a system to changes in the surroundings, i.e., mechanical or chemical reservoirs and heat baths

(7) H. Jung, Dissertation, Aachen, 1957; H. A. Buchdahl, *Z. Physik*, **152**, 425 (1958); G. Falk and H. Jung, "Handbuch der Physik," Vol. III, Part 2, S. Flügge, Ed., Springer-Verlag, Berlin, 1959, p 119.

(8) T. Ehrenfest-Afanassjewa, *Z. Physik*, **33**, 933 (1925); "Die Grundlagen der Thermodynamik," E. J. Brill, Leiden, 1956; B. Crawford and I. Oppenheim, *J. Chem. Phys.*, **34**, 1621 (1961); P. T. Landsberg, *Nature*, **201**, 485 (1964); U. M. Titula and N. G. van Kampen, *Physica*, **31**, 1029 (1965).

(subscript R in (4.3)), must be discussed for energetically isolated systems. The conditions for energetic isolation are expressed by the relations

$$\begin{aligned} dE_R &= -dE & dL_R &= -\kappa(f)d\Lambda \\ dS_R &\geq -dS & dN_{\alpha,R} &= -dN_\alpha \end{aligned} \quad (4.3)$$

From the fundamental relation (4.2) for system and reservoirs and from the relations of (4.3) one obtains

$$0 \geq d\pi = (f - f_R)\kappa d\Lambda + (T - T_R)dS + \sum_{\alpha=1}^A (\mu_\alpha - \mu_{\alpha,R})dN_\alpha \quad (4.4)$$

The independent variables of the differential form (4.4) are the variables of the system (physical length, Λ , entropy, S , mole numbers, N_α). In (4.4), force, f_R , temperature, T_R , and chemical potential, $\mu_{\alpha,R}$, of the reservoirs are parameters. For an external equilibrium between system and reservoirs, the total entropy must attain its maximal value, and the differential form must vanish. In that case, force, temperature, and chemical potentials of system and reservoirs are equal. Theorem 2(iv) provides, therefore, in cases of external equilibrium, linkage relations between two pairs of conjugated variables. For the discussion of experimental results it may be easier to choose force, temperature, and mole numbers of the system as independent variables. If from the equations of state, temperature, $T = T(\Lambda, S, N_\alpha)$, and force, $f = f(\Lambda, S, N_\alpha)$, are inserted in the differential form (4.4), one easily obtains with (2.6) linkage relations which relate conjugated mechanical quantities with conjugated chemical (4.5) or conjugated thermal quantities (4.6)

$$-\kappa(f) \left(\frac{\partial \Lambda}{\partial N_\alpha} \right)_{f,T,N_{\alpha'}} = \left(\frac{\partial \mu_\alpha}{\partial f} \right)_{T,N_\alpha} \quad (4.5)$$

$$\kappa(f) \left(\frac{\partial \Lambda}{\partial T} \right)_{f,N_\alpha} = \left(\frac{\partial S}{\partial f} \right)_{T,N_\alpha} \quad (4.6)$$

A comparison of (3.1) and (3.2) with (4.5) yields immediately

$$-L_{N,\alpha} = \left(\frac{\partial \mu_\alpha}{\partial f} \right)_{T,N_\alpha} \quad (4.7)$$

Equations from (4.7) are teinochemical ($\tau\epsilon\iota\nu\epsilon\iota\nu =$ to elongate, to stretch) relations.⁹ They are special cases, for a PES, of the relations which Gibbs^{10,11} has deduced on the basis of Maxwell relations between deformation and concentration and between chemical potential and tension. Linkage relations, such as (4.7), were experimentally tested on synthetic systems¹² and on models of natural contractile systems.¹³

Until the present time, however, all deductions of linkage relations between conjugated mechanical and chemical quantities have incorrectly assumed that internal energy is a function of state. However, the increase a system endures on a closed pathway, during which the system and reservoirs are isolated and during which the exchange numbers are constrained, is expressed, with Stoke's theorem, according to (4.2), (4.5), and (4.6)

$$\oint dE = - \left[\iint f \frac{f'}{\kappa} dT dS + \sum_{\alpha=1}^A \iint f \frac{f'}{\kappa} d\mu_\alpha dN_\alpha \right] \quad (4.8)$$

According to (4.4) a sum of independent addends can never be positive. We conclude from this fact that the mechanical work supplied to the reservoirs $dW_R = -f_R \kappa(f) d\Lambda$ is never greater than the mechanical work $-dW = f \kappa(f) d\Lambda$ extracted from the system

$$dW_R \leq -dW = -dE + T dS + \sum_{\alpha=1}^A \mu_\alpha dN_\alpha \quad (4.9)$$

From (4.8) and (4.9), one gets for the mechanical work supplied to the reservoirs during each cycle which a system with constrained exchange numbers endures

$$\oint dW_R \leq \iint \left(1 + \frac{f'}{\kappa} \right) dT dS + \iint \left(1 + \frac{f'}{\kappa} \right) d\mu_\alpha dN_\alpha \quad (4.10)$$

This relation shows that it is never possible, during cyclic processes, to store completely the chemical energy, $\iint d\mu_\alpha dN_\alpha$, or the thermal work, $\iint dT dS$, which is at the disposal of a PES, as mechanical energy into reservoirs.

The factor $1 + f'/\kappa$ in (4.10) is a quantity which cannot be discussed by thermodynamic analysis, but it must be ascertained by experiment. It is assumed that f'/κ is never positive. Under this intuitive assumption, it would never be possible to achieve a better efficiency of a heat converter than the well-known Carnot machine driven by a gas or liquid. However, the case $f'/\kappa > 0$ is possible on thermo-

(9) W. Kuhn, H. J. Kuhn, G. Ebner, and D. H. Walters, *Z. Elektrochem.*, **64**, 658 (1960).

(10) J. W. Gibbs, "The Scientific Papers," Vol. I, Dover Publications, New York, N. Y., 1961.

(11) W. B. Wiegand, *Trans. Inst. Rubber Ind.*, **1**, 141 (1925); W. W. Barbas, *Trans. Faraday Soc.*, **38**, 194 (1942); F. L. Warburton, *Proc. Phys. Soc. (London)*, **58**, 589 (1946); G. Gee, *Trans. Faraday Soc.*, **42**, 585 (1946); A. Katchalsky, S. Lifson, I. Michaeli, and M. Zwicky, "Size and Shape Changes of Contractile Polymers," A. Wassermann, Ed., Pergamon Press Ltd., London, 1961, p. 1.

(12) W. Kuhn, G. Ebner, H. J. Kuhn, and D. H. Walters, *Helv. Chim. Acta*, **43**, 502 (1960); **44**, 325 (1961).

(13) W. Kuhn, I. Toth, and H. J. Kuhn, *ibid.*, **45**, 2345 (1962); W. Kuhn, I. Toth, and A. Ramel, *Nature*, **199**, 1154 (1963).

dynamic foundations because (4.10) satisfies the first and the second law of thermodynamics.

5. Conclusions

The concept of length in the thermodynamics of elastic bodies which has been deduced in this paper for a PES should be extended to the general case of an elastic body. It will be the modulus κ of (3.2) which must, in a general theory, be applied to all components of the empirical deformation tensors. A construction which is analogous to that of physical length will then provide a physical deformation tensor. The thermodynamic interpretation of physical deformation tensors will give the same linkage relations between pairs of conjugated quantities as Gibbs¹⁰ has deduced. Specific internal energy of elastic bodies, however, is no

longer a function of state, and a quantitative conversion of chemical into mechanical work of reservoirs during cyclic processes with elastic bodies is not possible.

As soon as physical length or physical deformation tensors are experimentally established, one must discuss the theory of dynamic equilibria again since the force of inertia depends on accelerations, *i.e.*, length changes, in a field of force. Such increases can perhaps be measured with the modulus κ , which is universal in the thermodynamics of elastic bodies. It is certain that one has to introduce into the statistical theory of elastic bodies a new probability factor which accounts for the necessary randomness of length. This probability factor is either a consequence of the elementary dynamic laws or it is a property of mechanical ensembles. In such ways eq 3.2, with its classical beauty, may give us new physical insights.

Kinetics of Formation and Growth of Colloidal Silver Bromide Particles. II¹

by E. J. Meehan and Grace Chiu

School of Chemistry, University of Minnesota, Minneapolis, Minnesota 55455 (Received August 2, 1965)

The kinetics of formation and growth of colloidal particles of silver bromide has been investigated. In sols formed both in aqueous medium and in the presence of ethanol or of acetone, the number of particles at a given time is proportional to the initial supersaturation, over wide limits. The rate of particle growth due to Ostwald ripening has been determined over the period 2 min to 1 day.

Introduction

Studies on the kinetics of formation and growth of colloidal particles of silver bromide have been reported previously in which light-scattering methods were used for the continuous measurement of particle size as a function of time.² The present paper gives results of further study of this problem, the main emphasis being on the effects of concentration of sol and of the presence of complexing agents, colloid stabilizer, and organic solvents upon number of colloid particles, particle size, and growth. The unexpected

result has been found that over wide limits the number of colloidal particles is directly proportional to the initial supersaturation, described already in a brief communication.³ Also, the rate of particle growth as a result of Ostwald ripening has been determined.

(1) Taken from the Ph.D. Thesis of G. Chiu, Jan 1962.

(2) E. J. Meehan and W. H. Beattie, *J. Phys. Chem.*, **65**, 1522 (1961).

(3) E. J. Meehan and G. Chiu, *J. Am. Chem. Soc.*, **86**, 1443 (1964).

Experimental Section

Reagents and Preparation of Sols. Analytical reagent grade potassium bromide and silver nitrate, dried at 110° for 2 hr, were used to prepare 0.1 M stock solutions in redistilled water. The solutions were filtered through 0.45- μ pore size Millipore filters and were stored in polyethylene bottles. Acetone was AR grade. Ethanol and ammonia were reagent grade. Disodium dihydrogen ethylenediaminetetraacetate (EDTA, Eastman Kodak Co.) was recrystallized. Polyvinylpyrrolidone (PVP, Antara Chemicals) was Type NP-K30 with a number-average molecular weight of 4×10^4 . It was used without purification. The pH of a 1% aqueous solution was 3.7. The scattering at an angle of 90° was negligible compared to that of the most dilute sol investigated, and the solution was transparent (1 cm thickness) over the range 240–1000 m μ . Potentiometric measurements (± 0.5 mv) using a silver electrode in solutions of silver nitrate in the absence and presence of PVP (up to 0.01%), compared to control measurements in solutions of silver nitrate, potassium cyanide, and PVP, indicated that no reaction occurred between Ag(I) and PVP.

The solutions of silver and bromide, plus other reagents when used, were brought to 25°. Under dim white light one solution was added either by pipet or microburet to 25 ml of the other solution contained in a 250-ml beaker and stirred as described previously.² The use of Pyrex or polyethylene beakers gave the same results. Time was measured from the beginning of the addition, which took about 30 sec; the first measurement was made at about 2 min. The sols were kept in the dark at 25° between measurements. Ethanol or acetone, when present, was added in equal amounts to both silver and bromide before mixing. The concentrations of ethanol and acetone are expressed as per cent by volume. Several of the radius-time curves given in this paper have been found to be reproducible within 10% by various workers in this laboratory over a period of several years, indicating that dust or impurities in the reagents do not affect the results.

Light-Scattering Measurements. A calibrated Aminco light-scattering microphotometer was used to measure scattered intensity at 436 and 546 m μ . Transmission measurements were made in a Beckman DU spectrophotometer fitted with 4-mm aperture plates, using cells of path length from 0.1 to 50 cm as required. The methods used for size determination were specific forward scattering, specific turbidity, dissymmetry, and polarization ratio, the choice being determined by particle size and concentration.⁴ Exact Mie scattering calculations for the appropriate range of

size and refractive index are available.⁵ For calculations in ethanol-water or acetone-water mixtures, the Mie functions corresponding to silver bromide in water were used. From the refractive indices of the solvents, the maximum resulting error in radius for small particles is calculated to be 3%.

Results

Figures 1–5 present typical radius-time curves for sols prepared under a variety of conditions. In the presence of an excess of bromide (Figures 1 and 2) the initial growth became more rapid with decreasing concentration of sol. In 10^{-5} – 10^{-6} M sols (10% excess of bromide) all the particle growth occurred within 2 min or less. The effect of preparing a sol (10^{-3} M) in the presence of ethanol is shown in Figure 3. In up to 50 vol % ethanol the 2-min radii decreased slightly with increasing ethanol content, but soon after mixing, the radius-time curves became practically parallel. In 90% ethanol, however, the rate of growth after the initial period was substantially larger than in 0–50% ethanol. The effect of acetone (not shown) was determined only in dilute sols. As compared to the growth pattern in water, the presence of acetone caused a pronounced reduction in the initial rate of growth and slow growth occurred for several hours after mixing.

Presence of ammonia during formation of a 10^{-3} M sol (Figure 4) changed the growth pattern to that of a very dilute sol in the absence of ammonia; practically all the growth occurred in 2 min. Qualitatively similar results were obtained in 10^{-4} and 10^{-5} M sols (not shown). The behavior in the presence of EDTA was completely different. In a typical experiment 2.2×10^{-4} M potassium bromide was added to an equal volume of 2.0×10^{-4} M silver nitrate containing 4×10^{-3} M EDTA. The pH of the mixture was 9.4. The main silver species in solution was calculated⁶ to be 2.6×10^{-6} M AgY^{3-} , where Y is the anion of EDTA. The radius at 2 min was only 0.011 μ and the particles grew rapidly; after 3 hr the radius was 0.15 μ and the sol began to settle.

Effect of PVP. Under certain conditions PVP is an effective stabilizer for silver halide sols.^{7,8} Under some circumstances the rapid growth that occurs after mixing the reactants (Figures 1 and 2) could be pre-

(4) E. J. Meehan and W. H. Beattie, *J. Phys. Chem.*, **64**, 1006 (1960).

(5) E. J. Meehan and Z. Z. Hugus, *J. Opt. Soc. Am.*, **51**, 260 (1961).

(6) J. Bjerrum, G. Schwarzenbach, and L. G. Sillén, "Stability Constants," Parts I and II, The Chemical Society, London, 1958.

(7) B. Jirgensons, *Makromol. Chem.*, **6**, 30 (1951).

(8) F. Evva, *Z. Wiss. Phot., Photophysik, Photochem.*, **52**, 1 (1957).

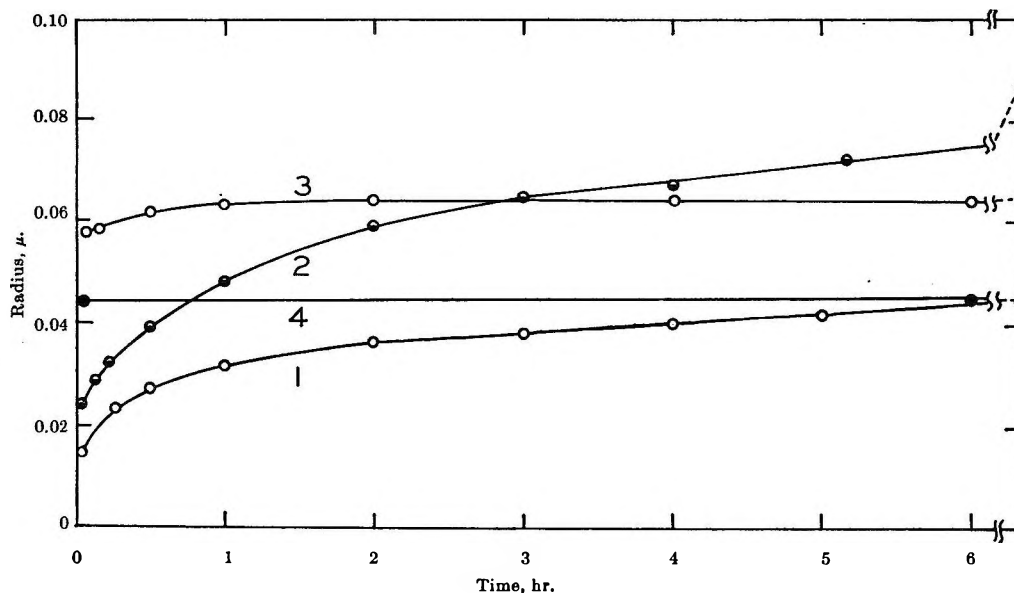


Figure 1. Particle radius vs. time; silver nitrate added to 10% excess of potassium bromide. Concentration of sol: 1, $10^{-3} M$; 2, $10^{-4} M$; 3, $10^{-5} M$; and 4, $5 \times 10^{-6} M$.

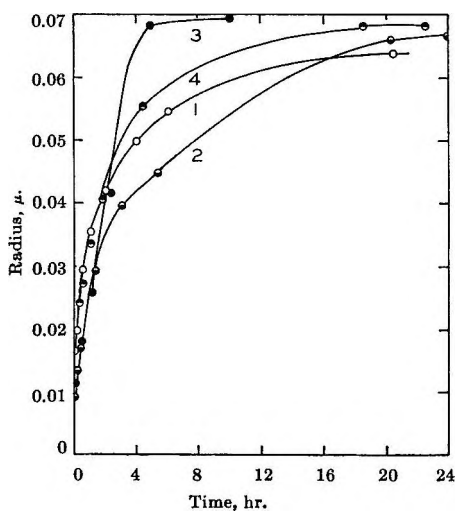


Figure 2. Particle radius vs. time; silver nitrate added to potassium bromide. Concentration of bromide in excess, $5 \times 10^{-3} M$; concentration of sol: 1, $5 \times 10^{-3} M$; 2, $5 \times 10^{-4} M$; 3, $5 \times 10^{-5} M$; and 4, $5 \times 10^{-6} M$.

vented completely by the addition of PVP. However, the effectiveness of PVP depended markedly upon the conditions of its addition, as shown by the following results. Approximately $10^{-5} M$ sols with 100% excess either of silver or of bromide were formed by adding by pipet 1 ml of $10^{-3} M$ potassium bromide (or silver nitrate) with or without PVP, the solution being stirred at 500 rpm. Stirring was continued for 20 sec. If neither solution contained PVP, 1 ml of PVP solution was added 20 sec after mixing. In all cases the final

concentration of PVP was about $10^{-5}\%$. The intensity scattered at an angle of 40° (i_{40}) was measured. In the absence of PVP, i_{40} increased at least eightfold within 30 min after mixing. Table I summarizes the results. (In this table, a sol is called "stable" if i_{40} changed by less than 1%/hr and "unstable" if i_{40} increased about as rapidly as in the absence of PVP.)

Table I: Stability of $Ca. 10^{-5} M$ Sols with $Ca. 10^{-5}\%$ PVP

| Solution added | Solution to which addition was made | |
|----------------|-------------------------------------|------------------------|
| | $AgNO_3$ | $AgNO_3 + PVP$ |
| KBr | Stable ^a | Unstable |
| KBr + PVP | Stable for a few hours | Stable for a few hours |
| | KBr | KBr + PVP |
| $AgNO_3$ | Stable ^a | Stable |
| $AgNO_3 + PVP$ | Unstable | Stable |

^a PVP added immediately after formation of sol.

The stability of sols prepared by adding silver nitrate to a solution of potassium bromide plus PVP was remarkably dependent upon the concentration of PVP, as shown in Figure 5. The addition of silver nitrate containing PVP to potassium bromide produced an unstable sol (Table I). However, when from 10^{-5} to $10^{-2}\%$ PVP was added at various times from 0.5 min to 3 hr after silver nitrate, the particle size became constant immediately and changed less

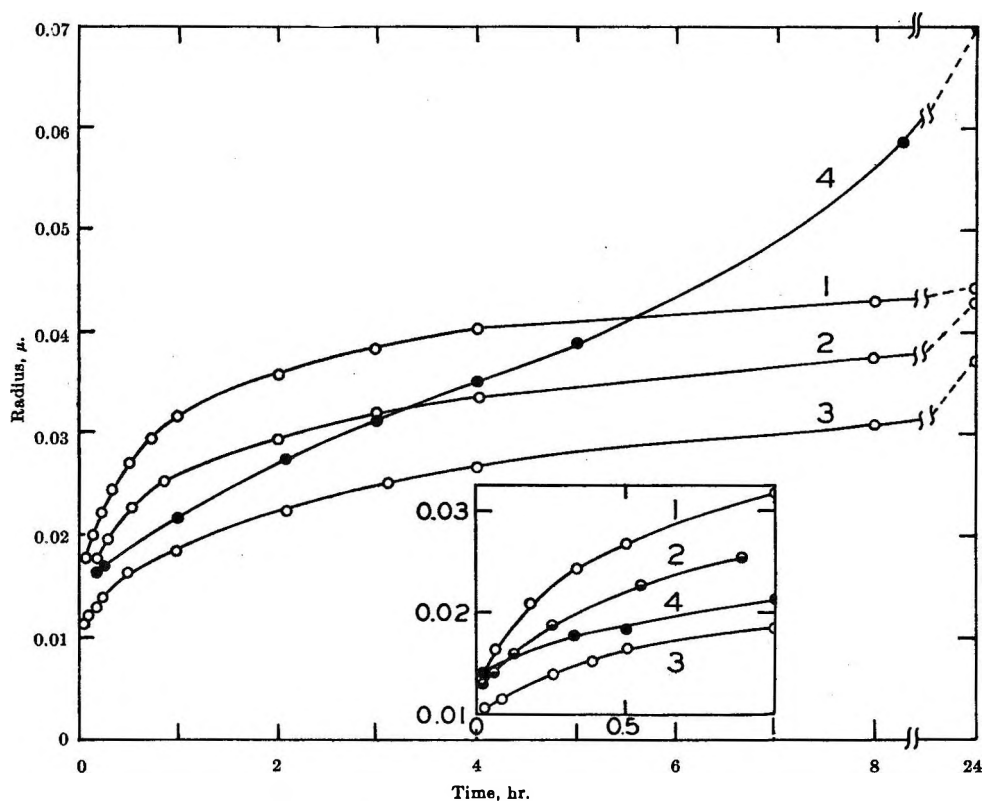


Figure 3. Particle radius vs. time: silver nitrate added to 10% excess of potassium bromide. Concentration of sol, $10^{-3} M$. Ethanol (vol %): 1, 0; 2, 10; 3, 50; and 4, 90.

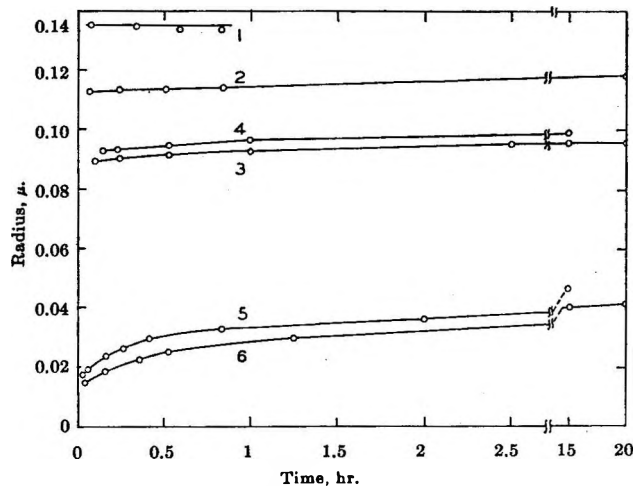


Figure 4. Particle radius vs. time. Potassium bromide (10% excess) added to silver nitrate. Concentration of sol, $10^{-3} M$. Concentration of ammonia: 1, 0.1 M ; 2, 0.05 M ; 3, 0.025 M ; 4, 0.005 M ; 5, 0.0005 M ; and 6, 0.

than 20% in the next 20 hr. Results at varied concentrations of reactants and PVP are summarized in Table II.

Numerous experiments in which the number and size of colloidal particles were measured before and after

Table II: Stability of Sols (Excess of Bromide): PVP Added 1 Min after Silver Nitrate

| [AgBr], M | [KBr], M | PVP, % | Change in radius from 2 min to 24 hr, % |
|----------------|---------------|-----------------------|---|
| 10^{-4} | 10^{-5} | 0 | 200 |
| | | 10^{-5} | 110 |
| 10^{-3} | 10^{-4} | 10^{-4} - 10^{-1} | 4-7 |
| | | 0 | 200 |
| 10^{-3} | 10^{-5} | 10^{-4} | 200 |
| | | 10^{-3} - 10^{-1} | 17-24 |
| 10^{-3} | 10^{-6} | 0 | 180 |
| | | 10^{-2} - 10^{-1} | 1-3 |
| | | 10^{-2} - 10^{-1} | 5 |

the addition of PVP showed that the addition of PVP did not change either number or size.

Previous work showed that upon dilution of fresh sols with water or with potassium bromide solution, a pronounced and almost discontinuous increase in radius occurred.² The dilution effects were observed also in the presence of gelatin, but the peculiar effects were completely eliminated when the sol was diluted with PVP solution.

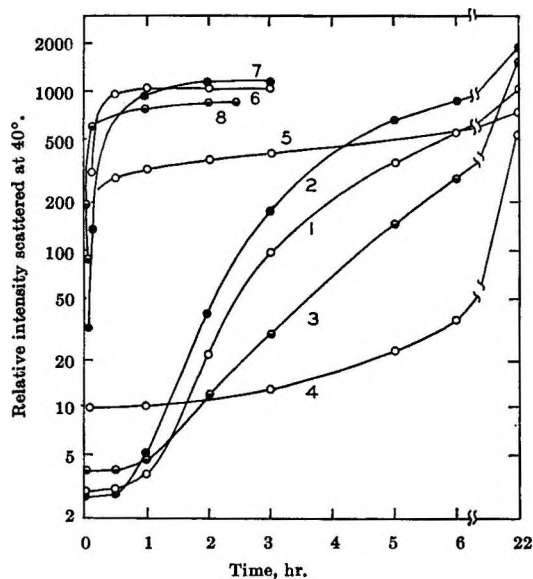


Figure 5. Relative i_{40} vs. time for 100% excess of silver nitrate added to potassium bromide containing PVP. Concentration of sol, $1.2 \times 10^{-5} M$. Concentration of PVP (wt %): 1, 10^{-2} ; 2, 10^{-3} ; 3, 10^{-4} ; 4, 10^{-5} ; 5, 10^{-5} ; 6, 10^{-7} ; 7, 10^{-8} ; and 8, 0.

Discussion

The growth curves for times greater than 2 min belong to two classes. In one class the radius is relatively small at 2 min and attains a limiting value only after some hours or days. In the other class the limiting radius is practically attained at 2 min and no further growth occurs. How the size, number, and growth patterns are related to concentration and supersaturation is discussed below.

Since the formation of colloidal silver bromide (as shown by conductance) is complete well within 2 min,^{2,9} the total number of colloidal particles can be calculated from the concentration of suspension and the average radius. The calculation is not exact because the sols are not homogeneous. However, the distribution of sizes in such sols is not broad.⁴ Assuming that the particles are spherical and have the bulk density 6.473 g ml^{-1} , the value of n , the number of particles per milliliter of suspension, is given by the relation

$$\log n = 9.84 + \log c - 3 \log r \quad (1)$$

where c is molar concentration of colloidal material and r is radius in microns. The relation between n and supersaturation is considered next.

In this paper supersaturation σ is defined as the concentration of silver bromide at the instant of mixing, divided by the solubility at equilibrium, s . Other workers have defined the supersaturation of the

slightly soluble ionic substance AB as the square root of the ratio of the ion activity products in the supersaturated state to the saturated state.^{10,11} (In the experiments of the present paper, ionic strengths are low and no activity corrections are required.) When equimolar amounts of A^+ and B^- are mixed, and if AB is completely dissociated, the two definitions of supersaturation are identical. The definitions are not the same, however, when the amounts of A^+ and B^- are unequal. For example, if the solubility product $S_{AB} = 10^{-10}$ and the initial concentrations of A^+ and B^- are 2×10^{-3} and $1 \times 10^{-3} M$, respectively, the equilibrium solubility is $10^{-7} M$. Since the sol concentration is $10^{-3} M$, supersaturation as defined in this paper is 10^4 , whereas according to the definition of La Mer, *et al.*,^{10,11} it is $\sqrt{(2 \times 10^{-3})(1 \times 10^{-3})/10^{-10}} = 140$. Moreover, the latter definition does not take into account the possibility of incomplete dissociation of AB or, even more important, the formation of complexes either with A^+ or with B^- . For example, consider a suspension made by mixing equal volumes of $0.01 M$ silver nitrate and $0.02 M$ potassium bromide. S_{AgBr} is 5.0×10^{-13} .¹² At the instant of mixing, $[Ag^+] = 5 \times 10^{-3} M$ and $[Br^-] = 1 \times 10^{-2} M$. The second definition of supersaturation^{10,11} yields $\sigma = \sqrt{5 \times 10^{-3} \times 10^{-2}/5 \times 10^{-13}} = 1 \times 10^4$. Since $[Br^-]$ at equilibrium = $5 \times 10^{-3} M$, $[Ag^+]$ at equilibrium = $1 \times 10^{-10} M$, but this does not correspond at all to the solubility. The concentration of undissociated silver bromide is $1 \times 10^{-8} M$ and that of $AgBr_2^-$ is $5 \times 10^{-8} M$.¹³ Hence the actual solubility is $6 \times 10^{-8} M$ and the supersaturation as defined in this paper is $5 \times 10^{-3}/6 \times 10^{-8} = 8.3 \times 10^4$.

Supersaturations were calculated as described above. Equilibrium constants for the formation of $AgNH_3^+$, $Ag(NH_3)_2^+$, and AgY^{3-} were taken from the IUPAC tables.⁶ Solubilities in the presence of ethanol and acetone were calculated from the data of Krahtovil and Tezak.¹⁴ In the mixed solvents the complex bromides are much more stable than they are in water. Therefore, when bromide is present in excess, the solubility in the mixed solvents is larger than it is in aque-

(9) G. H. Jonker and H. R. Kruyt, *Discussions Faraday Soc.*, **18**, 170 (1954).

(10) V. K. La Mer and R. H. Dinegar, *J. Am. Chem. Soc.*, **73**, 380 (1951).

(11) D. H. Klein, L. H. Gordon, and T. H. Walnut, *Talanta*, **3**, 177 (1959).

(12) B. B. Owens and S. R. Brinkley, Jr., *J. Am. Chem. Soc.*, **60**, 2229 (1938).

(13) E. Berne and I. Ledin, *Z. Naturforsch.*, **8a**, 719 (1953).

(14) J. Krahtovil and B. Tezak, *Arhiv Kemi*, **26**, 243 (1954).

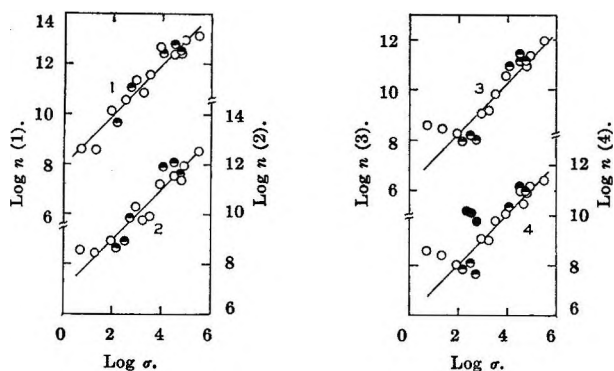


Figure 6. $\log n$ vs. $\log \sigma$ for silver nitrate added to potassium bromide: O, aqueous; \odot , with ethanol or acetone; \bullet , with EDTA. Time: 1, 2 min; 2, 1 hr; 3, 6 hr; and 4, 1 day.

ous solution, despite the fact that S_{AgBr} in the mixed solvents is much smaller than it is in water.

In sols prepared by addition of silver nitrate to an excess of potassium bromide, in the absence or presence of ethanol or acetone, n is directly proportional to σ over wide limits (Figure 6). At a given time t , the data (silver added to bromide, above a certain minimum σ , *vide infra*) are represented by

$$\log n = a(t) + \log \sigma \quad (2)$$

which applies up to $\log \sigma = 5.5$. The values of $a(t)$ and the approximate lower limit of validity of eq 2 are

| | 2 min | 1 hr | 6 hr | 1 day |
|------------------------------|-------|------|------|-------|
| $a(t)$ | 7.96 | 6.98 | 6.31 | 6.06 |
| Lower limit of $\log \sigma$ | 0.7 | 1.0 | 1.5 | 2.0 |

The dependence of $a(t)$ upon t is represented well within experimental error by

$$a(t) = 6.38 - 0.684 \log t(\text{sec}) \quad (3)$$

Combining eq 1-3 there is obtained

$$\log r(\mu) = 1.15 + \frac{1}{3} \log s + 0.23 \log t \quad (4)$$

where s is the molar solubility at equilibrium, equal as stated above to total dissolved silver in all forms. Equation 4 may be written in the equivalent form

$$r(\text{cm}) = (1.4 \times 10^{-3}) s^{1/3} t^{0.23} \quad (5)$$

The effects of temperature upon growth rates in a $5 \times 10^{-3} M$ silver bromide sol in $5 \times 10^{-4} M$ bromide have shown that the slow growth (at times greater than 37 min) is due to Ostwald ripening, while the initial rapid growth (at 32 sec) is a fast flocculation.² The present results indicate that for similar sols the slow growth process is dominant at times as short as 2 min.

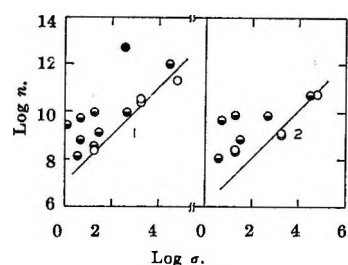


Figure 7. $\log n$ vs. $\log \sigma$ for potassium bromide added to silver nitrate: O, aqueous; \odot , with ammonia; \bullet , with EDTA. Time: 1, 4 min, and 2, 1 day.

Nielsen¹⁵ has given an approximate theoretical treatment of the growth rate due to Ostwald ripening. When the rate is determined by dissolution and reprecipitation, and the rates of surface reactions are of no consequence, Nielsen has found that the radius r should be given approximately by the expression

$$r^3 \cong \frac{\gamma v^2 D s t}{k T} \quad (6)$$

where s is the equilibrium solubility in molecules per cubic centimeter, γ is the surface energy, ergs per square centimeter, v the mean ionic volume, D the diffusion coefficient, k the Boltzmann constant, and T the temperature. The present work (eq 5) confirms the predicted dependence upon s . Using the numerical estimates: $\gamma = 40$ ergs cm^{-2} , $v = 10^{-22}$ cm^{-3} , $D = 10^{-5}$ $\text{cm}^2 \text{sec}^{-1}$, $s = 10^{-16}$ molecule $\text{cm}^{-3} = 1.6 \times 10^{-8} M$, and $kT = 4 \times 10^{-14}$ erg, Nielsen's eq 6 yields $r \cong 10^{-6} t^{1/3}$. For the same value of s , the experimental eq 5 becomes $r = 3.5 \times 10^{-6} t^{0.23}$.

As stated already, eq 2-5 apply above a certain minimum σ . At very small σ , practically all the particle growth occurs within 2 min or less, which accounts for the deviations at low σ from the straight lines of Figure 6. It is of interest also to note that 1-day-old sols prepared in the presence of EDTA have a particle number larger by 10-20-fold than sols of the same σ prepared without EDTA.

Sols prepared by the addition of excess of potassium bromide to silver nitrate have somewhat fewer particles initially than those prepared by the reverse order (Figure 7). At a given σ , the value of n at 4 min in the former case is about the same as at 1 hr in the latter. However, after 1 day of growth the n - σ relation is practically the same for both modes of addition. Sols prepared in the presence of ammonia (Figure 7) appear to deviate from the n - σ relation observed in the absence of ammonia. In general, the number of

(15) A. E. Nielsen, "Kinetics of Precipitation," Pergamon Press Inc., New York, N. Y., 1964, pp 108-115.

particles at a given σ is larger in the presence than in the absence of ammonia.

Nothing can be concluded from these experiments about the rate of nucleation. The experimental fact² that fast flocculation is occurring at 35 sec means that the number of particles observed at 2 min is determined not only by the number of primary nuclei formed

during mixing but also by the rate of fast flocculation. The fact that the observed value of n varies linearly with σ , whereas according to generally accepted nucleation theory the number of primary nuclei should vary exponentially with σ , indicates that the rate of fast flocculation also must vary exponentially with the supersaturation.

Electron Spin Resonance Studies of γ -Irradiated High Surface Area

Silica. I. Identification of Defects

by G. M. Muha

Esso Research and Engineering Company, Linden, New Jersey (Received August 2, 1965)

Electron spin resonance (esr) studies have been made of the defects introduced in a high surface area silica by γ -irradiation. The esr spectrum has been analyzed in terms of contributions from four distinct types of defects in the glass structure. Two of these defects are thought to be formed in the silica network by the trapping of an electron in an oxygen vacancy. There is some evidence that $\sim 10\%$ of the oxygen vacancies have nearby hydroxyl groups. The remaining two defects are thought to consist of holes trapped in silicon-oxygen and boron-oxygen bonds. The evidence for the former assignment is not conclusive. The boron in the latter case occurs as an impurity in the silica. It is found to be trigonally coordinated in contrast to the tetrahedral coordination observed in other glasses. This result is explained in terms of the low concentration of network modifier present. The spectrum arising from the B-O defect is described by an axially symmetric spin Hamiltonian with $g_{||} = 2.0100$, $g_{\perp} = 2.0023$, $A_{||} = 1.40 \times 10^{-3} \text{ cm}^{-1}$, and $A_{\perp} = 1.25 \times 10^{-3} \text{ cm}^{-1}$. The relationship between this B-O defect and the Al-O defect found in irradiated smoky quartz is briefly considered.

I. Introduction

Electron spin resonance (esr) techniques have been used in a number of cases to study the nature of the paramagnetic defects introduced in glasses by ionizing radiation. For example, spectra have been reported for fused silica,¹⁻³ alkali borate,⁴⁻⁶ aluminosilicate,^{7,8} and phosphate^{9,10} glasses. Quite often hyperfine effects are observed. In these cases, the interpretation of the spectrum is usually based on concepts de-

veloped in the study of defects in alkali halide crystals, *viz.*, electrons or holes trapped at vacancies in the lattice.

(1) J. S. van Wieringen and A. Kats, *Philips Res. Repts.*, **12**, 432 (1957).

(2) R. A. Weeks and C. M. Nelson, *J. Am. Ceram. Soc.*, **43**, 399 (1960).

(3) P. O. Frömau, R. Pettersson, and T. Vännngard, *Arkiv Fysik*, **15**, 559 (1959).

In the work described in the present paper, a description is given of the paramagnetic defects introduced by Co^{60} irradiation in a Vycor-type glass. This material is chemically similar to fused silica but differs physically in that it has a high surface area. This latter property enables one to study the effects of various gases on the observed defects; this work is described in the following paper¹¹ (hereafter referred to as II). The remarkable surface properties of this irradiated glass have previously been reported.¹²

The material used in the present study, usually referred to as "porous glass," is prepared¹³ by heating an alkali borosilicate glass above the annealing point to cause phase separation and then leaching the boric oxide rich phase with acid. The resulting material possesses a porous structure of high silica content containing some residual boron.

II. Experimental Section

The esr spectra were obtained with a Strand Model 600 X-band spectrometer equipped with a Varian V-4531 variable-temperature cavity. The magnetic field was provided by a Harvey Wells L-128 magnet. Field modulation at 6 kc/sec and a 3-sec time constant were used in all cases. The modulation amplitude and microwave power level were set below the point where line broadening or saturation effects would be observed in the recorded spectrum. First derivative presentation was used in recording the spectra.

The magnetic field was calibrated by a Harvey Wells F502 nmr gaussmeter, the frequency of which was monitored by a Hewlett-Packard 524C frequency counter. The g values were obtained by comparison with a DPPH sample ($g = 2.0036$) taped to the outside of the sample tube.

All samples used in this study were prepared by Yates using methods described in detail in II. The material was taken from a single lot of Corning 7930 porous glass containing about 3% boron plus other impurities of much lower concentration. For present purposes, it is sufficient to note that the esr spectrum was obtainable only if the irradiated sample was held under vacuum—if not, no signal was observed. Under vacuum, the samples are stable for periods in excess of 45 days as judged by the reproducibility of this esr spectrum. No esr signal was observed in samples that had not been irradiated.

III. Results and Discussion

A typical spectrum of a Co^{60} -irradiated porous glass sample is given in Figure 1. The spectrum consists of a sharp asymmetric line and five somewhat broader

lines superimposed on a broad background. In addition, several weaker lines are observed within the group of five lines along with another line in the region of 3388 gauss. A search at lower fields revealed no lines due to the presence of paramagnetic impurities.¹⁴

All samples became reddish violet from the radiation treatment. The sample coloration as well as the shape and intensity of the esr lines was stable at room temperature for periods in excess of 45 days, provided the sample was held under vacuum.

The spectrum of a porous-glass sample sintered so as to have essentially zero surface area was also obtained. This spectrum resembled that shown in Figure 1 except that the group of five lines was broadened so as to appear to overlap. The weak lines within the group of five lines could not be observed. The single line at highest field remained. In contrast to the behavior of the high surface area samples, the sintered sample was stable in air.

A. The Sharp Asymmetric Line. The sharp asymmetric line and the single weak line at highest field may be judged to be independent of the other lines in the spectrum by their behavior under conditions of saturation. At 77°K, it was possible to set the microwave power at a level so that these two lines were almost completely removed while the broad background and the group of five lines were reduced in intensity by less than 30%. A second piece of evidence concerning this point is offered in II. There it is shown that the addition of CH_3OH vapor to the sample "bleaches" these two lines but leaves the broad background and group of five lines essentially unchanged.

An expanded trace of the asymmetric line is given in Figure 2. The line is seen to be typical of that obtained from polycrystalline material with an anisotropic g tensor. On the basis of an analysis of the line shape,¹⁵ the curve can be described as Lorentzian with

(4) G. O. Karapetyan and D. M. Yudin, *Fiz. Tverd. Tela*, **4**, 2647 (1962); *Soviet Phys.-Solid State*, **4**, 1943 (1963).

(5) S. Lee and P. J. Bray, *J. Chem. Phys.*, **39**, 2863 (1963).

(6) S. Lee and P. J. Bray, *ibid.*, **40**, 2982 (1964).

(7) S. Lee and P. J. Bray, *Phys. Chem. Glasses*, **3**, 37 (1962).

(8) G. O. Karapetyan, S. A. Stepanov, and D. M. Yudin, *Fiz. Tverd. Tela*, **6**, 1531 (1964); *Soviet Phys.-Solid State*, **6**, 1197 (1964).

(9) G. O. Karapetyan and D. M. Yudin, *Fiz. Tverd. Tela*, **3**, 2827 (1961); *Soviet Phys.-Solid State*, **3**, 2063 (1962).

(10) Y. Nakai, *Bull. Chem. Soc. Japan*, **37**, 1089 (1964).

(11) G. M. Muha and D. J. C. Yates, *J. Phys. Chem.*, **70**, 1399 (1966).

(12) D. J. C. Yates and P. J. Lucchesi, *J. Am. Chem. Soc.*, **86**, 4258 (1964).

(13) M. E. Nordberg, *J. Am. Ceram. Soc.*, **27**, 299 (1944).

(14) R. H. Sands, *Phys. Rev.*, **99**, 1222 (1955).

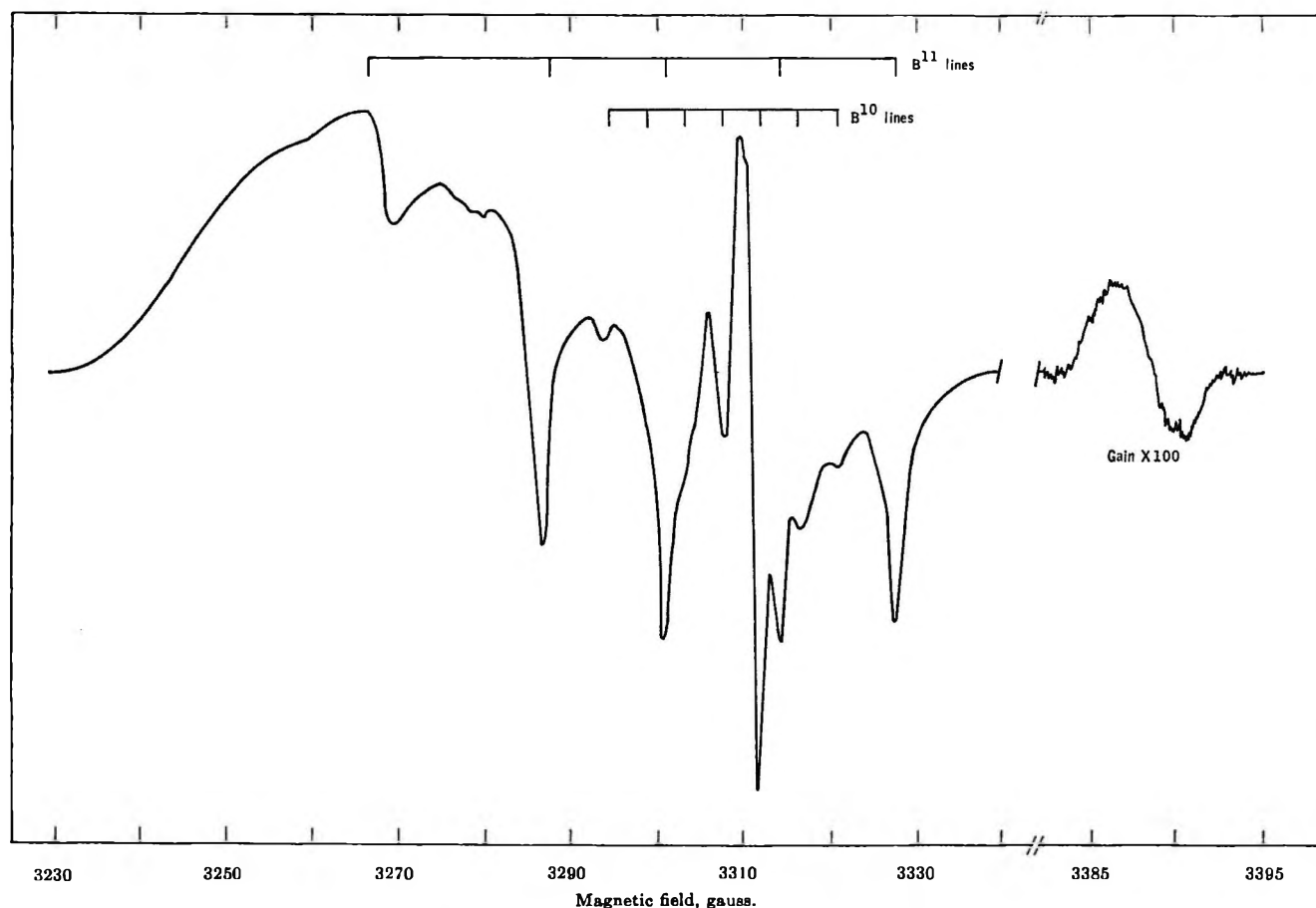


Figure 1. Esr spectrum of γ -irradiated porous glass obtained at room temperature. Note the changes in the vertical and horizontal scales for the line at highest field.

$g_{11} = 2.0016$, $g_{\perp} = 2.0003$, and a single-crystal line width of approximately 1.3 gauss. The g values were measured at the peaks of the derivative presentation and therefore necessarily include some error. This error has been estimated¹⁶ to be less than 10% of the g value variation, an amount of little importance for the present application.

A line of the type described here for porous glass has been reported in a variety of other irradiated materials containing the SiO_2 network. Examples include irradiated borosilicate⁵ and aluminosilicate glasses,⁷ fused silica,^{1,16} and Amersil.¹⁶ In addition, during the course of the present work, similar lines were obtained from other high surface area silicas including Quso-G30¹⁷ and Cabosil HS5.¹⁸ All of these samples exhibit an easily saturated line of approximately 1-gauss width and a g value near 2.001. From this evidence, it is concluded that the defect is associated with the SiO_2 network rather than with network modifiers, impurities, or peculiarities of a high surface area sample.

Weeks and Nelson² have studied radiation-induced defects in the SiO_2 network in fused silica and single-crystal quartz. For the latter material, they were able to show the presence of two paramagnetic centers which were labeled E_1' and E_2' . In addition, a direct correlation was established between the optical absorptions at 2120 and 2300 Å and the E_1' and E_2' centers, respectively. Tentative models^{2,19,20} have been proposed for the two centers which are consistent with the experimental data but offer some difficulty with respect

(15) J. W. Searl, R. C. Smith, and S. J. Wyard, *Proc. Phys. Soc. (London)*, **78**, 1174 (1961).

(16) R. A. Weeks and C. M. Nelson, *J. Appl. Phys.*, **31**, 1555 (1960).

(17) Obtained from the Philadelphia Quartz Co., Philadelphia 6, Pa. This material is prepared by an unspecified precipitation technique. It has a typical surface area of 270 m^2/g .

(18) Obtained from the Cabot Corp., Boston, Mass. This material is prepared by burning silicon tetrachloride. It has a typical surface area of 340 m^2/g .

(19) R. A. Weeks, *Phys. Rev.*, **130**, 570 (1963).

(20) R. A. Weeks and E. Lell, *J. Appl. Phys.*, **35**, 1932 (1964).

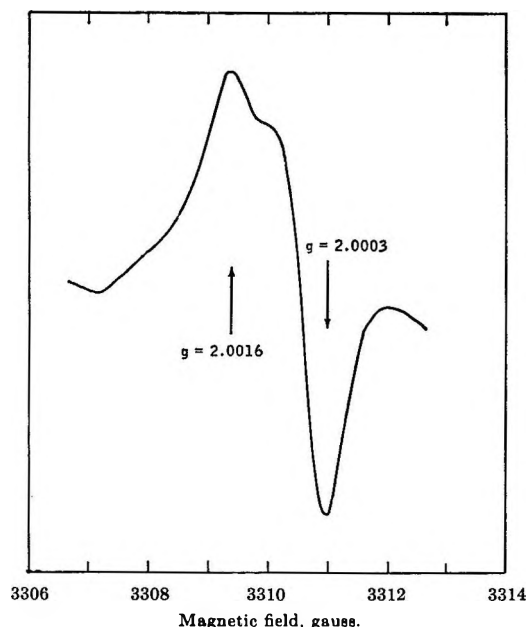


Figure 2. Expanded view of the center portion of the spectrum shown in Figure 1. This sharp, asymmetric line is thought to arise from an electron trapped in an oxygen vacancy.

to the electronic wave function involved.²¹ Both defects are thought to be similar in that they involve an unpaired electron trapped in an oxygen vacancy; they differ in the number of other silicon and oxygen atoms missing in the vicinity of the center.¹⁹

In the case of fused silica, the two centers cannot be resolved² because of the averaging effect over the anisotropic interactions. The optical absorptions can be resolved, and, on this basis, the identification with the single-crystal results is made. In fused silica, the E_1' center predominates.^{2,16,22}

In the porous glass used in this work, attempts²³ to resolve discrete bands in the optical region of the spectrum due to radiation changes were unsuccessful. A comparison of the g values for porous glass with those reported^{2,21} for the E_1' ($g_1 = 2.0003$, $g_2 = 2.0006$, $g_3 = 2.0018$) gives good agreement. Further, an integrated version of the spectrum shown in Figure 2 is in reasonable agreement with the calculated line shape for an E_1' center distributed in a glass.¹⁶ On the basis of these two observations, it will be assumed that the sharp asymmetric line corresponds to one of the E' centers previously reported, *viz.*, an electron trapped in an oxygen vacancy. Other details concerning nearby molecules or vacancies are as yet unknown.

B. High-Field Line. The weak line at high field is 78 gauss ($g = 1.96$) above the asymmetric line and has an over-all width of approximately 10 gauss. Its integrated intensity is estimated to be 10% of that of

the asymmetric line. A search for a corresponding line about the same distance below the asymmetric line was inconclusive. This region fell on the rapidly rising slope of the broad background.

The present work provided no direct evidence concerning the nature of the paramagnetic species responsible for this line. It may be structurally similar to the E' center assumed to give rise to the asymmetric line since, as noted above, similar chemical and relaxation behaviors are observed.

The large shift of the line from the region $g = 2$ suggests that a hyperfine interaction may be involved. Such interactions have been reported in other silicas. For example, in a Co^{60} -irradiated Corning 7943 silica, a pair of lines 5 gauss wide and separated by 75 gauss have been reported.²⁴ Deuterium substitution confirmed that the doublet was due to a proton interaction. The intensity of this doublet has been shown²⁰ to depend upon the presence of hydroxyl groups in the silica as shown by the presence of a 2.7- μ adsorption band.

Infrared studies of porous glass²⁵ also show the presence of a large number of hydroxyl groups. Little change is detected in the frequency or intensity of the OH band after Co^{60} irradiation.²³ The parallel between the infrared and esr results for porous glass and the Corning 7943 silica, coupled with the similar relaxation and chemical behavior noted for the assumed E' center, suggests the following interpretation. The high-field line arises from an E' site containing a nearby hydroxyl group. The intensity relative to the asymmetric line then implies that roughly 10% of the E' sites contain hydroxyl groups. The simplicity of this picture is attractive, but the hypothesis clearly requires more experimental evidence.

C. Group of Five Lines. A group of five lines similar to those observed in the spectrum of porous glass has previously been reported for irradiated borosilicates.⁵ In the latter case, a comparison of the spectra obtained at X- and K-band microwave frequencies with isotopically enriched B^{10} samples demonstrated conclusively that the five lines arise from an anisotropic boron hyperfine interaction.

(21) R. H. Silsbee, *J. Appl. Chem.*, **32**, 1459 (1961).

(22) R. A. Weeks and E. Sonders, Proceedings of the First International Conference on Paramagnetic Resonance, Jerusalem, Israel, North-Holland Publishing Co., Amsterdam, 1963, p 869.

(23) D. J. C. Yates, unpublished work.

(24) (a) A. J. Shuskus, O. R. Gilliam, and P. W. Levy, *Bull. Am. Phys. Soc.*, **6**, 246 (1961); (b) the Si^{29} hyperfine interaction observed in single-crystal quartz is strongly anisotropic and has not been observed in glasses.² On this basis, the possibility that the line under consideration in this section arises from a Si^{29} hyperfine interaction is rejected.

(25) N. Sheppard and D. J. C. Yates, *Proc. Roy. Soc. (London)*, **A238**, 69 (1956).

For porous glass, an analysis of the five-line spectrum based on a similar anisotropic hyperfine interaction will be presented. The validity of this approach will be shown by the explanation of the position and intensities of other weaker lines observed in the spectrum.

Of the group of five lines, the four lines on the high-field side are centered at $g = 2.0023$ with an approximately equal splitting of 13.4 gauss. If these peaks are due to the $H_{\perp}(M)$ contribution (notation of ref 5) of the B^{11} hyperfine transitions, then the line widths permit a resolution such that the 18% abundant B^{10} ($I = 3$) transitions should also be observed. The seven B^{10} lines would have a splitting relative to the B^{11} lines of $\sim 1/3$ (ratio of the magnetogyric ratios). Three lines with approximately the correct intensity and falling within 5% of the predicted positions are observed (Figure 1). The predicted positions of the remaining four lines are in a region overlapped by the asymmetric line and the B^{11} lines.

The remaining line of the group of five lines lies at lowest field and is assigned to the $H_{\parallel}(M = 3/2)$ contribution. At room temperature, the other three accompanying peaks are not directly observable. At 77°K, the spectral resolution is increased sufficiently to show the presence of another line of the same phasing and intensity as the lowest field line (Figure 3a). At room temperature, this line overlaps with a B^{10} line causing the latter to appear somewhat more intense than the other two B^{10} lines that are observed. This additional peak is assigned to the $H_{\parallel}(M = -3/2)$ contribution. The possibility that this line is due to one of the $M_I = \pm 1/2$ components is ruled out, for, in this case, the magnitude of the splitting involved would allow all four components to be observed.

If this assignment is correct, the $H_{\parallel}(M)$ components are centered at $g = 2.0100$ and separated by 14.9 gauss. A sketch of the theoretical line shapes (neglecting relaxation processes) using the parameters obtained above is given in Figure 3b. The unequal intensities of the perpendicular components of the B^{11} lines when observed at 77°K (Figure 3a) may be due to a partial overlapping with parallel components.

The line width at 77°K allowed considerable precision in the measurements of the splittings of the four $H_{\perp}(M)$ components. As noted above, these splittings are only approximately equal. For example, by using the results from five different samples, the spacings between the four lines were found to be 13.62 ± 0.08 , 13.28 ± 0.08 , and 13.36 ± 0.08 (and in that order from low to high field).²⁶ These variations in the splittings do not correspond to quadrupole or second-order effects.²⁷ They may arise from a shift in the apparent

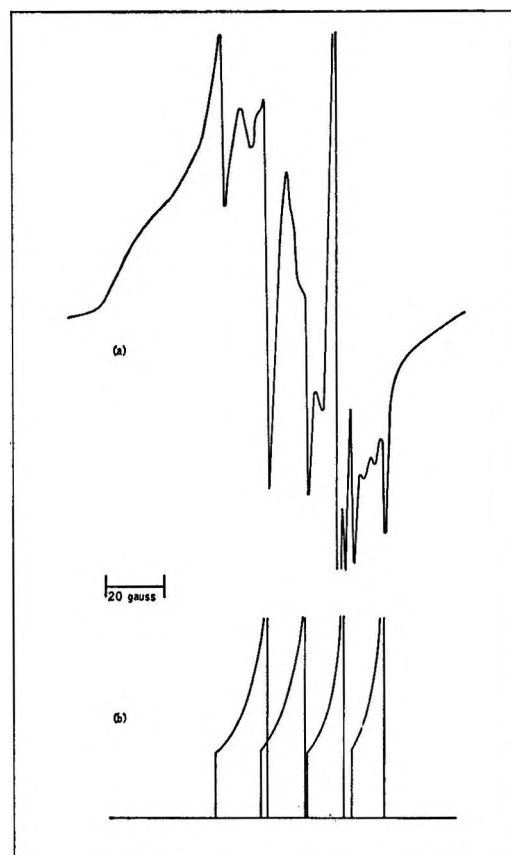


Figure 3. (a) ESR spectrum of γ -irradiated porous glass at 77°K showing increased resolution. (b) Theoretical line shapes (neglecting relaxation processes) computed using magnetic parameters given in eq 1.

center of the line due to the differences in the amount of overlapping of parallel and perpendicular components for each hyperfine line.

In the case of irradiated borosilicate glass,⁵ the observed B^{11} line widths were considerably greater than obtained here for irradiated porous glass. In addition, the line width did not narrow at 77°K in contrast to porous glass where a narrowing by a factor of ~ 2 is observed. The difference in behavior of the two glasses may be attributed to their difference in structure and chemical treatment prior to irradiation. In the case of porous glass, the relatively open structure may lessen line broadening due to dipolar interactions with neighboring atoms. Similarly, the strong dehydration treatment given porous glass before irradiation

(26) The value for $A_{\perp}/g_{\pm} = 13.4$ gauss quoted above is the simple average of these three spacings. The variation in the spacings makes a meaningful estimate of the experimental error in the magnetic parameters difficult. If it is arbitrarily decided to estimate the error as a tenth of the line width, the error would correspond to 0.2 gauss at 77°K.

(27) B. Bleaney, *Phil. Mag.*, **42**, 441 (1951).

tion¹¹ presumably would decrease dipolar broadening due to water molecules trapped in the glass structure.

Since B¹¹ has a considerable quadrupole moment, the question of a quadrupolar interaction deserves further consideration. The effect of this interaction²⁷ is to cause the hyperfine spacings to become unequal and to introduce weak lines corresponding to $\Delta M_I = \pm 1, \pm 2$. An estimate of the magnitude of the expected effects at arbitrary orientation of the crystalline axis relative to the applied field can be made by using the upper limit of the range in B¹¹ quadrupole constants reported in nmr studies.^{28, 29}

This estimate indicates that both the shift in the position of the lines and the intensities of the extra lines are small effects. In the following, it will be assumed that the integration over all orientations also gives a small effect, and, consequently, the quadrupole effects are not discretely observable in the spectrum.³⁰

Finally, then, the five-line spectrum can be described by the spin Hamiltonian

$$\mathcal{H} = \beta [g_{\parallel} H_z S_z + g_{\perp} (H_x S_x + H_y S_y)] + A_{\parallel} I_z S_z + A_{\perp} (I_x S_x + I_y S_y) \quad (1)$$

with $I = 1/2$, $g_{\parallel} = 2.0100$, $g_{\perp} = 2.0023$, $A_{\parallel} = 1.40 \times 10^{-3} \text{ cm}^{-1}$, and $A_{\perp} = 1.25 \times 10^{-3} \text{ cm}^{-1}$.

D. Broad Background Line. A line similar to that making up the broad background in Figure 1 has been reported in a wide variety of silicate-based glasses.^{1, 3, 5, 7, 31} The apparent g value varies with the material but is always greater than that of the free electron. The line width depends upon chemical composition, typical values lying in the range from 12 to 51 gauss. Also, the line width is reported to be independent of microwave frequency³¹ in some samples, but depends upon frequency in others.¹

The integrated intensity of the broad line observed in this work is too large to be explained in terms of a contribution from the polycrystalline averaging of the intensity of the boron lines discussed above. Rather, it is believed that this broad background represents an additional line, independent of the other lines described above.

The evidence for this statement lies principally in the following observations. First, the intensity of the background line (per unit radiation dose) was always significantly higher if the glass was not acid leached.³² No other features of the spectrum were observed to change. An effect similar to this has been observed in aluminosilicate⁷ glasses and fused silica.¹ In these cases, the intensity of the background line was found to depend on the alumina content and water content, respectively. Secondly, as discussed in part II, the

initial effect of carbon monoxide on the acid-leached sample is to remove most (but not all) of the broad background but to leave the other lines unchanged.

In γ -irradiated synthetic fused silica, a similar broad background has been attributed to defects intrinsic to the SiO network.^{20, 31} The line width can be explained by the anisotropy in the g tensor.³¹ In other silicas¹ and in aluminosilicate glasses,⁷ the resonance is thought to arise from holes trapped on non-bridging oxygen atoms.

In the case of porous glass, the present experimental results do not allow a definite assignment to be made. In part II, it is shown that hydrogen or deuterium added to the irradiated sample causes a "bleaching" of both the B¹¹ spectrum and the broad background line. Since the effect of carbon monoxide indicates the B¹¹ spectrum and the broad background are independent, while the hydrogen results suggest they are chemically similar, a reasonable hypothesis would be that the broad background arises from a Si-O defect which is the counterpart of the B-O defect. On the basis of electronegativity values, the Si-O bond is intermediate between the B-O and Al-O bonds in covalent character. Since spectra for holes trapped on an oxygen bound to tetrahedrally coordinated boron⁵ and aluminum⁷ have been reported, a similar defect in the case of silicon might be expected. The above hypothesis is then consistent with this observation concerning the covalent nature of the bonding involved. The parallel is not complete, however, for in the silicon case, a cation is not required for charge compensation in the unirradiated material.

IV. Boron-Oxygen Defect

In a previous section, it was concluded that the five-line spectrum was the result of a B¹¹ hyperfine interaction. In the present section, an attempt will be made to interpret the parameters in the spin Hamiltonian given in eq 1.

The boron hyperfine interaction observed in the glass is small compared to that observed in the free atom. Therefore, it is assumed that the "magnetic electrons" occupy extended molecular orbitals³³ in-

(28) K. S. Pennington and H. E. Petch, *J. Chem. Phys.*, **36**, 2151 (1962).

(29) E. Brun and S. Ghose, *ibid.*, **40**, 3031 (1964).

(30) Other intense lines in polycrystalline spectra sometimes arise at angles other than 0 or $\pi/2$ if the g and A tensors are specially related. Since no intense "extra" lines were observed in this study, the point is not considered. For an approximate treatment of this effect, see H. R. Gersmann and J. D. Swalen, *J. Chem. Phys.*, **36**, 3221 (1962).

(31) R. A. Weeks, *J. Appl. Phys.*, **27**, 1376 (1956).

(32) All parameters being reported in this paper have been obtained from samples that were acid leached. For a description of the leaching process, see ref. 12.

volving nearest neighbors, presumably oxygen. The contribution of boron to the molecular orbital may be approximated by $\phi = \zeta(a|2s\rangle + b|2p\rangle)$. In this expression, ζ is a measure of the contribution of the boron atomic orbitals to the hyperfine interaction.

The principal values of the g tensor are equal or greater than the free-electron value. In the absence of any information concerning the excited states mixed into the ground state by the spin-orbit coupling, it will be assumed³⁴ that the condition $g_{||} > g_{\perp} = g_e$ implies that a hole is involved. The anisotropy in the hyperfine tensor implies the hole interacts preferentially with only one of the boron nearest neighbors.⁶ A simple model fitting this description would be a hole trapped in a boron-oxygen bond. The system to be treated then involves seven electrons distributed in four orbitals. The hyperfine interaction for this system is represented by the operator³⁵ where the symbols

$$\mathcal{H} = g_e \beta_e g_n \beta_n \left[\frac{3(\vec{r} \cdot \vec{S})(\vec{r} \cdot \vec{I})}{r^5} - \frac{\vec{S} \cdot \vec{I}}{r^3} + \frac{8\pi}{3} \delta(r) \vec{S} \cdot \vec{I} \right] \quad (2)$$

have their usual significance. To express the interaction as a function of the spin coordinates only, the orbital coordinates are integrated out.³⁶ To simplify the integration, contributions to the matrix elements involving cross terms of boron and oxygen orbitals are neglected. Since the interaction falls off rapidly with distance, the approximation seems justified.³⁷ Comparison of the results of the integration with eq 1 gives the equalities

$$\begin{aligned} A_{||} &= \zeta^2(a^2\alpha + 2b^2\beta) \\ A_{\perp} &= \zeta^2(a^2\alpha - b^2\beta) \\ \alpha &= \frac{8\pi}{3} |\psi(0)|^2 g_e \beta_e g_n \beta_n \\ \beta &= \frac{2}{6} \langle r^{-3} \rangle g_e \beta_e g_n \beta_n \end{aligned} \quad (3)$$

where $\langle r^{-3} \rangle$ is taken over a boron 2p orbital.

From an SCF calculation (including configuration interaction) for boron,³⁸ $|\psi(0)|^2$ can be estimated as $9.56 \times 10^{24} \text{ cm}^{-3}$. The value $\langle r^{-3} \rangle$ for boron has been estimated⁵ from atomic beam data as $5.41 \times 10^{24} \text{ cm}^{-3}$. Based on these values, the results $\alpha = 6.77 \times 10^{-2} \text{ cm}^{-1}$ and $\beta = 1.83 \times 10^{-3} \text{ cm}^{-1}$ are obtained. If the isotropic hyperfine interaction is defined as $A' = \frac{1}{3}(A_{||} + 2A_{\perp}) = 1.30 \times 10^{-3} \text{ cm}^{-1}$, then the value of $\zeta^2 a^2$ must be 0.0192. A similar algebraic manipulation gives $\zeta^2 b^2 = 0.0273$ and finally $h = a^2/b^2 = 0.7$. For sp^2 and sp^3 hybrids, h would equal 0.500 and 0.333, respectively. A 5% increase in the experimental value of $A_{||}$ would give the theoretical ratio for the sp^2 hybrid, whereas a larger error (14%) would be required

to fit the sp^3 case. The latter error is equivalent to 1.4 times the line width and thus seems unjustifiably large.³⁹ Therefore, in the following it will be assumed that the B^{11} hyperfine interaction arises from a trigonally coordinated boron.

It is interesting to consider the difference in the hyperfine parameters reported here for porous glass and those reported for sodium borate glass by Lee and Bray.⁵ By using their experimental parameters, a calculation similar to that given above gives a per cent anisotropy $[(A_{||} - A_{\perp})/A']$ of 20% compared to a theoretical value of 21% for an sp^3 hybrid. This is in good agreement with their suggestion that a tetrahedrally coordinated boron was involved in the sodium borate case. In an nmr study, Silver and Bray⁴⁰ showed that the ratio of the concentration of four- to three-coordinated boron atoms in this type of glass is an increasing function of the concentration of the network modifier (Na_2O) present. This result suggests that the difference in coordination observed by esr in the porous glass and sodium borate glass can be understood in terms of the low sodium content (typically 50–400 ppm) of the porous glass. The explanation is in agreement with the present theory of the role of Na_2O as a network modifier.⁴⁰

If it is assumed that the hybridization for the case of porous glass is exactly sp^2 , then $a^2 = 1/3$ and $\zeta = 0.24$. A similar calculation for the sodium borate glass assuming sp^3 hybridization ($a^2 = 1/4$) gives $\zeta = 0.28$. The lower value of ζ for the sp^2 hybrid presumably reflects the increased electropositive character of the sp^3 hybrid relative to the sp^2 hybrid, *viz.*, a hole is more strongly "attracted" to the former since it has a higher electron density due to the formation

(33) K. W. H. Stevens, *Proc. Roy. Soc. (London)*, **A219**, 542 (1953); J. Owen, *ibid.*, **A227**, 183 (1955).

(34) C. P. Slichter, "Principles of Magnetic Resonance," Harper and Row Publishers, Inc., New York, N. Y., 1963, Chapter 7.

(35) S. M. Blinder, *J. Mol. Spectry.*, **5**, 17 (1960).

(36) B. Bleaney and K. W. H. Stevens, *Rept. Progr. Phys.*, **16**, 108 (1953); W. V. Smith, P. P. Sorokin, I. L. Gelles, and G. J. Lasher, *Phys. Rev.*, **115**, 1546 (1959).

(37) (a) M. Tinkham, *Proc. Roy. Soc. (London)*, **A236**, 549 (1956); (b) A. H. Maki and B. R. McGarvey, *J. Chem. Phys.*, **29**, 31 (1958).

(38) I. I. Glembotskii, V. V. Kibartas, and A. P. Yutsis, *Z. Eksperim. i Teor. Fiz.*, **29**, 617 (1955); *Soviet Phys. JETP*, **2**, 476 (1956).

(39) (a) From eq 3 we find $A_{||}/A_{\perp} = (h\alpha + 2\beta)(h\alpha - \beta)^{-1}$. With this expression, it is readily shown that any attempt to fit the data to the sp^3 case by varying the value of $|\psi(0)|^2$ over a reasonable range will automatically result in a better fit for the sp^2 case. For example, if SCF wave functions without configuration interaction^{39b} are used, a 10% increase in $A_{||}$ is required to fit the sp^3 ratio, but only a 2% increase is needed to fit the sp^2 case. In this discussion, we are assuming the major errors occur in $A_{||}$ and $|\psi(0)|^2$ since A_{\perp} is obtained from measurements on well resolved lines while $\langle r^{-3} \rangle$ is computed from experimental data. (b) F. W. Brown, J. H. Bartlett, Jr., and C. G. Dunn, *Phys. Rev.*, **44**, 296 (1933).

(40) A. H. Silver and P. J. Bray, *J. Chem. Phys.*, **29**, 984 (1958).

of the fourth bond.³ An independent estimate of this effect can be obtained if it is assumed that the electronegativity difference of the two hybrids is proportional to the shortening of the equilibrium bond length relative to the "normal" covalent radii.⁴¹ X-Ray studies of the $\text{Na}_2\text{O}-\text{B}_2\text{O}_3$ system⁴² have shown that the B-O distance increases from 1.39 to 1.48 Å as the boron coordination changes from three to four. The ratio of these two distances is 0.94, which is in agreement with the value of 0.86 obtained from the ratio of the ζ values.

The closeness of the agreement is probably coincidental; more significant is the fact that the difference in the hyperfine parameters is in the right direction and of the correct order of magnitude. The difference in the g values is in the wrong direction to be explained in terms of electronegativity. (The expected trend in these parameters is discussed more fully later in this section.) This contradiction may not be significant, for the difference is small and the error in measuring g for both cases may be relatively large.

No attempt will be made to attach significance to the absolute magnitude of ζ . At the present time, the available theory is inadequate to explain this quantity completely in terms of bond parameters.⁴³

The oxygen atom involved must either be in a nonbridging position or bridging the trigonal boron to a silicon atom. A bridge between two trigonal borons would result in a total nuclear spin of 3. A bridge between a trigonal and tetrahedral boron would give the hyperfine parameters for the latter case. Both of these possibilities are contrary to the experimental evidence. If the oxygen is nonbridging, then prior to irradiation it probably existed as part of a hydroxyl group. The effect of the γ radiation might be to remove the hydrogen leaving the paramagnetic defect. This hypothesis concerning the removal of the cation by irradiation has previously been suggested to account for the color centers observed in smoky quartz.⁴⁴

The question of the bridging or nonbridging nature of the oxygen could be resolved in principle, at least, if the orientation of the principal axes of the g tensor relative to the B-O bond axis was known. This information is not obtained in experiments using glasses, and therefore an independent check of the validity of the seven-electron B-O bond model is not possible. That this model is at least consistent with the results reported above, *i.e.*, $g_{\parallel} > g_{\perp} = g_e$, can be shown by the following calculation.

The boron contribution to the molecular orbital describing the B-O bond is expected to be small as judged from the (relatively) small hyperfine coupling constants experimentally determined. In the follow-

ing, this contribution will be neglected. The problem then becomes one involving seven electrons in the four oxygen 2s, 2p levels. The four levels are described by arbitrary linear combinations suitably orthonormalized

$$\varphi_k = a_{k1}S + a_{k2}P_x + a_{k3}P_y + a_{k4}P_z$$

For the ground state, the antisymmetrized product wave function

$$|4, \sigma\rangle = \mathcal{A}(\varphi_1\alpha, \varphi_1\beta, \dots, \varphi_4\sigma)$$

is chosen. In the ket vector, the integral indicates in which of the φ_k orbitals the odd electron (with spin σ) is located. Excited states are described by antisymmetrized products with the hole transferred to one of the other orbitals.

With these wave functions, the shift of the g tensor from the free-electron value is given to first order by the expression⁴⁵

$$\Delta g_{ij} = -\lambda \sum_n \frac{\langle 0|L_i|n\rangle \langle n|L_j|0\rangle}{E_n - E_0}$$

where λ is the spin-orbit coupling constant of the hole, $|0\rangle$ is the ground-state wave function, and the summation is taken over all the excited states $|n\rangle$. The magnitude of the energy differences to the excited states is unknown. As a first approximation, they may be taken to be equal. The results would then be valid to the extent that the ratios of all pairs of the ΔE_n values are ~ 1 . A straightforward computation of Δg_{ij} then shows that, in the principal axis system, the g shift has two values equal to zero and a third value greater than zero. Since $\lambda < 0$, the seven-electron model is consistent with the experimental results insofar as the approximations used above are valid.

A comparison of the results for the g tensor in porous glass and in sodium borosilicate glass (Table I) indicates that the oxygen spin-orbit effects are little influenced by the boron hybridization. This lends credence to the discussion of the defect in terms of a simple B-O bond.

Also included in Table I are the data for the Al-O defect in irradiated smoky quartz. In the latter case, it was suggested that the paramagnetic effects were due to a hole trapped on an oxygen atom integral to an AlO_4 tetrahedral unit. It is noted that the

(41) V. Schomaker and D. P. Stevenson, *J. Am. Chem. Soc.*, **63**, 37 (1941); H. O. Pritchard and H. A. Skinner, *Chem. Rev.*, **55**, 745 (1955).

(42) J. Biscoe and B. E. Warrer, *J. Am. Ceram. Soc.*, **21**, 287 (1938).

(43) H. S. Jarett, *Solid State Phys.*, **14**, 215 (1963).

(44) M. C. M. O'Brien, *Proc. Roy. Soc. (London)*, **A231**, 404 (1955).

(45) M. H. L. Pryce, *Proc. Phys. Soc. (London)*, **A63**, 25 (1950).

Table I: Experimental Values of the Spin-Hamiltonian Parameters for Three Types of Related Materials

| Bond | Proposed metal hybridization | $g_{ }$ | g_{\perp} | $A_{ }$, cm ⁻¹ | A_{\perp} , cm ⁻¹ | Ref |
|------|------------------------------|----------|-------------|--------------------------------|-----------------------------------|-----------|
| B-O | sp ² | 2.0100 | 2.0023 | 1.40×10^{-3} | 1.25×10^{-3} | This work |
| B-O | sp ³ | 2.0121 | 2.0024 | 1.59×10^{-3} | 1.31×10^{-3} | 5 |
| Al-O | sp ³ | 2.06 | 2.00 | 4.8×10^{-4} | 5.6×10^{-4} | 44 |

Al-O defect exhibits a greater g shift and a lower hyperfine coupling relative to the B-O defect. Interdependence of the hyperfine and g tensors has previously been noted in the covalent transition metal complexes.^{33,37a} With these materials, the effect was explained by introducing covalent effects in terms of the degree of mixing of ligand orbitals with the orbitals of the central ion in the LCAO-MO approximation. The theoretical treatment of the problem^{43,46} is more complex than first proposed, but in compounds exhibiting large covalent effects, the existence of a correlation between the magnetic parameters and the degree of covalency seems established.⁴⁷ This correlation shows that the isotropic g value increases and the isotropic hyperfine coupling constant decreases with increased ionic character of the bond. On the basis of the electronegativity differences, the B-O and Al-O bonds should possess 44 and 63% ionic character, respectively. The results given in Table I are in agreement with this correlation based on the isotropic parameters.

A comparison of the principal values of the hyper-

fine tensor shows a disagreement in that $|A_{||}| > |A_{\perp}|$ for the B-O defect but the reverse for the Al-O case. This disagreement can be explained in terms of the direction of the metal sp hybrid involved.⁴⁴ In the B-O case, the hybrid orbital is taken parallel to the bond axis; in the Al-O case, it is chosen orthogonal to the axis.⁴⁴ This difference suggests that the relative importance of the two mechanisms which contribute to the hyperfine interaction is different in the two cases.^{43,48} Such a result would not be unexpected, for the aluminum and boron cases differ in the principal quantum number, interatomic distance, and the availability of d orbitals.

Acknowledgment. The author wishes to thank Dr. M. T. Melchior for several helpful discussions and suggestions concerning certain aspects of this problem.

(46) K. DeArmond, B. B. Garrett, and H. S. Gutowsky, *J. Chem. Phys.*, **42**, 1019 (1965).

(47) D. Kivelson and R. Nieman, *ibid.*, **35**, 149 (1961).

(48) C. Keffer, T. Oguchi, W. O'Sullivan, and J. Yamashita, *Phys. Rev.*, **115**, 1553 (1959).

Electron Spin Resonance Studies of γ -Irradiated High Surface Area

Silica. II. Effect of Adsorbed Molecules

by G. M. Muha and D. J. C. Yates

Esso Research and Engineering Company, Linden, New Jersey (Received August 2, 1965)

Electron spin resonance techniques have been used to study the effect of added gases on the paramagnetic defects introduced in a high surface area silica by γ -irradiation. A previous study has established the relationship between these defects and the lines observed in the esr spectrum of the irradiated solid. Hydrogen, deuterium, and methanol are chemisorbed at well-defined sites. The possible reactions involved are discussed. Carbon monoxide is chemisorbed to give one of two paramagnetic products depending on previous surface treatment. The sites for carbon monoxide adsorption are not observed in the esr spectrum of the irradiated silica before gas addition. Oxygen, nitric oxide, ammonia, ethylene, and acetylene do not affect the esr spectrum. The absence of an effect with the first two gases listed suggests that the sites observed by esr, under our experimental conditions, are located in the bulk of the material.

I. Introduction

The effect of ionizing radiation on the physical and chemical properties of high surface area solids has received considerable attention in recent years.¹ Usually, marked changes in the surface properties and chemical activity are observed. These changes are explained in terms of concepts developed from radiation-damage studies in crystalline solids, such as lattice vacancies, interstitial atoms and ions, trapped electrons, and holes. One objective of these studies has been to develop an understanding of the relationship between radiation-induced defects and the active sites responsible for the change in adsorption properties and catalytic activity. In this connection, it has been suggested² that, in a broad sense, two types of mechanisms may be distinguished. The first involves direct chemical interaction with one of the radiation-induced defects. The second involves sites present before, and structurally unmodified by irradiation, which however exhibit a change in their activity after the radiation treatment. The latter activation process might occur because of the introduction of local variations in the Fermi level^{3,4} due to the presence of nearby defects.

In the case of high surface area oxides, a variety of physical methods have been used to study these

effects: for example, adsorptive capacity,^{2,5} hydrogen-deuterium exchange,^{2,6} infrared,⁷ and electron spin resonance.⁸⁻¹⁴ Of the various methods, esr has received the most attention to date, presumably because of its high sensitivity and ability to observe paramagnetic species whether in the adsorbate or adsorbent.

- (1) E. H. Taylor, *Nucleonics*, **20**, 53 (1962).
- (2) H. W. Kohn and E. H. Taylor, *Actes Congr. Intern. Catalyse, 8^e, Paris, 1960*, 1461 (1961).
- (3) F. F. Vol'kenshtein, "The Electronic Theory of Catalysis on Semiconductors," The Macmillan Co., New York, N. Y., 1963.
- (4) M. Boudart, *J. Am. Chem. Soc.*, **74**, 1531 (1952).
- (5) D. B. Rosenblatt and G. J. Dienes, *J. Catalysis*, **4**, 271 (1965).
- (6) H. W. Kohn and E. H. Taylor, *ibid.*, **2**, 32 (1963); *J. Phys. Chem.*, **63**, 500, 966 (1959).
- (7) D. J. C. Yates and P. J. Lucchesi, *J. Am. Chem. Soc.*, **86**, 4258 (1964).
- (8) H. W. Kohn, *J. Chem. Phys.*, **33**, 1588 (1960).
- (9) V. B. Kazansky, G. B. Pariisky, and V. V. Voevodsky, *Discussions Faraday Soc.*, **31**, 203 (1961).
- (10) P. H. Emmett, R. Livingston, H. Zeldes, and R. J. Kokes, *J. Phys. Chem.*, **66**, 921 (1962).
- (11) G. K. Boreskov, V. B. Kazansky, Yu. A. Mishchenko, and G. B. Pariisky, *Dokl. Akad. Nauk SSSR*, **157**, 384 (1964).
- (12) G. B. Pariisky and V. B. Kazansky, *Kinetika i Kataliz*, **5**, 93 (1964).
- (13) D. N. Stamires and J. Turkevich, *J. Am. Chem. Soc.*, **86**, 757 (1964).
- (14) J. H. Lunsford, *J. Phys. Chem.*, **68**, 2312 (1964).

The present work derived from a previous infrared study⁷ of ethylene adsorbed on γ -irradiated porous glass. In that work, it was reported that, with certain types of samples, ethylene would chemisorb only if the glass had been previously irradiated. Also, as mentioned in that study, esr studies with the same samples could not distinguish any effect of the ethylene on the esr spectrum although pronounced effects were observed with other gases. The present paper is a more detailed report of these observations. We have found examples in which it is possible to (a) differentiate between direct chemical and physical interactions at a previously well-characterized radiation-induced defect and (b) observe the appearance of a new paramagnetic species forming at some site(s) not directly observable by esr. This new species is not formed in the absence of radiation treatment.

In the preceding paper¹⁵ (hereafter referred to as I), an analysis of the esr spectrum of the γ -irradiated porous glass is presented. Three distinguishable paramagnetic defects were identified: (a) an electron trapped on a silicon atom with at least one oxygen atom missing (Si site), (b) a hole trapped predominantly on an oxygen atom bonded to a trigonally coordinated boron atom (B-O site), and (c) a hole trapped in the Si-O network (Si-O site). Defects b and c are thought to be formed by the removal of a hydrogen atom from a hydroxyl group. A high-field line is observed in the esr spectrum which is not explained by the three defects listed above. For purposes of this paper, it is sufficient to note that the behavior of the defect responsible for this line is identical with that of the Si site described above. A more detailed discussion of this parallel behavior is given in part I.

II. Experimental Section

The porous glass used in these experiments was obtained from the Corning Glass Co. It had major chemical components of SiO₂ (96.2%), B₂O₃ (3%), R₂O₃-RO₂ (0.7%), and sodium (50 ppm). Porous glass (Corning 7930) normally contains ~0.5% Na₂O. The material used in these experiments was a special type kindly supplied by Dr. M. E. Nordberg, Corning Glass Co., Corning, N. Y. It differs from the Corning 7930 in that it received a more extensive acid leaching. Throughout the present paper, the term acid leached refers to a further acid treatment in our laboratory.⁷ The term unleached glass refers to the material "as received."

The samples were of the same lot and received the same chemical pretreatment (leaching with 1 *N* nitric acid) and radiation dosage (between 20 and 60 Mr) as those described in the infrared work.⁷ Over the

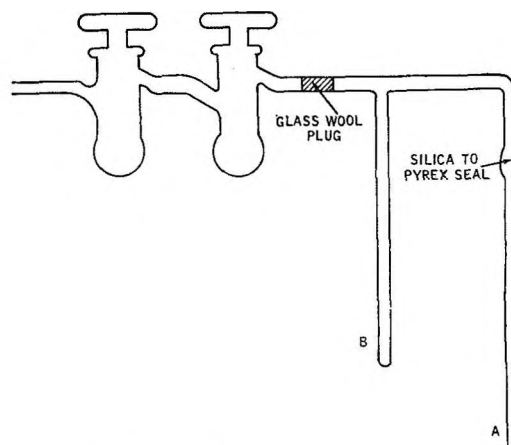


Figure 1. Silica-Pyrex cell.

range of radiation dosage used in these experiments, the strength of the esr lines increased with increasing dosage.

The radiation treatment induced an intense, narrow esr signal in the fused-quartz sample cell which was identical with the Si-site line observed in porous glass. It was removed by thermal bleaching at 550° for 30 min. This bleaching treatment necessitated the use of a special sample cell design (Figure 1) to attain reproducibility in the spectra after irradiation and before any gases were added. The double stopcocks were found necessary to maintain a good vacuum in the cell under radiation conditions. The cell was continuously evacuated during the bleaching of side arm A, the sample having previously been transferred to side arm B. With this treatment, the intensities were found to be reproducible for periods in excess of 45 days. If the stopcocks were opened to the atmosphere, all signals disappeared rapidly (<20 min).

The sample was in the form of chips and coarse powder of such dimensions as to fit in the 4-mm i.d. fused-silica tube (side arm A). Sufficient gas was added in all cases to ensure saturation of the surface as shown by a residual gas pressure in the cell of 1-10 cm. The vacuum system and gases used were the same as described previously.⁷ The esr equipment and spectrum calibration techniques used are given in part I. The radiation treatment and subsequent sample storage were at room temperature.

III. Results and Discussion

A. Hydrogen and Deuterium Experiments. The pronounced effect of hydrogen and deuterium on the esr spectrum of the irradiated glass is shown in Figure 2. It is seen that the group of five lines (B-O sites)

(15) G. M. Muha, *J. Phys. Chem.*, **70**, 1390 (1966).

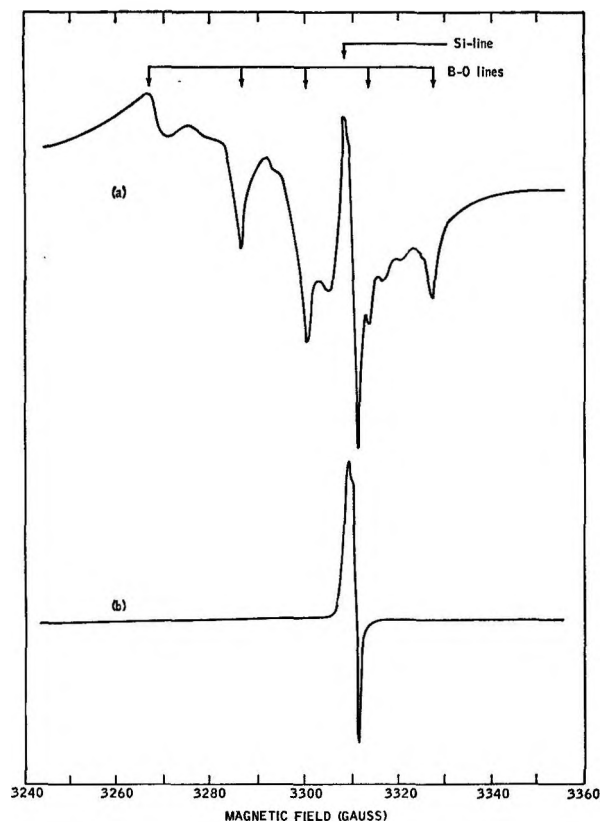


Figure 2. ESR spectrum of irradiated porous glass (a) before gas addition and (b) after addition of hydrogen. The lines arising from the Si sites and B-O sites are indicated above spectrum a. The Si-O sites give rise to the broad background observed in spectrum a.

and the broad background (Si-O sites) have been removed, while the sharp asymmetric line (Si sites) is unchanged. The effect is not reversible in the sense that pumping out the hydrogen does not bring back the lost lines. An effect not noted in Figure 2 is a change of sample color from the reddish violet of the irradiated state to the translucent white of the unirradiated state. It is of interest to note that the color disappeared very rapidly (<1 sec) with hydrogen but took slightly longer (3-5 sec) with deuterium.

If the irreversible nature of this process is taken to imply that strong chemisorption is involved, then the observed esr effect may be explained in terms of a reaction between the hole trapped on oxygen and the added hydrogen to form a hydroxyl group. It is clear that this result would be expected from the chemistry of the situation. Moreover, it is simply the reverse of the manner in which these defects are thought to be formed. A schematic illustration of the proposed situation is given in Figure 3. This same hypothesis of hydroxyl formation was previously suggested to explain some results with silica gel² although in that case no

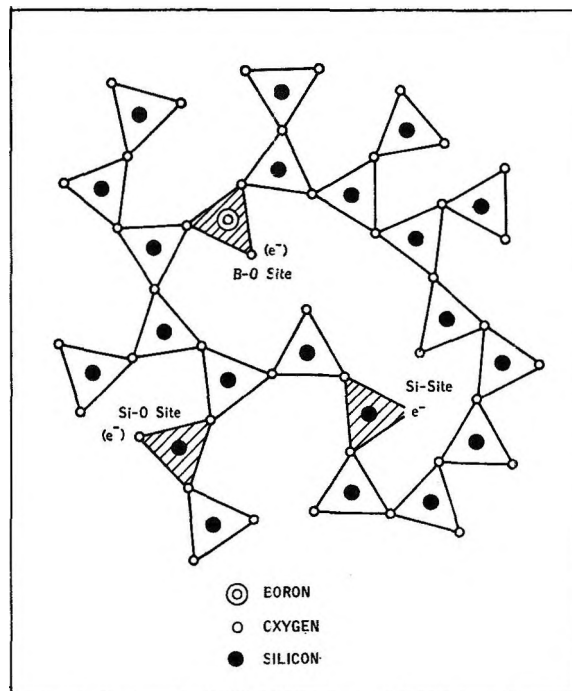


Figure 3. Schematic representation of three proposed defects (shaded) in irradiated porous glass. For clarity, all defects are shown in nonbridging positions although evidence on this point is not directly obtainable from the present experiments. The symbol e^- represents an unpaired electron; the symbol (e^-) represents a trapped hole.

direct evidence concerning the nature of the sites was available.

Some consideration must be given to the remaining hydrogen atom since only one from each molecule is used to form a hydroxyl group. Presumably, it could give the characteristic hyperfine splitting observed at 77°K in irradiated, highly divided solids⁸⁻¹⁰ and at room temperature in bulk fluorides.¹⁶ No such hyperfine splitting was observed with our samples after adding hydrogen at room temperature. This effect is probably due to the remaining hydrogen atoms having reacted with some other defects or impurities. This type of chemical interaction between diffusing molecules and trapped species has been observed at high temperatures in unirradiated fused quartz.¹⁷

The explanation of the results has so far been considered in terms of a chemical reaction. Alternatively, it might be desirable to describe the results in terms of the electronic band structure of the solid with the trapped holes acting as acceptor levels in the forbidden

(16) J. L. Hall and R. T. Schumacher, *Phys. Rev.*, **127**, 1892 (1962); B. Welber, *ibid.*, **136**, A1408 (1964).

(17) R. W. Lee, R. C. Frank, and D. E. Swets, *J. Chem. Phys.*, **36**, 1062 (1962); R. W. Lee, *ibid.*, **38**, 448 (1963).

gap and the incoming hydrogen as the electropositive donor filling the level.^{3,4} In this application of the band theory approximation, the antibonding and bonding combinations of the silicon-oxygen wave functions make up the conduction and valence bands, respectively. The two oxygen nonbonding orbitals are located within the forbidden gap and are normally full. Radiation removes an electron from one of these orbitals leaving a hole.

B. Oxygen, Nitric Oxide, Nitrogen, and Ammonia Experiments. In contrast with the marked effects noted in the case of hydrogen addition, the spectrum of the irradiated solid at room temperature was unaffected by the addition of oxygen, nitric oxide, nitrogen, or ammonia. The negative results for oxygen and nitric oxide are considered remarkable in light of the usual effects of these paramagnetic gases on esr spectra. These effects may be approximately separated into two types,¹⁸ collision broadening and quasi-chemical reactions. In the former case, the esr line broadens such that the total integrated intensity remains constant. Reported examples include the effect of oxygen on silicon surfaces¹⁹ and γ -irradiated zeolites.¹³ In the quasi-chemical reaction case, the line decreases in height at constant relative width; examples have been found in the study of pyrolyzed carbons.¹⁸

In the present study, upon adding oxygen, both a line broadening of the B-O lines and a true chemical effect at the Si-site lines were expected. The latter would arise by the filling of the oxygen vacancy associated with the Si sites. Examples illustrating these effects have been reported. Instances are the formation of the Si-A center in irradiated silicon single crystals²⁰ and the effect of oxygen on irradiated silica gel⁸ at room temperature. The absence of these effects in porous glass might occur if the defects were located in the bulk of the solid sufficiently far away from the surface so that a negligible quantity of oxygen or nitric oxide could diffuse in. In agreement with this, it is of interest to note that one of the defects in γ -irradiated zeolites is not affected by oxygen addition.¹³ It should be stressed that the above observation is not inconsistent with the rapid reaction of H₂ and D₂. These latter gases can rapidly diffuse in silicas over the largest distances involved in porous glass (30 Å).

The reactivity of the porous-glass sites in the absence of vacuum precluded the direct testing of the idea that these defects are not located on the surface. As an alternative, the chemical reactivity toward oxygen of the Si site in a nonporous piece of fused quartz was determined. An irradiated section of the fused-quartz tube that had not been thermally bleached was subjected to 500 lb of oxygen pressure at room tem-

perature for 30 min. Before the oxygen treatment, the cell gave an esr line essentially identical with that from the Si site in porous glass. Immediately after the oxygen treatment, the esr line was totally absent; on standing for 20 min at room temperature in the atmosphere, the line returned to nearly its initial intensity with no change in line shape. The conclusion drawn from this experiment is that the principal effect of oxygen under these conditions is to give a collision broadening of the esr line.²¹

The reason for the absence of a reaction between the added oxygen and the Si site in the fused quartz is unknown. The evidence for the description of the Si site as an oxygen vacancy is very strong. It is based on results with a wide variety of glasses and single-crystal samples.²² The absence of a chemical reaction might be explained in terms of the inaccessibility of the site to oxygen molecules, the possibly unfavorable kinetics of the reaction between the oxygen molecules and the site, or both. In the case of porous glass, the extreme lability of these samples on exposure to the atmosphere suggests that the hydroxyl group is an important factor in any discussion of this effect. Hydroxyl groups are suggested since oxygen and nitrogen have no effect, leaving water vapor as the remaining major atmospheric component. A dependence of the esr intensity on the *preirradiation* concentration of hydroxyl groups in the sample has been reported for a series of fused silicas.²²

C. Ethylene and Acetylene Experiments. The room temperature addition of ethylene or acetylene produced no observable effect on the esr spectrum of the irradiated samples, whether the glass had been previously acid leached or not. These results were unexpected, as an infrared study⁷ of the same material under identical conditions of pretreatment had shown that ethylene was strongly adsorbed and polymerized to form products containing up to 13 carbon atoms. The polymerization was thought to proceed through a free-radical mechanism because of the observed inhibiting effects of nitric oxide and oxygen. The addition of nitric oxide or oxygen to the ethylene-containing samples also showed no effect on the esr spectrum.

The failure to observe a signal from the polymerizing radical would have to be explained in terms of a line-

(18) D. J. E. Ingram, "Free Radicals as Studied by Electron Spin Resonance," Butterworth and Co. Ltd., London, 1958, p 210.

(19) K. A. Müller, P. Chan, R. Kleiner, D. W. Ovenall, and M. J. Sparnaay, *J. Appl. Phys.*, **35**, 2254 (1964).

(20) G. D. Watkins and J. W. Corbett, *Phys. Rev.*, **121**, 1001 (1961).

(21) Some caution in this respect must be exercised as the effect of hydrostatic pressure of gases on γ -irradiated silica has, to our knowledge, not been investigated.

(22) R. A. Weeks and E. Lell, *J. Appl. Phys.*, **35**, 1932 (1964).

broadening mechanism since the sensitivity of the spectrometer was more than sufficient to observe a signal calculated on the basis of the infrared intensities. The modulation amplitude for the experiments was such that a line up to 100 gauss in width would have been observed.

From the absence of any effect on the esr spectrum of the irradiated glass, it is concluded that the chemisorption occurs at some site(s) different from the three identified by esr. To check this point further, ethylene was admitted to a sample that had previously had hydrogen adsorbed. No effect was observed in the esr spectrum. Previous infrared work⁷ showed that this treatment has no effect on the ethylene adsorption.

D. Carbon Monoxide Experiments. The adsorption of carbon monoxide on an acid-leached sample of irradiated porous glass gave birth to a new line which grows to full intensity over a period of ~ 30 min. During this period, the sample color and the intensity of the lines attributed to B-O and Si sites do not appear to change. The broad background line attributed to the Si-O sites decreases to about half of its previous intensity. These results are shown in Figure 4a. After standing for 18 hr (Figure 4b), the new line does not change in intensity or shape. However, the B-O line, the rest of the Si-O line, and the sample color disappear. The integrated intensity of the new line is very much greater than that of the sample before gas addition, but the shape of the line renders quantitative estimation difficult. The line appears to consist of at least four components centered about $g = 2.00$.

A different type of spectrum is obtained if an unleached sample is used (Figure 5a). In this case, the intensity of the new line grows to its final value in ~ 24 hr, but the B-O and Si-O sites are undisturbed. The line from the Si site is obscured by the new line and its fate is not known. The integrated intensity is much greater than in the original sample, but, as opposed to the acid-leached case, the color remains. The line is of the shape expected for an axially symmetric g tensor,²³ and on this basis, the values $g_{\parallel} = 1.995$ and $g_{\perp} = 2.002$ are estimated. These results have been reproduced in at least four samples of each type and appear to be insensitive to most features of sample preparation except for the omission or inclusion of the acid-leaching step.

In both the acid-leached and unleached samples, pumping out the carbon monoxide produced no change in the spectra. However, if hydrogen is then added, the two types of samples behave differently. The spectrum of the leached sample shows no change, but the unleached sample gives a new spectrum (Figure 5b) and changes color to the translucent white of the

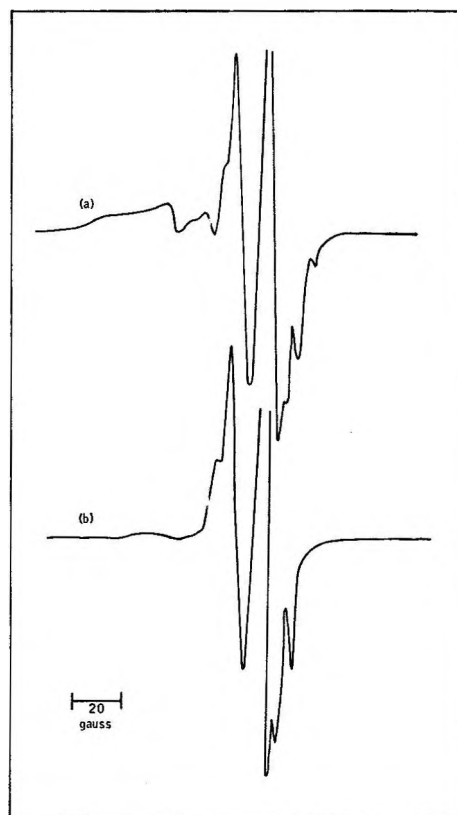


Figure 4. ESR spectrum obtained from a sample containing carbon monoxide adsorbed on acid-leached, irradiated porous glass (a) after 30 min and (b) after 18 hr. The vertical scale is the same in both (a) and (b). The Si site lines in both (a) and (b) have been shortened for clarity.

unirradiated glass. If the order of gas addition is reversed, *i.e.*, hydrogen followed by carbon monoxide, no new line is observed. Only the simple spectrum of Figure 2b is observed. This result is obtained for both the leached and unleached glasses.

At the present time, we can offer no detailed explanation of these results; work is continuing on the problem. However, some general observations can be made. (a) The fact that the color disappears for both leached and unleached glass together with the B-O and Si-O lines suggests that the color may be related to the presence of these defects. (b) The slow disappearance of the B-O and residual Si-O lines in the acid-leached samples after the "carbon monoxide line" has reached full intensity suggests that some additional reactions continue after the adsorption (as observed by esr) is complete. These additional reactions may involve products from the chemisorption which then diffuse to the Si-O and B-O sites to react. (c) The spectrum

(23) J. W. Searl, R. C. Smith, and S. J. Wyard, *Proc. Phys. Soc. (London)*, **A78**, 1174 (1961).

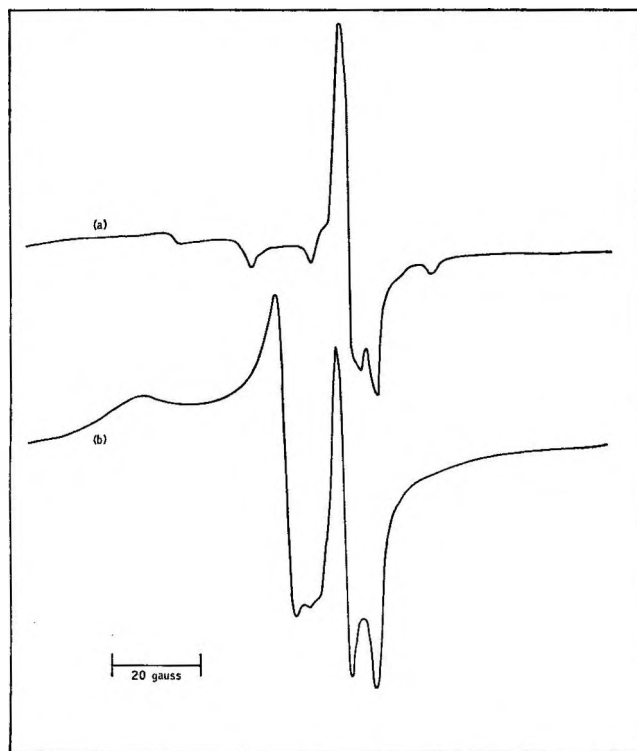


Figure 5. ESR spectrum of carbon monoxide adsorbed on unleached porous glass (a) after 24 hr, followed by (b) pumping off excess carbon monoxide, then adding hydrogen.

obtained from the addition of hydrogen to carbon monoxide on the unleached sample (Figure 5b) does not appear to be related in any simple fashion to the ESR spectrum of the formyl radical produced by the photolysis of hydrogen iodide in solid carbon monoxide.²⁴ (d) The higher intensity of the new line suggests that adsorption or radical generation is occurring at sites not directly observable by ESR. They may be diamagnetic or have too broad a paramagnetic resonance to be observed. These sites are deactivated by hydrogen, at least as far as carbon monoxide adsorption is concerned. This is another example, together with ethylene, of adsorption on a site not detectable by ESR. The adsorption of carbon monoxide may be dependent on some peculiarities of its electronic structure involving the lone electron pair since the isoelectronic nitrogen molecule has no effect.

E. Methanol Experiments. In the results discussed so far, the added gases have affected only the Si-O and B-O sites; direct evidence of any effect at the Si site has not been presented. An example will be discussed in which only the line due to the Si site is affected, all the other features of the spectrum being essentially unchanged.

The addition of methanol vapor to a sample of un-

leached, irradiated porous glass results in a slow decrease in the intensity of the line from the Si site concomitant with a loss in resolution between the parallel and perpendicular component. After 18 hr, a weak, symmetric line (indicated by the arrow in Figure 6) remains, and no further changes are observed. Pumping out the methanol does not change the spectrum, which is interpreted as evidence that chemisorption has taken place. No definite conclusions can be drawn concerning the origin of the residual line as it does not exhibit the anisotropy of the original line.

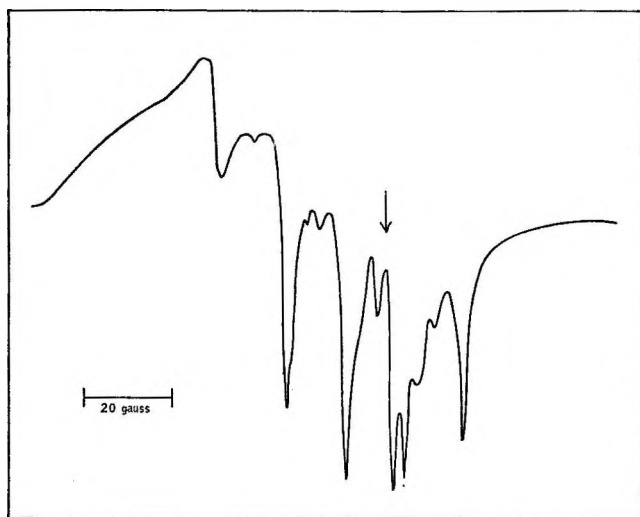


Figure 6. ESR spectrum observed 18 hr after addition of methanol to unleached, irradiated porous glass.

The present experiments do not suggest a unique mechanism for the disappearance of the main part of the line, for at least two possibilities must be considered. First, a direct chemical interaction of methanol with the Si sites may be involved. For example, methyl groups are known to exchange with the surface hydroxyl groups in unirradiated porous glass.²⁵ This seems improbable in the present experiments, as oxygen has no apparent effect on the Si sites. An indirect interaction is probably involved. For example, the methanol could be adsorbed to give a product not detectable by ESR plus other products which could react with the Si sites. This indirect effect would be analogous to the suggested secondary reaction at the B-O and Si-O sites after carbon monoxide adsorption.

The sites for methanol adsorption are probably not

(24) F. J. Adrian, E. L. Cochran, and V. A. Bowers, *J. Chem. Phys.*, **36**, 1661 (1962).

(25) M. Folman and D. J. C. Yates, *Proc. Roy. Soc. (London)*, **A246** 32 (1958).

the same as for carbon monoxide, as will now be shown. The addition of carbon monoxide to a methanol-treated sample results in the same spectrum as found in the absence of methanol (Figure 5a). The addition of methanol to a carbon monoxide-treated sample has no observable effect in the esr spectrum.

The results reported here for the unleached glass have been found reproducible as shown by identical results for three samples from the same batch of glass.

No experiments have yet been made with acid-leached samples.

The variety of results obtained in all of these experiments with irradiated silica depending on such factors as sequence of gas addition, surface preparation technique, secondary reactions, etc., suggest that extreme caution should be exercised in interpreting the results from any one experiment using esr, infrared spectroscopy, or other physical techniques.

Kinetics of the Water-Gas Equilibrium Reaction. I. The Reaction of Carbon Dioxide with Hydrogen

by G. L. Tingey

Battelle Memorial Institute, Pacific Northwest Laboratory, Richland, Washington (Received October 29, 1965)

The kinetics of the reaction of CO₂ with H₂ to form CO and H₂O were determined over the temperature range from 400 to 1050°. The temperature dependence of the rate of reaction suggests two separate reaction paths. One is predominant at temperatures below 800° and the second is predominant above 800°. The effect of CO₂, H₂, CO, and H₂O concentrations on the rate were determined in both temperature regions. The rate of the reaction in units of moles per liter per second can be expressed as the sum of the expressions

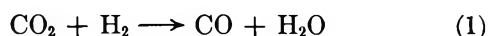
$$\frac{d[\text{CO}]}{dt} = 7.6 \times 10^4 e^{-39,200/RT} [\text{H}_2]^{1/3} [\text{CO}_2]$$

$$\frac{d[\text{CO}]}{dt} = 1.2 \times 10^{13} e^{-78,000/RT} [\text{H}_2]^{1/3} [\text{CO}_2]$$

The effect of a graphite surface was also investigated. No change in rate was observed when the graphite was reasonably pure. However, impurities caused a substantial increase in the rate. A homogeneous mechanism appears to be responsible for the high-temperature reaction and the data agree very well with the rate constants obtained from flame studies. The low-temperature mechanism is apparently due to trace quantities of oxygen in the gas.

Introduction

Carbon dioxide reacts with hydrogen yielding water vapor and carbon monoxide at a significant rate above 500°.



The kinetics of this reaction have been studied by Graven and Long.¹ These authors also reviewed the earlier work. We have investigated this reaction and find results somewhat different from those of Graven and Long. In the present study we have obtained rate data for the reaction under a variety of conditions and have suggested a reaction mechanism compatible with the experimental findings. We have also suggested reasons for the differences in results of this work and those of previous workers.

Experimental Section

Materials. Coleman grade CO₂, pure grade H₂, and CP grade CO were obtained from the Matheson Co. Bureau of Mines Grade A helium was used as a diluent. Each of the gases was analyzed by gas chromatography to determine the impurity levels.

A gas mixture was obtained by metering desired quantities of each gas through calibrated flow meters into the apparatus (see Figure 1). The resultant gas mixture was passed over copper turnings at 300° to remove trace quantities of oxygen. Any water formed over the copper was removed in a trap containing magnesium perchlorate. If the temperature of the copper turnings was above 350°, the copper catalysis of reaction 1 gave a rate which is significant compared

(1) W. M. Graven and F. J. Long, *J. Am. Chem. Soc.*, **76**, 2260, 6421 (1954).

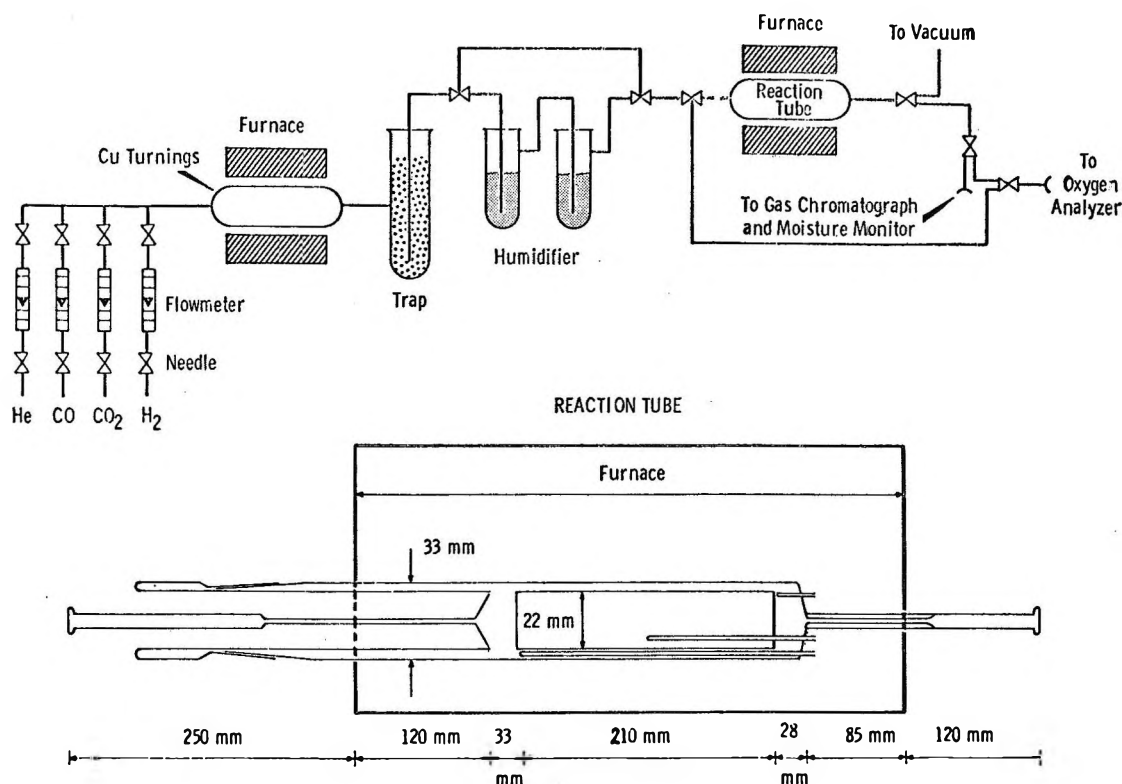


Figure 1. Apparatus.

to the homogeneous rate in the reaction tube. However, if the temperature of the copper turnings was reduced to 300° , the copper-catalyzed rate was negligibly low.

For those experiments in which water vapor was added to the gas mixture, distilled water was placed in the humidifier. Dissolved gases were first removed by bubbling helium through the water for several hours. The water vapor was added to the stream by bubbling the gas mixture through the liquid. The partial pressure of water vapor was taken as the vapor pressure at the temperature of the humidifier bath.

Analysis. The gases were analyzed on a Burrell Model K-7 gas chromatograph. When equipped with a 2.4-m column packed with 5-A molecular sieve and a 3-m column packed with silica gel, this instrument is capable of detecting gases at concentrations as low as 1 or 2 ppm in the gas stream. Above 100 ppm the accuracy is limited to about 3% by the uncertainty in the gas calibrating mixtures. Water vapor in the gas stream was determined by an electrolytic moisture analyzer capable of analyses in the range of 100–10,000 ppm with a precision of about 10%. An electrolytic technique was also used to detect oxygen concentrations as low as 5 ppm.

Nature of the Experiment. In order to cover the wide

range of temperatures desired, it was necessary to use two techniques of investigation: (1) a static technique for temperatures from 400 to 660° , and (2) a flow technique for temperatures above 580° .

For experiments in the static system, the purified gases were mixed in small (~ 8 ml) Pyrex ampoules equipped with break-seals. The ampoules were outgassed at $\sim 450^\circ$ to remove adsorbed gases, then filled with the gas mixture and maintained at the desired temperature in a tube furnace for several hours until the conversion was sufficient for analysis of the carbon monoxide formed.

A schematic diagram of the flow system is shown in Figure 1. The desired gases were metered, mixed, and passed through the purification tube containing copper turnings and into the drying trap. At this point the gas stream could be diverted into a humidifier or passed directly into the reaction chamber.

A detailed diagram of one of the reaction chambers is also shown in Figure 1. This tube was constructed of quartz and was designed to enable a graphite rod 1.9 cm in diameter and 15.2 cm long to be placed inside the chamber. The inlet and outlet tubes were small bore so that they occupied only 1.4% of the total volume of the reaction chamber. The temperature was monitored by three chromel–alumel thermocouples placed

in wells along the reaction zone. The temperature profile in the reaction zone was adjusted by placing shunt wires external to the furnace across the heating coils. In this manner the temperature was maintained constant within $\pm 5^\circ$ along the length of the reaction zone. The reaction chamber contained a quartz cylinder (see Figure 1) so that the gases passed down a 0.5-cm annulus around the cylinder. It is expected that the temperature profile across this small annular distance is easily constant within $\pm 5^\circ$.

The flow in the annulus around the quartz cylinder was well within the laminar region but some turbulence may have occurred at the ends of the cylinder. The linear velocity of the gases for most experiments exceeded 10 cm/sec, so back-diffusion should not be of major concern.

The experiments were designed to determine the rate expressions for the reaction. The order of the reaction with respect to both reactants as well as the effect of products on the rate were studied. The Arrhenius parameters were determined from the reaction rates at temperatures from 400 to 1050°.

The effect of a graphite surface on the reaction rate was determined by placing a sample of nuclear graphite² in the reaction tube. The extent of conversion was maintained at less than 1% in all experiments except those of rate *vs.* contact time and those at the highest temperature studied. The extent of conversion was kept within this limit by adjusting contact time (flow rate) and concentration (helium dilution) as the temperature was varied. The total pressure was maintained at 760 ± 15 torr.

Analyses were attempted for both products in all of the flow experiments. The molar quantity of water vapor was found to be equal, within experimental uncertainty, to that of the CO in every case except those in which one of the products was added initially or when graphite was present. Since the analyses for CO were more precise than those for H₂O, the CO yields were used in the calculation whenever possible.

Results and Discussion

When flow techniques are used, it is difficult to know the reaction time precisely since heat-up times and cool-down times are difficult to establish accurately. In this study, the reaction time was determined from a series of experiments in which the flow rate was varied while the temperature and reactant concentrations were held constant. Figure 2 is a plot of the CO produced as a function of the time required for a molecule of gas to pass through the reaction chamber.

Even though the data are linear, an apparent induction period of 0.3 sec is observed for the larger re-

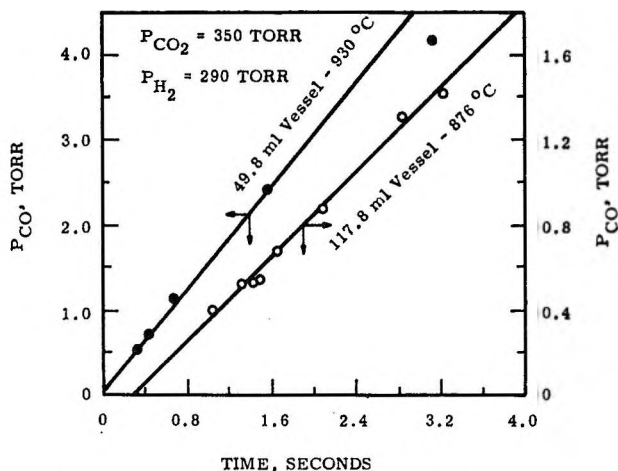


Figure 2. Effect of reaction time on the rate.

action chamber. Graven and Long¹ also reported this induction period and attributed it to the time required to build up the concentration of atoms and radicals. However, since we fail to observe an induction period when a reaction tube about one-half the size and designed for longer preheating is used, it appears more likely that the apparent induction period is due to a combination of heat-up time, cool-down time, and time required to reach steady state. The reaction time used for our calculations was the difference between the total time in the reaction furnace and the induction period observed for that reaction chamber. Since the induction period was small compared to the reaction time, a substantial error in the induction period would not change the results substantially. The scatter in the data may be partially due to changes in the heat-up and cool-down time as the gas composition changes. Helium was used as a diluent to decrease the time required for heating and cooling since it has a high heat conductivity and a low heat capacity.

Another difficulty in determining reaction times when flow techniques in the laminar region are used arises because the gas next to the wall flows at a lower velocity than the gas in the center of the stream. Bosworth³ has treated this phenomenon mathematically for a cylindrical vessel. Initially, the reaction vessel used for our study did not contain the quartz cylinder. The results were widely scattered and not reproducible. However, when the quartz cylinder was

(2) TSX grade nuclear graphite manufactured by Carbon Products Division of Union Carbide Corp. This graphite has an apparent density of 1.70 g/cm³ and an ash content of 2 to 8 ppm. R. E. Nightingale, Ed., "Nuclear Graphite," Academic Press, New York, N. Y., 1962, p 85.

(3) R. C. L. Bosworth, *Phil. Mag.*, **39**, 847 (1948).

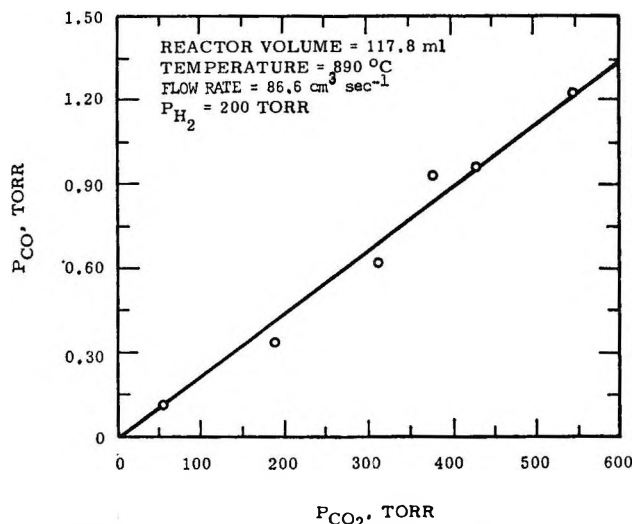


Figure 3. Effect of carbon dioxide concentration on the reaction rate.

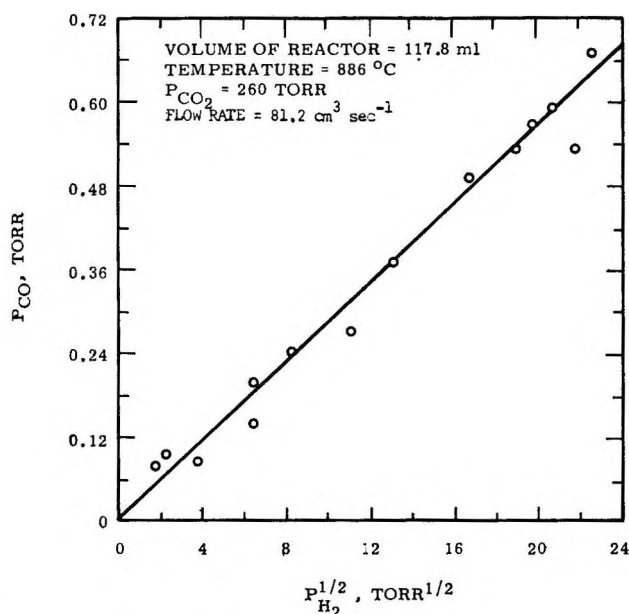


Figure 4. Effect of hydrogen concentration on the reaction rate.

inserted the results improved markedly. Although the flow down the annulus around the cylinder was still well within the laminar region, there was probably turbulent flow at both ends. We were not able to calculate the spread of residence times for our geometry but with an annular distance of only 0.5 cm, diffusion across the annulus may be sufficient to prevent a large concentration gradient.

Experiments were performed to determine the dependence of the rate of product formation on the reactant and product concentrations. Figures 3 and 4

show the results of these experiments. The rate exhibits a first-order dependence upon CO_2 concentration in the range from 50 to 500 torr and a one-half-order dependence upon H_2 in the concentration range from 4 to 500 torr. Figure 5 shows the effect of CO concentration on the reaction rate. These data show an initial inhibition by CO causing a 15% decrease in the rate when the CO pressure is 40 torr with no further decrease in rate with additional CO pressure. In contrast to this, Graven and Long¹ reported a 75% decrease in the rate when the CO pressure was about 120 torr, with no indication of a saturation of the effect. We also studied the effect of H_2O on the reaction rate. Although the data were not nearly so precise when water was added, there was no observable change ($\pm 5\%$) in the rate at pressures of H_2O up to 20 torr.

Since the data shown in Figures 2 through 5 were all taken at temperatures above 800° and give information about mechanism II only, we performed a series of experiments at 775° to determine the rate expression for mechanism I. Although the order with respect to CO_2 was unchanged, the order with respect to H_2 was one-third rather than one-half as found at the higher temperature. Inhibition by CO was also investigated and the relative decrease in rate with increase in CO pressure was approximately the same as that observed at the higher temperature.

The Arrhenius parameters derived from Figure 6 were ascertained from the data over a temperature range from 400 to 1050° . The Arrhenius plot was not linear as we expected; rather there was a definite change of slope at about 800° . The data, however, are fit reasonably well by the addition of two straight lines. We have interpreted this result as an indication of two separate reaction paths occurring simultaneously. One of these reaction paths (hereafter referred to as mechanism I) has a frequency factor of $7.6 \times 10^4 M^{-1/2} \text{sec}^{-1}$ and an activation energy of 39.2 kcal mole⁻¹ and is predominant at lower temperatures. The second path (mechanism II) has a frequency factor of $1.2 \times 10^{13} M^{-1/2} \text{sec}^{-1}$ and an activation energy of 78.0 kcal mole⁻¹ and is predominant at temperatures above 800° .

Effect of Graphite on the Reaction Rate. Long and Sykes⁴ and Ingles⁵ have studied the effect of carbon on the rate of the reverse reaction, $CO + H_2O \rightarrow CO_2 + H_2$. These authors reported a large effect by the carbon, not only on the rate but also on the form of the rate expression. It is apparent that impurities in

(4) F. J. Long and K. W. Sykes, *Proc. Roy. Soc. (London)*, **A215**, 111 (1952).

(5) O. G. Ingles, *Trans. Faraday Soc.*, **48**, 706 (1952).

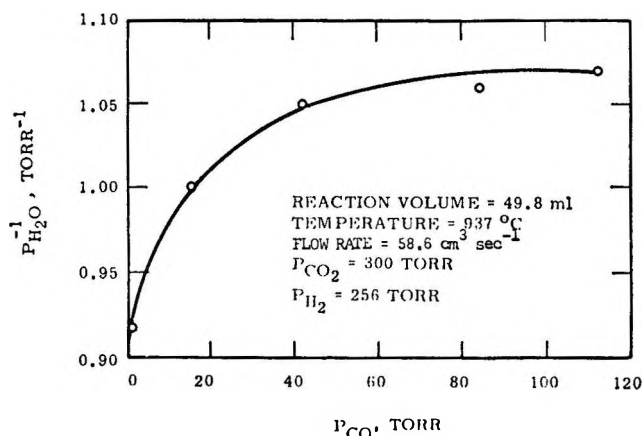


Figure 5. Effect of carbon monoxide concentration on the reaction rate.

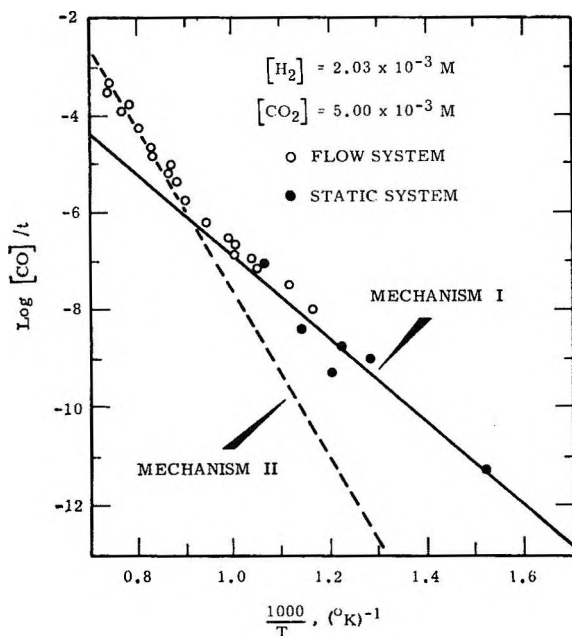


Figure 6. Effect of temperature on the reaction rate.

the carbon play a major role in the catalysis since different carbon samples affected the rate differently.

We have studied the effect of TSX nuclear grade graphite² on the kinetics of the reaction of CO₂ with H₂. When the graphite sample was handled with care to prevent contamination of its surface, the rate was the same as that observed in the absence of graphite. The graphite rod was slightly oxidized by the CO₂ as indicated by larger quantities of carbon monoxide than water in the effluent gas. However, there was no significant difference in the rate of water formation from that found when the graphite was not present. However, if the graphite becomes slightly contaminated by touching with bare hands or by machining,

a substantial enhancement of the rate is observed. This study indicates that impurities are responsible for any catalytic effect observed, and that if the graphite sample is reasonably free of impurities no change in the rate is found.

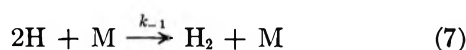
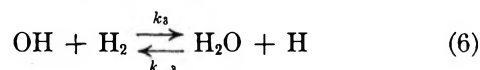
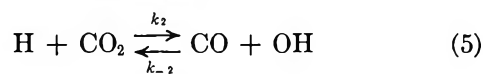
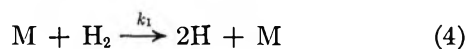
Mechanistic Considerations. If one neglects the small inhibition observed when CO is added to the gas mixture, the rate for the total reaction is the sum of the following equations, (1) the low-temperature process (mechanism I)

$$\frac{d[\text{CO}]}{dt} = \frac{d[\text{H}_2\text{O}]}{dt} = 7.6 \times 10^4 e^{-39,200/RT} [\text{H}_2]^{1/2} [\text{CO}_2] \quad (2)$$

and (2) the high-temperature process (mechanism II)

$$\frac{d[\text{CO}]}{dt} = \frac{d[\text{H}_2\text{O}]}{dt} = 1.2 \times 10^{13} e^{-79,000/RT} [\text{H}_2]^{1/2} [\text{CO}_2] \quad (3)$$

The most widely accepted mechanism, first suggested by Bradford,⁶ is



If the concentrations of OH and H are assumed to be in a stationary state, the rate from this mechanism is given by

$$\frac{d[\text{CO}]}{dt} = \left(\frac{k_1}{k_{-1}} \right)^{1/2} [\text{H}_2]^{1/2} \times \left[\frac{k_2 k_3 [\text{H}_2] [\text{CO}_2] - k_{-2} k_{-3} [\text{CO}] [\text{H}_2\text{O}]}{k_{-2} [\text{CO}] + k_3 [\text{H}_2]} \right] \quad (8)$$

Kaskan and Browne⁷ have reviewed the literature on the kinetics of several reactions including 4 through 7 above. They suggest the following values for the rate constants

$$k_1 = 3.6 \times 10^{15} T^{-0.82} e^{-103,200/RT} \quad (M^{-1} \text{ sec}^{-1})$$

$$k_2 = 2.7 \times 10^{14} T^{-0.79} e^{-30,700/RT} \quad (M^{-1} \text{ sec}^{-1})$$

$$k_{-2} = 3.2 \times 10^9 e^{-6300/RT} \quad (M^{-1} \text{ sec}^{-1})$$

(6) B. W. Bradford, *J. Chem. Soc.*, 1557 (1933).

(7) W. E. Kaskan and W. G. Browne, Report R64SD37, Space Science Laboratory, General Electric Co., July 1964.

$$k_3 = 6.3 \times 10^{10} e^{-5900/RT} \quad (M^{-1} \text{ sec}^{-1})$$

$$k_{-3} = 2.4 \times 10^{11} e^{-20,700/RT} \quad (M^{-1} \text{ sec}^{-1})$$

$$k_{-1} = 5.0 \times 10^{12} T^{-1} \quad (M^{-2} \text{ sec}^{-1})$$

In the present study with an average pressure of CO_2 and H_2 of 250 torr and the pressure of CO and H_2O not exceeding 1 torr, the ratio

$$\frac{k_2 k_3 [\text{CO}_2] [\text{H}_2]}{k_{-2} k_{-3} [\text{CO}] [\text{H}_2\text{O}]}$$

calculated from the rate constants suggested by Kaskan⁷ varies from about 10^4 at 400° to 10^5 at 900° . Equation 8 can therefore be simplified to yield

$$\frac{d[\text{CO}]}{dt} = \left(\frac{k_1}{k_{-1}} \right)^{1/2} \frac{k_2 [\text{H}_2]^{1/2} [\text{CO}_2]}{1 + \frac{k_{-2} [\text{CO}]}{k_3 [\text{H}_2]}} \quad (9)$$

Furthermore, in the temperature range of interest here, $k_{-2}/k_3 \sim 0.04$. Therefore, no observable inhibition by CO is predicted until the CO/H_2 ratio is 2 to 3, and a ratio of 25 would be required to decrease the rate by a factor of 2. Therefore, for application to the present study, eq 9 can be further simplified

$$\frac{d[\text{CO}]}{dt} = \left(\frac{k_1}{k_{-1}} \right)^{1/2} k_2 [\text{H}_2]^{1/2} [\text{CO}_2] \quad (10)$$

This expression is of the same form as eq 3, the experimentally observed rate at the higher temperatures.

If the specific rate constant is calculated for this mechanism from the values given in Kaskan's review,⁷ the following result is obtained

$$\left(\frac{k_1}{k_{-1}} \right)^{1/2} k_2 = 7.2 \times 10^{15} T^{-0.70} e^{-82,300/RT} \quad (11)$$

In the temperature range from 600 to 1050° , this expression is very nearly equivalent to

$$5.0 \times 10^{12} e^{-80,600/RT} \quad (12)$$

The calculated activation energy (80.6 kcal/mole) is surprisingly close to the observed value (78.0 kcal/mole). The value of the observed preexponential term (1.2×10^{13}) is also reasonably close to the calculated value (5×10^{12}).

Equation 8 is derived from Bradford's⁶ mechanism assuming a stationary state for H and OH . However, an estimate⁸ of the time required to reach steady state by the homogeneous rate, k_1 , shows that it is at least of the same order as the total reaction time and, therefore, this assumption may not be valid. On the other hand, the data shown in Figure 2 indicate that the steady state is reached in not more than 0.3 sec

compared with the estimated time of several seconds. It seems probable, therefore, that some other initiation reaction is involved in the mechanism, at least in the early stage of the reaction. One possible initiation reaction to be considered is the dissociation of H_2 on the vessel surface. Although we have not specifically studied surface effects, Graven and Long¹ failed to find an enhancement of the rate by increasing the surface areas. However, in their studies the rates were increased, possibly by an initiation process involving O_2 which may have masked any effect of surface area.

Other processes of initiation may be proposed which involve impurities in the gas stream. However, since the one-half order dependence on H_2 concentration is observed, it appears that the impurity must be effective only in rapidly bringing the system to a stationary state and then the homogeneous dissociation of H_2 controls the rate.

We have attempted to treat the kinetics without assuming stationary-state conditions by computer techniques but have not yet been successful. A comparison of the results obtained in this work and that of Graven and Long¹ is given in Table I.

Table I: Kinetic Parameters for Mechanism II

| | This work | Graven and Long ¹ | Calcd from ref 7 |
|--|----------------------|------------------------------|----------------------|
| Rate, $M \text{ sec}^{-1}$ | | | |
| 900° | 3.6×10^{-2} | 10.8×10^{-2} | 2.4×10^{-2} |
| 1050° | 1.6 | 1.6 | 1.2 |
| E^* , kcal/mole | 78 | 56 | 80.6 |
| Preexponential factor, $M^{-1/2} \text{ sec}^{-1}$ | 1.2×10^{13} | 2.9×10^9 | 5.0×10^{12} |

Low-Temperature Mechanism. Although we have not studied the low-temperature reaction in sufficient detail to suggest a specific mechanism, a few comments about the mechanism are in order. The reaction in this region appears to be first order in CO_2 and somewhat less than one-half order in H_2 . It appears likely that mechanism I may involve the surface of the vessel or an impurity in the gas stream.

Other workers^{1,9} have suggested that the reaction rate is strongly affected by O_2 . We briefly investigated the rate of the reaction as a function of the

(8) S. W. Benson, "The Foundation of Chemical Kinetics," McGraw-Hill Book Co., Inc., New York, N. Y., 1960, p 53.

(9) G. Hadman, H. W. Thompson, and C. N. Hinshelwood, *Proc. Roy. Soc. (London)*, **A137**, 57 (1932).

oxygen concentration and found a very large acceleration in the rate. At 790° the rate was increased by a factor of 22 when the amount of O₂ was increased from less than 5 ppm to 11 ppm. At 950°, the rate increased by a factor of about 5 or 6 for the same increase in O₂. Since the reaction is strongly affected by small concentrations of O₂, it is possible that low-temperature results were affected by O₂ even though the gas mixtures contained less than 5 ppm. The mechanism involving O₂ is probably very complicated and we will not speculate on its specific nature in this paper.

Correlations with Other Work. Although the form of the rate expression for mechanism II is not greatly different from that found by Graven and Long,¹ there are significant differences in the rates and in the activation energy. A comparison of the results obtained in this work and that of Graven and Long¹ is given in Table I. The rate reported by Graven and Long is about four times that which we observed at 850°. At 1050° the respective rates are approximately equal. In addition, they reported an activation energy of 56 kcal/mole compared to 78 kcal/mole which we observed in the same temperature region. The differences in the data could be explained if the oxygen

concentration were about 6 to 8 ppm higher in the gases used by Graven and Long than by ourselves. The rate would therefore be higher at temperatures where the oxygen-accelerated reaction contributes significantly to the total rate. An activation energy midway between the high-temperature and low-temperature values observed in our study is characteristic of the reaction in a temperature region where a crossover from mechanism I to mechanism II takes place.

Although we are unable to explain the difference in CO inhibition between the two studies, the kinetic rate constants obtained from other studies⁷ show that CO inhibition should not be observed. This is in reasonable agreement with our observations.

Acknowledgments. This paper is based on work performed under U. S. Atomic Energy Commission Contract AT(45-1)-1830. Permission to publish is gratefully acknowledged. Acknowledgment is also given to L. D. Raven and L. A. Charlot who performed much of the experimental work. The help of Dr. R. E. Nightingale in preparing the manuscript is appreciated.

Infrared Spectroscopic Investigations of Zeolites and Adsorbed

Molecules. II. Adsorbed Carbon Monoxide¹

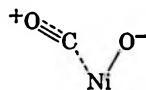
by C. L. Angell and Paul C. Schaffer

Union Carbide Research Institute, Tarrytown, New York 10592 (Received September 3, 1965)

On adsorbing carbon monoxide on X- and Y-type zeolites containing a variety of cations, two types of adsorption can be observed by infrared spectroscopy. The first, occurring on bivalent cation-containing zeolites, gives rise to a higher than gas-phase frequency infrared band. The actual frequency depends on the nature of the cation and the zeolite and can be correlated with the strength of the electric field near the cation. The origin of the high-frequency band is explained to be the polarization of the carbon monoxide molecule in the electric field. The second type of adsorption occurs on all zeolites examined and seems to be associated with two separate adsorption sites. Examples of the use of the high-frequency band for locating the cations in the zeolite structure are given.

Introduction

When carbon monoxide is adsorbed on transition metal oxides or on some transition metals in the presence of oxygen a band appears²⁻⁴ at about 2200 cm^{-1} . Its appearance at a higher than gas phase frequency is rather surprising. Several explanations have been offered and were reviewed by Eischens⁵ recently; the high-frequency band was ascribed to (I) a structure of the type



(II) a dipolar molecule, $^{-}\text{C}\equiv\text{O}^{+}$, attracted to the surface by the oxygen ions in ZnO ; or (III) the $(\text{CO})^{+}$ ion. We have found that CO on bivalent cation containing X- and Y-type zeolites also gives a band at about 2200 cm^{-1} . Its actual position depends on which bivalent cation is present and to a smaller extent on the type (X or Y) of zeolite. Univalent-cation zeolites do not show this band. In addition, there are bands at 2170 and 2120 cm^{-1} regardless of the cation composition, even including the case of decationized Y-zeolite. The precise frequency of the 2200- cm^{-1} band can be correlated with the radius of the bivalent cation. We infer that the frequency shift is primarily due to a distortion of the carbon monoxide molecule in the electrostatic field of the cation and that the distortion and frequency

shift are proportional to the strength of the electrostatic field at the adsorption site. The great advantage of zeolites over other ionic crystals in the elucidation of this phenomenon is that one is able to leave the general structure unchanged while varying the nature of the cation.

Experimental Section

The zeolite materials, the preparation of the pellets, and the spectrometers used have been described in part I.⁶ The samples were flash activated; they were evacuated at room temperature very briefly (pressure $\sim 10^{-3}$ torr), heated to 500° in less than 10 min, kept at this temperature under vacuum for about 3 hr (final pressure $\sim 5 \times 10^{-6}$ torr), and then allowed to cool under vacuum. The carbon monoxide, of CP grade from Mathieson, was analyzed and found to contain a small amount, 0.17%, of carbon dioxide, which was not

(1) The major portion of this work was presented (Abstract B7) at the Symposium on Molecular Structure and Spectroscopy, June 15-19, 1964, Columbus, Ohio.

(2) C. E. O'Neill and D. J. C. Yates, *Spectrochim. Acta*, **17**, 953 (1961).

(3) (a) J. H. Taylor and C. H. Amberg, *Can. J. Chem.*, **39**, 535 (1961); (b) L. H. Little and C. H. Amberg, *ibid.*, **40**, 1997 (1962).

(4) R. P. Eischens and W. A. Pliskin, *Advan. Catalysis*, **9**, 662 (1957).

(5) R. P. Eischens, *Science*, **146**, 486 (1964).

(6) C. L. Angell and P. C. Schaffer, *J. Phys. Chem.*, **69**, 3463 (1965).

removed. Extra short path length (1 mm) cells, described previously,⁶ were used because of the very strong gas phase spectrum of CO. Also, a new 2-cm cell was constructed in which measurements could be made on samples at liquid-nitrogen temperature; there was no provision for activating the sample *in situ* in this cell, however, and the samples, preactivated, had to be loaded into it in a vacuum drybox. In the region 2200–2000 cm^{-1} , slit widths of 0.040 to 0.100 mm were used, corresponding to spectral resolutions of 0.5 to 1.2 cm^{-1} . Band positions could be determined to $\pm 1 \text{ cm}^{-1}$, while band intensities were reproducible to $\pm 2\%$ of transmittance.

Results

None of the zeolite samples chemisorbed CO, and a pressure of about 200 torr was used to observe the CO bands. With minor exceptions, all the zeolites tested, including X- and Y-zeolites that contained uni-, bi- or trivalent cations⁷ and Y-zeolites that were partly or almost fully decationized, showed the two bands at 2170 and 2120 cm^{-1} unchanged in frequency, intensity, and shape. The exceptions were NaX (2164–2121 cm^{-1}), BaY (2105 cm^{-1}), and SrY (2098 cm^{-1}). In several cases the 2170- cm^{-1} band could not be resolved from the high-frequency band (see Table I and Figure 1). At room temperature the 2170- cm^{-1} band is about 1.5 times as strong as the 2120- cm^{-1} band (Figure 2). On cooling to liquid-nitrogen temperature, both bands show increases owing to increased CO adsorption (for example, MnY zeolite at room temperature and at 300 torr adsorbs 7 cc of CO/g of zeolite, while at -75° and the same pressure the adsorption is 52 cc/g), but the

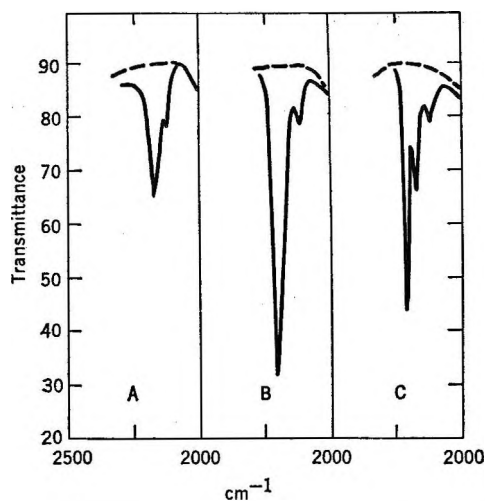


Figure 1. Spectra of carbon monoxide adsorbed on zeolites in the C-O stretching region: A, NaY; b, CaY; and C, ZnY.

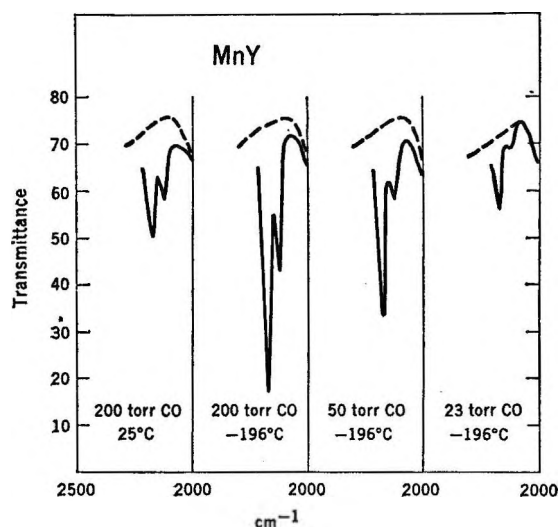


Figure 2. Spectra of carbon monoxide adsorbed on MnY zeolite. Variation of the two cation-independent bands with temperature and pressure; ratio of band heights 1.55:2.64:3.28:4.35.

Table I: Carbon Monoxide Adsorbed on Zeolites

| Cation | Frequencies ^a on Y-zeolite, cm^{-1} | | Frequencies ^a on X-zeolite, cm^{-1} | | Ionic radius, Å (Goldschmidt) |
|------------------|---|------|---|------|-------------------------------|
| | 2170 | 2120 | 2164 | 2121 | |
| Decationized | | | | | |
| Na ⁺ | 2172 | 2122 | 2164 | 2121 | 0.98 |
| Li ⁺ | 2172 | | | | 0.70 |
| Mg ²⁺ | 2213 | 2170 | 2205 | 2173 | 0.78 |
| Ca ²⁺ | 2197 | 2172 | 2192 | 2104 | 1.06 |
| Sr ²⁺ | 2186 | 2098 | | | 1.27 |
| Ba ²⁺ | 2178 | 2105 | 2172 | 2112 | 1.43 |
| Mn ²⁺ | 2208 | 2173 | 2119 | 2203 | 0.91 |
| Fe ²⁺ | 2198 | 2172 | | | 0.83 |
| Co ²⁺ | 2208 | 2172 | 2119 | 2204 | 0.82 |
| Ni ²⁺ | 2217 | 2172 | 2120 | 2211 | 0.78 |
| Zn ²⁺ | 2214 | 2170 | 2118 | | 0.83 |
| Cd ²⁺ | 2209 | 2170 | 2120 | | 1.03 |

^a Frequencies are accurate to $\pm 1 \text{ cm}^{-1}$.

2170- cm^{-1} band grows considerably faster until it is approximately four times the size of the 2120- cm^{-1} band.

In addition to the above ubiquitous bands, the zeolites containing bivalent cations showed a band of higher frequency (Figure 1). This is also due to weak adsorption, since the band disappears on pumping at room temperature, although not as readily as the other

(7) Zeolite Y [described in U. S. Patent 3,130,007 (1964)] has sodium ions as the structural cations. The notation BaY, CdY, etc., is used throughout this paper to denote zeolites prepared from zeolite Y by ion-exchange substitution of Ba²⁺, Cd²⁺, etc., cations for the Na⁺ cations of zeolite Y.

two bands. On cooling the samples in the presence of excess CO, the 2200-cm⁻¹ band from CoY and NiY (as typical examples) did not increase while the other two bands increased manyfold. The 2200-cm⁻¹ band also did not decrease when the gas pressure was decreased at low temperature, but the other two bands did decrease. Clearly, the CO molecules responsible for the cation-dependent band and for the other two bands are distinct, and infrared methods provide a means of distinguishing between them. When a sample of a 22% exchanged CoY (6.3 bivalent cations per unit cell) and a sample of a 20% exchanged NiY (5.7 bivalent cations per unit cell) were exposed to CO, the high-frequency bands did appear although much smaller than on the respective more highly exchanged zeolite samples. On the other hand, a 35% exchanged CaX sample (15 bivalent cations per unit cell) did not show any trace of the corresponding high-frequency band.

It was also noticed that small amounts of water present (<1%) eliminated the high-frequency CO band on the zeolites.

Discussion

It is known from the spectrum of CO⁺ that the removal of an electron from the CO molecule strengthens the CO bond and raises the stretching frequency⁸ (from 2143 cm⁻¹ in CO to 2184 cm⁻¹ in CO⁺), the electron being removed from the weakly antibonding lone-pair orbital of the carbon atom. In the case of CO adsorbed on zeolites we measure a partial electron transfer to the bonding cation. Although the dipole moment of the carbon monoxide molecule is very small (~0.1 D.), we assume that it is the carbon (negative) end that approaches the positive charge. The orientation of the CO units in all metal carbonyls strongly confirms this assumption. Since the position of the high-frequency band is dependent on the nature of the cation (see Table I), some property of the cation was searched for that would determine the strength of the interaction with CO. The sum of the first and second ionization potentials of the metal, *i.e.*, the electron affinity of the bivalent cation, and the ionic radius of the cation, *i.e.*, the distances to which the CO molecule can approach the cation, were thought to be suitable parameters. When the frequency of the CO band was plotted against the ratio of ionization potential to ionic radius, a not very satisfactory plot was obtained. This method, of course, takes into account only the bare cation and does not differentiate between X- and Y-zeolites. In order to achieve such differentiation, instead of using the field due to the bare ion, fields inside the zeolite were used as calculated by

Pickert, *et al.*^{9a} These calculations have determined the field as a function of distance from the cation, taking into account all the atoms present in the zeolite structure. The positions used for the Ca²⁺ were those determined in an X-ray study of a dehydrated Ca²⁺-exchanged single crystal of faujasite (Si/Al = 2.5)^{9b} and described by Pickert, *et al.*^{9a} This method gives different curves for the X- and Y-zeolites, the field always being lower in the X-type zeolite (see Rabo, *et al.*¹⁰). In order to determine the strength of the field at the CO molecule, the radius of the cation was taken, then 1.5 Å was added to this (1.5 Å is about the expected van der Waals radius of the carbon atom and we are concerned with an orbital on the carbon atom); the field strength at this point was found from the curve calculated. When the CO frequencies were plotted against field strength, a reasonably straight line was obtained (Figure 3) with the X- and Y-zeolites now separated, although in terms of a linear relationship one would expect a larger difference in frequency for corresponding X- and Y-zeolites than experimentally obtained. The line also extrapolated reasonably to the gas phase value.

Attempts were made to take care of the possibility that smaller cations are positioned somewhat deeper in the oxygen ring surrounding them. Therefore, instead of the radius *R* of the bivalent cation, a quantity R^2/R_{Ca} (which we will call reduced radius) was used. This was thought to take care of an approach of a smaller cation toward the oxygen atoms or the moving away of a larger cation from the oxygen atoms. For example, with a cation smaller than the Ca²⁺ ion the CO could approach closer by the difference of the respective radii; if, in addition, the cation was to move closer to the oxygen atoms than the Ca²⁺ positions, then the CO could approach to the framework by twice the difference of the cation radii. It was realized that this procedure is not fully justified, since moving the cation toward the framework will result in a "shielding" field due to the framework that is different from the one used in the field calculation based on the calcium cation positions. However, plots of CO frequencies against field strengths calculated this way, using the Pauling radii or the Goldschmidt radii of

(8) G. Herzberg, "Molecular Spectra and Molecular Structure. I. Spectra of Diatomic Molecules," D. van Nostrand Co. Inc., Princeton, N. J., 1950, p 522.

(9) (a) P. E. Pickert, J. A. Rabo, E. Dempsey, and V. Schomaker, *Actes Congr. Intern. Catalyse, 3^{me}, Amsterdam, 1964*, 714 (1965).
(b) R. Dodge, to be published.

(10) J. A. Rabo, P. E. Rickert, D. N. Stamires, and J. E. Boyle, *Actes Congr. Intern. Catalyse, 2^e, Paris, 1960*, 2055 (1960).

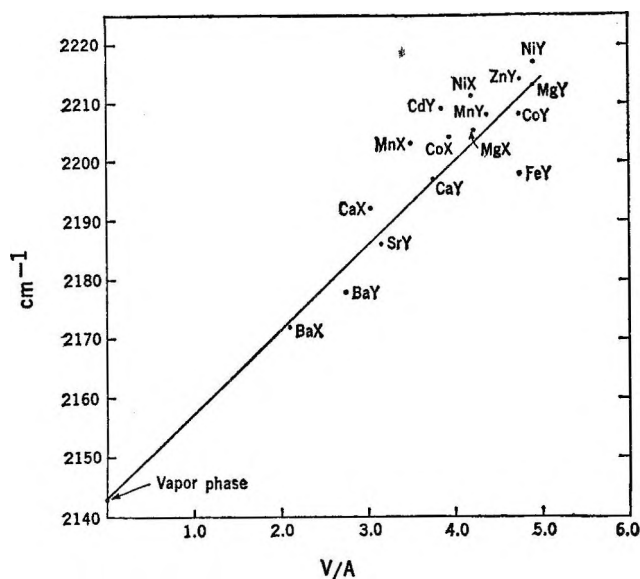


Figure 3. Plot of CO frequencies against field strength (in volts per angstrom) using Goldschmidt radii.

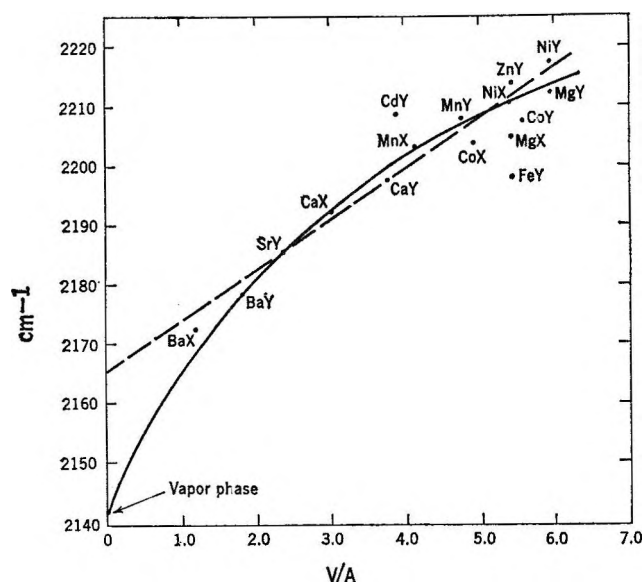


Figure 4. Plot of CO frequencies against field strength (in volts per angstrom) using reduced Goldschmidt radii.

bivalent cations, gave definite improvement over the previous plots, although FeY and CdY were still considerably off the line (see Figure 4). The Goldschmidt values gave somewhat better agreement. The slopes between X- and Y-zeolite points now practically coincide with the slope of the main line. However, a straight line extrapolates to about 2164 cm^{-1} and not to the gas phase value, but a slightly curved line going through this gas value fits the points just as well as a straight line.

Both lines of Figures 3 and 4 are considered a good enough relationship to suggest that the CO frequency shift depends only on the field strength and is therefore a polarization effect. This is also in good agreement with the weak adsorption of CO on all the zeolites studied, since a polarization phenomenon would require a small amount of energy. The picture that we have in mind is the polarization of the carbon monoxide molecule in the electrostatic field, *i.e.*, a transfer or moving away of both electrons in the lone-pair orbit of the carbon atom away from the carbon under the effect of the field and the movement of electrons from the oxygen toward the carbon atom thereby strengthening the bond between C and O atoms.

A molecular orbital picture of bonding in metal carbonyls has been presented by several authors,^{11,12} in which first the lone-pair orbital of each carbon atom donates an electron to the metal atom (σ bonding), then the accumulated negative charge on the metal atom causes back-donation of electrons into the π orbitals of the C-O bonds (π bonding). In our case only the first step need occur, since there will be no accumulation (rather a partial neutralization) of charge on the cation. Therefore, this phenomenon isolates the σ -bonding effect and shows that it gives rise to weak bonding between the metal and carbon atoms while raising the C-O bond strength.

This linear relation between frequency and field strength seems to hold fairly well for the closed shell (alkaline earth metal) cations, but it is not very surprising that among the transition metal cations there are considerable deviations. Cations with partially filled d orbitals are not expected to behave as spherical charged particles, but the d orbitals might interact with the CO molecule in a way that could be considered back-donation. At the moment, however, we are unable to present any correlation between the d orbitals and the positions of the Fe^{2+} , Co^{2+} , or Ni^{2+} on the plots of Figures 3 and 4.

It is unfortunate that the metal ion to carbon atom force constant cannot be calculated directly from an infrared band, since it is impossible to observe the metal-carbon stretching vibration, the transmission through a pellet of the zeolite being too small in the region of the expected band (around 33μ).

Now let us look at the two bands mentioned that occur when CO is adsorbed on any zeolite. Blyholder and Neff¹³ have observed similar bands in physical

(11) G. Blyholder, *J. Phys. Chem.*, **68**, 35 (1964).

(12) L. Orgel, "An Introduction to Transition-Metal Chemistry, Ligand-Field Theory," Methuen and Co. Ltd., London, 1960, p 135.

(13) G. Blyholder and L. D. Neff, *J. Chem. Phys.*, **36**, 3503 (1962).

adsorption of CO on iron and have suggested that these bands represent the P and R branches of rotational structure due to the rotation of the adsorbed CO. This is an unlikely explanation, since restricted rotation in one or maybe two dimensions could not give rise to P and R branches in just the same places as for free gas molecules (2175 and 2115 cm^{-1}). In addition, the P-R separation would be expected to decrease on going to lower temperatures, contrary to the observed fact that the band positions are unchanged on lowering the temperatures. Also, the ratio of intensities of the P and R branches should be independent of pressure at a given temperature, contrary to results found on zeolites (changing from 2.64 to 4.35 at -196° on MnY, Figure 2). Since these two bands occur on all zeolites, even decationized Y, the adsorbate cannot be associated with the cations in this case but must be connected with the oxygen atoms of the structure. How then does the 2170- cm^{-1} band arise when we have ascribed higher than gas phase frequencies as due to the donation of electrons away from the carbon atom? It is tentatively suggested that the 2170- cm^{-1} band arises from the CO molecule being attached by its oxygen atom to the surface oxygens,¹⁴ this way achieving the same change as attachment to a positive charge through the carbon atom would do. The 2120- cm^{-1} band then could represent a carbon monoxide molecule attached to surface oxygen through its carbon atom resulting in a weakening of the CO bond and the decrease of the stretching frequency. If the CO molecules would attach in two different orientations to the same sites, then the proportion of the two types of molecules should only be determined by their respective energies, and the intensity ratio of the bands arising from them should be independent of pressure. The definite dependence of this ratio on pressure (Figure 2) indicates that the molecules must attach to two *different* sites, and the adsorption represented by the 2170- cm^{-1} band is nearer to saturation at 200 torr than the one represented by the 2120- cm^{-1} band. The nature of the two sites cannot be determined from the present experiments.

In the X- and Y-type zeolites there are several different types of cationic sites,¹⁵ referred to as site I, site II, and site III. Sites I are in the centers of the hexagonal prisms joining the truncated octahedra of the (Si,Al) O_2 framework, sites II are on six-membered rings on the unjoined hexagonal faces of the octahedra, and sites III are on the walls of the channels (see Figure 8 of ref 15). Cations in site I are definitely not available to any molecules for direct interaction, while, of course, those in site II and III (surface cations) are quite open to the approach of molecules of adsorbing gas. Since X-ray examinations have not fully located

all the bivalent cations to the corresponding sites, it is interesting that the carbon monoxide adsorption offers a method of establishing the distribution of cations between the various sites. This is especially important when the monovalent cations originally present have been only partially replaced by bivalent cations. Is there any preference for the bivalent cations to go into site I, where a much tighter coordination with the surrounding oxygens is possible?

It has been shown that univalent cations do not give rise to an extra high-frequency carbon monoxide band. Therefore, the appearance of this band is an indication that there are bivalent cations in the surface (site II or site III) positions. The 22% exchanged CoY contains 6 Co^{2+} and 45 Na^+ cations per unit cell. It is also known that there are 16 site I, 32 site II, and 48 site III per unit cell.¹⁶ Since it is assumed that in site I a cation could not be reached by any adsorbed molecule, the appearance of a band at 2208 cm^{-1} is an indication that there must be Co^{2+} cations in surface sites. Since there are fewer Co^{2+} cations (6) than there are sites I (16), the above results show that Co^{2+} has no overwhelming preference for site I. The appearance of the extra high frequency band in the case of a 20% exchanged NiY indicated the same thing for the distribution of Ni^{2+} cations. On the other hand, the results obtained with 35% exchanged CaX indicate that the distribution of Ca^{2+} cations is significantly different from the other two mentioned. In this case, there are 15 Ca^{2+} cations per unit cell but still the extra CO band does not appear, indicating that the Ca^{2+} ions must be in the site I (hidden) positions. Measurements of heats of adsorption of CO carried out at Linde¹⁶ have shown that this CaX sample has the same heat of adsorption as a NaX sample, and more than 35% Ca^{2+} cations are needed before a heat of adsorption characteristic of CaX zeolite can be observed. The above spectroscopic results are in complete agreement with this.

The proven dependence of the CO frequency on the cation present clearly establishes that the carbon monoxide molecules must be attached to the cations. The displacement of cation-adsorbed carbon monoxide by small amounts of water also constitutes a proof that the first amounts of water are adsorbed on the cations. This is in agreement with our observation⁶ that small amounts of water do not affect the 3640- cm^{-1} OH band.

Acknowledgments. The authors wish to express

(14) C. H. Amberg and D. A. Seanor, ref 9a, p 450.

(15) D. W. Breck, *J. Chem. Educ.*, **41**, 678 (1964).

(16) R. Neddenriep, private communication.

their sincere thanks to Drs. Verner Schomaker and Jule Rabo for many helpful discussions and constructive

criticism, and to Dr. Edith Flanigen for many of the zeolite samples.

Radiolysis of Oxalate Alkaline Solutions in the Presence of Oxygen

by Z. D. Draganić, I. G. Draganić, and M. M. Kosanić

Boris Kidric Institute of Nuclear Sciences, Vinča, Yugoslavia (Received September 24, 1965)

The radiation yields of carbon dioxide, molecular hydrogen, and hydrogen peroxide were measured over the pH range from 9.5 to 14 in aqueous solutions of various oxalate and oxygen concentrations. The results obtained confirmed the change in the nature of hydroxyl radical with increasing pH. The basic form is replaced by ion radical O^- whose fate is determined in reactions with oxygen molecules and oxalate ions. The rate constant ratio $k_{O^-+O_2}/k_{O^-+C_2O_4^{2-}}$ was calculated from the experimental data. A cube root dependence of the molecular hydrogen yields, measured as a function of the oxalic acid concentration, was observed. The experimental results were quantitatively consistent with a simple reaction scheme which allowed determination of the primary yields in water γ radiolysis in the pH region 9.5–14.

Introduction

In radiation chemistry of aqueous solutions there is an increasing interest in the pH influence on the radical yields in alkaline medium. Haissinsky and his collaborators studied tellurous acid,¹ platinum salts,² potassium iodate,³ and potassium permanganate.⁴ As suggested in experiments with phosphites,⁵ all these systems indicate that after pH 12 the radical yields increase while the molecular yields decrease. Dainton and Watt^{6,7} studied aqueous solutions of acrylamide and potassium ferrocyanide and ferricyanide, with and without N_2O . They found that the molecular product yields remained practically unchanged in alkaline media but that the free-radical yields increased. Similar results were obtained at pH 13 by Hughes and Willis⁸ in the ferrocyanide-methanol system. Hayon⁹ recently found in different alkaline solutions an increase in the primary free-radical yields and a decrease in molecular product yields. Cheek and Linnenbom¹⁰ studied hypobromite solutions and found no change either in primary molecu-

lar or in free-radical yields over a pH region from neutral to alkaline.

Evidence has been accumulating also concerning the nature of the hydroxyl radical in alkaline media. Hochanadel¹¹ has confirmed the existence of the O^- ion radical in his study of the radiolysis and photolysis of hydrogen peroxide solutions. This species was originally proposed by Hart, *et al.*¹² Its existence was

- (1) M. Haissinsky and P. Patigny, *J. Chim. Phys.*, **59**, 675 (1962).
- (2) M. Haissinsky, *ibid.*, **60**, 402 (1963).
- (3) M. Haissinsky, J. Jové, and W. Szymanski, *ibid.*, **61**, 572 (1964).
- (4) M. Haissinsky and J. Petit, *ibid.*, **62**, 222 (1965).
- (5) M. Haissinsky, *ibid.*, **62**, 224, 1141, 1149 (1965).
- (6) F. S. Dainton and W. S. Watt, *Nature*, **195**, 1924 (1962).
- (7) F. S. Dainton and W. S. Watt, *Proc. Roy. Soc. (London)*, **A275**, 447 (1963).
- (8) G. Hughes and C. Willis, *Discussions Faraday Soc.*, **36**, 223 (1963).
- (9) E. Hayon, *Trans. Faraday Soc.*, **61**, 734 (1965).
- (10) C. Cheek and V. Linnenbom, *J. Phys. Chem.*, **67**, 1856 (1963).
- (11) C. J. Hochanadel, *Radiation Res.*, **17**, 286 (1962).

confirmed by the recent pulse-beam experiments of Czapski and Dorfman¹³ and Rabani and Matheson.¹⁴ Supporting the existence of this species we also cite the experiments by Hughes and Willis⁸ as well as some of our own observations on the pH influence on decomposition of oxalate ions in absence of oxygen.¹⁵ However, only Adams, *et al.*,¹⁶ have measured some relative rate constant ratios for the O^- ion radical.

Our earlier experiments¹⁷ showed that radiation-induced decomposition of oxalate ions, in oxygenated aqueous solutions, was practically due only to reaction with hydroxyl radicals. These experiments were carried out at $pH < 10$. Subsequent studies have shown that this system can also give information on initial radical and molecular yields at $pH > 10$. The purpose of this study was to use the simple reaction scheme and the complete material balance for the determination of the primary free-radical and molecular yields in the pH region 9.5–14. The competition data enabled calculation of the relative rate constant ratio for the O^- ion-radical reactions with oxygen molecules and oxalate ions.

Experimental Section

Solutions. The water used was triply distilled in a continuous Pyrex system (alkaline permanganate, acid dichromate, and finally without any additive). The oxalic acid (Merck AR) was recrystallized before use. The alkaline solutions were made by means of sodium hydroxide, freshly prepared by dissolving sodium (Carlo Erba AR) in triply distilled water in a nitrogen atmosphere. The pH of the solution was measured by a Beckman GS pH meter with an E2 electrode. The introduction of the given amount of oxygen and sodium hydroxide in deaerated solution was performed by standard techniques. The ampoules were completely filled, leaving no gas space.

The solubility of oxygen varied with the concentration of oxalic acid and with the pH of the solution. The initial oxygen concentration in 47 mM solutions was 0.60 ± 0.02 mM. In studies of the oxygen concentration influence, it varied from 0.3 to 0.8 mM. In experiments with ^{14}C , the solutions were saturated with atmospheric air.

Irradiations. The samples were irradiated in the 2-kurie irradiation source at Vinča.¹⁸ The absorbed dose rate, as determined with a Fricke dosimeter [$G(Fe^{3+}) = 15.5$], was 2.10^{19} $ev\ ml^{-1}\ hr^{-1}$.

Analyses. The gas products, H_2 and CO_2 , and the O_2 initially present were determined on a Perkin-Elmer 154 DG gas chromatograph. Argon or helium was used as carrier gas on a silica gel column.¹⁹ Since careful sample preparation did not give reproducible

initial concentrations of CO_2 , we paid special attention to the determination of blank corrections. Generally, ten samples were prepared as a series and three or four unirradiated samples of each series were analyzed for CO_2 . The observed CO_2 content was considered the blank and was plotted at the zero absorbed dose.

The amount of H_2O_2 was measured spectrophotometrically by the iodide method developed by Ghormley.²⁰ The molar extinction coefficient at 24° was determined to be $25,810\ l.\ mole^{-1}\ cm^{-1}$. The presence of oxalic acid slowed down the iodide oxidation so that the optical measurements were made about 30 min after the preparation of the solutions. An unirradiated sample of oxalic acid was used as a reference solution. Reference samples were prepared and measured simul-

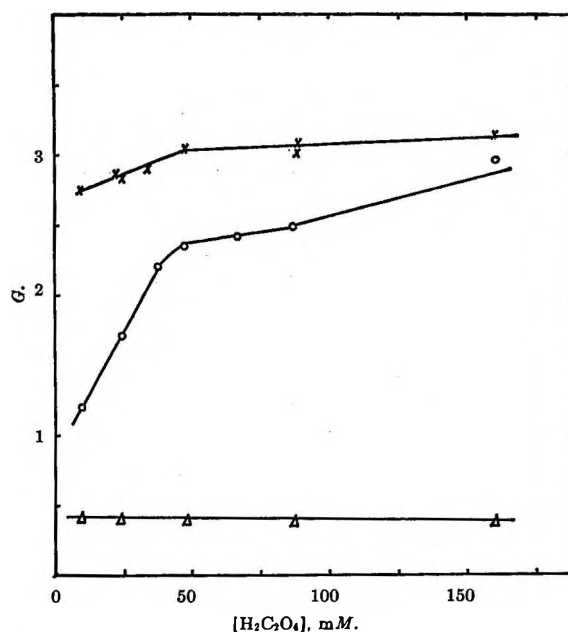


Figure 1. Influence of oxalate ion concentration on measured yields of H_2O_2 , CO_2 , and H_2 at $pH\ 12.0$; O_2 present decreases from 0.61 to 0.52 mM with oxalate concentration: X, H_2O_2 ; O, CO_2 ; and Δ , H_2 .

(12) E. Hart, S. Gordon, and D. Hutchison, *J. Am. Chem. Soc.*, **75**, 6165 (1953).

(13) G. Czapski and L. Dorfman, *J. Phys. Chem.*, **68**, 1169 (1964).

(14) J. Rabani and M. Matheson, *J. Am. Chem. Soc.*, **86**, 3175 (1964).

(15) I. Draganić, *J. Chim. Phys.*, **56**, 18 (1959).

(16) G. E. Adams, J. W. Boag, and B. D. Michael, *Trans. Faraday Soc.*, **61**, 492 (1965).

(17) Z. D. Draganić, I. G. Draganić, and M. M. Kosanić, *J. Phys. Chem.*, **68**, 2085 (1964).

(18) B. Radak and I. Draganić, *Bull. Inst. Nucl. Sci. Inst. "Boris Kidrić"* (Belgrade), **13**, 77 (1962).

(19) Lj. Petković, M. Kosanić, and I. Draganić, *ibid.*, **15**, 9 (1964).

(20) A. O. Allen, C. J. Hochanadel, J. A. Ghormley, and T. W. Davis, *J. Phys. Chem.*, **56**, 575 (1952).

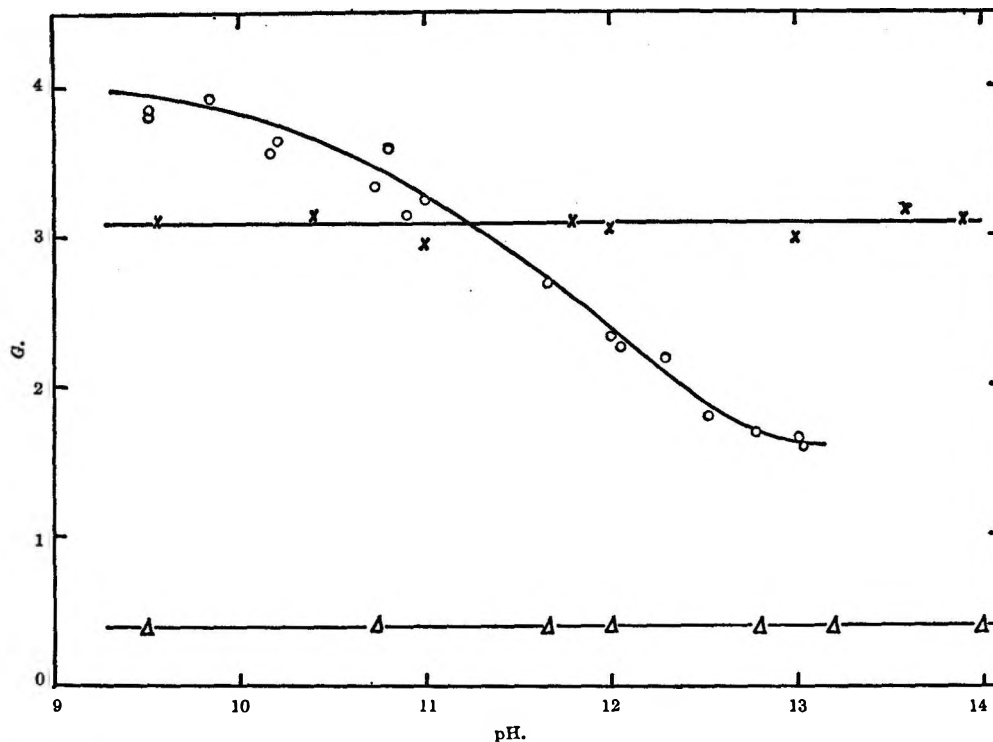


Figure 2. Irradiation yields of CO_2 , H_2O_2 , and H_2 measured in 47 mM sodium oxalate with $0.60 \pm 0.02 \text{ mM O}_2$ present: \times , H_2O_2 ; \circ , CO_2 ; and Δ , H_2 .

taneously with irradiated ones in order to avoid errors due to the oxidation of iodide by atmospheric oxygen. At pH 13–14, the solutions were first acidified with a 0.6 M oxalic acid solution and then measured in the usual way. In this case the molar extinction coefficient was $22,900 \text{ l. mole}^{-1} \text{ cm}^{-1}$. The decrease in the extinction coefficient is due mainly to the presence of an excess of oxalate salts. We have noticed that the impurities in potassium iodide of different origin can also contribute to this decrease.

In experiments where ^{14}C was used as a radioactive tracer, we used $\text{NaH}^{14}\text{CO}_3$ and $\text{H}^{14}\text{COONa}$ (Amersham). The specific activity was $5 \mu\text{curies ml}^{-1}$. The radioactivity counting was performed on a 2π proportional flow counter.

Results

General. As in our previous work at $\text{pH} < 10$, only carbon dioxide, hydrogen peroxide, and hydrogen were found in the solutions irradiated under initial conditions (doses from 0.35×10^{18} to $4.65 \times 10^{18} \text{ ev ml}^{-1}$). Figure 1 shows the influence of the initial oxalate ion concentration on the yields measured at pH 12. In these experiments the oxygen concentrations decreased from 0.61 to 0.52 mM with an increase of the oxalate concentration from 9.8 to 160 mM. This decrease is a result of the reduced solubility of oxygen which was introduced under constant pressure and temperature.

As in the previous measurements in acid and neutral media, only a slight influence of oxalate ion concentration on the hydrogen peroxide and hydrogen yields was observed. However, the influence on the carbon dioxide yields is pronounced. As can be seen in Table I, this is caused not only by the change of the initial oxalate ion concentration but also by the change of the oxalate/oxygen ratio. No influence of the initial oxygen concentration could be observed on the yields of hydrogen peroxide and of molecular hydrogen.

Table I: The Effect of Oxygen Concentration on Measured Yields of CO_2 at pH 13 and at Different Oxalate Concentrations

| Oxygen, mM | Oxalate, mM | $G(\text{CO}_2)$ |
|------------|-------------|------------------|
| 0.30 | 45.0 | 2.20 |
| 0.40 | 46.1 | 1.83 |
| 0.60 | 47.0 | 1.65 |
| 0.79 | 46.6 | 1.16 |
| 0.38 | 89.9 | 2.52 |
| 0.53 | 88.7 | 2.08 |
| 0.82 | 90.6 | 1.72 |

Figure 2 shows the pH influence on the measured yields in oxalate solutions ($\sim 47 \text{ mM}$) in the presence of oxygen ($0.60 \pm 0.02 \text{ mM}$). The 47-mM solutions

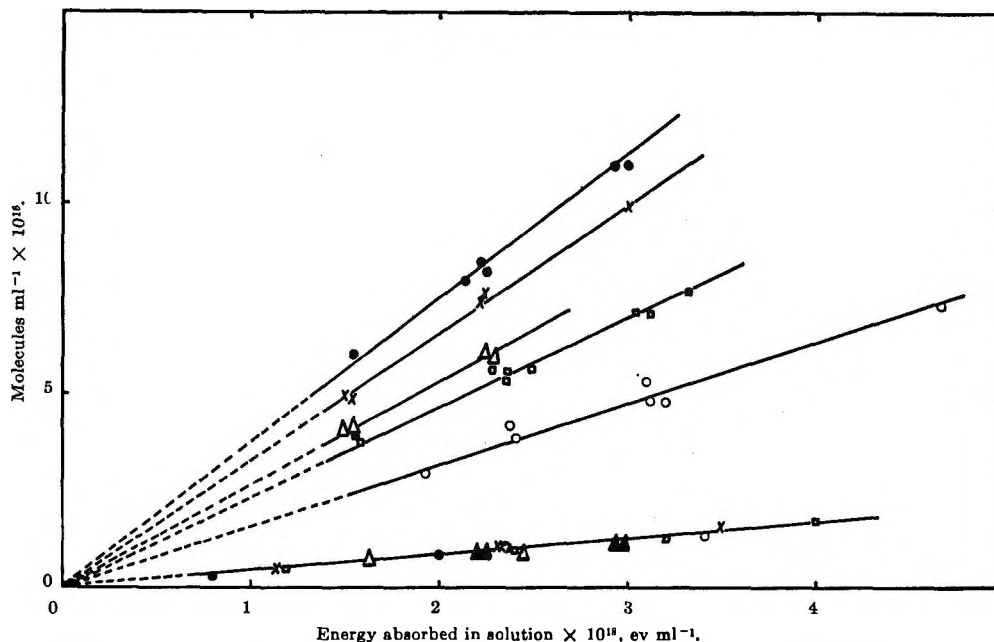


Figure 3. Influence of dose on the formation of CO_2 (upper curves) and H_2 (lower curve) in 47 mM oxalate solutions at different pH values: \bullet , 9.5; \times , 10.74; Δ , 11.66; \square , 12.0; \circ , 13.0; and \blacktriangle , 14.

were used, as larger concentrations would require larger corrections in CO_2 measurements and introduce more inaccuracy in yields calculation. This concentration was considered as the lowest one reasonably well placed in the plateau region (Figure 1).

As seen in Figure 2, data for the whole pH region are given only for molecular hydrogen and hydrogen peroxide, since only these measurements were reliable for $\text{pH} > 13$. The experimental scatter of CO_2 results is a consequence of the relatively low yields and the high blank corrections. At $\text{pH} 12\text{--}13$ the correction was of the same order of magnitude as the effect measured ($\sim 3 \times 10^{16}$ molecules ml^{-1}). At $\text{pH} 14$ this ratio is so unfavorable that measurement of $G(\text{CO}_2)$ was considered meaningless and therefore not done.

Products in Gas Phase. The concentrations of the gas products formed increased linearly with dose, as seen in Figure 3. The radiation yields decrease from 3.9 to 1.6 when the initial pH increases from 9.5 to 13. By adding different amounts of CO_2 before irradiation, the carbon dioxide content was varied in some cases severalfold. No visible influence was observed on the yields measured.

The hydrogen yield in 47 mM oxalate solutions was found to be 0.4, independent of the changes in pH value in the studied region. However, as seen in Figure 4, there is a cube-root dependence on the initial oxalate concentration. It allowed us to derive from the intercept the value 0.44 as the initial yield.

Products in Liquid Phase. The linear part of the

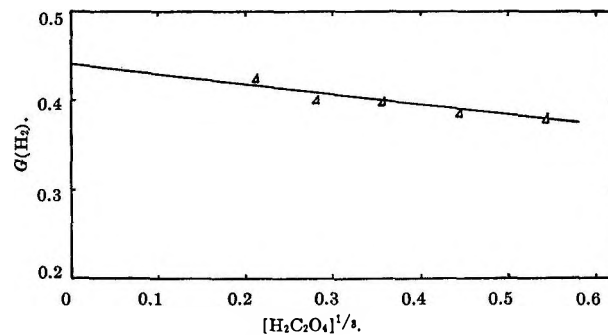


Figure 4. Cube root plot: measured molecular hydrogen yields at $\text{pH} 12$, as a function of oxalate ion concentration. Oxygen present: 0.61–0.52 mM.

H_2O_2 vs. dose curve was found to be considerably shorter in alkaline than in neutral and acid media. After an absorbed dose of 0.7×10^{18} ev ml^{-1} , the measured yields decrease with increasing dose. In calculating the initial yields we have used the corrected values, obtained as $G(\text{H}_2\text{O}_2)$ readings at zero dose on diagrams where H_2O_2 yields were plotted against dose. As can be seen in Figure 2, the hydrogen peroxide yields are pH independent and, within experimental error, equal to 3.10. We have obtained in our preceding work¹⁷ somewhat lower $G(\text{H}_2\text{O}_2)$ values for $\text{pH} 9.5$ and 9.8. The reason for this was that in calculation we used the uncorrected values obtained by measurements at doses higher than 0.7×10^{18} ev ml^{-1} .

We attempted to prove the presence of ozone in

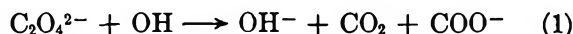
irradiated solutions at pH 12.0, 12.5, and 13.0. These measurements were made according to Taube and Bray's method,²¹ 5 or 10 sec after irradiation. No ozone could be measured.

Figure 5 shows data from measurements of the radioactivity of oxalate precipitated after irradiation. In oxalic acid solutions of different pH values, carbon dioxide or sodium formate labeled with ¹⁴C were used as the source of carboxyl radicals.

It is seen that no activity higher than the background was measured. It was easy, however, to follow the formation of labeled oxalic acid in the absence of oxygen.²² The radioactivity of the samples was a function of the dose and of the other relevant parameters such as the pH value of the solution and the source of the carboxyl radical. Possible sources considered were carbon dioxide and formate ion.

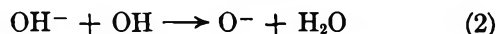
Discussion

Mechanism. These results, as well as earlier studies at pH < 10, indicate that the decomposition of oxalate ions in aqueous solutions results from the reaction with the hydroxyl radical

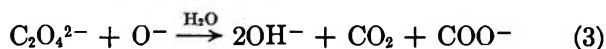


We have neglected the relatively slow reaction with short-lived reducing species, evident from the small $G(\text{H}_2)$ decrease shown in Figure 4. Observations in acid medium, where this decrease was much more pronounced, have shown that this reaction may be neglected. An intermediate, probably $\text{HOOC-C}(\text{OH})_2$, is formed which reacts with oxygen, producing oxalate and O_2^- , the net effect being as if oxygen has reacted directly with short-lived reducing species.

The data for $G(\text{CO}_2)$, presented in Figure 2, show that the decomposition of oxalate ions decreases strongly with increasing pH. The re-formation of oxalic acid is not likely to be the reason for this decrease, as confirmed by experiments with carbon-14 as tracer²² (Figure 5). Also, no change in the nature of oxalate ion should occur as the oxalic acid is completely dissociated after pH 6. Hence, the decrease observed could be explained only by the change in the nature of oxidizing short-lived species in reaction 1. The scavenging of OH radicals by OH^- ions



has been reported by various authors.^{9,11-16,23} In our case, as the pH increases, reaction 1 is replaced by the less efficient reaction



The high and constant yields of hydrogen peroxide at

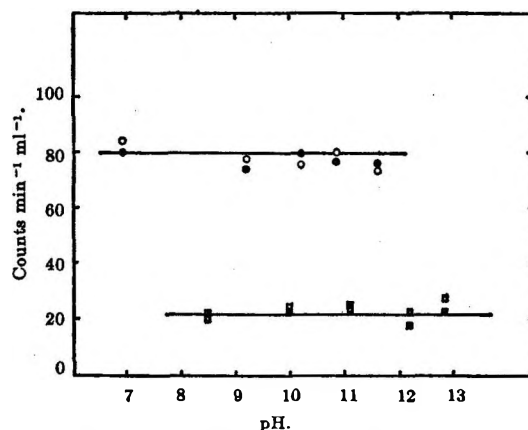
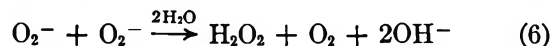
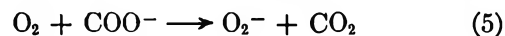
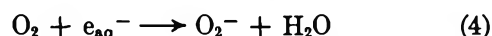


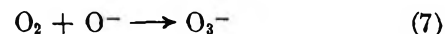
Figure 5. Radioactivity of oxalate precipitates: pH influence. O, $\text{H}^{14}\text{COONa}$; \square , $^{14}\text{CO}_2$; solid symbols denote blanks.

all pH values studied indicate its formation by the following reactions.



Experiments with ¹⁴C proved in particular the efficiency of reaction 5.

The decrease in $G(\text{CO}_2)$ and the constant $G(\text{H}_2\text{O}_2)$ with increasing pH, as seen in Figure 2, suggest an additional reaction of the O^- ion radical in which it disappears while hydrogen peroxide is being formed. That this is a reaction with the oxygen initially present in our solutions is shown by the influence of oxygen concentration on $G(\text{CO}_2)$ yields (Table I). In competition with reaction 3, this reaction could most probably be



Czapski and Dorfman¹³ pointed to such a possibility in their experiments with oxygenated alkaline aqueous solutions. They identified a species as being O_3^- with a maximum in the absorption spectrum at 430 m μ . The same phenomenon was also observed in pulse-beam experiments by Adams and Boag.²⁴

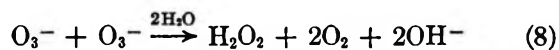
The hydrogen peroxide yields we measured indicate that the ion radical O_3^- must react in a way which leads to the formation of hydrogen peroxide

(21) H. Taube and W. C. Bray, *J. Am. Chem. Soc.*, **62**, 3357 (1940).

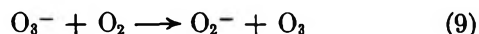
(22) Z. D. Draganić and M. Nenadović, *Intern. J. Appl. Radiation Isotopes*, in press.

(23) F. S. Dainton and S. A. Sills, *Proc. Chem. Soc.*, 223 (1962).

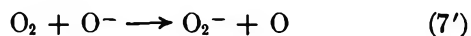
(24) G. A. Adams and J. W. Boag, *ibid.*, 112 (1964).



or

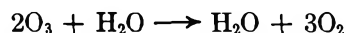


Nothing, however, would be changed in the material balance if reactions 7 and 9 were substituted by



However, we prefer to consider reactions 8 and 9 as more probable since the data on the identification of O_3^- are very convincing and there is no direct evidence available for reactions 7' and 9'.

Our experiments do not allow us to distinguish whether the fate of O_3^- is in reaction 8 or 9. The constant yield of H_2O_2 molecules only shows that O_3^- must react in a way in which half of a H_2O_2 molecule is formed for each O_3^- consumed, as this is the case both in reaction 8 and 9. In case of reaction 9, radiolysis would produce ozone. Its chemistry, particularly in alkaline solutions, is not well known. It is certain that it is unstable and by decomposition it produces oxygen²⁵



Therefore, although we were not able to detect ozone, we cannot exclude reaction 9.

Several authors have pointed to the high reaction rates of the primary reducing species with CO_2 in aqueous solutions,²⁶⁻²⁹ and the special precautions needed in work with alkaline solutions.³⁰ As our blank tests have shown, initial concentrations of CO_2 can be considerable (about 0.05 mM at pH 12). The CO_2 formed during irradiation and absorbed in the solution also has to be taken into account. Therefore, although the concentration of oxygen present in our solutions is considerably larger than that of carbon dioxide, it is evident that a fraction of solvated electrons must be consumed in reaction with carbon dioxide. However, as the product of this reaction is the COO^- ion radical, which disappears by reaction 5, the material balance is the same if we had only reaction 4. Also, at pH > 11 carbon dioxide is in carbonate form, which does not react with solvated electrons.^{22,27} The constant hydrogen peroxide yield we measured in alkaline solutions implies that even if it did react, the result would still be the same as in neutral solutions. The product formed should disappear in reaction with oxygen, producing CO_2 and 0.5 mole of H_2O_2 . This explains why the presence of CO_2 is not important for the kinetic treatment of the results.

Another question is to what extent the presence of bicarbonate contributes to the partial removal of hydroxyl radicals, thus reducing the decomposition yield of the oxalate ion. It has been shown recently^{24,31-33} that the bicarbonate and carbonate ions react efficiently with OH radicals, producing HCO_3^- and CO_3^- ion radicals, the rate constant being 1.10^7 and 3.10^8 $\text{M}^{-1} \text{sec}^{-1}$, respectively. However, these reactions can be hardly significant under our working conditions. The oxalate concentration is much larger than that of carbon dioxide, and the rate for oxalate-hydroxyl reaction is much higher. The CO_2 measurements in experiments with artificially enriched blanks also confirm that variations of carbon dioxide content initially present do not influence $G(\text{CO}_2)$ within the 10% dispersion observed. It should also be mentioned that

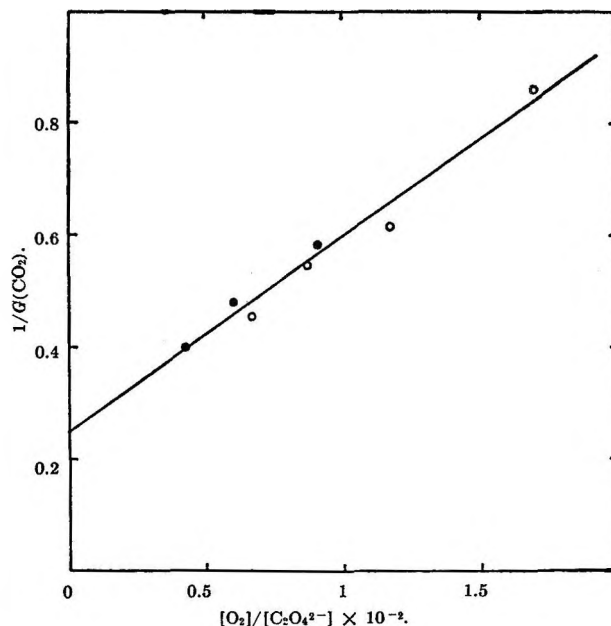


Figure 6. Competition between oxygen and oxalate for O^- at pH 13: \circ , 46 mM oxalate; and \bullet , 89 mM oxalate.

(25) O. L. Forcheimer and H. Taube, *J. Am. Chem. Soc.*, **76**, 2099 (1954).

(26) S. Gordon, E. J. Hart, M. S. Matheson, J. Rabani, and J. K. Thomas, *Discussions Faraday Soc.*, **36**, 193 (1963).

(27) G. Scholes, M. Simić, and J. J. Weiss, *ibid.*, **36**, 214 (1963).

(28) E. J. Hart, J. K. Thomas, and S. Gordon, *Radiation Res., Suppl.*, **4**, 74 (1964).

(29) J. J. Weiss, *ibid.*, **4**, 141 (1964).

(30) J. H. Baxendale, *ibid.*, **4**, 114 (1964).

(31) G. E. Adams, J. W. Boag, and B. D. Michael, *Trans. Faraday Soc.*, **61**, 1617 (1965).

(32) J. K. Thomas, *ibid.*, **61**, 702 (1965).

(33) J. P. Keene, Y. Raef, and A. J. Swallow, "Pulse Radiolysis," Proceedings of the International Symposium held at Manchester, April 1965, Academic Press, Inc., London, 1965.

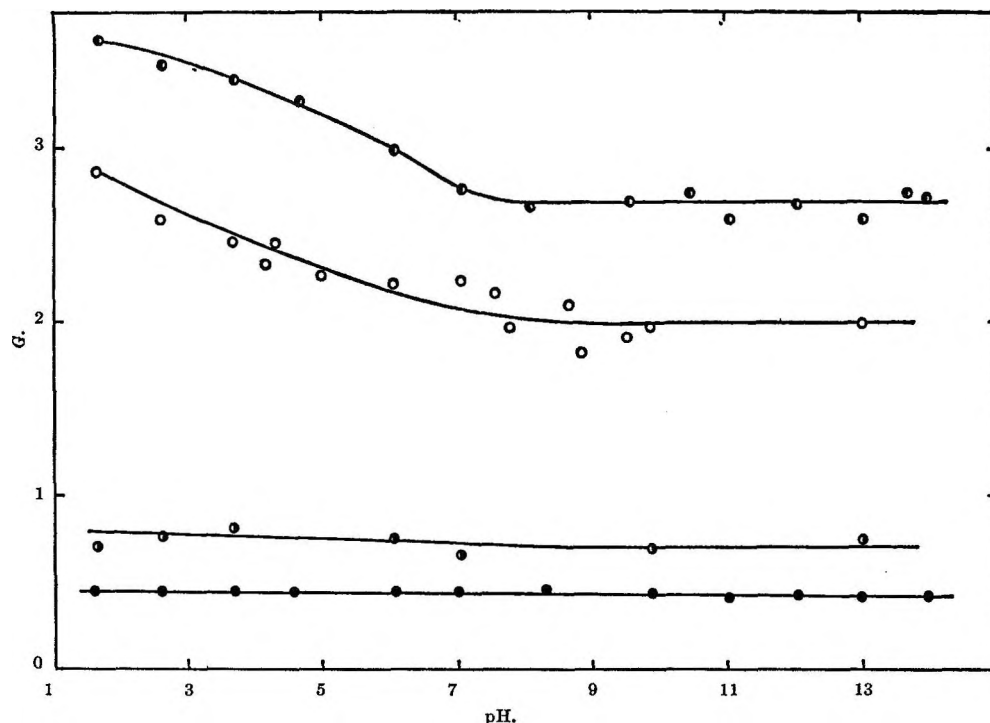


Figure 7. Primary radical and molecular yields from pH 1.6 to 14, derived from oxalic acid-oxygen system: \circ , $G_H + G_{e_{aq}^-}$; \circ , G_{OH} ; \circ , $G_{H_2O_2}$; and \bullet , G_{H_2} .

$G(H_2O_2)$ did not show any changes in experiments with CO_2 -enriched blanks.

The reaction scheme proposed and the experimental data obtained allow, by usual stationary-state kinetic treatment, the calculation of primary yields in water γ radiolysis.

Yield of Primary Molecular Hydrogen. From equations 1-9 it is seen that

$$G(H_2) = G_{H_2} \quad (10)$$

Equation 10 and the experimental data from Figure 2 give 0.40 for G_{H_2} in the whole pH region studied. However, this value requires a correction, because of the oxalate ion concentration influence on the second-order recombination reaction in which molecular hydrogen is produced (Figure 4). Extrapolation to zero scavenger concentration gives 0.44. This is within 2% experimental error consistent with values derived from the same system at pH < 10. Therefore, we consider for the pH region 9.5 to 14 that the primary molecular hydrogen yield is the same as it was found in acid and neutral media

$$G_{H_2} = 0.45$$

Yield of Primary Reducing Species. All short-lived reducing species react with oxygen, as given by eq 4 and 4'. From the reaction scheme we can derive

$$G(H_2O_2) = G_{H_2O_2} + 0.5(G_{e_{aq}^-} + G_H + G_{OH}) \quad (11)$$

On the assumption that the equation for the material balance

$$G_{OH} + 2G_{H_2O_2} = G_{e_{aq}^-} + G_H + 2G_{H_2} \quad (12)$$

is also correct for alkaline solutions, we obtain from eq 10-12

$$G_H + G_{e_{aq}^-} = G(H_2O_2) - G(H_2) \quad (13)$$

This equation and the data from Figure 2 give

$$G_H + G_{e_{aq}^-} = 2.7$$

for the whole pH region studied (9.5-14). The lower value given for pH 9.8 in the preceding work¹⁷ was due to the noninitial conditions in hydrogen peroxide measurements.

Yield of Primary Oxidizing Species and k_1/k_3 Rate Constant Ratio. From eq 11 and 13 we can also derive

$$G_{OH} + 2G_{H_2O_2} = G(H_2O_2) + G(H_2) \quad (14)$$

The yields of hydrogen peroxide and molecular hydrogen measured at pH 9.5-14 show that we can calculate for the whole region

$$G_{OH} + 2G_{H_2O_2} = 3.55$$

From eq 1-7 we have

$$G(\text{CO}_2) = 2G_{\text{OH}} \left\{ \frac{1}{1 + \frac{k_2[\text{OH}^-]}{k_1[\text{C}_2\text{O}_4^{2-}]} + \frac{1}{1 + \frac{k_7[\text{O}_2]}{k_3[\text{C}_2\text{O}_4^{2-}]}} - \frac{1}{\left(1 + \frac{k_2[\text{OH}^-]}{k_1[\text{C}_2\text{O}_4^{2-}]}\right)\left(1 + \frac{k_7[\text{O}_2]}{k_3[\text{C}_2\text{O}_4^{2-}]}\right)} \right\} \quad (15)$$

For $k_2[\text{OH}^-] \ll k_1[\text{C}_2\text{O}_4^{2-}]$, eq 15 becomes $G(\text{CO}_2) = 2G_{\text{OH}}$ in accordance with observations at pH < 10. For $k_2[\text{OH}^-] \gg k_1[\text{C}_2\text{O}_4^{2-}]$, we have

$$G(\text{CO}_2) = \frac{2G_{\text{OH}}}{1 + \frac{k_7[\text{O}_2]}{k_3[\text{C}_2\text{O}_4^{2-}]}} \quad (16)$$

In these calculations we had to assume that reaction 2 is not an equilibrium, which may be the case owing to the fairly large oxygen and oxalate concentrations.

The reciprocal form of eq 16 and experimental data given in Table I were used for plotting the graph in Figure 6. The least-squares method was used to obtain the slope of the curve, 34.91, and the intercept, 0.25, on the ordinate. Hence, we obtain $k_7/k_3 = 140$. We can also derive $G_{\text{OH}} = 2.0$ for pH 13, where these measurements were made. By using eq 14 and the experimental data for hydrogen peroxide and molecular hydrogen formation, the hydroxyl radical yield allows a calculation of the primary peroxide yield, $G_{\text{H}_2\text{O}_2} = 0.75$. One can see that the primary yields of oxidizing species obtained at pH 13 are in good agreement with the values derived from the same system at pH varying from 10 to neutral.¹⁷

Summary of Primary Yields in Water γ Radiolysis Derived from the Oxalate-Oxygen System at pH 1.6-14.

Figure 7 summarizes the data obtained in this work at pH > 9 and given in the preceding work¹⁷ at pH < 10.

It can be seen that the yields of short-lived species continually decrease from acid to neutral medium. When passing from neutral to alkaline media, no change in radical yields is observed. Molecular yields, however, remain practically unchanged in the whole pH region studied.

The oxalate-oxygen system is unique in that measurements to evaluate the radical and molecular yields may be made over the entire pH scale. However, some comparisons of the results obtained are still possible.

(1) In acid (pH 1.6) and neutral (pH 7) media, the yields derived from the oxalate-oxygen system are in good agreement with generally accepted values.³⁴ The free-radical yields determined in this work decrease steadily over the pH range acid to neutral. The steady decrease is contrasted with the sharp decrease observed at about pH 2 obtained in solutions of ferrous sulfate,³⁵ nitrous oxide,³⁶ and various solutes reported by Hayon.³⁷

(2) The results with the oxalate-oxygen system indicate no change in primary radical and molecular yields when the pH passes from neutral to alkaline, like hypobromite solutions.¹⁰

(3) The primary yields for alkaline medium derived from the aqueous oxalate-oxygen system are only in partial agreement with those derived from other systems.¹⁻⁹

(34) A. O. Allen, "The Radiation Chemistry of Water and Aqueous Solutions," D. Van Nostrand Co., Inc., New York, N. Y., 1961.

(35) W. G. Rothschild and A. O. Allen, *Radiation Res.*, **8**, 101 (1958).

(36) F. S. Dainton and D. B. Peterson, *Proc. Roy. Soc. (London)*, **A267**, 443 (1962).

(37) E. Hayon, *Trans. Faraday Soc.*, **61**, 723 (1965).

Effect of Pressure on Conductance. II. Walden Products and

Ionic Association in Methanol¹

by James F. Skinner and Raymond M. Fuoss

Contribution No. 1777 from the Sterling Chemistry Laboratory, Yale University, New Haven, Connecticut
(Received September 28, 1965)

The equivalent conductances of NaBr, Me₄NBr, Bu₄NBr, and Bu₄NBPh₄ in methanol have been measured at 31° up to 5000 kg/cm² from about 5 to 25 × 10⁻⁴ N. All the salts exhibit a decrease in conductance with increasing pressure, the relative decrease being nearly independent of concentration. The data were treated by the Fuoss-Onsager equation for unassociated electrolytes to determine the limiting conductances. For Bu₄NBPh₄, the Walden product is essentially constant up to 5000 kg/cm² over a more than threefold increase in solvent viscosity. The Walden products for the three bromides increase with pressure, presumably a consequence of the ability of the unsolvated bromide ion being able to slip through voids in the liquid. Analysis of the data, using the Fuoss-Kraus modification of the Ostwald dilution law, showed association for all four salts at 1 atm. For Me₄NBr and Bu₄NBPh₄, the association constant was independent of pressure, for NaBr it increases fivefold at 5000 kg/cm², and for Bu₄NBr, it decreases nearly to zero at maximum pressure.

Although a fairly substantial amount of data on the pressure dependence of conductance has accumulated in the literature, there has been no systematic study of the validity of Walden's rule over the range of viscosities available for a given solvent through application of hydrostatic pressure. A large number of investigations have been carried out on the pressure dependence of conductance in water, but many of these were done at only one concentration or on weak electrolytes. Korber² measured the conductances of a number of alkali halides at 3000 kg/cm² over a wide range of concentrations and found that at low concentrations the conductance went through a maximum with increasing pressure as the special water structure is destroyed. At higher concentrations, the maximum became less pronounced. There were, however, too few concentrations in the dilute region to permit extrapolation to infinite dilution. Adams and Hall³ measured the pressure dependence of conductance in water for a number of salts as a function of concentration, but their data were also at too high concentration to permit extrapolation. More recently, Ellis⁴ found that the limiting conductance of potassium chloride

in water went through a maximum at about 1000 kg/cm² in an investigation to 3000 kg/cm². The Walden product for this system shows an increase of 9% at 3000 kg/cm². Fisher^{5,6} has confirmed Ellis' findings on potassium chloride. It should be pointed out that at 5000 kg/cm² and 25° the viscosity of water has increased by about 30%, whereas for methanol under these conditions the increase is about 350%. This should, of course, magnify the pressure dependence of the Walden product. Horne⁷ has predicted that at pressures above about 2000 kg/cm², where the structure of water has been destroyed, Walden's rule should be obeyed by inorganic salts. Brummer⁸

(1) Grateful acknowledgment is made for the support of this work by the Directorate of Chemical Sciences, Air Force Office of Scientific Research Grant No. AF-AFOSR-244-63.

(2) F. Korber, *Z. Physik. Chem.*, **67**, 212 (1909).

(3) L. H. Adams and R. E. Hall, *J. Phys. Chem.*, **35**, 2145 (1931).

(4) A. J. Ellis, *J. Chem. Soc.*, 3689 (1959).

(5) F. H. Fisher, *J. Phys. Chem.*, **66**, 1607 (1962).

(6) F. H. Fisher and D. F. Davis, *ibid.*, **69**, 2595 (1965).

(7) R. A. Horne, *Nature*, **200**, 418 (1963).

(8) S. B. Brummer, *J. Chem. Phys.*, **42**, 1636 (1965).

has determined the limiting conductance to 1900 kg/cm² in N,N-dimethylformamide for a number of salts at different temperatures in order to calculate activation energies. A lack of data on the pressure dependence of viscosity for the solvent, however, prohibits calculation of the Walden product as a function of pressure. Skinner and Fuoss⁹ have measured conductance in diethyl ether and benzene over a range of solute concentrations to 5000 kg/cm², but the high degree of association in these solvents of low dielectric constant precludes extrapolation.

In the present investigation, methanol was chosen as the solvent because literature data are available for the pressure dependence of density, dielectric constant, and viscosity. The value of the dielectric constant is such that ionic association should be low. The concentration range was chosen such that limiting conductances could be determined ($\kappa a < 0.2$). The results show that for Bu₄NBPh₄ the Walden product remains constant within experimental error up to 5000 kg/cm², while for NaBr there is an increase in $\Lambda_0\eta$ of 47%; Me₄NBr and Bu₄NBr illustrate intermediate cases. Although the precision of the data was too low for evaluation of the ion-pair association constant from the extended Fuoss equation, use of the modified Ostwald dilution law did show substantial association. For NaBr, the association constant increases with pressure; for Bu₄NBr, it decreases; for the other two salts, the association was independent of pressure.

Experimental Section

The pressure-generating system and the temperature control of the autoclave have been previously described.⁹ Solvent and solution resistances were measured on a Shedlovsky conductance bridge¹⁰ and were extrapolated to infinite frequency (R vs. f^{-1}) from values at 1, 2, 5, and 10 kc. The conductance cell for the present work consisted of the previous Teflon piston and cylinder⁹ with a different electrode plug screwed into the bottom. The electrodes were two square pieces (1.5 × 1.5 cm) of 0.5-mm bright platinum, mounted vertically about 1 cm apart, each on two platinum rods cemented into the Supramica plug with epoxide. One rod for each electrode came through the plug to act as an electrical lead, dipping into a mercury cup. Supramica absorbs water so a cell calibration with aqueous potassium chloride was impossible. Treiner and Fuoss¹¹ have measured the conductance of tetrabutylammonium bromide in acetonitrile at 25°. Their data were used to determine the constants of the Fuoss-Onsager equation for unassociated electrolytes¹²; the following equation reproduces the data within ±0.2%.

$$\Lambda = 161.0 - 350c^{1/2} + 274c \ln(14.26c) + 858c \quad (1)$$

The high-pressure cell was then calibrated at 25° with tetrabutylammonium bromide in acetonitrile at three concentrations (16, 21, and 26 × 10⁻⁴ M) giving a cell constant of 0.1623 ± 0.0002 cm⁻¹ which was assumed to be valid at 31°, the temperature at which the measurements were made. The cell constant was also assumed to be independent of pressure within our precision of about 1%. (The electrodes are mounted on a rigid ceramic base, 1 cm apart and centered in a tube 2.5 cm in diameter. The movable Teflon plunger is 10–13 cm distant from the top of the electrodes, so any change in fringe field due to its motion should have a trivial effect on the cell constant.) Over the period required for the measurements, the temperature was constant to 31.0 ± 0.5°; the conductance values can be assumed to be accurate to about 1%. Solutions were prepared by weight in separate flasks before transferring to the cell. Vapor corrections were applied to all solutions. The solvent density corresponding to the relevant pressure was used to convert weight concentration to molarity.

Methanol was dried by refluxing 2-l. batches over 12 g of aluminum powder and 3 g of mercuric chloride for at least 6 hr under nitrogen. The solvent was used directly after distillation; it had a conductance of 7 × 10⁻⁸ mho, which amounts to only 0.2% of the lowest specific conductance involved. Solvent correction was therefore neglected. Sodium bromide (Harshaw Chemical Co.) was used as received, as random cuttings from crystals grown from melts. Tetramethylammonium bromide (Eastman 670) was recrystallized twice from a 1:1 mixture of methanol and absolute ethanol (5 g of salt/110 ml of solvent). The salt was dried at 40° and 15 mm for 2 days. Tetrabutylammonium bromide (Eastman 7377) was recrystallized twice in the following manner. A sample (20 g) of the salt was dissolved in 100 ml of boiling benzene and precipitated by addition of 300 ml of hot *n*-hexane. After filtration, the precipitate was dried for 1 week at 40° and 15 mm pressure. Tetrabutylammonium tetrabenzylboride was from laboratory stock; it was purified in the manner described by Coplan.¹³

The pressure dependences of the solvent properties (density, dielectric constant, and viscosity) have been calculated from literature data. Bridgman¹⁴ meas-

(9) J. F. Skinner and R. M. Fuoss, *J. Phys. Chem.*, **69**, 1437 (1965).

(10) J. E. Lind, Jr., and R. M. Fuoss, *ibid.*, **65**, 999 (1961).

(11) C. Treiner and R. M. Fuoss, *Z. Physik. Chem.*, **228**, 343 (1965).

(12) R. M. Fuoss, L. Onsager, and J. F. Skinner, *J. Phys. Chem.*, **69**, 2581 (1965).

(13) M. A. Coplan and R. M. Fuoss, *ibid.*, **68**, 1177 (1965).

ured the relative volumes of methanol at 30° to 12,000 kg/cm². Literature values^{15,16} of the density of methanol at 1 atm at 30 and 31° are 0.7818 and 0.7809 g/ml. From Bridgman's data and the 30° value, densities at 30° to 5000 kg/cm² were calculated and then fitted to the Tait equation¹⁷ by the method of least squares.

$$1 - \rho(1)/\rho(P) = A \log [(B + P)/(B + 1)] \quad (2)$$

where $\rho(1)$, $\rho(P)$ are the densities at 1 and P kg/cm² and A and B are empirical constants, both independent of temperature within experimental error over small temperature ranges. For methanol at 30°, the values of $A = 0.242$ and $B = 981$ kg/cm² were obtained. These values of A and B were used together with the 31° density at 1 atm to calculate densities at 31° and any pressure for the present work. Values at integral pressures are given in Table I.

Table I: Properties of Methanol to 5000 Kg/Cm²

| Pressure P , kg/cm ² | Density ρ , g/ml | 31° dielectric constant ϵ' | Viscosity 100 η |
|--------------------------------------|--------------------------|--|-------------------------|
| 1 | 0.7809 | 31.45 | 0.502 |
| 1000 | 0.8430 | 34.00 | 0.738 |
| 2000 | 0.8840 | 35.86 | 0.980 |
| 3000 | 0.9156 | 37.38 | 1.25 |
| 4000 | 0.9415 | 38.67 | 1.49 |
| 5000 | 0.9639 | 39.81 | 1.79 |

The dielectric constant¹⁸ of methanol at 25° is 32.63, and the derivative,¹⁸ $d(\log \epsilon')/dT$, in this range, is given as 0.260×10^{-2} . A value of 31.45 can be calculated at 31° which agrees well with a value graphically interpolated from literature values¹⁸⁻²⁰ at 20, 25, and 35°. The pressure dependence of the dielectric constant of methanol has been measured by Kyropoulos²¹ at 20° to 3000 kg/cm² and by Hartmann and co-workers²⁰ at 20 and 35° to 1800 kg/cm². These three separate sets of data were fitted to the Owen-Brinkley²² modification of the Tait equation

$$1 - \epsilon'(1)/\epsilon'(P) = A' \log [(B + P)/(B + 1)] \quad (3)$$

where $\epsilon'(1)$, $\epsilon'(P)$ are the dielectric constants at 1 and P kg/cm² and A' and B are empirical constants. The least-squaring gave for Kyropoulos (20°), Hartmann (20°), and Hartmann (35°) values of $A' = 0.313$, 0.257, and 0.241, respectively, and of $B = 1356$, 940, and 770 kg/cm², the data being fitted to 0.1% in all cases. To determine the sensitivity of the dielectric constant calculated from (3) to the values of A' and B , values at 4000 kg/cm² were computed, using the

above three sets of constants and the value 31.45 for $\epsilon'(1)$. The results were 38.67, 38.59, and 38.86, showing that the calculated values of $\epsilon'(P)$ are relatively insensitive to large variations in A' and B . The values obtained from Kyropoulos' data were chosen because his work covers a higher pressure range; these values of A' and B together with the 31° dielectric constant value were used to calculate dielectric constants at any pressure from (3). Values at integral pressures are given in Table I.

Graphical interpolation from values of the viscosity of methanol^{15,16,19} at 10, 20, 25, 30, and 40° gave a value of 0.502 cp at 31°. Bridgman^{23,24} measured the pressure dependence of the viscosity of methanol at 30° to 10,000 kg/cm². It was assumed that the pressure dependence would be independent of temperature over a small temperature range. From a graphical interpolation of Bridgman's data on a $\log [\eta_0(P)/\eta_0(1)]$ against pressure plot and the 1-atm value at 31°, it was possible to calculate viscosities at integral pressures. These values are listed in Table I. The following interpolation equation reproduces Bridgman's values at 1, 1000, and 4000 kg/cm² and the values in Table I to 1%; it was used to calculate viscosities.

$$\eta_0(P) = 0.502 + 0.228 \times 10^{-3} P + 0.005 \times 10^{-6} P^2 \quad (4)$$

The conductance data are given in Tables II-V. Pressures are given in kilograms per square centimeter and concentrations in equivalents per liter; Λ is equivalent conductance. For a given run, the weight concentration w was, of course, constant. In order to obtain the equivalent conductances given in the tables, 1000 times the observed specific conductance was divided by $c = w\rho$, where ρ is the density calcu-

(14) P. W. Bridgman, *Proc. Am. Acad. Arts Sci.*, **49**, 1 (1913-1914).

(15) J. Timmermans, "Physico-Chemical Constants of Pure Organic Compounds," Elsevier Publishing Co. Inc., New York, N. Y., 1950.

(16) "International Critical Tables," McGraw-Hill Book Co., Inc., New York, N. Y., 1933.

(17) H. S. Harned and B. B. Owen, "Physical Properties of Electrolytic Solutions," 3rd ed, Reinhold Publishing Corp., New York, N. Y., 1958.

(18) "Table of Dielectric Constants of Pure Liquids," National Bureau of Standards, Circular 514, U. S. Government Printing Office, Washington, D. C., 1951.

(19) A. Weissberger, "Organic Solvents," 2nd ed, Interscience Publishers, Inc., New York, N. Y., 1955.

(20) H. Hartmann, A. Neumann, and G. Rinck, *Z. Physik. Chem.*, **44**, 204, 218 (1965).

(21) S. Kyropoulos, *Z. Physik*, **40**, 507 (1926).

(22) B. B. Owen and S. R. Brinkley, *Phys. Rev.*, **64**, 32 (1943).

(23) P. W. Bridgman, "Physics of High Pressure," G. Bell and Sons Ltd., London, 1958, p 344.

(24) P. W. Bridgman, *Proc. Am. Acad. Arts Sci.*, **77**, 117 (1949).

lated from (2), using the relevant pressure. It should be noted that the 1-atm values before and after pressurizing agree to better than 1% in most cases, although the conductance changes under pressure by as much as a factor of 3.5.

Table II: Conductance of NaBr in Methanol at 31°

| P | 10 ^c | Δ | P | 10 ^c | Δ |
|------|-----------------|-------|------|-----------------|-------|
| 1 | 25.47 | 97.0 | 1 | 19.44 | 98.2 |
| 1027 | 27.54 | 75.4 | 1048 | 21.05 | 75.8 |
| 1979 | 28.80 | 63.4 | 1993 | 22.00 | 63.9 |
| 3129 | 29.98 | 53.9 | 3094 | 22.86 | 52.7 |
| 4078 | 30.77 | 46.4 | 4120 | 23.51 | 45.2 |
| 4922 | 31.38 | 41.4 | 4851 | 23.92 | 40.5 |
| 1 | 25.47 | 96.8 | | | |
| 1 | 14.78 | 99.9 | 1 | 11.99 | 100.2 |
| 1002 | 15.96 | 77.2 | 963 | 12.92 | 78.3 |
| 2011 | 16.74 | 63.8 | 1955 | 13.55 | 65.1 |
| 3129 | 17.40 | 52.9 | 3094 | 14.10 | 54.2 |
| 4085 | 17.86 | 45.8 | 4078 | 14.49 | 47.1 |
| 4858 | 18.18 | 40.8 | 4904 | 14.77 | 42.1 |
| 1 | 14.78 | 97.0 | 1 | 11.99 | 100.1 |
| 1 | 11.58 | 101.7 | 1 | 9.97 | 102.1 |
| 927 | 12.45 | 79.6 | 998 | 10.76 | 79.3 |
| 1983 | 13.10 | 65.2 | 2021 | 11.29 | 65.6 |
| 3108 | 13.62 | 54.1 | 3090 | 11.72 | 55.3 |
| 4064 | 13.98 | 46.9 | 4077 | 12.04 | 48.0 |
| 4918 | 14.26 | 41.6 | 4774 | 12.24 | 43.5 |
| 1 | 11.58 | 100.2 | 1 | 9.97 | 102.1 |
| 1 | 7.27 | 103.2 | 1 | 5.60 | 104.2 |
| 1005 | 7.85 | 79.8 | 1011 | 6.05 | 80.8 |
| 1941 | 8.21 | 67.1 | 1976 | 6.33 | 67.9 |
| 3094 | 8.54 | 55.6 | 3094 | 6.58 | 56.5 |
| 4085 | 8.78 | 48.2 | 4074 | 6.76 | 49.2 |
| 4795 | 8.93 | 43.7 | 4880 | 6.89 | 44.2 |
| 1 | 7.27 | 102.9 | 1 | 5.60 | 103.0 |

Discussion

In methanol, with a dielectric constant of 31.45, association of ions to pairs is slight or negligible (depending on the salt), and the change of conductance with pressure should be primarily a consequence of the change in viscosity. If the sphere-in-continuum model correctly described ionic solutions in methanol, the Walden product, $\Lambda_{0\eta}$, would be independent of pressure as also would be the radii calculated by Stokes' equation. It is well known that the product is only approximately constant for a given electrolyte in a series of solvents, the constancy being better in general the larger the ions. Water and other hydrogen-bonded solvents show a special pattern: the product usually is considerably larger for them than for aprotic solvents. Destruction of hydrogen-bonded structures²⁵ by the

Table III: Conductance of Me₄NBr in Methanol at 31°

| P | 10 ^c | Δ | P | 10 ^c | Δ |
|------|-----------------|-------|------|-----------------|-------|
| 1 | 24.46 | 118.0 | 1 | 19.89 | 119.1 |
| 907 | 26.46 | 93.0 | 1027 | 21.51 | 92.0 |
| 1934 | 27.83 | 76.1 | 1969 | 22.49 | 76.0 |
| 3080 | 28.97 | 62.7 | 3117 | 23.40 | 62.0 |
| 4106 | 29.79 | 53.5 | 4127 | 24.06 | 53.0 |
| 5055 | 30.45 | 46.8 | 5062 | 24.59 | 46.5 |
| 1 | 24.64 | 117.8 | 1 | 19.89 | 118.5 |
| 1 | 17.31 | 120.7 | 1 | 15.21 | 121.8 |
| 1019 | 18.71 | 92.9 | 1005 | 16.42 | 93.6 |
| 1976 | 19.57 | 76.9 | 1969 | 17.19 | 77.3 |
| 3108 | 20.36 | 63.0 | 3104 | 17.89 | 63.3 |
| 4078 | 20.91 | 53.7 | 4155 | 18.41 | 53.9 |
| 4816 | 21.27 | 48.0 | 5076 | 18.80 | 47.4 |
| 1 | 17.31 | 118.9 | 1 | 15.21 | 122.4 |
| 1 | 12.41 | 123.2 | 1 | 10.13 | 123.7 |
| 977 | 13.37 | 95.6 | 977 | 10.92 | 96.4 |
| 1983 | 14.03 | 78.1 | 1969 | 11.46 | 80.3 |
| 3108 | 14.59 | 64.2 | 3108 | 11.92 | 65.8 |
| 4190 | 15.03 | 54.3 | 4120 | 12.25 | 56.2 |
| 4950 | 15.30 | 48.6 | 4936 | 12.49 | 50.0 |
| 1 | 12.41 | 123.7 | 1 | 10.13 | 124.2 |
| 1 | 7.51 | 125.9 | | | |
| 1012 | 8.12 | 96.6 | | | |
| 2004 | 8.50 | 79.1 | | | |
| 3108 | 8.83 | 65.4 | | | |
| 4134 | 9.09 | 55.9 | | | |
| 4851 | 9.24 | 50.4 | | | |

ionic fields, which leads to an effective viscosity near the ion which is less than the macroscopic viscosity of the solvent, could account for the higher relative mobility in such solvents. The constancy of the product also fails in general for small ions in mixed solvents. When the ions are of about the same size as the solvent molecules, the packing of the latter and the shape and size of the gaslike regions ("holes") in the liquid will, of course, determine the average resistance to ionic motion which one measures through the conductance. Finally, for all polar solvents, there is an electrostatic drag on the ions due to the nonzero relaxation time of the dielectric through which they are moving.²⁶ Many previous investigations of the behavior of the Walden product were based on measurements in mixed solvents; possible complications here are selective solvation for the ions by one component of the mixture, or unmixing in the ionic fields which would concentrate the more polar com-

(25) H. S. Frank, *Proc. Roy. Soc. (London)*, **A247**, 481 (1958).

(26) (a) R. M. Fuoss, *Proc. Natl. Acad. Sci. U. S.*, **45**, 807 (1959);
(b) R. Zwanzig, *J. Chem. Phys.*, **38**, 1603 (1963).

Table IV: Conductance of Bu_4NBr in Methanol at 31°

| <i>P</i> | 10 ⁴ <i>c</i> | Λ | <i>P</i> | 10 ⁴ <i>c</i> | Λ |
|----------|--------------------------|-----------|----------|--------------------------|-----------|
| 1 | 27.00 | 88.6 | 1 | 24.15 | 88.9 |
| 854 | 28.90 | 69.7 | 991 | 26.06 | 67.6 |
| 1814 | 30.33 | 57.3 | 1934 | 27.27 | 56.1 |
| 3076 | 31.73 | 46.1 | 3097 | 28.41 | 47.9 |
| 4127 | 32.66 | 39.2 | 4113 | 29.21 | 39.6 |
| 4851 | 33.22 | 35.7 | 4785 | 29.68 | 36.1 |
| 1 | 27.00 | 88.3 | 1 | 24.15 | 88.9 |
| 1 | 19.30 | 90.1 | 1 | 15.25 | 91.6 |
| 700 | 20.46 | 73.3 | 1023 | 16.49 | 68.4 |
| 1835 | 21.71 | 57.8 | 1948 | 17.23 | 56.8 |
| 3092 | 22.69 | 46.5 | 3094 | 17.94 | 46.7 |
| 4190 | 23.39 | 39.6 | 4071 | 18.43 | 40.4 |
| 4869 | 23.76 | 35.9 | 4936 | 18.80 | 35.6 |
| 1 | 19.30 | 90.9 | 1 | 15.25 | 91.6 |
| 1 | 11.73 | 92.8 | 1 | 8.59 | 94.9 |
| 309 | 12.08 | 83.1 | 1034 | 9.29 | 70.8 |
| 1160 | 12.78 | 66.9 | 1997 | 9.73 | 58.3 |
| 1976 | 13.27 | 56.9 | 3090 | 10.10 | 48.3 |
| 3094 | 13.79 | 46.8 | 4092 | 10.38 | 41.2 |
| 4103 | 14.18 | 39.9 | 4711 | 10.54 | 37.0 |
| 4192 | 14.42 | 36.2 | | | |
| 1 | 11.73 | 91.7 | | | |
| 1 | 6.02 | 95.9 | | | |
| 1030 | 6.51 | 71.5 | | | |
| 1948 | 6.80 | 59.2 | | | |
| 3094 | 7.08 | 48.7 | | | |
| 4036 | 7.27 | 42.3 | | | |
| 4781 | 7.40 | 38.0 | | | |
| 1 | 6.02 | 96.2 | | | |

Table V: Conductance of Bu_4NBPh_4 in Methanol at 31°

| <i>P</i> | 10 ⁴ <i>c</i> | Λ | <i>P</i> | 10 ⁴ <i>c</i> | Λ |
|----------|--------------------------|-----------|----------|--------------------------|-----------|
| 1 | 25.20 | 67.6 | 1 | 20.27 | 68.9 |
| 935 | 27.10 | 47.6 | 1005 | 21.89 | 47.3 |
| 1948 | 28.47 | 35.8 | 1944 | 22.90 | 36.6 |
| 3101 | 29.63 | 27.1 | 3108 | 23.85 | 27.7 |
| 4092 | 30.45 | 22.2 | 4120 | 24.51 | 22.7 |
| 4960 | 31.07 | 18.9 | 4922 | 24.98 | 19.5 |
| 1 | 25.20 | 67.1 | 1 | 20.27 | 68.7 |
| 1 | 16.90 | 71.4 | 1 | 15.53 | 71.8 |
| 970 | 18.22 | 49.2 | 1065 | 16.83 | 48.0 |
| 1976 | 19.12 | 37.2 | 1955 | 17.55 | 37.7 |
| 3101 | 19.88 | 28.9 | 3139 | 18.29 | 28.6 |
| 4089 | 20.43 | 23.7 | 4201 | 18.82 | 23.1 |
| 4957 | 20.84 | 20.1 | 4830 | 19.10 | 20.5 |
| 1 | 16.90 | 71.1 | 1 | 15.53 | 71.1 |
| 1 | 12.75 | 72.4 | 1 | 10.72 | 73.5 |
| 1019 | 13.79 | 49.3 | 1027 | 11.59 | 50.8 |
| 1997 | 14.43 | 38.0 | 1969 | 12.12 | 38.7 |
| 3146 | 15.02 | 29.1 | 3115 | 12.61 | 29.7 |
| 4078 | 15.41 | 24.3 | 4085 | 12.95 | 24.5 |
| 4830 | 15.68 | 21.1 | 4957 | 13.22 | 20.9 |
| | | | 1 | 10.72 | 73.4 |
| 1 | 9.46 | 74.3 | | | |
| 970 | 10.20 | 50.9 | | | |
| 1990 | 10.70 | 38.4 | | | |
| 3094 | 11.12 | 29.7 | | | |
| 4092 | 11.43 | 24.3 | | | |
| 4915 | 11.65 | 20.8 | | | |
| 1 | 9.46 | 73.7 | | | |

ponent near the ions.^{27,28} By working in a single solvent of moderately high dielectric constant, however, and changing the viscosity by increasing the pressure, the chemical environment of the ions remains unchanged. Our experimental results represent such a situation.

The data of Tables II-V show a common pattern for all four salts at all concentrations: as the pressure increases, the conductance decreases. Furthermore, the relative decrease is almost independent of concentration; in the three-dimensional surface which shows Λ as a function of P and c , the Λ - P curves, which are the intersections of planes at constant concentration with this surface, are nearly parallel. This can also be seen by considering the ratios, $\Lambda(5000 \text{ kg/cm}^2)/\Lambda(1 \text{ atm})$, for the different salts at the highest and lowest concentrations measured. For sodium bromide, the ratio is 0.423 and 0.425 for 1-atm concentrations 25.5 and 5.60×10^{-4} ; for Me_4NBr , 0.397 and 0.400 for concentrations 24.6 and 7.51×10^{-4} ; for Bu_4NBr , 0.404 and 0.396 for concentrations 27.0 and 6.02×10^{-4} ;

and for Bu_4NBPh_4 , 0.280 and 0.280 for concentrations 25.2 and 9.46×10^{-4} . The much greater decrease for the last salt is reflected in the behavior of its Walden product as contrasted to that of the products for the other three, as will be shown later. In Figure 1 are shown Λ - P curves at selected concentrations (see caption) for the four salts. We note that the relative decrease in conductance is greatest for Bu_4NBPh_4 , the salt with the largest ions. The curves are, of course, much simpler than those reported for solutions in solvents of lower dielectric constant,^{9,29} where, in addition to changes in viscosity, increasing pressure also changes the extent of ion association as a consequence of increasing dielectric constant.

In order to discuss the effects of pressure in a more quantitative fashion, the effect of concentration must be eliminated, so that molecular parameters can be studied. The concentration range was chosen to per-

(27) J. B. Hyne, *J. Am. Chem. Soc.*, **85**, 304 (1963).(28) H. K. Bodenseh and J. B. Ramsey, *J. Phys. Chem.*, **67**, 140 (1963).(29) C. M. Apt, *et al.*, *ibid.*, **66**, 1210 (1962).

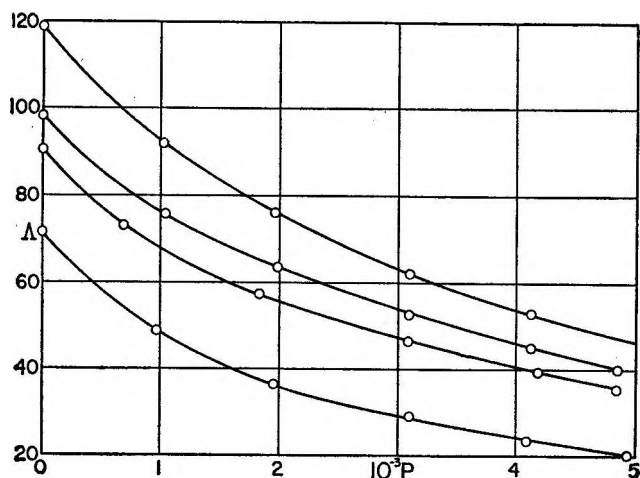


Figure 1. Pressure (kilograms per square centimeter) dependence of conductance in methanol at 31°. Top to bottom: Me₄NBr at 0.001989 *N*; NaBr at 0.001944 *N*; Bu₄NBr at 0.001930 *N*; and Bu₄NBPh₄ at 0.001690 *N*.

mit extrapolation for limiting conductance; however, the raw data of Tables II–V cannot be immediately analyzed, because the volume concentration, for the fixed-weight concentration of a given run, increases with pressure due to the compression of the solution. Consequently, large-scale plots of $\Lambda\eta$ against pressure were made for each run, and values of this variable were then read off at round values of pressure (1000–5000 kg/cm²). The necessary viscosities were calculated by means of (4). From the interpolated $\Lambda\eta$ values, the conductances were then computed at the round pressures. Finally, the volume concentrations were computed from the initial weight concentrations and the densities at round pressures, using (2) to calculate the densities. (Interpolation was made on $\Lambda\eta$ -*P* plots rather than on Λ -*P* plots, because the former are relatively much less steep and hence permit more precise interpolation.)

The Λ -*c* values at integral pressures were then analyzed by means of the equation¹²

$$\Lambda = \Lambda_0 - Sc^{1/2} + E'c \ln(6E_1'c) + Lc \quad (5)$$

which is valid for unassociated electrolytes, in order to obtain the limiting conductances given in Table VI.

If association occurs, eq 5 must be replaced by

$$\Lambda = \Lambda_0 - Sc^{1/2}\gamma^{1/2} + E'c\gamma \ln \tau^2\gamma + Lc\gamma - K_A c\gamma e^{-2\tau}\Lambda \quad (6)$$

which, for small values of the association constant K_A where γ (the fraction of free ions) approaches unity, becomes to a good approximation

$$\Lambda = \Lambda_0 - Sc^{1/2} + E'c \ln \tau^2 + (L - K_A\Lambda_0)c \quad (7)$$

Table VI: Pressure Dependence of Limiting Conductance and Ion-Ion Contact Parameter

| <i>P</i> , kg/cm ² | Λ_0 | | αL | Λ_0 |
|----------------------------------|---------------------|-----------|-------------|-------------|
| | NaBr | | | |
| 1 | 110.8 ± 0.2 | 2.9 ± 0.3 | 134.9 ± 0.1 | |
| 1000 | 84.5 ± 0.2 | 3.4 ± 0.4 | 103.1 ± 0.3 | |
| 2000 | 70.0 ± 0.2 | 1.9 ± 0.7 | 84.6 ± 0.1 | |
| 3000 | 58.9 ± 0.3 | 0.5 ± 0.4 | 70.1 ± 0.2 | |
| 4000 | 53.5 ± 0.4 | ... | 60.7 ± 0.2 | |
| 5000 | 45.7 ± 0.5 | ... | 51.8 ± 0.2 | |
| | Λ_0 | | αL | Λ_0 |
| | Bu ₄ NBr | | | |
| 1 | 102.6 ± 0.2 | 2.3 ± 0.3 | 83.0 ± 0.4 | |
| 1000 | 76.2 ± 0.3 | 3.4 ± 0.7 | 57.1 ± 0.2 | |
| 2000 | 61.8 ± 0.2 | 3.5 ± 0.7 | 43.3 ± 0.2 | |
| 3000 | 51.1 ± 0.1 | 3.8 ± 0.5 | 33.8 ± 0.2 | |
| 4000 | 44.5 ± 0.1 | 3.8 ± 0.8 | 27.9 ± 0.2 | |
| 5000 | 38.0 ± 0.1 | 4.0 ± 0.7 | 22.9 ± 0.1 | |

Inspection of (5) and (7) shows that the right-hand sides of both have the same functional dependence on concentration; in other words, when association is slight

$$\Lambda' = \Lambda_{\text{obsd}} + Sc^{1/2} - E'c \ln \tau^2 \quad (8)$$

$$= \Lambda_0 + (L - K_A\Lambda_0)c \quad (9)$$

is still a linear function of *c*, but with a coefficient obviously smaller than *L*. The latter in turn is a function of *a*, the contact distance. Consequently, the value of *L* obtained by empirical analysis of conductance data by means of (5) is a diagnostic test for slight association: if *L* is too small (*i.e.*, gives absurdly small contact distances), then association is present. (For higher degrees of association, the Λ' -*c* plots become curved.) The data for both Me₄NBr and Bu₄NBPh₄ gave very small (or even negative) values for the linear coefficient, and we conclude that these salts are associated. Sodium bromide gives a reasonable *a* value for 1–1000 kg/cm² but at higher pressures, *L* (and hence *a*) drops to unrealistic values; hence the association constant of sodium bromide in methanol *increases* with increasing pressure. For Bu₄NBr, on the other hand, the 1-atm value of *a* looks too small; as the pressure increases, the value of this parameter increases. Therefore Bu₄NBr is somewhat associated in methanol at 1 atm, and the association *decreases* with increasing pressure.

The precision of the data (hopefully ±0.5%) was too low to permit analysis by the program for eq 6, the equation for associated electrolytes. Consequently, they were analyzed by the Fuoss-Kraus equation³⁰

$$F(z)/\Lambda = 1/\Lambda_0 + c\Delta f^2 K_A/\Lambda_0^2 F(z) \quad (10)$$

which is a fair approximation to (6) because it has been shown¹² that the $Ec \log c$ and Lc terms of (6) nearly compensate each other at moderate dielectric constant. The values of Λ_0 from Table VI were used to compute $F(z)$; the $F/\Lambda - c\Delta f^2/F$ plots were linear, with some scatter. From their slopes, the association constants shown in Figure 2 were obtained.

Two effects of pressure are visible, one which increases association and one which decreases it. Increasing dielectric constant, as has already been shown⁹ experimentally, decreases association. The dielectric constant of methanol increases by 27% on going to 5000 kg/cm²; assuming $\hat{d} = 4$, the Boltzmann factor e^b in the association constant decreases to about one-third for this increase in D (from 260 to 80). This can account for most of the decrease in K_A for Bu_4NBr shown in Figure 2. Sodium bromide, in contrast, associates more with increasing pressure. If one assumes that the free ions are solvated, and that the ion pairs are unsolvated (or solvated to a smaller extent), the accompanying decrease in volume on association would be favored by increasing pressure, and therefore K_A should increase with increasing pressure. The two other salts, Me_4NBr and Bu_4NBPh_4 , show a moderate association which is independent of pressure. Noncoulombic association and no solvation would account for such behavior; this is, of course, *ad hoc* speculation. Fisher^{5,6} found that the association constants for magnesium and manganese sulfates in water decrease approximately to half on going to 2000 kg/cm². One thing is clear: a wide variety of solutes and solvents must be investigated before

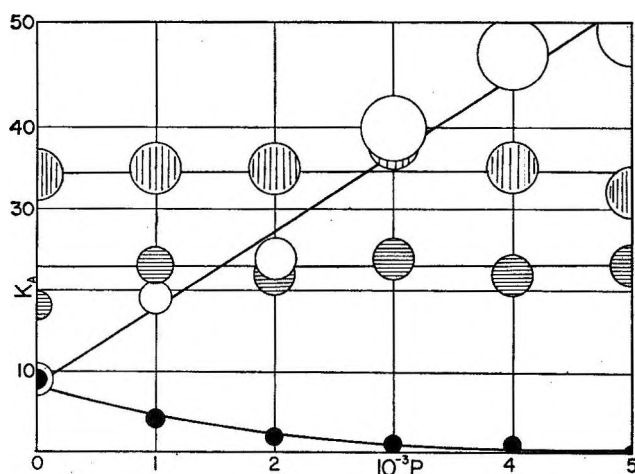


Figure 2. Pressure dependence of association constants: open circles, NaBr ; vertical crosshatch, Bu_4NBPh_4 ; horizontal crosshatch, Me_4NBr ; and solid circles, Bu_4NBr .

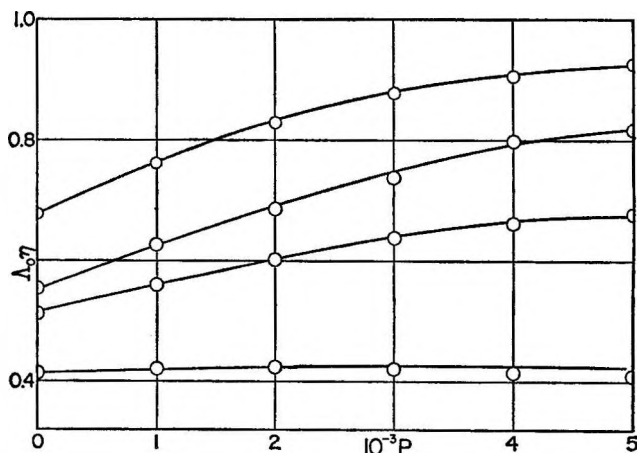


Figure 3. Pressure dependence of Walden products. Top to bottom: Me_4NBr , NaBr , Bu_4NBr , and $\text{Bu}_4\text{N} \cdot \text{BPh}_4$.

generalizations concerning the effects of pressure on ionic association can be made.

The Walden products are shown as a function of pressure in Figure 3. The values at 1 atm of 0.557, 0.515, and 0.417 for NaBr , Bu_4NBr , and Bu_4NBPh_4 , respectively, agree well with the literature values of 0.554,³¹ 0.519,³² and 0.414.¹³ The sequence correlates with size for the three quaternary salts ($\text{Me}_4\text{NBr} > \text{Bu}_4\text{NBr} > \text{Bu}_4\text{NBPh}_4$) in the expected way. The fact that the Walden product for sodium bromide is intermediate between the values of the two quaternary bromides suggests that the sodium ion is highly solvated, which is the conclusion also drawn from the increase in association constant with pressure for this salt.

Next, we consider the dependence of the Walden products on pressure. For Me_4NBr , NaBr , and Bu_4NBr , $\Lambda_0\eta$ increases with pressure; that is, the conductance does not decrease as rapidly as the macroscopic fluidity ($1/\eta$) decreases. Since the product for Bu_4NBPh_4 is substantially independent of pressure, these large ions evidently do behave like Stokes spheres in methanol. Consequently, the pressure dependence of $\Lambda_0\eta$ for the other three salts must be mostly a property of the bromide ions. We note also that the curves of Figure 3 are concave-down, and appear to be approaching an asymptotic value (where classical hydrodynamics would describe the system). Suppose a hybrid model represents the solvent: a continuous phase in which the ionic motion is hydrodynamic and in which

(30) R. M. Fuoss and C. A. Kraus, *J. Am. Chem. Soc.*, **55**, 476 (1933); R. M. Fuoss, *ibid.*, **57**, 488 (1935).

(31) A. R. Gordon, R. E. Jerris, D. R. Muir, and J. P. Butler, *ibid.*, **75**, 2855 (1953).

(32) M. A. Coplan, Dissertation, Yale University, 1963.

there are also empty spaces through which an ion can jump. Then the mobility of the bromide ion at 1 atm would be too high, in the sense that its average mobility as measured by conductance would be greater than that calculated for a sphere of a certain radius in the continuum, because it would slip through the holes in the methanol and thereby gain extra traversed distance without paying for it in friction. As pressure is increased, the free volume decreases. Schematically, if x represents the fraction of holes, and if the motion in the continuum is Stokesian, we could write

$$\Lambda_0 = (1 - x)A/\eta + Bx$$

As pressure increases, $(1 - x)$ and η increase; if the viscosity increases faster than x decreases, it is clear that $\Lambda_0\eta$ would increase at first and then level off at the value A at pressures where x was effectively zero.

The relaxation effect²⁶ also contributes to the change of Walden product with pressure, because it depends on dielectric constant which increases with increasing pressure. Coetzee and Cunningham³³ give 61.93 and 57.72 as the limiting mobilities in acetonitrile of the tetrabutylammonium ion and the tetraphenylboride ion, respectively (ratio, 1.073); if we assume that the ratio of mobilities is the same in methanol and is independent of pressure, single ion mobilities as a function of pressure can be calculated from the limiting conductances given in Table VI. From these, Stokes radii are calculated by the equation

$$R_s^\pm = 0.8194 + 10^{-3}/\lambda_0\eta_0 \quad (11)$$

The latter depend on the dielectric relaxation of the solvent²⁶

$$R_s = R_\infty + S/\epsilon_0 \quad (12)$$

where

$$S = B(\tau/\eta)(1 - \epsilon_\infty/\epsilon_0)/R_\infty^3 \quad (13)$$

and R_∞ is the radius of the equivalent sphere. In (13), the relaxation time (τ) is proportional to the viscosity η , B is a numerical constant, and the ratio $\epsilon_\infty/\epsilon_0$ of high-frequency to static dielectric constants is small compared to unity for polar liquids; hence, S is sub-

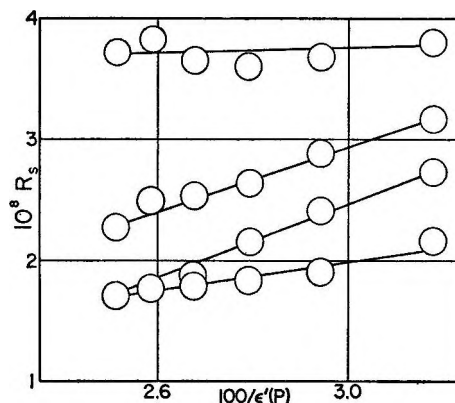


Figure 4. Pressure dependence of Stokes radii. Top to bottom: Bu_4N^+ , Na^+ , Br^- , and Me_4N^+ .

stantially independent of pressure. Figure 4 shows the Stokes radii plotted against reciprocal dielectric constant. For both Bu_4N^+ and BPh_4^- (not shown; the points lie 7% above the corresponding Bu_4N^+ points), R_s^\pm is nearly independent of pressure, as expected: first, because both ions are very large compared to methanol molecules, and second, because S is small on account of the R_∞^3 in the denominator. For Me_4N^+ , a positive slope appears, while Na^+ and Br^- show still stronger positive slopes. For the latter, S is found to be 150×10^{-3} , which is much larger than was found for similar ions in dioxane-water mixtures, where the dielectric constant was varied by changing solvent composition.^{34,35} Furthermore, the lines for Na^+ and Br^- in Figure 4 extrapolate to negative intercepts at $\epsilon^{-1} = 0$. The effect of dielectric relaxation is necessarily present, but for these two ions, it obviously is completely eclipsed by the compression effect discussed in the preceding paragraph. Other systems must be studied before generalizations may be attempted.

(33) J. F. Coetzee and G. P. Cunningham, *J. Am. Chem. Soc.*, **87**, 2529 (1965).

(34) J. E. Lind, Jr., and R. M. Fuoss, *J. Phys. Chem.*, **66**, 1727 (1962).

(35) T. L. Fabry and R. M. Fuoss, *ibid.*, **68**, 971 (1964). Corrections: Figure 1, abscissa scale is 1, 3, 5, 7, 9. Six lines below (6), read $R_\infty = 1.86$. Three lines above (7), read 10^{-10} . Read (7) as $R^+ = R_\infty + S/D$.

Intramolecular Hydrogen Bonding in the Hydrogen Anions of Some Carboxylic Acids in Water and Water-Methanol Mixtures. Evidence from Proton Magnetic Resonance

by Brian L. Silver, Z. Luz, S. Peller, and J. Reuben

Isotope Department, The Weizmann Institute of Science, Rehovoth, Israel (Received September 28, 1966)

Proton chemical shifts of the noncarboxylic hydrogens of a number of carboxylic acids were measured as a function of the degree of neutralization in water and methanol-water mixtures. Except for formic acid, the proton resonances for the monocarboxylic acids were shifted upfield upon neutralization of the acid. In phthalic, pyromellitic, and maleic acids, a downfield shift was observed upon half-neutralization. These results are interpreted in terms of intramolecular hydrogen bonding in the hydrogen anions of these acids.

Introduction

Intramolecular hydrogen bonding has often been invoked to account for the anomalous acid dissociation constants of some dicarboxylic acids.^{1,2} For example, the ratio, K_1/K_2 , of the first to the second ionization constants for maleic and fumaric acids are 20,200 and 23.2, respectively.³ This was explained in terms of internal hydrogen bonding in the monoanion of the *cis* (maleic) acid, which in comparison with the fumarate ion is stabilized relative to its dianion. Although the ratios K_1/K_2 have also been quantitatively accounted for by electrostatic interactions,⁴ more direct evidence for the existence of intramolecular hydrogen bonds has come from infrared and nmr spectroscopy. In aqueous solution, infrared measurements indicate that the maleate monoanion, but not maleic acid, is internally hydrogen bonded.⁴ Forsen^{5,6} has examined the monoanions of several dicarboxylic acids in dimethyl sulfoxide by nmr spectroscopy. A separate peak was observed for the carboxyl hydrogen of the monoanions of maleic, phthalic, and a number of alkyl-substituted succinic acids at about -15 ppm from water. This strong low-field shift is indicative of involvement of this proton in a strong hydrogen bond. Attempts to observe a separate nmr signal for the carboxylic proton in aqueous or methanol solutions failed, because of fast proton exchange with water.⁶ In the present paper we

bring forward nmr evidence to show that in these solvents intramolecular hydrogen bonding occurs in the hydrogen anions of some acids having two adjacent carboxyl groups. The evidence comes from changes in the chemical shifts of the nondissociating protons of these compounds.

It is generally known that the resonance of a proton bonded to the α -carbon of a carboxylic acid is shifted toward higher field in going from the free acid to the fully ionized molecule.⁷ In aliphatic acids this effect is also observed with hydrogens bonded to the β -carbon atom, but the shifts are about half of those for an α -hydrogen, while shifts of γ -hydrogens are usually not detected. In unsaturated systems the effect is transmitted over more bonds, and shifts can be observed for protons that are separated from the carboxyl group by as many as six bonds. For example, the methyl proton of *p*-toluic acid is shifted by $+2$ cps on

(1) E. J. King, "Acid-Base Equilibria," Pergamon Press Ltd., London, 1965, Chapter 7.

(2) G. C. Pimentel and A. L. McClellan, "The Hydrogen Bond," W. H. Freeman & Co., San Francisco, Calif., 1960, Chapter 5.

(3) L. Hunter, *Chem. Ind.* (London), 155 (1953).

(4) R. E. Rodd, R. E. Miller, and W. F. K. Wynne-Jones, *J. Chem. Soc.*, 2790 (1961).

(5) S. Forsen, *J. Chem. Phys.*, 29, 948 (1958).

(6) L. Ebersson and S. Forsen, *J. Phys. Chem.*, 64, 767 (1960).

(7) See, for example, D. Leussing and C. K. Stansfield, *J. Am. Chem. Soc.*, 86, 2805 (1964), and references therein.

going from the acid to the anion. These upfield shifts may be explained in terms of the inductive effect of the carboxyl group. The carboxylate ion will repel electrons more strongly than the un-ionized carboxyl group, thus increasing the shielding of the protons in the rest of the molecule. The dropping off of this effect along a chain of bonds is consistent with the generally observed attenuation of inductive effects as reflected in other observables, *e.g.*, chemical reactivity.⁸

In contrast to the above facts we have observed that in certain carboxylic acids, upon titration there is a *downfield* shift of protons in the rest of the molecule. This occurs almost exclusively in unsaturated carboxylic acids in which two carboxyl groups are bonded to adjacent carbon atoms and are in the *cis* configuration. We give examples of such cases and interpret the results in terms of intramolecular hydrogen-bonded cyclic structures in the monoanions of these acids.

Experimental Section

Nmr Spectra. Proton magnetic resonance spectra were recorded at 60 Mc/sec on a Varian A-60 nmr spectrometer. The temperature in the probe was approximately 32°. The proton chemical shift was measured relative to the proton signal of tetramethylammonium ion contained in the solution as an internal reference. The tetramethylammonium (TMA) ion was introduced either in the form of TMA bromide (0.1 *M*), or as the hydroxide in the cases where TMA hydroxide was used as the titrating base. The accuracy of the measurements is estimated at 1 cps.

In many cases the relevant hydrogen gave a single peak or a simple multiplet structure and the chemical shift was directly measurable, *e.g.*, formic, acetic, propionic acid, etc. In some aromatic systems the spectrum of the ring protons was more complicated, being A_2B_2 in phthalic and *p*-chlorobenzoic acid and A_2B in 1,2,3-benzenetricarboxylic acid. In these cases the chemical shifts were derived by a standard nmr spectra analysis.⁹ The concentration of the carboxylic acids was in the range 0.05–0.2 *M*. No dependence of shift on concentration was observed in the above range. In general, TMA hydroxide was used as titrating base; in some cases sodium or potassium hydroxide was used and the same shifts were observed as with TMA hydroxide.

Preparation of Solutions. Proton chemical shifts of the compounds were measured as a function of the degree of neutralization of the acid. Spectra were taken of solutions containing different ratios of the carboxylic acid to its conjugate base at constant total

concentration of the carboxylic compound. The solvents used were water or a methanol–water mixture containing 66 vol. % methanol. For each compound spectra were also taken in solutions containing excess added HCl, NaOH, or TMA hydroxide. No effect on the chemical shifts was found due to excess acid or base. The shifts in excess HCl were the same as those for the free carboxylic acids, and the shifts in excess base were the same as those in the completely ionized carboxylic acids. In some cases the solutions were unstable, either precipitating slowly or, in the case of acidified solutions of maleic and fumaric acids, showing new peaks in the spectra on standing. These solutions were therefore prepared immediately before recording their spectra.

Results

The results of the shift measurements are summarized in Table I. The results in 66% methanol–water mixture for phthalic, pyromellitic, maleic, and fumaric acid are also plotted in Figures 1–4. Some of the results are discussed in more detail below.

Aliphatic Saturated Acids. In all cases the observed proton shifts varied strictly linearly as a function of added base up to complete neutralization of the carboxylic acid, and therefore the shifts are only tabulated for the un-ionized and completely ionized acid. As seen from Table I, addition of strong acid (HCl) to the un-ionized compounds or excess base to the completely ionized compounds results in no significant alteration in the shifts. As an example, consider the results for butyric acid, which illustrates the

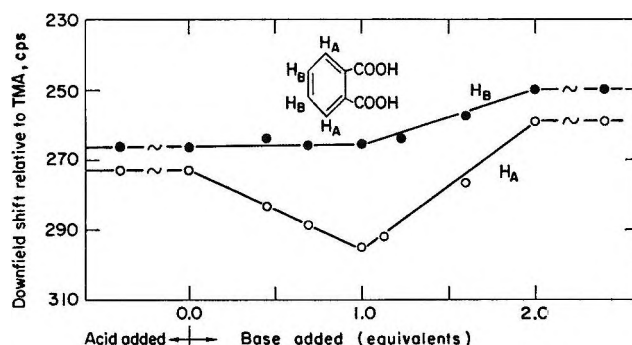
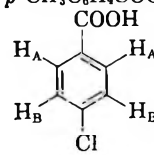
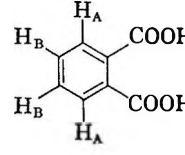
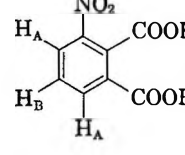
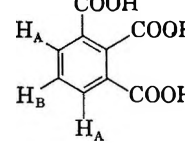


Figure 1. Chemical shift of protons A and B of phthalic acid relative to TMA as a function of degree of neutralization. The solution was 0.1 *M* in phthalic acid and the solvent was a methanol–water mixture containing 66 vol. % methanol.

(8) C. K. Ingold, "Structure and Mechanism in Organic Chemistry," Cornell University Press, Ithaca, N. Y., 1953, p 60 ff.

(9) J. A. Pople, W. G. Schneider, and H. J. Bernstein, "High Resolution Nuclear Magnetic Resonance," McGraw-Hill Book Co., Inc., New York, N. Y., 1959, Chapter 6.

Table I: Proton Chemical Shifts^a of the Noncarboxylic Protons of Some Carboxylic Acids

| Acid | Proton ^b | Solvent | Excess of acid, | Equiv of base | | | | | Excess of base, |
|-------------------------|---|------------------------|-----------------|---------------|------|-----|-----|-----|-----------------|
| | | | | 0 | 1 | 2 | 3 | 4 | |
| Formic | | H ₂ O | 311 | 313 | 338 | ... | ... | ... | 336 |
| | | Aq MeOH ^c | 304 | 304 | 340 | ... | ... | ... | 340 |
| Acetic | | H ₂ O | -65 | -65 | -76 | ... | ... | ... | -76 |
| | | Aq MeOH | -69 | -69 | -79 | ... | ... | ... | -79 |
| Propionic | CH ₃ CH ₂ COOH | H ₂ O | -48 | -48 | -61 | ... | ... | ... | -61 |
| | CH ₃ CH ₂ COOH | | -126 | -126 | -129 | ... | ... | ... | -129 |
| Butyric | CH ₃ CH ₂ CH ₂ COOH | Aq MeOH | 6 | 6 | 0 | ... | ... | ... | 0 |
| | CH ₃ CH ₂ CH ₂ COOH | | -34 | -34 | -36 | ... | ... | ... | -36 |
| | CH ₃ CH ₂ CH ₂ COOH | | -75 | -75 | -75 | ... | ... | ... | -75 |
| Succinic | | H ₂ O | -31 | -31 | -41 | -48 | ... | ... | -48 |
| | | Aq MeOH | -36 | -36 | -43 | -50 | ... | ... | -50 |
| Maleic | | H ₂ O | 196 | 193 | 186 | 168 | ... | ... | 168 |
| | | Aq MeOH | 189 | 189 | 186 | 163 | ... | ... | 163 |
| Fumaric | | H ₂ O | 220 | 219 | 211 | 199 | ... | ... | 199 |
| | | Aq MeOH | 214 | 214 | 207 | 200 | ... | ... | 200 |
| Toluic | <i>p</i> -CH ₃ C ₆ H ₄ COOH | Aq MeOH | 12 | 12 | 10 | ... | ... | ... | 10 |
| <i>p</i> -Chlorobenzoic |  | A Aq MeOH ^d | 274 | 274 | 269 | ... | ... | ... | 269 |
| | | B | 268 | 268 | 263 | ... | ... | ... | 262 |
| Phthalic |  | A H ₂ O | 278 | 278 | 278 | 260 | ... | ... | 260 |
| | | B | 271 | 271 | 266 | 256 | ... | ... | 256 |
| | | A Aq MeOH | 274 | 274 | 294 | 259 | ... | ... | 259 |
| | | B | 266 | 266 | 265 | 250 | ... | ... | 250 |
| 3-Nitrophthalic |  | A Aq MeOH | 308 | 308 | 303 | 282 | ... | ... | 282 |
| | | B | 275 | 275 | 266 | 256 | ... | ... | 256 |
| Hemimellitic |  | A Aq MeOH | 300 | 300 | 292 | 273 | 260 | ... | 260 |
| | | B | 268 | 268 | 263 | 255 | 248 | ... | 248 |
| Trimesic | | Aq MeOH | 331 | 331 | 330 | 325 | 320 | ... | 320 |
| Pyromellitic | | H ₂ O | 299 | 299 | 296 | 293 | 283 | 268 | 267 |
| | | Aq MeOH | 291 | 294 | 315 | 313 | 385 | 361 | 361 |

^a Shifts are in cycles per second and are referred to tetramethylammonium (TMA) ions as an internal reference. A positive number indicates a downfield shift. ^b The shifts refer to the italic proton where there is more than one equivalent set of protons. ^c A methanol-water mixture containing 66 vol. % methanol unless otherwise stated. ^d A methanol-water mixture containing 95 vol. % methanol.

usual behavior of monocarboxylic acids. Upon titration, the α -protons are shifted upfield by 6 cps, the β -protons by 3 cps, and the γ -protons are not affected within experimental error. The same type of behavior is followed by acetic and propionic acid. An exception to the general behavior is formic acid, which

shows a downfield shift on titration. A linear upfield shift upon titration of the two carboxyl groups is also observed in succinic acid.

Phthalic Acid. Phthalic acid gives an A₂B₂ spectrum, from which the chemical shifts of protons A and B were obtained.⁹ From the known effects of

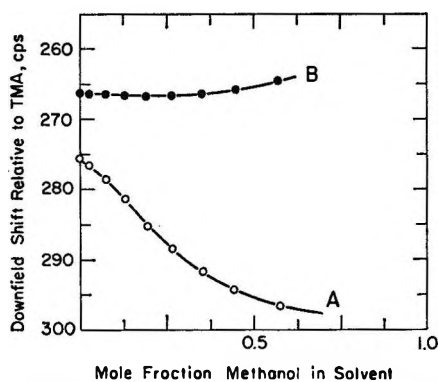


Figure 2. Chemical shifts of protons A and B of the hydrogen phthalate ion relative to TMA, and a water-methanol mixture, as a function of the mole fraction of methanol. The concentration of phthalate was 0.05 M.

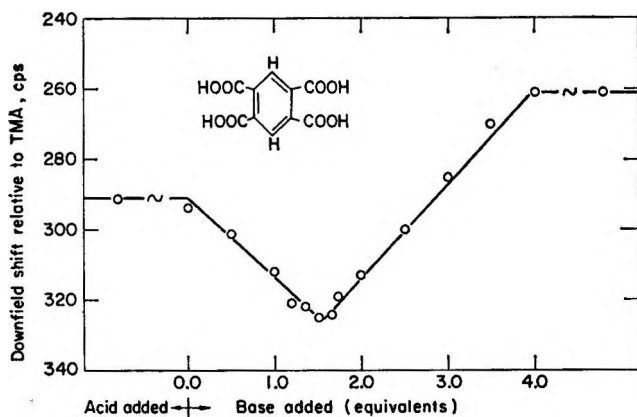


Figure 3. Chemical shifts of the aromatic proton of pyromellitic acid. Experimental details are the same as those in Figure 1.

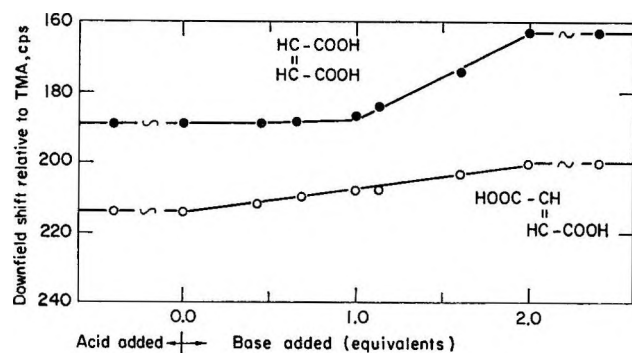


Figure 4. Chemical shifts of the carbon-bonded protons of maleic and fumaric acid. Experimental details are the same as in Figure 1.

ring substituents on the chemical shift of aromatic protons¹⁰ it is expected that the protons adjacent to the carboxyl group will be shifted to low field relative

to the other pair of protons of phthalic acid. The assignment of the labels A and B is based on this reasoning.

3-Nitrophthalic Acid. This acid gives very nearly an A₂B spectrum over the whole range of titration instead of the expected ABC spectrum. The two A protons correspond to positions 4 and 6 on the aromatic ring, and B to position 5. This assignment follows from a consideration of substituent effects on aromatic protons.¹⁰

The other acids not specifically mentioned above gave simple, immediately interpretable spectra.

Discussion

Before discussing the chemical implications of the results, a general description of the shifts of the monocarboxylic acids is given. Probably the simplest behavior is exhibited by the monocarboxylic aliphatic acids. In these compounds titration of the single acidic hydrogen results in an upfield shift of the resonances of some of the other hydrogen atoms of the molecule as described above. An exception is formic acid, where the nonacidic hydrogen is directly bonded to the carboxylic carbon atom, and this case is discussed below. In all cases the observed shift is strictly proportional to the fractions of the ionized form. Owing to fast proton exchange between the ionized and nonionized forms, only one set of lines is observed with shifts that are weighted averages of the shifts of the two species. Thus, the observed shift when the acid is completely ionized is the shift of the acid anion, RCOO⁻ while the shift observed before the addition of the base is the shift of the nonionized acid RCOOH. The largest shifts are observed in the protons attached to the α -carbon atom, being of the order of +10 cps. There is no significant effect upon changing the solvent from water to 66 vol. % methanol. The shift diminishes along a carbon chain, being of the order of +2 to +3 cps for a β -proton and less than 1 cps for a γ -proton.

Proton chemical shifts have been interpreted mainly in terms of two parameters:¹¹ (1) the electron density around the proton, and (2) the anisotropic magnetic susceptibility of neighboring groups. It is unlikely that the magnetic susceptibility of C-H and C-O bonds of the aliphatic side chain will be modified upon ionization of a carboxyl group. Therefore, the observed shifts are probably explicable in terms of changes in electronic density at the proton in question upon ionization of the carboxyl group. The total screening of

(10) See ref. 9, p 259.

(11) See ref. 9, pp 175-183.

a proton due to a single electron is estimated at about 20 ppm,¹¹ *i.e.*, 1200 cps at 60 Mc/sec. The observed shifts of the α -proton thus correspond to an increase of 0.5–1% of an electronic charge.

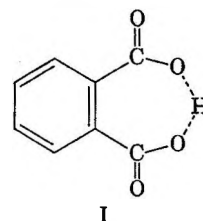
In formic acid the proton resonance of the carbon-bonded hydrogen is shifted considerably downfield from the usual aliphatic proton resonance. This shift is similar to that found for the proton of the aldehydes and has been explained as being due to the marked magnetic anisotropy of the carbonyl bond.¹² Apparently, the downfield shift of the carbon-bonded proton of formic acid is due to a change in the magnetic anisotropy of the carboxyl group upon ionization. For more distant hydrogens, *e.g.*, α -protons, the effect is probably very small, since it drops off as the inverse cube of the distance.¹²

Upfield shifts are also observed on titration of monocarboxylic aromatic acids. In these compounds, owing to the high polarizability of the π -electron system, the shifts are observed at greater distances from the carboxyl group than in aliphatic systems. Thus, in *p*-chlorobenzoic acid, ring hydrogens in the *meta* position to the carboxyl group are shifted by +5 cps as compared to <1 cps for the γ -hydrogen of butyric acid which is separated by the same number of bonds from the carboxyl group. The methyl hydrogens of *p*-toluic acid, although separated by six bonds from the carboxyl group, are nevertheless also shifted upfield by 2 cps.

The main interest of the present work lies in the finding that for carboxylic acids having adjacent carboxyl groups attached in the *cis* position to a double bond, titration of the first hydrogen results in a downfield shift of some of the protons in the rest of the molecule. This anomalous behavior will be interpreted in terms of the existence of intramolecular hydrogen bonding in the monoanions of these acids. Consider the results for phthalic acid which are plotted in Figure 1. In 66% methanol, titration of the first hydrogen results in a linear downfield shift of protons A while protons B are almost unshifted. Titration of the second hydrogen results in a linear upfield shift for both sets of protons. The over-all result for protons A and B is an upfield shift of +16 cps for the dianion as compared to the undissociated acid. Although the same over-all shift upon complete titration is observed in pure water as solvent, upon titration of the first hydrogen proton A is almost unshifted while proton B behaves almost the same as in 66% methanol (*cf.* Table I). In Figure 2 the chemical shifts of protons A and B for the monoanion are plotted as a function of the mole fraction of methanol in the solvent. It is seen that the chemical shift of proton B is rela-

tively insensitive to change in solvent while the downfield shift of proton A increases smoothly by about 20 cps from pure water to 75 vol. % methanol. In fact, this downfield shift is slightly greater than it appears from the figure, since in methanol the resonance of the A protons of the undissociated acid are shifted slightly upfield (4 cps in 66% methanol, *cf.* Table I).

The results can be interpreted in terms of a hydrogen-bonded structure for the monoanion, of type I, in which the two carboxyl groups are approximately coplanar with the aromatic ring. The p orbitals of the carbox-



ylic carbon and oxygen atoms perpendicular to the plane of the molecule will overlap with the adjacent aromatic π orbitals to form a conjugated ring. The two adjacent conjugated systems are reminiscent of the naphthalene molecule and, as in naphthalene, proton α is shifted downfield relative to β , owing to ring currents in the adjacent ring,^{13a} so we expect that in the cyclic structure of the phthalate monoanion, proton A will be shifted downfield owing to currents around the ring formed by the carboxyl groups. Since the effect of the ring current decreases as the cube of the distance, protons B being further from the center of the carboxylic ring will be much less affected than protons A. Molecular models suggest that structure I may be slightly strained if the carboxyl groups are accurately coplanar, but the strong hydrogen bond between the two carboxyl groups and resonance stabilization is expected to encourage their coplanarity.

The explanation of the observed results does not necessarily require the concept of a carboxylic ring current. An alternative interpretation can be based on the idea of a difference in the average anisotropic susceptibilities of the carboxyl group between the free acid and the hydrogen anions.^{13b} In the free acid hydrogen bonding is not strong enough to prevent free rotation of the carboxyl groups. In the monoanion the strong hydrogen bond considerably restricts the rotational freedom and the carbonyl group will have a much greater probability of lying in the plane of the aromatic ring. In this position the H_A proton will

(12) L. M. Jackman, "Applications of Nuclear Magnetic Resonance Spectroscopy in Organic Chemistry," Pergamon Press, 1959, Chap. 7.

(13) (a) Reference 9, p 251. (b) We thank a referee for suggesting this alternative explanation.

experience the greatest downfield shift due to the C=O magnetic anisotropy.

The proton involved in this hydrogen-bonded structure is expected to show a strong downfield shift. In fact, Forsen⁵ was able to observe a separate peak for the carboxylic proton of potassium hydrogen phthalate in dimethyl sulfoxide at -15.15 ppm relative to an external water reference. An analogous planar structure is very unlikely for the dianion because of the electrostatic repulsion of the two carboxyl groups. A hydrogen bond may conceivably be formed in the undissociated acid but it will be much weaker.

The stability of the intramolecular hydrogen bond in the monoanion will be affected by the nature of the solvent. Solvents which are capable of forming strong hydrogen bonds will compete effectively for the carboxylic proton and thus will rupture the intramolecular bond. The resulting solvated complex will not necessarily have the two carboxyl groups coplanar. In solvents less capable of hydrogen bonding, the intramolecular hydrogen bond will be more favored, relative to bonding to the solvent. Thus, it is expected that, *e.g.*, in methanol the hydrogen-bonded cyclic structure will be more favored than in pure water and thus the fraction of the hydrogen bonded form will be greater and will give a bigger downfield contribution to the observed shift. Therefore, the resonance of proton A will be shifted downfield in methanol relative to solvent water. In fact, as seen in Figure 2 the downfield shift of proton A increases with increasing proportion of methanol in the solvent. For the monoanion in dimethyl sulfoxide, where hydrogen bonding to solvent is probably weaker than to water or methanol, proton A is shifted downfield by 44.4 cps¹⁴ from proton B as compared to 32 cps in 75 vol. % methanol.

Intramolecular hydrogen bonding for the monoanion of phthalic acid in water has also been suggested by Hunter³ to explain the larger K_1 of phthalic acid as compared to its *meta* and *para* isomers. It should be noted that in contrast to the above conclusions King¹ states that the ratio K_1/K_E (where K_E is the acid dissociation constant of the monoester of phthalic acid) is only 2.2 , indicating no hydrogen bonding in the monoanion of phthalic acid.

In pyromellitic acid (1,2,4,5-benzenetetracarboxylic acid) it is possible for two hydrogen-bonded rings to be formed, and similar behavior to that observed in phthalic acid is expected. As seen from Figure 3, addition of 2 equiv of base results in a downfield shift of the aromatic hydrogens. Complete titration results in a net upfield shift. The continuous downfield shift upon addition of almost 2 equiv of base indicates that the first and second ionizations occur on opposite

sides of the molecule, resulting in a structure having two hydrogen-bonded rings. The maximum downfield shift does not occur at exactly half neutralization. While the explanation of this behavior is not clear to us, it may be due to the third ionization constant in 66% methanol-water being close to the second, and thus at the half-neutralization point there is a significant proportion of triply ionized molecules with only one hydrogen-bonded ring. As in phthalic acid, the downfield shift of the aromatic proton is much greater in 66% methanol than in water.

In hemimellitic acid (1,2,3-benzenetricarboxylic acid) the aromatic protons show an A_2B spectrum. On titration in 66% methanol both sets of protons move downfield almost linearly with equivalents of base (*cf.* Table I) contrary to the behavior expected by analogy with phthalic and pyromellitic acids. Examination of a molecular model shows that if two of the carboxyl groups form a structure coplanar with the benzene ring, strong steric interference occurs with the remaining carboxyl group. Thus, the formation of coplanar hydrogen-bonded rings may be discouraged in this molecule. Similarly, 3-nitrophthalic acid gives no downfield shift on titration of one hydrogen in 66% methanol-water (*cf.* Table I). The nitro group has approximately the same size and shape as a carboxyl group and will be expected to have the same steric effects. Neither of these acids is soluble enough in water to permit nmr measurements.

Trimesic acid (1,3,5-benzenetricarboxylic acid) has three equivalent protons, giving a single resonance line. Since there are no adjacent carboxyl groups, no cyclic structure can be formed. The resonance peak moves linearly upfield upon titration, with an over-all shift of 11 cps. This shift is very small compared with hemimellitic acid (40 cps for the A proton, and 20 cps for the B proton). Presumably less charge goes into the π system in the symmetrical 1,3,5 acid since electrostatic repulsion will tend to keep the charges on the periphery of the molecule.

Maleic acid, having two *cis*-carboxyl groups attached to a double bond, can form a cyclic hydrogen-bonded structure of the type discussed above, while fumaric acid, its *trans* isomer, cannot do so. These two acids are expected to show different behavior upon titration. From Figure 4 it is seen that in 66% methanol-water the proton resonance of fumaric acid moves linearly upfield with titrating base, and in maleic acid neutralization of one hydrogen gives practically no shift, while neutralization of the second hydrogen

(14) Calculated for 60 Mc/sec from ref 5 in which the shift is given at 40 Mc/sec.

results in a strong high-field shift. If one allows for a probable upfield shift of 13 cps (half the net shift between the un-ionized and double ionized acid) due to the inductive effect of the charge on the carboxyl group, the contribution of the carboxylic ring current (or the change in C=O time-averaged anisotropy) is estimated as a downfield shift of 10 cps. In water the downfield shift of the monoanion of maleic acid is slightly less than in methanol, but otherwise the behavior is similar. As above, these results can be interpreted as indicating intramolecular hydrogen bonding in the maleate monoanion. Such a model has also been put forward to account for the values of K_1/K_2 for fumaric and maleic acid.¹⁵ In water this ratio is 20,200 for maleic and 23.2 for fumaric acid, *i.e.*, the second dissociation of maleic acid is highly discouraged, compared to fumaric acid, presumably by a strong intramolecular hydrogen bond. In 50 wt % aqueous ethanol the ratios are¹⁵ 22×10^6 and 62 for maleic and fumaric acids, respectively. Thus, in the ethanol-water mixture the internally hydrogen-bonded structure is even more stable than in water. This is consistent with the present results. Infrared studies in aqueous solution also indicate that the maleate ion

is internally hydrogen bonded but that maleic acid is not.⁴

Finally, the infrared spectra¹⁶ and K_1/K_2 values¹⁶ for succinic acid and its alkyl derivatives show that in these compounds there is strong intramolecular hydrogen bonding both in water and alcohols. Since the C-C bond is saturated, a conjugated Π system cannot be formed in this case and thus no ring currents of the type described for phthalic acid are expected. Actually, a linear upfield shift is observed upon titration.

In summary, in those systems where internal hydrogen bonding can be expected to create a conjugated structure resulting in downfield shifts of neighboring hydrogens, such shifts have in fact been observed. Though the magnitude of the shifts cannot be related quantitatively in a simple way with the proportion of hydrogen-bonded molecules, the results indicate that this method can be applied to study hydrogen bonding in other favorable cases.

(15) L. Ebersson, *Acta Chem. Scand.*, **13**, 211 (1959).

(16) L. Ebersson, *ibid.*, **13**, 224 (1959).

Photochemistry of the Fluoro Ketones. 1,1,3,3-Tetrafluoroacetone¹

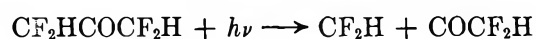
by G. O. Pritchard and J. T. Bryant

Department of Chemistry, University of California, Santa Barbara, California (Received September 28, 1965)

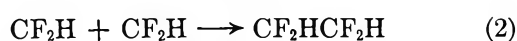
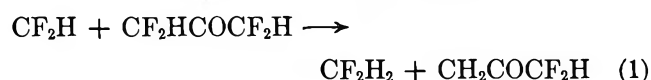
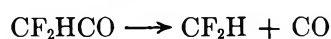
In the photolysis of the title ketone, CF_2H radicals recombine to give $\text{C}_2\text{F}_4\text{H}_2$, and disproportionate to give CF_2H_2 and CF_2 , but the elimination of HF is negligible under the conditions used. The activation energy for hydrogen atom abstraction by CF_2H radicals from the ketone is $6.9 \text{ kcal mole}^{-1}$. The ϕ_{CO} is unity over a 15-fold pressure variation at room temperature and remains close to unity up to 300° . This behavior is compared with acetone, trifluoroacetone, and hexafluoroacetone.

Introduction

After the primary photochemical step



the following reactions are of interest



In a preliminary account² it was shown that reaction 4 was very minor, indicating that the elimination of HF from the vibrationally excited $\text{CF}_2\text{HCF}_2\text{H}^*$ was not significant under the conditions used. In the previous investigation of the photolysis of $\text{CFH}_2\text{-COCF}_2\text{H}_2$, the rapid elimination of HF from $\text{CFH}_2\text{-CFH}_2^*$ was observed.³ The possible disproportionation reaction between two CFH_2 radicals appeared to be unimportant.³ However, Bellas, Strausz, and Gunning (BSG)⁴ have observed a disproportionation reaction between two CF_2H radicals in the Hg-photosensitized decomposition of CF_2HCl , so that the occurrence of reaction 3 in our system must be considered.

Experimental Section

The apparatus and procedure have been described previously.³ A pure sample of the ketone was supplied by E. I. du Pont de Nemours and Co.,⁵ and its mass spectrum is recorded in Table I. Ketone pressures

used varied between 1 and 10 cm in the kinetic experiments.

After photolysis, CO was separated at -195° and measured and checked on the mass spectrometer. Mass spectrometer analysis of a cut taken at -145° indicated pure CF_2H_2 with a trace of SiF_4 , for which a correction was made. $\text{C}_2\text{F}_4\text{H}_2$ was collected at -100° ; its mass spectrum is recorded in Table I, and it shows a very large transference peak at m/e 33 (CFH_2^+). The -145 and -100° fractions were also separated and characterized by vpc on a 0.5-m 3% squalane on 60-80 mesh alumina column, to ensure that the observed transference peak was not due to CF_2H_2 in the ethane sample.

In neither the -145° nor the -100° fractions was there any mass spectrometric evidence for $\text{CFH}=\text{CF}_2$, which has a large parent ion peak at m/e 82, and a base ion peak at m/e 63 ($\text{C}_2\text{F}_2\text{H}^+$). It was also proved to be absent by vpc characterization. When the system was dosed with $\text{C}_2\text{F}_3\text{H}$ prior to photolysis of the ketone, it was identified unambiguously in the product analysis in the -145° fraction, both by mass spectrometry and vpc.

In the quantum yield experiments the incident intensity varied between 1.9 and 2.8×10^{13} quanta/cc

(1) This work was supported by a grant from the National Science Foundation.

(2) G. O. Pritchard and J. T. Bryant, *J. Phys. Chem.*, **69**, 1085 (1965).

(3) G. O. Pritchard, M. Venugopalan, and T. F. Graham, *ibid.*, **68**, 1786 (1964).

(4) M. G. Bellas, O. P. Strausz, and H. E. Gunning, *Can. J. Chem.*, **43**, 1022 (1965).

(5) We are greatly indebted to Mr. Roy J. Plunkett for arranging this gift.

Table I: Mass Spectrum of $C_2F_4H_2$ and $(CF_2H)_2CO^a$

| m/e | Relative abundance | | Probable positive ion |
|-------|--------------------|---------------|-----------------------|
| | $C_2F_4H_2$ | $(CF_2H)_2CO$ | |
| 12 | 11 | 15 | C^+ |
| 13 | 14 | | CH^+ |
| 15 | 24 | | CH_2^+ |
| 25 | 10 | | C_2H^+ |
| 26 | 12 | | $C_2H_2^+$ |
| 29 | | 95 | CHO^+ |
| 31 | 122 | 90 | CF^+ |
| 33 | 464 | 170 | CFH_2^+ |
| 43 | 25 | | C_2F^+ |
| 50 | 13 | 31 | CF_2^+ |
| 51 | 1000 | 1000 | CF_2H^+ |
| 60 | | 103 | C_2FHO^+ |
| 61 | | 22 | $C_2FH_2O^+$ |
| 63 | 33 | | $C_2F_2H^+$ |
| 69 | 34 | 15 | CF_3^+ |
| 79 | | 132 | $C_2F_2HO^+$ |
| 82 | 45 | | $C_2F_3H^+$ |
| 83 | 259 | 128 | $C_2F_3H_2^+$ |
| 100 | | 14 | $C_2F_4^+$ |
| 101 | 53 | 36 | $C_2F_4H^+$ |
| 102 | 11 | | $C_2F_4H_2^+$ |
| 130 | | 59 | $C_3F_4H_2O^+$ |

^a Peaks at $m/e < 1\%$ of 51 and isotope peaks have been omitted. No isotope corrections have been made.

sec, depending upon the particular filter combination employed. Some difficulty was encountered with changes in transmission with time of the solution filters employed,³ so that all solutions were renewed before each quantum yield determination. Also, further problems were encountered with changes in transmission of the filters during an experiment due to thermal effects created by the lamp. Procedures were standardized by photolyzing the CF_2HCOCF_2H and acetone under exactly identical conditions in order to achieve reproducible data.

Based on $\log I_0/I = \epsilon cl$, ϵ for CF_2HCOCF_2H is 14.3 l. mole⁻¹ cm⁻¹ at 3153 Å, which is λ_{max} .

Results and Discussion

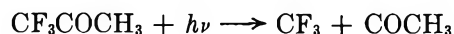
Quantum Yields. The results of these experiments are reported in Table II. The mass-balance (mb) ratios will be discussed in the next section. As was mentioned in the Experimental Section, some difficulties were encountered with the actinometry, but we consider that ϕ_{CO} is close to unity at all temperatures. To verify this, we undertook a series of experiments all conducted over a 14-hr period at room temperature in which fresh solution filters were used in each run. With a 15-fold pressure variation we obtained the values given in Table III. The experiment

at 0.72 cm is the least accurate owing to the small percentage absorption (<10%) of the incident light.

The ϕ_{CO} data present an unexpected picture, as with acetone, difluoroacetone, trifluoroacetone, and hexafluoroacetone the ϕ_{CO} is less than unity at room temperature, and only approaches unity at elevated temperatures. After the initial electron excitation of the ketone molecules, the quantum yields of CO depend upon the extent to which various kinds of radiative and radiationless transitions occur, and upon the lifetime, and the consequent possible reactions, of the acetyl radicals

In hexafluoroacetone⁶ ϕ_{CO} varies from 0.1 to 0.5 over the pressure drop 50 to 5 mm at room temperature, and ϕ_{CO} only approaches unity and is independent of pressure at 219°. These effects were largely correlated with the fluorescence efficiency (increasing with pressure, decreasing with temperature) of hexafluoroacetone,⁷ although processes involving collisional deactivation, internal conversion, and intersystem crossing were also evident.^{7b} While postulating the participation of the triplet state,^{7b} Okabe and Steacie^{7a} did not observe any phosphorescence. However, at low temperatures phosphorescence is observed, the phosphorescence quantum yield being 0.51 at -78°. The participation of the CF_3CO radical is unimportant,⁶ but under certain conditions it can be detected.⁹

The emission from trifluoroacetone has been investigated, and it is very similar (for 3130-Å excitation) to that for acetone.¹⁰ The fluorescence yield is independent of temperature and pressure (which is not readily explainable¹⁰), and the phosphorescence yield decreases with increasing temperature. Also, in the photolysis of trifluoroacetone the primary process appears to be



and $(CH_3CO)_2$ has been isolated as a product at 45°. ϕ_{CO} in CF_3COCH_3 photolysis reaches unity at ~200° but increases further with rising temperature.¹² In CH_3COCH_3 photolysis $\phi_{CO} = 1$ at 100°, but the reac-

(6) P. B. Ayscough and E. W. R. Steacie, *Proc. Roy. Soc. (London)*, **A234**, 476 (1956).

(7) (a) H. Okabe and E. W. R. Steacie, *Can. J. Chem.*, **36**, 137 (1958); (b) G. Giacometti, H. Okabe, and E. W. R. Steacie, *Proc. Roy. Soc. (London)*, **A250**, 287 (1959).

(8) P. G. Bowers and G. B. Porter, *J. Phys. Chem.*, **68**, 2982 (1964).

(9) B. G. Tucker and E. Whittle, *Trans. Faraday Soc.*, **61**, 484 (1965).

(10) P. Auloos and E. Murad, *J. Phys. Chem.*, **65**, 1519 (1961).

(11) E. A. Dawidowicz and C. R. Patrick, *J. Chem. Soc.*, 4250 (1964).

(12) R. A. Sieger and J. G. Calvert, *J. Am. Chem. Soc.*, **76**, 5197 (1954).

Table II

| Pressure of ketone, ^a cm | Temp, °C | Time, sec | Products, moles × 10 ⁴ | | | | | Mb ^b | |
|--|-------------|--------------|-----------------------------------|--------------------------------|--|-----------------|--|-----------------|--|
| | | | CO | CF ₂ H ₂ | C ₂ F ₄ H ₂ | φ _{CO} | φ _{CF₂H₂} | | φ _{C₂F₄H₂} |
| 5.20 | 24 | 3600 | 15.5 | 2.36 | 14.7 | 0.96 | 0.14 | 0.78 | 1.11 |
| 5.00 | 100 | 3600 | 6.06 | 1.73 | 4.04 | 0.67 | 0.19 | 0.45 | 0.87 |
| 4.80 | 169 | 3660 | 7.64 | 2.77 | 3.45 | 0.79 | 0.28 | 0.36 | 0.69 |
| 5.20 | 191 | 3600 | 10.0 | 3.03 | 4.21 | | | | 0.61 |
| 5.00 | 203 | 3600 | 8.94 | 3.30 | 3.11 | 0.88 | 0.32 | 0.31 | 0.51 |
| 3.40 | 242 | 2940 | 6.15 | 2.77 | 2.11 | | | | 0.60 |
| 5.98 | 245 | 3600 | 12.9 | 6.36 | 3.42 | 0.94 | 0.46 | 0.25 | 0.54 |
| 5.56 | 266 | 3600 | 10.9 | 8.86 | 3.12 | 0.87 | 0.71 | 0.25 | 0.72 |
| 2.80 | 297 | 3600 | 6.58 | 4.30 | 2.31 | | | | 0.72 |
| 5.36 | 300 | 3606 | 10.1 | 10.1 | 2.83 | 0.86 | 0.86 | 0.24 | 0.81 |

^a Reaction volume was 156 cc. ^b Mb represents $[\frac{1}{2}(\text{CF}_2\text{H}_2 - 0.19\text{C}_2\text{F}_4\text{H}_2) + 1.19\text{C}_2\text{F}_4\text{H}_2]/\text{CO}$.

Table III

| Pressure of ketone, cm | φ _{CO} |
|---------------------------|-----------------|
| 0.72 | 1.25 |
| 3.40 | 0.98 |
| 5.92 | 0.96 |
| 7.94 | 1.10 |
| 10.0 | 0.99 |

tions of the CH₃CO radical below this temperature are well known, partially accounting for φ_{CO} = 0.1 at room temperature.¹³

Radiative emission from CFH₂COCFH₂ has not been studied, but φ_{CO} was less than unity below 100°, which was accounted for in part by the participation of the CFH₂CO radical.³ It thus appears that the behavior of CF₂HCOCF₂H at room temperature, based on φ_{CO}, compares to that which would have been expected at least above 100° from a consideration of the other ketones we have discussed. It would be interesting to measure φ_{CO} for CF₂HCOCF₂H at say -100°, but at this temperature its vapor pressure would be less than 5 × 10⁻² mm (bp 58°). The multiplicity of the dissociative state of CF₂HCOCF₂H was not distinguishable in these experiments, but by comparison with the other ketones discussed where information is available from the radiative processes, both singlet and triplet molecules may decompose. When phosphorescence does occur, the temperature dependence certainly indicates a lower lying triplet energy state from which decomposition occurs with some activation energy.

If one assumes that decomposition occurs largely *via* the conversion of electronic energy into vibrational

energy which becomes distributed throughout the molecule,¹⁴ it is not evident why tetrafluoroacetone should undergo this internal conversion so much more efficiently than hexafluoroacetone at room temperature. Once the excitation is largely of a vibrational nature, CF₂HCOCF₂H will decompose more readily owing to the reduction in the number of effective oscillators in the molecule compared with CF₃COCF₃.

A comparison with the other ketones is difficult owing to the participation of the acetyl radical, but some of the reduction in the φ_{CO} in acetone and trifluoroacetone is due to radiative processes. It further cannot be assumed that there is no variance in the C-C bond strengths in the different ketones; perhaps this consideration applies particularly to the C-C bonds in the various acetyl radicals, where the residual vibrational energy may play a very important role in determining the dissociative fate of the radicals.¹⁵

Kinetic Data. The results of experiments carried out without the solution filters, in which the incident intensity of absorbing radiation was thereby increased by a factor of about 20, based on comparative values of R_{CO}, are recorded in Table IV. An Arrhenius plot of $h_1/k_2^{1/2} = R_{\text{CF}_2\text{H}_2}/R^{1/2}_{\text{C}_2\text{F}_4\text{H}_2}$ [ketone], where R = mean rate of formation, for the data in Tables II and IV showed distinct curvature at low temperatures, indicating an additional source of CF₂H₂, which was of more importance at low temperatures. Including

(13) D. S. Herr and W. A. Noyes, Jr., *J. Am. Chem. Soc.*, **62**, 2052 (1940).

(14) P. Seybold and M. Gouterman, *Chem. Rev.*, **65**, 413 (1965).

(15) As the various bond dissociation energies [except for acetone and acetyl, J. A. Kerr and J. G. Calvert, *J. Phys. Chem.*, **69**, 1022 (1965)] are not known, and the factors governing the partition of the excess vibrational energy between the various pairs of methyl and acetyl radicals are not understood exactly, further speculation is not warranted.

Table IV

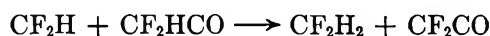
| Pressure of ketone, ^a cm | Temp, °C | Time, sec | Products, moles × 10 ⁶ | | | Mb ^b |
|--|-------------|--------------|-----------------------------------|--------------------------------|--|-----------------|
| | | | CO | CF ₂ H ₂ | C ₂ F ₄ H ₂ | |
| 1.92 | 22 | 600 | 10.9 | 1.79 | 9.32 | 1.02 |
| 9.28 | 23 | 300 | 15.6 | 2.56 | 13.8 | 1.05 |
| 3.58 | 116 | 120 | 9.97 | 1.70 | 8.14 | 0.98 |
| 6.00 | 123 | 180 | 10.2 | 2.07 | 7.67 | 0.92 |
| 0.94 | 125 | 600 | 6.08 | 1.10 | 5.26 | 1.04 |
| 3.32 | 127 | 300 | 9.21 | 1.78 | 7.49 | 0.99 |
| 10.5 | 131 | 180 | 10.2 | 2.92 | 9.56 | 1.17 |
| 4.44 | 153 | 120 | 10.1 | 1.87 | 8.37 | 1.00 |
| 1.96 | 164 | 600 | 9.84 | 1.83 | 7.74 | 0.96 |
| 9.30 | 164 | 180 | 9.87 | 3.13 | 7.05 | 0.94 |
| 6.32 | 165 | 360 | 14.9 | 3.13 | 11.6 | 0.96 |
| 2.88 | 241 | 300 | 6.79 | 1.75 | 4.25 | 0.81 |
| 1.40 | 242 | 600 | 7.16 | 1.67 | 5.04 | 0.89 |
| 9.70 | 251 | 90 | 15.5 | 5.00 | 7.58 | 0.70 |
| 3.42 | 277 | 120 | 8.57 | 2.82 | 4.88 | 0.79 |
| 4.02 | 305 | 120 | 10.1 | 3.83 | 5.22 | 0.76 |

^{a,b} See footnotes a and b of Table II.

reaction 3 in the mechanism, we may write, at a single temperature

$$R_{CF_2H_2}/R_{C_2F_4H_2} = k_1[\text{ketone}]/k_2^{1/2}R^{1/2}_{C_2F_4H_2} + k_3/k_2$$

Plots of $R_{CF_2H_2}/R_{C_2F_4H_2}$ vs. $[\text{ketone}]/R^{1/2}_{C_2F_4H_2}$, taken from the data in Table IV, are linear (see Figure 1), with intercepts at $k_3/k_2 = 0.18$ to 0.19 . This is in exact agreement with the value given by BSG,⁴ $k_3/k_2 = 0.17$ to 0.20 , independent of temperature. An Arrhenius plot of the function $k_1/k_2^{1/2} = (R_{CF_2H_2} - 0.19R_{C_2F_4H_2})/R^{1/2}_{C_2F_4H_2}[\text{ketone}]$ for all of the data in Tables II and IV is given in Figure 2. A straight line is obtained, independent of the intensity, from which a least-squares treatment yields $k_1/k_2^{1/2} = 2.2 \times 10^3 e^{-6900/RT}$ mole^{-1/2}cc^{1/2}sec^{-1/2}. These parameters are completely in line with other fluoro ketone hydrogen-atom abstraction data.³ Also recorded in Figure 2 are the values of $k_1/k_2^{1/2}$ obtained from the slopes in Figure 1. It is further seen from Figure 1 that reaction 3 constitutes the only measurable source of CF₂H₂ at room temperature. The ratio $R_{CF_2H_2}/R_{C_2F_4H_2} = k_3/k_2$ at room temperature is independent of the intensity, as the experiment conducted at 24° in Table II yields a value of $R_{CF_2H_2}/R_{C_2F_4H_2} = 0.18$. This correlates with the fact that CF₂HCO radicals do not play an important part in the mechanism ($\phi_{CO} = 1$ at room temperature), as a process such as



would show an intensity dependence. Also, the pressure independence of $R_{CF_2H_2}/R_{C_2F_4H_2}$ at room tempera-

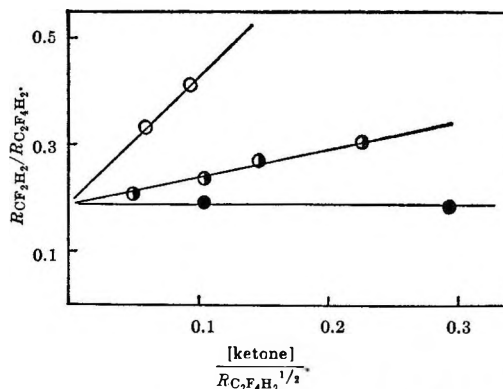


Figure 1. Plot of $R_{CF_2H_2}/R_{C_2F_4H_2}$ vs. $[\text{ketone}]/R^{1/2}_{C_2F_4H_2}$: O, 241–242°; ◐, 123–131°; and ●, 22–23°.

ture indicates the relative unimportance of CF₂H₂ produced by a radical interacting with a ketone molecule adsorbed on the wall; such a process has been suggested in acetone photolysis.¹⁶

The ease of the disproportionation (reaction 3) must be associated with its exothermicity. The considerable stabilization of CF₂, compared to CH₂, has recently been emphasized,¹⁷ suggesting that the CF₂-H bond is weak, compared to the CF₂H-H bond, which is about 103 kcal mole⁻¹.¹⁸

(16) P. Ausloos and E. W. R. Steacie, *Can. J. Chem.*, **33**, 47 (1955).

(17) I. P. Fisher, J. B. Homer, and F. P. Lossing, *J. Am. Chem. Soc.*, **87**, 957 (1965); J. P. Simons, *Nature*, **205**, 1308 (1965).

(18) A. M. Tarr, J. W. Coomber, and E. Whittle, *Trans. Faraday Soc.*, **61**, 1182 (1965).

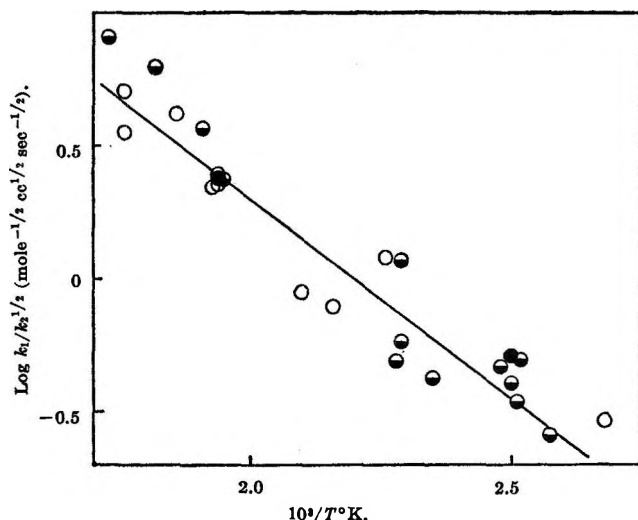
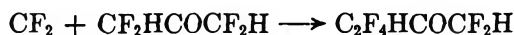


Figure 2. Arrhenius plot of $\log k_1/k_2^{1/2}$ vs. $10^3/T^\circ\text{K}$: O, filtered radiation; ●, unfiltered radiation; and ●, from slopes in Figure 1.

We were not able to ascertain the fate of the CF_2 species produced in reaction 3. They may predominantly recombine with CF_2H to produce $\text{C}_2\text{F}_4\text{H}$. This radical could abstract a hydrogen atom, suggesting an increasing error in $R_{\text{C}_2\text{F}_4\text{H}_2}$ by reaction 2, with increasing temperature. However, at room temperature, the radical would be expected to recombine with a CF_2H , producing $\text{C}_3\text{F}_6\text{H}_2$. Although a careful search was made, we were not able to detect the formation of any C_3 fluorocarbon in the system. $\text{C}_3\text{F}_6\text{H}_2$ was isolated and characterized by BSG⁴ in the Hg-photosensitized decomposition of CF_2HCl , produced by the consecutive addition of two CF_2H groups to CF_2 .⁴ It may be that



is a particularly efficient process. The data of BSG⁴ do not rule out the possible reaction



and in fact their data on the cross-combination ratio for CF_2H and CF_2Cl radicals shows a slight increase with pressure.⁴

The temperature dependence of reaction 1 is reflected in the $\phi_{\text{CF}_2\text{H}_2}$ and $\phi_{\text{C}_2\text{F}_4\text{H}_2}$ values and in the mass balance values. A decrease of the latter with temperature is expected owing to the removal of CF_2H radicals by



The mechanism predicts values of the mass balance to be unity at room temperature, independent of the pressure and the intensity, which is the case. The

smaller decrease in the mass balance with temperature in Table IV over Table II is again a reflection of the different intensities employed.

HF Elimination. In agreement with our data BSG⁴ did not report the formation of any $\text{C}_2\text{F}_3\text{H}$ in their system, indicating the very small occurrence of reaction 4 under the conditions used. In conventional unimolecular reaction rate theory, one may say that $\text{CF}_2\text{HCF}_2\text{H}^*$ has more effective oscillators than $\text{CFH}_2\text{-CFH}_2^*$ (from which the rapid elimination of HF was observed³), thereby reducing the probability of its attaining the critical configuration leading to HF elimination before collisional stabilization occurs. A 10-fold decrease in the relative rate of HCl elimination has recently been reported¹⁹ for $\text{C}_2\text{H}_5\text{Cl}^*$ and $\text{C}_2\text{H}_4\text{-Cl}_2^*$, which again may be correlated with an increase in the effective oscillators.²⁰ The data^{2,3,19} have been treated theoretically from this standpoint,²¹ and the calculations provide excellent confirmation of the experimental findings. Benson and Haugen²¹ find that the relative rates of HF elimination under similar conditions from $\text{C}_2\text{F}_5\text{H}^*$ to $\text{C}_2\text{F}_2\text{H}_4^*$ to $\text{C}_2\text{F}_3\text{H}_3^*$ to $\text{C}_2\text{F}_4\text{H}_2^*$ vary approximately as 400:50:7:1. The treatment assumes a constancy in the C-C bond dissociation energies. However, the HF elimination data from CF_3CH_3^* obtained initially by Alcock and Whittle²² showed slightly more elimination than we obtained³ with $\text{C}_2\text{F}_2\text{H}_4^*$ under similar conditions, leading us to suggest that $\text{C}_2\text{F}_4\text{H}_2^*$ appeared to be anomalous.² The rate of HF elimination is strongly dependent at any particular temperature upon the pressure and the quenching efficiency^{3,23} of the molecules in the system. Giles and Whittle²³ find values of $R_{\text{CF}_3\text{CH}_3}/R_{\text{CF}_2=\text{CH}_2}$ varying by a factor of 20 at 150° by changing the nature and the pressure of the quenching molecules. It has also been emphasized²³ that any particular system must be carefully calibrated to obtain correct HF elimination data, as the olefin produced may be rapidly consumed by radical addition reactions, rendering the analysis erroneously low.

At much higher temperatures (1200–1600°K) the rapid elimination of HF from $\text{C}_2\text{F}_5\text{H}^*$ has been observed by Tschuikow-Roux,²⁴ who, in the shock-

(19) D. W. Setser, R. Littrell, and J. C. Hassler, *J. Am. Chem. Soc.*, **87**, 2062 (1965).

(20) G. O. Pritchard, J. T. Bryant, and R. L. Thommarson, *J. Phys. Chem.*, **69**, 2804 (1965).

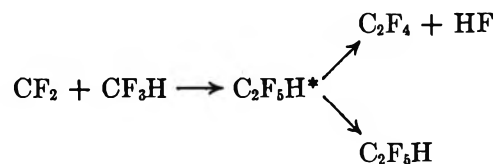
(21) S. W. Benson and G. Haugen, *ibid.*, **69**, 3898 (1965).

(22) W. G. Alcock and E. Whittle, *Trans. Faraday Soc.*, **61**, 244 (1965).

(23) R. D. Giles and E. Whittle, *ibid.*, **61**, 1425 (1965).

(24) E. Tschuikow-Roux, *J. Chem. Phys.*, **42**, 3639 (1965).

tube decomposition of fluoroform, proposes the reaction sequence



and $R_{\text{C}_2\text{F}_4}/R_{\text{C}_2\text{F}_5\text{H}} > 50$.

No quantitative kinetic data are presently available on the pyrolysis of alkyl fluorides,²¹ although the

elimination of HF from CF_3CH_3^* has been observed in the flow pyrolysis of $\text{CF}_3\text{N}=\text{NCH}_3$ at 560° .²⁵

Acknowledgments. We are indebted to a referee for some particularly helpful comments, to Drs. O. P. Strausz and G. Haugen for sending prepublication copies of their manuscripts, and to Dr. J. Heicklen for a helpful discussion.

(25) A. H. Dinwoodie and R. N. Haszeldine, *J. Chem. Soc.*, 2266 (1965).

Arsenic(IV) as an Intermediate in the Photochemical Oxidation of Ferrous Sulfate in the Presence of Arsenic Acid

by R. Woods

Chemistry Department, University of Melbourne, Parkville N. 2, Victoria, Australia (Received October 4, 1965)

The photochemical oxidation of ferrous sulfate in the presence of arsenic acid yields arsenic(III) in addition to iron(III). A complex of iron(II) and arsenic acid is postulated to be the photoactive species leading to arsenic(V) reduction. The stability constant and quantum yields of iron(III) and arsenic(III) of this complex were found to be 1.9, 1.8, and 0.9, respectively. The effect of oxygen on the quantum yields gives evidence to show that arsenic(IV) is formed as an intermediate in the photolysis.

The intermediate formation of the 4+ oxidation state of arsenic, produced by the oxidation of arsenic(III) by hydroxyl- or sulfate-free radicals has been postulated for a number of chemically and photochemically induced reactions.¹⁻⁷ No studies are found in the literature on the reduction of arsenic(V) to arsenic(IV).

Experimental Section

Materials. Ferrous sulfate was prepared by adding an excess of iron wire (99.9% Fe) to sulfuric acid solution under an atmosphere of nitrogen. The solution was filtered, acidified with sulfuric acid, and stored under nitrogen. The iron(III) in the ferrous sulfate

was always less than $5 \times 10^{-3}\%$ of the total iron concentration.

Arsenic acid was prepared by the prolonged boiling

- (1) M. Daniels and J. Weiss, *J. Chem. Soc.*, 2467 (1958).
- (2) M. Daniels, *J. Phys. Chem.*, 66, 1473, 1475 (1962).
- (3) L. J. Csanyi, *Discussions Faraday Soc.*, 29, 146 (1960).
- (4) R. Woods, I. M. Kolthoff, and E. J. Meehan, *J. Am. Chem. Soc.*, 85, 2385 (1963).
- (5) R. Woods, I. M. Kolthoff, and E. J. Meehan, *ibid.*, 85, 3334 (1963).
- (6) R. Woods, I. M. Kolthoff, and E. J. Meehan, *ibid.*, 86, 1698 (1964).
- (7) R. Woods, I. M. Kolthoff, and E. J. Meehan, *Inorg. Chem.*, 4, 697 (1965).

of arsenic trioxide with aqua regia. The aqua regia solution was taken to dryness. The solution was again taken to dryness with nitric acid and twice with water, and the residue was dissolved in water. The arsenic(III) in the arsenic acid was always less than $2 \times 10^{-3}\%$ of the total arsenic concentration.

Nitrogen used for deoxygenating the cell was purified from traces of oxygen by passage over a column of finely divided copper deposited on infusorial earth and heated at 200°. The oxygen content was thereby reduced to the order of $4 \times 10^{-5}\%$.

Photolysis. The reaction vessel consisted of a 5-cm cell fitted with polished silica windows. A side arm containing a Teflon stopcock was used for adding and removing the reaction mixture. Nitrogen or oxygen was bubbled through the solution in the cell by means of a fine glass capillary inserted through the stopcock. The cell was thermostated at 25° in a water bath and irradiated with a low-pressure mercury lamp at constant intensity. A 0.01 *N* uranyl oxalate actinometer solution, irradiated in the same cell, was used to measure the light intensity, the quantum yield at 2537 Å being taken as 0.60.⁹ The intensity was determined to be 2.33×10^{-5} einstein l.⁻¹ min.⁻¹.

Analysis. Iron(III) was determined spectrophotometrically as the sulfate at 303 mμ with a Shimadzu QR50 spectrophotometer. The extinction coefficient in 1 *M* sulfuric acid was determined as 2190 *M*⁻¹ cm.⁻¹. All solutions were adjusted to 1 *M* in sulfuric acid before determining the iron(III). The spectrum of iron(III) is affected by the presence of arsenic acid, the absorption peak at 303 mμ disappearing at the higher arsenic acid concentrations (Figure 1).

However, the extinction coefficient at 303 mμ is unaffected if the arsenic acid concentration is ≤ 0.1 *M* (Figure 1) and the higher arsenic acid solutions were diluted before analysis to give a solution containing 0.1 *M* arsenic acid.

Arsenic(III) was determined polarographically using a dropping-mercury electrode.¹⁰ The diffusion current was found to be dependent on the sulfuric acid concentration, and all solutions were adjusted to 1 *M* in sulfuric acid before analysis. Gelatin in a concentration of 0.01% was used as a maximum suppressor. The current was measured at -0.75 v vs. sce and was shown to be proportional to arsenic(III) concentration in the range 2×10^{-5} to 2×10^{-4} *M*. Iron(III) is also reduced at the dme at this potential. However, it is reduced at much more positive potentials, before the arsenic(III) wave appears, and its diffusion current was determined and subtracted from the total current at -0.75 v.

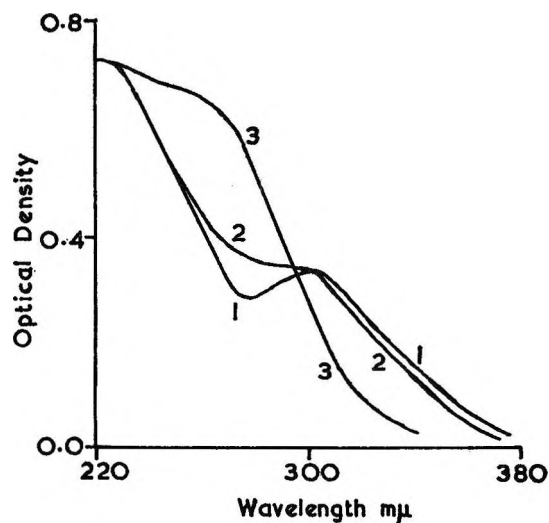


Figure 1. Ultraviolet spectrum of 1.5×10^{-4} *M* iron(III) in 1 *M* H₂SO₄ in the presence of (1) 0, (2) 0.1, and (3) 1.0 *M* arsenic(V).

Results

Arsenic(III) is formed during the photolysis of ferrous sulfate in the presence of arsenic acid. Prolonged irradiation of arsenic acid alone, or in the presence of the free-radical-capture agent, acrylonitrile, does not yield arsenic(III) and therefore the primary photochemical process resulting in the formation of arsenic(III) involves iron(II).

Iron(III) is also a photolysis product. The molar extinction coefficient of iron(III) is on the order of 200 times that of iron(II) and therefore acts as an inner filter. Jortner and Stein¹¹ conclude that, in the photooxidation of ferrous sulfate at high acidity, the role of iron(III) can be fully accounted for by its inner filter effect and derived an equation relating the initial rate of formation of iron(III) to the experimental rates, for complete light absorption

$$[\text{Fe}^{3+}] = (2AI_0/B)t/[\text{Fe}^{3+}] - 2/B$$

where I_0 is the light intensity, A the initial quantum yield, $[\text{Fe}^{3+}]$ the iron(III) formed in time t , and

$$B = \epsilon_{\text{Fe}^{3+}}/\epsilon_{\text{Fe}^{2+}}[\text{Fe}^{2+}]$$

$\epsilon_{\text{Fe}^{3+}}$ and $\epsilon_{\text{Fe}^{2+}}$ being the molar extinction coefficients of iron(III) iron(II), respectively. A plot of $[\text{Fe}^{3+}]$ against $t/[\text{Fe}^{3+}]$ extrapolated to zero $[\text{Fe}^{3+}]$ gives the

(8) F. R. Meyer and G. Ronge, *Z. Angew. Chem.*, **52**, 637 (1939).

(9) E. J. Bowen, "Chemical Aspects of Light," Oxford University Press, London, 1946, p 283.

(10) J. J. Lingane, *Ind. Eng. Chem., Anal. Ed.*, **15**, 583 (1943).

(11) J. J. Jortner and G. Stein, *J. Phys. Chem.*, **66**, 1258, 1264 (1962).

value of $1/AI_0$ from which the initial quantum yield, A , can be calculated. All initial quantum yields were determined in this manner.

The ratio of the rates of formation of iron(III) and arsenic(III) were found to be independent of time in all cases. The initial quantum yields of arsenic(III), A' , were determined from the initial iron(III) quantum yields and this ratio.

The effect of arsenic acid concentration, at constant iron(II) and sulfuric acid, on the initial quantum yields was determined (Table I).

Table I: Effect of Arsenic Acid Concentration ($1.25 \times 10^{-1} M$ $FeSO_4$; $1 M$ H_2SO_4)

| [As(V)], <i>M</i> | Quantum yields | |
|----------------------|------------------------|----------------------------|
| | Iron(III), <i>A</i> | Arsenic(III), <i>A'</i> |
| 0 | 0.223 | 0.0 |
| 0.02 | 0.288 | 0.039 |
| 0.05 | 0.370 | 0.090 |
| 0.10 | 0.490 | 0.175 |
| 0.20 | 0.72 | 0.30 |
| 0.30 | 0.86 | 0.36 |
| 0.40 | 0.98 | 0.45 |
| 1.00 | 1.29 | 0.64 |

The effect of iron(II) concentration on the ratio of iron(III) to arsenic(III) produced was determined (Table II). In this case the initial quantum yields were not derived as the purpose of this investigation was to ascertain whether the effect of arsenic acid tabulated above was due to competition between iron(II) and arsenic(V).

Table II: Effect of Iron(II) Concentration ($1 M$ H_2SO_4)

| [As(V)], <i>M</i> | [Fe ²⁺], <i>M</i> | $\frac{d[Fe(III)]/dt}{d[As(III)]/dt}$ |
|----------------------|----------------------------------|---------------------------------------|
| 0.02 | 1.25×10^{-1} | 6.7 |
| | 1.25×10^{-2} | 6.3 |
| | 1.25×10^{-3} | 6.3 |
| 0.05 | 1.25×10^{-1} | 4.0 |
| | 1.25×10^{-2} | 3.9 |
| | 1.25×10^{-3} | 3.9 |

Changing the iron(II) concentration 100-fold does not affect the ratio of iron(III) to arsenic(III) produced, and therefore the increase in quantum yield with increase in arsenic acid concentration is not due to competition between iron(II) and arsenic(V).

The effect of sulfuric acid concentration on the rate

Table III: Effect of Sulfuric Acid Concentration ($1.25 \times 10^{-1} M$ $FeSO_4$)

| [As(V)], <i>M</i> | [H ₂ SO ₄], <i>M</i> | $\frac{d[Fe(III)]/dt}{d[As(III)]/dt}$ | <i>A</i> | <i>A'</i> |
|----------------------|--|---------------------------------------|----------|-----------|
| 0.02 | 0.3 | 6.6 | | |
| | 1.0 | 6.7 | | |
| | 3.0 | 6.6 | | |
| 1.00 | 0.3 | | 1.24 | 0.62 |
| | 1.0 | | 1.29 | 0.64 |
| | 3.0 | | 1.35 | 0.67 |

of iron(III) to arsenic(III) produced and on the initial quantum yields was investigated (Table III).

There is no significant change in quantum yield or in the ratio of iron(III) to arsenic(III) formed with sulfuric acid concentration in the range 0.3 to 3.0 M .

The effect of oxygen on the quantum yield was determined (Table IV). The solution was saturated with oxygen at 1 atm, the concentration of oxygen in the sulfuric acid solution being calculated from the data given by Seidell.¹²

The effect of acidity on the rate constant ratio k_{13}/k_{12} was investigated (Table V).

The molar extinction coefficient of ferrous sulfate in the presence of arsenic acid was determined at 2537 Å (Table VI). The effect of arsenic acid on the iron(II) spectrum in 1 M sulfuric acid is shown in Figure 2.

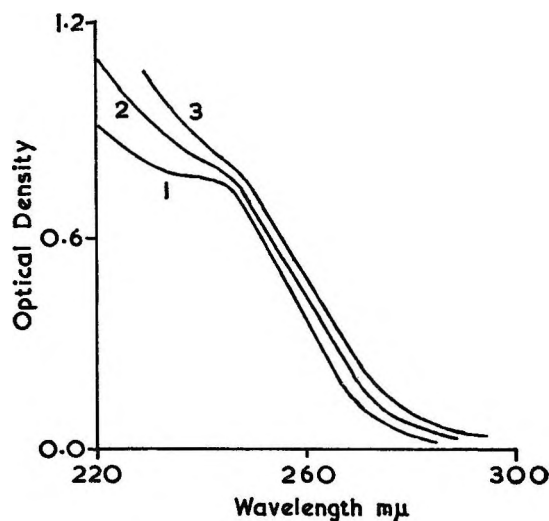


Figure 2. Ultraviolet spectrum of $4 \times 10^{-3} M$ iron(II) in $1 M$ H_2SO_4 in the presence of (1) 0, (2) 0.5, and (3) 1.0 M arsenic(V).

(12) A. Seidell, "Solubilities," D. Van Nostrand Co., Inc., New York, N. Y., 1955, p 1355.

Table IV: Effect of Oxygen Concentration (1 M H₂SO₄; Oxygen-Saturated Solutions 1.0 × 10⁻³ M O₂)

| [As(V)], M | [Fe ²⁺], M | A | | A' | | A _{O₂} /A _{N₂} | k ₁₃ /k ₁₂ ^a |
|---------------|---------------------------|----------------|----------------|----------------|----------------|--|---|
| | | N ₂ | O ₂ | N ₂ | O ₂ | | |
| 0.2 | 1.25 × 10 ⁻³ | | | | | 2.0 | |
| | 1.25 × 10 ⁻² | | | | | 1.8 | |
| | 3.75 × 10 ⁻² | 0.64 | 1.07 | 0.27 | 0.13 | | 40 |
| | 7.5 × 10 ⁻² | 0.72 | 1.07 | 0.30 | 0.19 | | 44 |
| | 1.25 × 10 ⁻¹ | 0.72 | 1.02 | 0.30 | 0.23 | | 38 |
| 0.05 | 1.25 × 10 ⁻¹ | 0.37 | 0.60 | 0.090 | 0.068 | | 40 |

^a k₁₃/k₁₂ is the ratio of the rate constants for the reactions of arsenic(IV) with oxygen and iron(II) (see Discussion).

Table V: Effect of Sulfuric Acid Concentration on k₁₃/k₁₂ (0.2 M As(V))

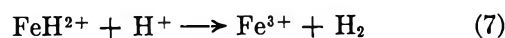
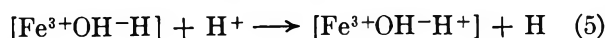
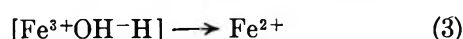
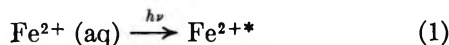
| [Fe ²⁺], M | [H ₂ SO ₄], M | % O ₂ | A | | A' | | k ₁₃ /k ₁₂ |
|---------------------------|---|------------------------|----------------|----------------|----------------|----------------|----------------------------------|
| | | | N ₂ | O ₂ | N ₂ | O ₂ | |
| 3.75 × 10 ⁻² | 3.0 | 0.7 × 10 ⁻³ | 0.73 | 1.03 | 0.31 | 0.21 | 26 |
| 7.5 × 10 ⁻² | 1.0 | 1.0 × 10 ⁻³ | | | | | 40 |
| | 0.3 | 1.2 × 10 ⁻³ | 0.56 | 1.07 | 0.25 | 0.15 | 46 |

Table VI: Effect of Arsenic Acid Concentration on the Molar Extinction Coefficient of Iron(II) at 2537 Å in 1 M Sulfuric Acid

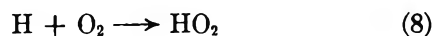
| [As(V)] M | ε, M ⁻¹ cm ⁻¹ |
|--------------|--|
| 0 | 15.0 |
| 0.25 | 15.6 |
| 0.50 | 16.1 |
| 0.75 | 16.7 |
| 1.00 | 16.9 |

Discussion

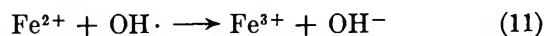
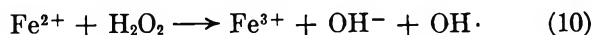
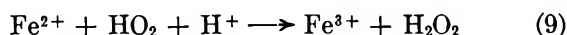
The photooxidation of ferrous sulfate has been extensively investigated by a number of workers.^{11,13-15} Jortner and Stein¹¹ give evidence to show that, at high acidity in the absence of oxygen, the photolysis is accounted for by the mechanism



In the presence of oxygen, the intermediate hydrogen atom can react to form hydroperoxy radical



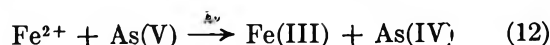
the subsequent reactions being



The ratio of the rate constants for reactions 8 and 6, k₈/k₆, was found to be 10³. In the presence of sufficient oxygen for reaction 8 to be very much faster than reaction 6, therefore, the initial quantum yield of iron(III) formation is twice that in the absence of oxygen.

The ultraviolet irradiation, at 2537 Å, of ferrous sulfate in the presence of arsenic acid yields arsenic(III). Arsenic acid is not photochemically reduced in the absence of iron(II) under the experimental conditions, and therefore the primary photolytic process involves iron(II).

The difference between the quantum yields in oxygen-free and oxygen-saturated solution can be interpreted by the intermediate formation of arsenic(IV) in the over-all mechanism, as follows, the reactions leading to arsenic(IV) formation being represented by the stoichiometric relationship

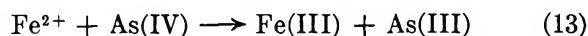


(13) E. Hayon and J. Weiss, *J. Chem. Soc.*, 3866 (1960).

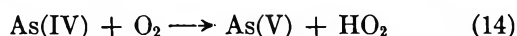
(14) M. Lefort and P. Douzou, *J. Chim. Phys.*, 53, 536 (1956).

(15) L. J. Heidt, M. G. Mullin, W. B. Martin, Jr., and A. M. J. Beatty, *J. Phys. Chem.*, 66, 336 (1962).

Previous investigations^{4,6,7} have shown that arsenic(IV) will oxidize iron(II)



and, in the absence of oxygen, this will be the only significant reaction involving arsenic(IV). Arsenic(IV) can also reduce iron(III),⁵⁻⁷ but this reaction will be insignificant in these experiments owing to the excess of iron(II) over iron(III), present in the reaction mixture. Arsenic(IV) also reacts with dissolved oxygen to give hydroperoxo radical (or As(IV)O_2) which has similar properties to hydroperoxo radical.^{5,7}



If the oxygen to iron(II) concentration ratio is sufficient for reaction 14 to be very much faster than reaction 13, arsenic(IV) will be quantitatively converted to hydroperoxo radical which will oxidize three ferrous ions. In this case the initial quantum yield of iron(III) will be twice that in the absence of oxygen, reactions 12 + 14 + 9 + 10 + 11, compared with 12 + 13, respectively, in accordance with the experimental results (Table IV). This result also shows that oxygen does not effect the primary photolytic process. It should be noted that oxidation of arsenic(III) by hydroxyl-free radical^{1,2,5-7} formed by reaction 10 will not compete with reaction 11 as there is a large excess of iron(II) over arsenic(III) in the reaction mixture.

At lower oxygen to iron(II) concentration ratios, there will be competition between iron(II) and oxygen for arsenic(IV). The initial quantum yield of arsenic(III) is a measure of the arsenic(IV) reacting with iron(II), as arsenic(IV) reacting with oxygen is oxidized to arsenic(V), while the difference between the initial yields of arsenic(III) in the presence and absence of oxygen is a measure of the arsenic(IV) reacting with oxygen.

$$\frac{\text{As(IV) reacting with O}_2}{\text{As(IV) reacting with Fe}^{2+}} = \frac{k_{14}[\text{O}_2]}{k_{13}[\text{Fe}^{2+}]} = \frac{A'_{\text{N}_2} - A'_{\text{O}_2}}{A'_{\text{O}_2}}$$

Therefore

$$\frac{k_{14}}{k_{13}} = \frac{[\text{Fe}^{2+}]}{[\text{O}_2]} \left(\frac{A'_{\text{N}_2} - A'_{\text{O}_2}}{A'_{\text{O}_2}} \right)$$

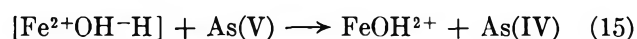
The ratio k_{14}/k_{13} is found to be independent of the ratio $[\text{Fe}^{2+}]/[\text{O}_2]$ (Table IV) in accordance with the proposed mechanism, the ratio in 1 M sulfuric acid being 40. The ratio k_{14}/k_{13} is independent of arsenic acid concentration, and therefore the postulated complex of iron(II) with arsenic acid (*vide infra*) reacts with arsenic(IV) at approximately the same rate as the uncomplexed ferrous ion. The rate constant ratio is dependent on sulfuric acid concentration (Table

V), suggesting that some complexing of iron(II) with sulfate occurs at the higher acidity, the reactivity of the complex with arsenic(IV) being greater than for the uncomplexed species.

The mechanism of reaction 12, resulting in arsenic(IV) formation, could be accounted for by postulating that either of the intermediates H or FeH^{2+} , formed by the photooxidation of ferrous sulfate (reactions 4 and 6) reduces arsenic(V) to arsenic(IV). However, these reactions anticipate competition either between arsenic(V) and iron(II) for H or between arsenic(V) and hydrogen ion for FeH^{2+} , respectively, contrary to the experimental results (Tables II and III). Furthermore, either of these reactions giving arsenic(IV) followed by reaction 13 does not explain the experimental increase in initial quantum yield of iron(III) when arsenic(V) is present.

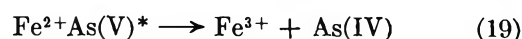
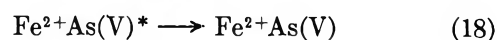
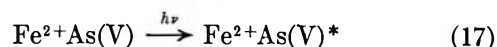
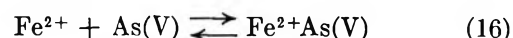
A chain mechanism would be necessary to account for this increase, but such a chain reaction is not apparent from previous investigations of reactions involving arsenic(IV).^{4,6,7}

It could also be postulated that the hydrogen atom formed in the solvent cage before dissociation into the bulk solution is scavenged by arsenic acid



This reaction explains, qualitatively, the increase in initial quantum yield of iron(III) and the absence of competition between arsenic(V) and iron(II) or acidity. However, this reaction would be competition with secondary recombination. The kinetics of such competition have been investigated by Noyes,¹⁶ who derived a relationship between the increase in quantum yield and the square root of the scavenger concentration. This relationship was confirmed for scavenging of this same intermediate by hydrogen ion.¹¹ However, the increase in quantum yield found here is approximately linearly related to the arsenic acid concentration at low arsenic acid concentrations (Figure 3) and not to its square root.

The photolysis can be explained by the formation of a photoactive complex of iron(II) with arsenic acid, the photochemical process represented by reaction 12 being



(16) R. M. Noyes, *J. Am. Chem. Soc.*, **77**, 2042 (1955); **78**, 5846 (1956).

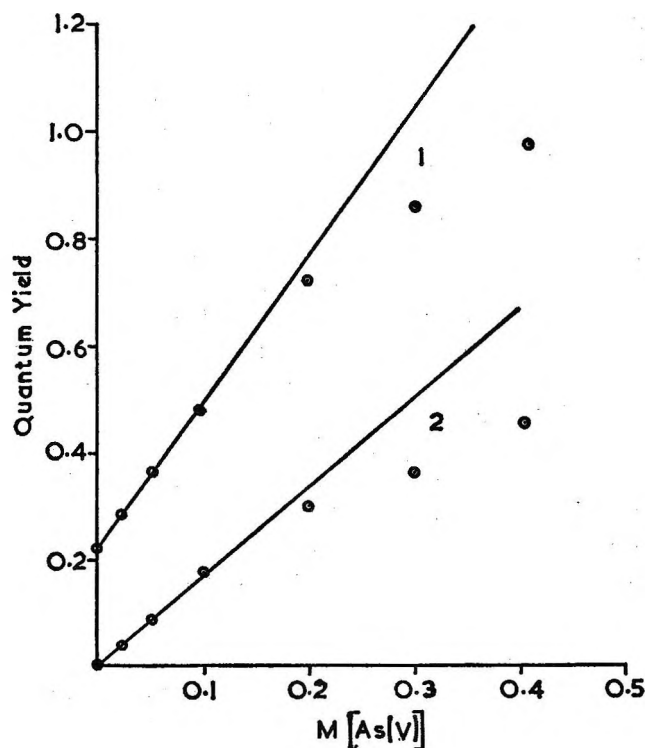


Figure 3. Plot of initial quantum yield in oxygen-free solution of (1) iron(III) and (2) arsenic(III) against arsenic(V) concentration.

In this case, the light absorbed by Fe²⁺, considering initial values and therefore the absence of iron(III), will be given by

$$I_{\text{Fe}^{2+}} = \frac{I_0}{1 + \frac{\epsilon_2}{\epsilon_1} \frac{[\text{Fe}^{2+}\text{As(V)}]}{[\text{Fe}^{2+}]}} = \frac{I_0}{1 + \frac{\epsilon_2}{\epsilon_1} K[\text{As(V)}]}$$

where ϵ_1 and ϵ_2 are the molar extinction coefficients of Fe²⁺ and Fe²⁺As(V), respectively, and K is the stability constant of Fe²⁺As(V)

$$K = \frac{[\text{Fe}^{2+}\text{As(V)}]}{[\text{Fe}^{2+}][\text{As(V)}]}$$

Also the light absorbed by Fe²⁺As(V) is

$$I_{\text{Fe}^{2+}\text{As(V)}} = \frac{I_0}{1 + \frac{\epsilon_1}{\epsilon_2} \frac{[\text{Fe}^{2+}]}{[\text{Fe}^{2+}\text{As(V)}]}} = \frac{I_0 \frac{\epsilon_2}{\epsilon_1} K[\text{As(V)}]}{1 + \frac{\epsilon_2}{\epsilon_1} K[\text{As(V)}]}$$

The initial rate of formation of iron(III), AI_0 , will be given by

$$AI_0 = A_1 I_{\text{Fe}^{2+}} + A_2 I_{\text{Fe}^{2+}\text{As(V)}}$$

where A_1 and A_2 are the initial quantum yields of iron(III) of Fe²⁺ and Fe²⁺As(V), respectively. Thus

$$A = \frac{A_1}{1 + \frac{\epsilon_2}{\epsilon_1} K[\text{As(V)}]} + \frac{A_2 \frac{\epsilon_2}{\epsilon_1} K[\text{As(V)}]}{1 + \frac{\epsilon_2}{\epsilon_1} K[\text{As(V)}]} \quad (\text{I})$$

Therefore the quantum yield is independent of total iron(II) concentration and acidity.

At low arsenic(V) concentration eq I simplifies to

$$A = A_1 + A_2 \frac{\epsilon_2}{\epsilon_1} K[\text{As(V)}]$$

anticipating the linear relationship between A and arsenic acid concentration shown in Figure 3. At the higher arsenic acid concentrations the denominator term in eq I becomes significant, and the relationship departs from linearity. Rearranging eq I gives

$$\frac{A - A_1}{[\text{As(V)}]} = \frac{\epsilon_2}{\epsilon_1} K(A_2 - A) \quad (\text{II})$$

A plot of $(A - A_1)/[\text{As(V)}]$ against A is shown in Figure 4. A linear plot is obtained in accordance with this relationship. From the slope and intercept the values $A_2 = 1.8$ and $(\epsilon_2/\epsilon_1)K = 2.14$ are obtained.

The same treatment can be made for the initial quantum yield of arsenic(III), A' ; in this case $A_1' = 0$.

$$A' = \frac{A_2' \frac{\epsilon_2}{\epsilon_1} K[\text{As(V)}]}{1 + \frac{\epsilon_2}{\epsilon_1} K[\text{As(V)}]} \quad (\text{III})$$

Rearranging eq III gives

$$\frac{A'}{[\text{As(V)}]} = \frac{\epsilon_2}{\epsilon_1} K(A_2' - A') \quad (\text{IV})$$

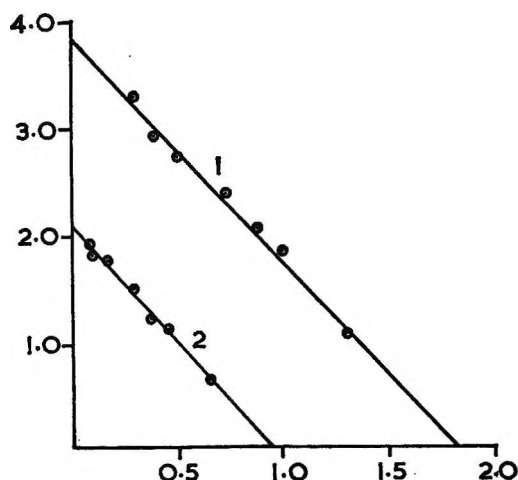


Figure 4. Plot of $(A - A_1)/[\text{As(V)}]$ (ordinate) against A , curve 1, and $A'/[\text{As(V)}]$ (ordinate) against A' , curve 2.

A plot of $A'/[As(V)]$ against A' is also shown in Figure 4, the slope and intercept giving the values $A'_2 = 0.9$ and $(\epsilon_2/\epsilon_1)K = 2.23$.

The ratio A_2/A'_2 is 2, as the arsenic(IV) formed oxidizes a second iron(II); the values of $(\epsilon_2/\epsilon_1)K$ are in good agreement.

The extinction coefficient ratio ϵ_2/ϵ_1 can be obtained from the experimental molar extinction coefficient, ϵ , at 2537 Å.

$$\epsilon[Fe(II)] = \epsilon_1[Fe^{2+}] + \epsilon_2[Fe^{2+}As(V)]$$

where $[Fe(II)]$ is the total iron(II) concentration in the solution. Therefore

$$\epsilon = \frac{\epsilon_1 + \epsilon_2 K [As(V)]}{1 + K [As(V)]} \quad (V)$$

The variation of the extinction coefficient with arsenic acid concentration is too small to estimate K from this equation. However, substituting the value of $(\epsilon_2/\epsilon_1)K = 2.2$ determined above in eq V gives

$$K = \left\{ \frac{\epsilon_1}{\epsilon} (1 + 2.2 [As(V)]) - 1 \right\} / [As(V)] \quad (VI)$$

Values of K derived from eq VI are 1.96, 1.92, 1.84, and 1.84 at arsenic acid concentrations of 0.25, 0.50,

0.75, and 1.00 M , respectively, giving an average value of $K = 1.9$.

The postulation of a photoactive complex between iron(II) and arsenic acid interprets, both qualitatively and quantitatively, the photochemical oxidation of ferrous sulfate in the presence of arsenic acid.

The quantum yields are little affected by acidity in the range 0.3 to 3.0 M sulfuric acid (Table III), suggesting that a complex of undissociated arsenic acid, rather than an arsenate ion, is involved. Complexes of undissociated phosphoric acid with thorium ($Th^{4+} \cdot H_3PO_4$)¹⁷ and with cobalt pentaammine ($Co(NH_3)_5 \cdot H_3PO_4^{3+}$)¹⁸ have been characterized.

The initial quantum yields for the iron(II) arsenic acid complex were determined to be 1.8 and 0.9 for iron(III) and arsenic(III), respectively. The fraction of excited ions that dissociate, k_{19}/k_{18} , is therefore 0.9; this fraction is much greater than for the aquo-ferrous ion.

Acknowledgment. The author is indebted to Professor A. S. Buchanan for advice during the course of this work and in the preparation of the manuscript.

(17) E. L. Zebroski, H. W. Alter, and F. K. Heumann, *J. Am. Chem. Soc.*, **73**, 5646 (1951).

(18) W. Schmidt and H. Taube, *Inorg. Chem.*, **2**, 698 (1963).

Structure and Transition in the Solid State of a Helical Macromolecule

by A. J. McKinnon and V. Tobolsky

Frick Chemical Laboratory, Princeton University, Princeton, New Jersey (Received October 7, 1966)

Results of X-ray, infrared, volume-temperature, and modulus-temperature measurements on solid films of poly- γ -benzyl-L-glutamate cast from chloroform solution are reported. It is concluded that these films contain paracrystalline and mesomorphic regions. The latter maintain a relative molecular disposition similar to that in the cholesteric mesomorphic phase in concentrated solution. In the solid, the structure may be idealized as composed of planes of molecules parallel to the film surface, the molecules in any one plane being parallel. Adjacent parallel planes of molecules have a small twist relative to one another about an axis perpendicular to the sheets of molecules. In the paracrystalline phase there is no helical twist, so that the molecules are all parallel and packed in a slightly distorted hexagonal array.

Introduction

Poly- γ -benzyl-L-glutamate (PBG) has been studied by many physical methods, including dynamic mechanical measurements on solid films¹ and solutions.² In dilute isotropic solution (in many solvents, including chloroform) it is well established^{3,4} that the molecule is a rigid helix, the preponderance of evidence identifying the helix as an α helix. It is also well known that in more concentrated solutions PBG forms mesomorphic phases^{5,6} akin to cholesteric liquid crystals. Recently, despite some suggestions to the contrary,⁶ the conformation in the mesomorphic phase has been identified as that of the α helix.⁷ At still higher concentrations in certain solvents, a so-called "paracrystalline" phase exists.^{6,7} In the solid, X-ray and electron diffraction evidence identifies the molecular structure once again as α helical.⁸⁻¹⁰ Discussion of the molecular arrangement and packing of helical molecules in the solid state has been confined to oriented films⁸ and fibers¹⁰ in which it is stated that the structure is paracrystalline.¹⁰ On the other hand, there has been no detailed discussion of the structure of the un-oriented solid.

We report in this paper results of several physicochemical studies on solid films of PBG cast from chloroform solution. We conclude, from the information in the literature together with our own results, that the solid contains paracrystalline and mesomorphic regions. The mesomorphic regions probably maintain the same

relative molecular disposition as in the cholesteric mesomorphic phase in concentrated solution as discussed by Robinson, *et al.*⁵

In the mesomorphic phase of concentrated solutions of PBG the molecules are packed, in any small region, approximately parallel, but with a small helical twist relative to one another about an axis perpendicular to the molecular axis. The array is not crystalline, but very far from random, as is characteristic of liquid crystals in general. At the highest concentrations at which observations have been made (about 50 wt % of PBG) the freedom of movement of the molecules is

- (1) R. G. Saba, J. A. Sauer, and A. E. Woodward, *J. Polymer Sci.*, **A1**, 1483 (1963).
- (2) N. W. Tschoegl and J. D. Ferry, *J. Am. Chem. Soc.*, **86**, 1474 (1964).
- (3) See, for example, P. Doty and W. B. Gratzer, "Polyamino Acids, Polypeptides and Proteins," M. A. Stahmann, Ed., University of Wisconsin Press, Madison, Wis., 1962, pp 111-119.
- (4) B. R. Jennings and H. G. Jerrard, *J. Phys. Chem.*, **69**, 2817 (1965).
- (5) (a) C. Robinson, *Trans. Faraday Soc.*, **52**, 571 (1956); (b) C. Robinson, J. C. Ward, and R. B. Beevers, *Discussions Faraday Soc.*, **25**, 29 (1958); (c) C. Robinson, *Tetrahedron*, **13**, 219 (1961).
- (6) V. Luzzati, M. Cesari, G. Spach, F. Masson, and J. M. Vincent, *J. Mol. Biol.*, **3**, 566 (1961).
- (7) D. A. D. Parry and A. Elliott, *Nature*, **206**, 616 (1965).
- (8) C. H. Bamford, A. Elliott, and W. E. Hanby, "Synthetic Polypeptides," Academic Press Inc., New York, N. Y., 1956, Chapter VIII.
- (9) D. F. Parsons and U. Martius, *J. Mol. Biol.*, **10**, 53C (1964).
- (10) A. Elliott, R. D. B. Fraser, and T. P. MacRae, *ibid.*, **11**, 821 (1965).

extremely small.^{5b,c} It is easy to envisage that a somewhat similar structure is retained in the solid when all solvent is removed.

The mesomorphic regions of the solid films we have made may be idealized as composed of planes of molecules parallel to the surface. In any given plane the molecules lie parallel to each other over small regions. Adjacent parallel planes of molecules have a small twist relative to one another about an axis perpendicular to the molecular sheets. Ideally this twist is constant from plane to plane and in the concentrated solutions produces characteristic birefringence.

The paracrystalline phase differs only in having no helical twist, so that the molecules are all parallel and packed in a slightly distorted hexagonal array.¹⁰ The evidence for these conclusions will be presented below.

Experimental Section

Films of PBG (Pilot Chemicals, Watertown, Mass., Lot No. G-58, $M_v = 338,000$) about 0.075 cm thick were cast from concentrated chloroform solution on a mercury surface. After casting, the films were heated at 100° *in vacuo* for at least 12 hr to remove all traces of solvent; this was verified since no chlorine could be detected by analysis.

Ten-second creep modulus measurements were made with a Gehman testing apparatus,¹¹ with Dow-Corning silicone oil as the heating medium. Specific volume-temperature measurements were made by measuring the buoyant weight of a sample immersed in a silicone oil (of known density at all temperatures) and were checked by pycnometry.

Infrared spectra were measured on a Perkin-Elmer Model 237-B recording spectrograph, using very thin (1–2 μ) films cast on AgCl plates, and X-ray photographs were made on flat plate and cylindrical cameras.

Results and Discussion

X-Ray Diagrams. Figure 1 shows flat-plate X-ray photographs of a PBG film at room temperature, with (a) the X-ray beam perpendicular to the PBG film plane (N position),⁸ and (b) the X-ray beam parallel to the PBG film plane (E position).

Photograph a shows five continuous diffraction rings, the three at lowest angle corresponding to the first three equatorials of the list given by Bamford, *et al.*⁸ The fourth has a spacing (5.26 Å) equivalent to that of the strong near-meridional reflection of the fifth-layer line of the fiber photograph,^{9,10} and the outer diffuse ring corresponds to a superposition of the very diffuse and broad off-meridional streak also on the fifth-layer line with the outermost equatorials. (See ref

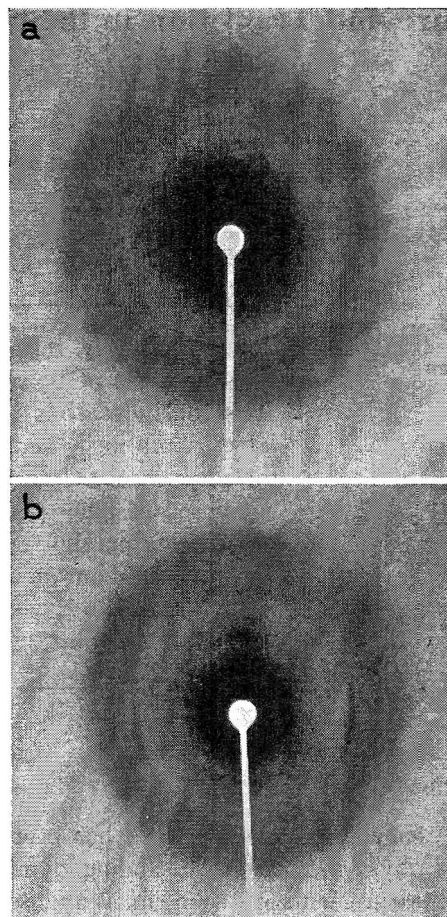


Figure 1. Flat-plate X-ray photographs of PBG film at room temperature (25°): (a) X-ray beam perpendicular to plane of PBG film; and (b) X-ray beam parallel to plane of horizontal PBG film.

10 for discussion of the fiber diagram.) Photograph b shows these reflections segregated into equatorial, near-meridional, and off-meridional reflections, and together with (a) indicates uniplanar orientation of the molecules in the plane of the PBG film.

Though our photographs do not show different equatorials in the N and E positions, as found by Bamford, *et al.*,⁸ for doubly oriented specimens made by "unidirectional wiping," the presence of spots superimposed on arcs on the equator of photograph b, and the asymmetry in intensity on the equator when the film plane is at a small angle to the beam (as in photo b), indicates some preference for the (110) plane of the paracrystalline regions to lie in the plane of the film. This is in agreement with the orientation found by Bamford, *et al.*, and also with the most likely structure proposed for the mesomorphic phase in solution.^{5b}

(11) S. D. Gehman, D. E. Woodford, and C. S. Wilkinson, Jr., *Ind. Eng. Chem.*, **39**, 1108 (1947).

The appearance of photo a is not unlike the normal pattern from a semicrystalline polymer, where crystalline and disordered regions give rise to rings and halos. It is at first glance tempting to conclude that the halos in this case come from the mesomorphic regions. Unfortunately, however, the halo can also occur in a completely paracrystalline material. It is possible to consider the halo on the X-ray diagram as arising from the diffuse streaks which occur on the layer lines of an oriented paracrystalline fiber. Our photos thus do not prove or disprove the existence of mesomorphic regions. On the other hand, the observation of several equatorials is evidence that the sample does consist at least partly of regions of parallel paracrystalline alignment of the molecules, since fewer equatorials might be expected from a completely mesomorphic material. This is supported by the fact that though the cholesteric structure in solution gives only the first, most intense, equatorial,^{5b,6} the paracrystalline phase gives several sharp equatorial reflections indexing on a hexagonal net. The X-ray diagrams seem to demonstrate the existence of paracrystalline regions.

The orientation observed in the film may be ascribed to the spontaneous self-orientation of the mesomorphic phase in chloroform solution at the liquid-air interface.^{5a} The preferred direction of the axis of torsion in this phase is perpendicular to the surface. The poorly developed "double orientation" may be traced to variations in the direction of the axis of torsion within the semimicroscopic texture of the mesomorphic phase.

Infrared Spectrum. The infrared spectrum of a very thin film of PBG showed peaks at 1656 (amide I) and 1549 cm^{-1} (amide II) which, together with the absence of a peak at 1690 cm^{-1} , due to nonhydrogen-bonded carbonyl absorption, indicate a helical conformation^{12,13} (intramolecular hydrogen bonding) at room temperature (25°). No shift in these peaks was observed at 100°. If there were any appreciable amount of random coil regions, one would expect on a statistical basis to observe some 1690- cm^{-1} absorption.

We also find no indication from the infrared spectrum of the presence of any β phase (intermolecular hydrogen bonding), nor does there appear to be evidence from any other source for β phase in high molecular weight PBG. For example, Blout and Asadourian¹³ were unable to detect β phase in the solid above a molecular weight of 28,000, and concluded that β phase in PBG was confined to very low molecular weight material. Though these methods may be insensitive to the presence of small breaks in the helix, the evidence indicates that the molecules in solid films of PBG exist as nearly completely rigid helices. This is sup-

ported by the occurrence of the α -helical conformation in the mesomorphic phase in concentrated solution.

Specific Volume. Reported values for the specific volume of solid PBG vary from 0.785¹⁴ to 0.850¹ and 0.870 cc/g .⁸ By contrast, the specific volume calculated from the X-ray data is 0.766 cc/g .¹⁰ Our measurements on our own films at 25° all lie in the range 0.786 \pm 0.003 cc/g , which is virtually identical with the partial specific volume in solution.^{8,14} Compared with the X-ray specific volume, our films have about 2% free volume.

Since heating *in vacuo* is said to promote crystallization,^{8,10} presumably with a consequent decrease in specific volume, it is likely that the exact value of the film density depends on the procedure by which the films are made. The fact that all solid films made thus far have higher specific volumes than the X-ray value indicates the existence of some phase other than the paracrystalline phase responsible for the X-ray diagram.

When we consider that the molecules are helical and have all possible orientations in the plane of the film, as shown by Figure 1a, the question of the molecular packing and the small free volume in the films becomes extremely interesting. Random packing of rigid helices would lead to enormous free volume. If there are noncrystalline regions in the films, these regions must be packed very efficiently. Such an efficient packing is provided by the concept that the noncrystalline regions are mesomorphic in structure.

Specific Volume vs. Temperature. Figure 2 shows the specific volume-temperature relation around the transition temperature for a typical sample and indicates a discontinuity in slope at 12°. This behavior is typical of a glasslike transition.

This transition occurs in a material which is still at least very largely helical above the transition temperature so that major internal rotations in the molecular backbone cannot take place. A possible explanation of the transition is the onset of side-chain rotations, which is in accord with the interpretations of proton magnetic resonance spectra^{15,16} and dielectric dispersion.¹⁷

(12) C. H. Bamford, A. Elliott, and W. E. Hanby, ref 8, Chapter V.

(13) E. R. Blout and A. Asadourian, *J. Am. Chem. Soc.*, **78**, 955 (1956).

(14) J. H. Bradbury, M. D. Fenn, and I. Gosney, *J. Mol. Biol.*, **11**, 137 (1965).

(15) J. A. E. Kail, J. A. Sauer, and A. E. Woodward, *J. Phys. Chem.*, **66**, 1292 (1962).

(16) K. Hikichi, *J. Phys. Soc. Japan*, **19**, 2169 (1964).

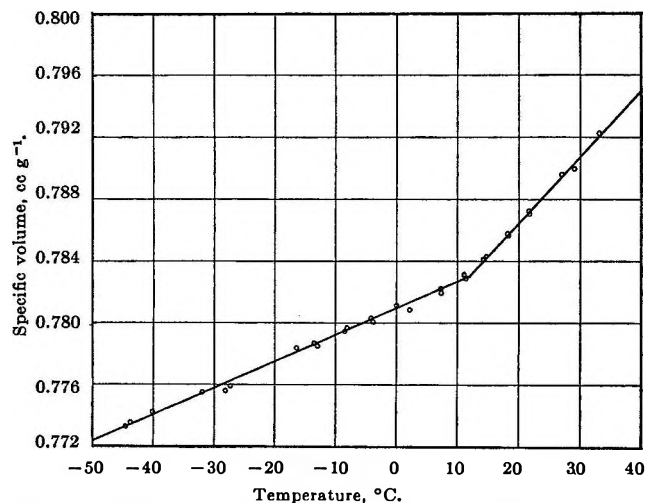


Figure 2. Specific volume of solid PBG film vs. temperature.

If the solid were entirely paracrystalline, or if the transition occurred only in paracrystalline regions, a first-order solid-solid phase change, possibly diffuse, with an associated volume change might be expected. Our data do not show this type of behavior, but only a change of coefficient of expansion from $2.4 \times 10^{-4} \text{ deg}^{-1}$ below the transition to $5.1 \times 10^{-4} \text{ deg}^{-1}$ above. This suggests that the side-chain motions start to occur in the mesomorphic regions.

Modulus-Temperature Curve. Figure 3 shows $3G$ ($G = 10\text{-sec}$ creep modulus) as a function of temperature. There is a well-defined and reproducible decrease in modulus by a factor of about 10 in the region $0\text{--}30^\circ$. Above 100° the modulus remains constant

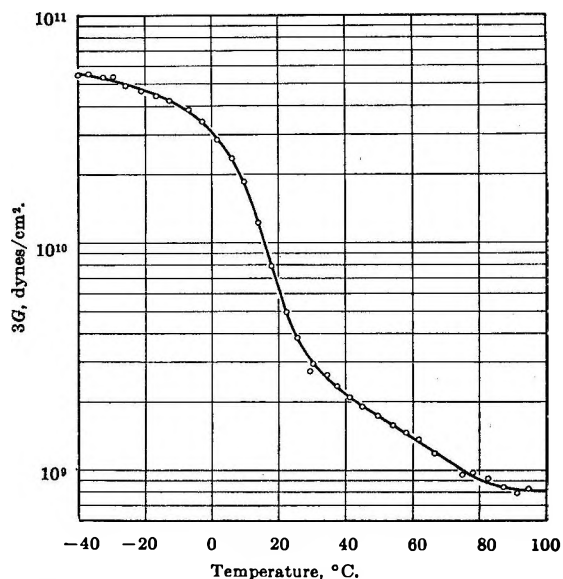


Figure 3. $3G$ as a function of temperature for PBG film. G is the 10-sec shear creep modulus.

until decomposition becomes severe about 200° . This modulus transition, which is compatible with a glasslike transition at about 12° , confirms previous work by dynamic measurements.¹

Acknowledgment. We wish to acknowledge the partial support of a fellowship from the Wool Research Organization of New Zealand and the U. S. Department of Agriculture.

(17) K. Hikichi, K. Saito, M. Kaneko, and J. Furuichi, *J. Phys. Soc. Japan*, **19**, 577 (1964).

Theoretical Calculations on Ions and Radicals. I. A Restricted Hartree-Fock Perturbation Method for the Calculation of Spin Densities

by J. E. Bloor, B. R. Gilson,

Cobb Chemical Laboratory, University of Virginia, Charlottesville, Virginia

and P. N. Daykin

British Columbia Research Council, Vancouver 8, British Columbia, Canada (Received October 11, 1965)

A restricted Hartree-Fock perturbation method, employing semiempirical SCFMO closed shell MO's to calculate the necessary matrix elements, is described and used to compute the spin densities and charge densities of 16 hydrocarbon ions. The results are very similar to those calculated by the "improved unrestricted Hartree-Fock" method of Snyder and Amos. Statistical analysis of the empirical relationship between esr hyperfine splitting constants and theoretical parameters show that the Colpa and Bolton expression, which includes both a charge and a spin density term, and the equation of Giacometti, Nordio, and Pavan introducing a nearest-neighbor term, are no improvement over the simple McConnell relationship.

Introduction

The indirect measurement of electron distributions by the measurement of electron spin resonance hyperfine splitting constants is a very powerful tool in the elucidation of the molecular structure of ions and radicals.¹⁻³ Often, however, particularly in the case of transients and of complex organic radicals containing heteroatoms, it is not possible to obtain enough hyperfine structure to assign unambiguously all the hyperfine splitting constants to particular atoms in the ion or radical under examination.⁴ Under such circumstances it is very helpful to have the assistance of theoretical calculations of electron spin densities (ρ) in order to calculate theoretical hyperfine splitting constants a_p^H using the McConnell⁵ equation

$$a_p^H = Q_{CH}^H \rho_p \quad (1)$$

or one of the other relationships⁶⁻⁸ which have been proposed for relating splitting constants to electron distributions.

Up to the present, the majority of calculations have been carried out using Hückel molecular orbitals (HMO's) to calculate spin and charge densities.^{2,3,6-10} Calculations have also been reported using a valence

bond method¹¹ and an "improved unrestricted Hartree-Fock method" (UHF),^{12,13} but apart from calculations on the pyrene¹⁴ anion, no systematic investigation of the use of the restricted Hartree-Fock (RHF) method has been reported.

The semiempirical RHF method with configuration

- (1) I. D. Morozova, *Russ. Chem. Rev.*, **31**, 575 (1962).
- (2) A. Carrington, *Quart. Rev. (London)*, **17**, 67 (1963).
- (3) P. H. Rieger and G. K. Fraenkel, *J. Chem. Phys.*, **37**, 2795, 2811 (1962); **39**, 609 (1963).
- (4) E. Ehrenberg, "Electronic Aspects of Biochemistry," B. Pullman, Ed., Academic Press, New York, N. Y., 1964, p 379.
- (5) H. M. McConnell, *J. Chem. Phys.*, **24**, 764 (1956).
- (6) J. P. Colpa and J. R. Bolton, *Mol. Phys.*, **6**, 273 (1963).
- (7) G. Giacometti, P. L. Nordio, and M. V. Pavan, *Theoret. Chim. Acta (Berlin)*, **1**, 404 (1963).
- (8) J. R. Bolton, *J. Chem. Phys.*, **42**, 309 (1965).
- (9) F. Schneider, K. Möbius, and M. Plato, *Angew. Chem. Intern. Ed.*, **4**, 856 (1965).
- (10) T. C. Sayetta and J. D. Memory, *J. Chem. Phys.*, **40**, 2748 (1964).
- (11) J. C. Schug, T. H. Brown, and M. Karplus, *ibid.*, **35**, 1873 (1961); **37**, 330 (1962).
- (12) A. T. Amos and G. G. Hall, *Proc. Roy. Soc. (London)*, **A263**, 483 (1961); A. T. Amos, *Mol. Phys.*, **5**, 91 (1962); L. C. Snyder and A. T. Amos, *J. Chem. Phys.*, **41**, 1773 (1964).
- (13) L. C. Snyder and A. T. Amos, *ibid.*, **42**, 3670 (1965).
- (14) H. Ben Jemia and R. Lefebvre, *J. Chim. Phys.*, **68**, 755 (1962).

interaction (CI), however, has been used widely and successfully¹⁵ in calculating ground-state and excited-state properties of many molecules.

In the work described here we have utilized the self-consistent field (SCF) MO's obtained from closed-shell RHF calculations of this type, to construct excited configurations for hydrocarbon radical anions and cations, and then we have introduced electron correlation (and therefore negative spin densities) into the ground state of the radical by allowing it to interact with the excited species using perturbation theory.¹⁶⁻¹⁸ We have applied the procedure to a number of hydrocarbon radical ions for which experimental hyperfine splitting constants are available in order to establish the reliability of the method, compared to other procedures, in predicting and assigning hyperfine splitting constants. We have also investigated, by statistical analysis, whether, as suggested by Colpa and Bolton⁶ and by Giacometti, Nordio, and Pavan,⁷ the addition of extra terms to the simple McConnell relationship⁵ (1) leads to any substantial improvement in the calculated hyperfine splitting constants. In succeeding papers we will present the results of calculations using the same RHF perturbation procedure on radicals and ions containing heteroatoms. As will be clearly demonstrated by this later work, we believe that the major advantage of this method over other procedures is that we can make use of experimental data on the neutral molecule (transition energies, ionization potentials, reduction potentials, and charge densities obtained from nmr measurements) to determine heteroatom parameters which can then be used in calculations on radical species derived from these neutral molecules.

Method

The basic equations used are a fairly straightforward application of perturbation theory within the framework of the semiempirical restricted Hartree-Fock theory as used by Longuet-Higgins and Pople¹⁶ in calculating the excited states of odd-alternant hydrocarbon radicals and ions. By using closed-shell SCF MO's and their orbital energies in the calculations, many of the molecular repulsion integrals, which would have to be included if HMO's were used, do not have to be computed and so calculations on large molecules can be carried out quite quickly. In our calculations we allowed configurations of three types to interact with the ground state. Configurations of the type

$${}^1\Psi_i^m = |\psi_1\bar{\psi}_1 \dots \psi_i\bar{\psi}_m \dots \psi_m|; \quad i < m \quad (2)$$

where the m th MO is the one containing the unpaired spin in the ground state, affect both spin and charge densities.

Configurations of the type

$${}^2\Psi_i^k = \frac{1}{\sqrt{2}}\{|\psi_1\bar{\psi}_1 \dots \psi_i\bar{\psi}_k \dots \psi_m| + |\psi_1\bar{\psi}_1 \dots \psi_k\bar{\psi}_i \dots \psi_m|\}; \quad i < m < k \quad (3)$$

interact with ground state to affect the charge densities only, while doubly excited configurations of the type

$${}^3\Psi_i^k = \frac{1}{\sqrt{6}}\{2|\psi_1\bar{\psi}_1 \dots \psi_i\psi_k \dots \bar{\psi}_m| - |\psi_1\bar{\psi}_1 \dots \psi_i\bar{\psi}_k \dots \psi_m| - |\psi_1\bar{\psi}_1 \dots \bar{\psi}_i\psi_k \dots \psi_m|\}; \quad i < m < k \quad (4)$$

interact with the ground state to affect the spin densities.

The excited state energies relative to the ground state may be written as

$$\begin{aligned} \langle {}^1\Psi_i^m | H | {}^1\Psi_i^m \rangle - \langle \Psi_0 | H | \Psi_0 \rangle &= E_m^{\text{SCF}} - E_i^{\text{SCF}} - 2\langle ii | mm \rangle + \langle im | im \rangle + \langle mm | mm \rangle \\ \langle {}^2\Psi_i^k | H | {}^2\Psi_i^k \rangle - \langle \Psi_0 | H | \Psi_0 \rangle &= E_k^{\text{SCF}} - E_i^{\text{SCF}} - \langle ii | kk \rangle + \langle mm | kk \rangle - \langle ii | mm \rangle - \\ &\quad \frac{1}{2}\langle mk | mk \rangle + \frac{1}{2}\langle im | im \rangle \\ \langle {}^3\Psi_i^k | H | {}^3\Psi_i^k \rangle - \langle \Psi_0 | H | \Psi_0 \rangle &= E_k^{\text{SCF}} - E_i^{\text{SCF}} - \langle ii | kk \rangle + \langle mm | kk \rangle - \langle ii | mm \rangle + \\ &\quad \frac{3}{2}\langle mk | mk \rangle + \frac{1}{2}\langle im | im \rangle \end{aligned}$$

and the matrix of elements of interaction with the ground state as

$$\langle {}^1\Psi_i^m | H | \Psi_0 \rangle = \langle im | mm \rangle \equiv {}^1A_{im}$$

$$\langle {}^2\Psi_i^k | H | \Psi_0 \rangle = \sqrt{2}\langle ik | mm \rangle - \frac{1}{\sqrt{2}}\langle im | km \rangle \equiv {}^2A_{ik}$$

$$\langle {}^3\Psi_i^k | H | \Psi_0 \rangle = -\sqrt{\frac{3}{2}}\langle im | km \rangle \equiv {}^3A_{ik}$$

where $\langle im | lk \rangle \equiv \int \psi_i(1)\psi_m(1)1/r_{12}\psi_l(2)\psi_k(2)dV_{12}$.

The spin densities and charge densities can then be written as (5) and (6), respectively

$$\rho_p^\pi = c_{mp}^2 - 2\left[\sum_{i < m} \frac{{}^1A_{im}}{E_i^m - E_0} c_{ip}c_{mp} + \sqrt{\frac{2}{3}}\sum_{i < m} \sum_{k > m} \frac{{}^3A_{ik}}{E_i^k - E_0} c_{ip}c_{kp}\right] \quad (5)$$

(15) For an extensive bibliography, see R. G. Parr, "Quantum Theory of Molecular Electronic Structure," W. A. Benjamin, Inc., New York, N. Y., 1963.

(16) H. C. Longuet-Higgins and J. A. Pople, *Proc. Phys. Soc. (London)*, **A68**, 591 (1951); A. Carrington and J. C. P. Smith, *Mol. Phys.*, **9**, 137 (1965).

(17) W. D. Hobe, *ibid.*, **7**, 325 (1964).

(18) G. J. Hoijtink, *ibid.*, **1**, 157 (1958).

$$q_p^\pi = c_{mp}^2 + 2 \sum_{i=1}^{m-1} c_{ip}^2 - 2 \left[\sum_{i < m} \frac{{}^1A_{im}}{E_i^m - E_0} c_{ip}c_{mp} + \sqrt{2} \sum_{i < m} \sum_{k > m} \frac{{}^2A_{ik}}{E_i^k - E_0} c_{ip}c_{kp} \right] \quad (6)$$

These equations were programmed in the Automath language and the calculations of ρ_p^π and q_p^π were carried out on a Honeywell 1400 computer.¹⁹

The molecules for which the calculations were performed and the numbering system used are given in Figure 1. For naphthalene, anthracene, naphthacene, phenanthrene, and pyrene, the closed shell SCFMO's obtained by Hoyland and Goodman²⁰ were used. For perylene, biphenyl, azulene, acenaphthalene, and fluoranthene, the closed shell SCFMO's were calculated using a constant resonance integral (β_{pq}) for nearest neighbors and the Nishimoto-Mataga²¹⁻²³ (NM) method of calculating repulsion integrals was used. The success of such calculations in predicting the properties of the neutral

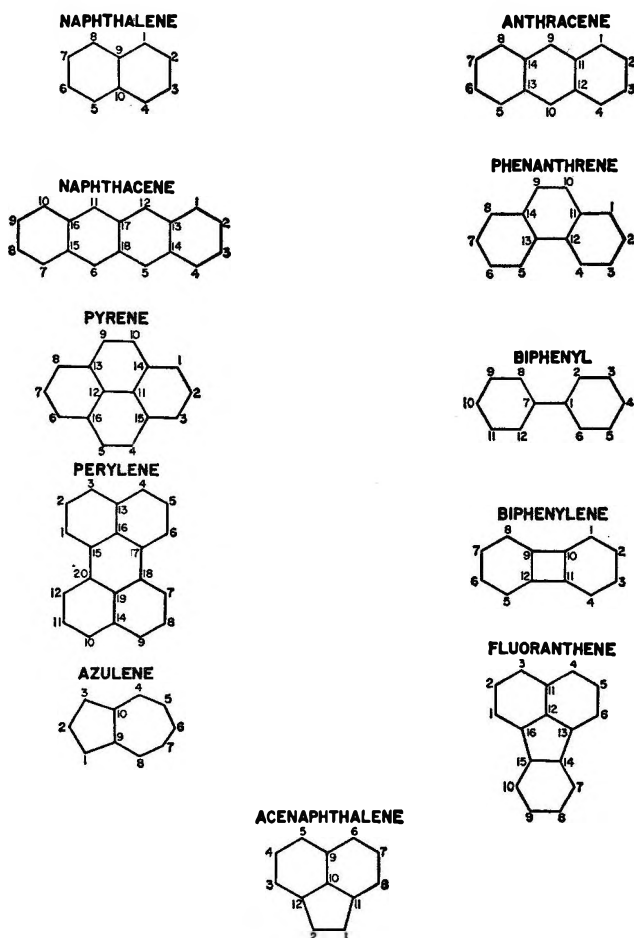


Figure 1. Numbering system used.

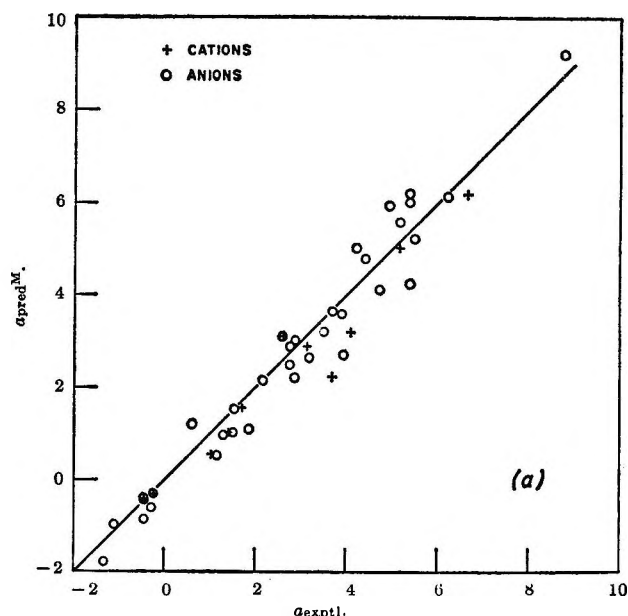


Figure 2A. Comparison between experimental coupling constants (a_{exptl}) and the values (a_{pred}^M) calculated from the simple McConnell relationship, eq 1.

hydrocarbons of molecules has been discussed elsewhere.²³⁻²⁵ We have found very little difference in the atomic orbital coefficients calculated by either method. Also, the plots (Figure 2) of experimental hyperfine constants *vs.* theoretical values calculated by using spin densities and charge densities calculated by both procedures in eq 1, 7, and 8 are indistinguishable from one another.

As an example of a typical calculation for a radical ion, we have summarized our results for the naphthalene anion in Table I. The relatively small depression of the ground state by excited configurations of types 1 and 2 shows that the closed shell SCFMO's are good approximations to the open shell MO's. The results for the spin and charge densities for the other radical anions of Figure 1 are summarized in Table II.

(19) Facilities are available for using these programs at the Franklin Institute Computing Center, Philadelphia, Pa., and in ALGCL at the University of Virginia, Charlottesville, Va.

(20) SCFMO's supplied by Prof. L. Goodman, calculated as described in J. R. Hoyland and L. Goodman, *J. Chem. Phys.*, **36**, 12 (1962).

(21) K. Nishimoto and N. Mataga, *Z. Physik. Chem. (Frankfurt)*, **12**, 335 (1957).

(22) L. S. Forster and K. Nishimoto, *J. Am. Chem. Soc.*, **37**, 1459 (1965).

(23) J. E. Bloor, P. N. Daykin, and P. Boltwood, *Can. J. Chem.*, **42**, 121 (1964).

(24) J. E. Bloor and N. Brearley, *ibid.*, **43**, 1761 (1965).

(25) J. E. Bloor, *ibid.*, in press, and work to be published.

Table I: Naphthalene Anion Excited Configurations and π -Electron Density Contributions after CI

| Con-figuration ^a | Energy, ev | Depression of ground state by con-figuration | Contribution to spin density ^b | | Contribution to charge density ^c | |
|-----------------------------|------------|--|---|------------|---|------------|
| | | | Position 1 | Position 2 | Position 1 | Position 2 |
| $1\Psi_2^8$ | 7.39 | 0.000 | ... | ... | 0.0000 | 0.0000 |
| $2\Psi_1^8$ | 7.18 | 0.000 | ... | ... | 0.0022 | 0.0010 |
| $2\Psi_4^8$ | 3.88 | 0.024 | ... | ... | 0.0013 | 0.0174 |
| $2\Psi_3^7$ | 6.49 | 0.052 | ... | ... | 0.0014 | 0.0196 |
| $2\Psi_3^{10}$ | 9.92 | 0.007 | ... | ... | 0.0088 | 0.0040 |
| $2\Psi_5^9$ | 7.26 | 0.025 | ... | ... | 0.0187 | 0.0187 |
| $2\Psi_1^8$ | 12.86 | 0.001 | 0.0013 | -0.0006 | ... | ... |
| $2\Psi_4^8$ | 9.55 | 0.030 | 0.0005 | -0.0071 | ... | ... |
| $2\Psi_3^7$ | 6.66 | 0.001 | 0.0001 | -0.0012 | ... | ... |
| $2\Psi_3^{10}$ | 10.81 | 0.035 | 0.0111 | -0.0050 | ... | ... |
| $2\Psi_6^9$ | 7.10 | 0.013 | 0.0081 | -0.0081 | ... | ... |

^a Defined by eq 2-6. ^b Calculated from individual terms of eq 5. ^c Calculated from individual terms of eq 6.

Calculation of Hyperfine Coupling Constants

Until recently, the simple relationship (eq 1) suggested by McConnell⁴ to relate the hyperfine splitting constant a_p^H of a hydrogen atom attached to a carbon atom p to the π -electron spin density ρ_p^π at that position was widely accepted.¹⁻³ However, in an attempt to explain the observed generally greater coupling constants for the cations of alternant hydrocarbons than those of the corresponding values for anions, Colpa and Bolton⁶ carried out a theoretical analysis of the nature of the interaction between the π -electron system and the C-H σ -orbitals. They arrived at a relationship (7), in which the hyperfine splitting constant a_p^H was also dependent on the excess charge density q_p^π , defined by $\Delta q_p^\pi = q_p^\pi - 1$, where q_p is calculated as in (6)

$$a_p^H = (Q_{CH}^H + K\Delta q_p^\pi)\rho_p^\pi \quad (7)$$

This equation (7) was claimed to represent the data for hydrocarbon anions and cations considerably better than (1). However, it has recently been shown by Higuchi²⁶ and by Lefebvre²⁷ that the theoretical derivation of (7) was incorrect because of sign errors and that the theory actually predicts a_p^H values for anions to be greater than for cations.

More recently, Bolton⁸ has attempted to rationalize (7) by postulating a first-order excess-charge effect which is due to the increase in the effective nuclear charge of the $2p\pi$ -orbital on the neutral carbon atom on cation formation. However, this hypothesis is not as convincing as the previous theory, since corresponding changes in other parameters such as the core integrals and two-center integrals undoubtedly occur and are neglected in the derivation of (7).

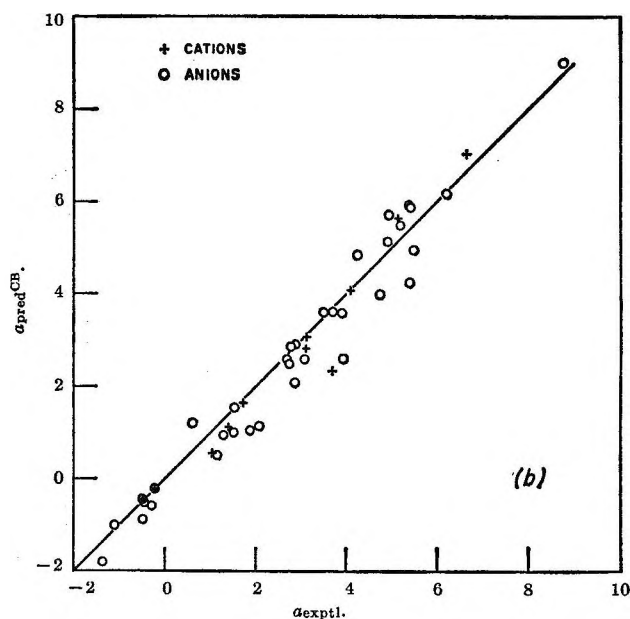


Figure 2B. Comparison between experimental coupling constants (a_{exptl}) and the values ($a_{\text{pred}}^{\text{CB}}$) calculated from the Colpa-Bolton relationship, eq 7.

In another attempt to improve on (1), Giacometti, *et al.*,⁷ postulated that the hyperfine splitting constant should be calculated from

$$a_p^H = Q_{CH}^H \rho_p^\pi \pm N' \left(\sum_j c_{mj} c_{mp} \right) \quad (8)$$

where the atoms j are the neighboring carbon atoms to p , and c_{mj} is the coefficient of AO j in the MO ψ_m which contains the unpaired electron. At the present

(26) J. Higuchi, *J. Chem. Phys.*, **39**, 345 (1963).

(27) R. Lefebvre, in footnote, ref 8.

Table II: Comparison of Observed and Theoretical Hyperfine Splitting Constants for Hydrocarbon Radical Ions

| Radical ion | Atom ^a | $\Delta q(\text{anion})^b$ | $\rho_p^{\pi c}$ | a_{expt}^d | | $a_{\text{H}^{\pi}}(M)^e$ | | $a_{\text{H}^{\pi}}(\text{CB})^f$ | | $a_{\text{H}^{\pi}}(\text{GNP})^g$ | |
|-----------------------------|-------------------|----------------------------|------------------|---------------------|--------|---------------------------|--------|-----------------------------------|--------|------------------------------------|--------|
| | | | | Anion | Cation | Anion | Cation | Anion | Cation | Anion | Cation |
| Naphthalene ^h | 1 | 0.164 | 0.233 | 4.95 | | 5.95 | | 5.71 | | 4.91 | |
| | 2 | 0.103 | 0.042 | 1.87 | | 1.07 | | 1.06 | | 1.52 | |
| Anthracene ^h | 1 | 0.074 | 0.112 | 2.76 | 3.12 | 2.86 | 2.86 | 2.87 | 3.08 | 2.98 | 3.13 |
| | 2 | 0.119 | 0.040 | 1.53 | 1.40 | 1.03 | 1.03 | 1.01 | 1.13 | 1.01 | 1.08 |
| | 9 | 0.183 | 0.242 | 5.41 | 6.65 | 6.19 | 6.19 | 5.88 | 6.99 | 6.03 | 6.45 |
| Tetracene ^h | 1 | 0.062 | 0.060 | 1.55 | 1.72 | 1.53 | 1.53 | 1.55 | 1.64 | 1.66 | 1.95 |
| | 2 | 0.078 | 0.020 | 1.15 | 1.06 | 0.52 | 0.52 | 0.52 | 0.56 | 0.81 | 0.85 |
| | 5 | 0.157 | 0.197 | 4.25 | 5.17 | 5.03 | 5.03 | 4.84 | 5.62 | 5.25 | 5.05 |
| Pyrene ^h | 1 | 0.152 | 0.162 | 4.75 | | 4.13 | | 3.99 | | 3.98 | |
| | 2 | 0.042 | -0.038 | -1.09 | | -0.97 | | -0.99 | | -1.81 | |
| | 4 | 0.085 | 0.085 | 2.08 | | 2.16 | | 2.16 | | 2.20 | |
| Biphenyl ⁱ | 2 | 0.074 | 0.097 | 2.75 | | 2.47 | | 2.48 | | 2.56 | |
| | 3 | 0.055 | -0.019 | -0.45 | | -0.49 | | -0.50 | | 0.78 | |
| | 4 | 0.176 | 0.204 | 5.50 | | 5.22 | | 4.97 | | 5.08 | |
| Phenanthrene ^h | 1 | 0.106 | 0.143 | 3.71 | | 3.66 | | 3.61 | | 3.68 | |
| | 2 | 0.067 | -0.034 | -0.43 | | -0.86 | | -0.86 | | -0.49 | |
| | 3 | 0.162 | 0.119 | 2.88 | | 3.03 | | 2.91 | | 3.10 | |
| | 4 | 0.062 | 0.048 | 0.63 | | 1.22 | | 1.23 | | 1.43 | |
| | 9 | 0.154 | 0.188 | 4.43 | | 4.81 | | 4.64 | | 4.74 | |
| Biphenylene ⁱ | 1 | 0.053 | -0.013 | -0.21 | -0.21 | -0.33 | -0.33 | -0.33 | -0.34 | 0.00 | 0.05 |
| | 2 | 0.113 | 0.083 | 2.86 | 3.69 | 2.12 | 2.12 | 2.09 | 2.32 | 2.27 | 2.46 |
| Perylene ⁱ | 1 | 0.089 | 0.102 | 3.08 | 3.10 | 2.60 | 2.60 | 2.59 | 2.82 | 2.76 | 2.89 |
| | 2 | 0.038 | -0.018 | -0.46 | -0.46 | -0.47 | -0.47 | -0.48 | -0.50 | -1.23 | -1.04 |
| | 3 | 0.128 | 0.145 | 3.53 | 4.10 | 3.70 | 3.70 | 3.62 | 4.08 | 3.79 | 3.96 |
| Acenaphthalene ⁱ | 1 | 0.144 | 0.104 | 2.70 | | 2.66 | | 2.58 | | 2.86 | |
| | 3 | -0.003 | 0.166 | 5.40 | | 4.25 | | 4.24 | | 4.29 | |
| | 4 | 0.070 | -0.038 | (0) | | -0.98 | | -0.99 | | -0.62 | |
| | 5 | 0.118 | 0.236 | 5.40 | | 6.02 | | 5.92 | | 5.97 | |
| | 7 | 0.030 | -0.010 | (0) | | -0.25 | | -0.26 | | 0.08 | |
| Fluoranthene ⁱ | 1 | 0.080 | 0.141 | 3.90 | | 3.59 | | 3.60 | | 3.67 | |
| | 2 | 0.067 | -0.024 | (0) | | -0.62 | | -0.62 | | -0.28 | |
| | 3 | 0.118 | 0.219 | 5.20 | | 5.59 | | 5.49 | | 5.54 | |
| | 7 | 0.030 | -0.010 | (0) | | -0.25 | | -0.26 | | 0.08 | |
| | 8 | 0.097 | 0.038 | 1.30 | | 0.96 | | 0.96 | | 1.22 | |
| Azulene ⁱ | 1 | 0.155 | -0.024 | -0.27 | | -0.61 | | -0.59 | | | |
| | 2 | 0.160 | 0.106 | 3.95 | | 2.71 | | 2.61 | | | |
| | 4 | 0.063 | 0.240 | 6.22 | | 6.12 | | 6.18 | | | |
| | 5 | 0.034 | -0.069 | -1.34 | | 1.76 | | -1.80 | | | |
| | 6 | 0.134 | 0.362 | 8.83 | | 9.24 | | 9.00 | | | |

^a Numbering system as given in Figure 1. ^b $\Delta q = q_p^{\pi} - 1$, where q_p^{π} is defined in eq 6. The value of Δq for the cation is $-\Delta q$ (anion) for alternant hydrocarbons. ^c Defined by eq 5. ^d Sources listed in ref 13. ^e Calculated using the simple McConnell relationship (eq 1) with numerical coefficients of Table III, line 4. ^f Calculated using the equation of Colpa and Bolton (eq 7) with numerical coefficients of Table III, line 3. ^g Calculated using the equation of Giacometti, Nordio, and Pavan (eq 8) with numerical coefficients of Table III, line 6. ^h SCFMO's calculated in ref 20. ⁱ SCFMO's calculated using NM method of calculating repulsion integrals with a constant resonance integral (see ref 24, 25).

time, it is impossible to calculate the necessary exchange integrals accurately enough to assess reliably the importance of these extra terms on theoretical grounds. The justification (if any) of the use of multiterm equations must therefore be established empirically by showing that either (7) or (8), or both, as compared to (1), substantially improve the agreement between calculated and experimental hyperfine splitting constants.

Results of Statistical Calculations

We have investigated the relative merits of (1), (7), and (8) by determining by statistical analysis the best regression lines in each case. Experimental hyperfine splitting constants and both our own theoretical spin and charge densities, as given in Table III, and those reported by Snyder and Amos, as calculated using their "improved unrestricted Hartree-Fock method," were used in separate calculations. A total of 49

Table III: Statistical Analysis of Relationships between Experimental Hyperfine Splitting Constants and Theoretical Parameters

| Source of spin-density data | Q_{CH}^H ^a | K ^a | N ^a | C ^a | Mean error ^b | Standard error ^c | Correlation ^d |
|--------------------------------|-------------------------|------------------|------------------|------------------|-------------------------|-----------------------------|--------------------------|
| This work ^e | 24.55 | -11.52 | ... | 0.373 | 0.329 | 0.440 | 0.982 |
| This work ^f | 23.85 | ... | ... | 0.363 | 0.372 | 0.470 | 0.974 |
| This work ^g | 26.57 | -12.57 | ... | ... | 0.388 | 0.515 | 0.989 |
| This work ^h | 25.99 | ... | ... | ... | 0.413 | 0.531 | 0.988 |
| This work ⁱ | 24.44 | ... | 2.129 | 0.336 | 0.380 | 0.496 | 0.971 |
| This work ^j | 26.36 | ... | 1.782 | ... | 0.424 | 0.545 | 0.986 |
| Snyder and Amos ^{g,k} | 23.91 | -10.64 | ... | 0.400 | 0.383 | 0.482 | 0.973 |
| Snyder and Amos ^{f,k} | 23.07 | ... | ... | 0.411 | 0.418 | 0.516 | 0.969 |
| Snyder and Amos ^{g,k} | 26.25 | -11.28 | ... | ... | 0.419 | 0.557 | 0.985 |
| Snyder and Amos ^{h,k} | 25.42 | ... | ... | ... | 0.443 | 0.590 | 0.988 |

^a From the equation $a_p^H = (Q_{CH}^H + K\Delta q_p)\rho_p\pi + N\Sigma c_{op}c_{oq} + C$; the signs of numbers obtained from Snyder and Amos' paper are adjusted to conform to our convention. Theoretically, C should be 0. The summation term includes q values which are nearest neighbors only. ^b Defined as $(1/n)\Sigma(a_{pred} - a_{exp})$, E. Brunner and F. Dörr, *Ber. Bunsenges.*, **68**, 468 (1964). ^c Defined as $\sqrt{(1/n)\Sigma(a_{pred} - a_{exp})^2}$. ^d ρ_{mult} defined according to standard statistical procedure. ^e Best line regardless of values of Q , K , C , for $N = 0$. ^f Best line ignoring the term in $\epsilon\rho$, *i.e.*, best line for $K = N = 0$. ^g Best line through the origin, *i.e.*, best line for $C = N = 0$. ^h Best line for $K = C = N = 0$. ⁱ Best line for $K = 0$. ^j Best line for $K = C = 0$. ^k The spin density values used are the ρ_{sa} calculated in ref 13 by annihilating the major spin states.

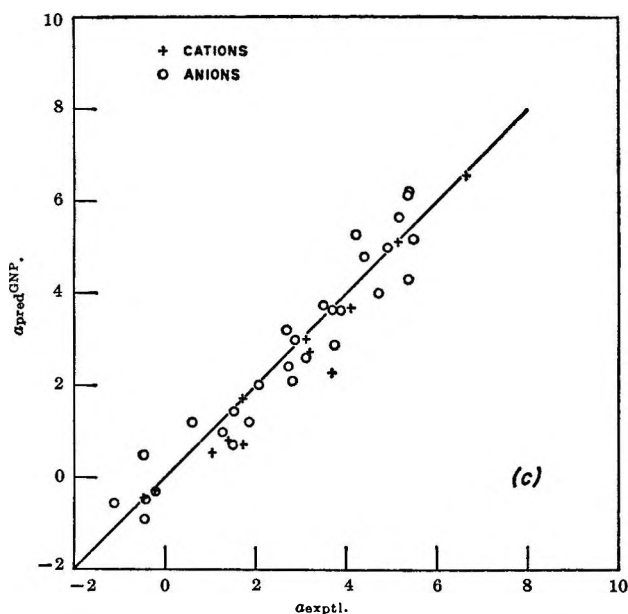


Figure 2C. Comparison between experimental coupling constants ($a_{exptl.}$) and the values (a_{pred}^{GNP}) calculated from the Giacometti-Nordio-Pavan relationship, eq 8.

positions in 16 hydrocarbon radical ions were used. Two different approaches were followed: (a) the best line with an intercept permitted was calculated (*i.e.*, a constant C was permitted as an additional term to (1), (7), and (8)), and (b) the regression line was forced through the origin by requiring $C = 0$, as demanded by current theories of hyperfine splitting constants.

It was noted that when C was allowed to be varied

for best fit, a value of approximately 0.3 to 0.4 was obtained for all three equations. This indicates the presence of some factor; perhaps a solvent effect, or nonnearest-neighbor effects, must be taken into account in addition to the factors entering into the theoretical treatments. Forcing the regression lines through the origin results in slightly higher correlation coefficients, but also increases the standard error by approximately 5–10%. In addition, imposing the restriction of zero intercept does increase the magnitude of the $Q_{CH}^H \sigma-\pi$ parameter to a value close to that which Bolton and Fraenkel²⁸ found necessary to fit their experimental C^{13} splittings. The higher Q_{CH}^H values obtained for $C = 0$ are also closer to the value of 26.20 obtained by Fessenden and Schuler²⁹ for the isopropyl radical, in which the unpaired electron is on a carbon atom with two other carbon atoms and one hydrogen atom as nearest neighbors: a condition close to the environment of the unpaired electrons in the hydrocarbon anions.

The value of Q_{CH}^H calculated using the simple McConnell relation (1) is changed only slightly by either of the additions demanded by (7) and (8); the slight change does bring the statistically best Q_{CH}^H value closer to that required to fit the calculated values of C^{13} splittings to the experimental one for anthracene.²⁸

Comparison of the data for the regression lines

(28) J. R. Bolton and G. K. Fraenkel, *J. Chem. Phys.*, **40**, 3307 (1964).

(29) R. W. Fessenden and R. H. Schuler, *ibid.*, **39**, 2147 (1963).

obtained using the UHF calculations and our RHF data shows that there is no significant difference between the regression coefficients for both sets of theoretical data. Both sets of calculations, moreover, predict experimental a_p^H values equally well, and both sets show that adding either the charge density-dependent term (as in (7)) or the nearest-neighbor term (as in (8)) results in no great statistical improvement in the calculation of hyperfine splitting constants. This lack of improvement is clearly seen by inspection of the graphs in Figure 2.

The finding that the addition of the extra terms to (1) does not substantially improve the calculation of hyperfine splitting constants suggests the possibility that the larger splitting constants observed for hydrocarbon positive ions are due to other causes than internal charge-density effects or nearest-neighbor effects as reflected in (7) and (8). Examination of the literature shows that all the hydrocarbon positive-ion esr measurements were made on cations produced in concentrated sulfuric acid; the esr measurements on anions were measured in polar organic solvents such as acetonitrile or N,N-dimethylformamide. At present we have no knowledge of the effect that changing from a medium of concentrated sulfuric acid to acetonitrile would have on a^H hyperfine splitting constants. It is, however, known that such a change can bring about large changes in other coupling constants. For example, Zweig³⁰ and his collaborators found that, for the sulfur analog of Wurster's blue cation radical, a change of medium from sulfuric acid to acetonitrile brought about a change in the a^{CH_3} coupling constant from 5.33 to 4.56 gauss. This may be an extreme case, but it demonstrates the necessity of eliminating this

possibility by performing measurements for both hydrocarbon cations and anions in the same solvent.

Conclusions

At present, we conclude that there is a very high correlation between experimental hyperfine splitting constants and spin densities both as calculated by the RHF perturbation method described here and the "improved UHF method" of Snyder and Amos. Both treatments, moreover, appear to be subject to similar errors, such as the prediction of too low splitting constants for the 2-positions of the polyacene anion radicals. The introduction of extra terms into the simple McConnell relationship (1) as in (7) and (8) leads to very little improvement in the statistical relationship, and the main justification for including these extra terms is that they predict Q_{CH}^H values which are in slightly better agreement with values found experimentally from C^{13} splitting constants of the isopropyl radical than the values obtained using the simple McConnell relationship. We believe, however, that the results support the possibility that other factors (such as solvent effects), not so far taken into consideration, could influence the magnitude of the hyperfine splitting constants; further experimental and theoretical work is clearly desirable.

Acknowledgments. It is a pleasure to acknowledge financial support for this work from the National Research Council of Canada, The Franklin Institute, and Smith Kline and French Laboratories, Philadelphia, Pa.

(30) A. Zweig, W. G. Hodgson, W. H. Jura, and D. L. Maricle, *Tetrahedron Letters*, 1821 (1963).

The Thermal Decomposition of Methyl Ketene

by P. G. Blake and K. J. Hole

Chemistry Department, University College, Cardiff, Wales (Received October 12, 1965)

The thermal decomposition of methyl ketene has been studied in a static system over the ranges 360–540° and 20–200 mm pressure. In carbon-coated vessels the primary decompositions are to carbon dioxide and pentadiene-2,3 and to carbon monoxide and butene-2, respectively. The decompositions are similar in rate, that to CO having the higher activation energy. Subsequent reactions of the olefins produce many other products, especially at higher temperatures. Both decompositions are of three-halves order and are inhibited by isobutene. A chain mechanism is therefore suggested and the low Arrhenius parameters are obtained, and the independence of the rate on surface/volume ratio indicates that the chains begin and end on the carbon surface.

Introduction

Kinetic work on the lower ketenes has been largely confined to ketene itself; in particular, the photolysis of ketene has been extensively studied, since this is a good source of methylene radicals.^{1,2} The pyrolysis of ketene produces mainly carbon dioxide and allene, but carbon monoxide becomes a major product at higher temperatures.^{3,4} It was proposed that carbon dioxide and allene were formed by a bimolecular process, and that methylene radicals, produced by the subsequent decomposition of allene, attacked ketene ultimately giving carbon monoxide.

Only the photolysis of methyl ketene has so far been investigated. Kistiakowsky and his co-workers^{5,6} have shown the carbon monoxide, ethylene, butene-2, and acetylene are the main products and proposed a mechanism involving the ethylidene radical.

The thermal decomposition of methyl ketene is reported here. It was thought to be of interest to compare this with the photolytic study and also with the pyrolysis of ketene. Biradicals have been postulated in the latter and in the thermal decomposition of diazomethane and diazoethane, and the possibility exists that they might be formed in this case.

Experimental Section

Materials. Methyl ketene was prepared by the pyrolysis of propionic anhydride at 390–420°. The product was purified by redistillation *in vacuo* at –80 to –90° to prevent polymerization, only the middle fraction being retained and stored at –196°. The litera-

ture boiling point⁷ of –56° is incorrect and seems to correspond to the temperature at which rapid exothermic dimerization of the liquid begins. An approximate boiling point of –23° was obtained by extrapolating vapor pressure measurements in the range –105 to –70° to 760 mm on a $\log p-1/T$ plot. The methyl ketene was completely absorbed by anhydrous magnesium perchlorate and was shown by gas chromatography not to contain more than 1% of ketene. The ultraviolet spectrum was closely similar to that obtained by Kistiakowsky and Chong. It seems advisable to prepare methyl ketene at as low a temperature as possible to reduce ketene formation to a minimum, and 400° gives a purer product than 550°.

Nitric oxide was prepared by treating saturated aqueous sodium nitrite solution with 10% sulfuric acid in the presence of mercury, and purified by passing through soda lime, silica gel, and a trap at –78°. The infrared spectrum showed that all NO₂ had been removed.

Isobutene, obtained from the Distillers Co. Ltd., was

- (1) J. Chanmugam and M. Burton, *J. Am. Chem. Soc.*, **78**, 509 (1956).
- (2) H. M. Frey, *Progr. Reaction Kinetics*, **2**, 137 (1964).
- (3) J. R. Young, *J. Chem. Soc.*, 2909 (1958).
- (4) W. B. Guenther and W. D. Walters, *J. Am. Chem. Soc.*, **81**, 1310 (1959).
- (5) G. B. Kistiakowsky and B. H. Mahan, *ibid.*, **79**, 2412 (1957).
- (6) D. P. Chong and G. B. Kistiakowsky, *J. Phys. Chem.*, **68**, 1793 (1964).
- (7) A. D. Jenkins, *J. Chem. Soc.*, 2563 (1952).

purified by distillation. Gas chromatography indicated the presence of traces of other olefins.

Apparatus and Technique. The high-vacuum apparatus was of a conventional static type. The reaction vessel was situated in an electrically heated aluminum-bronze block thermostat, the temperature of which was controlled by a platinum resistance thermometer and Sunvic proportional controller RT2. Vessel temperatures were measured by a standardized chromel-alumel thermocouple and Doran potentiometer. Temperature fluctuations during a run did not exceed $\pm 0.25^\circ$ at 540° .

An unpacked silica vessel and one packed with silica tubes were used, both of ca. 150 cc volume and having surface/volume ratios of 1.5 and 10.1 cm^{-1} , respectively. A mean dead space of 2.1% was corrected to the appropriate temperature and allowance was made for it.

A rapid surface reaction took place on silica and both vessels were coated with relatively thick carbon films by the repeated and prolonged pyrolysis of isobutene in them until the rate of decomposition of methyl ketene fell to a constant and reproducible value, which was the same in both vessels. Air must be excluded between as well as during runs if reproducible results are to be obtained.

Greaseless taps with P.T.F.E. diaphragms were used near the reaction vessel; otherwise, glass high-vacuum taps were employed. Pressures were read to ± 0.1 mm using a glass spiral manometer with mirror attachment.

The usual procedure was to admit methyl ketene to the vessel, make frequent readings of the pressure, and pump out the whole of the gas for analysis after the appropriate reaction time (30 sec to 10 min). Most attention was paid to the early stages of the decomposition and rate constants were calculated from initial rates.

Analysis. Samples were transferred to the analytical section of the apparatus, which consisted of two Ward-Le Roy stills, a mercury diffusion pump, a McLeod gauge, a Toepler pump-gas buret, and a gas chromatograph, and had take-off points for external analysis. Products were identified by a combination of infrared, mass spectrometric, and gas chromatographic techniques.

Hydrogen was occasionally measured by analyzing the permanent gas fraction on an A.E.I. MS3 mass spectrometer. CO, CO₂, CH₄, C₂H₄, C₂H₆, and methyl ketene were measured on the unfrozen sample to reduce the risk of dimerization. Methyl ketene was estimated by the infrared absorption of the $>\text{C}=\text{C}=\text{O}$ group at 2150 cm^{-1} , using a Perkin-Elmer Infracord 137. The absorption is strong and no dimerization occurred in the

infrared cell at the low pressures used; for the same reason, absorption in this region by CO was quite undetectable.

CO, CO₂, CH₄, C₂H₄, and C₂H₆ were measured by gas chromatography using a 1.2-m activated silica gel column at 25° , a katharometer detector, and hydrogen as a carrier gas. C₃ to C₅ hydrocarbons were analyzed on a duplicate run by freezing down in the Ward stills to room temperature and pumping into the gas buret. Methyl ketene and CO₂ were removed by absorption on soda lime and the hydrocarbons separated on a 6.1-m column of dinonyl phthalate on kieselguhr at 25° .

An attempt was made to estimate methyl ketene dimer in the system using the vapor phase infrared absorption of the carbonyl group in the lactone ring at 1750 cm^{-1} , but, owing to the low volatility of the liquid dimer at room temperatures, the results are very approximate.

Results

The decomposition was studied between 360 and 540° and from 20 to 200 mm pressure. Some semiquantitative runs were also made at lower temperatures.

Products. Some representative results are given in Table I. The major products were CO₂, CO, pentadiene-2,3, butene-2, ethylene, butadiene-1,2, and methane; smaller amounts of methyl ketene dimer, propylene, ethylene, isobutene, hydrogen, pentadiene-1,3, and propane were formed. The principal products were produced at substantially the same rate in packed and unpacked vessels, but there were variations of up to 40% in minor products, and, in particular, no pentadiene-1,3 was found in the packed vessel.

At lower temperatures CO₂ predominates, and the initial rate of formation of pentadiene-2,3 is approximately that of CO₂ and is equal to it at 361° (Figure 1). However, polymerization and decomposition of pentadiene-2,3 cause its concentration to pass through a maximum, and it is reduced to a minor product at high temperatures.

The ratio CO/CO₂ increases with temperature, eventually exceeding unity at high temperatures and large percentage reaction (Figure 2), and butene-2 pressure increases with CO, although it again passes through a maximum. Butadiene-1,2 is the only other major product below 400° , but CH₄ and C₂H₄ increase with temperature and become the major hydrocarbon products above 500° . There is no relation between pressure change and methyl ketene reacted, and there is an initial pressure decrease at all but the highest temperatures.

Kinetics. The rates of decomposition of methyl ketene and of formation of CO and CO₂ are the same in

Table I: Principal Products of Methyl Ketene Decomposition (All Pressures Are in Millimeters)

| Time, min | $\Delta\text{CH}_3\text{CHCO}$ | Δp | CO | CO ₂ | C ₂ H ₄ | C ₂ H ₆ | C ₃ H ₆ | C ₃ H ₈ | CH ₄ |
|--|--------------------------------|------------|-----|-----------------|-------------------------------|-------------------------------|-------------------------------|-------------------------------|-----------------|
| 406.2°, $p_{\text{CH}_3\text{CHCO}}$ 100 mm, unpacked vessel | | | | | | | | | |
| 1 | 48.2 | -5.9 | 4.5 | 12.4 | 8.2 | 2.9 | 1.4 | 0.3 | 0 |
| 2 | 60.7 | -14.4 | 5.7 | 17.4 | 5.8 | 2.5 | 1.3 | 0.9 | 0.5 |
| 5 | 79.0 | -24.0 | 7.0 | 21.4 | 5.1 | 4.5 | 2.4 | 1.2 | 0.8 |
| 406.2°, $p_{\text{CH}_3\text{CHCO}}$ 100 mm, packed vessel | | | | | | | | | |
| 1 | 51.6 | -5.3 | 4.3 | 11.7 | 5.9 | 1.0 | 0.6 | 0.2 | 0.2 |
| 2 | 65.6 | -12.1 | 6.0 | 17.4 | 7.8 | 3.3 | 1.8 | 0.2 | 0.2 |
| 5 | 84.7 | -16.3 | 7.7 | 18.6 | 4.9 | 4.0 | 2.1 | 0.3 | 0.3 |
| 457.3°, $p_{\text{CH}_3\text{CHCO}}$ 50 mm, unpacked vessel | | | | | | | | | |
| 2 | 32.6 | -2.5 | 5.0 | 9.1 | 4.1 | 1.4 | 0.6 | 0.9 | 0.8 |
| 487.2°, $p_{\text{CH}_3\text{CHCO}}$ 50 mm, packed vessel | | | | | | | | | |
| 1 | 30.8 | -1.6 | 4.5 | 6.5 | 2.4 | 2.3 | 1.1 | 0.3 | 0.6 |
| 2 | 36.7 | -0.9 | 7.3 | 8.1 | 1.6 | 3.4 | 1.4 | 1.8 | 1.7 |

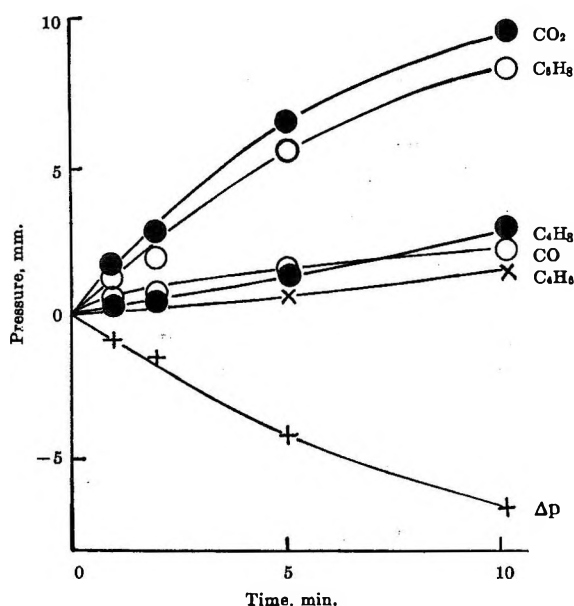


Figure 1. Product-time curves for the decomposition of 50 mm of methyl ketene at 361.0°.

both vessels within about 10%, despite the sevenfold difference in surface/volume ratio. The kinetic order was 1.5 in each case and rate constants obtained from initial rates are given in Table II. Below about 500° an order of 1.5 was also obeyed during the course of each run, since plots of $[\text{CH}_3\text{CHCO}]^{-1/2}$ vs. time were linear. At higher temperatures there was some curvature, but the decomposition of methyl ketene is then so rapid that rate constants will not be very accurate.

The Arrhenius parameters are given by

$$k_{\text{CO}} = 10^{5.9} \exp(-24,200/RT) \text{ l.}^{1/2} \text{ mole}^{-1/2} \text{ sec}^{-1}$$

$$k_{\text{CO}_2} = 10^{3.4} \exp(-14,800/RT) \text{ l.}^{1/2} \text{ mole}^{-1/2} \text{ sec}^{-1}$$

$$k_{\text{CH}_3\text{CHCO}} = 10^{3.9} \exp(-14,900/RT) \text{ l.}^{1/2} \text{ mole}^{-1/2} \text{ sec}^{-1}$$

in the unpacked vessel, being averages of the (similar) values at 20, 50, and 100 mm pressure, and by

$$k_{\text{CO}} = 10^{6.2} \exp(-25,100/RT) \text{ l.}^{1/2} \text{ mole}^{-1/2} \text{ sec}^{-1}$$

$$k_{\text{CO}_2} = 10^{3.7} \exp(-13,700/RT) \text{ l.}^{1/2} \text{ mole}^{-1/2} \text{ sec}^{-1}$$

$$k_{\text{CH}_3\text{CHCO}} = 10^{4.4} \exp(-16,100/RT) \text{ l.}^{1/2} \text{ mole}^{-1/2} \text{ sec}^{-1}$$

in the packed vessel. The values from $k_{\text{CH}_3\text{CHCO}}$ are of little significance since dimerization was occurring and making a larger contribution at lower temperatures.

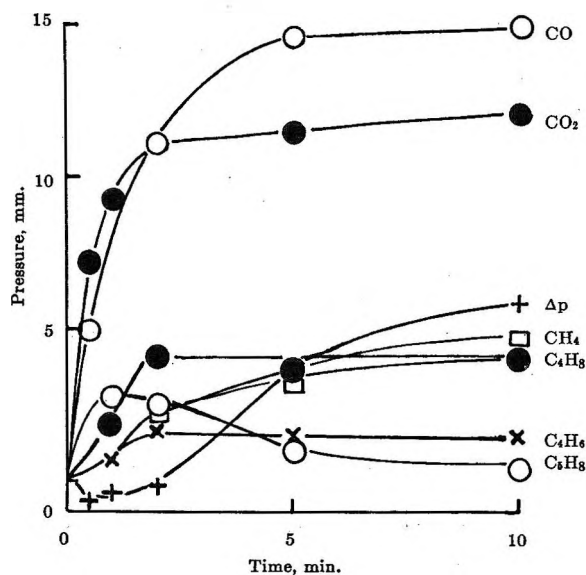
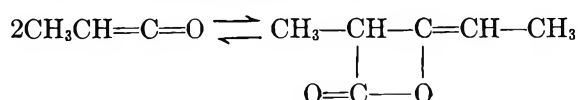


Figure 2. Product-time curves for the decomposition of 50 mm of methyl ketene at 487.2°.

Table II: Some Three-Halves-Order Rate Constants for Methyl Ketene Decomposition and CO and CO₂ Formation [k (l.^{1/2} mole^{-1/2} sec⁻¹) Has Been Multiplied by 10]

| $p_{\text{CH}_3\text{CHCO}}$, mm | T , °C | Vessel | $k_{\text{CH}_3\text{CHCO}}$ | k_{CO_2} | k_{CO} |
|--------------------------------------|-------------|----------|------------------------------|-------------------|-----------------|
| 50 | 361.7 | Unpacked | 0.55 | 0.21 | 0.03 |
| 50 | 406.2 | Packed | 1.26 | 0.46 | 0.12 |
| 100 | 406.2 | Unpacked | 1.18 | 0.40 | 0.12 |
| 50 | 457.3 | Unpacked | 2.39 | 0.83 | 0.32 |
| 50 | 457.3 | Packed | 2.68 | 0.91 | 0.30 |
| 20 | 487.2 | Unpacked | 3.65 | 1.62 | 0.98 |
| 50 | 487.2 | Packed | 3.80 | 1.34 | 0.95 |
| 100 | 487.2 | Unpacked | 3.27 | 1.38 | 0.87 |
| 50 | 502.3 | Packed | 5.24 | 1.76 | 1.24 |
| 50 | 542.3 | Packed | 8.50 | 2.51 | 2.51 |

Methyl Ketene Dimer. The pressure drop at 360 and 406° and the condensation observed on product removal suggested that dimer was present. An attempt was made to study the equilibrium



at various low temperatures, in order to measure K and ΔH for the dimerization, and thus estimate equilibrium pressures of dimer in the reacting system, but it became clear that other equilibria were involved and it was not possible to measure the equilibrium constant.

Appreciable pressures of dimer were found in the range 275–406°, the amounts decreasing with increasing temperature. Product element balances struck at 360 and 406° without allowing for dimer are deficient in C, H, and O by 40 and 25%, respectively. If the dimer is assumed to contain the missing oxygen, then C and H as well as O now balance, and observed pressures agree closely with those calculated from the products and methyl ketene gone. Although it was not possible to measure dimer with any accuracy, estimates made are compatible with the above procedure.

The oxygen deficiency falls with increasing temperature and vanishes at 542°. This, coupled with the fact that ΔH is negative for dimerization (inferred from the liquid phase) implies that dimer pressure decreases to very small values at the top of the temperature range. Carbon and hydrogen deficiencies above 500° were about 40%, reflecting the complex polymerizations of the olefinic products.

Inhibition of the Decomposition. Isobutene and nitric oxide were used and the effect on the rates of formation of CO and CO₂ and of disappearance of methyl ketene is shown in Table III. Rate constants in the presence of isobutene are only quoted to two figures since the

analytical points were more scattered. Both reactions are inhibited, and the average values are 32% for CO and 38% for CO₂.

Table III: Effect of Isobutene on Rates of Decomposition of Methyl Ketene and Formation of CO and CO₂ [k (l.^{1/2} mole^{-1/2} sec⁻¹) Has Been Multiplied by 10]

| T , °C | $p_{\text{CH}_3\text{CHCO}}$, mm | $p_{i\text{-C}_4\text{H}_8}$, mm | $k_{\text{CH}_3\text{CHCO}}$ | k_{CO} | k_{CO_2} |
|-------------|--------------------------------------|--------------------------------------|------------------------------|-----------------|-------------------|
| 406.2 | 50 | 0 | 1.3 | 0.14 | 0.42 |
| 406.2 | 50 | 200 | 1.1 | 0.10 | 0.22 |
| 487.2 | 50 | 0 | 3.5 | 0.92 | 1.5 |
| 487.2 | 50 | 200 | 3.0 | 0.59 | 1.1 |
| 502.3 | 50 | 0 | 5.6 | 1.2 | 1.7 |
| 502.3 | 50 | 200 | 4.8 | 0.7 | 1.2 |

Results with nitric oxide were not reproducible, slight inhibition resulting at first, but later runs being accelerated. Nitric oxide is known to attack carbon surfaces at these temperatures⁸ and this is the probable cause of the effect observed.

Discussion

The results show that both carbon dioxide and carbon monoxide are produced by processes of three-halves order which are inhibited by isobutene, and that approximately stoichiometric amounts of pentadiene-2,3 and butene-2, respectively, are formed at the same time. Reaction rates are independent of surface/volume ratio in carbon-coated vessels but the low Arrhenius constants suggest that the surface is involved.^{9,10} It thus seems probable that the decomposition of methyl ketene is a surface-initiated radical chain reaction, and that heterogeneous termination of chains must predominate, since the rate remains independent of surface/volume ratio. It will be simpler to discuss the mechanisms of CO₂ and CO formation separately, and then to consider the decomposition as a whole.

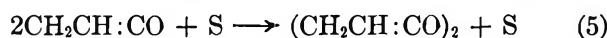
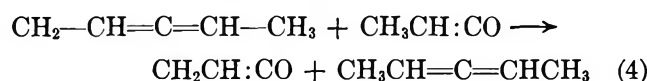
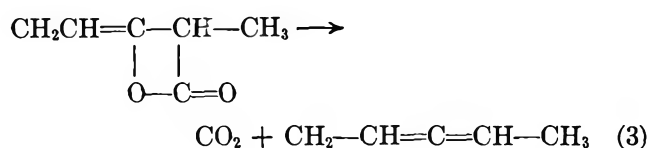
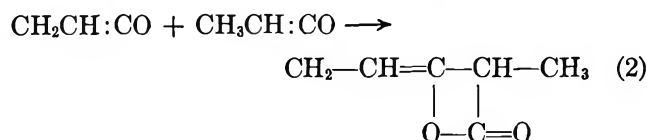
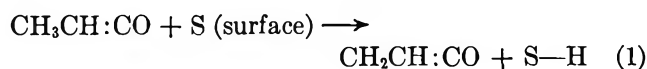
The Formation of Carbon Dioxide. The fact that pentadiene-2,3 is formed in amounts equal to CO₂ suggests an intermediate state resembling the lactone dimer above. The dimer could be formed first and then decompose, or the transition state could resemble the dimer. However, a simple molecular process of the above type would obey second-order kinetics and be unaffected by inhibitors. The ketene decomposition

(8) H. Watts, *Trans. Faraday Soc.*, 54, 93 (1958).

(9) S. Glasstone, K. J. Laidler, and H. Eyring, "The Theory of Rate Processes," McGraw-Hill Book Co., Inc., New York, N. Y., 1941, p 389.

(10) P. G. Ashmore, "Catalysis and Inhibition of Chemical Reactions," Butterworth and Co. Ltd., London, 1963, pp 19, 24.

was said to be second order, but the results of Young fit an order of 1.5 rather better. In methyl ketene, at least, a simple process must be ruled out, but the nature of the products makes it most probable that a cyclic intermediate must play some part in the decomposition. The following mechanism is proposed



If the steady-state approximation is made for the radicals involved, the rate of decomposition is given by

$$\frac{-d[\text{CH}_3\text{CHCO}]}{dt} = k_1 S [\text{CH}_3\text{CHCO}] + 2k_2 \left(\frac{k_1}{k_5} \right)^{1/2} [\text{CH}_3\text{CHCO}]^{3/2}$$

If the chains are long enough for the first term to be neglected

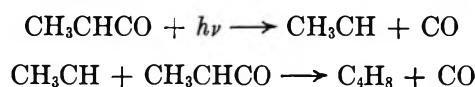
$$\frac{-d[\text{CH}_3\text{CHCO}]}{dt} = 2k_2 \left(\frac{k_1}{k_5} \right)^{1/2} [\text{CH}_3\text{CHCO}]^{3/2}$$

The mechanism predicts the observed products, order, inhibition, and independence of surface. The surface sites in initiation need not necessarily be the same as in termination. In this event the rate equation above must be multiplied by $(S_1/S_5)^{1/2}$, where S_1 and S_5 are the "concentrations" of the respective sites, and the independence of rate on surface/volume is maintained. The over-all activation energy $E = E_2 + 1/2(E_1 - E_5)$, and the A factor equals $2A_2(A_1/A_5)^{1/2}$ or $2A_2(A_1/A_5)^{1/2} (S_1/S_5)^{1/2}$ if initiation and termination sites are not the same. E_5 will be near zero and E_2 , for the radical addition, probably between 3 and 7 kcal/mole, which makes $E_1 \sim 20$ kcal since $E \sim 15$ kcal. The initiating step suggested is essentially one of hydrogen abstraction by a solid free radical and a low value for E_1 is understandable. In any event the large (negative) heats of adsorption mean that activation energies at the

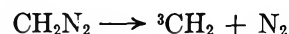
surface are often less than half of the corresponding homogeneous value. The very low value of A ($10^{3.4}$ l.^{1/2} mole^{-1/2} sec⁻¹) reflects the surface initiation (A_1), or the low value of S_1/S_5 , and also the low probability of reaction 2, the addition of a radical to a carbon-carbon double bond with the formation of a four-membered ring.

The Formation of Carbon Monoxide. Both stoichiometry and the measurement of products associate the formation of butene-2 with that of CO, and the results at 406° conform to the 1 to 2 ratio expected.

The formation of butene in the photolysis of methyl ketene by the steps



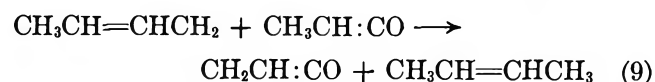
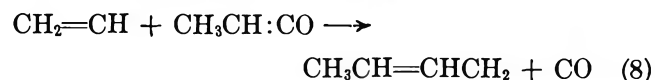
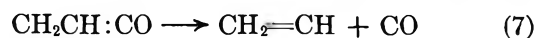
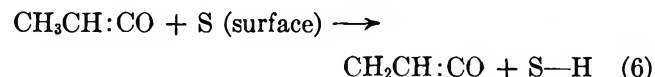
and the evidence for methylene and ethylidene in the pyrolysis of diazomethane and diazoethane^{11,12} suggest that butene may be formed by a similar process in this case. However, the activation energy of the pyrolysis of diazomethane is 35 kcal mole⁻¹, which is equal to the heat of the reaction¹³



and the corresponding heat for methyl ketene is estimated to be $+68 \pm 5$ kcal. This seems to rule out the direct formation of ethylidene, since the activation energy for CO formation is only 24 kcal.

The CO pressure-time curve was sigmoid in ketene pyrolysis and it was suggested that CO resulted from the attack of radicals formed by the decomposition of the product allene on ketene. In methyl ketene the maximum rate of formation of CO is at the beginning of the reaction and the above explanation is not tenable.

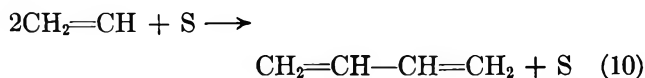
The following chain mechanism is advanced to account for the formation of CO



(11) B. S. Rabinovitch and D. W. Setzer, *J. Am. Chem. Soc.*, **83**, 750 (1961).

(12) R. F. Barrow, T. G. Pearson, and R. H. Purcell, *Trans. Faraday Soc.*, **35**, 880 (1939).

(13) G. von Bunau, P. Potzinger, and G. O. Schenk, *Tetrahedron*, **21**, 1293 (1965).



Steady-state treatment leads to

$$\frac{-d[\text{CH}_3\text{CHCO}]}{dt} = 2k_a \left(\frac{k_8}{k_{10}} \right)^{1/2} [\text{CH}_3\text{CHCO}]^{1/2}$$

if the chains are long, and predicts an over-all activation energy equal to $E_8 + 1/2(E_6 - E_{10})$, and an A factor of $2A_8(A_6/A_{10})^{1/2}$. These values will be considered below.

The Decomposition as a Whole. Chain mechanisms have been proposed to account for the CO_2 and CO formation. The decomposition must, however, be regarded as a whole and the effects of cross interactions must be considered. Only one chain-initiating step has been postulated; the termination processes are of the same type and, although cross-termination between the vinyl and CH_2CHCO radicals must be equally possible, this should not seriously affect the mechanism. Reactions 4 and 9, the abstraction of hydrogen from methyl ketene by the large olefinic radical, are the same in both cases, and the essential differences between the CO_2 and CO forming reactions are in steps 2 and 7, and 3 and 8. In (2), the CH_2CHCO radical adds to methyl ketene, in (7) it decomposes giving CO . In (3), the cyclic radical suffers unimolecular decomposition to CO_2 and in (8) the vinyl radical displaces CO from methyl ketene.

The observation that the activation energy for CO is 9.4 kcal higher and the A factor $10^{2.4}$ higher than for CO_2

must be explained. An exact comparison of the individual expressions for the activation energy cannot now be made since, for example, the addition of CH_2CHCO radicals to methyl ketene, which eventually leads to CO_2 , competes with their unimolecular decomposition to CO . However, it seems likely on general grounds that the addition will have the lowest activation energy and A factor of reactions 2, 3, 7, and 8, and that this is responsible for the difference in the Arrhenius equations for CO_2 and CO .

Since the kinetics of the steps postulated above are largely unknown and must be inferred from known cases, the suggested mechanisms are tentative in character, but appear to provide the most satisfactory explanation of the experimental results. One general difficulty is that it is not easy to see why homogeneous termination of the chains does not occur, since the radicals seem to be too large to need third body stabilization. The nondependence of rate on surface/volume ratio and the need for surface initiation suggest that this process cannot be important at the relatively low pressures studied.

Minor Products. The minor products are compatible with the above mechanism, but the complexity of the reactions undergone by olefins around 500° makes a detailed consideration of them unprofitable.

Acknowledgment. K. J. H. wishes to thank the Department of Scientific and Industrial Research for a maintenance grant.

The N-Isopropylcarbazole-Picryl Chloride System

by Paul Cherin and Michael Burack

Fundamental Research Laboratory, Xerox Corporation, Webster, New York (Received October 18, 1965)

N-Isopropylcarbazole (NIPC) combines with picryl chloride (PC) to form a 1:1 charge-transfer complex. Although NIPC crystallizes in an orthorhombic form, space group $Ic2a$, and the complex NIPC-PC crystallizes in a monoclinic form, space group $P2_1/c$, the crystal structures are believed to be very similar. The probable stacking arrangement of molecules in each case is described.

N-Isopropylcarbazole (NIPC) and picryl chloride (PC) combine to form a charge-transfer complex having a molecular ratio of 1:1. In combining, the NIPC becomes the electron donor, and the PC, the electron acceptor. The NIPC-PC combination occurs in both the solid state and in solution; this has been confirmed by Sharp¹ using absorption techniques and by Hoegl² who utilized differential thermal analysis. This article is devoted to the solid state aspects of the NIPC-PC system only.

Single crystals of the parent compounds (NIPC and PC), as well as the complex, have been prepared and studied by X-ray diffraction methods. The NIPC and PC molecules are of similar size; a molecule of PC could easily replace NIPC without disrupting the NIPC structure to any great extent, which facilitates their molecular combination in the solid state. Our studies of the charge-transfer complex (NIPC-PC) revealed a remarkable similarity between its lattice parameters and that of the parent compound NIPC.

Experimental Procedure

Single crystals of both NIPC and NIPC-PC were grown from solution. Although different solvents were tried in preparing the solution, dichloromethane proved to be the most effective. The solution was allowed to evaporate and yielded needle-like crystals of NIPC and NIPC-PC in the respective experiments. Subsequent examination with a polarizing microscope suggested a crystallographic axis parallel to the needle direction. For this reason, the crystals were mounted on fibers which were parallel to the needle direction. X-Ray photographs of the mounted crystals were taken with Weissenberg and precession cameras. The resulting photographs were used subsequently to deter-

mine the space group and the approximate lattice parameters of the crystals.

Polycrystalline samples were studied with a diffractometer, and the resulting data permitted a precise determination of the unit-cell dimensions. The density of NIPC and NIPC-PC was determined by suspending the respective crystals in a mixture of solvents. The densities were then measured with a pycnometer.

Discussion and Findings

The systematic absences for pure NIPC were observed to be of the type, $h + k + l = 2n + 1$ for reflections in general, with $l(k) = 2n + 1$ for $0kl$, and $h(l) = 2n + 1$ for $hk0$ reflections, respectively. This suggests that the NIPC space group is either $Ic2a$ or $Icma$. A piezoelectric measurement was made and found to be positive, and that fact led to the conclusion that the noncentrosymmetric space group $Ic2a$ was correct.

The systematic absences for NIPC-PC (1:1 ratio) were found to be of the type $k = 2n + 1$ for $0k0$ reflections and $l = 2n + 1$ for $h0l$ reflections. This indicated that the space group of the NIPC-PC unit cell was $P2_1/c$.

Conventional nomenclature was used in designating the axes of the monoclinic cell containing NIPC-PC; the axes of the orthorhombic cell were designated to illustrate the similarity to those of the monoclinic cell. Table I lists the refined unit-cell dimensions. Picryl chloride (PC) unit-cell dimensions were taken from the work reported by Golder, Zdanov, and Umanskij.³

(1) J. H. Sharp, *J. Phys. Chem.*, **70**, 584 (1966).

(2) H. Hoegl, Battelle Memorial Institute, Geneva, private communication.

(3) G. A. Golder, G. S. Zdanov, and M. M. Umanskij, *Dokl. Akad. Nauk SSSR*, **92**, 311 (1953).

Table I: Unit-Cell Dimensions

| Material | Space group | a, Å | b, Å | c, Å | β , deg | Z | ρ_{obsd} , g/cm ³ | ρ_x , g/cm ³ |
|----------|--------------------|--------------|---------------|--------------|---------------|---|--|------------------------------|
| NIPC | Ic2a | 18.01 ± 0.02 | 7.963 ± 0.006 | 16.82 ± 0.01 | 90 | 8 | 1.14 | 1.15 |
| PC | P2 ₁ /c | 11.10 | 6.83 | 12.62 | 102.5 | 4 | ... | ... |
| NIPC-PC | P2 ₁ /c | 18.12 ± 0.07 | 6.962 ± 0.013 | 16.70 ± 0.08 | 100.1 ± 0.1 | 8 | 1.47 | 1.46 |

An independent set of PC unit-cell dimensions was derived as a check against the referent data and, although a slight difference between the referent data and our data exists, it was concluded that the differences were not significant enough for separate discussion. The d spacings for NIPC are tabulated in Table II, and those for NIPC-PC are listed in Table III.

Table II: d Spacings and X-Ray Data for N-Isopropylcarbazole (NIPC)

| hkl | d_{obsd} | d_{calcd} | I/I_1 |
|----------------|-------------------|--------------------|---------|
| 101 | 12.32 | 12.30 | 5 |
| 200 | 9.02 | 9.01 | 15 |
| 002 | 8.44 | 8.42 | 100 |
| 202 | 6.15 | 6.15 | 6 |
| 211 | 5.62 | 5.62 | 55 |
| 112 | 5.53 | 5.51 | 10 |
| 103 | 5.36 | 5.36 | 2 |
| 400 | 4.51 | 4.51 | 3 |
| 004 | 4.21 | 4.21 | 18 |
| 312 | 4.16 | 4.17 | 50 |
| 303 | 4.10 | 4.10 | 5 |
| 402 | 3.97 | 3.97 | 13 |
| 204 | 3.81 | 3.81 | 7 |
| 114 } 220 } | 3.64 | 3.64 } 3.64 } | 4 |
| 501 | 3.52 | 3.52 | 2 |
| 222 | 3.34 | 3.34 | 1 |
| 321 | 3.26 | 3.26 | 6 |
| 123 } 413 } | 3.21 | 3.20 } 3.21 } | 3 |

The unit-cell dimensions of the charge-transfer complex are very similar to the parent compound, NIPC; the major difference between them being in the lengths of their b axes. This condition suggests that only minor structural differences exist between the two.

The major cleavage planes of the NIPC cell are parallel to the ab planes. This suggests the possibility that the essentially planar NIPC molecule is parallel to the ab planes. The intensity distribution of the $00l$ reflections observed on Weissenberg photographs

Table III: d Spacings and X-Ray Data for Charge-Transfer Complex NIPC-PC

| hkl | d_{obsd} | d_{calcd} | I/I_0 | hkl | d_{obsd} | d_{calcd} | I/I_1 |
|--------------|-------------------|--------------------|---------|----------------|-------------------|--------------------|---------|
| 100 | 17.88 | 17.80 | 58 | 31 $\bar{2}$ | 4.19 | 4.20 | 15 |
| 200 | 8.96 | 8.91 | 39 | 10 $\bar{4}$ | 4.16 | 4.16 | 6 |
| 002 | 8.24 | 8.20 | 100 | 20 $\bar{4}$ | 4.02 | 4.01 | 3 |
| 10 $\bar{2}$ | 8.06 | 8.02 | 42 | 10 $\bar{4}$ | 3.85 | 3.86 | 2 |
| 102 | 7.03 | 7.01 | 31 | 41 $\bar{1}$ | 3.78 | 3.78 | 6 |
| 20 $\bar{2}$ | 6.68 | 6.65 | 8 | | | | |
| 110 | 6.50 | 6.47 | 2 | 410 } 312 } | 3.75 | 3.75 } | 3 |
| 11 $\bar{1}$ | 6.17 | 6.16 | 6 | 402 | 3.66 | 3.66 | 1 |
| 300 | 5.94 | 5.94 | 5 | 500 | 3.56 | 3.57 | 1 |
| 202 | 5.57 | 5.57 | 4 | 50 $\bar{2}$ | 3.50 | 3.50 | 2 |
| 210 | 5.48 | 5.48 | 12 | 204 } | | | |
| 21 $\bar{1}$ | 5.40 | 5.38 | 4 | 021 | 3.40 | 3.40 | 23 |
| 012 | 5.30 | 5.32 | 8 | 12 $\bar{1}$ | 3.36 | 3.36 | 6 |
| 211 | 5.04 | 5.04 | 3 | 121 | 3.32 | 3.32 | 4 |
| 21 $\bar{2}$ | 4.81 | 4.81 | 3 | | | | |
| 310 | 4.52 | 4.52 | 3 | 314 } 313 } | 3.27 | 3.26 } | 2 |
| | | | | 400 } | 4.46 | 4.46 } | 13 |
| 302 } | 4.46 | 4.46 } | 13 | 11 $\bar{3}$ | 4.32 | 4.32 | 2 |
| 400 } | 4.46 | 4.46 } | 13 | 22 $\bar{1}$ | 3.22 | 3.22 | 10 |
| 11 $\bar{3}$ | 4.32 | 4.32 | 2 | | | | |

seem to confirm this implication. The intensity of the $00l$ reflections decrease rather uniformly as a function of $(\sin \theta)/\lambda$. It is interesting to note that this observation is an exception to the findings of Boeyens and Herbstein⁴ in which they indicated that, in general, the short dimension (usually about 6.7 to 7.4 Å) was the stacking direction for π -molecular compounds. Our findings are suggestive of molecular stacking in the moderately long c direction for both NIPC and NIPC-PC.

Further indirect evidence that the stacking direction is not parallel to the short axis was yielded by thermal diffuse scattering. Boeyens and Herbstein reported that oscillation photographs taken about the short direction, the needle axis of π -molecular crystals, showed strong thermal diffuse scattering from planes located on the second-layer line with spacings of about 3.2 to 3.5 Å. In contrast, NIPC and NIPC-PC show

(4) J. C. A. Boeyens and F. H. Herbstein, *J. Phys. Chem.*, **69**, 2153 (1965).

strong thermal diffuse scattering in planes distributed throughout reciprocal space in a more complex manner.

Analysis based on the data accumulated and presented in this note leads us to suspect that the planar molecules of NIPC are almost parallel to the ab planes; but, because the van der Waals width of the molecule across the benzene rings is 9.3 Å, and because the length of the b dimension is only 8 Å, it is necessary that the NIPC molecules be slightly tilted out of the ab plane. Taking the van der Waals radius of the hydrogen atom to be 1.2 Å, the tilt was calculated to be approximately 15° .

The structure of the NIPC-PC complex is believed to be very similar to the parent NIPC structure. This belief is supported by the similarity in the lattice parameters, and by the relative intensities of the $h00$, $0k0$, and $00l$ reflections observed on the Weissenberg photographs. It is further believed that the PC molecules replace alternate NIPC molecules in the

structure to maintain the π -bond interaction that exists in solution. In addition because the short axis is only 7 Å in the 1:1 complex, the molecules must be tilted out of the ab plane to a greater extent than in the parent NIPC crystal, assuming our basic model is correct.

Summary

The crystal structure of the charge-transfer complex, NIPC-PC, appears to be similar to its parent compound, NIPC, and the molecules lie in stacks as in the case of other similar compounds. It would seem, however, that the short dimension is not in the stacking direction.

Acknowledgments. The authors wish to thank J. Weigl and J. Sharp, Xerox Corporation, for their encouragement and many valuable discussions, and H. Hoegl, Battelle Memorial Institute, for his help in obtaining samples.

Ion-Solvent Size Ratio as a Factor in the Thermodynamics of Electrolytes

by B. E. Conway and R. E. Verrall

Department of Chemistry, University of Ottawa, Ottawa, Canada (Received October 19, 1965)

The possibly significant role of nonelectrostatic effects in the thermodynamics of electrolytes composed of large ions is pointed out. Such effects can arise from a nonideal configurational entropy of mixing if either the cation or the anion (or both) has a size appreciably greater than that of the solvent molecules. These effects, which can persist to moderately high dilutions, are suggested as one of the contributing factors leading to positive deviations from the Debye-Hückel limiting law at low concentrations as exhibited, for example, by some tetraalkylammonium salts. Other factors in the nonideality of these solutions are also considered, and may be of comparable importance.

Introduction

Recent and earlier work on the thermodynamics of solutions of tetraalkylammonium salts¹⁻⁶ has revealed unexpected deviations from the Debye-Hückel theory for activity and osmotic coefficients in the "limiting law" concentration range.

An inherent difficulty arises in the deduction of the experimental results for activity and osmotic coefficients. The emf method involves difficulties,⁴ so that reliance must be put on the isopiestic method which loses precision below *ca.* 0.1 *m*. The extrapolation which is then normally necessary for calculation of the activity coefficient relative to the infinite dilution reference state then requires the assumption of the applicability of the Debye-Hückel limiting law or a related form of this equation. However, for the very salts involved here, the limiting law cannot be assumed to be applicable until concentrations very much lower than 0.1 *m* are reached.

Although some of the deviations referred to above are negative ones,¹⁻³ which cannot be explained in terms of the classical framework of the electrostatic theory of long-range coulombic interactions, it seems that unusually large *positive* deviations from the Debye-Hückel limiting law are exhibited⁴⁻⁶ by some of the salts. The negative deviations can, however, be accounted for by the "structure-enforced" ion-pairing concept (incipient micelle formation) developed by Diamond⁸ and Frank⁷ and associated with the structure-promoting effects which these ions have on water. Also, ion pairing is indicated in some cases⁶ from the conductance and activity coefficient behavior

but not in other cases.⁸ Frank⁷ has suggested that: (a) the nearest-neighbor interaction theory^{9,10} of electrolytes which applies to simple electrolytes with small ions at moderate concentrations, giving a $c^{1/3}$ rather than a $c^{1/2}$ law for \log [activity coefficient], may also be applicable to lower concentrations¹¹ when the ions are large and hence may give rise to apparent deviations from the Debye-Hückel theory in the conventional limiting-law concentration region; and (b) mutual salting-in (*cf.* the effect discussed by Diamond³)

(1) J. Lange, *Z. Physik. Chem.*, **A168**, 147 (1934); B. Ebert and J. Lange, *ibid.*, **A139**, 584 (1928).

(2) V. E. Bower and R. A. Robinson, *Trans. Faraday Soc.*, **59**, 1717 (1963).

(3) R. M. Diamond, *J. Phys. Chem.*, **67**, 2513 (1963).

(4) M. A. V. Devanathan and M. J. Fernando, *Trans. Faraday Soc.*, **58**, 784 (1962). [However, this work has been criticized by Stokes (see R. H. Stokes, *ibid.*, **59**, 761 (1963)) and is inconsistent with the data of ref 2.]

(5) S. Lindenbaum and G. E. Boyd, *J. Phys. Chem.*, **66**, 911 (1964).

(6) B. J. Levien, *Australian J. Chem.*, **18**, 1161 (1965).

(7) H. S. Frank, "Chemical Physics of Ionic Solutions," B. E. Conway and R. G. Barradas, Ed., The Electrochemical Society, John Wiley and Sons, Inc., New York, N. Y., 1966, in press; see also H. S. Frank, *J. Phys. Chem.*, **67**, 1554 (1963).

(8) H. M. Daggett, E. J. Blair, and C. A. Kraus, *J. Am. Chem. Soc.*, **73**, 799 (1951).

(9) H. S. Frank and P. T. Thompson, *J. Chem. Phys.*, **67**, 1554 (1963); see also H. S. Frank and P. T. Thompson, "Structure of Electrolytic Solutions," W. Hamer, Ed., The Electrochemical Society, John Wiley and Sons, Inc., New York, N. Y., 1959, p 113.

(10) J. E. Desnoyers and B. E. Conway, *J. Phys. Chem.*, **68**, 2305 (1964).

(11) Limitingly the $c^{1/3}$ relation will go over to the normal $c^{1/2}$ law at sufficiently low concentrations (see ref 9).

of the tetraalkylammonium ions will lead to similar deviations.

All three of these suggestions are, we believe, cogent for the types of electrolytes we are considering here. However, in the present paper we wish to point out another factor, the *relative size* of the solute and solvent species, which will be of quite general significance and has seemingly been neglected in previous theories of electrolyte solutions. Presumably this is because the well-known electrostatic theories of long-range ion-ion interactions and those of short-range ion-solvation effects^{10,12,13} have hitherto always provided a satisfactory basis for discussion of the thermodynamics of inorganic electrolytes, the small ions of which are usually of a size comparable to that of the solvent molecules in the case of aqueous solutions. However, with tetraalkylammonium salts, the cations will be approximately some 5 [in the case of $(\text{CH}_3)_4\text{N}^+$] to 21 [in the case of $(\text{C}_6\text{H}_{11})_4\text{N}^+$] times larger than the solvent water molecules. The relative ion size factor, we shall show, can lead to appreciable positive deviations from the limiting law at quite high dilutions for the larger R_4N^+ ions.

The Relative Size Factor in the Entropy of Mixing

Until 1937,¹⁴ it was commonly believed that all athermal solutions would always be regular; *i.e.*, the relative size of "solute" and "solvent" would not influence the ideality of the entropy of mixing.

Fowler and Rushbrooke¹⁴ pointed out that this would not be the case and provided a theory of the deviations from ideality which would result for solutions of a "dimer" in its corresponding "monomeric" solvent. Calculations for this case have also been given more recently.¹⁵ More detailed treatments for other cases were given by Guggenheim.¹⁶ Hitherto such effects have not been considered for electrolyte solutions (but see ref 19 below) for the reasons stated above. In the case of large ions, they will, however, be quite significant as we show below.

For an ion composed of r groups (which we shall call the r -mer) each occupying a solvent lattice position, the relative partial molar free energy $\Delta\mu_r$ can be written in the usual way as

$$\Delta\mu_r = \mu_r - \mu_r^\circ = RT \ln [a_r/a_r^\circ] \quad (1)$$

where a_r° is the activity or fugacity of pure r -mer, a_r is that for the r -mer in the mixture of r with a solvent 1, and μ_r° is the chemical potential of r -mer in the standard state. $\Delta\mu_r$ is given from the statistical-mechanical lattice theory^{16,17} as

$$\Delta\mu_r = RT \ln \frac{N_r}{N_r + N_1/r} \left(\frac{N_r + N_1/r}{N_r + N_1/q} \right)^{zq/2} \quad (2)$$

for a mixture of N_r moles of r -mer in N_1 moles of solvent. The parameters z , q , and r are related by

$$q = r - \frac{2r}{z} + \frac{2}{z} \quad (3)$$

from which it will be noted (see below) that q is always less than r (because r is a positive integer > 1), except when it is equal to r which arises when $r = 1$ (ordinary regular solution case for solute and solvent having the same size) or when $z = \infty$ ^{18,19} (Flory's approximation²⁰); in eq 3, z is the coordination number for the lattice and q is a parameter defining the number zq of pairs of neighboring sites of which one is a member of the r -fold group constituting the r -mer and the other is not; in the athermal solution all configurations are, of course, assumed to have the same energy.

When $z = \infty$,¹⁸ volume fraction lattice statistics will apply, and the relation corresponding to eq 2, which must be derived by differentiating the appropriate expression¹⁶ for the free energy of mixing, is

$$\Delta\mu_r/RT = \ln \frac{N_r}{N_r + N_1/r} - (r - 1) \frac{N_1/r}{N_r + N_1/r} \quad (4)$$

The ideal solution law corresponding to eq 2 is

$$\Delta\mu_{r,i}/RT = \ln \frac{N_r}{N_r + N_1} \quad (5)$$

so that comparison of the terms in eq 2 or 4 and those in (5) gives the rational activity coefficient for the r -

(12) J. A. V. Butler, *J. Phys. Chem.*, **33**, 1015 (1929).

(13) R. H. Stokes and R. A. Robinson, *J. Am. Chem. Soc.*, **70**, 1870 (1948).

(14) R. H. Fowler and G. S. Rushbrooke, *Trans. Faraday Soc.*, **33**, 1272 (1937).

(15) D. H. Trevena, *Proc. Phys. Soc. (London)*, **84**, 969 (1964); see also D. H. Everett and M. Penney, *Proc. Roy. Soc. (London)*, **A212**, 164 (1952), for related experimental work.

(16) E. A. Guggenheim, "Mixtures," Oxford University Press, Oxford, 1951. It is to be noted that a somewhat different expression from that of Guggenheim was given by Fowler and Rushbrooke,¹⁴ but the qualitative predictions of these treatments are similar. Lattice theories are necessarily somewhat artificial in so far as the solute molecules are regarded as being constrained to fit among sites on the solvent "lattice." Nevertheless, this type of approach has been highly successful particularly for polymer solutions. Its application to large electrolyte ions is therefore justified, at least in the semiquantitative terms developed here.

(17) F. T. Wall, "Chemical Thermodynamics," W. H. Freeman, San Francisco, Calif., 1965, pp 376-383; see also M. O'Keefe, *J. Phys. Chem.*, **70**, 596 (1966).

(18) When $z = \infty$, the term in parentheses is unity since $q = r$, so that volume fraction statistics then apply as investigated by Glueckauf¹⁹ for hydrated small ions.

(19) E. Glueckauf, *Trans. Faraday Soc.*, **51**, 1235 (1955).

(20) P. J. Flory, *J. Chem. Phys.*, **10**, 51 (1942).

mer, and we shall denote this quantity by f_{ne} to stress its nonelectrostatic origin. In these terms, it will be seen from eq 2 or 4 that negative deviations from Raoult's law for the r -mer will always result. We require, however, the activity coefficient (to be denoted by γ) which is relative to the infinite dilution reference state in order to relate it to the Debye-Hückel activity coefficient; hence, we require that the thermodynamic behavior be related to the Henry's limiting law case¹⁷ rather than to the Raoult's law behavior of the solute. Hence, if the limiting value of f_{ne} (to be denoted by f_{ne}^0) as $N_r \rightarrow 0$ in finite N_1 can be obtained, γ can be evaluated as f_{ne}/f_{ne}^0 . An explicit result for γ_{ne} in these terms cannot easily be obtained from eq 2 and 5. We can proceed, however, by evaluating a quantity a/a_0 [cf. eq 1] from eq 2 where a/a_0 is a ratio of hypothetical vapor pressure of r -mer in the solution to that in the pure state. The ratio a/a_0 can be calculated from eq 5 (Raoult's law case) and 2 and then plotted against molar concentration c . For the non-ideal solution (eq 2), $(a/a_0)/c$ can also be plotted against c and extrapolated to $c = 0$ to give a limiting slope k_H of the plot of a/a_0 vs. c . The actual values of a/a_0 calculated from eq 2 at finite c can then be compared with the values that would arise if $a/a_0 = k_H c$ applied at all *finite* concentrations (Henry's law case). The ratio of these two values of a/a_0 at any concentration then gives γ_{ne} at that concentration. It follows by geometrical calculations (cf. ref 17; particularly Figure 18-1) that this ratio of a/a_0 values is equal to the ratio f_{ne}/f_{ne}^0 , which is the activity coefficient contribution γ_{ne} required for relation to the electrostatic Debye-Hückel mean activity coefficient γ_e and the experimental mean activity coefficient γ where $\gamma = \gamma_e \gamma_{ne}$.

In the limiting case of $z = \infty$,¹⁸ an approximate analytical result can be obtained²¹ for γ_{ne} . From eq 4 and 5

$$RT \ln f_{ne} = \Delta\mu_r - \Delta\mu_{r,i} \quad (6)$$

so that

$$\ln f_{ne} = \ln \frac{N_r}{N_r + N_1/r} - \ln \frac{N_r}{N_r + N_1} - \frac{(r-1)N_1/r}{N_r + N_1/r} \quad (7)$$

Then for $\ln f_{ne}^0$ as $N_r \rightarrow 0$

$$\ln f_{ne}^0 \doteq \ln r - (r-1) \quad (8)$$

Hence

$$\ln [f_{ne}/f_{ne}^0] = \ln \gamma_{ne} =$$

$$\ln \frac{(N_r + N_1)}{rN_r + N_1} + (r-1) \frac{N_r}{N_r + N_1/r} \quad (9)$$

As a limiting case, by expanding the \ln term in a series and taking only the first term (noting that $(N_r + N_1)/(rN_r + N_1) < 1$)

$$\ln \gamma_{ne} \doteq (r-1)^2 \frac{N_r}{rN_r + N_1} \quad (10)$$

results as a rough but simple approximation.

We now make a more complete numerical exploration of the properties of eq 2 and 4 in relation to eq 5 in order to determine if the effects discussed above are likely to be significant enough to explain the experimental positive deviations from the limiting electrostatic law observed in some cases. We consider three values of $r = 5, 10,$ and 20 with $z = 12$ and 6 (cf. ref 16); $z = 6$ is probably a reasonable compromise value for water, bearing in mind the local tetrahedral coordination ($z = 4$) and any effect the ion itself will have on the local water structure. With these values, q values are obtained as shown in Table I.

Table I

| r | Values of q | | |
|-----|---------------|----------|--------------|
| | $z = 6$ | $z = 12$ | $z = \infty$ |
| 5 | 3.67 | 4.33 | 5 |
| 10 | 7.0 | 8.5 | 10 |
| 20 | 13.67 | 16.83 | 20 |

The values of γ_{ne} have been plotted as a function of c for various values of z and r in Figure 1 taking $N_1 = 55.5$ moles of water. Substantial deviations ($\gamma_{ne} > 1$) from the Debye-Hückel result arise at moderate concentrations ($0.1 m$), and for larger values of r they persist to quite low concentrations ($0.01 m$).

It may also be noted that the partial molar volumes \bar{V}_2 of tetraalkylammonium salts which have recently been measured^{22,23} exhibit quite anomalously large negative linear dependencies on molar concentration c (slope term h) after the usual limiting-law $c^{1/2}$ term²⁴ has been eliminated. From the magnitudes of these h coefficients of c ,²³ e.g.

(21) We are indebted to a referee for the suggestion of calculating a limiting analytical result for this case.

(22) W. Y. Wen and S. Saito, *J. Phys. Chem.*, **68**, 2639 (1964).

(23) B. E. Conway, R. E. Verrall, and J. E. Desnoyers, *Trans. Faraday Soc.*, in press.

(24) O. Redlich and D. M. Meyer, *Chem. Rev.*, **64**, 221 (1964).

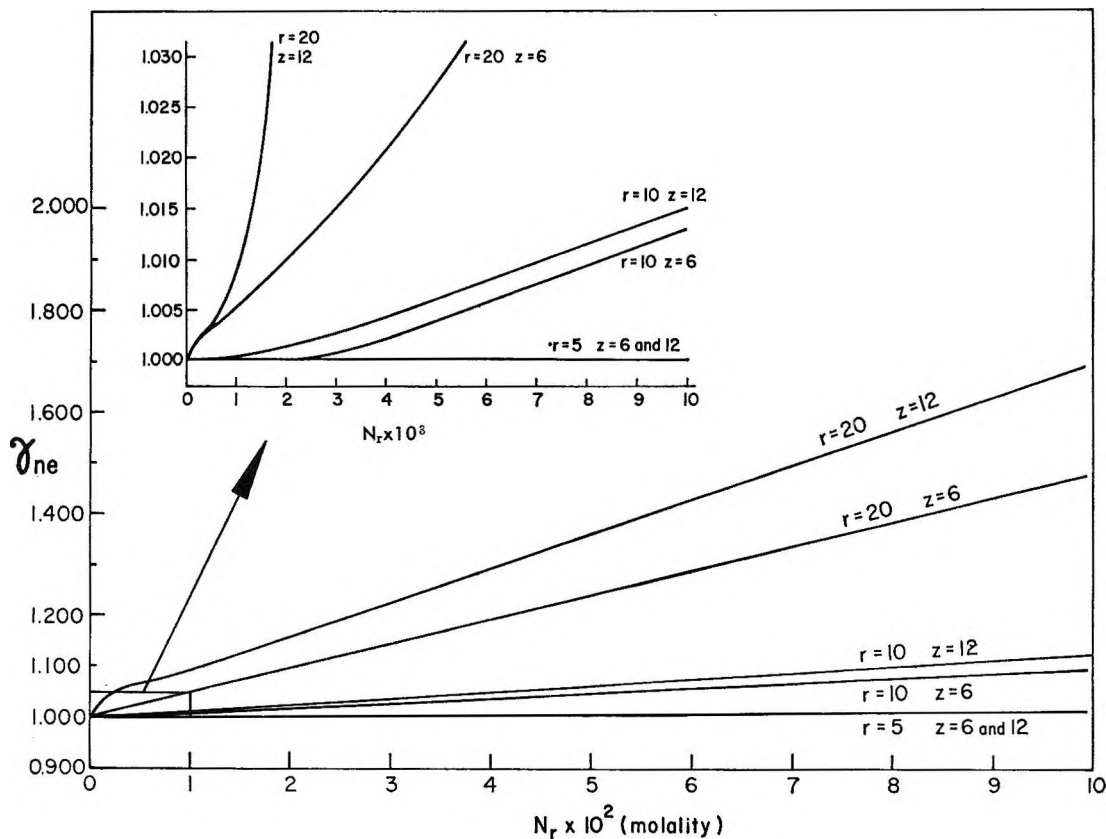


Figure 1. Values of γ_{ne} as a function of concentration calculated from the lattice theory for various values of r and z .

$$\bar{V}_2 = 107.32 + 2.792c^{1/2} - 4.6c \quad (\text{Me}_4\text{NCl})$$

$$\bar{V}_2 = 166.90 + 2.792c^{1/2} - 21.0c \quad (\text{Et}_4\text{NCl})$$

$$\bar{V}_2 = 182.87 + 2.792c^{1/2} - 28.1c \quad (n\text{-Pr}_4\text{NCl})$$

$$\bar{V}_2 = 294.14 + 2.792c^{1/2} - 50.3c \quad (n\text{-Bu}_4\text{NCl})$$

it is clear that these linear contributions will persist quite significantly into the limiting-law concentration region (0.0001–0.002 M) and in fact give substantial deviations from the limiting-law slope for \bar{V} in this concentration range. Since the ion size factor can give rise to an appreciable concentration-dependent term in the nonideal partial molal free energy of the solute r -mer ion, the derivative of this contribution with respect to pressure may give a corresponding contribution to the difference $\bar{V} - \bar{V}^0$ for various finite concentrations. For the tetraalkylammonium salts, h is experimentally found to become more negative with increasing r , *i.e.*, in the series Me to Bu; γ_{ne} for a given z becomes larger with increasing r or for a given r increases with increasing z . Very qualitatively, the observed effects could hence arise, in part, if r or z effectively became smaller with increasing pressure.

However, with regard to the partial molar volumes,

Wen and Saito²⁵ have shown that the apparently anomalous behavior of the hydrophobic tetraalkylammonium salts is partly eliminated when they are made more hydrophilic by terminal substitution of OH groups (tetraethanolammonium salts). In the thermodynamic behavior of the tetraalkylammonium salts, some specificity is also exhibited with regard to the nature of the coanion,²³ so that cation size effects need not be the only, or the main, reason for the anomalies in the activity coefficients. It seems that such specific effects must probably arise from *self*-salting-out effects between the anions and the cations; two kinds of effects can arise: one is connected with the local change of water activity brought about by hydration effects at the anion (conventional salting-out effect^{12,26}), and the other (also dependent on ion size) is due to the fact that the large cation is less polarizable than an equal volume of solvent and hence tends to be displaced away from a nearby coanion (cavity salting-out effect¹⁰). This is effectively a repulsive energy term

(25) W. Y. Wen and S. Saito, *J. Phys. Chem.*, **69**, 3539 (1965).

(26) B. E. Conway, J. E. Desnoyers, and A. C. Smith, *Phil. Trans. Roy. Soc. London Ser. A*, **256**, 389 (1964).

which must be added to the normal interionic attractive term but which diminishes the latter. This second effect will be proportional to the volume of the cation, and the first effect will be larger the more hydrated the anion. The sharing of structure-enhanced regions of the solution which can account for cation-anion (and cation-cation) association³ will be equivalent to a salting-in effect.²⁷ The first two effects will give rise to *positive* deviations from the Debye-Hückel prediction of γ , in the same direction, that is, as the direct ion-solvent size ratio effect.

The contribution of the latter effect, through γ_{ne} , seems of the right order of magnitude to explain *part* of the observed deviations from Debye-Hückel behavior at low concentrations. However, it is worth noting that relative size effects in binary mixtures of nonelectrolytes^{28,29} give rise to smaller deviations from ideality than would be predicted in terms of the statistical lattice theories, particularly when the molecules are spherical, and indeed for completely spherical molecules in a continuum the lattice theory would not be meaningful. However, in ref 28, a rather different experimental situation is involved from that considered here. In the present case, although Me_4N^+ is almost spherical, the higher members, *e.g.*, $n\text{-Bu}_4\text{N}^+$, certainly are not, and they must present to the solution a group of four chains in a variety of conformations but in an over-all tetrahedral configuration. Also, our treatment might be criticized on the basis that cal-

culations have been made using equations for particle⁸ in a linear arrangement rather than for four *n*-alkyl groups linked tetrahedrally. This limitation may not, however, be so serious as it may seem since Guggenheim¹⁶ has calculated the activities of solvent in solutions of linear tetramers and tetrahedral (but pyramidal) tetramers and finds surprisingly little difference between the calculated thermodynamic behavior of such species. Thus, for molecules having a given value of r , the effect of shape on the theoretical results for $\Delta\mu_1$ (or $\Delta\mu_r$) and the entropy of mixing is relatively small in comparison with the difference between the values of these functions for the r -mer and the values of the respective quantities for the corresponding ideal solution.

Acknowledgment. Grateful acknowledgment is made to the National Research Council, Canada, for support of this work and related experimental studies on partial molal volumes.²³ R. E. V. acknowledges the award of Province of Ontario Graduate Fellowships. We are indebted to Professor E. A. Guggenheim for discussion, in correspondence, on lattice statistics problems and to Dr. J. E. Desnoyers for his comments on this paper.

(27) J. E. Desnoyers, C. Jolicœur, and G. E. Pelletier, *Can. J. Chem.*, **43**, 3232 (1965).

(28) K. Shinoda and J. H. Hildebrand, *J. Phys. Chem.*, **61**, 789 (1957).

(29) J. H. Hildebrand and R. L. Scott, "Regular Solutions," Prentice-Hall, Inc., New York, N. Y., 1962.

The Reaction of Pyrophoric Lead with Oxygen

by J. Charles, P. W. Kopf, and S. Toby¹

School of Chemistry, Rutgers, The State University, New Brunswick, New Jersey 08903
(Received October 20, 1965)

Pyrophoric lead was prepared by the thermal decomposition of lead citrate *in vacuo*. The properties of the pyrophoric lead, as measured by stoichiometry of oxygen uptake, rate constant, and esr signal, were independent of preparation temperature above 400°. Pyrophoricity was found in samples with preparation temperatures much above the melting point of lead, showing that the material cannot consist simply of finely divided lead. Analysis showed approximately 20 wt % of carbon was present, but it was found that the carbon does not take part in the oxidation. First-order disappearance of oxygen was found over an initial pressure range of 0.02 to 1 torr and a range of temperatures from -115 to 75°. The rate constant obeyed the Arrhenius law, $k = (3.1 \pm 1) \exp[(2900 \pm 200)/RT] \text{ sec}^{-1}$. The large negative entropy of activation is comparable to the over-all entropy of reaction.

Introduction

Lead metal in a form which combusts spontaneously when exposed to air has been known since the last century. In the last 50 years three references²⁻⁴ to the preparation and properties of pyrophoric lead have appeared. No serious attempts have been made to find the conditions which give the most active material, nor are there any quantitative data published on the chemical composition or reactivity of pyrophoric lead.

The uptake of oxygen by pyrophoric lead is extremely rapid at room temperature, presumably because the metal is extremely finely divided. The kinetics of the reaction, at least in its initial stages, give an insight into a metal oxidation process which is free of the usual complexities due to diffusion of oxygen through films of oxide. Since pyrophoric lead contains carbon, however, it is important to establish that the oxidation process involves the lead only and in this paper evidence is presented to show that the carbon plays no part.

Experimental Section

Lead citrate, formate, and tartrate were decomposed by heating approximately 50-g samples at temperatures ranging from 300 to 600° in a vacuum system with continuous pumping. There was a large initial increase in pressure and the reaction was considered

complete when after several hours the pressure in the system had fallen to less than 10^{-3} torr.

Rates of oxygen uptake were measured by exposing pyrophoric lead to pure oxygen (Matheson Research Grade) and measuring pressure on a thermocouple gauge (A. F. Smith Co., Rochester, N. Y., Model 1013) which had been calibrated against a McLeod gauge.

Rates of oxygen uptake were measured in a system of 580-cm³ volume using approximately 0.25-g pyrophoric lead samples and a range of initial oxygen pressures from 0.02 to 2 torr. In the initial experiments the pyrophoric lead samples were placed at the bottom of vertical tubes fitted with break-seals and arranged so that the oxygen would pass through about 25 cm of thermostated tubing before coming in contact with the lead. Occasional erratic results were obtained which were thought to be due to local heating accompanying the exothermic (52.5 kcal mole⁻¹) reaction. This was minimized by placing the pyrophoric lead in a thin layer in the horizontal portion of an L-shaped tube.

(1) To whom correspondence should be addressed.

(2) G. R. Levi and A. Celeri, *Atti Accad. Naz. Lincei, Mem., Classe Sci. Fis. Mat. Nat.*, [6] 7, 350 (1928); *Chem. Abstr.*, 22, 2299 (1928).

(3) G. R. Levi and G. Rossi, *Gazz. Chim. Ital.*, 68, 576 (1938); *Chem. Abstr.*, 33, 1566 (1939).

(4) N. I. Glistenko, *Tr. Voronezhsk. Gos. Univ.*, 42, 31 (1956); *Chem. Abstr.*, 53, 8903 (1959).

Reproducibility improved, and the fact that rate constants for oxygen uptake were found to be approximately independent of initial oxygen pressure was taken as evidence that thermostating was satisfactory. This point is returned to in the Results.

Carbon and lead determinations were carried out as follows. Air was slowly admitted to a weighed sample of pyrophoric lead. After reweighing, the sample was shaken with 1:1 nitric acid. The mixture was filtered and the washed residue, shown by simple chemical tests to be pure carbon, was weighed. The filtrate was analyzed for lead gravimetrically as sulfate.

Electron spin resonance (esr) spectra were measured at 350 Mc/s.

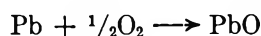
Results

Lead formate, when decomposed at 325°, gave massive lead and carbon. Lead tartrate decomposed over the range 300–425° gave a feebly pyrophoric material. Lead citrate gave an active pyrophoric material when decomposed in the range 300–600°, and all subsequent experiments were performed with pyrophoric lead prepared from citrate. The product was a black powder.

Analysis of several samples of pyrophoric lead gave the percentage by weight of lead as 83.5 ± 1 , the remainder being carbon. The percentage gain in weight on exposure to oxygen was 5.6 ± 0.4 .

In Figure 1 some properties of pyrophoric lead are plotted against temperature of preparation.

The efficiency of pyrophoric lead as an oxygen getter was calculated by assuming that all oxygen removed was due to



The actual weight of oxygen taken up divided by the stoichiometrically expected amount gave the getter efficiency, and this was plotted in Figure 1A.

The rates of oxygen uptake were found to follow first-order kinetics. The rate constants for room temperature uptake are plotted as a function of preparation temperature in Figure 1B.

The esr spectra of pyrophoric lead samples sealed in Pyrex tubes *in vacuo* were measured relative to a DPPH standard. The results are plotted as a function of preparation temperature in Figure 1C. In addition, oxygen was admitted to some samples; after oxidation had occurred, the excess oxygen was pumped off, and the esr spectra were reexamined. No significant difference was found.

The validity of the first-order rate law was tested over a variety of initial pressures and amounts of oxygen removed. Figure 2A shows a first-order plot for

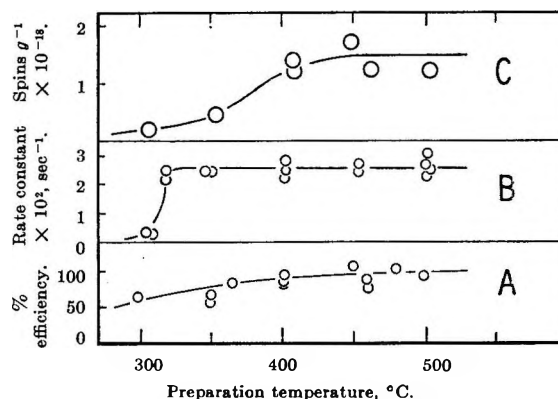


Figure 1. Reactivity of pyrophoric lead as a function of preparation temperature: A, per cent efficiency as a getter; B, first-order rate constant for uptake of oxygen; and C, electron spin resonance signal, spins per gram.

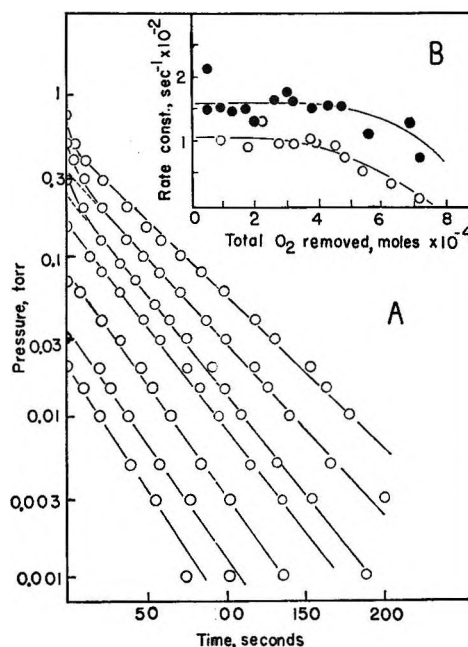


Figure 2. Test of first-order rate law of reaction between pyrophoric lead and oxygen at room temperature: A, varying initial pressures; and B, varying amounts of oxygen removed.

a 40-fold range of initial pressures. At the higher pressures a slight deviation from linearity occurred initially, but this disappeared after about 20 sec. The deviation may have been caused by a slight rise in temperature as the lead oxidized. As a precaution, initial oxygen pressures were kept below 0.25 torr when rate constants were measured at different temperatures.

The constancy of the rate constant with oxygen uptake is shown in Figure 2B and shows little change

Table I: Distribution of Rate Constants from Different Samples of Pyrophoric Lead

| Range of k at 25° $\times 10^3, \text{sec}^{-1}$ | 0-0.5 | 0.6-1.0 | 1.1-1.5 | 1.6-2.0 | 2.1-2.5 | 2.6-3.0 | 3.1-3.5 | 3.6-4.0 | 4.1-4.5 |
|--|-------|---------|---------|---------|---------|---------|---------|---------|---------|
| No. of samples | 0 | 2 | 5 | 5 | 8 | 5 | 1 | 1 | 1 |

up to about 4×10^{-4} mole of oxygen removed. This corresponded to approximately 30% of the lead reacted.

The reproducibility of rate constants measured from 28 different samples of pyrophoric lead is indicated in Table I. The values of k cluster around 0.015–0.025 and samples giving rate constants in this range at 25° were used in studies at other temperatures.

The data shown in Figure 2B were obtained from two different samples and show that, for a given sample, good reproducibility was obtained.

Using pyrophoric lead samples prepared at 450° , rates of oxygen uptake were measured in the range -196 to 75° , using a bath of the appropriate temperature around the sample. The oxygen uptake was fastest at -196° , being so rapid that it was difficult to measure. We suspected that most of the rapid pressure decrease was due to adsorption. A sample of pyrophoric lead which had been exposed to air for several days was therefore exposed to oxygen at -196° , and the result is shown in Figure 3. This clearly represents adsorption, and the results at -196° were therefore discounted. Pressure–time curves at -140° similarly showed that most of the oxygen uptake was due to adsorption. However, at -115° and above, oxidation predominated over adsorption and could be corrected for. A pressure–time plot taken at -78° is shown in Figure 3. An adsorption plot is also shown and is of small importance, amounting to a correction of less than 5%.

The adsorption that occurred was presumably due to the presence of carbon. As an additional check on possible interaction between the carbon and lead, a BET surface determination of pyrophoric lead before and after oxidation was made. The values obtained were 66 and $68 \text{ m}^2 \text{ g}^{-1}$, respectively, equal within the experimental error.

The fact that the -196° adsorption curve in Figure 3 is steeper than the reaction curves and does not follow first-order kinetics suggests that the reaction rate constants measured from -115 to 75° have real significance.

The rate constants obtained in the range -115 to 75° are shown as an Arrhenius plot in Figure 4. The parameters obtained are $E = 2.9 \pm 0.2 \text{ kcal mole}^{-1}$ and $A = 3.1 \pm 1 \text{ sec}^{-1}$.

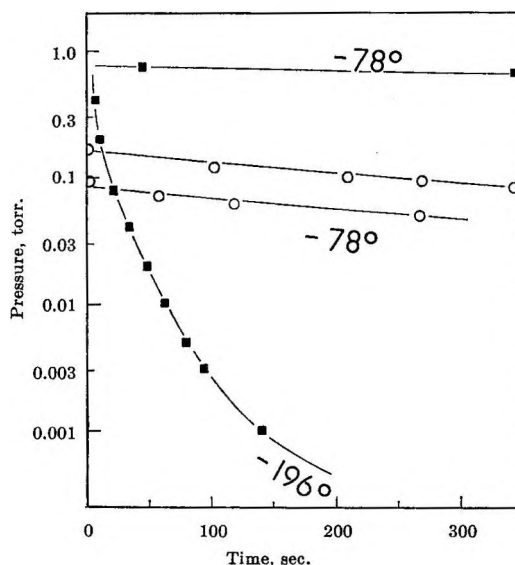


Figure 3. Reactivity of pyrophoric lead prepared at 400° : O, first-order plots of oxygen uptake at -78° ; and ■, first-order plots of oxygen adsorption at -78° and -196° by oxidized pyrophoric lead.

Discussion

Pyrophoric lead prepared by decomposition of lead citrate *in vacuo* at temperatures above 350° is spectacularly reactive, giving sparks and flames when poured into air.

The getter efficiency approaches 100% as indicated in Figure 1A, showing that PbO was the only product of oxidation. This agrees with the observation of Levi and Celeri² that X-ray analysis of pyrophoric lead exposed to air showed only Pb and PbO.

The esr intensities shown in Figure 1C are of interest. We obtained typical carbon resonance lines with a g value close to 2.00. ESR signals from carbon are well known,⁵ but we believe this is the first time that the esr signal from a pyrophoric metal has been noted. Ingram^{5a} gives typical values of 5×10^{19} spins/g for an active charcoal prepared *in vacuo*, and this may be compared with our values of 1×10^{18} spins/g for pyrophoric lead containing 20 wt % carbon. Levi and

(5) (a) D. J. E. Ingram, "Free Radicals as Studied by Electron Spin Resonance," Butterworth & Co. (Publishers) Ltd., London, 1958, pp 207–215; (b) K. Antonowicz, *J. Chem. Phys.*, **36**, 2046 (1962).

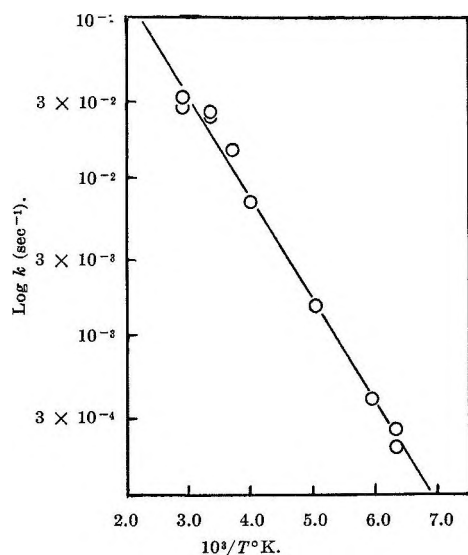


Figure 4. Arrhenius plot of rate constant for reaction between pyrophoric lead and oxygen.

Rossi³ in an X-ray study found that pyrophoric lead had too large a particle size to show a pattern significantly different from that of massive lead. This contrasts with pyrophoric nickel, which is extremely finely divided.

The importance of the carbon is emphasized by the fact that pyrophoric lead can be prepared at temperatures well above the melting point of lead without coalescing of the metal. Although pyrophoric lead contains about 20% carbon by weight, the percentage by volume may be as high as 90%. Thus, the lead appears to be strongly adsorbed on a carbon matrix, which prevents the lead particles from coalescing. However, the fact that the carbon plays no part in the oxidation process is indicated by the following: (a) the stoichiometry of oxygen uptake indicates that only PbO is formed; (b) the esr signal is typical for carbon and shows no change after the lead is oxidized; and (c) the BET specific surface is high (of the order of one-tenth that of charcoal) and shows no change after oxidation.

Relationship between Metallic Surface and Oxidation Law. The oxidation of a metal follows a rate law which depends on the state of the oxide formed and on the temperature.⁶ At low temperatures most metals follow a logarithmic law of oxygen uptake with time. As the temperature increases, the state of the oxide and the rate of diffusion through the oxide may change. The oxidation law may then become cubic, parabolic, or linear. The "linear" law refers to a linear growth of oxide at constant oxygen pressure. This corresponds to the first-order law in oxygen found in the present

work, for, if a given fraction of the collisions of the oxygen molecules with the lead result in reaction, then it follows that at an oxygen pressure of p the rate $\propto p \propto dp/dt$ so that a first-order law results.

Even if the temperature is held constant, the oxidation law obeyed may depend on the state of subdivision of the metal. Copper at 150° obeys a cubic law,⁶ but a study made on the low-pressure oxidation of copper foil which had been abraded in air and then reduced, gave a linear law⁷ in the range 140–300°. A recent study⁸ of the reaction of oxygen with evaporated films of lead gave a linear law at 230° and a complex logarithmic law in the range –78 to 100°. The present work gives a linear law for finely divided lead in the latter range. It is possible that finely divided materials in general obey linear oxidation laws, for it is interesting to note that a recent investigation of the reaction between lead sulfide and oxygen gave a complex law for sulfide samples of low specific surface and a linear law for samples of high specific surface.⁹ In the case of the oxidation of metals, it is meaningless to make a comparison of rate constants for metals which obey different oxidation laws. It is suggested that a study of the oxidation of metals in finely divided states will yield parameters which are directly comparable and which are functions of the metals rather than of the state of the oxide formed.

Kinetic Parameters. The rate data obtained in the present study are for the early stages of the reaction, before lead depletion becomes important. This corresponds to a system containing an unlimited supply of available metal.

The activation energy of 2.9 kcal mole⁻¹ found is considerably less than reported values for lead. In the range 250–320° Weber and Baldwin's¹⁰ parabolic rate constants give $E = 43$ kcal mole⁻¹. Anderson and Tare⁸ reported $E = 11$ kcal mole⁻¹ from the linear law obtained at two temperatures, 230 and 275°. Our low value suggests that the restriction on reaction between pyrophoric lead and oxygen appears to lie in the entropy rather than the enthalpy of activation. If we assume the transition state theory formulation with a transmission coefficient of unity, then the observed A factor corresponds to $\Delta S^* = -55$ cal deg⁻¹ mole⁻¹ at 300°K. This large negative value is not un-

(6) O. Kubaschewski and B. E. Hopkins, "Oxidation of Metals and Alloys," Academic Press Inc., New York, N. Y., 1962.

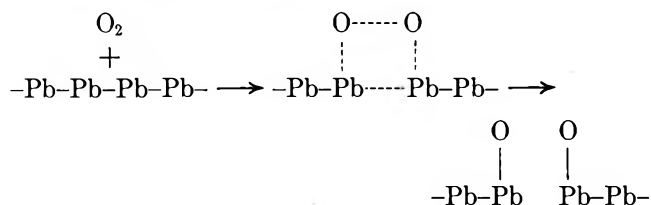
(7) F. J. Wilkins and E. K. Rideal, *Proc. Roy. Soc. (London)*, **A128**, 394 (1930).

(8) J. R. Anderson and V. B. Tare, *J. Phys. Chem.*, **68**, 1482 (1964).

(9) L. J. Hillenbrand, *J. Chem. Phys.*, **41**, 3971 (1964).

(10) E. Weber and W. M. Baldwin, *J. Metals*, **4**, 854 (1952).

reasonable since the transition state presumably resembles the products far more than the reactants.



The entropy change for the removal of a mole of oxygen is $\Delta S_0 = -48 \text{ cal deg}^{-1} \text{ mole}^{-1}$, which is reasonably close to the value of ΔS^* found.

Finally, it may be mentioned that the rapid removal of oxygen (half-life ~ 30 sec) by pyrophoric lead sug-

gests its use for removal of oxygen from, for example, streams of other gases. Although pyrophoric lead does not react with oxygen as quickly as "flashed" barium metal,¹¹ it does react much faster than does sodium and is simpler to handle.

Acknowledgments. We wish to thank Mr. E. Bretz and Dr. M. J. D. Low, both of this department, for help with the esr measurements and BET surface determinations. We are most grateful to the National Science Foundation for their support of this work through Grants GE-4048 and GE-7997.

(11) See, for example, L. F. Ehrke and C. M. Slack, *J. Appl. Phys.*, **11**, 129 (1940).

Infrared Study of the Reaction of Hydrogen Chloride with the Surface

of γ -Alumina and Its Effect on Surface "Acid" Sites¹

by J. B. Peri

Research and Development Department, American Oil Company, Whiting, Indiana (Received October 25, 1965)

Chemisorption of HCl on dry γ -alumina and the effects thereof on surface sites of possible catalytic importance were studied by infrared and gravimetric techniques. Chemisorption affected preexisting hydroxyl (or deuterioxy) groups selectively and formed new hydroxyl groups and water. Desorption of HCl and water on heating normally left new hydroxyl groups plus chloride. All hydroxyl groups could, however, be removed by suitable treatment. The activity of HCl-treated alumina for isomerization of adsorbed 1-butene increased with decreasing hydroxyl content, and the 1-butene isomerized more rapidly than it exchanged hydrogen with residual deuterioxy groups. " α sites" on alumina were affected by chloride so that carbon dioxide adsorbed thereon exhibited higher frequencies (2377 and 2392 cm^{-1} vs. original 2370 cm^{-1}). Changes in these sites probably explain changes in activity.

Introduction

γ -Alumina and other transition aluminas are commonly treated with halides to enhance their "acidity" and catalytic activity. The strong acid sites which exist on "dry" γ -alumina appear to be aluminum ions

(Lewis acids) partially exposed at a few special sites in the surface.² A recent model explains how such

(1) Presented at 150th National Meeting of the American Chemical Society, Atlantic City, N. J., Sept 1965.

sites could be produced during dehydration of the surface.³ The enhanced acidity of halide-treated alumina has been variously attributed to protons from adsorbed hydrogen halide,^{4,5} to acidic hydroxyl groups held by the same aluminum ion that holds a chloride ion,⁶ or to exposed aluminum ions whose acid strength has been inductively enhanced through replacement of an adjacent oxide ion by a halide ion.⁷

Little direct evidence supports any of these hypotheses. Greater retention of ammonia by fluoride-treated alumina than by pure alumina has been claimed to show enhanced acidity of preexisting (Lewis) acid sites,⁷ but replacement of halide by NH₂⁻ could complicate such measurements.⁸ Changes in the majority of surface acid sites could also differ from changes in the few "acid-base" sites of greatest catalytic importance.⁸

Infrared study has shown that molecular CO₂ can be strongly held by a few sites ("α sites") on dry γ -alumina and silica-alumina.⁹ These α sites appear to be important catalytically, although they represent only a small fraction of the surface.¹⁰ They normally contain a reactive oxide ion (or ions) in close proximity to an exposed cation. Changes in their number or nature should be reflected by changes in the spectrum of adsorbed CO₂.

Further investigation of the effect of chloride treatment on the surface of γ -alumina seemed advisable. Infrared and related study was made of the effects of treating transparent plates of highly dried γ -alumina aerogel with dry HCl gas and of the adsorptive and catalytic behavior of the resulting chlorided alumina. Exchange of the surface hydroxyl groups with deuterium provided further information.

Experimental Section

Most of the cells, equipment, and procedures have been described previously.¹⁰⁻¹² Perkin-Elmer Model 12C and 112 spectrometers were supplemented with a Beckman IR-9 spectrometer. A simple quartz cell, provided with a suitable inlet and outlet for the HCl, was used in the flow experiments. A small cell with CaF₂ windows was used in conjunction with the Beckman IR-9 in the CO₂ adsorption experiments. The aerogel plate, mounted in a Vycor holder, was moved from a furnace section to the window section by tilting the cell. CO₂ bands were removed from the spectrometer background by flushing with CO₂-free air.

Preparation and properties of the γ -alumina aerogel have been described.¹² The HCl (Matheson, anhydrous) was dried and purified by passage over naphthalene, glass wool at -78.5°, and P₂O₅, and was

degassed by repeated freezing and evacuation before use, except in flow experiments. Deuterium, 1-butene, and CO₂ were as previously described.^{2,10}

The aerogel plate used in the gravimetric study in cell C² was calcined in oxygen at 600° for 1 hr and subsequently evacuated at 800° for 1 hr. The total number of surface hydroxyl groups was then determined by equilibrium exchange at 600° with D₂ gas to be 5.6×10^{19} , and the total surface area, determined by N₂ adsorption at -195.6°, was 72 m². The dry sample weighed 0.246 g. Thus, specific surface area was 293 m²/g. About 6% (if 100% = 1.25×10^{15} OH/cm²) of the surface remained covered with hydroxyl and deuterioxyl groups. The alumina was then again exchanged with fresh D₂ at 600°, to convert essentially all remaining hydroxyl groups to deuterioxyl. After the spectrum had been scanned, dry HCl was admitted to the cell in small amounts while the alumina was held at 42°. Changes in the weight and spectra were followed concurrently. Equilibration time was at least 30 min and usually longer. Periodically the cell was evacuated or the gaseous HCl was frozen in a trap cooled with either liquid N₂ or Dry Ice and acetone to determine the extent of chemisorption and to check for the possible presence of H₂O or permanent gases.

To permit measurement of band intensities in the OD stretching and H₂O bending regions, where the bands of interest were superimposed on a very broad "tail" from hydrogen-bonded hydroxyl (or deuterium-bonded deuterioxyl) absorption, base lines were estimated by inspection.

Results

HCl Adsorption at 50° or Below. Adsorption of HCl on "dry" alumina at 50° or below was characterized mainly by the appearance of a very broad, intense band attributed to hydrogen-bonded hydroxyl groups. This band was centered around 3500 cm⁻¹ but extended to

(2) J. B. Peri, *Actes Congr. Intern. Catalyse, 2^e, Paris, 1960*, 1, 1333 (1961).

(3) J. B. Peri, *J. Phys. Chem.*, **69**, 220 (1965).

(4) R. Hay and C. Montgomery, *Ind. Eng. Chem.*, **37**, 335 (1945).

(5) A. Oblad, I. Messenger, and N. Brown, *ibid.*, **39**, 1462 (1947).

(6) K. G. Miasserov, O. E. Morozova, and Al. A. Petrov, *J. Gen. Chem. USSR*, **25**, 2165 (1955).

(7) A. N. Webb, *Ind. Eng. Chem.*, **49**, 261 (1957).

(8) J. B. Peri, *J. Phys. Chem.*, **69**, 231 (1965).

(9) J. B. Peri, presented at 145th National Meeting of the American Chemical Society, New York, N. Y., Sept 1963.

(10) J. B. Peri, *Proc. 3rd Intern. Congr. Catalysis, Amsterdam, 1964*, 1, 1100 (1965).

(11) J. B. Peri and R. B. Hannan, *J. Phys. Chem.*, **64**, 1526 (1960).

(12) J. B. Peri, *ibid.*, **69**, 211 (1965).

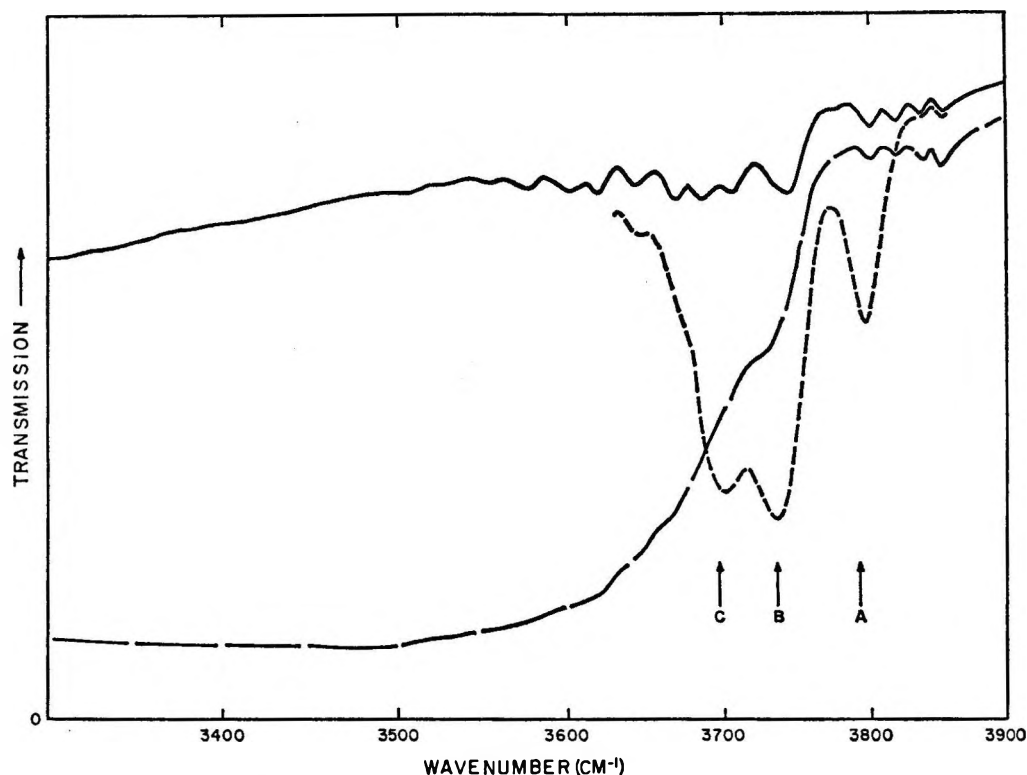


Figure 1. Initial adsorption of HCl (OH stretching bands): - - - -, before D_2 exchange; —, deuterated surface; and — · —, +26% HCl monolayer.

below 2000 cm^{-1} . No band assignable to HCl was detected, although one could have been had HCl existed in major amounts on the surface. Bands arising from Cl-O or Al-Cl linkages would not be expected in the region of the spectrum accessible in this study.

The growth of the broad hydroxyl band at 3500 cm^{-1} was paralleled by reduction of the intensities of isolated hydroxyl bands originally present. Slight shifts in the frequencies of the isolated hydroxyl bands were also noted. Desorption of chemisorbed HCl by heating and evacuation invariably eliminated some or all of the hydroxyl bands selectively, in a manner resembling that observed previously during attempted desorption of CCl_4 .¹¹

To study this process in greater detail, HCl was adsorbed on and desorbed from deuterated alumina, where changes in existing groups could be more easily distinguished from formation of new hydroxyl groups. Enough dry HCl to yield a surface coverage of 26% (if 100% = 6.25×10^{14} molecules/cm²) was admitted to cell C and chemisorbed fairly rapidly on the aerogel at 42° —adsorption was 95% complete after 5 min and 99.8% complete after 40 min.

The resulting spectra are shown in Figures 1 and 2. No further changes were observed after 16 hr of con-

tact. Adsorption of HCl was apparently quantitative. The isolated deuteroyl bands remained, although markedly decreased in intensity (after allowing for an underlying band), but the central band appeared slightly lower in frequency. No corresponding isolated hydroxyl bands were produced.

The reduction in intensity was calculated for the individual deuteroyl bands shown in Figure 2. The high-frequency band (A) was apparently reduced to 49% of original intensity, the central band (B) to 67%, and the low-frequency band (C) to 55%. The "tail" at frequencies below the isolated deuteroyl bands appears to be caused by deuterium-bonded O-D stretching, although overlap from the broad hydrogen-bonded hydroxyl stretching band at 3500 cm^{-1} still contributes.

Further additions of HCl caused further reduction in the intensities of the isolated deuteroyl bands, further shift of the central band to slightly lower frequency, and progressive increase (roughly proportional to the extent of chemisorption) in the intensity of the broad hydroxyl stretching band. As shown in Figure 3, the high-frequency (A) and low-frequency (C) deuteroyl bands had disappeared completely when 55% of the surface was covered with chemisorbed HCl. The central band (B) remained, although reduced to

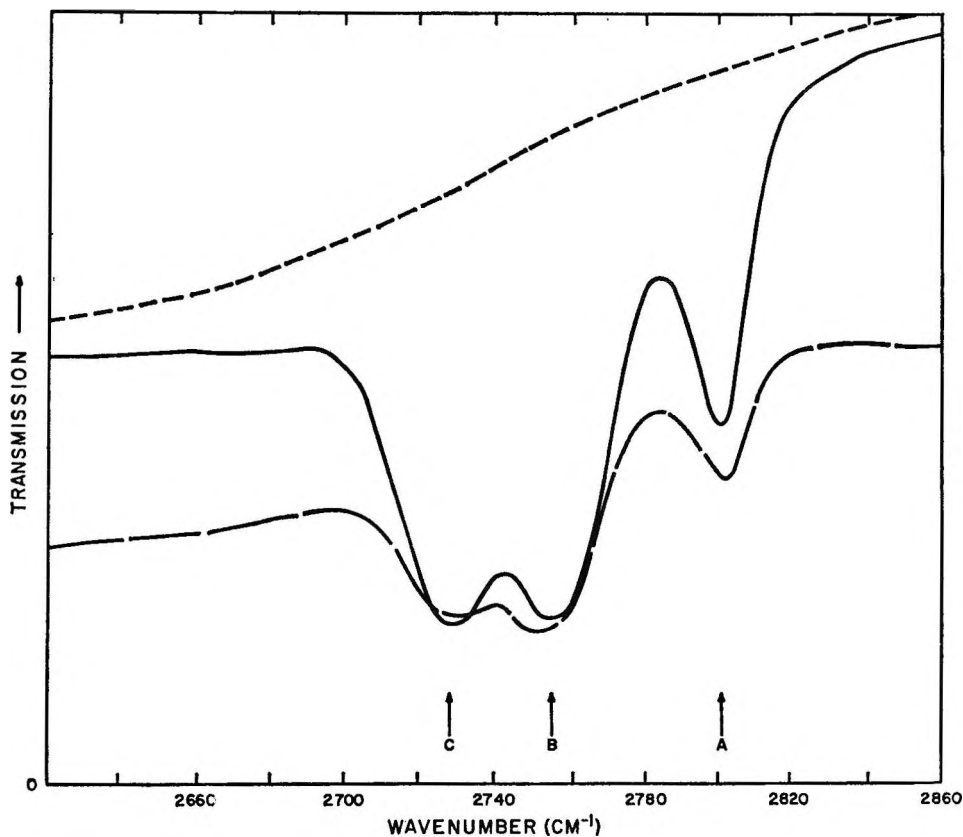


Figure 2. Initial adsorption of HCl (OD stretching bands): - - -, before D₂ exchange; —, deuterated surface; and — · —, +26% HCl monolayer.

about 35% of its original intensity. Further addition of HCl gave a total surface coverage of 80% after 3 days. At this point, the B band had almost disappeared. With 152 torr of HCl in the cell, surface coverage of 88% was achieved and the B band was gone. Elimination of this band thus required almost a complete monolayer of adsorbed HCl. Evacuation for 1 hr left 76% of the surface covered and partially restored the B band. No corresponding isolated hydroxyl bands were observed throughout the adsorption, even though isolated deuteroyl bands persisted and substantial amounts of HCl were present in the cell.

Figure 4 shows the adsorption isotherm obtained during the spectroscopic study described above. Equilibration time was normally 1 hr. The apparent "B point" lies at about 66% monolayer coverage. Similar data, obtained after subsequent evacuation of the cell at 800°, showed slightly decreased adsorption, mainly reflecting slightly lower surface area (274 vs. 293 m²/g) of the aerogel.

Adsorption of HCl was repeated on a different sample of deuterated aerogel, using cell A² in the Model 112 spectrometer. The detailed changes described above in the hydroxyl and deuteroyl stretching bands were

confirmed, and a band was found at 1630 cm⁻¹, apparently caused by H₂O. The intensity of this band was apparently closely proportional to the extent of chemisorption of HCl, as shown in Figure 5. The curves were obtained by subtracting the original spectrum from spectra obtained at the coverages shown. No band for HDO deformation was detected at, or near, the expected frequency (1400–1450 cm⁻¹).

Desorption of HCl. After adsorption of HCl to 88% monolayer, cell C was evacuated and the alumina was heated to desorb HCl and/or H₂O. Weight and spectral changes were again followed concurrently. Representative spectra for the hydroxyl stretching region are shown in Figure 6. (No deuteroyl bands remained.) The spectrum obtained under identical conditions after original drying at 800°, but before the D₂ exchange and HCl adsorption, is shown for comparison. The high-frequency (A) hydroxyl band, which had not appeared on adsorption of HCl, did not appear on desorption. New hydroxyl groups had clearly been formed by HCl addition at lower temperatures, as shown by the intensity of the hydroxyl bands left after evacuation at 400 and 500°, but evacuation at 800° left fewer hydroxyl groups than had initially

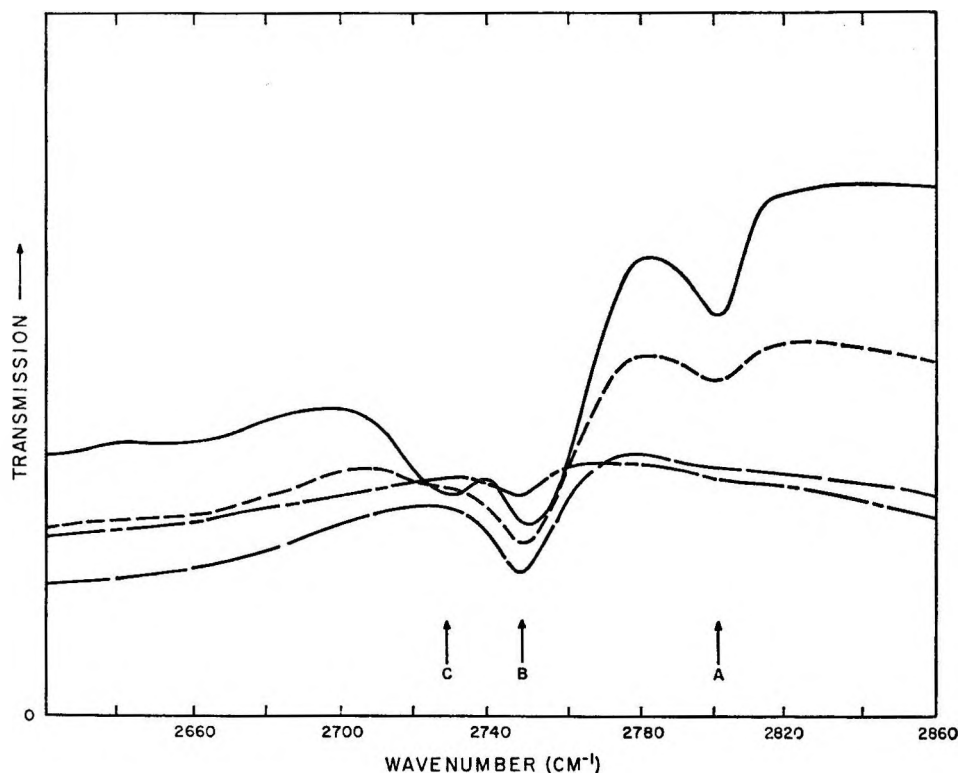


Figure 3. Further adsorption of HCl (OD stretching bands): —, 26% monolayer; ----, 43% monolayer; — · —, 55% monolayer; and - - -, 76% monolayer (after evacuation for 1 hr at 42°).

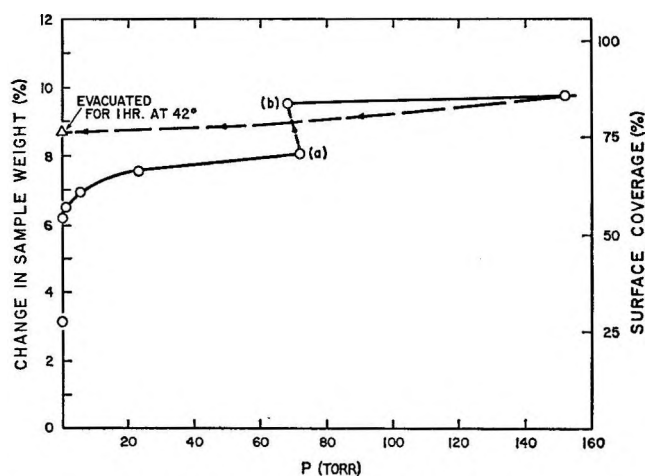


Figure 4. Adsorption of HCl; (b) = (a) + 72 hr.

been present before D₂ exchange. Only two major bands remained. One corresponded to the original B band, reduced to about 43% of its original intensity. The other appeared to be the C band, but was slightly lower in frequency, and had about 55% of its original intensity. The net reduction in the hydroxyl content caused by the adsorption and desorption of HCl was, as indicated by absorbance changes, about 60%.

Changes in weight during desorption are shown in

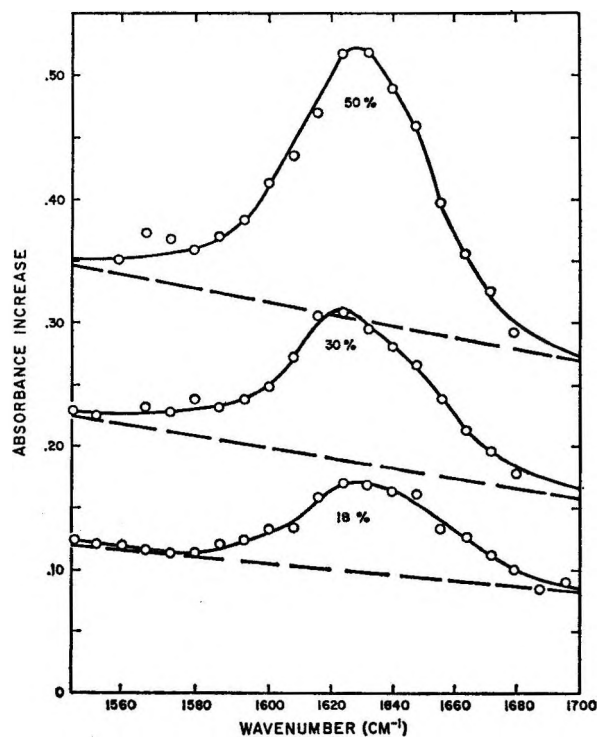


Figure 5. H₂O bending region. The percentage of the surface covered with HCl is indicated along each curve.

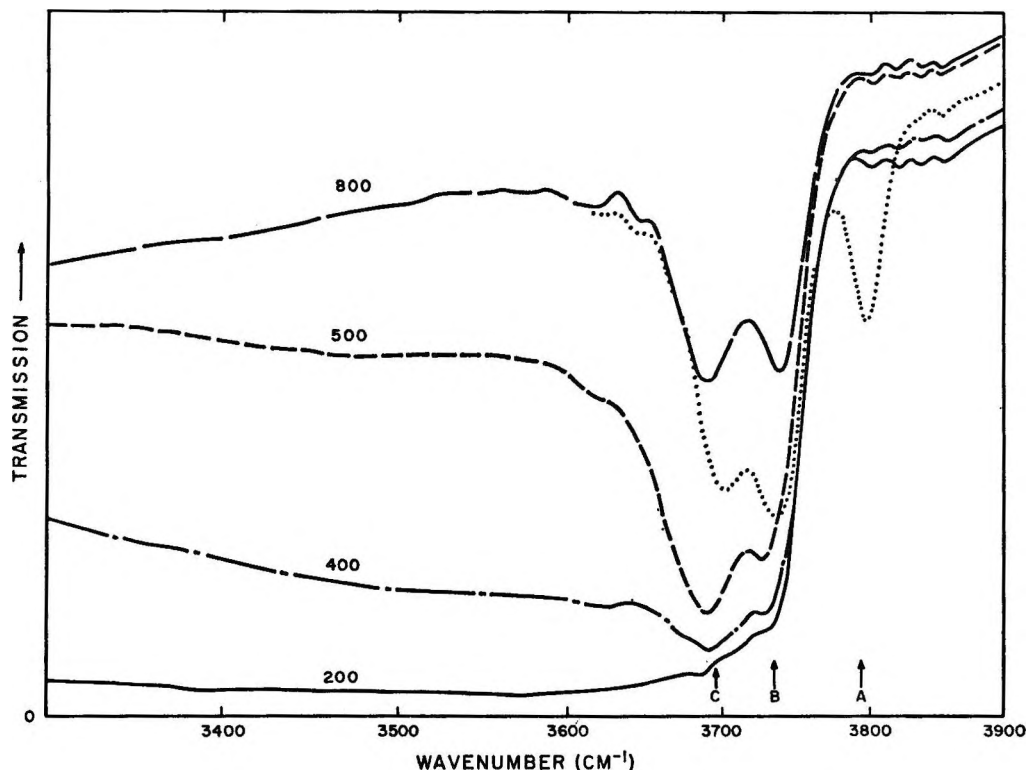


Figure 6. Desorption of HCl and H₂O (OH stretching bands):, curve before D₂ exchange. The temperatures at which the sample was evacuated are indicated above the curves in Centigrade degrees.

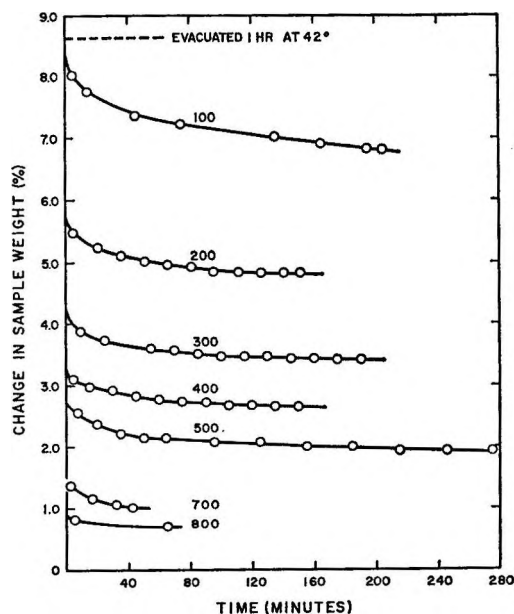


Figure 7. Desorption of HCl (and H₂O); the temperature at which the sample was evacuated are given above the curves in Centigrade degrees.

Figure 7. After evacuation at 800°, the sample was about 0.7% heavier than its original 800° dry weight. Replacement of hydroxyl groups can account for

about 60% of the increase. The remaining 40% must represent replacement of oxide ions. Final retention of chloride was 6.6% monolayer (if 100% = 1.25×10^5 Cl⁻/cm²). The gas desorbed on heating was mainly HCl (judged from the pressure reduction on cooling). A small amount of H₂O, which was probably also present, would not readily have been detected.

Reaction of Dry Alumina with Dry HCl at Higher Temperatures. Several experiments were designed to study reaction of HCl with alumina at high temperatures. An aerogel plate was dried under vacuum at 800°, cooled to 600°, and treated with HCl at 30 torr for 15 min. A spectrum was recorded, and the cell was then evacuated for 15 min. After a spectrum had again been recorded, the HCl treatment was repeated, and the cell was evacuated for 30 min. Finally, the cell was evacuated for 15 min at 800°. The spectra recorded are shown in Figure 8. After treatment with HCl at 600°, the A and B bands had vanished, leaving a band slightly lower in frequency than the original C band. Evacuation at 800° removed this final band.

In other experiments, alumina was calcined at 600° in O₂, dried in flowing N₂, and treated (while in the infrared beam) with flowing dry HCl at progressively higher temperatures. Spectra, recorded at intervals, showed gradual reduction in the intensity of the hy-

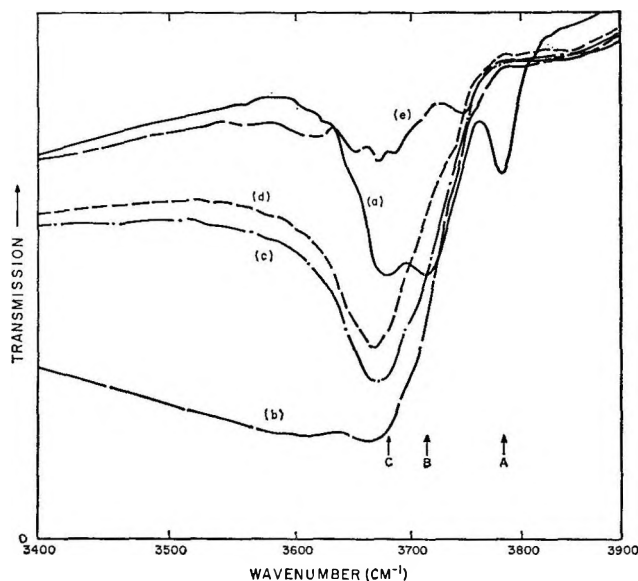


Figure 8. Removal of hydroxyl by HCl and evacuation (all spectra were recorded at 600°): a, original; b, 30 torr of HCl in cell; c, evacuated 15 min; d, evacuated 30 min after further HCl treatment; and e, evacuated at 800°.

droxyl bands. After almost 1 hr in dry HCl at 700° some hydroxyl groups remained but were being slowly eliminated. The temperature was then raised to 800°, and a spectrum was recorded immediately. The transparency of the aerogel was found to be decreasing rapidly. The cell was rapidly cooled to 290°, and a spectrum was again recorded (with increased slit width). Isolated and slightly perturbed hydroxyl groups had been eliminated completely, but a strong band corresponding to hydrogen-bonded hydroxyl groups remained. The originally transparent aerogel now resembled chalk, indicating large loss of surface area.

The Effect of Surface Chloride on the Adsorption of CO₂. Figure 9 illustrates how pretreatment of alumina with HCl affected subsequent adsorption of CO₂. The spectra were obtained, after pretreatment as discussed below, first with 2 torr of CO₂ in the cell and again after brief evacuation as indicated. (The small bands near 2350 cm⁻¹ in the initial spectra may represent CO₂ somehow entrapped in the γ -alumina.¹²)

Molecular CO₂ held (on α sites) on pure alumina predried at 800° yielded the spectra in Figure 9a. When the alumina was first exposed to 12 torr of HCl at room temperature for 15 min and then dried at 600° (1.5 hr), much less CO₂ was subsequently strongly held at room temperature as shown by Figure 9b, but a new band was noted at 2392 cm⁻¹. Subsequent heating of the alumina at 800° under vacuum (0.5 hr) appeared to restore some of the original α sites, as shown by increased CO₂ retention. The frequency of the CO₂

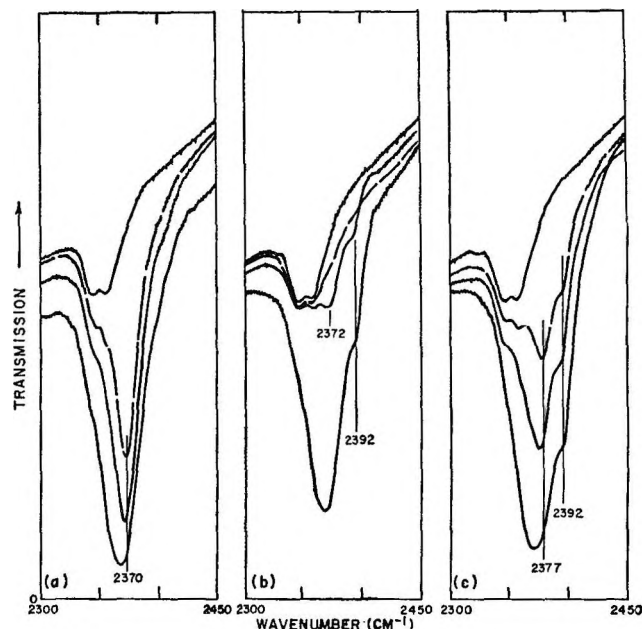


Figure 9. Adsorption of CO₂ on alumina: a, dried at 800°; b, HCl-treated at <50°, dried at 600°; and c, HCl-treated at 600°, dried at 800°. The uppermost spectra are before addition CO₂; the others are (reading up) after addition of 2 torr of CO₂, after 1-min evacuation, and after 15-min evacuation (dashed line).

band near 2372 cm⁻¹ seemed, however, to be slightly higher than on the original alumina. The alumina was then heated in 30 torr of HCl at 600° for 0.5 hr, dried by evacuation at 800° for 0.5 hr, cooled, and reexposed to CO₂. The spectra then obtained are shown in Figure 9c. They show two bands, corresponding to strongly held CO₂, near 2377 and 2392 cm⁻¹. Throughout these experiments, frequency shift for adsorbed CO₂ was also reflected by the increased width (arising from extension to higher frequency) of the band caused by more weakly held CO₂.

Changes were also noted in other bands which typically result from chemisorption of CO₂ on alumina.^{12,13} These will be discussed elsewhere, but, in general, HCl pretreatment tended to reduce or eliminate bands that usually reflect formation of carbonates and other chemisorbed CO₂ species.

Catalytic Activity of HCl-Treated Alumina. Chlorided alumina was tested for activity for double bond isomerization of 1-butene (8–10 torr) at room temperature by following changes in the C–H stretching bands of adsorbed butene. Results were only qualitative, because the activity was usually too high for accurate measurement.

(13) N. D. Parkyns, *Proc. 3rd Intern. Congr. Catalysis, Amsterdam, 1964*, 1, 914 (1965).

Alumina predried at 800°, saturated with dry HCl at room temperature, and then dried by evacuation at 600° showed activity comparable to that of pure alumina dried at 600°. A substantial hydroxyl band, slightly lower in frequency than the normal C band, remained as described previously. When HCl-treated alumina was first exchanged with deuterium to produce the corresponding deuterioxyl band, addition of 1-butene led to slow exchange with the deuterioxyl groups. This exchange, as found previously for pure alumina,² occurred much more slowly than isomerization of the butene.

When alumina pretreated as above with HCl was dried at 800°, fewer hydroxyl groups remained than on pure alumina similarly dried, but 1-butene isomerized somewhat more rapidly than on pure alumina and may also have polymerized slightly.

When the alumina was first treated with HCl (10 torr) at 600° and subsequently dried at 800°, virtually all hydroxyl groups were removed, but 1-butene isomerized more rapidly on this chlorided alumina than on pure alumina dried at the same temperature. Some of the adsorbed "butene" could not be desorbed at 200°.

Pentane was not isomerized at 100° or lower by alumina treated with HCl at 600° or lower, regardless of the temperature of subsequent drying.

Discussion

Adsorption of HCl at room temperature on dry γ -alumina creates new hydroxyl groups and H₂O, as shown by the intensity of the 3500-cm⁻¹ band and the rough proportionality of the 3500- and 1630-cm⁻¹ bands to the amount of HCl chemisorbed. If only reaction and/or exchange (with subsequent hydrogen bonding) of preexisting deuterioxyl groups had occurred, less increase in these hydroxyl or H₂O bands should have been observed as the number of unaffected deuterioxyl groups decreased.

The band produced at 1630 cm⁻¹ (H₂O deformation) indicates that some of the hydroxyl must have been present as H₂O. The proportion so held cannot readily be determined, however, since the ratio of absorptivities of the stretching and bending bands depends strongly on how H₂O is held. The stretching/bending ratios calculated at HCl coverages ranging from 20 to 50% average about 9. Comparison with ratios calculated from published data¹⁴ for ice at -9° (10.7) and liquid H₂O at 60 (2.3) and 3° (3.2) shows that nearly all hydroxyl could have been present as "icelike" H₂O molecules. Only about 30% of the total hydroxyl content need have been H₂O resembling liquid H₂O, however.

HCl did not react with the original deuterioxyl groups in strong preference to bare oxide surface. The first addition (Figures 1 and 2) represented twice the amount needed to react with all the deuterioxyl groups, but the maximum reduction in the intensity of any deuterioxyl band was only 50%. Reaction and exchange of all the original deuterioxyl groups could have produced only 15% of a monolayer of H₂O. New hydroxyl groups were, however, formed by chemisorption of HCl, and additional H₂O was apparently produced from these.

All the original deuterioxyl groups were accessible because they were ultimately eliminated, or their vibration frequencies were grossly altered through deuterium bonding, as HCl was adsorbed. The failure of corresponding isolated hydroxyl stretching bands to appear shows either that proton interchange between HCl and surface deuterioxyl groups could not occur readily at 42° (reduction in deuterioxyl band intensities being caused only by deuterium bonding), or that the hydroxyl groups and H₂O formed by chemisorption of HCl were not mobile on the surface. The latter seems much more probable.

Comparison of CO₂ adsorption on chlorided alumina with that on pure alumina predried at 800° indicates that the character of some of the α sites was altered by chloride and also that the total number of α sites was not greatly changed. Fewer α sites were present on chlorided alumina dried at 600°, presumably because more chloride and hydroxyl ions remained on the surface to shield aluminum ions. Changes in the nature of the α sites may explain changes in the catalytic activity produced by chloride.

Comparison of the rate of 1-butene isomerization on chlorided alumina with that on pure alumina predried at 800° supports previous findings that surface hydroxyl groups on alumina are not, *per se*, active for butene isomerization.²

Interpretation based on a model surface previously proposed for dry alumina,³ although highly speculative, can apparently explain most of the details of HCl chemisorption.

Figure 10a represents a "dry" alumina surface 6% covered with deuterioxyl ions. The significance of such representation has been explained previously.³ The isolated deuterioxyl (and hydroxyl) bands designated A, B, and C in the spectra (*e.g.*, in Figures 1 and 2) have been postulated to correspond to deuterioxyl (or hydroxyl) ions which have differing configurations of nearest neighbors as indicated by letter in

(14) J. J. Fox and A. E. Martin, *Proc. Roy. Soc. (London)*, **A174**, 234 (1940).

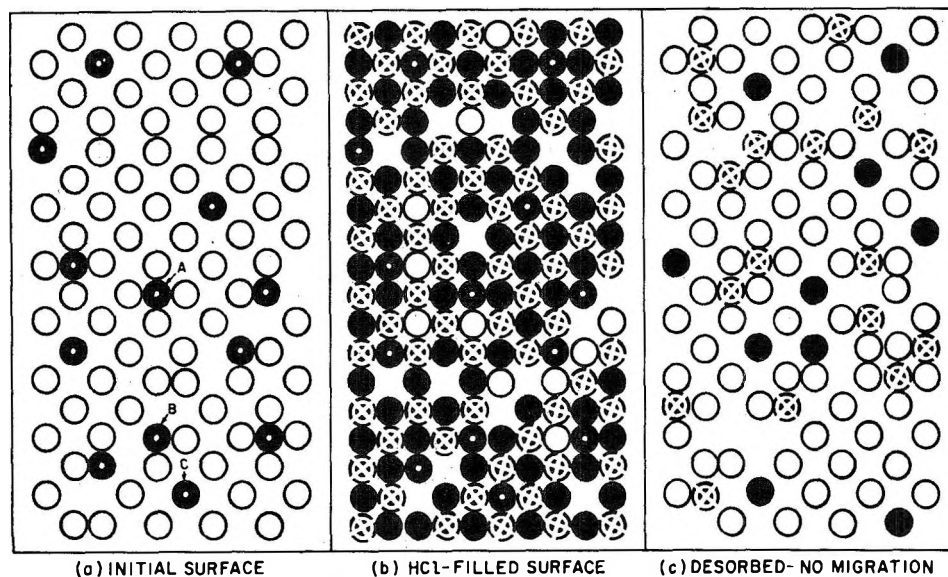


Figure 10. Chemisorption of HCl on a model surface: ●, deuterioxy; ◐, hydroxyl; O, oxide; and ⊗, chloride.

Figure 10a. Chemisorption of HCl forms a hydroxyl ion from an oxide ion and attaches a chloride ion at an adjoining vacant site. Reduction in the intensity of the isolated deuterioxy bands is presumably caused by the formation of hydroxyl ions from oxide ions immediately adjoining A- and B-site deuterioxy ions (permitting HDO formation or deuterium bonding) or by the attachment of chloride ions at vacant sites adjoining B- or C-site hydroxyl ions (permitting DCl formation or deuterium bonding).

Completely random chemisorption fails to explain the adsorption isotherm or the selective disappearance of the isolated deuterioxy bands. Packing effects are probably important. A surface completely filled with hydroxyl and chloride ions would be extremely crowded. Two chloride ions could probably not easily be held on two sites which immediately adjoin. Strongly held H_2O plus an oxide ion should require less space than two hydroxyl ions. Adsorption of HCl in widely spaced rows covering 25% of the surface sites would place either a chloride or hydroxyl ion immediately adjacent to about 50% of randomly distributed deuterioxy ions on A or C sites. Covering 50% of the surface could eliminate A and C deuterioxy bands through deuterium-bond formation to hydroxyl or chloride ions. The B-site deuterioxy ions, however, usually adjoin pair-vacancy defects. To fill both vacant sites in such a defect, two chloride ions must be held on adjoining sites. Because this should be difficult, some of the vacant sites (plus unreacted oxide ions) probably remain. Some B-site deuterioxy ions should thus remain relatively unaffected until pair vacancies are ultimately filled.

Figure 10b represents limiting random chemisorption of HCl to form hydroxyl and chloride ions on the surface of Figure 10a, subject to the restriction that two or more chloride ions cannot directly adjoin one another. About 78% of the surface is covered by chemisorbed HCl. With no restriction on adjoining chloride ions, the coverage could increase to 83%, the remaining 17% being unavailable because of preexisting deuterioxy ions and statistical exclusions (no vacant site directly adjoining an oxide ion). If, because of crowding, H_2O (or HDO) is formed whenever two hydroxyl ions (or OH^- and OD^-) directly adjoin, ~30% of the total hydrogen on the surface would be in H_2O .

On heating, H_2O (or HDO) is assumed to be preferentially desorbed wherever it can be formed as above from hydroxyl pairs. Desorption of HCl occurs through random combination of hydroxyl ions with chloride ions on immediately adjacent sites. Figure 10c illustrates the effects to be expected after removal of all possible H_2O and/or HCl. All A-site hydroxyl or deuterioxy ions have disappeared, but the number of C-site ions is over twice as great as originally. This appears consistent with the spectra (Figure 7) recorded after evacuation at 500° . Few, if any, B-site hydroxyl ions would be expected, but a few E-site hydroxyl³ ions are left which can readily convert to B-site hydroxyl by a single-space proton move. (No similar mechanism can regenerate an A-site hydroxyl.) At higher temperatures migration of ions would permit further elimination of HCl and should tend to minimize surface defects. Removal of HCl from the surface of Figure 10c to reduce the number of hydroxyl groups

to the extent found experimentally after evacuation at 800° (~2.5% hydroxyl monolayer) left 6.5% monolayer of chloride in good agreement with experiment. Because chloride ions should, like hydroxyl ions, reduce surface defects,³ they should often be held in domain boundaries and would, in this case, adjoin vacancy defects.

In the absence of mobility of oxide ions in regular domain areas, water can only be formed and desorbed through reaction of HCl with existing hydroxyl ions or with oxide ions at oxide defects. Hence, less than 20% of a typical dry surface can be filled with chloride ions. Depending on the extent of predrying, the maximum increase in the dry weight of typical (300 m²/g) alumina as a result of HCl treatment should be 2.2–3.2%. If oxide ions in regular domain areas become mobile, however (as apparently occurs at 700–800°), extensive chloride substitution can occur, leading to bulk reaction of the alumina.

Conclusion

Dry, chloride-treated alumina holds "acid" sites that are generally similar to those on dry γ -alumina. CO₂ adsorption shows that some of the α sites found on dry γ -alumina are modified by chloride and become more like the similar sites found on silica-alumina. At least some of these sites are probably catalytically active, but whether chloride-modified sites are more effective because of enhanced acidity of aluminum ions or for some other reason is not clear.

The effect of chloride undoubtedly depends on the method of addition and the amount retained. The chloride-alumina system is very complex and can involve free aluminum chloride or bulk oxychlorides as well as simple substitution of chloride for surface hydroxyl or oxide ions. Further study is, of course, needed.

Acknowledgment. The assistance of Mr. J. Kekich in the experimental work is gratefully acknowledged.

Liquid Ammonia Solutions. III. The Nature of Solutions of the Alkali and Alkaline Earth Iodides

by J. T. Nelson, R. E. Cuthrell, and J. J. Lagowski

Department of Chemistry, University of Texas, Austin, Texas (Received October 25, 1966)

The spectra of liquid ammonia solutions of the alkali and alkaline earth iodides, except CaI_2 , exhibit an absorption band at about 2500 Å, the position and intensity of which is temperature dependent; the position of the band is also dependent upon the concentration of added inert salt. Analysis of the data indicates that the band arises from a charge-transfer-to-solvent transition. The absence of this band in solutions of CaI_2 suggests that a molecular complex is present in this system.

Introduction

The position of the first ultraviolet absorption band for the iodide ion is solvent and temperature dependent; this band has been described as arising by a charge-transfer-to-solvent (ctts) mechanism.¹ We present here the results of a detailed study of the ultraviolet absorption band reported² for iodide ions in liquid ammonia which support this model.

Experimental Section

The spectra of liquid ammonia solutions containing iodide ions were determined using the equipment³ and rinsing technique⁴ previously described. The temperature of the solution in the optical cell was determined with a calibrated thermistor probe sealed into a glass well.

Commercially available reagent grade lithium, sodium, potassium, rubidium, cesium, calcium, strontium, and barium iodides were dried at 200° *in vacuo* and stored in a glove box containing helium which was equilibrated with sodium-potassium alloy. Lithium and potassium perchlorates were dried at 200 and 300°, respectively, and stored in a glove box.

Results and Discussion

Liquid ammonia solutions of the alkali metal iodides, as well as of SrI_2 and BaI_2 , exhibit an absorption band at about 2500 Å, the position of which is temperature dependent (Table I). The general characteristics of the band, however, do not vary with the nature of the cation. Within experimental error, solutions of

LiI , NaI , KI , CsI , SrI_2 , and BaI_2 obey Beer's law in the concentration range $1-10 \times 10^{-5} m$ at -78° (Table II), indicating that the iodide ion and aggregates containing this species cannot be distinguished spectrophotometrically under these conditions.⁵ However, the addition of a 100-fold excess of inert salt (KClO_4 or LiClO_4) lowers the wavelength of the iodide absorption band by 6-8 Å at a given temperature (Table I).

The temperature dependence of the band maximum is characteristic of ctts spectra, the transition corresponding to excitation of an electron to the first layer of solvent molecules. Platzman and Franck⁶ proposed a model for the excited state of the solvated iodide ion in which the electron moves in an orbital centered on iodine and defined largely by the field of the polarized solvent molecules around the ion. Smith and Symons^{1a-c} suggested that the excited electron is trapped in a solvent cavity. In this interpretation the excited

(1) (a) M. Smith and M. C. R. Symons, *Discussions Faraday Soc.*, **24**, 206 (1957); (b) *Trans. Faraday Soc.*, **54**, 338 (1958); (c) *ibid.*, **54**, 346 (1958); (d) G. Stein and A. Treinen, *ibid.*, **55**, 1086 (1959).

(2) W. Jolly, University of California Radiation Laboratory Report, 1952, p 2008.

(3) E. C. Fohn, R. E. Cuthrell, and J. J. Lagowski, *Inorg. Chem.*, **4**, 1002 (1965).

(4) (a) D. F. Burow and J. J. Lagowski, *Advances in Chemistry Series*, No. 50, American Chemical Society, Washington, D. C., 1965, p 125; (b) R. E. Cuthrell, Ph.D. Dissertation, The University of Texas, 1964.

(5) R. E. Cuthrell, E. C. Fohn, and J. J. Lagowski, *Inorg. Chem.*, **5**, 111 (1966).

(6) R. Platzman and J. Franck, *Z. Physik*, **138**, 411 (1954).

Table I: Values of λ_{\max} at -50° and the Temperature Dependence of the Iodide Ion Band in Solutions of Alkali and Alkaline Earth Iodides

| Compd | λ_{\max} , Å ^a | $\frac{d\lambda_{\max}}{dt}$, Å deg ⁻¹ | $\frac{dE_{\max}}{dt}$, cal deg ⁻¹ |
|---------------------------------------|--------------------------------------|---|--|
| LiI | 2500 | 1.28 ± 0.05 | -59.0 |
| LiI + LiClO ₄ ^b | 2493 | 1.42 ± 0.07 | -72.6 |
| NaI | 2500 | 1.36 ± 0.04 | -62.8 |
| KI | 2500 | 1.34 ± 0.06 | -61.5 |
| RbI | 2499 | 1.24 ± 0.05 | -56.0 |
| RbI + KClO ₄ ^b | 2491 | 1.31 ± 0.03 | -66.8 |
| RbI + LiClO ₄ ^b | 2493 | 1.33 ± 0.10 | -67.8 |
| CsI | 2499 | 1.39 ± 0.02 | -64.0 |
| CsI + LiClO ₄ ^b | 2491 | 1.32 ± 0.03 | -67.4 |
| SrI ₂ | 2485 | 0.74 ± 0.03 | -32.0 |
| BaI ₂ | 2501 | 1.06 ± 0.08 | -30.3 |

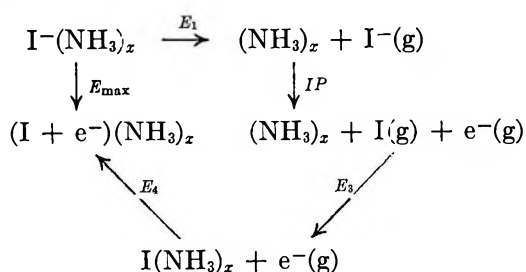
^a Measured at -50° . ^b Using a 100-fold excess of inert salt.

Table II: Molal Extinction Coefficient^a at 2475 Å for Iodide Ion in Liquid Ammonia at -78°

| Compd | $\epsilon \times 10^{-4}$ ^b |
|------------------|--|
| KI | 1.86 ± 0.06 |
| CsI | 1.81 ± 0.04 |
| SrI ₂ | 1.70 ± 0.06 |
| BaI ₂ | 1.73 ± 0.07 |

^a Determined from the slope of the Beer's law plots. ^b Calculated per equivalent of iodide ion.

electron is constrained to move within a solvent cavity containing an iodine atom, the energy of the transition being approximated by a simple electron-in-a-square-well model from the energy cycle shown in Scheme I.^{1a,b} In this cycle $I^-(NH_3)_x$ represents the iodide

Scheme I

ion in a cavity composed of x ammonia molecules, $(NH_3)_x$ the cavity consisting of similarly oriented solvent molecules, $I(NH_3)_x$ an iodine atom in the cavity, and $(I + e^-)(NH_3)_x$ an iodine atom plus an electron occupying the same cavity. The energy required to

remove the ion from the cavity leaving the latter intact is represented by E_1 , the ionization potential of the iodide ion by IP , the energy gained by replacing the iodine atom in the cavity by E_3 , the energy required to put the electron into the lowest orbital defined by the first solvation shell by E_4 , and the energy of the transition by E_{\max} . It follows that

$$E_{\max} = IP + E_1 + E_3 + E_4 \quad (1)$$

The energy of an electron in a well of radius r_0 is given⁷ by

$$E = \bar{n}^2/8mr_0^2 \quad (2)$$

where the other symbols have their usual meanings. By previous arguments^{1c}

$$E_4 = -E_1 + h^2/8mr_0^2 \quad (3)$$

since the relaxation time of the solvent cavity is very much less than the time required for the transition. Assuming E_3 to be negligibly small^{1a-c} and substituting eq 3 into eq 1 gives

$$E_{\max} = IP + h^2/8mr_0^2 \quad (4)$$

The absorption band for ammonia-iodide systems occurs at 2475 Å at -78° . Using 72.3 kcal/mole for the ionization potential of the iodide ion, the radius of the solvent cavity is calculated to be 4.48 Å, which extrapolates to 4.80 Å at 25° . The latter value should be compared with the value of 4.05 Å reported for the water-iodide system at 25° .^{1c}

The observed decrease in E_{\max} with temperature (Table I) suggests that, on the basis of the model proposed by Smith and Symons, the radius of the solvent cavity decreases with temperature. It might be expected that the radius of the cavity would become essentially that of the iodide ion at $0^\circ K$ and that the value of E_{\max} should approach that for the alkali metal iodides at $0^\circ K$. The extrapolated value of E_{\max} at $0^\circ K$ is 130 kcal/mole, which is in good agreement with the values of 134.5 ± 1 kcal/mole calculated for a variety of solvents^{1c} and 135.3 kcal/mole observed for crystalline KI at $20^\circ K$.⁸ The extrapolated value of E_{\max} corresponds (eq 4) to a cavity radius of 3.89 Å.

Stein and Treinen⁹ point out that the value of the cavity radius for the iodide ion in water calculated from the energy cycle shown in Scheme I is about 1 Å greater than any value expected. A modified Platz-

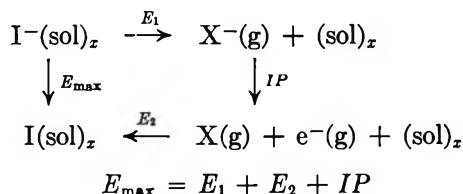
(7) K. Pitzer, "Quantum Chemistry," Prentice-Hall, Inc., Englewood Cliffs, N. J., 1960, p 512.

(8) H. Fesefeldt, *Z. Physik*, **64**, 623 (1930).

(9) G. Stein and A. Treinen, *Trans. Faraday Soc.*, **55**, 1086 (1959).

man and Franck⁶ model incorporating the concept^{1a-c} of a variable-radius parameter was suggested based on the energy cycle shown in Scheme II; all energy terms

Scheme II



are relative to a nonpolarizing electron in the medium at infinite distance from the ions. The energy, E_1 , is the sum of the potential energy of the ion due to the persistent polarization of the organized medium and the electronic polarization caused by the ion in solution; E_2 is the energy involved in introducing the radical into the organized medium (taken to be equal, but of opposite sign, to the heat of solvation of the radical) and introducing the electron to its excited level.⁶ Equation 5 is the basic relationship of the Stein and Treinen theory

$$E_{\text{max}} = IP - L_x + \frac{e^2}{r} \left(\frac{1}{2} + \frac{1}{2D_{\text{op}}} - \frac{1}{D_s} \right) - \frac{e^2}{2\bar{R}_e} \left(1 - \frac{1}{D_{\text{op}}} \right) - \left(\frac{\pi^2 m e^4}{2h^2} \right) \left(\frac{1}{D_{\text{op}}} - \frac{1}{D_s} \right)^2 \quad (5)$$

where L_x is the heat of solvation of the iodine radical, D_{op} and D_s are the optical and static dielectric constants, respectively, \bar{R}_e is the mean distance (5.8 Å) of the electron from the center of the cavity for the 2s state (chosen by Platzman and Franck for the halides), and the remaining terms have their usual significance. Assuming that the difference in the heat of solvation by ammonia and by water for the iodide ion (*i.e.*, *ca.* -4 kcal/mole¹⁰) is the same as for an iodine atom, and using -4.5 kcal/mole for the heat of hydration of an iodine atom,¹¹ L_x can be estimated as -8.5 kcal/mole. Equation 5 can be used to calculate the cavity radius for the iodide ion in liquid ammonia using the data for the static^{4a} and optical dielectric constants¹² that appear in the literature. The results of this calculation for several temperatures appear in Table III. The cavity radius calculated from eq 5 is markedly smaller than that calculated on the basis of Smith and Symons' model (eq 4). The interpretation of ctt spectra of anions in aqueous solutions according to eq 5 has yielded anion radii that correspond to the apparent ionic radii obtained from partial ionic volumes.⁹ Extrapolation of the cavity radius calculated from eq 5 to absolute zero gives a value of 2.43 Å; the crystallographic radius of the iodide ion is 2.16 Å.¹³ There

are no independent data available on apparent ionic volumes for species dissolved in liquid ammonia.

Table III: Iodide Ion Cavity Radius

| Temp, °C | E_{max} , Å | Cavity radius, Å | |
|----------|----------------------|------------------|------|
| | | Eq 4 | Eq 5 |
| 25 | 2599 | 4.80 | 3.04 |
| -78 | 2475 | 4.48 | 2.84 |
| -273 | 2204 | 3.89 | 2.43 |

The absorbance at the band maximum decreases with increasing temperature, as might be expected on the basis of the decrease in the density of the solution with temperature. However, the extinction coefficient at the band maximum decreases with increasing temperature even after a correction is made for the change in density. Thus, for example, ϵ_{max} for KI varies linearly from a value of 1.86×10^4 at -72.2° to 1.58×10^4 at -38.0° . A variation of this nature has been interpreted^{1c} in terms of an increase in the breathing vibrations of the cavity with temperature, which affects the relative shape of the configuration-coordinate curve for the ground and excited states.

The presence of excess cations causes a slight decrease in the value of E_{max} for the iodide ion (Table I), a phenomenon which has been observed in other solvents.^{1b} On the basis of the model suggested, it would appear that under these conditions cations can influence the potential field about, and the effective radius of, the cavity. An obvious suggestion is that cations become incorporated in the solvent layer at higher over-all cation concentrations. However, the temperature dependence of the iodide band in solutions containing excess cations is the same as that for solutions containing only the alkali and alkaline earth iodides. The absorption bands attributed to an iodide-containing, contact ion pair occur at about 2900 Å; the band position is virtually temperature independent. The band associated with iodide-containing, solvent-shared ion pairs is significantly less sensitive to temperature than is the position of the band attributed to solvent-separated ion pairs.¹⁴ Thus, it is likely that the slight shift in the position of the iodide

(10) W. Jolly, *Chem. Rev.*, **50**, 351 (1952).

(11) H. L. Friedman, *J. Chem. Phys.*, **21**, 319 (1953).

(12) D. F. Burow, Ph.D. Dissertation, The University of Texas, 1966.

(13) L. Pauling, "The Nature of the Chemical Bond," 3rd ed, Cornell University Press, Ithaca, N. Y., 1960, p 514.

(14) G. Stein and A. Treinen, *Trans. Faraday Soc.*, **56**, 1393 (1960).

band in solutions containing excess cations arises from slight, nonspecific perturbations by the cation on the solvent cage of the iodide ion.¹⁴

The spectral characteristics of solutions of BaI_2 and SrI_2 are different from those of the alkali iodides, the extinction coefficients of solutions of the former compounds being about 6% less than those of the latter compounds. The marked change in the temperature dependence of BaI_2 and SrI_2 solutions suggests that either the nature of the species or the cavity (or both) has been altered. It is possible that the band observed for BaI_2 and SrI_2 solutions is due, in part, to solvent-shared ion pairs, because the band attributed to these species is far less sensitive to temperature

changes than is the band associated with free solvated iodide ion.¹⁵

The spectra of liquid ammonia solutions of CaI_2 are featureless in the ultraviolet region, indicating that the concentration of solvated iodide ions is negligible in this system. This observation leads to the suggestion that the predominating species present are solvated molecules, probably of the type $\text{CaI}_2 \cdot 4\text{NH}_3$, where the calcium atom is octahedrally coordinated.

Acknowledgment. We gratefully acknowledge the support of the National Science Foundation in the form of a grant (NSF G-15734).

(15) T. R. Griffiths and M. C. R. Symons, *Mol. Phys.*, 3, 90 (1960).

Thermodynamic Properties of Nonaqueous Solutions. II. Free Energies, Entropies, and Activity Coefficients of Selected Alkali Metal Halides in Anhydrous N-Methylformamide¹

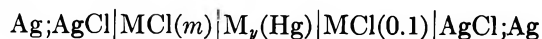
by Eugene Luksha and Cecil M. Criss²

Department of Chemistry, University of Vermont, Burlington, Vermont (Received October 26, 1965)

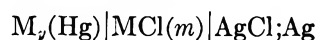
Electrode potentials have been measured for cells of the type $M_v(\text{Hg})|\text{MX}(\text{NMF})|\text{AgX};\text{Ag}$ where M is Li, Na, K, or Cs and X is either Cl^- or Br^- . These potentials have been combined with data in the literature to evaluate standard potentials for cells of the type $M|\text{MX}(\text{NMF})|\text{AgX};\text{Ag}$, from which standard free energies of formation and activity coefficients of LiCl, NaCl, KCl, CsCl, and NaBr in anhydrous N-methylformamide have been obtained. The activity coefficients were determined from 0.01 to approximately 0.1 *m*. Activity coefficients for KCl solutions were extended to saturation by means of the cell $\text{Ag};\text{AgCl}|\text{KCl}(m_1)|\text{K}_v(\text{Hg})|\text{KCl}(m_2)|\text{AgCl};\text{Ag}$. The free energies have been used in conjunction with heat data to obtain the standard partial molal entropies of the corresponding electrolytes.

Introduction

Electromotive force studies in solvents with dielectric constants greater than that of water are exceedingly rare. Mandel and Decroly³ have examined the platinum-hydrogen and silver-silver chloride electrodes in formamide (dielectric constant, *D* 109.5). The same electrodes have been studied by Dawson and co-workers^{4,5} in N-Methylacetamide (*D* 165.5 at 40°). Pavlopoulos and Strehlow⁶ have studied the platinum-hydrogen and cadmium-cadmium chloride electrodes as well as several metal electrodes in formamide. The only electromotive force studies in the very high dielectric constant solvent, N-methylformamide (*D* 182.4),⁷ have been those of Povarov and co-workers⁸ who studied cells of the types



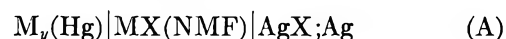
and



where M represents either Na or Cs for the first of these cells and Cs for the second.

In the first paper of this series,⁹ the heats of solution of several alkali metal halides in anhydrous N-methyl-

formamide were reported. In a continuation of the study of the thermodynamic properties of alkali metal halides in this solvent, electromotive forces have been measured for cells of the type



where M is Li, Na, K, or Cs, and X is either Cl^- or Br^- . Standard potentials of the corresponding metals relative to the silver-silver halide electrode have been

(1) This paper represents part of the work submitted by E. Luksha to the Graduate School of the University of Vermont in partial fulfillment of the requirement for the degree of Doctor of Philosophy.

(2) To whom correspondence should be directed: Department of Chemistry, University of Miami, Coral Gables, Fla.

(3) M. Mandel and P. Decroly, *Nature*, **182**, 794 (1958); *Trans. Faraday Soc.*, **56**, 29 (1960).

(4) L. R. Dawson, R. C. Sheridan, and H. C. Eckstrom, *J. Phys. Chem.*, **65**, 1829 (1961).

(5) L. R. Dawson, W. H. Zuber, Jr., and H. C. Eckstrom, *ibid.*, **69**, 1335 (1965).

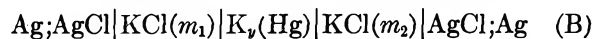
(6) T. Pavlopoulos and H. Strehlow, *Z. Physik. Chem. (Frankfurt)*, **2**, 89 (1954).

(7) G. R. Leader and J. F. Gormley, *J. Am. Chem. Soc.*, **73**, 5731 (1951).

(8) Y. M. Povarov, A. I. Gorbanev, Y. M. Kessler, and I. V. Safonova, *Dokl. Akad. Nauk SSSR*, **142**, 1128 (1962); **155**, 1411 (1964).

(9) R. P. Held and C. M. Criss, *J. Phys. Chem.*, **69**, 2611 (1965).

determined, and activity coefficients and the standard free energies of formation have been obtained for the solvated salts, LiCl, NaCl, KCl, CsCl, and NaBr. From the free energies and the known heats of solution,⁹ partial molal entropies of these salts in anhydrous N-methylformamide have been calculated. In addition, activity coefficients for KCl have been extended to concentrations up to saturation by use of the concentration cell



Experimental Section

Materials. N-Methylformamide was prepared in the same manner as that described previously.⁹ The solvent generally had a conductance ranging from 3×10^{-6} to 5×10^{-6} ohm⁻¹ cm⁻¹. The solvent was not used if the conductance exceeded 8×10^{-6} ohm⁻¹ cm⁻¹. Conductance values reported in the literature range from 10^{-3} to 4×10^{-7} ohm⁻¹ cm⁻¹.^{7,8,10-12} Karl Fischer titrations indicated the water content to be less than 0.003%. Automatically recorded warming curves, analyzed by the usual extrapolation methods, showed an average melting range of -3.52 to -2.99° . The solvent had a density of 0.9986 ± 0.0001 g/cc, which agrees with the most recent literature value.¹¹

Methods used in purifying LiCl, NaCl, KCl, CsCl, and NaBr have been described elsewhere.⁹ Analyses indicated that the chloride salts were bromide free.¹³

Amalgams were prepared from triply distilled mercury which had been bubbled through nitric acid and distilled once again. Potassium and sodium amalgams were prepared by the electrolysis of concentrated solutions of their carbonates, the carbonate solutions having been prepared from recrystallized reagent grade carbonate salts. Lithium and cesium amalgams were prepared by electrolysis of concentrated solutions of their chlorides. The amalgams were washed with conductivity water and anhydrous methanol, dried *in vacuo* at about 300° , and filtered directly into the dropping electrode reservoir through a capillary tube. Spent mercury was recovered by bubbling through nitric acid.

In some cases the amalgam compositions had to be adjusted to specified values. This was carried out by diluting an amalgam of known composition with pure mercury until the desired composition was obtained.

Each batch of amalgam was analyzed several times to determine the alkali metal content. These analyses were accomplished by decomposing a weighed amount of amalgam in 0.1 M standard HCl solution and back-titrating the excess acid with standard NaOH solution. The analyses agreed within 1%.

Electrodes. The silver-silver halide electrodes were prepared by the electrolytic method described by Ives and Janz.¹⁴ The electrodes were fabricated from 24 gauge platinum wire sealed in lead glass standard-taper joints. About 1 cm of wire was exposed. Electrical contact with the potentiometer leads was made through Wood's metal in the contact tube. At least six electrodes were prepared at a time, and those with a bias potential greater than 0.15 mv were discarded. All electrodes were stored in conductivity water until ready for use. Silver-silver iodide electrodes were made in a similar manner. However, because of the high solubility of AgI in the presence of iodides, these electrodes were rendered useless for measurements in N-methylformamide.

The dropping amalgam electrode consisted of a fine capillary joined to a standard taper joint which fitted into the top of the cell. The capillary was joined to the amalgam reservoir through a stopcock.

Apparatus. The apparatus for cell A was of all-glass construction, designed similarly to that of Izmailov and Ivanova.¹⁵ It had three openings fitted with standard taper joints. Two of these were for electrodes, the remaining one for filling the cell. The concentration cell was similar in design to that of Harned.¹⁶ Both cells were thermostated in a water bath at $25.00 \pm 0.01^\circ$ and both were coated externally with Siliclad (Clay Adams, Inc.) to eliminate electrical leakage from the water bath. All electromotive force measurements were made with a Leeds and Northrup Type K-3 potentiometer, using an unsaturated CdSO₄ (Epply Laboratory) cell as a standard. The potentiometer was frequently checked against three such cells. Since the impedances of the amalgam cells were high, a Keithley Instruments Model 151 microvoltmeter was connected in series with the positive terminal of the potentiometer and the positive terminal of the study cell. In order to reduce the noise to a tolerable level and at the same time maintain a high input impedance, the microvoltmeter was shunted with a 100-kilohm resistor. The voltage sensitivity of this circuitry was 0.01 mv. A standard cell was connected

(10) C. M. French and K. H. Glover, *Trans. Faraday Soc.*, **51**, 1418 (1955).

(11) I. Sinyakov, A. I. Gorbanev, Y. M. Povarov, and Y. M. Kessler, *Izv. Akad. Nauk SSSR, Otd. Khim. Nauk*, 1514 (1961).

(12) A. Strack, K. Swanda, and L. W. Bahe, *J. Chem. Eng. Data*, **9**, 416 (1964).

(13) D. J. G. Ives and J. Janz, "Reference Electrodes—Theory and Practice," Academic Press Inc., New York, N. Y., 1961.

(14) See ref. 13, pp 205-207.

(15) N. A. Izmailov and E. F. Ivanova, *Zh. Fiz. Khim.*, **29**, 1422 (1955).

(16) H. S. Harned, *J. Am. Chem. Soc.*, **51**, 417 (1929).

in series with reversed polarity to reduce the potential, since the electromotive force of the study cell was beyond the range of the potentiometer. Every precaution was taken against electrical leakage; the guarded circuits provided in the instrument were used effectively.

Procedure. Before each measurement, the cell was washed with distilled water, rinsed with anhydrous methanol, and then dried in an air oven at 125°. After removal from the oven, the cell was flushed with dry nitrogen and the dropping amalgam and silver-silver halide electrodes (cell A) or the two dropping amalgam electrodes (cell B) were immediately inserted into their respective compartments. Preparation of the silver-silver halide electrodes immediately prior to insertion in the cell involved removing the electrodes from storage in conductivity water and soaking them for a few minutes in pure anhydrous N-methylformamide and then for a few minutes in a solution of the same composition as that in the cell. Since the silver halide coating was very thin and the electrodes were not porous, a brief soaking period was sufficient for the removal of water.

Solutions of the alkali metal halides were prepared by the addition of a weighed quantity of salt to 50.00 ml of N-methylformamide in an apparatus that could easily be mated to a third opening in the cell by means of a standard taper joint. This apparatus reduced to an absolute minimum contact between the atmosphere and the solution and was used to fill the cell immediately after the electrodes were inserted. Precautions were taken to avoid contaminating the cell solutions with grease.

Potential measurements were generally initiated within a few minutes after the cell was placed in the thermostat. Readings were taken approximately every 5 min. All cells studied generally came to equilibrium within 45 min. After equilibrium was established, the potentials rarely varied by more than 0.3 mV from an average value during the period of observation. The cells were observed for a period of 1 hr, in general, and in a few cases as long as 3 hr.

Amalgam flow rates for each cell were varied from a continuous flow to a few drops per minute. In contrast to other investigators,^{17,18} who have studied dropping amalgam electrodes in other nonaqueous solvents, no effect could be observed on the electromotive force of the cells because of flow rate, except for the lithium cell. The flow rate of the lithium amalgam electrode affected the potential only at low concentrations, but since electromotive force measurements at the lower concentrations were not used in the extrapolation to infinite dilution for reasons discussed

below, the phenomenon was of little practical consequence.

Results and Discussion

All the amalgam electrodes exhibited abrupt decreases in electromotive force at low concentrations. This decrease occurred at about 0.01 *m* for the sodium, potassium, and cesium amalgams and at about 0.02 *m* for the lithium amalgam. This same phenomenon has been observed for this type of electrode by other investigators in methanol and formamide,^{6,15,17} but the cause of the behavior is not understood. The fact that the sharp potential drop of these electrodes occurs only at the lower concentrations leads one to suspect that it is a result of an increase in the metal ion concentration around the electrode surface, caused by decomposition of the amalgam. This accounts for the fact that the effect is more pronounced in dilute solutions, but does not explain the failure of the increased amalgam flow rate to correct the condition. Experimental points that showed this behavior were neglected in the extrapolations and in most cases are not presented in the data.

At concentrations greater than 0.02 *m* for the lithium cell and concentrations greater than 0.01 *m* for the other cells, the data are treated best by the method of Hitchcock.¹⁹

The electromotive force of a cell containing a 1:1 electrolyte and having its electrodes in their standard states is given by

$$E = E^\circ - \frac{2RT}{n\mathcal{F}} \ln m\gamma_{\pm} \quad (1)$$

where the symbols have their usual meanings. The expanded Debye-Hückel equation gives the mean activity coefficient as

$$\log \gamma_{\pm} = -\delta_{\gamma} \sqrt{m} + Cm$$

where

$$\delta_{\gamma} = 1.8248 \times 10^6 \frac{d_0^{1/2}}{(DT)^{3/2}} \quad (2)$$

C is a constant, *m* is the molality, *d*₀ and *D* are the density and dielectric constant of the solvent, respectively. For N-methylformamide at 25°, *D* 182.47 and *d*₀ 0.9986 g/cc, giving a value of 0.1439 (kg/mole)^{1/2} for δ_{γ} . Substitution of eq 2 into (1) and rearranging terms gives

(17) J. H. Wolfenden, C. P. Wright, N. L. Ross Kane, and R. S. Buckley, *Trans. Faraday Soc.*, **23**, 491 (1927).

(18) G. Scatchard and R. F. Tefft, *J. Am. Chem. Soc.*, **52**, 2265 (1930).

(19) D. I. Hitchcock, *ibid.*, **50**, 2076 (1928).

$$E + \frac{2RT}{n\mathcal{F}} \ln m - \frac{(2.303)2RT\delta_r\sqrt{m}}{n\mathcal{F}} = E^\circ - \frac{(2.303)2RTCm}{n\mathcal{F}} \quad (3)$$

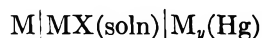
and substitution of the appropriate constants into eq 3 leads to

$$E + 0.11832 \log m - 0.01702\sqrt{m} = E^\circ - 0.11832Cm \quad (4)$$

Since an amalgam electrode is employed, the measured potential is not the electromotive force represented by E in eq 4, but rather a potential, E' , related to E by

$$E' = E - E'' \quad (5)$$

where E'' is the potential of a cell of the type



for some amalgam concentration y . To "correct" the observed potential to that which one would obtain for a pure metallic electrode, the value E'' must be added to the observed potential. Making this substitution and setting the left-hand side of eq 4 equal to E''' gives

$$E''' = E^\circ - 0.11832Cm \quad (6)$$

The resultant potentials then refer to a cell employing a pure metallic electrode and may be written as

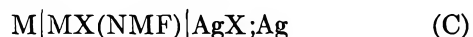


Table I summarizes the data. The first three columns give the molality of the cell solution, the measured potential, and the amalgam concentration of the dropping electrode, respectively. The fourth column gives the potential required to correct the observed potential to that for a pure metallic electrode. The fifth column gives the values of E''' in eq 6, and the sixth column gives the potentials for cells of type C.

Cesium and lithium amalgams were adjusted to the exact compositions shown in Table I in order to be compatible with potential data for the single amalgam concentrations listed in the literature.^{20,21} Three separate batches of lithium amalgam used for the measurements gave reproducible results. Only one batch of cesium amalgam was used in the measurements. Three batches of sodium amalgam were used. Two of these were used for the sodium chloride cell (only one measurement was made with one batch) and one for the sodium bromide cell. Only one batch of potassium amalgam was used in the measurements for cell A. Sodium amalgam cell data were corrected to the standard state electrode using the data of Richards

Table I: Electromotive Force Data for Electrolytes in N-Methylformamide at 25°

| m | E' | y , wt % | E'' | E''' | E |
|----------|---------|---------------|--------|--------|--------|
| LiCl | | | | | |
| 0.006573 | 2.41457 | 0.0350 | 0.9502 | 3.1052 | 3.3648 |
| 0.01126 | 2.39854 | 0.0350 | 0.9502 | 3.1164 | 3.3487 |
| 0.01750 | 2.38061 | 0.0350 | 0.9502 | 3.1207 | 3.3080 |
| 0.01933 | 2.37692 | 0.0350 | 0.9502 | 3.1220 | 3.3271 |
| 0.02617 | 2.36598 | 0.0350 | 0.9502 | 3.1262 | 3.3162 |
| 0.02914 | 2.36092 | 0.0350 | 0.9502 | 3.1265 | 3.3111 |
| 0.03505 | 2.35159 | 0.0350 | 0.9502 | 3.1264 | 3.3018 |
| 0.04309 | 2.34127 | 0.0350 | 0.9502 | 3.1264 | 3.2915 |
| 0.05130 | 2.33519 | 0.0350 | 0.9502 | 3.1289 | 3.2854 |
| 0.08755 | 2.31114 | 0.0350 | 0.9502 | 3.1312 | 3.2616 |
| NaCl | | | | | |
| 0.01229 | 2.17255 | 0.1291 | 0.8625 | 2.8071 | 3.0351 |
| 0.02488 | 2.13750 | 0.1291 | 0.8625 | 2.8075 | 3.0000 |
| 0.03671 | 2.11853 | 0.1291 | 0.8625 | 2.8080 | 2.9810 |
| 0.03742 | 2.12728 | 0.1636 | 0.8542 | 2.8094 | 2.9815 |
| 0.05897 | 2.09596 | 0.1291 | 0.8625 | 2.8089 | 2.9585 |
| 0.07924 | 2.07976 | 0.1291 | 0.8625 | 2.8072 | 2.9423 |
| 0.07963 | 2.08090 | 0.1291 | 0.8625 | 2.8086 | 2.9434 |
| 0.08106 | 2.07940 | 0.1291 | 0.8625 | 2.8080 | 2.9419 |
| 0.09913 | 2.06931 | 0.1291 | 0.8625 | 2.8077 | 2.9318 |
| KCl | | | | | |
| 0.009616 | 2.22877 | 0.3024 | 1.0328 | 3.0213 | 3.2616 |
| 0.01928 | 2.19384 | 0.3024 | 1.0328 | 3.0214 | 3.2266 |
| 0.02751 | 2.17613 | 0.3024 | 1.0328 | 3.0215 | 3.2089 |
| 0.03318 | 2.16757 | 0.3024 | 1.0328 | 3.0223 | 3.2004 |
| 0.04041 | 2.15792 | 0.3024 | 1.0328 | 3.0224 | 3.1907 |
| 0.04829 | 2.14923 | 0.3024 | 1.0328 | 3.0226 | 3.1820 |
| 0.06297 | 2.13690 | 0.3024 | 1.0328 | 3.0233 | 3.1697 |
| 0.07018 | 2.13094 | 0.3024 | 1.0328 | 3.0227 | 3.1637 |
| CsCl | | | | | |
| 0.009015 | 2.11136 | 0.1875 | 1.119 | 2.9868 | 3.230 |
| 0.01846 | 2.07576 | 0.1875 | 1.119 | 2.9873 | 3.195 |
| 0.03003 | 2.05144 | 0.1875 | 1.119 | 2.9874 | 3.170 |
| 0.03983 | 2.03727 | 0.1875 | 1.119 | 2.9872 | 3.156 |
| 0.05229 | 2.02387 | 0.1875 | 1.119 | 2.9873 | 3.143 |
| 0.06436 | 2.01373 | 0.1875 | 1.119 | 2.9875 | 3.133 |
| 0.07092 | 2.00879 | 0.1875 | 1.119 | 2.9872 | 3.128 |
| NaBr | | | | | |
| 0.008701 | 2.11872 | 0.2353 | 0.8402 | 2.7135 | 2.9589 |
| 0.02227 | 2.07056 | 0.2353 | 0.8402 | 2.7127 | 2.9108 |
| 0.03142 | 2.05409 | 0.2353 | 0.8402 | 2.7135 | 2.8943 |
| 0.04295 | 2.03784 | 0.2353 | 0.8402 | 2.7128 | 2.8780 |
| 0.05441 | 2.02700 | 0.2353 | 0.8402 | 2.7136 | 2.8672 |
| 0.07589 | 2.00927 | 0.2353 | 0.8402 | 2.7123 | 2.8495 |

and Conant²² and Lewis and Kraus.²³ Similar corrections for the potassium amalgam cell were made

(20) G. N. Lewis and F. G. Keyes, *J. Am. Chem. Soc.*, **35**, 340 (1913).

(21) H. E. Bent, G. S. Forbes, and A. F. Forziatti, *ibid.*, **61**, 709 (1939).

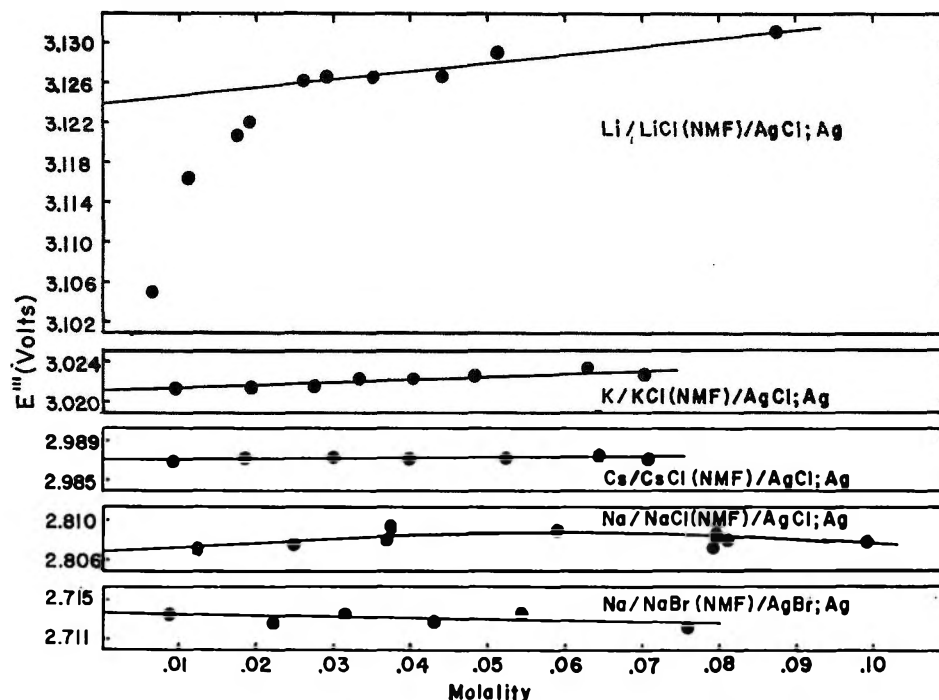


Figure 1. E''' vs. molality for cells of type C.

using the data of Bent and Gelfellan²⁴ and Lewis and Keyes.²⁵ The existence of potential data as a function of amalgam concentration made it unnecessary for sodium and potassium amalgams to be adjusted.

Figure 1 shows values of E''' plotted against the molality and extrapolated to infinite dilution by the method of least squares to obtain E° . Since the potentials below 0.01 m for all cells suffer very large decreases (as much as 50 mv), they have been omitted from Table I and Figure 1 and were not included in the least-squares treatment. Although the decrease in potential for the lithium cell occurs in solutions more than 0.02 m , the really abrupt decrease occurs only at concentrations below 0.01 m ; consequently, the data are shown down to a concentration of about 0.01 m but have not been included in the least-squares treatment. Because of the apparent curvature of E''' vs. m for the sodium chloride cell at higher concentrations, the two points for the most concentrated solu-

tions were not included in the least-squares treatment. The standard electrode potentials for the various cells evaluated by this treatment are given in Table II.

Smoothed values of the electromotive force, E , for cells of type C have been calculated from smoothed values of E''' at round values of the molality and are given in Table III.

Activity Coefficients of Electrolytes in N-Methylformamide

The smoothed electromotive forces listed in Table III are useful for obtaining activity coefficients of the corresponding salts in N-methylformamide. Rearrangement of eq 1 gives

$$\log \gamma_{\pm} = \frac{E^\circ - E_m}{0.11832} - \log m \quad (7)$$

from which γ_{\pm} for the various electrolytes have been evaluated. These are listed also in Table III, along with the few corresponding values for NaCl and CsCl reported in the literature.⁸

From the knowledge of activity coefficients in dilute solutions, activity coefficients at higher concentrations can be evaluated from cell B by the relationship

Table II: Standard Potentials for Cells of Type C

| Cell | E° |
|----------------------|-----------|
| Li LiCl(NMF) AgCl;Ag | 3.1237 |
| Na NaCl(NMF) AgCl;Ag | 2.8067 |
| K KCl(NMF) AgCl;Ag | 3.0212 |
| Cs CsCl(NMF) AgCl;Ag | 2.987 |
| Na NaBr(NMF) AgBr;Ag | 2.7135 |

(22) T. W. Richards and J. B. Conant, *J. Am. Chem. Soc.*, **44**, 601 (1922).

(23) G. N. Lewis and C. A. Kraus, *ibid.*, **32**, 1458 (1910).

(24) H. E. Bent and E. S. Gelfellan, *ibid.*, **55**, 3989 (1933).

(25) G. N. Lewis and F. G. Keyes, *ibid.*, **34**, 119 (1912).

Table III: Smoothed Values of E and Activity Coefficients for Round Concentrations for Cell C

| m | LiCl | | NaCl | | | KCl | | CsCl | | | NaBr | |
|------|--------|----------------|--------|----------------|------------------|--------|----------------|-------|----------------|------------------|--------|----------------|
| | E | γ_{\pm} | E | γ_{\pm} | γ_{\pm}^a | E | γ_{\pm} | E | γ_{\pm} | γ_{\pm}^a | E | γ_{\pm} |
| 0.01 | 3.3629 | 0.951 | 3.0455 | 0.958 | 0.964 | 3.2598 | 0.962 | 3.225 | 0.967 | 0.969 | 2.9517 | 0.969 |
| 0.02 | 3.3288 | 0.923 | 3.0110 | 0.938 | 0.963 | 3.2251 | 0.945 | 3.190 | 0.954 | 0.963 | 2.9167 | 0.958 |
| 0.03 | 3.3094 | 0.898 | 2.9911 | 0.922 | | 3.2051 | 0.929 | 3.170 | 0.945 | | 2.8963 | 0.951 |
| 0.04 | 3.2959 | 0.876 | 2.9772 | 0.906 | | 3.1910 | 0.921 | 3.156 | 0.936 | | 2.8819 | 0.943 |
| 0.05 | 3.2857 | 0.854 | 2.9666 | 0.890 | 0.950 | 3.1802 | 0.906 | 3.145 | 0.929 | 0.952 | 2.8707 | 0.938 |
| 0.06 | 3.2776 | 0.834 | 2.9580 | 0.878 | | 3.1715 | 0.895 | 3.136 | 0.922 | 0.944 | 2.8616 | 0.934 |
| 0.07 | 3.2709 | 0.815 | 2.9498 | 0.883 | 0.945 | 3.1642 | 0.885 | 3.128 | 0.916 | 0.940 | 2.8540 | 0.929 |
| 0.08 | 3.2652 | 0.796 | 2.9430 | 0.881 | | | | | | | 2.8473 | 0.925 |
| 0.09 | 3.2602 | 0.780 | 2.9369 | 0.883 | | | | | | | | |
| 0.10 | | | 2.9313 | 0.885 | 0.940 | | | | | | | |

^a Literature values (see ref 8).

$$E = \frac{RT}{n\mathcal{F}} \ln \frac{a_1}{a_2} = \frac{RT}{n\mathcal{F}} \ln \frac{m_1}{m_2} + \frac{RT}{n\mathcal{F}} \ln \frac{\gamma_{\pm,1}}{\gamma_{\pm,2}} \quad (8)$$

where the subscripts refer to the respective cell solutions. Results of such measurements for cell B are listed in Table IV. The first column gives the potential, E , for the cell and the remaining columns give the molalities, m_1 and m_2 , and activity coefficients, $\gamma_{\pm,1}$ and $\gamma_{\pm,2}$ of the reference and test solutions, respectively.

A comparison of the activity coefficients obtained from this work and those in the literature shows the present data to have somewhat lower values than those previously reported.⁵ In view of the uncertainties in amalgam cell measurements in nonaqueous solutions, the disagreement is not large.

Table IV: Electromotive Force Data and Activity Coefficients for the Cell, $\text{Ag}_2\text{AgCl}|\text{KCl}(m_1)|\text{K}_2\text{Hg}|\text{KCl}(m_2)|\text{AgCl};\text{Ag}$

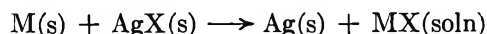
| E | m_1 | $\gamma_{\pm,1}$ | m_2 | $\gamma_{\pm,2}$ |
|----------|---------|------------------|---------|------------------|
| 0.01469 | 0.05570 | 0.899 | 0.04096 | 0.919 |
| -0.02525 | 0.05585 | 0.899 | 0.09247 | 0.888 |
| -0.05172 | 0.05593 | 0.899 | 0.1532 | 0.898 |
| -0.07341 | 0.05526 | 0.899 | 0.2333 | 0.889 |

In the first paper of this series,⁹ the heats of solution for sodium halide salts and lithium chloride showed limiting slopes considerably exceeding the theoretical values, suggesting ionic association for these electrolytes in anhydrous N-methylformamide. Examination of the activity coefficients of the same electrolytes leads one to the conclusion that ionic association exists to only a slight extent, if at all. This is in agreement with the conclusion drawn by Dawson and co-workers⁵ from their study of activity coefficients of HCl in N-

methylacetamide. However, if one assumes that the deviations in activity coefficients from the Debye-Hückel theory are primarily caused by a slight amount of ionic association, then because of the decreasing order in activity coefficients as one goes from CsCl LiCl, one would expect that ionic association would be greatest for LiCl and smallest for CsCl. The possibility of ionic association in this solvent is being investigated further and will be reported in a future communication.

Standard Free Energies and Entropies of the Solvated Electrolytes

The general reaction for cell C is



and the corresponding standard free-energy change for this reaction is

$$\Delta F^\circ = \Delta F^\circ_{\text{MX}(\text{soln})} + \Delta F^\circ_{\text{Ag}(s)} - \Delta F^\circ_{\text{M}(s)} - \Delta F^\circ_{\text{AgX}(s)} = -n\mathcal{F}E^\circ$$

Table V: Standard Free Energies and Heats of Formation and Partial Molal Entropies of Alkali Metal Halides in N-Methylformamide

| Salt | ΔF_f° , kcal/mole | ΔH_f° , kcal/mole ^a | S° , eu |
|------|--------------------------------|---|---------------------|
| LiCl | -98.4 | (-110.8) ^b | (-8.7) ^b |
| NaCl | -90.96 | -99.51 | 10.3 |
| KCl | -95.89 | -103.86 | 15.1 |
| CsCl | -95.11 | -102.7 | 21.3 |
| NaBr | -85.5 | -90.40 | 13.8 |

^a From heat of solution data of ref 9 and heats of formation of crystalline salts from ref 26. ^b Estimated.

The standard free energy of formation of a solvated salt MX is then given by

$$\Delta F^\circ_{MX(\text{soln})} = \Delta F^\circ_{AgX(s)} - n\bar{S}E^\circ$$

Values for the standard free energies of formation have been calculated for the corresponding solvated salts and are listed in Table V. The standard free energies of formation for the silver halides were obtained from Latimer.²⁶

Heats of solution for LiCl, NaCl, KCl, CsCl, and NaBr previously reported,⁹ when combined with the heats of formation of the crystalline salts²⁶ and free-

energy data obtained in this work, give the standard partial molal entropies for the corresponding salts. These entropies are also listed in Table V. The entropy given for LiCl is in considerable doubt since the heat of solution used in its evaluation is only an estimate.

Acknowledgment. The authors are grateful to the U. S. Atomic Energy Commission, which supported this work through Contract AT-(30-1)-3019.

(26) W. M. Latimer, "The Oxidation States of the Elements and their Potentials in Aqueous Solutions," 2nd ed, Prentice-Hall Inc., New York, N. Y., 1959.

Transference Numbers and Ionic Conductances in Formamide at 25°¹

by J. M. Notley and M. Spiro

Department of Chemistry, Imperial College of Science and Technology, London S.W.7, England
(Received October 27, 1965)

The cation and anion constituent transference numbers of potassium chloride were measured at 25° at five concentrations from 0.01 to 0.1 *N* by the direct moving-boundary method, using as solvent formamide specially freed from ionic impurities. The addition of water had little effect on the results. The limiting transference numbers were combined with equivalent conductances from the literature to give individual ionic conductances in formamide. Ionic solvation numbers were calculated from them by means of the Robinson and Stokes modification of Stokes' law. The conductances and viscosities of 24 uni-univalent salts in formamide, measured by Davis, *et al.*, were reexamined so as to give limiting conductances and viscosity B_η coefficients. The concentration dependence of conductance in formamide was found to be strongly affected by the viscosity correction.

Introduction

To attain a better understanding of ion-solvent interaction, we need accurate data on the properties of electrolytes at infinite dilution and, if at all possible, on the properties of single ions because cation-solvent and anion-solvent interactions are different. For most properties of electrolytes, the fraction to be attributed to the individual ions is uncertain except in the case of conductance where an unambiguous assignment can be made by means of transference numbers. Un-

fortunately, although there are accurate conductance data for dozens of nonaqueous solvents, transference numbers of comparable accuracy exist only for a few: methanol² (dielectric constant, ϵ 31.5), ethanol³ (ϵ

(1) Presented in Sept 1965 at the 16th Meeting of C.I.T.C.E. in Budapest, Hungary.

(2) J. A. Davies, R. L. Kay, and A. R. Gordon, *J. Chem. Phys.*, **19**, 749 (1951); J. Smisko and L. R. Dawson, *J. Phys. Chem.*, **59**, 84 (1955).

(3) J. R. Graham and A. R. Gordon, *J. Am. Chem. Soc.*, **79**, 2350 (1957); J. Smisko and L. R. Dawson, *J. Phys. Chem.*, **59**, 84 (1955).

24.3), dimethylformamide⁴ (ϵ 36.7), and nitromethane⁵ (ϵ 36.7) at 25° and liquid ammonia ($\epsilon \approx 22$) at much lower temperatures.⁶ Since no accurate transference numbers were available for solvents of dielectric constant higher than that of water, we set out to determine them in formamide at 25° (ϵ 109.5,⁷ viscosity η 3.30 cp⁸).

When this project was planned, the transference numbers of KCl in formamide were known to a few units per cent from emf⁹ and Hittorf¹⁰ work and from reasoning based on Stokes' law.¹¹ During the course of our research a further Hittorf study of the same system was published.^{12, 12a} We have instead used the much more accurate moving-boundary method.

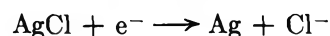
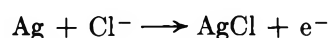
Experimental Section

All runs were carried out in an oil-filled glass-sided thermostat at $25 \pm 0.01^\circ$ kept constant to $\pm 0.002^\circ$. The general transference technique is described by Spiro,¹³ the optical assembly being illustrated in his Figure 12 and the rising boundary cell in his Figure 15. However, a new current regulator was designed and the circuit is shown in Figure 1. The EL 360 pentode was chosen because it can stand applied potentials as large as 4500 v; most other valves are not recommended by their manufacturers for use above 550 v. The current through the EL 360 is controlled by the voltage across resistance B amplified by the EF 91 valve. The potential source consisted of 20 120-v dry batteries. Currents from 30 μ a to 2.5 ma could be selected by setting the range switch at A in the appropriate position and by the proper choice of the grid bias potential on the EF 91 valve. The impedance of the regulator ranged from 150 to 1000 megohms, so that a change of 1 megohm in the resistance of the cell during a run altered the current by only 0.1–0.7%. During an experiment the current was determined at regular time intervals by measuring the potential drop across a standard 1000-ohm resistor in series with the cell.

A series of preliminary experiments was carried out to find suitable following solutions for a leading solution of KCl in formamide. Autogenic experiments, attractive because of their inherent simplicity, failed to throw up a viable system: cadmium, silver, and thallium anodes were ruled out by virtue of the known insolubility of their chloride salts, mercury became covered with a gray deposit and gave no visible boundary, zinc produced a visible but curved boundary and copper, which formed a curious thick boundary, was unsuitable because it dissolves spontaneously in formamide containing oxygen and because its electrode reaction produces a mixture of Cu(I) and Cu(II).¹⁴ Sheared boundaries were more successful. Visible

cation boundaries were seen between KCl and LiCl (falling boundary) or PbCl₂ (rising), but not between KCl and NaCl (falling) or BaCl₂ (rising). Anion boundaries appeared when the following salt was potassium picrate (KPic) (rising) or potassium benzene sulfonate (rising) though not when it was HCOOK (rising or falling), CH₃COOK (rising or falling), or KI (rising). Potassium iodate reacted with the solvent. The cation and anion boundaries selected for quantitative study were KCl \leftarrow PbCl₂ and KCl \leftarrow KPic; they were easy to see even at very low currents.

Of the several possible electrodes investigated, those of the Cd|Cd(OOCCH₃)₂ type, while nongassing, were rejected because of slow volume changes caused by diffusion.¹⁵ Platinum anodes at low current densities did not gas either, but there is some difference of opinion in the literature¹⁶ as to the product formed and this affects the calculation of the volume correction. Silver was finally chosen as the nongassing anode and silver chloride (made by dipping a platinum electrode repeatedly into the molten salt) as the nongassing cathode. Experiments confirmed that the expected electrode reactions



proceeded quantitatively in formamide solutions.

-
- (4) J. E. Prue and P. J. Sherrington, *Trans. Faraday Soc.*, **57**, 1795 (1961).
- (5) S. Blum and H. I. Schiff, *J. Phys. Chem.*, **67**, 1220 (1963).
- (6) E. C. Franklin and H. F. Cady, *J. Am. Chem. Soc.*, **26**, 499 (1904); J. L. Dye, R. F. Sankuer, and G. E. Smith, *ibid.*, **82**, 4797 (1960); **83**, 5047 (1961); J. B. Gill, *Chem. Commun.* (London), **7** (1965).
- (7) G. R. Leader, *J. Am. Chem. Soc.*, **73**, 856 (1951).
- (8) G. F. Smith, *J. Chem. Soc.*, 3257 (1931).
- (9) T. Pavlopoulos and H. Strehlow, *Z. Physik. Chem.* (Frankfurt), **2**, 89 (1954).
- (10) L. R. Dawson and C. Berger, *J. Am. Chem. Soc.*, **79**, 4269 (1957); C. Berger, Ph.D. Dissertation, University of Kentucky, 1952.
- (11) L. R. Dawson, E. D. Wilhoit, and P. G. Sears, *J. Am. Chem. Soc.*, **79**, 5906 (1957).
- (12) R. Gopal and O. N. Bhatnagar, *J. Phys. Chem.*, **68**, 3892 (1964).
- (12a) NOTE ADDED IN PROOF. G. P. Johari and P. H. Tewari, *J. Phys. Chem.*, **70**, 197 (1966), published a third set of Hittorf results while the present paper was in press.
- (13) M. Spiro, "Determination of Transference Numbers," Chapter 46 in A. Weissberger, Ed., "Physical Methods of Organic Chemistry," 3rd ed., Interscience Publishers, New York, N. Y., 1960.
- (14) H. Röhler, *Z. Elektrochem.*, **16**, 419 (1910).
- (15) M. Selvaratnam and M. Spiro, *Trans. Faraday Soc.*, **61**, 360 (1965).
- (16) K. Schaum and H. Schneider, *Ber.*, **56**, 2460 (1923); S. Tajima and N. Baba, *Electrochim. Acta*, **7**, 355 (1962); D. E. Couch, *ibid.*, **9**, 327 (1964).

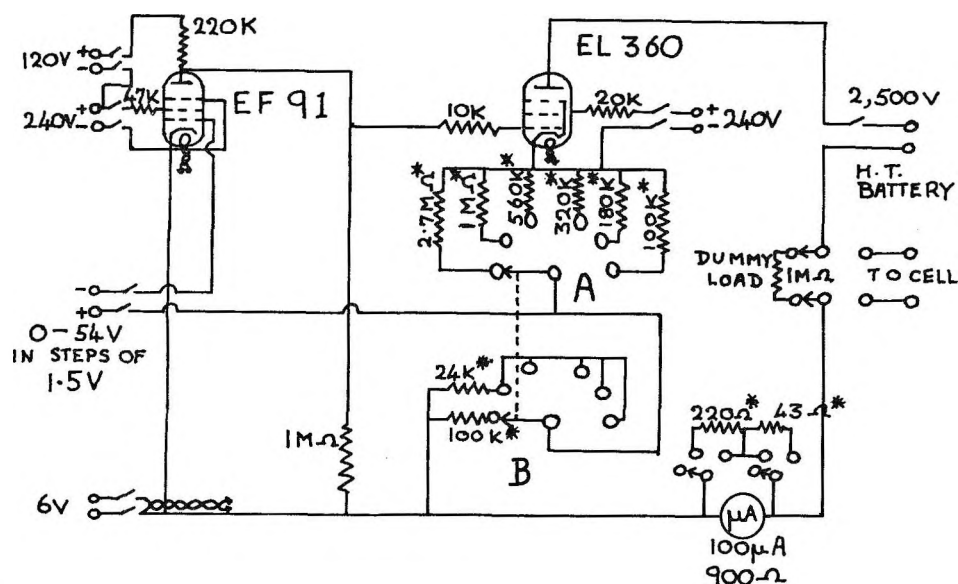


Figure 1. Circuit diagram of electronic current regulator. Resistances marked with an asterisk are high-stability ones with a 1% tolerance, and k stands for kilohms.

Thus¹³ the corrected transference numbers at any normality, c_{KCl} , are given by the equations

$$T_{\text{K}}^{\text{KCl}} = T_{\text{K}}^{\text{KCl}}(\text{obsd}) - c_{\text{KCl}}\Delta V$$

(anode or cathode closed)

$$T_{\text{Cl}}^{\text{KCl}} = T_{\text{Cl}}^{\text{KCl}}(\text{obsd}) + c_{\text{KCl}}\Delta V \text{ (anode closed)}$$

where

$$\Delta V = V_{\text{AgCl}} - V_{\text{Ag}} - T_{\text{K}}^{\text{KCl}}\bar{V}_{\text{KCl}}^{\text{KCl}}$$

From molal and partial molal data in the literature^{17,18} and the average transference number found in this paper, we obtain

$$\Delta V = +0.0019 \text{ l. } f^{-1}$$

BDH AnalaR KCl was dried at 160°; a sample showed only a trace (ca. 10⁻³%) of acidity. Lead chloride was prepared by mixing solutions of AnalaR lead nitrate and hydrochloric acid, washed, dried at 110° and then more fully at 250° under a stream of dry HCl gas, and finally allowed to cool under dry nitrogen. Potassium picrate was formed by adding a solution of AnalaR potassium hydroxide to a hot solution of AnalaR picric acid; the solid which appeared on cooling was twice recrystallized from water and dried at 120°. The salts dissolved rapidly in formamide if a shaking machine was used, although lead chloride had first to be shaken to a dry powder before the solvent was added. The solutions were made up at 25° in calibrated Pyrex volumetric flasks and transferred to the cell by pressure of dry nitrogen.

BASF formamide (fp 2.25°) was dried with Union

Carbide 3A Molecular Sieves and deionized by means of a mixed bed of Amberlite ion-exchange resins loaded, respectively, with H⁺ and HCONH⁻ ions. Details of the purification process are given elsewhere.¹⁹ The purified solvent, fp 2.3°, could be tapped off in liter quantities and had a water content (160 ppm or 0.009 M) and specific conductance ($2 \times 10^{-7} \text{ ohm}^{-1} \text{ cm}^{-1}$) lower than any in the literature. The specific conductance of the solvent slowly increased on standing and it was therefore measured, whenever a run was carried out, on a sample of the same batch of formamide that had been used to make up the KCl solution. This was the value used to calculate the solvent correction which was less than 0.25% for the most dilute solution.

Results

The results of 40 transference runs are summarized in Table I. At each concentration of KCl, and for each type of boundary, the transference numbers were found to be independent of current when the latter was changed by a factor of 2 and independent also of a variation of at least 15% in the normality of the following electrolyte. Further purification of the solvent by triply recrystallizing it had no effect either. The average deviation from the mean transference number was 0.0004. The sum of the cation and anion transference numbers is seen to be close to unity in all

(17) L. G. Longworth, *J. Am. Chem. Soc.*, **54**, 2741 (1932).

(18) R. Gopal and R. K. Srivastava, *J. Phys. Chem.*, **66**, 2704 (1962).

(19) J. M. Notley and M. Spiro, *J. Chem. Soc.*, **B**, 362 (1966).

Table I: Summary of Transference Measurements on KCl in Formamide at 25°

| cKCl | 10 ³ cPbCl ₂ | Current, ma | T _K ^a | 10 ³ cKPic | Current, ma | T _{Cl} ^a | T _K + T _{Cl} | "Best" T _K |
|---------|------------------------------------|-------------|-----------------------------|-----------------------|-------------|------------------------------|----------------------------------|-----------------------|
| 0.01017 | 7.2-10.0 | 0.08-0.15 | 0.4242 | 7.7-10.0 | 0.05-0.11 | 0.5768 | 1.0010 | 0.4238 |
| 0.02008 | 17.0-20.0 | 0.15-0.29 | 0.4233 | 14.9-17.8 | 0.11-0.21 | 0.5771 | 1.0004 | 0.4231 |
| 0.05002 | 43-51 | 0.38-0.75 | 0.4216 | 35-45 | 0.25-0.54 | 0.5782 | 0.9998 | 0.4217 |
| 0.08027 | 47-65 | 0.64-1.22 | 0.4204 | 43-70 | 0.48-0.93 | 0.5792 | 0.9996 | 0.4206 |
| 0.1005 | 79-95 | 0.75-1.50 | 0.4201 ^b | 56-92 | 0.50-1.06 | 0.5795 | 0.9996 | 0.4203 |

^a With volume and solvent corrections applied. ^b A run carried out with triply recrystallized formamide of fp 2.4° gave 0.4203.

cases, an important check on the reliability of the measurements, and the "best" values in the last column were obtained by dividing the mean cation transference number by ($T_K + T_{Cl}$). It is these values which are used in the calculations following.

The figures in Table II demonstrate that the addition of small quantities of water was without significant effect on the transference numbers. This is consistent with earlier reports^{9,20} that the presence of up to 1% of water (0.6 *M*) had no appreciable effect on conductances and emf's in formamide. It seems likely, therefore, that further drying of the solvent used in the present work would not have altered the results listed in Table I.

Table II: Effect of the Addition of Water

| cKCl | Water content, <i>M</i> | T _K | T _{Cl} |
|---------|-------------------------|----------------|-----------------|
| 0.01017 | 0.008 | | 0.5768 |
| | 0.053 | | 0.5767 |
| | 0.10 | | 0.5779 |
| 0.1002 | 0.010 | 0.4201 | 0.5795 |
| | 0.13 | 0.4203 | 0.5799 |

Discussion

Comparison with Previous Results. The data are set out in Table III, and the apparently large disagreement between different determinations requires some comment.

The only indirect method is that based on the assumption that the ions Me_3PhN^+ and $PhSO_3^-$ are equimobile in formamide. There is no independent evidence to support this assumption; in water the limiting ionic conductances of the two ions^{21,22} differ by 7% and, since one ion has a large polar group exposed to solvation influences while the other has not, no conclusions can be drawn as to their relative mobilities in other media. There is some hope that the re-

cently synthesized salt $(i-Am)_4N^+B(i-Am)_4^-$ will prove to be more equimobile than others yet tried²³ but its solubility in formamide is unknown.

The rather high transference number derived from cells with transference is probably accounted for by the fact that results obtained by this method are very sensitive to small errors in emf.¹³ The Hittorf method, too, based as it is on concentration differences, makes precision difficult. An uncertainty of as little as 0.2% in the concentrations of the electrode and middle compartments leads to an uncertainty of 4% in the final transference number if the concentration at each end of the cell changes by one-tenth during electrolysis. Dawson and Berger,¹⁰ who encountered some problems with potentiometric titrations for chloride in the presence of formamide, found that the cation transference numbers calculated from the anolyte and catholyte portions differed on average by 7%. Gopal and Bhatnagar¹² measured the composition of the anode chamber only and determined the potassium content gravimetrically as the dipotassium sodium cobaltinitrite, a method which has not been recommended²⁴ for work of high accuracy in the case of aqueous solutions. Both groups of Hittorf workers analyzed only one middle compartment and appear not to have varied the current or time of electrolysis for any given solution. Equal mixing between both electrode compartments and the middle section, brought about by diffusion, convection, or vibration, would therefore have remained undetected and led to low results. When all these points are borne in mind, the results in Table III are seen not to differ by more than can reasonably be attributed to experimental error.

(20) F. H. Verhoek, *J. Am. Chem. Soc.*, **58**, 2577 (1936).

(21) G. H. Jeffery and A. I. Vogel, *J. Chem. Soc.*, 400 (1932).

(22) M. J. McDowell and C. A. Kraus, *J. Am. Chem. Soc.*, **73**, 2170 (1951); P. G. Sears, E. D. Wilhoit, and L. R. Dawson, *J. Chem. Phys.*, **23**, 1274 (1955).

(23) J. F. Coetzee and G. P. Cunningham, *J. Am. Chem. Soc.*, **86**, 3403 (1964); **87**, 2529 (1965).

(24) R. Belcher and A. J. Nutten, *Anal. Chim. Acta*, **4**, 475 (1950).

Table III: Comparison of Transference Numbers of KCl in Formamide at 25° Obtained by Different Methods

| Method | Concn range, <i>M</i> | Results | Ref |
|---|--------------------------|--------------------------------------|------------|
| Conductance of Me ₃ PhN ⁺ +PhSO ₃ ⁻ | | $T_{K^{\circ}} = 0.415$ | 11 |
| Cell with transference | Not given | $T_{K^{\circ}} = 0.45$ | 9 |
| Hittorf | 0.20–0.59 | $T_{K^{\circ}} = 0.406, b^a = 0.072$ | 10 |
| Hittorf | 0.1–0.5 | $T_{K^{\circ}} = 0.419, b = 0.014$ | 12 |
| Hittorf | 0.03–0.14 | $T_{K^{\circ}} = 0.409, b = 0.013$ | 12a |
| Moving boundary | 0.01–0.1 | $T_{K^{\circ}} = 0.427, b = 0.054$ | This paper |

^a See eq 1.

Variation with Concentration. The "best" potassium transference numbers in Table I, when plotted against \sqrt{c} , exhibit a similar anabatic deviation from the Debye-Hückel-Onsager (DHO) limiting slope as do the cation transference numbers of NaCl and LiCl in water¹⁷ (those of KCl in water form a poor basis for comparison because they are so close to 0.5). Again, as for salts in aqueous solution, a plot against concentration of the Longworth¹⁷ function $T_{K^{\circ}}$ is a straight line, *i.e.*

$$T_{K^{\circ}} = \frac{T_{K^{\circ}}\Lambda' + \beta\sqrt{c}}{\Lambda' + 2\beta\sqrt{c}} = T_{K^{\circ}} + bc \quad (1)$$

where

$$\Lambda' = \Lambda^{\circ} - (\alpha\Lambda^{\circ} + 2\beta)\sqrt{c}$$

and where c stands for normality, Λ for equivalent conductance of the electrolyte, superscript $^{\circ}$ for infinite dilution, and α and β for the relaxation and electrophoretic DHO coefficients. In formamide at 25° these equal 0.1391 and 6.91, respectively. The plot of $T_{K^{\circ}}$ vs. c is shown in Figure 2. The results can also be fitted by the Stokes transference equation,²⁵ although this requires an improbably large distance of closest approach of 8 Å. A smaller distance of 6 Å can be accommodated if uncertainties of 0.1% are assigned to each transference number.

Conductance and Viscosity of Electrolytes. Before deriving single ionic conductances by combining the limiting transference number with limiting equivalent conductances, we need to examine the latter critically. There exist three main sets of conductance data for 1:1 electrolytes in formamide: those of Dawson, *et al.*,^{11,26} of Tewari and Johari,²⁷ and of Davis, *et al.*^{28,29} The last group measured the conductances of over 30 electrolytes in formamide and it was thought worthwhile to treat their results for simple 1:1 salts by present day methods. Since the equivalent conductances of Davis, Putnam, and Jones²⁸ are in reciprocal Siemens units³⁰ (Λ of 0.02 *N* aqueous KCl taken as

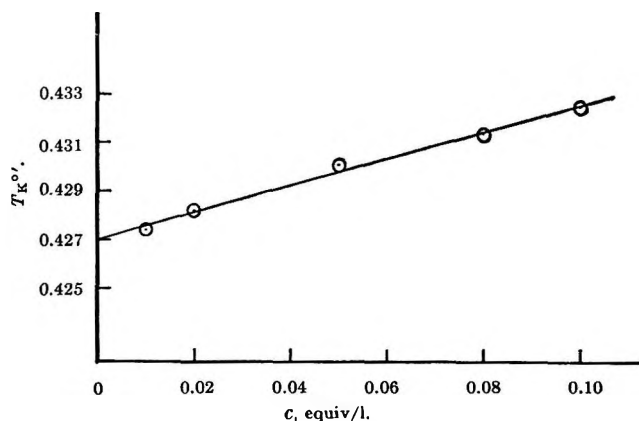


Figure 2. Plot of Longworth function $T_{K^{\circ}}$ vs. normality of KCl.

129.7 at 25°) and those of Davis and Johnson²⁹ in (old) reciprocal ohms (Λ of the same solution equals 137.9), both sets were converted to the Jones and Bradshaw standard.³¹ The figures so obtained have been extrapolated by the Shedlovsky equation³²

$$\Lambda^{\circ} = \frac{\Lambda + 2\beta\sqrt{c}}{1 - \alpha\sqrt{c}} = \Lambda^{\circ} + B_{\Lambda}c \quad (2)$$

In drawing the lines greater weight was given to the points at 0.25, 0.1, 0.02, and 0.01 *N* and lesser weight to those at 0.005 *N* and below where the solvent cor-

(25) R. H. Stokes, *J. Am. Chem. Soc.*, **76**, 1988 (1954).

(26) L. R. Dawson, T. M. Newell, and W. J. McCreary, *ibid.*, **76**, 6024 (1954).

(27) P. H. Tewari and G. P. Johari, *J. Phys. Chem.*, **67**, 512 (1963).

(28) P. B. Davis, W. S. Putnam, and H. C. Jones, *J. Franklin Inst.*, **180**, 567 (1915).

(29) P. B. Davis and H. I. Johnson, Carnegie Institution of Washington Publication No. 260, Carnegie Institution of Washington, Washington, D. C., 1918, p 71.

(30) H. C. Jones, *et al.*, Carnegie Institution of Washington Publication No. 210, Carnegie Institution of Washington, Washington, D. C., 1915, pp 51, 102.

(31) G. Jones and B. C. Bradshaw, *J. Am. Chem. Soc.*, **55**, 1780 (1933).

(32) T. Shedlovsky, *ibid.*, **54**, 1405 (1932).

Table IV: Intercepts and Slopes of Shedlovsky Plots for Some Electrolytes in Formamide at 25°, from the Data of Davis, *et al.*^{28,29}

| Salt | Λ° | B_A | B_η | $B_A(\text{cor})$ | Lit. comparison | | |
|---|-----------------|-------|----------|-------------------|-----------------|-------|-----|
| | | | | | Λ° | B_A | Ref |
| LiNO ₃ | 26.2 | 10 | 0.47 | 22 | 25.5 | | 27 |
| LiOOCH ²⁹ | 24.0 | -11 | 0.49 | 1 | | | |
| NaBr | 27.4 | 3 | 0.59 | 19 | | | |
| NaI | 26.4 | 10 | 0.38 | 20 | 26.74 | 14.3 | 11 |
| NaNO ₃ ²⁹ | 27.7 | 9 | 0.47 | 22 | 27.5 | | 27 |
| NaOOCH ²⁹ | 25.3 | 0 | 0.53 | 13 | | | |
| NaOOCPh ²⁹ | 19.9 | 4 | 0.85 | 21 | | | |
| NaO ₃ SPh ²⁹ | 20.3 | 11 | 0.69 | 25 | 20.46 | 8.6 | 11 |
| KCl | 29.4 | 9 | 0.38 | 20 | 29.85 | 8.8 | 11 |
| KI | 29.1 | 12 | 0.25 | 19 | 29.31 | 14.8 | 11 |
| KSCN | 29.9 | 14 | 0.25 | 21 | | | |
| KNO ₃ ²⁹ | 29.9 | 3 | 0.4 | 15 | 30.1 | | 27 |
| RbCl | 29.8 | 10 | 0.41 | 22 | | | |
| RbBr | 30.2 | 7 | 0.3 | 16 | | | |
| RbI | 29.3 | 15 | 0.39 | 26 | | | |
| RbNO ₃ | 30.1 | 8 | 0.23 | 15 | | | |
| CsCl | 30.5 | 8 | 0.41 | 21 | | | |
| CsNO ₃ | 31.0 | 6 | 0.30 | 15 | | | |
| NH ₄ Br | 32.2 | 10 | 0.23 | 17 | 31.7 | | 27 |
| NH ₄ I | 31.9 | 15 | 0.3 | 25 | | | |
| NH ₄ NO ₃ ²⁹ | 33.4 | 4 | 0.15 | 9 | 33.7 | | 27 |
| NH ₄ OOCH ²⁹ | 31.1 | -12 | 0.25 | -4 | | | |
| Me ₄ NCl | 29.6 | 12 | 0.3 | 21 | | | |
| Et ₄ NI | 26.6 | 6 | 0.24 | 12 | | | |

rection was large. The Λ° intercepts are usually uncertain by a few tenths of a unit and the slopes by 1-4 units. The results are summarized in Table IV in which they are also compared with those of later researches wherever overlap occurs. The agreement is quite fair, the Λ° values of Davis, *et al.*, being an average 0.3 unit less than those of Dawson and 0.2 unit greater than those of Tewari and Johari. By implication, therefore, the more modern values differ more from each other than they do from those obtained 50 years ago, and this may be related to the fact that the specific conductance of the formamide employed has not been much better, of the order of 10^{-5} ohm⁻¹ cm⁻¹. We believe that it can be drastically reduced only by ion exchange (as in the present paper) or by some other technique such as zone refining.

The empirical Shedlovsky slopes in Table IV, and those published elsewhere,¹¹ are unexpectedly low. If we assume that to a first approximation the conductance of a completely dissociated electrolyte follows the Robinson and Stokes equation³³

$$\Lambda = \Lambda^\circ - (\alpha\Lambda^\circ + 2\beta)\sqrt{c}/(1 + Ba\sqrt{c}) \quad (3)$$

then the slope B_A should equal $(\alpha\Lambda^\circ + 2\beta)Ba$. Thus, since B in formamide is 0.2783, the distance a of closest approach corresponding to the average positive Shed-

lovsky slope of 9 is only 1.8 Å, less than the sums of the crystal radii. The reason lies in the neglect of the viscosity correction, for the equivalent conductances in (2) should be replaced by^{34,35}

$$\Lambda(1 + B_\eta c)$$

where B_η is given by the Jones and Dole equation^{35,36}

$$\eta = \eta^\circ(1 + A\sqrt{c} + B_\eta c) \quad (4)$$

Here η is the viscosity of the solution, η° that of the solvent, and A is the Falkenhagen interionic coefficient.

Davies, *et al.*,^{28,29} have measured the viscosities of the electrolyte solutions listed in Table IV and we have calculated the B_η coefficients from their data at 0.1 and 0.25 *N* using eq 4. The Falkenhagen A parameter was small and was evaluated by means of the theoretical equation³⁶ and the ionic conductances in Table

(33) R. A. Robinson and R. H. Stokes, *J. Am. Chem. Soc.*, **76**, 1991 (1954).

(34) R. M. Fuoss and F. Accascina, "Electrolytic Conductance," Interscience Publishers, Inc., New York, N. Y., 1959, Chapter XV.

(35) R. H. Stokes and R. Mills, "Viscosity of Electrolytes and Related Properties," Pergamon Press Ltd., Oxford, 1965, Chapters 4-6.

(36) H. S. Harned and B. B. Owen, "The Physical Chemistry of Electrolytic Solutions," 3rd ed, Reinhold Publishing Corp., New York, N. Y., 1958, pp 236-242.

VI. The results are given in column 4 of Table IV; they are of some interest in the absence of much information on B_η coefficients in nonaqueous solvents.³⁶ That their accuracy is not very high can be seen by inspection of the original viscosity data, by the fact that the viscosity of the samples of solvent formamide employed with different solutes ranged from 3.194 to 3.338 cp, and by the absence of any pronounced tendency in the B_η values toward additivity. In spite of this, the ionic B_η coefficients in Table V reproduce the observed values of the salts as a whole with a mean deviation of 0.04. The exact choice of subdivision into the ionic contributions is, of course, partly subjective and may require amendment when more information becomes available. The results are consistent with the concept of greater structure making (greater solvation) by the smaller anions and cations. The figures for the tetraalkylammonium ions are curious: in aqueous solution B_η is 0.12 and 0.38 for Me_4N^+ and Et_4N^+ , respectively,³⁵ and the anomalously low value for Et_4N^+ in formamide would, if it is not due to experimental error, lead one to postulate structure breaking. There are no negative values, as there are in water, to suggest this effect for other ions.

Table V: Ionic B_η Coefficients in Formamide at 25°

| Cation | B_η | Anion | B_η |
|-------------------------|----------|-------------------|----------|
| Li^+ | 0.34 | Cl^- | 0.20 |
| Na^+ | 0.36 | Br^- | 0.15 |
| K^+ | 0.18 | I^- | 0.11 |
| Rb^+ | 0.18 | SCN^- | 0.07 |
| Cs^+ | 0.21 | NO_3^- | 0.10 |
| NH_4^+ | 0.12 | HCOO^- | 0.15 |
| Me_3N^+ | 0.1 | PhCOO^- | 0.49 |
| Et_4N^+ | 0.13 | PhSO_3^- | 0.33 |

Returning to the problem of conductance, the incorporation of the viscosity correction into the Shedlovsky equation (2) introduces an additional term which changes the slope from B_A to

$$B_A(\text{cor}) = B_A + \Lambda^\circ B_\eta$$

The average numerical slope (excluding two abnormally low values) is thereby increased to 19 (Table IV) with a corresponding increase in the distance of closest approach to 3.8 Å, a much more reasonable figure than before. This is useful evidence in favor of including a viscosity term in the conductance equation; in aqueous solutions its effect is only of the order of 10% and therefore marginal while in many other solvents the B_η coefficients are not known.

Some of the Shedlovsky slopes in Table IV and elsewhere¹¹ are very small or even negative. Although raised by the viscosity correction, they do not become large enough to yield reasonable distances of closest approach and it seems likely that in these instances there is some ion pairing in solution. It is easily shown that, to a first approximation, its effect on the Shedlovsky slope B_A is to decrease it by an amount $\Lambda^\circ K_{\text{as}}$, where K_{as} is the association constant. It follows that lithium and ammonium formates in formamide possess association constants of the order of unity, and so does Bu_4NI .¹¹ This surprising result—in a solvent of dielectric constant 109.5—is supported by the signs of slight association shown by Et_4NI in Table IV and fits in with similar observations reported for tetraalkylammonium halides in other hydrogen-bonded solvents.³⁷

Single Ionic Conductances. The limiting cation transference number of KCl obtained from Figure 2 (0.427), together with the limiting equivalent conductances in the literature^{11,27} and in Table IV, allow one to draw up a set of individual ionic conductances. These are given in Table VI, in square centimeters per international ohm per equivalent. The only conductances that do not fit are those of NH_4Br and NH_4NO_3 or, to put it another way, the ionic conductance of the ammonium ion varies according to the salt chosen.

Table VI: Limiting Ionic Equivalent Conductances in Formamide at 25°

| Cation | λ_+° | Anion | λ_-° |
|---------------------------|-------------------|---------------------------|-------------------|
| Li^+ | 8.5 | Cl^- | 17.1 |
| Na^+ | 10.1 | Br^- | 17.2 |
| K^+ | 12.7 | I^- | 16.6 |
| Rb^+ | 12.8 | SCN^- | 17.2 |
| Cs^+ | 13.5 | NO_3^- | 17.4 |
| NH_4^+ | 15.6 | HCOO^- | 15.3 |
| Me_3N^+ | 12.5 | CH_3COO^- | 11.9 |
| Et_4N^+ | 10.0 | PhCOO^- | 9.8 |
| Bu_4N^+ | 6.8 | PhSO_3^- | 10.4 |
| Me_3PhN^+ | 10.7 | | |
| H^+ | 10.8 ^a | | |
| Tl^+ | 15.8 | | |

^a The conductance of HCl at 25° was obtained by interpolation of the data of Dawson, Newell, and McCreary.²⁶

Only one equation exists that helps us to understand isothermal conductivities—Stokes' law

$$\lambda_\pm^\circ \eta^\circ = |z_\pm| eF / 6\pi r_s \quad (5)$$

(37) R. L. Kay and D. F. Evans, paper read at the 16th Meeting of C.I.T.C.E., Budapest, Sept 1965.

in which e is the protonic charge, F Faraday's constant, z_{\pm} the charge number, and r_s the Stokes radius of the ion. The product $\lambda_{\pm}^{\circ}\eta^{\circ}$, Walden's product, should be independent of medium for any ion large enough to be unsolvated, but Table VII shows that for the tetraalkylammonium ions it is higher in formamide than it is in water, methanol, ethanol, or nitromethane. There is a hint in the literature⁴ that in dimethyl sulfoxide, another viscous solvent, the Walden product for Bu_4N^+ may also be rather high. A blanket explanation would simply be that Stokes' law is not applicable even to ions as big as Bu_4N^+ in cases where the solvent molecule itself, or perhaps the time-averaged solvent agglomerate, is large. On the molecular scale there are at least two factors out of which other interpretations could be compounded: iceberg formation, which would reduce the Walden product for Bu_4N^+ in water and perhaps in other media or, alternatively, structure breaking, which might raise the mobility in formamide. There is just a suggestion of the latter effect in the viscosity coefficients discussed above, but clearly more and accurate data for several alkylammonium ions are required before definite conclusions can be drawn.

Table VII: Properties of Tetraalkylammonium Ions

| Ion | $\lambda^{\circ}\eta^{\circ}$ (in H_2O , | $\lambda^{\circ}\eta^{\circ}$ (in HCONH_2) | r_s | r_{cor}/r_s |
|-------------------------|---|---|-------|----------------------|
| | MeOH , EtOH , and MeNO_2) | | | |
| Me_4N^+ | 0.333-0.402 | 0.413 | 1.99 | 1.74 |
| Et_4N^+ | 0.292-0.299 | 0.330 | 2.49 | 1.61 |
| Bu_4N^+ | 0.171-0.214 | 0.224 | 3.65 | 1.35 |

In contradistinction to the large R_4N^+ ions, the alkali metal and halide ions move more slowly in formamide than would have been expected from their mobilities in water and the viscosities of the two media. However, Stokes' law is no longer valid for small ions, and Robinson and Stokes³⁸ have devised a method of allowing for this. In brief, it rests upon the assumption that tetraalkylammonium ions are unsolvated; their bare radii are taken to be the correct hydrodynamic values, r_{cor} , and a plot of r_{cor}/r_s vs. r_s is constructed. The correct radii of other ions, whose r_s values are known and that lie in the range covered by the plot, can then be read off. Figure 3 shows the graph for water given by Robinson and Stokes³⁸ and one for formamide based on the data for the Me_4N^+ , Et_4N^+ , and Bu_4N^+ ions in Table VII. Although the discussion in the previous paragraph casts some doubts

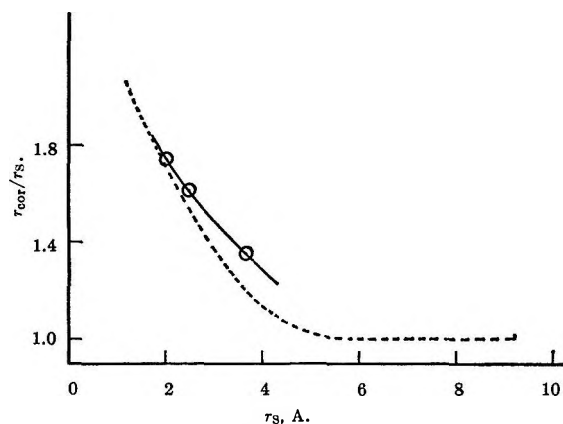


Figure 3. Correction graphs for Stokes' law. The full line is based on the data for the tetraalkylammonium ions in Table VII, the dashed curve is that given for water by Robinson and Stokes.³⁸

on the main postulate of the method, it is certainly an improvement over the direct use of Stokes' law and the formamide curve in Figure 3 was therefore used to derive the corrected radii in Table VIII. The volumes of the net solvation shells are then

$$V = \frac{4}{3}\pi(r_{\text{cor}}^3 - r_{\text{cryst}}^3)$$

and effective solvation numbers n have been calculated by dividing these volumes by the average volume of a formamide molecule in the pure solvent, 66.2 \AA^3 . This ignores any electrostrictive contraction of the solvent molecules next to the ions. The last column in Table VIII lists for comparison the corresponding hydration numbers in water. A similar calculation of solvation numbers in formamide (and other solvents) was carried out by Gopal and Husain,³⁹ who used Walden's rule to obtain the conductances of the tetraalkylammonium ions. Their graph of r_{cor}/r_s vs. r_s was therefore identical with that for water and their

Table VIII: Solvation of Ions in Formamide at 25°

| Ion | r_{cryst}^{38} | r_s | r_{cor} | n | n_{water}^{38} |
|---------------|-------------------------|-------|------------------|-----|-------------------------|
| Li^+ | 0.60 | 2.92 | 4.41 | 5.4 | 7.0 |
| Na^+ | 0.95 | 2.46 | 3.99 | 4.0 | 5.0 |
| K^+ | 1.33 | 1.96 | 3.43 | 2.5 | |
| Rb^+ | 1.48 | 1.94 | 3.40 | 2.3 | |
| Cs^+ | 1.69 | 1.84 | 3.28 | 1.9 | |
| H^+ | 0.00 | 2.30 | 3.80 | 3.5 | |

(38) R. A. Robinson and R. H. Stokes, "Electrolyte Solutions," 2nd ed, Butterworth and Co. Ltd., London, 1959, pp 120-126, 461.

(39) R. Gopal and M. M. Husain, *J. Indian Chem. Soc.*, **40**, 981 (1963).

solvation numbers were consequently smaller than those in Table VIII.

The relatively low conductances of the monoatomic ions in formamide, and their greater hydrodynamic radii, are now seen to be due to the greater size of the formamide molecules in the solvation shells, an effect which more than compensates for the decrease in solvation numbers. This latter decrease does not mean, incidentally, that formamide molecules are less strongly attached to ions than are water molecules, for there is some independent evidence to the contrary. First, it has already been pointed out that small quantities of water do not significantly alter emf's,^{9,20} conductances,²⁰ or transference numbers (Table II) in formamide, and second, salts such as CdCl₂ and CuSO₄ crystallize from water-formamide mixtures with formamide, and not water, of crystallization.⁴⁰

An ion deserving special mention is H⁺, which, as has already been pointed out elsewhere,^{26,41} shows little or no abnormal mobility in formamide. Its solvation number in Table VIII seems reasonable and solids of composition HCl·HCONH₂,⁴² HCl·2HCONH₂,⁴³ and HBr·2HCONH₂⁴⁴ have been referred to

in the literature. The ion HCONH⁻, too, appears to migrate normally.¹⁴

An important application of the ionic conductances in Table VI is in the choice of suitable electrolytes for salt bridges in emf work. The two main criteria for minimizing liquid junction potentials are equal or nearly equal conductances of anion and cation and high solubility. Sodium benzoate and sodium benzenesulfonate qualify well in terms of conductance but have solubilities of the order of 0.5 *M* only, and ammonium iodide (solubility 7 *M*⁴⁵) and ammonium formate (solubility 3 *M*) therefore seem to be better candidates for formamide solutions.

Acknowledgment.—We thank the Science Research Council for the award of a studentship to J. M. N.

(40) M. Nardelli, L. Cavalca, and L. Coghi, *Riv. Sci.*, **27**, 2144 (1957); M. Nardelli and L. Coghi, *ibid.*, **29**, 134 (1959).

(41) M. Mandel, *Discussions Faraday Soc.*, **39**, 220 (1965).

(42) P. L. Magill, *Ind. Eng. Chem.*, **26**, 611 (1934).

(43) H. H. Bosshard and H. Zollinger, *Helv. Chim. Acta*, **42**, 1659 (1959).

(44) P. Walden, *Z. Elektrochem.*, **26**, 72 (1920).

(45) R. Gopal and M. M. Husain, *J. Indian Chem. Soc.*, **40**, 272 (1963).

Condensed-Phase Behavior of the Aluminum Chloride-Zirconium

Chloride System^{1,2}

by A. J. Shor, William T. Smith, Jr., and M. A. Bredig

Reactor Chemistry and Chemistry Divisions, Oak Ridge National Laboratory, Oak Ridge, Tennessee, and the Department of Chemistry, University of Tennessee, Knoxville, Tennessee. (Received October 28, 1965)

According to thermal, differential thermal, and X-ray analysis, Al_2Cl_6 and ZrCl_4 form a simple eutectic system, without solid intermediary compounds but possibly with some limited solid solution. The composition of the eutectic at 165° is approximately 75 mole % Al_2Cl_6 . In disagreement with earlier literature data, visual observation above the liquidus showed the presence of only one liquid phase. Semiquantitative interpretation, with the use of the heats of fusion of the components, of the liquidus in terms of activities suggests that these largely molecular chlorides interact in the liquid to form mixtures of essentially un-ionized complex molecules $\text{ZrCl}_4 \cdot (\text{AlCl}_3)_n$, $n = 1, 2, 3$, and 4, with higher values of n possible at high aluminum chloride concentration.

Except for a cursory effort by Korshunov, Reznik, and Morozov,³ few data are given in the literature on the solid-liquid phase behavior of the aluminum chloride-zirconium chloride system. Information on such salt systems is especially significant as a result of increased interest in reprocessing of nuclear fuel elements containing aluminum or zirconium by methods dependent on the high relative volatility of their chloride salts. Experimental difficulties arising from high vapor pressures developed at moderate temperatures has limited the study of these systems in the past. This paper reports the solid-liquid phase diagram for the aluminum chloride-zirconium chloride system. Activities of ZrCl_4 and Al_2Cl_6 in the melts are estimated and implications in relation to ZrCl_4 - AlCl_3 complexing in liquid solution are discussed. Discrepancies in the phase diagram between this study and the results of previous investigators are ascribed principally to the disturbing effects of the extensive supercooling observed throughout the range of composition.

Experimental Section

Chemicals. Aluminum chloride was prepared from the elements, using high purity (99.99%) aluminum metal and carefully dried chlorine gas. Zirconium chloride (U. S. Industrial Chemicals Co., Reactor Grade) was purified by repeated sublimations. Melting points and freezing points obtained by thermal analy-

sis of the pure materials were 192 ± 1 and $437 \pm 1^\circ$ compared to published values of 192.6 and 438° for aluminum chloride and zirconium chloride, respectively.^{4,5} The purity of the salts was also confirmed by chemical and spectrochemical analyses. The salt mixtures were prepared in a helium atmosphere dry-box where the moisture level was maintained at or below 30 ppm by volume.

Apparatus and Procedures. Phase reaction temperatures were determined principally by differential thermal analysis. These observations were supplemented and extended by thermal analysis and visual observations of phase changes. Interaction with atmospheric moisture and oxygen and loss of salt through volatilization were prevented by sealing the mixtures in evacuated quartz tubes or nickel capsules.

(1) Research sponsored by the U. S. Atomic Energy Commission under contract with the Union Carbide Corporation.

(2) In part a revision of a thesis by A. J. S., submitted in partial fulfillment of the requirements for the degree of Master of Science, University of Tennessee, Dec 1964.

(3) B. G. Korshunov, A. M. Reznik, and I. S. Morozov, *Tr. Mosk. Inst. Tonkoi Khim. Tekhol.*, 7, 127 (1958).

(4) R. E. Kirk and D. F. Othmer, "Encyclopedia of Chemical Technology," Vol. I, The Interscience Encyclopedia, Inc., New York, N. Y., 1952.

(5) "Gmelins Handbuch der Anorganischen Chemie," 8th ed, Zirconium System No. 42, Verlag Chemie, GmbH., Weinheim, 1958, p 285.

The capsules were provided with thermocouple wells. Calibrated stainless steel sheathed chromel–alumel thermocouples were assembled in a differential-temperature network using Al_2O_3 as a reference substance. A Rubicon Type B high-precision potentiometer was employed for instrumental calibration and in direct thermal analysis measurements. High purity lead obtained from the National Bureau of Standards as well as reagent grade LiCl and NaCl was used for temperature standardization and to aid in interpretation of differential thermal analysis curves. Visual observations were made by immersing quartz capsules in a well-stirred bath of LiNO_3 – NaNO_3 – KNO_3 eutectic mixture which was heated and cooled at a rate of about $1^\circ/\text{min}$ through the temperature range of interest.

Measurements and Accuracy. Mainly heating curves were used for the estimation of both eutectic and liquidus transition temperatures. Since very marked supercooling was observed, particularly for the eutectic and the aluminum chloride liquidus transitions, heating curves were exclusively used for the aluminum-rich region. Segregation of the components on freezing led to spurious points on the subsequent heating curves. These extraneous points were eliminated by rapid cooling of the melts before the heating runs. The observations of liquidus and eutectic temperatures are considered reliable within $\pm 3^\circ$.

Results and Discussion

Both melting and freezing point observations for a series of aluminum chloride–zirconium chloride mixtures are listed in Table I, and the phase diagram derived therefrom is shown in Figure 1. Data are plotted as temperature in degrees Centigrade *vs.* mole per cent Al_2Cl_6 , aluminum chloride being known^{6,7} to exist as the dimer both in the liquid and gaseous state.

In disagreement with the phase diagram reported by Korshunov, *et al.*,³ and with a very similar diagram reported more recently for HfCl_4 – AlCl_3 by Morozov, Tverskov, and Kurapova,⁸ visual observation failed to give any evidence for the existence of equilibria between two liquid phases. The data from thermal analysis also are representative of a simple phase diagram, showing a eutectic at 165° and 75 mole % Al_2Cl_6 . In order to judge the reliability of visual observation for finding two liquids in equilibrium with each other, it is to be pointed out that, in the earlier work on aluminum halide systems with various second components,^{9–11} visual observation did furnish support for the existence of a miscibility gap derived from thermal data.

X-Ray diffraction measurements both at room and

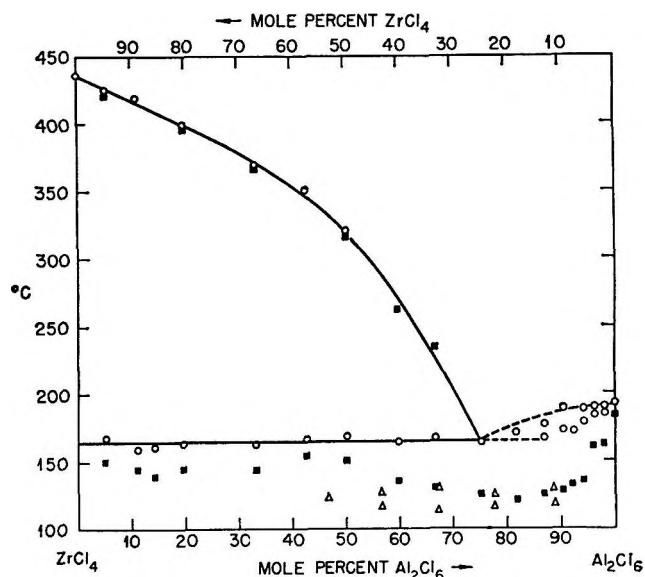


Figure 1. Binary condensed-phase diagram for the zirconium tetrachloride–aluminum chloride system: O, behavior on heating; ■, behavior on cooling; and Δ , data of Korshunov, *et al.*³

elevated temperatures gave no evidence of the formation of solid intermediary compounds, such as reported for other systems involving aluminum chloride.^{9–11} However, especially for the aluminum-rich mixtures, formation of solid solutions was not excluded and may be suggested by the thermal data discussed below. The most probable form of such solutions, a simple random substitution, to a limited extent (Figure 1), of $3\text{Zr}^{4+} + 1$ vacancy for 4Al^{3+} in the (ionic¹²) lattice of solid aluminum chloride, $\text{AlCl}_3(\text{c})$, would have hardly been detectable by X-rays.

As mentioned above, the significance of the thermal analysis data for the aluminum chloride liquidus is greatly affected by the fact that, because of the large

(6) W. Hückel, "Structural Chemistry of Inorganic Compounds," Elsevier Publishing Co., Amsterdam, 1950, p 1680.

(7) R. L. Harris, R. E. Wood, and H. L. Ritter, *J. Am. Chem. Soc.*, **73**, 3151 (1951).

(8) I. S. Morozov, V. A. Tverskov, and G. I. Kurapova, *Russ. J. Inorg. Chem.*, **9** (9), 1184 (1964). The diagram showing a large miscibility gap must be wrong if for no other reason than that the melting point depression of Al_2Cl_6 by HfCl_4 , shown is 70 times larger than is compatible with the known heat of fusion of Al_2Cl_6 .

(9) J. Kendall, E. D. Crittenden, and H. K. Miller, *J. Am. Chem. Soc.*, **45**, 963 (1923). The existence of compounds with equivalent ratios other than 1:1, proposed by these authors, seems poorly supported. In particular, the " A_2B_y " compounds are in disagreement with the phase rule.

(10) I. N. Belyaev, *Russ. Chem. Rev.*, **29**, 428 (1960). See remarks in the preceding footnote.

(11) H. Houtgraaf and A. M. DeRoos, *Rec. Trav. Chim.*, **12**, 963 (1953).

(12) W. Blitz and A. Voigt, *Z. Anorg. Allgem. Chem.*, **126**, 39 (1923).

supercooling, heating data had to be used with their inherent faults, which are related to the slow establishment of equilibrium. The thermal effects which were entered in the diagram of Figure 1 as being due to the Al_2Cl_6 liquidus might seem to lend themselves to the alternate interpretation as a monotectic horizontal, *i.e.*, two immiscible liquids in equilibrium with solid aluminum chloride as reported for various other systems involving Al_2Cl_6 .⁹⁻¹¹ However, the recorder tracings from both the thermal and the differential thermal analysis runs (heating), especially around 90 mole % Al_2Cl_6 , *i.e.*, in the middle of the range between pure Al_2Cl_6 and the eutectic, did not show the simultaneous presence of two invariant temperature points, namely, a monotectic and a eutectic. That this was not due to poor resolution is proven by the fact that in heating runs with samples containing less than 90 mole % Al_2Cl_6 that had been cooled slowly, two well-resolved peaks did appear. As the peak at the higher temperature was not present in the heating runs with previously rapidly cooled samples, it could, of course, not be interpreted as a monotectic reaction. Instead, it was attributed to the melting of more or less pure solid aluminum chloride formed as a result of segregation on slow freezing. For compositions higher in Al_2Cl_6 than 90 mole %, the temperatures at which melting made itself felt in both the differential and direct thermal analysis runs (heating) were increasingly higher than the eutectic temperature (Figure 1). This is taken to reflect one or the other of two possible situations: one, in the absence of solid solution, the amount of eutectic melt became gradually smaller with higher Al_2Cl_6 concentration, and its thermal effect was increasingly overshadowed by the liquidus effect; or, alternately, and perhaps more plausibly, the rising temperatures may represent the aluminum chloride solidus, *i.e.*, the zirconium chloride solution in solid aluminum chloride as mentioned above. The Al_2Cl_6 liquidus data given represent the temperatures at which the difference between the sample and the reference thermocouple, that first arose on heating through the eutectic (or the solidus) temperature, began to diminish. This peak in the differential temperature was then interpreted as the end of the melting process, namely, the crossing of the liquidus.

The finding of complete miscibility in the liquid state of this system by both visual observation and thermal analysis is further supported by the considerations that follow. The existence of liquid-miscibility gaps has been reported for a number of binary systems involving aluminum chloride or bromide, particularly at high aluminum halide concentrations.^{9,10} These cases are all characterized by the second component

being a typical salt, an electrolyte such as an alkali metal halide, MX, which forms a stable solid complex salt $\text{M}(\text{AlX}_4)$ with the aluminum halide. The apparent largely nonionic, molecular character of ZrCl_4 , somewhat similar to Al_2Cl_6 in its relatively high volatility (subl pt 331° , as compared with the boiling point of 1400° for KCl) is consistent with the failure to observe coexistence of two liquids. The molecular nature of ZrCl_4 prevents the formation of a salt-like solid compound, *e.g.*, $\text{Zr}(\text{AlCl}_4)_4$, that would correspond to the existing solid salt KAlCl_4 . The great similarity of the Zr^{4+} and Al^{3+} ions, both with noble gas electron shells, in the ratio of charge to size, *i.e.*, in polarizing power, produces a near balance in their competition for chloride ions. With the very dissimilar pair $\text{K}^+-\text{Al}^{3+}$ this balance is very heavily in favor of Al^{3+} , enabling complex salt formation. Also, if indeed a salt-like solid, *e.g.*, of the composition $\text{Zr}(\text{AlCl}_4)_4$, would form, it would be expected to be stable enough thermally to be observed in equilibrium with liquid. No such solid compound was found, yet in the cases in which aluminum chloride did form a liquid phase in equilibrium with a liquid phase rich in the other component (*e.g.*, KCl ⁹ and even nitrosyl chloride¹¹), solid salt-like intermediate compounds such as $\text{K}(\text{AlCl}_4)$ and $\text{NO}(\text{AlCl}_4)$ did make their appearance. Their solubility, as well as that of liquids of similar composition, in the nonpolar liquid Al_2Cl_6 was always very small.

The interpretation of the liquidus data with the use of the heats of fusion ΔH_m (assumed to be temperature independent), namely, 17,000 and 9000 cal mole⁻¹ for Al_2Cl_6 ¹³ and ZrCl_4 ,¹⁴ at the melting points $T_0 = 466$ and 709°K , respectively, in terms of the activities of the two components suggests considerable interaction in the liquid phase. These activities, a , were computed from the liquidus temperatures, T , at various compositions by means of the approximate equation

$$\ln a = \frac{\Delta H_m}{R} \left(\frac{1}{T_0} - \frac{1}{T} \right)$$

The experimental activities obtained in this manner are compared in Figure 2 with activities calculated for various solution models. The limiting slope, near $a = 1$, for $a(\text{ZrCl}_4)$ is twice unity, *i.e.*, corresponds to the monomeric dissolution, without ionization, of ZrCl_4 and AlCl_3 in the nonpolar solvent ZrCl_4 . Because of the experimental difficulties discussed above, the

(13) National Bureau of Standards Circular 500, U. S. Government Printing Office, Washington, D. C., 1952, p 731.

(14) A. A. Palko, A. D. Ryon, and D. W. Kuhn, *J. Phys. Chem.*, **62**, 319 (1958).

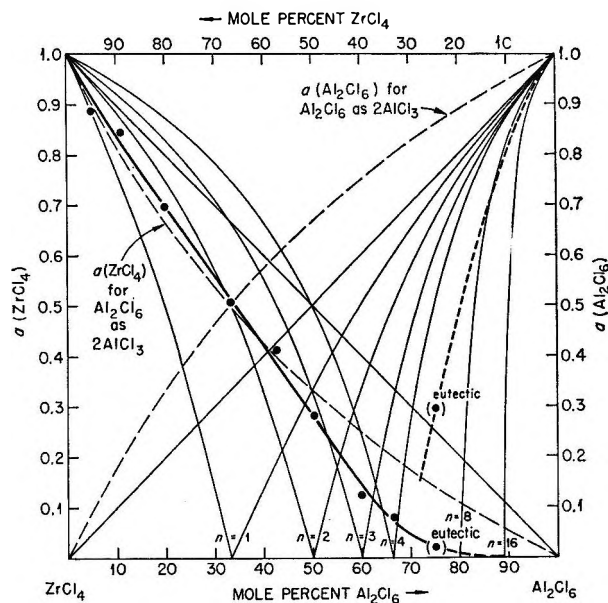


Figure 2. Comparison of experimental activities of zirconium tetrachloride and aluminum chloride with those of various models (Al_2Cl_6 as 2AlCl_3 , or as $\text{ZrCl}_4 \cdot (\text{AlCl}_3)_n$, $n = 1, 2, 3$, and 4 , or even higher). The dotted line for $a(\text{Al}_2\text{Cl}_6)$ corresponds to the dotted Al_2Cl_6 liquidus of Figure 1.

limiting slope for $a(\text{Al}_2\text{Cl}_6)$ is not established. However, with increasing ZrCl_4 concentration, a very strong negative deviation from Raoult's law for ideal mixing of Al_2Cl_6 and ZrCl_4 occurs in $a(\text{Al}_2\text{Cl}_6)$ such that at the eutectic, 75 mole % Al_2Cl_6 , as derived mainly from the intersection of the ZrCl_4 liquidus with the eutectic horizontal, this activity assumes a rather low value ($a \approx 0.3$, $\gamma \approx 0.4$; limited solid solubility would lower these figures slightly). On the other hand, the activity of ZrCl_4 , on addition of Al_2Cl_6 all the way up to 45 mole % Al_2Cl_6 , decreases at what appears to be the rate expected for ideal mixing of monomeric AlCl_3 with the ZrCl_4 (dotted line, Figure 2). Above 45 mole %, it decreases much more rapidly and above 70 mole % appears to approach zero activity asymptotically. We shall see that the simple interpretation of $a(\text{ZrCl}_4)$ below 45 mole % Al_2Cl_6 in terms of the monomeric species cannot be correct. Instead, we wish to suggest an interpretation in terms of the formation, in the liquid phase, of a series of complexes between the two chlorides, namely, $\text{ZrCl}_4 \cdot n\text{AlCl}_3$, $n = 1, 2, 3$, and 4 , with the—possibly terminal—formation, near 67 mole % Al_2Cl_6 , of the compound $\text{ZrCl}_4 \cdot 4\text{AlCl}_3$, or $\text{Zr}(\text{AlCl}_4)_4$. A slightly modified formula, $\text{Zr}(\text{ClAlCl}_3)_4$, might be used to express the plausible assumption of a highly symmetrical molecule in which both aluminum and zirconium occupy the centers of altogether five interconnected chlorine tetrahedra in such a way

Table I: Liquidus and Eutectic Temperatures and Zirconium Tetrachloride Activity in the Zirconium Tetrachloride-Aluminum Chloride System

| Compn, mole % | AlCl_3 | Al_2Cl_6 | Transition temp, °C | | | | Activ- ities, ^a $a(\text{ZrCl}_4)$ | Activity coef- ficient, $\gamma(\text{ZrCl}_4)$ |
|---------------|-----------------|--------------------------|---------------------|-----|-------------------|------|---|--|
| | | | On heating Eut | Liq | On cooling Liq | Eut | | |
| 0 | 0 | ... | 437 | 435 | ... | 1.00 | 1.00 | |
| 10 | 5.3 | 167 | 425 | 420 | 150 | 0.89 | 0.94 | |
| 20 | 11.1 | 159 | 419 | 417 | 144 | 0.84 | 0.94 | |
| 25 | 14.3 | 160 | ... | ... | 139 | ... | ... | |
| 33 | 19.8 | 163 | 399 | 396 | 144 | 0.70 | 0.87 | |
| 50 | 33.3 | 162 | 369 | 366 | 143 | 0.51 | 0.77 | |
| 60 | 42.8 | 166 | 350 | ... | 154 | 0.42 | 0.73 | |
| 67 | 50.4 | 168 | 320 | 317 | 150 | 0.28 | 0.56 | |
| 75 | 60.0 | 164 | ... | 262 | 135 | 0.13 | 0.33 | |
| 80 | 66.7 | 167 | ... | 234 | 130 | 0.08 | 0.24 | |
| 86 | 75.4 | 163 | ... | ... | 125 | 0.02 | 0.08 | |
| 90 | 81.8 | 170 | ... | ... | 120 | ... | ... | |
| 93 | 87.0 | 170 | 177 | ... | 125 | ... | ... | |
| 95 | 90.5 | 172 | 188 | ... | 127 | ... | ... | |
| 96 | 92.3 | 171 | ... | ... | 132 | ... | ... | |
| 97 | 94.2 | 178 | 188 | ... | 135 | ... | ... | |
| 98 | 96.1 | 183 | 189 | ... | 160 | ... | ... | |
| 99 | 98.0 | 185 | 189 | ... | 162 | ... | ... | |
| 100 | 100.0 | ... | 193 | 183 | ... | 0 | ... | |

^a See text for method of calculation.

that each of the four AlCl_4 tetrahedra which surround the zirconium, again in tetrahedral arrangement, shares one of its corners with the central, ZrCl_4 , tetrahedron. However, the suspicion seems justified that with the first additions of ZrCl_4 to Al_2Cl_6 even larger complexes, with additional AlCl_3 ($n = 5, 6, 7$, and 8) might form. Such larger clusters may well be responsible for the large increase in supercooling (Figure 1). This probably is also associated with an increased viscosity. (Salts $\text{M}^+(\text{Al}_2\text{Cl}_7)^-$ have been reported⁹).

The activity of ZrCl_4 does not follow the curve for $n = 4$, nor, for that matter, any one of those for $n = 1, 2$, or 3 , but crosses them. This might be expected, as the competition between the many ZrCl_4 molecules for the few AlCl_3 groups available at low Al_2Cl_6 concentration must lead to the more or less simultaneous formation of the various lower complexes, $\text{ZrCl}_{(4-n)}(\text{ClAlCl}_3)_n$, beginning with a preponderance of $n = 1$ and continuing with rising n toward the formation, near the composition of 67 mole % Al_2Cl_6 , of $\text{Zr}(\text{ClAlCl}_3)_4$.

The apparent agreement, then, at concentrations up to 45 mole % Al_2Cl_6 , mentioned above, of the experimental $a(\text{ZrCl}_4)$ with the curve calculated for an ideal solution of independent monomeric AlCl_3 molecules in ZrCl_4 (dotted line in Figure 2) must be considered

purely (if strangely) coincidental: if AlCl_3 and ZrCl_4 were the species present, the experimental activity for aluminum chloride would have had to follow the line marked " $a(\text{Al}_2\text{Cl}_6)$ for Al_2Cl_6 as 2AlCl_3 " all across the diagram. Actually this activity, mainly by the position of the eutectic, is shown to be much smaller at all compositions below 67 mole % Al_2Cl_6 . The presence of monomeric AlCl_3 is also unlikely on theoretical grounds, as with only three ligands it would represent a coordinatively most unsaturated species.

Acknowledgments. The authors express their gratitude to Mr. R. E. Thoma of the Oak Ridge National Laboratory for the loan of the differential thermal analysis equipment and helpful discussions. Especially helpful advice was received from Professor J. E. Ricci of New York University, but the conclusions of the paper do not necessarily reflect his opinions. Mr. A. S. Dworkin of Oak Ridge National Laboratory made a valuable contribution to the experimental work.

Gas-Liquid Partition Chromatography of Perdeuterioethane. Isotope Effects on Vaporization from Solution¹

by W. Alexander Van Hook and James T. Phillips

Chemistry Department, University of Tennessee, Knoxville, Tennessee 37916 (Received November 1, 1965)

Gas-liquid chromatographic separation factors for the system C_2H_6 - C_2D_6 have been obtained over the temperature range 0 to -130° on a variety of liquid partition columns. The isotope effects were pronounced functions of the temperature. The logarithm of the separation factors varied by more than a factor of 3 when the substrate was changed from highly polar (such as CH_3CHO) to nonpolar (such as 2,3,4-trimethylpentane) liquids. These results and some earlier results of Liberti, Cartoni, and Bruner on the system C_6H_6 - C_6D_6 (*J. Chromatog.*, **12**, 8, 1963) are interpreted with the aid of the statistical theory of isotope effects in condensed systems and consistency with the theory is demonstrated.

The gas chromatographic fractionation of compounds isotopically substituted with deuterium (and/or tritium) has received considerable attention. The literature has been summarized by Van Hook and Kelly^{2a} and Bentley, Saha, and Sweeley.^{2b} The technique is of interest both as a method of practical analysis of isotopic mixtures and for the investigation of isotope effects in solution and the intermolecular forces which give rise to them. Most of the effort to date has been devoted to development of techniques and analytical methods, and very few results have been discussed in the context of the theory of isotopic separations. In the present work we wish to present some chromato-

graphic data for the system C_2H_6 - C_2D_6 on a number of liquid phases and point out its consistency with the statistical theory of isotope effects in condensed systems.³ We shall then consider some results of Liberti, Cartoni, and Bruner⁴ on the system C_6H_6 -

(1) Presented at the 150th National Meeting, American Chemical Society, Atlantic City, N. J., Sept 1965.

(2) (a) W. A. Van Hook and M. E. Kelly, *Anal. Chem.*, **37**, 508 (1965); (b) R. Bentley, N. C. Saha, and C. C. Sweeley, *ibid.*, **37**, 1118 (1965).

(3) J. Bigeleisen, *J. Chem. Phys.*, **34**, 1485 (1961).

(4) A. Liberti, G. P. Cartoni, and F. Bruner, *J. Chromatog.*, **12**, 8 (1963).

C_2D_6 in the same framework. The theory has been shown to fit quantitatively the isotope effect on vapor pressure over a broad temperature range for a number of systems displaying higher order quantum effects, including the deuterated ethylenes⁵ and deuterated ethanes.⁶ It is of interest to determine whether the predictions of the theory extend to isotope effects on the process of vaporization from dilute solution.

Experimental Section

The experimental techniques and apparatus have been described previously.^{2a} In the present investigation, 50-ft coiled copper columns were employed. The liquid was supported on firebrick in all cases. The columns employed are summarized in Table I and the results shown in Figure 1. The data were obtained over as wide a temperature range as possible on each column, and the columns employed were varied over as wide a range in relative retention as possible. (The relative retention shows a crude inverse correlation with the polarity of the solvent.) The net result is that the chromatographic conditions for a good part of the data are far from optimal and the precision is poor. It is about one order of magnitude less than that for the vapor pressure measurements which are also shown in Figure 1.

Table I: Characteristics of Packed Columns

| Code | Column | Wt % liquid | Rel. retention ^a at -78° |
|---------------------|----------------------------------|-------------|-------------------------------------|
| MCP | Methylcyclopentane | 15 | 41 |
| TMP | 2,3,4-Trimethylpentane | 13 | 42 |
| EtOH | Ethyl alcohol | 33 | 7 |
| CH ₃ CHO | Acetaldehyde | 20 | 1 |
| Eutectic | Ethyl alcohol-acetaldehyde (8:2) | 20 | 5 |

^a Relative retention is defined as $[(t_{C_2H_6}/t_{N_2})_{col} x (t_{N_2}/t_{C_2H_6})_{col}] / [(t_{CH_3CHO}/t_{N_2})_{col} x (t_{N_2}/t_{CH_3CHO})_{col}]$ [(moles of CH₃CHO/100 g of firebrick)/(moles of x/100 g of firebrick)].

The temperatures are limited on one hand by the freezing point of the liquid coating and on the other by the point at which its vapor pressure becomes appreciable. Direct comparisons with the vapor pressure data are therefore possible in most cases only over a rather limited range. On any given column the precision is poorest at the temperature extremes. This follows from the short retentions (and small absolute separations) at high temperatures or from the excessive peak broadening at the lower ones caused by ex-

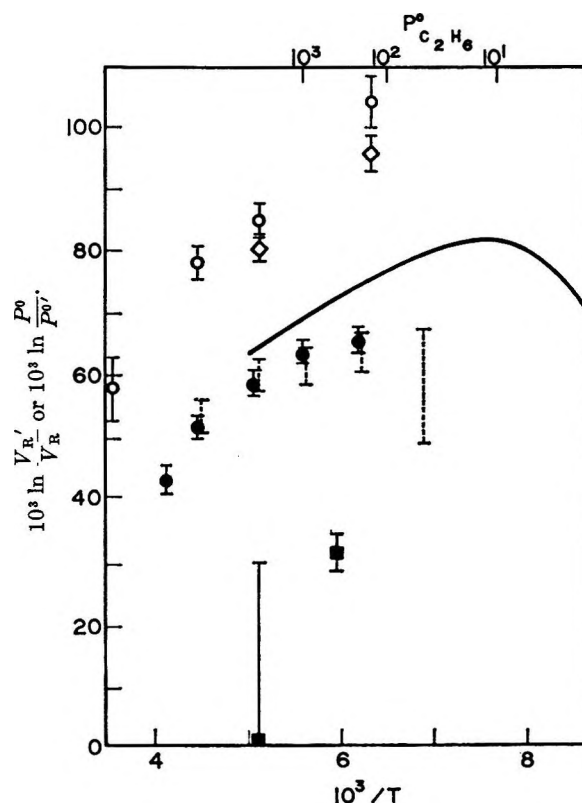


Figure 1. Separation factors for C_2D_6 - C_2H_6 : ■, 15% acetaldehyde on firebrick; ●, 33% ethyl alcohol on firebrick; ▮, 20% 8:2 ethyl alcohol-acetaldehyde on firebrick; —, vapor pressure ratios of pure liquids; ◇, 13% 2,3,4-trimethylpentane on firebrick; and ○, 15% methylcyclopentane on firebrick.

tremely long retention times and low ethane vapor pressures.

The difficulties are compounded when polar substrates are employed. Both the relative effect and the absolute retention times are lowered (Table I and Figure 1). The net result is that the actual measured separation may change by as much as a factor of 150 in going from nonpolar to very polar columns of comparable temperature, length, and solvent concentration. Such effects could be minimized only by going to inconveniently long columns and high pressure drops for the more polar materials.

Results

The data in Figure 1 are natural logarithms of ratios of the corrected retention volumes, $V_R^{D,H}$, for the sub-

(5) (a) J. Bigeleisen, S. V. Ribnikar, and W. A. Van Hook, *J. Chem. Phys.*, **38**, 489 (1963); (b) J. Bigeleisen, M. J. Stern, and W. A. Van Hook, *ibid.*, **38**, 497 (1963); (c) M. J. Stern, W. A. Van Hook, and M. Wolfsberg, *ibid.*, **39**, 3179 (1963).

(6) W. A. Van Hook, *ibid.*, **44**, 234 (1966).

stituted and unsubstituted molecules. The ratio, V_R^H/V_R^D is readily identified⁷ with the ratio of activities

$$V_R^H/V_R^D = \gamma_D P_D^\circ / \gamma_H P_H^\circ \quad (1)$$

where $\gamma_{H,D}$ refers to the activity coefficients and $P_{H,D}^\circ$ to the vapor pressures of the pure compounds. Significant nonideality in the solutions is demonstrated. Thus, at -100° γ_D/γ_H varies from 1.02 for the nonpolar columns to 0.96 for the polar CH_3CHO column. The most precise data was obtained with the EtOH column. It clearly demonstrates the pronounced curvature predicted by the theory as do the results on 2:8 $\text{2CH}_3\text{-CHO-EtOH}$ solvent. This latter column was prepared so that the temperature could be lowered below the freezing point of EtOH or CH_3CHO while maintaining a reasonably polar substrate. At these lower temperatures, however, the precision suffers owing to the low absolute vapor pressure of ethane and the concomitant poor resolution and peak tailing.

The extremely poor precision at the higher temperature on the CH_3CHO column is due to the very low relative retention and small isotope effect.

Discussion

A theoretical approach to isotope effects on activities in condensed systems has been made by Bigeleisen.³ He specifically considered the case of pure compounds. The theory leads on the basis of a cell model for the condensed phase, neglect of gas imperfections, terms involving molar volume effects, anharmonicities, etc., to

$$\frac{P'}{P} = \frac{\prod_{\text{internal frequencies}}^{3N-6} \left[\frac{(u/u')_c}{(u/u')_g} \right] \left[\frac{\exp(u' - u)_c/2}{\exp(u' - u)_g/2} \right]}{\prod_{\text{external liquid frequencies}}^6 \frac{u}{u'} \left[\exp\left(\frac{u' - u}{2}\right) \right] \left[\frac{1 - \exp(-u')}{1 - \exp(-u)} \right]} \times \quad (2)$$

where the prime denotes the lighter isotope, $u = h\nu/kT$, and c and g refer to the condensed or gas phases, respectively.

Equation 2 connects the force fields describing the motion of an isolated molecule in the gas phase or a condensed phase molecule in the cell defined by its neighbors to the pressure ratio. These fields are different owing to the intermolecular forces which become effective in the condensed phase. In the pure state they are exclusively "solute-solute" forces, but for the case of an infinitely dilute solution they will be exclusively solvent-solute. The latter case is of interest. It is nicely approximated in gas chroma-

tography. We sidestep a lengthy derivation paralleling that of Bigeleisen³ and directly combine (1) and (2) to give

$$\frac{V_R}{V_R'} = \frac{\gamma' P^{\circ'}}{\gamma P^\circ} = \frac{P'}{P} = \text{(right-hand side of eq 2)} \quad (3)$$

If the $3N$ frequencies of the system can be factored into two distinct sets, (2) reduces to

$$\ln \frac{V_R}{V_R'} = \ln \frac{P'}{P} = \frac{A}{T^2} - \frac{B}{T} \quad (4)$$

where the A term is interpreted as a first-order quantum correction appropriate for those modes of $u < 2\pi$. For ethane, A should take the form

$$A = \frac{1}{24} \left(\frac{h}{k} \right)^2 \left\{ \sum_{\text{ext}} (\nu_i'^2 - \nu_i^2) + (\delta(\nu_{\text{IR}}'^2) - \delta(\nu_{\text{IR}}^2)) \right\}$$

The sum is over the $i = 6$ low-lying lattice frequencies and the second term is due to the internal rotation, where $\delta(\nu^2) = \nu_c^2 - \nu_g^2$. In the development which follows, the lattice frequencies may be taken as the average Debye frequencies (if the Debye ν_{max} frequencies are employed, the coefficients for these frequencies should be multiplied by 0.6). An Einstein distribution is assumed for the rotational or librational frequencies and the internal rotation is treated in the harmonic oscillator approximation.

The B term in eq 2 is the contribution from the changes in zero point energy of the large (*i.e.*, $h\nu/kT > 2\pi$) internal frequencies on condensation, given by

$$B = \left(\frac{h}{2k} \right) \left\{ [\Sigma \nu_g' - \Sigma \nu_c'] - [\Sigma \nu_g - \Sigma \nu_c] \right\}$$

The sums are over-all internal frequencies except the internal rotation.

Equation 4 shows that important contributions arise both from the zero point shifts on condensation of the $3n - 7$ high-energy ($u > 2\pi$) modes and from the seven (hindered translations, librations, and internal rotation) lower-energy modes. For ethane there is a net red shift in molecular vibrational frequencies on condensation and the terms are of opposite sign. Inverse isotope effects with concomitant maxima, deviations from the rule of the mean, and isotope effects between equivalent isomers are therefore expected. All of these effects are nicely exhibited by the ethane vapor pressure data⁶ and within the experimental precision by the chromatographic data (except that deviations from the rule of the mean and the vapor pressure iso-

(7) A. I. M. Keulmans, "Gas Chromatography," Reinhold Publishing Corp., New York, N. Y., 1959, p 172.

tope effect between equivalent isomers were not measured chromatographically).

Van Hook⁶ has discussed the applicability of eq 2 and 4 to the vapor pressure ratios of the deuterated ethanes and concludes that equations such as (4) afford reasonable fits to the high-temperature ($\geq 150^\circ\text{K}$) data. Thus for the case $\text{C}_2\text{D}_6\text{-C}_2\text{H}_6$ plotted in Figure 1 we have from force field *A* of ref 6

$$\ln \left(\frac{P_{\text{C}_2\text{H}_6}}{P_{\text{C}_2\text{D}_6}} \right) = \frac{(346)_{\text{TR}} + (282)_{\text{IR}}}{T^2} - \frac{(16.1)_{\text{ZPE}}}{T} \quad (5)$$

where T and R refer to the external translational and rotational contribution, IR to that from the internal rotation, and ZPE to the contribution from the internal modes. At 200°K , eq 5 gives -0.0646 and, at 150°K , -0.0791 . The complete equation (2) shows -0.0651 and -0.0809 , while a refined treatment which empirically takes into account the change in anharmonicity of the lattice frequencies with temperature gives -0.0642 and -0.0783 . The experimental data show -0.0638 and -0.0783 . The point, without belaboring the issue, is that the data in this paper can be discussed well within the chromatographic precision (± 0.003 in the most favorable cases) in the context of an approximate equation of the form of (4). We, of course, expect different values of the *A* and *B* parameters for each different condensed phase owing to changes in the average cell size (*A* term) or in the solute-solvent intermolecular dispersion or dipole-induced dipole forces (*B* term). Thus significant deviations from ideality are expected. In particular, one might expect that as the polarity of the solvent is increased that the inverse isotope effect will decrease since the bending modes and internal rotation will be blue shifted with respect to the neat liquid owing to the dipole-induced dipole forces (or incipient hydrogen bonding, if you will).

The chromatographic data display the expected trends discussed above. Unfortunately, they are not precise enough to allow meaningful fits to (4) to be made and values of *A* and *B* to be determined. It is also unfortunate that no spectroscopic data on ZPE shifts on condensation of ethane into solution are available. These factors preclude the possibility of model calculations designed to make numerical tests of the correlation. On a more qualitative level it is clear that all five sets of data are consistent with the prediction of substantial curvature in $1/T$ vs. $\ln R$ plots. For the EtOH and eutectic columns, such curvature is unambiguously demonstrated. (An immediate consequence is that the interpretation of the slopes of such plots in terms of isotope effects on heats

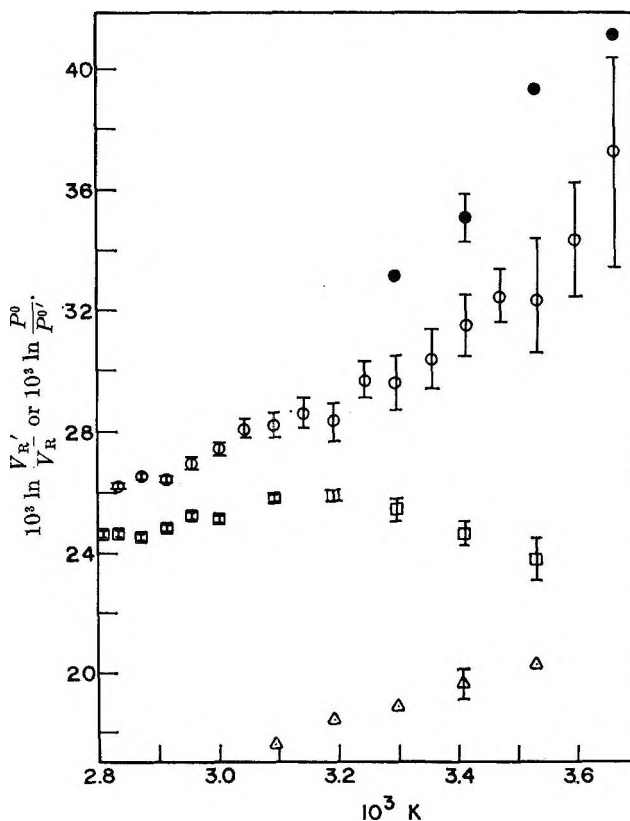


Figure 2. Separation factors for $\text{C}_6\text{D}_6\text{-C}_6\text{H}_6$: ●, capillary column with squalane;⁴ □, vapor pressure data of Davis and Schiessler;⁹ ○, vapor pressure data of Ingold, *et al.*;⁸ Δ, capillary column with silicone 702.⁴ A single point not shown for capillary column dinonyl phthalate⁴ is at $10^3/T = 3.42$ and $6 < 10^3 \ln (V_{\text{C}_6\text{H}_6}/V_{\text{C}_6\text{D}_6}) < 8$.

of vaporization, etc., should be made only with extreme caution since in general a straight-line relationship is not to be expected.) In addition, the deviations from ideality are in the expected direction; *i.e.*, as the polarity of the solvent increases, the magnitude of the inverse isotope effect falls off in the order $\text{MCP} \gtrsim \text{TMP} > \text{EtOH} > \text{CH}_3\text{CHO}$.

Although the chromatographic data are not precise enough to define the changes in the *A* and *B* terms which occur when one goes from the neat liquid to the solvents, it does unambiguously demonstrate that changes occur at least in the *B* term; *i.e.*, the entire effect cannot be accounted for simply by changes in the *A* term, although it is to be expected that some changes also occur in this term.

[Thus, consider the nonpolar columns. At 200°K , $\ln (P_{\text{D}}/P_{\text{H}}) \cong 0.080$. If one assumes that all changes occur in *A*, then $A \rightarrow 0$ and $\ln (P_{\text{D}}/P_{\text{H}}) \cong 16/200 \cong 0.08$. For *A* to approach zero, the internal rotation ν_4 would have to red shift 15 to 25 cm^{-1} from its value

in liquid ethane to compensate for the contribution of the hindered translations and rotations. This is unreasonably large. It amounts to a red shift of 3 to 13 cm^{-1} with respect to the gas for this low-frequency mode. Infrared studies⁸ of spectral shifts on condensation for such low frequency modes invariably show blue shifting with respect to the gas phase, even for van der Waals bonded liquids.

Similarly, for the CH_3CHO column at 165°K an A term of 1768 ($^\circ\text{K}$)² would be predicted if B remained 16°K. Assuming that the internal rotational mode and the external modes increased in the same ratio, this would require a blue shift in ν_4 from 290 cm^{-1} in liquid C_2H_6 to 543 cm^{-1} in CH_3CHO . Such a change is untenably large. We conclude that an important part of the total solvation effect must result in changes of the zero point energy shifts on condensation, that is in the B term.]

It is of interest to consider the benzene-perdeuterio-benzene system which has been investigated by Liberti, Cartoni, and Bruner.⁴ They measured separation factors on coated capillary columns between 273 and 323°K. Their results for squalane and Dow-Corning 702 silicone oil are shown in Figure 2 together with the available vapor pressure data.^{9,10} The authors give no estimate of the precision of their data, but from the reproductions of their chromatograms we note a separation between peaks (20°) of about 1 min. Assuming an error of ± 2 sec in measuring peak separation, we calculate the error bars shown in the figure. It is impossible to estimate the precision of the points at the other temperatures. A comparison of the 20° point with the ethane data indicates an improvement in precision of more than a factor of 5 in going from the packed column to the capillary technique. Liberti, *et al.*, also measured a single point on dinonyl phthalate solvent at 20°. From the reproduction of the chromatogram we estimate a separation of 0.2 to 0.3 min at a retention time of 36 min, or in units of $10^8 \ln(P_D/P_H)$ an effect of 6 to 8. Thus, for the benzene system, as well as for ethane, the logarithm of the inverse isotope effect varies by a factor of 3 to 5 in going from nonpolar to highly polar solvents, and varies in the direction predicted by our earlier remarks. Significant shifts in the zero point term are indicated.

Liberti, *et al.*, compared their results to the vapor pressure data of Ingold, *et al.*⁹ This data are shown in Figure 2 where the bars indicate an uncertainty of ± 0.1 mm in one of the pressures entering the ratio. The higher precision data of Davis and Schiessler¹⁰ are also shown. The bars indicate an uncertainty of ± 0.03 mm. We believe that the later data are to be preferred since the shape of the curve agrees with the

predictions of the theory. The maximum shown by (2) is apparent, while the plot of the earlier data (Figure 2) shows a definite trend toward concave upwards. This later shape is theoretically untenable.

One result of the change of basis is that significant changes occur in the reported ratios of the activity coefficients. The new values are given in Table II.

Table II: Isotope Effect on Activity Coefficient of Benzene

| $10^8 \ln$ ($P_{\text{C}_6\text{D}_6}/$ $P_{\text{C}_6\text{H}_6}$) ^a | ($\gamma_{\text{C}_6\text{D}_6}/\gamma_{\text{C}_6\text{H}_6}$) _{squalane} | ($\gamma_{\text{C}_6\text{D}_6}/\gamma_{\text{C}_6\text{H}_6}$) _{silicone 702} | $T,$ $^\circ\text{K}$ |
|--|---|---|--------------------------|
| [21.6] ^b | 1.0198 (1.0073) ^c | ... | 273.2 |
| 23.8 | 1.0150 (1.0061) | 0.9965 (0.9880) | 283.2 |
| 24.6 | 1.0106 (1.0041) | 0.9950 (0.9887) | 293.2 |
| 25.4 | 1.0077 (1.0031) | 0.9935 (0.9890) | 303.2 |
| 25.9 | ... | 0.9926 (0.9894) | 313.2 |
| 25.8 | ... | 0.9919 (0.9895) | 323.2 |

^a Data of Davis and Schiessler. ^b Extrapolated. ^c Parenthesized values are from Liberti, *et al.*,⁴ based on vapor pressures of Ingold, *et al.*⁸

We do not wish to consider a detailed fit of the theory to the data of Davis and Schiessler. From the curvature in Figure 2 it is evident that the A term is significant in comparison with the magnitude of the zero point contribution. It is unfortunate that the chromatographic data are not available over a wider temperature range in order to determine whether the apparent linearity in the T^{-1} plots persists or whether it is an artifact. If the former is the case, it would appear that the "A" frequencies are significantly lower in the solutions than in the neat liquids.¹¹ This is in addition to large changes in the zero point (B) contributions.

We conclude that chromatographic studies of isotopic molecules afford a convenient method of study of isotope effects in solution. Capillary techniques offer improved precision over packed columns, but the results obtained with both methods are in agreement with the predictions of the theory both in regard to the temperature dependence and to the solvent dependence. This is an important result, for it establishes a foundation for the rational selection of columns and

(8) W. G. Fateley, I. Matsubara, and R. E. Witkowski, *Spectrochim. Acta*, **20**, 1461 (1964).

(9) C. K. Ingold, G. G. Rarsin, C. L. Wilson, and C. R. Bayley, *J. Chem. Soc.*, 915 (1936).

(10) R. T. Davis, Jr., and R. W. Schiessler, *J. Phys. Chem.*, **57**, 966 (1953).

(11) NOTE ADDED IN PROOF. A. Liberti (private communication) informs us that he considers the precision of his data which we quote above as better than 10.5 sec. In that event, the curves are nicely linear and a very small A term is indicated.

conditions for the separation of isotopically substituted molecules. More quantitative tests of the theory of isotope effects in condensed systems as applied to solutions must await precise data over a broad temperature range on systems on which the vapor pressure ratios themselves are thoroughly understood. The capillary-column benzene results discussed above indicate that such a program could be

practically implemented. In the case of benzene vapor pressure, data on other isotopic benzenes would be useful in constructing a detailed fit to the theory. Such a fit would be necessary for any detailed interpretation of the chromatographic data.

Acknowledgment. This research was supported by the Petroleum Research Fund, administered by the American Chemical Society.

Vibrational Intensities. XII. An Optical-Mechanical System from Infrared Attenuated Total Reflection Measurements

by A. C. Gilby, John Burr, Jr., and Bryce Crawford, Jr.

Molecular Spectroscopy Laboratory, Department of Chemistry, University of Minnesota, Minneapolis, Minnesota 55455 (Received November 1, 1966)

An infrared optical system is described for making precise measurements at a variable angle of incidence of the reflectivity of the surface of a sample covered by a transparent material of high refractive index. The incident beam contains rays spread over a range of about 1° . The average angle of incidence can be varied from 11 to 75° and be reproduced to better than $0.5'$ of arc. The optical elements are all standard mirrors except for the hemicylinder placed over the sample. Construction, alignment, and performance are described.

The molecular properties which may be studied by determining integrated intensities of gas phase infrared absorptivities are displayed also in the absorption bands of condensed phases; we must add, however, on the side of basic factors the effect of intermolecular forces, and on the side of observed phenomena the variation of refractive index through an absorption band. We have chosen to study these phenomena using the technique of attenuated total reflection (ATR), as advocated by Fahrenfort,¹ to determine accurately the two bulk optical constants, refractive index and attenuation index, of substances in condensed phases. In this paper we describe the instrument we have constructed and its performance.

General Design

In order to use the ATR method, two conditions must be met. First, the sample must be in good optical contact with a transparent window of high refractive index and, second, the light incident on the window-to-sample boundary must be as near parallel as possible and at an angle of incidence which can be varied over a wide range and known to the order of minutes of arc. The first condition is easily met when the sample is a liquid and the window a solid such as KRS-5 or germanium. Solid samples are not so easy.

(1) J. Fahrenfort, *Spectrochim. Acta*, **17**, 698 (1961); J. Fahrenfort and W. M. Vissar, *ibid.*, **18**, 1103 (1962).

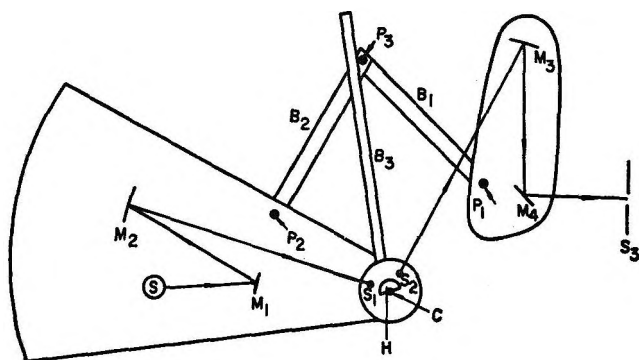


Figure 1. Optical system of ATR apparatus.

If a high-index liquid, transparent through a useful range of the infrared, could be found, the problem would be solved. So far we have concentrated on optical polishing of the sample and window before placing them in contact. This work with oriented single crystals as samples will be described in a later paper. The optical system to be described is equally applicable to liquid or solid samples.

The second condition is met most easily if the apparatus is built on a comfortably large scale. Figure 1 shows the general plan of the system. M_2 and M_3 are standard Perkin-Elmer spherical mirrors, 7.6 cm diameter and 28.5 cm radius of curvature. M_1 and M_4 are plane mirrors. H is the hemicylinder, usually a KRS-5 single crystal 0.75 in. in diameter. It is important that it should be close to a true half cylinder, say within 0.002 or 0.003 in. As in Fahrenfort's design, an image of the Nernst glower S is formed at S_1 such that light becomes almost parallel inside the hemicylinder.[†] To a good approximation, the distance of S_1 from the axis of the hemicylinder is given by $rn/(n-1)$ where r is the radius of the hemicylinder and n is its refractive index at the frequency of the infrared light to be used. Light internally reflected from the flat back face of the hemicylinder is reimaged at S_2 , and mirrors M_3 and M_4 transfer this image to S_3 , the entrance slit of a Perkin-Elmer Model 12C monochromator modified for double-pass operation.

The curvature of the hemicylinder only affects light in a plane perpendicular to its axis. However, this does not result in additional light losses because there is a compensating effect due to the astigmatism introduced by the two spherical mirrors M_2 and M_3 . The amount of astigmatism is determined by how far the spheres are used off-axis. Rays are focussed in a horizontal plane at S_1 , S_2 , and S_3 , whereas in a vertical plane they are focussed very close to the back surface of the hemicylinder and then close to S_3 .

The entire system is mounted on an aluminum base-

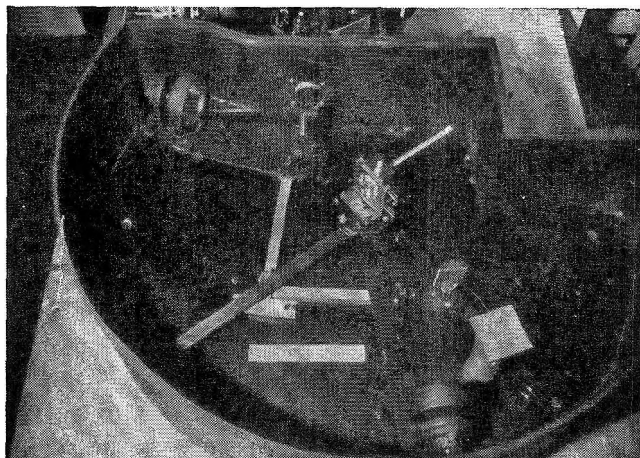


Figure 2. Optical system of ATR apparatus.

plate and surrounded by a wall and lid so that it can be flushed out with dry nitrogen. The system rests on adjustable feet and is bolted to the base of the monochromator. (See Figure 2.)

Construction and Alignment

Mechanical System for Varying the Angle of Incidence. A 1-in. diameter brass shaft is mounted vertically in a ball bearing in the center of the base plate. Inside this is a concentric steel shaft supported by two ball bearings recessed into the ends of the brass shaft. Attached to the brass shaft is an aluminum plate supporting the glower and M_1 and M_2 . This subsidiary base plate is kept parallel to the main base plate and its weight is supported by two ball-bearing wheels which run in a circle on the main base plate. Rotation of the source optics is controlled by a 7-in. diameter worm gear beneath the base plate and a micrometer drive graduated to read to 1' of arc. The micrometer can be adjusted by hand or driven by a synchronous motor in order to scan reflectivity *vs.* angle of incidence.

The sample table is attached to the inner steel shaft and all play is eliminated from the inner assembly by a spring which is attached to the bottom free end of the shaft and pushes upward on the lower ball bearing. The sample table can rotate freely or it can be locked to a system of pivoted bars which rotate it at half the speed of the source optics. B_1 and B_2 are brass bars pivoted together at P_3 . B_1 is pivoted to the base plate at P_1 and B_2 is pivoted to the moving source optics at P_2 . Two ball-bearing wheels at the end of B_1 ensure that the pivot axes are kept vertical. The pivots are made from ball bearings and short lengths of $3/8$ -in. rod press-fitted together. There are no set screws. Drill rod is used at P_1 and P_2 and a permanent cylindrical magnet, ground to size, at P_3 . It is important

to have P_1P_3 and P_2P_3 the same length, probably to better than 0.001 in. Similarly, P_1C and P_2C must be equal and this is achieved by using a template to fit over the shafts before screwing the housings for the ball bearings at P_1 and P_2 into place. B_3 , a precision-ground steel bar, is attached to a collar beneath the sample table. The sample table can rotate within this collar or be locked in a fine-adjustable position with respect to it. The other end slides in contact with the permanent magnet P_3 with its weight supported by a brass collar on P_3 . The edges of B_3 are accurately parallel to the center line CP_3 .

Supporting the Sample and Hemicylinder in the Correct Position. In the case of liquid samples, the cell is made from a solid block of brass with a cavity in the middle of the front face reached by holes from the top. The hemicylinder is cemented over the cavity so that its back face is in the same plane as the front face of the cell. Lines engraved on the front face of the cell help in replacing the hemicylinder reproducibly. The finished cell is chromium plated (Figure 3).

The cell and hemicylinder must now be attached to the sample table in the correct orientation. This is done by the cell holder. The bottom, one side, and the front face of the cell are held in contact with the cell holder by spring clips and the cell holder fits in an adjustable position on the sample table. The cell holder has a square base which fits inside a large square well in the top of the sample table. Set screws in the base of the cell holder provide vertical adjustments so that the hemicylinder axis can be made parallel to the rotation axis. Horizontal adjustments are made with set screws projecting inward from the sides of the well in the sample table.

The hemicylinder and rotational axes coincide when two points along the hemicylinder axis are stationary when the sample table is freely rotated. It is not easy to make this alignment with the hemicylinder in place, so the cell is replaced in turn by each of two flat pieces of brass, one twice as tall as the other, and each with a line engraved representing the position the hemicylinder axis will take with respect to the cell holder. To test when the point at the top end of each line is stationary during rotation we observe it in relation to a fixed pointer held just above it.

Optical Alignment and Angle Calibration. A mercury lamp is placed in an optically equivalent position to the detector and the monochromator is set so that the green line emerges from the entrance slit. For good definition of the angle of incidence, the entrance slit is straight and the exit slit is curved. Mirror M_4 is adjusted so that light falls symmetrically on M_3 . This is done with the aid of a screen, ruled symmetrically with vertical

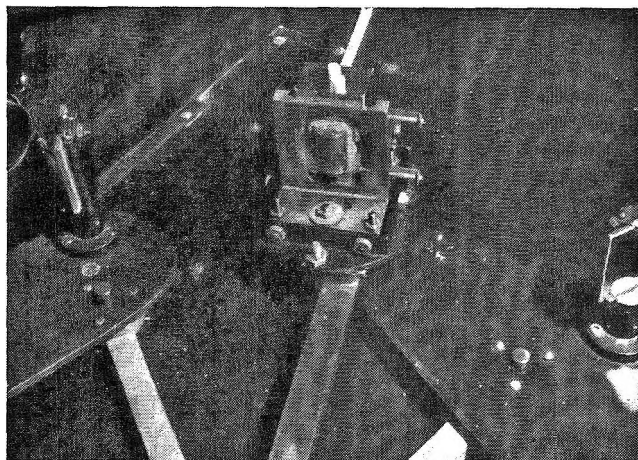


Figure 3. Liquid cell for ATR measurements.

lines, which fits over M_3 . The mask is removed and M_3 is adjusted to direct the light over the rotation axis (using one of the engraved pieces of brass in place of the hemicylinder and cell). The light is focussed the correct distance in front of the axis by focussing it on a screen supported by a piece of brass which projects forward from the cell holder by the calculated distance. With the glower as source the same procedure is followed to align M_1 and M_2 . Next, the source optics are rotated to the 90° angle-of-incidence position. With the cell holder empty and rotated to face M_3 , the mercury light passes directly from M_3 to M_2 . M_3 is masked except for a 0.25-in. central hole, and M_2 is covered with a screen ruled with vertical lines. The 90° position is calibrated by finding the position of the micrometer when the light falls centrally on M_2 . The result is reproducible to within $0.5'$ of arc. A plane mirror is placed in the cell holder and, with the source optics rotated to some smaller angle of incidence, the sample table is rotated and locked onto the bisecting bar B_3 so that the light is again centered on M_2 . When the screen is removed from M_2 , the green light should fall centrally on the glower for all angles of incidence and, provided the performance tests, described below, are satisfactory, the apparatus is ready to operate.

Interchangeability of Hemicylinders. To use hemicylinders of different refractive indices without realigning the mirrors, each hemicylinder must focus parallel light the same distance from its axis. If this fixed distance is x , we can find the proper radius of a hemicylinder of known refractive index from $r = x(n - 1)/n$. Thus, a germanium hemicylinder must be made almost 1 in. in diameter if it is to be interchangeable with a 0.75-in. diameter KRS-5 hemicylinder.

Performance Tests on the System

Measurements made with this system in order to determine optical constants are described in a following paper; before such measurements can be made we must investigate the performance of the instrument as otherwise we cannot assign confidence limits to our results. We need to know how well the light beam is collimated and we need to check that the angle calibration and alignment of the optical system are still satisfactory after the hemicylinder has been placed in position. Scanning the reflectivity *vs.* angle at a fixed wavelength, referred to as an "angle scan," yields much useful information concerning the performance of the instrument.

(1) *Determination of the Degree of Nonparallelism of the Light in the Incident Beam.* Ideally, the curve of reflectivity *vs.* angle of incidence with a nonabsorbing sample, such as air, in the cell would show a discontinuity of slope at the critical angle. In practice, the beam of light is made up of many rays of slightly differing angle of incidence so that the reflectivity curve is rounded at this point and the slope just below the critical angle is less steep. We can estimate the extent of the angle spread by synthesizing reflectivity curves from the Fresnel equations² assuming an even distribution of light energy within various ranges of angles of incidence until we find one which reproduces the observed curve. Since the monochromator does not transmit both polarizations equally, we have to measure the instrument polarization before we can compute synthetic reflectivity curves. This is done by

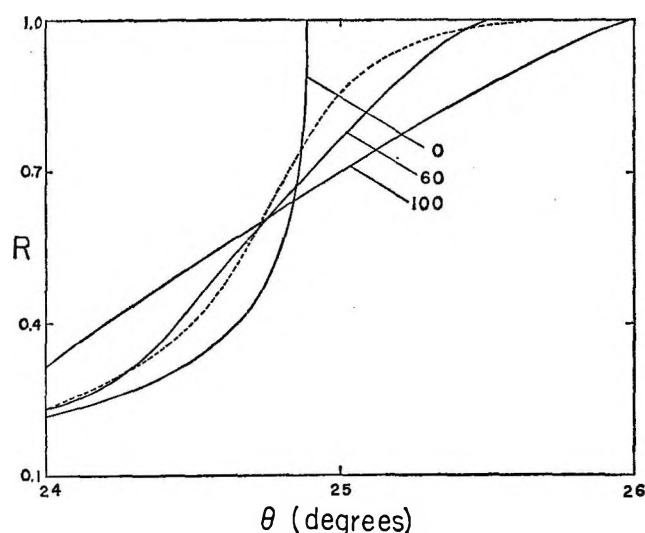


Figure 4. Synthetic (solid lines) and observed (dashed line) angle-scan curves for a KRS-5 hemicylinder. The numbers on the synthetic curves represent the minutes of arc over which the reflectivities were averaged in calculating the curves.

placing a polarizer in front of the detector, as described in the following paper. Figure 4 shows a portion of the observed and calculated curves and also the ideal curve for parallel light. Thus the observed curve (for KRS-5) is reasonably approximated if we assume an angle spread of 0.5° on either side of the average angle.

The spread of angles of the beam in the horizontal plane can be minimized by correctly focussing M_2 and M_3 . However, there is also a contribution from the spread of angles in the vertical plane. Since 9° is subtended by M_2 and M_3 at S_1 and S_2 , the vertical angle spread could be as much as 3.5° for KRS-5 and 2.5° for germanium after refraction by the hemicylinder. The effect would be negligible at grazing angles and maximum at near normal angles of incidence. Actually, our estimation of the angle-spread effect involves measurements of reflectivities at low angles of incidence where the effect should be greatest for the usable range of the hemicylinder, and so, in practice, vertical angle spread is found to be not as important as it might be.

The spread of angles determined in this way was found to increase with increase in mechanical slit width.

A rough calculation shows that a lateral displacement of the image of the entrance slit by as little as 0.1 mm produces a systematic change in the angle of incidence of $20'$ of arc. This figure is for a KRS-5 hemicylinder 0.75 in. in diameter. A smaller KRS-5 hemicylinder would give rise to a larger shift but the shift is the same for any set of interchangeable hemicylinders. This calculation suggests that the finite width of the spectrometer entrance slit, say 0.1 or 0.2 mm, will contribute significantly to the over-all spread of angles of incidence of rays which reach the detector.

The steepest observed slope, just below the critical angle for KRS-5 in contact with air, is about 0.02 in reflectivity per minute of arc. Photometric uncertainty limits our reflectivity measurements to ± 0.005 and so uncertainty in angle would be the dominant source of random error in reflectivity measurements made at this angle incidence. This example shows the importance of knowing the angle of incidence and also that the angle reproducibility of the system has not been over-designed.

(2) *Check on Angle Calibration.* The comparison between synthetic and observed angle scans also provides a check on the calibration of the average angle of incidence. In spite of the discrepancy between the observed and calculated angle-scan curves, which

(2) See M. Born and E. Wolf, "Principles of Optics," Pergamon Press Ltd., London, 1959, or the following paper in this series.

probably means that our assumption about the energy distribution within the angle spread was not altogether correct, it is still possible to use this approach to calibrate with an accuracy of about 5' of arc. This assumes that the observed angle-scan curve should be symmetric with respect to the synthetic curves. Figure 4 suggests that the observed curve is displaced approximately 3' of arc to lower angle from the 60' angle-spread curve.

(3) *Check on Alignment of Instrument.* An angle scan provides a sensitive test of alignment. A slight displacement of the hemicylinder axis from the rotation axis or a lateral displacement of the image of the entrance slit from its correct position will result in intensity variations over the totally reflected region of the scan. A longitudinal displacement of the slit image will increase the angle spread and further reduce the slope just below the critical angle. Calculation shows that the angle spread is increased by about 1° for 1 mm out-of-focus for the 0.75-in. diameter KRS-5 hemicylinder. The effect is larger for a smaller diameter KRS-5 hemicylinder, and for a set of interchangeable hemicylinders the spread is proportional to the refractive index.

(4) *Optical Homogeneity of Hemicylinder.* Tests with crossed polarizers placed just before and after the

KRS-5 hemicylinder indicate that it does not depolarize the light. Tests with crossed polarizers placed before M_3 and at the detector show that the optical components located between the hemicylinder and detector also have no effect on the state of polarization.

(5) *Energy Losses and Spectral Resolution in the System.* The only serious energy losses are the reflection losses at the curved surfaces of the hemicylinder which, for KRS-5, amount to about 30%. Using appropriate prism materials in our monochromator, we found we could, with a reasonable signal-to noise ratio, use a spectral slit width of about 2 cm^{-1} over most of the spectrum.

Acknowledgments. We are most grateful for support provided to this program by the National Science Foundation through Grant GP-3411. Part of the material reported here is taken from a dissertation to be submitted to the Graduate Faculty of the University of Minnesota by J. B. in partial fulfillment of the requirements for the degree of Doctor of Philosophy. We wish particularly to express our thanks to Mr. F. O. Grapp for his help in the design and construction of this instrument, and to thank Dr. A. Clifford and Mr. William Krueger for their contributions in the study of its actual performance.

Vibrational Intensities. XIII. Reduction of Attenuated Total Reflection Data to Optical Constants

by A. C. Gilby, John Burr, Jr., William Krueger, and Bryce Crawford, Jr.

Molecular Spectroscopy Laboratory, Department of Chemistry, University of Minnesota, Minneapolis, Minnesota 55465 (Received November 1, 1965)

A set of procedures is described which have been developed to obtain optical constants (refractive index extinction coefficient) for isotropic samples from attenuated total reflection measurements in the region of infrared absorption bands. Data are presented for the 675- and 1035-cm⁻¹ bands of benzene, the 760-cm⁻¹ band of CHCl₃, and the 770-cm⁻¹ doublet of CCl₄.

The optical constants, refractive index, and extinction coefficient of condensed phases in the infrared region have received considerable attention in the past few years, quite properly in view of the potential information they offer about intramolecular and intermolecular forces. The methods of study have included spectral absorption, reflection, and dispersion measurements in the region of absorption bands, with interpretation using various approaches. Each technique has its advantages and its difficulties, which we will not discuss here; after consideration, we have taken as our technique of choice the measurement of attenuated total reflection (ATR), whose possibilities Fahrenfort¹ has called attention to, and we have constructed the instrument described in the preceding paper. We wish here to set forth the procedures we have developed in obtaining optical constants from reflectivities, to point out the sources of error and the means of minimizing their effect, and to present data for the optical constants of four well-known liquid phase infrared bands. The basic method is capable of extension to oriented anisotropic crystals, on which we shall report later; the present discussion we confine to isotropic nonmagnetic samples.

Method for Obtaining the Optical Constants

The reflectivity (intensity ratio of reflected to incident light) of an isotropic sample depends on its complex refractive index, which we write as $\hat{n}_2 = n_2(1 + ik_2)$ where $i = \sqrt{-1}$.² In order to determine the extinction coefficient n_2k_2 and the real part of the re-

fractive index n_2 from reflectivity measurements, two experimental data are needed at each frequency. Fahrenfort has discussed pairs of possible experiments¹ and he favors using light polarized perpendicular to the plane of incidence at two different angles of incidence (see Figure 1). For this state of polarization, it is possible to solve simultaneously the Fresnel equation (eq 1) for the two angles of incidence and express algebraically each optical constant in terms of measured quantities. However, a prism spectrometer, such as the double-passed Perkin-Elmer 12C used in this work, discriminates against the perpendicularly polarized light, so that even with an ideal polarizer less than one-third of the energy remains. Because of this, we chose to make measurements with unpolarized light at two angles of incidence even though this means a longer calculation to determine the optical constants. The geometry of the situation at the boundary between the high-index hemicylinder, medium 1, and the sample, medium 2, is shown in Figure 1. The reflectivity R_s of light polarized perpendicular to the plane of incidence and R_p of light

(1) J. Fahrenfort, *Spectrochim. Acta*, **17**, 698 (1961); J. Fahrenfort and W. M. Vissar, *ibid.*, **18**, 1103 (1962); J. Fahrenfort, in "Infrared Spectroscopy and Molecular Structure," M. Davis, Ed., Elsevier Publishing Co., New York, N. Y., 1963, Chapter XI.

(2) Different authors have used many different names for the optical constants. Some measure of conformity is achieved if we adhere to the following: we will call \hat{n}_2 the *complex refractive index*, n_2 the *refractive index*, n_2k_2 the *extinction coefficient*, and k_2 the *attenuation index*. The Bouguer-Lambert law of absorption states that $I/I_0 = e^{-\alpha x}$, where the absorption coefficient $\alpha = 4\pi\nu n_2k_2$ and ν is the wave-number in reciprocal centimeters of the light in a vacuum.

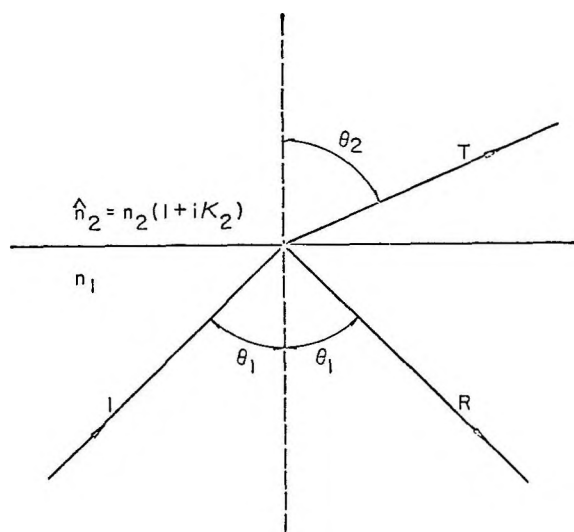


Figure 1. Ray diagram between the boundary of hemicylinder and sample.

polarized at right angles are given by the Fresnel equations (eq 1) which come directly from Maxwell's equations and certain boundary conditions. The

$$R_s = \frac{|\hat{n}_1 \cos \theta_1 - \hat{n}_2 \cos \theta_2|^2}{|\hat{n}_1 \cos \theta_1 + \hat{n}_2 \cos \theta_2|^2}$$

$$R_p = \frac{|\hat{n}_2 \cos \theta_1 - \hat{n}_1 \cos \theta_2|^2}{|\hat{n}_2 \cos \theta_1 + \hat{n}_1 \cos \theta_2|^2} \quad (1)$$

complex angle θ_2 is removed from these equations by using Snell's law: $\hat{n}_1 \sin \theta_1 = \hat{n}_2 \sin \theta_2$. Regarding unpolarized light as the sum of equal parts of parallel and perpendicular polarized light, we would obtain the reflectivity of unpolarized light as the simple average of the separate reflectivities: $R = (R_s + R_p)/2$. However, the spectrometer does not transmit both polarizations equally and, if we define the instrument sensitivity, S , by the ratio of perpendicular polarized energy to parallel polarized energy reaching the detector when the ATR element is totally reflecting, then the reflectivity we actually measure is given by

$$R = R_s[S/(1 + S)] + R_p[1/(1 + S)] \quad (2)$$

From measurements of reflectivity at two angles of incidence, $\theta_1 = \theta_a$ and $\theta_1 = \theta_b$, we have two equations

$$R_a = f(\theta_a, n_1, n_2, n_2 K_2, S) \quad R_b = f(\theta_b, n_1, n_2, n_2 K_2, S) \quad (3)$$

No algebraic relations have been found which separately express n_2 and $n_2 K_2$ in terms of measured quantities and so we use a "brute force" method of solution programmed in FORTRAN II for use with a CDC 1604 computer. The measurements of reflectivity at oblique angles of incidence are made using the apparatus described in the previous paper.

The reliability of the optical constants obtained depends on the choice of hemicylinder index n_1 and the two angles of incidence θ_a and θ_b . These must be chosen so that uncertainties in the various experimental measurements have the least effect on the value of the optical constants. The procedure we use consists of the following steps.

(I) Measurement of instrument polarization. This need be done only once for a given spectral region.

(II) Survey scans of the reflectivity through the absorption band at various angles of incidence.

(III) Choice of experimental conditions (n_1 , θ_a , θ_b) by rule of thumb followed by measurement of reflectivities.

(IV) Calculation of optical constants using a computer program which we call OPCONST2.

(V) Use of these results to predict, by calculation, the experimental conditions which will give the least uncertainty in the optical constants. The computer program used for this is called TABLE. If the calculation predicts the conditions used in step III, we do not need to redetermine the optical constants. This is not usually the case, however, and we proceed to steps VI and VII.

(VI) Final measurements of reflectivities using the calculated optimum experimental conditions.

(VII) Calculation of optical constants, estimation of the errors, and correction of the results for known systematic errors.

The important points are discussed more fully in the paragraphs below.

Measurement of Instrument Polarization (Step I). Before we calculate the optical constants we must know the factor S , and so we measure the energy reaching the detector with a polarizer in the beam. There are three possible locations for a polarizer: between source and hemicylinder, hemicylinder and entrance slit, or exit slit and detector. Because of uncertainties arising from displacement of the polarized beam, the first two positions are not attractive. This leaves the last alternative. The polarizer was made by Perkin-Elmer and consists of six AgCl plates inclined at Brewster's angle. When the polarizer is rotated to change the state of polarization, the ellipsoid is refocused for maximum response from the thermocouple. We believe that this polarizer system is good when used for light polarized parallel to the plane of incidence (horizontal plane) but is not as reliable for the other state of polarization. This may be a further source of systematic error, but calculations show that the optical constants are not particularly sensitive to changes in S of the order of 10%. It can be shown that the maximum error of 2% in R is caused

by an error of 10% in S . The measurement of S is made with the hemicylinder in place and the cell empty. Although S is almost constant throughout an absorption band for our prism instrument, it may vary rapidly with frequency for a grating instrument. There is no evidence that the hemicylinder contains strained zones which depolarize the light.

Choosing Experimental Conditions by Rule of Thumb (Step III). In the results section to follow we show how the best two angles of incidence are close together in regions of low absorption and widely separated in regions of high absorption. The two angles are chosen so that they give widely separated reflectivities which are quite sensitive, but not too sensitive, to small changes in the angle. This choice represents a compromise. Great sensitivity of reflectivity to angle will minimize the effect of photometric errors, but it will accentuate the effect of errors in the measurement of the angle and uncertainties due to the unavoidable spread of angles of incidence within the incident beam. High sensitivity of reflectivity to angle only occurs when the sample is weakly absorbing. In general, several different pairs of angles are needed to measure a band.

Measurement of Reflectivities. The band is scanned in separate sections corresponding to the frequency range of each pair of angles. With the instrument, if necessary thoroughly flushed with dry nitrogen, we scan the reflected intensity at each angle with the cell empty. Next the cell is filled and, while the force optics are refocused, the shutter-closed trace is recorded. Finally, the reflected intensity of the hemicylinder-sample boundary is measured and the cell is emptied. The whole process is repeated with different colored pen ink and if the two traces do not superimpose the whole run is discarded. Reflectivities are measured at regular frequency intervals from these traces and used in step IV with the main program, OPCONST2, to calculate the optical constants.

Computer Program for Calculation of Optical Constants (Step IV). A flow diagram of the calculation is given in Figure 2. First we make a preliminary guess at n_2 and n_2k_2 . This is easy on the wing of a band because n_2k_2 will be small and an estimate of the critical angle gives an approximate value for n_2 . The computer uses these values to calculate R_a and R_t by eq 3 and compares them with the experimentally observed values. The optical constants are then adjusted one at a time to find how each affects the agreement with observation and then repeated changes in n_2 and n_2k_2 are made along a line of steepest descent toward the solution. This line is followed until the new value of n_2 and n_2k_2 cease to give better agreement and a new

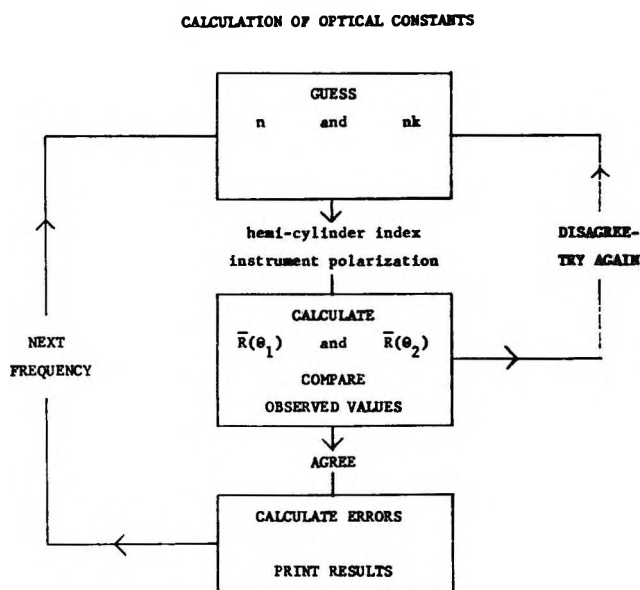


Figure 2. Flow diagram for program OPCONST2.

direction is chosen. The area of search is repeatedly narrowed until very small changes in n_2 and n_2k_2 , such as 3×10^{-5} , do not give better agreement. These are the values taken for the optical constants at that frequency. This completes the calculation at this frequency, and the optical constants just found are used as the initial guesses for the next point in the spectrum. The calculation proceeds at about 2000 iterations/min. In general, the stronger the band the more cycles are needed. The following two examples of speed are from benzene: (1) optical constants were calculated for 100 separate points between 736 and 630 cm^{-1} in 15 min with an average of 400 iterations/point; (2) 81 points between 1080 and 940 cm^{-1} took 5 min with an average of 200 iterations/point.

Prediction of Best Experimental Conditions by Calculation (Step V). In this step we take the optical constants obtained in step IV and use them in program TABLE. This computer program selects the pair of angles which minimize the effect on the optical constants of the various sources of experimental error. Each source of error is assessed for its effect on the observed reflectivity and, from the uncertainty in the two reflectivities, we calculate the uncertainty in the optical constants. The appropriate partial derivatives are found numerically by testing the sensitivity of reflectivity to small changes in the optical constants.

Sources of Experimental Error. There are two obvious main causes of error, of which the first, the photometric accuracy, is entirely similar to that involved in any quantitative spectroscopy. A reflectivity is the ratio of two intensity measurements and,

from reproducibility considerations, we assume an uncertainty of ± 0.005 in the value of an observed reflectivity.

The second main cause of error is peculiar to this type of measurement; the inevitable uncertainty in the angle of incidence must be considered. Actually, there are two factors under this heading. They are (1) the unavoidable range of angles of incidence within the beam, and (2) the absolute value of the average angle of incidence. By regarding the absolute angle calibration as a source of experimental error, to be considered when choosing the best pair of angles, we can avoid angles where the R vs. θ_1 curve is very steep. If we do this, we can regard the spread of angles within the beam as a systematic error for which we can largely correct (step VII).

Consideration of the Fresnel equations shows that when $n_2\kappa_2$ is small the reflectivity can change very rapidly with small changes in angle of incidence. For instance, when $n_2\kappa_2 = 0.001$, the maximum reflectivity change, which occurs close to the critical angle, is about 0.025 per minute of arc. As the absorption increases, the effect is much less serious. When $n_2\kappa_2$ is 0.01, the maximum slope of R vs. θ_1 is about 0.009 per minute and when $n_2\kappa_2$ is 0.1 it is about 0.001 per minute. These slopes, which are only slightly dependent on n_2 and n_1 , are appropriate for a KRS-5 hemicylinder, n_1 2.374, with n_2 of about 1.5. They are slightly larger if the difference between n_2 and n_1 increases. In practice, the slope near the critical angle of the observed curve for a weakly absorbing sample is found to be less steep because of the range of angle of incidence. The 0.025 per minute slope in the example above would appear with our apparatus as 0.015 per minute. This means that if we were to measure the reflectivity at this angle, an error of only 0.33' of arc would change the reflectivity by an amount equal to the photometric uncertainty. With a plane mirror in place of the hemicylinder-sample boundary, we can calibrate the angle of incidence of the chief ray reproducibly to 0.5' of arc. However, when the hemicylinder is placed in position, we may cause small changes in the average angle of incidence. To minimize the effect of this uncertainty on the measured reflectivities we should choose angles where the reflectivity is not particularly sensitive to angle change. This is in conflict with the best choice to minimize the effect of photometric uncertainty and it is the job of program TABLE to find the best compromise. Since we have a spread of angles of incidence of about 1° , we do not simply use the slope of R vs. θ_1 at the average angle θ_a or θ_b . Instead, we find the slope at θ_a , $\theta_a + 30'$, and $\theta_a - 30'$ and use the greatest slope in the calculation,

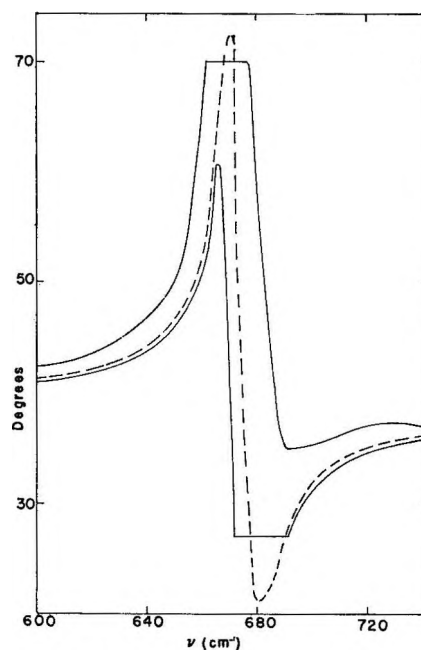


Figure 3. Best angles of incidence for the 675 cm^{-1} band of liquid benzene, using KRS-5 elements, from program TABLE. The best lower angles occur just below the critical angles (dashed curve), while the best higher angles occur above the critical angles. The straight-line positions of the best-angle curves occur because the calculations were limited to angles of incidence within the possible experimental range for the KRS-5 hemicylinder ($27\text{--}70^\circ$).

and similarly for θ_b . Typical best-angle values for a strong band are shown in Figure 3. In choosing the best angles we assume that the uncertainty in the reflectivity is 0.005. The uncertainty in the angle of incidence was assumed in all the error calculations to be $\pm 1'$ of arc. This figure was used more as a sensitivity factor than as a known error. Later, we felt that angles of incidence were uncertain to $\pm 3'$ of arc but were reproducible to within $\pm 1'$ and that the angle between the two angles of incidence was known to within $\pm 1'$. Actually, the errors in optical constants were found to depend mostly on the error of this angle difference. However, the errors due to the angle errors should probably be scaled up somewhat.

The value of the hemicylinder index will affect markedly the values for the best angles, but will not seriously affect the limits of error if appropriate best values are used. Thus, the calculated errors in n_2 and $n_2\kappa_2$ at the best angles for the 1035-cm^{-1} C_6H_6 band are the same for either KRS-5 (n_1 2.37) or AgCl (n_1 1.98) hemicylinders. For the 675-cm^{-1} C_6H_6 band, there is an interval of approximately 3 cm^{-1} where the Ge (n_1 4.00) hemicylinder shows about one-

third of the errors calculated with the KRS-5 hemicylinder.

We shall consider the systematic errors introduced by the spread of angles of incidence in step VII. Errors in measurement of instrument polarization are discussed in step I, but the effect of nonsystematic errors in this measurement are expected to be very small and so we do not include them in calculating the best angles. The values of n_1 are calculated by the computer for each frequency from published dispersion formulas which are presumed to be accurate.³

Final Calculation of Optical Constants and Their Reliability (Step VII). At this point we consider the small correction which may be necessary because of the nonparallelism of the incident light. The extent of this was described in the previous paper which described the apparatus. In principle, if we know the energy distribution for the various angles of incidence within the beam, we can express the reflectivity in terms of the average angle of incidence and the optical constants n_2k_2 and n_2 . Each part of eq 3 would then become a summation of the contribution to the over-all reflectivity from each of a number of closely spaced angles of incidence within the beam. In practice, this would make the iterative part of the program considerably slower and we use an alternative approach. During the iterative process, we assume that the beam is parallel with a well-defined angle of incidence and so calculate values of n_2k_2 and n_2 as described earlier. We can then correct the reflectivities to absorb most of the effect of the angle spread as follows. By assuming that the incident beam of light has a uniform energy distribution over a range of angles of $\pm 0.5^\circ$ on either side of the central angle, the calculated R vs. θ_1 curve agreed roughly with the observed curve. Using the optical constants just obtained, we calculate the reflectivity at $(\theta_1 - 30')$ and $(\theta_1 + 30')$. We then fit a quadratic through these points to represent that part of the R vs. θ_1 curve and calculate the mean value of this curve over the $60'$ angle range. This is shown in Figure 4. \bar{R} is, therefore, the reflectivity we would have observed experimentally if the true reflectivity curve had passed through R_m , R , and R_p . In fact, the observed reflectivity R is the reflectivity of the true curve averaged over $60'$ and we can estimate the true reflectivity at θ_b as $R + (R - \bar{R})$. We do this for R_{θ_a} also and evaluate corrected optical constants from them. If the angles were chosen as described above so as to avoid very steep parts, and consequently regions of high curvature, of the R vs. θ_1 curve, the corrections are always small and this very crude procedure appears to correct for the major part of this known systematic error.

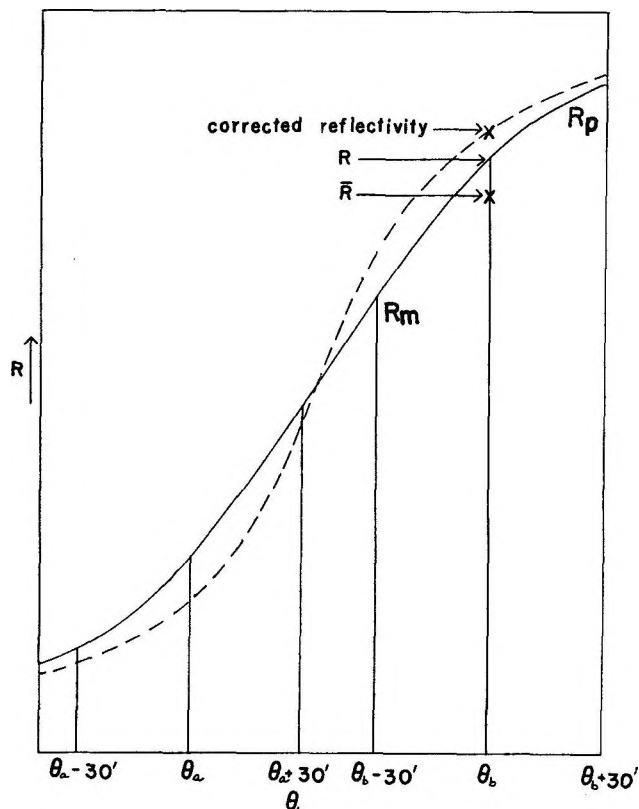


Figure 4. Correction of observed reflectivities for angle-spread effect. The solid line is the observed curve, and the dashed line represents the curve which would be observed with parallel light.

The uncertainty in the optical constants is calculated assuming ± 0.005 uncertainty in photometric accuracy and $\pm 1'$ of arc uncertainty in the angle of incidence. Except at very low absorption, photometric errors are more important than angle errors.

Results of Measurements on Well-Known Bands

The data presented here have been obtained during the development of the method described in the previous section and the earlier results were obtained using a less elaborate procedure. All measurements were made at room temperature with the liquid at $25 \pm 1^\circ$.

1. *The 760-Cm⁻¹ Band of Liquid Chloroform.* In the work on this band, steps I-IV were used. The angles of incidence were chosen intuitively. The errors in the optical constants were calculated assuming uncertainties in the observed reflectivities ranging from ± 0.001 to ± 0.010 . Figure 5 shows the calcu-

(3) For KRS-5, see E. K. Plyler, *J. Res. Bur. Std.*, **41**, 125 (1949); L. W. Tilton, E. K. Plyler, and R. E. Stephens, *ibid.*, **43**, 81 (1949). For AgCl, see H. Schröter, *Z. Physik.*, **67**, 24 (1931); L. W. Tilton, E. K. Plyler, and R. E. Stephens, *J. Opt. Soc. Am.*, **40**, 540 (1950). For Ge, see C. D. Salzberg and J. J. Villa, *ibid.*, **47**, 244 (1957).

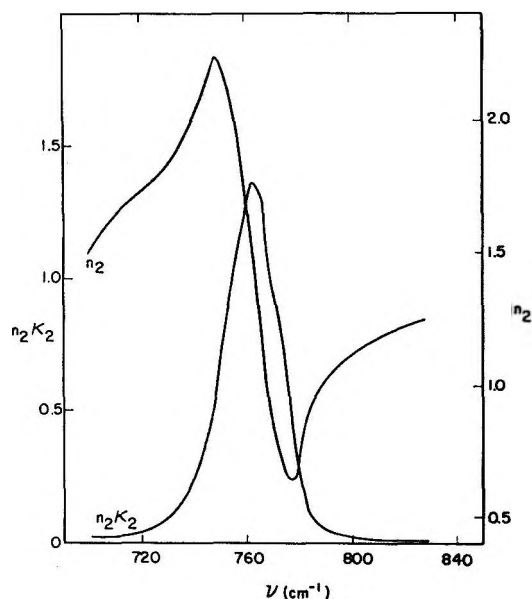


Figure 5. Optical constants for the 760-cm⁻¹ band of liquid chloroform.

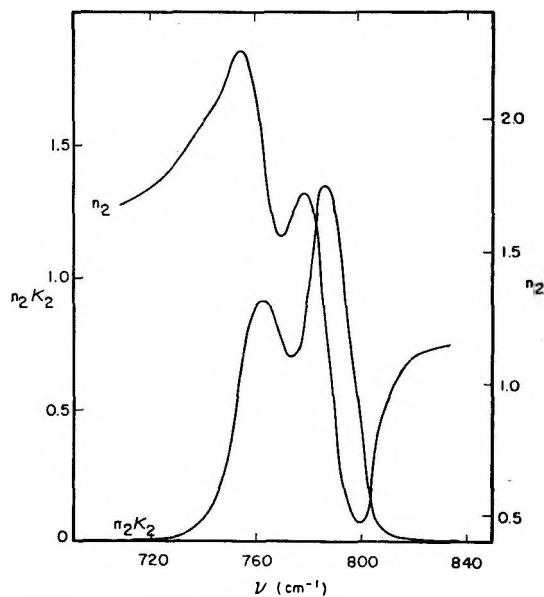


Figure 7. Optical constants for the 770-cm⁻¹ doublet of liquid carbon tetrachloride.

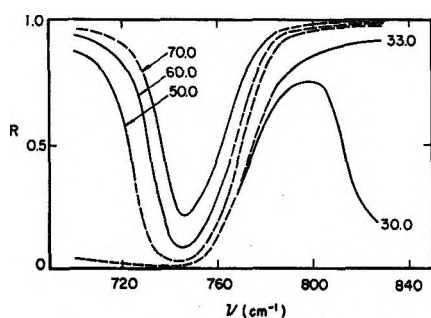


Figure 6. Observed and synthetic (dashed segments) reflectivities for the 760-cm⁻¹ band of liquid chloroform. Numbers near curves give the angles of incidence.

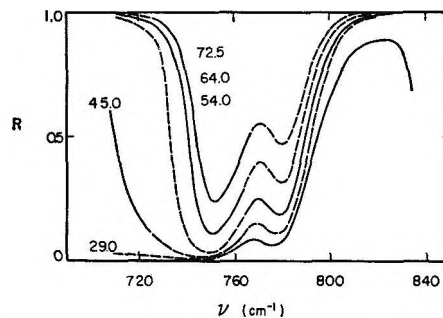


Figure 8. Observed and synthetic (dashed segments) reflectivities for the 770-cm⁻¹ doublet of liquid carbon tetrachloride. Numbers near curves give the angles of incidence.

lated optical constants. The solid lines in Figure 6 show the reflectivities actually measured, and the dotted lines are reflectivities calculated from the optical constants. The data are listed in Table I.

2. *The 770-Cm⁻¹ Doublet of Liquid Carbon Tetrachloride.* The data for this band were obtained using the same procedure as the chloroform band, involving steps I-IV (Figure 7). It is interesting to note that the relative intensity of the two components is reversed in the reflection spectrum shown in Figure 8. The data are given in Table II.

3. *The 675-Cm⁻¹ Band of Liquid Benzene.* In studying this band, we first developed the full procedure described, steps I-VII. This band was first measured under the same conditions as the CHCl₃ and CCl₄ bands reported above. However, a rather large scatter in the results, difficulties in reproducing the results,

and the fact that the integrated intensity was consistently higher than that obtained by other methods prompted a more thorough investigation. Calculations showed that a poor choice of angles of incidence would result in very large uncertainties in the optical constants and this led to the development of step V. When the angles were chosen by calculation rather than by intuition, the optical constants showed far less scatter. In this case, the best angles were chosen by program TABLE considering photometric uncertainty only and did not take into account the uncertainty in angle of incidence. This omission would have negligible effect where n_2K_2 is greater than 0.05. The data are listed in Table III.

4. *The 1035-Cm⁻¹ Band of Liquid C₆H₆.* Here also the final measurements involved the complete procedure, steps I-VII (see Figures 9-14). At first,

Table I: Optical Constants for the 760-Cm⁻¹ Band of Liquid Chloroform

| ν , cm ⁻¹ | n_{2k2} | $\sigma(n_{2k2})$ | n_2 | $\sigma(n_2)$ |
|-------------------------------|-----------|-------------------|-------|---------------|
| Angles of incidence: 30°, 33° | | | | |
| 828 | 0.005 | 0.001 | 1.244 | 0.001 |
| 824 | 0.006 | 0.001 | 1.231 | 0.001 |
| 820 | 0.007 | 0.001 | 1.239 | 0.001 |
| 816 | 0.009 | 0.001 | 1.200 | 0.001 |
| 812 | 0.011 | 0.001 | 1.186 | 0.001 |
| 808 | 0.014 | 0.001 | 1.166 | 0.003 |
| 804 | 0.019 | 0.001 | 1.138 | 0.002 |
| 800 | 0.024 | 0.001 | 1.104 | 0.001 |
| 796 | 0.034 | 0.001 | 1.061 | 0.003 |
| 794 | 0.042 | 0.001 | 1.033 | 0.006 |
| 792 | 0.050 | 0.003 | 1.010 | 0.011 |
| 790 | 0.061 | 0.003 | 0.979 | 0.012 |
| 788 | 0.080 | 0.002 | 0.933 | 0.008 |
| 786 | 0.103 | 0.005 | 0.887 | 0.016 |
| 784 | 0.129 | 0.009 | 0.853 | 0.026 |
| Angles of incidence: 30°, 70° | | | | |
| 782 | 0.200 | 0.011 | 0.755 | 0.021 |
| 780 | 0.283 | 0.023 | 0.694 | 0.029 |
| 778 | 0.412 | 0.023 | 0.637 | 0.020 |
| 776 | 0.564 | 0.027 | 0.647 | 0.018 |
| 774 | 0.727 | 0.029 | 0.672 | 0.009 |
| 772 | 0.822 | 0.037 | 0.756 | 0.004 |
| 770 | 0.948 | 0.019 | 0.824 | 0.005 |
| 768 | 1.013 | 0.026 | 0.917 | 0.007 |
| Angles of incidence: 60°, 70° | | | | |
| 766 | 1.268 | 0.111 | 1.170 | 0.018 |
| 764 | 1.328 | 0.149 | 0.312 | 0.006 |
| 762 | 1.364 | 0.189 | 1.482 | 0.013 |
| 760 | 1.249 | 0.104 | 1.641 | 0.007 |
| 758 | 1.072 | 0.177 | 1.777 | 0.022 |
| 756 | 1.175 | 0.069 | 1.952 | 0.016 |
| 754 | 0.974 | 0.070 | 2.066 | 0.022 |
| 752 | 0.693 | 0.094 | 2.103 | 0.023 |
| 750 | 0.717 | 0.052 | 2.191 | 0.021 |
| 748 | 0.673 | 0.022 | 2.246 | 0.014 |
| 744 | 0.384 | 0.016 | 2.145 | 0.002 |
| 742 | 0.338 | 0.024 | 2.092 | 0.003 |
| 740 | 0.255 | 0.013 | 2.039 | 0.006 |
| 738 | 0.201 | 0.007 | 1.989 | 0.005 |
| 736 | 0.176 | 0.006 | 1.936 | 0.005 |
| 734 | 0.139 | 0.005 | 1.913 | 0.007 |
| 732 | 0.117 | 0.004 | 1.874 | 0.010 |
| 730 | 0.108 | 0.003 | 1.817 | 0.008 |
| 728 | 0.083 | 0.004 | 1.816 | 0.014 |
| Angles of incidence: 50°, 60° | | | | |
| 726 | 0.065 | 0.002 | 1.792 | 0.003 |
| 724 | 0.056 | 0.001 | 1.767 | 0.002 |
| 720 | 0.044 | 0.001 | 1.726 | 0.002 |
| 716 | 0.036 | 0.001 | 1.686 | 0.007 |
| 712 | 0.035 | 0.003 | 1.624 | 0.021 |
| 708 | 0.029 | 0.002 | 1.599 | 0.029 |
| 704 | 0.030 | 0.006 | 1.525 | 0.071 |
| 700 | 0.029 | 0.008 | 1.463 | 0.118 |

Table II: Optical Constants for the 770-Cm⁻¹ Doublet of Liquid Carbon Tetrachloride

| ν , cm ⁻¹ | n_{2k2} | $\sigma(n_{2k2})$ | n_2 | $\sigma(n_2)$ |
|---------------------------------|-----------|-------------------|-------|---------------|
| Angles of incidence: 29°, 54° | | | | |
| 834 | 0.006 | 0.002 | 1.146 | 0.002 |
| 830 | 0.006 | 0.001 | 1.128 | 0.003 |
| 826 | 0.008 | 0.001 | 1.094 | 0.008 |
| 822 | 0.013 | 0.001 | 1.039 | 0.008 |
| 818 | 0.016 | 0.003 | 1.007 | 0.025 |
| 814 | 0.027 | 0.001 | 0.946 | 0.012 |
| 810 | 0.048 | 0.002 | 0.852 | 0.025 |
| 806 | 0.101 | 0.008 | 0.718 | 0.038 |
| 804 | 0.166 | 0.021 | 0.618 | 0.058 |
| 802 | 0.300 | 0.062 | 0.494 | 0.069 |
| 800 | 0.432 | 0.111 | 0.465 | 0.080 |
| 798 | 0.560 | 0.152 | 0.485 | 0.077 |
| 796 | 0.723 | 0.085 | 0.512 | 0.036 |
| 794 | 0.958 | 0.054 | 0.571 | 0.014 |
| 792 | 1.056 | 0.060 | 0.690 | 0.013 |
| 790 | 1.255 | 0.130 | 0.855 | 0.024 |
| 788 | 1.331 | 0.131 | 1.065 | 0.037 |
| 786 | 1.349 | 0.127 | 1.290 | 0.057 |
| 784 | 1.305 | 0.098 | 1.514 | 0.039 |
| 782 | 1.094 | 0.044 | 1.667 | 0.027 |
| 780 | 0.957 | 0.030 | 1.707 | 0.024 |
| 778 | 0.856 | 0.011 | 1.721 | 0.004 |
| 776 | 0.720 | 0.013 | 1.676 | 0.006 |
| 774 | 0.706 | 0.021 | 1.637 | 0.004 |
| 772 | 0.695 | 0.019 | 1.591 | 0.004 |
| 770 | 0.745 | 0.043 | 1.557 | 0.015 |
| 768 | 0.794 | 0.039 | 1.575 | 0.008 |
| 766 | 0.876 | 0.017 | 1.636 | 0.009 |
| 764 | 0.903 | 0.015 | 1.734 | 0.009 |
| 762 | 0.915 | 0.045 | 1.855 | 0.028 |
| 760 | 0.827 | 0.046 | 1.960 | 0.029 |
| Angles of incidence: 64°, 72.5° | | | | |
| 758 | 0.851 | 0.130 | 2.164 | 0.044 |
| 756 | 0.766 | 0.166 | 2.252 | 0.084 |
| 754 | 0.598 | 0.078 | 2.250 | 0.037 |
| 752 | 0.501 | 0.055 | 2.245 | 0.027 |
| 750 | 0.369 | 0.049 | 2.190 | 0.007 |
| 748 | 0.263 | 0.043 | 2.141 | 0.006 |
| 746 | 0.187 | 0.015 | 2.106 | 0.008 |
| 744 | 0.162 | 0.017 | 2.049 | 0.015 |
| 742 | 0.115 | 0.013 | 2.017 | 0.019 |
| 740 | 0.085 | 0.010 | 1.981 | 0.025 |
| 738 | 0.060 | 0.004 | 1.950 | 0.019 |
| 736 | 0.044 | 0.007 | 1.924 | 0.040 |
| Angles of incidence: 45°, 64° | | | | |
| 734 | 0.038 | 0.002 | 1.873 | 0.010 |
| 732 | 0.028 | 0.001 | 1.853 | 0.009 |
| 730 | 0.021 | 0.002 | 1.827 | 0.010 |
| 728 | 0.015 | 0.002 | 1.803 | 0.008 |
| 726 | 0.013 | 0.002 | 1.784 | 0.007 |
| 724 | 0.011 | 0.002 | 1.769 | 0.006 |
| 720 | 0.008 | 0.001 | 1.739 | 0.004 |
| 716 | 0.005 | 0.002 | 1.713 | 0.001 |
| 712 | 0.005 | 0.005 | 1.691 | 0.001 |
| 708 | 0.001 | 0.001 | 1.676 | 0.001 |

Table III: Optical Constants for the 675-Cm⁻¹ Band of Liquid Benzene

| ν , cm ⁻¹ | n_{2k2} | $\sigma(n_{2k2})$ | n_2 | $\sigma(n_2)$ | ν , cm ⁻¹ | n_{2k2} | $\sigma(n_{2k2})$ | τ_2 | $(\sigma\tau_2)$ |
|-------------------------------|-----------|-------------------|-------|---------------|-------------------------------|-----------|-------------------|----------|------------------|
| Angles of incidence: 30°, 40° | | | | | Angles of incidence: 55°, 70° | | | | |
| 736 | 0.006 | 0.001 | 1.391 | 0.019 | 670 | 1.083 | 0.127 | 2.429 | 0.100 |
| 732 | 0.007 | 0.001 | 1.390 | 0.019 | 669 | 0.697 | 0.124 | 2.292 | 0.072 |
| 728 | 0.008 | 0.001 | 1.381 | 0.018 | 668 | 0.512 | 0.102 | 2.211 | 0.036 |
| 724 | 0.009 | 0.001 | 1.373 | 0.017 | 667 | 0.387 | 0.067 | 2.136 | 0.008 |
| 720 | 0.012 | 0.001 | 1.362 | 0.016 | 666 | 0.280 | 0.036 | 2.088 | 0.011 |
| 716 | 0.012 | 0.001 | 1.345 | 0.014 | 665 | 0.228 | 0.018 | 2.034 | 0.012 |
| 712 | 0.014 | 0.001 | 1.335 | 0.013 | 664 | 0.194 | 0.010 | 1.980 | 0.009 |
| 708 | 0.017 | 0.001 | 1.314 | 0.010 | 662 | 0.137 | 0.005 | 1.905 | 0.006 |
| 704 | 0.021 | 0.001 | 1.295 | 0.008 | 660 | 0.093 | 0.004 | 1.865 | 0.007 |
| 700 | 0.029 | 0.001 | 1.260 | 0.005 | 658 | 0.069 | 0.005 | 1.819 | 0.013 |
| 696 | 0.042 | 0.002 | 1.213 | 0.003 | 656 | 0.060 | 0.006 | 1.762 | 0.026 |
| 692 | 0.063 | 0.002 | 1.148 | 0.004 | 654 | 0.044 | 0.006 | 1.755 | 0.035 |
| 688 | 0.124 | 0.005 | 1.033 | 0.010 | Angles of incidence: 40°, 55° | | | | |
| 684 | 0.341 | 0.021 | 0.840 | 0.021 | 654 | 0.041 | 0.005 | 1.771 | 0.024 |
| 680 | 0.834 | 0.060 | 0.841 | 0.011 | 650 | 0.028 | 0.002 | 1.728 | 0.017 |
| Angles of incidence: 30°, 70° | | | | | 646 | 0.023 | 0.001 | 1.694 | 0.013 |
| 684 | 0.340 | 0.025 | 0.854 | 0.022 | 642 | 0.020 | 0.001 | 1.655 | 0.008 |
| 682 | 0.496 | 0.028 | 0.842 | 0.016 | 638 | 0.015 | 0.001 | 1.644 | 0.007 |
| 680 | 0.768 | 0.032 | 0.885 | 0.011 | 634 | 0.012 | 0.001 | 1.629 | 0.006 |
| 679 | 0.843 | 0.031 | 0.950 | 0.010 | 630 | 0.011 | 0.001 | 1.619 | 0.005 |
| 678 | 0.986 | 0.033 | 1.042 | 0.010 | 626 | 0.009 | 0.001 | 1.603 | 0.004 |
| 677 | 1.041 | 0.034 | 1.177 | 0.011 | 622 | 0.008 | 0.001 | 1.593 | 0.004 |
| 676 | 1.189 | 0.038 | 1.277 | 0.012 | 618 | 0.007 | 0.001 | 1.585 | 0.003 |
| 675 | 1.321 | 0.045 | 1.532 | 0.016 | 614 | 0.005 | 0.001 | 1.577 | 0.003 |
| 674.5 | 1.345 | 0.048 | 1.664 | 0.018 | 610 | 0.007 | 0.001 | 1.571 | 0.003 |
| 674 | 1.307 | 0.051 | 1.750 | 0.019 | | | | | |
| 673 | 1.232 | 0.058 | 1.925 | 0.023 | | | | | |
| 672 | 1.117 | 0.067 | 2.064 | 0.028 | | | | | |
| 671 | 0.925 | 0.083 | 2.196 | 0.038 | | | | | |
| 670 | 0.782 | 0.100 | 2.256 | 0.050 | | | | | |

the best angles were chosen so as to minimize only the photometric uncertainties as described for the 675-cm⁻¹ band. However, the 1035-cm⁻¹ band is far less intense than the 675-cm⁻¹ band and so the reflectivity, particularly on the wings of the band, is very sensitive to the angle of incidence when it is close to the critical angle and very insensitive to angle elsewhere. In these regions of low absorption, the two predicted "best" angles were very close together, in some cases only 0.5° apart.

The plots of the optical constants *vs.* wavenumber obtained at these "best" angles showed discontinuities at changes of angle pair. The incorporation into the procedure of the effects due to the uncertainty in the average angle of incidence and the nonparallelism of the incident light (as described in steps V and VI) gave a continuous extinction coefficient curve; however, the refractive index curve still showed discontinuities. Since the angle-spread corrections for n_{2k2} were rather large (50% along the high-frequency wing),

the band was remeasured at angles of incidence picked to minimize the angle-spread corrections in n_{2k2} without introducing extraordinarily large photometric errors. It is these data which are presented in this work. It is not possible to account for the discontinuities at 1060 and 940 cm⁻¹ in the refractive index curve (Figure 13) in terms of the calculated errors; however, it is just in these regions that the angle-spread corrections become quite large. The corrected optical constants for this band are given in Table IV.

Comparison with Other Data. In comparing our results with those of others who have studied these and related phenomena with a similar purpose, it is not quite clear just what property is the one of basic significance. We shall follow the present usual pattern and compare integrated absorption coefficients

$$A = (1/C) \int_{\text{band}} \alpha d\nu = (4\pi/C) \int n_{2k2} \nu d\nu \quad (4)$$

where α is the Bouguer-Lambert absorption coefficient²

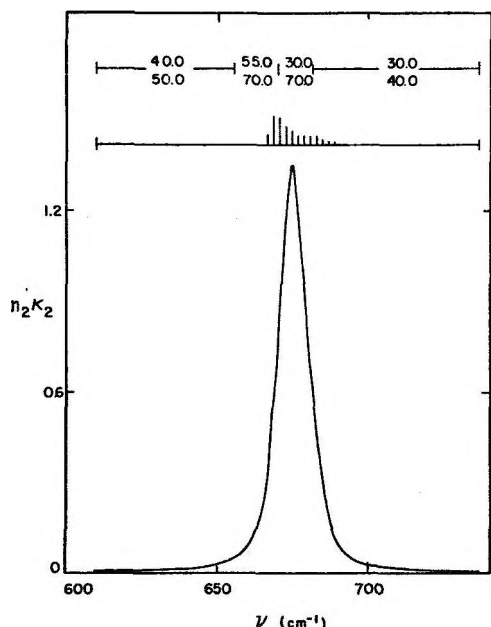


Figure 9. Extinction coefficient *vs.* wavenumber for the 675-cm⁻¹ band of liquid benzene. The numbers above the curve give the angles of incidence, and the vertical lines represent the calculated errors.

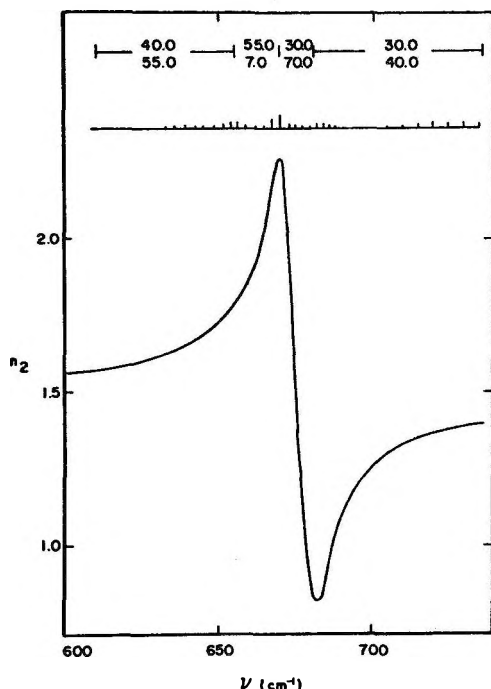


Figure 10. Refractive index *vs.* wavenumber for the 675-cm⁻¹ band of liquid benzene. The numbers above the curve give the angles of incidence, and the vertical lines represent the calculated errors.

in reciprocal centimeters, *C* is the concentration of the sample in micromole per cubic centimeter, and ν is the vacuum wavenumber in reciprocal centimeters.

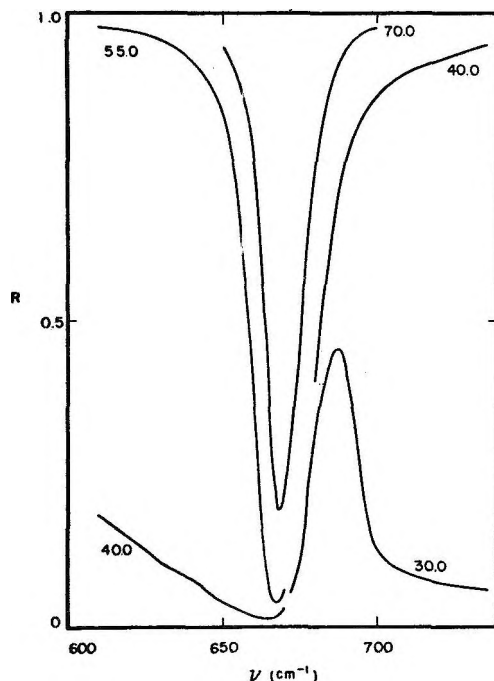


Figure 11. Observed reflectivities for the 675-cm⁻¹ band of liquid benzene. Numbers near curves give the angles of incidence.

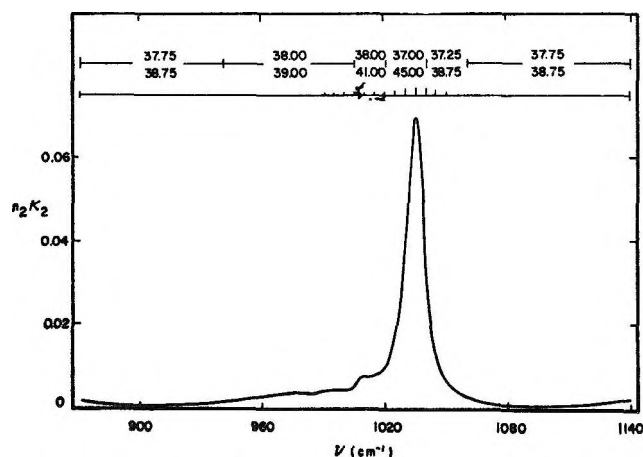


Figure 12. Extinction coefficient *vs.* wavenumber for the 1035-cm⁻¹ band of liquid benzene. The numbers above the curve give the angles of incidence, and the vertical lines represent the calculated errors.

Actually, our values were obtained by integrating the extinction coefficient to obtain the cross-section we prefer

$$\Gamma = (1/C) \int (\alpha/\nu) d\nu = (4\pi/C) \int n_2 K_2 d\nu \quad (5)$$

and computing *A* from the approximate relation $A = \nu_0 \Gamma$, with ν_0 the band-center wavenumber.

The four bands involved have been examined by several methods. Dispersion studies, in which ob-

Table IV: Optical Constants for the 1035-Cm⁻¹ Band of Liquid Benzene

| ν , cm ⁻¹ | n_{2k2} | $\sigma(n_{2k2})$ | n_2 | $\sigma(n_2)$ | ν , cm ⁻¹ | n_{2k2} | $\sigma(n_{2k2})$ | n_2 | $\sigma(n_2)$ |
|-------------------------------------|-----------|-------------------|--------|---------------|-------------------------------------|-----------|-------------------|--------|---------------|
| Angles of incidence: 37.75°, 38.75° | | | | | Angles of incidence: 37.0°, 45.0° | | | | |
| 1140 | 0.0025 | 0.0003 | 1.4587 | 0.0007 | 1034 | 0.0676 | 0.0019 | 1.4634 | 0.0034 |
| 1132 | 0.0020 | 0.0003 | 1.4578 | 0.0007 | 1033 | 0.0597 | 0.0017 | 1.4755 | 0.0034 |
| 1124 | 0.0013 | 0.0003 | 1.4571 | 0.0007 | 1032 | 0.0512 | 0.0015 | 1.4827 | 0.0034 |
| 1116 | 0.0011 | 0.0003 | 1.4565 | 0.0007 | 1031 | 0.0436 | 0.0014 | 1.4854 | 0.0034 |
| 1108 | 0.0009 | 0.0003 | 1.4558 | 0.0007 | 1030 | 0.0369 | 0.0012 | 1.4875 | 0.0034 |
| 1100 | 0.0006 | 0.0003 | 1.4554 | 0.0007 | Angles of incidence: 38.0°, 41.0° | | | | |
| 1092 | 0.0009 | 0.0003 | 1.4548 | 0.0007 | 1031 | 0.0440 | 0.0015 | 1.4852 | 0.0026 |
| 1084 | 0.0008 | 0.0003 | 1.4544 | 0.0007 | 1030 | 0.0371 | 0.0013 | 1.4866 | 0.0023 |
| 1080 | 0.0010 | 0.0003 | 1.4540 | 0.0008 | 1028 | 0.0271 | 0.0009 | 1.4873 | 0.0020 |
| 1076 | 0.0008 | 0.0003 | 1.4540 | 0.0008 | 1026 | 0.0208 | 0.0008 | 1.4828 | 0.0018 |
| 1072 | 0.0012 | 0.0003 | 1.4530 | 0.0011 | 1022 | 0.0126 | 0.0006 | 1.4765 | 0.0013 |
| 1068 | 0.0012 | 0.0003 | 1.4526 | 0.0012 | 1018 | 0.0086 | 0.0005 | 1.4708 | 0.0010 |
| 1064 | 0.0020 | 0.0004 | 1.4497 | 0.0027 | 1014 | 0.0078 | 0.0005 | 1.4682 | 0.0010 |
| Angles of incidence: 37.25°, 38.75° | | | | | 1010 | 0.0074 | 0.0005 | 1.4661 | 0.0010 |
| 1064 | 0.0024 | 0.0003 | 1.4442 | 0.0008 | Angles of incidence: 38.0°, 39.0° | | | | |
| 1060 | 0.0030 | 0.0003 | 1.4426 | 0.0008 | 1010 | 0.0072 | 0.0005 | 1.4662 | 0.0009 |
| 1056 | 0.0038 | 0.0004 | 1.4407 | 0.0008 | 1006 | 0.0061 | 0.0005 | 1.4651 | 0.0009 |
| 1052 | 0.0054 | 0.0004 | 1.4386 | 0.0009 | 998 | 0.0044 | 0.0004 | 1.4627 | 0.0009 |
| 1050 | 0.0062 | 0.0005 | 1.4370 | 0.0011 | 990 | 0.0040 | 0.0004 | 1.4618 | 0.0009 |
| 1048 | 0.0082 | 0.0005 | 1.4342 | 0.0013 | 982 | 0.0037 | 0.0004 | 1.4604 | 0.0009 |
| 1046 | 0.0107 | 0.0006 | 1.4314 | 0.0017 | 972 | 0.0037 | 0.0004 | 1.4604 | 0.0009 |
| 1044 | 0.0159 | 0.0008 | 1.4270 | 0.0024 | 960 | 0.0028 | 0.0003 | 1.4602 | 0.0009 |
| Angles of incidence: 37.0°, 45.0° | | | | | 948 | 0.0019 | 0.0003 | 1.4596 | 0.0010 |
| 1046 | 0.0120 | 0.0011 | 1.4291 | 0.0016 | 940 | 0.0016 | 0.0003 | 1.4588 | 0.0013 |
| 1044 | 0.0169 | 0.0012 | 1.4252 | 0.0020 | Angles of incidence: 37.75°, 38.75° | | | | |
| 1042 | 0.0249 | 0.0013 | 1.4197 | 0.0025 | 940 | 0.0017 | 0.0003 | 1.4555 | 0.0007 |
| 1041 | 0.0298 | 0.0014 | 1.4192 | 0.0025 | 928 | 0.0013 | 0.0003 | 1.4541 | 0.0007 |
| 1040 | 0.0370 | 0.0015 | 1.4170 | 0.0027 | 916 | 0.0011 | 0.0003 | 1.4532 | 0.0007 |
| 1039 | 0.0455 | 0.0016 | 1.4195 | 0.0027 | 904 | 0.0010 | 0.0003 | 1.4522 | 0.0007 |
| 1038 | 0.0541 | 0.0018 | 1.4213 | 0.0029 | 892 | 0.0011 | 0.0003 | 1.4516 | 0.0008 |
| 1037 | 0.0642 | 0.0019 | 1.4271 | 0.0031 | 880 | 0.0013 | 0.0003 | 1.4502 | 0.0010 |
| 1036 | 0.0684 | 0.0019 | 1.4417 | 0.0031 | 868 | 0.0025 | 0.0004 | 1.4470 | 0.0020 |
| 1035 | 0.0694 | 0.0019 | 1.4537 | 0.0034 | | | | | |

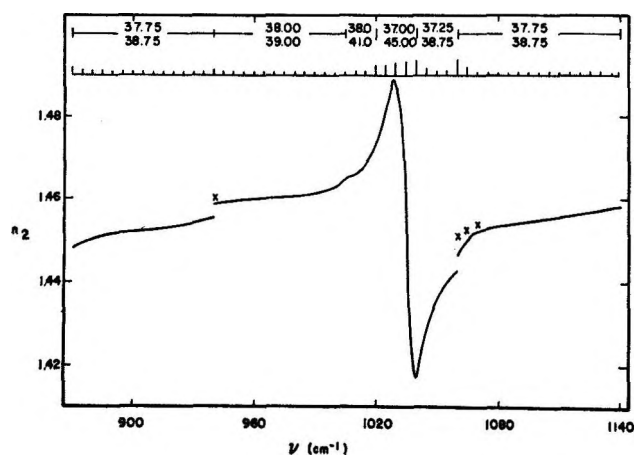


Figure 13. Refractive index vs. wavenumber for the 1035-cm⁻¹ band of liquid benzene. The numbers above the curve give the angles of incidence, and the vertical lines represent the calculated errors. The crosses (X) are points uncorrected for the angle-spread effect.

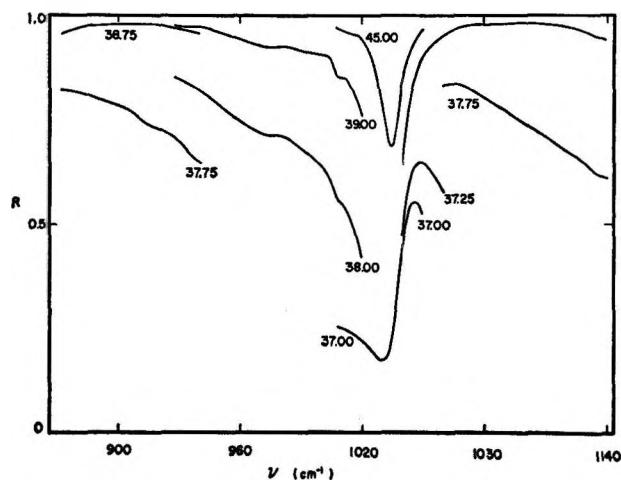


Figure 14. Observed reflectivities for the 1035-cm⁻¹ band of liquid benzene. Numbers near curves give the angles of incidence.

Table V: Comparison of Integrated-Intensity Results^a

| Method | C ₆ H ₆ (675 cm ⁻¹) | C ₆ H ₆ (1035 cm ⁻¹) | CHCl ₃ | CCl ₄ |
|-------------------|--|---|-------------------------|-------------------------|
| Fit to dispersion | 14.1 ± 1.2 ^b | 1.8 ± 0.7 ^b | 28.1 ± 2.2 ^c | 46.0 ± 2.3 ^d |
| Fit to reflection | 16.5 ^e | ... | 34.2 ^e | 47.7 ^e |
| Absorption | 9.54 ± 0.14 ^f | 1.15 ± 0.01 ^f | ... | ... |
| | 10.58 ± 0.83 ^g | 1.19 ± 0.08 ^g | | |
| ATR | ... | 1.23 ^h | ... | ... |
| | | 1.12 ⁱ | | |
| This work | 14.2 ± 0.6 | 1.29 ± 0.09 | 28.6 | 46.6 |

^a All entries in centimeters per micromole. ^b Reference 5. ^c Reference 6. ^d Reference 4. ^e Reference 7. ^f Integration over band with wing correction. ^g Integrated area obtained by Ramsay's method, ref 8. ^h Reference 9. ⁱ Reference 10.

served refractive-index values are fitted by the Drude equations and the A values are obtained as parameters, were applied by Kagarise to CCl₄,⁴ and by Schatz and co-workers to benzene⁵ and to chloroform.⁶ The same basic Drude model was applied to observations of the normal reflection spectrum by Schatz, Maeda, Hollenberg, and Dows,⁷ for the stronger bands of several liquids. The absorption spectrum of liquid benzene was studied by Hisatsune and Jayadevappa,⁸ who used several modifications of the band-integration process in order to correct for wing difficulties.

The problem of the wings of the band affects any band-integration process, of course, including ours. We found it especially annoying in the case of the weak 1035-cm⁻¹ benzene band, with the accompanying hot band on the low-frequency side. The value given in Table V, 1.29 cm/μmole, was obtained by eliminating the hot band; if it was included, a value of 1.54 ± 0.11 cm/μmole was found. We are inclined to blame the less-than-ideal agreement with the two other reported ATR values for this weak band on this same question of what to include in the integration.^{9,10}

Acknowledgments. Portions of this paper are taken from dissertations to be submitted by J. B. and by W. K. to the Graduate Faculty of the University of Minnesota in partial fulfillment of the requirements for the degree of Doctor of Philosophy. The work is part of a research program which receives support, which we deeply appreciate, from the National Science Foundation through Grant GP-3411. Our grateful thanks go to Professor J. Overend and Dr. A. Clifford of this laboratory, to Dr. David Powell, now of the College of Wooster, Wooster, Ohio, and to Dr. I. Suzuki of the University of Tokyo, for their helpful discussions and contributions during the work.

- (4) R. E. Kagarise, *J. Chem. Phys.*, **31**, 1258 (1959).
- (5) P. N. Schatz, *ibid.*, **32**, 894 (1960).
- (6) L. P. Lindsay, S. Maeda, and P. N. Schatz, to be published.
- (7) P. N. Schatz, S. Maeda, J. L. Hollenberg, and D. A. Dows, *J. Chem. Phys.*, **34**, 175 (1961).
- (8) I. C. Hisatsune and E. S. Jayadevappa, *ibid.*, **32**, 565 (1960).
- (9) J. Fahrenfort and W. M. Vissar, *Spectrochim. Acta*, **18**, 1103 (1962).
- (10) P. A. Flournoy, *J. Chem. Phys.*, **39**, 3156 (1963).

Vibrational Intensities. XIV. The Relation of Optical Constants to Molecular Parameters

by A. A. Clifford and Bryce Crawford, Jr.

Molecular Spectroscopy Laboratory, Department of Chemistry, University of Minnesota, Minneapolis, Minnesota 55465 (Received November 1, 1965)

A method is described in which optical constants for condensed phases can be corrected for dielectric effects. This involves transformation to the complex "local susceptibility," which is defined as the ratio of the polarization to the "internal field." The local susceptibility can then be fitted to a Van Vleck and Weisskopf band shape, using a simple graphical technique, and molecular parameters obtained. The results of this procedure, applied to the attenuated total reflection (ATR) data from the preceding paper, are given.

It has long been recognized that the absorption of light by molecules in the condensed phase is significantly affected by electric fields due to the surrounding absorbed particles. This dielectric effect has given rise both to difficulties in rationalizing band shapes and to methods for making dielectric corrections to absorption maxima¹ and intensities.² Now that it is possible by various methods, including attenuated total reflection (ATR), to make accurate measurements of both real and imaginary parts of the complex refractive index, \hat{n} [$=n(1 + i\kappa)$], a further attempt to fit experimental data to theoretically predicted behavior can be made.

A number of models for absorption have been previously discussed. These include the damped harmonic oscillator, the Lorentz oscillator,³ and a modification of the latter, translated into quantum mechanical terms, by Van Vleck and Weisskopf.⁴ All these models give rise directly to expressions relating the polarization of the dielectric, $\hat{\mathbf{P}}$, to the field felt by the molecules, the "local field" or "internal field," $\hat{\mathbf{E}}_i$. We may usefully define their ratio as the "local susceptibility," \hat{C} ($=C' + iC''$). For example, the Van Vleck and Weisskopf model gives

$$\frac{\hat{\mathbf{P}}}{\hat{\mathbf{E}}_i} = \hat{C} = S \left[\frac{\nu_0 - i\gamma}{(\nu_0 - \nu) - i\gamma} + \frac{\nu_0 + i\gamma}{(\nu_0 + \nu) + i\gamma} \right] \quad (1)$$

where S is the strength factor and the function in brackets we can call the shape factor. ν is the vacuum wavenumber of the incident radiation and ν_0 is the wave-

number corresponding to the oscillator's "natural frequency." γ represents a damping constant also expressed as a wavenumber which is related to the mean collision or relaxation time, τ , thus

$$\gamma = 1/2\pi c\tau$$

The strength factor is given by

$$S = N/3h\nu_0 c |\mu_{ij}|^2 \quad (2)$$

with N the concentration of oscillators per cubic centimeter and μ_{ij} the electric-moment matrix element for the transition.

Calculating the Local Susceptibility

In the gas phase the refractive index, n , is essentially unity; hence, to a good approximation, the absorption coefficient is proportional to the imaginary part of the local susceptibility and can be used directly in band-shape considerations. In condensed phases, however, we need to calculate the local susceptibility more rigorously. The problem is one of obtaining a value for the local field; for this we naturally first turned to the Lorentz-Lorenz equation and have as yet found it

(1) J. G. Kirkwood, cited by W. West and R. T. Edwards, *J. Chem. Phys.*, **5**, 14 (1937); E. Bauer and M. Magat, *J. Phys. Radium*, **9**, 319 (1938).

(2) P. N. Schatz, *Spectrochim. Acta*, **21**, 617 (1965); S. R. Polo and M. K. Wilson, *J. Chem. Phys.*, **23**, 2376 (1955).

(3) H. A. Lorentz, "The Theory of Electrons," G. E. Stechert, New York, N. Y., 1923.

(4) J. H. Van Vleck and V. F. Weisskopf, *Rev. Mod. Phys.*, **17**, 227 (1945).

Table I: Optical Constants and Local Susceptibilities, Experimental and Calculated, for the 678-Cm⁻¹ Band of Liquid Benzene

| Fre- quency, cm ⁻¹ | n | nk | C' | | C'' | |
|-------------------------------------|-------|-------|---------|---------|--------|--------|
| | | | Exptl | Calcd | Exptl | Calcd |
| 630 | 1.619 | 0.011 | 0.0838 | 0.0841 | 0.0012 | 0.0011 |
| 632 | 1.626 | 0.012 | 0.0845 | 0.0848 | 0.0013 | 0.0012 |
| 634 | 1.628 | 0.012 | 0.0847 | 0.0854 | 0.0013 | 0.0013 |
| 636 | 1.635 | 0.013 | 0.0855 | 0.0862 | 0.0014 | 0.0014 |
| 638 | 1.643 | 0.015 | 0.0863 | 0.0870 | 0.0016 | 0.0016 |
| 640 | 1.649 | 0.017 | 0.0870 | 0.0879 | 0.0018 | 0.0018 |
| 642 | 1.655 | 0.020 | 0.0876 | 0.0889 | 0.0021 | 0.0020 |
| 644 | 1.678 | 0.020 | 0.0900 | 0.0900 | 0.0021 | 0.0022 |
| 646 | 1.694 | 0.023 | 0.0917 | 0.0912 | 0.0024 | 0.0025 |
| 648 | 1.719 | 0.025 | 0.0942 | 0.0926 | 0.0025 | 0.0029 |
| 650 | 1.728 | 0.028 | 0.0951 | 0.0942 | 0.0028 | 0.0033 |
| 652 | 1.754 | 0.033 | 0.0977 | 0.0960 | 0.0032 | 0.0038 |
| 654 | 1.772 | 0.041 | 0.0995 | 0.0981 | 0.0039 | 0.0045 |
| 656 | 1.762 | 0.060 | 0.0986 | 0.1005 | 0.0058 | 0.0053 |
| 658 | 1.819 | 0.069 | 0.1040 | 0.1034 | 0.0064 | 0.0064 |
| 660 | 1.865 | 0.093 | 0.1083 | 0.1068 | 0.0083 | 0.0078 |
| 662 | 1.905 | 0.137 | 0.1122 | 0.1109 | 0.0118 | 0.0098 |
| 664 | 1.980 | 0.194 | 0.1190 | 0.1160 | 0.0156 | 0.0127 |
| 666 | 2.088 | 0.280 | 0.1285 | 0.1224 | 0.0205 | 0.0169 |
| 668 | 2.211 | 0.512 | 0.1419 | 0.1304 | 0.0331 | 0.0234 |
| 670 | 2.256 | 0.782 | 0.1535 | 0.1404 | 0.0464 | 0.0341 |
| 672 | 2.064 | 1.117 | 0.1613 | 0.1517 | 0.0712 | 0.0528 |
| 674 | 1.750 | 1.307 | 0.1641 | 0.1595 | 0.1018 | 0.0868 |
| 676 | 1.277 | 1.189 | 0.1264 | 0.1430 | 0.1538 | 0.1413 |
| 678 | 1.042 | 0.986 | 0.0645 | 0.0707 | 0.1694 | 0.1788 |
| 680 | 0.885 | 0.768 | 0.0028 | -0.0020 | 0.1462 | 0.1421 |
| 682 | 0.848 | 0.487 | -0.0211 | -0.0192 | 0.0865 | 0.0878 |
| 684 | 0.840 | 0.341 | -0.0250 | -0.0118 | 0.0583 | 0.0537 |
| 686 | 0.925 | 0.214 | -0.0112 | -0.0007 | 0.0352 | 0.0349 |
| 688 | 1.033 | 0.124 | 0.0057 | 0.0092 | 0.0196 | 0.0240 |
| 690 | 1.099 | 0.087 | 0.0157 | 0.0171 | 0.0133 | 0.0175 |
| 692 | 1.148 | 0.063 | 0.0230 | 0.0234 | 0.0094 | 0.0132 |
| 694 | 1.181 | 0.051 | 0.0279 | 0.0285 | 0.0075 | 0.0103 |
| 696 | 1.213 | 0.042 | 0.0325 | 0.0326 | 0.0061 | 0.0083 |
| 698 | 1.238 | 0.036 | 0.0361 | 0.0360 | 0.0051 | 0.0068 |
| 700 | 1.261 | 0.029 | 0.0393 | 0.0389 | 0.0041 | 0.0057 |
| 702 | 1.278 | 0.024 | 0.0416 | 0.0413 | 0.0033 | 0.0048 |
| 704 | 1.295 | 0.021 | 0.0440 | 0.0434 | 0.0029 | 0.0041 |
| 706 | 1.310 | 0.019 | 0.0460 | 0.0452 | 0.0026 | 0.0036 |
| 708 | 1.314 | 0.017 | 0.0466 | 0.0468 | 0.0023 | 0.0031 |
| 710 | 1.317 | 0.016 | 0.0470 | 0.0481 | 0.0022 | 0.0028 |
| 712 | 1.335 | 0.014 | 0.0494 | 0.0494 | 0.0019 | 0.0025 |
| 714 | 1.339 | 0.013 | 0.0499 | 0.0505 | 0.0017 | 0.0022 |
| 716 | 1.345 | 0.012 | 0.0507 | 0.0514 | 0.0016 | 0.0020 |
| 718 | 1.350 | 0.012 | 0.0514 | 0.0523 | 0.0016 | 0.0018 |
| 720 | 1.362 | 0.011 | 0.0530 | 0.0531 | 0.0014 | 0.0016 |

quite adequate in explaining our results. (An unsuccessful attempt to improve upon it is outlined later.) This equation relates the local field, \hat{E}_i , to the macroscopic field, \hat{E} ; thus

$$\hat{E}_i = \hat{E} = (4\pi/3)\hat{P}$$

and hence we have

$$1/\hat{C} = 1/\hat{\chi} - (4\pi/3)$$

$\hat{\chi}$ being the usual macroscopic electric susceptibility; or, in more familiar form:

$$\hat{C} = 3/4\pi[(\hat{\epsilon} - 1)/(\hat{\epsilon} + 2)] \quad (3)$$

where $\hat{\epsilon} (= \epsilon' + i\epsilon'')$ is the complex dielectric constant. Separating into real and imaginary parts

$$C' = 3/4\pi \left[1 - \frac{3(\epsilon' + 2)}{(\epsilon' + 2)^2 + \epsilon''^2} \right]$$

$$C'' = \frac{9\epsilon''}{4\pi[(\epsilon' + 2)^2 + \epsilon''^2]} \quad (4)$$

So, by using Maxwell's relation, $\hat{\epsilon} = \hat{n}^2$, and then eq 4 experimental refractive index data can be transformed into values of the (Lorentz-Lorenz) local susceptibility. An example is given for the 678-cm⁻¹ band of benzene in Table I and Figure 1, using the ATR data from the preceding paper. Transformation to local susceptibility apparently produces similar though changed traces. In particular the plot of C'' against frequency is more symmetrical than the corresponding plot for $n\kappa$. Also the frequency which gives the maximum value of C'' is seen to be slightly different from the absorption "band center."

A Graphical Method for Comparison of Experimental Results with the Van Vleck and Weisskopf Band Shape

Basic Equations. Having transformed our data into variables which are more relevant to theoretical considerations we may now attempt to understand the band shape. For the infrared region the Van Vleck and Weisskopf expression is likely to be the most useful.

Equation 1 gives the contribution of a single transition to the local susceptibility. In practice, we must take into account other transitions and also a contribution due to nonresonant or Debye absorption. Fortunately, if the other bands are sufficiently remote and we choose frequencies high enough so that nonresonant absorption is negligible, the local susceptibility resulting from them will be a constant real quantity which we can call K . Equation 1 now becomes

$$\hat{C} = K + S \left[\frac{\nu_0 - i\gamma}{(\nu_0 - \nu) - i\gamma} + \frac{\nu_0 + i\gamma}{(\nu_0 + \nu) + i\gamma} \right] \quad (5)$$

Separating into real and imaginary parts, we obtain

$$C' = K + 2S \left[\frac{\gamma^4 + \gamma^2(2\nu_0^2 + \nu^2) + \nu_0^2(\nu_0^2 - \nu^2)}{\gamma^4 + 2\gamma^2(\nu_0^2 + \nu^2) + (\nu_0^2 - \nu^2)^2} \right] \quad (6)$$

$$C'' = 2S \left[\frac{\nu\gamma(\gamma^2 + \nu_0^2 + \nu^2)}{\gamma^4 + 2\gamma^2(\nu_0^2 + \nu^2) + (\nu_0^2 - \nu^2)^2} \right] \quad (7)$$

From eq 6 and 7 the following relation can be readily derived.

$$C' = K + 2S + (1/\gamma)C'' \nu \left[\frac{\nu_0^2 - \nu^2 - \gamma^2}{\nu_0^2 + \nu^2 + \gamma^2} \right] \quad (8)$$

For the majority of condensed phase bands, at normal temperatures, and provided we confine ourselves

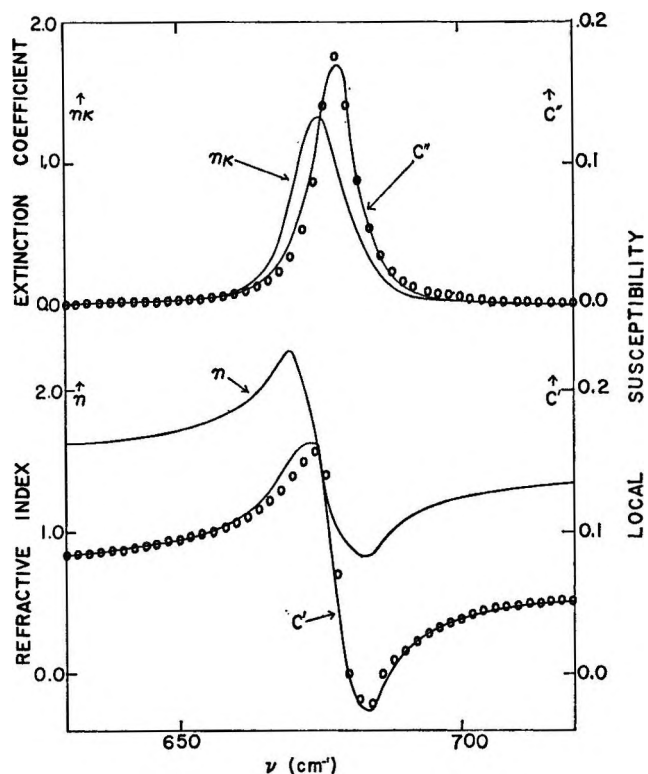


Figure 1. Optical constants and local susceptibilities for the 678-cm⁻¹ band of liquid benzene. For the local susceptibilities, the line represents experimental data and the circles are calculated points.

to frequencies in the far-infrared and higher, $\gamma^2 \ll \nu_0^2$. For example, ν_0^2/γ^2 is approximately 4×10^4 for the benzene 678-cm⁻¹ band. Thus, if we create a weighted susceptibility

$$C^{\circ} = \nu \left[\frac{\nu_0^2 - \nu^2}{\nu_0^2 + \nu^2} \right] C'' \quad (9)$$

then it will be very nearly true that

$$C' = K + 2S + (1/\gamma)C^{\circ} \quad (10)$$

Obtaining a Value for ν_0 . To calculate the weighted susceptibility we need the true frequency of the transition, ν_0 , which in a condensed phase is not always the same as the frequency of maximum absorption. It can be seen from eq 5 that for C'' to be a maximum

$$\nu = \sqrt{\nu_0^2 + \gamma^2} \approx \nu_0 \quad (11)$$

since $\nu_0^2 \gg \gamma^2$. ν_0 is thus obtained from the C'' maximum and an effective dielectric correction is easily made. This correction will not, of course, take into account the change of the potential function of the molecule as it moves into the condensed phase. What it will do is to give a corrected frequency shift

Table II: Band Parameters Obtained from ATR Data Using the Plotting Technique^a

| | Fre- quency of $n\kappa$ maxi- mum, cm ⁻¹ | ν_0 , cm ⁻¹ | γ , cm ⁻¹ | $10^{12}\tau$, sec | K | $10^4S'$ | $10^4S''$ | Γ^c | Γ^{liq} | Γ^{pw} | Γ (gas phase) |
|---------------------------|---|-------------------------------|--------------------------------|------------------------|---------|----------|-----------|------------|----------------|---------------|----------------------------|
| Benzene | 674 | 678 | 3.91 | 1.36 | 0.0691 | 108 | 98 | 15,400 | 21,000 | 15,800 | 12,600 ^b |
| Benzene | 1035 | 1035 | 5.56 | 0.96 | 0.0647 | 4.37 | 4.32 | 990 | 1,100 | 850 | 820 ^b |
| Chloroform | 762 | 769 | 6.95 | 0.76 | 0.0604 | 206 | 190 | 30,100 | 37,200 | 30,000 | 36,000 ^c |
| Main band | 786 | 792 | 5.84 | 0.91 | 0.0235 | 182 | 135 | 30,100 | 58,000 | 44,400 | 49,500 ^d |
| Carbon tetra- chloride | | | | | | | | | | | |
| Subsidiary peak | (762) | (766) | (10.3) | (0.52) | (0.106) | (69) | (91) | (14,800) | | | |

^a Intensities (Γ) are given in square centimeters per mole. ^b J. Overend in "Infra-red Spectroscopy and Molecular Structure," M. Davies, Ed., Elsevier Publishing Co., Amsterdam, 1963. Chapter X. ^c J. Morcillo, J. Herranz, and J. F. Biarge, *Spectrochim. Acta*, 15, 110 (1959). ^d L. P. Lindsay and P. N. Schatz, *ibid.*, 20, 1421 (1964).

from which a more precise evaluation of intermolecular forces in the condensed phase can be made.

The extent of this correction in some bands can be seen by comparing columns 2 and 3 of Table II. The figures in Table II have been calculated from the ATR data for the four bands published in the preceding paper. In the case of the weak benzene 1035-cm⁻¹ band the correction is negligible. In the other cases it amounts to a shift of a few wavenumbers to higher frequencies.

The C^o-C' Plots. Values of C^o can now be calculated throughout a band and plots of C^o against C' can be drawn. According to eq 10 this should give a straight line of slope γ . Plots for the four bands mentioned are given in Figure 2. Acceptable straight lines are obtained in all cases with, however, partial deviations produced by the "hot" band on the benzene 1035-cm⁻¹ figure and by the minor peak of the carbon tetrachloride doublet. These off-line points are therefore not included in the calculation of the values of γ which are shown in Table II.

Calculation of Intensities. The absorption cross section Γ , calculated in the gas phase from the Bouguer-Lambert absorption coefficient α

$$\Gamma = (1/C_m) \int \alpha d \ln \nu = (1/C_m l) \int \ln(I_0/I) d \ln \nu \quad (12)$$

with C_m the molar concentration of the gas,⁵ is physically significant since it bears the simple relationship

$$\Gamma = 8\pi^3 N_0 / 3hc |\mu_{ij}|^2 \quad (13)$$

to the electric-moment matrix element μ_{ij} .

For the condensed phase, our model indicates that the same cross section, for which relation 13 will hold,

can be calculated from the strength factor S of the local susceptibility; we find

$$\Gamma^c = 8\pi^3 \nu_0 (M/d) S \quad (14)$$

where ν_0 is the wavenumber and M and d are the molecular weight and the density. Γ^c is, of course, the intensity corrected for the dielectric effect, which is otherwise obtained using the Polo-Wilson equation.²

Values of S can be obtained now that ν_0 and γ are known by plotting C' and C'' against the real and imaginary parts of the shape factor. As can be seen from eq 6 and 7, both these plots should give a slope of $2S$. Figure 3 gives an example of such plots for the benzene 678-cm⁻¹ band. The straight-line behavior again represents a test of the approach.

In this way two slightly different values of S , as shown in Table II, are obtained from each band. S' is the value obtained from the real part and S'' from the imaginary part of the local susceptibility. Then from the average of S' and S'' , Γ^c can be obtained using eq 14. These are shown in Table II alongside values (Γ^{liq}) obtained by the conventional technique of eq 12.

Comparison of Experimental and Theoretical Local Susceptibilities. Plots of the real part of the local susceptibility against the shape factor will also give values for the contribution to the local susceptibility from outside the band, K , shown also in Table II. Now that all the parameters in the Van Vleck and Weisskopf equation have been determined, theoretical values of the local susceptibility can be calculated and compared with experimental values. These are shown for the 678-cm⁻¹ benzene band in Table I and Figure 1.

(5) B. L. Crawford, Jr., *J. Chem. Phys.*, 29, 1042 (1958).

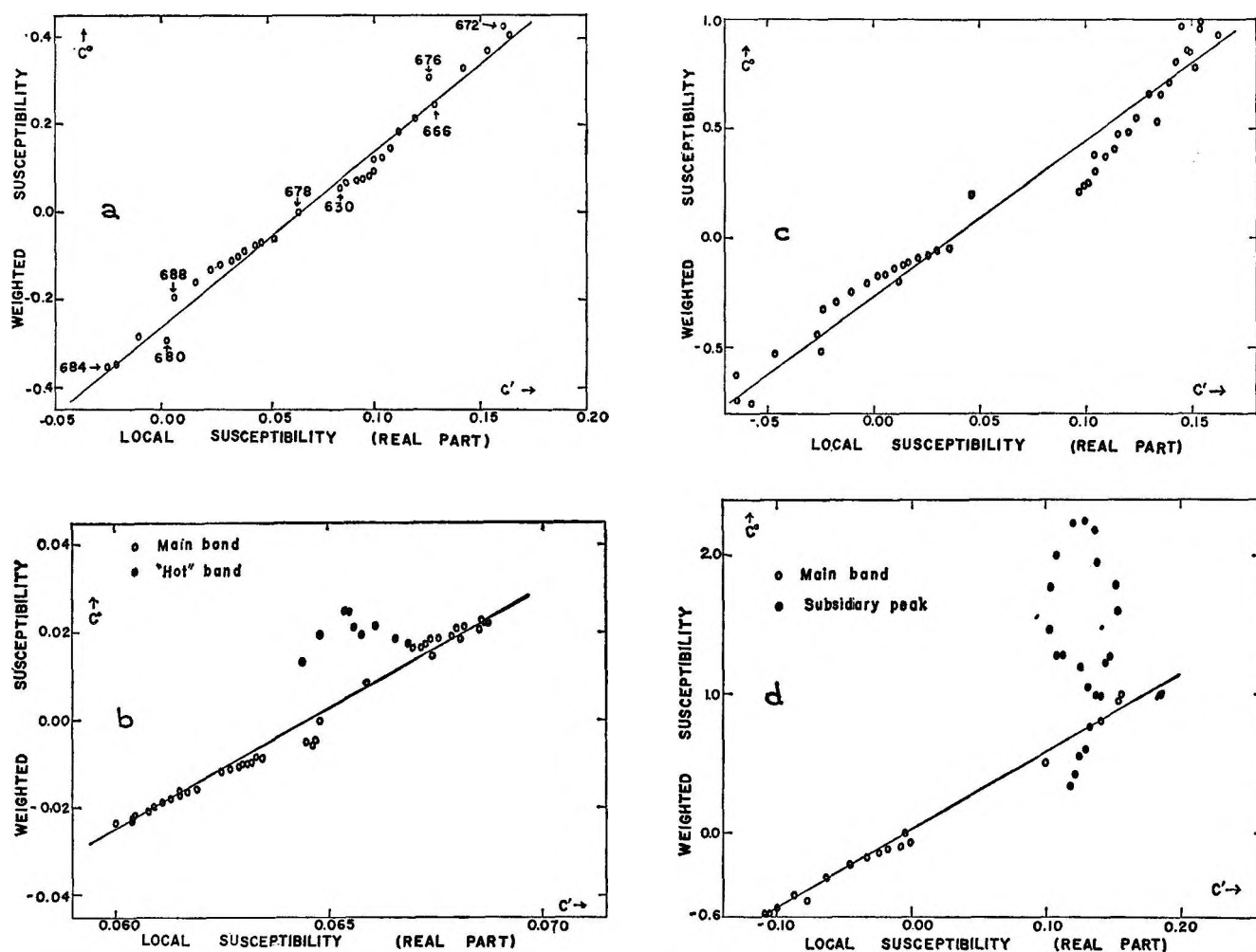


Figure 2. Plots of the weighted susceptibility against the real part of the local susceptibility for the (a) benzene 678-cm⁻¹, (b) benzene 1035-cm⁻¹, and (c) chloroform 762-cm⁻¹ bands, and (d) the carbon tetrachloride 792-cm⁻¹ doublet.

The region at the lower frequency side of the band center, where the biggest deviations occur, is also the region where the experimental results are the least reliable. The agreement at the edges of the band is particularly gratifying.

Comparison with Other Methods of Obtaining Intensities

Our present approach offers very real advantages, aside from the pleasure of finding such a nice fit to a simple model, since the value of Γ^c is not obtained by an integration and hence avoids those problems of "integration limits" and "wing corrections" which have long plagued the student of intensities. It does, of course, assume a particular model, subject to a "straight-line" test and this may not be possible in all cases. It is worth mentioning, therefore, that a generalized Γ^c can be obtained from the integral, over the band, of the imaginary part of the local susceptibility using the following expression

$$\Gamma^c = 8\pi^2(M/d)\int C''d\nu \quad (15)$$

which is independent of a particular band-shape model; this reduces appropriately to the gas phase Γ of eq 12 and the Van Vleck-Weisskopf Γ^c of eq 14.

Also it has been argued by Schatz² that the Polo-Wilson equation will adequately correct for dielectric effects, on the basis of the Lorentz-Lorenz field, in spite of the variation of the refractive index, n , throughout the band, provided the appropriate value of n is used. Thus, our graphical method and the Polo-Wilson equation should give the same result. This is seen to be essentially true by comparing the values of Γ^c and Γ^{PW} (obtained by a Polo-Wilson correction to Γ^{liq}) in Table II. We attribute the discrepancy in the benzene 1035-cm⁻¹ band case to integration difficulties, because of the associated hot band. We also feel that, as well as integration problems, the Polo-Wilson method suffers from lack of precision due to the dif-

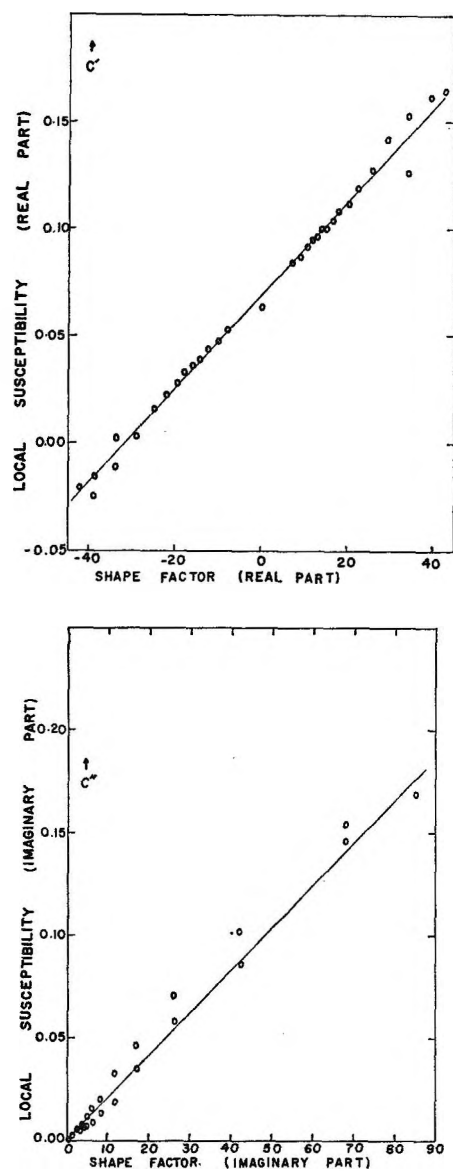


Figure 3. Plots of the local susceptibility against the shape factor for the liquid benzene 678-cm^{-1} band.

ficulty which arises in practice of assigning the correct value to n .

Values for gas phase intensities are also given in Table II, although these are not expected to equal the corrected liquid phase intensities in all cases because of nondielectric or "chemical" action.⁶ We have not needed to rely here on theoretical considerations to predict when both intensities should be the same and hence to decide whether the Lorentz-Lorenz correction was adequate. Instead, our criterion has been "straight-line" behavior: a point which is amplified later.

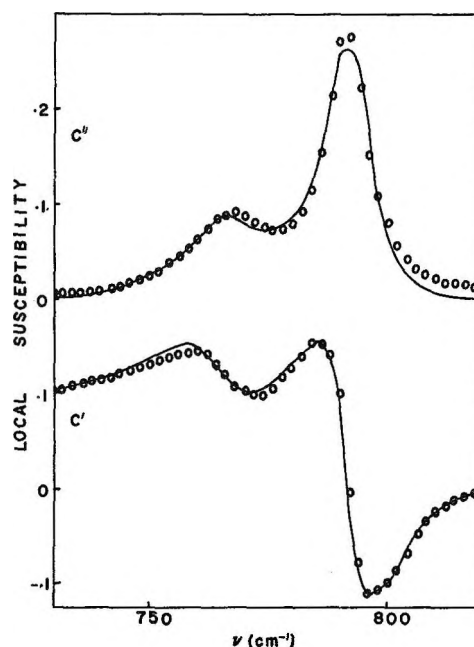


Figure 4. Comparison of experimental and theoretical local susceptibilities for the carbon tetrachloride 792-cm^{-1} doublet. The line represents experimental data and the circles are calculated points.

Treatment of Data for Adjacent Bands

The method outlined in the last section only applies, strictly speaking, to single remote bands. Thus, the carbon tetrachloride doublet main band did not give good plots. However, some approximate parameters were obtained both for the main band and the subsidiary peak. Data for the subsidiary peak are given in parentheses in Table II.

These values were later refined by least squares to fit the local susceptibility data. The final parameters are shown in Table III, and Figure 4 shows how the experimental and calculated values compared at the end of the refinement process. As mentioned in the preceding paper, these data were not obtained by the later techniques and are not so reliable as the benzene data. We are therefore satisfied by the agreement obtained. Again we note an advantage of the present approach over integration procedures, in that overlapping bands can be analyzed in terms of their separate intensities, without the subjective curve sketching which has been resorted to.⁷

Improvement of the Method

The four bands studied so far have obeyed the as-

(6) W. B. Person, *J. Chem. Phys.*, **28**, 319 (1958); A. D. Buckingham, *Proc. Roy. Soc. (London)*, **A248**, 169 (1958).

(7) E.g., A. D. Dickson, I. M. Mills, and B. L. Crawford, Jr., *J. Chem. Phys.*, **27**, 445 (1957).

Table III: Band Parameters Obtained for the Carbon Tetrachloride 792-Cm⁻¹ Doublet by Least-Squares Refinement^a

| | ν_0 cm ⁻¹ | γ cm ⁻¹ | $10^{12}\tau$ sec | $10^6 S$ | Γ^0 | K |
|-----------------|-----------------------------|------------------------------|----------------------|----------|------------|--------|
| Main band | 791.2 | 5.2 | 1.02 | 180 | 34,000 | 0.0596 |
| Subsidiary peak | 766.6 | 10.3 | 0.52 | 107 | 19,600 | |

^a Intensities (Γ) are given in square centimeters per mole.

assumptions of the Lorentz-Lorenz field and the Van Vleck and Weisskopf band shape to within the reliability of the experimental data. However, two possible improvements were explored.

Improvements to the Lorentz-Lorenz Field. For an isotropic medium, the local field at a point in a dielectric can in general be expressed by³

$$\hat{E}_i = \hat{E} - a(4\pi/3)\hat{P} \quad (16)$$

where a is a scalar which depends on the arrangement of charged particles around the point under consideration. In the cases where the Lorentz-Lorenz equation holds, a , of course, becomes unity. Using eq 16, the local susceptibility is given by

$$\hat{C} = 3/4\pi \left[\frac{\hat{\epsilon} - 1}{a\hat{\epsilon} - a + 3} \right] \quad (17)$$

This was used to calculate C with values of a slightly different from unity. This, however, gave $C^0 - C'$ plots which were worse straight lines than those obtained previously.

The Effect of a Range of Relaxation Times. Models of dielectrics in which molecules are assumed to have a range of relaxation times are often used to explain nonresonant absorption data.⁸ Application of this idea to resonant absorption was mentioned by Van Vleck and Weisskopf.⁴ Equation 5 would become in this case

$$\hat{C} = K + \int_{\text{range of } \gamma} \hat{C}(\gamma) d\gamma \quad (18)$$

where

$$\hat{C}(\gamma) = S(\gamma) \left[\frac{\nu_0 - i\gamma}{(\nu_0 - \nu) - i\gamma} + \frac{\nu_0 + i\gamma}{(\nu_0 + \nu) + i\gamma} \right]$$

and $S(\gamma)$ has only positive values.

Separating into real and imaginary parts, one obtains instead of (10)

$$C' = K + 2 \int S(\gamma) d\gamma + \left[\frac{\int \frac{C(\gamma)'' d\gamma}{\gamma}}{\int C(\gamma)'' d\gamma} \right] C^0$$

Thus, to a first approximation, the slope of a $C^0 - C'$ at any point will be

$$\left[\frac{\int \frac{C(\gamma)'' d\gamma}{\gamma}}{\int C(\gamma)'' d\gamma} \right]^{-1}$$

At the center of the band, as $\nu \rightarrow \nu_0$, $C(\gamma)'' \rightarrow 2S(\gamma)\nu/\gamma$. The slope will therefore be

$$\frac{\int \frac{S(\gamma) d\gamma}{\gamma}}{\int \frac{S(\gamma) d\gamma}{\gamma^2}}$$

At the edges of the band $C(\gamma)'' \rightarrow 2S(\gamma)\nu\gamma(\nu_0^2 + \nu^2)/(\nu_0^2 - \nu^2)$ and the slope becomes

$$\frac{\int S(\gamma)\gamma d\gamma}{\int S(\gamma) d\gamma}$$

From Schwarz's inequality it follows that

$$\frac{\int S(\gamma)\gamma d\gamma}{\int S(\gamma) d\gamma} \geq \frac{\int \frac{S(\gamma) d\gamma}{\gamma}}{\int \frac{S(\gamma) d\gamma}{\gamma^2}}$$

and thus the slope of the $C^0 - C'$ plot should be greater at the edges of the band than in the band center, with the straight line becoming a figure eight. Actually the deviations from linearity are, if anything, in the opposite direction and the data do not therefore suggest a range of relaxation times.

Physical Significance of the Results

Physically speaking, our fit of the Van Vleck and Weisskopf band shape indicates that we are observing single transitions and that rotational motion is effectively suppressed. These systems therefore are more significantly described in terms of the angular position of the molecules rather than their angular momenta and they approximate to Shimizu's "Debye limit."⁹

Recently some interesting work has been done in which band shapes have been discussed in terms of time-correlation functions.⁹ In these terms, the treatment outlined here is equivalent to the application of a damped-oscillator correlation function to the local

(8) H. Fröhlich, "Theory of Dielectrics," 2nd ed, Oxford University Press, London, 1958; C. P. Smith, "Dielectric Behaviour and Structure," McGraw-Hill Book Co., Inc., New York, N. Y., 1955; C. J. F. Böttcher, "Theory of Electric Polarisation," Elsevier Publishing Co., Amsterdam, 1952; K. S. Cole and R. H. Cole, *J. Chem. Phys.*, **9**, 341 (1941).

(9) R. G. Gordon, *ibid.*, **43**, 1307 (1965); H. Shimizu, *ibid.*, **43**, 2453 (1965).

susceptibility. (Compare Frölich's derivation of equations for the dielectric constant and loss in the region of resonant absorption.⁶) The small deviations from the Van Vleck and Weisskopf band shape of the data presented here compared with the probable errors do not justify transformation for further investigation of a correlation function. However, this may be worthwhile with other ATR data, especially where partial rotation appears to be significant.¹⁰ It seems likely that correlation functions derived from the local susceptibility, when this can be adequately calculated, rather than from the absorption coefficient, will prove to be more fruitful for strong bands in condensed phases.

Acknowledgments. We gratefully acknowledge the financial support for this work obtained from the National Science Foundation through Grant GP-3411 and would also like to thank our colleagues in this

laboratory, especially Dr. John Overend, for many helpful discussions.

Addendum

It has been brought to our attention that the idea of transforming a spectrum to correct for dielectric effects is not a new one. Bakhshiev, Girin, and Libov¹¹ have used expressions for the internal field to calculate what they call true absorption spectra. Their method of obtaining the true absorption spectra using the Lorentz-Lorenz field is identical, except for a constant factor, with that for the imaginary part of the (Lorentz-Lorenz) local susceptibility as described in this paper.

(10) *E.g.*, W. J. Jones and N. Shepperd, *Trans. Faraday Soc.*, **56**, 625 (1959).

(11) N. G. Bakhshiev, O. P. Girin, and V. S. Libov, *Opt. Spectry.* (U.S.S.R.), **14**, 255, 336, 395 (1963); **16**, 549 (1964).

Proton Resonance Spectrum of Butatriene^{1a}

by Stephen G. Frankiss^{1b} and Ikuo Matsubara

Mellon Institute, Pittsburgh, Pennsylvania (Received November 8, 1965)

The proton resonance spectrum of butatriene at -55° is reported. The long-range *trans* (H,H') and *cis* (H,H') coupling constants are equal to 8.95 cps, which agrees well with Karplus' calculated value (7.8 cps). The proton chemical shifts of ethylene, allene, and butatriene are briefly discussed.

The long-range coupling constants ($J_{HH'}$) between protons separated by π -electronic structure have been the subject of several recent experimental²⁻³ and theoretical^{9,10} studies. Karplus, in particular, has emphasized the importance of the contributions of π -electron terms ($J_{HH'}[\pi]$) to these coupling constants.¹⁰ He has estimated the values of $J_{HH'}[\pi]$ in a few systems and has predicted a large (7.8 cps) value for $J_{HH'}[\pi]$ in butatriene. Although the observation of $J_{HH'}$ in butatriene would provide a useful check of his theory, the only reported attempt to observe its spectrum was

thwarted by its rapid polymerization.¹¹ We have found, however, that at low temperatures (below

(1) (a) This work was supported by the National Science Foundation under Grant GP-1628; (b) Department of Chemistry, University College, Gower St., London, W.C.1, England, to whom all communications should be sent.

(2) D. F. Koster and A. Danti, *J. Phys. Chem.*, **69**, 486 (1965), and references quoted therein.

(3) M. W. Hanna and J. K. Harrington, *ibid.*, **67**, 940 (1963).

(4) R. K. Kullnig and F. C. Nachod, *ibid.*, **67**, 1361 (1963).

(5) A. A. Bothner-By and R. K. Harris, *J. Am. Chem. Soc.*, **87**, 3451 (1965), and references quoted therein.

-50°), the rate of polymerization is sufficiently slow that satisfactory spectra may be obtained.

Experimental Section

Butatriene was prepared by the method of Schubert, *et al.*,¹² and was purified by low-temperature bulb-to-bulb distillations *in vacuo*. Its infrared¹³ and nmr spectra were used as purity criteria; only one very weak extraneous peak was observed, at τ 8.4 in the nmr spectrum.

The compound was studied in 5-mm Pyrex tubes as a pure liquid at -55° and as a dilute solution (*ca.* 1% v/v) in tetramethylsilane (TMS) at -55 and 37° . The spectrum of a dilute solution (*ca.* 5% v/v) of allene (Matheson) in TMS was also measured. The spectra were obtained on a Varian A-60 spectrometer and were measured using a full-scale sweep width of 50 cps. The calibration was by means of audio side bands; the reported frequencies are the average values of at least six measurements.

Results

Butatriene was studied with ^{13}C in natural abundance, and so its proton spectrum consists of a strong line due to $^{12}\text{CH}_2\text{CC}^{12}\text{CH}_2$ and weak lines from $^{13}\text{CH}_2\text{CC}^{12}\text{CH}_2$. Only the outer lines in the $^{13}\text{CH}_2\text{CC}^{12}\text{CH}_2$ spectrum were observed (Table I); the low-field part of the spectrum is illustrated in Figure 1.

The spectrum of $^{13}\text{CH}_2\text{CC}^{12}\text{CH}_2$ was analyzed as an $\text{A}_2\text{B}_2\text{X}$ type (though it approximated to $\text{A}_2\text{K}_2\text{X}$) using the LAOCOON II program.¹⁴ It was assumed that $J_{\text{BX}} = -2.4$ cps and $J_{\text{AA}} = 2.0$ cps (by analogy with similar coupling constants in ethylene^{15,16}). The calculated spectrum is not, however, very sensitive to these two parameters.

The calculated peak positions are given in Table I, along with the derived values of ν_{A} , J_{AB} (*trans*), and J_{AB} (*cis*).

Table I: Peak Positions^a in the Hydrogen Spectrum of $^{13}\text{CH}_2\text{CC}^{12}\text{CH}_2$ and the Derived Parameters^b

| Obsd | Calcd | Peak | Obsd | Calcd |
|-------|-------|------|------|-------|
| -94.8 | -94.9 | 1 | 95.9 | 95.8 |
| -93.9 | -93.9 | 2 | 94.8 | 94.8 |
| -85.9 | -85.9 | 3 | 86.8 | 86.8 |
| -85.0 | -85.0 | 4 | 85.9 | 85.9 |
| -76.9 | -77.0 | 5 | 77.9 | 77.9 |
| -76.2 | -76.2 | 6 | 77.2 | 77.1 |

^a Measured in cps relative to $^{12}\text{CH}_2\text{CC}^{12}\text{CH}_2$; 1% $^{13}\text{CH}_2\text{CC}^{12}\text{CH}_2$ in TMS has τ 4.800 ± 0.001 at 37° and τ 4.775 ± 0.001 at -55° ; 5% $^{13}\text{CH}_2\text{C}^{12}\text{CH}_2$ in TMS has τ 5.457 ± 0.001 at 37° .

^b The derived parameters are $\nu_{\text{A}} - \nu_{\text{B}} = 0.47$ cps; J_{AB} (*trans*) = 8.95 cps; $J_{\text{AX}} = 170.9$ cps; J_{AB} (*cis*) = 8.95 cps.

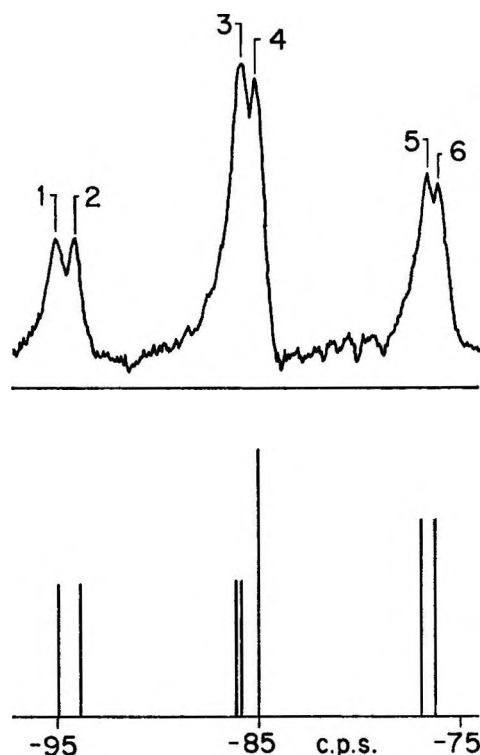


Figure 1. Low-field part of the spectrum of $^{13}\text{CH}_2\text{CC}^{12}\text{CH}_2$: upper part, observed; lower part, calculated.

Discussion

The *trans* (H, H') and *cis* (H, H') coupling constants in butatriene are both equal to 8.95 cps. There is good agreement between this value (if it assumed to be positive) and Karplus' calculated value (7.8 cps) for $J_{\text{HH}'}[\pi]$ in butatriene.¹⁰ This result therefore confirms the importance of the contribution of π -electron terms to long-range coupling constants between protons separated by π -electronic structure.

- (6) N. Muller and D. E. Pritchard, *J. Chem. Phys.*, **31**, 768 (1959).
- (7) E. I. Snyder, L. J. Altman, and J. D. Roberts, *J. Am. Chem. Soc.*, **84**, 2004 (1962).
- (8) R. C. Hirst and D. M. Grant, *ibid.*, **84**, 2009 (1962).
- (9) H. M. McConnell, *J. Mol. Spectry.*, **1**, 11 (1957); *J. Chem. Phys.*, **30**, 126 (1959).
- (10) M. Karplus, *J. Am. Chem. Soc.*, **82**, 4431 (1960); *J. Chem. Phys.*, **33**, 1842 (1960).
- (11) E. I. Snyder and J. D. Roberts, *J. Am. Chem. Soc.*, **84**, 1582 (1962).
- (12) W. M. Schubert, T. H. Liddicoet, and W. A. Lanka, *ibid.*, **76**, 1929 (1954).
- (13) F. A. Miller and I. Matsubara, *Spectrochim. Acta*, **22**, 173 (1966).
- (14) S. Castellano and A. A. Bothner-By, *J. Chem. Phys.*, **41**, 3863 (1964).
- (15) R. M. Lynden-Bell and N. Sheppard, *Proc. Roy. Soc. (London)*, **A269**, 385 (1962).
- (16) G. S. Reddy and J. H. Goldstein, *J. Mol. Spectry.*, **8**, 475 (1962).

The directly bound (C,H) coupling constants J_{CH} [H_2 -(CC) $_nH_2$] for ethylene, allene, and butatriene increase monotonically with n , but the proton chemical shifts do not show such a simple correlation (Table II). Since it has been suggested that an increase in J_{CH} can be correlated with a decrease in the local diamagnetic shielding of the proton,¹⁷ these results indicate that the proton chemical shifts between the three compounds contain significant contributions from long-range shielding. Pople has shown that part of the low-field proton

chemical shift from ethane to ethylene can be explained by the larger anisotropy of the atomic susceptibility of carbon in ethylene than in ethane.¹⁸ A similar calculation shows that, within the limitations of the dipolar approximation, the anisotropy of ethylenic carbon can account for part (0.3) of the increase in τ (0.8) from ethylene to allene, but it predicts a small increase (0.1) in τ from allene to butatriene, whereas a significant decrease (-0.7) is observed. A possible explanation for this decrease is that the terminal carbon atoms in butatriene might be more anisotropic than in allene. This could be the result of conjugation between the terminal pairs of π -electrons in the excited states of butatriene.

Acknowledgment. We thank Dr. A. A. Bothner-By for the use of the LAOCOON II program and Dr. D. F. Koster for his advice. S. G. F. thanks I.C.I. for a Research Fellowship during the tenure of which part of this work was done.

Table II: τ Values and Directly Bound (C,H) Coupling Constants in Ethylene, Allene, and Butatriene

| Compound | τ | J_{CH} , cps |
|-----------------------------------|-------------------|--------------------|
| CH ₂ CH ₂ | 4.66 ^a | 156.4 ^a |
| CH ₂ CCH ₂ | 5.46 | 168.2 ^b |
| CH ₂ CCCH ₂ | 4.80 | 170.9 |

^a See ref 15. ^b E. B. Whipple, J. H. Goldstein, and W. E. Stewart, *J. Am. Chem. Soc.*, **81**, 4761 (1959).

(17) J. H. Goldstein and G. S. Reddy, *J. Chem. Phys.*, **36**, 2644 (1962).

(18) J. A. Pople, *Discussions Faraday Soc.*, **34**, 7 (1963).

Nitrous Oxide Dosimetry. Effects of Temperature, Pressure, and Electric Field¹

by F. T. Jones² and T. J. Sworski³

Union Carbide Corporation, Nuclear Division, Research Center, Tuxedo, New York (Received November 8, 1965)

The N₂O dosimeter was calibrated for 1-Mev electrons by ionization measurements. $G_{N_2} = 10.0 \pm 0.2$, $G_{O_2} = 4.0 \pm 0.4$, $G_{NO} = 3.9 \pm 0.3$, and $G_{-N_2O} = 12.0 \pm 0.4$ are initial yields at 24° and 600 torr. All yields increase with increasing temperature. The ratio G_{NO}/G_{O_2} increases from 1.0 at 24° and 600 torr to greater than 2.0 above 150°. Therefore, owing to reaction between NO and O₂, the volatile products after trapping at -196° consist of only N₂ and O₂ at 24° and only N₂ and NO above 150°. Although G_{-N_2O} and G_{N_2} are essentially independent of pressure from 50 to 600 torr, G_{O_2} decreases and G_{NO} increases with decreasing pressure. The G value for O₂ volatile after trapping at -196° decreases from 2.0 at 600 torr to 0.9 at 50 torr at 24°. Product yields are increased by electrical fields insufficient to induce secondary ionization but sufficient to induce electronic excitation. The pressure dependence for G_{N_2} and G_{NO} at $X/p \sim 11$ v cm⁻¹ torr⁻¹ is consistent either with ultimate dissociative electron capture of all electrons and bimolecular deactivation of N₂O* or with no significant electron capture and termolecular deactivation of N₂O* with $\tau_{N_2O^*} \sim 10^{-9}$ sec.

Introduction

A ferrous sulfate solution in air-saturated 0.4 *M* sulfuric acid is commonly used as a radiation dosimeter. Reported values for $G(Fe^{3+})$ of 15.6 ± 0.3^4 and 15.8 ± 0.3^5 for ⁶⁰Co γ radiation and 15.45 ± 0.11^6 for 2-Mev electrons indicate the excellent agreement achieved in calibrations of this dosimeter.

Harteck and Dondes⁷ proposed the use of N₂O for gas phase dosimetry. Energy absorption in gases can be determined by measurement of the rate of ionization during radiolysis. This technique, however, has produced a wide disparity in calibrations of the nitrous oxide dosimeter: $G(N_2) = 12.4 \pm 0.4$ for ⁶⁰Co γ -radiation⁸ and $G(N_2) = 11.3 \pm 0.4$ for 70-kvp X-rays,⁹ both calibrated by ionization measurements, are much larger than $G(N_2) = 10.3 \pm 0.3$ reported by Harteck and Dondes⁷ (all G values are recalculated on the basis of $W_{N_2O} = 32.9$).

Experimental techniques have been developed in our laboratory¹⁰ which enable dosimetry in the gas phase to be carried out by ionization measurements with a precision of better than $\pm 1\%$ with an electron accelerator. We, therefore, calibrated the nitrous oxide dosimeter and determined the effects of temperature, pressure, and electrical field.

Experimental Section

Materials. Nitrous oxide (Matheson Co.) was introduced into the vacuum system through a column of KOH pellets and followed by repeated degassing of the condensed solid at 77°K and subsequent distilling at 193°K until N₂, O₂, NO, and NO₂ could not be detected by the analytical methods used for these products of irradiation.

Analysis. Products not condensable at 77°K were analyzed by either combustion analysis or mass spectrometry. Combustion analysis was employed for samples containing only N₂ and O₂. Hydrogen, puri-

(1) Presented at the 151st National Meeting of the American Chemical Society, Pittsburgh, Pa., March 1966.

(2) Department of Chemistry, Stevens Institute of Technology, Hoboken, N. J.

(3) Chemistry Division, Oak Ridge National Laboratory, Oak Ridge, Tenn.

(4) C. J. Hochanadel and J. A. Ghormley, *J. Chem. Phys.*, **21**, 880 (1953).

(5) R. M. Lazo, H. A. Dewhurst, and M. Burton, *ibid.*, **22**, 1370 (1954).

(6) R. H. Schuler and A. O. Allen, *ibid.*, **24**, 56 (1956).

(7) P. Harteck and S. Dondes, *Nucleonics*, **14**, No. 3, 66 (1956).

(8) G. R. A. Johnson, *J. Inorg. Nucl. Chem.*, **24**, 461 (1962).

(9) B. J. Burt and J. F. Kircher, *Radiation Res.*, **9**, 1 (1958).

(10) G. G. Meisels, *J. Chem. Phys.*, **41**, 51 (1964).

fied by diffusion through a palladium thimble, was added to the sample and the mixture was burned by recirculation over a heated platinum wire. The pressure drop on combustion was a measure of O_2 content and the remainder of the sample was assumed to be N_2 . For samples containing NO, analyses were carried out on an Atlas CH4 mass spectrometer.

Oxides of nitrogen were determined by dissolution of the irradiated samples in 0.1 N NaOH followed by spectrophotometric analysis for nitrite ion at 520 $m\mu$ by the α -naphthylamine-sulfanilic acid reagent.¹¹ Expansion of the sample into a previously evacuated bulb of known volume followed by addition of 0.1 N NaOH through a side arm in the bulb gave consistently lower results than expected from stoichiometry. Therefore, 0.1 N NaOH was added directly to the irradiation cell. Although this technique required that cells be disassembled, cleaned, and reassembled after each irradiation, the nitrite yields gave good material balance.

Irradiations. The radiation source was a 1.0-Mev van de Graaff electron accelerator. Irradiation cells for use at room temperature and high-voltage equipment were similar to those used by Meisels.¹⁰ These cells were sufficiently large to permit chemical analysis of the gas and consisted of Pyrex cylinders, 4.11 cm in i.d. and 2.05 cm in length, fitted with amalgamated lead gaskets and 0.013-cm aluminum windows. For irradiations above room temperature, a stainless steel cell 2 in. in diameter and 4 in. in length shown in Figure 1 was fitted at one end with a 0.013-cm aluminum window by means of a compression seal. The window was sealed, without gasket since lead gaskets are unsuitable at high temperatures, between an outer ring and a flange on the cell which had been machined to provide a small raised lip. Ionization currents were measured between the cylindrical cell wall and a tungsten rod projecting axially through a vacuum-tight Kovar seal at one end. The cell was coated outside with a refractory cement and wrapped with electrical heating tape to give temperature uniformity to $\pm 2^\circ$ at 300° as measured by thermocouples imbedded in the refractory cement.

Results

Dosimetry. Application of an electric field during radiolysis induced positive and negative charges to drift to the cathode and anode, respectively. A measurable ion current increases with increasing ratio of the electric field, X , to the pressure, p , until all ions are collected at the windows and a plateau is reached in a plot of ionization current, i , as a function of X/p . The saturation current i_s , measured at the plateau, together with the energy required to produce one ion pair in nitrous oxide ($W_{N_2O} = 32.9^{10}$), is a measure of the rate

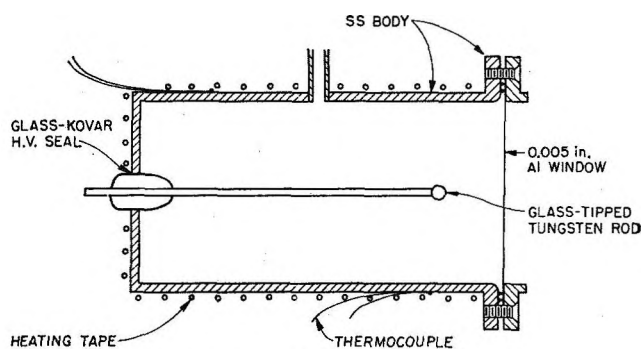


Figure 1. High-temperature irradiation cell.

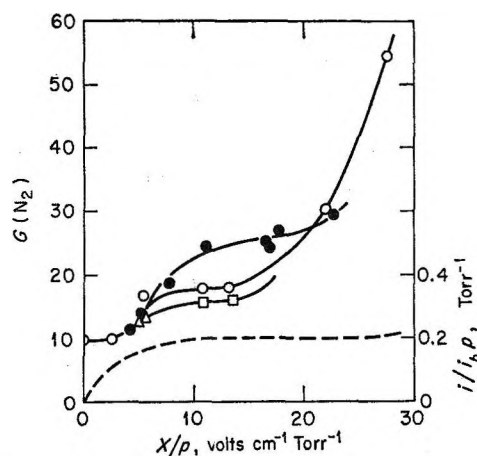


Figure 2. Dependence of $G(N_2)$ on X/p and pressure at 24° . Pressures of N_2O in torr: ●, 50; ○, 100; □, 200; and △, 500.

of energy absorption during radiolysis. Under our experimental conditions, i_s was a linear function of both the accelerator beam current i_b and the pressure. A typical plot of $i/i_b p$ as a function of X/p is shown in Figure 2.

i_s was not measured for the samples in which products of radiolysis were determined. The presence of an electric field during radiolysis markedly affects product formation as shown in Figure 2 for $G(N_2)$ as a function of X/p . There is a striking difference between the effect of an electric field on N_2O and that on C_2H_4 previously reported¹² from this laboratory. The decomposition of C_2H_4 is only slightly affected by an electric field up to $X/p \sim 15$ and then product yields increase sharply with increase in X/p from 15 to the onset of secondary ionization at 27 v cm^{-1} torr $^{-1}$. In sharp contrast, there is a stepwise increase in $G(N_2)$ from N_2O at

(11) B. F. Rider and M. G. Mellon, *Ind. Eng. Chem., Anal. Ed.*, **18**, 96 (1946).

(12) G. G. Meisels and T. J. Sworski, *J. Phys. Chem.*, **69**, 2867 (1965).

field strengths below $15 \text{ v cm}^{-1} \text{ torr}^{-1}$ superimposed on a further sharp increase in $G(\text{N}_2)$ with increase in X/p from 15 to the onset of secondary ionization. The onset of the first increase occurs at about the same value of X/p for all pressures, but the magnitude of the stepwise increase is highest at the lowest pressure. Since this increase sets in before the ionization current has reached its saturation value i_b , dosimetry measurements should be carried out in the absence of electric fields.

Thus, to determine energy absorption with high accuracy, i_b should be monitored continuously during the irradiation but without application of an electric field. This was accomplished by using a second irradiation cell to monitor i_b , a procedure employed by Boag.¹³ Two identical cells were mounted in tandem in the path of the accelerator beam: the first cell adjacent to the beam port of the accelerator monitored the accelerator beam by a continuous recording of i_a and the second cell was used to determine product yields. Chemical yields were not determined in the first cell and electrical fields were eliminated in the second cell by electrically connecting both windows together to ground. The attenuation of i_b by the first cell was determined in a series of calibration runs by measurement of i_a in both cells simultaneously (using two high-voltage supplies and two X-Y recorders) as a function of nitrous oxide pressure and accelerator beam current. A constant ratio of 0.370 ± 0.001 was determined for the energy absorbed in the second cell relative to the first—at the same N_2O pressures—over the range 22 to 600 torr and independent of i_b . Most of the experiments were carried out with the same N_2O pressure in both cells but it was also ascertained that (a) i_a was directly proportional to N_2O pressure in each cell as shown in Table I and (b) G values measured in the second cell were, within experimental error, independent of N_2O pressure in the first cell, at least from 50 to 200 torr.

Table I: Dependence of i_a/i_b on Pressure

| N_2O pressure, torr | Range of i_b , μa | i_a/i_b | $i_a/i_b P$, torr^{-1} |
|---|-----------------------------------|-----------------|-------------------------------------|
| 22.0 | 0.08–8.00 | 4.29 ± 0.01 | 0.195 ± 0.001 |
| 98.0 | 0.02–2.00 | 19.3 ± 0.1 | 0.197 ± 0.001 |
| 147 | 0.02–1.00 | 29.0 ± 0.2 | 0.197 ± 0.001 |

Effect of Pressure. Primary products in the radiolysis of N_2O are N_2 , O_2 , and NO .¹⁴ A slow, thermal reaction of NO and O_2 to form NO_2 occurs in the gas phase. NO and O_2 react rapidly when the irradiated sample is condensed with liquid N_2 ,⁹ a common practice in analysis for

N_2 and O_2 . G values determined after reaction of NO and O_2 to form NO_2 will be denoted by $G(\text{N}_2)$, $G(\text{O}_2)$, and $G(\text{NO})$.

Values for $G(\text{N}_2)$ and $G(\text{O}_2)$ at 24° and pressures of 50, 200, and 600 torr are listed in Table II. No effect of radiation intensity was observed over at least an eight-fold variation in i_b from 0.5 to $4.0 \mu\text{a}$ [7.5×10^{18} to $6.0 \times 10^{19} \text{ ev g}^{-1} \text{ min}^{-1}$] at 600 torr, or over smaller variations in intensity at other pressures. The results in Table II show a decrease in $G(\text{N}_2)$ at large doses and indicate an initial value for $G(\text{N}_2)$ of 10.0 ± 0.2 independent of pressure, within experimental error, from 200 to 600 torr. Lower values for $G(\text{N}_2)$ at 50 torr are attributed principally to a nonlinearity of $G(\text{N}_2)$ with dose at the higher doses employed, although a slight decrease in $G(\text{N}_2)$ with decrease in pressure cannot be ruled out. $G(\text{O}_2)$, however, markedly decreases with decreasing pressure: $G(\text{O}_2) = 2.0 \pm 0.2$ at 600 torr, $G(\text{O}_2) = 1.5 \pm 0.2$ at 200 torr, and $G(\text{O}_2) = 0.9 \pm 0.1$ at 50 torr.

Effect of Temperature. The stainless steel irradiation cell was used at high temperatures. N_2O in con-

Table II: Dependence of N_2 and O_2 Yields on Pressure^a

| Pressure, torr | Dose, 10^{20} ev/g | $G(\text{N}_2)$ | $G(\text{O}_2)$ |
|-------------------|---------------------------------|-----------------|-----------------|
| 600 | 0.288 | 10.1 | 1.96 |
| | 0.361 | 10.0 | 2.07 |
| | 0.594 | 10.0 | 1.82 |
| | 0.741 | 10.1 | 2.13 |
| | 1.12 | 9.95 | 2.16 |
| | 1.20 | 9.76 | 2.04 |
| | 1.75 | 9.49 | 1.94 |
| | 200 | 1.13 | 10.1 |
| 1.15 | | 9.92 | 1.39 |
| 1.44 | | 10.0 | 1.56 |
| 1.50 | | 10.0 | 1.50 |
| 2.18 | | 10.2 | 1.61 |
| 2.91 | | 9.67 | 1.73 |
| 4.70 | | 9.40 | 1.79 |
| 50 | | 2.94 | 9.50 |
| | 4.42 | 9.42 | 0.96 |
| | 5.99 | 9.25 | 0.90 |
| | 8.55 | 9.00 | 0.91 |
| | 11.6 | 9.21 | 1.07 |
| | 17.4 | 8.84 | 1.03 |

^a Irradiations at 24° . Products volatile from trap at -196° .

(13) J. W. Boag in "Radiation Dosimetry," G. J. Hine and G. L. Brownell, Ed., Academic Press Inc., New York, N. Y., 1956, Chapter 4.

(14) G. R. Gedye, *Trans. Faraday Soc.*, **27**, 474 (1931); *J. Chem. Soc.*, 3016 (1931).

tact with stainless steel is stable up to at least 200°. Thermal decomposition and catalytic decomposition on the cell wall becomes serious above 250°. The effect of temperature on the N₂O dosimeter was examined from 24 to 200°.

At low radiation intensities, $i_b \sim 0.005 \mu\text{a}$, it was possible to measure i as a function of X/p by applying a high voltage to the central electrode and measuring the ion current collected on the cell wall. Since the electric field in the cell approximates cylindrical symmetry and because the collection efficiency may be low in certain regions of the cell, i_a could not be determined with the accuracy obtained with the parallel plate electrodes. Nevertheless, at a given density of N₂O, the largest change in i_a observed on increasing the temperature from 24 to 200° was less than 15%. Since this was the limit of accuracy for determinations of i_a in this cell, it was assumed that $W_{\text{N}_2\text{O}}$ is independent of temperature and, likewise, that energy absorption is independent of temperature.

Values for $G(\text{N}_2)$, $G(\text{O}_2)$, and $G(\text{NO})$ as a function of temperature at N₂O density corresponding to a pressure of 400 torr at 24° are listed in Table III. $G(\text{N}_2)$ increases with increase in temperature. $G(\text{O}_2)$ decreases with increase in temperature and is essentially zero at temperatures above 150°. $G(\text{NO})$ is measurable at 150° and increases with increase in temperature.

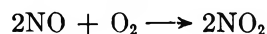
Table III: Dependence of Measured N₂, O₂, and NO Yields on Temperature^a

| Temp, °C | $G(\text{N}_2)$ | $G(\text{O}_2)$ | $G(\text{NO})$ |
|-------------|-----------------|-----------------|----------------|
| 24 | 10.0 | 2.0 | 0.00 |
| 70 | 12.4 | 1.0 | 0.00 |
| 100 | 14.1 | 0.53 | 0.00 |
| 150 | 17.9 | 0.03 | 0.13 |
| 200 | 21.1 | 0.08 | 6.20 |

^a N₂O density corresponding to a pressure of 400 torr at 24°. Products volatile from trap at -196°. Total radiation dose = 0.96×10^{20} ev/g.

Formation of Oxides of Nitrogen.—The yield of oxides of nitrogen was determined by total dissolution of sample in 0.1 N NaOH followed by analysis for the nitrite ion. Nitrite analyses were carried out only at 600 torr of N₂O at doses between 4.28×10^{20} and 12.6×10^{20} ev/g. No effect of dose was observed within the limits of experimental error.

Assuming that NO and NO₂ are the only products of radiolysis besides N₂ and O₂ and that the following reactions go to completion, the yield of oxides of nitro-



gen was measured to be $G(\text{NO} + \text{NO}_2) = 3.9 \pm 0.3$ at 24°.

With $G(\text{N}_2) = 10.0$ and $G(\text{O}_2) = 2.0$, stoichiometry requires that $G(\text{NO} + \text{NO}_2) = 4.0$ in excellent agreement with the observed value. Material balance was, therefore, achieved in this system.

Discussion

Values reported here for $G(\text{O}_2)$ and $G(\text{NO})$ represent only the excess of either O₂ or NO over the amount required by stoichiometry for formation of NO₂. The following relationship is required by stoichiometry.

$$G(\text{NO}_2) = 2/3G(\text{N}_2) - 1/3G(\text{NO}) - 4/3G(\text{O}_2) \quad (\text{I})$$

Initial yields of the primary products of irradiation are denoted by G_{N_2} , G_{NO} , and G_{O_2} . These are related to the observed yields after reaction of NO with O₂ is complete by the relationships II–IV.

$$G_{\text{N}_2} = G(\text{N}_2) \quad (\text{II})$$

$$G_{\text{O}_2} = G(\text{O}_2) + 1/2G(\text{NO}_2) \quad (\text{III})$$

$$G_{\text{NO}} = G(\text{NO}) + G(\text{NO}_2) \quad (\text{IV})$$

Effect of Temperature. $G(\text{N}_2) + G(\text{O}_2)$ varies only slightly with increase in temperature up to 150° since an increase in $G(\text{N}_2)$ is accompanied by a decrease in $G(\text{O}_2)$ as shown in Table III. For this reason, N₂O decomposition—measured by the yield of noncondensable gas at liquid N₂ temperature—appears to be temperature independent up to about 150°. When G_{NO} exceeds $2G_{\text{O}_2}$ and $G(\text{NO})$ becomes appreciable, as shown in Table III for 200°, the yield of noncondensable gas will markedly increase with increase in temperature. Thus, the sharp increase in noncondensable gas above 150° previously attributed¹⁵ to an increase in $G(\text{N}_2) + G(\text{O}_2)$ is here attributed to $G(\text{N}_2) + G(\text{NO})$.

G_{N_2} , G_{O_2} , G_{NO} , and $G_{-\text{N}_2\text{O}}$ increase with increase in temperature as shown in Figure 3. The results approximate an Arrhenius dependence with apparent activation energies of approximately $E_{\text{N}_2}^a = 1.2$, $E_{\text{O}_2}^a = 0.75$, $E_{\text{NO}}^a = 2.2$, and $E_{-\text{N}_2\text{O}}^a = 1.5$ kcal/mole. This effect of temperature is larger than reported by Wourtz, in good agreement with the results of Flory¹⁵ and less than reported by Gorden and Ausloos.¹⁷

A priori, one would not expect that thermal energy would make a significant contribution to the elemen-

(15) D. A. Flory, *Nucleonics*, **21**, No. 12, 50 (1963).

(16) E. Wourtz, *Radium*, **11**, 332 (1919).

(17) R. Gorden, Jr., and P. Ausloos, *J. Res. Natl. Bur. Std.*, **A69**, 79 (1965).

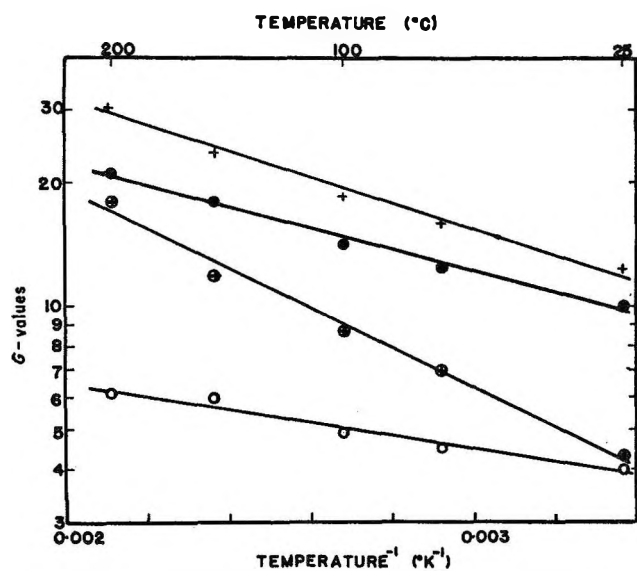
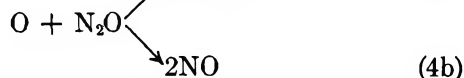
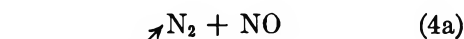
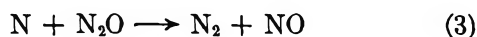


Figure 3. Dependence of initial G values on temperature. N_2O concentrations were constant at 400 torr at 24° : \circ , G_{O_2} ; \odot , G_{NO} ; \bullet , G_{N_2} ; and $+$, G_{-N_2O} .

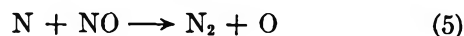
tary processes in radiation chemistry. The marked effect of temperature must be attributed to subsequent reactions of ionic or free-radical intermediates. The net effect of ionization and excitation has been assumed¹⁴ to result in two over-all processes (eq 1 and 2) which have



also been postulated^{18,19} as primary photochemical processes. Reactions of N and O atoms with N_2O (eq 3 and 4) are endothermic if N and O atoms are in the



ground state.²⁰ N atoms react with NO ²¹ (eq 5),



while O atoms must recombine. As the temperature is increased and reactions 3 and 4 become more probable, G_{-N_2O} would increase with a limiting yield at high temperatures equal to twice the value observed at low temperatures.

Figure 3 shows that G_{-N_2O} increases by more than a factor of 2 between 24 and 200° . Gorden and Ausloos¹⁷ report that G_{N_2} increased by almost a factor of 8 between 40 and 376° . These increases are too large to explain by the sequence of reactions 1-4. Gorden and

Ausloos¹⁷ have postulated an ionic chain reaction. Our large increase in the ratio G_{NO}/G_{O_2} with increase in temperature is consistent with their reaction mechanism.

Effect of Pressure. Table IV shows initial yields for 50, 200, and 600 torr N_2O , calculated from the data in Table II. Although Table II does show all values less than 10.0 for $G(N_2)$ at 50 torr, a plot of N_2 concentration against dose shows that all data for 50, 200, and 600 torr fall on the same curve, indicating a common initial yield. While G_{N_2} and G_{-N_2O} remain essentially constant over this pressure range, G_{O_2} decreases and G_{NO} increases as the pressure is lowered. The effect of pressure is to alter the product distribution without affecting G_{-N_2O} .

Table IV: Effect of Pressure on Primary Product Yields^a

| Pressure, torr | G_{N_2} | G_{NO} | G_{O_2} | G_{-N_2O} |
|----------------|-----------|----------|-----------|-------------|
| 600 | 10.0 | 4.0 | 4.0 | 12.0 |
| 200 | 10.0 | 4.6 | 3.9 | 12.3 |
| 50 | 10.0 | 5.5 | 3.6 | 12.7 |

^a Primary is used here only to denote product yields before secondary reaction of NO with O_2 .

Effects of Electrical Fields. Application of an electrical field causes the thermal electrons to gain energy as a result of diffusive displacements and to acquire a drift velocity in the direction of the field. At values of X/p greater than $25 \text{ v cm}^{-1} \text{ torr}^{-1}$, the energy distribution of these electrons is such that secondary ionization becomes significant, as indicated by the increase in $i_a/\nu_b p$ at $X/p = 30$ in Figure 2. The increase in product G values at values of X/p less than required for the onset of significant secondary ionization is attributable principally to molecular excitations.¹² Typical molecular excitations due to absorption of high-energy radiation lie very high, include superexcited states, and are principally optically allowed states.^{22,23} In sharp contrast, molecular excitations due to collisions with electrons accelerated by an electrical field lie very low, and optically forbidden states become important. For

(18) W. A. Noyes, Jr., *J. Chem. Phys.*, **5**, 807 (1937).

(19) M. Zelikoff and L. M. Aschenbrand, *ibid.*, **22**, 1680 (1954).

(20) J. P. Doering and B. H. Mahan, "Chemical Reactions in the Lower and Upper Atmosphere," Stanford Research Institute Symposium, Interscience Publishers, Inc., New York, N. Y., 1961, Paper No. 21.

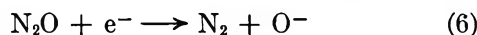
(21) J. P. Doering and B. H. Mahan, *J. Chem. Phys.*, **36**, 1682 (1962).

(22) R. L. Platzman, *Vortex*, **23**, 372 (1962).

(23) R. L. Platzman, *Radiation Res.*, **17**, 419 (1962).

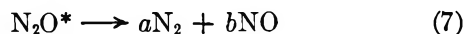
example, the dissociation of H_2 by an electrical field was quantitatively explained by Poole²⁴ with the theory of Emeleus, Lunt, and Meek²⁵ assuming that only triplet states of H_2 ($3\Sigma_g^+$ and $3\Sigma_u^+$) dissociate while singlet states undergo radiative transitions to the ground state.

The large stepwise increase in G_{N_2} and G_{NO} at X/p less than $15 \text{ v cm}^{-1} \text{ torr}^{-1}$ is in qualitative agreement with both the observations of Williams and Essex²⁶ and Burt and Kircher⁹ and their postulate that excitation and dissociation of N_2O is induced by electrons accelerated in an electrical field. However, the further and larger increase in G_{N_2} and G_{NO} with concomitant increase in G_{O_2} from $X/p \sim 15 \text{ v cm}^{-1} \text{ torr}^{-1}$ to the onset of secondary ionization was not observed by either Williams and Essex²⁶ or Burt and Kircher⁹ and is in disagreement with their conclusion that yields would not increase at higher values of X/p . They assumed that all electrons are captured before reaching the electrodes by dissociative electron capture²⁷ (eq 6) and that a limiting ratio of

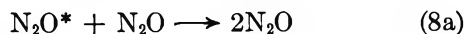


dissociative excitation to dissociative electron capture is reached at X/p less than $15 \text{ v cm}^{-1} \text{ torr}^{-1}$.

If dissociative attachment is the ultimate fate of all electrons in N_2O at the pressures used in this work, then for a given value of X/p the number of excited molecules formed by each electron before attachment should be constant: $G_{N_2O^*} = kG_{e^-}$, where $G_{N_2O^*}$ and G_{e^-} are the numbers of excited N_2O molecules and electrons, respectively, formed per 100 ev absorbed from the accelerator electron beam, and k is a constant which would depend only on X/p . The marked dependence of G_{N_2} and G_{NO} on pressure at $X/p \sim 11$ shown in Figures 2 and 4 indicates collisional deactivation of N_2O^* in competition with the dissociation of N_2O^* which ultimately yields a molecules of N_2 and b molecules of NO .



Assuming deactivation occurs by collision with another



N_2O molecule, then ΔG_{N_2} , the enhancement in G_{N_2} at fixed X/p , should be given by

$$1/\Delta G_{N_2} = A(1 + k_{8a}[N_2O]/k_7) \quad (Va)$$

where $A = akG_{e^-}$ is a constant at fixed X/p and $[N_2O]$ is the pressure in torr. An analogous relationship can be derived for ΔG_{NO} .

On the other hand, if attachment does not occur to any significant extent, then it can be assumed that $G_{N_2O^*} = \alpha_e l G_{e^-}$ where α_e is the number of N_2O^* formed per unit path length by each electron owing to energy

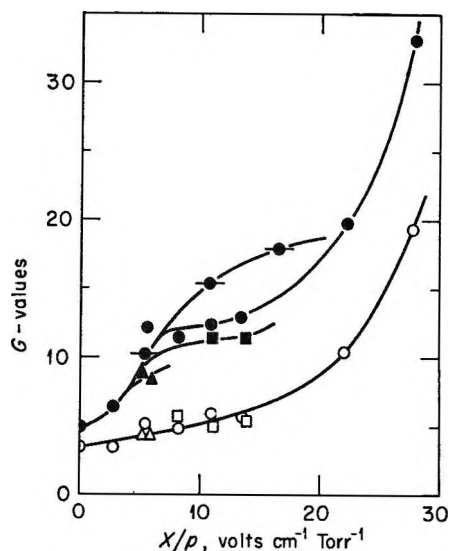
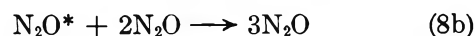


Figure 4. Dependence of G_{NO} (dark symbols) and G_{O_2} (light symbols) on X/p and pressure. Pressures of N_2O in torr: \circ , 50; \square , 100; \square , 200; and Δ , 500.

absorbed from the electrical field, and l is the average path length for electrons in the irradiation cell. Then α_e for excitation is analogous to the "first Townsend coefficient,"²⁸ α_i for ionization and α_e/p should be a function only of X/p , just as is α_i/p . However, the results are quantitatively inconsistent with bimolecular deactivation of N_2O^* since G_{N_2} and G_{NO} would then be expected to increase with increase in pressure. Suppose that collisional deactivation is termolecular, as pro-



posed by Callear and Robb²⁹ for $C_2H_4^*$. Then ΔG_{N_2} at fixed X/p should be given by the following relationship

$$[N_2O]/\Delta G_{N_2} = B(1 + k_{8b}[N_2O]^2/k_7) \quad (Vb)$$

where $B = [N_2O]/aG_{N_2O^*} = [N_2O]/a\alpha_e l G_{e^-}$ is constant as explained above.

The limited data in Figures 2 and 4 preclude quantitative evaluation of the constants in equations Va or Vb. Qualitatively, however, the pressure dependence of ΔG_{N_2} and ΔG_{NO} at $X/p \sim 11$ yields approximate values for k_{8a}/k_7 or k_{8b}/k_7 . Then the lifetime of N_2O^* can be estimated by assuming a value for (a) k_{8a} of

(24) H. G. Poole, *Proc. Roy. Soc. (London)*, **A163**, 424 (1937).

(25) K. G. Emeleus, R. W. Lunt, and C. A. Meek, *ibid.*, **A156**, 394 (1936).

(26) N. T. Williams and H. Essex, *J. Chem. Phys.*, **16**, 1153 (1948).

(27) N. E. Bradbury and H. E. Tatel, *ibid.*, **2**, 835 (1934).

(28) L. B. Loeb, "Fundamental Processes of Electrical Discharge in Gases," John Wiley and Sons, Inc., New York, N. Y., 1939.

(29) A. B. Callear and J. C. Robb, *Discussions Faraday Soc.*, **17**, 21 (1954).

about $10^{11} M^{-1} \text{sec}^{-1}$ for bimolecular deactivation or (b) k_{3b} about $10^8 M^{-2} \text{sec}^{-1}$ assuming termolecular deactivation, as predicted by most treatments³⁰ and assuming 100% efficiency in deactivation. By either of the above treatments, an average lifetime $\tau_{N_2O^*} \sim 1/k_7 \sim 10^{-9} \text{sec}$ results. The results of the present work are therefore consistent with either electron attachment to N_2O or no significant attachment but a termolecular quenching mechanism.

N₂O Dosimetry. The values of $G(N_2) = 10.0 \pm 0.2$, $G(O_2) = 2.0 \pm 0.2$, and $G(-N_2O) = 12.0 \pm 0.4$ measured for small conversions at 24° and 600 torr are in good agreement with determinations of $G(N_2 + O_2) = 11.9 \pm 0.7$ by Flory,¹⁵ $G(N_2) = 9.7$ by Moseley and Truswell,³¹ $G(-N_2O) = 12.0 \pm 0.3$ by Harteck and Dondes,⁷ and $G(-N_2O) = 12.3 \pm 1.3$ by Gedye.¹⁴ The disagreement with the determinations of $G(N_2) = 12.4 \pm 0.4$ by Johnson⁸ and $G(N_2) = 11.3$ by Burt and Kircher⁹ (both values recalculated on the basis of $W_{N_2O} = 32.9^{10}$) established by the method of ionization currents may be due to the cylindrical geometry of the ionization chambers used by these workers, making it necessary to extrapolate the ionization current to infinite voltage⁸ to obtain a value for the current corre-

sponding to saturation. The collection efficiency in ionization chambers of this design may be quite low,¹³ giving rise to a low apparent dose and high apparent G values. In addition, the problem of circumventing the enhancement in chemical yields which results when a voltage is applied to nitrous oxide under irradiation must also be met. The effects of wall thickness and cell diameter in small cells may be responsible for the differences between the present work and the values $G(N_2) = 11.0 \pm 0.4$, determined by Hearne and Hummel,³² and $G(N_2) = 13.1 \pm 0.2$, determined by Kubose.³³ Wourtsel's¹⁶ original result of 1.74 molecules of N_2O decomposed/ion pair has been corrected to 2.7 by Mund,³⁴ giving a value of $G(-N_2O) = 8.2$ which is considerably lower than any other thus far reported.

(30) See, for example, L. S. Kassel, "The Kinetics of Homogeneous Gas Reactions," Chemical Catalog Co., New York, N. Y., 1932.

(31) F. Moseley and A. E. Truswell, Atomic Energy Research Establishment, Harwell, England, Report No. AERE-R 3078 (1960).

(32) J. A. Hearne and R. W. Hummel, *Radiation Res.*, **15**, 254 (1961).

(33) D. Kubose, *Trans. Am. Nucl. Soc.*, **7**, 318 (1964).

(34) W. Mund, *J. Phys. Chem.*, **30**, 890 (1926).

Diffusion of Iron in Single-Crystal Nickel Oxide

by K. J. Richards and F. E. Wagstaff

*Metallurgy and Ceramics Research Laboratory, Aerospace Research Laboratories,
Wright-Patterson Air Force Base, Ohio (Received November 12, 1965)*

The diffusion of Fe^{55} in nickel oxide, NiO, has been studied in air in the temperature range 1000 to 1400°, utilizing a decrease in surface activity method. The measured diffusion coefficients can be expressed as $D = 1.81 \times 10^{-3} \exp(-44.5 \text{ kcal}/RT) \text{ cm}^2 \text{ sec}^{-1}$. Over the temperature range investigated the diffusivity of iron was appreciably greater than the reported values for nickel self-diffusion, but the temperature dependence of the diffusion coefficients was essentially the same.

Introduction

A considerable amount of study has been devoted to the various physical properties of NiO and the other monoxides of the iron-group transition metal oxides, primarily because of the variable-valence property of the cations which permits these compounds to behave as intrinsic nonstoichiometric semiconductors when equilibrated with an oxidizing atmosphere. The detailed nature of the lattice point defects in these materials is still, however, a matter of conjecture, as are the diffusion mechanisms.

We have chosen to study the effect of ion properties on the diffusion behavior of substitutional impurities in order to gain further insight into the predominant transport processes in NiO. The experimental approach has been to measure in pure nickel oxide the diffusivity of iron impurity which is present in extremely small concentrations, using the radioactive tracer, Fe^{55} . Because of the low concentrations, interaction effects between impurity ions are negligible, resulting in the simplest type of chemical diffusion. Such diffusion measurements are free from the complications often accompanying the more frequently employed type of chemical diffusion experiment which employs very much larger concentration gradients than are needed with tracers. The results of such experiments are thus more amenable to theoretical interpretation.

Experimental Section

The decrease in surface activity method was used to measure the diffusion coefficient for Fe^{55} in NiO. When applicable, this technique offers some definite experimental advantages over the more frequently used

sectioning methods. Experimentally, in the decrease in surface activity method, a vanishingly thin deposit of radioactive tracer is made on a flat surface of a semi-infinite specimen. The decrease in the intensity of the radiation from this "active" face due to the diffusion of the tracer into the specimen is then measured by counting the "active" surface before and after a diffusion anneal. Under these experimental conditions, the appropriate solution to the diffusion equation for the distribution of radioactivity in the specimen after a diffusion anneal is

$$C = Q(\pi Dt)^{-1/2} \exp(-x^2/4Dt) \quad (1)$$

where C is the concentration of tracer at a depth, x , from the initial radioactive deposit, Q is the number of tracer atoms per unit area initially deposited, and D and t are, respectively, the diffusion coefficient and the diffusion time.

Owing to absorption of radiation by the specimen, the activity measured at the "active" surface decreases as the tracer diffuses into the crystal. If the absorption of radiation follows Lambert's law, it has been shown¹ that the ratio of the surface activity after and before a diffusion anneal is

$$A/A_0 = \text{erfc}(\mu^2 Dt)^{1/2} \quad (2)$$

where $\text{erfc}(y) \equiv \exp(y^2) [1 - \text{erf}(y)]$. $\text{erf}(y)$ is the Gaussian error integral and μ is the linear absorption coefficient for the tracer radiation in the diffusion specimen. D can therefore be evaluated by measuring

(1) J. Steigman, W. Shockley, and F. C. Nix, *Phys. Rev.*, **56**, 13 (1939).

the decrease in surface activity as a function of time at a particular temperature.

An additional experimental convenience of this method which is implicit in (2) but which does not seem to have been generally recognized or applied is that a single sample can be used for diffusion measurements at more than one temperature. Since a unique value of the activity ratio is determined for a particular product, Dt , a constant time, τ , can be chosen to represent the entire previous thermal history of the sample, and eq 2 can be rewritten as

$$A/A_0 = \operatorname{erfc}(\mu^2 D[\tau + t])^{1/2} \quad (3)$$

If A_0 is known, only a single diffusion anneal is needed to evaluate D . If neither A_0 or τ are known, D can still be determined by measuring the activity after consecutive diffusion anneals at the same temperature.

It should be remembered that for eq 3 to be applicable, the distribution of tracer in the specimen must be accurately described by eq 1. This has been shown to be the case over the temperature range covered in this study for previous studies of self-diffusion in $\text{NiO}^{2,3}$ and the related systems of CoO and FeO^4 . In addition, the results of this study show the diffusivity to be time independent, which is a requirement of the applicability of eq 2.

The diffusion measurements were made on a single crystal of NiO which was supplied by the Air Force Cambridge Research Laboratories. The crystal was grown by the flame-fusion method from powder of unspecified purity. Emission spectrographic analysis of this crystal showed the following cation impurity concentrations: Al (10 ppm), Na (10 ppm), K (50 ppm), Li (<1 ppm). Impurities such as Fe, Co, and Si were not found; however, the detection limit for these elements was only of the order of 10–50 ppm. The diffusion samples were cut from the single-crystal boule in the form of thin plates approximately 1.5 mm thick. The diffusion surface was then carefully ground and polished to a surface roughness of the order of 0.1 μ .

As discussed previously, the application of eq 2 and 3 requires that the tracer radiation follow an exponential absorption law. The isotope employed in this study, Fe^{55} , meets this requirement exactly. The tracer was obtained from Nuclear Science and Engineering Corp., Pittsburgh, Pa., as a high specific activity (2.76 mcuries/ml), carrier free (<0.2 mg/ml) solution of Fe^{55} in 0.5 N HCl, containing less than 0.0001% Fe^{59} . The Fe^{55} emits 0.0059-Mev Mn $K\alpha$ X-radiation with a half-life of 2.7 years. The linear absorption coefficient for this radiation in NiO was calculated using the equation

$$\mu = \rho(W_{\text{Ni}}\mu_{\text{Ni}} + W_{\text{O}}\mu_{\text{O}}) = 672 \text{ cm}^{-1} \quad (4)$$

where ρ is the density of NiO (6.80 g/cm³), W_{Ni} and W_{O} are the weight fractions of Ni and O, and μ_{Ni} and μ_{O} are the mass absorption coefficients.⁵

The diffusion couples were prepared by the vacuum evaporation of a vanishingly thin layer of radioactive iron onto the prepared surface of the specimen. An aliquot of the tracer to be deposited was placed in an alumina evaporation cup and converted to a nitrate by successive evaporation and dissolution in nitric acid. The final nitrate solution was taken to dryness and reduced in hydrogen at a temperature of about 1000° prior to evaporation. The tracer deposition was performed with an electron-beam-heated evaporation source. With this system, about 40,000 counts/min of the tracer were evaporated onto the prepared surface of each sample. This deposit was fixed by heating the crystals in air at 800° for 10 min. The amount of Fe^{55} actually deposited was very small. An approximate calculation, based on the supplier's radiochemical assay of the tracer, indicates that, if all the deposited Fe^{55} were equally distributed in the first micron of the specimen, only of the order of one in 10⁵ cation sites would be occupied by a tracer ion. These very low concentrations, effectively infinite dilution, make it possible to equate the measured interdiffusion coefficient to the diffusion coefficient for iron in nickel oxide.

The diffusion anneals were performed in air in the temperature range 1000–1400° in a silicon carbide resistance furnace. The sample temperature was measured with a platinum-rhodium thermocouple placed adjacent to the "active" face of the crystal. This indicated a sample temperature variation of $\pm 1^\circ$ during diffusion anneals and a heat-up time from room temperature to final anneal temperature of approximately 30 sec. To ascertain the effect of surface evaporation, one diffusion anneal was performed on a sample with activity deposited on opposite sides of the crystal. A thin platinum washer was sandwiched between one surface and another inactive one. No appreciable activity was detected on the inactive sample, and the decreases in the surface activity on the opposing faces were statistically the same. The surface activity measurements were made in a thin-window, gas-flow proportional counter using 2π geometry. Since at a constant oxygen pressure the sample

(2) J. S. Choi and W. J. Moore, *J. Phys. Chem.*, **66**, 1308 (1962).

(3) M. T. Shim and W. J. Moore, *J. Chem. Phys.*, **26**, 802 (1957).

(4) R. E. Carter and F. D. Richardson, *Trans. AIME*, **194**, 1244 (1954).

(5) B. D. Cullity, "Elements of X-Ray Diffraction," Addison-Wesley Publishing Co., Inc., Reading, Mass., 1956, p 466.

composition depends on the temperature, under these experimental conditions, the observed temperature dependence of the diffusivity of iron in nickel oxide resulted from variations in both the mobility and concentration of the diffusing species. This experimental method (*i.e.*, making measurement at a constant oxygen pressure) parallels that employed in the reported studies of self-diffusion in nickel oxide.^{2,3,6} It was not felt that the available data on the effect of pressure and temperature on defect concentrations in NiO were sufficiently accurate to permit the unambiguous measurement of the temperature dependence of mobility at constant defect compositions.

Results and Discussion

Some of the diffusion coefficients were measured using specimens which had had a prediffusion anneal while others were determined from samples which had no thermal history subsequent to the preparation of the diffusion couple. Typical data on the time dependence of the decrease in surface activity for two such specimens are shown in Figure 1. The diffusion coefficients determined at 1100° for these two samples were essentially the same, which is additional verification of the applicability of eq 2 to this system. It was also found in this study that there was no statistically significant variation in the diffusion coefficients determined from isothermal anneals that produced mean diffusion penetrations, \sqrt{Dt} , varying from 4 to 50 μ . The lack of any systematic effect of either the prediffusion anneal or the diffusion time on the experimentally determined diffusivities implies that compositional equilibrium in NiO is attained at rates somewhat faster than are found for the transport of iron through this material. This is in agreement with the observation of Mitoff⁷ that above about 1000° electrical conductivity measurements on NiO could not be made rapidly enough to avoid the effect of compositional variations resulting from a change in temperature.

The diffusivity was found to obey the Arrhenius equation, $D = D_0 \exp(-E/RT)$, over the temperature range of the experiment. The diffusion parameters and their corresponding probable errors as determined by a least-squares analysis of the data were: $D_0 = (1.81 \pm 0.02) \times 10^3 \text{ cm}^2/\text{sec}$ and $E = 44.5 \pm 0.2 \text{ kcal/mole}$. Since one of the primary objectives of this study was to determine the effect of the properties of the impurity on the diffusion parameters, it is interesting to compare these results for iron with the reported values for self-diffusion in nickel oxide,^{2,3,6} though obviously only tentative conclusions can be drawn from one comparison. Iron is larger in both ionic radius and polarizability than nickel, but these ions are

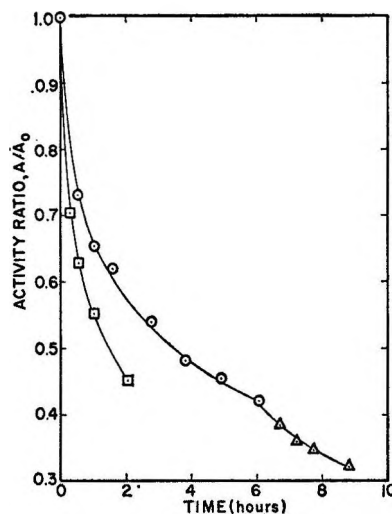


Figure 1. Typical surface activity vs. time curves. Solid lines were calculated from eq 3 using values of D determined from eq 5. \circ , 1072°; \triangle , 1150°; and \square , 1150°.

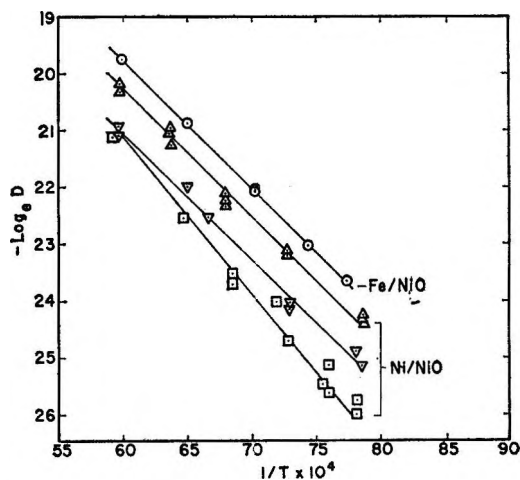


Figure 2. Comparison of the diffusivities for iron and nickel in NiO. Solid lines represent reported Arrhenius equations, $D = D_0 \exp(-E/RT)$. \square , data of Lindner and Akerstrom⁶; ∇ , data of Shim and Moore³; \triangle , data of Choi and Moore²; and \circ , this work.

isotypes, existing in both divalent and trivalent states. Using a sectioning technique, Choi and Moore² reported $D(\text{Ni}/\text{NiO}) = 1.83 \times 10^{-3} \exp(-45.6 \text{ kcal}/RT)$. In earlier studies, employing the decrease in surface activity method, Shim and Moore³ reported $D = 4.4 \times 10^{-4} \exp(-44.2 \text{ kcal}/RT)$ and Lindner and Åkerström⁶ found $D = 1.72 \times 10^{-2} \exp(-56.0 \text{ kcal}/RT)$. The impurity and self-diffusion data for

(6) R. Lindner and Å. Åkerström, *Discussions Faraday Soc.*, **23**, 133 (1957).

(7) S. P. Mitoff, *J. Chem. Phys.*, **35**, 882 (1961).

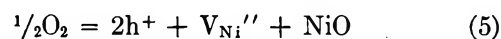
nickel oxide are summarized in Figure 2 for the temperature range covered in this study. It is apparent that the diffusivities measured by Shim and Moore³ and Lindner and Åkerström⁶ are in closer agreement than it would appear from the reported Arrhenius equations, although there is definitely a systematic difference in their results. The data of Moore and his co-workers^{2,3} are assumed to provide the more reliable measure of the apparent activation energy (≈ 45 kcal/mole) since they were obtained by two different experimental techniques using both single- and polycrystalline specimens.

Analysis of the data for iron diffusion is complicated by the temperature dependence of the numbers of defects as well as their mobilities. Because of the very low iron concentrations, however, and the relatively high intrinsic defect population arising from the ease of oxidation of divalent nickel, the total defect concentrations are controlled by the nickel oxide. Thus, since the measured energies for impurity and self-diffusion are essentially identical, the temperature dependence of the Fe and Ni mobilities is also the same, which implies the same transport process. It is not surprising to find that these closely related substitutional ions, Fe and Ni, have nearly the same activation energy since similar observations have been reported for homovalent ion diffusion in many materials ranging from metals to ionic crystals.

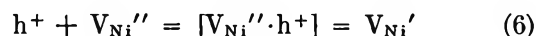
The absence of impurity-impurity interaction effects at the very low concentrations of iron employed in this investigation certainly contributes to minimizing the effect of the ion properties on the energies for substitutional impurity mobility. In addition, size effects would be reduced by the polarization of the ion in the direction of the adjacent vacancy (a vacancy mechanism is assumed). On the other hand, it might be expected that related ion properties such as polarizability, ionization potentials, and ionic radius would have an effect on other factors contributing to impurity diffusion, *e.g.*, local vibrational frequencies and relative impurity-defect concentrations. As can be seen in Figure 2, in NiO the diffusivity of the iron ions was appreciably greater than that of the nickel ions. Unfortunately, the magnitude of this effect is obscured by the systematic differences in the reported self-diffusion data. A similar increase in the diffusivity of the iron group transition ions in MgO with increasing ionic radius has been observed by Wuensch and Vasilos.⁸

In attempting to explain these effects, it should be remembered that the measured diffusivities are determined by the fraction of ions able to move as well as by their mobility. These factors, in turn, are related to the predominant lattice defects and their

specific concentrations. It is generally accepted that cation diffusion in the transition metal oxides proceeds by a vacancy mechanism and that the reactions that control the vacancy concentration in NiO can be written



and



where h^+ is an electron hole, assumed here to be Ni^{3+} , and V_{Ni}'' and V_{Ni}' are, respectively, doubly ionized and singly ionized (hole-vacancy associate) vacancies. The predominant type of vacancy will be determined by the relative values of the equilibrium constants for eq 5 and 6. From a study of the electrical resistivity of NiO, Mitoff⁷ concluded that the nickel vacancies in this material were doubly ionized. However, as pointed out by Choi and Moore,² the data (at least at higher oxygen pressures) are in better accord with the view that the cation vacancies are all singly ionized. This has been substantiated by the recent work of Duquesnoy and Marion⁹ on the variation of electrical conductivity in NiO as a function of oxygen partial pressure.

Since diffusion of an ion *via* normal lattice sites can only occur if there is a vacancy adjacent to the ion, the fact that the available data seem to indicate that essentially every nickel vacancy is associated with an electron hole immediately suggests the hole-vacancy associate as a possible diffusing species that is consistent with the observed differences in the diffusivity of Fe and Ni in NiO. The rate-controlling transport mechanism would involve the transposition of the vacancy and the hole. The diffusion coefficient can be expressed as

$$D = 2pa^2\nu f \exp(-\Delta H^*/RT) \quad (7)$$

a is the jump distance (the same for iron and nickel), ν is the effective vibration frequency along the transport coordinate of the hole-vacancy associate (ν is assumed to include the entropy effect), f is the correlation factor for diffusion, p is the fraction of tracer ions able to move, and ΔH^* is the activation energy for exchange of a tracer ion with a vacancy. Because of the similarities in the activation energies for diffusion of Fe and Ni, the transport mechanism must be the same for both ions; however, the specific concentration of the defects involved might differ. Also, as a consequence of the high relative mobility of the hole around the

(8) B. J. Wuensch and T. Vasilos, *J. Chem. Phys.*, **36**, 2917 (1962).

(9) A. Duquesnoy and F. Marion, *Compt. Rend.*, **256**, 2862 (1963).

vacancy (electron transfer),¹⁰ the correlation factor, f , would be a purely geometrical factor. On this basis, it is only p and ν that would contribute to the differences in Fe and Ni diffusion. Although the total concentration of vacancies and holes is fixed at constant temperature and P_{O_2} , the specific concentration of Fe^{3+} [*i.e.*, $Fe^{3+}/(Fe^{3+} + Fe^{2+})$] would always be greater than Ni^{3+} because of its lower ionization potential; this would contribute to a greater total diffusivity of iron. The frequency factor, ν , would also produce an effect in the same direction. Since the difference in mass of these ions is not significant, the ion of larger ionic radius, iron, would be expected to have a greater effective vibrational frequency along the diffusion coordinate.

Although these factors are in qualitative agreement with the experimental observations, the available data do not exclude a number of alternative mechanisms, involving different exchange processes and different lattice defects. An "interstitialcy" mechanism or phenomenologically equivalent process is certainly a pos-

sibility. Azaroff,¹¹ for example, has pointed out that the diffusion paths of least resistance in fcc structures must consist of alternating tetrahedral and octahedral voids, and Roth¹² from a neutron diffraction study of the closely related oxide, FeO, has deduced that this lattice contains iron interstitials in the ratio of one interstitial (as Fe^{3+}) to every two vacancies. It is also possible that transport involves a vacancy mechanism, but the diffusing defects are quite complex. In this regard, for example, O'Keeffe and Moore¹³ have speculated on the existence of a triple vacancy ($V_O V_O V_{Ni}$) to explain the results of a study of oxygen diffusion in NiO. Additional definitive experimentation is obviously needed to provide the basis of a consistent mechanistic interpretation of the diffusion processes in nickel oxide.

(10) F. J. Morin, *Phys. Rev.*, **93**, 1199 (1954).

(11) L. V. Azaroff, *J. Appl. Phys.*, **32**, 1658 (1961).

(12) W. L. Roth, *Acta Cryst.*, **13**, 140 (1960).

(13) M. O'Keeffe and W. J. Moore, *J. Phys. Chem.*, **65**, 1438 (1961).

Spin-Free Quantum Chemistry.^{1a} III. Bond Functions and the Pauling Rulesby F. A. Matsen, A. A. Cantu,^{1b} and R. D. Poshusta^{1c}*Molecular Physics Group, The University of Texas, Austin, Texas 78712 (Received November 12, 1965)*

The Pauling rules which evaluate matrix elements for a spin-free Hamiltonian over anti-symmetric Slater bond functions are derived in the spin-free formulation of quantum chemistry. In this formulation a vector bond diagram is replaced by a two-columned Young tableau. The Slater bond function for this bond diagram is replaced by a spin-free bond function projected from a spin-free primitive function by a "structure projector." The structure projector is an element in the permutation algebra which is constructed with reference to the two-columned tableau. Matrix elements over two spin-free bond functions contain an algebraic element called the "bracket element" which is a product of the adjoint of the structure projector for the first bond function and the structure projector for the second bond function. The coefficients (the Pauling numbers) of the $N!$ permutation operators in the expansion of the bracket element are evaluated by group theoretical methods.

1. Historical Introduction

The bond function, introduced by Slater² in 1931, has been one of the most important tools of quantum chemistry. It embraces the concepts of the electron pair, the chemical bond, the pure bond state, and resonance among pure bond states. We review briefly the construction of Slater bond functions and the evaluation of matrix elements for a spin-free Hamiltonian over these functions using a method due to Pauling.³

We first construct a vector bond diagram, denoted by D_x , in which the first N integers are arranged in order in a circle. A certain number, say p , of pairs of integers are connected by arrows. See Table I. The spin state of the system is given by

$$S = N/2 - p \quad (1.1)$$

We next construct a spin-orbital product, denoted by $|\Sigma\rangle$, with a β orbital assigned to the tail and an α orbital assigned to the head of each arrow in D_x . We denote a permutation on the spin coordinates in $|\Sigma\rangle$ by

$$|\Sigma;P\rangle \equiv P|\Sigma\rangle \quad (1.2)$$

We designate by $R\mathcal{E}D_x$ those permutations which permute paired spin orbitals and which thus reverse the arrows in D_x .

Next we form a spin-bond function

$$|\Sigma;x\rangle \equiv \frac{1}{2^{p/2}} \sum_{R \in \mathcal{E}D_x} (-1)^R |\Sigma;R\rangle \quad (1.3)$$

where the sum extends over all possible arrow reversals and $(-1)^R$ is plus or minus one depending on whether R is an even or an odd number of reversals. See Table I.

Next we select a spin-free primitive function which we denote by $|\gamma\rangle$. For simplicity, we may take $|\gamma\rangle$ to be an orbital product with all orbitals distinct, but this is not necessary. A permutation⁴ on the electron coordinates is denoted by

$$|\gamma;P\rangle \equiv P|\gamma\rangle \quad (1.4)$$

We complete the construction of a Slater bond function forming the antisymmetrized function

$$|\gamma\Sigma x;A\rangle \equiv (1/\sqrt{N!}) \sum_P (-1)^P |\gamma;P\rangle |\Sigma x;P\rangle \quad (1.5)$$

If $|\gamma\rangle$ is an orbital product, (1.5) can be expressed as a linear combination of Slater determinants.

$$|\gamma\Sigma x;A\rangle = \frac{1}{2^{p/2}} \sum_{R \in \mathcal{E}D_x} (-1)^R \left(\begin{array}{c} |\gamma\rangle \\ |\Sigma;R\rangle \end{array} \right) \quad (1.6)$$

(1) (a) Supported by the Robert A. Welch Foundation of Houston, Texas, and the National Aeronautics and Space Administration; (b) Jefferson Chemical Co. Fellow; (c) National Science Foundation Postdoctoral Fellow.

(2) J. C. Slater, *Phys. Rev.*, **38**, 1109 (1931).

(3) L. Pauling, *J. Chem. Phys.*, **1**, 280 (1933).

Table I: Spin-Bond Functions for $N = 4, p = 2 (S = 0)^a$

| κ | D_κ and $ \Sigma\rangle$ | $ \Sigma; \kappa\rangle$ |
|----------|---|--|
| I | $1 \longrightarrow 2$ $4 \longleftarrow 3$ $ \Sigma\rangle = \beta(1)\alpha(2)\beta(3)\alpha(4)$ | $\frac{1}{2}[\beta(1)\alpha(2)\beta(3)\alpha(4) - \beta(2)\alpha(1)\beta(3)\alpha(4) - \beta(1)\alpha(2)\beta(4)\alpha(3) + \beta(2)\alpha(1)\beta(4)\alpha(3)]$ |
| II | $1 \downarrow \quad \uparrow 2$ $4 \downarrow \quad \uparrow 3$ $ \Sigma\rangle = \beta(1)\alpha(2)\beta(3)\alpha(4)$ | $\frac{1}{2}[\beta(1)\alpha(2)\beta(3)\alpha(4) - \beta(4)\alpha(2)\beta(3)\alpha(1) - \beta(1)\alpha(3)\beta(2)\alpha(4) + \beta(4)\alpha(3)\beta(2)\alpha(1)]$ |
| III | $1 \searrow \quad \nearrow 2$ $4 \swarrow \quad \nwarrow 3$ $ \Sigma\rangle = \beta(1)\alpha(2)\alpha(3)\beta(4)$ | $\frac{1}{2}[\beta(1)\alpha(2)\alpha(3)\beta(4) - \beta(3)\alpha(2)\alpha(1)\beta(4) - \beta(1)\alpha(4)\alpha(3)\beta(2) + \beta(3)\alpha(4)\alpha(1)\beta(2)]$ |

^a Note that by Rumer's rule, $|\Sigma; III\rangle = |\Sigma; II\rangle - |\Sigma; I\rangle$.

See Table II. If $|\gamma\rangle$ is an orbital product, D_κ can be represented by an orbital bond diagram in which the integers in D_κ are replaced by the orbitals to which the electrons are assigned in D_κ . See Table III.

Table II: Slater Bond Functions $N = 4, p = 2 (S = 0)$ (Orbital Product Primitive Function)^a

$|\gamma\rangle = a(1)b(2)c(3)d(4) \equiv abcd$
 $|\Sigma\rangle = \beta(1)\alpha(2)\beta(3)\alpha(4) \equiv \beta\alpha\beta\alpha$ for $\kappa = I$ and II
 $|\Sigma\rangle = \beta(1)\alpha(2)\alpha(3)\beta(4) \equiv \beta\alpha\alpha\beta$ for $\kappa = III$

| κ | $ \gamma\Sigma\kappa; A\rangle$ |
|----------|--|
| I | $\frac{1}{2} \left\{ \binom{abcd}{\beta\alpha\beta\alpha} - \binom{abcd}{\alpha\beta\beta\alpha} - \binom{abcd}{\beta\alpha\alpha\beta} + \binom{abcd}{\alpha\beta\alpha\beta} \right\}$ |
| II | $\frac{1}{2} \left\{ \binom{abcd}{\beta\alpha\beta\alpha} - \binom{abcd}{\alpha\alpha\beta\beta} - \binom{abcd}{\beta\beta\alpha\alpha} + \binom{abcd}{\alpha\beta\alpha\beta} \right\}$ |
| III | $\frac{1}{2} \left\{ \binom{abcd}{\beta\alpha\alpha\beta} - \binom{abcd}{\alpha\alpha\beta\beta} - \binom{abcd}{\beta\beta\alpha\alpha} + \binom{abcd}{\alpha\beta\beta\alpha} \right\}$ |

^a Note that by Rumer's rule, $|\gamma\Sigma III; A\rangle = |\gamma\Sigma II; A\rangle - |\gamma\Sigma I; A\rangle$.

The number of independent Slater bond functions which can be obtained from a given spin-free primitive function $|\gamma\rangle$ is

$$f_N^S = \frac{N!(2S + 1)}{\left(\frac{N}{2} - S\right)! \left(\frac{N}{2} + S + 1\right)!} \quad (1.7)$$

or

$$f_N^p = \frac{N!(N - 2p + 1)}{p!(N - p + 1)!} \quad (1.8)$$

Table III: Bond Orbital Diagrams $|\gamma\rangle = a(1)b(2)c(3)d(4)$

| κ | D_κ |
|----------|---|
| I | $a \longrightarrow b$ $d \longleftarrow c$ |
| II | $a \quad b$ $\downarrow \quad \uparrow$ $d \quad c$ |
| III | $a \quad b$ $\diagdown \quad \diagup$ $d \quad c$ |

Any Slater bond function can be expressed as a linear combination of f_N^p linearly independent bond functions. In particular for N even and $p = N/2$, a Slater bond function for a diagram containing crossed bonds can be expressed as a linear combination of Slater bond functions for diagrams with uncrossed (or canonical) bond diagrams. The latter is known as Rumer's rule. See Tables I and II.

A matrix element for a spin-free Hamiltonian over Slater bond functions, has the form

$$\langle \gamma\Sigma\kappa; A | \mathbf{H} | \gamma\Sigma\kappa'; A \rangle = \sum_P (P)_{\kappa\kappa'} \langle \gamma | \mathbf{H} | \gamma; P \rangle \quad (1.9)$$

Here $\langle \gamma | \mathbf{H} | \gamma; P \rangle$ is a spin-free matrix element. $(P)_{\kappa\kappa'}$ is a numerical coefficient, which we call a "Pauling number." It is independent of $|\gamma\rangle$ and depends only on $D_\kappa, D_{\kappa'}$, and P . Pauling has given rules for the determination of $(P)_{\kappa\kappa'}$ for the case of N even and $p = N/2 (S = 0)$. He obtained the $(P)_{\kappa\kappa'}$ for N odd and $p = [(N - 1)/2] (S = 1/2)$ from the case of $p = (N + 1)/2$ by deleting permutations involving the $(N + 1)$ th (or ghost) orbital.

The Pauling rules for obtaining $(P)_{\kappa\kappa'}$ are given in the following paragraphs.

(a) Form the vector bond diagram $D_{\kappa*} \equiv PD_\kappa$, by permuting the integers in D_κ , according to P and returning the integers to their original order carrying along the new head and tail assignments. Superimpose D_κ and $D_{\kappa*}$ and label the superposition $[D_\kappa D_{\kappa*}]$.

(b) Reverse arrows in $[D_\kappa D_{\kappa*}]$ so that the arrows are head to head and tail to tail. Label the new superposition $[D_\kappa D_{\kappa*}]$ and denote the number of arrow reversals by r .

(4) A permutation $P = \begin{pmatrix} 1 & 2 & \dots & N \\ P(1) & P(2) & \dots & P(N) \end{pmatrix}$ on the electron coordinates of an orbital product function takes an electron coordinate i and converts it to $P(i)$ all within the same orbital.

(c) Count the number of islands (the number of disjoint sets of linked integers) in $[D_k D_{k^*}]$. Denote the number of islands by i .

(d) Apply Pauling's rule

$$(P)_{xx'} = (-1)^{P+r(1/2)(N/2)-i} \quad (1.10)$$

See Table VIII.

In this paper we have derived, besides a formula for the Pauling numbers for arbitrary N and p , the Pauling rules using theorems from the permutation group algebra. While the derivation is more complicated than Pauling's original derivation, it demonstrates clearly the role of permutational symmetry which is implicit in the Pauling development.

The general formulation of spin-free quantum chemistry was presented in paper I⁵ of this series. In paper II,⁶ three electron problems were considered in detail.

2. A Brief Introduction to Spin-Free Quantum Chemistry

A spin-free Hamiltonian for an N -electron system commutes with the permutations on the coordinates of all the N electrons. We denote this group of permutations by S_N . The eigenstates of the spin-free Hamiltonian are grouped in sets, called permutation states, each characterized by a partition of N . We designate a partition of N by

$$[\lambda] = [\lambda^1, \lambda^2, \dots, \lambda^N] \quad (2.1)$$

where λ^i is a positive integer or zero such that

$$\lambda^1 \geq \lambda^2 \geq \dots \geq \lambda^N \geq 0 \quad (2.2)$$

and

$$\sum \lambda^i = N \quad (2.3)$$

See Table IV.

The set of all linear combinations of permutation operators of S_N form an algebra⁷ called the permutation algebra which we denote by A_N . An element of A_N is

$$X = \sum_P (X)_P P \quad (2.4)$$

where $(X)_P$ is a numerical coefficient. A_N can be decomposed into a direct sum of invariant subalgebras $A_N^{[\lambda]}$ each indexed by a partition $[\lambda]$ of N . That is

$$A_N = \sum_{[\lambda]} A_N^{[\lambda]} \quad (2.5)$$

The invariant subalgebras have the important property that if $X^{[\lambda]}$ is an element of $A_N^{[\lambda]}$ and $Y^{[\lambda']}$ is an element in $A_N^{[\lambda']}$ then

$$X^{[\lambda]} Y^{[\lambda']} = 0 \text{ for } [\lambda] \neq [\lambda'] \quad (2.6)$$

Table IV

| Partitions and some tableaux for $N = 4$ | | | |
|--|---|---|---|
| $[\lambda]$ | $\tau_r^{[\lambda]}$ | | |
| $[1^4] = [1,1,1,1]$ | $\begin{array}{ c } \hline 1 \\ \hline 2 \\ \hline 3 \\ \hline 4 \\ \hline \end{array}$ | ... | |
| $[2,1^2] = [2,1,1,0]$ | $\begin{array}{ c } \hline 1 2 \\ \hline 3 \\ \hline 4 \\ \hline \end{array}$ | $\begin{array}{ c } \hline 1 3 \\ \hline 2 \\ \hline 4 \\ \hline \end{array}$ | $\begin{array}{ c } \hline 1 4 \\ \hline 2 \\ \hline 3 \\ \hline \end{array}$... |
| $[2^2] = [2,2,0,0]$ | $\begin{array}{ c } \hline 1 2 \\ \hline 3 4 \\ \hline \end{array}$ | $\begin{array}{ c } \hline 1 4 \\ \hline 2 3 \\ \hline \end{array}$ | $\begin{array}{ c } \hline 1 3 \\ \hline 2 4 \\ \hline \end{array}$... |
| Excluded partitions and tableaux | | | |
| $[3,1] = [3,1,0,0]$ | $\begin{array}{ c } \hline 1 2 3 \\ \hline 4 \\ \hline \end{array}$ | $\begin{array}{ c } \hline 1 2 4 \\ \hline 3 \\ \hline \end{array}$ | $\begin{array}{ c } \hline 1 3 4 \\ \hline 2 \\ \hline \end{array}$... |
| $[4] = [4,0,0,0]$ | $\begin{array}{ c } \hline 1 2 3 4 \\ \hline \end{array}$ | ... | |

A function projected by an element of $A_N^{[\lambda]}$ is said to lie in the $[\lambda]$ th permutation state. For example, the functions

$$|\gamma; X^{[\lambda]}\rangle \equiv X^{[\lambda]}|\gamma\rangle \quad (2.7)$$

and

$$|\gamma; Y^{[\lambda']}\rangle \equiv Y^{[\lambda']}|\gamma\rangle \quad (2.8)$$

lie in permutation states $[\lambda]$ and $[\lambda']$, respectively. A matrix element between two such functions is, by (2.6)

$$\begin{aligned} \langle \gamma; X^{[\lambda]} | \mathbf{H} | \gamma; Y^{[\lambda']} \rangle &= \langle \gamma | \mathbf{H} X^{[\lambda]\dagger} Y^{[\lambda']} | \gamma \rangle \\ &= 0 \text{ for } [\lambda] \neq [\lambda'] \end{aligned} \quad (2.9)$$

Here $X^{[\lambda]\dagger}$ is the adjoint of $X^{[\lambda]}$ which also lies in $A_N^{[\lambda]}$. Equation 2.9 shows that a spin-free Hamiltonian does not mix different permutation states.

Young⁷ has devised a simple method for the construction of elements in $A_N^{[\lambda]}$. We arrange the first N integers in rows of length λ^i . See Table IV. This array is called a Young tableau and is designated by

(5) Paper I: F. A. Matsen, "Advances in Quantum Chemistry," Vol. I, P. O. Lowdin, Ed., Academic Press, New York, N. Y., 1964.

(6) Paper II: F. A. Matsen, *J. Phys. Chem.*, **68**, 3282 (1964).

(7) For a thorough discussion of permutation algebras, see D. E. Rutherford, "Substitutional Analysis," Edinburgh, 1948. See also F. A. Matsen and R. D. Poshusta, "Algebras, Ideals and Quantum Mechanics with Applications from the Symmetries Group," Molecular Physics Group Technical Report, University of Texas, Austin, Texas, to be published.

the symbol $T_r^{[\lambda]}$. We next construct the algebraic element

$$E_r^{[\lambda]} \equiv N_r^{[\lambda]} P_r^{[\lambda]} \tag{2.10}$$

Here $N_r^{[\lambda]}$ is the antisymmetric sum of the permutations on the integers in the columns and $P_r^{[\lambda]}$ is the symmetric sum of the permutations on the integers in the rows of $T_r^{[\lambda]}$. See Table V. Young has shown that for any element X of A_N , the element

$$X_r^{[\lambda]} \equiv E_r^{[\lambda]} X \tag{2.11}$$

is an element in $A_N^{[\lambda]}$.

We note that

$$\sigma_{r'r} E_r^{[\lambda]} = E_{r'}^{[\lambda]} \sigma_{r'r} \tag{2.12}$$

where $\sigma_{r'r}$ is the permutation⁸ that converts $T_r^{[\lambda]}$ into $T_{r'}^{[\lambda]}$. That is

$$T_{r'}^{[\lambda]} = \sigma_{r'r} T_r^{[\lambda]} \tag{2.13}$$

The σ 's have the following rule of combination

$$\sigma_{r'r'} \sigma_{r''r''} = \sigma_{r''r'} \tag{2.14}$$

From the fact that there are two, and only two, spin states for an electron and as a consequence of the anti-symmetry principle, the only permutation states that occur in nature are those for which

$$[\lambda] = [2^p, 1^{N-2p}] \quad 0 \leq p \leq N/2 \tag{2.15}$$

Here p is called the permutation quantum number. It is related to the spin quantum number by the expression

$$p = N/2 - S \tag{2.16}$$

The set of permutation states characterized by $[\lambda] = [2^p, 1^{N-2p}]$ replaces, in spin-free quantum chemistry, the spin states in conventional theory.

The tableaux associated with permutation states $[\lambda] = [2^p, 1^{N-2p}]$ are two columned tableaux containing p rows of length two and $N - 2p$ rows of length one. See Table IV.

3. Spin-Free Bond Functions

In the spin-free formulation of quantum chemistry, the vector bond diagram D_x is replaced by a Young tableau, $T_x^{[\lambda]}$. A bond diagram with p bonds is replaced by a tableau containing p rows of length two and $N - 2p$ rows of length one. The partition of such a tableau is $[\lambda] = [2^p, 1^{N-2p}]$. Each pair of integers connected by an arrow in D_x is placed in the same row of $T_x^{[\lambda]}$ with the tail integer in the first column. The paired integers are placed in any order in the rows of length two and the unpaired integers in any order in the rows of length one. See Table VI. We associate

Table V

A Young operator for $[\lambda] = [2^2]$

$$T_r^{[\lambda]} = \begin{array}{|c|c|} \hline 1 & 2 \\ \hline 3 & 4 \\ \hline \end{array}$$

$$\begin{aligned} E_r^{[\lambda]} &= N_r^{[\lambda]} P_r^{[\lambda]} \\ &= [\{s - (13)\}\{s - (24)\}][\{s + (12)\}\{s + (34)\}] \\ &= s - (13) - (24) + (13)(24) + (12) - (123) - \\ &\quad (142) + (1423) + (34) - (134) - (243) + \\ &\quad (1324) + (12)(34) - (1234) - (1432) + \\ &\quad (14)(23) \end{aligned}$$

A Young operator for $[\lambda] = [2, 1^2]$

$$T_r^{[\lambda]} = \begin{array}{|c|c|} \hline 1 & 2 \\ \hline 3 & \\ \hline 4 & \\ \hline \end{array}$$

$$\begin{aligned} E_r^{[\lambda]} &= [s - (13) - (14) - (34) + (134) + (143)][s + \\ &\quad (12)] \\ &= s - (13) - (14) - (34) + (134) + (143) + \\ &\quad (12) - (123) - (124) - (12)(34) + \\ &\quad (1234) + (1243) \end{aligned}$$

with $T_x^{[\lambda]}$ any element in $A_N^{[\lambda]}$ called a structure projector

$$\kappa \equiv \epsilon(\sigma_{I\kappa}) E_I^{[\lambda]} \sigma_{I\kappa} \tag{3.1}$$

where

$$\epsilon(\sigma_{I\kappa}) \equiv (-1)^{\sigma_{I\kappa}} \tag{3.2}$$

is the parity of $\sigma_{I\kappa}$.⁹ Here

$$\begin{array}{|c|c|} \hline 1 & 2 \\ \hline 3 & 4 \\ \hline \vdots & \vdots \\ \hline \vdots & \vdots \\ \hline 2p-1 & 2p \\ \hline \vdots & \vdots \\ \hline \vdots & \vdots \\ \hline N & \\ \hline \end{array} \tag{3.3}$$

(8) The objects in a tableau are numbers. A permutation P on a tableau takes a number i and converts it to $P(i)$ all within the same position in the tableau.

(9) The proof that κ is independent of the order of rows of length two or one is straightforward. Let $T_x^{[\lambda]}$ be a tableau that differs from $T_x^{[\lambda]}$ in the arrangement of the rows. Then (suppressing $[\lambda]$) $N_x = N_x, P_{\hat{x}} = P_x, \sigma_{x\hat{x}} N_{\hat{x}} = \epsilon(\sigma_{x\hat{x}}) N_{\hat{x}}$, and $\sigma_{x\hat{x}} = \sigma_{I\kappa} \sigma_{x\hat{x}}$. Thus by (2.12) and (2.14)

$$\begin{aligned} \hat{\kappa} &= \epsilon(\sigma_{I\hat{\kappa}}) N_I P_I \sigma_{I\hat{\kappa}} = \epsilon(\sigma_{I\hat{\kappa}}) \sigma_{I\hat{\kappa}} N_{\hat{\kappa}} P_{\hat{\kappa}} \\ \hat{\kappa} &= \epsilon(\sigma_{I\kappa} \sigma_{x\hat{x}}) \sigma_{I\kappa} \sigma_{x\hat{x}} N_{\hat{\kappa}} P_{\hat{\kappa}} = \epsilon(\sigma_{I\kappa}) \sigma_{I\kappa} N_x P_x = \kappa \end{aligned}$$

Table VI

Structure projectors for $[\lambda] = [2^2]$;
 $p = 2$ ($S = 0$), $f_N^p = 2$

| κ | D_{κ} | $T_{\kappa}^{[\lambda]}$ | $\sigma_{I\kappa}$ | $(-1)^{\sigma_{I\kappa}}$ | Projector, κ |
|----------|---|--|--------------------|---------------------------|------------------------|
| I | 1. \rightarrow .2 4. \leftarrow .3 | $\begin{bmatrix} 1 2 \\ 3 4 \end{bmatrix}$ | δ | 1 | $E_I^{[\lambda]}$ |
| II | 1. \downarrow .2 4. \uparrow .3 | $\begin{bmatrix} 1 4 \\ 3 2 \end{bmatrix}$ | (24) | -1 | $-E_I^{[\lambda]}(24)$ |
| III | 1. \swarrow .2 4. \searrow .3 | $\begin{bmatrix} 1 3 \\ 4 2 \end{bmatrix}$ | (243) | 1 | $E_I^{[\lambda]}(243)$ |

I = $\delta - (13) - (24) + (13)(24) + (12) - (123) - (142) + (1423) + (34) - (134) - (243) + (1324) + (12)(34) - (1234) - (1432) + (14)(23)$

II = $-(13) + \delta + (13)(24) - (24) - (132) + (23) + (1342) - (234) - (143) + (14) + (1243) - (124) - (1432) + (14)(23) + (12)(34) - (1234)$

III = $+(23) - (132) - (234) + (1342) + (123) - (12) - (1423) + (142) + (243) - (1324) - (34) + (134) + (1243) - (124) - (143) + (14)^a$

Structure projectors for $[\lambda] = [2,1^2]$;
 $p = 1$ ($S = 1$), $f_N^p = 3$

| | | | | | |
|-----|--|---|----------|---|---------------------------|
| I | 1. \rightarrow .2 4. .3 | $\begin{bmatrix} 1 2 \\ 3 \\ 4 \end{bmatrix}$ | δ | 1 | $E_I^{[\lambda]}$ |
| II | 1. \downarrow .2 4. .3 | $\begin{bmatrix} 2 3 \\ 1 \\ 4 \end{bmatrix}$ | (132) | 1 | $E_I^{[\lambda]}(132)$ |
| III | 1. \leftarrow .2 4. \leftarrow .3 | $\begin{bmatrix} 3 4 \\ 1 \\ 2 \end{bmatrix}$ | (13)(24) | 1 | $E_I^{[\lambda]}(13)(24)$ |

I = $+\delta - (13) - (14) - (34) + (134) + (143) + (12) - (123) - (124) - (12)(34) + (1234) + (1243)$

II = $+(13) - \delta - (134) - (143) + (14) + (34) + (132) - (23) - (1324) - (1432) + (14)(23) + (243)$

III = $+(13)(24) - (24) - (1342) - (1423) + (142) + (234) + (1324) - (243) - (132) - (14)(23) + (1432) + (23)^b$

^a Note that by Rumer's rule, **III** = **II** - **I**. ^b Note that for $[\lambda] = [2,1^2]$, **I**, **II**, and **III** are linearly independent.

and

$$T_{\kappa}^{[\lambda]} = \sigma_{\kappa I} T_I^{[\lambda]} \quad (3.4)$$

The structure projector projects spin-free bond functions from a primitive function. Thus

$$|\gamma; \kappa\rangle \equiv \frac{1}{\sqrt{C}} \kappa |\gamma\rangle \quad (3.5)$$

where

$$C = 2^p p! (N - p)! \quad (3.6)$$

Spin-free functions for $N = 4$ are given in Table VII. Matrix elements computed with functions 3.5 are identical with those obtained with Slater bond functions.⁵

Table VII: Spin-Free Bond Functions, $[\lambda] = [2^2]$

$$|\gamma\rangle = a(1)b(2)c(3)d(4) \equiv abcd$$

$$|\gamma; \text{I}\rangle = 1/4 \{abcd - cbad - adcb + cdab + bacd - cabd - bdca + dcba + abdc - dbac - acdb + dcab + badc - dabc - bcda + dcba\}$$

$$|\gamma; \text{II}\rangle = 1/4 \{-cbad + abcd + cdab - adcb - bcad + acbd + bdac - adbc - cbda + dbca + cabd - dacb - bcda + dcba + badc - dabc\}$$

$$|\gamma; \text{III}\rangle = 1/4 \{abcd - bcad - adbc + bdac + cabd - bacd - cbda + bdca + acdb - dcab - abdc + dbac + cabd - dacb - bcda + dcba\}^a$$

^a Note that by Rumer's rule $|\gamma; \text{III}\rangle = |\gamma; \text{II}\rangle - |\gamma; \text{I}\rangle$.

4. Matrix Elements over Spin-Free Bond Functions

The matrix elements for a spin-free Hamiltonian over spin-free bond functions $|\gamma; \kappa\rangle$ and $|\gamma; \kappa'\rangle$ can be conveniently expressed in terms of an element $A_N^{[\lambda]}$ which we denote by $Z_{\kappa\kappa'}$ and which we call the "bracket operator." Thus

$$\langle \gamma; \kappa | \mathbf{H} | \gamma; \kappa' \rangle = \langle \gamma | \mathbf{H} | \gamma; Z_{\kappa\kappa'} \rangle \quad (4.1)$$

where the bracket operator is by (3.5) and (2.9)

$$Z_{\kappa\kappa'} \equiv \frac{\kappa^\dagger \kappa'}{C} \equiv \sum_P (P)_{\kappa\kappa'} P \quad (4.2)$$

Here¹⁰

$$\kappa^\dagger = \sigma_{\kappa I} E_I^\dagger \epsilon(\sigma_{\kappa I}) = \sigma_{\kappa I} P_I N_I \epsilon(\sigma_{\kappa I}) \quad (4.3)$$

By (2.11), (2.9), and (2.15)

$$Z_{\kappa\kappa'} = 0 \text{ unless } p = p' \quad (4.4)$$

(10) Hereafter, we suppress $[\lambda]$ in $T_{\kappa}^{[\lambda]}$, $P_{\kappa}^{[\lambda]}$, $N_{\kappa}^{[\lambda]}$, $E_{\kappa}^{[\lambda]}$, and $\epsilon_{\kappa}^{[\lambda]}$ (see (5.3)).

i.e., unless D_x and $D_{x'}$ contain the same number of bonds. We can obtain the Pauling numbers $(P)_{xx'}$ for all permutation states and for all permutations by direct expansion of (4.2). We note that $Z_{xx'}$ is independent of the form of the spin-free primitive function $|\gamma\rangle$. The values of the Pauling numbers for the states of $N = 4$ are given in Table VIII.

An off-diagonal bracket element can be expressed in terms of a diagonal bracket element. By (4.2), (3.1), and (2.12) we have

$$\begin{aligned} Z_{xx'} &= \epsilon(\sigma_{xx'})\epsilon(\sigma_{I_x'\sigma_{x'I}})E_I^\dagger E_I\sigma_{I_x'}/C \\ &= \epsilon(\sigma_{xx'})E_x^\dagger E_x\sigma_{xx'}/C \\ &= \epsilon(\sigma_{xx'})Z_{xx}\sigma_{xx'} \end{aligned} \tag{4.5}$$

5. Group Theoretical Formulation of the Pauling Numbers

The diagonal bracket element Z_{xx} is an element in an invariant subalgebra $A_N^{[\lambda]}$ and as such can be expanded in an orthogonal matrix basis⁶ $\{e_{rs}^{[\lambda]}; r, s = 1 \text{ to } f^{[\lambda]}\}$ of $A_N^{[\lambda]}$. Here

$$e_{rs}^{[\lambda]} = (f^{[\lambda]}/N!) \sum_P [P]_{rs}^{[\lambda]} P \tag{5.1}$$

where $[P]_{rs}^{[\lambda]}$ is the (r, s) th element in the matrix representing P in the orthogonal irreducible representation $\Gamma^{[\lambda]}$. Thus

$$Z_{xx} = \sum_r \sum_s^{f^{[\lambda]}} [Z_{xx}]_{rs}^{[\lambda]} e_{rs}^{[\lambda]} \tag{5.2}$$

For $T_x^{[\lambda]}$ we define the idempotent element (see (A3))

$$\epsilon_x \equiv (1/2^p)P_x \tag{5.3}$$

and we note that

$$\epsilon_x Z_{xx} \epsilon_x = \epsilon_x P_x N_x N_x P_x \epsilon_x = P_x N_x N_x P_x = Z_{xx} \tag{5.4}$$

It is noted in Appendix A that for a given T_x there exists a form of the irreducible representation $\Gamma^{[\lambda]} = \Gamma_x^{[\lambda]}$ such that

$$[\epsilon_x]_{rs}^{[\lambda]} = \delta_{r1}\delta_{s1} \tag{5.5}$$

Then by (5.4) and (5.5) we have

$$\begin{aligned} [Z_{xx}]_{rs}^{[\lambda]} &= [\epsilon_x Z_{xx} \epsilon_x]_{rs}^{[\lambda]} \\ &= \sum_t \sum_u [\epsilon_x]_{rt}^{[\lambda]} [Z_{xx}]_{tu}^{[\lambda]} [\epsilon_x]_{us}^{[\lambda]} \\ &= \delta_{r1}\delta_{s1} [Z_{xx}]_{11}^{[\lambda]} \end{aligned} \tag{5.6}$$

On the substitution of (5.6) into (5.2) we obtain

$$Z_{xx} = [Z_{xx}]_{11}^{[\lambda]} e_{11}^{[\lambda]} \tag{5.7}$$

On the substitution of (5.1) and (B6) into (5.7)

$$Z_{xx} = \sum_P [P]_{11}^{[\lambda]} P \tag{5.8}$$

where $[P]_{11}^{[\lambda]} \in \Gamma^{[\lambda]}$. We obtain an off-diagonal bracket element by substituting (5.8) into (4.5)

$$\begin{aligned} Z_{xx'} &= \epsilon(\sigma_{xx'})Z_{xx}\sigma_{xx'} \\ &= \sum_P \epsilon(\sigma_{xx'}) [P]_{11}^{[\lambda]} P \sigma_{xx'} \\ &= \sum_P \epsilon(\sigma_{xx'}) [P \sigma_{x'x}]_{11}^{[\lambda]} P \end{aligned} \tag{5.9}$$

We compare (5.9) with (4.2) to obtain

$$(P)_{xx'} = \epsilon(\sigma_{xx'}) [P \sigma_{x'x}]_{11}^{[\lambda]} \tag{5.10}$$

Equation 5.10, which is true for a given x and any x' , relates the Pauling numbers for arbitrary N and p (spin state) to an irreducible representation $\Gamma_x^{[\lambda]}$ of the permutation group S_N . $\Gamma_x^{[\lambda]}$ was assumed to be an orthogonal representation with condition (5.5). It can be shown that the orthogonality requirement is not necessary and only condition (5.5) is needed to obtain (5.10). In the next section we go on to the special case treated by Pauling, $p = N/2$, and derive his rule from eq 5.10.

6. Explicit Evaluation of the Pauling Numbers for $p = N/2$

For $p = N/2$ (N even) we have an explicit form for $[P \sigma_{x'x}]_{11}^{[\lambda]}$ and hence for $(P)_{xx'}$. The case for $p = (N - 1)/2$ (N odd) is obtained by deleting permutations involving the $(N + 1)$ th integer in the formulation for $p = (N + 1)/2$. We begin by considering tableaux T_x and $T_{x'}$ and a permutation P . We define a tableau

$$T_{x^*} \equiv P T_{x'} = P \sigma_{x'x} T_x \tag{6.1}$$

Thus

$$\sigma_{x^*x} = P \sigma_{x'x} \tag{6.2}$$

Next we construct new tableaux as

$$\begin{aligned} T_{\hat{x}} &\equiv \sigma_{\hat{x}x} T_x \\ T_{\hat{x}^*} &\equiv \sigma_{\hat{x}^*x^*} T_{x^*} \end{aligned} \tag{6.3}$$

where $\sigma_{\hat{x}x}$ transposes along rows in T_x , $\sigma_{\hat{x}^*x^*}$ transposes along rows and rearranges rows in T_{x^*} so that $T_{\hat{x}}$ and $T_{\hat{x}^*}$ have identical first columns. Next we permute on the second column of $T_{\hat{x}}$ so as to make it identical with $T_{\hat{x}^*}$. This is done with $\sigma_{\hat{x}\hat{x}^*}$.

$$T_{\hat{x}^*} = \sigma_{\hat{x}\hat{x}^*} T_{\hat{x}} \tag{6.4}$$

By (A41)

$$[\sigma_{x^*x}]_{11}^{[\lambda]} = [\sigma_{\hat{x}\hat{x}^*}]_{11}^{[\lambda]} = (-1/2)^q \tag{6.5}$$

where q is the minimum number of transpositions on

Table VIII: The Pauling Numbers $(P)_{xx'}$ for the Structures in Table VI

| xx' | g | (12) | (13) | (23) | (123) | (132) | (14) | (24) | (34) | (124) | (142) |
|-----------------|--------|--------|--------|--------|--------|--------|--------|--------|--------|--------|--------|
| $p = 2 (S = 0)$ | | | | | | | | | | | |
| I I | 1 | 1 | $-1/2$ | $-1/2$ | $-1/2$ | $-1/2$ | $-1/2$ | $-1/2$ | 1 | $-1/2$ | $-1/2$ |
| I II | $1/2$ | $1/2$ | -1 | $1/2$ | $1/2$ | -1 | $1/2$ | -1 | $1/2$ | -1 | $1/2$ |
| II I | $1/2$ | $1/2$ | -1 | $1/2$ | -1 | $1/2$ | $1/2$ | -1 | $1/2$ | $1/2$ | -1 |
| II II | 1 | $-1/2$ | $-1/2$ | 1 | $-1/2$ | $-1/2$ | 1 | $-1/2$ | $-1/2$ | $-1/2$ | $-1/2$ |
| $p = 1 (S = 1)$ | | | | | | | | | | | |
| I I | 1 | 1 | $-1/2$ | $-1/2$ | $-1/2$ | $-1/2$ | $-1/2$ | $-1/2$ | -1 | $-1/2$ | $-1/2$ |
| I II | $-1/2$ | $-1/2$ | 1 | $-1/2$ | $-1/2$ | 1 | $1/2$ | 0 | $1/2$ | 0 | $1/2$ |
| I III | 0 | 0 | $-1/2$ | $1/2$ | $1/2$ | $-1/2$ | $1/2$ | $-1/2$ | 0 | $-1/2$ | $-1/2$ |
| II I | $-1/2$ | $-1/2$ | 1 | $-1/2$ | 1 | $-1/2$ | $1/2$ | 0 | $1/2$ | $1/2$ | 0 |
| II II | 1 | $-1/2$ | $-1/2$ | 1 | $-1/2$ | $-1/2$ | -1 | $-1/2$ | $-1/2$ | $1/2$ | $1/2$ |
| II III | $-1/2$ | $1/2$ | 0 | $-1/2$ | 0 | $1/2$ | $1/2$ | 1 | $-1/2$ | $-1/2$ | -1 |
| III I | 0 | 0 | $-1/2$ | $1/2$ | $-1/2$ | $1/2$ | $1/2$ | $-1/2$ | 0 | $-1/2$ | $-1/2$ |
| III II | $-1/2$ | $1/2$ | 0 | $-1/2$ | $1/2$ | 0 | $1/2$ | 1 | $-1/2$ | -1 | $-1/2$ |
| III III | 1 | -1 | $-1/2$ | $-1/2$ | $1/2$ | $1/2$ | $-1/2$ | $-1/2$ | 1 | $1/2$ | $1/2$ |

the second column of $T_{\hat{k}}$ into which $\sigma_{\hat{k}^* \hat{k}}$ can be decomposed. In terms of the three tableau operations defined and by (2.14)

$$\sigma_{x^* x} = \sigma_{x^* \hat{k}^*} \sigma_{\hat{k}^* \hat{k}} \sigma_{\hat{k} x} \quad (6.6)$$

Note that $\sigma_{x \hat{k}} = \sigma_{\hat{k} x}$.

Consider the parity $\epsilon(\sigma_{\hat{k}^* x^*}) \epsilon(\sigma_{\hat{k} x}) = \epsilon(\sigma_{\hat{k}^* x^*} \sigma_{\hat{k} x})$. Since the permutations in $\sigma_{\hat{k}^* x^*}$ that rearrange rows are of even parity, then the parity is just $(-1)^r$, where r is the sum of the number of transpositions on rows contained in $\sigma_{\hat{k}^* x^*}$ and $\sigma_{\hat{k} x}$. By (6.2) and (6.6)

$$(-1)^{\sigma_{x^* x}} = (-1)^{P + \sigma_{xx'}} = (-1)^{r+q} \quad (6.7)$$

Then by (6.2)

$$\epsilon(\sigma_{xx'}) \equiv (-1)^{\sigma_{xx'}} = (-1)^{P+r+q} \quad (6.8)$$

Finally by (5.10), (6.2), (6.5), and (6.8) we obtain

$$(P)_{xx'} = (-1)^{P+r} (1/2)^q \quad (6.9)$$

In summary $(P)_{xx'}$ is computed in the following manner. (a) Form tableau $T_{x^*} \equiv PT_{x'}$. (b) Permute integers along rows in T_{x^*} and permute integers along rows and rearrange rows in T_{x^*} so that the resulting tableaux $T_{\hat{k}}$ and $T_{\hat{k}^*}$ have identical first columns. Denote the sum of the transposition along rows by r . (c) Determine the minimum number of transpositions on the second column of $T_{\hat{k}}$ necessary to make it identical with $T_{\hat{k}^*}$. Denote the number of these transpositions by q . (d) Apply eq 6.9.

To obtain Pauling's rule we replace the tableaux by their equivalent vector bond diagrams. We note first that r determines the number of arrow reversals required to obtain the superposition $[D_{\hat{k}} D_{\hat{k}^*}]$. We

note further that $\sigma_{\hat{k}^* \hat{k}}$ determines the number of islands. For $\sigma_{\hat{k}^* \hat{k}} = g$, $[D_{\hat{k}} D_{\hat{k}^*}]$ contains $N/2$ islands. Each transposition in $\sigma_{\hat{k}^* \hat{k}}$ reduces the number of islands by one. Consequently if $\sigma_{\hat{k}^* \hat{k}}$ contains q transpositions

$$i = (N/2) - q \quad (6.10)$$

We substitute (6.10) into (6.9) and make use of the relation between Young tableaux and vector bond diagrams to obtain the Pauling rule, eq 1.10.

7. Conclusions

We have formulated spin-free bond functions whose matrix elements with a spin-free Hamiltonian are identical with those obtained with the spin-containing Slater bond functions. We have given a spin-free group theoretical derivation of the Pauling rules for these matrix elements.

The results of this paper together with the results obtained in papers I and II of this series further establish the existence of a valid, operative spin-free quantum chemistry. A belief in the existence of a spin-free quantum chemistry can prevent improper use of spin concepts in discussions of electron dynamics of chemical systems and can develop a clearer view of the forces which operate in these systems.

The mathematical tools [the theory of the permutation (symmetric) group] used in the spin-free formulation of quantum chemistry were in existence before the discovery of spin. It would have been possible, therefore, for quantum chemistry to have been developed without knowledge of the existence of spin. The use of spin and the antisymmetry principle is an indirect way of introducing permutation group theory into quantum chemistry.

| (134) | (143) | (234) | (243) | (1234) | (1432) | (1324) | (1423) | (1342) | (1243) | (12)(34) | (13)(24) | (14)(23) |
|-----------------|-------|-------|-------|--------|--------|--------|--------|--------|--------|----------|----------|----------|
| $p = 2 (S = 0)$ | | | | | | | | | | | | |
| -1/2 | -1/2 | -1/2 | -1/2 | -1/2 | -1/2 | 1 | 1 | -1/2 | -1/2 | 1 | 1 | 1 |
| 1/2 | -1 | -1 | 1/2 | -1 | -1 | 1/2 | 1/2 | 1/2 | 1/2 | 1/2 | 1/2 | 1/2 |
| -1 | 1/2 | 1/2 | -1 | -1 | -1 | 1/2 | 1/2 | 1/2 | 1/2 | 1/2 | 1/2 | 1/2 |
| -1/2 | -1/2 | -1/2 | -1/2 | -1/2 | -1/2 | -1/2 | -1/2 | 1 | 1 | 1 | 1 | 1 |
| $p = 1 (S = 1)$ | | | | | | | | | | | | |
| 1/2 | 1/2 | 1/2 | 1/2 | 1/2 | 1/2 | 0 | 0 | 1/2 | 1/2 | -1 | 0 | 0 |
| -1/2 | -1 | 0 | 1/2 | 0 | -1 | -1/2 | 1/2 | -1/2 | 1/2 | 1/2 | 1/2 | -1/2 |
| 1/2 | 1/2 | 1/2 | -1/2 | 1/2 | 1/2 | 1 | -1 | -1/2 | -1/2 | 0 | 1 | -1 |
| -1 | -1/2 | 1/2 | 0 | -1 | 0 | 1/2 | -1/2 | -1/2 | -1/2 | 1/2 | 1/2 | -1/2 |
| 1/2 | 1/2 | -1/2 | -1/2 | 1/2 | 1/2 | 1/2 | 1/2 | 0 | 0 | 0 | 0 | -1 |
| 0 | -1/2 | 1/2 | 1 | 0 | -1 | -1/2 | 1/2 | 1/2 | -1/2 | 1/2 | -1/2 | 1/2 |
| 1/2 | 1/2 | -1/2 | 1/2 | 1/2 | 1/2 | -1 | 1 | -1/2 | -1/2 | 0 | 1 | -1 |
| -1/2 | 0 | 1 | 1/2 | -1 | 0 | 1/2 | -1/2 | -1/2 | 1/2 | 1/2 | -1/2 | 1/2 |
| -1/2 | -1/2 | -1/2 | -1/2 | 1/2 | 1/2 | 0 | 0 | 1/2 | 1/2 | -1 | 0 | 0 |

Appendix A

The Evaluation¹¹ of $(P)_{xx'}$

For a tableau T_β with partition $[\beta] = [\beta^1, \beta^2, \dots, \beta^N]$ we define a subgroup of S_N composed of the elements which permute the integers along the rows of T_β . We designate the group by G_β and note that its order is

$$n^\beta = \beta^1! \beta^2! \dots \beta^N! \tag{A1}$$

and its index is

$$n_\beta = N! / n^\beta \tag{A2}$$

We denote by the symbol $\Pi^{j\beta}$ ($j = 1$ to n^β) a generator of the j th left coset of G_β . The symmetric idempotent of G_β is

$$\varepsilon_\beta = (1/n^\beta) P_\beta \tag{A3}$$

With ε_β and the $\Pi^{j\beta}$ we generate a set of elements

$$\varepsilon_\beta^j = \Pi^{j\beta} \varepsilon_\beta \quad j = 1 \text{ to } n_\beta \tag{A4}$$

which are the basis of a subalgebra, A_{N^β} of A_N . These elements are also the basis for a representation Γ^β of S_N . The representation is generally reducible. That is

$$\Gamma^\beta = \sum_{[\lambda]} f^{[\beta][\lambda]} \Gamma^{[\lambda]} \tag{A5}$$

where

$$f^{[\beta][\lambda]} = (1/N!) \sum_P \chi^{[\beta]}(P) \chi^{[\lambda]}(P) \tag{A6}$$

is the number of times $\Gamma^{[\lambda]}$ occurs in Γ^β and $\chi^{[\beta]}(P)$ and $\chi^{[\lambda]}(P)$ are characters in Γ^β and $\Gamma^{[\lambda]}$, respectively. We note that $\chi^{[\beta]}(P)$ and hence $f^{[\beta][\lambda]}$ depend only on the partition $[\beta]$ associated with G_β and not with G_β itself.

We can choose an irreducible representation of S_N which is canonical to the symmetric idempotent ε_β of G_β . That is, we can choose a representation such that

$$[\varepsilon_\beta]_{rs}^{[\lambda]} = \delta_{rs} \text{ for } r, s \leq f^{[\beta][\lambda]} \tag{A7}$$

$$= 0 \text{ for } r, s > f^{[\beta][\lambda]} \tag{A8}$$

We designate this representation by $\Gamma_\beta^{[\lambda]}$. Murnaghan¹² has shown that¹³

$$f^{[\beta][\lambda]} = 0 \text{ for } [\beta] > [\lambda] \tag{A9}$$

$$= 1 \text{ for } [\beta] = [\lambda] \tag{A10}$$

Consider first a tableau with $[\beta] = [3, 1^{N-3}]$

$$T_\beta = \begin{array}{|c|c|c|} \hline e & f & g \\ \hline \cdot & & \\ \hline \cdot & & \\ \hline \cdot & & \\ \hline \cdot & & \\ \hline \cdot & & \\ \hline \cdot & & \\ \hline \cdot & & \\ \hline \cdot & & \\ \hline \end{array} \tag{A11}$$

Here

(11) M. Kotani, "Calculations Fonctions d'Onde Moleculaire," CNRS, Paris, 1958; Encyclopedia of Physics, Vol. XXXVII/2, Springer-Verlag, Berlin, 1961. In these references Professor Kotani has developed eq A19 and a form of (A38). In the first reference he invoked the antisymmetry principle and then used representation theory. In the second reference his argument is based on the properties of spin eigenfunctions. Our derivation of these relations, while exploiting the Kotani approach, is entirely group theoretical and spin free.

(12) F. D. Murnaghan, "The Theory of Group Representations," Johns Hopkins University, Baltimore, Md., 1938.

(13) Partitions are ordered according to the dictionary order. Thus for $N = 4$, $[1^4] < [2, 1^2] < [2^2] < [3, 1] < [4]$.

$$G_\beta = \{g, (ef), (eg), (fg), (efg), (egf)\} \quad (\text{A12})$$

and

$$\varepsilon_\beta = 1/6\{g + (ef) + (eg) + (fg) + (efg) + (egf)\} \quad (\text{A13})$$

$$= 1/6\{g + (eg) + (fg)\}\{g + (ef)\} \quad (\text{A14})$$

In representation form (A14) becomes

$$[\varepsilon_\beta]_{rs}^{[\lambda]} = 1/6 \sum_t ([g]_{rt}^{[\lambda]} + [(eg)]_{rt}^{[\lambda]} + [(fg)]_{rt}^{[\lambda]}) \times ([g]_{ts}^{[\lambda]} + [(ef)]_{ts}^{[\lambda]}) \quad (\text{A15})$$

We consider now an irreducible representation with $[\lambda] = [2^{N/2}]$. We wish to make the representation canonical to the idempotent ε_x of G_x with

$$T_x = \begin{array}{|c|c|} \hline l & l' \\ \hline m & m' \\ \hline n & n' \\ \hline \cdot & \cdot \\ \hline \cdot & \cdot \\ \hline \end{array} \quad (\text{A16})$$

and $[\kappa] = [2^{N/2}]$.

Let A_t be a transposition on a row; *i.e.*, $A_t = (ll')$, (mm') , \dots . Then

$$A_t P_x = P_x A_t = P_x \quad (\text{A17})$$

and thus

$$A_t Z_{xx} = Z_{xx} A_t = Z_{xx} \quad (\text{A18})$$

Then by (5.6)

$$[A_t]_{it}^{[\lambda]} = [A_t]_{it}^{[\lambda]} = \delta_{it} \quad (\text{A19})$$

Let C_t be a transposition between rows; *i.e.*, $C_t = (lm)$, $(l'm')$, (lm') , etc. Given a C_t , consider an A_t which contains one of the integers in C_t . Then there is a $C_{t'}$ which consists of the remaining integers in A_t and C_t and is given by

$$A_t C_{t'} = C_t A_t \quad (\text{A20})$$

The tableau in (A11) is completely arbitrary; thus we take it to be the one with

$$\begin{aligned} (ef) &= A_t \\ (eg) &= C_t \\ (fg) &= C_{t'} \end{aligned} \quad (\text{A21})$$

Since

$$[g]_{rt}^{[\lambda]} = \delta_{rt} \quad (\text{A22})$$

then by (A15) and (A19)

$$[\varepsilon_\beta]_{it}^{[\lambda]} = 2/6(\delta_{it} + [C_t]_{it}^{[\lambda]} + [C_{t'}]_{it}^{[\lambda]}) \quad (\text{A23})$$

Since $[\beta] = [3, 1^{N-3}] > [\kappa] = [2^{N/2}]$, we have by (A8) and (A10)

$$[\varepsilon_\beta]_{it}^{[\lambda]} = 0 \quad (\text{A24})$$

Then by (A23)

$$[C_t]_{it}^{[\lambda]} + [C_{t'}]_{it}^{[\lambda]} = -\delta_{it} \quad (\text{A25})$$

We make use of the above relations to evaluate $[\sigma_{x^*x}]_{it}^{[\lambda]}$ of (6.5). By analogy to (3.1) and referring to (6.1) and (6.3) we have

$$\begin{aligned} \kappa^* &= \epsilon(\sigma_{xx^*})\kappa\sigma_{xx^*} \\ \hat{\kappa}^* &= \epsilon(\sigma_{x^*x^*})\kappa^*\sigma_{x^*x^*} \\ \hat{\kappa} &= \epsilon(\sigma_{x\hat{x}})\kappa\sigma_{x\hat{x}} \end{aligned} \quad (\text{A26})$$

The $\hat{\kappa}$'s (with carets) differ at most by sign from the κ 's because $\sigma_{x\hat{x}}$ transposes along rows of $T_{\hat{x}}$ and $\sigma_{x^*x^*}$ transposes along rows and rearranges rows of $T_{\hat{x}^*}$.

$$\hat{\kappa} = \epsilon(\sigma_{x\hat{x}})\kappa \quad (\text{A27})$$

$$\hat{\kappa}^* = \epsilon(\sigma_{x^*\hat{x}^*})\kappa^* \quad (\text{A28})$$

Then

$$Z_{xx^*} = \epsilon(\sigma_{x\hat{x}})\epsilon(\sigma_{x^*\hat{x}^*})Z_{\hat{x}\hat{x}^*} \quad (\text{A29})$$

and

$$Z_{xx} = Z_{\hat{x}\hat{x}} \quad (\text{A30})$$

Note that since $\varepsilon_x = \varepsilon_{\hat{x}}$

$$\Gamma_x^{[\lambda]} = \Gamma_{\hat{x}}^{[\lambda]} \quad (\text{A31})$$

By analogy to (5.9) and by employing (A29) and (A30) we have

$$Z_{xx^*} = \epsilon(\sigma_{xx^*}) \sum_P [P\sigma_{x^*x}]_{it}^{[\lambda]} P \quad (\text{A32})$$

and

$$\begin{aligned} Z_{xx^*} &= \epsilon(\sigma_{x\hat{x}})\epsilon(\sigma_{x^*\hat{x}^*})Z_{\hat{x}\hat{x}^*} \\ &= \epsilon(\sigma_{x\hat{x}})\epsilon(\sigma_{x^*\hat{x}^*})\epsilon(\sigma_{\hat{x}\hat{x}^*})Z_{\hat{x}\hat{x}\hat{x}^*\hat{x}^*} \\ &= \epsilon(\sigma_{xx^*})Z_{\hat{x}\hat{x}\hat{x}^*\hat{x}^*} \\ &= \epsilon(\sigma_{xx^*})Z_{xx}\sigma_{\hat{x}\hat{x}^*} \\ &= \epsilon(\sigma_{xx^*}) \sum_P [P\sigma_{\hat{x}\hat{x}^*}]_{it}^{[\lambda]} P \end{aligned} \quad (\text{A33})$$

On equating (A32) with (A33) and for $P = g$ we have

$$[\sigma_{x^*x}]_{it}^{[\lambda]} = [\sigma_{\hat{x}^*\hat{x}}]_{it}^{[\lambda]} \quad (\text{A34})$$

Now $\sigma_{\hat{x}^*\hat{x}}$ can be decomposed into a product of some minimum number, say g , of transpositions on the second column of $T_{\hat{x}}$. These are transpositions of the type C_t but on $T_{\hat{x}}$.

$$\sigma_{x^*x} = C_1 C_2 \dots C_q \tag{A35}$$

For C_q consider the A_q which contains the integer of C_q not found in $C_1, C_2, \dots,$ and C_{q-1} . Then by (A20) and since A_q will commute with $C_1, C_2, \dots,$ and C_{q-1} , we have

$$C_1 C_2 \dots C_q A_q = A_q C_1 C_2 \dots C_q \tag{A36}$$

Thus by (A19) and (A31)

$$[C_1 C_2 \dots C_q]_{II}^{[\lambda]} = [C_1 C_2 \dots C_{q'}]_{II}^{[\lambda]} \tag{A37}$$

Further by (A37) and (A25)

$$\begin{aligned} & [C_1 C_2 \dots C_q]_{II}^{[\lambda]} \\ &= 1/2 \{ [C_1 C_2 \dots C_q]_{II}^{[\lambda]} + [C_1 C_2 \dots C_{q'}]_{II}^{[\lambda]} \} \\ &= 1/2 \sum_t [C_1 C_2 \dots C_{q-1}]_{It}^{[\lambda]} \{ [C_q]_{II}^{[\lambda]} + [C_{q'}]_{II}^{[\lambda]} \} \\ &= 1/2 \sum_t [C_1 C_2 \dots C_{q-1}]_{It}^{[\lambda]} (-\delta_{II}) \\ &= -1/2 [C_1 C_2 \dots C_{q-1}]_{II}^{[\lambda]} \end{aligned} \tag{A38}$$

Similarly, we have the existence of an A_{q-1} such that

$$C_1 C_2 \dots C_{q-1} A_{q-1} = A_{q-1} C_1 C_2 \dots C_{(q-1)} \tag{A39}$$

Thus by the above procedure we have

$$[C_1 C_2 \dots C_q]_{II}^{[\lambda]} = (-1/2)^2 [C_1 C_2 \dots C_{q-2}]_{II}^{[\lambda]} \tag{A40}$$

Doing this q times, by (A35), (A34) becomes

$$[\sigma_{x^*x}]_{II}^{[\lambda]} = (-1/2)^q \tag{A41}$$

Appendix B

Evaluation of $[Z_{xx}]_{II}^{[\lambda]}$

By (4.5) and (4.2)

$$\begin{aligned} Z_{xx} &= E_x^\dagger E_x / C \\ &= \frac{P_x N_x N_x P_x}{2^p p! (N-p)!} = \frac{P_x N_x P_x}{2^p} \end{aligned} \tag{B1}$$

By (5.7)

$$Z_{xx} = [Z_{xx}]_{II}^{[\lambda]} e_{II}^{[\lambda]} \tag{B2}$$

so

$$P_x N_x P_x = 2^p [Z_{xx}]_{II}^{[\lambda]} e_{II}^{[\lambda]} \tag{B3}$$

Now by p 65 of ref 5

$$\begin{aligned} (P_x N_x P_x)^2 &= 2^p (P_x N_x)^2 P_x \\ &= \frac{2^p N!}{f^{[\lambda]}} P_x N_x P_x \end{aligned} \tag{B4}$$

Then by (B3) and (B4)

$$\begin{aligned} (P_x N_x P_x)^2 &= \frac{2^{2p} N!}{f^{[\lambda]}} [Z_{xx}]_{II}^{[\lambda]} e_{II}^{[\lambda]} \\ &= (2^p [Z_{xx}]_{II}^{[\lambda]})^2 e_{II}^{[\lambda]} \end{aligned} \tag{B5}$$

or

$$[Z_{xx}]_{II}^{[\lambda]} = \frac{N!}{f^{[\lambda]}} \tag{B6}$$

Spin-Free Quantum Chemistry. IV. The p^n Electron Configuration¹

by F. A. Matsen

Molecular Physics Group, The University of Texas, Austin, Texas 78712 (Received December 2, 1965)

For the p^n electron configuration, spin-free kets are constructed which are symmetry adapted with respect to the symmetric group, S_n ; the unitary group in three dimensions, $U(3)$; the rotation group in three dimensions, $R(3)$; and the rotation group in two dimensions, $R(2)$. Fractional parentage coefficients given by Jahn and van Wieringen are employed in the construction. Each nonexcluded ket is characterized by a partition $[\lambda] = [2^p, 1^{n-2p}]$ which indexes irreducible representations of S_n and $U(3)$ and by the numbers L and M , which index the irreducible representations of $R(3)$ and $R(2)$. The coulomb matrix elements are obtained as a function of n , p , and L by expressing the coulomb interaction in terms of the Casimir operators of $SU(3)$ and $R(3)$, $V \approx \{n(n-1)/2\}F^0 - (12/50)\{3G(SU(3)) - (1/2)G(R(3)) - 5n/6\}F^2$. This is equivalent to the dipole interaction operator of Van Vleck, $V \approx \{n(n-1)/2\}F^0 - (2/50)\{5n(n-1)/2 + 3\sum_{i<j} \vec{l}_i \cdot \vec{l}_j - 12\sum_{i<j} \vec{s}_i \cdot \vec{s}_j\}F^2$. It is of pedagogical interest that the treatment of the problem presented here employs explicitly neither the concept of spin angular momentum nor the concept of orbital angular momentum. Model interactions inside the p shell are also discussed.

Introduction

We consider systems for which a spin-free Hamiltonian is applicable. An n -particle spin-free Hamiltonian commutes with the group of permutations, S_n , on the spin-free particle indices. That is

$$[H, P] = 0, P \in S_n \quad (1)$$

Products of orbitals (one-particle kets) are often employed in the construction of a vector space for a many-particle system. We use spin-free orbitals for the construction and designate an orbital product by

$$|k(n)\rangle \equiv |k_1\rangle |k_2\rangle \cdots |k_n\rangle \quad (2)$$

We restrict ourselves to q distinct orbitals so that the dimension of the orbital product vector space is q^n . We transform this basis of the space to a basis that is symmetry adapted with respect to S_n . We employ for this the theory of the unitary group.^{2,3}

A unitary transformation on the set of q orbitals expressed in operator form is

$$U|k\rangle = \sum_{k'} [U]_{k'k} |k'\rangle \quad (3)$$

The set of all $q \times q$ unitary matrices whose elements

are $[U]_{k'k}$ constitute the unitary group $U(q)$. An irreducible representation $\Gamma^{[\lambda]}(U(q))$ is characterized by a partition

$$[\lambda] = [\lambda^1, \lambda^2, \dots, \lambda^q] \quad (4)$$

and has dimension

$$g^{[\lambda]} = \prod_{i<j} (x_i - x_j) / (q-1)!(q-2)! \dots 2 \quad (5)$$

where

$$x_i = \lambda^i - i + q \quad (6)$$

Consider the transformation of an orbital product by the direct product operator

$$U^n \equiv U \otimes U \otimes \dots \otimes U, n \text{ times} \quad (7)$$

This is written

(1) Supported by the Robert A. Welch Foundation, Houston, Texas, and The National Aeronautics and Space Administration. The previous paper in this series is F. A. Matsen, A. A. Cantu, and R. D. Poshusta, *J. Phys. Chem.*, **70**, 1558 (1966).

(2) M. Hamermesh, "Group Theory," Addison-Wesley Publishing Co., Reading, Mass., 1962.

(3) F. D. Murnaghan, "The Unitary and Rotation Groups," Spartan Books, Washington, D. C., 1962.

$$U^n |k(n)\rangle = \sum_{k'(n)}^{q^n} [U^n]_{k'(n)k(n)} |k'(n)\rangle \quad (8)$$

where

$$[U^n]_{k'(n)k(n)} = [U]_{k_1'k_2} [U]_{k_2'k_2} \dots [U]_{k_n'k_n} \quad (9)$$

We designate the matrix whose elements are given in (9) by $[U]^n$. Thus

$$[U]^n = [U] \otimes [U] \otimes \dots \otimes [U], n \text{ times} \quad (10)$$

$[U]^n$ provides a q^n dimensional representation $\Gamma^n(U(q))$, a representation which is normally reducible. The reduction is

$$\Gamma^n(U(q)) = \sum_{[\lambda]} f^{[\lambda]} \Gamma^{[\lambda]}(U(q)) \quad (11)$$

where the frequency is

$$f^{[\lambda]} = n! \prod_{i < j} (x_i - x_j) / \prod_i (x_i!) \quad (12)$$

It follows that

$$q^n = \sum_{[\lambda]} f^{[\lambda]} g^{[\lambda]} \quad (13)$$

See Table I.

Table I: Analysis of $\Gamma^n(U(3))$; $q^n = 81$

| $[\lambda]$ | $g^{[\lambda]}$ | L | $f^{[\lambda]}$ | $f^{[\lambda]}g^{[\lambda]}$ |
|---------------------|-----------------|---------|-----------------|------------------------------|
| [4] | 15 | 0, 2, 4 | 1 | 15 |
| [3,1] | 15 | 1, 2, 3 | 3 | 45 |
| [2 ²] | 6 | 0, 2 | 2 | 12 |
| [2,1 ²] | 3 | 1 | 3 | 9 |
| [1 ⁴] | 0 | 0 | 1 | $\frac{0}{81}$ |

We now transform the product basis $\{|k(x)\rangle\}$ to a basis which is symmetry adapted with respect to $U^n(q)$.

$$|k(n); [\lambda] t \rho\rangle = \sum_{k'(n)}^{q^n} |k'(n)\rangle \langle k'(n) | [\lambda] t \rho\rangle \quad (14)$$

These elements transform under $U^n(q)$ according to

$$U^n |k(n); [\lambda] t \rho\rangle = \sum_{\rho'}^{g^{[\lambda]}} [U]_{\rho' \rho}^{[\lambda]} |k(n); [\lambda] t \rho'\rangle \quad (15)$$

Here $[U]_{\rho' \rho}^{[\lambda]}$ is the $(\rho' \rho)$ th element in the $g^{[\lambda]} \times g^{[\lambda]}$ matrix representing U in $\Gamma^{[\lambda]}(U(q))$. The kets which are symmetry adapted with respect to $U^n(q)$ are also symmetry adapted with respect to S_n . Thus

$$P |k(n); [\lambda] t \rho\rangle = \sum_{t'}^{f^{[\lambda]}} [P]_{t' t}^{[\lambda]} |k(n); [\lambda] t' \rho\rangle \quad (16)$$

Here $[P]_{t' t}^{[\lambda]}$ is the $(t' t)$ th element in the $f^{[\lambda]} \times f^{[\lambda]}$ matrix representing P in $\Gamma^{[\lambda]}(S_n)$. The partition $[\lambda]$ in a ket identifies both the irreducible representation of $U(q)$ and the irreducible representation of S_n .

For a spin-free Hamiltonian

$$\langle k(n); [\lambda'] t' \rho' | H | k(n); [\lambda] t \rho \rangle = \delta([\lambda'] [\lambda]) \delta(t' t) \langle k(n); [\lambda] \rho' | H | k(n); [\lambda] \rho \rangle \quad (17)$$

Thus the $q^n \times q^n$ representation of the spin-free Hamiltonian is broken up into $(f^{[\lambda]} g^{[\lambda]}) \times (f^{[\lambda]} g^{[\lambda]})$ blocks, each characterized by a partition $[\lambda]$. These blocks are in turn broken up into $f^{[\lambda]}$ identical blocks of dimension $g^{[\lambda]} \times g^{[\lambda]}$, each characterized by the index t . In consequence, each eigenket is $f^{[\lambda]}$ -fold degenerate and is characterized by a partition $[\lambda]$. A ket characterized by a partition $[\lambda]$ is said to be in the $[\lambda]$ th permutation state.

Systems with Spherical Symmetry

A system with spherical symmetry is a system such that

$$[H, R] = 0, R \in R(3) \quad (18)$$

where $R(3)$ is the rotation group in three dimensions. For a spherically symmetric system the one-particle kets are of the form

$$|\gamma LM\rangle = |\gamma L\rangle |LM\rangle \equiv f_{\gamma L}(r) Y_{LM}(\theta, \phi) \quad (19)$$

These kets transform under $R(3)$ according to

$$R |\gamma LM\rangle = \sum_{M'=-L}^L [R]_{M' M}^L |\gamma LM'\rangle \quad (20)$$

where $[R]_{M' M}^L$ is the $(M' M)$ th element in the $f^L \times f^L$ dimensional matrix representing R in $\Gamma^L(R(3))$ and where

$$f^L = 2L + 1 \quad (21)$$

The kets in (19) are also symmetry adapted with respect to $R(2) \subset R(3)$. Its irreducible representation $\Gamma^M(R(2))$ are one-dimensional and are indexed by M . One-electron kets with a given γ and L are said to belong to the γL shell. For $L = 0, 1, 2, \dots$, the shells are referred to as s, p, d, \dots , shells. We designate a product of n one-particle spherical orbitals by

$$|\gamma(n) L(n) M(n)\rangle \equiv |\gamma(n) L(n)\rangle |L(n) M(n)\rangle \equiv |\gamma_1 L_1 M_1\rangle |\gamma_2 L_2 M_2\rangle \dots |\gamma_n L_n M_n\rangle \quad (22)$$

Product kets with a fixed $|\gamma(n) L(n)\rangle$ are said to belong to the $\gamma(n) L(n)$ configuration.

Now $R(3)$ is a proper subgroup of $U(q)$ so that

$$\Gamma^{[\lambda]}(U(g)) = \sum_L f^{[\lambda]L} \Gamma^L(R(3)) \quad (23)$$

and

$$g^{[\lambda]} = \sum_L f^{[\lambda]L} f^L = \sum_L (2L + 1) f^{[\lambda]L} \quad (24)$$

A ket which is symmetry adapted with respect to $U^n(g)$ and $R^n(3)$ is written

$$|\gamma(n)L(n); [\lambda]t\sigma LM\rangle = |\gamma(n)L(n)\rangle \sum_{M(n)} |L(n)M(n)\rangle \langle L(n)M(n)| [\lambda]t\sigma LM\rangle \quad (25)$$

Here we have replaced ρ in eq 14 by σLM . The range of σ is $f^{[\lambda]L}$. If $f^{[\lambda]L} = 1$, σ is suppressed.

For a Hamiltonian that commutes with $R^n(3)$ and S_n

$$\langle \gamma(n)L(n); [\lambda]tL'M'\sigma' | H | \gamma(n)L(n); [\lambda]tLM\sigma \rangle = \delta(L'L) \delta(M'M) \times \langle \gamma(n)L(n); [\lambda]L\sigma' | H | \gamma(n)L(n); [\lambda]L\sigma \rangle \quad (26)$$

Each $([\lambda], t)$ block of dimension $g^{[\lambda]} \times g^{[\lambda]}$ is factored into $(f^{[\lambda]L} f^L) \times (f^{[\lambda]L} f^L)$ blocks, each characterized by L . Each L block is factored in f^L identical blocks of dimension $f^{[\lambda]L} \times f^{[\lambda]L}$. In consequence, each of the $f^{[\lambda]L}$ eigenkets of a $([\lambda], t)$ block is f^L -fold degenerate and is characterized by an integer L . Such an eigenket is said to be in the L th $R(3)$ (angular momentum) state and the M th $R(2)$ (z component of angular momentum) state.

The symmetry adapted kets for a configuration p^n can be obtained from the symmetry-adapted kets for p^{n-1} by means of the fractional parentage coefficients given by Jahn and van Wieringen.⁴ Here the index t is taken to be the Yamanouchi symbol

$$t = (t_n, t_{n-1}, \dots, t_i, \dots, t_1) \quad (27)$$

which identifies one of the $f^{[\lambda]}$ standard Young tableaux. Here t_i is the row occupied by the i th integer in the t th standard tableau. The Yamanouchi symbols are ordered as follows: t comes before t' for $t_n > t'_n$, or for $t_{n-1} > t'_{n-1}$ if $t_n = t'_n$, etc. See Table II.

The symbols associated with p^{n-1} are starred. The index t^* is obtained from t by deleting t_n . Thus

$$t^* = (t_{n-1}, \dots, t_i, \dots, t_1) \quad (28)$$

$$|p^n; [\lambda]tLM\rangle = \sum_{L^*} |p^{n-1}p[\lambda^*]t^*L^*; LM\rangle \langle p^{n-1}p[\lambda^*]L^* | p^n[\lambda]L \rangle \quad (29)$$

where

Table II: Young Tableaux and Yamanouchi Symbols for $m = 4$

| | Young tableaux | |
|--|---|--------|
| $[\lambda] = [4]; f^{[4]} = 1$ | $\begin{array}{ c c c c } \hline 1 & 2 & 3 & 4 \\ \hline \end{array}$ | (1111) |
| $[\lambda] = [3,1]; f^{[3,1]} = 3$ | $\begin{array}{ c c c } \hline 1 & 2 & 3 \\ \hline 4 \\ \hline \end{array}$ | (2111) |
| | $\begin{array}{ c c c } \hline 1 & 2 & 4 \\ \hline 3 \\ \hline \end{array}$ | (1211) |
| | $\begin{array}{ c c c } \hline 1 & 3 & 4 \\ \hline 2 \\ \hline \end{array}$ | (1121) |
| $[\lambda] = [2^2]; f^{[2^2]} = 2$ | $\begin{array}{ c c } \hline 1 & 2 \\ \hline 3 & 4 \\ \hline \end{array}$ | (2211) |
| | $\begin{array}{ c c } \hline 1 & 3 \\ \hline 2 & 4 \\ \hline \end{array}$ | (2121) |
| $[\lambda] = [2,1^2]; f^{[2,1^2]} = 3$ | $\begin{array}{ c c } \hline 1 & 2 \\ \hline 3 \\ \hline 4 \\ \hline \end{array}$ | (3211) |
| | $\begin{array}{ c c } \hline 1 & 3 \\ \hline 2 \\ \hline 4 \\ \hline \end{array}$ | (3121) |
| | $\begin{array}{ c c } \hline 1 & 4 \\ \hline 2 \\ \hline 3 \\ \hline \end{array}$ | (1321) |
| $[\lambda] = [1^4]; f^{[1^4]} = 1$ | $\begin{array}{ c } \hline 1 \\ \hline 2 \\ \hline 3 \\ \hline 4 \\ \hline \end{array}$ | (4321) |

$$|p^{n-1}p[\lambda^*]t^*L^*; LM\rangle = \sum_{M^*} |p^{n-1}; [\lambda^*]t^*L^*M^*\rangle |pM - M^*\rangle \times \langle L^*1M^*M - M^* | LM \rangle \quad (30)$$

where $\langle L^*1M^*M - M^* | LM \rangle$ is a Clebsch-Gordon coefficient. Table III contains fractional parentage coefficients for the p^n configurations for those permutation states $[\lambda] = [2^p, 1^{n-2p}]$ that are allowed for electrons. Table IV gives the spin-free symmetry adapted kets for the configuration p^3 .

The integer p is called the permutation quantum number and replaces the spin quantum number S in

(4) H. A. Jahn and H. van Wieringen, *Proc. Roy. Soc. (London)*, **A209**, 502 (1951).

Table III: Fractional Parentage Coefficients $\langle p^{n-1}p[\lambda^*]L^*[p^n[\lambda]L] \rangle$ for the Electron Configuration p^n

| $n = 2$ | | | | | | |
|---------------------|-----|----------|-----|---------------|---------------|-----------|
| $[\lambda]$ | p | t | L | $[1]S$ | $[1]P$ | $[1]D$ |
| [2] | 1 | (11) | S | 1 | 0 | 0 |
| [2] | 1 | (11) | D | 0 | 0 | 1 |
| [1 ²] | 0 | (21) | P | 0 | 1 | 0 |
| $n = 3$ | | | | | | |
| $[\lambda]$ | p | t | L | $[2]S$ | $[2]D$ | $[1^2]P$ |
| [2,1] | 1 | (211) | P | $\sqrt{4/9}$ | $-\sqrt{5/9}$ | 0 |
| [2,1] | 1 | (121) | P | 0 | 0 | 1 |
| [2,1] | 1 | (211) | D | 0 | 1 | 0 |
| [2,1] | 1 | (121) | D | 0 | 0 | 1 |
| [1 ³] | 0 | (321) | S | 0 | 0 | 1 |
| $n = 4$ | | | | | | |
| $[\lambda]$ | p | t | L | $[21]P$ | $[21]D$ | $[1^3]S$ |
| [2 ²] | 2 | (2211) | S | 1 | 0 | 0 |
| [2 ²] | 2 | (2121) | S | 1 | 0 | 0 |
| [2 ²] | 2 | (2211) | D | $-\sqrt{1/4}$ | $\sqrt{3/4}$ | 0 |
| [2 ²] | 2 | (2121) | D | $-\sqrt{1/4}$ | $\sqrt{3/4}$ | 0 |
| [2,1 ²] | 1 | (3211) | P | $\sqrt{3/8}$ | $\sqrt{5/8}$ | 0 |
| [2,1 ²] | 1 | (3121) | P | $\sqrt{3/8}$ | $\sqrt{5/8}$ | 0 |
| [2,1 ²] | 1 | (1321) | P | 0 | 0 | 1 |
| $n = 5$ | | | | | | |
| $[\lambda]$ | p | t | L | $[2^2]S$ | $[21]D$ | $[21^2]P$ |
| [2 ² ,1] | 2 | (32211) | P | $\sqrt{1/6}$ | $\sqrt{5/6}$ | 0 |
| [2 ² ,1] | 2 | (23211) | P | 0 | 0 | 1 |
| $n = 6$ | | | | | | |
| $[\lambda]$ | p | t | L | $[21^2]P$ | | |
| [2 ³] | 3 | (332211) | S | 1 | | |

the conventional formulation. The two quantum numbers are related by

$$p = n/2 - S \tag{31}$$

Coulomb Matrix Elements

The 3^n kets associated with the configuration p^n are degenerate in zero order. This degeneracy is split in first order by the coulombic interaction

$$V = \sum_{i < j} e^2/r_{ij} \tag{32}$$

The coulombic interaction expressed in irreducible tensorial operator form⁶ is

$$V = e^2 \sum_{i < j} \sum_K (r_{<}^K/r_{>}^{K+1}) \vec{C}^K(i) \cdot \vec{C}^K(j) \tag{33}$$

where

$$\vec{C}^K(i) \cdot \vec{C}^K(j) \equiv \sum_{Q=-K}^K (-1)^Q C_Q^K(i) C_Q^K(j) \tag{34}$$

and

$$C_Q^K(i) \equiv \left(\frac{4\pi}{4K+1} \right)^{1/2} Y_{KQ}(\theta_i, \phi_i) \tag{35}$$

The matrix elements over the symmetry adapted kets as given in (25) are

$$\langle p^n; [\lambda'] t' L' M' | V | p^n; [\lambda] t L M \rangle = \delta([\lambda'] | [\lambda]) \delta(t' t) \delta(L' L) \delta(M' M) \sum_K \Phi^K(p^n[\lambda] L) F^K \tag{36}$$

where

$$F^K = e^2 \iint f_{\gamma p}^2(r_i) (r_{<}^K/r_{>}^{K+1}) f_{\gamma p}^2(r_j) d\tau_i d\tau_j \tag{37}$$

and

$$\Phi^K(p^n[\lambda] L) = \sum_{i < j} \sum_{m'(n)} \sum_{m(n)} \times \langle l(n) m'(n) | [\lambda] t L M \rangle \langle l(n) m(n) | [\lambda] t L M \rangle \times \langle l(n) m'(n) | \vec{C}^K(i) \cdot \vec{C}^K(j) | l(n) m(n) \rangle \tag{38}$$

We apply the Wigner-Eckart theorem to obtain

$$\langle p m_i' | C_Q^K(i) | p m_i \rangle = (-1)^{1-m_i'} \begin{pmatrix} 1 & K & 1 \\ m_i' & Q & m_i \end{pmatrix} \times \langle p | \vec{C}^K(i) | p \rangle \tag{39}$$

Here $\begin{pmatrix} 1 & K & 1 \\ m_i' & Q & m_i \end{pmatrix}$ is a 3- J symbol which must satisfy the triangular condition $\Delta(1K1)$. Further, since $\vec{C}^K(i)$ is an axial vector

$$\Phi^K(p^n[\lambda] L) = 0 \text{ for } K \neq 0, 2 \tag{40}$$

For $K = 0$

$$\langle p m_i' | C_0^0(i) | p m_i \rangle = \delta(m_i' m_i) \tag{41}$$

so

$$\Phi^0(p^n[\lambda] L) = \frac{n(n-1)}{2} \tag{42}$$

For $K = 2$, the $\Phi^2(p^n[\lambda] L)$ can be evaluated by expanding the symmetry adapted kets in terms of the fractional parentage coefficients. This is tedious and unnecessary since we can obtain a general expression for $\Phi^2(p^n[\lambda] L)$ by exploiting the group properties of $U(3)$ and its subgroups. Our treatment follows closely that of Bayman⁶ and Judd.⁵

(5) B. R. Judd, "Operator Techniques in Atomic Spectroscopy," McGraw-Hill Book Co., Inc., New York, N. Y., 1963.

(6) B. F. Bayman, "Groups and Their Applications to Spectroscopy," Nordita, Copenhagen, 1960.

Table IV: Spin-Free Kets for p^3 Which Are Symmetry-Adapted to $U(3)$, $R(3)$, and S_n

| | $ 11\rangle 11\rangle 10\rangle$ | $ 11\rangle 10\rangle 11\rangle$ | $ 10\rangle 11\rangle 11\rangle$ | $ 11\rangle 11\rangle 1\bar{1}\rangle$ | $ 11\rangle 10\rangle 10\rangle$ | $ 10\rangle 11\rangle 10\rangle$ | $ 11\rangle 1\bar{1}\rangle 11\rangle$ | $ 1\bar{1}\rangle 11\rangle 11\rangle$ | $ 10\rangle 10\rangle 11\rangle$ | $ 11\rangle 10\rangle 1\bar{1}\rangle$ | $ 10\rangle 11\rangle 1\bar{1}\rangle$ |
|------------------------------------|----------------------------------|----------------------------------|----------------------------------|--|----------------------------------|----------------------------------|--|--|----------------------------------|--|--|
| $ p^3; [21](2,1,1)D2\rangle$ | $\sqrt{2/3}$ | $-1/\sqrt{6}$ | $-1/\sqrt{6}$ | | | | | | | | |
| $ p^3; [21](1,2,1)D2\rangle$ | 0 | $1/\sqrt{2}$ | $-1/\sqrt{2}$ | | | | | | | | |
| $ p^3; [21](2,1,1)D1\rangle$ | | | | $1/\sqrt{3}$ | $1/\sqrt{12}$ | $1/\sqrt{12}$ | $-1/\sqrt{12}$ | $-1/\sqrt{12}$ | $-1/\sqrt{3}$ | | |
| $ p^3; [21](1,2,1)D1\rangle$ | | | | 0 | $1/2$ | $-1/2$ | $1/2$ | $-1/2$ | 0 | | |
| $ p^3; [21](2,1,1)P1\rangle$ | | | | $-1/\sqrt{3}$ | $1/\sqrt{12}$ | $1/\sqrt{12}$ | $1/\sqrt{12}$ | $1/\sqrt{12}$ | $-1/\sqrt{3}$ | | |
| $ p^3; [21](1,2,1)P1\rangle$ | | | | 0 | $1/2$ | $-1/2$ | $-1/2$ | $1/2$ | 0 | | |
| $ p^3; [21](2,1,1)D0\rangle$ | | | | | | | | | | $1/2$ | $1/2$ |
| $ p^3; [21](1,2,1)D0\rangle$ | | | | | | | | | | $1/\sqrt{12}$ | $-1/\sqrt{12}$ |
| $ p^3; [21](2,1,1)P0\rangle$ | | | | | | | | | | $-1/\sqrt{12}$ | $-1/\sqrt{12}$ |
| $ p^3; [21](1,2,1)P0\rangle$ | | | | | | | | | | $1/2$ | $-1/2$ |
| $ p^3; [1^3](3,2,1)S0\rangle$ | | | | | | | | | | $1/\sqrt{6}$ | $-1/\sqrt{6}$ |
| $ p^3; [21](2,1,1)D\bar{1}\rangle$ | | | | | | | | | | | |
| $ p^3; [21](1,2,1)D\bar{1}\rangle$ | | | | | | | | | | | |
| $ p^3; [21](2,1,1)P\bar{1}\rangle$ | | | | | | | | | | | |
| $ p^3; [21](1,2,1)P\bar{1}\rangle$ | | | | | | | | | | | |
| $ p^3; [21](2,1,1)D\bar{2}\rangle$ | | | | | | | | | | | |
| $ p^3; [21](1,2,1)D\bar{2}\rangle$ | | | | | | | | | | | |

An effective Hamiltonian for the p^n configuration is

$$V \approx \frac{n(n-1)}{2}F^0 + \chi^2 F^2 \tag{43}$$

where

$$\begin{aligned} \chi^2 &\equiv \sum_{i < j} \vec{C}^2(i) \cdot \vec{C}^2(j) \\ &= \sum_{i < j} \sum_{K > 0} \vec{C}^K(i) \cdot \vec{C}^K(j) - \sum_{i < j} \sum_{\substack{K > 0 \\ \text{odd}}} \vec{C}^K(i) \cdot \vec{C}^K(j) \end{aligned} \tag{44}$$

We replace the axial vector $\vec{C}^K(i)$ by a polar vector $\vec{v}^K(i)$ which differs from $\vec{C}^K(i)$ by the fact that its reduced matrix elements admit odd K and by a numerical factor

$$A^K = (3\sqrt{2K+1}) \begin{pmatrix} 1 & K & 1 \\ 0 & 0 & 0 \end{pmatrix} \tag{45}$$

In particular

$$(A^2)^2 = 12/50 \tag{46}$$

Then

$$\begin{aligned} \chi^2 &\approx (12/50) \left\{ \sum_{i < j} \sum_{K > 0} \vec{v}^K(i) \cdot \vec{v}^K(j) - \sum_{i < j} \sum_{\substack{K > 0 \\ \text{odd}}} \vec{v}^K(i) \cdot \vec{v}^K(j) \right\} \end{aligned} \tag{47}$$

The $\vec{v}^K(i)$ are the generators for $U(3)$ and its subgroups, the unimodular unitary group $SU(3)$ and the rotation group $R(3)$. The Casimir operator for $SU(3)$ is written as

$$G(SU(3)) = (1/3) \left\{ \sum_{i < j} \sum_{K > 0} \vec{v}^K(i) \cdot \vec{v}^K(j) + (1/2) \sum_i \sum_{K > 0} (\vec{v}^K(i))^2 \right\} \tag{48}$$

The Casimir operator for $R(3)$ is

$$G(R(3)) = 2 \left\{ \sum_{i < j} \sum_{\substack{K > 0 \\ \text{odd}}} \vec{v}^K(i) \cdot \vec{v}^K(j) + (1/2) \sum_i \sum_{\substack{K > 0 \\ \text{odd}}} (\vec{v}^K(i))^2 \right\} \tag{49}$$

Hence

$$\begin{aligned} \chi^2 &= (12/50) \left\{ 3G(SU(3)) - (1/2)G(R(3)) - (1/2) \sum_i \sum_{\substack{K > 0 \\ \text{even}}} (\vec{v}^K(i))^2 \right\} \end{aligned} \tag{50}$$

The third term depends only on n , since

$$\langle pm_i | (\vec{v}^K(i))^2 | pm_i \rangle = \delta(m'm)(2K+1)/3 \tag{51}$$

Then

$$\chi^2 = (12/50) \{ 3G(SU(3)) - (1/2)G(R(3)) - 5n/6 \} \tag{52}$$

Since the kets $|p^n; [\lambda]tLM\rangle$ are symmetry adapted to $U(3)$ (hence to $SU(3)$) and to $R(3)$, the respective Casimir operators are diagonal in this representation. In particular

$$\begin{aligned} \langle p^n; [\lambda']t'L'M' | G(SU(3)) | p^n; [\lambda]tLM \rangle &= \\ &\delta([\lambda'][\lambda])\delta(t't)\delta(L'L)\delta(M'M) \times \\ &(1/6)[4n - 4n^2/3 - 2p(p-n-1)] \end{aligned} \tag{53}$$

| | | | | | | | | | | | | | |
|--|----------------------------------|--|--|--|--|--|--|--|--|--|--|--|--|
| $ 11\rangle 1\bar{1}\rangle 10\rangle$ | $ 10\rangle 10\rangle 10\rangle$ | $ 1\bar{1}\rangle 11\rangle 10\rangle$ | $ 1\bar{1}\rangle 10\rangle 11\rangle$ | $ 10\rangle 1\bar{1}\rangle 11\rangle$ | $ 11\rangle 1\bar{1}\rangle 1\bar{1}\rangle$ | $ 10\rangle 10\rangle 1\bar{1}\rangle$ | $ 1\bar{1}\rangle 11\rangle 1\bar{1}\rangle$ | $ 1\bar{1}\rangle 10\rangle 10\rangle$ | $ 10\rangle 1\bar{1}\rangle 10\rangle$ | $ 1\bar{1}\rangle 1\bar{1}\rangle 11\rangle$ | $ 1\bar{1}\rangle 10\rangle 1\bar{1}\rangle$ | $ 10\rangle 1\bar{1}\rangle 1\bar{1}\rangle$ | $ 1\bar{1}\rangle 1\bar{1}\rangle 10\rangle$ |
| 0 | 0 | 0 | $-1/2$ | $-1/2$ | | | | | | | | | |
| $1/\sqrt{3}$ | 0 | $-1/\sqrt{3}$ | $-1/\sqrt{12}$ | $1/\sqrt{12}$ | | | | | | | | | |
| $1/\sqrt{3}$ | 0 | $1/\sqrt{3}$ | $-1/\sqrt{12}$ | $-1/\sqrt{12}$ | | | | | | | | | |
| 0 | 0 | 0 | $1/2$ | $-1/2$ | | | | | | | | | |
| $-1/\sqrt{6}$ | 0 | $1/\sqrt{6}$ | $-1/\sqrt{6}$ | $1/\sqrt{6}$ | | | | | | | | | |
| | | | | | $1/\sqrt{12}$ | $1/\sqrt{3}$ | $1/\sqrt{12}$ | $-1/\sqrt{12}$ | $-1/\sqrt{12}$ | $-1/\sqrt{3}$ | | | |
| | | | | | $-1/2$ | 0 | $1/2$ | $-1/2$ | $1/2$ | 0 | | | |
| | | | | | $1/\sqrt{12}$ | $-1/\sqrt{3}$ | $1/\sqrt{12}$ | $1/\sqrt{12}$ | $1/\sqrt{12}$ | $-1/\sqrt{3}$ | | | |
| | | | | | $1/2$ | 0 | $-1/2$ | $1/2$ | $-1/2$ | 0 | | | |
| | | | | | | | | | | | $1/\sqrt{6}$ | $1/\sqrt{6}$ | $-\sqrt{2}/3$ |
| | | | | | | | | | | | $-1/\sqrt{2}$ | $1/\sqrt{2}$ | 0 |

and $r_2 = r_3 = 3/2$ (60)

$$\langle p^n; [\lambda'] t' L' M' | G(R(3)) | p^n; [\lambda] t L M \rangle = \delta([\lambda'] [\lambda]) \delta(t' t) \delta(L' L) \delta(M' M) \times (1/2) L(L+1) \quad (54)$$

These are the Slater-Condon values.

Then

$$\chi^2 = -(1/60) \{ 8n^2 - 14n + 3L(L+1) + 12p(p-n-1) \} \quad (55)$$

Since $F^2 > 0$, the Hund rule follows from (55): states with lowest permutation quantum number (p) lie the lowest and, in a given permutation state, states with the highest R_3 quantum number (L) lie the lowest.

We are interested in the relative splitting in a p^n configuration so we neglect all terms that depend only on n and write the interaction in the p shell as

$$V = 3(\alpha + \beta)G(SU(3)) - 2\beta G(R(3)) \quad (56)$$

Its eigenvalues in the symmetry adapted basis are

$$\langle |V| \rangle = -(\alpha + \beta)p(p-n-1) - \beta L(L+1) \quad (57)$$

The relative term values for the p^n configuration are listed in Table V. We define the ratios

$$r_2 = r_4 \equiv \frac{E(^1S) - E(^1D)}{E(^1D) - E(^3P)} = \frac{3\beta}{\alpha - \beta} \quad (58)$$

and

$$r_3 \equiv \frac{E(^2P) - E(^2D)}{E(^2D) - E(^4S)} = \frac{4\beta}{3(\alpha - \beta)} \quad (59)$$

For the coulombic interaction $\alpha = 3\beta$, so

Table V: Relative Model Interaction Term Values (for the Coulombic Interaction $\alpha = 3\beta$)

| n | $[\lambda]$ | p | L | Term symbol | $\langle V \rangle$ |
|-----|---------------------|-----|-----|-------------|-----------------------|
| 2 | [2] | 1 | 0 | 1S | $2\alpha + 2\beta$ |
| | | 1 | 2 | 1D | $2\alpha - 4\beta$ |
| 3 | [1 ²] | 0 | 1 | 3P | -2β |
| | [2,1] | 1 | 1 | 2P | $3\alpha + \beta$ |
| | | 1 | 2 | 2D | $3\alpha - 3\beta$ |
| 4 | [1 ³] | 0 | 0 | 1S | 0 |
| | [2 ²] | 2 | 2 | 1D | 6α |
| | | 2 | 0 | 1S | $6\alpha + 6\beta$ |
| 5 | [2,1 ²] | 1 | 1 | 3P | $4\alpha + 2\beta$ |
| | | 2 | 1 | 3P | $8\alpha + 6\beta$ |
| 6 | [2 ³] | 3 | 0 | 1S | $12\alpha + 12\beta$ |

Model Interactions

The choice of basis kets restricted to a single configuration ignores the effect of configuration interaction. In consequence, the relative splitting calculated for a single configuration need not agree with experiment. For example, in the first row of the periodic table the experimental r_i are $r_2 = r_3 = 1.14$ compared to $3/2$ and $r_4 = 0.5$ compared to $2/3$.

One can introduce empiricism into the theory and postulate a model interaction of the form of (56) but one in which the ratio of α to β is determined by experiment. Thus if we set α equal to 3.67β , agreement with experiment is obtained.

The concept of a model interaction has been widely used in nuclear theory where the explicit nature of the interaction is not known. The concept of the model interaction was introduced into atomic spectroscopy by Bacher and Goudsmit.⁷ A recent review of the use of model interaction in atomic spectra has been given by Racah.⁸

Equivalent Forms of the Interaction in the p Shell

The coulombic interaction, V , inside a p^n configuration can be expressed in a number of distinct but equivalent forms, which were first formulated by Van Vleck.⁹ On substitution of (31), eq 55 becomes

$$\chi^2 = -(1/60)\{5n^2 - 20n + 3L(L + 1) + 12S(S + 1)\} \quad (61)$$

By angular momentum theory

$$L(L + 1) \approx L^2 \quad (62)$$

and

$$S(S + 1) \approx S^2 \quad (63)$$

With (62) and (63), (61) becomes

$$\chi^2 = -(1/60)\{5n^2 - 20n + 3L^2 + 12S^2\} \quad (64)$$

Again by angular momentum theory and on restriction to the p shell

$$L^2 = \sum_i l_i^2 + 2\sum_{i<j} \vec{l}_i \cdot \vec{l}_j \approx 2n + 2\sum_{i<j} \vec{l}_i \cdot \vec{l}_j \quad (65)$$

and

$$S^2 = \sum_i s_i^2 + 2\sum_{i<j} \vec{s}_i \cdot \vec{s}_j \approx 3n/4 + 2\sum_{i<j} \vec{s}_i \cdot \vec{s}_j \quad (66)$$

On substituting (65) and (66) into (64) we obtain

$$\chi^2 = -(2/60)\{5n(n - 1)/2 + 3\sum_{i<j} \vec{l}_i \cdot \vec{l}_j + 12\sum_{i<j} \vec{s}_i \cdot \vec{s}_j\} \quad (67)$$

The form given in eq 67 is called the dipole-dipole interaction. This form (and the others given above) are a consequence of the restricted single configuration space upon which the coulomb operator is forced to operate. It is not to be regarded as a true interaction.

It is of pedagogical interest that the p^n problem can be formulated without reference to spin angular momentum or to orbital angular momentum. The spin angular momentum states of conventional theory are replaced by symmetry states associated with the symmetric (permutation) group and the orbital angular momentum states are replaced by the symmetry states of the rotation group.

(7) R. F. Bacher and S. Goudsmit, *Phys. Rev.*, **46**, 948 (1934).

(8) C. Racah, *J. Quant. Spectry. Radiative Transfer*, **4**, 617 (1964). (See also J. S. Griffith, "The Theory of Transition Metal Ions," Cambridge University Press, Cambridge, England 1961.)

(9) J. H. Van Vleck, *Phys. Rev.*, **45**, 416 (1934).

Intramolecular Kinetic Carbon Isotope Effect in the Gas Phase

Decomposition of Deuteriooxalic Acid

by Gabriel Lapidus,^{1a} Donald Barton,^{1b} and Peter E. Yankwich

Noyes Laboratory of Chemistry, University of Illinois, Urbana, Illinois 61801 (Received November 18, 1965)

The intramolecular C¹³ kinetic isotope effect has been measured between 127 and 180° in the decomposition to carbon dioxide and formic acid of oxalic acid-*d*₂ vapor at an initial pressure of 0.8 mm. This isotope effect is small, 0.5% maximum, but has a temperature dependence so large that it inverts within the experimental range. It is shown that ordinary isotope effect theory and assumptions of low pressure effects, such as described by Rabinovitch and his co-workers, are inadequate to explain the results or would not come into play, respectively. It is postulated that multiple reaction paths are responsible for the phenomena observed.

Introduction

Recently, we reported results on the kinetics of the decompositions of oxalic acid^{2a} and of oxalic acid-*d*₂^{2b} in the gas phase at pressures near 1 mm. Comparison of the two sets of rate constants for the temperature range 127–156° revealed a small deuterium isotope effect normal in direction, $k_H > k_D$, at low temperatures, which disappears near 145°, and is *inverted*, $k_D > k_H$, at higher temperatures.

In an attempt to explain this unusual phenomenon, we showed that: the size of the temperature dependence of k_H/k_D could be accounted for by combination of kinetic, equilibrium (*e.g.*, between cyclic and noncyclic structures arising through intramolecular intercarboxyl hydrogen bonding), and tunneling isotope effects; the observed magnitude of $(k_H/k_D - 1)$ is reasonable if there were impressed on the above combination a virtually temperature-independent inverse isotope effect such as that described and observed by Rabinovitch and his co-workers.³⁻⁷

Since the Rabinovitch effect should appear only in the low-pressure region of a gaseous unimolecular decomposition, and since we have no information on the rate of the oxalic acid pyrolysis as a function of pressure, it seemed possible that study of the temperature dependence of C¹³ kinetic isotope effects might reveal additional information about the reaction mechanism. Under the experimental conditions accessible to us,^{2a} only the *intramolecular* carbon isotope effect

(that arising in the bifunctionality of the reagent and determined from measurements on the isotopic constitution of the products) could be studied conveniently.

We expected the intramolecular carbon kinetic isotope effect to be small (of the order of 1%) because there is but one C-C bond in the oxalic acid molecule, and it must always be broken during the pyrolysis to carbon dioxide and formic acid; this isotope effect depends only upon the structural and related energetic differences between isotopically isomeric forms of activated molecules.

Consider now a possible statistical inverse intramolecular carbon isotope effect in this decomposition. A number of factors operate to ensure its smallness: first, the reduced mass effect is only about 5% of that for hydrogen isotopy in the same molecule; second, the

(1) (a) Research associate, 1960–1963. (b) Visiting assistant professor, 1960–1962, Department of Chemistry, Memorial University of Newfoundland, St. John's, Newfoundland.

(2) (a) G. Lapidus, D. Barton, and P. E. Yankwich, *J. Phys. Chem.*, **68**, 1863 (1964); (b) G. Lapidus, *et al.*, *ibid.*, **69**, 407 (1966).

(3) B. S. Rabinovitch, D. W. Setser, and F. W. Schneider, *Can. J. Chem.*, **39**, 2609 (1961).

(4) B. S. Rabinovitch and J. H. Current, *ibid.*, **40**, 557 (1962).

(5) F. W. Schneider and B. S. Rabinovitch, *J. Am. Chem. Soc.*, **84**, 4215 (1962).

(6) J. H. Current and B. S. Rabinovitch, *J. Chem. Phys.*, **38**, 1967 (1963).

(7) F. W. Schneider and B. S. Rabinovitch, *J. Am. Chem. Soc.*, **85**, 2365 (1963).

differences between the quantum statistical densities of energy states which contribute to the isotopically *isomeric* decomposition modes (characteristic of the *intramolecular* isotope effect) are much smaller than the corresponding differences which contribute to the isotopic decomposition modes characteristic of the *intermolecular* isotope effect; third, a consideration similar to the second operates through the isotopic and isotopically isomeric critical energies, $(E_0)_i$.

We expected, therefore, that in the decomposition of oxalic acid- d_2 the above factors and the additional suppression of nonclassical effects because of the substitution of D for H should serve to eliminate or to reduce to marginal observability a statistical inverse intramolecular carbon isotope effect; these considerations operate whether the actual decomposition is homogeneous or heterogeneous (the latter possibility having been mentioned but not explored in the earlier work on the rate of the reaction²). Were such an expectation sound, and in the absence of an as yet unsuspected mechanism for inversion of primary kinetic isotope effects, any isotope fractionation observed could be attributed to an ordinary kinetic origin; though small, such an isotope effect should be a monotonic function of temperature and should not invert.

Experimental Section

Reagent. Fisher Analytical grade oxalic acid was purified by vacuum sublimation at 110°, and labeled to at least 99.3 atom % D in both carboxyl groups by repeated evaporation to dryness from solution in 99.5% deuterium oxide. The material was dried *in vacuo* and stored over magnesium perchlorate until used.

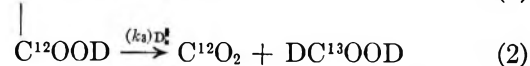
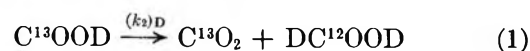
Apparatus and Procedure. The apparatus and procedures were identical with those employed in the kinetics studies^{2a} with two exceptions: (1) because the intramolecular isotope effect is determined from measurements on the final products, run times were extended so that the decomposition was 99.9% or more; (2) all samples of carbon dioxide were equilibrated with standard water to reduce to *nil* the variation in the correction applied for the presence of O¹⁷.

Because the reaction was taken essentially to completion, higher temperatures could be employed than in the kinetics studies, and experiments were carried out between 127 and 180°. At 180°, k_D is about $4.6 \times 10^{-3} \text{ sec}^{-1}$, but thermal equilibration is so rapid under the conditions employed that there is inappreciable reaction during warm-up even at this temperature. There is, however, a total of $1.3 \pm 0.4\%$ reaction during the sublimation and injection steps, which occur, effectively, at a temperature of 130°. Correction for

this effect proved too small to have significant influence on the results reported below.

Isotope Analyses. The procedures employed have been detailed in earlier publications from this laboratory.⁸⁻¹⁰ Because preliminary experiments showed the carbon isotope effects to be very small, extra precision was achieved by replacing the dc amplifiers of the original mass spectrometer with a slaved pair of vibrating-reed electrometers (Applied Physics Corp., Pasadena, Calif.).

Notation and Calculations. The isotopic rate constant ratio sought was $(k_2/k_3)_D$ in the notation of Lindsay, McElcheran, and Thode¹¹



Let $(X_C)_t$ be the mole fraction of C^{13}O_2 in carbon dioxide product collected up to any time t , and $(X_F)_t$ be the corresponding mole fraction of DC^{13}OOD derived from measurements on carbon dioxide obtained by combustion (in a Pregl-like apparatus) of the formic acid product. Then

$$\frac{(X_C)_t}{(X_F)_t} = (k_2/k_3)_D \quad (3)$$

that is, this ratio of isotopic rate constants results from the indicated quotient of mole fractions for any time t , whether it corresponds to partial or complete decomposition.

Results

The results obtained at seven temperatures are collected in Table I and plotted as the open points in Figure 1. Bands representing the results obtained for the intermolecular hydrogen isotope effect are shown for comparison. The line through the intramolecular carbon isotope effect results is a least-squares fit to all of the data except those for 180°; its equation is

$$L(k_2/k_3)_D = (3.20 \pm 0.14)\theta - (7.61 \pm 0.34) \quad (4)$$

where $L(x) = 100 \ln x$, and $\theta = 10^3/T(^{\circ}\text{K})$; the average scatter of the experimental results from the least-squares line is ± 0.06 in $\ln x$, equivalent to ± 0.0006 in $(k_2/k_3)_D$. Like the deuterium isotope effect observed earlier,² this carbon isotope effect is relatively small, apparently normal in sense¹¹ at low

(8) P. E. Yankwich and R. L. Belford, *J. Am. Chem. Soc.*, **75**, 4178 (1953).

(9) P. E. Yankwich and R. L. Belford, *ibid.*, **76**, 3067 (1954).

(10) P. E. Yankwich and J. L. Copeland, *ibid.*, **79**, 2081 (1957).

(11) J. G. Lindsay, D. E. McElcheran, and H. G. Thode, *J. Chem. Phys.*, **17**, 589 (1949).

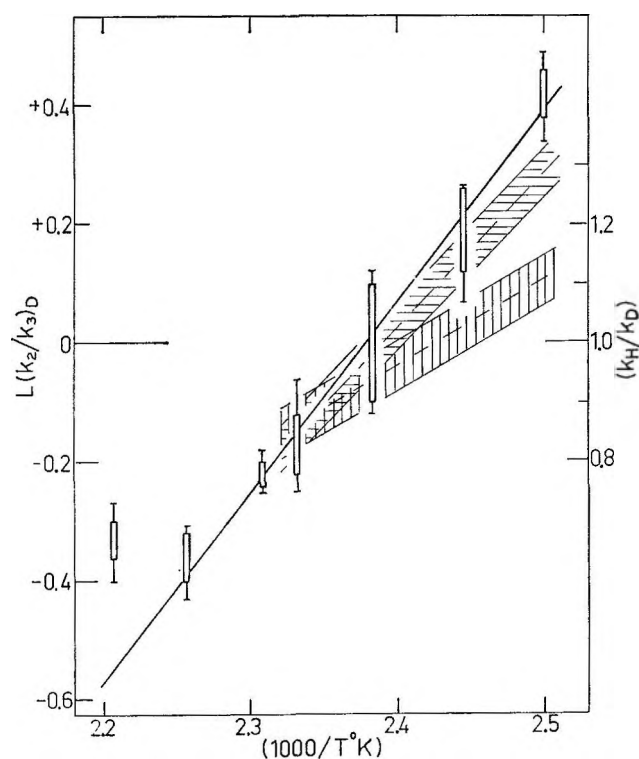


Figure 1. Temperature dependence of the intramolecular carbon isotope effect, $L(k_2/k_3)_D$, in the decomposition of oxalic acid- $d_2(g)$. The vertical rectangles encompass average deviations from the mean; horizontal bars indicate maximum and minimum results observed. Solid line is least-squares fitted to all data except those for 180° . The bands represent smoothed average results for the intermolecular rate constant ratio (k_H/k_D) ; their vertical widths encompass average deviations from the mean results at all temperatures. The upper band (horizontal shading) is least-squares fit to the original data; the lower band (vertical shading) is based on corrected results for $(k_H)_{av}$ at 134.1° . Estimated inversion temperatures are $(k_2/k_3)_D$, $147 \pm 5^\circ$; k_H/k_D , upper band, $145 \pm 13^\circ$, lower band, $139 \pm 9^\circ$.

temperatures, but inverted at higher temperatures. The inversion temperatures are similar for the two isotopic rate constant ratios.

Discussion

Although isotope effect inversion is uncommon, it can be brought about, for reaction along a single chemical path, in a number of ways: by equilibria precedent to the rate-determining step, by equilibrium-related structural changes upon activation, by an appropriate isotope shift pattern in the vibrational modes of the normal and activated molecules,¹² or through a statistical phenomenon such as that described by Rabinovitch and his co-workers.³⁻⁷ In a gaseous reaction, the C^{13} intramolecular isotope effect should not be affected by the first two, and we believe that our use of deuteriooxalic acid has removed or reduced

drastically the possibility of occurrence of the last. The temperature dependence of an ordinary kinetic isotope effect is due to the vibrational isotope shifts and bears an almost uniform relation to the magnitude of the effect.¹³⁻¹⁶ The temperature dependence ob-

Table I: Intramolecular Isotope Effect in $(COOD)_2(g)$ Decomposition

| Run temp, °C | $(k_2/k_3)_D$ | $Av (k_2/k_3)_D$ |
|--------------|---------------|-----------------------|
| 126.6 | 1.00492 | 1.00417 ± 0.00040 |
| | 1.00340 | |
| | 1.00422 | |
| | 1.00427 | |
| | 1.00470 | |
| | 1.00392 | |
| | 1.00379 | |
| 134.1 | 1.00258 | 1.00194 ± 0.00063 |
| | 1.00068 | |
| | 1.00236 | |
| | 1.00212 | |
| 146.4 | 1.00118 | 0.99996 ± 0.00102 |
| | 0.99915 | |
| | 0.99938 | |
| | 0.99880 | |
| | 1.00123 | |
| 155.6 | 0.99941 | 0.99825 ± 0.00051 |
| | 0.99835 | |
| | 0.99783 | |
| | 0.99751 | |
| 160.0 | 0.99749 | 0.99782 ± 0.00020 |
| | 0.99789 | |
| | 0.99765 | |
| | 0.99823 | |
| | 0.99784 | |
| 170.0 | 0.99606 | 0.99641 ± 0.00041 |
| | 0.99659 | |
| | 0.99574 | |
| | 0.99674 | |
| | 0.99692 | |
| 180.0 | 0.99666 | 0.99669 ± 0.00030 |
| | 0.99728 | |
| | 0.99674 | |
| | 0.99601 | |
| | 0.99648 | |

(12) H. C. Urey, *J. Chem. Soc.*, 562 (1947).

(13) J. Bigeleisen and M. Wolfsberg, *Advan. Chem. Phys.*, **1**, 15 (1958).

(14) P. E. Yankwich and H. S. Weber, *J. Am. Chem. Soc.*, **78**, 564 (1956).

(15) P. E. Yankwich and R. M. Ikeda, *ibid.*, **81**, 1532 (1959).

served in these experiments is enormous even when compared with the largest fractionation observed, that at the lowest temperature. Neither ordinary isotope effect theory nor assumption of an effect related to the possibility that 1 mm is well into the *low-pressure* region for the decomposition can explain this extreme relative temperature dependence. Since chemical reactions on surfaces and in the gas phase have the fundamental similarity that both require the modification of extant molecular force fields upon activation, one does not expect new *kinds* of isotope fractionation effects to arise where the reaction proceeds along a single chemical path involving a surface; therefore, the above conclusions concerning isotope effect inversion are valid equally for homogeneous and heterogeneous reactions.

We believe that this unusual isotope effect is due to accessibility to the reaction of at least two decomposition paths; that is, at least two pairs of isotopically isomeric activated molecules yield products in this decarboxylation. If this notion is correct, the deviant result at 180° may actually be due to the final predominance of one path over the other(s) as the temperature is increased; the different decomposition paths may involve activated molecules similar or drastically different in structure. In our first paper on this reaction,^{2a} it was pointed out that there might be a heterogeneous component to the observed reaction rate; a combination of heterogeneous and homogeneous

mechanisms provide one kind of decomposition-path duality which could explain the inverting intramolecular isotope effect. In the same place, we indicated (for an assumed unimolecular mechanism) our preference for a reaction coordinate in which there was intramolecular hydrogen atom transfer from one carboxyl group to the carbonyl oxygen of the other; another kind of decomposition-path duality would be provided were reaction to occur simultaneously *via* a reaction coordinate we did not favor at that time, *viz.*, direct intramolecular hydrogen transfer to carbon.

Though the quality of these data is high, the temperature range of the experiments covers only one region of the isotope effect spectrum anticipated for the reaction model mentioned above, and no detailed treatment is possible. Similarly, the linear form assumed for representation of the temperature dependence as in eq 4, though customary and adequate for our limited purposes here, may be incorrect; a graph with very slight upward curvature would improve the fit at 127 and 170°, but would not affect the deviant character of the observations at 180°.

Acknowledgments. Mrs. Nancy Neilson performed the mass spectrometric analyses. We are indebted to our colleague Dr. L. B. Sims for helpful suggestions and discussion. This research was supported by the U. S. Atomic Energy Commission.

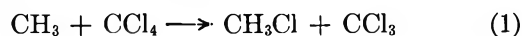
Abstraction of Halogen Atoms by Methyl Radicals

by D. M. Tomkinson and H. O. Pritchard¹

Chemistry Department, University of Manchester, Manchester 13, England (Received November 19, 1965)

Previous work on the abstraction of chlorine atoms by methyl radicals has been extended to include the abstraction of bromine and iodine atoms, mainly from halogenated methanes. The results obtained for CF₃Br and CF₃I suggest that in general, $D(\text{CF}_3\text{-X})$ is about 4 kcal/mole greater than $D(\text{CH}_3\text{-X})$. Several new recombinations of methyl with halogenated methyl radicals in which elimination of HX occurs have been observed.

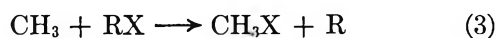
It was previously shown by Tomkinson, Galvin, and Pritchard² that reactions of the type



could be conveniently studied using di-*t*-butyl peroxide as a thermal source of methyl radicals. The measured rate constants were related to that of the recombination reaction



In the present work, rate constants for reactions of the type



were measured relative to the rate constants for reaction 1 by decomposing peroxide in the presence of mixtures of RX and CCl₄ and analyzing for the relative rates of formation of CH₃X and CH₃Cl, and so on.

Experimental Section

The experimental procedure was identical with that used previously² with the exception that analyses were performed using a vapor phase chromatograph instead of a mass spectrometer. Column packings, temperatures, and flow conditions were chosen to suit each particular determination (see ref 3 for full details).

Results

Since almost all the rate constants determined in this work are related to the previously measured rate constants for reaction 1, we felt it advisable to check the Arrhenius parameters for this reaction using chromatographic instead of mass spectrometric analysis. A least-squares Arrhenius plot on the results of 15 experiments carried out between 90 and 145° gave

$E_1 - \frac{1}{2}E_2 = 12.4 \pm 0.8$ kcal/mole and $\log (A_1/A_2^{1/2})$ ($\text{ml}^{1/2} \text{mole}^{-1/2} \text{sec}^{-1/2}$) = 6.5. The activation energy obtained is not significantly different from that obtained previously, *viz*, 13.4 ± 0.8 kcal/mole (the error limits quoted in Table I of ref 2 were incorrect and should all have been about ± 0.8 kcal/mole). There is, however, a discrepancy of about a factor of 2.5 in the observed values of $k_1/k_2^{1/2}$ at any temperature; this may have arisen in the mass spectrometer calibration, since all the vpc calibrations were repeated and carefully rechecked, but unfortunately we could not confirm this because the mass spectrometer used was no longer operational. (The previous rate constants for C₂Cl₆ and CCl₃COCCl₃ were also too low by the same factor.) The mass spectrometer results were scaled by adding 0.415 to the $\log (k_1/k_2^{1/2})$ values, giving a homogeneous set of 28 points corresponding to $E_1 - \frac{1}{2}E_2 = 12.9 \pm 0.7$ kcal/mole and $\log (A_1/A_2^{1/2})$ ($\text{ml}^{1/2} \text{mole}^{-1/2} \text{sec}^{-1/2}$) = 6.7. In the new experiments, variations of about a factor of 5 in both the peroxide and the carbon tetrachloride concentrations were made without any effect on the observed rate constants. We also note in passing that ethylene is a by-product (*ca.* 0.5–1% yield) of the thermal decomposition of di-*t*-butyl peroxide, and in experiments where both the temperature and the halide concentration were high, the amount of ethylene formed was comparable to the ethane.

(1) To whom correspondence should be addressed: Centre for Research in Experimental Space Science, York University, Toronto 12, Ontario, Canada.

(2) D. M. Tomkinson, J. P. Galvin, and H. O. Pritchard, *J. Phys. Chem.*, **68**, 541 (1964).

(3) Full details of all mixtures studied and analysis systems used are given by D. M. Tomkinson, Ph.D. Thesis, University of Manchester, 1965.

Initially, a survey of reactivities relative to CCl_4 at 130° was carried out by comparing various bromides with CCl_4 . Then the reactivities of iodides and other chlorides were established by comparing these molecules with bromides.³ A summary of the relative reactivities is shown in Table I, and it is clear that the trends are similar to those found in the liquid phase.⁴ The third column of this table shows the reactivities of several hydrogen-containing iodides, but similar figures could not be obtained for chlorides and bromides because hydrogen abstraction was usually the dominant process.

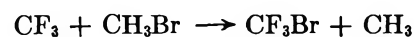
Table I: Relative Rates^a for the Reaction, $\text{CH}_3 + \text{RX} \rightarrow \text{CH}_2\text{X} + \text{R}$, at 130° in the Gas Phase

| Chlorides | | Bromides | | Iodides | |
|-------------------------------------|------|-----------------------------|------|---|------|
| CFCl_3 | ~0.1 | CF_3Br | 2 | $\text{C}_6\text{H}_5\text{I}$ | 1.5 |
| $\text{CFCl}_2\text{CF}_2\text{Cl}$ | ~0.1 | CF_2Br_2 | 13 | <i>n</i> - $\text{C}_3\text{H}_7\text{I}$ | 140 |
| C_2Cl_4 | ~0.1 | CF_2ClBr^b | 17 | <i>sec</i> - $\text{C}_3\text{H}_7\text{I}$ | 270 |
| $\text{C}_6\text{H}_5\text{CCl}_2$ | 0.5 | CCl_3Br^b | 1000 | CF_3I | 2150 |
| C_2Cl_6 | 0.7 | $\text{CCl}_2\text{Br}_2^b$ | 2300 | CH_2I_2 | 2800 |
| CCl_4 | 1 | CBr_4 | 4300 | | |
| $\text{CCl}_3\text{COCCl}_3$ | 5 | | | | |
| CCl_3CN^c | 7 | | | | |

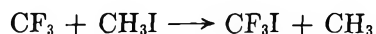
^a Per molecule, *not* per halogen atom. ^b Reaction of CH_3 radicals with these molecules individually does not produce detectable quantities of CH_3Cl . ^c Reaction of CH_3 radicals with CCl_3CN alone does not produce detectable quantities of CH_3CN .

Temperature coefficients were studied for a number of competing pairs of halides, and Arrhenius parameters, determined relative to that for CCl_4 , are listed in Table II. Also shown in Table II is our reassessment of the previous results on hexachloroethane and hexachloroacetone, and a new determination for benzotrifluoride. The most striking feature about the chlorides is the very close similarity between the activation energies for chlorine abstraction and the activation energies for hydrogen abstraction from the corresponding hydrocarbon. The pattern presented by the bromides is also reasonable, except perhaps the low figures for CF_2Br_2 (where complications could possibly arise owing to the stability of the CF_2 radical). The reactivity of CF_3I is reasonable in comparison with CF_3Br .

Dissociation Energies. Recently, Alcock and Whittle⁵ have measured the activation energies of the two reactions

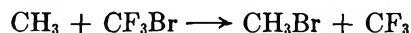


$$E = 8.3 \pm 0.3 \text{ kcal/mole}$$

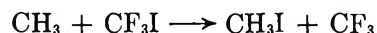


$$E = 3.3 \pm 0.2 \text{ kcal/mole}$$

and our measurements show that the activation energies for the reverse reactions are



$$E \simeq 12.5 \pm 1.0 \text{ kcal/mole}$$



$$E \simeq 7.5 \pm 1.0 \text{ kcal/mole}$$

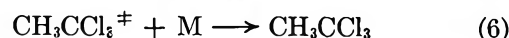
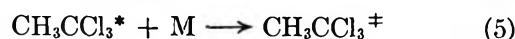
We conclude therefore that

$$[D(\text{CF}_3\text{-Br}) - D(\text{CH}_3\text{-Br})] \simeq$$

$$[D(\text{CF}_3\text{-I}) - D(\text{CH}_3\text{-I})] \simeq 4 \text{ kcal/mole}$$

This result is consistent with the higher value for $D(\text{CF}_3\text{-H})$ derived from chlorination and bromination studies on fluoroform⁶ and supported by preliminary results from these laboratories on the iodination of fluoroform.⁷ On the other hand, there is published evidence that $D(\text{CF}_3\text{-X}) \simeq D(\text{CH}_3\text{-X})$ for $\text{X} = \text{iodine}$,⁸ $\text{X} = \text{bromine}$,⁹ and $\text{X} = \text{hydrogen}$,^{10,11} some of which is not too easy to refute.

Elimination Following Radical Combination. Two products which are formed as a result of the thermal decomposition of di-*t*-butyl peroxide in the presence of carbon tetrachloride are large amounts of isobutylene oxide and some 1,1-dichloroethylene; at the same time, there was always more CH_4 than would have been formed by the decomposition of peroxide alone. The formation of these two molecules and the extra methane is consistent with the following set of reactions.



(4) F. W. Evans, R. J. Fox, and M. Szwarc, *J. Am. Chem. Soc.*, **82**, 6414 (1960).

(5) W. G. Alcock and E. Whittle, *Trans. Faraday Soc.*, **61**, 244 (1965).

(6) P. Corbett, A. M. Tarr, and E. Whittle, *ibid.*, **59**, 1609 (1963), and personal communication.

(7) C. A. Goy and H. O. Pritchard, unpublished data.

(8) R. K. Boyd, G. W. Downs, J. S. Gow, and C. Horrex, *J. Phys. Chem.*, **67**, 719 (1963).

(9) A. H. Sehon and M. Szwarc, *Proc. Roy. Soc. (London)*, **A209**, 110 (1951).

(10) G. O. Pritchard, H. O. Pritchard, H. I. Schiff, and A. F. Trotman-Dickenson, *Trans. Faraday Soc.*, **52**, 849 (1956).

(11) G. O. Pritchard and R. L. Thommarson, *J. Phys. Chem.*, **68**, 568 (1964).

Table II: Arrhenius Parameters for the Gas Phase Reaction, $\text{CH}_3 + \text{RX} \rightarrow \text{CH}_3\text{X} + \text{R}$, over the Temperature Range 90–145°

| Molecule | Reaction no. | Log A (ml mole ⁻¹ sec ⁻¹) ^a | E, kcal/mole |
|------------------------------------|--------------|--|--|
| CCl_4 | 1 | $\frac{1}{2} \log A_2 + 6.7 \approx 13.4$ | $\frac{1}{2}E_2 + 12.9 \pm 0.7 \approx 12.9 \pm 0.7$ |
| CCl_3CN | 3g | $\log A_{3d} - 0.3 \approx 12.9$ | $E_{3d} + 3.3 \pm 0.5 \approx 10.4 \pm 1.0$ |
| C_2Cl_6 | 1a | $\frac{1}{2} \log A_2 + 5.1 \approx 11.8$ | $\frac{1}{2}E_2 + 10.1 \pm 0.9 \approx 10.1 \pm 0.9$ |
| $\text{CCl}_3\text{COCCl}_3$ | 1b | $\frac{1}{2} \log A_2 + 5.9 \approx 12.6$ | $\frac{1}{2}E_2 + 9.7 \pm 0.8 \approx 9.7 \pm 0.8$ |
| $\text{C}_6\text{H}_5\text{CCl}_3$ | 1c | $\frac{1}{2} \log A_2 + 3.6 \approx 10.3$ | $\frac{1}{2}E_2 + 7.6 \pm 0.8 \approx 7.6 \pm 0.8$ |
| CF_3Br | 3a | $\log A_1 - 0.1 \approx 13.3$ | $E_1 - 0.4 \pm 0.5 \approx 12.5 \pm 1.0$ |
| CBr_4 | 3b | $\log A_{3f} + 0.4 \approx 14.2$ | $E_{3f} + 0.4 \pm 0.4 \approx 7.9 \pm 1.1$ |
| CCl_2Br_2 | 3c | $\log A_{3f} + 0 \approx 13.8$ | $E_{3f} + 0.1 \pm 0.4 \approx 7.6 \pm 1.1$ |
| CCl_3Br | 3d | $\log A_1 - 0.2 \approx 13.2$ | $E_1 - 5.8 \pm 0.5 \approx 7.1 \pm 0.9$ |
| CF_2Br_2 | 3e | $\log A_1 - 2.4 \approx 11.0$ | $E_1 - 6.5 \pm 0.5 \approx 6.4 \pm 1.0$ |
| CF_3I | 3f | $\log A_{3d} + 0.6 \approx 13.8$ | $E_{3d} + 0.4 \pm 0.4 \approx 7.5 \pm 1.0$ |

^a Per molecule, not per halogen atom.

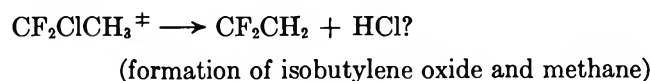
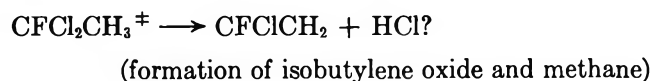
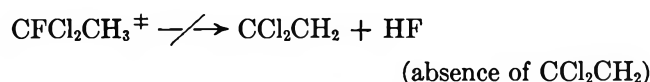
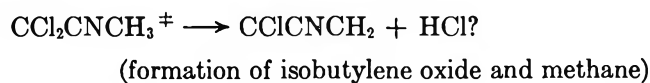
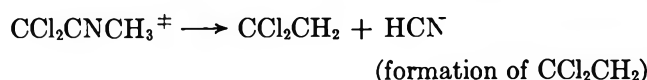
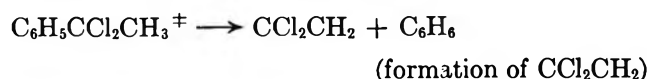
The possible existence of such a reaction sequence was first investigated by Galvin and Pritchard^{2,12}; however, the first authentic example was discovered by Pritchard, Venugopalan, and Graham,¹³ and numerous other examples have been found since (see, *e.g.*, ref 5 and, 14–17).

However, all the HCl formed in reaction 7 will not remain in the system, as it will be readily attacked by methyl radicals, *i.e.*



The principal fate of the chlorine atoms is that they abstract from the peroxide substrate, which is itself very resistant to methyl radical attack,¹⁸ forming more HCl, more CH_4 , etc. From the work of Hogg and Kebarle,¹⁹ we know that under such conditions one of the major products of free-radical attack on di-*t*-butyl peroxide is isobutylene oxide—whereas in the thermal decomposition of the peroxide on its own, where the methyl radical concentration is maximal, only traces of isobutylene oxide are formed.

In addition to reaction 7, possible evidence was found for similar reactions as follows.



The system is too complicated for any quantitative information concerning these reactions to be obtainable.

- (12) J. P. Galvin, Ph.D. Thesis, University of Manchester. 1963.
 (13) G. O. Pritchard, M. Venugopalan, and T. F. Graham. *J. Phys. Chem.*, **68**, 1786 (1964).
 (14) G. O. Pritchard and J. T. Bryant, *ibid.*, **69**, 1085 (1965).
 (15) G. O. Pritchard, J. T. Bryant, and R. L. Thommarson, *ibid.*, **69**, 2804 (1965).
 (16) R. D. Giles and E. Whittle, *Trans. Faraday Soc.*, **61**, 1425 (1965).
 (17) D. W. Setser, R. Littrell, and J. C. Hassler, *J. Am. Chem. Soc.*, **87**, 2062 (1965).
 (18) G. O. Pritchard, H. O. Pritchard, and A. F. Trotman-Dickenson, *J. Chem. Soc.*, 1425 (1954).
 (19) A. M. Hogg and P. Kebarle, *J. Am. Chem. Soc.*, **86**, 4558 (1964).

Polymer Formation in Irradiated Liquid Pyridine

by Carol K. Pearce and Joseph E. Ellison, Jr.

Institute for Exploratory Research, U. S. Army Electronics Command, Fort Monmouth, New Jersey 07703
(Received November 22, 1965)

Pyridine was exposed at room temperature to γ or X-radiation with total dosages of $3.5\text{--}73 \times 10^{19}$ ev/g, using dose rates from 2.47×10^{17} to 1.46×10^{21} ev/g hr. The molecular weight of the polymer formed increased with increasing dose, evidence of hydrogenation was found, and the polymer yield $G_{\text{pyridine}} = 3.66$ was determined. Three bipyridine isomers were detected in the polymer. The bipyridine yields were dependent on total dose and also on dose rate. The experimental results are consistent with a mechanism involving $\text{C}_5\text{H}_4\text{N}\cdot$ and $\text{C}_5\text{H}_6\text{N}\cdot$ radicals.

Introduction

Radiolysis studies on benzene have shown it to be a compound that is relatively stable to radiation. When the benzene ring is modified by the introduction of a nitrogen heteroatom to form pyridine, this stability is apparently diminished. Thus values were found for $G_{\text{polymer}} = 3.48^1$ and $3.8,$ ² though for benzene $G_{\text{polymer}} = 0.99.$ ¹ In contrast to the polymer yields, gas yields were reported to be comparable to those from benzene. G_{H_2} for pyridine was calculated from Klots and Johnson's data¹ to be 0.024, and Antoine² found a value of 0.025, compared to that for benzene of 0.0378.³ Further, values of $G_{\text{C}_2} = 0.0341^1$ and 0.045^2 were found for pyridine, and for benzene $G_{\text{C}_2} = 0.0194^1$ was determined. Also, G_{HCN} was reported² to be 0.020 for pyridine. Antoine concluded² from the G_{C_2} and G_{HCN} values for pyridine that rupture of the pyridine ring was of little importance in the formation of the radiolysis products.

For a better understanding of the effect of radiation on liquid pyridine, a more detailed knowledge of the polymer radiolysis fraction is necessary. Other than a finding of $G_{2,2'\text{-bipyridine}} = 1.1,$ ² no analysis of this fraction has been reported. Results of our investigation of the nongaseous fraction formed upon irradiation of liquid pyridine are presented in this article.

Experimental Section

Pyridine used in this investigation was Fisher Certified Reagent grade, redistilled from anhydrous barium oxide using a 50-plate Bruun bubble-cap column, except for those samples irradiated under a nitrogen

atmosphere. The pyridine used in these latter samples was the Eastman Spectro Grade chemical, dried with Molecular Sieves Type 4A and used without further purification. Benzene was Fisher Certified Reagent which was stored over freshly cut sodium after purification by redistillation and fractional crystallization. The polypyridines used for calibration were 2,2'-bipyridine (Fisher CP grade) and 2,2',2''-terpyridine (G. Frederick Smith reagent); 2,3'-bipyridine⁴ and 2,4'-bipyridine^{5,6} were prepared according to the literature.

Irradiations were accomplished with a 100-curie cesium-137 source ($2.47\text{--}4.05 \times 10^{17}$ ev/g hr), a 3.5-kurie cobalt-60 source ($1.92\text{--}8.92 \times 10^{18}$ ev/g hr), or the X-radiation from 1.5-mev Van de Graaff electrons impinging on a lead target ($5.9\text{--}14.6 \times 10^{20}$ ev/g hr). FeSO_4 dosimetry ($G_{\text{Fe}^{2+} \rightarrow \text{Fe}^{3+}} = 15.6$) was used with appropriate corrections for electron density. Air-free samples were exposed. Cells constructed from 25-ml or 50-ml round-bottom Pyrex flasks were evacuated to the order of 10^{-6} mm and filled by vacuum distillation with previously purified and degassed (freeze-thaw technique) liquid. Other samples used for some of the studies of the bipyridine fraction were sealed under a nitrogen atmosphere after having been

- (1) C. E. Klots and R. H. Johnson, *J. Phys. Chem.*, **67**, 1615 (1963).
- (2) F. Antoine, *Compt. Rend.*, **258**, 4742 (1964).
- (3) T. Gäumann and R. H. Schuler, *J. Phys. Chem.*, **65**, 703 (1961).
- (4) C. R. Smith, *J. Am. Chem. Soc.*, **52**, 397 (1930).
- (5) C. R. Smith, *ibid.*, **46**, 414 (1924).
- (6) P. Krumholz, *ibid.*, **73**, 4449 (1951).

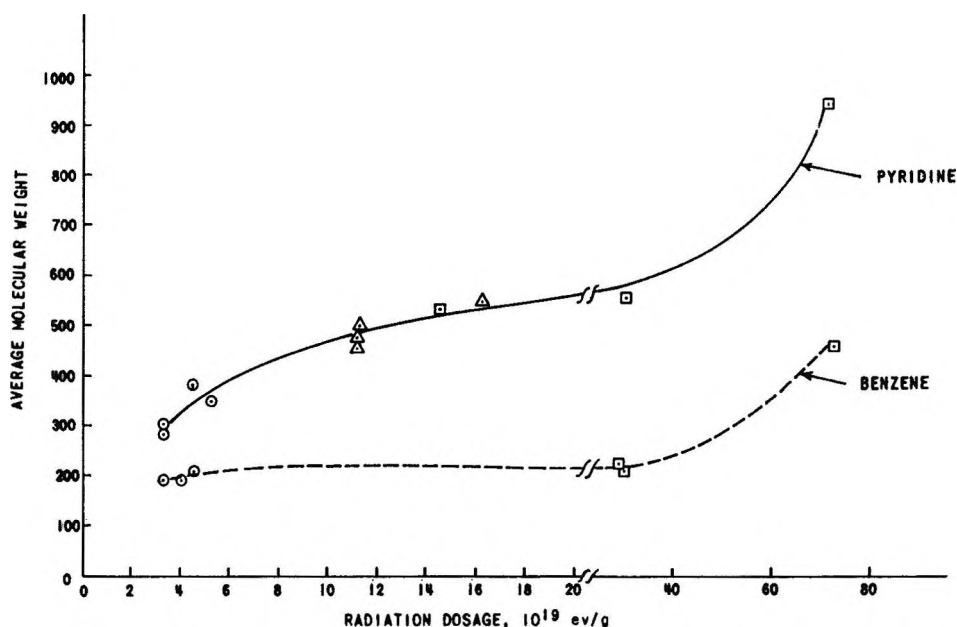


Figure 1. Variation in average molecular weight of radiolysis polymers with absorbed radiation dosage for pyridine and benzene: \circ , cesium-137 γ -radiation; \square , 1.5-mev Van de Graaff electrons; and Δ , cobalt-60 γ -radiation.

flushed for 2 hr with dried, CO_2 -free nitrogen. Exposures were done at room temperature.

After irradiation, excess pyridine was distilled off under vacuum and the reddish brown residue was analyzed. Analyses were conducted immediately upon isolation of the residue if possible, or else the products were stored under dry nitrogen or in a vacuum desiccator until used to avoid undue exposure to air. A Perkin-Elmer vapor fractometer Model 154C, using columns packed with Carbowax 1500 on glass beads, was employed for the gas chromatographic analyses. The Fractometer utilized a thermistor detector; supplemental heat was applied to the outlet line to prevent condensation of the bipyridines (boiling points from 272 to 305 $^\circ$) before they were collected for ultraviolet analysis. In this way the 2,2', 2,3', and 2,4'-bipyridines were separated; 3,3'- and 4,4'-bipyridine (and presumably the 3,4' isomer, which has a similar boiling point) appeared together after the "2" isomers. 2,2',2''-Terpyridine was not separated at all. Ultraviolet absorption spectra of the gc fractions in 0.02 M NH_4OH solution were measured on a Cary Model 11 recording spectrophotometer and compared with the spectra of known bipyridines and with those recorded in the literature.⁷

Molecular weight determinations were done by the isothermal distillation technique⁸ with urea comparison solutions. Microhydrogenation determinations⁹ of the extent of unsaturation were made, using platinum oxide catalyst and glacial acetic acid solvent. Com-

bustion microanalyses for carbon, hydrogen, and nitrogen were obtained with the F & M Scientific Corp. Model 180 carbon, hydrogen, and nitrogen analyzer.

Results

Our determination of the polymer yield, *i.e.*, $G_{\text{pyridine} \rightarrow \text{polymer}}$, gave an average value of 3.66 ± 0.54 for dosages of $3.5\text{--}75 \times 10^{19}$ ev/g, which is in general accord with earlier work.^{1,2} As expected, the average molecular weight increased with dosage (Figure 1). Within experimental error, no dose rate effect on the polymer yield was found. The average molecular weight of the pyridine polymer increased more rapidly, however, than that of the benzene polymer for corresponding doses. This fact indicated more extensive interaction of pyridine, resulting in polymer molecules with longer chains than is true for benzene. A not unexpected change in the polymer was found in one pyridine sample inadvertently exposed to air both during and after irradiation. Here G_{pyridine} rose to 5.35, and the average molecular weight was 688, in contrast to a value of 535 for a comparable dose in the absence of air.

At lower doses (3.0×10^{19} ev/g), bipyridines evidently contribute largely to the total polymer. We were

(7) P. Krumholz, *J. Am. Chem. Soc.*, **73**, 3487 (1951).

(8) S. J. Clark, "Quantitative Methods of Organic Microanalysis," Butterworth & Co. (Publishers) Ltd., London, 1956, p 203 ff.

(9) C. L. Ogg and F. J. Cooper, *Anal. Chem.*, **21**, 1400 (1949).

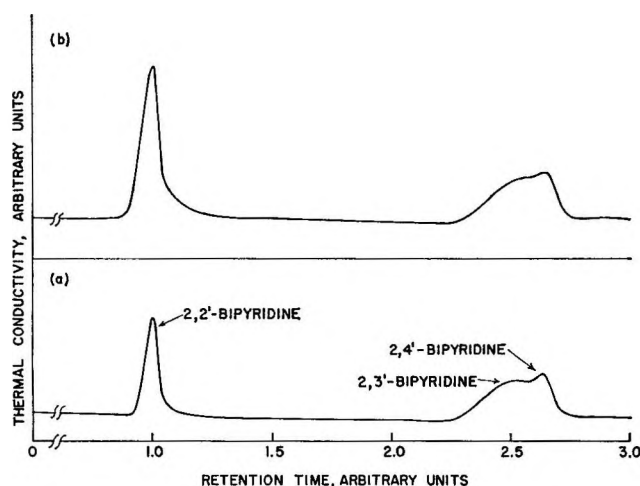


Figure 2. Gas chromatogram of (a) bipyridine calibration solution, 0.13 *M* in 2,2', 2,3', and 2,4'-bipyridines, and (b) pyridine radiolysis products.

able to separate three bipyridines (the 2,2', 2,3', and 2,4' isomers) in these cases with gas chromatographic techniques (Figure 2). Identification of the bipyridines was made by comparison of the retention times with calibration solutions and by ultraviolet absorption spectra of the three fractions as indicated above. We determined the quantity of bipyridines present by calibration of the gas chromatograms with bipyridine standards. At higher doses, lower yields (Figure 3) of bipyridines were detected, seemingly in contradiction to the finding of Antoine² that the 2,2'-bipyridine yield increased linearly with dose. Although the dosages used in Antoine's work were not indicated, apparently they were in the lower range, since a molecular weight of 150 was obtained for the polymer. An increase in dose rate also appeared to lower the bipyridine yield (Figure 3).

Combustion and hydrogenation microanalyses were made on the pyridine radiolysis polymer as shown in Table I. For comparison with the higher molecular weight fraction, hexapyridines with eight double bonds saturated, $C_{30}H_{36}N_6$, and with 12 double bonds saturated, $C_{30}H_{44}N_6$, have molecular weights of 483 and 491, respectively, and ten and six double bonds per molecule, respectively. The experimental results indicate the radiolysis polymer formed in this particular dose range ($1.18\text{--}1.69 \times 10^{20}$ ev/g) included compounds polymerized at least to the hexapyridine stage, with both longer and shorter chains probably present. That extensive hydrogenation occurred is shown in the deviation of the empirical formula from that for polypyridines, $C_{5n}H_{2+3n}N_n$. The amount of hydrogen found was much greater than that for a

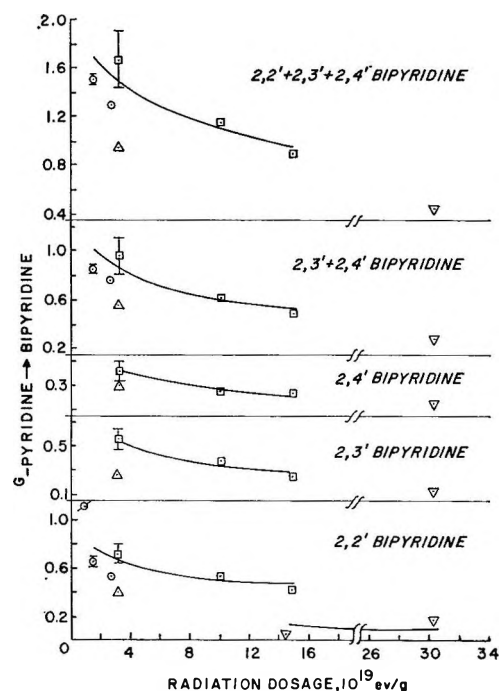


Figure 3. Dependence of radiolysis yields of bipyridines upon radiation dosage and dose rate: \circ , $2.47\text{--}3.33 \times 10^{17}$ ev/g hr cesium-137 radiation (the 2,3'- and 2,4'-bipyridines were not resolved for these samples, but appeared together); \square , $1.63\text{--}1.71 \times 10^{18}$ ev/g hr cobalt-60 radiation; \triangle , 8.92×10^{18} ev/g hr cobalt-60 radiation; ∇ , $5.90\text{--}6.12 \times 10^{20}$ ev/g hr Van de Graaff X-radiation; and \circ , yield determined by Antoine.²

polypyridine. Also, the hydrogenation data showed fewer double bonds per molecule than would be expected (three times the number of pyridine rings) if only polypyridines were present. Similar conclusions may be drawn from the data for the lower dose range ($3.22\text{--}3.48 \times 10^{19}$ ev/g).

Table I: Analysis of Pyridine Radiolysis Polymer

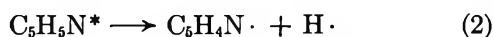
| Av mol wt | % hydrogen | % nitrogen | % carbon | Formula | Moles of hydrogen/mole of polymer |
|------------------|-------------------|--------------------|--------------------|---------------------------|-----------------------------------|
| 550 | 7.13 ^a | 16.65 ^a | 76.21 ^a | $C_{34.5}H_{38.9}N_{6.5}$ | ... |
| 500 | 6.85 ^b | 18.32 ^b | 74.82 ^b | $C_{31.1}H_{33.4}N_{6.5}$ | 6.8 |
| 460 | 6.96 | 17.41 | 75.63 | $C_{29}H_{31.8}N_{6.4}$ | 7.2 |
| 475 | 6.84 | 18.83 | 74.33 | $C_{29.4}H_{32.2}N_{6.4}$ | 7.6 |
| 305 ^c | 6.59 | 19.23 | 74.18 | $C_{18.8}H_{19.9}N_{4.2}$ | ... |
| 305 ^c | ... | ... | ... | ... | 5.0 |
| 295 ^c | ... | ... | ... | ... | 5.1 |

^a Average of three determinations. ^b Average of two determinations. ^c Estimated from Figure 1.

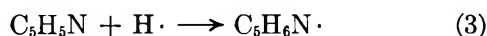
Any contribution to the polymer molecules by fragments from fracture of the pyridine ring has been assumed to be minor. That ring fracture was not extensive² has been noted before. The high average molecular weight of the polymer also argues for chains constructed of pyridine-size units, rather than of smaller fragments. Yields noted above show that bipyridines accounted for almost one-half the 100-ev yield for the total polymer found at 3.0×10^{19} ev/g. The average molecular weight from Figure 1 was approximately 290 for the total polymer, compared to 156 for bipyridine, so that the amount of high molecular weight compounds present must be appreciable.

Discussion

To formulate a mechanism for the radiolysis of pyridine, the analyses reported above and the radiolysis product and radical yields must be considered along with certain facets of the reactivity of pyridine itself. Formation of radicals as a result of initial ionization and excitation radiation processes comprises the primary radiation process (eq 1 and 2).

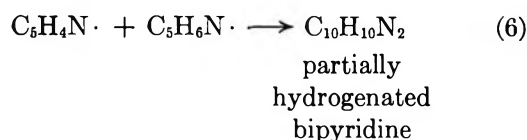
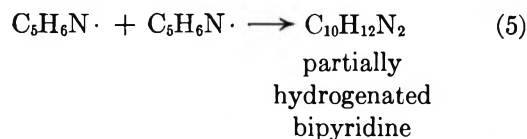
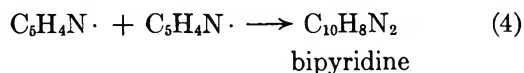


Reaction of hydrogen atoms with unexcited or "solvent" pyridine can occur quickly.



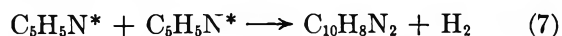
Reaction 3 can occur even at low temperatures^{10,11} so that $\text{C}_5\text{H}_4\text{N}\cdot$ and $\text{C}_5\text{H}_6\text{N}\cdot$ radicals are the precursors for those radiolysis products formed by radical reactions. The radical yield in the radiolysis of pyridine has been determined¹¹ by esr techniques at -170 to -160° to be $G_R = 0.7$, compared to a comparable value of 0.2 for benzene.¹⁰ This radical yield for pyridine is higher than the yields for some other aromatic compounds derived from benzene, but it is much lower than the yields from most other classes of organic compounds.¹⁰ The yield was attributed to $\text{C}_5\text{H}_4\text{N}\cdot$ and $\text{C}_5\text{H}_6\text{N}\cdot$, and it was postulated that H atoms added to the pyridine 4-position to form the latter radical.

The 100-ev radical yield for irradiated pyridine at room temperature has been determined² by stable free-radical techniques to be 3.3 and, for benzene, 0.7. These yields approximate the polymer yields in both the pyridine and benzene cases. Radical-radical reactions might then be assumed to account solely for the polymer formation, for example



Such a mechanism would lead to some inconsistency with the yields and identity of the bipyridine isomers found experimentally. The only bipyridines found were the 2,2', 2,3', and 2,4' isomers. If these isomers had formed chiefly through (4), the yields of the 2,3'- and 2,4'-bipyridines would give some indication of the amount of 3- and 4- $\text{C}_5\text{H}_4\text{N}\cdot$ present. Assuming 3- and 4- $\text{C}_5\text{H}_4\text{N}\cdot$ interact in proportions similar to those found from the radiolysis bipyridines for 2- $\text{C}_5\text{H}_4\text{N}\cdot$, the 3,3', 3,4', and 4,4'-bipyridine yields can be estimated for (4). The estimated amounts of these bipyridines would have been detected on the gas chromatogram, especially since these three isomers would not have been resolved but would have appeared together. Further, a large contribution of hydrogenated bipyridines to the dimer product would be implied by reactions 5 and 6. The molecular weight determinations and bipyridine yields indicated a sizable amount of rather high molecular weight compounds must be present. A dimer yield much greater than the bipyridine yield alone would be difficult to reconcile with these results. Indeed, had hydrogenated bipyridines been present, some evidence should have appeared on the chromatograms. No such evidence was found (Figure 2). Radical-radical reactions apparently do not dominate the early steps of the radiolysis.

Reactions of excited pyridine molecules could form bipyridines (eq 7), but if so the contribution must be a



minor one. The hydrogen yield in pyridine radiolysis is even smaller than that for benzene.^{1,2}

That the reactions between solvent pyridine and the radicals resulting from primary and secondary radiation processes are a major source of the higher radical and product yields for pyridine may be inferred from other studies. Comparisons of the reactivity of pyridine and benzene with methyl radicals¹² and hydrogen

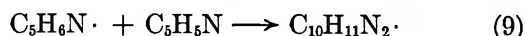
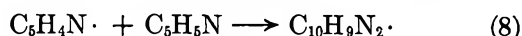
(10) V. V. Voevodskii and Yu. N. Molin, *Radiation Res.*, **17**, 366 (1962).

(11) V. A. Sharpatyi, S. A. Safarov, and K. G. Ianova, *Dokl. Akad. Nauk SSSR*, **147**, 863 (1962).

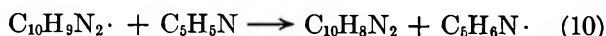
(12) M. Levy and M. Szwarc, *J. Am. Chem. Soc.*, **77**, 1949 (1955).

atoms^{1,13} indicate a value for pyridine about three times greater than that for benzene. Phenyl radicals attack pyridine and benzene about equally, however.¹⁴ Kalkwarf¹⁵ determined "protection indices" for a number of compounds based upon their reactivity, relative to erioglaucone, with radicals generated in the radiolysis of water. The protection index for pyridine was 0.169, and for benzene it was 0.11. The higher value for pyridine was attributed to the more rapid reaction of pyridine with uncharged radicals as shown by molecular orbital calculations. Comparing the indices for pyridine and benzene, we find pyridine to be about 1.5 times as reactive with these particular radicals as benzene. The relative reactivity of benzene and pyridine with radicals appears to be influenced by the nature of the radicals.

We have already noted the much higher molecular weights found for the pyridine radiolysis polymer compared to the benzene polymer. This was interpreted as evidence of a longer chain length, or more extensive reaction, for the pyridine case. Further, we have calculated the average number of polymer molecules formed per 100-ev input from our data for pyridine ($G' = 0.60$) and for benzene ($G' = 0.33$). Comparing our G' values, we find about 1.8 more polymer molecules are formed for pyridine than for benzene. The relative number of polymer molecules formed appears to agree within an order of magnitude with the relative reactivities of radicals with pyridine and benzene, whether the reactivities are deduced from Kalkwarf's data or from a median of the values for hydrogen atoms and larger (phenyl) radicals. The median reactivity concept would resemble the actual radiolysis situation most closely. Qualitatively, the agreement in values was interpreted to mean reactions between radicals and solvent pyridine are a more important part of the pyridine radiolysis mechanism than is true for benzene. The greater propensity for radicals and hydrogen atoms to react with pyridine, as well as the higher primary radical yields, would account for the high yields and the high molecular weights observed. Reactions of the primary radiolysis radicals with solvent pyridine (8 and 9) are consistent with the known chemistry of



pyridine and with the products resulting from radiolysis. Further reaction of the $\text{C}_{10}\text{H}_9\text{N}_2\cdot$ radical would produce the bipyridine isomers found.



Radical attack on pyridine occurs at all three posi-

tions.¹⁶ Phenyl radicals yield about 54% of 2-phenylpyridine, 32% of the 3 isomer, and 14% of the 4 isomer. The partial rate factors calculated¹⁴ from these yields for the attack of phenyl radicals on pyridine with respect to benzene are 1.69 at the 2-position, 1.0 at the 3-position, and 0.87 at the 4-position. From these factors, experimental values of the atom-localization energies at each position have been determined. These values substantially agree with those calculated from molecular orbital theory, affirming that the yields of isomers result from radical substitution. In the radiolysis of pyridine, we have obtained 43% 2,2'-bipyridine, 31% 2,3'-bipyridine, and 26% 2,4-bipyridine. If only reactions 8 and 10 were involved in the production of bipyridine, we might expect percentage yields closer to those found in the phenyl radical case. The trend of attack at the 2-, 3-, and 4-positions appears similar in both instances, and this similarity in order may signify that reactions 8 and 10 are of major importance in the radiolysis mechanism. Indeed, assuming the primary radiolysis radicals attack pyridine to form bipyridines in the same ratio with respect to benzene as do phenyl radicals, partial rate factors can be calculated¹⁴ from the bipyridine radiolysis yields. The factors so calculated with respect to benzene are 1.34, 0.97, and 1.64 for the 2-, 3-, and 4-positions, respectively. The values and the relation between them are quite different from those for the attack of phenyl radicals on pyridine, which as noted above agreed with molecular orbital theory. However, part of the 2,4'-bipyridine yield, all of which had been ascribed to attack at the 4-position in determining partial rate factors, may in reality be due to attack at the 2-position. If only 14% of the total bipyridine yield is attributed to the 4-position to correspond to the phenyl radical case, and the remainder of the 2,4'-bipyridine yield is combined with the 2,2' isomer yield for a total of 55% at the 2-position, the partial rate factors become 1.72, 0.97, and 0.87 at the 2-, 3-, and 4-positions, respectively. Thus, the major part of the bipyridine radiolysis yields can be explained by the attack of the $2\text{-C}_5\text{H}_4\text{N}\cdot$ and $4\text{-C}_5\text{H}_4\text{N}\cdot$ radicals on pyridine, though a contribution from radical-radical reactions may be present also.

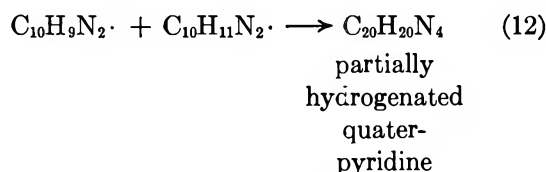
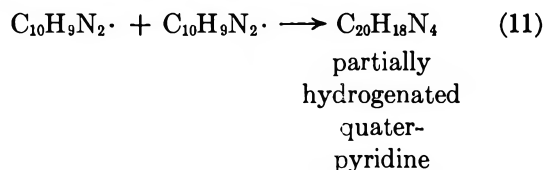
(13) C. E. Klots, Y. Raef, and R. H. Johnson, *J. Phys. Chem.*, **68**, 2040 (1964).

(14) D. R. Augood, D. H. Hey, and G. H. Williams, *J. Chem. Soc.*, 2094 (1952).

(15) D. R. Kalkwarf, Proceedings of the 2nd United Nations International Conference on Peaceful Uses of Atomic Energy, Geneva, Vol. 29, United Nations, New York, N. Y., 1958, p 379.

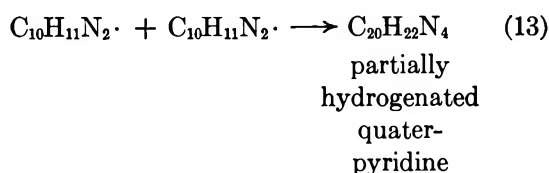
(16) R. A. Barnes, "Pyridine and Its Derivatives," Part I, E. Klingsberg, Ed., Interscience Publishers, Inc., New York, N. Y., 1960, Chapter 1.

The apparent dependence of the bipyridine yield on total dose and dose rate (Figure 3) indicated an interference with reaction 10, possibly

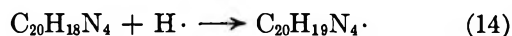


The bipyridine yield may rise to a maximum according to reactions 8 and 10 and then decrease with increasing dose through reactions 8, 11, and 12. This would be in accord with Antoine's report² of a linear increase with dose. Antoine found a $G_{2,2'\text{-bipyridine}} = 1.1$, presumably as noted before at a lower dose than used in this work, and at a different dose rate.

The higher hydrogenated polypyridines also can result from other radical-radical reactions, as



Hydrogen atom and radical attack on molecular products could occur also, for example



and undergo subsequent radical reactions to form the ultimate radiolysis products.

Much work remains to be done to clarify the mechanism by which radiolysis products are formed in pyridine. Particularly interesting would be the development of extremely sensitive detection techniques for the separation and identification of the bipyridines other than those determined here. All the bipyridine isomers are polar, high-boiling compounds, and all except 2,2'-bipyridine have similar boiling points. For these reasons, even the gas chromatographic separations reported here proved extremely difficult to accomplish. Kinetic studies, especially those involving isotopically labeled compounds and the evaluation of temperature effects, would be enlightening. We anticipate future work here will further develop the pyridine radiolysis mechanism.

Acknowledgments. The authors express their appreciation for useful discussions on various phases of this work with Professor Richard F. Firestone, Ohio State University, Department of Chemistry. Assistance in performing the irradiations was given by Mr. Charles Olsen and Mr. Joseph Crotchfelt of the Institute for Exploratory Research.

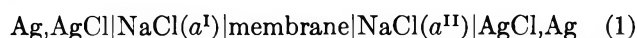
Membrane Potentials. Measurement of Electromotive Force of Cells Containing "Untreated" Collodion Membrane*

by N. Lakshminarayanaiah

Department of Pharmacology, Schools of Medicine, University of Pennsylvania, Philadelphia, Pennsylvania
(Received November 23, 1965)

Measurements of membrane potentials, counterion transport numbers, and solvent transport numbers for the system $\text{KCl(aq)}|\text{collodion membrane}|\text{KCl(aq)}$ are presented and used to test the Scatchard theory of membrane potential. The agreement between the observed and calculated emf's of appropriate membrane cells, although initially very poor, proved satisfactory later when proper amends were made for the change in the physical structure of the membrane brought about by the applied electric field.

Of the several theories formulated in recent years to describe the electrical potentials arising across permselective membranes of high fixed charge density, the theory of Scatchard,¹ which is based on the application of well-established principles of classical thermodynamics used in the consideration of liquid-liquid junction potentials to the treatment of isothermal diffusion potentials generated across membranes, has been shown² to be very satisfactory in describing the emf's of membrane cells of the type



containing cross-linked sodium phenolsulfonate membranes of medium fixed charge density. The equation of the Scatchard theory predicting the emf of membrane cell of type 1, although not from first principles, was cast by Hills, *et al.*,³ into the form

$$E = -\frac{2RT}{F} \int_I^{\text{II}} (\bar{l}_+ - 10^{-3}m_{\pm}M\bar{l}_w) d \ln a_{\pm} \quad (2)$$

(where E is the emf of the membrane cell 1, F is the Faraday, m_{\pm} is the mean molality of the electrolyte solution of activity a_{\pm} , \bar{l}_+ and \bar{l}_w are the transference numbers of counterion and solvent, respectively, in the membrane phase, and M is the molecular weight of solvent), a form in which it was derived earlier by Lorimer, *et al.*,⁴ by applying the principles of thermodynamics of irreversible processes to transport phenomena across membranes.

Unlike the fixed charge theory of membrane potential

expounded by Teorell⁵ and Meyer and Sievers,⁶ the Scatchard theory is very general and stipulates no special property, as, for example, presence of a number of ionogenic groups, in regard to the structure of the membrane. In view of this, it is no surprise to find the theory to be satisfactory in describing the emf's of membrane cells even in high salt environment in which there is incomplete ionic selectivity of the membrane. Conversely, it may be presumed that the Scatchard theory would be equally successful in describing the emf's of cells containing membranes carrying few or nil fixed charge groups. This paper therefore describes the extent of success achieved in integrating eq 2 by using values of \bar{l}_+ and \bar{l}_w measured as functions of activity of the external electrolyte solution of KCl employing untreated collodion membranes carrying only stray and end carboxylic groups.⁷

* Presented at the Tenth Annual Meeting of the Biophysical Society held at Boston, Mass., Feb. 23-25, 1966.

(1) G. Scatchard, *J. Am. Chem. Soc.*, **75**, 2883 (1953).

(2) N. Lakshminarayanaiah and V. Subrahmanyam, *J. Polymer Sci.*, **A2**, 4491 (1964).

(3) G. J. Hills, P. W. M. Jacobs, and N. Lakshminarayanaiah, *Proc. Roy. Soc. (London)*, **A262**, 246 (1961).

(4) J. W. Lorimer, E. I. Boterenbrood, and J. J. Hermans, *Discussions Faraday Soc.*, **21**, 141 (1956).

(5) T. Teorell, *Proc. Soc. Exptl. Biol. Med.*, **33**, 282 (1935); *Proc. Natl. Acad. Sci. U. S.*, **21**, 152 (1935); *Progr. Biophys. Biophys. Chem.*, **3**, 305 (1953).

(6) K. H. Meyer and J. F. Sievers, *Helv. Chim. Acta*, **19**, 649, 665, 987 (1936).

(7) K. Sollner, I. Abrams, and C. W. Carr, *J. Gen. Physiol.*, **24**, 467 (1940).

Experimental Section

The preparation of collodion membranes is described elsewhere.⁸ Membranes used in this study had an exchange capacity of 0.2 mequiv/g of wet membrane.

Methods already outlined^{2,8} were followed to determine meaningful values for the transport numbers of K⁺ counterion (\bar{t}_+) and water (\bar{t}_w). These were measured as functions of external electrolyte (KCl) concentration.

Membrane potentials were measured using half cells and procedures described in our previous publications.^{2,9}

Results and Discussion

The emf of the cell Ag, AgCl|KCl(m^I)|membrane|KCl(m^{II})|AgCl, Ag at 25° for various values of molality of the external solutions are given in Table I. The untreated collodion membranes have low fixed charge concentration and are therefore expected to show low selectivity toward counterions. The observed emf of the membrane cell is compared with the E_{\max} value in Figure 1. The so-called E_{\max} value given by

$$E_{\max} = -\frac{2RT}{F} \ln \frac{a_{\pm}^{II}}{a_{\pm}^I} \quad (3)$$

is the maximum possible value of electrical potential arising across an ideally permselective membrane across which there is negligible transport of co-ions and solvent. The drop in selectivity with the mean external activity is very marked compared to the smooth decrease in selectivity exhibited by cross-linked polymethacrylic acid membrane of high fixed charge density of nearly 3 m (also shown in Figure 1). The collodion

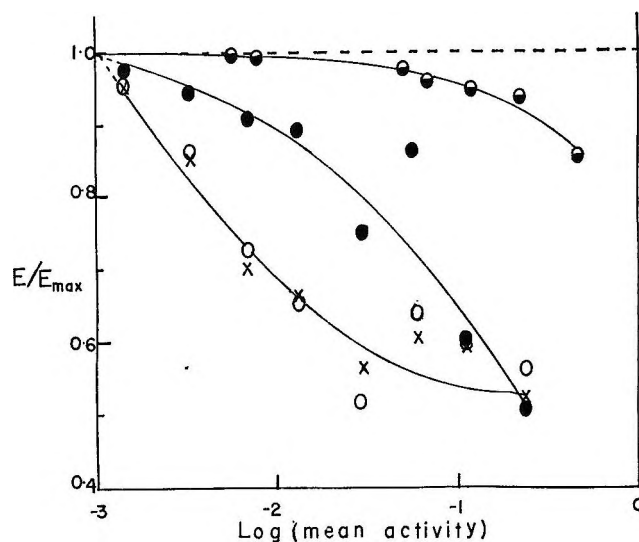


Figure 1. The variation of E/E_{\max} with mean external activity: ●, observed values with polymethacrylic acid of high fixed charge density taken from ref 9; ●, observed values of this study; ○, calculated values from observed transport numbers; X, observed values with membranes used in counterion transport number determinations.

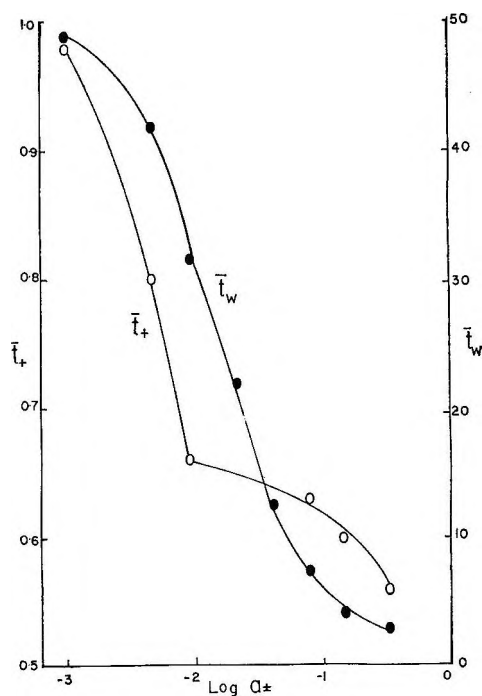


Figure 2. Counterion and solvent transport numbers as a function of external activity.

Table I: Emf's of the Cell Ag, AgCl|KCl(m^I)|membrane|KCl(m^{II})|AgCl, Ag at 25°

| Cell no. | m ^I , mole kg ⁻¹ | m ^{II} , mole kg ⁻¹ | a _± ^I , mole kg ⁻¹ | a _± ^{II} , mole kg ⁻¹ | E, mv |
|----------|--|---|---|--|-------|
| 1 | 0.002004 | 0.001002 | 0.001912 | 0.000969 | 34.0 |
| 2 | 0.00501 | 0.002004 | 0.00464 | 0.001912 | 43.0 |
| 3 | 0.01002 | 0.00501 | 0.00905 | 0.00464 | 31.0 |
| 4 | 0.02005 | 0.01002 | 0.01742 | 0.00905 | 30.0 |
| 5 | 0.0502 | 0.02005 | 0.0410 | 0.01742 | 33.0 |
| 6 | 0.1004 | 0.0502 | 0.0773 | 0.0410 | 28.1 |
| 7 | 0.201 | 0.1004 | 0.145 | 0.0773 | 19.5 |
| 8 | 0.507 | 0.201 | 0.331 | 0.145 | 21.5 |

membrane, being not very permselective, is not able to keep the co-ions out of the membrane phase even in a very low salt external environment to the same extent as ion-exchange membranes of high fixed charge density. The Scatchard theory has taken the factors causing this

(8) N. Lakshminarayanaiah and K. R. Brennen, *Electrochim. Acta*, in press.

(9) G. J. Hills, P. W. M. Jacobs, and N. Lakshminarayanaiah, *Proc. Roy. Soc. (London)*, **A262**, 257 (1961).

decrease in selectivity, *viz.*, transport of co-ion and solvent, into account in formulating eq 2. Using the values of \bar{l}_+ and \bar{l}_w determined by electrolysis experiments and given in Figure 2, the cell emf may be evaluated quite realistically, but the difficulty lies in integrating eq 2. From the data of Figure 2, it is possible to derive, by interpolation, the required values of \bar{l}_+ and \bar{l}_w for each of the membrane interfaces concerned, but the variation of these quantities across the membrane is not known and can only be obtained from a knowledge of the steady-state diffusion profile in the membrane. This profile may be assumed to be linear between the two solution activities with which the two membrane faces are in equilibrium. Thus, the corresponding variation of \bar{l}_+ and \bar{l}_w in the membrane may be inferred from the known variation of these quantities with the external solution molality (see Figure 2). Using the values so derived, eq 2 was integrated numerically by means of Simpson's rule. The results expressed as a ratio E/E_{\max} are shown in Figure 1. These values are significantly lower than the observed values and are outside the limits of experimental variation which was $\pm 2\%$.

In the previous study with high fixed charge membranes,⁹ where the calculated values of emf were also lower than the observed values, several possibilities existing to cause this disagreement have been discussed. However, in the recent paper² this lack of agreement was shown to be due to use of improper values of \bar{l}_+ and \bar{l}_w , whereas in this work the effects of both back-diffusion and concentration polarization leading to membrane polarization, which made the transport numbers of the previous study⁹ improper, have been eliminated.

The causes for this unsatisfactory agreement therefore were sought elsewhere. In a number of experiments carried out to determine \bar{l}_+ , when high currents especially were employed to eliminate back electrolyte diffusion by shortening the time of electrolysis experiment, sudden changes in current flow were observed. The membranes used in this study have very high impedance (specific conductance $k \approx 10^{-10}$ ohm⁻¹ cm⁻¹) and consequently required application of high dc voltages (>100) to get the required current flow (15–20 ma). The sudden change in current during an experiment was found to be due to a change in the physical structure of the membrane. Determination of the membrane impedance after the electrolysis experiment showed that the membrane had become more conducting than it was before the transport number determination. This pointed to the fact that the membrane had become more porous. As a result, when these membranes were used in the above cell (1), lower cell emf's were observed. These values, also expressed as E/E_{\max} and shown in Figure 1, agreed reasonably well with the calculated values. Thus, it is found that, provided proper corrections are made where they are due as shown in this study, eq 2 of the Scatchard theory describes satisfactorily the emf's of cells of type 1 containing membranes of low fixed charge density.

Acknowledgments. The work was supported in part by U. S. Public Health Service Grant NB-03321 from the National Institute of Neurological Diseases and Blindness and by Grant GB-865 from the National Science Foundation.

The Significant Structure Theory Applied to the Hydrides of Elements of the Fifth Group

by Mu Shik Jhon, Joe Grosh, Taikyue Ree, and Henry Eyring

Department of Chemistry, University of Utah, Salt Lake City, Utah (Received December 1, 1965)

The significant structure theory has been applied to the liquid state of PH_3 , AsH_3 , and SbH_3 . The molar volume, vapor pressure, specific heat, entropy, and critical properties for the liquids are all calculated. Surface tensions of the liquids are calculated by a modification of earlier techniques. Good agreement with experimental observations is obtained.

Introduction

The significant structure theory of liquids has been developed^{1,2} and successfully applied to a number of liquids. Lately, Lee, *et al.*,³ have applied significant structure theory to liquid NH_3 and calculated all thermodynamic properties and the surface tension. Good agreement with observed values was found. This paper is one of a series of studies applying this theory to various common and uncommon liquids² and is the second of a sequence dealing with hydrides belonging to one family.

The Partition Function

According to the significant structure theory of liquid, the partition function of a liquid is

$$f = (f_s)^{V_s N/V} (f_g)^{(V-V_s)N/V}$$

Here, f_s and f_g are the partition functions of "solid-like" and "gas-like" structure; respectively, V is the molar volume of the liquid, V_s is the molar volume of the solid at the melting temperature, and N is Avogadro's number. Except for liquid ammonia, each of the hydrides of the nitrogen family has a normal entropy of fusion and a solid state transition.⁴ This indicates that these compounds probably rotate in the solid state at the melting point. Therefore, the usual rotation term is included in both the gas and solid terms. For simplicity, the system was treated as an Einstein solid. Accordingly, the partition function takes the following form.

$$f = \left\{ \frac{e^{E_s/RT}}{(1 - e^{-\theta/T})^3} \frac{8\pi^2(8\pi^3 ABC)^{1/2}(kT)^{3/2}}{3h^3} \times \prod_{i=1}^6 \frac{1}{1 - e^{-h\nu_i/kT}} [1 + n(X-1)e^{-\frac{aE_s}{(X-1)RT}}] \right\}^{N/X} \times \left\{ \frac{(2\pi mkT)^{3/2}}{h^3} \frac{eV}{N} \frac{8\pi^2(8\pi^3 ABC)^{1/2}(kT)^{3/2}}{3h^3} \times \prod_{i=1}^6 \frac{1}{1 - e^{-h\nu_i/kT}} \right\}^{(1-1/X)N} \quad (1)$$

Here, E_s and θ are the energy of sublimation and the Einstein characteristic temperature, respectively. a is a dimensionless constant which, for simple liquids is calculable from the model. A , B , and C are the three principal moment of inertia, ν_i is the internal molecular vibration frequency, m is the molecular mass, $X = V/V_s$, N is Avogadro's number, and n is the number of nearest neighbors around a molecule of the liquid at the melting point.

(1) (a) H. Eyring and T. Ree, *Proc. Natl. Acad. Sci. U. S.*, **47**, 526 (1961); (b) H. Eyring and R. P. Marchi, *J. Chem. Educ.*, **40**, 562 (1963).

(2) D. Henderson, H. Eyring, and D. Felix, *J. Phys. Chem.*, **66**, 1128 (1962); T. R. Thomson, H. Eyring, and T. Ree, *ibid.*, **67**, 2701 (1963); T. S. Ree, T. Ree, and H. Eyring, *ibid.*, **68**, 1163, 3262 (1964); *J. Chem. Phys.*, **41**, 524 (1964); R. P. Marchi and H. Eyring, *J. Phys. Chem.*, **68**, 221 (1964); S. H. Lin, H. Eyring, and J. Davis, Jr., *ibid.*, **68**, 3617 (1964); Y. L. Wang, T. Ree, T. S. Ree, and H. Eyring, *J. Chem. Phys.*, **42**, 1926 (1965); S. M. Ma and H. Eyring, *ibid.*, **42**, 1920 (1965). (See also the series of papers appearing in *Proc. Natl. Acad. Sci. U. S.* from 1958 to the present.)

(3) H. Lee, M. S. Jhon, and S. Chang, *J. Korean Chem. Soc.*, **8**, 85 (1964).

(4) Landolt-Bornstein, "Zahlen Werte und Funktion aus Physik, Chemie, Astronomie, Geophysik und Technik," Vol. II, Part 3, Springer-Verlag, Berlin, 1956.

The parameters n , a , θ , E_s , and V_s are calculated in a manner described by Chang, *et al.*,^{5,6} and the values are given in Table I. The calculations were made using an IBM 7040 computer.

Results

(a) *Volume and Pressure.* The Helmholtz free energy A is given by

$$A = -kT \ln f \quad (2)$$

Table I: Parametric Values

| | PH ₃ | AsH ₃ | SbH ₃ |
|------------------|-------------------------|-------------------------|-------------------------|
| n | 11.45 | 11.514 | 11.58 |
| θ , °K | 62.67 | 39.63 | 33.50 |
| V_s , cc | 41.44 | 42.13 | 49.75 |
| a | 0.1257×10^{-2} | 0.9950×10^{-3} | 0.7491×10^{-3} |
| E_s , cal/mole | 3964 | 4528 | 5565 |

A is plotted against V for a constant T , and a common tangent to the points corresponding to the liquid and vapor phases is drawn. The vapor pressure is given by the slope of the common tangent, and the abscissas of the two points of the common tangent indicate the volume of the liquid and vapor (Figure 1). By using eq 1, calculations of the molar volumes and vapor pressures at various temperatures were made. The calculated results are plotted in Figures 2 and 3 and show close agreement with experimental values.⁷⁻¹⁰

(b) *Entropy.* Entropies of the liquid S_l are calculated from eq 1 and 2 using the relation

$$S_l = -\left(\frac{\partial A}{\partial T}\right)_V = \frac{\partial}{\partial T} (kT \ln f)_V \quad (3)$$

In Figure 4, the calculated entropies of liquids are compared with the observed values⁴ of PH₃ and AsH₃. There is excellent agreement between theory and experiment.

(c) *The Critical Points Properties.* The critical point was found by setting the first and second derivatives of pressure with respect to volume at constant temperature equal to zero, and finding the values of P , V , and T satisfying these two conditions by a trial and error technique using an IBM 7040 computer. Since this calculation requires the second and third derivatives of the partition function, the critical point constitutes a fairly severe test of the theory. The calculated results are listed in Table II. The observed data^{7,11} available at present show satisfactory agreement with the calculated values.

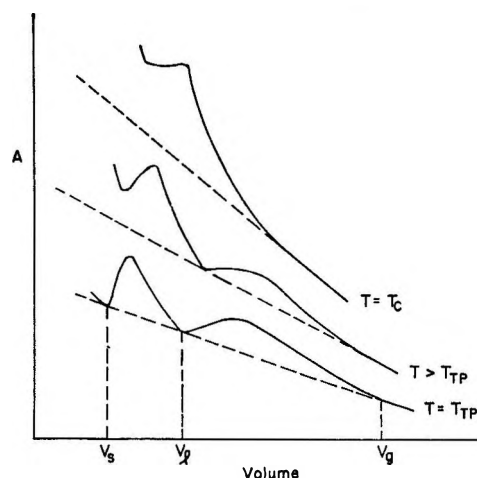


Figure 1. The schematic representation of Helmholtz free energy vs. volume T_c and T_{TP} are the temperatures at the critical point and triple point, respectively.

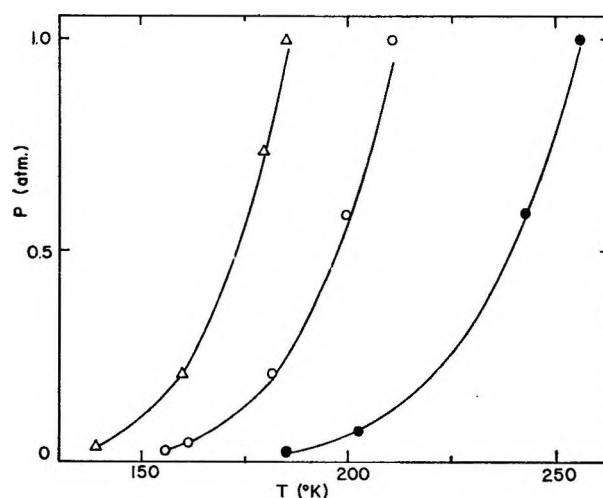


Figure 2. Vapor pressures of the liquids of PH₃, AsH₃, and SbH₃ vs. temperature. The observed values for PH₃ (Δ), AsH₃ (O), and SbH₃ (\bullet) are from ref 7, 8, and 9, respectively. The solid lines represent calculated values.

(d) *Heat Capacity.* Differentiation of the expression for entropy with respect to temperature at con-

(5) S. Chang, H. Park, W. K. Paik, S. H. Park, M. S. Jhon, and W. S. Ahn, *J. Korean Chem. Soc.*, **8**, 33 (1964); M. S. Jhon and S. Chang, *ibid.*, **8**, 85 (1964); W. Paik and S. Chang, *ibid.*, **8**, 29 (1964); W. S. Ahn and S. Chang, *ibid.*, **8**, 125 (1964).

(6) M. S. Jhon, J. Grosh, T. Ree, and H. Eyring, *J. Chem. Phys.*, **44**, 1465 (1966).

(7) "Lange's Handbook of Chemistry," 10th ed, McGraw-Hill Book Co., Inc., New York, N. Y., 1961.

(8) R. H. Sherman and W. F. Giaque, *J. Am. Chem. Soc.*, **77**, 2154 (1955).

(9) A. A. Durrant and T. G. Pearson, *J. Chem. Soc.*, 731 (1934).

(10) D. MacIntosh and B. D. Steele, *Z. Physik. Chem.*, **55**, 129 (1906).

(11) S. Skinner, *Proc. Roy. Soc. (London)*, **42**, 283 (1887).

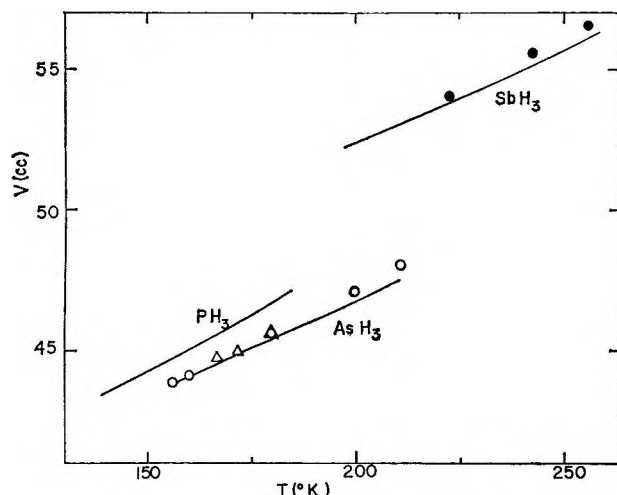


Figure 3. Molar volumes of the liquids of PH_3 , AsH_3 , and SbH_3 vs. temperature: The observed values (Δ) are from ref 10, while the \circ and \bullet are from ref 8 and 9. The solid lines represent calculated values.

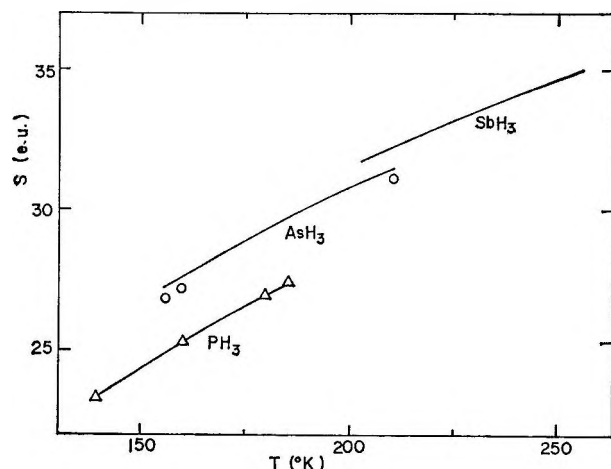


Figure 4. Entropies of the liquids of PH_3 , AsH_3 , and SbH_3 vs. temperature. The experimental data (Δ , \circ) are from ref 4; the solid lines represent calculated values.

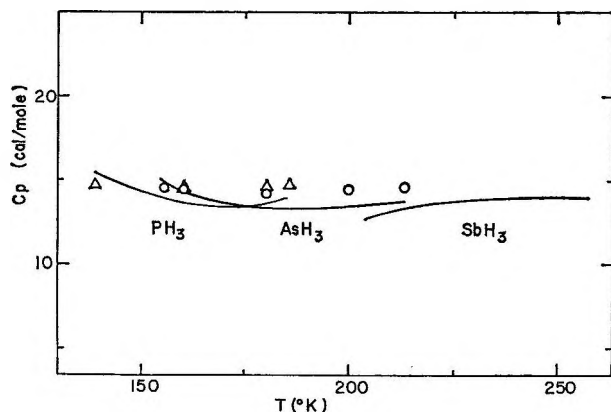


Figure 5. Heat capacities of the liquids of PH_3 , AsH_3 , and SbH_3 vs. temperature. The experimental data (Δ , \circ) are from ref 4; the solid lines represent calculated values.

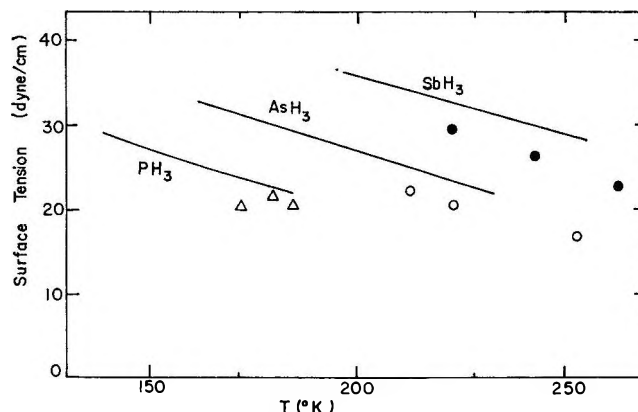


Figure 6. The surface tensions of the liquids of PH_3 , AsH_3 and SbH_3 . The observed values (Δ , \circ , \bullet) are from ref 9; the solid lines represent calculated values.

Table II: Calculated and Observed Critical Constants^a

| | T_c , °K | P_c , atm | V_c , cc |
|----------------|---------------|----------------|---------------|
| PH_3 | | | |
| Calcd | 350.72 | 75.82 | 137.17 |
| Obsd | 327.15 | 64.50 | 155.95 |
| Δ , % | 7.20 | 17.55 | 12.04 |
| AsH_3 | | | |
| Calcd | 420.7 | 139.3 | 89.39 |
| SbH_3 | | | |
| Calcd | 505.15 | 91.05 | 164.45 |

^a The observed critical data for the liquids of AsH_3 and SbH_3 are not available.

stant volume, multiplied by T , yields C_v . This, in turn, can be converted to C_p by the use of the compressibility β and the coefficient of expansion α , both of which can be calculated from the partition function as shown in the equation.

$$C_p = C_v + TV \frac{\alpha^2}{\beta}$$

Figure 5 shows the results obtained. The calculated results give good agreement with observed values.⁴ Thus, our model gives good results even for the heat capacity which involves the second derivative of the partition function.

(e) *Surface Tension.* The method¹² developed here for the calculation of surface tension is an improvement of the method used by Chang, *et al.*¹³ The calculated

(12) J. Grosh, M. S. Jhon, T. Ree, and H. Eyring, to be published.

(13) S. Chang, T. Ree, H. Eyring, and I. Matzer in "Progress in International Research on Thermodynamics and Transport Phenomena," Academic Press, New York, N. Y., 1962, p 88.

results are shown in Figure 6. Again, the calculated results are in good agreement with the observed values.³

Discussion

We next discuss the parameters found in these calculations.

We assumed $n = 12V_s/V_m$ for a close packed structure, V_s and V_m being the solid volume and the liquid volume at the melting point, respectively. The values of θ are expected to be a little less than those in the solid. Even if the force constants k_r were about equal for the hydrides, the θ values would decrease from PH_3 down to SbH_3 , since $\theta = \langle h/2\pi k \rangle (k_r/m)^{1/2}$. This tendency is observed in our values for θ . The values for E_s are expected to increase from PH_3 to SbH_3 as is observed. It is interesting to see that the parametric E_s values are nearly equal to the sum (in calories/mole)⁴ of ΔH (fusion) and ΔH (vaporization): 4359 to 3767 cal for PH_3 and 5098 to 4293 cal for AsH_3 ; the datum for ΔH_f is not available for SbH_3 .

The E_s value³ for liquid ammonia is exceptionally

high. This is due to the hydrogen-bond formation in liquid ammonia.

The values found for a are close to those which would be obtained from the formula¹⁴

$$a = \frac{n - 1}{Z} \frac{1}{Z} \frac{(V_m - V_s)^2}{V_s V_m}$$

where Z is taken to be 12.

The usual calculation³ of surface tension of liquid ammonia deviates from experiment. This was improved by considering the molecular orientation of surface molecules.³ However, for the nonpolar molecules such as PH_3 , AsH_3 , and SbH_3 , the simple model for the surface tension give excellent agreement with the observed values (Figure 6).

Acknowledgments. The authors express their thanks to the National Science Foundation under Grant GP-3698 and the Atomic Energy Commission under Contract No. AT(11-1)-1144 for supporting this work.

(14) T. S. Ree, T. Ree, H. Eyring, and R. Perkins, *J. Phys. Chem.* **69**, 3322 (1965).

A Hydrogen Electrode in Ice^{1a}

by P. N. Krishnan,^{1b} I. Young, and R. E. Salomon

Department of Chemistry, Temple University, Philadelphia, Pennsylvania (Received December 6, 1966)

The preparation and behavior of a hydrogen electrode in ice is reported. In order to compensate for the slow diffusion of hydrogen in ice, powdered platinum was placed on the ice-gaseous hydrogen interface. The cell potential followed the Nernst equation at the temperature of the measurements. The net reaction only involves the transport of hydrogen from the high- to the low-pressure side.

Introduction

The hydrogen electrode is normally regarded as an oxidation-reduction electrode at which equilibrium is established between the electrons in a noble metal, hydrogen ions in an aqueous solution, and dissolved molecular hydrogen.² In practice, the noble metal must serve the role of a catalyst and for this reason, as well as for reasons of its nobility, platinized platinum is used. The solution is saturated with hydrogen by continuous bubbling in the vicinity of the platinum solution interface. The operation of the electrode depends upon the existence of both dissolved hydrogen and hydrogen ions at the platinum solution interface. The extension of the temperature range of this electrode to below the freezing point of the solution would require that fairly rapid transport of hydrogen from every metal-ice interfacial region to the gaseous hydrogen phase could occur. Such a transport could in principle take place either through the ice or through the platinum; however, the rates of diffusion would be too low to be of use.^{3,4} Platinum and palladium electrodes can be frozen into ice and in various forms are used as ohmic contacts for conductivity measurements.⁵⁻⁸ The potential difference between a pair of these electrodes in the same piece of ice is at the mercy of the accidental difference in hydrogen concentrations in them. A potential of the order of 10 mv is almost always found to exist between two apparently identical platinum wires when they are frozen into the same sample of pure or electrolyte-doped ice. Simple metallic electrodes cannot be used, therefore, in any potential measurements in ice involving a few millivolts. For instance, the results of measurements of thermogalvanic potentials in ice using brass electrodes⁹ now appear to be

in doubt.¹⁰ It was therefore of interest to develop a thermodynamically reversible electrode for use in ice. In the absence of a known reversible electrode, which could be used as a reference, it was necessary to prepare two such electrodes and place them in the same sample and then to compare the experimental potential difference with that predicted by theory. Since protons are the only mobile species in pure and impure ice,^{11,12} the obvious electrode to use is a hydrogen electrode. The major experimental problem to be solved was the development of a method whereby gaseous hydrogen can enter and leave every region separating metal and ice. In order to achieve this end, it is necessary to keep the diffusion path as small a value as possible. It was found that precooled fine platinum powder,

(1) (a) This work was supported by the Office of Saline Water, U. S. Department of the Interior. (b) This research is part of a dissertation to be submitted to the Temple University Graduate Board in partial fulfillment of the requirements for the degree of Doctor of Philosophy.

(2) J. G. David and G. J. Janz, "Reference Electrodes—Theory and Practice," Academic Press, New York, N. Y., and London, 1961, p 71.

(3) W. Kuhn and M. Thurkau, *Helv. Chim. Acta*, **41**, 938 (1958).

(4) R. M. Barrer, "Diffusion In and Through Solids," The Macmillan Co., New York, N. Y., 1941, p 168.

(5) R. S. Bradley, *Trans. Faraday Soc.*, **53**, 687 (1957).

(6) G. W. Gross, private communication.

(7) H. Engelhardt, Ph.D. Thesis, Physics Department, Technische-Hochschule, Munich, Germany, 1965.

(8) J. H. L. Johnstone, *Proc. Trans. Nova Scotian Inst.*, **13**, 126 (1912).

(9) J. Latham and B. J. Mason, *Proc. Roy. Soc. (London)*, **A260**, 523 (1963).

(10) G. W. Gross, *J. Geophys. Res.*, **70**, 2291 (1965).

(11) J. C. Decroloy, H. Granicher, and C. Jaccard, *Helv. Phys. Acta*, **30**, 465 (1957).

(12) E. J. Workman, F. H. Truby, and W. Drost-Hansen, *Phys. Rev.*, **94**, 1073 (1954).

sprinkled on the surface, was suitable in this regard. The largest diffusion path required would have a length of the order of the grain circumference. The powder would be kept in equilibrium with a controlled pressure of hydrogen.

Experimental Section

The 10^{-4} M NaCl solutions were placed in the U tube shown in Figure 1 and boiled under reduced pressure for several minutes to remove dissolved air. The tube was closed off and the bottom tip was placed in a Dry Ice-acetone bath for the purpose of seeding. The seeded tip was placed in a constant-temperature bath maintained at -6° . The bath level was slowly raised (4 mm/hr) by the dropwise addition of coolant from an external reservoir. In this manner a flat surface was maintained during the entire growth period and the resultant sample was free of gross flaws and was found, by observation through crossed polaroids, to be strain free. Powdered platinum black (99.98% pure, with an average particle size of 15μ , supplied by the J. Bishop Co.) which was precooled to -6° was sprinkled on the surface to a height of about 2.5 mm. A broom of fine platinum wires, spot-welded to a heavy platinum wire, made contact to the powder. The heavy wires were sealed into side arms and brought to the outside where they were connected to a Cary Model 31 vibrating reed electrometer. The U tube was surrounded by a grounded concentric copper tube for purposes of shielding. All leads were shielded. Two plastic plugs with small openings which were kept above the platinum-ice interface helped to reduce convection.

Both sides of the tube were evacuated and the stopcocks were closed. The tube was then slowly brought to -10° and kept at that temperature for several days. During this time the potential difference varied erratically. When hydrogen at 1 atm pressure was introduced into both sides of the tube the potential difference reached zero after a period of about 30 min. When one side arm was maintained at a fixed pressure and the pressure of the other varied, the potential responded sluggishly and reached a steady value after a 30-min period. The results obtained in a typical run are given in Table I. Attempts to study the temperature dependence of the cell potential were limited by the contraction of the sample and the subsequent leakage of hydrogen along the tube walls.

Discussion

The electrode system described differs from one in which two hydrogen electrodes are immersed in an aqueous liquid electrolyte in one important respect.

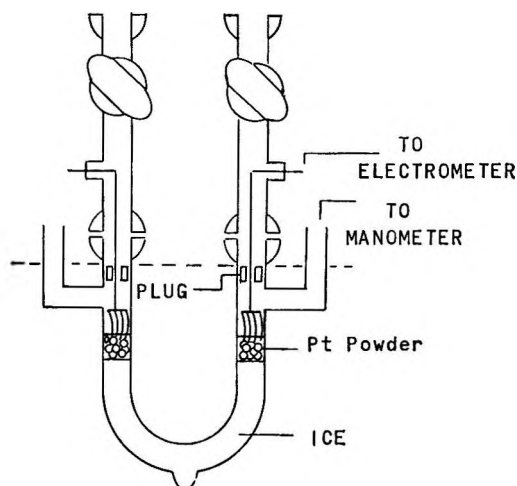


Figure 1. Diagram of the cell.

Table I: Potential of the Cell at Various Hydrogen Pressures

| Pressure (P_1), cm | Pressure (P_2), cm | $\log (P_1/P_2)$ | Potential, calcd | Potential, obsd |
|------------------------|------------------------|------------------|------------------|-----------------|
| 77.0 | 12.5 | 0.7896 | 20.64 | 20 |
| 77.0 | 17.6 | 0.6410 | 16.6 | 16 |
| 77.0 | 31.2 | 0.3924 | 9.2 | 12 |
| 77.0 | 72.0 | 0.0290 | 0.78 | 2 |
| 9.8 | 77.2 | 0.8964 | -23.4 | -24 |
| 21.9 | 77.2 | 0.5472 | -14.3 | -15 |
| 62.2 | 77.2 | 0.0938 | -2.43 | -6 |
| 77.0 ^a | 4.1 | 1.2737 | 33.0 | 30 |
| 77.0 ^a | 30.2 | 0.4065 | 10.6 | 10 |

^a Repeated using the same system.

In both pure and doped ice the current is carried entirely by protons and the passage of 1 f of charge results in the transport of 1 equiv of hydrogen without any other changes in the ice. Hence, corrections for liquid junction potentials are not required even if significant concentration gradients exist across the ice sample. Unlike its relative in aqueous solution, whose potential can be varied by varying the hydrogen ion activity, the ice-hydrogen electrode potential depends only on the hydrogen pressure (and, of course, the temperature). In the fourth column of Table I, the potential of the cell calculated on the basis of the Nernst equation is given. In spite of a precision which was limited to about 1 mv, the agreement between theoretical and experimental cell potentials is fairly good. The cell resistance was quite high and was found to be due to the intergranular resistance of the platinum powder. This high resistance (typically of the order of 10^8 ohms) limited the precision with which the measurements could be carried out.

A factor which may be of significance in the operation of this cell is the liquid-like layers purported to exist on an ice interface at temperatures below 0°. These films of water on ice have often been invoked to explain the phenomena of regelation and would be expected to enhance the transport of hydrogen to every interfacial region. These same layers may be responsible in some

measure for the spurious potentials observed when various electrodes are frozen into ice.

The electrode described should be of use in the measurement of thermogalvanic potentials in ice. The results of this investigation are in accord with the position that protons are the only mobile carriers in ice.

(13) W. A. Weyl, *J. Colloid Sci.*, **6**, 389 (1951).

Further Studies on the Decarboxylation of Oxalic Acid in Polar Solvents

by Louis Watts Clark

Department of Chemistry, Western Carolina College, Cullowhee, North Carolina (Received December 6, 1965)

Rate constants and activation parameters are reported for the decarboxylation of oxalic acid in propylene glycol, 1,4-butanediol, and 2,3-butanediol. The results of this investigation are compared with previous data on the reaction in seven additional solvents, as well as in the vapor phase. Inductive and steric effects of the various solvents are discussed.

In the past, kinetic studies have been carried out on the decarboxylation of oxalic acid in at least 15 nonaqueous solvents. These include dioxane,¹ glycerol,² dimethyl sulfoxide, triethyl phosphate, aniline, N-methylaniline, N,N-dimethylaniline, quinoline,³ 6-methylquinoline, 8-methylquinoline,⁴ *o*-cresol, *m*-cresol, *p*-cresol, ethylene glycol, and 1,3-butanediol.⁵ Recently, Haleem and Yankwich have repeated the experiments using the solvent glycerol.⁶ Lapidus, Barton, and Yankwich have also studied the decarboxylation of oxalic acid in the vapor phase and have proposed a unimolecular mechanism for the reaction.⁷

In an effort to gain a better understanding of the mechanism and energetics of this reaction, further experimentation has been carried out in this laboratory on the decarboxylation of oxalic acid in three additional polar solvents, propylene glycol, 1,4-butanediol, and 2,3-butanediol. A comparison of the results of this investigation (reported herein) with previous data sheds light on the mechanism of the reaction and leads to a better understanding of other heterolytic reactions.

Experimental Section

Reagents. (1) Anhydrous oxalic acid, reagent grade, 100.0% assay, was used in this research. To ensure perfect dryness it was stored in a desiccator containing sulfuric acid. (2) The solvents were highest purity quality and were redistilled at atmospheric pressure directly into the dried reaction flask immediately before the beginning of each decarboxylation experiment.

Apparatus and Technique. The details of the apparatus and technique used in this research have been described previously.⁸ In these experiments, a sample

(1) A. Dinglinger and E. Schröder, *Z. Physik. Chem.*, **A179**, 401 (1937).

(2) L. W. Clark, *J. Am. Chem. Soc.*, **77**, 6191 (1955).

(3) L. W. Clark, *J. Phys. Chem.*, **61**, 699 (1957).

(4) L. W. Clark, *ibid.*, **62**, 633 (1958).

(5) L. W. Clark, *ibid.*, **67**, 1255 (1963).

(6) M. A. Haleem and P. E. Yankwich, *ibid.*, **69**, 1729 (1965).

(7) G. Lapidus, D. Barton, and P. E. Yankwich, *ibid.*, **68**, 1863 (1964).

of oxalic acid weighing 0.1618 g (corresponding to 40.0 ml of CO₂ at STP on complete reaction, based upon the actual molar volume of CO₂ at STP, 22,264 ml) was weighed into a fragile glass capsule weighing approximately 0.1 g and blown from 7-mm soft glass tubing. The course of the reaction was followed by measuring the volume of CO₂ evolved at atmospheric pressure and at the temperature of a water-jacketed buret. The buret was calibrated by the National Bureau of Standards at 20.0°. Water maintained at 20.0 ± 0.05° by means of a cooling coil and an electronic relay was circulated through the water jacket during the experiment. The temperature of the oil bath was controlled to within ±0.005° using a completely transistorized temperature control unit equipped with a sensitive thermistor probe. A thermometer which also had been calibrated by the National Bureau of Standards was used to read the temperature of the oil bath. Appropriate corrections and calibrations were carefully applied to this thermometer in order to reduce errors in temperature readings to a minimum. About 60.0 g of solvent, saturated with dry CO₂ gas, was used in each experiment.

Results

Decarboxylation experiments were carried out in each solvent at four different temperatures over about a 30° range. The experiments were repeated two or three times at each temperature. In the case of each of the solvents the log ($V_{\infty} - V_t$) was a linear function of time over about the first 80% of the reaction. The average rate constants, calculated in the usual manner from the slopes of the experimental logarithmic plots, are brought together in Table I. The parameters of the absolute reaction rate equation⁹

$$k = \frac{\kappa T}{h} e^{-\Delta H^*/RT} e^{\Delta S^*/R}$$

based upon the data in Table I, are shown in Table II, along with previously published data which are pertinent to the discussion.

Discussion

A comparison of the activation parameters for the decarboxylation of oxalic acid vapor and the decarboxylation of oxanilic acid melt (lines 1 and 2 of Table II) reveals that the smaller molecule (oxalic acid) has the *lower* entropy of activation. Since an increase in molecular complexity is generally accompanied by a decrease in the entropy of activation,¹⁰ we would have expected the decarboxylation of oxalic acid to have a *higher* entropy of activation than that of oxanilic acid. This inversion, however, finds a ready

Table I: Apparent First-Order Rate Constants for the Decarboxylation of Oxalic Acid in Several Solvents

| Solvent | Temp, °C (cor) | $k \times 10^4$ (av), sec ⁻¹ |
|------------------|-------------------|--|
| Propylene glycol | 118.38 | 2.67 |
| | 128.75 | 3.97 |
| | 137.64 | 5.35 |
| | 148.65 | 7.68 |
| 2,3-Butanediol | 130.30 | 1.81 |
| | 138.51 | 3.26 |
| | 149.85 | 7.03 |
| | 160.17 | 13.64 |
| 1,4-Butanediol | 139.56 | 0.96 |
| | 152.93 | 2.62 |
| | 160.03 | 4.71 |
| | 169.48 | 8.43 |

Table II: Activation Parameters for the Decarboxylation of Oxalic Acid and Related Acids Alone and in Several Solvents

| System | ΔH^* , kcal/ mole | ΔS^* , eu/ mole |
|--|---------------------------------|-------------------------------|
| 1. Oxanilic acid (melt) ^a | 40.1 | 21.4 |
| 2. Oxalic acid (vapor) ^b | 29.2 | -6.6 |
| 3. Oxalic acid in glycerol ^c | 27.6 | -4.9 |
| 4. Oxalic acid in glycerol ^d | 26.4 | -7.8 |
| 5. Oxalic acid in ethylene glycol ^e | 17.6 | -30.0 |
| 6. Oxalic acid in propylene glycol ^f | 10.3 | -49.1 |
| 7. Oxalic acid in quinoline ^g | 38.9 | 15.75 |
| 8. Oxalic acid in 1,4-butanediol ^f | 25.5 | -15.8 |
| 9. Oxalic acid in dimethyl sulfoxide ^g | 40.6 | 20.7 |
| 10. Oxalic acid in 1,3-butanediol ^g | 29.3 | -4.9 |
| 11. Oxalic acid in triethyl phosphate ^g | 28.85 | -5.8 |
| 12. Oxalic acid in 2,3-butanediol ^f | 22.63 | -20.2 |

^a L. W. Clark, *J. Phys. Chem.*, **66**, 1543 (1962). ^b See ref 6. ^c See ref 6. ^d See ref 2. ^e See ref 5. ^f Present research, based on Table I. ^g See ref 3.

explanation in the fact that dicarboxylic acids tend to associate past the dimer stage.¹¹ The polymerization of oxalic acid could conceivably yield a larger entity for taking part in the rate determining step than would the dimerization of oxanilic acid. The higher enthalpy of activation in the case of the decarboxylation of oxanilic acid may be explained on the basis of the

(8) L. W. Clark, *J. Phys. Chem.*, **60**, 1150 (1956).

(9) S. Glasstone, K. J. Laidler, and H. Eyring, "The Theory of Rate Processes," McGraw-Hill Book Co., Inc., New York, N. Y., 1941, p 14.

(10) L. P. Hammett, "Physical Organic Chemistry," McGraw-Hill Book Co., New York, N. Y., 1940, p 126.

(11) W. Hückel, "Theoretical Principles of Organic Chemistry," Vol. II, Elsevier Publishing Co., New York, N. Y., 1958, p 329.

+*E* effect exerted by the unshared pair of electrons on the nitrogen atom which would tend to neutralize the effective positive charge on the carbonyl carbon atom of the anilide.

The decarboxylations of oxalic acid in ethylene glycol and in propylene glycol (lines 4 and 5 of Table II) are accompanied by very large negative entropies of activation which may no doubt be attributed to extensive polymerization of these two solvents. The decrease in ΔH^* and in ΔS^* on going from ethylene glycol to propylene glycol may be explained on the basis of the inductive and steric effects of the methyl group in propylene glycol. One would naturally expect that the presence of two methyl groups on opposite sides of the glycol (as in 2,3-butanediol) would further accentuate these effects and result in lowering still more the enthalpy and entropy of activation of the reaction. Actually, however, it is found that both the enthalpy and entropy of activation for the reaction in 2,3-butanediol are *higher* than they are in either ethylene glycol or propylene glycol (line 12 of Table II). When the two hydroxyl groups are separated by one or two carbon atoms, as in 1,3-butanediol (line 10) and 1,4-butanediol (line 8), the enthalpy as well as the entropy of activation of the oxalic acid reaction are larger than they are in those compounds in which the two hydroxyl groups are located on adjacent carbon atoms (ethylene glycol, propylene glycol, and 2,3-butanediol—lines 4, 5, and 12 of Table II).

These anomalous results find a ready explanation when it is observed that the various systems shown in Table II are actually representatives of four different reaction series: (1) the decarboxylation of oxalic acid (vapor) and oxanilic acid (melt) (a derivative of oxalic acid); (2) the decarboxylation of oxalic acid in the related solvents glycerol, ethylene glycol, and propylene glycol; (3) the decarboxylation of oxalic acid in quinoline and in 1,4-butanediol; (4) the decarboxylation of oxalic acid in dimethyl sulfoxide, triethyl phosphate, 1,3-butanediol, and 2,3-butanediol. Plots of enthalpy vs. entropy of activation for these four reaction series are shown in Figure 1.

Line III of Figure 1 combines the two reaction series: (1) the decarboxylation of oxalic acid (vapor) and oxanilic acid (melt), and (2) the decarboxylation of oxalic acid in the related solvents glycerol, ethylene glycol, and propylene glycol. The enthalpy of activation axis for the first series has been shifted purposely in such a manner as to superimpose it upon the second series. This device helps to point out the interesting fact that the two lines connecting the parameters have very nearly equal slopes. (It is often found in kinetic studies that a change in the structure of reactant or

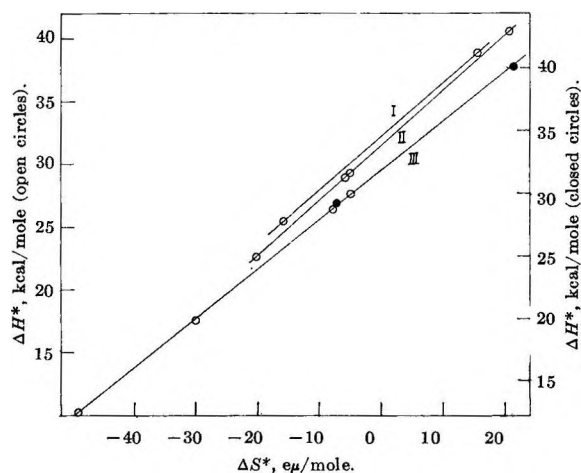


Figure 1. Enthalpy vs. entropy of activation plots for the decarboxylation of oxalic acid and related compounds: line I, oxalic acid in 1,4-butanediol and in quinoline; line II, oxalic acid in 1,3-butanediol, 2,3-butanediol, triethyl phosphate, and dimethyl sulfoxide; line III (open circles), oxalic acid in glycerol (two sets of data), in ethylene glycol, and in propylene glycol; (closed circles), oxalic acid (vapor) and oxanilic acid (melt).

solvent results in the formation of a second line parallel to the original line.¹²) The slope of this line is 393°K or 120°C. This is the so-called isokinetic temperature of the reaction series,¹³ *i.e.*, the temperature at which the rate constants for all the reactions conforming to the line are equal. The intercept of the isokinetic temperature line on the zero entropy of activation axis yields ΔF° , the free energy of activation at the isokinetic temperature of all the reactions conforming to the line.¹² Substitution of this value in the absolute reaction rate equation⁹ enables the rate of reaction at the isokinetic temperature to be calculated. For the decarboxylation of oxalic acid and its derivative in the absence of solvent ΔF° is found to be 31.8 kcal/mole. For that of oxalic acid in glycerol and the two glycols ΔF° is 29.5 kcal/mole. The respective calculated rate constants at 120° in sec⁻¹ for these two reaction series turn out to be 0.000017 and 0.000324. In other words, at 120°, oxalic acid would react nineteen times as fast in glycerol and the glycols as it would in the absence of solvent. Glycerol and the glycols thus *lower the free energy of activation at the isokinetic temperature* for the decarboxylation of oxalic acid.

The decrease in ΔS^* for the decarboxylation of oxalic acid from 15.75 eu/mole in quinoline to -15.8 eu/mole

(12) J. Leffler, *J. Org. Chem.*, **20**, 1202 (1955).

(13) S. L. Freiss, E. S. Lewis, and A. Weissberger, Ed., "Technique of Organic Chemistry," Vol. VIII, Part I, "Investigations of Rates and Mechanisms of Reactions," 2nd ed, Interscience Publishers, Inc., New York, N. Y., 1961, p 207.

in 1,4-butanediol (lines 7 and 8 in Table II) points to the extensive linear polymerization of the diol. The $\Delta H^* - \Delta S^*$ plot for the decarboxylation of oxalic acid in these two solvents has a slope of 423°K or 150°C (line I of Figure 1).

The large positive entropy of activation for the decarboxylation of oxalic acid in dimethyl sulfoxide (line 9 of Table II) may be attributed to the simplicity of the solvent molecule and its lack of association in the absence of hydrogen bonding. The negative entropy of activation for the reaction in triethyl phosphate (line 11) may be attributed to the steric effect of the three methyl groups. Similarly, the decrease in the entropy of activation on going from 1,3-butanediol (line 10) to 2,3-butanediol (line 12) may be attributed to the greater steric hindrance to the reaction in the latter diol due to the presence of the two methyl groups flanking the nucleophilic center. A plot of enthalpy of activation *vs.* entropy of activation for the decarboxylation of oxalic acid in these four solvents (line II of Figure 1) has a slope of 438°K or 165°C.

The problem of the validity of an observed linear enthalpy-entropy of activation relationship has been critically analyzed by Petersen, *et al.*¹⁴ They have shown that (because of experimental error) the range of ΔH^* values for a given reaction series must be much greater than twice the maximum possible error in ΔH^* before any assurance as to the validity of the relationship can be entertained. The maximum possible error in ΔH^* can be calculated by means of the equation

$$\delta = 2R \frac{T'T}{T' - T} \alpha \quad (1)$$

where δ is the maximum possible error in ΔH^* (in the positive direction), R is the gas constant, T' and T are the upper and lower temperature limits respectively, and α is the maximum fractional error in the rate constant. For purposes of discussion we may take as a typical system in the present research the decarboxylation of oxalic acid in 2,3-butanediol (Table I). If we assume a maximum fractional error in the rate constant of 0.05, δ (according to eq 1) is found to be 1.14 kcal/mole and 2δ is thus 2.28 kcal/mole. In Table III are shown the range of ΔH^* values for each of the four reaction series shown in Table II, and the ratio $d\Delta H^*/2\delta$ in each case. The fact that this ratio is much greater than unity for each series inspires considerable confidence in the validity of the observed linear relationships shown in Figure 1.

It is interesting to note that several other reaction series have been reported previously having the same isokinetic temperatures as those found in this research

Table III: Validity Tests of Several Linear $\Delta H^* - \Delta S^*$ Plots According to Petersen, *et al.*¹⁴

| Reaction series | $d\Delta H^*$, kcal/ mole | 2δ , kcal/ mole | $d\Delta H^*/$ 2δ | Figure 1 ref |
|-------------------------------------|----------------------------------|------------------------------|-----------------------------|-----------------|
| 1. Oxalic acid (vapor) | 11.9 | 2.28 | 5.2 | Line III |
| 2. Oxalic acid + glycerol | 17.3 | 2.28 | 7.6 | Line III |
| 3. Oxalic acid + quinoline | 13.4 | 2.28 | 5.9 | Line I |
| 4. Oxalic acid + dimethyl sulfoxide | 17.0 | 2.28 | 7.4 | Line II |

Table IV: Isokinetic Temperatures of Several Reaction Series—Decarboxylation Reactions

| System | Isokinetic temp | |
|---|-----------------|-----|
| | °K | °C |
| Cinnamalmalonic acid in cresols ^a | 468 | 195 |
| | 453 | 180 |
| Oxalic acid in dimethyl sulfoxide, etc. ^b | 438 | 165 |
| Malonic acid in nitro compounds ^c | | |
| Oxalic acid in quinoline, etc. ^b | 423 | 150 |
| Benzylmalonic acid in quinoline, etc. ^d | | |
| Malonanilic acid in quinoline, etc. ^c | | |
| Oxalic acid in various solvents ^f | | |
| β -Resorcylic acid in various solvents ^g | | |
| Malonic acid in acids ^h | | |
| Picolinic acid in various solvents ⁱ | | |
| | 408 | 135 |
| Oxalic acid and oxanilic acid along ^j | 393 | 120 |
| Oxalic acid in glycerol, etc. ^b | | |
| Benzylmalonic acid in acids, cresols ^a | | |
| Malonanilic acid in acids, cresols ^c | | |
| Benzylmalonic acid in aniline derivatives ^d | 378 | 105 |
| Malonanilic acid in aniline derivatives ^e | | |

^a L. W. Clark, *J. Phys. Chem.*, **67**, 1481 (1963). ^b This research. ^c L. W. Clark, *J. Phys. Chem.*, **62**, 368 (1958). ^d L. W. Clark, *ibid.*, **70**, 627 (1966). ^e L. W. Clark, *ibid.*, **68**, 2150 (1964). ^f L. W. Clark, *ibid.*, **66**, 1543 (1962). ^g L. W. Clark, *ibid.*, **67**, 2831 (1963). ^h L. W. Clark, *ibid.*, **68**, 3048 (1964). ⁱ L. W. Clark, *ibid.*, **69**, 2277 (1965). ^j See ref 7 and L. W. Clark, *ibid.*, **66**, 1543 (1962).

(see Table IV). The sixteen different reaction series listed in Table IV yield five isokinetic temperatures separated from one another by 15° intervals. In general, the higher isokinetic temperatures are associated with stronger mutual attractions between the electrophile-nucleophile pairs.

Acknowledgment. Acknowledgment is made to the Donors of the Petroleum Research Fund, administered by the American Chemical Society, for support of this research.

(14) R. C. Petersen, J. H. Markgraf, and S. D. Ross, *J. Am. Chem. Soc.*, **83**, 3819 (1961).

Short-Range Order in Fused Salts. I. Coordination States of Nickel(II) in Molten Zinc Chloride-Potassium Chloride Mixtures¹

by C. A. Angell and D. M. Gruen

Chemistry Division, Argonne National Laboratory, Argonne, Illinois (Received December 6, 1965)

Absorption spectra of Ni(II) in molten KCl-ZnCl₂ mixtures have been obtained as a function of temperature and of melt composition in the range 4000-40,000 cm⁻¹. Spectra have been obtained over the entire composition range from pure liquid ZnCl₂ to pure liquid KCl. The extremes in the temperature range studied were 250 to 900°. Observed spectral changes have been interpreted to indicate the existence of (a) a two-species equilibrium involving Ni(II) in octahedral and distorted tetrahedral sites, and (b) transformation by a continuous distortion mechanism of an octahedral Ni(II) species to a highly distorted tetrahedral species. The effect of Cl⁻ polarization by Zn(II) and of volume changes on the coordination behavior of Ni(II) is discussed. A simple technique for handling and weighing small samples of highly hygroscopic materials is described.

Introduction

The elucidation of short-range order in fused salts on the basis of 3d-ion absorption spectra has been discussed in previous publications.^{2,3} It is well known that the visible absorption spectra of these ions are strongly dependent on the ligand field in which they find themselves. Since the ligand field is determined to a good first approximation by the number and configuration of the nearest neighbor anions, the spectra observed in a given melt can provide detailed information on the coordination state of a 3d ion and can reveal the dependence of this state on the properties of the solvent. The present study will show in detail how the absorption spectrum of Ni(II) is affected by the forces determining the short-range order in ionic melts and the means by which changes in the local order can be brought about.

Spectral studies have shown^{2,3} that, in alkali chloride melts at high temperatures, the divalent 3d ions are surrounded by four chloride ions in tetrahedral or distorted tetrahedral symmetry, while in the molecular Al₂Cl₆ melt the 3d ions are octahedrally coordinated. Of particular interest are certain intermediate situations observed, for example, in the LiCl-KCl eutectic in the range 400-700° where temperature-dependent equilibria involving both tetrahedral and octahedral coordination states of a number of 3d ions

have been shown to occur.² The importance of solvent composition has been illustrated by studies in AlCl₃-KCl melts, where profound changes in coordination take place over relatively small ranges of composition.³

In order to obtain more detailed information on the various factors influencing coordination changes, we have sought other fused salt solvents in which effects due to temperature and composition could be systematically investigated.

Our previous work has resulted in the recognition of the strong dependence of the coordination behavior of the 3d ions on the polarizing power of the melt cations. This suggests that one might vary the polarizing power in a controlled fashion in order to influence the energetics of coordination number changes. In particular, it would appear that the conditions for the concurrent existence of four- and six-coordinated 3d ion species in measurable concentrations are most readily fulfilled in melts whose cation charge-to-radius ratios, z_+/r_+ , are intermediate between those of alkali ions, such as K(I) with $z_+/r_+ = 0.8$ and Al(III) with $z_+/r_+ = 6.0$. Thus, MgCl₂ ($z_+/r_+ = 3.2$), ZnCl₂ ($z_+/r_+ = 2.7$), or

(1) Based on work performed under the auspices of the U. S. Atomic Energy Commission.

(2) D. M. Gruen and R. L. McBeth, *Pure Appl. Chem.*, **6**, 23 (1963).

(3) H. A. Øye and D. M. Gruen, *Inorg. Chem.*, **4**, 1173 (1965).

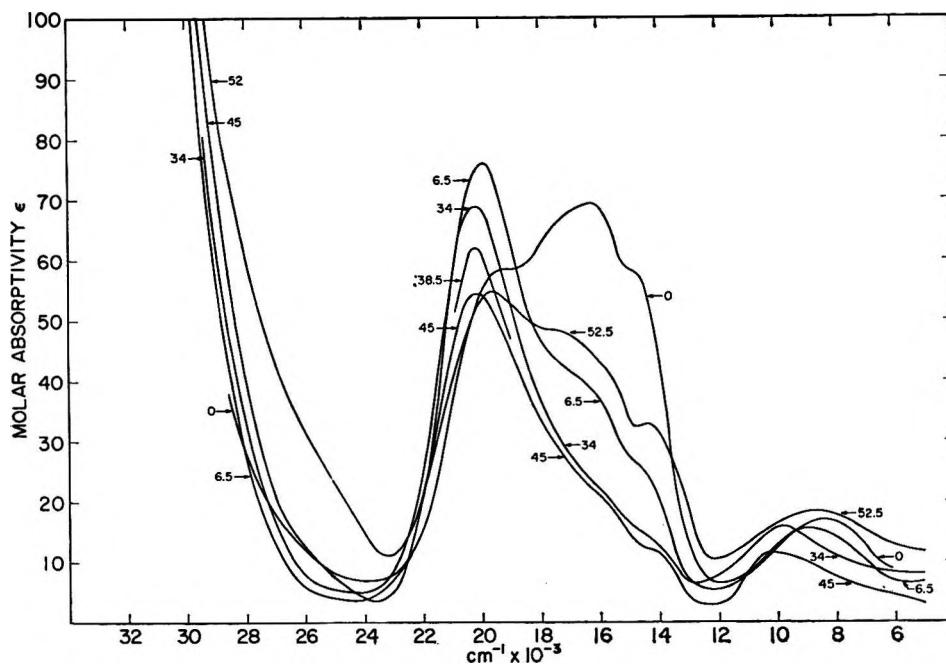


Figure 1. Spectra of Ni(II) in KCl-ZnCl₂ melts at 320°. KCl contents are given in mole per cent.

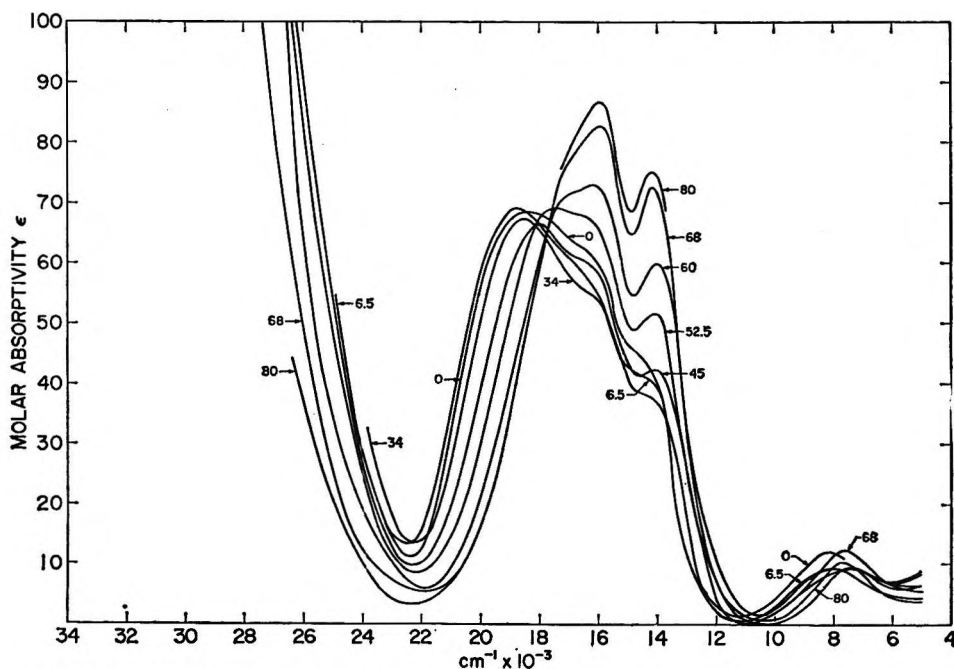


Figure 2. Spectra of Ni(II) in KCl-ZnCl melts at 700°. KCl contents are given in mole per cent.

the divalent transition metal chlorides themselves ($z_+/r_+ = 2.7-2.4$) would appear to be suitable components in binary solvent systems with either AlCl₃ or KCl as the second component. Of these, ZnCl₂ is of interest since many binary systems involving ZnCl₂ have unusually low liquidus temperatures. Such systems therefore offer wide temperature intervals

as well as suitable ranges of solvent cation potentials for study.

For the purposes of the present investigation, the Ni(II) ion is particularly advantageous since the energy separations between absorption bands in octahedral and tetrahedral crystal fields are large enough to prevent extensive overlapping. As will be seen, this

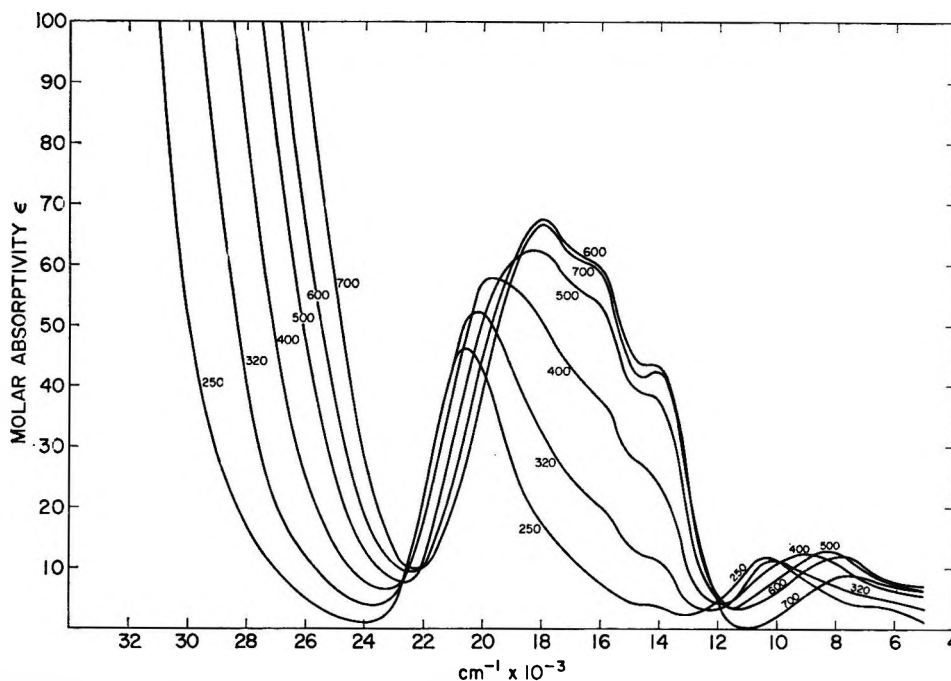


Figure 3. Spectra of Ni(II) in 45.3 mole % KCl-54.7 mole % ZnCl₂ melt as a function of temperature in the range 250-700°.

circumstance enables one to draw important distinctions concerning the manner in which the Ni(II) configuration changes in the ZnCl₂-KCl system chosen for the present study.

Results

Spectra of Ni(II) in the ZnCl₂-KCl system are shown as a function of composition in Figures 1 and 2 and as a function of temperature at fixed compositions (45.3, 52.5, and 58 mole % KCl) in Figures 3-5. Spectra at 34, 60, 68, 80, and 90 mole % KCl have also been studied as a function of temperature and will be referred to in the Discussion section. The spectra given in Figures 1-5 were selected because they best illustrate the important features encountered in this system. Measurements at 320° (Figure 1) and at 700° (Figure 2) show that the spectra of Ni(II) in molten ZnCl₂-KCl depend in a complicated way both on the composition and temperature of the solvent. For example, in going from pure ZnCl₂ to ~6.5 mole % KCl, pronounced spectral changes occur at the fixed temperature of 320°. Presumably, the structure of pure liquid ZnCl₂ changes drastically on addition of small amounts of KCl, and these changes are reflected in the Ni(II) spectrum. A detailed discussion of the spectra in this composition range will be given in a subsequent paper. The spectral changes observed at 320° on further addition of KCl (up to 45 mole %) can be described as due primarily to a reduction in the intensity of the 6.5 mole % spectrum. At still higher

KCl contents (52.5 mole %), the spectrum shifts to lower energies and the oscillator strength increases.

On the other hand, the spectrum of Ni(II) in liquid ZnCl₂ at 700° (curve marked 0 in Figure 2) is affected only to a minor extent by KCl additions up to 45 mole %. These observations are in accord with other evidence^{4,5} which shows that ZnCl₂ is much less associated at 700° than at 320°.

Comparisons of 320 and 700° spectra at fixed compositions reveal the pronounced effect of temperature on the energies and intensities of the absorption maxima. Temperature effects are presented in greater detail in Figures 3-5 for the fixed compositions 45.3, 52.5, and 58.0 mole % KCl.

The spectra at fixed compositions can be divided into two classes. The first class extends over the composition range 0 to about 50 mole % KCl. Isosbestic points are absent from this class of spectra as shown by the 45.3 mole % KCl composition (Figure 3). The spectra shift to lower energies with increasing temperature. However, the intensities may increase or decrease with temperature depending on composition. (Compare Figures 1 and 2.)

The second class of spectra which can be studied over the composition range 52-58 mole % KCl is exemplified by the 52.5 and 58 mole % compositions

(4) F. R. Duke and R. A. Fleming, *J. Electrochem. Soc.*, **104**, 251 (1957).

(5) D. E. Irish and T. F. Young, *J. Chem. Phys.*, **43**, 1766 (1965).

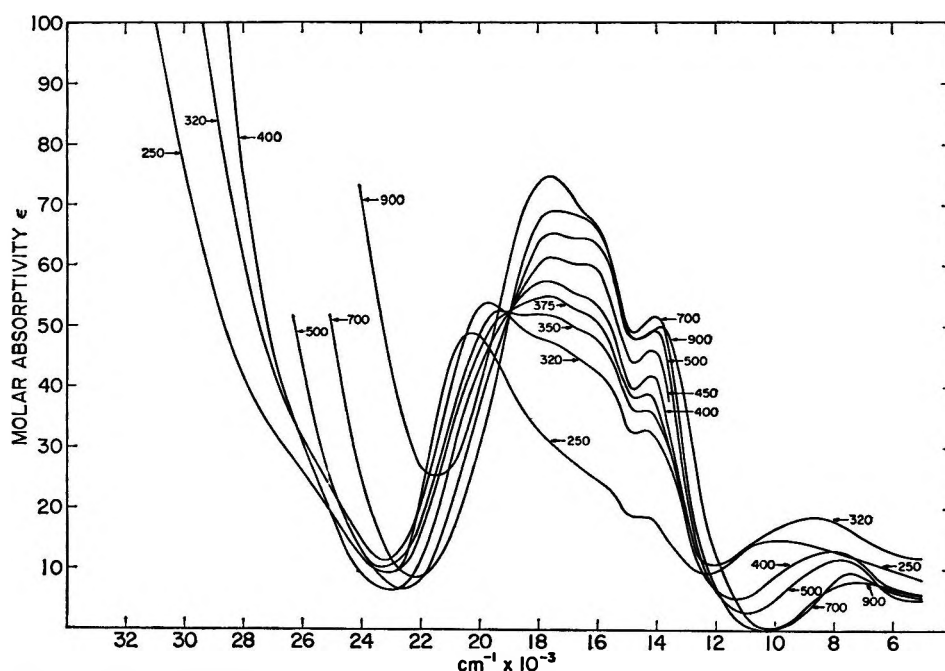


Figure 4. Spectra of Ni(II) in 52.5 mole % KCl-47.5 mole % ZnCl₂ melt as a function of temperature in the range 250-900°.

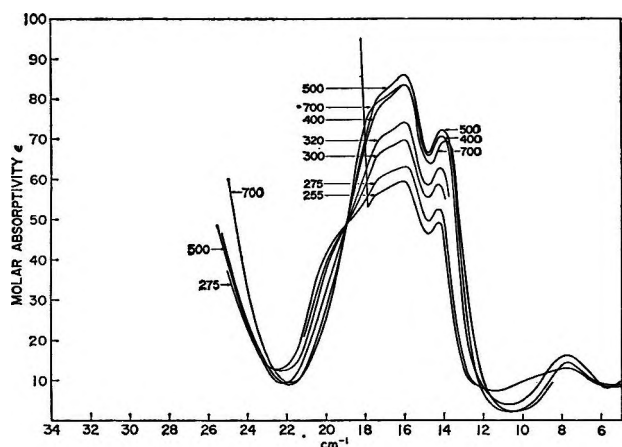


Figure 5. Spectra of Ni(II) in 58 mole % KCl-42 mole % ZnCl₂ melt as a function of temperature in the range 255-700°.

shown in Figures 4 and 5, respectively. These spectra are characterized by the presence of an isosbestic point for each composition. With increasing temperature, the absorption maxima decrease in energy while increasing in intensity.

The 250-400° temperature region in which many of the spectral changes described in the foregoing paragraphs occurred is not available for study at compositions with KCl contents greater than ~58 mole %. This is due to the increase in the liquidus temperature as shown in Figure 6, which gives the KCl-ZnCl₂ phase diagram determined by Shatilo and Ugai.⁶

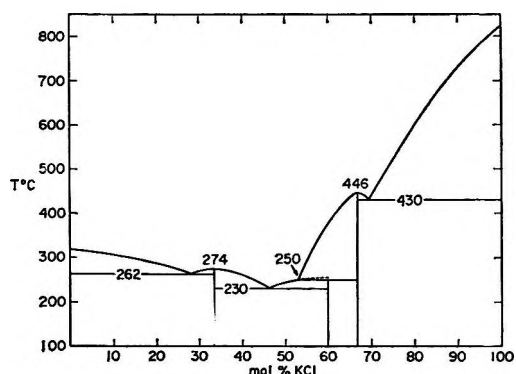


Figure 6. Phase diagram for the KCl-ZnCl₂ binary system.

At the higher temperatures accessible to measurement in the 60-100 mole % KCl region, the effects of temperature on the spectra are not very pronounced. Furthermore, the appearances of the spectra do not alter greatly with composition in the range 60-100 mole % KCl.

Discussion

Two of the spectral types seen in Figures 1-5 have been identified in previous work² on crystals of known structure as due to Ni(II) ions in either octahedral or tetrahedral chloride ion environments. In Figure 7, the spectra of Ni(II) in molten 68.4% KCl-31.6% ZnCl₂ at 550° (curve 1b) and in molten 45.3% KCl-

(6) V. A. Shatilo and Y'a A. Ugai, *Zh. Fiz. Khim.*, **23**, 744 (1949).

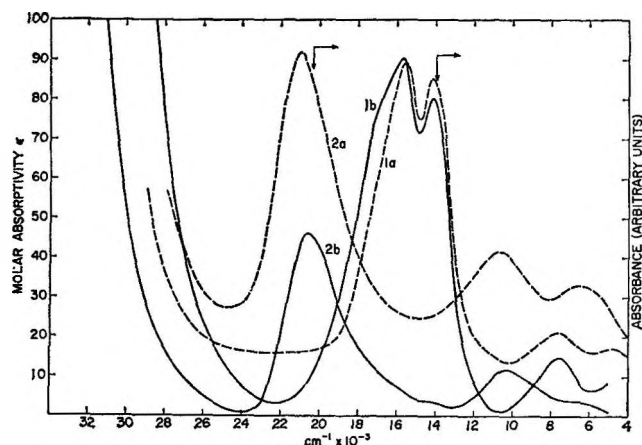


Figure 7. Comparison spectra of Ni(II) in melts and crystals. 1a and 2a are crystal spectra taken at 550° of Ni(II)-doped Cs_2MgCl_4 and $CsMgCl_3$, respectively. 1b and 2b are melt spectra in 68.4% KCl-31.6% $ZnCl_2$ at 550° and in 45.3% KCl-54.7% $ZnCl_2$ at 250°, respectively.

54.7% $ZnCl_2$ at 250° (curve 2b), are compared with the 550° spectra of Ni(II) in the crystal lattices of Cs_2MgCl_4 (curve 1a) and $CsMgCl_3$ (curve 2a), respectively. Since in these crystals, Ni(II) is known to substitute for Mg(II) at sites of essentially undistorted tetrahedral and octahedral symmetry, it is reasonable to conclude that the same configurations account for the melt spectra. However, not all the spectra shown in Figures 1-5 can be resolved in terms of these two coordination states. At least one other Ni-Cl coordination state is required to permit detailed discussion of the spectral changes which are observed on varying the temperature and composition of the melts. One possible configuration is square-planar $NiCl_4^{2-}$, and to obtain its spectrum in crystals, we attempted to substitute Ni(II) into the square-planar site of K_2PtCl_4 . These attempts were unsuccessful. The spectral identification procedure based on comparison of melt spectra with spectra in host lattices of known structure therefore cannot as yet be employed for the square-planar $NiCl_4^{2-}$ configuration. A crystal spectrum different from either the octahedral or tetrahedral spectrum of Ni(II) has been obtained, however, by quenching a 33 mole % KCl-67 mole % $ZnCl_2$ melt containing a low concentration of Ni(II). This melt has the composition of the congruently melting compound KZn_2Cl_5 which occurs in the phase diagram (Figure 6). The visible absorption spectrum of the crystalline compound doped with Ni(II) is shown in Figure 8. The absorption band at 22,300 cm^{-1} is due to Ni(II) in an octahedral site and is in fact the only absorption band observed if the melt is allowed to solidify slowly or if crystals obtained by quenching to

room temperature are annealed at a higher temperature. The peaks in the region 12,000-19,000 cm^{-1} in quenched crystals (Figure 8) are apparently due to Ni(II) in a severely distorted tetrahedral site. The distorted tetrahedral spectrum of Ni(II) in KZn_2Cl_5 is quite distinct from that of Ni(II) in Cs_2ZnCl_4 or K_2ZnCl_4 in which distortions from tetrahedral symmetry are small.^{2,7}

The principal new feature of the Ni(II) spectrum in KZn_2Cl_5 is the appearance of an absorption peak at 16,600 cm^{-1} . Unfortunately, the crystal structure of KZn_2Cl_5 is not known, but it is reasonable to suppose that in this compound, Zn(II) retains tetrahedral symmetry by linking tetrahedra through chlorine bridges. This is made plausible by the fact that the Co(II) spectrum in KZn_2Cl_5 is that of the well-characterized undistorted tetrahedral $CoCl_4^{2-}$ configuration. Because Ni(II) gains considerably more crystal-field stabilization energy by distorting than does Co(II), it is not unexpected to find the site symmetry about Ni(II) to be highly distorted. Apparently, the lattice energy of the compound KZn_2Cl_5 is such as to allow distortion to occur whereas little distortion can occur in the case of a substitutional Ni(II) impurity in the K_2ZnCl_4 lattice.

The configurations responsible for the high-temperature spectra of the 45.3 mole % KCl (Figure 3) and 52.5 mole % KCl (Figure 4) compositions are seen to transform to an octahedral configuration at temperatures below 300°. In the 58 mole % KCl melt (Figure 5) a transformation similar to that seen in Figures 3 and 4 appears to occur but is not complete at the lowest temperatures at which measurements can be made at this composition. An interpretation of these spectral changes in terms of different Ni(II) species will now be given.

It is easily shown that an equilibrium among two distinct light absorbing species results in an isosbestic (constant absorption) point at the wavelength at which the molar absorptances of the two species are equal. Isosbestic points at 19,000 cm^{-1} are, in fact, seen in Figure 4 between 320 and 600° and in Figure 5 between 255 and 600°, respectively. In Figure 3 (45.3 mole % KCl), however, no evidence of an isosbestic point is found. It appears that here, and also at higher $ZnCl_2$ contents (spectra not shown), the transformation occurs as a result of a continuous distortion of the chloride ion environment of Ni(II) with changing temperatures. Which of these two situations occurs depends, of course, on the energies of the states of intermediate configuration relative to those of the end

(7) D. M. Gruen and R. L. McBeth, *J. Phys. Chem.*, 63, 393 (1959).

members. Presumably, a two-species equilibrium occurs if intermediate configurations are of higher energy, *i.e.*, if there is an energy barrier to be crossed in the transformation. An interesting feature of the continuous distortion spectra is that the spectral bands of the intermediate configurations are no broader than those of the end members. Qualitatively, this can be interpreted to imply that the free energy along the distortion path changes rapidly with respect to kT so that virtually all of the Ni(II) ions in the melt have the same intermediate configuration. One may regard the additional broadness of the peak at 500° (Figure 3) as the result of a flattening of the free-energy path, resulting in a limited spreading out of configurations. Somewhere between 45.3 and 52.5% KCl this "flattening-out" of the free-energy path must pass over to a "col" separating "valleys," resulting ultimately in a two-species equilibrium. It thus appears that the two-species equilibrium region should be preceded on either side of its compositional range by regions of progressive distortion. Indications of the presence of such regions may, in fact, be seen in the spectral changes between 250 and 320° and between 700 and 900° in Figure 4.

As noted above, the spectra (Figures 3 and 4) in melts at temperatures below 300° show that Ni(II) ends up in an octahedral configuration. It should be pointed out that the energy of the most intense octahedral band (which is presumably an inverse function of the Ni-Cl distance) changes slightly with the temperature and with composition of the solvent.

The spectra of Ni(II) in high-temperature melts are also clearly dependent on the solvent composition. The difference between the high-temperature spectra in Figures 4 and 5 lies in the relative intensities of the peaks at 1600 and 1720 cm^{-1} . These high-temperature spectra differ from that of the undistorted tetrahedral species only in the presence of the 1720- cm^{-1} peak. Their similarity to the crystal spectrum of Figure 7 is obvious. The absorption at 1720 cm^{-1} of the "distorted tetrahedral" species decreases as the KCl content of the solvent increases, *i.e.*, as the composition approaches the K_2ZnCl_4 composition at 67% KCl.

The manner in which the measurements shown in Figure 5 were obtained is of interest to the understanding of the spectra involving a distorted tetrahedral species. The liquidus temperature for this composition (58% KCl) is 380° (Figure 6). However, in a remarkable instance of supercooling, the spectral changes could be followed, over a period of more than 1 hr, down to a temperature of 255°. At this temperature the sample suddenly crystallized to a homogeneous translucent mass. Inspection of the phase diagram

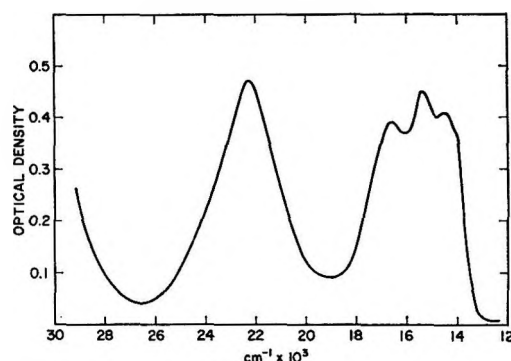


Figure 8. Room-temperature spectrum of Ni(II)-doped KZn_2Cl_5 . Sample obtained by quenching from the melt.

(Figure 6) shows that this is the temperature at which the peritectic compound $\text{K}_3\text{Zn}_2\text{Cl}_7$ (60 mole % KCl), becomes thermodynamically stable. It is tempting to speculate that a substantial energy barrier hinders nucleation of the K_2ZnCl_4 (67 mole % KCl) phase while there is no energy barrier to the nucleation of the $\text{K}_3\text{Zn}_2\text{Cl}_7$ phase in the 58 mole % KCl melt. The structure of K_2ZnCl_4 contains isolated ZnCl_4^{2-} ions. Since liquid of composition $2\text{ZnCl}_2 \cdot 3\text{KCl}$ contains insufficient chloride to form ZnCl_4^{2-} , there may be a tendency to form $\text{Zn}_2\text{Cl}_7^{3-}$ by corner linking of tetrahedra. Although there is no direct spectroscopic evidence, it is not unreasonable to suppose the existence of $\text{Zn}_2\text{Cl}_7^{3-}$ in the liquid.⁸ The energy barrier to nucleation of the K_2ZnCl_4 phase on this view would involve the Zn-Cl-Zn bond energy. We therefore suggest that the spectrum of the 58% KCl high-temperature end member is due to Ni(II) with a tetrahedral chloride environment distorted as a result of being corner linked to another tetrahedron. For statistical reasons, this will almost always be a $[\text{ZnCl}_4]$ tetrahedron. Presumably, the Ni(II) in such an environment is closer to the three unshared ligands than to the fourth shared ligand.

At higher ZnCl_2 contents, there will be a tendency to share additional corners. There can, of course, also be sharing of edges or faces. The varying degrees of distortion from tetrahedral symmetry to be expected on the basis of these considerations are presumably responsible for the complicated spectral changes seen in Figures 1-5.

The change from a two-species equilibrium to a continuous distortion transformation encountered in

(8) It may be noted that Raman spectra studies of this system [see, *e.g.*, J. R. Moyer, J. C. Evans, and G. Y-S. Lo, *J. Electrochem. Soc.*, 113, 158 (1966)] have so far been interpreted without the postulation of an average Zn-Cl coordination state represented by the $\text{Zn}_2\text{Cl}_7^{3-}$ formula, near the $2\text{ZnCl}_2 \cdot 3\text{KCl}$ composition, although the linking of $[\text{ZnCl}_4]$ tetrahedra by common chlorides has been used in previous interpretations of pure molten ZnCl_2 Raman spectra.⁵

the present study can help to provide a better understanding of charge distribution in ionic melts. With increasing ZnCl₂ content beyond the 60% KCl composition, the Ni(II) ions are increasingly coordinated to chloride ions which are already members of [Zn_xCl_y] tetrahedral groupings. Polarization of the chloride ions by the zinc ions lowers the charge density on the chloride ions, thus decreasing the ligand repulsion energies which tend to give symmetrical configurations. For this reason, distortions due to ligand field stabilization energies tend to become more pronounced with increasing ZnCl₂ content, a trend seen, for example, in comparing the high-temperature spectra of Figures 3 and 4. Distortions appear to be energetically more favored in the liquid than in the crystal lattice (Figure 8) and are seen to depend sensitively on the balance between crystal field energies and electrostatic repulsion energies of the ligands. The ligand charge density at the 45 mole % KCl composition is apparently small enough for the Ni(II) site to be distorted to such an extent that the energy barrier between the distorted tetrahedral site and the octahedral site is negligible. As observed above, this is the condition which permits the continuous transformation mechanism exemplified in Figure 5 to occur. Support for this conclusion may be derived from the fact that in LiCl-KCl solutions, where the chloride ligands are less polarized than in the ZnCl₂-containing melts, an octahedral-tetrahedral equilibrium has been observed⁹ which can be shown to involve an almost undistorted tetrahedral species.

It remains to comment on the reasons for the change of configuration and coordination number with temperature. The simplest view is that the octahedral configuration is a result of the 16-kcal octahedral site stabilization energy.² The decrease of the coordination number with increasing temperature is due to the addition of thermal energy which overcomes the crystal field energy and allows the anion-ligand repulsion energies to assert themselves. However, not only the internal energy of the system but also its volume changes with temperature. The effect of the volume factor on the coordination state of an ion is elucidated by the following argument.

It is well known that the increase in volume on fusion of ionic crystals is the result of a decrease in coordination number rather than an increase in nearest neighbor separations. This is taken to indicate that a proportion of holes, vacant quasi-lattice sites, or, less specifically, an amount of free volume has been introduced into the structure. If the temperature is raised, the liquid expands and, as the internuclear distances do not appear to increase significantly, the expansion is presumably accomplished by an increase

in "hole" or "free" volume. If the number of holes, as well as their mean size, increases, then the coordination number must decrease further. Conversely, if the free volume is reduced by lowering the temperature (or increasing the pressure), the coordination number must increase. If the crystallization temperature is reduced either by supercooling or by adding a second component, the tendency to increase the coordination number should be maintained unless the properties of the liquid change in some unexpected way. In practice it is found that if crystallization is severely inhibited, the liquid eventually becomes a glassy solid at a density slightly less than that of the corresponding crystalline solid. It is possible to relate this transformation to the effective disappearance of free volume or hole volume from the liquid.^{10,11} The coordination number should, therefore, reach a maximum value, approximating that of the crystalline material, at the glass transition temperature. These considerations are consistent with the fact that the present system, in which Ni(II) has for the first time been observed to undergo a complete change from four coordination to six coordination with changing temperature, is one in which the liquidus temperatures are unusually low, and in which a glass transformation is known to occur.¹² Indeed, these properties of the solvent system influenced its choice for this study.

In conclusion, we note that, except for the low-temperature results, the principal spectra observed in this study may be matched by spectra observed in previous studies in different solvents such as alkali halides^{7,13a} LiCl-KCl,^{2,9a} and MgCl₂-KCl.^{13b} The effects discussed above and their structural consequences are therefore apparently of general interest, rather than being specific to the ZnCl₂-KCl system.

It is hoped that further studies with other 3d ions in these low-melting solvents, and also optical studies at pressures up to 2 kbars, will throw further light on the factors determining local structure in melts.

(9) (a) C. R. Boston and G. P. Smith, *J. Phys. Chem.*, **62**, 409 (1958); (b) C. K. Jørgensen, *Mol. Phys.*, **1**, 410 (1958).

(10) D. Turnbull and M. H. Cohen, *J. Chem. Phys.*, **34**, 120 (1961).

(11) It is probably more fundamentally correct, and is even more intuitively reasonable, to relate the glass transformation to the effective disappearance from the liquid of configurational entropy, as suggested by J. H. Gibbs and E. A. Dimarzio [*ibid.*, **28**, 373 (1958)]. The configurational entropy in a fused salt must be intimately related to the free volume, and the views expressed here could be rephrased in terms of the loss of entropy in passing from a four-coordinate state to the more ordered six-coordinate octahedral configuration. In this view, however, the volume change itself becomes a reflection of the changing entropy content of the liquid.

(12) I. Schulz, *Naturwiss.*, **44**, 536 (1957); C. A. Angell *J. Phys. Chem.*, **68**, 1917 (1964).

(13) (a) G. P. Smith and C. R. Boston, *J. Chem. Phys.*, **43**, 4051 (1965); (b) D. M. Gruen and H. A. Øye, unpublished results.

Experimental Section

Materials. AR grade KCl and, separately, AR grade ZnCl_2 containing some water were fused under dry HCl gas and, in the case of ZnCl_2 , HCl gas was passed through the melt for 1–3 hr to ensure the removal of all water. After filtration, the melts were pelletized by dropping into liquid nitrogen held in storage vessels which were subsequently sealed after the N_2 had boiled off.

Procedure. As our current program requires the variation of composition in binary systems where both components may be hygroscopic, we have developed a convenient technique for transferring weighed quantities of beads of hygroscopic salt from storage vessel to cell without recourse to drybox handling. This system, which will be described below, is so simple to use that the potential difficulty of changing composition in doubly hygroscopic binary systems is no obstacle to the detailed examination of composition effects in such systems.

In the present work, the initial survey was made in two series of runs, one commencing with pure ZnCl_2 doped with NiCl_2 ($\sim 10^{-2} M$) to which KCl beads were systematically added up to 45.3 mole % KCl, and the other commencing with pure KCl plus NiCl_2 , to which ZnCl_2 beads were added until the KCl content had been reduced to 52.5%. The total Ni in each series was determined by analysis after the completion of the series. The composition region of special interest, 52.5–60% KCl, was examined in greater detail in a subsequent series.

Spectra of the melts were taken using a Cary 14H spectrophotometer and furnace design which have been described in previous publications.¹⁴ The spectra of solidified melts were taken using a Cary 14 ambient-temperature spectrophotometer. Flat sections of the solid salt were used, as the intensities were not sufficient to use KBr pellet techniques successfully.

Density. Density data necessary to obtain molar absorptivities from the optical densities of the solutions were obtained by use of a simple quartz densitometer. The data, and derived information on molar volume changes in this system, will be reported elsewhere.

Technique for Transferring Weighed Samples of Hygroscopic Materials. The system used in the transfer of beads from storage vessel, A, to weighing bottle, XY, is illustrated in Figure 9. A similar system is used to complete the transfer of weighed material to the optical cell. The principle of the transfer technique lies in being able to open and close the weighing bottle, Figure 9a, by rotating the cap X, relative to the body, Y, and thus to align or disalign the

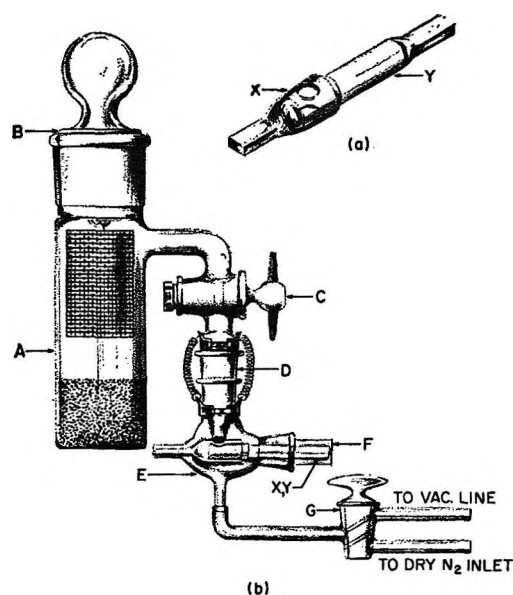


Figure 9. Apparatus for transfer of dry ZnCl_2 beads from storage vessel to weighing bottle. Wire-mesh basket suspended from cap B of vessel A contains silica gel or molecular sieve.

two holes in the cone and sleeve as illustrated. Since this action can easily be performed from outside a sealed system, a dry atmosphere can be maintained during the transfer process.

The procedure is as follows. The weighing bottle XY, with the holes aligned, is placed in the antechamber section E, and the porthole is closed with the cap F. The square ends of the weighing bottle are now located in similarly square recesses in the antechamber E, and cap F is located so that rotation of cap F about the sleeve joint opens or closes the weighing bottle as required. The antechamber E is then attached to the vessel A at the sleeve joint D and secured by springs. By operating the two-way tap G, which connects the antechamber to a vacuum pump and to a source of dry nitrogen gas, the antechamber is evacuated and refilled with dry nitrogen several times. The wide-bore Teflon tap C on the side arm of the storage vessel A has been kept closed up to this point. The approximate number of beads required for the desired composition change is now tipped into the side arm and transferred to the weighing bottle by opening the tap C. The weighing bottle is then closed by a rotation of antechamber cap F, tap C is closed, and the weighing bottle may be removed through the porthole and transferred to the balance for exact weight determination.

A device similar to the antechamber section is then used to transfer the beads from the weighing bottle to the melt in the optical cell. The only additional

(14) D. M. Gruen and R. L. McBeth, *J. Phys. Chem.*, **66**, 57 (1962).

feature is the connection of this device to the cell by means of a ball joint. This is necessary because the cell is usually in a vertical position in the furnace when the addition is made, so that a means of tipping the weighing bottle to let the beads run out must be provided.

Using ZnCl_2 glass beads, it is easy to detect shortcomings in transfer technique, since the beads are perfectly clear when kept dry, but quickly "frost" over on the surface on contact with traces of moisture. With due care it was possible to carry out the transfer from storage vessel to optical cell without any "frosting" being observed. As these transfers would normally be performed by drybox handling and weighing techniques, it is notable that to prevent the occurrence

of a similar frosting of their ZnCl_2 glass samples, Goldstein and Nakonecznyi¹⁵ found it necessary to first flush out their drybox for at least 3 days. ZnCl_2 is an extremely hygroscopic substance so that the efficacy of the system has been proven under severe conditions.

The use of beads, which are easy to prepare, is generally to be recommended in the manipulation of small quantities of salts, as the transfer operations are cleaner and more direct, and 100% transfer of weighed materials is always attained.

(15) M. Goldstein and M. Nakonecznyi, *Phys. Chem. Glasses*, **6**, 126 (1965).

Ultrasonic Absorption in Aqueous Polyethylene Glycol Solutions¹

by Gordon G. Hammes and Thomas B. Lewis

Department of Chemistry, Cornell University, Ithaca, New York, and Department of Chemistry and Research Laboratory of Electronics, Massachusetts Institute of Technology, Cambridge, Massachusetts
(Received December 9, 1965)

The ultrasonic absorption and velocity in aqueous solutions of polyethylene glycol of molecular weights 20,000 and 7500 have been measured over the frequency range 10 to 185 Mc/sec. A single relaxation process is observed over the concentration, temperature, and frequency range investigated. The high-frequency limiting value of the absorption always exceeds that of water, which suggests that the water structure is altered owing to the presence of polymer and/or further relaxation processes occur at higher frequencies than employed in this investigation. The relaxation times determined from the data are essentially independent of concentration, temperature, and molecular weight; the maximum of the absorption per wavelength is approximately proportional to the polymer concentration. Viscosity measurements on the polymer solutions and use of the Zimm theory of viscous relaxation indicates that viscous relaxation is not being observed. The relaxation process is attributed to a perturbation of the hydrogen-bonding equilibrium between polymer and solvent. Minimum volume changes of approximately ± 0.6 ml/mole of monomer are associated with this equilibrium. The general use of ultrasonic absorption measurements as a probe of microscopic solvent structure is considered.

Introduction

Ultrasonic attenuation measurements in poly-L-glutamic acid (PGA) solutions have been recently reported.² The observed chemical relaxation was attributed primarily to solvent-polymer interactions, that is, to perturbation of an equilibrium between solvent molecules bound to the polymer and the bulk solvent. Since PGA is a quite complex polymer, such an interpretation is difficult to make with certainty, and a simpler polymer, polyethylene glycol, has been selected for further study. Only three sources of ultrasonic relaxation are possible in aqueous polyethylene glycol solutions: macromolecule-macromolecule interactions, solvent-polymer interactions, and viscosity. These three processes can be distinguished experimentally, and the results obtained indicate solvent-polymer interactions are responsible for the observed ultrasonic relaxation. The use of ultrasonic attenuation measurements as a probe of microscopic solvent structure in the neighborhood of solutes is considered.

Experimental Section

Polyethylene glycol, E-6000 (E6) of Lot V-75 and

E-20,000 (E20) of Lot A200, with average molecular weights of 7500 and 20,000 respectively, were obtained from the Dow Chemical Co., Midland, Mich. Both polymers are characterized by a sharply peaked molecular weight distribution. At the temperatures used in this work, the bulk polymers are highly water-soluble solids. Ultrasonic measurements were made on 1.98 and 1.20 *m* (moles of monomer/1000 g of solvent) solutions at 10 and 25°. All solutions were prepared with doubly distilled water. Calibrated Cannon-Fenske viscometers were used to measure the solution viscosities.

The absorption and velocity measurements were obtained with the ultrasonic pulse system previously described.² A 2-Mc/sec X-cut quartz transducer was used for the measurements between 10 and 42 Mc/sec, while two 5-Mc/sec X-cut quartz crystals were used in the frequency range 35 to 185 Mc/sec. The procedure

(1) This work was supported in part by the Joint Services Electronics Program under Contract DA 36-039-AMC-03200(E) and in part by grants from the National Institutes of Health (GM07803 and 13292).

(2) J. J. Burke, G. G. Hammes, and T. B. Lewis, *J. Chem. Phys.*, **42**, 3520 (1965).

for determining the amplitude absorption coefficients and the ultrasonic velocities has been described in detail elsewhere.^{2,5} The absorption coefficients were reproducible to within $\pm 2\%$, with the data at low frequencies being somewhat less accurate owing to the decreased attenuation of the solutions. The measured velocities were reproducible to within 0.5%. The instrument was checked for absolute accuracy at periodic intervals using water and the accepted literature values for the absorption coefficient⁴ and velocity.⁵ These results were always within the limits of the quoted reproducibility. The temperature was maintained to $\pm 0.05^\circ$ with a Bronwill thermostating unit and a Whirlpool thermoelectric immersion cooler.

Results and Treatment of Data

Ultrasonic measurements of the pressure amplitude absorption coefficient, α , and the velocity of propagation, v , were obtained for the two molecular weights of the polymer at two concentrations and temperatures. The data are presented in Figures 1 and 2 in plots of α/f^2 vs. f , where f is the frequency. If only a single relaxation process is being observed in the frequency range investigated⁶

$$\alpha/f^2 = \frac{A\tau}{1 + (\omega\tau)^2} + B \quad (1)$$

where A and B are amplitude parameters, τ is the characteristic relaxation time, and ω is equal to $2\pi f$. Very often when chemical relaxation effects are observed B is equal to the value of α/f^2 of the pure solvent; however, in the polyethylene glycol solutions this constant always exceeded the value characteristic of the pure solvent.

For an analysis of the results, a useful procedure is to consider the absorption per wave length, $\mu = 2\alpha_R\lambda$, where λ is the wavelength and α_R is equal to $(\alpha/f^2 - B)f^2$. This quantity can be represented by

$$\mu = 2\mu_m \frac{\omega\tau}{1 + (\omega\tau)^2} \quad (2)$$

where μ_m is equal to $Av/2\pi$.

The data can be characterized by the three independent constants, B , μ_m , and τ . Values of μ_m and τ are obtained from plots of $\log \mu$ vs. $\log f$, which are symmetrical about $f = 1/2\pi\tau$. A typical plot of the data is presented in Figure 3 along with the corresponding theoretical curve. In practice, the three constants are varied to obtain a best fit of the data to a single relaxation curve. In all cases assumption of a single relaxation process is sufficient to characterize the data. The values of μ_m/c_0 , B , and τ obtained by this procedure, where c_0 is the polymer concentration in moles of

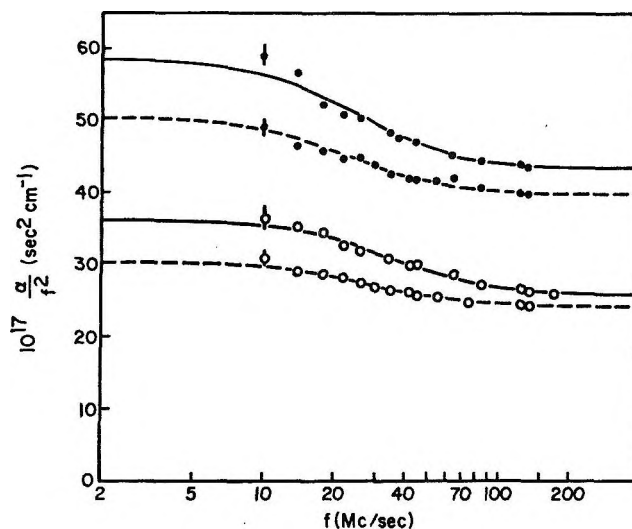


Figure 1. Ultrasonic absorption of aqueous solutions of polyethylene glycol of molecular weight 7500 as a function of frequency at 10° (\bullet) and 25° (\circ). Best-fit single-relaxation curves are indicated by the solid lines for the 1.98 m solutions and by dashed lines for the 1.20 m solutions.

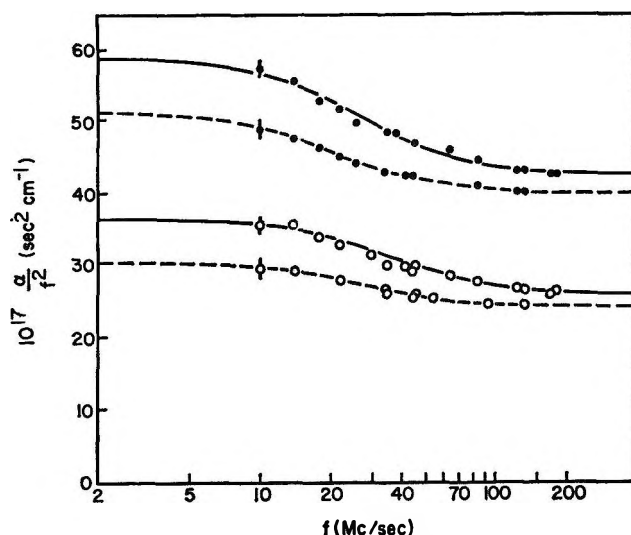


Figure 2. Ultrasonic absorption of aqueous solutions of polyethylene glycol of molecular weight 20,000 as a function of frequency at 10° (\bullet) and 25° (\circ). Best-fit single-relaxation curves are indicated for the 1.98 m solutions by the solid lines, and for the 1.20 m solutions by the dashed lines.

monomer/1000 g of solvent, are listed in Table I, together with the measured ultrasonic velocities. The

(3) T. B. Lewis, "Relaxation Spectra in Polymer Solutions," Ph.D. Thesis, Massachusetts Institute of Technology, 1965.

(4) J. H. Pinkerton, *Nature*, **160**, 128 (1947).

(5) M. Greenspan and C. E. Tschiegg, *J. Res. Natl. Bur. Std.*, **59**, 249 (1957).

(6) K. F. Herzfeld and T. A. Litovitz, "Absorption and Dispersion of Ultrasonic Waves," Academic Press Inc., New York, N. Y., 1959.

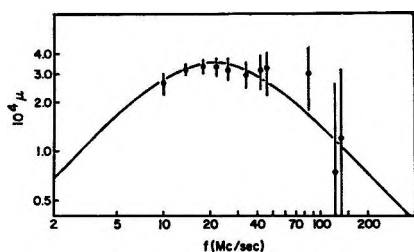


Figure 3. The absorption per wavelength of 1.20 *m* aqueous solution of polyethylene glycol, molecular weight 20,000, vs. frequency at 10°. The single-relaxation curve which best fits the data is indicated. Error brackets correspond to $\pm 2\%$ variation of the measured values of α/f^2 at each frequency.

estimated uncertainties in τ are $\pm 10\%$, in $\mu_m/c_0 \pm 15\%$, and in $B \pm 3\%$. Theoretical curves calculated with these parameters and eq 1 are included in Figures 1 and 2.

Table I: Ultrasonic Parameters

| c_0 , m | T , °C | $10^4 \mu_m/c_0$, m^{-1} | $10^{11} B$, sec^2/cm | $10^9 \tau$, sec | $10^7 \tau^2$, ^a sec | $10^{-5} v$, cm/sec |
|--------------|-------------|--------------------------------|-----------------------------|----------------------|-------------------------------------|-------------------------|
| E6 | | | | | | |
| 1.20 | 10 | 3.0 | 39.8 | 6.9 | 3.1 | 1.48 |
| 1.20 | 25 | 2.3 | 24.1 | 5.5 | 1.7 | 1.53 |
| 1.98 | 10 | 2.9 | 43.2 | 6.4 | 3.1 | 1.51 |
| 1.98 | 25 | 2.7 | 25.8 | 4.7 | 1.7 | 1.54 |
| E20 | | | | | | |
| 1.20 | 10 | 2.9 | 40.1 | 7.6 | 18 | 1.48 |
| 1.20 | 25 | 2.3 | 24.1 | 5.7 | 10 | 1.52 |
| 1.98 | 10 | 3.4 | 42.6 | 5.9 | 18 | 1.50 |
| 1.98 | 25 | 2.9 | 26.0 | 4.5 | 10 | 1.54 |

^a Calculated from the theory of Zimm.⁷

Viscosities of the polyethylene glycol solutions were measured at five concentrations for both molecular weights at both temperatures. The intrinsic viscosities, $[\eta]$, were determined by an extrapolation of $(\eta/\eta_{H_2O} - 1)/C'$ and $\ln(\eta/\eta_{H_2O})/C'$ to zero concentrations. Here η is the solution viscosity, η_{H_2O} the viscosity of water, and C' the concentration in grams per deciliter. A summary of the viscosity results is given in Table II.

Discussion

In all cases the absorption data can be ascribed to a single relaxation process. A consideration of the variations of the relaxation time, τ , and the maximum of the absorption per wavelength, μ_m , can provide some insight into the nature of the process

Table II: Viscosities of Polyethylene Glycol Solutions

| Poly- mer | T , °C | η , cp | | | | | $[\eta]$, dl/g |
|--------------|-------------|-------------|------|------|------|------|--------------------|
| | | 1.98 | 1.20 | 0.46 | 0.23 | 0.11 | |
| E6 | 10 | 5.43 | 3.42 | 1.96 | 1.62 | 1.46 | 0.22 |
| E6 | 25 | 3.40 | 2.19 | 1.30 | 1.09 | 0.98 | 0.19 |
| E20 | 10 | 11.2 | 5.80 | 2.60 | 1.89 | 1.58 | 0.39 |
| E20 | 25 | 6.88 | 3.62 | 1.68 | 1.25 | 1.06 | 0.34 |

occurring. The relaxation time is almost constant for the different conditions of molecular weight, concentration, and temperature. However, a slight trend to shorter times occurs as the temperature and concentration are increased; unfortunately, the precision of the measurements is not sufficient to establish these trends with certitude. The maximum of the absorption per wavelength divided by the monomer concentration, μ_m/c_0 , is also roughly constant within the experimental uncertainties. The concentration and temperature ranges investigated were limited by the fact that at lower concentrations and higher temperatures the amplitude of the relaxation process was too small to measure with precision, while at higher concentrations the polymer begins to influence the bulk solution properties and the variation of activity coefficients with concentration (which is unknown) is of importance in interpreting the data.

If the observed relaxation process is primarily due to viscous effects, the relaxation times should be comparable to those predicted by the theory of Zimm⁷ for the motion of a flexible polymer molecule in solution. This theory predicts a spectrum of relaxation times, although the amplitude associated with the longest relaxation time is expected to be much greater than that associated with shorter times. Values of the longest relaxation time calculated according to Zimm⁷ are included in Table I; the theoretical relaxation times are more than an order of magnitude longer than those observed. Moreover, if the observed process were due to a spectrum of viscosity relaxation times, the relaxation times should depend markedly on molecular weight. This is clearly inconsistent with the observed experimental results. A final possibility is that a "local viscosity" effect is being observed which would be independent of molecular weight. In this case, the same relaxation process should be observed in dielectric relaxation. Dielectric relaxation experiments have been carried out on solutions of polyethylene glycol in benzene and water.^{8,9}

(7) B. H. Zimm, *J. Chem. Phys.*, **24**, 269 (1956).

Relaxation has not been detected in the frequency range under consideration here although a dielectric relaxation effect attributed to orientation of short chain segments ("local viscosity" relaxation) has been observed in benzene at much shorter times ($\sim 10^{-11}$ sec). In the case of water as the solvent, the observed dielectric relaxation was attributed primarily to water, rather than to polymer. The "local viscosity" relaxation is a possible cause for the constant B being higher than that found for the pure solvent. That is, α/f^2 would presumably decrease further at very high frequencies due to this relaxation. Alternatively, the presence of polymer might change the relaxation characteristics of water itself, causing the observed increase in B .⁸

Polymer-polymer interactions also are probably not the source of the observed effect. A more distinct concentration dependence of the relaxation parameters would be expected if this were the case: the relaxation times would decrease markedly with increasing concentration and the maximum of the absorption per wave length, μ_m , would not be simply proportional to the polymer concentration. Moreover, some dependence of γ on molecular weight would be expected.

The primary process observed here most likely corresponds to solvent-polymer interactions. The perturbation by the sound wave would have the effect of shifting the equilibrium between water molecules bound to the polyethylene glycol and water in the bulk solvent. This would involve the breakdown of the water structure around the polymer and solvation of the polyethylene glycol by the water and is probably related to hydrogen-bonding interactions between the oxygens of the polymer and the hydrogens of the water. If this chemical process were rate limiting for the "local viscosity" dielectric relaxation, the dielectric and ultrasonic relaxation times would be identical.

If the ultrasonic relaxation is due to a chemical process, the maximum of the absorption per wavelength can be written as¹⁰

$$\mu_m = \frac{\pi \rho v^2 c_0 \Gamma}{R T \Gamma} \left[\Delta V^\circ - \frac{\beta}{\rho c_p} \Delta H^\circ \right]^2 \quad (3)$$

where ΔV° and ΔH° are the standard volume and enthalpy changes associated with the chemical process, ρ is the solution density, β is the thermal expansion coefficient of the solution, c_p is the constant-pressure specific heat of the solution, R is the gas constant, T is the absolute temperature, c_0 is the solute concentration, and Γ is a function of the equilibrium constant (and concentrations in general). For the process $A \rightleftharpoons B$, Eigen and de Maeyer¹⁰ show that the function Γ has a maximum value of about 0.25. Minimum values of the

bracketed quantity in eq 3 can be calculated with eq 3 and Γ equal to 0.25. The results, which are essentially independent of concentration, are summarized in Table III. Very often for aqueous solutions, the value of β is sufficiently small and ΔV° sufficiently large (10 to 20 ml/mole) so that the effect of the enthalpy term

Table III: Minimum Values of $\pm[\Delta V - (\beta/\rho c_p)\Delta H]^\circ$

| (PEG) ^b | T, °C | E6 | E20 |
|--------------------|-------|-----|-----|
| 1.20 | 10 | 0.6 | 0.6 |
| 1.20 | 25 | 0.6 | 0.6 |
| 1.98 | 10 | 0.6 | 0.7 |
| 1.98 | 25 | 0.6 | 0.6 |

^a Milliliters per mole of monomer. ^b Polyethylene glycol concentration in moles per 1000 g of solvent.

can be neglected. However, in the present case, no final conclusion concerning the magnitude of the volume and/or enthalpy change associated with the relaxation process can be reached, except that both are probably very small. The volume change associated with the solvent-polymer interactions can be roughly identified with the volume change which occurs on mixing polymer and solvent. Thermodynamic mixing properties for aqueous solutions of polyethylene glycol at 65° have been reported¹¹ and the results indicate that the volume change associated with mixing is approximately -1 ml/mole of monomer, which is of the same order of magnitude as the volumes reported in Table III.

The ultrasonic relaxation process observed in PGA solutions exhibited a distribution of relaxation times, but this relaxation was also attributed primarily to polymer-solvent interactions.² The results reported here tend to confirm this interpretation. The distribution of relaxation times in the case of PGA solutions is probably due to the presence of several different solvating sites and/or to a superposition of other relaxation processes which can occur in PGA solutions (cf. ref 2 for a more comprehensive discussion of this point).

Recently, Zana¹² made acoustic studies of polymers

(8) M. Davies, G. Williams, and G. D. Loveluck, *Z. Elektrochem.*, **64**, 575 (1960).

(9) W. H. Stockmayer, H. Yu, and J. E. Davis, Abstracts, 145th National Meeting of the American Chemical Society New York, N. Y., Sept 1963, p 7U.

(10) M. Eigen and L. de Maeyer in "Technique of Organic Chemistry," Vol. 8, Part 2, S. L. Friess, E. S. Lewis, A. Weissberger, Ed., Interscience Publishers, Inc., New York, N. Y., 1963.

(11) G. N. Malcolm and J. S. Rowlinson, *Trans. Faraday Soc.*, **53**, 921 (1957).

(12) R. Zana, *J. Chim. Phys.*, **62**, 612 (1965).

in organic solvents. Many of the results he reported cannot be explained in terms of a simple relaxation process, but others strongly suggest polymer-solvent interactions are being observed. This type of interaction is certainly not limited to macromolecules. Ultrasonic relaxation effects have been observed in alcohol-water solutions with data obtained over a limited frequency range.^{13,14} This relaxation behavior can also be attributed to a perturbation of intermolecular hydrogen bond equilibria. More definitive information about solvent-solute interactions, *e.g.*, local solvent structure and rates of elementary processes, can be found with appropriate small molecule solutes by use of the ultrasonic method.^{15,16} The study of

solute-solvent interactions with ultrasonic attenuation measurements on a more extensive scale may prove to be of general utility in the investigation of microscopic solvent structure. Further experiments with other systems are currently in progress.

Acknowledgements. The authors wish to thank Mr. Michael H. Auerbach for carrying out some preliminary experiments on the polyethylene glycol-water system.

(13) L. R. O. Storey, *Proc. Phys. Soc. (London)*, **B65**, 943 (1952).

(14) D. Sette, *Nuovo Cimento*, **1**, 800 (1955).

(15) G. G. Hammes and H. O. Spivey, *J. Am. Chem. Soc.*, **88**, 1621 (1966).

(16) G. G. Hammes and W. Knoche, in preparation.

The Interaction of Acridine Orange with Poly- α -L-glutamic Acid¹

by Gordon G. Hammes and Colin D. Hubbard

Department of Chemistry, Cornell University, Ithaca, New York, and the Department of Chemistry, Massachusetts Institute of Technology, Cambridge, Massachusetts (Received December 13, 1965)

A kinetic study has been made of the monomer-dimer reaction of acridine orange (AO) and of the reaction between poly- α -L-glutamic acid (PGA) and AO with the temperature-jump method. Related spectral measurements have also been made. The formation of the AO dimer is essentially diffusion controlled, which indicates the dye "stacking" occurs in 10^{-10} sec or less. The observed relaxation effect in the PGA-AO system can be described quantitatively by assuming two relaxation processes occur. Measurement of the relaxation times was made at pH 4.7, where PGA is predominantly in a helical conformation, and at pH 7.5 where PGA is in the form of a random coil. At both pH values, both relaxation times are independent of polyglutamic acid concentration at high concentrations of polymer, but show a marked dependence on the polyglutamic acid concentration when the polymer concentration is lowered. Only at low concentrations of PGA do the relaxation data show a significant dependence upon the acridine orange concentration. A possible mechanism of the PGA-AO interaction is one in which the rate-controlling steps in the over-all complex formation are intramolecular and probably involve the displacement of solvent molecules and/or counterions from the vicinity of the polymer. However, other plausible mechanisms involving dye stacking and polymer aggregation cannot be excluded. The same general mechanism appears to be operative for both the helical and random-coil forms of PGA, although the relaxation times are considerably longer for the former.

Introduction

Several investigators have examined the equilibrium properties of aqueous solutions of dyestuffs and polyanions. Acridine orange (AO), in particular, has been used for this purpose; this has resulted in an accumulation of data concerned with the spectra of AO bound to such polyanions as polyglutamic acid, polyadenylic acid, polyuridylic acid, RNA, DNA, etc.²

From changes in the visible absorption spectrum as the concentration of acridine orange is varied, it has been established that AO aggregates in aqueous solution.³

Parallel changes in the spectrum of AO upon addition of polyelectrolytes have led to the hypothesis that dye molecules bound to the polymer may be sufficiently closely located on the polymer molecule to interact with one another to form aggregates analogous to those found in free dye solution.^{2a} The phenomenon of AO molecules aggregating while bound to a polymer is generally termed "stacking." Bradley and Wolf^{2a}

have introduced a parameter called the "stacking tendency" as an arbitrary measure of the strength of interaction between such dye molecules. Other workers have suggested that the color changes occurring in AO when the amount of added polymer is varied can be attributed to interaction of the dye with different types of binding sites on the polymer.^{2b-d} This latter idea, however, is inconsistent with the results obtained with electrolytes having only one type of monomer unit.

By determining the kinetic parameters characteristic

(1) This work was supported by grants from the National Institutes of Health (GM 07803 and GM 13292).

(2) For example, (a) D. F. Bradley and M. K. Wolf, *Proc. Natl. Acad. Sci. U. S.*, **45**, 944 (1959); (b) R. F. Steiner and R. F. Beers, *Science*, **127**, 335 (1958); (c) R. F. Steiner and R. F. Beers, *Arch. Biochem. Biophys.*, **81**, 75 (1959); (d) R. F. Beers, D. D. Hendley, and R. F. Steiner, *Nature*, **182**, 242 (1958); (e) A. L. Stone and D. F. Bradley, *J. Am. Chem. Soc.*, **83**, 3627 (1961); (f) A. M. Michelson, *Ann. Rev. Biochem.*, **30**, 133 (1961).

(3) V. Zanker, *Z. Physik. Chem.*, **199**, 15 (1952).

of the reaction between poly- α -L-glutamic acid (PGA) and AO in aqueous solution and of the association reaction between two single dye molecules to form a dimeric dye molecule, we hoped to gain some insight into the nature of the complex species present at equilibrium and to obtain information about the mechanistic processes which lead to such species. Of particular interest are the rates and mechanism of stacking because of the importance of stacking in nucleic acid structures. The association of AO with itself and with PGA are both very rapid processes, so that the temperature-jump method was used for all kinetic measurements. Since at room temperatures and high salt concentration (approximately 0.1 M) PGA exists predominantly as an α helix in aqueous solution below about pH 5, and as a random coil above pH 7,⁴ the role of the polyanion structure in the dye-PGA interaction can be explored. However, the kinetic and spectral data obtained permit only qualitative features of the over-all mechanism of the AO-PGA interaction to be assessed.

Experimental Section

Materials. Acridine orange from the National Aniline Division was recrystallized twice from methanol. Poly- α -L-glutamic acid (Lot No. G-54, molecular weight given as 65,000) was obtained from Pilot Chemicals. All other materials were standard reagent grade chemicals. Deionized distilled water was used for the preparation of all solutions.

Spectra. The absorbancy of solutions was measured in the range 430–520 m μ at 25.0° with a Beckman Model DU spectrophotometer fitted with a thermostated cell housing. In practice, solutions were made simply by adding the appropriate amounts of stock solutions of polyglutamic acid and acridine orange to a buffer solution, which upon bringing to a standard volume was either 0.1 M sodium acetate-acetic acid (pH 4.7), or 0.1 M sodium acetate-tris(hydroxymethyl)-aminomethane (pH 7.5). All pH measurements were made with a Radiometer pH meter.

The over-all association constant for reactions between other polyanions and AO has been reported to be markedly decreased as the high ionic strength is increased:^{2a} therefore, the identification of complex species has been possible only at buffer concentrations less than or equal to 10⁻³ M. On the other hand, temperature-jump experiments require an ionic strength of about 0.1 M. Consequently, spectra of PGA-AO solutions were measured over a range of buffer concentration from 10⁻³ to 10⁻¹ M.

Kinetic Experiments. Details of the temperature-jump apparatus have been amply documented.⁵⁻⁷

Temperature-jump experiments to determine the rate constants for association and dissociation of dimeric AO were performed over a range of total AO concentration from 1.75 \times 10⁻⁵ to 5 \times 10⁻⁵ M in 0.1 M sodium acetate-acetic acid buffer (pH 4.7). The relaxation effect (observed at 446 m μ) has a relaxation time approaching the time resolution of the apparatus. To minimize any cavitation effects, solutions were made from freshly boiled distilled water. However, within experimental error, the relaxation times were identical with those determined when this precaution was omitted.

Before a series of kinetic runs on the PGA-AO system was performed, solutions of the background electrolyte, with and without AO and PGA, were introduced into the cell of the temperature-jump apparatus and tested to verify that no relaxation effects other than those relating to PGA-AO interactions were being observed. (Although a very fast relaxation process due to AO aggregation was observed with AO in buffer solution, the amount of free AO in solution when polymer is present is sufficiently small so that only a negligible amount of AO dimers is present and, consequently, this relaxation effect is not observed.) At both pH values investigated, 4.7 (α helix) and 7.5 (random coil), the relaxation spectrum was obtained over a range of PGA concentrations from about 5 \times 10⁻⁴ to 2 \times 10⁻² M (the molarity of PGA is expressed in terms of the monomer) and at AO concentrations of 5.0 \times 10⁻⁵ and 2.5 \times 10⁻⁵ M. All kinetic runs were performed at 25.0° in 0.1 M buffer. The wavelengths used for observation of the chemical relaxation were 495 m μ at pH 4.7 and 506 m μ at pH 7.5.

Because of the known sensitivity of acridine dyes to light, solutions containing AO were exposed to light for the absolute minimum of time; in the temperature-jump experiments the incident light was blocked from the cell during the period between successive temperature jumps.

Results and Treatment of Data. The large differences in spectra of other polyanion-AO complexes at low buffer concentration which occur upon varying the mole ratio of reactants have already been mentioned.^{2a} The peak observed at 440–450 m μ when the polymer/AO ratio ([P]/[AO]) is near 1, gives way with increase in [P]/[AO] to one at 460–470 m μ . Further increase in [P]/[AO] yields a band in the region of 500

(4) P. A. Doty, A. Wada, J. T. Yang, and E. R. Blout, *J. Polymer Sci.*, **23**, 851 (1957).

(5) G. G. Hammes and J. I. Steinfeld, *J. Am. Chem. Soc.*, **84**, 4639 (1962).

(6) G. G. Hammes and P. Fasella, *ibid.*, **84**, 4644 (1962).

(7) R. E. Cathou and G. G. Hammes, *ibid.*, **86**, 3240 (1964).

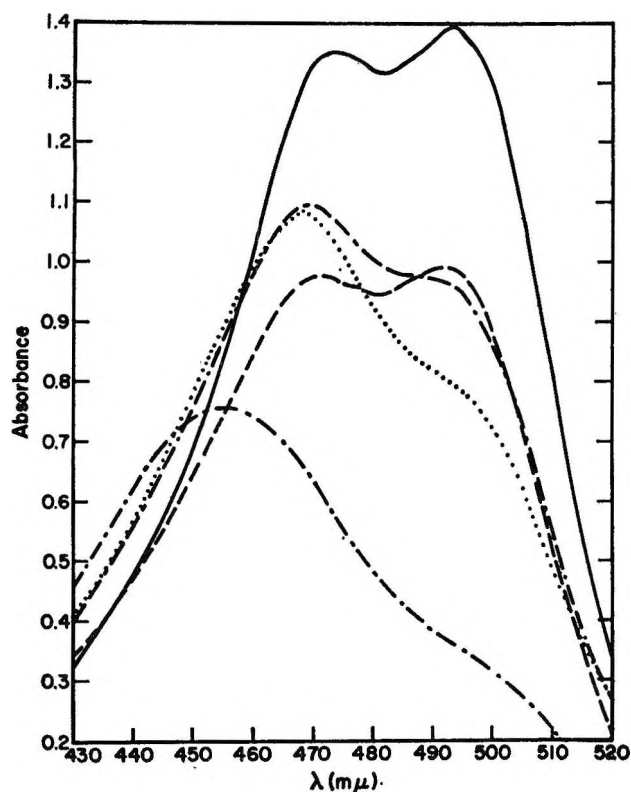


Figure 1. Spectra of solutions at pH 7.5, 25.0°, and $[AO] = 5.0 \times 10^{-6} M$: —, $[PGA] = 0$, 0.1 M buffer; ---, $[PGA] = 1.33 \times 10^{-3} M$, 0.1 M buffer; ····, $[PGA] = 1.33 \times 10^{-3} M$, 0.001 M buffer; - · - ·, $[PGA] = 3.37 \times 10^{-2} M$, 0.1 M buffer; and ·····, $[PGA] = 3.37 \times 10^{-2} M$, 0.001 M buffer.

$m\mu$, with a corresponding decline in the one at 460–470 $m\mu$. The value of the mole ratio required to produce these changes was found to be strongly dependent upon the particular polymer. The short-wavelength peak was considered to be characteristic of a highly stacked complex, while the longer-wavelength peaks were thought to represent the cases of two dye molecules interacting (dimer stacks) and no stacking, respectively. Observations on the PGA-AO system at pH 7.5 at buffer concentrations of $10^{-3} M$ are, in general, consistent with those for other systems described, although there was no evidence of a predominating peak near 500 $m\mu$ in our measurements. Some typical spectra are shown in Figure 1. It may be that a higher ratio of $[PGA]/[AO]$ than was used is required to produce the absorption band at 500 $m\mu$, or that only small amounts of unstacked complexes are formed when the polyanion is polyglutamic acid. Interpretation of kinetic data would be greatly facilitated by an exact knowledge of the species present at equilibrium, but unfortunately a characterization of

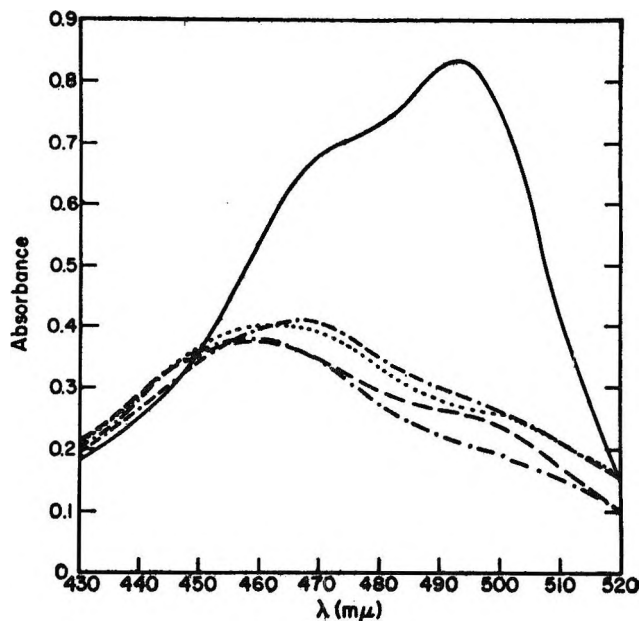


Figure 2. Spectra of solutions at pH 4.7, 25.0°, and $[AO] = 2.5 \times 10^{-5} M$: —, $[PGA] = 0$, 0.1 M buffer; ---, $[PGA] = 3.34 \times 10^{-4} M$, 0.1 M buffer; ····, $[PGA] = 3.34 \times 10^{-4} M$, 0.001 M buffer; - · - ·, $[PGA] = 2.0 \times 10^{-2} M$, 0.1 M buffer; and ·····, $[PGA] = 2.0 \times 10^{-2} M$, 0.001 M buffer.

the solutions used for the kinetic experiments in terms of the stacking model cannot be definitive owing to the dissociation of complexes and concomitant masking of the spectra which occurs at high buffer concentrations. It is difficult to ascertain whether the appearance of the band at 495 $m\mu$ should be attributed to free dye in monomeric form or to dye in monomeric form bound to polyglutamic acid or to a combination of both of these species. Most probably, solutions used for kinetic measurements contained a mixture of a small amount of dimer dye-polymer complex, single dye-polymer complex, and unbound dye.

The spectra afford little assistance in assessment of the composition of equilibrium solutions when the PGA is in a helical form since only negligible changes of peak intensity and peak position occur when the total PGA concentration is varied over two orders of magnitude, the total AO concentration is varied over a factor of 2, and the buffer concentration is changed from 10^{-1} to $10^{-3} M$ (see Figure 2). However, the parallel in kinetic behavior suggests that the complexes formed are similar to those formed at pH 7.5.

We will first consider the kinetic results obtained for the monomer-dimer system in acridine orange solutions. A plot of the logarithm of the amplitude of the light intensity change *vs.* time was linear for all

solutions, indicating a single relaxation process. For an association reaction of the type



the reciprocal relaxation time is

$$1/\tau = 4k_{12}[AO_M] + k_{21} \quad (2)$$

where $[AO_M]$ is the equilibrium concentration of the monomeric species. From previous data² the equilibrium constant for the dimerization reaction can be estimated to be $1.5 \times 10^4 M^{-1}$ at 25.0° , so that the concentrations of monomer and dimer species can be calculated for any value of the total acridine orange concentration. Figure 3 shows a plot of τ^{-1} vs. $4[AO_M]$ from which the following rate constants were determined: $k_{12} = 2.7 \times 10^8 M^{-1} \text{sec}^{-1}$ and $k_{21} = 1.8 \times 10^4 \text{sec}^{-1}$. The ratio of rate constants gives an equilibrium constant of $1.5 \times 10^4 M^{-1}$, in good agreement with the value cited above.

The relaxation spectrum of the PGA-AO system is considerably more complex than that of the AO system. For all solutions, a plot of the logarithm of the amplitude of the light intensity change vs. time was curved, but the assumption of two relaxation times was sufficient to represent the data quantitatively. A typical plot of the data is shown in Figure 4, together with the calculated theoretical curve assuming two relaxation times, that is, assuming the signal amplitude can be represented as $A_1 e^{-t/\tau_1} + A_2 e^{-t/\tau_2}$. The relaxation times were obtained by first determining the longer relaxation time from the linear portion of the curve at long times; the linear portion of the curve was then extended to shorter times and was subtracted from the experimental curve. The value of the shorter time can be determined from the resultant straight line.

The faster relaxation time at pH 7.5 could not be obtained very precisely since, except at very low concentrations of PGA, the relaxation time was of the order of $20 \mu\text{sec}$, which is close to the limit of time

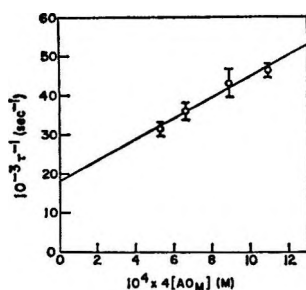


Figure 3. Plot of τ^{-1} vs. $4[AO_M]$ for the dimerization of acridine orange.

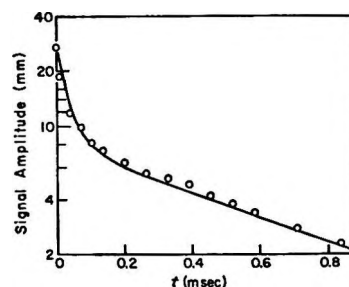


Figure 4. Plot of the logarithm of amplitude of light intensity change vs. time; $[PGA] = 2.7 \times 10^{-3} M$, $[AO] = 5.0 \times 10^{-6} M$ and pH 7.5. Circles are experimental points. The solid line is the theoretical curve obtained as described in the text. The equation for the theoretical curve is SA (millimeters) = $23.2e^{-t/0.06} + 7.6e^{-t/0.57}$, where t is in milliseconds.

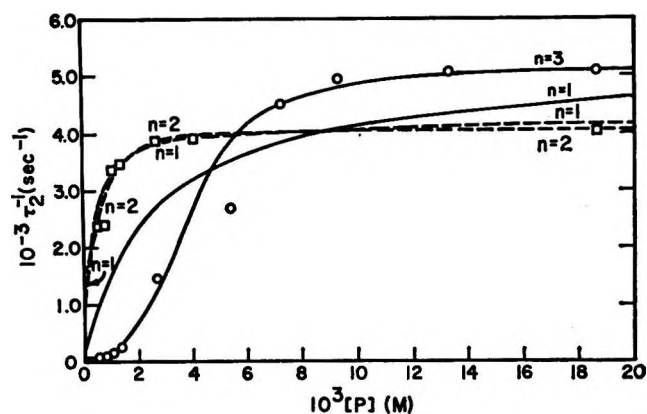


Figure 5. Plot of τ_2^{-1} vs. $[PGA]$ at pH 7.5 and 25.0° : for $[AO] = 5.0 \times 10^{-6} M$, circles are experimental points, solid lines are theoretical curves; for $[AO] = 2.5 \times 10^{-4} M$, squares are experimental points, dashed lines are theoretical curves. The theoretical curves are calculated with eq 6 and the values of n given in the figure.

resolution of the equipment. The estimated error in the other relaxation times is about $\pm 20\%$. In Figure 5, the values of $1/\tau_2$ are plotted against $[PGA]$ for both concentrations of AO employed. The over-all profiles are of similar form for both AO concentrations, but the relaxation times are quantitatively different at low concentrations of AO and PGA. Unfortunately, in the critical region of very low PGA concentration, relaxation data cannot be reliably obtained because the interaction between PGA and AO is very weak. At both AO concentrations τ_2 reaches a constant value of approximately $200\text{--}250 \mu\text{sec}$ at high concentrations of PGA.

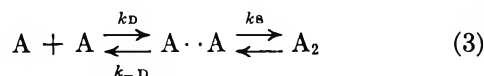
Relaxation times for dye interacting with the α -helical form of polyglutamic acid were an order of magnitude slower, which allowed both of the relaxation times to be quantitatively measured. Both τ_1

and τ_2 depend markedly upon the concentration of PGA until the ratio $[\text{PGA}]/[\text{AO}]$ is about 200, whereupon τ_1 remains constant at 400–500 μsec , while τ_2 reaches a concentration-independent value of about 3 msec. These concentration-independent limits are both also virtually independent of the acridine orange concentration. Again, as at pH 7.5, the relaxation times differ at low PGA and AO concentrations, but the $1/\tau$ -[PGA] profiles are of the same general form.

Discussion

The results obtained for the monomer-dimer AO system indicate that the aggregation process is quite rapid. The maximum possible value for the second-order rate constant is about $10^9 M^{-1} \text{sec}^{-1}$,⁸ so that dimer formation essentially is a diffusion-controlled process.

The over-all mechanism of complex formation can be depicted as



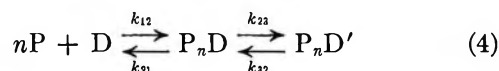
where $A \cdot A$ represents a complex which forms and dissociates at rates controlled by diffusion and k_S is the rate constant for "stacking." In order for the over-all association rate to be diffusion controlled, k_S must be much greater than k_{-D} . The magnitude of k_{-D} can be estimated as 10^{10}sec^{-1} ,⁹ so that the rate constant associated with "stacking" must be greater than 10^{10}sec^{-1} .

The mechanistic explanation for the relaxation spectra of the PGA-AO system is not so simple. If we assume that the actual relaxation processes being observed do not change as the PGA concentration is changed and that the relaxation times reach a constant limiting value at high PGA concentrations, the processes being observed are almost certainly *intramolecular*. In general terms, a plausible mechanism is one in which a dye molecule binds very rapidly to a site on the polymer; this process is followed by a slower intramolecular rearrangement. The question as to whether dimeric, monomeric, or both forms of AO bind directly to the polymer will be considered later, along with possible explanations for the occurrence of two relaxation times. In terms of this mechanism, a lower bound can be estimated for the second-order rate constant characterizing the initial combination of dye and polymer by assuming the relaxation time for this process is less than 10 μsec ; in this case

$$k > \sim \frac{1}{\tau[\text{PGA}]} \sim 10^8 M^{-1} \text{sec}^{-1}$$

which is similar to the value found for dimer forma-

tion in the AO system. (The rate constant for the PGA-AO interaction would be expected to be larger, since it involves a reaction between positively and negatively charged molecules.) An alternative mechanism is one in which the measured relaxation times are considered to be primarily associated with the combination of dye and polymer, but at high PGA concentrations other processes (for example, the transfer of a dye molecule between polymers) become coupled to this simple one-step mechanism causing a plot of τ^{-1} vs. [PGA] to level off rather than continuing as a straight line as predicted by the simple mechanism. For this mechanism, the characteristic second-order rate constant would be given approximately by the initial slopes of Figures 5–7. The *maximum* rate constant estimated by such a procedure is approximately $3 \times 10^6 M^{-1} \text{sec}^{-1}$, which is considerably less than the value found in the AO system. If direct dye transfer were involved, the rate would presumably be slower for the random coil because of unfavorable electrostatic interactions. Therefore, this type of mechanism seems unlikely. If we assume the relaxation times characterize an intramolecular process, a simple mechanism which is consistent with the dependence of the relaxation times upon the polymer concentration, but excludes the various possible aggregation states of the dye, can be formally written as



where P and D designate polymer and dye, respectively. Equation 4 means that n polymer molecules are associated with each dye molecule. Assuming the first step is equilibrated rapidly, the slow relaxation time for eq 4 can be written as (see Appendix for details)

$$1/\tau = k_{32} + \frac{k_{23}}{1 + \frac{k_{21}}{k_{12}([\text{P}]^n + n^2[\text{D}][\text{P}]^{n-1})}} \quad (5)$$

Since in the present experiments $n^2(\text{D})(\text{P})^{n-1}$ is usually much smaller than $(\text{P})^n$, eq 4 can be approximated as

$$1/\tau = k_{32} + \frac{k_{32}}{1 + \frac{k_{21}}{k_{12}[\text{P}]^n}} \quad (6)$$

Theoretical curves for n equal to 1, 2, and 3 were fit to the data by a trial and error procedure. Some of these curves are shown in Figures 5–7. In all cases the best fit is obtained for n equals to 2 or 3, although the fit is

(8) P. Debye, *Trans. Electrochem. Soc.*, **82**, 265 (1942).

(9) M. Eigen, *Z. Physik. Chem. (Frankfurt)*, **1**, 176 (1954).

Table I: Kinetic Parameters for the Polyglutamic Acid-Acridine Orange System

| $10^5[\text{AO}]$ M | pH | Relaxation process | k_{12}/k_{21} M^{-n} | k_{21} sec^{-1} | k_{32} sec^{-1} | n |
|--------------------------|-----|-----------------------|-----------------------------|-------------------------------|-------------------------------|-----|
| 2.5 | 4.7 | 1 | 5×10^2 | 2.3×10^3 | 3×10^2 | 1 |
| 2.5 | 4.7 | 1 | 3×10^7 | 2.2×10^3 | 9×10^2 | 3 |
| 5.0 | 4.7 | 1 | 3×10^2 | 2.8×10^3 | 50 | 1 |
| 5.0 | 4.7 | 1 | 1.3×10^7 | 2.4×10^3 | 6×10^2 | 3 |
| 2.5 | 4.7 | 2 | 1×10^3 | 3.1×10^2 | 20 | 1 |
| 2.5 | 4.7 | 2 | 4.5×10^6 | 2.9×10^2 | 1×10^2 | 2 |
| 5.0 | 4.7 | 2 | 7×10^2 | 3.7×10^2 | 20 | 1 |
| 5.0 | 4.7 | 2 | 2.5×10^3 | 3.6×10^2 | 5 | 2 |
| 2.5 | 7.5 | 2 | 3×10^3 | 4.2×10^3 | 2×10^2 | 1 |
| 2.5 | 7.5 | 2 | 1.6×10^6 | 4.1×10^3 | 1.6×10^3 | 2 |
| 5.0 | 7.5 | 2 | 4×10^2 | 4.7×10^3 | 50 | 1 |
| 5.0 | 7.5 | 2 | 2×10^7 | 5.1×10^3 | 50 | 3 |

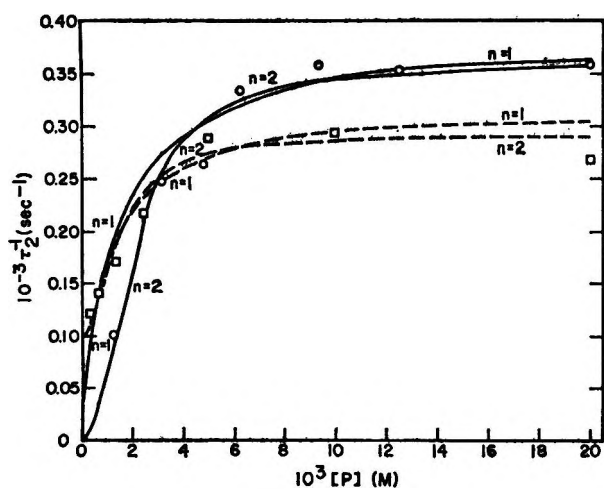


Figure 6. Plot of τ_2^{-1} vs. [PGA] at pH 4.7 and 25.0°: for $[\text{AO}] = 5.0 \times 10^{-5} M$, circles are experimental points, solid lines are theoretical curves; for $[\text{AO}] = 2.5 \times 10^{-5} M$, squares are experimental points, dashed lines are theoretical curves. The theoretical curves are calculated with eq 6 and the values of n given in the figure.

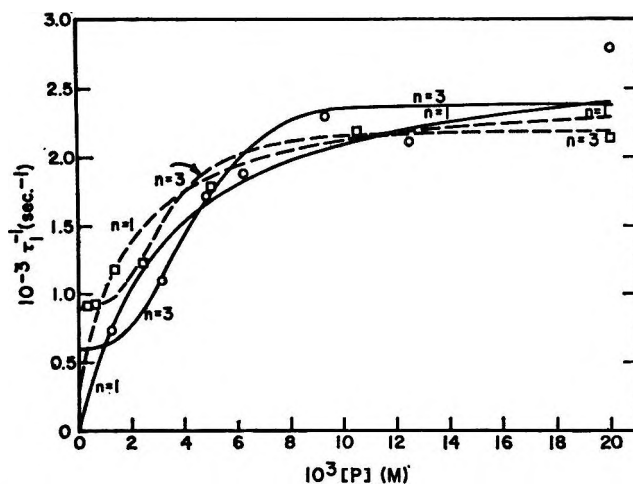
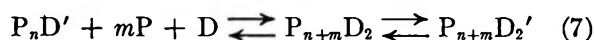


Figure 7. Plot of τ_1^{-1} vs. [PGA] at pH 4.7 and 25.0°: for $[\text{AO}] = 5.0 \times 10^{-5} M$, circles are experimental points, solid lines are theoretical curves; for $[\text{AO}] = 2.5 \times 10^{-5} M$, squares are experimental points, dashed lines are theoretical curves. The theoretical curves are calculated with eq 6 and the values of n given in the figure.

satisfactory for n equals 1 except for the case of τ_2^{-1} at pH 7.5 and $[\text{AO}] = 5.0 \times 10^{-5} M$, where the curve for n equals 1 is an unacceptable representation of the data. The values of k_{12}/k_{21} , k_{23} , and k_{32} which describe the data best are summarized in Table I. If n is equal to 1, the mechanism is easily understood: it simply implies that the rate-controlling step in complex formation is an intramolecular process, presumably desolvation and/or displacement of counterions. If n is equal to 2 or 3, the mechanism does not appear plausible since this implies two or three polymer molecules are binding a single dye molecule.

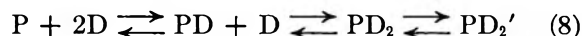
The above mechanism is obviously a gross simplification since it does not take into account the fact that two relaxation times are observed and that the relaxa-

tion times are dependent upon dye concentration. The mechanism can be modified by including the formation of dimer stacks, *i.e.*

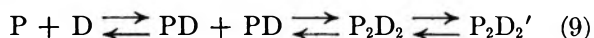


Calculation of the relaxation spectrum of this mechanism with several assumptions about the relative equilibration rates of the different steps yields quite cumbersome expressions, which depend upon the dye concentration in a complex manner, but reduce to a form similar to that of eq 5 in certain limits. The data are not precise enough to merit further refinement along these lines except to say that enough parameters are available so that the data can be fit about as well as the simple mechanism (eq 4) with n equal to 1.

Many other types of mechanism have been investigated in trying to correlate the experimental data. For example, a "stacking mechanism" such as



cannot be reconciled with the data. A rather improbable mechanism which yields a fit to the data similar to the above case where n is equal 1, is one in which two polymer chains, each with a bound dye molecule, interact to form a complex in which the two dyes are shared by the two polymers, *i.e.*



It does not appear likely that two random-coil polymer chains with or without bound dye molecules will combine, because of the unfavorable electrostatic conditions for such an interaction, although spectral data concerned with the interaction of polyadenylic acid and acridine orange led to the speculation that in the presence of excess of polyadenylic acid, bound dye is shared by the macromolecules.^{2b}

Another possible mechanism is one in which after a very rapid initial polymer-dye interaction, two consecutive intramolecular processes occur which represent the faster and slower relaxation processes, respectively.

This may be written



By making the assumptions that the initial step is equilibrated very rapidly compared with the last two, and that the final step is very slow compared with the previous one, expressions for both relaxation times can be derived which are similar to eq 6, when n equals 1.

Finally, we have considered the effect of including the monomer-dimer equilibrium of acridine orange in the mechanisms: in fact, this refinement produces only minor changes in the shapes of the theoretical curves regardless of what assumptions are made concerning the nature of the species being bound.

To conclude, an exhaustive examination of possible mechanisms of the PGA-AO interaction has not led to a quantitative fit of the data. This may be due to the fact that discrete relaxation times are not being measured. The results do seem to indicate that the initial PGA-AO interaction is quite rapid and is followed by relatively slow intramolecular processes. However, this simple mechanism is clearly not sufficient to explain all of the results quantitatively.

If the aggregation or "stacking" of acridine orange upon the polymer chain is responsible for the observed relaxation processes, then this occurs considerably more

slowly than in free solution. Conceivably "stacking" along the polymer chain could involve displacement of solvent and counterions and therefore might be slower than in the AO dimer. However, another possibility is that the rate-controlling steps being observed are involved in the actual mechanism of complex formation between AO and PGA, which would also involve displacement of solvent molecules and counterions. The actual "stacking" interaction probably occurs very rapidly as in the AO dimer ($k > 10^{10} \text{ sec}^{-1}$). Alternatively, polymer aggregation might be occurring, but this seems unlikely for PGA at high pH values. Unfortunately, our results yield no criterion upon which a distinction between the various mechanisms can be made.

The geometrical form of the polyglutamic acid appears to have a negligible part in influencing the overall mechanism or stoichiometry of the interaction with acridine orange, but does affect the magnitude of the kinetic parameters. A smaller electrostatic attraction of the cationic dye for the polymer when more of the carboxyl groups of the latter are protonated presumably accounts for the slower reaction of acridine orange with the helical form of the polymer. The observation that the spectrum of a solution of acridine orange at pH 12.8 is only negligibly changed by the presence of polyglutamic acid at a concentration of approximately $2 \times 10^{-2} M$ indicates that when acridine orange is essentially unprotonated, its interaction with polyglutamic acid is very weak. Furthermore, this suggests that the binding between PGA and AO is primarily electrostatic in nature.

Little conclusive information about the structure of PGA-AO complexes is available and reports about the form of the DNA-AO complex indicate the variance of opinion in this field^{2a,e,10-12} The results obtained here indicate that the structure of the complexes should be qualitatively similar for both geometrical forms of PGA.

A preliminary investigation of the interaction between polynucleotides and acridine orange by the temperature-jump method has shown that in these systems the relaxation effects are even more complex. However, hopefully, further studies of these and analogous systems will lead to clarification of the mechanism of interaction of the polyglutamic acid-acridine orange system.

(10) L. S. Lerman, *J. Mol. Biol.*, **3**, 18 (1961); *Proc. Natl. Acad. Sci. U. S.*, **49**, 94 (1963).

(11) S. F. Mason and A. J. McCaffery, *Nature*, **204**, 468 (1964).

(12) L. Stryer and E. R. Blout, *J. Am. Chem. Soc.*, **83**, 1411 (1961).

Appendix

Derivation of Equation 5

From eq 4, the rate law near equilibrium can be written as

$$\frac{-d\delta[P_n D']}{dt} = -k_{23}\delta[P_n D] + k_{32}\delta[P_n D'] \quad (\text{A1})$$

Mass conservation requires that

$$\delta[D] + \delta[P_n D] + \delta[P_n D'] = 0 \quad (\text{A2})$$

$$\delta[P] + n\delta[P_n D] + n\delta[P_n D'] = 0 \quad (\text{A3})$$

and differentiation of the equilibrium constant

$$k_{12}/k_{21} = K_{12} = \frac{[P_n D]}{[P]^n [D]} \quad (\text{A4})$$

gives

$$\delta[P_n D] = K_{12}[P]^n \delta[D] + nK_{12}[D][P]^{n-1} \delta[P] \quad (\text{A5})$$

Combination of eq A2, A3, and A6 yields

$$\delta[P_n D] = [(K_{12}/n)[P]^n + nK_{12}[D][P]^{n-1}] \delta[P] \quad (\text{A6})$$

Substitution of eq A3 into eq A1 gives

$$\frac{-d\delta[P_n D']}{dt} = \left[k_{32} + \frac{k_{23}}{1 + \frac{\delta[P]}{n\delta[P_n D]}} \right] \delta[P_n D'] \quad (\text{A7})$$

$$= \frac{1}{\tau} \delta[P_n D] \quad (\text{A8})$$

and use of eq A6 gives the expression for the relaxation time in eq 5.

Kinetics of Excited Molecules. V. Photochemistry of Hexafluoroacetone

by Peter G. Bowers¹ and Gerald B. Porter

Department of Chemistry, University of British Columbia, Vancouver, Canada (Received December 13, 1965)

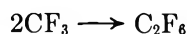
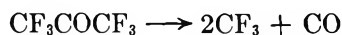
The photochemical decomposition of hexafluoroacetone has been examined over a wide pressure range at several different exciting wavelengths. A mechanism for the primary photochemical process is proposed to interpret these results and those of the emission spectra. All of the rate constants for the elementary reactions are evaluated. The natural lifetime of the triplet state is estimated to be about 0.03 sec. The RRR theory of unimolecular reactions is applied to the rate constants for dissociation of singlet excited molecules.

Introduction

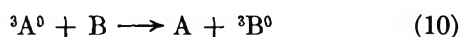
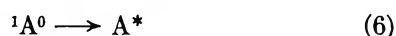
Various aspects of the photolysis of hexafluoroacetone (HFA) have been studied to elucidate the primary process.²⁻⁴ HFA is a particularly good substance for this type of investigation because its photochemistry is simple for low conversions, except at elevated temperatures.⁵ Carbon monoxide and hexafluoroethane, formed in equal amounts, are the only products, and the quantum yield of either can be assumed with certainty to represent the quantum yield of primary dissociation,

ϕ . The chemical mechanism of the reaction is adequately represented by the following two steps.

- (1) Holder of a University of British Columbia Fellowship, 1962-1963, and a National Research Council Bursary, 1963-1964.
- (2) P. B. Ayscough and E. W. R. Steacie, *Proc. Roy. Soc. (London)*, **A234**, 476 (1956).
- (3) G. Giacometti, H. Okabe, and E. W. R. Steacie, *Proc. Roy. Soc. (London)*, **A250**, 287 (1959).
- (4) H. Okabe and E. W. R. Steacie, *Can. J. Chem.*, **36**, 137 (1958).
- (5) A. S. Gordon, *J. Chem. Phys.*, **36**, 1330 (1962).



The simplest reaction sequence necessary to interpret the available data on the primary process is embodied in the following set.



The notation is that generally used for the primary process of the substance A, which here represents hexafluoroacetone. The superscripts 1 and 3 represent the multiplicity of the excited electronic states, while an asterisk denotes a molecule with more vibrational energy than a vibrationally equilibrated molecule with superscript zero. Reaction 10 occurs in the presence of a suitable acceptor, notably biacetyl.⁶ The scheme is simplified to the extent that some of the reactions must take place in a sequence of more elementary reactions.

The present work was undertaken to provide more information about the detailed primary process, particularly with respect to the dependence on temperature and exciting wavelength of the dissociation reactions 2 and 8.

Experimental Section

Some of the experimental details have been described previously.⁴ For most of the photolyses, HFA gas was prepared from its hydrate, obtained from Merck of Canada. In a few runs, Allied Chemical HFA gave completely concordant results.

Light from a BTH Type ME/D mercury lamp (for wavelengths longer than 2850 Å) or a Hanovia D517A compact arc (for shorter wavelengths) was focussed on the entrance slit of a fast grating monochromator. The emergent light passed through a 9863 Corning filter, and then along the axis of the reaction cell as a parallel beam approximately 1 cm in diameter, without touching the walls of the cell. It then impinged on a ferrioxalate actinometer to provide a measure of the

radiation transmitted by the cell and its contents, integrated over the duration of a run. The half-widths of the radiation used for excitation (about 50 Å) were determined with a second grating monochromator equipped with a photocell.

The cylindrical reaction vessels were made of Pyrex glass tubes, to which quartz windows were cemented with an epoxy resin. This procedure allowed the actual transmission properties of each window to be measured accurately before it was attached to the cell. Depending on the absorption coefficient and pressure of HFA, one of three cells, with lengths 4, 14, and 40 cm, but otherwise identical, was used to have the fraction of incident light absorbed in a conveniently measurable range. The absorption under conditions of the photolyses was monitored with an RCA 935 photocell. At very low pressures, however, it was necessary to measure the absorption coefficient in a 125-cm cell, and to determine the absorption in the photolysis cell through a Lambert's law extrapolation. Small deviations from Beer-Lambert law behavior were evident only at the very highest pressures of HFA used.

After reaction, C₂F₆ and unreacted HFA were condensed out by distilling the products into two traps in series at -196°. Carbon monoxide was collected in a calibrated McLeod-Toepler gauge. Gas chromatographic analysis showed that the carbon monoxide collected was pure.

Results

The photochemical data are presented in Figures 1-6, which show the reciprocal primary quantum yield as a function of pressure of HFA for a number of wavelengths of excitation at room temperature, and one wavelength at -78°.

Some general observations may be summarized as follows. (i) All the $1/\phi$ vs. pressure plots have a constant or positive decreasing slope. There is no evidence whatever that the slopes tend to zero at low pressure, even though extensive data were obtained down to 1 mm. (ii) ϕ^0 , the extrapolated primary quantum yield at zero pressure is very close to 1 (1.00 ± 0.03) at all wavelengths, with the possible exception of 3340 Å, where the extrapolation is unreliable. (iii) At high pressures the yield decreases to a limiting value, ϕ^∞ . At 3340, 3130, and 3020 Å, ϕ^∞ is 0.2, and this value is reached at progressively higher pressures. Curvature of the plot for 2804 Å is readily apparent, although the high-pressure limit was not reached. (iv) At 2652 Å, $1/\phi$ vs. pressure is linear up to 150 mm, where $\phi = 0.14$. There is a small systematic discrep-

(6) P. G. Bowers and G. B. Porter, *J. Phys. Chem.*, **68**, 2982 (1964).

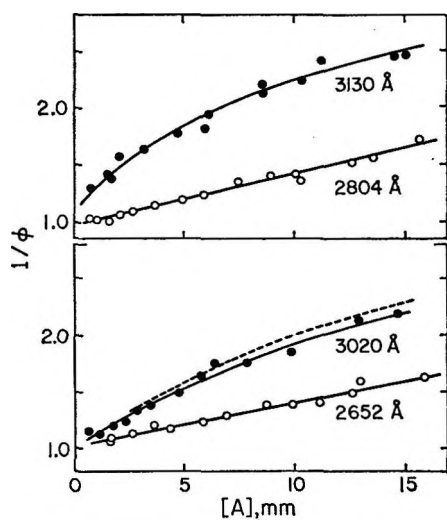


Figure 1. Reciprocal quantum yields for various wavelengths at 25° (lower pressures).

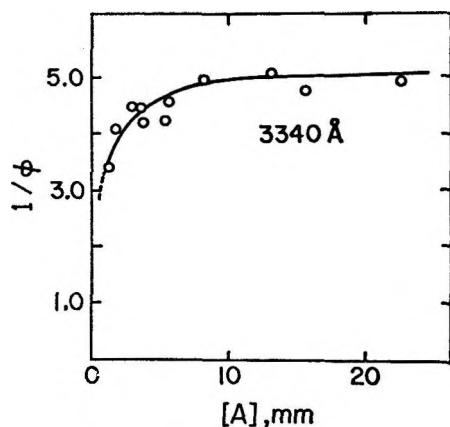


Figure 2. Reciprocal quantum yields at 3340 Å and 25°.

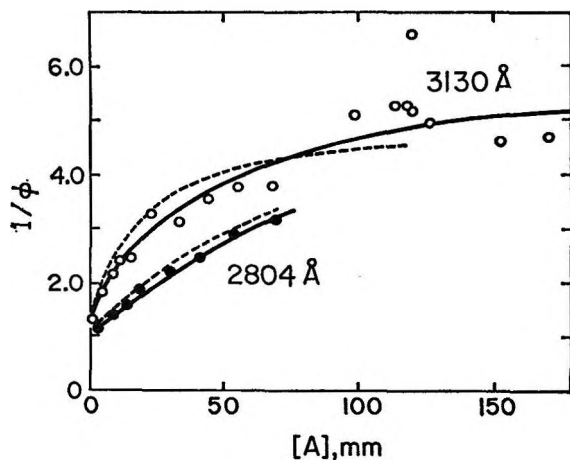


Figure 3. Reciprocal quantum yields at 25° at 2804 and 3130 Å (higher pressures).

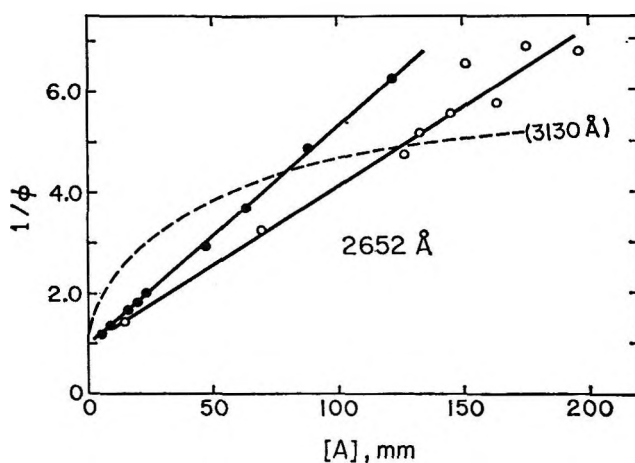


Figure 4. Reciprocal quantum yields at 2652 Å and 25° (higher pressures).

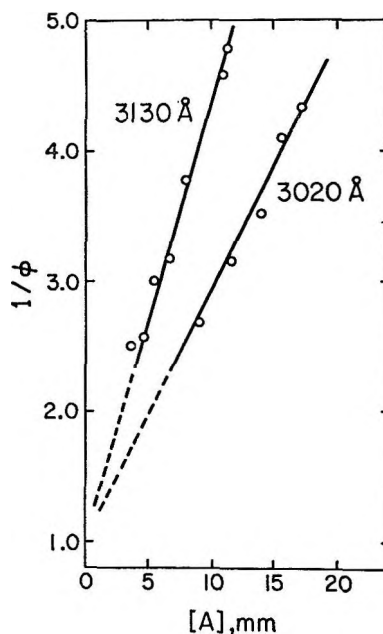


Figure 5. Reciprocal of HFA-biacetyl mixtures at 25° (3130 and 3020 Å).

any between the two sets of data in Figure 4. (v) In the presence of a low concentration of biacetyl (0.2–0.4 mm) the quantum yields at 25° using 3130- or 3020-Å radiation are decreased considerably, with $1/\phi$ then linear with pressure of HFA over the range examined. In these experiments, the fraction of light absorbed by the biacetyl was negligible. (vi) At -78° , with 3130-Å excitation, $1/\phi$ is linear with pressure of HFA. (vii) The quantum yields reported here are higher than those previously given for this compound^{2,3} with regard to the value of ϕ^∞ , for which Ayscough and Steacie found 0.04 at 25°, using 3130 Å.

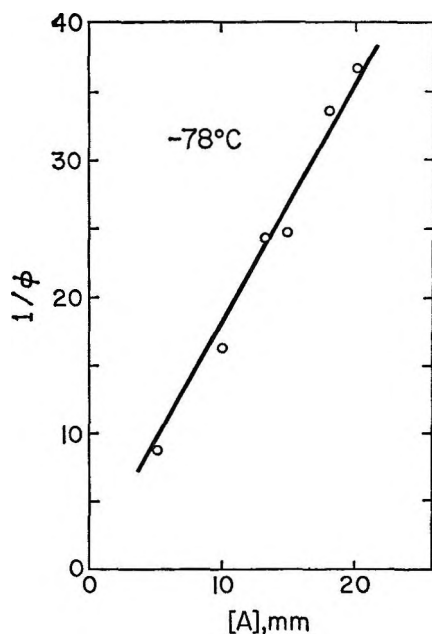


Figure 6. Photolysis of HFA at -78° using 3130-Å excitation.

Discussion

It has been shown⁷ that at low pressures a point of inflection should occur in a plot of $1/\phi$ against pressure if a weak (multistage) collision deactivation process is operative, rather than the strong collision mechanism implied by the reaction scheme above. Furthermore, a multistage process should lead to a zero slope at zero pressure. From our observations, an inflection, if present, could only occur in the pressure region below a few millimeters, and would then be too small an effect to support the idea of weak collisional deactivation.

Kutschke, *et al.*,⁸ have recently shown that a plot of $(1 - \phi)/[A]$ is a sensitive test for weak collisional deactivation, provided systematic errors in the quantum yield are small. Our data plotted in this way do not exhibit the expected behavior for weak collisions. This is not surprising because we find $1/\phi$ to extrapolate linearly to unity at all wavelengths. In the rest of this discussion, therefore, we shall assume that an excited singlet molecule cannot decompose (except *via* the triplet state) once it has suffered a collision.

The mechanism embodied in reactions 1 to 10 leads to the following expression for the primary quantum yield

$$\phi = \frac{k_2}{k_2 + k_3[A]} + \frac{k_3[A]}{k_2 + k_3[A]} \times \frac{k_4}{k_4 + k_5 + k_6} \frac{k_8}{k_7 + k_8 + k_9 + k_{10}[B]} \quad (I)$$

in which the first term is the quantum yield from direct

dissociation of excited singlet molecules, and the second the quantum yield *via* the triplet state. If only singlet dissociation occurs, eq I reduces to a simple linear form

$$1/\phi = 1 + k_3[A]/k_2 \quad (II)$$

The quantum yields for fluorescence and phosphorescence are

$$\phi_{\text{fluor}} = \frac{k_3[A]}{k_2 + k_3[A]} \frac{k_5}{k_4 + k_5 + k_6} \quad (III)$$

$$\phi_{\text{phos}} = \frac{k_3[A]}{k_2 + k_3[A]} \frac{k_4}{k_4 + k_5 + k_6} \times \frac{k_7}{k_7 + k_8 + k_9 + k_{10}[B]} \quad (IV)$$

When biacetyl is present, the second term in (I) is negligible, while ϕ_{phos} drops to zero, and biacetyl itself then shows sensitized phosphorescence.

As has been shown previously, the rate constant k_3 is temperature dependent. If we assume that the other reactions competing for the triplet state have very small activation energies, then Ayscough and Steacie's figures for the temperature variation of ϕ^{∞} lead to a value of about 11 kcal/mole for the activation energy associated with triplet dissociation. (This still holds true, whether reaction 9 is the true radiationless conversion process or a much faster pseudo-first-order reaction of a constant trace concentration of some quenching impurity.)

Since the triplet state of HFA has a long lifetime (see below), there is adequate time for the thermal unimolecular reaction 8 to occur. Thus triplet state dissociation is strongly temperature dependent, increasing as the temperature is raised. At a temperature of -78° , for example, there is no detectable dissociation *via* the triplet state, as evidenced by the linear $1/\phi$ vs. $[A]$ plot.

In order to test eq I and to arrive at values for the various rate constant ratios, it is convenient to abbreviate that equation to the form

$$\phi = \frac{a + b[A]}{a + [A]} \quad (V)$$

where

$$a = k_2/k_3$$

$$b = \frac{k_4}{k_4 + k_5 + k_6} \frac{k_8}{k_7 + k_8 + k_9 + k_{10}[B]}$$

(7) B. T. Connelly and G. B. Porter, *J. Chem. Phys.*, **33**, 81 (1960).

(8) A. N. Strachan, R. K. Boyd, and K. O. Kutschke, *Can. J. Chem.*, **42**, 1345 (1964).

Then, to obtain an equation which can be plotted as a linear function, eq V is rearranged to give the following

$$\frac{\phi}{1 - \phi} = \frac{b}{1 - b} + \frac{a}{(1 - b)[A]}$$

$$\frac{[A]}{1 - \phi} = \frac{a}{1 - b} + \frac{[A]}{1 - b}$$

Unfortunately, both equations utilize the quantity $1 - \phi$, which involves a large experimental error at low pressures where ϕ is nearly unity. However, the data do give reasonable least-squares lines, so that the parameters a and b can be determined at each wavelength, as shown in Table I. In the presence of biacetyl, the a values (5.3 and 3.0 mm at 3130 and 3020 Å, respectively) are obtained directly from the slopes of the lines in Figure 5 and compare reasonably with the values in Table I. It is evident that biacetyl in trace quantities has little effect on singlet excited HFA.

Table I: Values for the Parameters a and b under the Various Photolysis Conditions

| λ , Å | Temp., °C | a , mm | b |
|------------------|--------------|-------------|------|
| 3340 | 25 | ... | 0.19 |
| 3130 | 25 | 3.8 | 0.21 |
| 3130 | -78 | 0.61 | 0 |
| 3020 | 25 | 6.0 | 0.22 |
| 2804 | 25 | 17.3 | 0.12 |
| 2652 | 25 | 22.6 | 0 |

At 3130 Å and 33 mm of HFA it was found that⁹

$$\frac{k_3[A]}{k_2 + k_3[A]} \frac{k_4}{k_4 + k_5 + k_6} = 0.45 \quad (\text{VI})$$

Using the ratio k_2/k_3 from Table I, we find, therefore

$$k_5 + k_6 \simeq k_4$$

The fluorescence yield under the same conditions is 0.009,⁹ and hence from eq III

$$k_4 + k_6 \simeq 100k_5$$

The value of k_5 as determined from the integrated absorption coefficient is $1.8 \times 10^5 \text{ sec}^{-1}$. Thus, we can assign the values

$$k_4 \simeq k_6 \simeq 1.0 \times 10^7 \text{ sec}^{-1}$$

The lifetime of the HFA triplet state has been found from the phosphorescence decay to be $1.8 \times 10^{-3} \text{ sec}$ at room temperature.⁹ That is

$$k_7 + k_8 + k_9 = 5.5 \times 10^2 \text{ sec}^{-1}$$

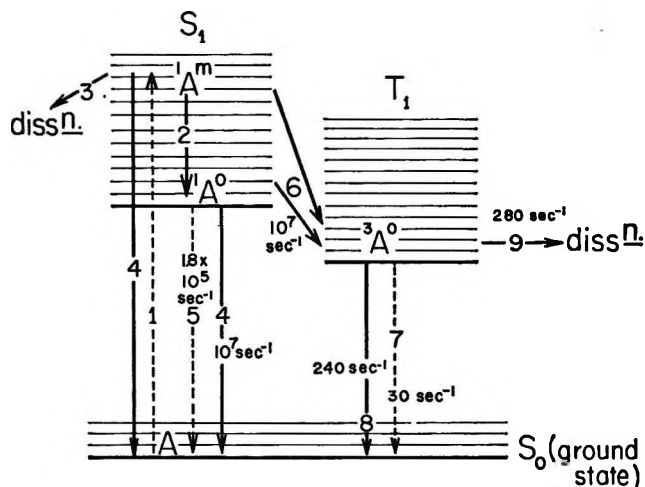


Figure 7. Rate constants for the primary processes in HFA at 25° estimated from absorption, emission, and dissociation data.

Furthermore, under the conditions where eq VI holds, the phosphorescence yield is 0.025,⁹ and so

$$\frac{k_7}{k_7 + k_8 + k_9} = 0.056$$

Combining these figures with the long wavelength value of b from Table I gives

$$k_7 = 30 \text{ sec}^{-1}$$

$$k_8 = 240 \text{ sec}^{-1}$$

$$k_9 = 280 \text{ sec}^{-1}$$

The results of these calculations are summarized in the Jablonski diagram, Figure 7. The fact that the rate constants for internal conversion (k_4) and intersystem crossing (k_6) are comparable is in contrast to recent findings for some aromatic molecules in solution,¹⁰ where internal conversion from the excited singlet state is apparently negligible. Despite the many experimental uncertainties inherent in the measurement of an intersystem crossing efficiency, we feel it unlikely that our value of 0.45 in eq VI is only half the true value. The actual values given to k_4 and k_6 ($\simeq 10^7 \text{ sec}^{-1}$) may be somewhat high, considering that k_2 at 3130 Å is only $3.8 \times 10^7 \text{ sec}^{-1}$ (see Table II), and yet the limiting low-pressure dissociation yield is very close to unity. The error here may arise in the calculation of k_5 from an integrated absorption coefficient.

The value of k_8 corresponds to an activation energy of 14.5 kcal/mole based on a "normal" frequency factor

(9) J. McIntosh and G. B. Porter, unpublished results.

(10) T. Medinger and F. Wilkinson, *Trans. Faraday Soc.*, **61**, 620 (1965).

of 10^{13} sec^{-1} . From the increase in ϕ_{phos} on cooling from room temperature to -78° , we find k_9 to have an activation energy of 0.6 kcal/mole.¹¹ The difference, $E_8 - E_9 = 14$ kcal/mole, is somewhat larger than the experimental value of 11 kcal for the activation energy for triplet dissociation deduced above.

The data of Table I do not fit the proposed mechanism at the shortest wavelengths, in that ϕ^∞ , instead of remaining constant at 0.21, decreases progressively. There is considerable scatter in these data, which arose from the low light intensities and consequent extended runs at 2800 and 2650 Å. Further, the limiting quantum yield is attained only at quite high pressures, so the conclusions with regard to the values of ϕ^∞ are uncertain. The original luminescence data³ showed that fluorescence (which is all that was observed) does occur down to 2537 Å. We have verified this result in our laboratories⁹ and have shown that both fluorescence and phosphorescence are observable at 2500 Å at room temperature and, somewhat enhanced, at -78° . Unfortunately, it has not yet been possible to verify whether the phosphorescence/fluorescence ratio decreases for short wavelength excitation, as we would expect if ϕ^∞ decreases. Because of these uncertainties, further discussion of the detailed behavior at short wavelengths is not possible at present.

The ratio k_2/k_3 is derived essentially from the slope of the linear function $1/\phi$ vs. $[A]$ (eq II), even though in practice, because of triplet dissociation, a more complicated function has to be considered. The separation of k_2 can only be done if a value of k_3 can be assumed. We adopt the strong collision degradation mechanism and use the kinetic theory bimolecular collision rate constant for k_3 . That is, with $\sigma = 6$ Å, $k_3 = 1.88 \times 10^{11}$ l./mole sec. The values of k_2 , given in Table II, are obtained by this procedure at each wavelength. For comparison, the rate constants of Ayscough and Steacie are also given.²

Table II: Rate Constants for Photodissociation

| Temp. °C | λ , Å | k_2 , sec ⁻¹ |
|-------------|-------------------|------------------------------|
| 107 | 3130 ² | 2.35×10^8 |
| 78 | 3130 ² | 1.25×10^8 |
| 53 | 3130 ² | 6.25×10^7 |
| 27 | 3130 ² | 3.01×10^7 |
| 25 | 3130 | 3.8×10^7 |
| -78 | 3130 | 4.7×10^6 |
| 25 | 3020 | 6.0×10^7 |
| 25 | 2804 | 1.7×10^8 |
| 25 | 2652 | 2.3×10^8 |
| 25 | 2640 ² | $\sim 3 \times 10^8$ |

The species $^1A^*$ dissociates from vibrationally excited (nonequilibrium) levels. The energy spread of the excited molecules depends upon the wavelength distribution of the "monochromatic" light, and on E , the thermal vibrational energy in the ground state. We shall consider perfectly monochromatic light in the calculations below; corrections for the widths of the exciting lines were found to be quite small ($<10\%$).

In the energy diagram, Figure 8, E_x is the energy of the exciting wavelength in excess of the zero-zero band, E_{00} . The tacit assumption is that the energy E_x is randomly distributed among the various vibrational degrees of freedom of the molecule. E_{min} is critical energy required for dissociation. A molecule with vibrational energy E_{min} or greater in a favorable internal mode (the carbon-carbon extension) is presumed to cross to an unstable state and undergo rapid predissociation.

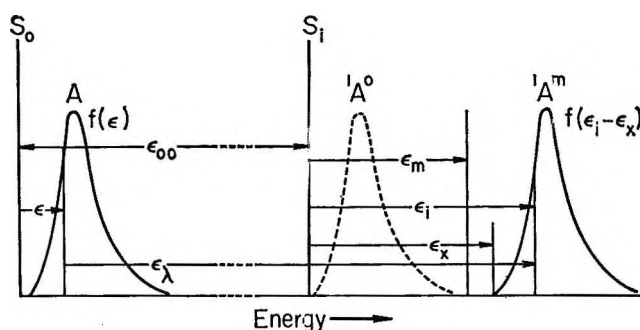


Figure 8. Energy diagram for photodissociation of S_1 .

The total vibrational energy relevant to the dissociation of $^1A^*$ is

$$E_1 = E_x(\lambda) + E(T)$$

Equation II then becomes

$$\frac{1}{\phi} = \left[\int_{E_c}^{\infty} \frac{k_2(E_1)f(E)}{k_2(E_1) + k_3[A]} dE_1 \right]^{-1} \quad (\text{VII})$$

where $k_2(E_1)$ is the specific rate constant for a molecule with vibrational energy E_1 .

In the general case, the lower limit of integration may be either E_{min} or E_x . The latter case arises if $E_{\text{min}} < E_x$, and is recognized by $\phi^0 = 1$. That is, in the absence of collisions, the optical contribution is sufficient to promote dissociation of all molecules, regardless of their thermal energy content. For HFA, ϕ^0 is close to unity at wavelengths 3130 Å or shorter, and this

(11) The quantum yields quoted in ref 6 are in error. The lifetime for phosphorescence increases from 1.8×10^{-3} sec at 25° to 2.7×10^{-3} sec at -60° .⁹

gives an upper limit to the critical energy E_{\min} . From the known value of E_{00} ,⁴ we get $E_{\min} < 8.6$ kcal/mole.

An important point is that if ϕ^0 is less than unity, then when $E_{\min} < E_x$ there may be a competing unimolecular process such as the internal conversion



with $k_{2a} \simeq k_2$. On the other hand, if $E_{\min} < E_x$, then some ${}^1A^*$ molecules simply have insufficient energy to decompose, and in this case k_{2a} may be quite negligible compared with k_2 . Under conditions of weak excitation, such an effect ($\phi^0 < 1$) is shown by ketene¹² and azoethane.¹³

Equation VII is approximately equivalent to

$$\frac{1}{\phi} = 1 + k_3[A]\langle 1/k_2 \rangle \quad (\text{VIII})$$

where the mean value is defined as

$$\langle 1/k_2 \rangle = \int_{E_x}^{\infty} \frac{g(E_1)}{k_2(E_1)} dE_1 \quad (\text{IX})$$

The function $g(E_1)$ is simply $f(E)$ shifted along the energy axis as shown in Figure 8, so that

$$g(E_1) = 0 \text{ for } E_1 < E_x$$

$$g(E_1) = f(E_1 - E_x) \text{ for } E_1 \geq E_x$$

To compute values of $\langle 1/k_2 \rangle^{-1}$ for comparison with k_2 (observed) requires explicit expressions for $k_2(E_1)$ and $f(E)$. This is the type of calculation done in detail by Rabinovitch,¹⁴ *et al.*, for chemically activated systems. Because the normal mode frequencies for HFA have not been measured for either ground or excited states, the classical general forms for $k_2(E_1)$ and $f(E)$ were used. Equation IX then becomes

$$\langle 1/k_2 \rangle = \int_{E_x}^{\infty} \left[1 - \frac{E_{\min}}{E_1} \right]^{1-s_1} \times$$

$$\left[\frac{E_1 - E_x}{kT} \right]^{s_2-1} \exp \left(\frac{E_1 - E_x}{\nu kT(s_2 - 1)} \right) dE_1 \quad (\text{X})$$

The index s_1 , on the RRK picture,¹⁵ is the number of normal modes exchanging energy with the breaking bond, while s_2 is the number contributing to the thermal energy in the ground state. In Figure 9, some computed values for the integral (X) are compared with the experimental data at 3130 Å. We would not expect the Arrhenius plot to be linear (hence our avoidance of the term "activation energy" for E_{\min}). In the high-temperature limit, where thermal energy is dominant, the slope could be interpreted in the usual way, whereas

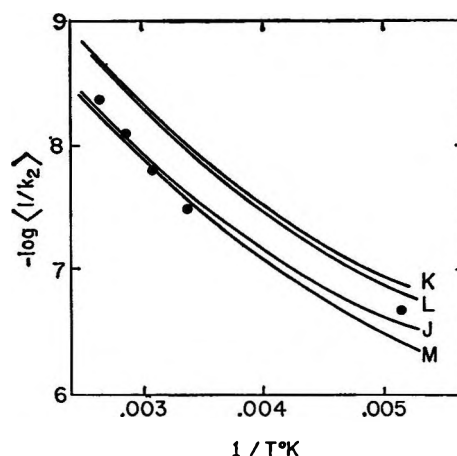


Figure 9. Calculated $k_2(T)$ values compared with experimental data. Curves K and L have been displaced upward 0.2 unit.

at low temperatures, $\langle 1/k_2 \rangle^{-1}$ approaches a limiting value determined only by the value of E_x (*i.e.*, by the exciting wavelength). The greatest slope and intercept in the experimental points thus provide lower limits for E_{\min} and the frequency factor ν . The figures are $E_{\min} > 5.7$ kcal/mole and $\nu > 3 \times 10^{11}$ sec⁻¹.

Order-of-magnitude agreement may be obtained between the calculated and observed values of $k_2(T)$ at 3130 Å, if rather more than half the normal modes are taken for the index s_1 (approximations J, K, L, and M in Figure 9 and Table III). However, the values for $k_2(\lambda)$ at 25°, calculated using any of these sets of approximations, are very much larger than those found experimentally. The best approximation is M, where ν was chosen to have its minimum possible value, based on temperature dependence (3×10^{11} sec⁻¹). The comparison is shown in Table IV. The calculated value of k_2 at 2652 Å is about 30 times too large.

Table III: Parameters Used in Calculating the Curves in Figure 9

| Curve | $10^{-14}\nu$, sec ⁻¹ | s_1 | s_2 | E_{\min} , cm ⁻¹ |
|-------|--------------------------------------|-------|-------|----------------------------------|
| J | 1.58 | 22 | 11 | 2500 |
| K | 1.00 | 15 | 10 | 3000 |
| L | 1.58 | 19 | 11 | 2750 |
| M | 3.2×10^{-3} | 15 | 18 | 3000 |

(12) W. A. Noyes, Jr., and A. N. Strachan, *J. Am. Chem. Soc.*, **76**, 3258 (1954).

(13) H. Cerfontain and K. O. Kutschke, *Can. J. Chem.*, **36**, 344 (1958).

(14) R. E. Harrington, B. S. Rabinovitch, and M. R. Hoare, *J. Chem. Phys.*, **33**, 744 (1960).

(15) L. J. Kassel, "Kinetics of Homogeneous Gas Reactions," Chemical Catalog Co., Inc., New York, N. Y., 1932.

Table IV: Calculated and Observed Rate Constants k_2 at 25° (Approximations M and N Differ only in the Values Assigned to s_1)

| λ , A | k_2 (obsd), sec ⁻¹ | M | | N | |
|------------------|------------------------------------|-------|--|-------|--|
| | | s_1 | $\langle k_2^{-1} \rangle^{-1}$, sec ⁻¹ | s_1 | $\langle k_2^{-1} \rangle^{-1}$, sec ⁻¹ |
| 3130 | 3.8×10^7 | 15 | 2.8×10^7 | 15 | 3.8×10^7 |
| 3020 | 6.0×10^7 | 15 | 4.8×10^8 | 17 | 1.4×10^8 |
| 2804 | 1.7×10^8 | 15 | 4.2×10^9 | 21 | 4.5×10^8 |
| 2652 | 2.3×10^8 | 15 | 8.6×10^9 | 24 | 5.4×10^8 |

Several reasons may exist for the apparent inefficiency of the "optical" vibrational energy in promoting dissociation. The original assumption that E_x is distributed randomly may in itself be reasonable, but clearly requires that *all* the normal modes be used in the RRK equation for $k_2(E_1)$. Another point is that the number of active modes may increase with increasing energy.¹⁶ The larger the total vibrational energy, the

greater is the possibility of exciting some of the higher vibrational frequencies. In approximation N, Table IV, the value of s_1 was increased from 15 at 3130 Å ($E_x = 3380 \text{ cm}^{-1}$) to its maximum value of 24 at 2652 Å ($E_x = 9140 \text{ cm}^{-1}$), and proportionately at intermediate wavelengths. Although this results in a much better correlation with the experimental values of $k_2(\lambda)$, such arbitrary adjustments carry little conviction. It is felt that a more realistic assessment of these rate constants must await a quantum statistical formulation based on the normal mode frequencies of the ground state of the molecule and an indication as to how these may change in the excited states.

Acknowledgment. This research was made possible through a grant from the National Research Council of Canada.

(16) E. K. Gill and K. J. Laidler, *Proc. Roy. Soc. (London)*, **A250**, 121 (1959).

Positive Hole Migration and Trapping in γ -Irradiated 3-Methylpentane at -196°

by David W. Skelly¹ and William H. Hamill

Department of Chemistry and the Radiation Laboratory,² University of Notre Dame, Notre Dame, Indiana 46556
(Received December 14, 1965)

In γ -irradiated glassy 3-methylpentane at -196° , toluene forms a cation T^+ with absorption maxima at 1075 and 425 $m\mu$ and carbon tetrachloride forms a cation C^+ with one band at 480 $m\mu$. The formulas of these ionic species are unknown. Both additives trap electrons, but no absorption attributable to anions was observed. At 2.4 mole % toluene, addition of carbon tetrachloride to 2.6 mole % increased OD(T^+) markedly, which is attributable to increased stabilization of T^+ by electron trapping. At 2.6 mole % CCl_4 , adding up to 2.4 mole % toluene tends to saturate OD(T^+) due to increased hole trapping, while OD(C^+) remains constant. The facts suggest that carbon tetrachloride traps only excited holes while toluene traps only ground-state holes. Other types of charge migration are considered.

Introduction

A considerable number of examples of a variety of typical ionic processes have been reported for γ -irradiated organic solids. Among these are the migration through an appropriate matrix of electrons and (positive) holes, and their trapping by the matrix or by solutes.³ To observe either anionic or cationic species, both must be stabilized. There are two recognizable mechanisms of hole trapping. One is proton transfer, *e.g.*, $CH_3OH^+ + CH_3OH \rightarrow CH_3OH_2^+ + CH_2OH$. The other is charge transfer to a molecule of lower ionization potential,³ *e.g.*, $C_6H_{14}^+ + C_6H_6 \rightarrow C_6H_{14} + C_6H_6^+$. Electrons can be trapped by simple attachment to form molecular anions, *e.g.*, $(C_6H_5)_2 + e^- \rightarrow (C_6H_5)_2^-$. They also react by dissociative resonance attachment, *e.g.*, $CH_3Cl + e^- \rightarrow CH_3 + Cl^-$.⁴ Electrons can also be trapped by a variety of glassy solids, including alkanes⁵ and ethers.³ In the 3-methylpentane (3MP) matrix, solvent-trapped electrons escape spontaneously (or diffuse) and react slowly with holes or with appropriate solutes.⁵

Much less is known about the behavior of holes. Since solvent-trapped electrons are observed in pure 3MP ($>0.6/100$ ev) there must be solvent-trapped holes, but no corresponding absorption band has been identified. There is no evidence for slow migration of holes, but solute cations form in good yield during, or immediately after, γ -irradiation.³ Also, two cation-forming additives compete with each other for holes.^{3,6}

Many cations can be photobleached,³ and this suggests electronic excitation of holes.

Toluene has a lower ionization potential than 3MP and traps holes, as expected. Carbon tetrachloride has a higher ionization potential than 3MP, but it also forms cations in this matrix.³ It will be shown that when both additives are present there is no apparent competition for the limited yield of migrating holes. The present work is concerned with this apparent anomaly which is attributed to migration of holes at two levels of excitation of 3MP.

Experimental Section

Phillips pure grade 3-methylpentane was treated with concentrated sulfuric acid until no change in color resulted. It was then washed with water, dried over calcium chloride, and passed through an 8-ft column of freshly activated silica gel, retaining the middle two-

(1) From the Ph.D. Dissertation of D. W. Skelly.

(2) The Radiation Laboratory of the University of Notre Dame is operated under contract with the U. S. Atomic Energy Commission. This is AEC Document No. COO-38-451.

(3) J. P. Guarino and W. H. Hamill, *J. Am. Chem. Soc.*, **86**, 777 (1964).

(4) J. B. Gallivan and W. H. Hamill, *Trans. Faraday Soc.*, **61**, 1960 (1965); D. W. Skelly and W. H. Hamill, *J. Chem. Phys.*, **43**, 2795 (1965).

(5) J. B. Gallivan and W. H. Hamill, *ibid.*, **44**, 1279 (1966).

(6) J. B. Gallivan and W. H. Hamill, *ibid.*, in press.

thirds. Toluene and carbon tetrachloride of reagent grade were used as received.

Samples were handled on a preparative vacuum line, distilled into cells formed from drawn 1 cm \times 1 cm Ultrasil tubing, sealed, plunged into liquid nitrogen, and γ irradiated (1.5 to 2.7×10^{18} ev g^{-1} min^{-1}). They were transferred to a windowed dewar flask filled with liquid nitrogen for examination using a Cary Model 14R recording spectrophotometer.

Results and Discussion

Both $C_6H_5CH_3$ and CCl_4 form cationic species in the γ -irradiated 3MP glassy matrix.³ They are presumed to be the molecular ions, but this has not been demonstrated, and they will be designated arbitrarily by T^+ and C^+ . The optical absorption bands lie at 425 and 1075 $m\mu$ for T^+ and at 480 $m\mu$ for C^+ . Each of these additives traps electrons, probably as $C_6H_5CH_3^-$ and Cl^- , since they depress the solvent-trapped electron band at $\lambda_{max} \sim 1.6 \mu$, or altogether prevent its appearance. Of these two additives, CCl_4 is the more efficient.

The promotion of the optical density at 1075 $m\mu$ of the $C_6H_5CH_3$ cation, $OD(T^+)$, by CCl_4 in a matrix containing 2.4 mole % $C_6H_5CH_3$ appears in Figure 1. At this concentration of $C_6H_5CH_3$, no measurable concentration of solvent-trapped electrons remains (less than $\sim 2\%$ of the yield in pure 3MP). It must be considered, however, that the matrix alone traps only $\sim 20\%$ of the electrons released. The limited yield of T^+ at 0% CCl_4 is to be attributed to partial trapping of electrons by toluene. As the concentration of CCl_4 increases, more electrons are trapped, less ion recombination occurs, and more T^+ survives. The very rapid increase in $OD(T^+)$ at small concentrations of CCl_4 can be attributed to a population of ion pairs which achieve greater than average charge separation. Each of these additives is bifunctional with respect to trapping electrons and holes, and their interaction is not evident from Figure 1. However, the two effects can be somewhat resolved by observing $OD(T^+)$ vs. per cent $C_6H_5CH_3$ at fixed concentrations of n -PrCl (0, 0.3, and 1.0 mole %), shown in Figure 2. The sigmoid nature of the dependence is marked at 0% PrCl, but diminishes with increasing concentration of PrCl, and practically disappears with 2.6% CCl_4 (upper curve of Figure 3). Since both $C_6H_5CH_3$ and the chlorides trap electrons, the result at 0% PrCl could represent the twofold effect of $C_6H_5CH_3$. That is, if $C_6H_5CH_3$ must both trap holes to form T^+ , and also trap electrons to protect T^+ from charge recombination, then the net dependence of $OD(T^+)$ on concentration of $C_6H_5CH_3$ will be approximately quadratic at first. At a sufficient concentration of chloride, $C_6H_5CH_3$ exhibits only its hole-trap-

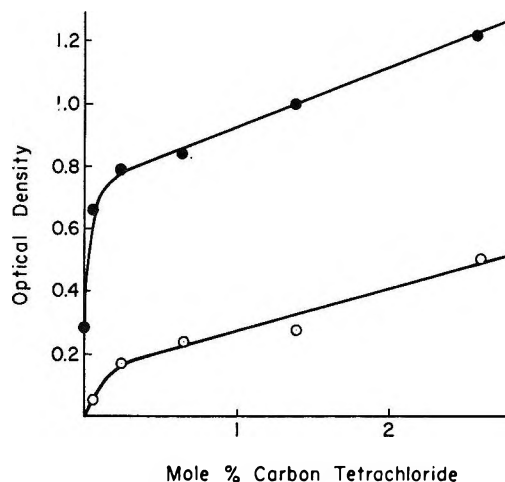


Figure 1. Optical density of toluene cation at λ_{max} 1075 $m\mu$ (●) and carbon tetrachloride cation at λ_{max} 480 $m\mu$ (○) for 2.4 mole % toluene in 3-methylpentane at -196° . Dose, 5.8×10^{18} ev g^{-1} .

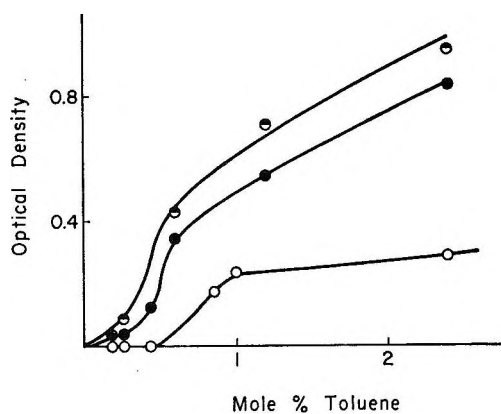


Figure 2. Optical density of toluene cation vs. mole per cent toluene in 3-methylpentane at -196° with (○) 0, (●) 0.3, and (◐) 1.0 mole % n -propyl chloride. Dose, 7.8×10^{18} ev g^{-1} .

ping function and $OD(T^+)$ will tend to be proportional to toluene concentration. This type of sigmoid concentration dependence is also consistent with results observed for benzene, p -xylene, and mesitylene which resemble $C_6H_5CH_3$ by trapping electrons as well as holes. Results are summarized in Table I.

When each of two solutes A and B can trap migrating positive holes to form cations A^+ and B^+ , it is to be expected that

$$N_{A^+}/N_{B^+} = \sigma_A N_A / \sigma_B N_B \quad (1)$$

where N and σ refer to number per unit volume and cross section. Just this kind of competitive behavior was observed for 2-methyl-1-pentene (2MP-1) and

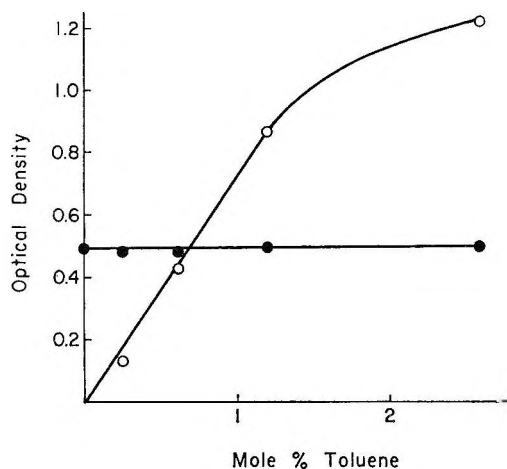


Figure 3. Optical densities of toluene cation (O) and carbon tetrachloride cation (●) vs. mole per cent toluene, at 2.6 mole % CCl_4 in 3-methylpentane at -196° . Dose, 5.8×10^{18} ev g^{-1} .

Table I: Cations of Benzene, *o*-Xylene, and Mesitylene in 3-Methylpentane at -196° ^a

| Aromatic hydrocarbon, mole % | <i>n</i> -Propyl chloride, mole % | OD ^b of cation |
|------------------------------|-----------------------------------|---------------------------|
| Benzene (0.29) | 0.3 | 0.05 |
| (0.73) | 0.3 | 0.42 |
| (2.9) | 0.3 | 0.79 |
| <i>p</i> -Xylene (1.20) | 0 | 0.00 |
| (0.20) | 0.3 | 0.00 |
| (0.55) | 0.3 | 0.40 |
| (1.10) | 0.3 | 0.68 |
| Mesitylene (0.19) | 0 | 0.00 |
| (0.19) | 0.3 | 0.00 |
| (0.48) | 0.3 | 0.26 |
| (1.90) | 0.3 | 0.66 |

^a Dose, 7.8×10^{18} ev g^{-1} . ^b λ_{max} (m μ) 925 (benzene), 1150 (xylene), and 1038 (mesitylene).

$\text{C}_6\text{H}_5\text{CH}_3$ in 3MP.⁶ It will be considered normal behavior and requires no further discussion.

When 2MP-1 concentration gradually increased with 1 mole % CCl_4 in 3MP a distinguishably different behavior was found since OD(C^+) decreased without a correlated increase in OD(2MP-1⁺). Results were approximately describable by

$$\text{OD}(\text{C}^+) = \text{constant } \sigma_c N_c / (\sigma_c N_c + \sigma_o N_o) \quad (2)$$

where *c* and *o* refer to CCl_4 and olefins but only the dependence upon concentration of 2MP-1 was adequately tested. The dependence of OD(2MP-1⁺) was sigmoid, but fitted no simple description.⁶

This type of behavior will be attributed to deactivation of the excited hole. A transient excited 2MP-1⁺ could, in principle, undergo charge exchange with 3MP to the lower conducting state of the hole which could then be trapped by a second encounter with 2MP-1 to give 2MP-1⁺. This assumption agrees with optical bleaching of 2MP-1⁺ in 3MP, although transfer to a second solute has not been achieved.⁶ The dependence of OD(2MP-1⁺) is plausibly quadratic for small concentrations of 2MP-1, in qualitative agreement with the assumed mechanism.

The results in Figure 3 follow still another pattern. At the large concentration of CCl_4 employed it must be considered that electrons are trapped very efficiently, and increasing amounts of $\text{C}_6\text{H}_5\text{CH}_3$ would not be expected to affect the total yield of stabilized cations by contributing to electron trapping. Neither eq 1 nor the analog of eq 2 is applicable, since OD(T^+) increases without diminishing OD(C^+).

Behavior of the third type can be assigned to two species of hole which are conducted by the matrix and differ in energy. The ionization potential $I(\text{CCl}_4)$ is unknown but presumably higher than $I(3\text{MP})$. Since C^+ forms as an indirect product of irradiation, its precursor conducting hole must correspond to an excited state of 3MP^+ which migrates by resonance charge transfer with 3MP. Toluene either does not interact with the excited hole, or has a near-resonant state and transmits it. Such an effect has been demonstrated by using optical excitation of T^+ in 3MP to transfer charge through the matrix to another solute.⁶ A hole of lower energy than $I(\text{CCl}_4)$, also conducted by 3MP, must be assigned as the precursor of T^+ . It behaves normally in competition with 2MP-1, as discussed.

The effects reported here cannot easily be generalized, or extended to rather different compositions. The possibility of trapping a hole depends upon the environment. Thus $\sim 2\%$ 2MP-1 traps holes in 3MP, but at $>10\%$ 2MP-1 becomes conducting again.⁶ Also, CCl_4 in a 3MP matrix forms C^+ , but $\sim 1\%$ 3MP in a CCl_4 matrix apparently forms 3MP^+ , as well as a species resembling C^+ .⁷ Inequalities of ground-state ionization potentials have often been invoked in radiation chemistry to account for energy transfer by charge exchange in the exothermic direction. This criterion does not exclude the possibility that C^+ may be CCl_4^+ , and be stabilized in 3MP, because intra- and intermolecular relaxation may lower the energy of the ion by an amount exceeding the difference of ionization poten-

(7) T. Shida and W. H. Hamill, unpublished results.

tials. The phenomena related to the hole in organic solids are clearly rather more complex than those for the

electron, and the mechanisms proposed are necessarily tentative.

Gravimetric Adsorption Studies of Thorium Oxide. II. Water

Adsorption at 25.00^o₁

by E. L. Fuller, Jr., H. F. Holmes, and C. H. Secoy

Reactor Chemistry Division, Oak Ridge National Laboratory, Oak Ridge, Tennessee (Received December 14, 1965)

The complex nature of water adsorption on thorium oxide has been studied using a sensitive microbalance. High-temperature sintering appears to produce a material which predominantly presents the 100 cubic face in the surface, upon which there are three distinct modes of adsorption. There is a rapid chemisorption, forming surface hydroxyl groups which are slowly hydrated. In addition and as a precursor for surface hydration, physical adsorption occurs.

The interaction of water with the surface of thorium oxide is somewhat complex and not well understood. Gravimetric adsorption studies have been made in an effort to interpret the effects of the past history on the nature of the surface. This work is in conjunction with the calorimetric² and electrokinetic³ studies reported earlier. It is well known that even the specific surface area of thorium oxide (calculated from nitrogen adsorption isotherms) varies considerably, depending on the mode of preparation and calcining temperature.^{4,5}

We have studied the nature of water vapor adsorption on two well-characterized samples of thorium oxide in an attempt to evaluate the stoichiometry and thermodynamics of the adsorbed species. In addition to the fundamental knowledge such data would offer, there is considerable interest in thorium dioxide as a heterogeneous catalyst.^{5,6}

Throughout this report we have assumed that a truly physically adsorbed water molecule occupies the theoretical 10.6 Å² rather than some value chosen to correlate the specific surface areas calculated from nitrogen and water isotherms (based on the 16.2 Å² occupied by a nitrogen molecule).⁷

The gravimetric apparatus and environmental controls used for this investigation have been described previously.⁸ The two samples studied thus far are samples A and D as described in ref 2b and 3 (14.7 and 2.20 m²/g, resulting from 650 and 1200° calcination, respectively).

When considered on a unit surface area basis, the two samples behaved identically when outgassed at 10⁻⁵ torr. The samples were held *in vacuo*, and the temperature was incrementally increased with the

(1) Research sponsored by the U. S. Atomic Energy Commission under contract with the Union Carbide Corp.

(2) (a) H. F. Holmes and C. H. Secoy, *J. Phys. Chem.*, **69**, 151 (1965); (b) H. F. Holmes, E. L. Fuller, Jr., and C. H. Secoy, *ibid.*, **70**, 436 (1966).

(3) H. F. Holmes, C. S. Shcup, Jr., and C. H. Secoy, *ibid.*, **69**, 3148 (1965).

(4) V. D. Allred, S. R. Buxton, and J. P. McBride, *ibid.*, **61**, 117 (1957).

(5) W. S. Brey, B. H. Davis, P. G. Schmidt, and C. G. Moreland, *J. Catalysis*, **3**, 303 (1964).

(6) M. E. Winfield, *Australian J. Sci. Res.*, **3**, 291 (1950).

(7) H. K. Livingston, *J. Am. Chem. Soc.*, **66**, 569 (1944).

(8) E. L. Fuller, Jr., H. F. Holmes, and C. H. Secoy, *Vacuum Microbalance Tech.*, **4**, 109 (1965).

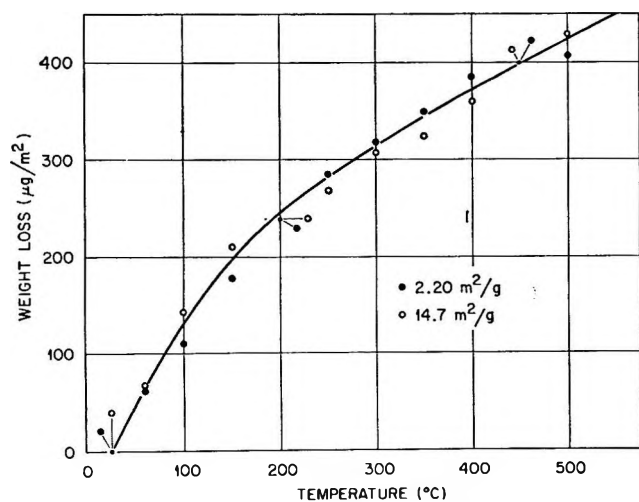


Figure 1. Weight loss on outgassing ThO_2 at 10^{-3} torr.

resulting weight loss shown in Figure 1. It was found necessary to maintain the sample at each temperature for at least 16 hr to obtain a steady weight. The excellent correlation for these widely diverse specific surface areas points out that this desorption is truly related to the surface of the samples. Also, it is evident that a temperature of 500° is far from adequate to remove all of the tenaciously bound water to produce a "dry" surface at this pressure, since there is no indication of an approach to a limiting weight at this temperature.

When the samples were heated to 500° *in vacuo*, a gray to black coloration began in the upper layers of the powder and penetrated more deeply with successive treatments at 500° , whereas maintaining the 500° temperature did not propagate the color. This color is undoubtedly due to a small amount of carbon since it can be removed with oxygen treatment at 400 to 500° with an accompanying weight loss. Also, raising the temperature to 1000° *in vacuo* will bleach the samples to their original white. We feel that the presence of this small amount of carbon (or its parent hydrocarbon) in no way invalidates our results since neither the surface area nor the energetics of water adsorption² are altered by its presence. Immediately upon cooling from 500° , the samples begin to gain weight slowly (6 to 7 $\mu\text{g}/\text{hr}$) even when exposed to the vacuum pumps, owing to the desiccating action of the activated surface.

A series of successive adsorption and desorption isotherms for water vapor on sample A at 25.00° was obtained. The first two of these, shown in Figure 2, indicate the complex nature of the process. This graph is constructed from data obtained 15 to 60 min after introduction or extraction of water vapor. For

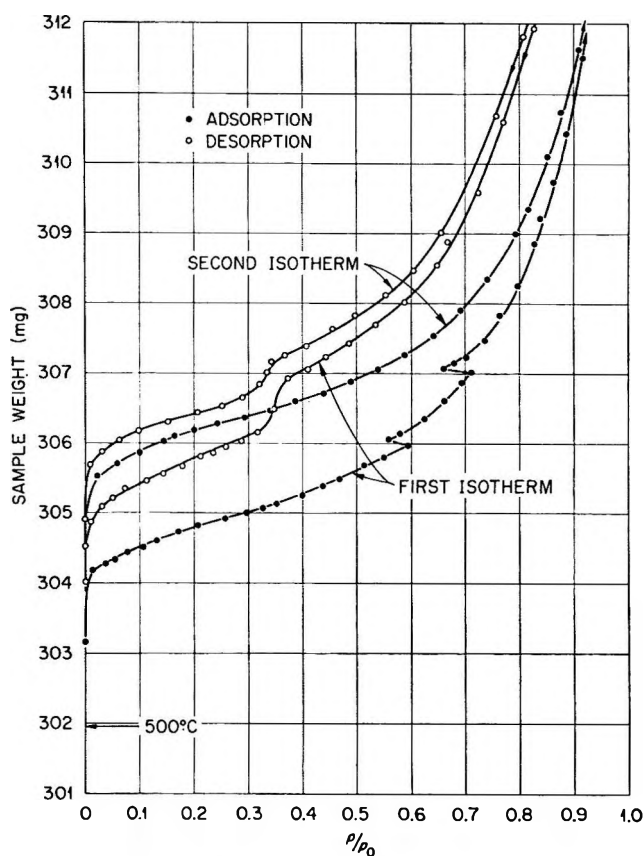


Figure 2. Water isotherms for sample A at 25.00° .

clarity, only about half of the experimental points are shown. The sharp discontinuities correspond to overnight stops in the isotherm construction. Although the data do not represent equilibrium isotherms, the curves have the general shape of type-II isotherms (Brunauer classification⁹) with high-pressure hysteresis due to capillary condensation. It appears that underlying a reversible physical adsorption process is a slow irreversible binding of water to the surface. The term irreversible, as used in this paper, applies to the bound water which cannot be removed at the temperature of the isotherm, and does not imply thermodynamic irreversibility. The kinetic nature of this binding is revealed in the overnight discontinuities in the lower isotherm and in the increasing vacuum weight after each excursion to higher pressures of water vapor. Although only the first two are shown in Figure 2, each successive isotherm failed to close upon the preceding one by a decreasing amount. The experiment was terminated prior to achieving complete closure of the adsorption and desorption branches as was done with sample D (see below).

(9) S. Brunauer, "The Adsorption of Gases and Vapors," Vol. I, Princeton University Press, Princeton, N. J., 1945.

The specific surface area calculated from these water isotherms (BET method¹⁰) decreased from 28.8 to 9.6 m²/g: The initial values are unquestionably high due to the inability of the BET theory to differentiate between chemical and physical adsorption and the comparatively large amount of water involved in the chemical process. A similar decrease in the specific surface area with higher surface water content has been observed for aluminum oxide.¹¹ This diminution of surface area from the 14.7 m²/g is probably real and due to the fact that irreversible binding of water effectively decreases the surface area. Classical treatment¹² of the capillary hysteresis desorption closure at a partial pressure of 0.35 shows quite a number of pores of radii as low as 10 Å.

A similar irreversible binding has been observed underlying the physical adsorption of water on silicon oxide by Barrett.¹³ His isotherms were normalizable (identical when each is referred to its own vacuum weight), whereas it is quite evident that thorium oxide isotherms are not normalizable.

Water vapor adsorption on sample D gave the same behavior as sample A in that each successive adsorption occurred at higher sample weight, owing to the slow underlying irreversible binding. Figure 3, which shows the initial and final isotherms only, indicates that the only schematic difference lies in the capillary hysteresis region (closure at $p/p_0 = 0.52$) where the higher calcination temperature has sintered out all pores of radii less than 50 Å.

Since each successive isotherm more closely approximates the preceding one, an attempt was made to obtain an isotherm involving only physical adsorption. Six months of repeated adsorption and desorption was required to construct the final reversible isotherm (the upper curve in Figure 3). The high-pressure hysteresis, due to capillary condensation, still persists, and the entire isotherm is reproducible to 1 µg over the entire pressure region. The final vacuum weight is only slightly dependent on temperature as observed experimentally at 18 and 32°. The rate of irreversible binding is a complex function of both the water vapor pressure and the amount of water previously bound. The rate is increased markedly with the first increments of pressure, but higher pressure increments have less accelerating effects. The rate diminishes appreciably as more water is bound under the physically adsorbed water.

Incremental increases in temperature to 1000° indicate that a "dry" weight of thorium oxide is achieved at 1000° *in vacuo*. Duval¹⁴ reports that a temperature of 950° must be achieved to obtain a tga (thermogravimetric analysis) curve for stoichio-

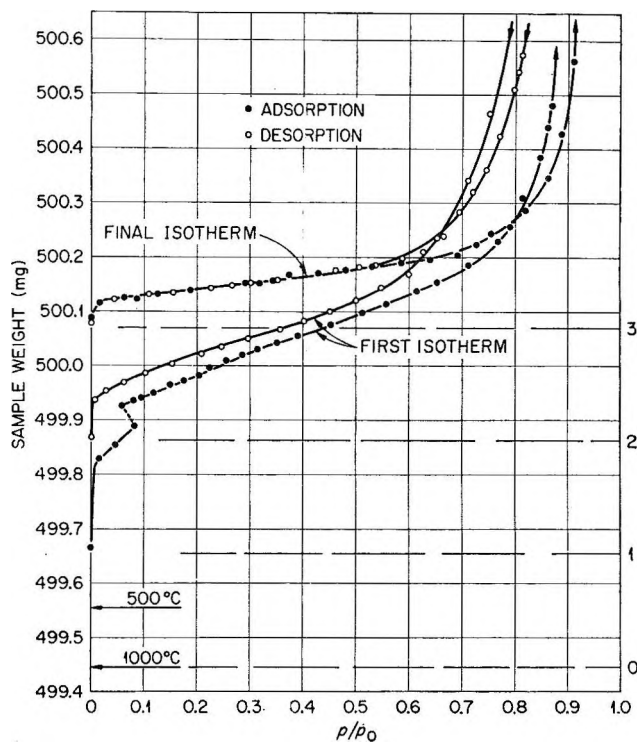


Figure 3. Water isotherms for sample D at 25.00°.

metric thorium oxide. When the sample was again exposed to water vapor at 25.00°, the same slow irreversible binding process began, and the isotherms essentially reproduce the initial ones. The process was not followed to completion for a second time.

The irreversible binding of water to the surface of thorium oxide must certainly be oriented to specific surface sites in light of the energetics of adsorption² and in view of the fact that it cannot be removed *in vacuo* without raising the temperature. These two facts preclude the concept that this water is held by physical forces of the van der Waals type. In attempting to calculate the area occupied by a chemisorbed molecule one must know which crystalline faces are present in the surface. No conclusive evidence has yet been forwarded to answer this problem for thorium oxide. The chemisorption capacity for water on thorium oxide is 192, 135, and 221 µg/m² for the 100, 110, and 111 surface planes, respectively, based on the

(10) S. Brunauer, P. H. Emmett, and E. Teller, *J. Am. Chem. Soc.*, **60**, 309 (1938).

(11) N. Hackerman and W. H. Wade, *J. Phys. Chem.*, **68**, 1592 (1964).

(12) J. H. deBoer, *Proc. Symp. Colston Res. Soc.*, **10**, 68 (1958).

(13) H. M. Barrett, A. W. Birnie, and M. Cohen, *J. Am. Chem. Soc.*, **62**, 2839 (1940).

(14) C. Duval, "Inorganic Thermogravimetric Analysis," 2nd ed, Elsevier Publishing Co., New York, N. Y., 1963.

face-centered-cubic lattice parameter for the bulk oxide ($a_0 = 5.597 \text{ \AA}$).

The right ordinate in Figure 3 is the equivalent monolayer capacity of sample D based on the exposure of the 100 plane in the surface and the specific surface area of $2.20 \text{ m}^2/\text{g}$. The excellent correlation of the final vacuum weight to that of the equivalent three chemisorbed layers lends credence to this model. The simplest and most straightforward interpretation of this result is that of a dissociative chemisorption to form two surface hydroxyl groups per surface thorium, which in turn are each hydrated with a water molecule in the final equilibrium state. This is the surface analog of a hydrated bulk hydroxide and satisfies the observed stoichiometry. It is hoped that concurrent infrared spectroscopic studies of these same materials will shed some light on the nature of the bonding of these nondissociated hydrating molecules on the surface. This model receives considerable support from the three distinct energetic adsorptions noted for high-temperature calcined thorium oxide.^{2b} In addition, this stoichiometric amount of water is just that required to build up one completed face-centered-cubic lattice unit on the surface above the 100 ThO_2 plane, with the hydroxide and water oxygen occupying image positions of the substrate oxide ions. Recent nmr studies¹⁵ have also shown that there is considerable rigid orientation of water on the surface of thorium oxide, which involves a slow hydration process.¹⁶ Furthermore, electrical conductivity studies on quite a number of oxides conclusively show that the hydration process does not involve electron transfer.¹⁷ Antoniou¹⁸ has observed that there is the equivalent of three chemisorbed layers of water in an immobile state on the surface of silica.

The model presented here proposes a third distinct type of adsorption: an immobile, associative type (much akin to bulk hydrogen bonding) in addition to the truly physical and chemical adsorption. Since physical adsorption occurs in addition, the additional nomenclature seems warranted. The slow kinetics of adsorption cannot normally be associated with a

true physical adsorption process, and the energetics^{2b} of this surface hydration are near that normally associated with hydrogen bonding.¹⁹ It appears that the hydrolysis of the surface oxide is relatively rapid but that the hydration of the surface hydroxyls is a slow process. This hydration involves physical adsorption as a precursor with an orientation to each individual hydroxyl group.

These extremely slow kinetics of associative adsorption from the gas phase should not be confused with the well-defined first-order kinetics observed calorimetrically² in liquid water. The former is present for both high and low surface area materials, regardless of porosity, whereas the latter is due to diffusion into pores and is observed only when small pores (dimensions near that of a water molecule) are present.

The small crystallite size (large specific surface area) and low firing temperature of sample A thwart any idealized quantitative treatment. Qualitatively, however, this material exhibits the same slow, irreversible behavior but the interactions are much more complex. This nonideal behavior is also noted in the net differential heats for this material.^{2b} It appears that one must deal with a material which has a low specific surface (resulting from a high-temperature calcination) to obtain data indicative of an ideal crystal plane surface.

The infeasibility of attempting to evaluate thermodynamic data from these isotherms is shown by the low vapor pressure of the initial adsorbed species and the prohibitive kinetics in arriving at equilibrium states. Equally impracticable is the practice of attempting to predict the amount of adsorption from predetermined isotherms.

(15) W. S. Brey and K. D. Lawson, *J. Phys. Chem.*, **68**, 1474 (1964).

(16) K. D. Lawson, Thesis, University of Florida, 1963.

(17) A. Bielanski, "Catalysis and Chemical Kinetics," Academic Press Inc., New York, N. Y., 1964, p 104.

(18) A. A. Antoniou, *J. Phys. Chem.*, **68**, 2754 (1964).

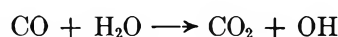
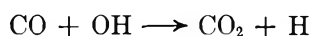
(19) G. C. Pimentel and A. L. McClellan, "The Hydrogen Bond," W. H. Freeman and Co., San Francisco, Calif., 1960, pp 206-225.

Photochemical Equilibrium Studies of Carbon Dioxide and Their Significance for the Venus Atmosphere

by Robert R. Reeves, Jr., Paul Harteck, Barbara A. Thompson, and Roger W. Waldron

Department of Chemistry, Rensselaer Polytechnic Institute, Troy, New York (Received December 16, 1965)

The photolysis of carbon dioxide has been studied using the 1633-A persistent line of bromine. Dissociation into carbon monoxide and oxygen accompanied by formation of ozone was readily observed. The O₃/O₂ ratio was comparable to that obtained on irradiation of oxygen alone. The addition of traces of moisture to the system resulted in a recombination back to CO₂. With moisture content of about 1 ppt the recombination to CO₂ was virtually complete. This was true with either excess CO or excess O₂. The system was studied at various temperatures from 25 to -72° beginning with pure CO₂ or with mixtures of CO and O₂. The mechanism for recombination in the presence of traces of H₂O may involve reactions such as



The addition of small amounts of H₂ also inhibits the dissociation of CO₂, tending to confirm the proposed mechanism. These results may contribute substantially to an understanding of the chemistry of the Venus atmosphere.

Introduction

The photochemistry of carbon dioxide has been studied for many years and has become of special interest more recently in connection with the chemistry of the Venus atmosphere. Groth² in 1937 and others in recent years³⁻⁵ have carried out investigations using the 1470-A line of xenon. Some have also utilized the 1236-A line of krypton^{4,5} and a hydrogen lamp emitting in the 1600-A region.⁵ Some questions still exist, however, as to the exact nature of the processes occurring in the photolysis. In particular, some workers have reported finding smaller amounts of oxygen produced than expected. The bromine lamp, recently developed in this laboratory,⁶ provides a high output intensity at 1633 A and thus can be used for photochemical equilibrium studies. Since none of the previous studies of carbon dioxide was carried to photochemical equilibrium, it seemed appropriate to investigate this system with the bromine lamp. This paper describes some results of this investigation.

Experimental Section

The bromine lamp has been described in detail elsewhere.⁶ Features of interest for the present study include the outer cooling jacket which permits irradiation at any desired temperature, the insulating vacuum jacket between the irradiation chamber and the discharge tube and a provision for withdrawal for analysis of small samples of the gas being irradiated at any time.

The gases used were obtained from Matheson Co. and were purified before use. CO₂ (Coleman grade) was purified by pumping away air at liquid nitrogen temperature, then separating from any water vapor by dis-

(1) Presented in part at the 150th National Meeting, American Chemical Society, Atlantic City, N. J., Sept 1965.

(2) W. Groth, *Z. Physik. Chem.*, **B37**, 307 (1937).

(3) H. Jucker and E. K. Rideal, *J. Chem. Soc.*, 1058 (1957).

(4) B. H. Mahan, *J. Chem. Phys.*, **33**, 959 (1960).

(5) P. Warneck, *Discussions Faraday Soc.*, **37**, 57 (1964); see also discussion on pp 217, 218.

(6) B. A. Thompson, R. R. Reeves, Jr., and P. Harteck, *J. Phys. Chem.*, **69**, 3964 (1965).

tillation at Dry Ice temperature. CO always contained trace amounts of iron carbonyl which could have interfered with the equilibrium observation. This impurity was therefore removed by bubbling the gas through sodium hydroxide solution, and the CO was then dried by passing through liquid oxygen traps. Oxygen, argon, and hydrogen were dried by passing through liquid oxygen traps and used without further purification. Small amounts of water were introduced when desired by using argon or oxygen directly from the cylinder, eliminating the liquid oxygen traps.

Irradiations were carried out on pure CO₂; mixtures of CO₂ and argon; mixtures of CO, O₂, and argon; and mixtures of CO₂, H₂, and argon. Argon served as a mass spectrometer reference and, in the case of the CO-O₂ mixtures, to lower the explosion limits. Most irradiations were performed at room temperature, but experiments were also made at -31 and -72°. Gas samples were analyzed using a Consolidated Electro-dynamics Corp. 21-130 mass spectrometer.

Where desirable, ozone was measured by bubbling the irradiated gas through potassium iodide solution and titrating the liberated iodine with standard sodium thio-sulfate.

Results

Irradiation of CO₂. When pure CO₂ was irradiated, dissociation occurred resulting in the formation of CO and O₂. O₃ was also present and the O₃/O₂ ratio was comparable to that obtained with pure O₂.⁶ The ratio of CO to O₂ was measured mass spectrometrically and, including the oxygen from the O₃, was found to be 2:1 in contrast to the results of some other workers⁶ who have reported finding less than the stoichiometric amount of oxygen. However, the experimental conditions in this work were quite different; in particular, a much greater fraction of the CO₂ was dissociated in this work than in previous experiments.

In all cases (about 20 experiments) the dissociation proceeded initially at a rate consistent with a quantum yield of 1 for CO₂ decomposition as determined by comparing the rate with the rate of ozone formation in a flowing system of pure O₂.⁶ This initial rate was maintained until a few per cent of the CO₂ had been decomposed. Back-reactions then began to compete and a stationary state was approached. A typical curve of CO/CO₂ ratio as a function of irradiation time is shown in Figure 1. This curve shows a CO/CO₂ ratio at the stationary state of about 0.13. However, although the initial rate of decomposition was always the same, the stationary-state CO/CO₂ ratio seemed to be rather erratic, ranging from a value of about 0.1 to about 0.35

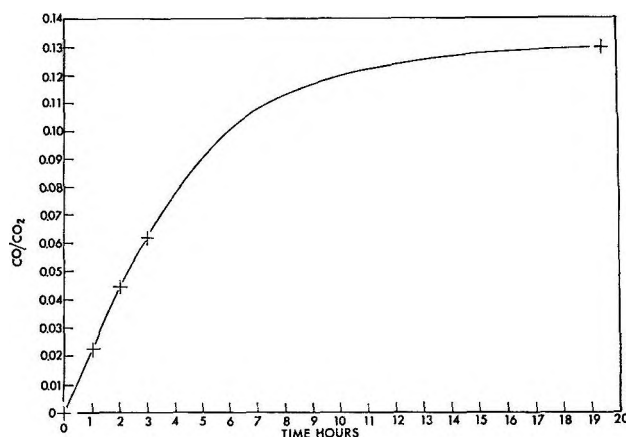


Figure 1. Typical dissociation curve for CO₂ irradiated with bromine lamp.

(O₂/CO₂ ~ 0.05-0.18). The value of 0.35 for CO/CO₂ was the maximum obtained in these experiments.

Irradiation of CO-CO₂ Mixtures. In an effort to understand the variable stationary-state decomposition observed with pure CO₂, it was decided to approach the equilibrium from the opposite direction, *i.e.*, beginning with mixtures of CO and O₂. All these experiments were done with a CO pressure of less than 150 mm. The initial O₂ pressure was varied from 50 to 100 mm, and argon was added to bring the total pressure into the 650-mm region. In all cases it was found that reaction to form CO₂ proceeded to completion. With excess CO, all the O₂ was consumed (O₂/CO₂ < 0.005) and with excess O₂, all the CO was consumed (CO/CO₂ < 0.01). A close examination of the mass spectra revealed the presence of small amounts of water vapor (~0.1%).

When the reaction gases were dried as carefully as possible (~0.01% H₂O), the stationary state was shifted slightly in the direction of increased decomposition (O₂/CO₂ ~ 0.03) and thus it was concluded that the reaction to form CO₂ was being catalyzed due to the presence of water. The fact that no higher degree of dissociation was obtained starting with CO-O₂ mixtures was probably due to the presence of minor traces of hydrogen-containing impurities in the CO.

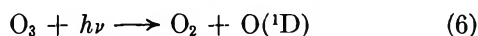
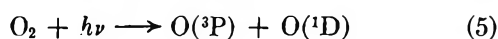
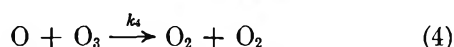
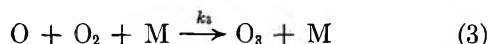
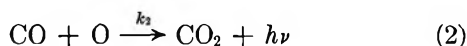
Irradiation of CO₂ with H₂ Added. To gain further insight into the nature of the recombination reactions, irradiations were carried out on pure CO₂ to which traces of hydrogen were added. This would react with the O atoms formed by CO₂ dissociation to produce OH radicals and H atoms. If these are really catalyzing the recombination to CO₂, then the addition of small amounts of H₂ should cause a radical shift in the equilibrium.

It was found that with as little as 0.1% H₂ present, the dissociation of CO₂ was completely inhibited (O₂/

$\text{CO}_2 < 0.005$). With 0.01% H_2 , dissociation occurred to a very small extent ($\text{O}_2/\text{CO}_2 \sim 0.02$). Thus the assumption of catalysis by water or its decomposition products seems correct. It should be noted that most of the added hydrogen remained in the form of H_2 , as could be observed mass spectrometrically, and only a small fraction was converted to H_2O during the time of irradiation.

Discussion

Steady-State Equilibrium. When CO_2 is irradiated with ultraviolet light, the following reactions occur and play a major role in defining the position of equilibrium.



It is assumed in the following discussion that all the $\text{O}(\text{D})$ atoms formed in reactions 1, 5, and 6 are immediately quenched to $\text{O}(\text{P})$ and do not affect the subsequent reactions. Wall effects are negligible under the conditions of these experiments and therefore have not been included in the above series of equations. An expression for the expected stationary-state ratio of CO to CO_2 can be derived from a steady-state treatment of these reactions. By setting up steady-state equations for CO_2 , O atoms, and O_3 , and combining the three equations, the following two relationships between CO , CO_2 , O_2 , and O_3 may be obtained.

$$\frac{(\text{O}_3)}{(\text{O}_2)} = \frac{\alpha_2 k_2 (\text{CO})}{\alpha_3 k_4 (\text{CO}_2)} \quad (\text{I})$$

$$\frac{(\text{CO})}{(\text{CO}_2)} = \frac{k_3 (\text{M}) - k_4 (\text{O}_3/\text{O}_2)}{\frac{\alpha_1 k_2}{\alpha_3} (\text{O}_3/\text{O}_2)} \quad (\text{II})$$

where α_1 , α_2 , and α_3 are the absorption coefficients of O_3 , O_2 , and CO_2 for the incident radiation. By substitution of (I) into (II), and application of the quadratic formula, the CO/CO_2 ratio is found to be

$$\frac{(\text{CO})}{(\text{CO}_2)} = \frac{-1 + \sqrt{1 + 4 \frac{\alpha_1 k_3 (\text{M})}{\alpha_2 k_4}}}{\frac{2\alpha_1 k_2}{\alpha_3 k_4}} \quad (\text{III})$$

By substitution of (III) into (I), the O_3/O_2 ratio is

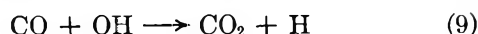
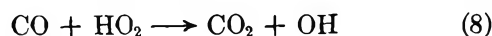
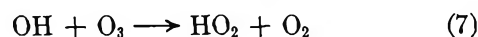
$$\frac{(\text{O}_3)}{(\text{O}_2)} = \frac{-1 + \sqrt{1 + 4 \frac{\alpha_1 k_3 (\text{M})}{\alpha_2 k_4}}}{2\alpha_1/\alpha_2} \quad (\text{IV})$$

Equation IV is identical with that calculated for the O_3/O_2 ratio in a pure $\text{O}_2\text{-CO}_3$ system by a similar steady-state treatment,⁷ showing that in a CO_2 system at photochemical equilibrium the O_3/O_2 ratio is independent of the CO_2 and CO .

The reported values of 20, 75, and 2.5 cm^{-1} for α_1 , α_2 , and α_3 at 1633 \AA ⁸ were substituted into eq III together with the following values for k_2 , k_3 , and k_4 . At 300°K the respective values were 10^{-18} and $10^{-14} \text{ cc/particle sec}$ and $3 \times 10^{-34} \text{ cc}^2/\text{particle}^2 \text{ sec}$; at 200°K the values were 10^{-18} , 10^{-14} , and 5×10^{-34} , respectively. The value of k_2 is that reported by Mahan and Solo⁹ and the same value was used at both temperatures because recent work in this laboratory has shown that the activation energy is very low.¹⁰ Exact values for the rate coefficients of reactions 3 and 4 are not generally agreed upon at present.¹¹ The above values were selected in the light of the data available. In any case, the conclusions drawn would not be substantially affected by small changes in the values of k_2 , k_3 , and k_4 . A pressure of 100 mm was assumed for the calculations.

Substitution of these values into eq III gives a steady-state CO/CO_2 ratio of 52 at 200°K and 28 at 300°K . Thus, under the experimental conditions used for this work the CO_2 should have been over 90% dissociated at steady state. Instead, as noted above, the maximum dissociation found was about 25% with evidence that recombination to CO_2 was being catalyzed by water or its decomposition products. It is clear from these results that for equilibrium studies the requirements for purity of systems are even more stringent than had been thought.

Recombination Mechanisms. The reactions most likely to be important in a water-catalyzed recombination include the following in addition to reactions 1-6.



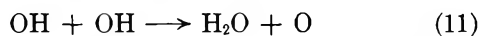
(7) P. Harteck, R. R. Reeves, Jr., and B. A. Thompson, to be published.

(8) K. Watanabe, M. Zelickoff, and E. C. Y. Inn, "Absorption Coefficients of Several Atmosphere Gases," Air Force Cambridge Research Center Technical Report No. 53-23, 1953.

(9) B. H. Mahan and R. B. Solo, *J. Chem. Phys.*, **37**, 2669 (1962).

(10) P. Harteck, R. R. Reeves, Jr., and A. S. Bergendahl, to be published.

(11) For discussion see F. Kaufman and J. R. Kelso, *Discussions Faraday Soc.*, **37**, 26 (1964), and A. Mathias and H. I. Schiff, *ibid.*, **37**, 38 (1964).



It should be noted that reactions 7 and 8 constitute a cycle as do reactions 9 and 10. Benson¹² has pointed out that reaction 8 is probably fast and reaction 10 is known to be very fast. Reaction 9 has a activation energy of at least 7 kcal¹³ and reaction 11 is known to be very fast also. The exact recombination mechanism may involve all these reactions as well as others of a similar nature.

Significance for the Venus Atmosphere. It is evident that an H atom or OH-catalyzed recombination mechanism could explain the peculiar composition of the Venus atmosphere, namely the high abundance of CO₂ with no more than a trace of either CO or O₂.¹⁴ These constituents might be expected to be present in the Venus atmosphere in relatively high concentrations owing to photodissociation of CO₂.

The most recent spectroscopic investigations¹⁵ from a balloon indicate the presence of trace amounts of atmospheric water vapor. For the above mechanism

only very small amounts of water need be present. Photodissociation of the water would produce OH radicals and H atoms which could be expected to be present in steady state down to the cloud layer. It is probable, therefore, that any oxygen or carbon monoxide formed in the Venus atmosphere reacts to regenerate CO₂ in the manner described above. These reaction schemes thus provide an explanation for the absence of both CO and O₂ from the Venus atmosphere in the abundances which might have been anticipated.

Acknowledgment. This work was carried out under a research grant from the National Aeronautics and Space Administration.

(12) S. W. Benson, "The Foundations of Chemical Kinetics," McGraw-Hill Book Co., Inc., New York, N. Y., 1960, p 461.

(13) See L. I. Avramenko and R. V. Kolesnikova, *Advan. Photochem.*, **2**, 32 (1964).

(14) P. Harteck, R. R. Reeves, Jr., and B. A. Thompson, "Photochemical Problems of the Venus Atmosphere," NASA Technical Note TN-D-1984, 1963.

(15) M. Bottema, W. Plummer, and J. Strong, *Astrophys. J.*, **139**, 1021 (1964).

Osmotic and Activity Coefficients of Acidopentaamminecobalt(III) Complexes

by L. H. Berka¹ and W. L. Masterton

Department of Chemistry, University of Connecticut, Storrs, Connecticut (Received December 21, 1965)

Osmotic coefficients, measured at 37°, and activity coefficients, derived therefrom, are reported for the compounds $[\text{Co}(\text{NH}_3)_5\text{A}]\text{X}_2$ where $\text{A}^- =$ acetate, propionate, or isobutyrate and $\text{X}^- = \text{NO}_3^-$, I^- , Br^- , or Cl^- . Below 0.1 *m*, the osmotic and activity coefficients of all of these compounds fall within a narrow range of each other. At higher concentrations, ϕ and γ_{\pm} appear to be independent of the organic ligand but vary with the anion in the order $\text{Cl}^- > \text{Br}^- > \text{I}^- > \text{NO}_3^-$. The osmotic and activity coefficients of these complex ion electrolytes are markedly lower than those of simple electrolytes of the same valence type. The data are interpreted in terms of association between cation and anion; calculated ion-pair dissociation constants fall between 0.05 and 0.1. The factors which are responsible for association of complex ion electrolytes are discussed. It is suggested that dispersion forces may play an important part in ion-pair formation.

Introduction

Osmotic and activity coefficients have been reported previously for the 2:1 complex ion electrolytes $[\text{Co}(\text{NH}_3)_5\text{NO}_2]\text{Cl}_2$, $[\text{Co}(\text{NH}_3)_5\text{Cl}](\text{ClO}_4)_2$, and $[\text{Co}(\text{NH}_3)_5\text{F}]\text{Cl}_2$.² It was found that the activity coefficients of these compounds are lower than those of simple 2:1 electrolytes and are more nearly comparable to those of simple 1:2 electrolytes. These results were interpreted qualitatively in terms of the relatively minor role of cation hydration in 1:2 and complex ion electrolytes and extensive association in the latter compounds as indicated by the low Debye-Hückel a^0 values required to fit the data at low concentrations.

As part of a continuing study of the thermodynamic properties of aqueous solutions of complex ion electrolytes, we have chosen a series of acidopentaamminecobalt(III) complexes, which may be represented by the general formula $[\text{Co}(\text{NH}_3)_5\text{A}]\text{X}_2$ where $\text{A}^- = \text{CH}_3\text{COO}^-$, $\text{CH}_3\text{CH}_2\text{COO}^-$, and $(\text{CH}_3)_2\text{CHCOO}^-$ and $\text{X}^- = \text{NO}_3^-$, I^- , Br^- , and Cl^- . These compounds offer a systematic approach to studying the effects of ligand and anion substitution on activity coefficients in both dilute and concentrated solutions. Several of these salts have aqueous solubilities exceeding 1 *m*; in no case does the rate of aquation of the complex cation exceed 1%/day³ at 37°.

Experimental Section

Compounds. (1) $[\text{Co}(\text{NH}_3)_5\text{CH}_3\text{COO}]\text{X}_2$ Series. (a)

$\text{X}^- = \text{NO}_3^-$. This was prepared by the method of Basolo, *et al.*³ *Anal.* Calcd: NH_3 , 26.0 Found: NH_3 , 25.9.

(b) $\text{X}^- = \text{I}^-$. This was prepared according to the method of Werner.⁴ *Anal.* Calcd: NH_3 , 18.6; I , 55.5. Found: NH_3 , 18.6; I , 55.4.

(c) $\text{X}^- = \text{Br}^-$. $[\text{Co}(\text{NH}_3)_5\text{CO}_3]\text{Br} \cdot \text{H}_2\text{O}$ ⁵ was treated with acetic acid; the desired product was precipitated by adding a concentrated solution of NaBr and was recrystallized from water using NaBr. *Anal.* Calcd: NH_3 , 23.5; Br , 44.0. Found: NH_3 , 23.4; Br , 44.3.

(d) $\text{X}^- = \text{Cl}^-$. A solution of the bromide salt was passed through a column of Amberlite IRA-400 resin in the chloride form. The product was brought out of solution by freeze-drying and was recrystallized from hot water. *Anal.* Calcd: NH_3 , 31.1; Cl , 25.9. Found for sample dried over P_2O_5 : NH_3 , 30.8; Cl , 25.4.

(2) $[\text{Co}(\text{NH}_3)_5\text{CH}_3\text{CH}_2\text{COO}]\text{X}_2$ Series. (a) $\text{X}^- = \text{NO}_3^-$. This was prepared by the method of Basolo, *et al.*³ *Anal.* Calcd: NH_3 , 25.0. Found: NH_3 , 25.0.

(1) Abstracted in part from the Ph.D. thesis of L. H. Berka.

(2) W. L. Masterton and J. A. Scola, *J. Phys. Chem.*, **68**, 14 (1964).

(3) Estimated from data given by F. Basolo, J. G. Bergmann, and R. G. Pearson, *ibid.*, **56**, 22 (1952).

(4) A. Werner, *Ber.*, **40**, 4111 (1907).

(5) A. Werner and N. Goslings, *ibid.*, **36**, 2380 (1903).

(b) $X^- = I^-$. A solution of KI was added to a solution of the nitrate salt. The product was recrystallized from hot water. *Anal.* Calcd: NH_3 , 18.1; I, 53.9. Found: NH_3 , 18.1; I, 53.8.

(c) $X^- = \text{Br}^-$. A solution of the iodide salt was shaken with solid AgBr. After filtration, the product was brought out of solution by freeze-drying. *Anal.* Calcd: NH_3 , 22.6; Br, 42.4. Found: NH_3 , 22.6; Br, 42.2.

(d) $X^- = \text{Cl}^-$. This was prepared by shaking a solution of the iodide salt with solid AgCl. The product was brought out of solution by freeze-drying. *Anal.* Calcd: NH_3 , 29.6; Cl, 24.6. Found: NH_3 , 29.6; Cl, 24.5.

(3) $[\text{Co}(\text{NH}_3)_5(\text{CH}_3)_2\text{CHCOO}]X_2$ Series. The method given by Basolo³ for the preparation of the nitrate salt gave a product which analyzed correctly for NH_3 but which was found to be contaminated by a relatively insoluble compound. Recrystallization gave a very poor yield owing to the high solubility ($>2.5 m$) of the nitrate. For these reasons, the procedure was modified first to prepare the iodide salt, which was then readily converted to the nitrate.

(a) $X^- = I^-$. Ten grams of $[\text{Co}(\text{NH}_3)_5\text{CO}_3]\text{NO}_3 \cdot 0.5\text{H}_2\text{O}$ was suspended in 17 ml of water and 37 ml of isobutyric acid was slowly added. The mixture was concentrated on the steam bath for 90 min, then cooled in ice. The solid product was removed by filtration and the iodide salt was precipitated from the filtrate using KI. The product was recrystallized twice from hot water. *Anal.* Calcd for $[\text{Co}(\text{NH}_3)_5(\text{CH}_3)_2\text{CHCOO}]I_2 \cdot 0.5\text{H}_2\text{O}$: NH_3 , 17.2; I, 51.4; C, 9.7; H, 4.7. Found: NH_3 , 17.2; I, 49.4; C, 9.9; H, 4.8.

(b) $X^- = \text{NO}_3^-$. Prepared by titrating a solution of the iodide to the equivalence point with AgNO_3 . After filtration, the product was brought out of solution by freeze-drying. *Anal.* Calcd: NH_3 , 24.0; C, 13.5; H, 6.2. Found: NH_3 , 24.0; C, 14.1; H, 6.0.

(c) $X^- = \text{Br}^-$. This preparation was analogous to that of $[\text{Co}(\text{NH}_3)_5\text{CH}_3\text{CH}_2\text{COO}]\text{Br}_2$. *Anal.* Calcd for $[\text{Co}(\text{NH}_3)_5(\text{CH}_3)_2\text{CHCOO}]\text{Br}_2 \cdot \text{H}_2\text{O}$: NH_3 , 20.8; Br, 39.1; C, 11.7; H, 5.9. Found: NH_3 , 20.7; Br, 38.0; C, 11.9; H, 5.9.

(d) $X^- = \text{Cl}^-$. This preparation was analogous to that of $[\text{Co}(\text{NH}_3)_5\text{CH}_3\text{CH}_2\text{COO}]\text{Cl}_2$. *Anal.* Calcd for $[\text{Co}(\text{NH}_3)_5(\text{CH}_3)_2\text{CHCOO}]\text{Cl}_2 \cdot 0.5\text{H}_2\text{O}$: NH_3 , 27.4; Cl, 22.7; C, 15.4; H, 7.5. Found: NH_3 , 27.3; Cl, 22.0; C, 15.8; H, 7.3.

Apparatus. Osmotic coefficients were measured at 37° with a Mechrolab vapor pressure osmometer. The method described previously² was modified as follows. Potassium chloride solutions rather than pure water

were used for both the reference bead and the solvent cup. A resistance reading, ΔR , was taken on a solution of complex ion electrolyte nearly isopiestic with the KCl solution used as a reference. The osmotic coefficient, ϕ , of the complex ion electrolyte is then given by

$$\phi = \frac{(2m\phi)_{\text{KCl}}}{3m} + k \frac{\Delta R}{3m} \quad (1)$$

The constant k in eq 1 was calculated from resistance readings taken with two KCl solutions of different concentrations.

Instead of using a ΔR reading to calculate ϕ directly, as was done previously, the ΔR reading, by this method, is used only to obtain a small correction to be added to the accurately known first term on the right of eq 1. Consequently, the error in ϕ introduced by an error in k is minimized.

For each compound, measurements were taken at approximately 0.01 m intervals in the range from 0.01–0.10 m . With the more soluble compounds, additional readings were taken at approximately 0.1 m intervals up to 1.0 m . Typical data are given in Table I.

Treatment of Data and Results

Smoothed Osmotic and Activity Coefficients. These quantities, obtained as described previously,² are given in Tables II–IV. The experimental error is estimated to be $\pm 1\%$ for ϕ and $\pm 3\%$ for γ_{\pm} in the concentration range 0.03–0.10 m , and $\pm 0.5\%$ for ϕ and $\pm 3\%$ for γ_{\pm} above 0.1 m . The values of a^0 obtained were virtually identical for all of the compounds studied, averaging $2.5 \pm 0.2 \text{ \AA}$.

Extent of Ion-Pair Formation. The fact that the osmotic and activity coefficients of these electrolytes are significantly lower than those of "normal" 2:1 electrolytes implies a considerable degree of association between cation and anion. This is confirmed by the small magnitude of the Debye–Hückel a^0 values required to fit the data at low concentrations. In these respects, the data reported here resemble those for other complex ion electrolytes studied previously.²

For the process $\text{MA}^+ \rightleftharpoons \text{M}^{2+} + \text{A}^-$ the ion-pair dissociation constant, K , is given by the expression

$$K = \frac{\alpha(1 + \alpha)m(\gamma_{\pm}'_{21})^3}{(1 - \alpha)(\gamma_{\pm}'_{11})^2} \quad (2)$$

where α is the degree of dissociation of the ion pair, and $\gamma_{\pm}'_{21}$ and $\gamma_{\pm}'_{11}$ are the mean activity coefficients of completely dissociated 2:1 and 1:1 electrolytes, respectively. Values of K for the 12 compounds reported here were calculated by the approach described in a previous article,⁶ making use of the equation

Table I: Measured Osmotic Coefficients of $[\text{Co}(\text{NH}_3)_5\text{CH}_3\text{CH}_2\text{COO}]\text{Cl}_2$

| m | ϕ | m | ϕ | m | ϕ | m | ϕ |
|--------|--------|--------|--------|-------|--------|-------|--------|
| 0.0103 | 0.863 | 0.0600 | 0.793 | 0.390 | 0.701 | 0.852 | 0.672 |
| 0.0104 | 0.878 | 0.0706 | 0.788 | 0.396 | 0.700 | 0.999 | 0.670 |
| 0.0202 | 0.844 | 0.0802 | 0.769 | 0.485 | 0.691 | 1.50 | 0.669 |
| 0.0302 | 0.826 | 0.100 | 0.766 | 0.570 | 0.687 | 1.81 | 0.671 |
| 0.0400 | 0.817 | 0.198 | 0.739 | 0.653 | 0.681 | 2.10 | 0.676 |
| 0.0503 | 0.805 | 0.295 | 0.715 | 0.732 | 0.677 | 2.40 | 0.681 |

Table II: Smoothed Osmotic and Activity Coefficients of $[\text{Co}(\text{NH}_3)_5\text{CH}_3\text{COO}]\text{X}_2$

| m | NO_3^- | | I^- | | Br^- | | Cl^- | |
|------|-----------------|----------------|--------------|----------------|---------------|----------------|---------------|----------------|
| | ϕ | γ_{\pm} | ϕ | γ_{\pm} | ϕ | γ_{\pm} | ϕ | γ_{\pm} |
| 0.03 | 0.829 | 0.563 | 0.833 | 0.570 | 0.833 | 0.568 | 0.820 | 0.552 |
| 0.04 | 0.812 | 0.526 | 0.817 | 0.533 | 0.816 | 0.531 | 0.805 | 0.515 |
| 0.05 | 0.800 | 0.498 | 0.805 | 0.505 | 0.803 | 0.502 | 0.794 | 0.487 |
| 0.07 | | | 0.788 | 0.464 | 0.783 | 0.459 | 0.777 | 0.446 |
| 0.10 | | | 0.776 | 0.424 | 0.763 | 0.415 | 0.760 | 0.404 |
| 0.20 | | | | | 0.722 | 0.333 | 0.725 | 0.326 |
| 0.30 | | | | | 0.697 | 0.289 | 0.699 | 0.283 |
| 0.40 | | | | | 0.678 | 0.259 | 0.678 | 0.253 |
| 0.50 | | | | | 0.662 | 0.237 | 0.664 | 0.232 |
| 0.60 | | | | | 0.650 | 0.220 | 0.661 | 0.217 |

Table III: Smoothed Osmotic and Activity Coefficients of $[\text{Co}(\text{NH}_3)_6\text{CH}_3\text{CH}_2\text{COO}]\text{X}_2$

| m | NO_3^- | | I^- | | Br^- | | Cl^- | |
|------|-----------------|----------------|--------------|----------------|---------------|----------------|---------------|----------------|
| | ϕ | γ_{\pm} | ϕ | γ_{\pm} | ϕ | γ_{\pm} | ϕ | γ_{\pm} |
| 0.03 | 0.829 | 0.563 | 0.829 | 0.565 | 0.829 | 0.565 | 0.830 | 0.565 |
| 0.04 | 0.812 | 0.525 | 0.813 | 0.528 | 0.813 | 0.528 | 0.814 | 0.529 |
| 0.05 | 0.798 | 0.496 | 0.800 | 0.499 | 0.800 | 0.499 | 0.802 | 0.500 |
| 0.07 | 0.777 | 0.452 | 0.780 | 0.456 | 0.781 | 0.456 | 0.784 | 0.458 |
| 0.10 | 0.754 | 0.407 | 0.760 | 0.412 | 0.761 | 0.412 | 0.766 | 0.415 |
| 0.20 | 0.703 | 0.320 | 0.719 | 0.330 | 0.724 | 0.332 | 0.735 | 0.339 |
| 0.30 | 0.667 | 0.272 | 0.692 | 0.285 | 0.701 | 0.289 | 0.718 | 0.298 |
| 0.40 | 0.641 | 0.240 | 0.667 | 0.254 | 0.681 | 0.259 | 0.704 | 0.270 |
| 0.50 | | | 0.642 | 0.229 | 0.664 | 0.237 | 0.692 | 0.250 |
| 0.60 | | | | | 0.648 | 0.219 | 0.682 | 0.234 |
| 0.80 | | | | | 0.625 | 0.193 | 0.672 | 0.210 |
| 1.0 | | | | | 0.618 | 0.176 | 0.670 | 0.196 |
| 1.2 | | | | | 0.609 | 0.163 | 0.670 | 0.186 |
| 1.6 | | | | | | | 0.671 | 0.168 |
| 2.0 | | | | | | | 0.674 | 0.156 |
| 2.4 | | | | | | | 0.681 | 0.148 |

$$\phi_{21} = \alpha\phi'_{21} + \frac{2}{3}(1 - \alpha)\phi'_{11} \quad (3)$$

where ϕ_{21} is the measured osmotic coefficient while ϕ'_{21} and ϕ'_{11} are calculated osmotic coefficients for completely dissociated 2:1 and 1:1 electrolytes, respectively.

The values of ϕ'_{21} , ϕ'_{11} , $\gamma_{\pm 21}$, $\gamma_{\pm 11}$ used in eq 2 and 3 to solve for K are given in Table V. These parameters are slightly smaller than those used in a previous paper,⁶

which was concerned with the calculation of ion-pair dissociation constants of "simple" 2:1 electrolytes. Presumably, the osmotic coefficient of a completely dissociated complex ion electrolyte should be somewhat smaller than that of a simple electrolyte such as CaCl_2 because of hydration effects. The entry of solvent

(6) W. L. Masterton and L. H. Berka, *J. Phys. Chem.*, in press.

Table IV: Smoothed Osmotic and Activity Coefficients of $[\text{Co}(\text{NH}_3)_5(\text{CH}_3)_2\text{CHCOO}]\text{X}_2$

| m | NO_3^- | | I^- | | Br^- | | Cl^- | |
|------|-----------------|----------------|--------------|----------------|---------------|----------------|---------------|----------------|
| | ϕ | γ_{\pm} | ϕ | γ_{\pm} | ϕ | γ_{\pm} | ϕ | γ_{\pm} |
| 0.03 | 0.823 | 0.557 | 0.830 | 0.565 | 0.822 | 0.555 | 0.827 | 0.560 |
| 0.04 | 0.805 | 0.519 | 0.814 | 0.528 | 0.806 | 0.517 | 0.811 | 0.523 |
| 0.05 | 0.791 | 0.489 | 0.801 | 0.499 | 0.793 | 0.488 | 0.799 | 0.495 |
| 0.07 | 0.769 | 0.444 | 0.781 | 0.456 | 0.774 | 0.445 | 0.781 | 0.453 |
| 0.10 | 0.745 | 0.398 | 0.759 | 0.411 | 0.754 | 0.401 | 0.763 | 0.410 |
| 0.20 | 0.697 | 0.313 | 0.715 | 0.328 | 0.716 | 0.321 | 0.732 | 0.334 |
| 0.30 | 0.664 | 0.266 | 0.683 | 0.282 | 0.691 | 0.278 | 0.715 | 0.293 |
| 0.40 | 0.636 | 0.234 | 0.657 | 0.249 | 0.671 | 0.249 | 0.701 | 0.266 |
| 0.50 | 0.611 | 0.210 | 0.633 | 0.225 | 0.654 | 0.227 | 0.690 | 0.246 |
| 0.60 | 0.588 | 0.190 | 0.614 | 0.206 | 0.640 | 0.210 | 0.680 | 0.230 |
| 0.80 | 0.552 | 0.162 | 0.593 | 0.180 | 0.630 | 0.187 | 0.669 | 0.207 |
| 1.0 | 0.535 | 0.144 | | | | | 0.671 | 0.194 |
| 1.5 | 0.484 | 0.113 | | | | | 0.671 | 0.169 |
| 2.0 | 0.450 | 0.094 | | | | | 0.671 | 0.152 |
| 2.5 | 0.427 | 0.081 | | | | | 0.672 | 0.141 |

water molecules into the first coordination sphere of an ion such as Ca^{2+} will have the effect of increasing the apparent values of ϕ and γ_{\pm} for CaCl_2 . The magnitude of this correction was estimated from the equations of Stokes and Robinson.⁷ In the concentration range covered here ($m \leq 0.1$), the effect is very small; the maximum correction in ϕ_{21} , for example, amounts to only -0.009 .

Table V: Osmotic and Activity Coefficients Calculated for Completely Dissociated Complex Ion Electrolytes

| Ionic strength | ϕ'_{21} | ϕ'_{11} | $\gamma'_{\pm 21}$ | $\gamma'_{\pm 11}$ |
|----------------|--------------|--------------|--------------------|--------------------|
| 0.010 | 0.938 | 0.969 | 0.818 | 0.903 |
| 0.015 | 0.928 | 0.964 | 0.789 | 0.886 |
| 0.020 | 0.920 | 0.959 | 0.765 | 0.873 |
| 0.030 | 0.909 | 0.952 | 0.732 | 0.851 |
| 0.040 | 0.901 | 0.948 | 0.706 | 0.836 |
| 0.050 | 0.894 | 0.944 | 0.686 | 0.822 |
| 0.060 | 0.888 | 0.942 | 0.669 | 0.812 |
| 0.080 | 0.882 | 0.938 | 0.643 | 0.794 |
| 0.100 | 0.877 | 0.934 | 0.622 | 0.780 |
| 0.120 | 0.872 | 0.931 | 0.605 | 0.768 |
| 0.150 | 0.867 | 0.928 | 0.585 | 0.753 |
| 0.180 | 0.864 | 0.925 | 0.570 | 0.741 |
| 0.210 | 0.862 | 0.924 | 0.557 | 0.732 |
| 0.240 | 0.861 | 0.924 | 0.546 | 0.725 |
| 0.270 | 0.860 | 0.923 | 0.537 | 0.717 |
| 0.300 | 0.861 | 0.923 | 0.529 | 0.710 |

Equations 2 and 3 were used to calculate K for each complex ion electrolyte at a series of molalities ranging from 0.03 to 0.10. The excellent agreement between calculated K values at different molalities (Table VI) is particularly striking.

Table VI: Calculated Values of the Dissociation Constant of $[\text{Co}(\text{NH}_3)_5\text{CH}_2\text{CH}_2\text{COO}]^{2+}$, Cl^-

| m | ϕ_{21} | α | K |
|------|-------------|----------|-------|
| 0.03 | 0.830 | 0.793 | 0.088 |
| 0.04 | 0.814 | 0.752 | 0.085 |
| 0.05 | 0.802 | 0.722 | 0.084 |
| 0.06 | 0.792 | 0.695 | 0.083 |
| 0.07 | 0.784 | 0.668 | 0.081 |
| 0.08 | 0.777 | 0.648 | 0.082 |
| 0.09 | 0.771 | 0.630 | 0.081 |
| 0.10 | 0.766 | 0.608 | 0.080 |

The ion-pair dissociation constants given in Table VII for the 12 electrolytes studied were calculated at $m = 0.1$, except for $[\text{Co}(\text{NH}_3)_5\text{CH}_2\text{COO}](\text{NO}_3)_2$, where, because of solubility limitations, the calculation was made at $m = 0.05$. Values of K were also calculated by the more involved thermodynamic approach described in ref 6 with virtually identical results.

Table VII: Dissociation Constants for $[\text{Co}(\text{NH}_3)_5\text{A}]^{2+}$, X^-

| | NO_3^- | I^- | Br^- | Cl^- |
|--------------------------------------|-----------------|--------------|---------------|---------------|
| CH_2COO^- | 0.080 | 0.097 | 0.075 | 0.071 |
| $\text{CH}_2\text{CH}_2\text{COO}^-$ | 0.064 | 0.071 | 0.072 | 0.080 |
| $(\text{CH}_3)_2\text{CHCOO}^-$ | 0.054 | 0.071 | 0.064 | 0.075 |

Discussion

Up to a molality of 0.1, the osmotic and activity coefficients of the compounds listed in Tables II-IV are

(7) R. H. Stokes and R. A. Robinson, *J. Am. Chem. Soc.*, **70**, 1870 (1948).

very close to one another, except for an indication of lower values for the nitrates. This is, of course, also true of the ion-pair dissociation constants listed in Table VII.

Above 0.1 *m*, ϕ and γ_{\pm} appear to change very little when one acid ligand is replaced by another. The agreement between the osmotic coefficients of the compounds $[\text{Co}(\text{NH}_3)_5\text{CH}_3\text{CH}_2\text{COO}]\text{Cl}_2$ and $[\text{Co}(\text{NH}_3)_5(\text{CH}_3)_2\text{CHCOO}]\text{Cl}_2$ over the entire concentration range from 0.03 to 2.00 *m* is particularly striking. A similar agreement is observed with $[\text{Co}(\text{NH}_3)_5\text{CH}_3\text{COO}]\text{Br}_2$ and $[\text{Co}(\text{NH}_3)_5\text{CH}_3\text{CH}_2\text{COO}]\text{Br}_2$ from 0.03 to 0.60 *m*. The equivalence of propionate and isobutyrate ligands is indicated in the first instance and that of acetate and propionate ligands, in the second.

On the other hand, at concentrations above 0.1 *m*, there is an appreciable change in ϕ or γ_{\pm} when one anion is replaced by another. Almost without exception, the osmotic coefficients decrease in the order $\text{Cl}^- > \text{Br}^- > \text{I}^- > \text{NO}_3^-$. At very high concentrations, the spread becomes particularly large. Compare, for example, the two compounds $[\text{Co}(\text{NH}_3)_5(\text{CH}_3)_2\text{CHCOO}]\text{Cl}_2$ and $[\text{Co}(\text{NH}_3)_5(\text{CH}_3)_2\text{CHCOO}](\text{NO}_3)_2$, whose osmotic coefficients at 2.0 *m* are, respectively, 0.671 and 0.450.

If one interprets the data at concentrations above 0.1 *m* solely in terms of varying extents of association between anion and cation, two conclusions can be drawn.

(1) Association is little affected by a change in ligand involving the replacement of one organic anion by another.

(2) Association appears to increase in the order $\text{Cl}^- < \text{Br}^- < \text{I}^- < \text{NO}_3^-$. This order is the reverse of what one would expect if the association were strictly coulombic, in which case, its extent should be inversely related to anionic size.

The most striking feature of these data is the fact that the osmotic and activity coefficients are considerably lower than those of most simple 2:1 electrolytes (*e.g.*, CaCl_2 , etc.). This becomes obvious at concentrations as low as 0.1 *m* where γ_{\pm} is about 0.41 ± 0.02 as compared to values of 0.50 or greater commonly observed with simple 2:1 salts.⁸ Furthermore, these complex ion electrolytes show no evidence of a minimum in activity coefficient at concentrations as high as 2.5 *m*; γ_{\pm} values for simple 2:1 salts ordinarily pass through a minimum somewhere between 0.1 and 1.0 *m* and then increase rapidly with increasing concentration. The activity coefficient of CaCl_2 , for example, after passing through a minimum of 0.448 at about 0.5 *m*, rises to 1.063 at 2.5 *m*; γ_{\pm} for $[\text{Co}(\text{NH}_3)_5(\text{CH}_3)_2\text{CHCOO}]\text{Cl}_2$ at 2.5 *m* is only 0.141.

The only simple 2:1 salts which resemble those studied here in the variation of ϕ and γ_{\pm} with concentration are ones which are extensively ion paired, notably the alkaline earth nitrates. Even with these compounds, the extent of ion pairing is much smaller. For example, the ion-pair dissociation constant of $\text{Ca}(\text{NO}_3)_2$ is estimated by Davies⁹ to be about 0.5; those for the compounds listed in Table VII fall between 0.05 and 0.1.

The question arises as to why these complex ion electrolytes ion pair to a much greater extent than simple salts of the same valence type. The answer cannot lie in the coulombic factor frequently invoked to explain relative extents of ion pairing. Complex cations of the type $[\text{Co}(\text{NH}_3)_5\text{A}]^{2+}$ must be at least as large as hydrated alkaline earth cations (*e.g.*, $\text{Ca}(\text{H}_2\text{O})_6^{2+}$, etc.).

Perhaps the simplest explanation of the effects observed here is that offered by Stengle and Langford¹⁰ to rationalize nmr studies which indicate that salts of $\text{Cr}(\text{en})_3^{3+}$ are extensively associated while those of $\text{Cr}(\text{H}_2\text{O})_6^{3+}$ are not. They suggest that hydrated cations can fit readily into the surrounding network of water molecules and consequently are unlikely to come into close contact with anions. Complex cations such as $\text{Cr}(\text{en})_3^{3+}$ or, in this case, $[\text{Co}(\text{NH}_3)_5\text{A}]^{2+}$, should not bond as readily with water molecules in the second coordination sphere and hence may be able to associate more readily with anions.

Carrying this idea one step further, it might be postulated that large ions such as $[\text{Co}(\text{NH}_3)_5\text{A}]^{2+}$, which cannot fit readily into the surrounding water structure, may create a cavity in the solvent large enough to accommodate simultaneously an anion. This type of "structure-enforced" ion pairing has been proposed by Diamond¹¹ to explain the abnormally low osmotic and activity coefficients of tetraalkylammonium iodides. Quite possibly, it may be characteristic of water solutions of complex ion electrolytes as well.

Both of these approaches treat ion pairing in terms of the effect of a large cation upon the surrounding water structure. We should like to suggest an alternative explanation which emphasizes instead the relatively strong noncoulombic forces which must exist between ions of the type dealt with here. It was reported earlier¹² that the neutral complex $[\text{Co}(\text{NH}_3)_5\text{A}]$

(8) R. H. Stokes, *Trans. Faraday Soc.*, **44**, 295 (1948).

(9) C. W. Davies, "Ion Association," Butterworth Inc., Washington, D. C., 1962.

(10) Thomas R. Stengle and C. H. Langford, *J. Phys. Chem.*, **69**, 3299 (1965).

(11) R. M. Diamond, *ibid.*, **67**, 2513 (1963).

(NO₂)₃] is strongly salted-in by alkali halides. The salt effects in these systems were explained largely in terms of dispersion forces between the complex molecule on the one hand and the ions of the salt on the other. Extending this idea to complex ion electrolytes, one might expect dispersion forces to make a significant contribution to the formation of ion pairs involving a large, highly polarizable cation such as [Co(NH₃)₆A]²⁺. This would explain, among other things, why the extent of association appears to increase in the order Cl⁻ < Br⁻ < I⁻ since this is the order of increasing polarizability of the anions.

In this connection, Rosseinsky¹³ has pointed out that, contrary to popular belief, ion-pair formation in salts of

the alkali or alkaline earth metals usually increases with the size of the cation. This lends support to our belief that, while coulombic forces and solvent structure effects are undoubtedly important in ion pairing, dispersion forces may play a much more significant role than has been generally recognized.

Acknowledgment. This work was supported in part by the Research Foundation of the University of Connecticut and by an NSF graduate fellowship awarded to L. H. B.

(12) W. L. Masterton and Robert N. Schwartz, *J. Chem. Phys.*, **69**, 1546 (1965).

(13) D. R. Rosseinsky, *J. Chem. Soc.*, 785 (1962).

Nitro-*p*-terphenyls. I. Dual Charge-Transfer Properties and Spectral Correlations

by Richard L. Hansen

Contribution No. 850 from the Central Research Laboratories, Minnesota Mining and Manufacturing Company, St. Paul, Minnesota 55119 (Received November 12, 1965)

Seven nitro-*p*-terphenyls have been found to form charge-transfer complexes with both electron donors and acceptors. The results of quantitative studies of complexes with tetracyanoethylene and with *N,N*-dimethyl-*p*-toluidine are reported. A partial interpretation of the absorption spectra of the nitroterphenyls has been made on the basis of their charge-transfer spectra and elementary molecular orbital theory.

Introduction

Organic charge-transfer complexes have been extensively investigated for a number of years. Typically, a given organic molecule acts as either an electron donor or an electron acceptor but seldom as both. In addition to intramolecular charge-transfer interactions in certain molecules, a limited number of compounds such as iodine can play a dual role and form self-complexes in which one molecule behaves as an electron donor toward a second molecule as acceptor.¹

Examples of materials possessing more general dual

charge-transfer properties are quite rare. The "charge-transfer" or "π-complex" theories developed by Mulliken,² by Dewar and Lepley,³ and enunciated by Briegleb⁴ intimate that organic molecules should be capable of functioning as both charge-transfer donors and ac-

(1) P. A. D. deMaine, *J. Chem. Phys.*, **24**, 1091 (1956).

(2) R. S. Mulliken, *J. Am. Chem. Soc.*, **72**, 600 (1950); **74**, 811 (1952); *J. Phys. Chem.*, **56**, 801 (1952).

(3) M. J. S. Dewar and A. R. Lepley, *J. Am. Chem. Soc.*, **83**, 4560 (1961).

(4) G. Briegleb, *Angew. Chem.*, **76**, 326 (1964).

ceptors; albeit, one of these roles may be dominant. In support of these views, Wentworth and Chen have reported that certain polycyclic aromatic hydrocarbons can behave as charge-transfer acceptors. However, the complexes were very weak, the uncertainties were large, and charge-transfer spectra could not be obtained.⁵ The donor abilities of aromatic hydrocarbons are well known.

Proceeding along these lines, we have found that several nitro-*p*-terphenyls, some of which are new, exhibit well-defined dual charge-transfer properties; e.g., they complex with tetracyanoethylene (TCNE), a typical acceptor, and with *N,N*-dimethyl-*p*-toluidine (DMT), a representative electron donor. These complexes are described below. The electronic absorption spectra of the nitroterphenyls are related to their charge-transfer properties. The ability of elementary molecular orbital theory to account for the properties of the nitroterphenyls is tested.

Following papers in this series will deal with polarographic studies of the nitroterphenyls and with the epr spectra of the radical anions derived from them.

Experimental Section

Materials. A mixture of 2-nitro- and 4-nitro-*p*-terphenyl was prepared by the method of France, Heilbron, and Hey.⁶ Fractional crystallization from either ethanol or benzene followed by chromatography on an alumina column gave 2-nitroterphenyl, mp 129–130° and 4-nitroterphenyl, mp 214–215°. The infrared spectra of these compounds displayed typical N–O stretching bands in KBr. In 4-nitroterphenyl these bands appeared at 1340 and 1517 cm⁻¹ but were at 1349 and 1527 cm⁻¹ in the 2-nitro isomer, suggesting that the nitro group is sterically hindered in the latter case.⁷

4,4''-Dinitro-*p*-terphenyl, mp 272–273°, was obtained by the direct nitration of *p*-terphenyl using a mixture of acetic and fuming nitric acids.⁶ Infrared bands were at 1342 and 1512 cm⁻¹.

3-Nitro-*p*-terphenyl was prepared as suggested by Gray and Lewis.⁸ Chromatography on alumina followed by recrystallization from methylene chloride gave nearly colorless plates: mp 176–177°; infrared bands, 1350 and 1522 cm⁻¹.

Nitro-*p*-terphenyls containing more than one nitro group in a given benzene ring have not been reported previously. The Ullmann biaryl coupling reaction, which in these cases involved heating a melt of 4-iodobiphenyl and the appropriate 1-chloronitrobenzene with copper, provided a convenient route to three of these compounds. The general technique has been described adequately.^{9,10} In each case the product

was purified by column chromatography and recrystallization from a methylene chloride-*n*-hexane mixture.

2,4-Dinitro-*p*-terphenyl was made at 210°. The yield was 6%: yellow needles; mp 150–151°; infrared bands, 1352 and 1530 cm⁻¹. *Anal.* Calcd for C₁₈H₁₂N₂O₄: C, 67.5; H, 3.8; N, 8.8. Found: C, 67.0; H, 4.0; N, 8.6. When 2,4-dinitrobromobenzene was used as the reactant, the yield was increased to 18%.

2,6-Dinitro-*p*-terphenyl was prepared at 185° in 46% yield. The yellow needles melted at 131–132°. Infrared bands were at 1356 and 1529 cm⁻¹. *Anal.* Found: C, 67.2; H, 3.7; N, 8.8.

The reaction between 4-iodobiphenyl and picryl chloride at 158° produced 2,4,6-trinito-*p*-terphenyl in 80% yield. The yellow needles melted at 179–180°. Infrared bands were at 1352 and 1557 cm⁻¹. *Anal.* Calcd for C₁₈H₁₁N₃O₆: C, 59.2; H, 3.0; N, 11.5. Found: C, 59.1; H, 3.3; N, 11.3.

p-Terphenyl and biphenyl were recrystallized and the *p*-terphenyl was then sublimed. Tetracyanoethylene was crystallized from chlorobenzene and sublimed. *N,N*-Dimethyl-*p*-toluidine was distilled under vacuum, saturated with nitrogen, and stored in a refrigerator. Spectro grade methylene chloride was used as received.

Equipment and Procedure. Differential absorption spectra were obtained in matched 1- or 5-cm cells on a Beckman Model DK-2A spectrophotometer. The cell holder was thermostated to ±0.2°, and the cell compartment was flushed with dry nitrogen for work below room temperature. Charge-transfer spectra were measured at 15, 25, and 35°. For the series of TCNE complexes, the nitroterphenyl concentration covered the range 4–36 × 10⁻³ *M*, and the TCNE concentration the range 4–26 × 10⁻³ *M*. In the case of the DMT complexes the nitroterphenyl concentration was held constant at either 1 × 10⁻³ or 4 × 10⁻³ *M*. The DMT concentration was varied in the range 10⁻² to 10⁻¹ *M*. The absorbance was reproducible to at least ±2% and in most cases to ±1% or better. Spectra of the parent nitroterphenyls were measured in the range of about 8–80 × 10⁻⁶ *M*.

Calculations. In the case of the TCNE complexes, data taken at ten wavelengths chosen to encompass the charge-transfer band were averaged by the matrix methods of Wallace¹¹ and Ainsworth.¹² Averaged

(5) W. E. Wentworth and E. Chen, *J. Phys. Chem.*, **67**, 2201 (1963).

(6) H. France, I. M. Heilbron, and D. H. Hey, *J. Chem. Soc.*, 1364 (1938).

(7) L. H. Bellamy, "The Infrared Spectra of Complex Molecules," John Wiley and Sons, Inc., New York, N. Y., 1958, p 300.

(8) G. W. Gray and D. Lewis, *J. Chem. Soc.*, 5156 (1961).

(9) P. E. Fanta, *Chem. Rev.*, **38**, 139 (1946).

(10) J. Forrest, *J. Chem. Soc.*, 566 (1960).

absorbances at three widely separated wavelengths were then treated according to the least-squares method of Liptay for the calculation of equilibrium constants and extinction coefficients.¹³ These computations were programmed for an IBM 705 computer.

Less elaborate analyses were needed for the series of DMT complexes. In these cases it was convenient to employ an excess of the amine. Equilibrium constants and extinction coefficients were obtained graphically at several wavelengths using the Scott modification of the Benesi-Hildebrand equation.¹⁴

Hückel molecular orbital calculations were performed for the nitroterphenyls and related molecules on a CDC 1604 computer using standard diagonalization techniques. The heteroatom parameters, $k_{CN} = 0.8$, $k_{NO} = 0.7$, $h_{N^+} = 2.0$, and $h_O = 1.0$, suggested by Streitwieser were used where required.¹⁵ In an effort to make the model more realistic, the effects of non-planarity on energy levels were investigated by varying H_{11}' , the resonance integral connecting the biphenyl and nitrobenzene moieties, between 1.0β and 0.0β in those molecules containing a 2-nitro group.¹⁶ For simplicity, coplanarity was otherwise assumed and no attempt was made to study the effects of simultaneous rotation about a carbon-nitrogen bond, for example.

Results

The stoichiometry of both series of complexes was

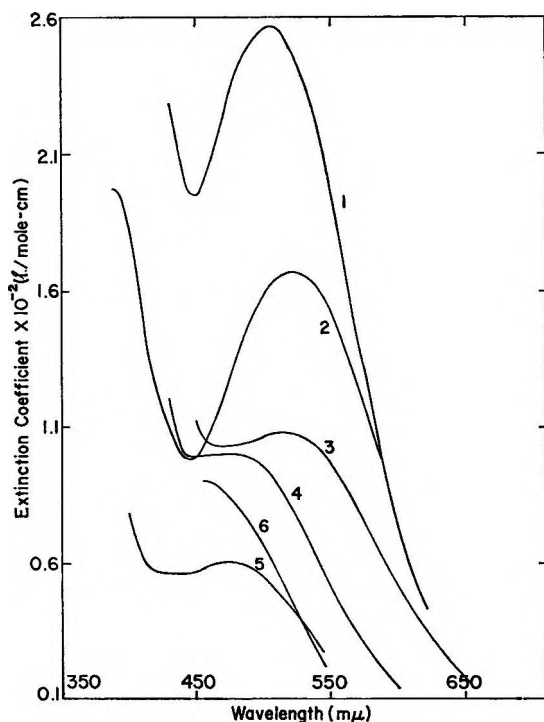


Figure 1. Charge-transfer spectra of nitroterphenyl-TCNE complexes in methylene chloride at 25°.

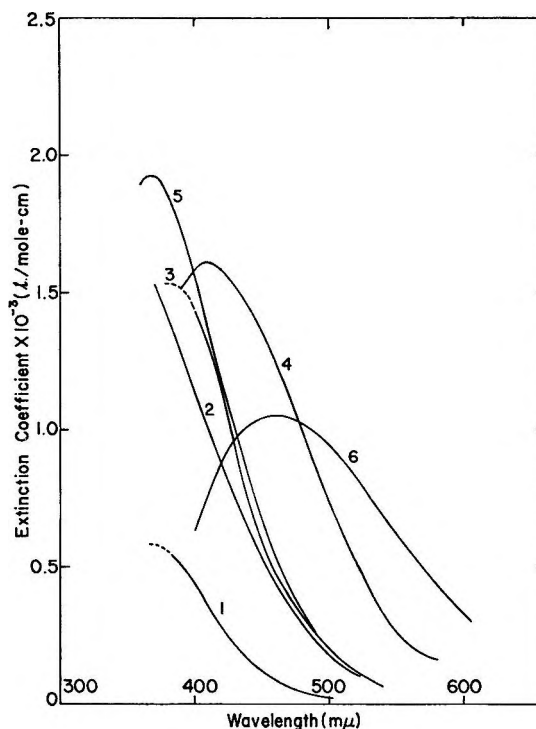


Figure 2. Charge-transfer spectra of nitroterphenyl-DMT complexes in methylene chloride at 25°.

1:1 with respect to the reactants. In the case of the TCNE complexes, a matrix ranking method was used which is mathematically accurate but can only be as certain as the spectroscopic data.^{11,12} In the case of the DMT complexes, the stoichiometry rests solely on the linear Scott plots obtained. The pitfalls involved in determining the stoichiometry, thermodynamic, and optical properties of complexes are well documented.¹⁷⁻²⁰ The charge-transfer spectra of the complexes of six of the nitroterphenyls with TCNE and DMT appear in Figures 1 and 2, respectively. The curves are identified by the compound numbers given in Table I. Parabolic extrapolations were made

- (11) R. M. Wallace, *J. Phys. Chem.*, **64**, 899 (1960).
- (12) S. Ainsworth, *ibid.*, **65**, 1968 (1961); **67**, 1613 (1963).
- (13) W. Liptay, *Z. Elektrochem.*, **65**, 375 (1961).
- (14) R. L. Scott, *Rec. Trav. Chim.*, **75**, 787 (1956).
- (15) A. Streitwieser, "Molecular Orbital Theory for Organic Chemists," John Wiley and Sons, Inc., New York, N. Y., 1961, p 117.
- (16) H. Suzuki, *Bull. Chem. Soc. Japan*, **35**, 1853 (1962), and previous papers.
- (17) W. B. Person, *J. Am. Chem. Soc.*, **87**, 167 (1965).
- (18) G. D. Johnson and R. E. Bowen, *ibid.*, **87**, 1655 (1965).
- (19) K. Conrow, G. D. Johnson, and R. E. Bowen, *ibid.*, **86**, 1025 (1964).
- (20) P. R. Hammond, *J. Chem. Soc.*, 479 (1964).

Table I: The Properties of Complexes with TCNE in Methylene Chloride at 25°

| Compd | Ct max, m μ | ϵ_{max} , l./mole cm | $f^a \times 10^3$ | K_x | $-\Delta H$, kcal/mole | $-\Delta F_x$, kcal/mole | ΔS_x , eu | $b^2/a^{2b} \times 10^2$ |
|----------------------------------|-----------------------|--|-------------------|-------------|--------------------------------|------------------------------|----------------------|--------------------------|
| 2-Nitroterphenyl (1) | 506 | 260 \pm 80 | 7 | 14 \pm 4 | 1.6 \pm 0.2 | 1.6 \pm 0.2 | 0 \pm 2 | 2.8 \pm 0.5 |
| 3-Nitroterphenyl (2) | 520 ~390 | 170 \pm 40 200 \pm 40 | 3 | 39 \pm 10 | 1.7 \pm 0.6 | 2.2 \pm 0.2 | 2 \pm 3 | 3 \pm 1 |
| 4-Nitroterphenyl (3) | 516 | 110 \pm 40 | 3 | 50 \pm 18 | 2.6 \pm 0.5 | 2.3 \pm 0.3 | -1 \pm 3 | 4.7 \pm 0.9 |
| 2,4-Dinitroterphenyl (4) | 480 | 100 \pm 9 | 2.2 | 32 \pm 3 | 1.2 \pm 0.1 | 2.1 \pm 0.1 | 3.1 \pm 0.9 | 4.0 \pm 0.2 |
| 2,6-Dinitroterphenyl (5) | 475 | 60 \pm 7 | 1.1 | 51 \pm 1 | 1.0 \pm 0.2 | 2.3 \pm 0.1 | 4.4 \pm 0.5 | 1.6 \pm 0.2 |
| 2,4,6-Trinitro- terphenyl (6) | 460 | 90 \pm 20 | 1.9 | 31 \pm 7 | 0.4 \pm 0.1 | 2.0 \pm 0.2 | 5 \pm 1 | 0.6 \pm 0.2 |
| 4,4''-Dinitroterphenyl (7) | <410 | | ... | | | | | |
| <i>p</i> -Terphenyl (8) | 557 382 | 800 \pm 300 1200 \pm 400 | 17 30 | 11 \pm 4 | 1.4 \pm 0.2 1.1 \pm 0.2 | 1.4 \pm 0.3 | 0 \pm 2 | 2.7 \pm 0.4 |
| Biphenyl (9) | 495 390 | 800 \pm 200 1000 \pm 200 | 19 22 | 8 \pm 2 | 1.7 \pm 0.1 1.2 \pm 0.1 | 1.2 \pm 0.2 | -2 \pm 1 | 2.9 \pm 0.2 |
| Benzene ^c (10) | 384 | 3570 | | 2.00 | 2.30 | 0.411 | -6 | |

^a Oscillator strength, $f = 4.3 \times 10^{-9} \epsilon_{\text{max}} \Delta \nu_{1/2}$, estimated by assuming band symmetry. ^b See text. ^c Taken from ref 24.

Table II: The Properties of Complexes with DMT in Methylene Chloride at 25°

| Compd | Ct max, m μ | ϵ_{max} , l./mole cm | $f^a \times 10^3$ | K_x | $-\Delta H$, kcal/mole | $-\Delta F_x$, kcal/mole | ΔS_x , eu | $b^2/a^{2b} \times 10^2$ |
|-------|-----------------------|--|-------------------|-----------------|----------------------------|------------------------------|----------------------|--------------------------|
| 1 | 370 | 580 \pm 30 | 16 | 1.06 \pm 0.04 | 0.4 \pm 0.2 | 0.03 \pm 0.02 | -1.2 \pm 0.7 | 0.5 \pm 0.3 |
| 2 | <360 | >1580 | .. | 0.74 \pm 0.04 | 0.5 \pm 0.3 | -0.18 \pm 0.03 | -2 \pm 1 | <0.6 |
| 3 | 385 | 1580 \pm 30 | 42 | 1.00 \pm 0.02 | 0.7 \pm 0.02 | 0.0 \pm 0.01 | -2.3 \pm 0.1 | 0.94 \pm 0.03 |
| 4 | 410 | 1600 \pm 200 | 58 | 1.3 \pm 0.2 | 1.0 \pm 0.1 | 0.14 \pm 0.06 | -2.8 \pm 0.6 | 1.4 \pm 0.2 |
| 5 | 370 | 1900 \pm 300 | 64 | 0.9 \pm 0.1 | 0.6 \pm 0.1 | -0.04 \pm 0.06 | -2.2 \pm 0.6 | 0.8 \pm 0.1 |
| 6 | 460 | 1100 \pm 200 | 37 | 4.4 \pm 0.6 | 1.8 \pm 0.4 | 0.89 \pm 0.08 | -3 \pm 1 | 2.9 \pm 0.6 |
| 7 | <390 | ... | ... | ... | | | | |

^a See note a, Table I. ^b See text.

to two of the charge-transfer (ct) maxima.²¹ The decomposition of overlapping charge-transfer bands and extrapolation to band maxima have also been described by Lepley²² and by Voigt and Reid.²³ Although 4,4''-dinitroterphenyl also formed complexes, the absorption maxima occurred at inaccessible wavelengths and the complexes were not studied quantitatively.

Optical and thermodynamic properties for both series of complexes appear in Tables I and II. The TCNE complexes of biphenyl and *p*-terphenyl were also investigated as potential models, the results appearing in Table I. In the latter cases, at least some of the data have appeared previously.^{24,25} The present results are comparable to those reported.

The product, $K_x \epsilon$, was measurable to a precision of

1-2% and heats of reaction were obtained from the variation of this quantity with temperature. The heat of reaction was slightly wavelength dependent for the TCNE complexes of biphenyl and *p*-terphenyl. This has been observed before in the case of the biphenyl complex,²⁵ the heat of reaction being slightly larger at long wavelengths. The equilibrium constants, which are more tenuous, were independent of wavelength.

(21) A. A. Gordus and R. B. Bernstein, *J. Chem. Phys.*, **22**, 790 (1954).

(22) A. R. Lepley, *J. Am. Chem. Soc.*, **86**, 2545 (1964).

(23) E. M. Voigt and C. Reid, *ibid.*, **86**, 3930 (1964).

(24) R. E. Merrifield and W. D. Phillips, *ibid.*, **80**, 2778 (1958).

(25) G. Briegleb, J. Czekalla, and G. Reuss, *Z. Physik. Chem. (Frankfurt)*, **30**, 333 (1961).

The quantity, b^2/a^2 , is a measure of the degree of electron transfer in the ground state.²⁶

Electronic absorption spectra of the nitroterphenyls were obtained in several solvents. Spectra in methylene chloride are shown in Figure 3. The spectra of the three mononitro compounds have been reported.²⁷ Our spectra differ somewhat from those reported previously.

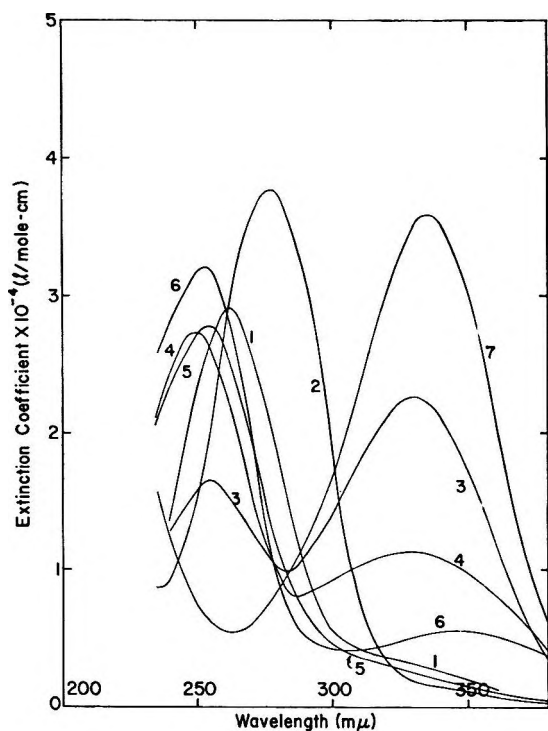


Figure 3. Absorption spectra of the nitroterphenyls in methylene chloride.

The absorption spectra all obeyed Beer's law over as much as 15-fold changes in concentration. No evidence was found for the formation of nitroterphenyl self-complexes at the concentrations employed.

The spectra consist generally of two bands with maxima near 330 and 250 $m\mu$. The 250- $m\mu$ bands underwent bathochromic shifts of 1–5 $m\mu$ in ethanol compared to *n*-hexane. Similar shifts were observed in the case of the 330- $m\mu$ bands, amounting to 16 $m\mu$ in the case of 4,4''-dinitroterphenyl but only 1 $m\mu$ in the case of 2,4-dinitroterphenyl. 2,4,6-Trinitroterphenyl was exceptional in that the 330- $m\mu$ band was shifted 11 $m\mu$ to shorter wavelengths in ethanol. For comparison, the spectrum of nitrobenzene contains two resolvable bands at 330 $m\mu$ ($\epsilon \sim 10^2$) and 250 $m\mu$ ($\epsilon \sim 10^4$), as well as a shoulder at about 280 $m\mu$ ($\epsilon \sim 10^3$).²⁸

Discussion

With the exception of 4,4''-dinitroterphenyl and possibly 2,4,6-trinitroterphenyl, all of the TCNE complexes display two charge-transfer bands although the second maximum was accessible only in the cases of biphenyl, *p*-terphenyl, and 3-nitroterphenyl. The appearance of two charge-transfer bands in TCNE complexes has been reported in several instances.^{25,29–31} As in other cases, this can be accounted for very well on the basis of elementary Hückel MO theory.

Interaction between the lowest vacant b_{2g} level of TCNE and the highest filled levels of the hydrocarbons (also b_{2g} symmetry) accounts for the frequencies of the first charge-transfer bands. This is illustrated in the upper curve of Figure 4 where the highest filled MO energies are correlated with the charge-transfer frequencies. The single charge-transfer band of the benzene-TCNE complex at 384 $m\mu$ is included.²⁴ The slope of the line shown through these points corresponds to $|\beta| = 2.47$ eV.

The next lower lying filled levels of biphenyl and terphenyl are degenerate at 1.00β in the Hückel model, at least one of the set possessing b_{1g} symmetry. Thus, one would expect a second charge-transfer band in each case at an energy close to that of the benzene-TCNE complex. In fact, these bands appear at 390 and 382 $m\mu$ for biphenyl and terphenyl, respectively.

Except for 4,4''-dinitroterphenyl, the results of Hückel calculations in the nitroterphenyl cases indicate that the highest filled levels are quite similar in symmetry and energy to the highest filled levels of biphenyl and terphenyl. The electron density at the nitro group(s) is low and the local symmetry of the biphenyl portion is b_{2g} . In the nitroterphenyls, as in biphenyl and terphenyl, the next lower lying filled M.O.'s are degenerate at 1.00β .

It is reasonable to assume that the nitroterphenyl-TCNE complexes, like the hydrocarbon complexes, require interaction between the lowest vacant TCNE orbital and the two highest filled MO's of the nitroterphenyl. The Hückel energy of the highest filled orbital is correlated with the frequency of the first charge-transfer band in Figure 4. The variation in

(26) G. Briegleb, "Elektronen Donator-Acceptor Komplexe," Springer-Verlag, Berlin, 1961, p 22.

(27) K. Iguchi, T. Nozaki, A. Imamura, and S. Takahashi, *Bull. Chem. Soc. Japan*, **35**, 1783 (1963).

(28) J. N. Murrell, "The Theory of the Electronic Spectra of Organic Molecules," John Wiley and Sons, Inc., New York, N. Y., 1963, p 186.

(29) A. R. Lepley, *Tetrahedron Letters*, No. 39, 2823 (1964).

(30) A. Zweig and J. E. Lehnson, *J. Am. Chem. Soc.*, **87**, 2647 (1965).

(31) E. M. Voigt, *ibid.*, **86**, 3611 (1964).

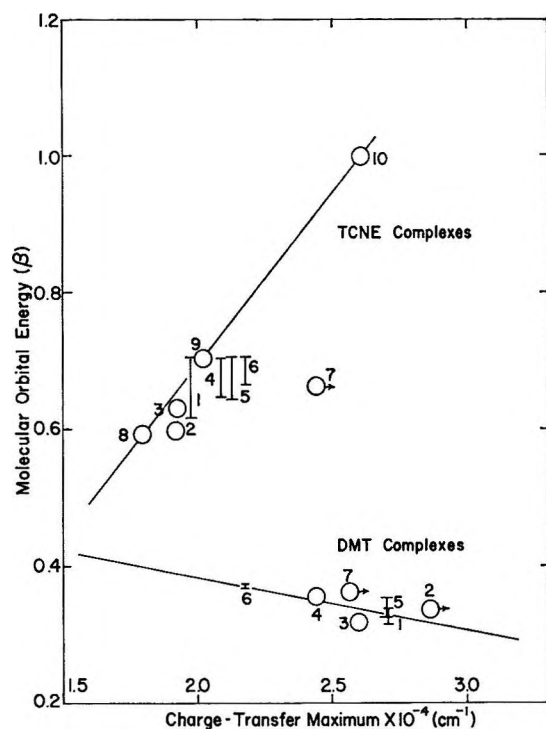


Figure 4. Relations between charge-transfer frequencies and molecular orbital energies.

the energies shown for the 2-nitro compounds illustrates the range when H_{11} is varied from 0.0β to 1.0β . 4,4''-Dinitroterphenyl is an obvious misfit.

A consideration of the energy of the highest filled orbital in 4,4''-dinitroterphenyl indicates that this compound should also exhibit a charge-transfer maximum with TCNE at a wavelength comparable to the other nitroterphenyls. The highest filled MO possesses b_{2g} symmetry in the point group V_h which also appears to be favorable. A significant difference between 4,4''-dinitroterphenyl and the others is that the MO's of the latter contain nodal planes cutting the $C_{1''}-C_4$ bond providing a favorable site for the TCNE molecule. This node is missing in the highest filled orbital of 4,4''-dinitroterphenyl.

The second charge-transfer maxima in all of the complexes are expected to occur near that of the benzene-TCNE complex at $384 m\mu$. In the single case in which it was accessible, the spectrum of the 3-nitroterphenyl-TCNE complex contains a second maximum at about $390 m\mu$.

The nitroterphenyl complexes with TCNE are more stable than the hydrocarbon complexes. All of these complexes are stabilized predominantly by van der Waal's forces in the ground state. In contrast to the hydrocarbons, all the nitroterphenyls except 4,4''-dinitroterphenyl should possess permanent electric

dipole moments. The induction forces stabilizing the nitroterphenyl complexes should be larger than the dispersion or London forces in the hydrocarbon complexes.

Complexing is also expected to produce an induced dipole moment oriented in the direction of charge transfer. As suggested by the work of Herndon and Sanders,³² the resultant dipole moment in a nitroterphenyl-TCNE complex may actually be smaller than in the uncomplexed state. Decreased solvation requirements in the complexed state may explain the more favorable entropies of formation observed for some of the complexes.³³

The complexes of the nitroterphenyls with DMT probably involve interaction between the highest filled MO of the amine and the lowest lying vacant orbital of the nitroterphenyl. Whereas the donor orbitals of the nitroterphenyls are similar to the donor orbitals in biphenyl and terphenyl, Hückel calculations suggest that the lowest vacant orbitals are quite a bit like the lowest vacant orbitals of the corresponding nitrobenzenes with high electron density at the nitro group(s). For example, in the case of 2,4-dinitroterphenyl, this orbital is identical with the lowest vacant orbital of *m*-dinitrobenzene even if the molecule is planar.

The correlation between the frequencies of the charge-transfer bands in the nitroterphenyl-DMT complexes and the calculated energy of the lowest vacant orbitals of the nitroterphenyls is shown in the lower portion of Figure 4. The slope of the line shown corresponds to $|\beta| = 16$ ev. If the Hückel treatment of the nitroterphenyls provided a reliable description of relative orbital energies, one would expect that a consistent value for $|\beta|$ would result from the nitroterphenyl correlations shown in Figure 4. A single value for $|\beta|$ does not appear to suffice to transpose relative Hückel energies to an absolute scale.

The stability of the complexes with DMT increases with the number of nitro groups in the molecule and these complexes are comparable in most respects to corresponding nitrobenzene complexes.³⁴

In molecules displaying dual charge-transfer properties utilizing their highest filled and lowest vacant molecular orbitals, a unique opportunity is afforded

(32) W. C. Herndon and H. W. Sanders, *J. Miss. Acad. Sci.*, **9**, 55 (1963).

(33) It is difficult to believe that ΔS could become a positive quantity due to this effect. It should be pointed out that the free energies and entropies of formation given in Tables I and II are scaled by the choice of standard state. A more conventional equilibrium constant in liters per mole units results by multiplying K_x by 0.065, the molar volume of the solvent. This leads to free energies which are more positive and entropies which are more negative.

(34) B. Dale, R. Foster, and D. Ll. Hammick, *J. Chem. Soc.*, 3986 (1954).

to relate the charge-transfer spectra to the electronic spectrum of the dual charge-transfer agent.

There is little doubt that the bands at 250 and 280 $m\mu$ in the spectrum of nitrobenzene are intramolecular charge-transfer bands of the type described by Nagakura.³⁵ Calculations confirm this,³⁶⁻³⁸ but the origin of the low-intensity band at 330 $m\mu$ is still unsettled.

The Hückel treatment of nitrobenzene gave results in fair agreement with the more sophisticated calculations of Peacock and Wilkinson.³⁶ The 330- $m\mu$ band should be a $\pi \rightarrow \pi^*$ transition involving a redistribution of charge in the nitro group.

In the nitroterphenyls the long wavelength $\pi \rightarrow \pi^*$ band should be quite different than the 330- $m\mu$ band of nitrobenzene. In each case an allowed transition from the highest filled to the lowest vacant molecular orbital is indicated. These should be regarded as intramolecular charge-transfer transitions; about 0.6 electron being transferred principally from the biphenyl ring system to the nitro group(s).

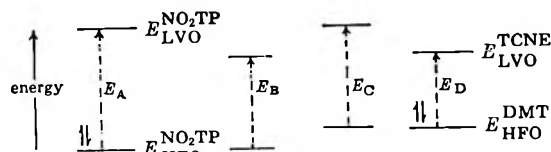
The intensities of the nitroterphenyl bands near 330 $m\mu$ are considerably higher than this band of nitrobenzene. The low intensity of the band in the case of 3-nitroterphenyl may be due to the lack of resonance coupling between the biphenyl ring system and the nitro group.

The Hückel treatment of three nitrobiphenyls indicates that a similar absorption band should be observed in those compounds as, in fact, it is.³⁹

A linear relation between the observed frequency of this band and the calculated energy of the transition is shown in Figure 5 where the effect of varying H_{11} is again illustrated. The correlation is very good, especially for the molecules most likely to be planar. The slope of the line shown corresponds to $|\beta| = 2.68$ ev.

If the models we have chosen are correct, it should be possible to calculate the frequency of this nitroterphenyl absorption band by an appropriate combination of charge-transfer frequencies; *viz.*

$$E_A = E_B + E_C - E_D$$



The frequency of the nitroterphenyl absorption band is E_A ; E_B and E_C are the corresponding charge-transfer maxima in the complexes with TCNE and DMT, respectively, while E_D is the frequency of the charge-transfer band in the TCNE-DMT complex.⁴⁰ The

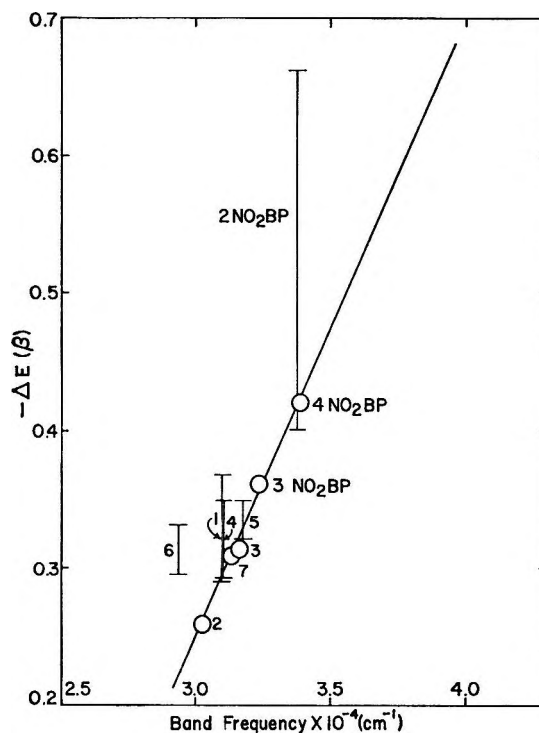


Figure 5. The correlation between the calculated and observed energies of the intramolecular charge-transfer band in the nitroterphenyls.

calculated results are compared with experiment in Table III. The calculated frequencies are slightly larger than those observed. This is not surprising since one would not expect stabilization energies of the complexes to cancel exactly. The disagreement in the cases of 3-nitroterphenyl and 4,4'-dinitroterphenyl is inordinately large, however. This is expected in the case of 4,4'-dinitroterphenyl since, as noted above, this compound does not give a charge-transfer band with TCNE involving the molecule's highest filled MO. In the case of 3-nitroterphenyl either the model chosen to represent the absorption band or one of the complexes may be in error.

It is not worthwhile to press the Hückel models to the extent of offering interpretations of the other absorption bands in the spectra of the nitroterphenyls.

(35) S. Nagakura and J. Tanaka, *J. Chem. Phys.*, **22**, 236 (1954); **23**, 1441 (1955).

(36) T. E. Peacock and P. T. Wilkinson, *Proc. Phys. Soc. (London)*, **78**, 460 (1960).

(37) S. Nagakura, M. Kojima, and Y. Maruyama, *J. Mol. Spectry.*, **13**, 174 (1964).

(38) R. Basu, *Theoret. Chim. Acta*, **2**, 87 (1964).

(39) D. F. Detar and H. J. Scheifele, Jr., *J. Am. Chem. Soc.*, **73**, 1442 (1951).

(40) This band was found to occur at 720 $m\mu$ in methylene chloride.

Table III: A Comparison between the Observed Nitroterphenyl Absorption Band and That Calculated from Charge-Transfer Spectra^a

| Compd | Long wavelength max. | |
|-------|----------------------|------------|
| | Calcd | Obad |
| 1 | 3.29 | ~3.13 (sh) |
| 2 | >3.31 | ~2.99 (sh) |
| 3 | 3.15 | 3.03 |
| 4 | 3.13 | 3.03 |
| 5 | 3.42 | ~3.13 (sh) |
| 6 | 2.96 | 2.90 |
| 7 | >3.61 | 2.99 |

^a All spectra were taken in methylene chloride.

In one case, however, the model seems particularly apt.

The spectrum of 4,4''-dinitroterphenyl contains only the band described above. The elementary theory indicates that the second absorption band should be a transition from the highest filled to the second vacant MO. In the point group V_h this should be ${}^1A_g \rightarrow {}^1A_g$ which is parity forbidden, accounting nicely for the absence of the band.

An interesting possibility for further study in materials with dual charge-transfer properties would be to determine if the nitroterphenyls are capable of simultaneously complexing with both TCNE and DMT. Our attempts to investigate this failed when it was found that the TCNE-DMT complex is not stable.

Nitro-*p*-terphenyls. II. The Relation between Charge-Transfer Properties and Polarographic Oxidation and Reduction Potentials

by Richard L. Hansen, P. E. Toren, and R. H. Young

Contribution No. 353 from the Central Research Laboratories, Minnesota Mining and Manufacturing Company, St. Paul, Minnesota 55119 (Received November 12, 1965)

Polarographic data have been obtained for seven nitro-*p*-terphenyls and related compounds. Linear correlations of oxidation and reduction potentials with charge-transfer frequencies and parameters arising from elementary molecular orbital theory have been demonstrated. Steric strain in certain of these molecules can be relieved by preferential twisting of a nitro group out of the aromatic ring plane or by rotation about a carbon-carbon bond.

Introduction

The singular ability of several nitro-*p*-terphenyls to perform both electron donor and acceptor roles in charge-transfer complexes was described in a previous article.¹

We have measured the polarographic oxidation and reduction potentials of these nitroterphenyls and have obtained similar data for several model compounds in order to relate their charge-transfer and elec-

trochemical properties. We also hoped to determine the sites of steric strain in certain of these molecules and to test the theoretical models which were employed.

The energy of a charge-transfer absorption band is given approximately by eq 1, where I_D is the ioni-

$$h\nu_{ct} = I_D - E_A + C \quad (1)$$

(1) Part I: R. L. Hansen, *J. Phys. Chem.*, **70**, 1646 (1966).

zation potential of the donor, E_A is the electron affinity of the acceptor, and C should be nearly constant in a series of related complexes with a given donor or acceptor. In elementary theory, ionization potentials and electron affinities should also be linearly related to polarographic oxidation and reduction potentials, respectively.² Thus, one expects that electrochemical and charge-transfer properties will be correlated. Actually, both oxidation potentials³ and reduction potentials⁴ have been correlated with charge-transfer frequencies, but it has not been possible to test both correlations with one series of compounds before. The relations between oxidation and reduction potentials and molecular orbital energy levels are well known in the case of aromatic hydrocarbons,^{5,6} but few attempts have been made to test these relations for molecules containing heteroatoms. In addition, oxidation potentials of aromatic nitro compounds appear not to have been reported before.

Experimental Section

Materials. The preparation and purification of the nitroterphenyls have been described as has the purification of the hydrocarbons.¹ The nitrobenzene was distilled while the other nitro compounds were commercial samples used as received.

Tetra-*n*-butylammonium perchlorate (TBAP) was prepared from tetrabutylammonium bromide and sodium perchlorate. The electrolytes were dried under vacuum and stored in a drybox.

Acetonitrile was purified by method D of Coetzee, *et al.*⁷ Karl Fischer titration indicated that the final product contained less than 0.002% water. The acrylonitrile and methacrylonitrile content combined was less than 5 ppm as determined by vapor phase chromatography. The dimethylformamide was distilled from anhydrous potassium carbonate.⁸ Both solvents were stored in a drybox.

Procedure. The polarographic measurements were made on deoxygenated solutions containing 1–5 mM substrate and 0.1 M supporting electrolyte. The solutions were made up in a drybox. DMF gave somewhat better defined reduction waves than did MeCN, while MeCN proved to be superior for obtaining the oxidation potentials.

Reduction potentials were obtained by conventional three-electrode polarography at a dropping mercury cathode. The voltage was referred to an aqueous saturated calomel electrode. The quantitative reductions were carried out on 10-ml samples using a mercury pool as the cathode. The applied potential corresponded to the plateau of the first polarographic wave and the current was integrated electronically.

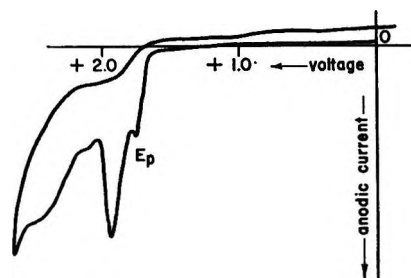


Figure 1. The current-voltage curve for 4-nitro-*p*-terphenyl.

The polarographic oxidations were done at a platinum disk anode having an area of 0.125 cm². An aqueous sce served as reference in the three-electrode system. A cyclic voltammetric method was used,⁹ and current-voltage curves were obtained at a scan rate of 3 v/min.

Results

The half-wave reduction potentials and the oxidation potentials of seven nitroterphenyls displaying dual charge-transfer properties are given in Table I together with supporting data for similar compounds. A typical current-voltage scan used in determining an oxidation potential is shown in Figure 1. It is clear that the oxidation of 4-nitroterphenyl is chemically irreversible since no reaction occurred on the cathodic going scans. This was the case for all of the compounds studied. Electrochemical reversibility was not investigated directly, but if the oxidations are reversible in the electrochemical sense, the E_p values will be related to classical half-wave potentials by an additive constant.¹⁰ Chemical irreversibility does not necessarily exclude the possibility that the electrode process may be reversible, *e.g.*, the reduction of 2,4,6-trinitroterphenyl, *vide infra*.

The diffusion current constants, I_D , and Tomes' criterion are consistent with electrochemically reversible one-electron reductions. Cyclic voltammetry in the case of 2,4,6-trinitroterphenyl, however, showed that

(2) A. Streitwieser, Jr., "Molecular Orbital Theory for Organic Chemists," John Wiley and Sons, Inc., New York, N. Y., 1961, p 173.

(3) A. Zweig, W. G. Hodgson, and W. H. Jura, *J. Am. Chem. Soc.*, **86**, 4124 (1964).

(4) M. E. Peover, *Trans. Faraday Soc.*, **58**, 1656, 2370 (1962).

(5) C. J. Hoijtink, *Rec. Trav. Chim.*, **74**, 1525 (1955).

(6) C. J. Hoijtink, *ibid.*, **77**, 555 (1958).

(7) J. F. Coetzee, G. P. Cunningham, D. K. McGuire, and G. R. Padmanabhan, *Anal. Chem.*, **34**, 1139 (1962).

(8) P. H. Rieger, I. Bernal, W. H. Reinmuth, and G. K. Fraenkel, *J. Am. Chem. Soc.*, **85**, 683 (1963).

(9) Z. Galus, H. Y. Lee, and R. Adams, *J. Electroanal. Chem.*, **5**, 17 (1963).

(10) H. Matsuda and Y. Ayabe, *Z. Elektrochem.*, **59**, 494 (1955).

Table I: Oxidation and Reduction Potentials

| Compound | Oxidation ^a $E(\text{peak})$, v vs. sce | Reduction ^b | | I_D^d |
|-------------------------------|---|---------------------------|----------------------------------|---------|
| | | $-E_{1/2}$, v vs. sce | $-(E_{1/4} - E_{1/2})^e$, mv | |
| Nitrobenzene (1) | | 1.12 ± 0.01 | 60 ± 4 | 3.0 |
| <i>m</i> -Dinitrobenzene (2) | | 0.83 ^g | 61 | 2.6 |
| <i>s</i> -Trinitrobenzene (3) | | 0.46 | 42 | 2.3 |
| 2-Nitrobiphenyl (4) | | 1.16 | 52 | 2.2 |
| 4-Nitrobiphenyl (5) | | 1.03 | 66 | 2.4 |
| 2-Nitroterphenyl (6) | 1.88 | 1.30 | 80 | 2.4 |
| 3-Nitroterphenyl (7) | 1.78 | 0.98 | 80 | 2.9 |
| 4-Nitroterphenyl (8) | 1.76 ± 0.01 ^f | 1.14 | 70 | 2.2 |
| 2,4-Dinitroterphenyl (9) | 1.86 | 0.81 | 60 | 2.9 |
| 2,6-Dinitroterphenyl (10) | 1.76 | 1.04 ^g | 72 | 2.3 |
| 4,4''-Dinitroterphenyl (11) | 2.06 | 1.02 | 66 | 2.4 |
| 2,4,6-Trinitroterphenyl (12) | 2.00 | 0.67 | 52 | 1.9 |
| Benzene (13) | 2.43 ^h | | | |
| Biphenyl (14) | 1.91 ⁱ | | | |
| <i>p</i> -Terphenyl (15) | 1.78 | | | |

^a In MeCN-TBAP. ^b In DMF-TBAP. ^c This should be 56 mv for a one-electron reversible electrochemical process: J. Tomes, *Collection Czech. Chem. Commun.*, **9**, 12, 81, 150 (1937). ^d $I_D = i_d/Cm^{2/3}t^{1/6}$ where i_d is the diffusional current, C is the substrate concentration, and the quantity $m^{2/3}t^{1/6}$ is characteristic of the dropping mercury electrode. ^e Second, poorly defined wave at -1.27 v. ^f Second wave at 1.95 v. ^g Small polarographic maximum. ^h H. Lund [*Acta Chem. Scand.*, **11**, 491, 1323 (1957)] reported a half-wave potential of 2.00 v; 0.43 v was added corresponding to the difference in the case of biphenyl. ⁱ Lund^h reported $E_{1/2} = 1.48$ v.

the reduction was chemically irreversible just as the oxidations were. None of the other reductions was investigated in this regard.

Quantitative reductions were carried out in the cases of nitrobenzene, 2,6-dinitro-, 4,4''-dinitro-, and 2,4,6-trinitroterphenyl in DMF. The integrated current showed that several electrons per molecule were passed through these solutions with no indication of an approaching end point except in the case of 2,4,6-trinitroterphenyl which gave a quantitative one-electron reduction. The use of sodium perchlorate as the electrolyte in place of the tetrabutylammonium salt gave the same results.

2,6-Dinitro- and 2,4,6-trinitroterphenyl gave rise to deeply colored solutions upon reduction in DMF, red in the case of the trinitro compound and violet in the other. On the basis of other experience, we believed these colors to be due to the free radical anions, the anticipated reduction products.¹¹ We were surprised to find that no epr signal could be detected in 0.2 mM solutions, whereas 1 mM solutions gave intense epr spectra. We can only conclude that the DMF contained an impurity in less than 1 mM concentration which reacted with the anion-radical reduction product.

Discussion

The relation between the frequencies of the charge-transfer bands in nitroterphenyl-*N,N*-dimethyl-*p*-tolui-

dine complexes¹ and the reduction potentials of the nitro compounds was found to be linear with ϵ correlation coefficient, $r = 0.90$. The least-squares correlation line was $\nu_{ct}(\text{cm}^{-1}) = (8 \pm 4) \times 10^3(-v) + (1.7 \pm 0.2) \times 10^4 \text{ cm}^{-1}$. The slope is unity when the charge-transfer frequencies are measured in electron volts. A similar correlation ($r = -0.93$) was found between the reduction potentials of the nitro compounds and the energies of their lowest vacant molecular orbitals calculated by the Hückel method.¹ A value for $|\beta|$ of 7 ± 2 eV was obtained from the slope.

Oxidation potentials are expected to be related to the energies of the highest filled molecular orbitals. The oxidation potentials of six compounds listed in Table I, including the three hydrocarbons and the three nitroterphenyls not containing 2-substitution, were found to be linearly related ($r = 0.94$) to the energies of their highest filled orbitals. The effective value of $|\beta|$ in this correlation was 1.8 ± 0.5 eV.

A linear correlation between the oxidation potentials of the donors and the frequencies of the long wavelength charge-transfer bands in complexes of TCNE with the nitroterphenyls and the three hydrocarbons appears in Figure 2.¹ In this case $r = 0.92$ and the least-squares line is $E_p(v) = (8 \pm 2) \times 10^{-5} \text{ cm}^{-1} +$

(11) Part III: R. L. Hansen, R. H. Young, and P. E. Toren, *J. Phys. Chem.*, **70**, 1657 (1966).

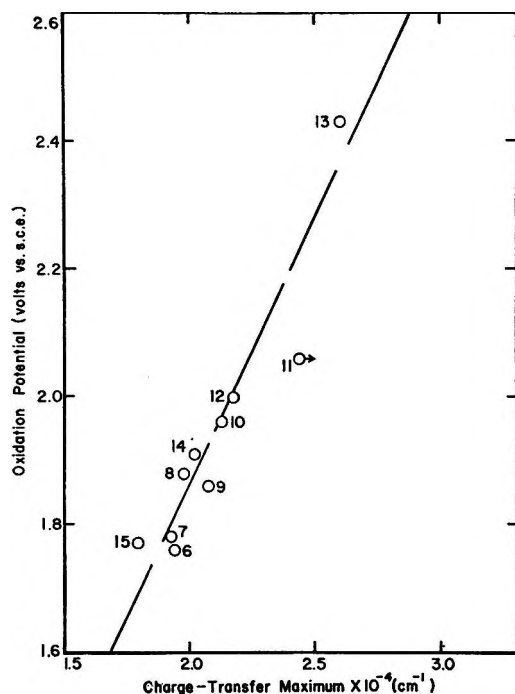


Figure 2. The relation between oxidation potentials and charge-transfer frequencies.

(0.15 ± 0.09) v. With comparable units of energy the slope is 0.6 ± 0.2 . Since 4,4'-dinitroterphenyl does not display a long wavelength charge-transfer band with TCNE,¹ the point corresponding to this compound, although shown in Figure 2, was not included in the correlation.

Pysh and Yang,¹² and more recently Neikam and co-workers¹³ have found linear relationships between half-wave oxidation potentials and photoionization potentials of aromatic hydrocarbons, but the slopes were not unity. It has been pointed out that the slope in these correlations need not be 1 if there are specific interactions at the electrode-solution interface.¹³ It has now been reported that aromatic hydrocarbons form charge-transfer complexes with platinum oxide,¹⁴ which may account for the slopes observed in the relations between oxidation potentials and charge-transfer frequencies or ionization potentials.

For aromatic nitro compounds, Geske and his co-workers have shown clearly that steric hindrance which causes decoupling of the nitro group from the aromatic ring shifts the reduction potential to a more negative voltage.¹⁵ Aside from the nitro group, the length of the conjugated system has little effect on the reduction potential in the present series of compounds. Compare nitrobenzene, 4-nitrobiphenyl, and 4-nitroterphenyl with reduction potentials of -1.12 , -1.03 , and -1.14 v.

The effects of steric hindrance on oxidation potentials have not been investigated systematically. In the methoxybenzenes, decoupling a methoxy substituent causes a decrease in the oxidation potential.³ In the nitroterphenyls the addition of a nitro group to an otherwise conjugated system seems to have little effect on the oxidation potential. Compare terphenyl, 3-nitroterphenyl, and 4-nitroterphenyl, all having oxidation potentials of 1.77 ± 0.01 v. The oxidation potential does reflect the extent of the hydrocarbon portion of the molecule, however, as shown by the oxidation potentials of benzene, biphenyl, and terphenyl.

These generalities are consistent with Hückel calculations which indicate that the lowest vacant MO in these nitro compounds is strongly associated with the nitro groups while the highest filled orbital is essentially a hydrocarbon orbital.¹

The nitroterphenyls which are substituted in the 2-position are expected to be noncoplanar due to steric hindrance. The strain may be relieved by rotation about the $C_1-C_{1'}$ bond, a C-N bond, or both. The first possibility should be revealed in the oxidation potential and the second in the reduction potential.

The nitroterphenyls can be divided into two broad groups on the basis of their oxidation potentials, those similar to biphenyl with oxidation potentials more anodic than about 1.85 v and the remainder similar to terphenyl. 2-Nitro-, 2,4-dinitro-, and 2,4,6-trinitroterphenyl are in the former group, suggesting that they are twisted about the $C_1-C_{1'}$ bond.

The effect on reduction potential of rotation about a C-N bond is illustrated by the more cathodic reduction potential of 2-nitroterphenyl as compared to either the 3- or 4-nitro isomers or nitrobenzene, and by the reduction potential of 2,6-dinitroterphenyl compared to *m*-dinitrobenzene.

The reduction potential of 2,4-dinitroterphenyl is identical with that of *m*-dinitrobenzene. The Hückel treatment of this molecule indicates that the lowest vacant molecular orbital is a "pure" *m*-dinitrobenzene level.¹ The reduction potential substantiates this while suggesting, as does the oxidation potential, that steric strain in this molecule is relieved almost exclusively by rotation about the $C_1-C_{1'}$ bond. In contrast, steric strain in the 2,6-dinitro isomer appears

(12) E. S. Pysh and N. C. Yang, *J. Am. Chem. Soc.*, **85**, 2124 (1963).

(13) W. C. Neikam, G. R. Dimeler, and M. M. Desmond, *J. Electrochem. Soc.*, **111**, 1190 (1964).

(14) I. T. Ernst, J. L. Garnett, and W. A. Sollich-Baumgartner, *J. Catalysis*, **3**, 568 (1964).

(15) D. H. Geske, J. L. Ragle, M. A. Bambenck, and A. L. Balch, *J. Am. Chem. Soc.*, **86**, 987 (1964).

to be relieved predominantly by rotation of the nitro groups out of the ring plane.

Comparison of the reduction potential of 2,4,6-trinitroterphenyl with that of *s*-trinitrobenzene suggests that the 2- and 6-nitro groups in this molecule are also twisted to some extent. Thus, both mechanisms for the relief of steric strain are operative in 2-nitro- and 2,4,6-trinitroterphenyl.

NOTES

Nitro-*p*-terphenyls. III. Electron Paramagnetic Resonance Spectra of the Radical Anions

by Richard L. Hansen, R. H. Young,
and P. E. Toren

Contribution No. 343 from the Central Research Laboratories,
Minnesota Mining and Manufacturing Company,
St. Paul, Minnesota 55119 (Received November 12, 1965)

The dual charge-transfer abilities and polarographic properties of several nitro-*p*-terphenyls can be explained reasonably well in terms of Hückel MO theory.^{1,2} A consequence of this model is that the lowest vacant MO's of these molecules should be essentially nitrobenzene levels. For example, the LVO of 2,6-dinitroterphenyl should be very similar to the LVO of *m*-dinitrobenzene with low electron density in the biphenyl portion of the molecule.

The lowest vacant molecular orbitals of aromatic nitro compounds have been extensively mapped by epr spectroscopy using the electrochemical anion-radical generation technique pioneered by Geske and Maki.³ We have used this technique to test the Hückel model. We also hoped to learn more about steric strain in these molecules.

Experimental Section

The materials which were used have been described.^{1,2} The anion radicals were generated by electrochemical reduction at potentials corresponding to the first polarographic waves of the nitroterphenyls.² The

It is not possible from these rather limited data to estimate angular degrees of noncoplanarity, but the intensity of the nitroterphenyl absorption band near 330 m μ seems to be decreased more dramatically by nitro group decoupling than by rotation about the C₁-C_{1'} bond. This band, regarded as an intramolecular charge-transfer band, is much more intense in 2,4-dinitroterphenyl than in the 2,6-dinitro isomer.¹

solutions in DMF were 1-5 mM in the nitro compound and contained 0.1 M tetrabutylammonium perchlorate. The reductions were conducted in a vessel similar to that described by Rieger and Fraenkel⁴ placed in the dual cavity of a Varian Model 4205 spectrometer. The reference contained peroxyamine disulfonate.

Results and Discussion

The epr spectra of seven nitro-*p*-terphenyls were analyzed in terms of N¹⁴ and proton hyperfine coupling constants. The results are summarized in Table I. The assignments have been made largely on the basis of analogies reported in the literature.

The hyperfine coupling constants of the mononitro compounds are similar to those reported for nitrobenzene,⁵ although the nitrogen coupling constants are smaller.

The effect on the N¹⁴ coupling constant of rotation about the C-N bond is well documented both experimentally and theoretically;⁶⁻⁸ noncoplanarity causes an increase in a_N . The nitrogen coupling constants of the three mononitro terphenyls do not follow the behavior expected on this basis, but vary in a manner

(1) Part I: R. L. Hansen, *J. Phys. Chem.*, **70**, 1646 (1966).

(2) Part II: R. L. Hansen, P. E. Toren, and R. H. Young, *ibid.*, **70**, 1653 (1966).

(3) D. H. Geske and A. H. Maki, *J. Am. Chem. Soc.*, **82**, 2671 (1960).

(4) P. H. Rieger and G. K. Fraenkel, *J. Chem. Phys.*, **39**, 609 (1963).

(5) P. Ludwig, T. Layloff, and R. H. Adams, *J. Am. Chem. Soc.*, **86**, 4568 (1964).

(6) D. H. Geske, J. L. Ragle, M. A. Bambenek, and A. L. Balch, *ibid.*, **86**, 987 (1964).

(7) D. H. Geske and J. L. Ragle, *ibid.*, **83**, 3532 (1961).

(8) P. H. Rieger and G. K. Fraenkel, *J. Chem. Phys.*, **39**, 609 (1963).

Table I: Coupling Constants of Nitro-*p*-terphenyl Anion Radicals in DMF

| Compd | Position | $ a_N $, gauss | $ a_H $, gauss |
|-------------------------------|-------------|--------------------|--------------------|
| 2-Nitroterphenyl | 2 | 8.82 ± 0.05 | |
| | 3 | | 3.0 ± 0.1 |
| | 4,6 | | 1.1 ± 0.1 |
| | 5 | | 4.2 ± 0.1 |
| 3-Nitroterphenyl | 3 | 9.27 ± 0.05 | |
| | 2,4 | | 3.18 ± 0.05 |
| | 5 | | 1.07 ± 0.05 |
| | 6 | | 4.05 ± 0.07 |
| 4-Nitroterphenyl ^a | 4 | 8.3 ± 0.1 | |
| | 2,6 | | 0.94 ± 0.06 |
| | 3,5 | | 3.1 ± 0.1 |
| | 2',6' | | 1.07 ± 0.05 |
| 2,4-Dinitroterphenyl | 2 | 3.3 ± 0.2 | |
| | 4 | 6.6 ± 0.4 | |
| 2,6-Dinitroterphenyl | 2,6 | 3.94 ± 0.05 | |
| | 3,5 | | 3.94 ± 0.05 |
| | 4 | | 0.96 ± 0.05 |
| 4,4''-Dinitroterphenyl | 4,4'' | 3.6 ± 0.2 | |
| | 3,5,3'',5'' | | 1.8 ± 0.1 |
| 2,4,6-Trinitroterphenyl | 2,6 | Zero | |
| | 4 | 5.3 ± 0.1 | |
| | 3,5 | | 3.1 ± 0.07 |
| | 2',6' | | 0.64 ± 0.08 |
| | 2'',6'' | | 0.32 ± 0.04 |

^a Hückel calculations give electron densities of 0.007 for C₂ and C₆ and 0.018 for C_{2'} and C_{6'} in a planar model.¹

more suggestive of the ability of the nitro group to interact with the biphenyl ring system. It has been reported that electron-withdrawing substituents *para* to the nitro group decrease a_N .⁹ The proton coupling indicates that the LVO of 4-nitroterphenyl does extend into the biphenyl ring system. The small nitrogen coupling in the 2- and 3-nitro isomers compared to nitrobenzene suggests a certain amount of delocalization in these cases as well, although splittings attributable to biphenyl protons were not detected.

Of the three dinitroterphenyls only 2,6-dinitroterphenyl gave a well resolved epr spectrum. In the other cases, the coupling constants which could be determined were assigned on the basis of the expected steric effect and by analogy to 4,4'-dinitrobiphenyl.⁸

In the case of 2,6-dinitroterphenyl the coupling constants are just slightly smaller than those reported for 2,6-dinitrotoluene,⁸ and a_N is identical with that of *m*-dinitrobenzene.⁸ The oxidation and reduction potentials of this material suggested that steric strain was relieved predominantly by rotation of the nitro

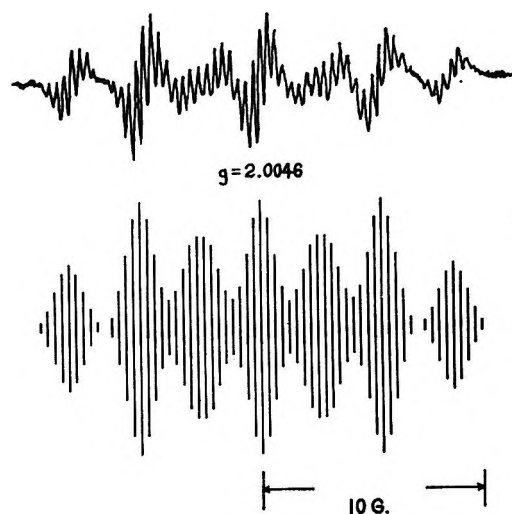


Figure 1. The epr spectrum of 2,4,6-trinitroterphenyl anion radical.

groups out of the ring plane.² The N¹⁴ coupling constant does not reveal decoupling of the nitro groups from the π -electron system. It is possible that the conformation of the anion is different than that of the neutral molecule. There is no evidence that the lowest vacant MO extends into the biphenyl ring system.

The epr spectrum of the 2,4,6-trinitroterphenyl anion radical is shown in Figure 1. The reconstruction is based on the coupling constants in Table I. It is significant that the 2- and 6-nitro groups are not revealed in the spectrum. Bernal and Fraenkel have also observed less than the expected number of nitro groups in the epr spectra of electrolytically generated nitromesitylene and nitrodurene anion radicals in DMF.¹⁰ However, their electrolyses were conducted at potentials corresponding to higher polarographic waves and evidently produced amino derivatives.¹¹ Glarum and Marshall have studied a series of polynitroaromatic anion radicals generated electrolytically and report coupling constants for all of the N¹⁴ nuclei expected,¹² although the alternating line width phenomenon¹³ was observed in some cases.

The alternating line width phenomenon cannot be ruled out in the present case although spectra obtained at several modulation amplitudes did not yield any new

(9) A. H. Maki and D. H. Geske, *J. Am. Chem. Soc.*, **83**, 1852 (1961).

(10) I. Bernal and G. K. Fraenkel, *ibid.*, **86**, 1671 (1964).

(11) This was pointed out by the referee. See R. D. Allendoerfer and P. H. Rieger, Abstracts, 150th National Meeting of the American Chemical Society, Atlantic City, N. J., Sept 1965.

(12) S. H. Glarum and J. H. Marshall, *J. Chem. Phys.*, **41**, 2182 (1964).

(13) J. H. Freed and G. K. Fraenkel, *ibid.*, **41**, 699 (1964).

lines. It may be significant that even though the polarographic reduction of 2,4,6-trinitroterphenyl was a one-electron reversible electrochemical process, cyclic voltammetry indicated chemical irreversibility.² If the spectrum we have obtained is that of the 2,4,6-trinitroterphenyl anion radical, it is evident that the lowest vacant MO is delocalized over the entire molecule, since proton splittings from all three benzene rings were observed.

We had also hoped to be able to report the nitroterphenyl cation-radical spectra. However, we have been unable to obtain spectra of these species in sulfuric acid or by electrochemical oxidation in acetonitrile or DMF.

Acknowledgment. We wish to thank Mr. George Filipovich for the use of the epr equipment.

Radiation Chemistry of Aqueous

Solution of Silver Ion¹

by Gideon Czapski² and A. O. Allen

Chemistry Department, Brookhaven National Laboratory, Upton, New York 11973 (Received October 15, 1965)

Little work has appeared on the radiation chemistry of solutions of silver salts. Shchegoleva, *et al.*,³ have reported a few experiments on the effect of alcohols on the yields of reduction. The reduction of silver ion by hydrogen atoms was demonstrated in 1928 by Bonhoeffer and Harteck⁴ and more recently by Littman, Carr, and Brady⁵ and by Czapski and Stein.⁶ The rate constant for the reaction of solvated electron with silver ion has recently been determined.^{7,8} The present results show that the chemistry is more complicated than might be anticipated from looking at a table of rate constants. Our attention was recently called to a paper by Ryabchikova, *et al.*,⁹ who irradiated relatively high concentrations of Ag⁺ (>0.1 M), with results in qualitative agreement with ours.

Experimental Section

The irradiations were made in two Co⁶⁰ γ -ray sources having dose rates of 5800 and 250 rads/min. The Pyrex irradiation cells were steam-cleaned and pre-irradiated. The water was triply distilled. The silver salts were of analytical grade and were used without further purification.

Irradiated solutions contained a brown precipitate which was removed on a fine sintered glass filter and

washed several times with distilled water. When the precipitate was washed with NH₄OH or 1 N HClO₄ solution, no silver was present in the washing, showing that there was no Ag₂O or hyponitrite in the precipitate, which was therefore assumed to consist entirely of metallic silver. The precipitate was dissolved in 30% HNO₃ containing a small amount of NaNO₂ to catalyze the dissolution of metallic silver, and the resulting solution was titrated for silver using 0.05 N KCNS. The limit of detection was 0.5 μ mole.

Nitrite ion was determined by the method of Shin.¹⁰ Hydrogen was determined by the method used by Schwarz, Losee, and Allen.¹¹ Attempts were made to determine peroxide both by the iodide method and by measuring the amount of oxygen produced on the addition of ceric sulfate to the solution. The results were not well reproducible and merely served to indicate roughly the amount of peroxide present. It is possible that the metallic silver and peroxide interact in a somewhat irreproducible manner.

Results

Results of the irradiation of silver perchlorate solution are shown in Table I. The yields of metallic silver were small at low concentration but increased with increasing concentration. The presence of air resulted in a reduction of the yield as compared to air-free solutions, as did also the addition of hydrogen peroxide to the air-free solution; $G(\text{Ag}^0)$ in 0.01 M Ag⁺ fell from 0.22 to 0.05, then to zero, as (H₂O₂) was increased from zero to 1 mM, then to 6 mM. The reduction in yield of hydrogen with increasing concentration of silver ion is expected¹² from the high rate of reaction of silver ions with solvated electrons.

(1) Research performed under the auspices of the U. S. Atomic Energy Commission.

(2) Department of Physical Chemistry, The Hebrew University, Jerusalem, Israel.

(3) I. S. Shchegoleva, A. V. Egunov, T. S. Glikman, and V. Ya Dain, *Dokl. Akad. Nauk SSSR*, **148**, 633 (1963).

(4) K. F. Bonhoeffer and P. Z. Harteck, *Z. Physik. Chem.*, **A139**, 64 (1928).

(5) F. E. Littman, E. M. Carr, and A. P. Brady, *Radiation Res.*, **7**, 107 (1957).

(6) G. Czapski and G. Stein, *Israel J. Chem.*, **2**, 15 (1964).

(7) S. Gordon, E. J. Hart, M. S. Matheson, J. Rabani, and J. K. Thomas, *Discussions Faraday Soc.*, **36**, 193 (1963).

(8) J. H. Baxendale, *et al.*, *Nature*, **201**, 468 (1964).

(9) G. G. Ryabchikova, V. I. Duzhenkov, and P. Ya. Glazunov, *Tr. Tashkentsk. Konf. po Mirnomu Ispol'z. At. Energii, Akad. Nauk Uz. SSR*, **1**, 361 (1961); *Chem. Abstr.*, **57**, 1787f (1962).

(10) M. B. Shin, *Ind. Eng. Chem. Anal. Ed.*, **13**, 33 (1941).

(11) H. A. Schwarz, J. P. Losee, and A. O. Allen, *J. Am. Chem. Soc.*, **76**, 4693 (1954).

(12) H. A. Schwarz, *Radiation Res. Suppl.*, No. 4, 103 (1964).

Table I: Product Yields G (molecules/100 ev) in AgClO_4 Solutions^a

| (AgClO_4) , M | Air free | | Air saturated $G(\text{Ag}^0)$ |
|-----------------------------|--------------------|-------------------|-----------------------------------|
| | $G(\text{Ag}^0)^b$ | $G(\text{H}_2)^c$ | |
| 0.001 | 0.07 | ... | 0.05 |
| 0.002 | 0.12 | ... | 0.07 |
| 0.0025 | ... | 0.38 | ... |
| 0.005 | 0.18 | 0.33 | ... |
| 0.01 | 0.22 | 0.30 | 0.14 |
| 0.02 | 0.32 | 0.28 | 0.17 |
| 0.05 | 0.45 | ... | ... |
| 0.1 | 0.57 | ... | 0.28 |
| 0.2 | 0.96 | ... | 0.37 |
| 0.5 | 1.56 | ... | ... |

^a Yields G of H_2O_2 were about 0.3 ± 0.15 ; of O_2 , 0.10 ± 0.05 .

^b Determined at about 175,000 rads total dose. At higher doses the yield falls off. ^c Yield constant from 50,000 to 300,000 rads.

Addition of a small amount of nitrite ion to the solutions resulted in an abrupt increase in the yield of metallic silver. Further addition of nitrite caused a gradual decrease in the yield, as shown in Figure 1. At the higher nitrite concentrations, $G(\text{Ag}^0)$ depends mainly on the ratio between nitrite and silver ion concentrations, while the absolute value of the silver ion concentration has only a slight effect on the yield, such as might be expected from an increase in the total yield of radicals due to scavenging of radicals from the spurs. However, at nitrite concentrations of $4 \times 10^{-4} M$ and below, the yield becomes independent of nitrite concentration and increases with silver ion concentration from a value of 2.8 at $10^{-3} M \text{Ag}^+$ to 5.8 at $2 \times 10^{-2} M$ or above. At low nitrite ion concentrations the yield remains almost constant as the nitrite is depleted and then suddenly falls to zero when the nitrite ion has been completely used up (Figure 2).

Table II shows that adding an inert salt to the nitrite solutions consistently increased the yield of metallic

Table II: Metallic Silver Yield as a Function of Ionic Strength

| (AgClO_4) , mM | (NaNO_2) , mM | (LiClO_4) , mM | μ | $G(\text{Ag}^0)$ |
|------------------------------|-----------------------------|------------------------------|-------|------------------|
| 2.65 | 26.5 | 80.0 | 0.109 | 2.38 |
| 2.65 | 26.5 | 0.0 | 0.029 | 2.15 |
| 5.0 | 10.0 | 15.0 | 0.03 | 3.34 |
| 5.0 | 10.0 | 0.0 | 0.015 | 3.13 |
| 10.0 | 10.0 | 30.0 | 0.05 | 4.48 |
| 10.0 | 10.0 | 20.0 | 0.04 | 4.44 |
| 10.0 | 10.0 | 10.0 | 0.03 | 4.40 |
| 10.0 | 10.0 | 0.0 | 0.02 | 4.25 |

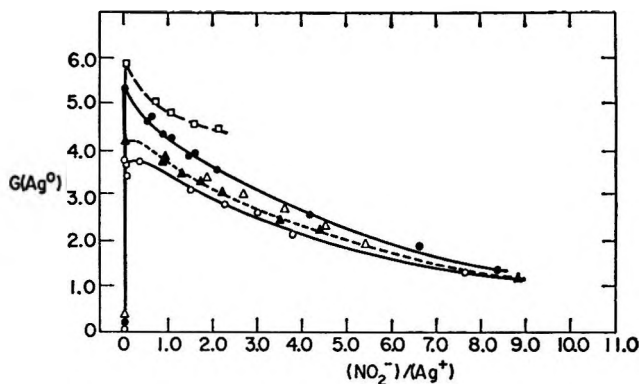


Figure 1. Dependence of metallic silver yield on the concentration ratio, nitrite to silver ion: O, $2.65 \times 10^{-3} M \text{AgClO}_4$, air free; Δ , $4.55 \times 10^{-3} M \text{AgClO}_4$, air free; \blacktriangle , $9.5 \times 10^{-3} M \text{AgClO}_4$, air free; \bullet , $1.9 \times 10^{-2} M \text{AgClO}_4$, air free; \square , $1.0 \times 10^{-2} M \text{AgClO}_4$, air saturated.

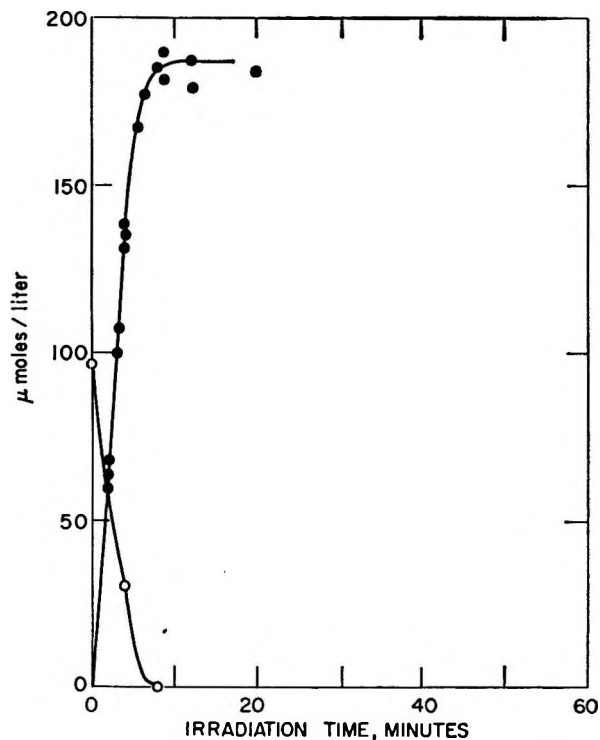


Figure 2. Metallic silver formation and nitrite consumption as a function of dose in air-free $10^{-2} M \text{AgClO}_4$, $0.97 \times 10^{-4} M \text{NaNO}_2$: \bullet , Ag^0 ; \circ , NO_2^- .

silver by an amount somewhat greater than the normal irreproducibility in this quantity.

The yield of metallic silver from a perchlorate solution is also increased by addition of ethanol to the solution, as was reported also by Shchegoleva, *et al.*,³ but a 300-fold higher concentration of ethanol than of nitrite is required to obtain the highest yield values (Figure 3).

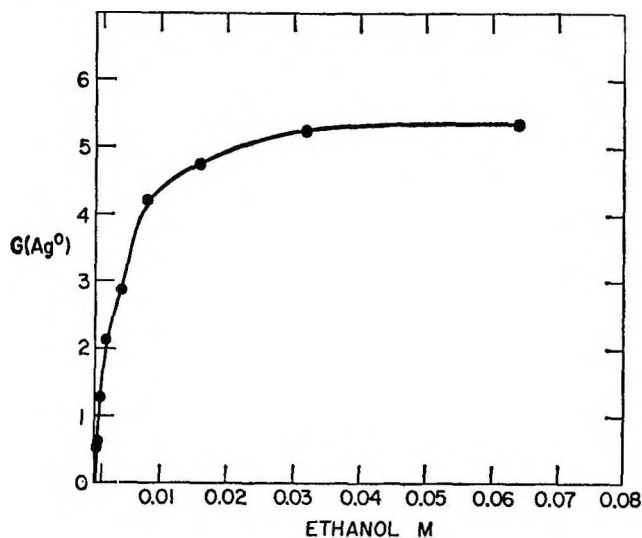


Figure 3. Metallic silver yield in air-free $10^{-2} M$ AgClO_4 solution as a function of ethanol concentration.

No effect of dose rate was found in any of the yields measured. All solutions were neutral and unbuffered; pH effects were not studied.

Discussion

The low yield of metallic silver produced in the absence of any added reducing agent presumably indicates that most of the silver which is reduced by the solvated electrons or hydrogen atoms formed from the water by radiation is reoxidized by the oxidizing radicals. The hydrogen peroxide also can apparently reoxidize the metallic silver, but much more slowly, so that part but not all of the molecular peroxide formed from radiation remains as such in solution. Some peroxide may also decompose catalytically. The net yield of metal is thus equal to the excess of reducing radicals over oxidizing radicals, $G_{e^-} + G_{\text{H}} - G_{\text{OH}}$, less part of the molecular peroxide yield $G_{\text{H}_2\text{O}_2}$.

The increase in $G(\text{Ag}^0)$ with increasing concentration of Ag^+ is reminiscent of the effect of Ag^+ in decreasing the yield of reduction of Ce^{IV} by radiation in H_2SO_4 solutions,^{13,14} although the latter effect occurs at lower concentrations of Ag^+ . Masters and Challenger¹⁴ listed a number of ways in which Ag^+ might interfere with Ce^{IV} reduction, but Sworski¹⁵ preferred to ascribe the entire effect to the occurrence in the spur of the reaction $\text{Ag}^+ + \text{OH} \rightarrow \text{Ag}^{\text{II}}$ in competition with $\text{OH} + \text{OH} \rightarrow \text{H}_2\text{O}_2$, thus decreasing $G_{\text{H}_2\text{O}_2}$. In the present case, scavenging of OH by Ag^+ will not increase the yield since OH, H_2O_2 , and Ag^{II} all act as oxidizing agents, but scavenging of e^- by Ag^+ , thereby effectively increasing G_{e^-} at the expense of H_2 formation, will increase $G(\text{Ag}^0)$. In fact, Table I shows that between 0.002 and 0.02 M Ag^+ , the increase in $G(\text{Ag}^0)$

is just twice the decrease in $G(\text{H}_2)$, as expected on this basis. However, above 0.1 M Ag^+ the increase in $G(\text{Ag}^0)$ is too large to be accounted for in this way; some other effect must contribute to the yield of reduction in concentrated solutions.

The addition of alcohol converts the oxidizing radicals into a reducing species, presumably by the reaction $\text{OH} + \text{C}_2\text{H}_5\text{OH} = \text{H}_2\text{O} + \text{C}_2\text{H}_4\text{OH}$. At sufficiently high alcohol concentration, the yield of metallic silver (apart from possible small contributions from H_2O_2) therefore becomes equal to the total yield of radicals, $G_{e^-} + G_{\text{H}} + G_{\text{OH}}$. Since a considerable concentration of alcohol is required to produce this high yield, it is clear that some other reagent is competing with the ethanol for reaction with OH. This can hardly be the metallic silver, which is present in much too low a concentration. We must therefore conclude that the OH radicals react with the silver ions to form divalent silver, and that this readily oxidizes metallic silver but does not readily react with alcohol. Ag^{II} formation by OH was proposed by others,^{9,15} though on evidence even more indirect.

Unlike alcohol, the nitrite ion brings the yield of metallic silver to its maximum value at very low concentrations. This can hardly be due to reaction of NO_2^- with OH, since the rate constant of this reaction is known not to be so much larger than that of the reaction of OH with ethanol.¹⁶ We must therefore suppose that it is the Ag^{II} which is reacting rapidly with the nitrite. Since Ag^{II} may presumably be a good two-electron oxidizing agent, it is reasonable to suppose that it acts directly on nitrite to give nitrate ion, being reduced at the same time to metallic silver.

With increasing nitrite concentration, two effects may then occur to reduce the yield. First, the nitrite begins to compete with the silver ions for reaction with the reducing radicals. The reduction product of nitrite thereby formed apparently does not react with silver ion to form metallic silver. The ionic strength effect indeed shows that a competition exists in this system between differently charged species for a charged radical, which must be the solvated electron. Secondly, the nitrite competes with the silver ion for reaction with OH. This reaction must occur, because the yield at high nitrite concentrations falls below the value of G_{OH} . The product of this reaction, which we may call NO_2 , therefore does not reduce silver ion

(13) G. L. Clark and W. S. Coe, *J. Chem. Phys.*, **5**, 97 (1937).

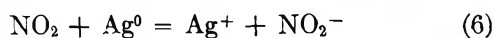
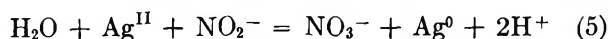
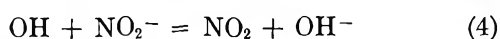
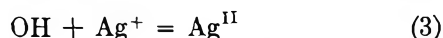
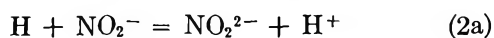
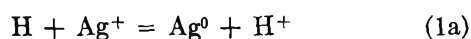
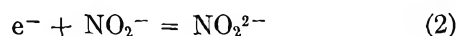
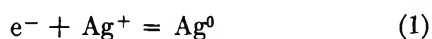
(14) B. J. Masters and G. E. Challenger, *J. Phys. Chem.*, **59**, 1093 (1955).

(15) T. J. Sworski, *Radiation Res.*, **4**, 483 (1956).

(16) G. E. Adams and J. Boag, *Proc. Chem. Soc.*, 112 (1964).

to metallic silver but probably rather oxidizes the metallic silver, as suggested by the fact that the oxidation of silver by concentrated nitric acid is catalyzed by the addition of a small amount of nitrite to the acid.

Our proposed reaction scheme for nitrite solutions is therefore



The fate of the NO_2^{2-} formed in reaction 2 is not known although it is clear from the work of Schwarz^{17,18} that it can react with NO_2 to regenerate nitrite ions. Possibly a low concentration of NO_2^{2-} may remain as such in solution (its sodium salt, Na_2NO_2 , has been prepared from liquid ammonia solution and is known to decompose with water to yield H_2 ¹⁹).

We attempted to fit the data to equations derived from the reaction scheme above, but there is so much scatter, owing to effects of ionic strength and scavenging, that an exact quantitative treatment seems hardly worthwhile. A value of about 8 for k_1/k_2 , derived from pulse radiolysis experiments,^{8,20} is not in disagreement with the present interpretation.

(17) H. A. Schwarz and A. O. Allen, *J. Am. Chem. Soc.*, **77**, 1324 (1955).

(18) H. A. Schwarz and A. J. Salzman, *Radiation Res.*, **9**, 502 (1958).

(19) D. M. Yost and H. Russel, Jr., "Systematic Inorganic Chemistry," Prentice-Hall, Inc., New York, N. Y., 1944, pp 52-58.

(20) J. K. Thomas, S. Gordon, and E. J. Hart, *J. Phys. Chem.*, **68**, 1524 (1964).

Evidence for the Existence of $^{11}B-^{10}B$

Coupling in NaB_3H_8 and B_4H_{10} ¹

by Arlan D. Norman and Riley Schaeffer

Contribution No. 1351 from the Department of Chemistry, Indiana University, Bloomington, Indiana 47405
(Received October 22, 1965)

Previously, it had been suggested that $^{11}B-^{10}B$ spin-spin coupling existed between the 1 and 3 boron

atoms of tetraborane-10 giving rise to septet fine structural features on the upfield doublet of the ^{11}B nmr spectrum.² This was later shown to be unlikely, owing to the absence of similar structure in the ^{11}B spectrum of B_4D_{10} , and the fact that no effect on the ^{11}B spectrum of B_4D_{10} was observed upon double irradiation at the ^{10}B resonance frequency.³ In a subsequent investigation it was shown that at high ^{10}B concentrations (ca. 85% ^{10}B) the fine structure of the B_4H_{10} doublet decreased, contrary to the effect expected if strong $^{11}B-^{10}B$ coupling existed.⁴ We have observed that the symmetrical nine-line ^{11}B spectrum of the $B_3H_8^-$ ion⁵ also exhibits decreased resolution as the ^{10}B concentration in the sample is increased. Recently, using $^{11}B-\{^{10}B\}$ nuclear magnetic double resonance we have obtained evidence which suggests that this loss of resolution in the $B_3H_8^-$ and B_4H_{10} spectra arises from weak ^{10}B coupling with the $^{11}B-^1H$ spin-coupled systems.

Experimental Section

Spectroscopic Techniques. The ^{11}B nuclear magnetic resonance spectra were obtained using a Varian Associates Model 4300B high-resolution field-sweep spectrometer operating at 19.24915 Mc/sec equipped with standard Varian variable temperature probe accessories. Chemical shifts were determined using external standards (relative to boron trifluoride diethyl etherate) and coupling constants were measured by the side-band method. Double irradiation experiments were carried out by transmitting up to 1 w of radiofrequency energy (H_2) from a temperature-stabilized General Radio Co. 0.5-50 Mc/sec variable frequency oscillator to the sample through a second transmitter coil attached to the low-temperature probe insert. Decoupling frequencies (H_2) were continuously monitored with a Hewlett-Packard Model 524C electronic counter.

Preparation of Samples. Samples of NaB_3H_8 in diethyl ether⁶ (ca. 2.8 M) of various $^{10}B-^{11}B$ isotopic contents were prepared by the reactions of appropriate mixtures of $^{10}B_2H_6$ (96% ^{10}B) and $^{11}B_2H_6$ (98% ^{11}B)

(1) Studies of Boranes. XXII; for paper XXI of this series see A. D. Norman and R. Schaeffer, *J. Am. Chem. Soc.*, **88**, 1143 (1965).

(2) R. E. Williams, S. G. Gibbins, and I. Shapiro, *ibid.*, **81**, 6164 (1959).

(3) J. S. Rigden, R. C. Hopkins, and J. D. Baldeschwieler, *J. Chem. Phys.*, **35**, 1532 (1961).

(4) R. C. Hopkins, J. D. Baldeschwieler, F. N. Tebbe, R. Schaeffer, and A. D. Norman, *ibid.*, **43**, 947 (1965).

(5) W. N. Lipscomb, "Boron Hydrides," W. A. Benjamin, Inc., New York, N. Y., p 127.

(6) W. V. Hough, L. J. Edwards, and A. D. McElroy, *J. Am. Chem. Soc.*, **80**, 1838 (1958).

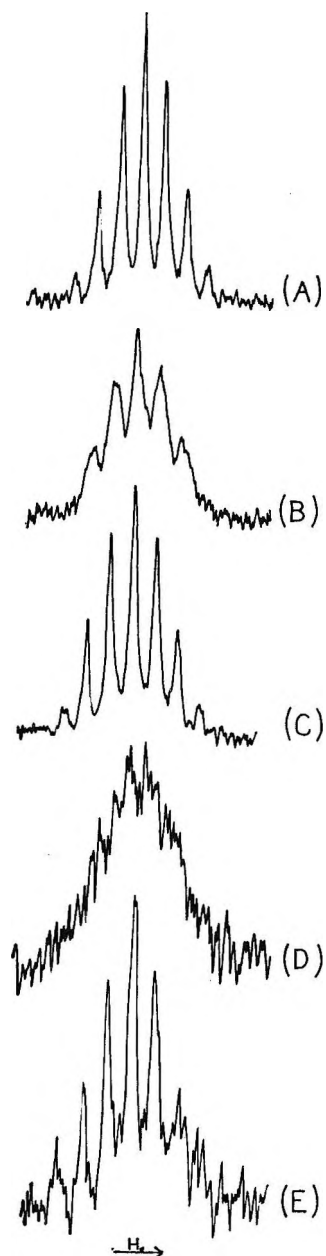


Figure 1. ^{11}B nmr spectra of NaB_3H_8 -diethyl ether solution; A, 2% ^{10}B -98% ^{11}B ; B, 61% ^{10}B -39% ^{11}B ; C, 61% ^{10}B -39% ^{11}B , ^{11}B - $\{^{10}\text{B}\}$ decoupled; D, 85% ^{10}B -15% ^{11}B ; and E, 85% ^{10}B -15% ^{11}B , ^{11}B - $\{^{10}\text{B}\}$ decoupled.

with sodium amalgam. A sample of B_4H_{10} enriched to 69% ^{10}B was prepared by pyrolysis of a mixture of $^{10}\text{B}_2\text{H}_6$ and $^{11}\text{B}_2\text{H}_6$ in a hot-cold reactor.⁷ $^{11}\text{B}_4\text{H}_{10}$ (18.8% ^{10}B -81.2% ^{11}B) was obtained from a laboratory supply. Tetraborane samples were purified by conventional fractional condensation techniques and were stored at -196° .

Data and Results

Triborohydride (B_3H_8^-). The ^{11}B nmr spectra of the

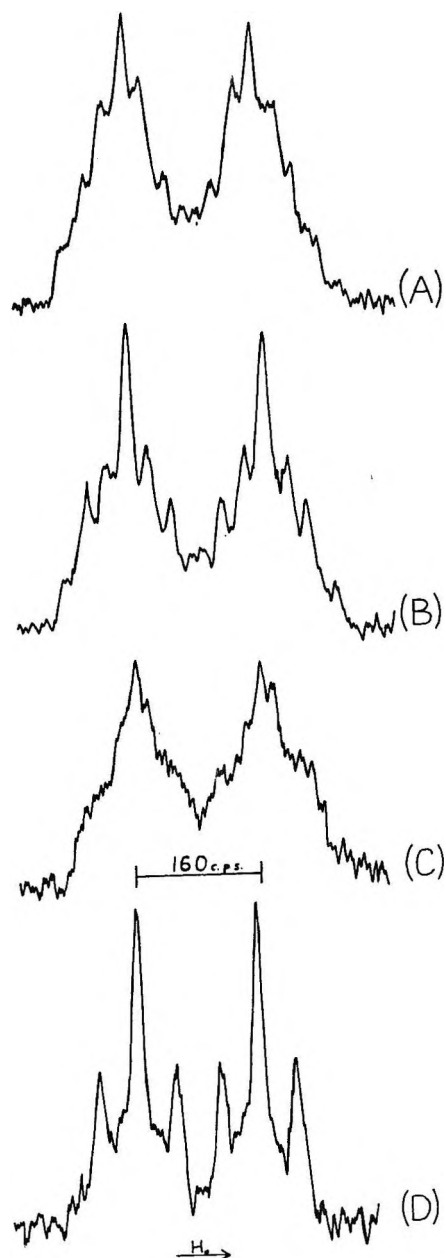


Figure 2. ^{11}B nmr spectra of B_4H_{10} ; A, 18.8% ^{10}B -81.2% ^{11}B ; B, 18.8% ^{10}B -81.2% ^{11}B , ^{11}B - $\{^{10}\text{B}\}$ decoupled; C, 61% ^{10}B -39% ^{11}B ; and D, 61% ^{10}B -39% ^{11}B , ^{11}B - $\{^{10}\text{B}\}$ decoupled.

diethyl ether- NaB_3H_8 solutions obtained prior to ^{11}B - $\{^{10}\text{B}\}$ decoupling are shown in Figures 1A, 1B, and 1D. In each case, the signal appears as a symmetrical multiplet ($\delta = 30.2 \pm 0.5$ ppm, $J = 32$ cps); however, as the ^{10}B content is increased, line broadening and subsequent loss of resolution occurs. The spectrum of 2% ^{10}B -98% ^{11}B NaB_3H_8 (1A) is resolved nearly

(7) M. S. Klein, B. C. Harrisor., and I. J. Solomon, *J. Am. Chem. Soc.*, **80**, 4149 (1958).

to base line, at 61% ^{10}B -39% ^{11}B (1A) resolution has decreased markedly, and at 85% ^{10}B -15% ^{11}B (1D) individual multiplet lines are no longer readily distinguishable. The relative intensities of the central lines in spectra 1A and 1B were found to be 29:57:70:57:29 \pm 1 in close agreement with the intensities calculated for the central lines of the nine-line multiplet expected to arise from coupling with eight equivalent protons. Low signal to noise ratios made line intensity measurements of spectrum 1D and the outermost four peaks of 1A and 1B difficult. In each of the above cases, the spectra were observed over a sufficiently wide range of radiofrequency field amplitudes (35 to 55 db below 0.5 w) to establish that the observed resolution loss was not due to radiofrequency field (H_1) saturation effects. At low temperatures (ca. -15°) resolution decreased, probably owing to increased viscosity of the diethyl ether solution.

The ^{11}B nmr spectra of the 61% ^{10}B -39% ^{11}B and 85% ^{10}B -15% ^{11}B NaB_3H_8 samples obtained when a strong radiofrequency field, H_2 , was applied at the ^{10}B resonance frequency are shown in Figures 1C and 1E. In these cases, ^{11}B - $\{^{10}\text{B}\}$ double resonance was obtained by sweeping the magnetic field, H_0 , and varying H_2 until the maximum effect on the spectrum was observed. Evidence of line sharpening and increased peak intensities was easily seen at H_2 frequencies ranging from 6.445890 to 6.445720 Mc/sec; however, the optimum frequency appeared to be 6.445790 Mc/sec \pm 10 cps. Within the limits of experimental error, the relative line intensities and 32-cps line spacings appeared unchanged in the ^{11}B - $\{^{10}\text{B}\}$ decoupled spectra.

Tetraborane (B_4H_{10}). The high-field doublets of the ^{11}B spectra of 18.8% ^{10}B -81.2% ^{11}B and 61% ^{10}B -39% ^{11}B B_4H_{10} samples measured prior to ^{11}B - $\{^{10}\text{B}\}$ double irradiation are shown in Figures 2A and 2C, respectively. Considerable secondary structure is exhibited in the spectrum of the 18.8% ^{10}B -81.2% ^{11}B material (2A) which partially collapses as the ^{10}B content of the tetraborane sample is increased.⁴ Hence, at 61% ^{10}B -39% ^{11}B , a doublet ($J = 157$ cps) exhibiting secondary broad triplet structure ($J = 47$ cps) is obtained (2C).

Application of ^{11}B - $\{^{10}\text{B}\}$ double resonance to the two B_4H_{10} samples resulted in the spectra shown in Figures 2B and 2D. In 2B, the two most intense center peaks show increased intensity relative to the remaining fine structure lines and over-all resolution of the signal is improved; however, in 2D a doublet ($J = 159$ cps) of triplets ($J = 50$ cps) is clearly shown. The optimum decoupling frequency (H_2) for B_4H_{10} was 6.445790 Mc/sec \pm 10 cps.

Acknowledgment. This work was supported by the National Science Foundation and by the National Aeronautics and Space Administration in the form of a traineeship for A. N. The authors wish to express appreciation to Arthur O. Clouse for assistance in obtaining nmr data.

Observations in Relation with Surface Phenomena of Rotating Liquids

by M. Borneas

*Faculty of Physics and Chemistry, Timisoara, Rumania
(Received March 4, 1966)*

We have shown in some preceding papers¹ that if a liquid is in rotation (quasi-static state), the surface tension changes its value, depending on frequency and temperature. We called this phenomenon a "roto-kinetic effect." We have shown that with all of the liquids studied, at low temperatures the roto-kinetic surface tension is greater than the static surface tension, except some minima. Above a certain temperature, characteristic for each liquid, the roto-kinetic effect disappears.

The appearance of an increased interaction at the surface of rotating liquids suggests the formation and ordering of molecular groups. The problem of ordering in liquid crystals has been very interestingly treated in a recent paper.² We assume that something analogous is happening in all liquids, that is, a separation of liquids in "crystals" and "noncrystals" cannot be so neat.

In our experiments the inertial field seems to be responsible for the ordering. However, a simple model of anisotropic and inhomogeneous groups which are directed under the centrifugal forces is not sufficient, because the roto-kinetic effect does not depend on the distance to the center of rotation. This we underline with the data presented in Tables I and II (errors ranging from 0.15 to 0.3%).

We presume that the groups appearing in liquids are temporal since they are disuniting and re-forming, a fact which is admitted by other authors too.³

(1) M. Borneas and E. Kalman, *Compt. Rend.*, **245**, 1710 (1957); M. Borneas and I. Băbuția, *ibid.*, **249**, 1036 (1959); *Studii Cercetari Chim. (Timisoara)*, **7**, 353 (1960); *Naturwiss.*, **47**, 373 (1960); *Acta Phys. Polon.*, **20**, 187 (1961).

(2) R. Williams, *J. Chem. Phys.*, **39**, 384 (1963).

(3) E. Darmais, "L'état liquide de la matière," Albin Michel, Paris, 1943.

Table I: Roto-kinetic Surface Tension of Ethyl Alcohol (dynes/cm) at 15.5°

| Tensiometer ring diameter, mm | Rotation frequency, rev/min | | | | | |
|-------------------------------|-----------------------------|-------|-------|-------|-------|-------|
| | 0 | 40 | 58 | 70 | 100 | 143 |
| 5.48 | 22.33 | 22.41 | 22.50 | 22.56 | 22.72 | 23.15 |
| 6.18 | 22.36 | 22.43 | 22.49 | 22.53 | 22.73 | 23.15 |
| 7.38 | 22.34 | 22.40 | 22.49 | 22.56 | 22.75 | 23.16 |
| 8.53 | 22.33 | 22.39 | 22.50 | 22.54 | 22.73 | 23.14 |
| 10.38 | 22.32 | 22.41 | 22.47 | 22.52 | 22.75 | 23.11 |
| 13.58 | 22.33 | 22.43 | 22.49 | 22.54 | 22.74 | 23.14 |

Table II: Roto-kinetic Surface Tension of Butyl Alcohol (dynes/cm.) at 21°

| Tensiometer ring diameter, mm | Rotation frequency, rev/min | | | | | |
|-------------------------------|-----------------------------|-------|-------|-------|-------|-------|
| | 0 | 40 | 58 | 70 | 100 | 143 |
| 5.48 | 24.62 | 24.72 | 24.80 | 24.85 | 25.05 | 25.55 |
| 6.18 | 24.65 | 24.74 | 24.80 | 24.84 | 25.07 | 25.59 |
| 7.38 | 24.64 | 24.74 | 24.76 | 24.86 | 25.05 | 25.58 |
| 8.53 | 24.61 | 24.68 | 24.79 | 24.88 | 25.08 | 25.55 |
| 10.38 | 24.63 | 24.68 | 24.79 | 24.82 | 25.04 | 25.57 |
| 13.58 | 24.63 | 24.71 | 24.79 | 24.85 | 25.06 | 25.56 |

At the temperature where the roto-kinetic effect disappears, there is a phase transition to an isotropic liquid phase. No existing mathematical theory is suitable to explain the surface phenomena described above.

Exchange of Chlorine between Hydrogen Chloride and Metal Chlorides^{1,2}

by J. R. Wilson and J. E. Willard

Department of Chemistry, University of Wisconsin, Madison, Wisconsin (Received April 19, 1965)

The exchange of halogen atoms between gaseous covalent molecules and a number of solid metal halides has been observed.³⁻¹⁴ That such exchange should occur is in some ways surprising. There is no detailed knowledge of the nature of metal halide surfaces or adequate theory for predicting the probability of their reaction with covalent molecules. With the aim of determining whether there are significant differences

in the rates of reaction which can be correlated with the nature of the chloride, we have investigated the exchange between HCl³⁶ and 25 solid metal chlorides. We have also tested the ability of several solid metal chlorides to catalyze vapor phase Friedel-Crafts reactions.

Experimental Section

Gaseous HCl was prepared from aqueous HCl-(Cl³⁶) by passing through P₂O₅ on a vacuum line. Its specific activity was determined in a glass annular counting jacket which surrounded a thin-walled Geiger tube. It was then exposed to the metal chloride sample in a 30-ml flat-bottomed quartz reaction vessel, which could be heated to any desired temperature. Following exposure it was returned to the counting jacket for determination of the activity. By repeated exposures of the HCl to the sample, followed by activity determinations, the exchange of Cl³⁶ was followed as a function of time and temperature. Transfers were made by freezing the gas into a tube on the desired vessel, with the aid of liquid nitrogen.

(1) This work was supported in part by the U. S. Atomic Energy Commission under Contract AT(11-1)-32, by the W. F. Vilas Trust of the University of Wisconsin, and by a Danforth Foundation Fellowship.

(2) Further details of the work are given in the Ph.D. Thesis of J. R. Wilson, University of Wisconsin, 1964, available from University Microfilms, Ann Arbor, Mich.

(3) These include the exchange of chlorine between HCl and NaCl,⁴ AlCl₃,⁵ ZrCl₄,⁶ and SnCl₄;⁷ of chlorine between Cl₂ and NaCl,⁴ and AgCl;⁸ of bromine between Br₂ and AgBr;⁹ of fluorine in a number of gas-solid systems;^{10,11} of iodine between CH₃I and AgI, PdI₂, TI₂, and PbI₂;¹² of bromine between CH₃Br and BaBr₂, CaBr₂, and AlBr₃;¹³ and of chlorine between alkyl chlorides and AlCl₃.¹⁴

(4) See for example and other references: (a) R. J. Adams and L. G. Harrison, *Trans. Faraday Soc.*, **60**, 1792 (1964); (b) L. W. Barr, I. M. Hoodless, J. A. Morrison, and R. Rudham, *ibid.*, **56**, 697 (1960).

(5) M. Blau, W. T. Carnall, and J. E. Willard, *J. Am. Chem. Soc.*, **74**, 5762 (1952).

(6) B. P. Dahlstrom, Jr., and J. E. Willard, unpublished.

(7) R. A. Howald and J. E. Willard, *J. Am. Chem. Soc.*, **77**, 2046 (1955).

(8) F. J. Johnston, Ph.D. Thesis, University of Wisconsin, 1952.

(9) (a) I. M. Kolthoff and A. S. O'Brien, *J. Am. Chem. Soc.*, **61**, 3409 (1939); (b) I. M. Kolthoff and A. S. O'Brien, *J. Chem. Phys.*, **7**, 401 (1939); (c) N. Davidson and J. Sullivan, *ibid.*, **17**, 178 (1949).

(10) (a) R. B. Bernstein and J. J. Katz, *J. Phys. Chem.*, **56**, 885 (1952); (b) R. M. Adams, I. Sheft, and J. J. Katz, *Proc. Intern. Conf. Peaceful Uses At. Energy, 2nd, Geneva*, **20**, 219 (1958); (c) I. Sheft, H. Hyman, R. M. Adams, and J. J. Katz, *J. Am. Chem. Soc.*, **83**, 291 (1961).

(11) (a) T. A. Gens, J. A. Wethington, A. R. Brose, and E. R. Van Artsdalen, *ibid.*, **79**, 1001 (1957); (b) T. A. Gens, J. A. Wethington, and A. R. Brosi, *J. Phys. Chem.*, **62**, 1593 (1958).

(12) I. Galiba, L. Latzkovits, and D. Gal, *Magy. Kem. Folyoirat*, **67**, 323 (1961).

(13) G. B. Kistiakowsky and J. R. van Wazer, *J. Am. Chem. Soc.*, **65**, 1729 (1943).

(14) (a) C. H. Wallace and J. E. Willard, *ibid.*, **72**, 5275 (1950); (b) M. Blau and J. E. Willard, *ibid.*, **73**, 442 (1951).

Table I: Exchange between HCl and Metal Chlorides^a

| | 30° | | | 100° | | | 200° | | | 300° | | |
|---------------------------------------|-----|----|-----|------|----|----|------|----|----|------|----|----|
| | 20 | 50 | 80 | 20 | 50 | 80 | 20 | 50 | 80 | 20 | 50 | 80 |
| LiCl | | | | | | | | | | | | 10 |
| NaCl | | | | | | | | | | | | b |
| KCl | | | | | | | | | | | | b |
| MgCl ₂ | 5 | | | 1 | 5 | | | | | | | |
| CaCl ₂ | | | | 1 | 8 | | * | * | | 3 | | |
| SrCl ₂ | 1 | 3 | 100 | * | * | 2 | | | | | | |
| SrCl ₂ ^c | | | | 2 | 80 | | | | | 100 | | |
| BaCl ₂ | | | | 1 | 3 | 60 | * | 2 | | 6 | | |
| BaCl ₂ ^c | | | | | | | * | * | | 2 | | |
| ScCl ₃ | 4 | | | * | 25 | | | | | | | |
| YCl ₃ | | | | 15 | | | | | | | | |
| LaCl ₃ | | | | | | | 120 | | | 2 | 5 | 30 |
| PrCl ₃ | | | | | | | 10 | | | * | 2 | 13 |
| NdCl ₃ | | | | | | | | | | 1 | 5 | 40 |
| GdCl ₃ | | | | | | | 5 | | | * | 2 | 5 |
| DyCl ₃ | | | | | | | 3 | 15 | | | | 10 |
| YbCl ₃ | | | | | | | | | | 1 | 6 | |
| HfCl ₄ | 35 | | | | 6 | 55 | | | | | | |
| CoCl ₂ | 1 | | | | 5 | 20 | | | | | | |
| CoCl ₂ (subl) ^d | | | | | | | | | | 80 | | |
| Cu ₂ Cl ₂ | | | | | | | 40 | | | 2 | 6 | 25 |
| AgCl ^{e, f} | | | | | | | | | | 100 | | |
| CdCl ₂ | | | | | | | 1 | 35 | | * | * | 5 |
| PbCl ₂ | 3 | 75 | | | | 10 | | | | | | |
| SbCl ₃ | 3 | 25 | | | | | | | | | | |
| BiCl ₃ | | | | 20 | | | | | | | | |
| GaCl ₃ ^f | | | | | | | | | | | | |
| TiCl ₃ ^f | | | | | | | | | | | | |
| GeCl ₃ ^f | | | | | | | | | | | | |
| SnCl ₄ ^f | | | | | | | | | | | | |

^a Numbers in the table show time in minutes required to achieve the per cent exchange indicated at head of column; * indicates too fast to measure. All of the measurements were made with 1.5×10^{-4} mole of HCl in a 30-ml reaction vessel and a solid-to-gas Cl ratio of 38:1 except for SbCl₃, BiCl₃, and Cu₂Cl₂, where the ratios were 70:1, 67:1, and 18:1, respectively. Estimated particle sizes were in the 5- μ range unless otherwise noted. ^b Gave readily measurable exchange at 380° and above. Annealing of NaCl in unlabeled HCl at 600° for 2 hr prior to exposure to labeled HCl did not change the exchange rate. ^c Fused samples. ^d This CoCl₂ which had been sublimed at 300°, forming sheets of stack-like crystals, gave only slow exchange at 300° or below, whereas the powder formed by dehydration of the hydrate gave rapid exchange at 300°. ^e AgCl also showed 20% transfer of activity in 5 min and 50% transfer in 50 min at 400°. ^f Readily observable exchange occurs in 1 hr or less at -78°.

Before and after each exposure to the metal chloride, the HCl pressure was determined. Normally it remained constant. Unless otherwise noted, 1.5×10^{-4} mole of HCl(Cl³⁶) was used in all runs, with sufficient metal chloride to give a ratio of chlorine in the gas to that in the solid of 1:38. With this ratio 97.4% of the Cl³⁶ is present in the solid when equilibrium distribution of activity is achieved.

The NaCl, KCl, LiCl, CdCl₂, and PbCl₂ used were reagent grade commercial materials. The AgCl was a single piece cut from a sheet obtained from the Harshaw Chemical Co. Anhydrous BaCl₂, SrCl₂, MgCl₂, CoCl₂, YCl₃, and ScCl₃ were prepared by dehydration of the hydrates *in vacuo*. The MgCl₂, YCl₃, and ScCl₃ were exposed to inactive HCl at ele-

vated temperature prior to use in order to convert any hydroxide to chloride.

The rare earth chlorides were prepared by treating the oxides with CCl₄ vapor at 500-600°. Commercial Cu₂Cl₂ was purified by recrystallization, and BiCl₃, SbCl₃, and HfCl₄ were purified by sublimation. Compounds which are liquids at room temperature (TiCl₄, GeCl₄, and SnCl₄) were vacuum distilled into the reaction vessel. GaCl₃ was prepared by the reaction of HCl gas on Ga metal.

Results

Exchange Studies. The data of Table I, based on curves of the type of Figure 1, show that exchange occurs for all of the chlorides tested, and give an indica-

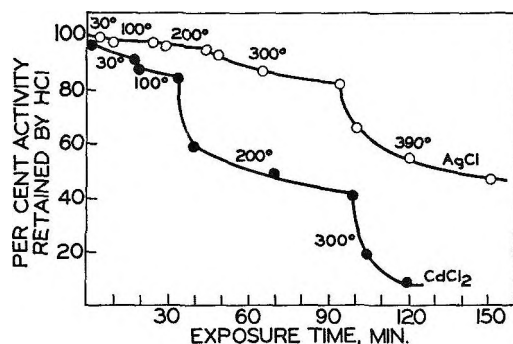


Figure 1. Transfer of Cl^{36} from $\text{HCl}(\text{Cl}^{36})$ to AgCl and CdCl_2 as a function of time and temperature. Ratio of Cl atoms in HCl to Cl atoms in metal chloride is 1:38.

tion of the minimum temperature ranges at which it can be readily observed. The comparisons are qualitative rather than quantitative, since the samples were prepared by different methods and the specific surface areas and defect concentrations were not the same. Except as otherwise noted, the estimated particle sizes were in the $5\text{-}\mu$ range.

A striking feature of the results is the fact that the alkaline earth chlorides all undergo exchange much more rapidly than the alkali metal chlorides, and that their exchange is readily observable at temperatures as low as 0.3 of the absolute melting point. This was true both for samples prepared by dehydration of the hydrates and for crystals of BaCl_2 and SrCl_2 prepared by cooling from the fused state, to ensure minimum surface area.

The evidence² indicates that the transfer of chlorine atoms at the surface of the samples of Table I was, in all cases, fast compared to diffusion of the atoms into the lattice. The most plausible mechanism for this rapid transfer involves attraction of the chlorine end of an HCl dipole to a positive lattice site, followed by departure of the proton in combination with a chlorine ion from another site. A mechanism of this type, involving induced dipoles, has been suggested to explain the fact that CCl_4 exchanges chlorine readily with the ionic surface of aluminum chloride, but not with dissolved or gaseous aluminum chloride.^{14a} The rapid exchange of HCl with the covalent species SnCl_4 , TiCl_4 , GaCl_3 , and GeCl_4 at -78° suggests that these compounds have ionic surfaces or that a different mechanism, such as complex formation, is available.

We have found no significant correlation of the observed exchange rates with available lattice parameters of the chlorides tested.²

Friedel-Crafts Studies. Studies with AlCl_3 ¹⁴ and with ZrCl_4 ⁶ have shown that they are capable of cata-

lyzing vapor phase Friedel-Crafts reactions as well as exchanging readily with HCl. To determine whether such catalytic effectiveness might be a general property of metal chlorides which exchange chlorine with HCl, the catalytic ability of additional compounds was investigated. These were chosen to include one compound which undergoes extensive exchange with HCl only at elevated temperature (NaCl), and five compounds representing different types which exchange at room temperature (BaCl_2 , SrCl_2 , ScCl_3 , HfCl_4 , and PbCl_2).

The NaCl , BaCl_2 , SrCl_2 , and PbCl_2 were each allowed to stand in contact with ethyl chloride and benzene vapors for times up to 6 months at 140° . The catalyst was present in large excess relative to the organic reactants which were present in equimolar amounts. The yield of ethylbenzene was a fraction of a per cent at most. ScCl_3 showed no catalytic activity when maintained with the organic materials for 18 hr at 100° . HfCl_4 gave a 30% yield of ethylbenzene in 16 hr at 30° . It is concluded that the ability of an inorganic chloride to exchange chlorine with HCl does not give information about its catalytic efficiency.

Chemical Shifts of Methyl Protons in Methylated Polynuclear Aromatic Hydrocarbons¹

by I. C. Lewis

Union Carbide Corporation, Carbon Products Division,
Parma Technical Center, Parma, Ohio 44130
(Received July 20, 1965)

The proton chemical shifts in polynuclear aromatic hydrocarbons have been the subject of considerable interest. The large downfield shifts exhibited by aromatic protons have been attributed to the effects of circulating ring currents involving the π electrons.^{2a} Aromatic proton shifts additionally reflect changes in the π -electron density at the attached carbon atom.^{2b}

The magnitude of the ring current effect has been accurately estimated for benzene.³ In the treatment of

(1) This research was sponsored in part by the Air Force Materials Laboratory, Research and Technology Division, Air Force Systems Command, U. S. Air Force.

(2) (a) J. A. Pople, W. G. Schneider, and H. J. Bernstein, "High-Resolution Nuclear Magnetic Resonance," McGraw-Hill Book Co., Inc., New York, N. Y., 1959; (b) T. Schaefer and W. G. Schneider, *Can. J. Chem.*, **41**, 966 (1963).

polycyclic hydrocarbons, the ring current intensity for each ring had originally been considered equal to that of benzene. Proton shifts in polynuclear hydrocarbons have been computed from a model based on this principle.^{2a} Recently, Jonathan, Gordon, and Dailey⁴ have refined these calculations and computed aromatic proton shifts, σ_π , for polycyclic hydrocarbons, based on ring current intensities determined individually for each polycyclic system. Only fair quantitative agreement was found between the calculated and measured values of σ_π .

The accurate determination of aromatic proton chemical shifts is complicated by spin-spin splittings. Furthermore, aromatic proton shifts are quite sensitive to nonuniform solvent effects⁵ and to steric effects.^{4,6} These factors present limitations to a quantitative test of the ring current model in polynuclear hydrocarbons. The ring current model can alternately be tested by the nmr absorptions of aromatic methyl protons which can be measured precisely and unambiguously. In addition, the protons in methylated aromatics have been found to be less susceptible to solvent effects than those of unsubstituted aromatics.^{7,8}

Maclean and Mackor⁹ measured the nmr spectra for a limited number of methylated aromatics at 40 Mc/sec and showed a relationship between the methyl proton shifts and those of the aromatic protons in the unsubstituted hydrocarbon. Durand, Parello, and Buu-Hoi¹⁰ have measured the methyl proton shifts for additional methylated polynuclear aromatics at 60 Mc/sec. These investigators found a relatively poor agreement between the experimental parameters and those computed from the ring current model in which the current intensity of benzene was employed for each ring unit.


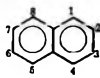
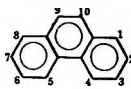
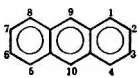
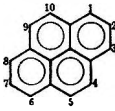
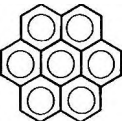
The present investigation reports methyl proton chemical shifts which have been determined at 60 Mc/sec for a variety of polycyclic methyl compounds. These quantities are shown to agree quite well with the refined σ_π values determined by Jonathan, *et al.*⁴

Experimental Section

The aromatic hydrocarbons employed in this study, with the exception of methylcoronene, were obtained from commercial sources and generally used as received. In a number of instances where the melting behavior indicated some impurity, the compounds were crystallized from organic solvents. Methylcoronene was synthesized by the Friedel-Craft methylation of coronene.¹¹

The solutions for measurement were made up to 5% of hydrocarbon in CCl₄ and contained (CH₃)₄Si as an internal standard. The spectrum for methylcoronene

Table I: Chemical Shifts of Methyl Groups Substituted on Aromatic Rings

| Ring system | Methyl substituent | δ , ppm | π |
|---|--------------------|-------------------|-------|
| Benzene  | 1 | 2.37 | 0.00 |
| | 1, 2 | 2.25 | |
| | 1, 3 | 2.30 | |
| | 1, 4 | 2.28 | |
| | 1, 3, 5 | 2.25 | |
| | 1, 2, 4, 5 | 2.15 | |
| | 1, 2, 3, 4, 5 | 2.13, 2.18 | |
| | 1, 2, 3, 4, 5, 6 | 2.17 | |
| Naphthalene  | 1 | 2.68 | 0.85 |
| | 2 | 2.50 | 0.42 |
| | 1, 2 | 2.47, 2.57 | |
| | 1, 5 | 2.70 | |
| | 1, 6 | 2.50, 2.63 | |
| | 2, 3 | 2.40 | |
| | 2, 3, 6 | 2.38, 2.47 | |
| Phenanthrene  | 1 | 2.73 | 0.99 |
| | 2 | 2.53 | 0.56 |
| | 3 | 2.62 | 0.61 |
| | 9 | 2.72 ^a | 0.99 |
| Anthracene  | 2 | 2.55 | 0.55 |
| | 9 | 3.05 | 1.83 |
| | 9, 10 | 3.05 | |
| Pyrene  | 1 | 2.93 | 1.55 |
| | 2 | 2.80 | 1.12 |
| | 4 | 2.87 | 1.40 |
| Coronene  | 1 | 3.30 ^b | 2.74 |

^a Data of ref 8. ^b Measured in CS₂ with reference to toluene.

- (3) J. S. Waugh and R. W. Fessenden, *J. Am. Chem. Soc.*, **79**, 849 (1957).
 (4) N. Jonathan, S. Gordon, and B. P. Dailey, *J. Chem. Phys.*, **36**, 2443 (1962).
 (5) A. A. Bothner-By and R. E. Glick, *ibid.*, **26**, 1651 (1957).
 (6) C. Reid, *J. Mol. Spectry.*, **1**, 18 (1957).
 (7) See ref 1, p 426.
 (8) F. F. Yew, R. J. Kurland, and B. J. Mair, *Anal. Chem.*, **36**, 843 (1964).
 (9) C. Maclean and E. L. Mackor, *Mol. Phys.*, **4**, 241 (1961).
 (10) P. Durand, J. Parello, and N. P. Buu-Hoi, *Bull. Soc. Chim. France*, 2438 (1963).
 (11) The author wishes to thank Mrs. S. Wallon for the synthesis of methylcoronene.

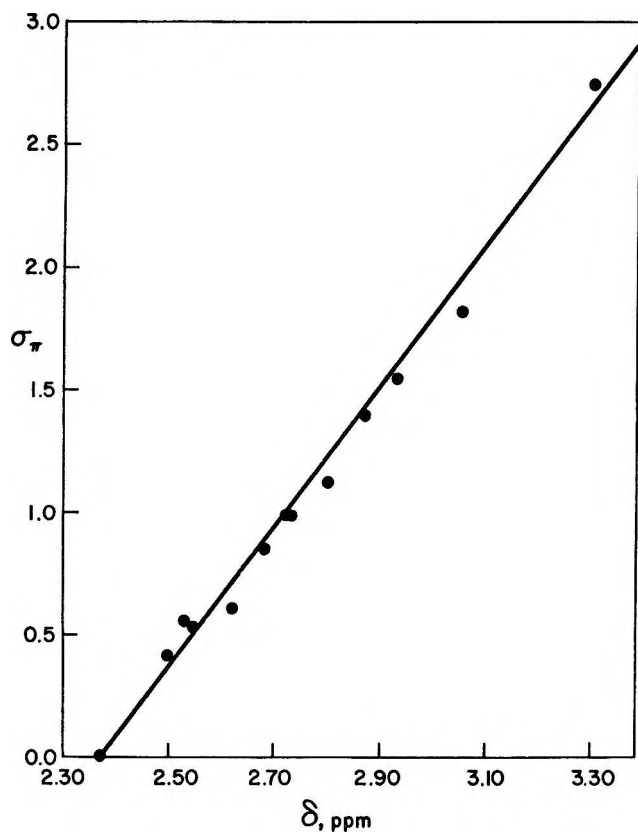


Figure 1. Relationship between computed aromatic proton shifts, σ_{π} , and methyl proton shifts, δ , in polycyclic hydrocarbons.

was obtained in CS_2 and measured relative to toluene in the same solvent. Spectra were recorded at 60 Mc/sec with a Varian A-60 spectrometer.

Results

Summarized in Table I are the chemical shifts, δ , in ppm for the protons of methyl groups substituted in various positions of six aromatic ring systems: benzene, naphthalene, phenanthrene, anthracene, pyrene, and coronene. Table I also lists the screening constants, σ_{π} , for the aromatic protons at the corresponding positions in the ring as calculated by Jonathan, *et al.*⁴

Figure 1 illustrates a comparison of the δ CH_3 values with the σ_{π} aromatic proton shifts. The linear agreement is quite good and provides further validation of the ring current model as well as of the conclusions of Maclean and Mackor pertaining to the relationship between aromatic methyl and aromatic proton chemical shifts. The nmr methyl data in Table I show a much poorer correlation with the aromatic proton chemical shifts computed from the single benzene ring current model.^{2a} The slope of the line in Figure 1 represents

the relative contribution of the circulating ring currents to the chemical shifts of the aromatic ring protons and the aromatic methyl protons. The magnitude of this slope can be estimated by employing the model of Johnson and Bovey¹² to calculate the ring current contributions to the aromatic methyl shifts.¹⁰ A comparison of these computed methyl shifts with those calculated for the ring protons⁴ leads to a slope of 2.1 which is in good agreement with the slope of 2.5 for the experimental methyl shift data in Figure 1.

Several polymethylated aromatics are also included in Table I. In general, additional methyl substitution in the ring shifts the methyl proton resonance upfield. This result is expected in view of the electron-releasing nature of the methyl group and has been described elsewhere.⁴

(12) C. E. Johnson and F. A. Bovey, *J. Chem. Phys.*, **29**, 1012 (1958).

Changes in Dielectric Relaxation during Dehydration and Rehydration of Rochelle Salt

by P. G. Hall and F. C. Tompkins

Department of Chemistry, Imperial College of Science and Technology, London, S.W.7, England (Received September 27, 1965)

Garner¹ has reviewed early gravimetric studies of the rehydration of dehydrated salt hydrates. Discontinuities in the plots of water uptake against time did not correspond to any known hydrates. With common alum,² multilayer adsorbed water controlled the rate of diffusion into the porous anhydride, but a phase transformation corresponding to $\text{Al}_2(\text{SO}_4)_3 \cdot 9.4\text{H}_2\text{O}$ produced a "glassy" modification which was very stable to further rehydration after dehydration. More recent investigations, also using gravimetric methods, with lead styphnate³ and manganous oxalate⁴ showed that the conditions of dehydration can have a pronounced effect on the subsequent rehydration.

This note concerns the use of a dielectric relaxation

(1) W. E. Garner, Ed., "Chemistry of the Solid State," Butterworth and Co. (Publishers) Ltd., London, 1955, Chapter 8.

(2) A. Bielanski and F. C. Tompkins, *Trans. Faraday Soc.*, **46**, 1072 (1950).

(3) T. B. Flanagan, *ibid.*, **55**, 114 (1959).

(4) T. B. Flanagan and M. K. Goldstein, *J. Phys. Chem.*, **68**, 663 (1964).

method for investigating the dehydration and rehydration of potassium sodium tartrate tetrahydrate (Rochelle salt). The ferroelectric nature of Rochelle salt has attracted wide interest⁵ and is known to be bound up with the water of crystallization. Previous dielectric studies of a variety of other crystal hydrates, generally aimed at distinguishing between "free" and "bound" water, are reviewed by Hasted.⁶

Experimental Section

The apparatus and dielectric cell design have been described previously.⁷ Fixed pressures of water vapor were established by controlling the temperature of the water reservoir connected to the cell. AR grade Rochelle salt was crushed before use. Changes in dielectric relaxation at constant frequency (0.90 Mc/sec) are reported as changes in Q^{-1} , with ΔQ^{-1} for the fully dehydrated sample taken as zero. The hydrate was dehydrated under vacuum at 22°.

Results and Discussion

Figure 1 shows the plots of ΔQ^{-1} against time for vacuum dehydration at 22° and subsequent rehydration at 22 and 0° using 20 and 4.58 mm of water vapor, respectively. Initially, the Q value corresponding to the tetrahydrate was out of range of the instrument; after pumping for about 20 min, ΔQ^{-1} decreased sharply to about 3×10^{-3} and remained at this value for several hours before decreasing to zero after continued pumping for over 48 hr. This indicates that part of the water of crystallization is firmly bound or structural water. ΔQ^{-1} is expected to decrease with decreasing amounts of water adsorbed on or taken up by the solid but the shape of the dehydration curve suggests that a change in relaxation time⁸ is superimposed on this. Since the more firmly bound water is likely to have a longer relaxation time than the loosely bound water, the sharp decrease in ΔQ^{-1} probably reflects a marked increase in relaxation time.

The presence of loosely bound water confirms other observations⁹ made with Rochelle salt. Structural determination¹⁰ shows that the water molecules are hydrogen bonded to oxygen atoms of the tartrate ion and that one of the water molecules differs from the other three in showing strong polarization along one direction of the crystal. Thus, the firmly bound water indicated by the present work may correspond to the monohydrate.

The rehydration curves are both characterized initially by a sharp increase in ΔQ^{-1} . This compares closely with the sharp initial increase in weight observed with the rehydration of dehydrated lead styphnate monohydrate, and is consistent with adsorption

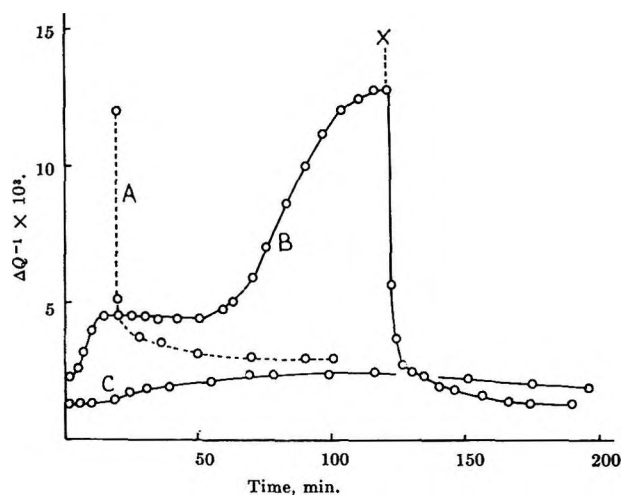


Figure 1. Dehydration and rehydration curves for Rochelle salt; variation of ΔQ^{-1} with time: A, dehydration, B, rehydration, 22°, 20 mm of water vapor; C, rehydration, 0°, 4.58 mm of water vapor; X indicates isolation of the cell from the reservoir.

and rehydration at a surface rendered porous by the dehydration process.³ Further increases in ΔQ^{-1} are considerably more marked with curve B, which shows sigmoid-like steps, until at the point marked X (where the cell was isolated from the reservoir) there is a sharp decrease which begins to be arrested at about the value corresponding to the firmly bound water.

With the rehydration experiments the solid is exposed to higher vapor pressures than the tetrahydrate equilibrium vapor pressures¹¹ of 7.5 mm at 22° and <4.0 mm at 0°. Therefore, the stepwise increase in ΔQ^{-1} may indicate the formation of the trihydrate in the surface layers; three inflections are evident with curve B. It is noted that a further increase in ΔQ^{-1} corresponding, on this basis, to tetrahydrate formation would be outside the range of the Q meter.

The hydrated surface region would be unstable with respect to the anhydrous interior, but as long as a continuous supply of water vapor is available, the hydrated region can be replenished faster than water

(5) H. D. Megaw, "Ferroelectricity in Crystals," Methuen and Co. Ltd., London, 1957, Chapter 2; W. J. Merz, *Progr. Dielectrics*, **4**, 103 (1962).

(6) J. B. Hasted, *ibid.*, **3**, 138 (1961).

(7) P. G. Hall and F. C. Tompkins, *J. Chem. Soc.*, (A), 36 (1966).

(8) Possible relaxation mechanisms for this type of heterogeneous dielectric are discussed in ref 7.

(9) L. F. Bates, *Sci. Progr.* (London), **30**, 465 (1936).

(10) (a) C. A. Beevers and W. Hughes, *Proc. Roy. Soc. (London)*, **A177**, 251 (1947); (b) M. P. Bernard, *Compt. Rend.*, **250**, 3819 (1960).

(11) H. H. Lowry and S. O. Morgan, *J. Am. Chem. Soc.*, **46**, 2152 (1924).

molecules are lost from the advancing trihydrate front by diffusion into the porous interior. However, once the supply of water vapor is cut off, the surface blocks of trihydrate rapidly disappear as the loosely bound water is dispersed into the porous interior, where it then becomes more firmly bound. Hence there results the steep drop in ΔQ^{-1} as the relaxation time increases. The sharp decrease is arrested at about the same ΔQ^{-1} value as the initial inflection at the beginning of rehydration, which provides further evidence that the firmly bound water corresponds to the monohydrate. After the arrest, the slow decrease in ΔQ^{-1} to about 1.5×10^{-3} is most probably due to there being insufficient water to form the monohydrate uniformly throughout the solid.

After the last data point shown for curve B, the cell was kept isolated at 22° for 24 hr before being reconnected to the reservoir, but no marked changes in ΔQ^{-1} were observed. This suggests that a transformation to a nonporous structure had occurred. This sample was then dehydrated under vacuum before being rehydrated to give curve C. With the latter, inflections following the initial rise are scarcely evident, perhaps as a result of the lower temperature and the consequent increase in relaxation time.

In spite of the narrowness of the data presented here, it is clear that the dielectric method may provide useful information concerning dehydration and rehydration of salt hydrates. Such a method has an advantage over the conventional gravimetric approach, in that changes in relaxation time can be followed.

Acknowledgment. This research was supported financially by the U. S. Air Force through its European Research Office.

Solubilities of Potassium, Triisoamylbutylammonium, and Tetrabutylammonium Tetrphenylborides and Picrates in Water and Methanol and Their Medium Effects at 25°

by Orest Popovych and Robert M. Friedman

Department of Chemistry, Brooklyn College of the City University of New York, Brooklyn 10, New York (Received October 4, 1965)

The solubilities reported here were determined as part of our study of medium effects for electrolytes in

nonaqueous solvents. While the title tetraphenylborides and picrates acquired importance as reference electrolytes in definitive conductometric studies,¹⁻⁶ there was little information on their solubilities. Except for those of potassium picrate (KPi) in water and methanol⁷ and of potassium tetraphenylboride (KBPh₄) in water,⁸ the solubilities are reported here for the first time.

Concentration of tetraphenylborides and picrates in saturated solutions was determined by ultraviolet and visible spectrophotometry, respectively. Using the association constants reported for methanolic solutions by Fuoss and co-workers,^{4,5} we calculated ionic concentrations and activities for the saturated methanolic solutions, as well as the corresponding medium effects.

Experimental Section

Materials. Reagent grade chemicals were used unless otherwise specified. Methanol (Matheson, spectro grade) was refluxed over aluminum amalgam and distilled, rejecting the initial and final 10%. Deionized water was redistilled.

Sodium tetraphenylboride (Fisher, 99.7%) was the starting material for the synthesis of other tetraphenylborides. KBPh₄ was prepared by treating NaBPh₄ with an excess of KCl in water; it was recrystallized three times from 3:1 acetone-water and dried *in vacuo* at 80°. Tetrabutylammonium tetraphenylboride (Bu₄NBPh₄) was synthesized as described in the literature.¹ *Anal.* Calcd: C, 85.52; H, 10.05; N, 2.49. Found for two batches: C, 85.52, 85.52; H, 9.85, 9.96; N, 2.50, 2.40. Triisoamylbutylammonium tetraphenylboride ((TAB)BPh₄) and picrate ((TAB)Pi) were synthesized and purified essentially by the method of Coplan and Fuoss.⁵ *Anal.* Calcd for (TAB)BPh₄: C, 85.54; H, 10.35; N, 2.32. Found: C, 85.89; H, 10.36; N, 2.40. Tetrabutylammonium picrate (Bu₄NPi) was prepared by exact neutralization of purified picric acid in water-methanol with methanolic Bu₄NOH (Matheson, 25%) and purified by recrystallization from 90% ethanol-water mixture. KPi was prepared by treating stoichiometric amounts of purified picric acid with standard aqueous KOH.

(1) F. Accascina, S. Petrucci, and R. M. Fuoss, *J. Am. Chem. Soc.*, **81**, 1301 (1959).

(2) H. Sadek and R. M. Fuoss, *ibid.*, **81**, 4507 (1959).

(3) R. M. Fuoss and E. Hirsch, *ibid.*, **82**, 1013 (1960).

(4) R. W. Kunze and R. M. Fuoss, *J. Phys. Chem.*, **67**, 911 (1963).

(5) M. A. Coplan and R. M. Fuoss, *ibid.*, **68**, 1177 (1964).

(6) J. F. Skinner and R. M. Fuoss, *ibid.*, **68**, 1882 (1964).

(7) A. Seidell, "Solubilities of Inorganic and Metal Organic Compounds" D. Van Nostrand Co., Inc., New York, N. Y., 1940.

(8) R. T. Pfaum and L. C. Howick, *Anal. Chem.*, **28**, 1542 (1956).

Table I: Solubilities of Electrolytes in Methanol and Water and Their Medium Effects at 25°

| Electrolyte | Solubility, <i>C</i> , moles/L | | α in CH ₃ OH | Ion-activity product, $(C\alpha f_{\pm})^2$ | | Medium effect, $\log m f_{\pm}^2$ (eq 3) |
|-----------------------------------|---|---|--------------------------------|---|-----------------------|--|
| | H ₂ O | CH ₃ OH | | H ₂ O | CH ₃ OH | |
| KBPh ₄ | 1.74×10^{-4} 1.78×10^{-4a} | 3.11×10^{-3} | 0.958 | 2.94×10^{-8} | 5.86×10^{-6} | -2.300 |
| KPi | 2.42×10^{-2} 2.41×10^{-2b} | 8.53×10^{-3} 1.03×10^{-2b} | 0.951 | 4.37×10^{-4} | 3.46×10^{-5} | +1.101 |
| (TAB)Pi | 2.26×10^{-4} | 0.392 | 0.680 | 4.92×10^{-8} | 1.23×10^{-2} | -5.398 |
| Bu ₄ NPi | 1.21×10^{-3} | 0.873 | 0.589 | 1.35×10^{-6} | 3.70×10^{-2} | -4.438 |
| (TAB)BPh ₄ | $1.4 \times 10^{-7?}$ (obsd) 1.08×10^{-7} (calcd) | 3.60×10^{-3} | 0.930 | 1.17×10^{-14} | 7.36×10^{-6} | -8.799 |
| Bu ₄ NBPh ₄ | $3.4 \times 10^{-6?}$ (obsd) 2.59×10^{-7} (calcd) | 2.58×10^{-3} | 0.940 | 6.69×10^{-14} | 4.62×10^{-6} | -7.839 |

^a See ref 8. ^b See ref 7.

The product was recrystallized three times either from water or from methanol and was used for solubility determination in the corresponding solvent. Purity of all salts was monitored by their spectra and electrolytic conductances in methanol.

Measurements. Saturation was achieved by shaking the salt suspensions on a Burrell wrist-action shaker in water-jacketed flasks through which water was circulated from a $25.00 \pm 0.01^\circ$ bath. About 2 weeks of vigorous shaking was found to be sufficient for saturation. The saturated solutions were filtered through Gelman Metrical filters of 0.20- μ pore size in a filtration syringe. Aliquots of the filtered solutions were immediately diluted (if necessary) with the solvent to proper spectrophotometric range and their spectra were recorded on a Cary spectrophotometer Model 14.

All work with tetraphenylborides was carried out in thoroughly deaerated solutions and containers. In spite of all precautions, however, (TAB)BPh₄ and Bu₄NBPh₄ usually decomposed upon prolonged equilibration with water, so that reliable results for their solubilities in water were difficult to obtain directly. Fortunately, the presence of decomposition could be readily recognized from the accompanying drastic changes in the ultraviolet spectra. Since hydrolytic decomposition of tetraphenylborides is known to be rapid in acid solutions, we attempted to measure the solubility of Bu₄NBPh₄ and (TAB)BPh₄ in aqueous 10^{-5} *M* NaOH. This method was successful part of the time.

Results and Discussion

Spectrophotometric analysis of most tetraphenylboride solutions took advantage of their characteristic ultraviolet peaks at about 266 and 274 $m\mu$ which are independent of the associated cation. At the two maxima, the molar absorptivities *a* were found to be 3.25×10^3 and 2.06×10^3 in water, and 3.00×10^3 and 2.12×10^3 in methanol, respectively. Similar values were reported for acetonitrile-water mixtures.⁸ Only the extremely dilute solutions of Bu₄NBPh₄ and (TAB)BPh₄ in water had to be analyzed in the more intense, though less characteristic, region of the spectrum at 225 $m\mu$ ($a = 2.22 \times 10^4$). Molar absorptivities of the picrate ion in water and methanol were determined from the absorbance of KPi and (TAB)Pi solutions in the 2×10^{-5} to 1×10^{-4} *M* range. For the broad picrate maximum at ~ 355 $m\mu$, *a* was found to be 1.44×10^4 and 1.56×10^4 in water and methanol, respectively. Beer's law was obeyed throughout.

The results in Table I were obtained as follows. Molar solubilities, *C*, were calculated from the above absorptivities and from the observed absorbances of the saturated solutions. For methanolic solutions, the degrees of ionic dissociation, α , were calculated from the literature values of the corresponding association constants.^{4,5} Once the ionic concentration $C\alpha$ was known, the conventional mean ionic activity coefficients f_{\pm} (molar scale) were estimated from the Debye-Hückel equation, which for methanolic solutions at 25° assumed the form

$$-\log f_{\pm}^2 = \frac{3.803(C\alpha)^{1/2}}{1 + 0.5099d(C\alpha)^{1/2}} \quad (1)$$

Reasonable values of the ion-size parameter d in methanol were adopted or estimated from the results of Fuoss and co-workers;^{2,3} they were 7, 6, 5.5, and 4.5 for R_4NBPh_4 , R_4NPI , $KBPh_4$, and KPI , in that order. For aqueous solutions, α was assumed to be unity and the Debye-Hückel activity coefficients were estimated using, for most cases, Kielland's⁹ ion-size parameters. For Bu_4N^+ , TAB^+ , and BPh_4^- , the parameters were estimated from Nightingale's data¹⁰ to be 9.4, 10, and 10, respectively. While the use of the Debye-Hückel equation for saturated (TAB)Pi and Bu_4NPI in methanol (ionic strengths 0.267 and 0.514, respectively) is open to criticism, it is not nearly so objectionable here as it would be for common electrolytes, composed of small ions. Solvation, which is the primary cause for deviations from the Debye-Hückel law at higher concentrations, is known to be negligible for ions of the size of TAB^+ , Bu_4N^+ , and PI^- . For the PI^- ion (which is the smallest one of the three) the solvation number was actually determined to be zero in several solvents, including methanol.¹¹

The medium effect for an electrolyte $m f_{\pm}^2$ is a measure of the free-energy change upon transferring 1 mole of the electrolyte from its standard state in water to its standard state in the nonaqueous solvent, methanol in this case. For a uni-univalent electrolyte

$$\Delta G^\circ = 2RT \ln m f_{\pm}^2 \quad (2)$$

and $m f_{\pm}^2$ can be obtained from the ratio of ionic activities a_{\pm} in saturated aqueous and nonaqueous solutions, designated by subscripts w and s, respectively.

$$\log m f_{\pm}^2 = \log m f_{cation} + \log m f_{anion} = \log \frac{(a_{\pm})_w^2}{(a_{\pm})_s^2} \quad (3)$$

The medium effects in the last column in Table I were calculated using eq 3. The striking feature of most medium effects (in logarithmic form) determined here is their negative sign, reflecting the fact that distribution of their ions favors the nonaqueous phase, despite the somewhat reduced dissociation and activity coefficients in the latter. Medium effects for most electrolytes are positive.

It should be noted that the medium effects for (TAB)- BPh_4 and for Bu_4NBPh_4 were obtained indirectly from those of other salts (eq 4). The indirect calculation takes advantage of the additivity of individual ionic medium effects in logarithmic form, e.g.

$$\log m f_{(TAB)BPh_4} = \log m f_{(TAB)PI} + \log m f_{KBPh_4} - \log m f_{KPI} \quad (4)$$

We resorted to this calculation because the two tetraalkylammonium tetraphenylborides were found to be susceptible to hydrolytic decomposition, which, coupled with their extremely low solubilities, would tend to make a direct solubility determination in water unreliable. The above calculation also leads to a possibly novel method of determining indirectly the solubility of a compound in a solvent in which it is too unstable for a prolonged equilibration required in a direct solubility determination. Thus, the solubilities of (TAB) BPh_4 and Bu_4NBPh_4 in water were derived with the aid of eq 3 from their calculated medium effects (eq 4) and their measured activities in methanol. The accuracy of the indirect procedure could be improved, of course, if the activities of the tetraalkylammonium picrates in saturated methanolic solutions were determined by some method more suitable for solutions of the order of $10^{-1} M$ than solubility measurements coupled with the Debye-Hückel law. However, an advantage of the indirect solubility determination lies in the fact that it can be checked *via* medium effects in any number of solvents.

Acknowledgment. Acknowledgment is made to the donors of the Petroleum Research Fund, administered by the American Chemical Society, for partial support of this research.

(9) J. Kielland, *J. Am. Chem. Soc.*, **59**, 1675 (1937).

(10) E. R. Nightingale, *J. Phys. Chem.*, **63**, 1381 (1959).

(11) P. Walden and E. J. Birr, *Z. Physik. Chem.*, **A153**, 1 (1931).

Effects of Divalent Cations on Multiionic Diffusion across a Weak-Acid Membrane¹

by T. M. Ellison² and H. G. Spencer

Department of Chemistry, Clemson University, Clemson, South Carolina (Received October 25, 1965)

The accumulation of divalent cations in weak-acid membranes has been shown to reduce appreciably the interdiffusion flux of univalent cations across the membranes.³ In this investigation the flux ratios are reported for multiionic systems of the type: 0.0500 M

(1) Presented at the Southeast-Southwest Regional Meeting of the American Chemical Society, Memphis, Tenn., Dec 1965.

(2) To whom correspondence should be addressed: Research and Development Directorate, U. S. Army Missile Command, Redstone Arsenal, Ala.

(3) H. G. Spencer and T. M. Ellison, *J. Phys. Chem.*, **69**, 2415 (1965).

Table I: Fluxes and Flux Ratios for the Multiionic Interdiffusion System:
0.0500 M ACl, 0.0500 M BCl-Membrane-0.1000 M CCl

| Univalent cation | | | Divalent cation salt ($2.5 \times 10^{-2} M$) | \bar{J}_A | \bar{J}_B (equiv cm $^{-2}$ sec $^{-1}$ 10 9) | \bar{J}_C | J_A/\bar{J}_B | | U_A/U_B in H $_2$ O |
|------------------|----------|----------|--|-------------|--|-------------|-----------------|----------|--------------------------|
| A | B | C | | | | | Calcd | Found | |
| Na | NMe $_4$ | K | None | 8.86 | 6.12 a | 14.98 | 3.6 | 1.45 | 1.36 |
| | | | CaCl $_2$ | 3.86 | 2.25 a | 6.11 | 2.9 | 1.71 | |
| | | | CuCl $_2$ | 0.65 | 0.65 a | 1.30 | 2.1 | 1.0 b | |
| K | NMe $_4$ | Na | None | 11.90 | 4.50 a | 16.40 | 4.2 | 2.65 | 2.02 |
| | | | CaCl $_2$ | 5.80 | 0.95 a | 6.75 | 4.5 | 6.00 | |
| | | | CuCl $_2$ | 0.96 | 0.48 a | 1.46 | 2.8 | 2.0 b | |
| K | Na | NMe $_4$ | None | 8.37 | 6.42 | 14.79 c | 1.2 | 1.30 | 1.48 |
| | | | CaCl $_2$ | 2.56 | 1.58 | 4.14 c | 1.5 | 1.62 | |
| | | | CuCl $_2$ | 0.96 | 0.96 | 1.92 c | 1.3 | 1.0 b | |

$^a \bar{J}_B = \bar{J}_C - \bar{J}_A$. b Low total flux limits precision of results. $^c \bar{J}_C = \bar{J}_A + \bar{J}_B$.

NaCl, 0.0500 M KCl-weak-acid membrane-0.1000 M NMe $_4$ Cl, with permutations of the cations. The presence of Ca $^{2+}$ or Cu $^{2+}$ ions (0.0025 M) on both sides of the membrane alters the flux ratios. An equation based on the Nernst-Planck equation predicts satisfactorily the trends in the flux ratios from conductivity data.

Experimental Section

The preparation of the poly(vinyl methyl ether-maleic acid) (PVM-MA)-poly(vinyl alcohol) (PVA) membranes and the materials, equipment, and general procedures used were the same as reported previously.³ The multiionic transport was investigated by placing a solution which was 0.0500 M in two univalent cations (Na $^+$, K $^+$, NMe $_4^+$) on one side of the membrane and a solution which was 0.1000 M in the third ion on the other side. Flame photometry was used to determine Na $^+$ and K $^+$ concentrations. By assuming the absence of anion flux and electric transference, the NMe $_4^+$ flux was calculated as the sum or difference of the Na $^+$ and K $^+$ ion fluxes. Divalent cation concentrations in both solutions were either zero or 0.0025 M. All multiionic diffusion measurements were made on membranes cut from the same sheet which was 45 μ thick. The accuracy of the Na $^+$ and K $^+$ ion fluxes was within 6% of the values reported. The sum or difference technique used to determine NMe $_4^+$ results in doubling the accuracy limits for NMe $_4^+$.

Results and Discussion

A theory for interdiffusion applicable to multiionic systems has been presented by Helfferich and Schlögl for a membrane behaving as a quasi-homogeneous phase in which anion groups are fixed.⁴ The modified flux equation is

$$\bar{J}_i = -\bar{D}_i \left(\frac{d\bar{C}_i}{dx} + Z_i \bar{C}_i \frac{F}{RT} \frac{d\phi}{dx} \right) \quad (1)$$

where \bar{D}_i is the self-diffusion coefficient of species i , \bar{C}_i is the normality of the i th ion in the pore liquid, Z_i is the charge on the species, and ϕ is the electrical potential. F , R , and T are the Faraday constant, the gas constants, and temperature in degrees Kelvin, respectively. The most serious simplification in eq 1 is that activity coefficients for every ionic species are assumed constant throughout the membrane.

A simple solution of the modified flux equation requires the imposition of a number of boundary conditions: (1) the flux is completely controlled by the membrane; (2) the concentration of the fixed groups, the concentration of divalent ions, and the diffusion coefficients of the monovalent ions are constant across the membrane; (3) convection and the presence of co-ions are disregarded; (4) electric current is absent; (5) the diffusing ions i and j do not associate with fixed or mobile species and coupled diffusion effects are not considered; and (6) stationary-state or constant-flux conditions are maintained. The resulting equation is

$$J_i = -K \bar{D}_A \bar{C}_A' / (e^{K\delta} - 1) \quad (2)$$

where K is a constant, $\bar{C}_A = \bar{C}_A'$ at $X = \delta$, and δ is the membrane thickness. The ratio of fluxes for two ions in a multiionic system is

$$\bar{J}_A/\bar{J}_B = \frac{\bar{D}_A \bar{C}_A'}{\bar{D}_B \bar{C}_B'} \quad (3)$$

Values of \bar{D}_i and \bar{C}_i determined from conductivity and

(4) F. Helfferich and R. Schlögl, *Discussions Faraday Soc.*, 21, 133 (1956).

equilibrium concentration data for the system investigated have been reported.³ The self-diffusion coefficients were calculated using the equation⁵

$$D_i = \frac{RT10^3 K \bar{i}_i}{|Z_i| F^2 \bar{C}_i} \quad (4)$$

where K is the specific conductance and \bar{i}_i is the transport number of species i in the membrane. In the conductivity measurements \bar{C}_i was constant across the membrane, *i.e.*, $\bar{C}_i = \bar{C}_i'$. Providing that $\bar{i}_A = \bar{i}_B$ for conductance of ions A^+ and B^+ in the membrane and assuming that $\bar{C}_i = \bar{C}_i'$, substitution of eq 4 into eq 3 yields

$$J_a/J_b = K_a/K_b \quad (5)$$

The experimental fluxes obtained for multiionic interdiffusion are shown in columns 1 and 2 of Table I. Experimental flux ratios and flux ratios calculated using eq 5 are given in columns 3 and 4, respectively. For comparison, the ratio of ionic mobilities in H_2O are shown in column 5.

The provision that $\bar{C}_i = \bar{C}_i'$ for a static system applies to a dynamic system may not represent a true model for multiionic interdiffusion. Also, interactions between solute ions in multicomponent systems may be appreciable as demonstrated by Wendt.⁶ However, the relation between single-ion interdiffusion coefficients as determined from conductivity data and flux ratios calculated for multiionic systems does predict the observed trends in experimental flux ratios. Where the self-diffusion coefficients for the competitively diffusing ions are nearly the same, as for Na^+ and K^+ , the calculated values are in good agreement with experimental values.

The total flux for the multiionic systems decreases in the presence of Ca^{2+} and to a greater extent with Cu^{2+} . This trend is in agreement with the decrease in flux for biionic interdiffusion in the presence of Ca^{2+} and Cu^{2+} reported previously.³ The barrier properties of the membrane as altered by complexing ions not only cause a decrease in the total flux but also affect the relative fluxes of the competitively diffusing univalent ions. The flux ratios are observed to increase in the presence of Ca^{2+} and decrease in the presence of Cu^{2+} .

Acknowledgment. Support by the National Institutes of Health under Grant RG 8774 is gratefully acknowledged.

Scaling in Carbon Monoxide and Nitrogen

by J. Goodisman

*Department of Chemistry, University of Illinois, Urbana, Illinois
(Received October 27, 1965)*

In a recent article,¹ the possibility of scaling the electronic wave function for a molecule for use on a second molecule isoelectronic to the first was discussed. Calculations were made for the pairs H_2 - He_2^{2+} and LiF - BeO . It was pointed out that the accuracy of the energy and other expectation values obtained from the scaled function could throw some light on the similarities or differences between the two molecules involved, and it was noted that the pair CO - N_2 would be a good candidate for such calculations. At about the same time as ref 1, self-consistent field calculations were published by Huo² on CO and BF . Less extensive calculations on N_2 , CO , and BF have been published by Nesbet.³ We here report the results of scaling on these wave functions.

Briefly, the scaling method is as follows: let $\psi_1(r;R)$ be a normalized electronic wave function (within the Born-Oppenheimer approximation) for molecule I. The scaled wave function ψ_{1s} is obtained by multiplying *all* coordinates by the scaling factor s .

$$\psi_{1s} = s^{3n/2} \psi_1(sr; sR) \quad (1)$$

Here, $s^{3n/2}$ is the normalizing factor with n the number of electrons, r refers to all electronic coordinates, and R and sR refer to the coordinates of the nuclei, which enter as parameters. Specializing to diatomic molecules, let molecule II be related to molecule I by having the charge on nucleus A multiplied by Z_A and the charge on nucleus B multiplied by Z_B . Then, scaling a wave function obtained for molecule I and using this to calculate the expectation value of the Hamiltonian for molecule II, we have

$$\bar{E}_s(R) = s^2 T_1(sR) + s C_1(sR) + s Z_A L_1^A(sR) + s Z_B L_1^B(sR) + s Z_A Z_B M_1(sR) \quad (2)$$

where sR is the internuclear distance for molecule I and R is that for molecule II, $T_1(sR)$ is the expectation value of electronic kinetic energy, $C_1(sR)$ is the expectation value of interelectronic repulsion, $L_1^A(sR)$ is the expectation value of the interaction of electrons with nucleus A, $L_1^B(sR)$ is the expectation value of the

(5) K. S. Spiegler and C. D. Coryell, *J. Phys. Chem.*, **57**, 687 (1953).
(6) R. P. Wendt, *ibid.*, **69**, 1227 (1965).

(1) J. Goodisman, *J. Phys. Chem.*, **69**, 2520 (1965).
(2) W. Huo, *J. Chem. Phys.*, **43**, 624 (1965).
(3) R. K. Nesbet, *ibid.*, **40**, 3619 (1964).

interaction of electrons with nucleus B, and $M_1(sR)$ is the nucleus-nucleus potential energy. All expectation values are for the Hamiltonian of molecule I, at an internuclear distance of sR .

In accordance with the variation principle, the value of s which minimizes $\bar{E}_s(R)$ with sR held fixed at R_0 is

$$s_0 = -[2T_1(sR)]^{-1}[C_1(sR) + Z_A L_1^A(sR) + Z_B L_1^B(sR) + Z_A Z^B M_1(sR)] \quad (3)$$

With this value of s , $\bar{E}_s(R) = -s_0^2 T_1(sR)$, where $R = R_0/s_0$. Thus, if we know the expectation values in (3) for molecule I at internuclear distance R_0 , we can calculate an energy for molecule II at internuclear distance R_0/s_0 . In addition, if $f(r)$ is a function homogeneous of degree i in the electronic coordinates whose expectation value for molecule I at R_0 is $\langle f \rangle_1^{sR}$, its expectation value for molecule II at R_0/s_0 is

$$\langle f \rangle_s^R = \langle f \rangle_1^{sR} / s^i \quad (4)$$

For instance, the operators for the electronic contribution of the dipole and quadrupole moments are homogeneous of degrees 1 and 2, while the nuclear contribution is in each case exactly calculable before and after

Table I

| A. Calculations for $N_2 \rightarrow CO$ | | | | |
|--|------------------------|-----------|------------------------|-------------------------------------|
| $R = R_{CO}$ (ao) | $sR = R_{N_2}$ (ao) | s | $\bar{E}_s(R)$, au | $Q^{\infty}(R)$, 10^{-28} esu |
| 1.9 | 1.744393 | 0.9181016 | -108.77378 | -2.35978 |
| | 1.868 | 0.9831579 | -109.45037 | -2.06478 |
| | 2.068 | 1.0884211 | -108.66208 | -1.69994 |
| 2.1 | 1.868 | 0.8895238 | -108.15949 | -2.52235 |
| | 2.068 | 0.9847619 | -109.41979 | -2.07666 |
| | 2.268 | 1.0800000 | -108.76676 | -1.73290 |
| 2.3 | 2.068 | 0.8991304 | -108.28212 | -2.49106 |
| | 2.268 | 0.9860870 | -109.33383 | -2.07868 |
| | 2.391607 | 1.0398291 | -109.18303 | -1.86499 |
| B. Calculations for $CO \rightarrow N_2$ | | | | |
| $R = R_{N_2}$ (ao) | $sR = R_{CO}$ (ao) | s | $\bar{E}_s(R)$, au | $Q^{N_2}(R)$, 10^{-28} esu |
| 1.9 | 1.808393 | 0.9517858 | -106.33909 | -1.54651 |
| | 1.932 | 1.0168421 | -106.05240 | -1.18271 |
| | 2.132 | 1.1221053 | -103.61866 | -0.61519 |
| 2.1 | 1.932 | 0.9200000 | -106.04849 | -1.44480 |
| | 2.132 | 1.0152381 | -105.96874 | -0.88990 |
| | 2.332 | 1.1104762 | -103.88725 | -0.45413 |
| 2.3 | 2.132 | 0.9269565 | -105.96991 | -1.06748 |
| | 2.332 | 1.0139130 | -105.83591 | -0.54476 |
| | 2.455607 | 1.0676552 | -104.39311 | -0.27038 |

Table II

| A. Comparisons with calculated results for CO | | | | |
|--|--------------------|------------------------|--------------------|-----------------------|
| R_{CO} | E_{CO} (SCF) | E_{CO} (scaling) | Q_{CO} (SCF) | Q_{CO} (scaling) |
| 1.8084 | -112.66220 | | -2.02948 | |
| 1.9 | | -109.48065 | | -1.99651 |
| 1.932 | -112.72952 | | -1.94022 | |
| 2.1 | | -109.44389 | | -2.01531 |
| 2.132 | -112.75878 | | -1.79077 | |
| 2.3 | | -109.35349 | | -2.02154 |
| 2.332 | -112.73211 | | -1.60514 | |
| B. Comparisons with calculated results for N_2 | | | | |
| R_{N_2} | E_{N_2} (SCF) | E_{N_2} (scaling) | Q_{N_2} (SCF) | Q_{CO} (scaling) |
| 1.868 | -108.94320 | | -1.32522 | |
| 1.9 | | -106.35619 | | -1.47599 |
| 2.068 | -108.97143 | | -1.19197 | |
| 2.1 | | -106.25835 | | -1.19933 |
| 2.268 | -108.92938 | | -1.03270 | |
| 2.3 | | -106.11754 | | -0.83612 |
| 2.3916 | -108.88528 | | -0.91728 | |

scaling. Choice of origin¹ may be important; for the quadrupole moment, we follow Nesbet³ in maintaining the origin at $16/28$ the distance from the C to the O nucleus.

As pointed out in ref 1, one should really be determining the value of s which minimizes $\bar{E}_s(R)$ for a fixed R , not a fixed sR . We do this by calculating $\bar{E}_s(R)$ from eq 2 for a particular R , starting from several different values of sR , and then fitting to a quadratic to get the minimum energy and best scaling factor. The expectation value of the quadrupole moment is obtained by quadratic interpolation of the values obtained from the scaled wave functions.

The energies and molecular quadrupole moments for CO calculated in this way from scaled N_2 wave functions are given in Table IA; the energies and molecular quadrupole moments for N_2 calculated from scaled CO wave functions are given in Table IB. We have also included, in Table II, comparison with the values obtained by direct calculation by Nesbet,³ whose expectation values we have used.

The similarities in physical and other properties between CO and N_2 have been frequently noted,^{4,5}

(4) For example, Y. K. Syrkin and M. E. Dyatkina, "Structure of Molecules and the Chemical Bond," translated and revised by M. A. Partridge and D. O. Jordan, Dover Publications, Inc., New York, N. Y., 1964, p 136; J. C. Slater, "Quantum Theory of Molecules and Solids," Vol. I, McGraw-Hill Book Co., Inc., New York, N. Y., 1963, p 134; J. D. Roberts and M. C. Caserio, "Basic Principles of Organic Chemistry," W. A. Benjamin, Inc., New York, N. Y., 1964, p 684.

and sometimes ascribed to similarities in electronic structure. Long and Walsh⁵ have argued that most of these properties follow from similar molecular size and external force field (which is expected from the relative positions of the C, O, and N atoms in the periodic table), while properties which reflect electronic structure, such as the effect of ionization on the bond strength, actually point up dissimilarities between the molecules.

The present results tend to bear out this idea. Similar electronic wave functions would imply very good results for the electronic properties of CO from scaled N_2 wave functions and *vice versa*. We note that the scaling factors are quite close to unity (compare ref 1), again reflecting similar molecular size, but that the agreement in energy is not very good. The energy errors are of the same order of magnitude as in the LiF-BeO pair,¹ which would certainly not be considered similar. Equilibrium internuclear distances are well predicted, but this again reflects only similar molecular sizes; the agreement for the molecular quadrupole is not very good.

The difference between the Hamiltonian for CO and N_2 is a one-electron operator, and perturbation theory has been employed to calculate its effect.⁶ Perturbation methods, because of their flexibility, can do much better than the present method, but it turns out that even energies as accurate as these reported here require considerable labor.

(5) L. H. Long and A. D. Walsh, *Trans. Faraday Soc.*, **43**, 342 (1947).

(6) T. Y. Chang and W. B. Brown, University of Wisconsin Theoretical Chemistry Institute Report WIS-TCI-114 (1965).

The Electron Spin Resonance Absorption of Solid 1,1-Diphenyl-2-picrylhydrazyl Mixtures. Surface and Aging Effects

by Kedma H. Bar-Eli and Karl Weiss

Tyco Laboratories, Inc., Waltham, Massachusetts 02154, and Photochemistry and Spectroscopy Laboratory, Northeastern University, Boston, Massachusetts 02115 (Received October 29, 1965)

Matsunaga and McDowell¹ have reported that the electron spin resonance spectra of mixtures of 1,1-diphenyl-2-picrylhydrazyl (DPPH) with zinc oxide and with nickel oxide show line broadening and an apparent loss of spins when compared with the spectra of DPPH itself. This effect has been ascribed to a

transfer of electrons between DPPH and the oxides. DPPH admixed with inert solids is widely employed as a standard in electron spin resonance spectroscopy.² In this note we show that an interaction leading to loss of spins can occur even with materials considered to be inert. The extent of spin loss depends on the nature of the material and on the method of mixing.

The measurements were made with a standard Varian V-4500 spectrometer using a single cavity. DPPH (Aldrich Chemical Co.) was used either as received or after recrystallization,^{2b} with identical results. Calcium carbonate (Mallinckrodt Analytical reagent), magnesium carbonate, basic (Fisher Certified), and potassium chloride (Baker Analyzed) were used without further treatment. The mixtures were examined in air as weighed samples of constant volume.

A Wig-L-Bug amalgamator (Crescent Dental Manufacturing Co.) served to prepare mixtures of varying DPPH content. For *unground* mixtures the components were merely shaken until homogeneous. For *ground* mixtures (1-min grinding time), a stainless steel ball was included. Once homogeneity was attained by either method, the esr signal amplitude was independent of further mixing. The average particle diameter of DPPH and mixtures with KCl is $>50 \mu$ before grinding and $\sim 5 \mu$ after grinding measured by a Fisher Sub-Sieve Sizer. The particle size of $MgCO_3$ mixtures was determined by the carbonate itself which is $<0.5 \mu$. Intensities were computed from the amplitude of the derivative curve and the line width, which was found to be invariant within each set of samples.³

The results are summarized in Figures 1 and 2 as plots of the specific intensity (I_{sp} , intensity per milligram of DPPH) against the weight fraction of DPPH in the mixture (X_D). The behavior of unground samples is illustrated by magnesium carbonate mixtures, which show the anticipated lack of dependence of I_{sp} on X_D . Fresh, ground mixtures with potassium chloride (Figure 1) also behave as expected. With ground magnesium carbonate and calcium carbonate mixtures, however, there is a marked decrease of I_{sp} with increasing dilution. That a rapid destruction of spins occurs during the grinding process is supported by a corresponding decrease in the apparent extinction coefficient of DPPH at $525 m\mu$ observed in chloroform extracts of the ground magnesium carbonate mixtures.

(1) Y. Matsunaga and C. A. McDowell, *Can. J. Chem.*, **38**, 724 (1960).

(2) (a) D. J. E. Ingram, "Free Radicals as Studied by Electron Spin Resonance," Butterworth and Co. Ltd., London, 1958, Chapter 3; (b) J. J. Lothe and G. Eia, *Acta Chem. Scand.*, **12**, 1535 (1958); (c) L. S. Singer, *J. Appl. Phys.*, **30**, 1463 (1959); (d) J. Zanchetta, A. Marchand, and A. Pacault, *Compt. Rend.*, **258**, 1496 (1964).

(3) *Cf.*, however, F. Bruin and M. Bruin, *Physica*, **22**, 129 (1956).

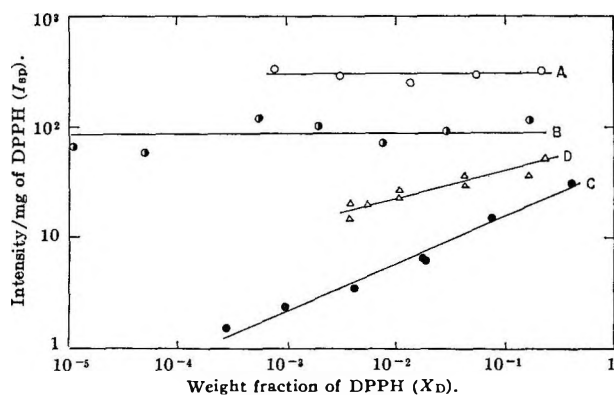


Figure 1. Specific intensity as a function of the weight fraction of DPPH for fresh mixtures: A, magnesium carbonate (unground); B, potassium chloride (ground); C, magnesium carbonate (ground); D, calcium carbonate (ground). I_{sp} is in arbitrary units. Curves coincide, but have been moved apart for clarity.

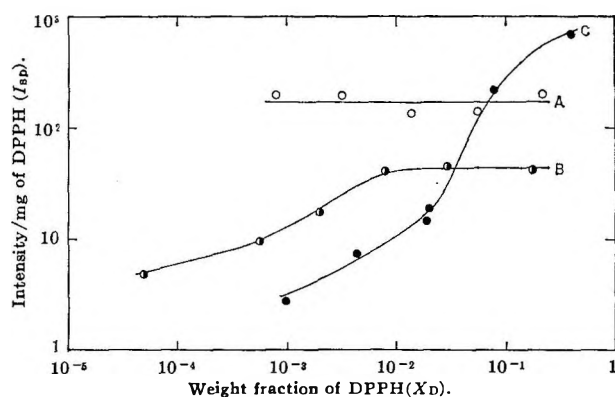


Figure 2. Specific intensity as a function of the weight fraction of DPPH for aged (1 month) mixtures. The labels are the same as in Figure 1. I_{sp} units and vertical positions of curves are arbitrary.

Storage of ground mixtures in air causes further decrease in I_{sp} (Figure 2). Again, the effect is most pronounced with magnesium carbonate. Although no change in line width resulted from the grinding, aging caused an increase from 1.9 gauss⁴ to 2.5 gauss.

It has been reported that DPPH in benzene solution reacts with surface-bound water and hydroxyl groups.^{5,6} The grinding effect increases in the order potassium chloride < calcium carbonate << magnesium carbonate, which is also the order of increasing water content of these materials. Since grinding can provide the intimate contact necessary for a rapid solid-solid interaction to occur, this sequence suggests that the surface reaction with water is primarily responsible for the permanent loss of spins. The data indicate that freshly prepared, ground mixtures of DPPH

with potassium chloride constitute useful standards over a wide range of composition.

Acknowledgments. This work was sponsored by the U. S. Air Force Cambridge Research Laboratories, Office of Aerospace Research, under Contracts AF19(628)-2845 and AF19(628)-3836.

(4) Cf. R. G. Bennett and A. Henglein, *J. Chem. Phys.*, **30**, 1117 (1959).

(5) J. G. Aston and D. N. Mitra, *J. Phys. Chem.*, **69**, 3219 (1965).

(6) T. Laederich and P. Traynard, *Compt. Rend.*, **259**, 1848 (1964).

Adsorption of Propane on Carbon Black

by G. L. Taylor and J. H. Atkins

Cabot Corporation, Cambridge, Massachusetts
(Received November 1, 1965)

Isosteric heats of adsorption of propane as a function of coverage were measured on a channel grade black, a 2700° heat-treated sample of the channel black, and two furnace grade carbon blacks. In addition, it was possible to determine the orientation of the propane molecule on the surface, checking it against a molecular model.

The carbon blacks used and their specific BET surface areas were Vulcan 6,¹ an ISAF oil furnace black with 115 m²/g; Regal 600,¹ an SCRF oil furnace black with 91.6 m²/g; Spheron 6,¹ a channel black with 106 m²/g; and Graphon,¹ a 2700° heat-treated Spheron 6 with 77.7 m²/g. Each of the first three samples have a heterogeneous surface with active adsorption sites which are involved in the reinforcement mechanism of polymers. Graphon has a homogeneous surface with few if any active sites.

The experimental isotherms were done on a recording adsorption balance² at the following bath temperatures: 194.6, 273.1, 283.1, 293.1, and 303.1°K. The isosteric heats of adsorption, Q_s , were determined by taking points of equal coverage from each of the isotherms and inserting the data into the following integrated form of the Clausius-Clapeyron equation

$$Q_s = \frac{2.303R(\log P_2 - \log P_1)}{1/T_1 - 1/T_2}$$

(1) Trade names of Cabot Corp.

(2) J. H. Atkins, presented at 148th National Meeting of American Chemical Society, Chicago, Ill., Sept 1964; Abstracts, p 9-I.

A plot of $\log P$ vs. $1/T$ results in a straight line of slope $Q_s/2.303R$. From our data, Q_s at any given coverage for each of the four samples is a constant over the temperature range of 194.6 to 303.1°K, since in all cases the four points fall on a straight line.

The values of Q_s as functions of coverage up to a half of a monolayer are illustrated in Figure 1.

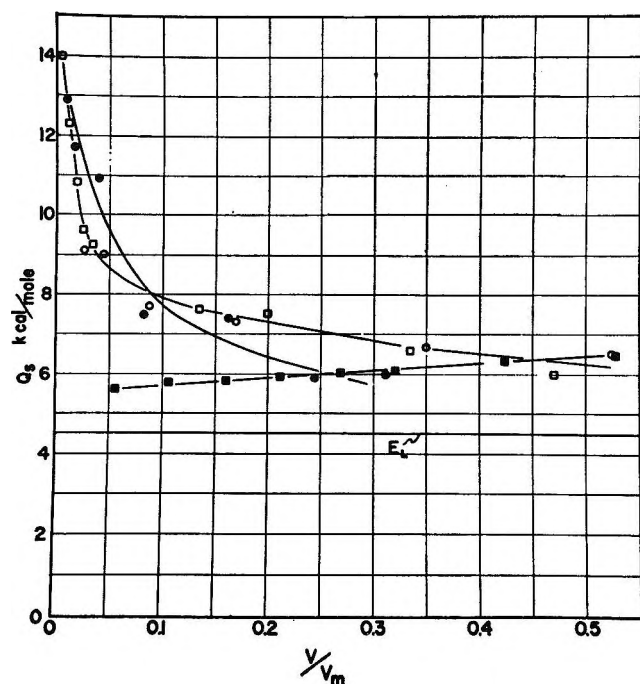


Figure 1. Q_s as a function of coverage for four carbon blacks: \square , Vulcan 6, $V_m = 14.90$ cc/g; \circ , Regal 600, $V_m = 11.45$ cc/g; \blacksquare , Graphon, $V_m = 9.40$ cc/g; and \bullet , Spheron 6, $V_m = 12.30$ cc/g.

With the active blacks the high initial isosteric heats of adsorption are explained by their heterogeneous surfaces with the first adsorbate molecules being adsorbed at the most active sites. From the initial Q_s values it appears that the initial adsorption occurs in small pores where two or more surfaces can interact with each adsorbate molecule.

The different slope of the isosteric heat curve for Graphon compared to those of the other adsorbents can be explained on the basis of a homogeneous surface where the heat of adsorption of propane is the same, no matter where it is adsorbed. The increase in the heat value as more of the surface is covered is due to adsorbate-adsorbate interaction. Similar results using *n*-butane on Graphon were found by Beebe and co-workers³ and by Pierce and Smith,⁴ who adsorbed ethyl chloride on the same material.

It is interesting to compare the experimental heats

of adsorption with the theoretical calculations of Kiselev and co-workers.⁵ Working with *n*-alkane molecules, they estimated that each CH_3 group would contribute 2.1 to 2.3 kcal/mole and each CH_2 group 1.7 to 1.9 kcal/mole. For propane, this is 6–6.5 kcal/mole. Allowing about 0.5–1 kcal/mole for a term in R.T. (to compensate for differences between potential energy and the isosteric heat) gives an expected heat of adsorption between 5 and 6 kcal/mole, in good agreement with the results of this paper.⁶

It is gratifying that the calorimetrically determined differential heats of adsorption of *n*-butane on Spheron 6 reported by Beebe and co-workers³ over the same range of coverages parallel our values using propane with the higher absolute value for the *n*-butane being explained by the additional CH_2 group.

The monolayer coverage by propane of each of the carbon black samples was determined by taking the *B* point from the 194.6°K isotherm. The surface areas of the samples were determined using a nitrogen BET technique and from this the specific surface area occupied by a propane molecule on each sample was calculated. These values are shown in Table I.

Table I

| Sample | V_m , cc | Surface area, m^2/g | A^2 per mole- cule | Shadow areas in A^2 per molecule | |
|-----------|---------------|---|-----------------------------------|--|------------------------------|
| | | | | a hori- zontal (mean) | b verti- cal (mean) |
| Vulcan 6 | 14.90 | 115.0 | 29.5 | | |
| Regal 600 | 11.45 | 91.6 | 30.5 | 30.3 | 11.8 |
| Spheron 6 | 12.30 | 106.0 | 31.8 | | |
| Graphon | 9.40 | 77.7 | 31.5 | | |

To corroborate the experimental propane specific surface areas, a molecular model of the propane was constructed using the Godfrey molecular models. The average area covered by this model was determined by photographing its shadow in different orientations. The value listed under a in Table I represents the shadow area of the propane molecule "lying down" on the surface, that under b represents an alternate configuration, standing on an end, with only one methyl

(3) R. A. Beebe, G. L. Kington, M. H. Polley, and W. R. Smith, *J. Am. Chem. Soc.*, **72**, 40 (1950).

(4) C. Pierce and N. R. Smita, *ibid.*, **75**, 846 (1953).

(5) N. N. Avgul, A. A. Isirikyan, A. V. Kiselev, I. A. Lygina, and D. P. Poshkus, *Izv. Nauk SSSR, Otd. Khim. Nauk*, 1314 (1957).

(6) The authors wish to thank the referee who called their attention to ref 4.

group in contact with the carbon surface. The agreement between the experimentally obtained values and that in column a leaves no doubt that the propane is horizontally oriented on the surface in the monolayer.

Doubly Charged Transition Metal Carbonyl Ions¹

by Robert E. Winters and Robert W. Kiser

Department of Chemistry, Kansas State University,
Manhattan Kansas 66504 (Received November 29, 1965)

The majority of positive ions formed in the ion source of the mass spectrometer bear a single charge. It is possible, however, to obtain doubly charged positive ions if in the initial ionization process two electrons are removed from the molecule. The absolute intensity of +2 ions is generally found to be much lower than +1 ions.² Mohler, *et al.*,³ have suggested that decomposition of doubly charged hydrocarbon ions to give two singly charged ions is the more probable process for the +2 ion breakdown scheme. No direct relationship between the intensity of the singly and doubly charged species is observed in hydrocarbons.^{4,5} In fact, not infrequently a rather intense doubly charged species is observed whereas the ion at twice its m/e value is quite small.⁴

The first evidence of a doubly charged ion decomposing into a second doubly charged species and a neutral fragment was reported by Beynon, *et al.*⁶ Meyerson and Vander Haar⁷ then found nine more instances where doubly charged ions disrupted to a neutral particle and a different doubly charged ion. This type of fragmentation has also recently been reported⁸ for azulene and naphthalene parent molecule +2 ions.

In order to examine the mode of decomposition of the doubly charged transition metal carbonyl ions, we have studied the 70-ev mass spectrum of tungsten hexacarbonyl. Earlier investigation⁹ of this monomeric carbonyl was unable to provide satisfactory data on the +2 ions due to the compound's low vapor pressure¹⁰ under the experimental conditions. We have now modified the inlet to the mass spectrometer in order to increase the sample pressure in the ion source. The results are interpreted in terms of successive unimolecular decomposition of the doubly charged ions by loss of neutral CO groups.

Experimental Section

Mass spectra were measured with approximately 70-ev electrons on a Bendix Model 12-100 time-of-flight mass spectrometer. The instrumentation has been described previously.¹¹ The solid tungsten hexacarbonyl was vaporized from a 15.2-cm stainless steel tube connected directly to the ion source of the mass spectrometer. This arrangement allowed external heating of the sample in order to increase its vapor pressure.

Results and Discussion

A comparison of the singly⁹ and doubly charged ions formed upon electron impact of tungsten hexacarbonyl is shown in Figure 1. The most intense ion in each spectrum is arbitrarily assigned an intensity of 100.¹² The intensities of all other peaks are given values relative to the most intense peak. Contrary to previous observations⁴ that no direct relationship exists between singly and doubly charged ions, a definite relation appears to exist between such ions from this metal carbonyl. Also, only the most intense singly charged $M(\text{CO})_x$ species were found as +2 ions in the mass spectra of $\text{Ni}(\text{CO})_4$ and $\text{Fe}(\text{CO})_5$,¹³ and $\text{Cr}(\text{CO})_6$ and $\text{Mo}(\text{CO})_6$.⁹ Such close similarity in the mass spectra suggests that the mode of formation of the doubly charged fragmentation ions is very similar to the process proposed earlier⁹ for the singly charged ions, *i.e.*, elimination of neutral CO groups. Such a decomposition scheme would require considerable charge to be associated with the metal atom. How-

(1) This report is based on work performed under contract with the U. S. Atomic Energy Commission, Contract No. AT(11-1)-751, with Kansas State University. Abstracted from the Ph.D. dissertation of R. E. Winters, Kansas State University, 1965.

(2) F. H. Field and J. L. Franklin, "Electron Impact Phenomena and the Properties of Gaseous Ions," Academic Press, Inc., New York, N. Y., 1957.

(3) F. H. Mohler, V. H. Dibeler, and R. M. Reese, *J. Chem. Phys.*, **22**, 394 (1954).

(4) J. H. Beynon, "Mass Spectrometry and Its Application to Organic Chemistry," Elsevier Publishing Co., Amsterdam, 1960.

(5) K. Bieman, "Mass Spectrometry: Organic Chemical Applications," McGraw-Hill Book Co., Inc., New York, N. Y., 1962.

(6) J. H. Beynon, G. R. Lester, and A. E. Williams, *J. Phys. Chem.*, **63**, 1861 (1959).

(7) S. Meyerson and R. W. Vander Haar, *J. Chem. Phys.*, **37**, 2458 (1962).

(8) R. J. Van Brunt and M. E. Wacks, *ibid.*, **41**, 3195 (1964).

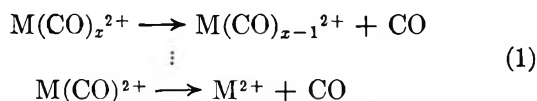
(9) R. E. Winters and R. W. Kiser, *Inorg. Chem.*, **4**, 157 (1965).

(10) T. N. Rezhikhina and V. V. Shvyrev, *Vestnik Moskov. Univ.*, **7** (6), *Ser. Fiz.-Mat. i Estestven. Nauk*, (4), 41 (1952).

(11) E. J. Gallegos and R. W. Kiser, *J. Am. Chem. Soc.*, **83**, 773 (1961); *J. Phys. Chem.*, **65**, 1177 (1961).

(12) The actual intensities of the singly charged ions are 4.27 times the intensities of the doubly charged ions.

(13) R. E. Winters and R. W. Kiser, *Inorg. Chem.*, **3**, 699 (1964).



ever, the second ionization potentials of several transition metal carbonyl species (Table I) strongly suggest that the second electron removed upon electron impact is an electron from an orbital largely associated with the metal atom. The first ionization potentials^{9,10} of these metal carbonyls have been reported also as being very near the ionization potentials of the metals. Note that within experimental error the second ionization potential of the $\text{M}(\text{CO})_x$ species corresponds to the second ionization potential of the respective metal atom.

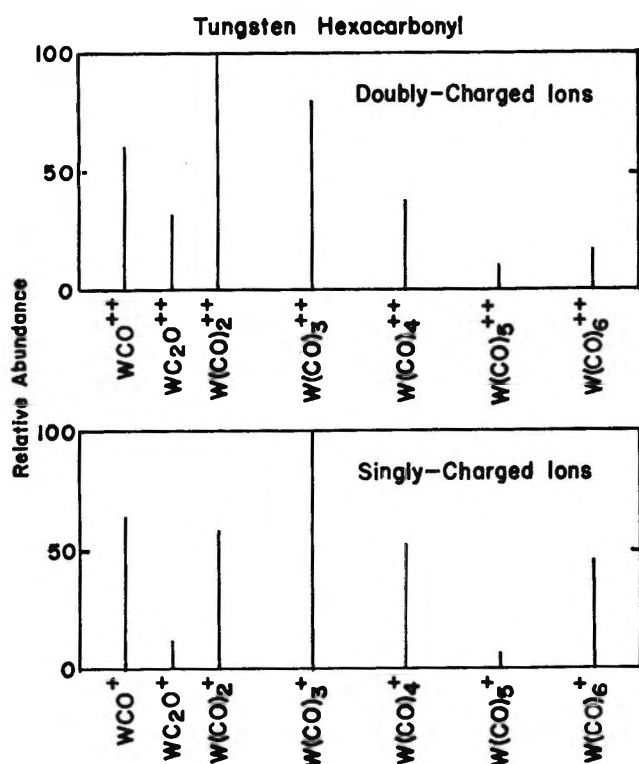


Figure 1. Mass spectra of doubly and singly charged ions from tungsten hexacarbonyl.

It appears, therefore, that the doubly charged transition metal carbonyl molecule ions decompose in a manner similar to that previously proposed for the singly charged positive ions, *i.e.*, by a series of consecutive unimolecular decompositions. The metastable transitions corresponding to such processes in both the singly and doubly charged ions have recently been observed.¹⁴

It is anticipated that the quasi-equilibrium theory of mass spectra¹⁵ may find new applications in the

Table I: Comparisons of the Second Ionization Potentials of Some $\text{M}(\text{CO})_x$ Species and the Metals

| $\text{M}(\text{CO})_x$ species | Second ionization potential, eV^a | Metal | Second ionization potential, eV^b |
|---------------------------------|--|-------|--|
| $\text{Ni}(\text{CO})_2$ | 17.6 ± 1.0 | Ni | 18.15 |
| $\text{Fe}(\text{CO})$ | 16.2 ± 2.0 | Fe | 16.18 |
| $\text{Cr}(\text{CO})$ | 17.3 ± 1.0^c | Cr | 16.49 |
| $\text{Mo}(\text{CO})$ | 16.4 ± 0.6 | Mo | 15.717 |
| $\text{Mo}(\text{CO})_2$ | 15.2 ± 0.6 | | 16.15 ^d |
| $\text{Mo}(\text{CO})_3$ | 15.4 ± 1.2 | | |

^a See ref 9 and 13. ^b C. E. Moore, "Atomic Energy Levels," National Bureau of Standards Circular 467, U. S. Government Printing Office, Washington, D. C. ^c D. R. Bidinosti and N. S. McIntyre, University of Western Ontario, personal communication, 1965. ^d M. A. Catalan and F. R. Rico, *Anales Real Soc. Espan. Fis. Quim.* (Madrid), **48A**, 328 (1952).

unimolecular decomposition of doubly charged ions. Such calculations are now underway in these laboratories.

(14) R. E. Winters and J. H. Collins, private communication; a paper describing this work has been submitted to *J. Phys. Chem.*

(15) H. M. Rosenstock, M. B. Wallenstein, A. L. Wahrhaftig, and H. Eyring, *Proc. Natl. Acad. Sci. U. S. A.*, **38**, 667 (1952); M. Vestal, A. L. Wahrhaftig, and W. H. Johnston, *J. Chem. Phys.*, **37**, 1276 (1962).

The Nature of the Acidic Sites on Silica-Alumina.

A Reevaluation of the Relative Absorption Coefficients of Chemisorbed Pyridine

by Michael R. Basila and Theodore R. Kantner

Gulf Research & Development Company, Pittsburgh, Pennsylvania
(Received December 2, 1965)

In a recent infrared spectroscopic study¹ of pyridine (PY) adsorbed on a synthetic silica-alumina (SA), we estimated the ratio of Lewis to Brønsted acid sites to be ~ 1 from the intensities of bands characteristic of the coordinately bonded (LPY) and protonated (BPY) chemisorbed pyridine at 1450 and 1545 cm^{-1} , respectively. This estimate was based on relative absorption coefficients derived by assuming identical absorption coefficients for the ν_{19a} mode which occurs at 1490 cm^{-1} for both chemisorbed species. Subsequent work

(1) M. R. Basila, T. R. Kantner, and K. H. Rhee, *J. Phys. Chem.*, **68**, 3197 (1964).

has shown that this assumption is incorrect and it is the purpose of this note to reevaluate the absorption coefficients. The experimental details of the work are given in our earlier paper.¹

Lewis-Brønsted Acid Site Distribution on SA. When a sample of SA containing chemisorbed PY is exposed to H₂O vapor a large proportion of the chemisorbed LPY is transformed to chemisorbed BPY.^{1,2} Inspection of the spectrum reveals that the 1490-cm⁻¹ band changes in intensity rather than remaining constant as one would expect if the absorption coefficients were identical in the two chemisorbed species. The intensity increase suggests that the BPY species has the greater absorption coefficient. It is possible to derive an expression for the relative absorption coefficients for the two species by substituting the relationships (1)–(3) into (4).

$$\epsilon_{1490}^L/\epsilon_{1450} = C = 0.25 \quad (1)$$

$$([\text{LPY}]_1 - [\text{LPY}]_2) = -([\text{BPY}]_1 - [\text{BPY}]_2) \quad (2)$$

$$A_{1450}^1 - A_{1450}^2 = l\epsilon_{1450}([\text{LPY}]_1 - [\text{LPY}]_2) \quad (3)$$

$$A_{1490}^1 - A_{1490}^2 = l\epsilon_{1490}^L([\text{LPY}]_1 - [\text{LPY}]_2) + l\epsilon_{1490}^B([\text{BPY}]_1 - [\text{BPY}]_2) \quad (4)$$

The resulting expression for the absorption coefficient ratio is

$$\frac{\epsilon_{1490}^B}{\epsilon_{1490}^L} = \frac{C(A_{1450}^1 - A_{1450}^2) - (A_{1490}^1 - A_{1490}^2)}{C(A_{1450}^1 - A_{1450}^2)} \quad (5)$$

In (1)–(5), A signifies the peak absorbance, l is the optical path length, and the superscripts 1 and 2 refer to the absorbancies before and after addition of H₂O. The value of C was determined from the spectrum of PY chemisorbed on potassium-poisoned SA where only the LPY species is observed.¹ The value of $\epsilon_{1490}^B/\epsilon_{1490}^L$ was estimated to be 6.0 ± 0.9 .

The ratio of Lewis to Brønsted acid sites may be estimated from the following equation.

$$\frac{[\text{LPY}]}{[\text{BPY}]} = \frac{6.0CA_{1450}}{A_{1490} - CA_{1450}} \quad (2)$$

Using (2), a value of 6.0 is calculated for the ratio $[\text{LPY}]/[\text{BPY}]$ on SA or in other words one out of every seven chemisorbed pyridine molecules is a protonated species.

Other Silica-Aluminas. In the course of our work we have studied several other commercial silica-aluminas. One would not expect the Lewis-Brønsted acid site distribution to be constant for such materials, especially in view of the variations in the composition and methods of preparation which usually exist between commercial catalysts. Our measurements are

consistent with this expectation. The results shown in Table I indicate that the Lewis sites predominate in all the silica-aluminas, but that a wide range in the ratio of Lewis to Brønsted sites exists.

Table I: Lewis-Brønsted Acid Site Distribution in Silica-Aluminas^a

| Catalyst | % Al ₂ O ₃ | SA, m ² /g | [LPY]/[BPY] |
|----------------------------|----------------------------------|-----------------------|-------------|
| American Cyanamid Triple A | 25 | 430 | 6.0 |
| Davison F-125 | 25 | 352 | 3.8 |
| Houdry S-90 | 12 | 421 | 4.2 |
| Houdry S-36 | 12 | 157 | 2.9 |

^a The catalyst samples were pretreated by heating from ambient to 500° over a 3-hr period with continuous evacuation, calcining in pure O₂ for at least 4 hr at 500°, and evacuating overnight at 500°.

(2) E. P. Parry, *J. Catalysis*, **2**, 371 (1963).

Nuclear Magnetic Resonance Studies of Inorganic Fluorides. II. Solvent Effects on $J(^{29}\text{Si}-^{19}\text{F})$ in Silicon Tetrafluoride^{1,2}

by T. D. Coyle, R. B. Johannesen, F. E. Brinckman, and T. C. Farrar

National Bureau of Standards, Washington, D. C.
(Received December 7, 1965)

Several recent reports^{3–6} have demonstrated the occurrence of solvent and temperature effects on nuclear spin coupling constants in a number of systems. The various mechanisms which may produce detectable changes in coupling constants by altering the average electronic structure of the molecules containing the coupled nuclei have been summarized by Gutowsky and co-workers.³ In this note we report our observa-

(1) Presented in part at the 150th National Meeting of the American Chemical Society, Atlantic City, N. J., Sept 1965.

(2) Part I: R. B. Johannesen, T. C. Farrar, F. E. Brinckman, and T. D. Coyle, *J. Chem. Phys.*, **44**, 962 (1966).

(3) H. S. Gutowsky, J. Jonas, F. Chen, and R. Meinzer, *ibid.*, **42**, 2625 (1965), and references cited therein.

(4) K. Kuhlmann and D. M. Grant, *J. Phys. Chem.*, **68**, 3208 (1964).

(5) S. L. Smith and R. H. Cox, *J. Mol. Spectry.*, **16**, 216 (1965).

(6) P. Bates, S. Cawley, and S. S. Danyluk, *J. Chem. Phys.*, **40**, 2415, (1964).

tions of a significant solvent dependence of the ^{29}Si - ^{19}F coupling constants in SiF_4 and related molecules. The results given here provide an example of medium effects on coupling constants involving fluorine and a directly bonded nucleus and suggest that such variations may be of quite general occurrence.

Listed in Table I are values of $J(^{29}\text{Si}-^{19}\text{F})$ for SiF_4 in a variety of solvents at 28° . The results were obtained from measurements of the splitting of the ^{29}Si satellites in the ^{19}F spectrum, using a Varian DP-60 spectrometer modified for frequency-sweep operation. The experimental procedures and error limits of the measurements have been described previously.² The sample tubes from which the data in Table I were obtained contained approximately 15 mole % SiF_4 in the indicated solvents. Owing to the volatility of the solute and unknown variations in solubility, the concentration of SiF_4 in the liquid phase was undoubtedly somewhat lower than 15% and varied to some extent between solvents.

Table I: $J(\text{Si}-\text{F})$ in SiF_4

| Solvent | J | Solvent | J |
|------------------------------------|--------|---|--------|
| Si_2OF_6 | 170.51 | SiF_2Br_2 | 174.51 |
| CF_3CN | 170.66 | $(\text{CH}_3)_4\text{Si}$ | 174.68 |
| CCl_3F^a | 170.78 | CCl_3F | 175.03 |
| CH_3SiF_3 | 171.12 | CH_2Cl_2 | 175.23 |
| SiF_3Br | 171.51 | CHCl_3 | 176.12 |
| $\text{C}_2\text{H}_5\text{SiF}_3$ | 172.01 | $\text{Si}_2\text{Cl}_5\text{F}-\text{Si}_2\text{Cl}_6$ (1:3) | 176.14 |
| $\text{CH}_2=\text{CHSiF}_3$ | 172.05 | SiFBr_3 | 176.45 |
| $(\text{CH}_3)_2\text{SiF}_2$ | 172.35 | CCl_4 | 176.83 |
| $(\text{CH}_3)_3\text{SiF}$ | 173.06 | Cyclo- C_6H_{12} | 176.88 |
| C_6F_6 | 173.44 | C_6H_6 | 176.98 |
| CCl_2F_2 | 173.67 | BBr_3 | 178.0 |
| $(\text{C}_2\text{H}_5)_2\text{O}$ | 173.70 | SiBr_4 | 178.61 |

^a Gas phase value.

An indication of the concentration dependence of J in four solvents is given in Table II. The measured value of the coupling constant is largest in the most dilute solutions. Because of the uncertainty in the liquid phase concentrations of SiF_4 and the experimental difficulties in measuring the satellite separation in more dilute solutions, extrapolation to infinite dilution is unreliable. It is apparent, however, that infinite dilution values of J would differ from the values at 15% nominal concentration to an extent that is small compared to the variations from solvent to solvent.

The values of the coupling constant in pure SiF_4 , measured in the manner reported earlier,² were 169.00 ± 0.08 and 168.84 ± 0.03 hertz for the gas at 30 and

Table II: Concentration Dependence of $J(\text{Si}-\text{F})$

| Solvent | SiF_4 concn (%) | J |
|---|--------------------------|--------|
| $(\text{C}_2\text{H}_5)_2\text{O}$ | 15 | 173.70 |
| | 50 | 172.71 |
| Cyclo- C_6H_{12} | 15 | 176.88 |
| | 25 | 176.77 |
| SiBr_4 | 17 | 178.61 |
| | 30 | 178.37 |
| $(\text{CH}_3)_4\text{Si}$ | 15 | 174.68 |
| | 31 | 174.27 |
| | 50 | 173.78 |
| CCl_3F (gas, 28°) | 15 | 170.78 |
| | (liq, -3°) | 171.40 |
| | (liq, -30°) | 172.10 |

110 atm, respectively. For liquid SiF_4 at -52° , the value was 169.97 ± 0.08 Hz. The "best" value for this parameter is thus 169–170 Hz, which is somewhat lower than previously reported values.^{7,8}

As the data in the tables show, addition of any of the 24 solvents studied to SiF_4 produces an increase in the apparent coupling constant. In contrast to the behavior noted in some previously reported examples of solvent dependence,^{5,6} there is no evident correlation of the values of J with solvent dielectric constant over the rather limited range of ϵ represented by the solvents listed. It is noteworthy that the smallest increases in $J(^{29}\text{Si}-^{19}\text{F})$ are produced by the most highly fluorinated solvents. For series of related solvents of formula $\text{SiX}_n\text{F}_{4-n}$ or $\text{CX}_n\text{F}_{4-n}$, $J(^{29}\text{Si}-^{19}\text{F})$ for the solute increases monotonically with increasing n . These observations suggest that the solvent effects may result, at least in part, from relatively specific intermolecular fluorine-fluorine interactions.³ We have also noted similar behavior in mixtures of the chlorofluorosilanes, where $J(^{29}\text{Si}-^{19}\text{F})$ for each species increases as the proportion of the more highly chlorinated compounds is increased.

It is highly probable that the observed solvent dependences reflect the composite effects of several factors which may alter the time-averaged electronic state of the solute molecules. In particular, the silicon and fluorine atoms, or both, may interact with appropriate donor or acceptor sites in the solvent molecules to an extent which will depend on local electrophilic and nucleophilic character in both solvent and solute

(7) E. L. Muetterties and W. D. Phillips, *J. Am. Chem. Soc.*, **81**, 1084 (1959).

(8) P. T. Inglefield and L. W. Reeves, *J. Chem. Phys.*, **40**, 2425 (1964).

(9) V. S. Watts and J. H. Goldstein, *ibid.*, **42**, 228 (1965).

species. In the case of basic solvents, donor-acceptor interactions involving the silicon d orbitals may be expected to predominate, leading in extreme cases to appreciable concentrations of well-defined complexes. In other cases, transitory formation of fluorine-bridged species may be significant. In view of the pronounced reactivity of many covalent inorganic halides as exemplified by electron-acceptor character, the occurrence of association through halogen bridges, and intermolecular ligand exchange, it is likely that similar solvent effects on coupling constants will be observed in many covalent fluorides.

The Dissociation Rate of Molecular Fluorine

by Daniel J. Seery

United Aircraft Research Laboratories, East Hartford, Connecticut
(Received December 7, 1965)

Recent measurements of the dissociation rate of molecular $F_2^{1,2}$ are considerably lower than would be expected by analogy with the other halogens. Since there is good reason to accept the validity of the experimental measurements, these unexpectedly low values for the dissociation rate constant warrant further analysis.

If the bond dissociation energy is considered as a guide to predict the dissociation rates, then the rate of dissociation of F_2 should be similar to that for I_2^3 and greater than those for Br_2^4 and Cl_2^5 . (The dissociation energy is 37 kcal for F_2 , 35.6 kcal for I_2 , 45.4 kcal for Br_2 , and 57.1 kcal for Cl_2 .) Inspection of Figure 1, however, shows that the dissociation rate of F_2 is a good deal slower than that for I_2 , and, as a matter of fact, it is not much greater than the dissociation rate of Br_2 .

A further indication that F_2 dissociation is quite different from the other members of the halogen family is given by a comparison of the experimental dissociation rates with those obtained from the theory of Benson and Fueno.⁶ Although this theory was developed for recombination reactions, dissociation rates can be readily obtained by using the principle of detailed balancing. The calculated dissociation rates are then within a factor of 2 of the experimental results for I_2 and Br_2 , whereas for F_2 the theory gives results approximately two orders of magnitude higher than experiment.

For all systems in which a chemical reaction takes place, there is a resultant perturbation of the normal

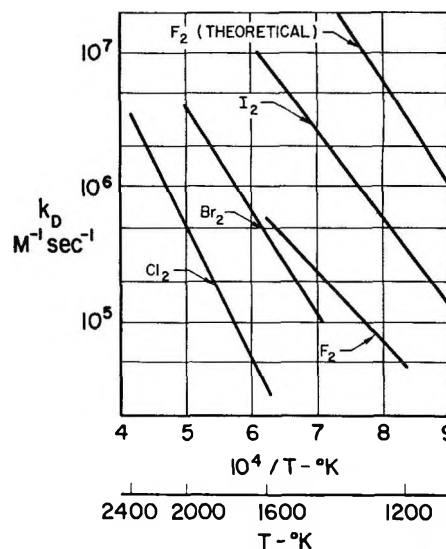


Figure 1. Dissociation rate constants vs. $1/T$. Sources of experimental data are given in the text. The theoretical values for F_2 were calculated using ref 6 as indicated in the text.

Boltzmann distribution of the vibrational levels. In the dissociation of a diatomic molecule, this perturbation is caused by the depopulation of the upper vibrational levels, and the extent of depopulation is in turn controlled by the upward transition rate (or "ladder climbing") of the vibrational levels. Of the several factors that can influence the rate of population of the vibrational levels, anharmonic effects⁷ seem to be the most important for an explanation of the relatively low dissociation rate for F_2 .

A plausible explanation of these low rates is that a rapid depopulation of the upper vibrational levels results in a "bottleneck" or minimum in the transition rate in the middle of the vibrational ladder. The argument originally formulated by Pritchard⁸ is the following. The number of transitions per unit time from $v = i$ to $v = j$ (where $j = i + 1$) is given by

$$N_{ij} = ZN_i P_{ij}$$

where Z is the number of collisions per unit time,

- (1) C. D. Johnson and D. Britton, *J. Phys. Chem.*, **68**, 3032 (1964).
- (2) D. J. Seery and D. Britton, to be published.
- (3) D. Britton, N. Davidson, W. Gehman, and G. Schott, *J. Chem. Phys.*, **25**, 804 (1956).
- (4) C. D. Johnson and D. Britton, *ibid.*, **38**, 1455 (1963).
- (5) M. van Thiel, D. J. Seery, and D. Britton, *J. Phys. Chem.*, **69**, 834 (1965).
- (6) S. W. Benson and T. Fueno, *J. Chem. Phys.*, **36**, 1597 (1962).
- (7) Anharmonic effects have been shown to have a substantial effect on the transition probability for a Morse potential; cf. F. H. Mies, *ibid.*, **40**, 523 (1964).
- (8) H. O. Pritchard, *J. Phys. Chem.*, **66**, 2111 (1962).

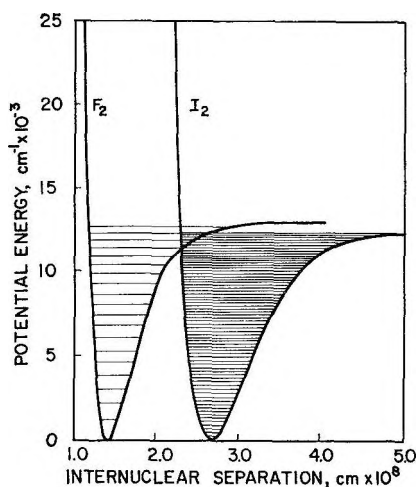


Figure 2. Potential energy curves for F_2 and I_2 . Curves are calculated by the method of H. M. Hulburt and J. O. Hirschfelder, *J. Chem. Phys.*, **9**, 61 (1941). See also J. O. Hirschfelder, *ibid.*, **35**, 1901 (1961).

N_i is the population of level i , and P_{ij} is the probability of transition from i to j and varies with $e^{-E_{ij}/RT}$ where E_{ij} is the energy difference between the levels. It then follows that as i increases, N_i will decrease, but P_{ij} will increase because E_{ij} decreases. Thus, under some circumstances, N_{ij} can have a minimum, implying that there is a rate-determining step in the middle of the activation ladder.

Consider the case of a diatomic molecule suddenly heated by shock wave. At the onset of dissociation, and before recombination is important

$$N_{j-3,j-2} > N_{j-2,j-1} > N_{j-1,j} < N_{j,j+1} < N_{j+1,j+2}$$

Thus, depending on the rate of increase of $P_{j,j+1}$, etc., there will be a reduction in the equilibrium population of upper vibrational levels. It should be emphasized (even as Pritchard does) that this situation is a direct result of the fact that diatomic molecules are anharmonic oscillators. It should further be pointed out that the probability of this situation developing for a given diatomic molecule will depend on just how anharmonic the molecule is. A comparison of the ratios of the zero-order vibrational frequency to the first anharmonicity constant⁹ shows that F_2 is by far the most anharmonic of the halogens. The ratio $\omega_e/\omega_e X_e$ is about five times larger for I_2 than for F_2 .

This anharmonicity of F_2 is also obvious in the separations and number of the vibrational energy levels as shown in Figure 2. I_2 has about 72 vibrational levels¹⁰ below the continuum and their separations range from 0.026 eV for $\Delta V_{1,2}$ to 0.016 eV for $\Delta V_{71,72}$. For a similar dissociation energy F_2 has 19 vibrational levels below the continuum whose separations range

from 0.107 eV for $\Delta V_{1,2}$ to 0.050 eV for $\Delta V_{18,19}$. The marked difference in anharmonicity indicates that a Pritchard-type "bottleneck" could develop for F_2 but is less likely for I_2 . This difference also helps to explain why the theory of Benson and Fueno, which uses harmonic oscillator transition probabilities, does not appear to be applicable to F_2 .

Another factor that helps to explain why the dissociation rate constants for F_2 are lower than I_2 is that for the latter, the possibility of nonnearest-neighbor vibrational transitions must be considered. It has been pointed out¹¹ that, when the separations of the vibrational levels are less than the thermal energy, vibrational transitions from and to next-nearest neighbors are important for the activation process. Furthermore, it should be noted that these relatively large separations of the vibrational levels for F_2 are close to the thermal energy ($1000^\circ K = 0.086$ eV) and this can also result in an over-all decrease in P_{ij} .

Acknowledgment. The author wishes to acknowledge several helpful discussions with Dr. H. J. Kolker, of United Aircraft Research Laboratories.

(9) For a compilation of the spectroscopic constants of the halogens, see W. H. Evans, T. R. Munson, and D. D. Wagman. *J. Res. Natl. Bur. Std.*, **55**, 147 (1955).

(10) The calculations of the vibrational energy levels for F_2 and I_2 were made from a simple two-term expansion using data from ref 9, and thus there is no pretense of high accuracy. An experimental study by R. D. Verma [*J. Chem. Phys.*, **32**, 738 (1960)] gives about 114 vibrational levels for I_2 . The major difference between Verma's work and the calculations used here occurs in the region close to the dissociation limit (approximately the top 30 levels) where Verma's data indicate a sharp increase in the number of levels and a concurrent decrease in the energy separation. Since a similar experimental study was not available for F_2 and since the more precise information on the vibrational levels would not affect the arguments presented here, it was decided to present the I_2 calculations in their present form.

(11) K. E. Schuler and G. H. Weiss, *ibid.*, **38**, 505 (1963).

Viscoelastic Behavior of Dilute Polystyrene Solutions in an Extended Frequency Range

by John D. Ferry, Larry A. Holmes, J. Lamb, and A. J. Matheson

Department of Electrical Engineering, The University, Glasgow W.2, Scotland, and the Department of Chemistry, University of Wisconsin, Madison, Wisconsin 53706 (Received December 22, 1965)

Dynamic viscoelastic measurements of dilute solutions of polymers in highly viscous solvents in the low audiofrequency range¹⁻³ give information about relatively long-range segmental motions which are

described by the theories of Rouse,⁴ Zimm,⁵ and Tschoegl.⁶ At much higher frequencies in such solvents, where the segmental motions do not respond to the oscillatory stress, the dynamic viscosity approaches a limiting value which is much less than the steady-flow viscosity but significantly greater than that of the solvent.^{7,8} This feature affects to some degree the interpretation of the low-frequency measurements. In order to reexamine the entire frequency range, we have combined here some low-frequency and high-frequency data on the same polymer samples.

Experimental Section

Low-frequency data for the storage and loss shear moduli of three polystyrenes with sharp molecular weight distribution, S-102, S-111, and S-108, have already been reported.² Another with higher molecular weight, S-1161, also generously provided by Dr. H. W. McCormick of the Dow Chemical Co., has now been similarly studied at a weight concentration of 1% in Aroclor 1248 at 10.2 and 24.9° in the frequency range from 0.1 to 400 cps, using the apparatus of Birnboim and Ferry.⁹ High-frequency measurements were made on solutions of S-102, S-108, and S-1161 by the torsional piezoelectric crystal as previously described;⁷ the frequency was 73 kc/sec and the temperature range from 30° down to the temperature at which the solution viscosity was about 15 poises. The Aroclors 1248 and 1232, used as solvents in these studies, are partially chlorinated diphenyls furnished by the Monsanto Co. The polymer molecular weights are given in Table I.

Table I: Parameters from High-Frequency Measurements, Reduced to 25°

| | Sample | | | |
|------------------------|--------------|-------|-------------------|--------|
| | S-102 | S-111 | S-108 | S-1161 |
| | 82 | 239 | 267 | 1200 |
| | Aroclor 1232 | | | |
| Concn, wt % | ... | ... | 2 | 1 |
| η_s , poise | ... | ... | 0.143 | 0.143 |
| η_∞ , poise | ... | ... | 0.181 | 0.162 |
| η , poise | ... | ... | 0.68 | 0.78 |
| | Aroclor 1248 | | | |
| Concn, wt % | 2 | 2 | 2 | 1 |
| η_s , poises | 2.60 | 2.60 | 2.2 ^a | 2.60 |
| η_∞ , poises | 3.79 | 3.8 | 3.15 ^a | 2.83 |
| η , poises | 7.79 | 12.9 | 15.1 | 15.4 |

^a The Aroclor 1248 low-frequency data for S-108 were obtained in a solvent lot with slightly lower viscosity (2.2 poises) than that used for the others. The value of η_∞ determined at high frequencies in the solvent lot of 2.60-poise viscosity has been corrected by the ratio 2.2/2.60.

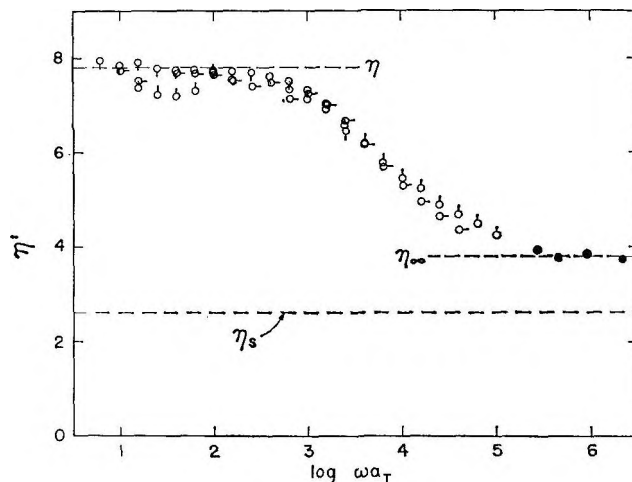


Figure 1. Dynamic viscosity plotted against logarithm of frequency reduced to 25° for 2% polystyrene S-102 in Aroclor 1248: \circ , low-frequency measurements at 6.4°; \odot , 10.0°; \circ , 25.0°; and \bullet , piezoelectric measurements.

Results

At the highest frequencies and lowest temperatures, the dynamic viscosity $\eta' (= G''/\omega$, where G'' is the dynamic loss modulus and ω is the radian frequency) approaches a limiting value η_∞ . This is illustrated in Figure 1 for sample S-102 at a concentration of 2%. Here reduction to 25° has been accomplished for measurements at other temperatures by multiplying the frequency by $\alpha_T = (\eta - \eta_s)T_0\rho_0/(\eta - \eta_s)_0T\rho$ and multiplying η' by $(\eta - \eta_s)_0/(\eta - \eta_s)$, where T is absolute temperature and ρ is density, and the subscript 0 refers to the reference temperature. The temperature superposition is less satisfactory than usual, but it is clear that η_∞ is substantially higher than η_s .

In Table I, similar limiting values of η_∞ are given for all the solutions of polystyrene in Aroclor studied here, together with the steady-flow solution viscosity η and the solvent viscosity η_s . For comparison there are included some results of Philippoff⁸ on a 2% solution of polystyrene S-111 in Aroclor 1248. As previously discussed, the difference $\eta_\infty - \eta_s$ is due to a contribution of the polymer chain to the viscosity associated with

- (1) N. W. Tschoegl and J. D. Ferry, *J. Phys. Chem.*, **68**, 867 (1964).
- (2) J. E. Frederick, N. W. Tschoegl, and J. D. Ferry, *ibid.*, **68**, 1974 (1964).
- (3) J. E. Frederick and J. D. Ferry, *ibid.*, **69**, 346 (1965).
- (4) P. E. Rouse, Jr., *J. Chem. Phys.*, **21**, 1272 (1953).
- (5) B. H. Zimm, *ibid.*, **24**, 269 (1956).
- (6) N. W. Tschoegl, *ibid.*, **39**, 149 (1963); **40**, 473 (1964).
- (7) J. Lamb and A. J. Matheson, *Proc. Roy. Soc. (London)*, **A281** 207 (1964).
- (8) W. Philippoff, *Trans. Soc. Rheol.*, **8**, 117 (1964).
- (9) M. H. Birnboim and J. D. Ferry, *J. Appl. Phys.*, **32**, 2305 (1961).

the volume-filling properties of the statistical coil independent of its motions, similar to the effect of rigid spheres in suspension as described by the Einstein equation.¹⁰

In comparing the frequency dependence of the storage (G') and loss (G'') shear moduli with the predictions of molecular theories,⁴⁻⁶ it has been customary¹⁻³ to represent the polymer contribution to the loss as $G'' - \omega\eta_s$, or $G'' - v_1\omega\eta_s$ where v_1 is the volume fraction of solvent, ordinarily negligibly different from unity; correspondingly, the normalized dynamic viscosity has been presented as $(\eta' - v_1\eta_s)/(\eta - v_1\eta_s)$. This procedure assumes that the entire polymer contribution to the solution viscosity can take part in the relaxation processes. However, since the molecular theories describe only that portion of loss associated with chain motions, it has been pointed out⁷ that the appropriate loss contribution should instead be $G'' - \omega\eta_\infty$, while the normalized dynamic viscosity should be $(\eta' - \eta_\infty)/(\eta - \eta_\infty)$. In Figure 2, G' and $G'' - \omega\eta_\infty$ are plotted in this manner for the data of Figure 1 at 6.4°; a single temperature is chosen because of the imperfect superposition with reduced variables, due probably to different temperature dependences of $(\eta - \eta_\infty)$ and η_∞ , that of η_∞ being probably closer to that of η_s . The solid curves are drawn from the theory of Tschoegl⁶ with $h = \infty$ (dominant hydrodynamic interaction) and $\epsilon = 0.065$; the agreement with the experimental data is much better than originally reported² where the theory was matched to $G'' - \omega v_1\eta_s$ (Figure 1 of ref 2).

The normalized dynamic viscosity is plotted as $(\eta' - \eta_\infty)/(\eta - \eta_\infty)$ for two other solutions in Figure 2, and in Figure 3 the storage shear modulus for all three solutions is plotted combining both low- and high-frequency measurements, for comparison with molecular theory. High-frequency measurements made in Aroclor 1232 have been reduced to equivalent values in Aroclor 1248 by multiplying the frequencies by $(\eta - \eta_s)_{1248}/(\eta - \eta_s)_{1232}$. At very low frequencies, substitution of η_∞ for $v_1\eta_s$ makes little difference, but at higher frequencies the frequency dependence is distinctly affected as previously shown.⁷

Strictly speaking, the nonzero slope for G' at high frequencies observed in Figure 3 is inconsistent with a constant limiting value of η_∞ (or direct proportionality of G'' to ω), since according to the phenomenological relations of viscoelasticity these quantities should be connected by the equation¹¹

$$d \log G'/d \log \omega =$$

$$F(G''/G')/(1 - d \log G''/d \log \omega) \quad (1)$$

where F is a factor not far from unity. If $d \log G''/d$

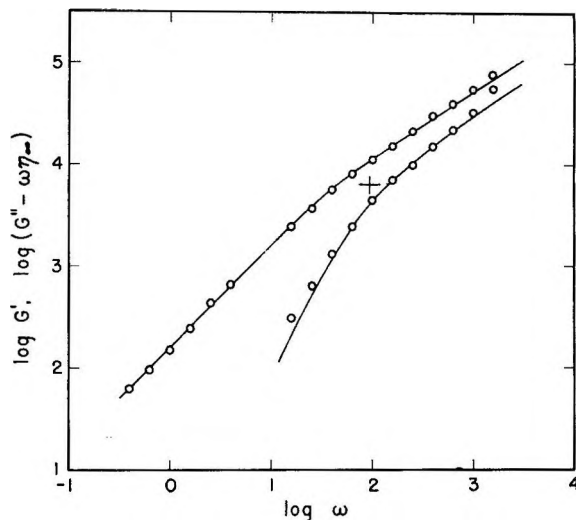


Figure 2. Frequency-dependent polymer contributions to the storage and loss moduli for 2% polystyrene in Aroclor 1248, at 6.4°, plotted logarithmically against frequency: solid curve, theoretical, with parameters from Table II.

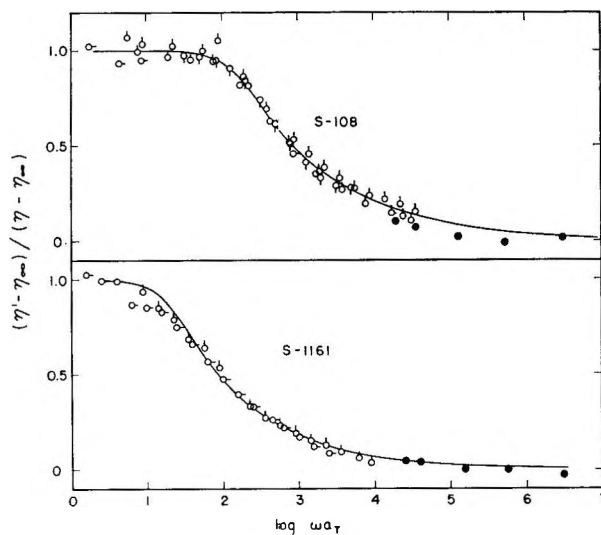


Figure 3. Normalized dynamic viscosity $(\eta' - \eta_\infty)/(\eta - \eta_\infty)$ plotted against logarithm of frequency reduced to 25° for two polystyrenes. Low-frequency measurements as follows: S-108, δ , 9.9° and 10.2°; \circ , 18.1°; \square , 20.0°; S-1161, δ , 10.2°; \circ , 24.9°; \bullet , piezoelectric measurements; solid curves are theoretical.

$\log \omega$ is 1 or $d \log \eta'/d \log \omega$ is zero, then $d \log G'/d \log \omega$ should be zero. However, in practice G'' (including the contribution of solvent to the loss) is at least an order of magnitude greater than G' in this region, so a small deviation from direct proportionality of G'' to

(10) A. Einstein, *Ann. Physik*, **19**, 289 (1906); **34**, 591 (1911).

(11) J. D. Ferry, "Viscoelastic Properties of Polymers," John Wiley and Sons, Inc., New York, N. Y., 1961, Chapter 4, eq 9 and 20.

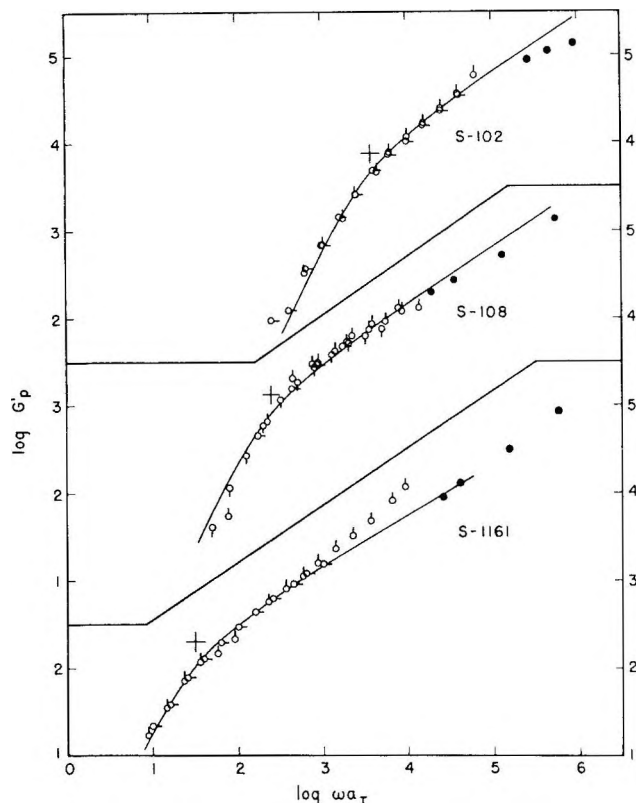


Figure 4. Storage shear modulus plotted logarithmically against frequency reduced to 25° for solutions of Figures 1 and 3, with same temperature key; curves theoretical. Cross denotes origin of dimensionless theoretical plot.

ω (or slight dependence of η' on ω) is still consistent with a substantial positive slope of $\log G'$ vs. $\log \omega$. In addition, the onset of solvent relaxation occurs¹² at a viscosity of about 10 poises at 100 kc/sec, and the solvent will thus make a small contribution to G' at the higher frequencies.

Discussion

Comparison with Molecular Theories when η_∞ is Taken into Account. Satisfactory agreement with the frequency dependence predicted by the Tschoegl theory with the parameters listed in Table II is evident in Figures 3 and 4. The shift from Zimm-like ($h = \infty$) to Rouse-like (h approaching 0) behavior with increasing molecular weight is observed as in the previous analysis² where η_∞ was not taken into account. The molecular weights M_{ve} in Table II are obtained by matching the coordinates of the experimental and theoretical curves as previously described;² they are still somewhat higher than the true molecular weights.¹³

Equivalent Hydrodynamic Sphere from η_∞ . The Einstein equation can be applied quantitatively to polymer solutions if each polymer molecule is regarded as being replaced by an equivalent hydrodynamic

Table II: Parameters from Fitting Tschoegl Theory

| Sample | S-102 | S-108 | S-1161 |
|--------------------|----------|----------|--------|
| $M \times 10^{-3}$ | 82 | 267 | 1200 |
| Concn, wt % | 2 | 2 | 1 |
| h | ∞ | ∞ | 2.5 |
| ϵ | 0.065 | 0.090 | 0.135 |
| $\log M_{ve}$ | 5.02 | 5.73 | 6.25 |
| $\log (M_{ve}/M)$ | 0.11 | 0.30 | 0.17 |

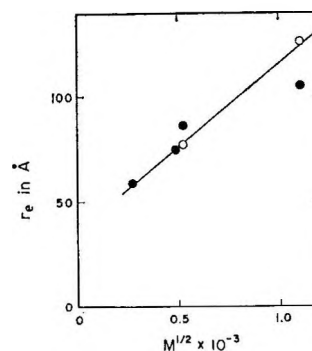


Figure 5. Effective Einstein radius plotted against square root of molecular weight: O, in Aroclor 1232; ●, in Aroclor 1248.

sphere, which makes the same contribution to the solution viscosity as does the polymer above the polymer relaxation region.⁷ Thus the nonrelaxing part of the polymer contribution to the solution viscosity, $\eta_\infty - \eta_s$, may be expressed by analogy with the Einstein equation as

$$\eta_\infty - \eta_s = 2.5V_2\eta_s \quad (2)$$

where V_2 is the volume fraction of the equivalent hydrodynamic spheres. This may be rearranged to give

$$\eta_\infty - \eta_s = \frac{2.5cN_0v_e\eta_s}{M} \quad (3)$$

where c is the concentration of polymer in grams per cubic centimeter, N_0 is Avogadro's number, v_e is the volume of the equivalent hydrodynamic sphere, and M is the molecular weight of the polymer. Equation 3 shows that $\eta_\infty - \eta_s$ is proportional to c for a given polymer-solvent system, as found experimentally by Philippoff.⁸ Equation 3 may also be used to calculate the radius of the equivalent hydrodynamic sphere, r_e ,

(12) A. J. Barlow, J. Lamb, and A. J. Matheson, unpublished work.

(13) NOTE ADDED IN PROOF. A very recent theory of A. Peterlin (*J. Chem. Phys.*, in press, and private communication) shows that the finite high-frequency intrinsic viscosity can be attributed to an internal viscosity associated with the Rouse-Zimm submolecules. It follows that the form of the frequency dependence is modified, so that neither $G'' - \omega\eta_s$ nor $G''' - \omega\eta_\infty$ can be expected to fit the Rouse-Zimm-Tschoegl theories precisely.

which is plotted against $M^{1/2}$ for solutions of polystyrene in Aroclor in Figure 5; the dependence is linear in the range covered. Earlier high-frequency data in solvents of low viscosity^{7,12} are in general consistent with this type of treatment, but for such solutions it has not yet been possible to determine η_{∞} by direct measurement.

More extensive measurements of the Einstein viscosity in several viscous solvents of different solvent power are required to investigate the dependence of η_{∞} on the molecular configuration of the polymer in

the various solvents. It would also be interesting to extend the measurements to higher frequencies to see if the onset of the relaxation of η_{∞} occurs close to the relaxation region of the solvent.

Acknowledgments. These studies were supported at Wisconsin by a grant from the U. S. Public Health Service, No. GM-10135, and at Glasgow by a grant from the National Engineering Laboratory of the Department of Scientific and Industrial Research.

COMMUNICATIONS TO THE EDITOR

Kinetics of Iodination of Mercury Dimethyl in Various Solvents

Sir: In previous calorimetric experiments, it was noted that the iodination of mercury dialkyls took place at markedly different rates in different solvents.¹ We report here measurements on the iodination of mercury dimethyl in five solvents over a temperature range of 23–45°.

The iodination takes place rapidly in all solvents in sunlight, but it was found following rigorous exclusion of light that there exists a genuine dark-reaction. This thermal reaction was followed by mixing known concentrations of iodine and of mercury dimethyl, each in the solvent concerned, in stoppered flasks inside a light-tight temperature-controlled box. The extent of the reaction was determined by removing samples at known times and determining the unused iodine colorimetrically. Tests showed that our sampling technique did not advance the percentage reaction appreciably, but if the solutions were left in the colorimeter for any length of time the superposition of the photochemical reaction, caused by the photometer light source, upon the genuine thermal reaction led to higher rate constants. In the concentration ranges used (10^{-3} to 10^{-2} mole/l. of each reactant) the reaction was found to be first order in each reactant, and a summary of the results obtained is given in Table I. The rate constants vary by a factor of about 100, but to within the experimental error, the activation energy for the reaction is independent of the solvent. The iodination of mercury dimethyl in carbon tetrachloride has been studied

previously by Razuvaev and Savitskii,² who found a slightly higher activation energy of 9.5 kcal/mole; their rate constants are consistently larger than ours (e.g. 0.116 instead of 0.073 at 28°) and it is not clear from their account whether they were aware of the existence of a photochemical reaction.

Table I

| Solvent | Dielectric constant | $\Delta H_{\text{soln}}(\text{I}_2)$, kcal/mole ^a | k at 28°, l. mole ⁻¹ min ⁻¹ | E , kcal/mole |
|----------------------|---------------------|---|---|-----------------|
| Cyclohexane | 2.05 | -5.8 | 0.069 ± 0.003 | 7.1 ± 1.0 |
| Carbon tetrachloride | 2.22 | -5.8 | 0.073 ± 0.004 | 7.7 ± 1.0 |
| Benzene | 2.30 | -4.25 | 0.40 ± 0.02 | 8.5 ± 1.0 |
| Chloroform | 4.64 | -5.1 | 1.49 ± 0.05 | 8.0 ± 1.0 |
| Ethanol | 25.8 | -1.65 | 6.95 ± 0.35 | 7.4 ± 1.0 |

^a K. Hartley and H. A. Skinner, *Trans. Faraday Soc.*, **46**, 621 (1950).

There is no obvious correlation between the rate constants and any simple physical property of the solvents. However, there is a reasonable correlation between the rate constants and the quantity $-\{\text{dielectric constant}/\Delta H_{\text{soln}}(\text{I}_2)\}$ which might suggest that a higher rate of reaction is favored by a higher degree of ionic dissociation and by a higher degree of complexing between the I_2 and the solvent.

The experiments in ethanol were repeated in 0.125 M

- (1) H. O. Pritchard, Ph.D. Thesis, University of Manchester, 1951.
 (2) G. A. Razuvaev and A. V. Savitskii, *Dokl. Akad. Nauk SSSR*, **85**, 575 (1953).

sodium iodide-ethanol solutions. The rate constant at 28° fell to 1.10 l. mole⁻¹ min⁻¹ with an over-all activation energy of 16.5 ± 1 kcal/mole. The simplest explanation of this effect is that the normal reaction involves I⁺, but in the presence of some 20-fold excess of NaI, this is suppressed and that an alternative but more difficult path involves the I⁻ ion.

(3) Centre for Research in Experimental Space Science, York University, Toronto.

DEPARTMENT OF CHEMISTRY
UNIVERSITY OF MANCHESTER
MANCHESTER, ENGLAND

ALLAN LORD³
H. O. PRITCHARD³

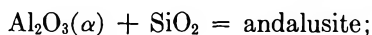
RECEIVED JANUARY 10, 1966

The Thermodynamic Properties of the Aluminum Silicates

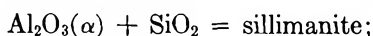
Sir: Using oxide melt solution calorimetry at 695°, the authors have succeeded in determining the enthalpies of formation of the three polymorphs of Al₂SiO₅ (kyanite, andalusite, and sillimanite) and of 3Al₂O₃·2SiO₂ (mullite). The results are



$$\Delta H_{968} = -2.37 \pm 0.15 \text{ kcal/mole}$$



$$\Delta H_{968} = -1.99 \pm 0.17 \text{ kcal/mole}$$



$$\Delta H_{968} = -1.51 \pm 0.15 \text{ kcal/mole}$$



$$\Delta H_{968} = +5.44 \pm 0.35 \text{ kcal/mole}$$

These data are in serious disagreement with the values quoted by Rossini, *et al.*,¹ which indicate heats of formation for the polymorphs of the order of -40 kcal/mole. On the basis of these results, and of entropy, heat content, and volume data taken from the literature, the *P-T* diagram for the Al₂O₃-SiO₂ system can be calculated for a wide range of temperatures and pressures.

When our new enthalpy data are combined with information on the free energy of formation of mullite (-5.6 kcal/mole, at 1823°K; Rein and Chipman²) we are able to derive a new value for the standard entropy of mullite, $S_{298}^\circ = 64.43$ cal/deg mole. The uncertainty in this value is estimated to be about ±0.5 cal/deg mole.

This result disagrees with the third-law value of the entropy given by Pankratz, Weller, and Kelley,³ 60.8 ± 0.8 cal/deg mole. However, this apparent discrepancy can be resolved in part by allowing for the disorder associated with the mixing of Si and Al on the tetrahedral sites of the mullite structure. The present work will be published in greater detail elsewhere.

(1) F. D. Rossini, *et al.*, National Bureau of Standards Circular 500, U. S. Government Printing Office, Washington, D. C., 1952.

(2) R. H. Rein and J. Chipman, *Trans. AIME*, **233**, 415 (1965).

(3) L. B. Pankratz, W. W. Weller, and K. K. Kelley, U. S. Bureau of Mines Report of Investigations, 6287, Mines Bureau, Pittsburgh, Pa., 1963.

INSTITUTE FOR THE STUDY OF METALS
UNIVERSITY OF CHICAGO
CHICAGO, ILLINOIS

J. L. HOLM
O. J. KLEPPA

RECEIVED MARCH 11, 1966